

25тн IAEA FUSION ENERGY CONFERENCE

D+2

13-18 October 2014 St. Petersburg, Russian Federation

Programme, Abstracts and Contributions





ic Energy Agency







25th IAEA Fusion Energy Conference St. Petersburg, Russian Federation October 13–18, 2014

Programme & Book of Abstracts & Linked Contributions

Version: September 14, 2015

Scan relevant QR to download the Conference4me app.



QR for Android



QR for iPhone

The **Conference4me** application provides a digital, mobile copy of the conference agenda and timetables, venue information, social network updates, and more. Download **Conference4me** from the Android Play Store or from iTunes, run the application and choose the *25th IAEA Fusion Energy Conference* from the list of conferences available for download. For more information about Conference4me, including QR codes for direct downloads, please see the official Conference4me website: http://Conference4me.psnc.pl

Thanks to PSNC for integrating this conference into the Conference4me smartphone conference application.

Colophon

This book has been assembled from the abstract sources submitted by the contributing authors. Layout, editing, and customized T_EX & LAT_EX macros used to typeset the book were developed by Dr. P. Knowles, LogrusData, Vienna, Austria.

Conference Secretariat

IAEA Scientific Secretaries:

Mr Ralf Kaiser Mr Richard Kamendje

Division of Physical and Chemical Sciences International Atomic Energy Agency Vienna International Centre, PO Box 100 1400 Vienna, Austria tel: +43 1 2600 21707 physics@iaea.org

IAEA Administration and Organization:

Ms Karen Morrison

Division of Conference and Document Services International Atomic Energy Agency Vienna International Centre, PO Box 100 1400 Vienna, Austria tel: +43 1 2600 21317 fax: +43 1 26007 K.Morrison@iaea.org

Local Organization

Host Government Officials:

Ms Marina Belyaeva

Mr Viacheslav Gutkov

Department for International Cooperation The State Atomic Energy Corporation "Rosatom" 24, Bolshaya Ordynka St. 119017 Moscow Russian Federation MPBelyaeva@rosatom.ru VAGutkov@rosatom.ru

Conference Site Issues:

25th IAEA FEC Support Center

bld. 40, 11, Ordzhonikidze St. Moscow, Russian Federation, 115419 tel: +7 499 922 89 95 Fec2014@atomexpo.com

Mr Alexey Kalashnikov

Department of International Scientific Programs The State Atomic Energy Corporation "Rosatom" 24, Bolshaya Ordynka St. 119017 Moscow Russian Federation ANKalashnikov@rosatom.ru

Ms Elena Starostina

25th IAEA FEC Support Center bld. 40, 11, Ordzhonikidze St. Moscow, Russian Federation, 115419 tel: +7 499 922 89 95 ENStarostina@atomexpo.com

Conference Location

Hotel Park Inn Pribaltiyskaya

14 Korablestroiteley St. Vasilyevsky Island St. Petersburg, Russia, 199226

Satellite Meetings

Satellite meetings can be held. Meeting rooms and times can be reserved at: http://www.fec2014.org/en/satellite_meetings/

Working Language & Resolution

Working Language: English

Resolution: No resolutions may be submitted for consideration on any subject; no votes will be taken

Participation in an IAEA Scientific Meeting

Governments of Member States and those organizations whose activities are relevant to the meeting subject matter are invited to designate participants in the IAEA scientific conferences and symposia. In addition, the IAEA itself may invite a limited number of scientists as invited speakers. Only participants designated or invited in this way are entitled to present papers and take part in the discussions.

Representatives of the press, radio, television or other information media and members of the public, the latter as "observers", may also be authorized to attend, but without the right to take part in the proceedings.

Scientists interested in participating in any of the IAEA meetings should request information from the Government authorities of their own countries, in most cases the Ministry of Foreign Affairs or national atomic energy authority.

IAEA Publications

All IAEA publications may be ordered from the Sales and Promotion Unit, International Atomic Energy Agency, P.O. Box 100, A-1400 Vienna, Austria Fax: +43 1 2600-29302 sales.publications@iaea.org www.iaea.org/Publications/index.html

Nuclear Fusion Journal

Participants have been invited to submit their paper for possible publication in the IAEA journal, Nuclear Fusion. Contributed papers that were not submitted for publication in Nuclear Fusion will be available as pdfs. Links on the abstract pages direct the reader either to the contribution paper or the Nuclear Fusion journal, as appropriate. If your institution does not have access to the journal, pdfs of these FEC derived articles can be requested from nf@iaea.org.

Name	Country/International Organization
Chair:	
Yutaka Kamada	Japan
Vice Chair:	
Alain Bécoulet	France
Enrique Ascesibar	Spain
Enrique Ascasibar Boyd Blackwell	Spain Australia
Dhiraj Bora	India
Vincent Chan	United States of America
Glenn Counsell	European Commission
Xuru Duan	China
Stephen Eckstrand	United States of America
Atsushi Fukuyama	Japan
Martin Greenwald	United States of America
Lorne Horton	European Commission
Katsumi Ida	Japan
Arne Kallenbach	Germany
Boris Kuteev	Russian Federation Russian Federation
Sergei Lebedev Hyeon Park	Korea, Republic of
Pravesh Patel	United States of America
Steven Sabbagh	United States of America
Keishi Sakamoto	Japan
Hiroyuki Shiraga	Japan
Joseph Snipes	ITER
Elisabeth Surrey	United Kingdom

This book contains all abstracts accepted by the FEC programme committee. Note that abstracts have been edited for style uniformity.

Overview of Contributions (as of September 14, 2015)

- 1 Keynote presentation
- 23 Overview talks
- 73 Regular talks
- 22 Rapporteured papers
- 4 Overview poster presentations
- 558 Regular poster presentations
 - 0 Post deadline talks
 - 12 Post deadline poster presentations
 - 5 Summary talks

Overview posters will be exhibited during the entire conference. All oral presentations will also be displayed as posters according to the programme.

The duration of oral presentations indicated in the programme already includes discussion time. Speakers are requested to make available the following times for discussions:

4' for overview presentation (total 25')

3' for regular oral presentation (total 20')

Rapporteur papers are identified by the letter "a" after the paper number. Rapporteured papers are identified by the letters "b" or "c" after the paper number.

Explanation of Abbreviations

- **O** Opening
- S Summary
- **OV** Overviews
- **OVP** Overview Posters
 - **EX** Magnetic Confinement Experiments
 - TH Magnetic Confinement Theory and Modelling For both **EX** and **TH**, subdivisions are:
 - C: Confinement
 - S: Stability

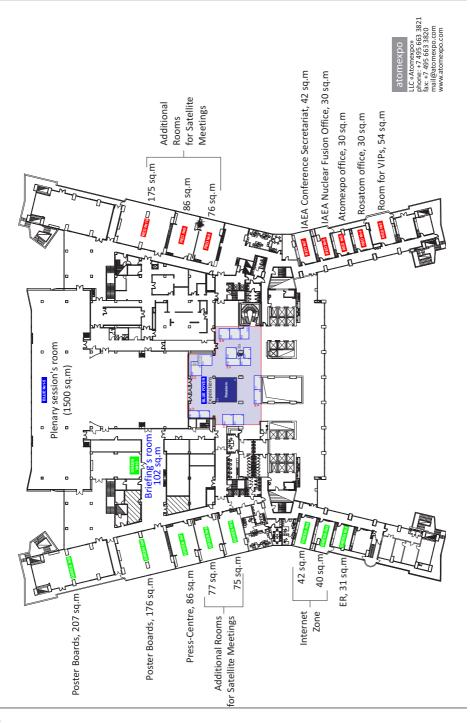
W: Wave–plasma interactions; current drive; heating; energetic particles **D**: Plasma–material interactions; divertors; limiters; scrape-off layer (SOL)

- FIP Fusion Engineering, Integration and Power Plant Design
- FNS Fusion Nuclear Physics and Technology
- **ICC** Innovative Confinement Concepts

IFE Inertial Fusion Experiments and Theory

MPT Materials Physics and Technology

- PD Post-Deadline contributions
- PPC Plasma Overall Performance and Control
- SEE Safety, Environmental and Economic Aspects of Fusion



Conference Timetable

Ing OV/3 P1 Overview: Inertial and OV/3 Inertial and Nagnetic Magnetic Magnetic P1 13 P1 13 P1 14 P1 13 P1 13 P1 14 P1 13 P1 14 P1 14 P1 13 P1 14 P1 14 P1 14 P1 13 P1 14 P1 14 P1 14	FIP/2 Heating and Disruption p. 22	P3	OCT. 16, 2014	+	Oct. 17, 2014		Oct. 18, 2014
ining Overview: ining Inertial and ining Inertial and Magnetic Husion P. 13 P. 13 P. 13 P. 13 P. 13 P. 13 P. 13 P. 13 P. 13 P. 14 Sector OV/4 P. 13 P. 14	Heating and Disruption p. 22		IFE/1	P5	EX/7-PPC/1	P7	FNS/1-MPT/1
p. 13 p. 14 n b. 13 view: al and n b. 13 n al bhysics n al bhysics <	p. 22	Posters	Inertial Fusion Experiments and Theory	Posters	Divertor & Exhaust Physics	Posters	Next Step Fusion Nuclear Technology
I EX/1 View: 3D Physics nn B. 13 nn D. 13 D. Physics B. 14 D. 13 D. 13 D. 13 D. 14 D. 13 D. 13 D. 14 D. 13 D. 13 D. 14 D. 13 D. 14 D. 14 D. 13 D. 15 D. 14 D. 14 D. 15 D. 15 D. 14 D. 14 D. 15 D. 15 D. 14 D. 14 D. 15 D. 15 D. 14 D. 15 D. 15 D. 16 D. 15 D. 17 D. 13 D. 18 D. 13 D. 19 D. 13 D. 13 D. 13 D. 14 D. 14 D. 15 D. 15 D. 16 D. 14 D. 17 D. 15 D. 18 D. 14 D. 17 <	L	p. 23	p. 34	p. 35	p. 47	p. 48	p. 61
I EX/1 View: 3D Physics view: 3D Physics an 3D Physics an 3D Physics an 3D Physics an 0 p. 13 p. 14 p. 13 p. 13 p. 13 p. 14 and 0	Co	Coffee Break					
Notew: Anticew: Anticew: antic Bosters Anticew: Anticew: D Prysics Anticew: Anticew: D Anticew: D <	EX/2-TH/1	P3	EX/5-TH/4	P5	EX/8, TH/6, PD	Ld	EX/11-TH/8
p. 13 p. 13 p. 14 p. 13 p. 13 p. 14 p. 13 p. 13 p. 13 p. 13 p. 13 p. 13 p. 13 p. 14 p. 14 p. 13 p. 14 p. 14	Core Turbulence	Posters	Runaway, Disruption & RF Physics	Posters	3D Physics & Post-Deadline Papers	Posters	Edge Turbulence
2 Posters iew: A Posters Magnetic Public Magnetic Public Posters Magnetic Public Posters Public Posters Public Posters Public Posters Public Posters Public Posters Public Posters Public Posters Public Posters Public Posters Public Posters Public	p. 22	p. 23	p. 34	p. 35	p. 47	p. 48	p. 62
Normal and Normal and Normal and Normal and Nagnetic etic frusion frust frusion frust fr		Lunch					
Alew: Alew: Al and Angnetic Fusion Alexie Al	EX/3-TH/2	P4	EX/6-TH/5	P6	EX/9-PPC/2	P8	
	Pedestal Physics	Posters	Transport & MHD	Posters	Operational Scenarios	Posters	Summary (13:30 – 15:40)
p. 10 p. 11 p. 17 p. 18 p. 27	p. 27	p. 29	p.40	p. 42	p. 55	p. 56	p. 63
	Co	Coffee Break	~				
FIP/1 OVP OV/5 P2 EX/4-	EX/4-TH/3	P4	FIP/3	P6	EX/10-TH/7	P8	
ITER Technology Overview: Diverte Magnetic SOL PI Fusion Eusion	Divertor & SOL Physics	Posters	New Devices & Technology	Posters	Energetic Particles Physics	Posters	Summary (16:10 - 17:40)
p. 18 p.	p. 28	p. 29	p. 41	p. 4 2	p. <mark>55</mark>	p. 56	p. 63
Nuclear Fusion Reception Board Meeting			Banquet				

Programme

Conference Registration — Hotel Park Inn Pribaltiyskaya, Blue Foyer

(16:00 - 19:00)

Sunday, October 12, 2014

MON

Conference Registration — Hotel Park Inn Pribaltiyskaya, Blue Foyer (07:30 – 18:30)

O/1: Opening

Chair	:: V. Gusev (l	Russian Fed.)		<i>Plenary Hall: Blue 1–5 (08:30 – 10:15)</i>
Time	Id	Presenter		Title
8:30	O/1	Host Government Representative	Russian Federation	Welcome Address
9:00	O/2	IAEA Representative	IAEA	Opening Address and Nuclear Fusion Prize Award
9:30	O/3	E. P. Velikhov	Russian Federation	Igor Kurchatov and the Russian Fusion Program

Coffee Break (10:15 – 10:45)

OV/1: Magnetic Fusion

Chair: A. Burdakov (Russian Fed.)

PDF Link: Discussion Plenary Hall: Blue 1–5 (10:45 – 12:30)

Chain: The Durau	(itubbiaii i cu	•)	1 ienary 11an Drac 1 0 (10.10 12.00)
Time Id	Presenter		Title
10:45 OV/1-1	L. Askinazi	Russian Federation	Fusion Research in Ioffe Institute
11:10 OV/1-2	O. Motojima	ITER	The ITER Project Construction Status
11:35 OV/1-3	F. Romanelli	European Commis- sion	Overview of the JET Results
12:00 OV/1-4	R. J. Buttery	USA	DIII-D Research to Address Key Challenges for ITER and Fusion Energy

Lunch Break (12:30 - 14:00)

NION

Monday, October 13, 2014

<mark>OV/2</mark> : Inertial a Chair: Y. Liu (Cl	nd Magnetic Fusi hina)	on	PDF Link: Discussion Plenary Hall: Blue 1–5 (14:00 – 16:10)
Time Id	Presenter		Title
14:00 OV/2-1	A. Krasilnikov	Russian Federation	Progress with the ITER Project Activity in Russia
14:25 OV/2-2	H. Zohm	Germany	Recent ASDEX Upgrade Research in Support of ITER and DEMO
14:50 OV/2-3	K. Ida	Japan	Overview of Transport and MHD Stability Study and Impact of Magnetic Field Topology in the Large Helical Device
15:15 OV/2-4	I. Chapman	UK	Overview of MAST Results
15:40 OV/2-5	E. Marmar	USA	Alcator C-Mod: Research in Support of ITER and Steps Beyond

Coffee Break (16:10 – 16:40)

FIP/1: ITER Technology

Chair: O. Filatov (Russian Fed.)

PDF Link: Discussion

Plenary Hall: Blue 1-5 (16:40 - 18:45)

 17:40 FIP/1-4Ra P. Bruzzone Switzerland Summary of the Test Results of ITER Conductors in SULTAN FIP/1-4Rb Research, Development and Production of ITER Toroidal Field Conductors and Poloidal Field Cables in Russia 18:00 FIP/1-5 A. Encheva ITER Overview of the Design Development, Prototype Manufacturing and Procurement of the ITER In-Vessel Coil 18:20 FIP/1-6Ra C. Sborchia ITER Progress in the Design and Manufacturi of High Vacuum Components for ITER FIP/1-6Rb 		(Itabbian I cal)		1 ioning 11init 2 inte 1 o (10110 - 10110)
Technology for ITER Full-Tungsten Divertor in Japan17:00 FIP/1-2J. P. GunnFranceSurface Heat Loads on Tungsten Monoblocks in the ITER Divertor17:20 FIP/1-3N. KoizumiJapanFull-Scale Trial Results to Qualify Optimized Manufacturing Plan for ITE Toroidal Field Coil Winding Pack in Japan17:40 FIP/1-4RaP. BruzzoneSwitzerlandSummary of the Test Results of ITER Conductors in SULTANFIP/1-4RbResearch, Development and Production of ITER Toroidal Field Conductors and Poloidal Field Cables in Russia18:00 FIP/1-5A. EnchevaITEROverview of the Design Development, Prototype Manufacturing and Procurement of the ITER In-Vessel Coil18:20 FIP/1-6RaC. SborchiaITERProgress in the Design and Manufactur of High Vacuum Components for ITER FIP/1-6Rb	Time Id	Presenter		Title
 Monoblocks in the ITER Divertor 17:20 FIP/1-3 N. Koizumi Japan Full-Scale Trial Results to Qualify Optimized Manufacturing Plan for ITE Toroidal Field Coil Winding Pack in Japan 17:40 FIP/1-4Ra P. Bruzzone Switzerland Summary of the Test Results of ITER Conductors in SULTAN FIP/1-4Rb Research, Development and Production of ITER Toroidal Field Conductors and Poloidal Field Cables in Russia 18:00 FIP/1-5 A. Encheva ITER Overview of the Design Development, Prototype Manufacturing and Procurement of the ITER In-Vessel Coil 18:20 FIP/1-6Ra C. Sborchia ITER Progress in the Design and Manufactur of High Vacuum Components for ITER Manufacturing Design and Progress of 	16:40 FIP/1-1	Y. Seki	Japan	Technology for ITER Full-Tungsten
 Optimized Manufacturing Plan for ITE Toroidal Field Coil Winding Pack in Japan 17:40 FIP/1-4Ra P. Bruzzone Switzerland Summary of the Test Results of ITER Conductors in SULTAN FIP/1-4Rb Research, Development and Production of ITER Toroidal Field Conductors and Poloidal Field Cables in Russia 18:00 FIP/1-5 A. Encheva ITER Overview of the Design Development, Prototype Manufacturing and Procurement of the ITER In-Vessel Coil 18:20 FIP/1-6Ra C. Sborchia ITER Progress in the Design and Manufacturing of High Vacuum Components for ITER FIP/1-6Rb 	17:00 FIP/1-2	J. P. Gunn	France	0
FIP/1-4RbConductors in SULTANFIP/1-4RbResearch, Development and Production of ITER Toroidal Field Conductors and Poloidal Field Cables in Russia18:00FIP/1-5A. EnchevaITER18:20FIP/1-6RaC. SborchiaITERProgress in the Design and Manufacturi of High Vacuum Components for ITER Manufacturing Design and Progress of	17:20 FIP/1-3	N. Koizumi	Japan	Optimized Manufacturing Plan for ITER Toroidal Field Coil Winding Pack in
 of ITER Toroidal Field Conductors and Poloidal Field Cables in Russia 18:00 FIP/1-5 A. Encheva ITER Overview of the Design Development, Prototype Manufacturing and Procurement of the ITER In-Vessel Coil 18:20 FIP/1-6Ra C. Sborchia ITER Progress in the Design and Manufactur of High Vacuum Components for ITER FIP/1-6Rb 	17:40 FIP/1-4Ra	P. Bruzzone	Switzerland	5
Prototype Manufacturing and Procurement of the ITER In-Vessel Coil 18:20 FIP/1-6Ra C. Sborchia ITER Progress in the Design and Manufactur of High Vacuum Components for ITER FIP/1-6Rb Manufacturing Design and Progress of	FIP/1-4Rb			Research, Development and Production of ITER Toroidal Field Conductors and Poloidal Field Cables in Russia
of High Vacuum Components for ITER FIP/1-6Rb Manufacturing Design and Progress of	18:00 FIP/1-5	A. Encheva	ITER	0 1
	18:20 FIP/1-6Ra	C. Sborchia	ITER	Progress in the Design and Manufacture of High Vacuum Components for ITER
	FIP/1-6Rb			Manufacturing Design and Progress of the First Sector for ITER Vacuum Vessel

40N	NOM	MOM	NOM	MOM	MOM	
101	MON	MON	MON	MON	MON	
101	IOM	MON	MON	MOI	MOI	
40	ОM	MО	OM	OM	MО	
ЛC	MC	MC	MC	MC	MC	
Ч	Ж	М	М	М	М	
V	Ň	Ž	Ž	Ž	Ž	
\sim	Ν	Σ	\geq	Σ	Σ	
	2	2	2	2	2	
	Į		4			

These posters will be displayed for the duration of the conference

Overview	Posters OVP		Poster Room: Green 8&9 (14:00 – 18:45)
Id	Presenter		Title
OV/1-1	L. Askinazi	Russian Federation	Fusion Research in Ioffe Institute
OV/1-2	O. Motojima	ITER	The ITER Project Construction Status
OV/1-3	F. Romanelli	European Commis- sion	Overview of the JET Results
OV/1-4	R. J. Buttery	USA	DIII-D Research to Address Key Challenges for ITER and Fusion Energy
OV/2-1	A. Krasilnikov	Russian Federation	Progress with the ITER Project Activity in Russia
OV/2-2	H. Zohm	Germany	Recent ASDEX Upgrade Research in Support of ITER and DEMO
OV/2-3	K. Ida	Japan	Overview of Transport and MHD Stability Study and Impact of Magnetic Field Topology in the Large Helical Device
OV/2-4	I. Chapman	UK	Overview of MAST Results
OV/2-5	E. Marmar	USA	Alcator C-Mod: Research in Support of ITER and Steps Beyond
OV/3-1	H. Azechi	Japan	Fast Ignition Realization EXperiment (FIREX) and Prospect to Inertial Fusion Energy in Japan
OV/3-2	P. Barabaschi	European Commis- sion	Status of JT-60SA Project
OV/3-3	B. Wan	China	Advance of H-Mode Physics for Long-Pulse Operation on EAST
OV/3-4	SW. Yoon	Korea, Republic of	Overview of KSTAR Results in 2013 Campaign
OV/4-1	M. Xu	China	Overview of HL-2A Recent Experiments
OV/4-2	S. Coda	Switzerland	The Science Program of the TCV Tokamak: Exploring Fusion Reactor and Power Plant Concepts
OV/4-3	S. A. Sabbagh	USA	Overview of Recent Physics Results from NSTX
OV/4-4	M. Kobayashi	Japan	3D Effects of Edge Magnetic Field Configuration on Divertor/SOL Transport and Optimization Possibilities for a Future Reactor

Monday, October 13, 2014

FEC-2014	Monday, C		
Id	Presenter		Title
OV/4-5	J. Sánchez	Spain	Transport, Stability and Plasma Control Studies in the TJ-II Stellarator
OV/5-1	P. Terry	USA	Overview of Gyrokinetic Studies on Electromagnetic Turbulence
OV/5-2	M. E. Puiatti	Italy	Overview of the RFX-Mod Contribution to the International Fusion Science Program
OV/5-3	B. Chapman	USA	Overview of Results from the MST Reversed Field Pinch Experiment
OV/5-4	G. Pucella	Italy	Overview of the FTU Results
OV/5-5	S. Pradhan	India	First Experiments in SST-1
OV/P-01	N. Nakajima	Japan	Overview of DEMO Activities of IFERC Project in BA Activities
OV/P-02	G. Zhuang	China	Overview of the Recent Research on the J-TEXT Tokamak
OV/P-03	V. Gusev	Russian Federation	Review of Globus-M Spherical Tokamak Results
OV/P-04	M. Gryaznevich	UK	Contribution to Fusion Research from IAEA Coordinated Research Projects and Joint Experiments

OV/3: Inertial and Magnetic Fusion PDF Link: Discussion Chair: M. Mori (Japan) Plenary Hall: Blue 1-5 (08:30 - 10:15) TUE Time Id Title Presenter 8:30 OV/3-1 H. Azechi Fast Ignition Realization EXperiment Japan (FIREX) and Prospect to Inertial Fusion Energy in Japan P. Barabaschi 8:55 OV/3-2 European Status of JT-60SA Project Commission 9:20 OV/3-3 B. Wan China Advance of H-Mode Physics for Long-Pulse Operation on EAST 9:45 OV/3-4 S.-W. Yoon Korea, Overview of KSTAR Results in 2013 Republic of Campaign

Coffee Break (10:15 – 10:45)

EX/1: 3D Physics

Chair: F. Waelbroeck (USA)

PDF Link: Discussion

Plenary Hall: Blue 1–5 (10:45 – 12:30)

Chair: F. Waelbro	JECK (USA)		Plenary Hall: Blue 1–5 (10:45 – 12:50)
Time Id	Presenter		Title
10:45 EX/1-1	M. R. Wade	USA	Recent Advances in the Understanding and Optimization of RMP ELM Suppression for ITER
11:05 EX/1-2	A. Kirk	UK	Effect of Resonant Magnetic Perturbations on Low Collisionality Discharges in MAST and a Comparison with ASDEX Upgrade
11:25 EX/1-3	T. E. Evans	USA	Comparative Studies of Edge Magnetic Islands and Stochastic Layers in DIII-D and LHD
11:45 EX/1-4	S. A. Sabbagh	USA	Physical Characteristics of Neoclassical Toroidal Viscosity in Tokamaks for Rotation Control and the Evaluation of Plasma Response
12:05 EX/1-5	Y. Jeon	Korea, Republic of	Successful ELM Suppressions in a Wide Range of q_{95} Using Low n RMPs in KSTAR and its Understanding as a Secondary Effect of RMP

Poster Sessi	on: P1	Poster Room: Green 8&9 (08:30 – 12:30)			
Id	Presenter		Title		
TH/P1-2	W. W. Heidbrink	USA	Developing and Validating Predictive Models for Fast Ion Relaxation in Burning Plasmas		
TH/P1-3	S. K. Tiwari	India	Current Drive by Electron Temperature Gradient Turbulence in Tokamak Pedestal Region		
TH/P1-5	Y. Liu	UK	Computation of Resistive Instabilities in Tokamaks with Full Toroidal Geometry and Coupling Using DCON		
TH/P1-7	M. Rajkovic	Serbia	Quantifying Self-Organization in Magnetically Confined Fusion Plasmas		
TH/P1-8	R. Farengo	Argentina	Redistribution of Energetic Particles Due to Internal Kink Modes		
TH/P1-9	M. Malkov	USA	From Micro to Macro: L-H Transition Dynamics and Power Threshold Scaling		
TH/P1-11	KC. Shaing	USA	Transport Theory for Energetic Alpha Particles and Superbananas in Tokamak Fusion Reactors with Broken Symmetry		
TH/P1-12	H. Wang	Japan	Simulation Study of a New Kind of Energetic Particle Driven Geodesic Acoustic Mode		
TH/P1-13	L. Sugiyama	USA	Nonlinear and Toroidal Mode Coupling Effects on $m = 1$, $n = 1$ Instabilities		
TH/P1-14	G. Giruzzi	France	Modelling of Pulsed and Steady-State DEMO Scenarios		
TH/P1-15	R. Singh	Korea, Republic of	On Anomalous Dissipation and Relaxation in ELMs		
TH/P1-16	T. Rafiq	USA	Comparison of Simulated and Experimental Temperature, Density and Toroidal Rotation Profiles in Tokamak Plasmas		
TH/P1-17	I. Katanuma	Japan	A Flute Instability under the $E \times B$ Shear Flow in an Open System		
EX/P1-18	A. Biancalani	Germany	Global Gyrokinetic Modeling of Geodesic Acoustic Modes and Shear Alfvén Instabilities in ASDEX Upgrade		
EX/P1-19	E. Viezzer	Germany	Radial Electric Field and Poloidal Impurity Asymmetries in the Pedestal of ASDEX Upgrade: Quantitative Comparisons between Experiment and Theory		

Id	Presenter		Title
EX/P1-20	B. Geiger	Germany	Experimental Quantification of the Impact of Large and Small Scale Instabilities on Confined Fast Ions in ASDEX Upgrade
EX/P1-21	T. Tala	Finland	Identification of Intrinsic Torques in ASDEX Upgrade H-Mode Plasmas
EX/P1-22	M. García-Muñoz	Spain	Fast-Ion Response to Externally Applied 3D Magnetic Perturbations in ASDEX Upgrade H-Mode Plasmas
EX/P1-23	W. Suttrop	Germany	Studies of Magnetic Perturbations in High-Confinement Mode Plasmas in ASDEX Upgrade
EX/P1-24	D. Mazon	France	W Impurity Poloidal Assymmetries Observed at ASDEX Upgrade Using Soft-X-Ray Tomography Reconstruction
EX/P1-25	G. Birkenmeier	Germany	Filament Transport in the SOL of ASDEX Upgrade
PPC/P1-26	M. Reich	Germany	Real-Time Control of NTMs Using ECCD at ASDEX Upgrade
EX/P1-27	A. Herrmann	Germany	Solid Tungsten Divertor-III for ASDEX Upgrade and Contributions to ITER
EX/P1-28	V. Rozhdestven- sky	Russian Federation	Nonthermal Microwave Emission Features under the Plasma Ohmic Heating and Lower Hybrid Current Drive in the FT-2 Tokamak
EX/P1-29	S. Lashkul	Russian Federation	Impact of Isotopic Effect on Density Limit and LHCD Efficiency in the FT-2 Experiments
EX/P1-30	A. Altukhov	Russian Federation	Poloidal Inhomogeneity of Turbulence in the FT-2 Tokamak by Radial Correlation Doppler Reflectometry and Full-f Gyrokinetic Modeling
TH/P1-31	M. K. Islam	Bangladesh	Analysis of Plasma Behavior in the Localized Non-Axisymmetric <i>B</i> Region of the GAMMA 10 Tandem Mirror
EX/P1-32	V. Bulanin	Russian Federation	Geodesic Acoustic Mode Investigation in the Spherical Globus-M Tokamak Using a Multi-Diagnostic Approach
EX/P1-33	N. Bakharev	Russian Federation	Fast Particle Behavior in Globus-M
TH/P1-34	V. Dyachenko	Russian Federation	The First Lower Hybrid Current Drive Experiments in the Spherical Tokamak Globus-M

	Id	Presenter		Title
TU	TH/P1-35	I. Senichenkov	Russian Federation	Integrated Modeling of the Globus-M Tokamak Plasma
[1]	EX/P1-36	A. Kuzmin	Japan	Determination of the System Function for the Particle Circulation Process Using Perturbation Technique in QUEST
	EX/P1-37	K. Hanada	Japan	Investigation of Progression from Low to High Hydrogen Recycling during Long Duration Discharges on a Spherical Tokamak, QUEST
	EX/P1-38	H. Idei	Japan	Fully Non-Inductive Current Drive Experiments Using 28 GHz and 8.2 GHz Electron Cyclotron Waves in QUEST
	EX/P1-39	K. Mishra	Japan	Self Organization of High β_p Plasma Equilibrium with an Inboard Poloidal Null Sustained by Fully Non-Inductive Current Drive in QUEST
	EX/P1-40	M. Spolaore	Italy	Turbulent Electromagnetic Filaments in Toroidal Plasma Edge
	EX/P1-41	R. Lorenzini	Italy	The Isotope Effect in the RFX-Mod Experiment
	EX/P1-42	G. Spizzo	Italy	Density Limit Studies in the Tokamak and the Reversed-Field Pinch
	EX/P1-43	S. Neudatchin	Russian Federation	Study of ITB Formation, Electron Heat and Density Flux Structure in New ECRH/ECCD Experiments at T-10 Tokamak
	EX/P1-44	L. Klyuchnikov	Russian Federation	Impurities Removal during Central ECR Heating in T-10
	EX/P1-45	A. Melnikov	Russian Federation	Study of GAM Radial Structure and Properties in OH and ECRH Plasmas in the T-10 Tokamak
	EX/P1-46	N. Ivanov	Russian Federation	Magnetic Island and Plasma Rotation under External Resonant Magnetic Perturbation in T-10 Tokamak
	EX/P1-47	S. Mirnov	Russian Federation	Experimental Investigation of the System of Vertical and Longitudinal Lithium Limiters as a Prototype of Plasma Facing Components of a Steady State Tokamak-Reactor on T-11M Tokamak
	EX/P1-48	A. Shcherbak	Russian Federation	Investigation of a Phenomenology of the Improved Confinement Regime in T-11M Tokamak

Id	Presenter		Title
EX/P1-49	A. Vertkov	Russian Federation	Development of Lithium CPS Based Limiters for Realization of a Concept of Closed Lithium Circulation Loop in Tokamak
EX/P1-50	I. Roy	Russian Federation	The Auxiliary Heating and Current Drive Systems on The Tokamak T-15 Upgrade
EX/P1-51	M. Inomoto	Japan	Generation of Energetic Electrons by Magnetic Reconnection with Presence of High Guide Field
TH/P1-52	M. Leconte	Korea, Republic of	Feedback of a Neoclassical Tearing Mode on Drift Wave – Zonal Flow Turbulence

Lunch Break (12:30 – 14:00)

OV/4 : Magnetic Fusion	
-------------------------------	--

Chair: M. Kwon (Korea, Republic of)

PDF Link: Discussion Plenary Hall: Blue 1–5 (14:00 – 16:10)

Time Id	Presenter		Title
14:00 OV/4-1	M. Xu	China	Overview of HL-2A Recent Experiments
14:25 OV/4-2	S. Coda	Switzerland	The Science Program of the TCV Tokamak: Exploring Fusion Reactor and Power Plant Concepts
14:50 OV/4-3	S. A. Sabbagh	USA	Overview of Recent Physics Results from NSTX
15:15 OV/4-4	M. Kobayashi	Japan	3D Effects of Edge Magnetic Field Configuration on Divertor/SOL Transport and Optimization Possibilities for a Future Reactor
15:40 OV/4-5	J. Sánchez	Spain	Transport, Stability and Plasma Control Studies in the TJ-II Stellarator

Coffee Break (16:10 – 16:40)

Time Id Presenter	Title
OV/5: Magnetic Fusion Chair: P. Kaw (India)	PDF Link: Discussion Plenary Hall: Blue 1–5 (16:40 – 18:45)
Time Id Presenter	Title
16:40 OV/5-1 P. Terry U	5A Overview of Gyrokinetic Studies on Electromagnetic Turbulence
17:05 OV/5-2 M. E. Puiatti Ita	ly Overview of the RFX-Mod Contribution to the International Fusion Science Program
17:30 OV/5-3 B. Chapman U	5A Overview of Results from the MST Reversed Field Pinch Experiment
17:55 OV/5-5 S. Pradhan In	dia First Experiments in SST-1
18:20 OV/5-4 G. Pucella Ita	ly Overview of the FTU Results

Poster Session: P2

Poster Room: Green 8&9 (14:00 – 18:45)

Id	Presenter		Title
TH/P2-1	C. Pan	China	The Combining Effect of the Inductive Electric Field and the Lower Hybrid Waves on the Impurity Ions Toroidal Rotation in the Lower Hybrid Current Drive Tokamak Plasmas
TH/P2-2	A. Y. Aydemir	Korea, Republic of	ELM Pacing with Periodic Plasma Column Displacements
TH/P2-5	Z. Gao	China	Frequency and Damping Rate of the Geodesic Acoustic Mode in Collisional Plasmas
TH/P2-6	M. Schneller	Germany	Study of Nonlinear Fast Particle Transport and Losses in the Presence of Alfvén Waves
TH/P2-7	F. Jenko	Germany	Can Gyrokinetics Really Describe Transport in L-Mode Core Plasmas?
TH/P2-9	T. Rhee	Korea, Republic of	A Reduced Model of ELM Mitigation by SMBI and Pellet Injection
TH/P2-10	A. Kuley	USA	Nonlinear Particle Simulation of Radio Frequency Waves in Fusion Plasmas
TH/P2-11	V. Pastukhov	Russian Federation	Influence of Boundary Conditions on Turbulent Transport and Plasma Energy Confinement Time Evolution in Tokamaks with Additional Heating: Simulations for T-10 and T-15 Tokamaks
TH/P2-12	N. Miyato	Japan	Nonlocal Transport from Edge to Core in Tokamak Plasmas

Tuesday, October 14, 2014

Id	Presenter		Title
TH/P2-13	H. He	China	Fishbone Modes in Plasmas with Dual Neutral Beam Injection Heating
TH/P2-14	Y. Kosuga	Japan	Progress on Transport Modeling by Trapped Ion Resonance Driven Turbulence
TH/P2-15	N. Aiba	Japan	MHD Instability Excited by Interplay between Resistive Wall Mode and Stable MHD Modes in Rotating Tokamak Plasmas
TH/P2-16	H. R. Strauss	USA	Toroidal Rotation Produced by Disruptions and ELMs
EX/P2-20	F. Turco	USA	Impact of NBI-Injected Fast Ions in the Stabilization of the Resistive Wall Mode in High- β_N Plasmas
EX/P2-21	D. Orlov	USA	Suppression of Type-I ELMs with Incomplete I-Coil Set on DIII-D
EX/P2-22	N. W. Eidietis	USA	Measurement of Radiated Power Asymmetry during Disruption Mitigation on the DIII-D Tokamak
EX/P2-24	S. Smith	USA	Full-f Neoclassical Simulations toward a Predictive Model for H-Mode Pedestal Ion Energy, Particle and Momentum Transport
EX/P2-26	T. W. Petrie	USA	Applying the Radiating Divertor Approach to Innovative Tokamak Divertor Concepts
EX/P2-27	D. L. Rudakov	USA	Reduction of Net Erosion of High-Z PFC Materials in DIII-D Divertor Due to Re-Deposition and Low-Z Coating
EX/P2-28	C. Paz-Soldan	USA	The Single Dominant Mode Picture of Non-Axisymmetric Field Sensitivity and its Implications for ITER Geometric Tolerances
EX/P2-29	S. Smith	USA	Electron Temperature Critical Gradient and Transport Stiffness
EX/P2-30	S. Mordijck	USA	Momentum and Particle Transport Across the ITG-TEM Turbulence Regimes in DIII-D H-Mode Plasmas
PPC/P2-31	A. M. Garofalo	USA	Compatibility of Internal Transport Barrier with Steady-State Operation in the High Bootstrap Fraction Regime on DIII-D
PPC/P2-32	J. E. Barton	USA	Physics-Model-Based Control of the Plasma State Dynamics for the Development and Sustainment of Advanced Scenarios in DIII-D

Id	Presenter		Title
PPC/P2-33	E. Kolemen	USA	Experimental Simulation of Burn Control Using DIII-D In-Vessel Coils
PPC/P2-34	T. C. Luce	USA	Expanding the Physics Basis of the Baseline Q=10 Scenario toward ITER Conditions
PPC/P2-35	J. Ferron	USA	High Internal Inductance for Steady-State Operation in ITER and a Reactor
PPC/P2-36	C. C. Petty	USA	Achieving Steady-State Conditions in High-Beta Hybrid Scenario in DIII-D
PPC/P2-37	A. M. Garofalo	USA	Advancing the Physics Basis of Quiescent H-Mode Through Exploration of ITER Relevant High Density Operation
TH/P2-38	R. Pinsker	USA	Off-Axis Current Drive with High Harmonic Fast Waves for DIII-D
EX/P2-39	X. Gong	China	Development of Fully Noninductive Scenario at High Bootstrap Current Fraction for Steady State Tokamak Operation on DIII-D and EAST
EX/P2-40	K. Razumova	Russian Federation	Heat Transport and Enhancement Confinement Regimes in Tokamak as a Result of Plasma Self-organization
EX/P2-41	P. Martin	Italy	Extreme Low-Edge Safety Factor Tokamak Scenarios via Active Control of Three-Dimensional Magnetic Field on RFX and DIII-D
EX/P2-42	L. Marrelli	Italy	Avoidance of Tearing Mode Locking and Disruption with Electro-Magnetic Torque Introduced by Feedback-Based Mode Rotation Control in DIII-D and RFX-Mod
TH/P2-44	Y. Xiao	China	Gyrokinetic Simulation of Microturbulence in EAST Tokamak and DIII-D Tokamak
TH/P2-45	T. Xia	China	Fluid Simulation of Particle and Heat Fluxes during Burst of ELMs on EAST and DIII-D
EX/P2-46	G. Mazzitelli	Italy	Thermal Loads on FTU Actively Cooled Liquid Lithium Limiter
EX/P2-47	C. Sozzi	Italy	Experiments on Magneto-Hydrodynamics Instabilities with ECH/ECCD in FTU Using a Minimal Real-Time Control System
EX/P2-48	D. Carnevale	Italy	Runaway Electron Control in FTU
EX/P2-49	F. Causa	Italy	Cherenkov Emission Provides Detailed Picture of Non-Thermal Electron Dynamics in the Presence of Magnetic Islands

Tuesday, October 14, 2014

Id	Presenter		Title
EX/P2-50	B. Esposito	Italy	On the Measurement of the Threshold Electric Field for Runaway Electron Generation in FTU
EX/P2-51	G. Granucci	Italy	Experiments and Modelling on FTU Tokamak for EC Assisted Plasma Start-up Studies in ITER-like Configuration
EX/P2-52	C. Mazzotta	Italy	Peaked Density Profiles Due to Neon Injection on FTU
EX/P2-54	S. Nowak	Italy	(N)TM Onset by Central EC Power Deposition in FTU and TCV Tokamaks

Wednesday, October 15, 2014

Chair: A. Litvak (Russian Fed.) Time Id Presenter Title 8:30 FIP/2-1 ITER Disruption Mitigation System S. Maruyama Developments and Design for ITER FIP/2-2Ra Y. Oda 8:50 Japan Prototype Development of the ITER EC System with 170 GHz Gyrotron FIP/2-2Rb Development of Dual Frequency Gyrotron and Launcher for the JT-60SA ECH/ECCD System FIP/2-2Rc Development of Over 1 MW and Multi-Frequency Gyrotrons for Fusion USA 9:10 FIP/2-3 S. Wukitch ICRF Actuator Development at Alcator C-Mod 9:30 FIP/2-4 A. Masiello European Progress Status of the Activities in EU for Commisthe Development of the ITER Neutral sion Beam Injector and Test Facility 9:50 FIP/2-5Ra H.Tobari Development of DC Ultra-High Voltage Japan Insulation Technology for ITER NBI FIP/2-5Rb Progress in Long Pulse Production of Powerful Negative Ion Beams for IT-60SA and ITER

FIP/2: Heating and Disruption

PDF Link: Discussion

Plenary Hall: Blue 1–5 (08:30 – 10:15)

Coffee Break (10:15 – 10:45)

EX/2 and TH/1: Core Turbulence PDF Link: Discussion Chair: E. Gusakov (Russian Fed.) *Plenary Hall: Blue 1–5 (10:45 – 12:30)* Time Id Presenter Title 10:45 EX/2-1 S. Inagaki Japan Dynamic Method to Study Turbulence and Turbulence Transport G. R. McKee 11:05 EX/2-2 USA Turbulence Behavior and Transport **Response Approaching Burning Plasma Relevant Parameters** 11:25 TH/1-1 Multi-Scale ITG/TEM/ETG Turbulence S. Maeyama Japan Simulations with Real Mass Ratio and β Value D. Ernst USA 11:45 EX/2-3 Controlling H-Mode Particle Transport with Modulated Electron Heating in DIII-D and Alcator C-Mod via TEM Turbulence 12:05 TH/1-2 P. Helander Germany Advances in Stellarator Gyrokinetics

WED

Poster Sess	ion: P3		Poster Room: Green 8&9 (08:30 – 12:30)
Id	Presenter		Title
EX/1-1	M. R. Wade	USA	Recent Advances in the Understanding and Optimization of RMP ELM Suppression for ITER
EX/1-2	A. Kirk	UK	Effect of Resonant Magnetic Perturbations on Low Collisionality Discharges in MAST and a Comparison with ASDEX Upgrade
EX/1-3	T. E. Evans	USA	Comparative Studies of Edge Magnetic Islands and Stochastic Layers in DIII-D and LHD
EX/1-4	S. A. Sabbagh	USA	Physical Characteristics of Neoclassical Toroidal Viscosity in Tokamaks for Rotation Control and the Evaluation of Plasma Response
EX/1-5	Y. Jeon	Korea, Republic of	Successful ELM Suppressions in a Wide Range of q_{95} Using Low <i>n</i> RMPs in KSTAR and its Understanding as a Secondary Effect of RMP
PPC/P3-2	A. R. Polevoi	ITER	Assessment of Operational Space for Long-Pulse Scenarios in ITER
EX/P3-3	X. Zhang	China	High Power ICRF Systems and Heating Experiments in EAST
EX/P3-4	G. Calabrò	Italy	EAST Snowflake Experiment: Scenario Development and Edge Simulations
EX/P3-5	B. Lyu	China	Core Plasma Rotation Characteristics of RF-Heated H-Mode Discharges on EAST
EX/P3-6	L. Xiang	China	Investigation of Argon Seeding in Different Divertor Configurations in EAST and Corresponding SOLPS 5.0 Modeling
EX/P3-7	G. Li	China	Studies of Impact of Edge Current Profiles, Plasma Shaping, Nonlinearity on Edge Localized Modes with BOUT++ Code
EX/P3-8	Y. Liang	Germany	ELM Mitigation by Lower Hybrid Waves in EAST
EX/P3-9	X. Gao	China	Study of Pedestal Turbulence on EAST Tokamak
EX/P3-10	L. Wang	China	Progress in Active Control of Divertor Power Load in the EAST Superconducting Tokamak
EX/P3-11	B. Ding	China	Investigation of LHW-Plasma Coupling and Current Drive Related to H-Mode Experiments in EAST

	Id	Presenter		Title
	EX/P3-12	Y. Xu	China	The Latest Development of EAST Neutral Beam Injector
WED	TH/P3-13	X. Gong	China	Theoretical Analysis of the ICRH Antenna's Impedance Matching for ELMy Plasmas on EAST
	EX/P3-14	R. Reichle	ITER	Redefinition of the ITER Requirements and Diagnostics for Erosion, Deposition, Dust and Tritium Measurements Accounting for the Change to Tungsten Divertor
	EX/P3-16	M. Wischmeier	Germany	Advancing Power Exhaust Studies from Present to Future Tokamak Devices
	EX/P3-17	G. Hogeweij	The Nether- lands	Impact of W on Scenario Simulations for ITER
	EX/P3-18	D. Campbell	ITER	Status of R&D for ITER Disruption Loads, Disruption Mitigation and Runaway Electron Avoidance
	PPC/P3-19	F. Köchl	Austria	Examination of the Entry to Burn and Burn Control for the ITER 15 MA Baseline and Other Scenarios
	PPC/P3-20	A. Mineev	Russian Federation	Study of ITER First Plasma Initiation Using a 3D Electromagnetic Model
	PPC/P3-21	Y. Gribov	ITER	Plasma Vertical Stabilization in ITER
	PPC/P3-22	M. Romanelli	UK	Evaluation of Fuelling Requirements and Transient Density Behavior in ITER Scenarios
	TH/P3-23	Y. Gott	Russian Federation	Asymmetry Current in ICRF Heating ITER Plasmas
	TH/P3-24	F. Köchl	Austria	Modelling of Transitions Between L- and H-Mode Including W Behaviour in ITER Scenarios
	TH/P3-25	P. Rodrigues	Portugal	A Systematic Approach to the Linear-Stability Assessment of Alfvén Eigenmodes in the Presence of Fusion-Born Alpha Particles for ITER-like Equilibria
	TH/P3-28	K. McClements	UK	Fast Particle-Driven Ion Cyclotron Emission (ICE) in Tokamak Plasmas and the Case for an ICE Diagnostic in ITER
	TH/P3-29	R. Dux	Germany	Influence of a Tungsten Divertor on the Performance of ITER H-Mode Plasmas

Id	Presenter		Title
TH/P3-30	T. Kurki-Suonio	Finland	ITER Energetic Particle Confinement in the Presence of ELM Control Coils and European TBMs
TH/P3-31	S. Konovalov	Russian Federation	Integrated Modelling of ITER Disruption Mitigation
TH/P3-32	P. Minashin	Russian Federation	Effect of Multi-Pass Absorption of Electron Cyclotron Heating Wave on Initial Stage of Discharge in ITER-like Tokamak
TH/P3-34	M. T. Kotschen- reuther	USA	X-Divertors in ITER — Without any Hardware Changes or Additions — and in Current Machines, and DEMO Reactors
TH/P3-35	V. Zhogolev	Russian Federation	Simulation of the Pre-Thermal Quench Stage of Disruptions at Massive Gas Injection and Projections for ITER
TH/P3-36	V. Vdovin	Russian Federation	Off-Axis Current Generation by Helicons and LH Waves in Core of Modern Tokamaks and Reactors FNSF-AT, ITER, DEMO and by Alfvén Waves in Pedestal Plasmas. Scenarios, Modeling and Antennae
TH/P3-37	V. Nesenevich	Russian Federation	On the Possibility of Alpha-Particle Confinement Study in ITER by NPA Measurements of Knock-on Ion Tails
TH/P3-38	P. Aleynikov	ITER	Kinetic Modelling of Runaway Electrons and their Mitigation in ITER
TH/P3-39	M. Isaev	Russian Federation	Alfvén Eigenmode Evolution in ITER Steady-State Scenario
TH/P3-40	B. Bazylev	Germany	Modelling of Melt Damage of Tungsten Armour under Multiple Transients Expected in ITER and Validations against JET-ILW Experiments
TH/P3-41	F. Imbeaux	France	Design and First Applications of the ITER Integrated Modelling & Analysis Suite
TH/P3-42	E. M. Bass	USA	Fusion Alpha Loss in ITER with Local Marginal Stability to Alfvén Eigenmodes
TH/P3-43	J. R. Martin-Solis	Spain	Formation and Termination of Runaway Beams in Tokamak Disruptions and Implications for ITER
TH/P3-44	Y. Liu	UK	Modelling Toroidal Rotation Damping in ITER Due to External 3D Fields

	Id	Presenter		Title
	TH/P3-45	R. Zagorski	Poland	Integrated Core-SOL-Divertor Modelling for ITER Including Impurity: Effect of Tungsten on Fusion Performance in H-Mode and Hybrid Scenario
VED	TH/P3-46	G. N. Throumoulopou los	Greece -	On the Equilibrium and Stability of ITER Relevant Plasmas with Flow
	EX/P3-47	M. Jakubowski	Germany	Influence of Magnetic Perturbations on Particle Pump-out in Magnetic Fusion Devices
	EX/P3-48	D. Douai	France	Experimental and Modelling Results on Wall Conditioning for ITER Operation
	EX/P3-49	B. Chapman	USA	Micro- and Macro-Instability, and Large Density and Beta in Improved Confinement MST RFP Plasmas
	EX/P3-50	M. Nornberg	USA	Predator-Prey Time Dynamics and Locking Control of Spontaneous Helical States in the RFP
	EX/P3-52	S. Masamune	Japan	Attainment of High Electron Poloidal β in Axisymmetric State and Two Routes to Self-Organized Helical State in Low-Aspect-Ratio RFP
	EX/P3-54	N. Kirneva	Russian Federation	High Density Regime in Ohmic TCV Discharges with Positive and Negative Triangularity
	EX/P3-55	A. Merle	Switzerland	From Edge Non-Stiffness to Improved IN-Mode: a New Perspective on Global Tokamak Radial Transport
	EX/P3-56	B. Duval	Switzerland	Progress in Snowflake Divertor Studies on TCV
	EX/P3-57	L. Porte	Switzerland	Multi-Diagnostic Study of Core Turbulence and Geodesic Acoustic Modes in the TCV Tokamak
	EX/P3-59	I. Furno	Switzerland	Basic Investigations of Turbulence and Interactions with Plasma and Suprathermal Ions in the TORPEX Device with Open and Closed Field Lines

Lunch Break (12:30 – 14:00)

Chair: R. Buttery	r, (USA)		Plenary Hall: Blue 1–5 (14:00 – 16:10)
Time Id	Presenter		Title
14:00 TH/2-1	V. Rozhansky	Russian Federation	Understanding of Impurity Poloidal Distribution in Edge Pedestal by Modeling
14:20 EX/3-1	E. Viezzer	Germany	Overview of Recent Pedestal Studies at ASDEX Upgrade
14:40 EX/3-2	J. Hughes	USA	Edge Instability Limiting the Pedestal Growth on Alcator C–Mod Experiment and Modeling
15:00 EX/3-3	C. Maggi	Germany	Pedestal Confinement and Stability in JET-ILW ELMy H-Mode Scenarios
15:20 TH/2-2	P. B. Snyder	USA	Super H-mode: Theoretical Prediction and Initial Observations of a New High Performance Regime for Tokamak Operation
15:40 TH/2-3	S. Parker	USA	Gyrokinetic Study of Edge Blobs and Divertor Heat-Load Footprint

Coffee Break (16:10 – 16:40)

EX/3 and TH/2: Pedestal Physics

	EX/4 and TH/3: Divertor & SOL Physics Chair: E. Marmar (USA)			PDF Link: Discussion Plenary Hall: Blue 1–5 (16:40 – 18:45)
	Time Id	Presenter		Title
L	16:40 EX/4-1	G. Matthews	UK	Melting of Tungsten by ELM Heat Loads in the JET Divertor
VEI	17:00			TBA
0	17:20 TH/3-2	P. Ricci	Switzerland	First-Principle Theory-Based Scaling of the SOL Width in Limited Tokamak Plasmas, Experimental Validation, and Implications for the ITER Start-up
	17:40 TH/3-3	L. Aho-Mantila	Finland	Assessment of Scrape-off Layer Simulations with Drifts against L-Mode Experiments in ASDEX Upgrade and JET
	18:00 EX/4-2	M. Goniche	France	Near-Field Physics of Lower-Hybrid Wave Coupling to Long-Pulse, High Temperature Plasmas in Tore Supra
	18:20 EX/4-3	A. Kreter	Germany	Fuel Retention and Erosion of Metallic Plasma-Facing Materials under the Influence of Plasma Impurities

Poster Sess	ion: P4		Poster Room: Green 8&9 (14:00 – 18:45)
Id	Presenter		Title
FIP/1-1	Y. Seki	Japan	Development of Tungsten Monoblock Technology for ITER Full-Tungsten Divertor in Japan
FIP/1-2	J. P. Gunn	France	Surface Heat Loads on Tungsten Monoblocks in the ITER Divertor
FIP/1-3	N. Koizumi	Japan	Full-Scale Trial Results to Qualify Optimized Manufacturing Plan for ITER Toroidal Field Coil Winding Pack in Japan
FIP/1-5	A. Encheva	ITER	Overview of the Design Development, Prototype Manufacturing and Procurement of the ITER In-Vessel Coils
FIP/1-6Ra	C. Sborchia	ITER	Progress in the Design and Manufacture of High Vacuum Components for ITER
FIP/1-6Rb	HJ. Ahn	Korea, Republic of	Manufacturing Design and Progress of the First Sector for ITER Vacuum Vessel
FIP/2-1	L. R. Baylor	USA	Disruption Mitigation System Developments and Design for ITER
FIP/1-4Rb	V. Vysotsky	Russian Federation	Research, Development and Production of ITER Toroidal Field Conductors and Poloidal Field Cables in Russia
EX/P4-1	G. Verdoolaege	Belgium	A New Methodology for Scaling Laws with Arbitrary Error Distributions: Case Study for the H-Mode Power Threshold
TH/P4-3	O. Agullo	France	Remote Generation of NTM Precursors by Interchange Turbulence
TH/P4-4	Y. Sarazin	France	Understanding Momentum Transport in Tokamak Plasmas
TH/P4-6	K. Dyabilin	Russian Federation	The Interpretation of the Tokamak Self-Consistent Pressure Profiles
TH/P4-7	T. E. Evans	USA	A Cross-Benchmarking and Validation Initiative for Tokamak 3D Equilibrium Calculations
TH/P4-9	A. Sadykov	Kazakhstan	Numerical Code "TOKSCEN" for Modeling of Plasma Evolution in Tokamak
TH/P4-10	C. Bourdelle	France	L to H Mode Transition: Parametric Dependencies of the Temperature Threshold

	Id	Presenter		Title
	TH/P4-11	I. Holod	USA	Global Gyrokinetic Simulations of Electromagnetic Instabilities in Tokamak Plasmas
WED	TH/P4-13	R. Paccagnella	Italy	Progresses in 3D Nonlinear Numerical Simulation of Tokamak Disruptions
0	TH/P4-14	R. I. Pinsker	USA	Full Wave Simulations for Fast Wave Heating and Power Losses in the Scrape-off Layer of Tokamak Plasmas
	TH/P4-15	D. Chandra	India	Modeling and Analytic Study of Plasma Flows on Tearing Mode Stability
	TH/P4-16	Z. Guo	Korea, Republic of	Turbulent Elasticity and the Physics of Time Delay
	TH/P4-17	I. Ivanova-Stanik	Poland	Influence of the Divertor Plate Material on the Plasma Performance in DEMO
	PPC/P4-19	R. Wenninger	Germany	Advances in the Physics Basis for the European DEMO Design
	EX/P4-20	P. Brunsell	Sweden	Resistive Wall Mode Studies Utilizing External Magnetic Perturbations
	EX/P4-21	P. Bagryansky	Russian Federation	Last Achievements in the Experiments with ECR Heating in the Gas Dynamic Trap
	EX/P4-22	S. Hussain	Pakistan	First Plasma Formation in Glass Spherical Tokamak (GLAST)
	EX/P4-23	A. Burdakov	Russian Federation	Status of GOL-3 Multiple Mirror Trap Experiments
	EX/P4-24	B. Blackwell	Australia	Structure and Scaling of Fluctuations in the MHD Range in the H-1NF HELIAC
	EX/P4-25	G. Navratil	USA	Active and Passive Experiments to Control the Helical Boundary of Wall-Stabilized Tokamak Plasma
	EX/P4-26	S. Ohshima	Japan	Observation of a Toroidally Symmetrical Electric Field Fluctuation with Radially Elongated Structure in Heliotron J
	EX/P4-27	S. Yamamoto	Japan	External Control of Energetic-Ion-Driven MHD Instabilities by ECH/ECCD in Heliotron J Plasmas
	EX/P4-28	S. Kobayashi	Japan	Parallel Flow Dynamics and Comparison with Neoclassical Transport Analysis in NBI Plasmas of Heliotron J
	EX/P4-29	T. Mizuuchi	Japan	A New Operation Regime for High-Density Plasma in Heliotron J

Id	Presenter		Title
EX/P4-30	M. Nagata	Japan	Non-Inductive Solenoid-Less Plasma Current Start-up on HIST Using Transient Coaxial Helicity Injection
ICC/P4-31	B. Victor	USA	Progress on HIT-SI and Imposed Dynamo Current Drive
EX/P4-33	Y. Yu	China	Observation of Zonal Flows in Core Plasma with Collective Scattering Density Fluctuation Measurement
EX/P4-34	S. Sharapov	UK	Instabilities and Transport of Fast Ions on MAST
EX/P4-35	J. Hillesheim	UK	Cross-Polarization Doppler Backscattering Measurements and Microtearing at the Top of the MAST H-Mode Pedestal
EX/P4-36	M. Valovic	UK	Pellet Fuelling of Plasmas Including ELM Mitigation in MAST
EX/P4-37	J. Harrison	UK	Improved Understanding of Edge Plasma Dynamics Through Visible Imaging on MAST
EX/P4-38	J. Hillesheim	UK	Influence of Flow Shear on the Structure of Ion-Scale Turbulence in MAST
TH/P4-39	M. J. Hole	Australia	Advanced Equilibrium Models for Anisotropy, Flow and Chaotic Fields
TH/P4-40	S. Saarelma	UK	Understanding the MAST H-Mode Pedestal Through Experiments and Modelling
EX/P4-41	M. Martinez	Spain	Analysis of Ion Energy Spectrum and Spikes in ECRH TJ-II Plasmas, with Fixed and Variable Magnetic Configuration
EX/P4-43	B. Zurro	Spain	Studying the Impurity Charge Dependence of Impurity Confinement in ECR Heated TJ-II Stellarator Plasmas
EX/P4-45	F. Castejón	Spain	Stable Plasmas in Theoretically Mercier-Unstable TJ-II Configurations
EX/P4-46	Á. Cappa	Spain	Influence of ECR Heating on NBI-Driven Alfvén Eigenmodes in the TJ-II Stellarator
EX/P4-47	T. Estrada	Spain	Limit Cycle Oscillations at the L-I-H Transition in TJ-II Plasmas: Triggering, Temporal Ordering and Radial Propagation
ICC/P4-48	S. Inoue	Japan	Numerical Study of Energy Transfer Mechanism of Magnetic Reconnection/Torus Plasma Merging under High Toroidal Magnetic Field

Id	Presenter		Title
TH/P4-49	O. Mishchenko	Germany	Global gyrokinetic particle-in-cell simulations of Alfvénic modes
FIP/P4-1	Y. Zhai	USA	Multi-Physics Engineering Analysis for an Integrated Design of ITER Diagnostic First Wall and Diagnostic Shield Module
FIP/P4-2	L. Hu	China	Progress on the ITER Diagnostic-Radial X-Ray Camera
FIP/P4-3	A. Garcia Carrasco	Sweden	Comprehensive First Mirror Test for ITER at JET with ITER-like Wall
FIP/P4-4	D. Gin	Russian Federation	Gamma-Ray Spectrometer in the ITER NPA System
FIP/P4-5	Y. Kawano	Japan	Overview of ITPA R&D Activities for Optimization of ITER Diagnostic Performance
FIP/P4-6	A. Litnovsky	Germany	Studies of Protection and Recovery Techniques of Diagnostic Mirrors for ITER
FIP/P4-7	I. Bolshakova	Ukraine	Experimental Evaluation of Long-Term and Stable Magnetic Sensors Operation in ITER-Relevant Conditions
MPT/P4-8	A. Razdobarin	Russian Federation	RF Discharge for In-Situ Mirror Surface Recovery in ITER
FIP/P4-9	I. Ricapito	European Commis- sion	Tritium Transport Modelling: First Achievements on ITER Test Blanket Systems Simulation and Perspectives for DEMO Breeding Blanket
FIP/P4-10	J. Chen	China	Behaviors of ITER EHF FW under High Heat Flux for Mock-ups Manufactured by HIP Joining Technology
FIP/P4-12	W. Chung	Korea, Republic of	Design Finalization and R&D Activities before the Start of Manufacture of ITER Thermal Shield
FIP/P4-13	SW. Kim	Korea, Republic of	Current Status of Final Design and R&D for ITER Blanket Shield Block in Korea
FIP/P4-15	N. Takeda	ITER	R&D Status on Remote Handling Technology for ITER Blanket Maintenance
MPT/P4-17	L. Begrambekov	Russian Federation	Protecting B ₄ C Coating for ITER Divertor Tiles. Deposition, Operation, Removal of Erosion Products
FIP/P4-20	A. Labusov	Russian Federation	Structural Analysis of the ITER Coil Power Supply System

Id	Presenter		Title
FIP/P4-21	Y. Nunoya	Japan	Advance in Japanese Superconductor for ITER
MPT/P4-23	C. Gustafsson	Spain	Experimental Assessment of Erosion Corrosion Parameters of Copper Alloys and Copper to Steel Joints at ITER Operational Conditions
FIP/P4-24	Y. Wang	China	Preparation for Preliminary Design of ITER GDC
FIP/P4-25	V. Rozov	ITER	Hybrid Integral-Differential Simulator of EM Force Interactions / Scenario-Assessment Tool with Pre-Computed Influence Matrix in Applications to ITER
FIP/P4-26	V. Belyakov	Russian Federation	Development of Predictive Simulator to Model Electromagnetic Transients for ITER Application
FNS/P4-27	A. Serikov	Germany	Neutronic Analyses for ITER Diagnostic Port Plugs

	Chair: M. Murakami (Japan)			Plenary Hall: Blue 1–5 (08:30 – 10:15)	
	Time	Id	Presenter		Title
	8:30	IFE/1-1	C. Li	USA	Effects of Ion Diffusion on Fusion Burn at the Shock Flash in Inertial-Confinement Fusion Implosions
TH	8:50	IFE/1-2	S. Fujioka	Japan	Experimental Platform for Efficient Heating of Fusion Fuel with Fast-Ignition Scheme
U	9:10	IFE/1-3	S. Krashenin- nikov	USA	Effect of Pre-Plasma on Intense Electron Beam Generation by Relativistic Laser Radiation
	9:30	IFE/1-4	E. Koresheva	Russian Federation	Conception of a Cryogenic Target Factory for IFE
	9:50	IFE/1-5	H. J. Kong	Korea, Republic of	A High-Energy and Highly Repetitive fs/ps Laser Using Optical Parametric Chirped-Pulse Amplification with a ns Beam Combined Pumping Laser for Fast Ignition

IFE/1: Inertial Fusion Experiments & Theory

Coffee Break (10:15 – 10:45)

EX/5 and TH/4: H Chair: B. Wan (C	• •	ysics PDF Link: Discussion Plenary Hall: Blue 1–5 (10:45 – 12:30)	
Time Id	Presenter		Title
10:45 EX/5-1	R. Granetz	USA	An ITPA Joint Experiment to Study Runaway Electron Generation and Suppression
11:05 TH/4-1	V. A. Izzo	USA	The Role of MHD in 3D Aspects of Massive Gas Injection for Disruption Mitigation
11:25 EX/5-2	C. Reux	France	Runaway Electron Generation with the ITER-like Wall and Efficiency of Massive Gas Injection at JET
11:45 EX/5-3	R. L. Tanna	India	Novel Approaches for Mitigating Runaway Electrons and Plasma Disruptions in Tokamak ADITYA
12:05 TH/4-2	A. Popov	Russian Federation	The Low Threshold Parametric Decay Instabilities Leading to Anomalous Absorption at ECRH in Toroidal Devices

Poster Sess	ion: P5		Poster Room: Green 8&9 (08:30 – 12:30)
Id	Presenter		Title
EX/2-1	S. Inagaki	Japan	Dynamic Method to Study Turbulence and Turbulence Transport
EX/2-2	G. R. McKee	USA	Turbulence Behavior and Transport Response Approaching Burning Plasma Relevant Parameters
EX/2-3	D. Ernst	USA	Controlling H-Mode Particle Transport with Modulated Electron Heating in DIII-D and Alcator C-Mod via TEM Turbulence
EX/3-1	E. Viezzer	Germany	Overview of Recent Pedestal Studies at ASDEX Upgrade
EX/3-2	J. Hughes	USA	Edge Instability Limiting the Pedestal Growth on Alcator C–Mod Experiment and Modeling
EX/3-3	C. Maggi	Germany	Pedestal Confinement and Stability in JET-ILW ELMy H-Mode Scenarios
EX/4-1	G. Matthews	UK	Melting of Tungsten by ELM Heat Loads in the JET Divertor
EX/4-2	M. Goniche	France	Near-Field Physics of Lower-Hybrid Wave Coupling to Long-Pulse, High Temperature Plasmas in Tore Supra
EX/4-3	A. Kreter	Germany	Fuel Retention and Erosion of Metallic Plasma-Facing Materials under the Influence of Plasma Impurities
FIP/2-2Ra	Y. Oda	Japan	Prototype Development of the ITER EC System with 170 GHz Gyrotron
FIP/2-2Rb	T. Kobayashi	Japan	Development of Dual Frequency Gyrotron and Launcher for the JT-60SA ECH/ECCD System
FIP/2-2Rc	T. Imai	Japan	Development of Over 1 MW and Multi-Frequency Gyrotrons for Fusion
FIP/2-3	S. Wukitch	USA	ICRF Actuator Development at Alcator C-Mod
FIP/2-4	A. Masiello	European Commis- sion	Progress Status of the Activities in EU for the Development of the ITER Neutral Beam Injector and Test Facility
FIP/2-5Ra	H. Tobari	Japan	Development of DC Ultra-High Voltage Insulation Technology for ITER NBI
FIP/2-5Rb	A. Kojima	Japan	Progress in Long Pulse Production of Powerful Negative Ion Beams for JT-60SA and ITER

	Id	Presenter		Title
	TH/1-1	S. Maeyama	Japan	Multi-Scale ITG/TEM/ETG Turbulence Simulations with Real Mass Ratio and β Value
	TH/1-2	P. Helander	Germany	Advances in Stellarator Gyrokinetics
	TH/2-1	V. Rozhansky	Russian Federation	Understanding of Impurity Poloidal Distribution in Edge Pedestal by Modeling
THU	TH/2-2	P. B. Snyder	USA	Super H-mode: Theoretical Prediction and Initial Observations of a New High Performance Regime for Tokamak Operation
	TH/2-3	S. Parker	USA	Gyrokinetic Study of Edge Blobs and Divertor Heat-Load Footprint
	TH/3-2	P. Ricci	Switzerland	First-Principle Theory-Based Scaling of the SOL Width in Limited Tokamak Plasmas, Experimental Validation, and Implications for the ITER Start-up
	TH/3-3	L. Aho-Mantila	Finland	Assessment of Scrape-off Layer Simulations with Drifts against L-Mode Experiments in ASDEX Upgrade and JET
	ICC/P5-1	V. Ilgisonis	Russian Federation	Tokamak with an Ergodic Central Area
	TH/P5-4	D. Morozov	Russian Federation	Thermal Equilibrium and Density Limit in Tokamak-Reactor
	TH/P5-6	T. Kiviniemi	Finland	Gyrokinetic Simulation of Phenomenology of GAMs
	TH/P5-7	C. Castaldo	Italy	Advances in Modeling of Nonlinear Effects in LHCD Experiments
	TH/P5-8	K. Imadera	Japan	Global Profile Relaxation Coupled with $E \times B$ Staircase in Toroidal Flux-Driven ITG Turbulence
	TH/P5-9	G. Hao	China	Finite Toroidal Flow Generated by Resistive Wall Tearing Modes in a Toroidal Plasma
	TH/P5-10	S. Guo	Italy	Progress in Theoretical Studies of Resistive Wall Modes for RFP plasmas and Comparison with Tokamaks
	TH/P5-12	G. M. Staebler	USA	Limit Cycle Oscillations and L/H Transitions from Two Dimensional Mean Field Momentum Transport Equations
	TH/P5-13	A. Matsuyama	Japan	Simulation of Energy-Dependent Stochastic Transport Induced by Low-Order MHD Instabilities for Runaway Electron Mitigation

Id	Presenter		Title
TH/P5-14	N. Kasuya	Japan	Numerical Diagnostics of Non-Diffusive Transport Process by Use of Turbulence Diagnostic Simulator
TH/P5-17	H. Miura	Japan	Two-Fluid Effects on Pressure-Driven Modes in a Heliotron Device
EX/P5-18	M. Halitovs	Latvia	Analysis of Tritium in Divertor Materials
EX/P5-20	A. B. Kukushkin	Russian Federation	Theoretical Model of ITER High Resolution H-Alpha Spectroscopy for a Strong Divertor Stray Light and Validation against JET-ILW Experiments
EX/P5-21	J. Ongena	Belgium	ICRF Discharge Production for Ion Cyclotron Wall Conditioning on JET
EX/P5-22	E. A. Lerche	Belgium	ICRH for Mitigation of Core Impurity Accumulation in JET-ILW
EX/P5-23	V. V. Plyusnin	Portugal	Parameters of Runaway Electrons in JET
EX/P5-24	E. Delabie	The Nether- lands	Overview and Interpretation of L-H Threshold Experiments on JET with the ITER-like Wall
EX/P5-25	C. Giroud	UK	Towards Baseline Operation Integrating ITER-Relevant Core and Edge Plasma within the Constraint of the ITER-like Wall at JET
EX/P5-26	S. Brezinsek	Germany	Beryllium Migration in JET ITER-like Wall Plasmas
EX/P5-27	T. Loarer	France	Plasma Isotopic Change over Experiments in JET under Carbon and ITER-like Wall Conditions
EX/P5-28	G. Kurskiev	Russian Federation	A Study of Core Thomson Scattering Measurements in ITER Using a Multi-Laser Approach
EX/P5-29	E. de la Luna	Spain	Comparative Study of High Triangularity H-Mode Plasma Performance in JET with Be/W Wall and CFC Wall
EX/P5-30	M. Lennholm	European Commis- sion	Real-Time Control of ELM and Sawtooth Frequencies: Similarities and Differences
EX/P5-31	S. Brezinsek	Sweden	An Overview of Erosion-Deposition Pattern in JET with ITER-like Wall
EX/P5-32	K. Schmid	Germany	WallDYN Simulations of Global Impurity Migration and Fuel Retention in JET and Extrapolations to ITER

	Id	Presenter		Title
	EX/P5-33	S. Gerasimov	UK	JET Asymmetrical Disruptions
	TH/P5-34	A. E. Järvinen	Finland	Comparison of H-Mode Plasmas in JET-ILW and JET-C with and without Nitrogen Seeding
	TH/P5-35	M. Groth	Finland	Steps in Validating Scrape-off Layer Simulations of Detached Plasmas in the JET ITER-like Wall Configuration
THU	TH/P5-36	E. Sorokina	Russian Federation	Long-Lived Ribbon Structure in JET Tokamak as a Manifestation of a Force-Free Magneto-Current Island
	TH/P5-37	S. Moradi	France	Core Micro-Instability Analysis of JET Hybrid and Baseline Discharges with Carbon Wall
	EX/P5-38	R. Sabot	France	Discriminating the Trapped Electron Mode Contribution in Density Fluctuation Spectra and Turbulent Transport
	EX/P5-39	P. Jacquet	UK	Maximization of ICRF Power by SOL Density Tailoring with Local Gas Injection
	EX/P5-40	E. Joffrin	France	Impact of Divertor Geometry on ITER Scenarios Performance in the JET Metallic Wall
	ICC/P5-41	V. Svidzinski	USA	Plasma Confinement by Pressure of Rotating Magnetic Field in Toroidal Device
	PPC/P5-42	D. Moreau	France	Combined Magnetic and Kinetic Control of Advanced Tokamak Steady State Scenarios based on Semi-Empirical Modeling
	ICC/P5-43	T. Asai	Japan	Control of Spontaneous Rotation in a Field-Reversed Configuration by Double-Sided Magnetized Plasmoid Injection
	EX/P5-46	C. Xiao	Canada	Plasma Current Start-up without Central Solenoid in the Iron Core STOR-M Tokamak
	EX/P5-48	E. Tsitrone	France	Preparing ITER Tungsten Divertor Operation in Tore Supra: Physics Basis for the WEST Project
	EX/P5-49	Y. Takase	Japan	Non-Inductive Plasma Start-up Experiments on the TST-2 Spherical Tokamak Using Waves in the Lower-Hybrid Frequency Range
	TH/P5-50	G. Ciraolo	France	Numerical Modeling for Divertor Design and in Support to the WEST Project
	FIP/2-4Rc	V. Toigo	Italy	Progress in the Realization of the PRIMA Neutral Beam Test Facility

Id	Presenter		Title
FIP/P5-1	R. Zanino	Italy	Design Studies towards the Geometrical Optimization of the Thermal-Hydraulic Performance of Cylindrical Hypervapotron-Type Collectors for Gyrotrons
MPT/P5-2	W. Osei-Mensah	Ghana	Radiation Responses for a Stainless Steel Composite as a Neutral Beam Injector Guard Wall of ITER
FIP/P5-3	T. Seki	Japan	ICRF Heating Experiment Using the Faraday Shield Less Antenna and New High Power Antenna in LHD
FIP/P5-4	V. Vdovin	Russian Federation	ICRF System on Tokamak T-15
FIP/P5-5	V. Vdovin	Russian Federation	Helicons Current Drive System in Tokamak T-15
SEE/P5-6	R. Hiwatari	Japan	Control Requirement of Tokamak Fusion Power Plant for Power Generation in Grid System
SEE/P5-8	E. Mukhin	Russian Federation	In-Situ Monitoring Hydrogen Isotope Retention in ITER First Wall
SEE/P5-9	W. J. Choi	Korea, Republic of	Formation of the Business Ecosystem of the Big Science in Korea: Focus on Nuclear Fusion and Accelerator Devices
SEE/P5-10	M. Nakamura	Japan	Analysis of Accident Scenarios of a Water-Cooled Tokamak DEMO
SEE/P5-12	J. Herb	Germany	Review of the Safety Concept for Fusion Reactor Concepts and Transferability of the Nuclear Fission Regulation to Potential Fusion Power Plants
SEE/P5-13	M. Ni	China	Tritium Safety Assessment for Fusion Reactor Based on Fuel Cycle and Environmental Dispersion Modelling
SEE/P5-15	D. Chen	China	Physics Design and Economic Assessment of a Long-Pulsed Fusion Power Plant

Lunch Break (12:30 – 14:00)

Thursday, October 16, 2014

	EX/6 and TH/5: T Chair: Y. Oh (Kor		PDF Link: Discussion Plenary Hall: Blue 1–5 (14:00 – 16:10)	
	Time Id	Presenter		Title
	14:00 EX/6-1	M. Valisa	Italy	Heavy Impurity Transport in the Core of JET Plasmas
TH	14:20 EX/6-2	M. Yoshida	Japan	Response of Ion and Electron Temperatures, Electron Density and Toroidal Rotation to Electron Cyclotron Heating in JT-60U
C	14:40 EX/6-3	Y. Shi	Korea, Republic of	Toroidal Rotation Profile Structure in L- and H-Mode KSTAR Plasmas
	15:00 TH/5-1	M. Honda	Japan	Integrated Modeling of Toroidal Rotation with the 3D Non-Local Drift-Kinetic Code and Boundary Models for JT-60U Analyses and Predictive Simulations
	15:20 EX/6-4	X. Ji	China	Interaction between Neoclassical Tearing Modes and Non-Local Transport in HL-2A
	15:40 TH/5-2	J. Garcia	France	Core Microturbulence and Edge MHD Interplay and Stabilization by Fast Ions in Tokamak Confined Plasmas

Coffee Break (16:10 – 16:40)

Chair: L. El-Gueb	0	y	<i>Plenary Hall: Blue</i> 1–5 (16:40 – 18:45)
Time Id	Presenter		Title
16:40 FIP/3-1	A. Dinklage	Germany	The Initial Programme of Wendelstein 7-X on the Way to a HELIAS Fusion Power Plant
17:00 FIP/3-2	E. Azizov	Russian Federation	Status of Upgrading Project of Tokamak T-15
17:20 FIP/3-3	R. Kemp	UK	DEMO Design Point Studies
17:40 FIP/3-4Ra	N. Asakura	Japan	Physics and Engineering Studies of the Advanced Divertor for a Fusion Reactor
FIP/3-4Rb			DEMO Concept Development and Assessment of Relevant Technologies
18:00 FIP/3-5Ra	K. Feng	China	Current Status of Chinese Solid Tritium Breeder TBM
18:20 FIP/3-6	K. Kim	Korea, Republic of	Design Concept of K-DEMO for Near-Term Implementation

FIP/3: New Devices & Technology

PDF Link: Discussion

Thursday, October 16, 2014

Poster Session: P6			Poster Room: Green 8&9 (14:00 – 18:45)	
Id	Presenter		Title	
IFE/1-1	C. Li	USA	Effects of Ion Diffusion on Fusion Burn at the Shock Flash in Inertial-Confinement Fusion Implosions	
IFE/1-2	S. Fujioka	Japan	Experimental Platform for Efficient Heating of Fusion Fuel with Fast-Ignition Scheme	
IFE/1-3	S. Krashenin- nikov	USA	Effect of Pre-Plasma on Intense Electron Beam Generation by Relativistic Laser Radiation	
IFE/1-4	E. Koresheva	Russian Federation	Conception of a Cryogenic Target Factory for IFE	
IFE/1-5	H. J. Kong	Korea, Republic of	A High-Energy and Highly Repetitive fs/ps Laser Using Optical Parametric Chirped-Pulse Amplification with a ns Beam Combined Pumping Laser for Fast Ignition	
TH/P6-1	P. Cahyna	Czech Republic	Modelling of Spatial Structure of Divertor Power Loads Caused by Edge-Localized Modes Mitigated by Magnetic Perturbations	
TH/P6-2	U. Daybelge	Turkey	Rotation Instability of Neoclassical Plasma Near Magnetic Separatrix	
TH/P6-4	A. Fukuyama	Japan	Kinetic Integrated Modeling of Burning Start-up Phase in Tokamaks	
TH/P6-8	T. Onjun	Thailand	Analysis of ITB and ETB Formations in Tokamak Plasma Using Bifurcation Concept	
TH/P6-9	L. Colas	France	Self-Consistent Modeling of Radio-Frequency Sheaths: Comparison with Tore Supra Measurements and Predictability for Future Machines	
TH/P6-10	S. Yi	Korea, Republic of	How Turbulence Spreading Decouples the Flux from the Local Gradient: a Nonlinear Gyrokinetic Simulation Study	
TH/P6-11	O. Meneghini	USA	Integrated Modeling of Tokamak Experiments with OMFIT	
TH/P6-12	J. Shiraishi	Japan	Extension of Kinetic-Magnetohydrodynamic Model to Include Toroidal Rotation Shear Effect and its Application to Stability Analysis of Resistive Wall Modes	
TH/P6-14	J. Zhu	China	Theoretical and Simulation Studies on the Wave and Particle Dynamics Associated with Alfvén Eigenmodes in Tokamak Plasmas	

Poster Session: P6

Poster Room: Green 8&9 (14:00 – 18:45)

Id	Presenter		Title
TH/P6-15	W. Tang	USA	New Physics Insights on Size-Scaling of Confinement Enabled by Computing at Extreme Scale
TH/P6-16	L. Chen	China	Nonlinear Excitation of Kinetic Geodesic Acoustic Modes by Drift Waves in Nonuniform Plasmas
EX/P6-17	B. LaBombard	USA	High Density LHRF Experiments in Alcator C-Mod and Implications for Reactor Scale Devices
EX/P6-19	T. Golfinopoulos	USA	New Insights into Short-Wavelength, Coherent Edge Fluctuations on Alcator C-Mod
EX/P6-20	L. E. Sugiyama	USA	Destabilization of Internal Kink by Suprathermal Electron Pressure Driven by Lower Hybrid Current Drive (LHCD)
EX/P6-21	D. Whyte	USA	New In-Situ Measurements for Plasma Material Interaction Studies in Alcator C-Mod
EX/P6-22	A. Hubbard	USA	Multi-Device Studies of Pedestal Physics and Confinement in the I-Mode Regime
TH/P6-24	K. C. Lee	Korea, Republic of	Analysis of Radial Electric Field Formation by Asymmetry of Neutral Beam Injection on KSTAR and NSTX Based on the Gyro-Center Shift
EX/P6-25	K. Mukai	Japan	Development of Impurity Seeding and Radiation Enhancement at Helical Divertor in LHD
EX/P6-26	N. Ohno	Japan	Plasma Structure Change and Intermittent Fluctuation near Magnetic Island X-Point under Detached Plasma Condition in LHD
EX/P6-27	M. Yokoyama	Japan	Comprehensive Understandings of Energy Confinement in LHD Plasmas through Extensive Application of the Integrated Transport Analysis Suite
EX/P6-28	I. Murakami	Japan	Development of Quantitative Atomic Modeling for Tungsten Transport Study Using LHD Plasma with Tungsten Pellet Injection
EX/P6-29	S. Ohdachi	Japan	Pressure Driven MHD Instabilities in Intrinsic and Externally Enhanced Magnetic Stochastic Region of LHD
EX/P6-30	M. Yoshinuma	Japan	Abrupt Reversal of Convective Flow of Carbon Impurity during Impurity-Hole Formation on LHD

	Id	Presenter		Title
	EX/P6-31	K. Fujii	Japan	Study of Neutral Hydrogen Transport in LHD Core Plasmas Based on High Dynamic-Range Balmer-Alpha Spectroscopy
	EX/P6-32	S. Sudo	Japan	Study of Transport Characteristics of Multiple Impurities Depending on the Impurity Source Location in LHD
THU	EX/P6-33	M. Shoji	Japan	Studies of Dust Transport in Long Pulse Discharges in the Large Helical Device
J	EX/P6-34	T. Shimozuma	Japan	Optimization of High Harmonic ECRH Scenario to Extend a Heating Plasma Parameter Range in LHD
	EX/P6-35	Y. Narushima	Japan	Experimental Observation of Plasma Response to Resonant Magnetic Perturbation and its Hysteresis in LHD
	EX/P6-36	X. Du	Japan	Interaction between Resistive Interchange Mode and Helically Trapped Energetic Ions and its Effects on the Energetic Ions and Bulk Plasmas in LHD
	EX/P6-37	S. Sakakibara	Japan	Characteristics of MHD Instabilities Limiting Beta Value in LHD
	TH/P6-38	S. Murakami	Japan	Integrated Heat Transport Simulation of High Ion Temperature Plasma of LHD
	TH/P6-39	G. Kawamura	Japan	Transport Simulation Analysis of Peripheral Plasma with the Open and the Closed LHD Divertor
	TH/P6-40	A. Ishizawa	Japan	Electromagnetic Gyrokinetic Analysis of Turbulent Transport in Finite- <i>beta</i> LHD Plasmas
	EX/P6-43	K. C. Lee	Korea, Republic of	Experimental Observation of Nonlocal Electron Thermal Transport in NSTX RF-Heated L-Mode Plasmas
	EX/P6-45	E. Fredrickson	USA	Parametric Dependence of Fast-Ion Transport Events on the National Spherical Tokamak Experiment
	PPC/P6-46	HS. Kim	Korea, Republic of	Development of Real Time Multiple Control Algorithm for Integrated Control of Plasma Profiles and Neoclassical Tearing Mode
	TH/P6-49	R. W. Harvey	USA	NBI and HHFW Fast Ion Temporal Dynamics Modeling with CQL3D-Hybrid-FOW in NSTX Discharges

THU

Id	Presenter		Title
TH/P6-50	A. W. Leonard	USA	Modeling Divertor Concepts for Spherical Tokamaks NSTX, NSTX-U, and ST-FNSF
TH/P6-52	D. Russell	USA	Modelling the Effect of Lithium on SOL Dynamics and the SOL Heat Flux Width Observed in NSTX
EX/P6-53	T. W. Petrie	USA	Impact of 3D Fields on Divertor Detachment in NSTX and DIII-D
EX/P6-54	G. Xu	China	The Role of Lithium Conditioning in Achieving High Performance, Long Pulse H-Mode Discharges in the NSTX and EAST Devices
TH/P6-55	B. Nelson	USA	Transient CHI Plasma Start-up Simulations and Projections to NSTX-U
EX/P6-56	Y. Tan	China	Study of the Alfvén Wave Coupling in the SUNIST Spherical Tokamak
EX/P6-57	A. Tukachinsky	Russian Federation	Alfvén Oscillations in the TUMAN-3M Tokamak Ohmic Regime
EX/P6-58	V. Kornev	Russian Federation	Effect of Horizontal Displacement on Fast Ion Confinement in TUMAN-3M
EX/P6-59	A. Belokurov	Russian Federation	GAM Evolution and LH-Transition in the TUMAN-3M Tokamak
TH/P6-60	J. Ongena	Belgium	Verification of the Simulated Radiated Power of the ICRH Antenna Design for Wendelstein 7-X with Experimental Results Using a Quarter Scale Mock-up Antenna
IFE/P6-2	Z. Zhang	Japan	Energy Transport by MeV Hot Electrons in Fast Ignition Plasma Driven with LFEX PW Laser
IFE/P6-3	H. Shiraga	Japan	Fast Ignition Experiments and Intense Hard-X-Ray Harsh Environment
IFE/P6-4	A. Morace	Japan	Plasma Mirror technology on a PW, multi-kJ class Laser to reduce the pre-formed plasma for application to Fast Ignition research.
IFE/P6-5	T. Johzaki	Japan	Control of Electron Beam Using Strong Magnetic Field for Efficient Core Heating in Fast Ignition
IFE/P6-6	H. Nagatomo	Japan	Computational Study of Magnetic Field Compression by Laser Driven Implosion

	Id	Presenter		Title
	IFE/P6-7	M. Murakami	Japan	High Compression of Matter by Hyperspherical Shock Waves for Application to Impact Ignition
	IFE/P6-8	A. Sid	Algeria	Stabilization Effect of Weibel Modes in Relativistic Laser Fusion Plasma
THU	IFE/P6-9	Y. Mori	Japan	1000 Times Enhancement of Fusion Reaction in Relation to Fast-Ion Heating Induced by a Direct-Irradiating Fast-Ignition Scheme
L	IFE/P6-10	Y. Nishimura	Japan	Counter Implosion of 500 μ m Diameter CD Shell and Fast Heating of its Core Plasma by Tailored DPSSL-Pumped Laser
	IFE/P6-11	R. Hanayama	Japan	1Hz Pellets Injection and Laser Synchronous System for Continuous Laser Confinement Fusion and Neutron Generation
	IFE/P6-12	T. Sekine	Japan	Conceptual Design of kilo-Joule Laser Driver for Inertial Fusion Mini-Reactor CANDY
	IFE/P6-13	M. Wölz	Germany	Increasing Laser Power Density towards IFE Requirements: High-Power Laser Diode Bars
	IFE/P6-16	M. Shmatov	Russian Federation	The Perspectives of the Use of the Advanced Fuels for Power Production

EX/7 and PPC/1: Divertor & Exhaust Physics Chair: W. Morris (UK)

PDF Link: Discussion Plenary Hall: Blue 1–5 (08:30 – 10:15)

Chair: w. Morris (UK)				Plenury = 10.13
Time Id Presenter			Title	
8:30	EX/7-1	A. Kallenbach	Germany	Partial Detachment of High Power Discharges in ASDEX Upgrade
8:50	EX/7-2	M. Wischmeier	Germany	Impurity Seeding on JET to Achieve Power Plant like Divertor Conditions
9:10	EX/7-3	H. Kasahara	Japan	Progress of High-Performance Steady-State Plasma and Critical PWI Issue in LHD
9:30	EX/7-4	A. W. Leonard	USA	Developing Physics Basis for the Radiative Snowflake Divertor at DIII-D
9:50	PPC/1-1	E. Kolemen	USA	Burning Plasma Relevant Control Development: Advanced Magnetic Divertor Configurations, Divertor Detachment and Burn Control

Coffee Break (10:15 – 10:45)

		D: 3D Physics &		
Time	r: A. Komori	Presenter		<i>Plenary Hall: Blue 1–5</i> (10:45 – 12:30) Title
		G. Huijsmans	ITER	Non-Linear MHD Simulations for ITER
	TH/6-1Rb			Non-Linear MHD Modelling of Edge Localized Modes and their Interaction with Resonant Magnetic Perturbations in Rotating Plasmas
11:05	EX/8-1	H. Park	Korea, Republic of	Simultaneous Measurement of the ELMs at Both High and Low Field Sides and ELM Dynamics in ELM Crash-Free Period in KSTAR
11:25	TH/6-2	K. Ichiguchi	Japan	Three-Dimensional MHD Analysis of Heliotron Plasma with RMP
11:45	PD/1-1	Presenter: tbd	Country	Title: tbd
12:05	PD/1-2	Presenter: tbd	Country	Title: tbd

Friday, October 17, 2014

	Poster Sessi	on: P7		Poster Room: Green 8&9 (08:30 – 12:30)
	Id	Presenter		Title
	EX/5-1	R. Granetz	USA	An ITPA Joint Experiment to Study Runaway Electron Generation and Suppression
	EX/5-2	C. Reux	France	Runaway Electron Generation with the ITER-like Wall and Efficiency of Massive Gas Injection at JET
	EX/5-3	R. L. Tanna	India	Novel Approaches for Mitigating Runaway Electrons and Plasma Disruptions in Tokamak ADITYA
FRI	EX/6-1	M. Valisa	Italy	Heavy Impurity Transport in the Core of JET Plasmas
	EX/6-2	M. Yoshida	Japan	Response of Ion and Electron Temperatures, Electron Density and Toroidal Rotation to Electron Cyclotron Heating in JT-60U
	EX/6-3	Y. Shi	Korea, Republic of	Toroidal Rotation Profile Structure in L- and H-Mode KSTAR Plasmas
	EX/6-4	X. Ji	China	Interaction between Neoclassical Tearing Modes and Non-Local Transport in HL-2A
	EX/9-1	A. Sips	European Commis- sion	Progress in Preparing Scenarios for ITER Operation
	EX/9-2	I. M. Ferreira Nunes	Portugal	Compatibility of High Performance Operation with JET ILW
	EX/9-3	C. Challis	UK	Improved Confinement in JET High Beta Plasmas with an ITER-like Wall
	EX/9-4	J. Schweinzer	Germany	Development of the Q=10 Scenario for ITER on ASDEX Upgrade (AUG)
	EX/9-5	G. Xu	China	A Long-Pulse H-Mode Regime with a New Coherent Mode Providing Continuous Transport across Pedestal in EAST
	EX/10-1	W. W. Heidbrink	USA	Alfvén Eigenmodes Can Limit Access to High Fusion Gain, Steady-State Tokamak Operation
	EX/10-2	M. Van Zeeland	USA	Fast Ion Transport during Applied 3D Magnetic Perturbations on DIII-D
	EX/10-3	M. Osakabe	Japan	Indication of Bulk-Ion Heating by Energetic Particle Driven Geodesic Acoustic Modes on LHD
	EX/10-4	W. W. Heidbrink	USA	Effects of MHD Instabilities on Neutral Beam Current Drive

Id	Presenter		Title
TH/4-1	V. A. Izzo	USA	The Role of MHD in 3D Aspects of Massive Gas Injection for Disruption Mitigation
TH/4-2	A. Popov	Russian Federation	The Low Threshold Parametric Decay Instabilities Leading to Anomalous Absorption at ECRH in Toroidal Devices
TH/5-1	M. Honda	Japan	Integrated Modeling of Toroidal Rotation with the 3D Non-Local Drift-Kinetic Code and Boundary Models for JT-60U Analyses and Predictive Simulations
TH/5-2	J. Garcia	France	Core Microturbulence and Edge MHD Interplay and Stabilization by Fast Ions in Tokamak Confined Plasmas
TH/7-1	Y. Todo	Japan	Multi-Phase Simulation of Alfvén Eigenmodes and Fast Ion Distribution Flattening in DIII-D Experiment
TH/7-2	Z. Lin	USA	Radial Localization of Alfvén Eigenmodes and Zonal Field Generation
FIP/3-3	R. Kemp	UK	DEMO Design Point Studies
FIP/3-4Rb	Y. Sakamoto	Japan	DEMO Concept Development and Assessment of Relevant Technologies
FIP/3-6	K. Kim	Korea, Republic of	Design Concept of K-DEMO for Near-Term Implementation
FNS/1-1	L. El-Guebaly	USA	Configuration Studies for an ST-Based Fusion Nuclear Science Facility
FNS/1-2Ra	J. Knaster	Japan	The Accomplishment of the Engineering Design Activities of IFMIF/EVEDA: the European-Japanese Project Towards a Li(d,xn) Fusion Relevant Neutron Source
MPT/1-2	X. Liu	China	Overview of Fusion Reactor Materials Study at SWIP
MPT/1-3	A. M. Ito	Japan	Molecular Dynamics and Density Functional Simulations of Tungsten Nanostructure Formation by Helium Plasma Irradiation
MPT/1-4	A. Hasegawa	Japan	Neutron Irradiation Effects on Grain-Refined W and W-Alloys
PPC/2-1	K. Nagaoka	Japan	Integrated Discharge Scenario for High-Temperature Helical Plasma on LHD
TH/P7-1	D. P. Brennan	USA	Energetic Particle Driven $n = 1$ MHD Instabilities in Tokamaks with Weakly Reversed Shear

	Id	Presenter		Title
	TH/P7-2	K. Hallatschek	Germany	Evolution and System Dependent Properties of Zonal Flows and GAMs in Tokamaks and Planet Atmospheres
	TH/P7-4	L. Zheng	USA	Finite Larmor Radius Effects on Low- <i>n</i> Magnetohydrodynamic Modes at H-Mode Pedestal with Plasma Rotation
	TH/P7-5	P. Beyer	France	Mechanisms and Dynamics of the External Transport Barrier Formation in Nonlinear Plasma Edge Simulations
FRI	TH/P7-6	C. Di Troia	Italy	Bayesian Derivation of Plasma Equilibrium Distribution Function for Tokamak Scenarios
	TH/P7-7	Y. Kosuga	Japan	A New Theory of Scale Selection: What Determines the Avalanche Scale?
	TH/P7-8	Y. Homma	Japan	Kinetic Modeling of Classical and Neo-Classical Transport for High-Z Impurities in Fusion SOL/Divertor Plasmas Using Binary Collision Method
	TH/P7-9	M. Nunami	Japan	Reduced Model for Gyrokinetic Turbulent Transport in Helical Plasmas
	TH/P7-10	L. Sugiyama	USA	Open Theoretical Issues and Solutions for Fusion Relevant Physics Regimes
	TH/P7-13	W. A. Cooper	Switzerland	Equilibrium and Fast Particle Confinement in 3D Tokamaks with Toroidal Rotation
	TH/P7-14	V. Pustovitov	Russian Federation	Energy Principle for the Fast Resistive Wall Modes in Tokamaks
	TH/P7-15	M. Lesur	Japan	Chirping Alfvén Eigenmodes Drive Convective and Diffusive Transport
	EX/P7-16	S. Kulkarni	India	Recent ICRH-Wall Conditioning, Second Harmonic Heating and Disruption Mitigation Experiments Using ICRH System in Tokamak ADITYA
	EX/P7-17	P. Dhyani	India	Disruption Control Using Biased Electrode in Aditya Tokamak
	EX/P7-18	Y. Liu	China	L-H Transition Triggered by Fishbone Mode in the NBI Heated HL-2A Plasmas
	EX/P7-19	Y. Xu	China	Neoclassical Tearing Modes Triggered by Intrinsic Error Field in the HL-2A Tokamak
	EX/P7-20	D. Yu	China	Evolution of the Ion Temperature in Pedestal during the ELM Mitigation by SMBI

Id	Presenter		Title
EX/P7-21	M. Jiang	China	The Observation of Synchronous Oscillation prior to Disruption in the HL-2A Tokamak
EX/P7-22	L. Nie	China	Comparison of ELM-Filament Mitigation between Supersonic Molecular Beam Injection and Pellet Injection in the HL-2A Tokamak
EX/P7-23	W. Zhong	China	The Role of Edge Plasma Instabilities in Dynamical Evolution of Pedestal in the HL-2A Tokamak
EX/P7-24	Y. Zhang	China	Measurements of Fast-Ion Losses Induced by MHD Instabilities Using Scintillator-Based Probe in the HL-2A Tokamak
EX/P7-25	L. Yu	China	Transition and Interaction of Low-Frequency MHD Modes during Neutral Beam Injection on HL-2A
EX/P7-26	Z. Cui	China	Study of Carbon Transport in the Scrape-off Layer of HL-2A with Impurity Sources Located at Limiter, Baffle and Divertor
EX/P7-27	W. Chen	China	Characterization and Nonlinear Interaction of Shear Alfvén Waves in the Presence of Strong Tearing Modes in Tokamak Plasmas
TH/P7-30	Z. Wang	China	Simulations and Validations of Transport during Fueling by SMBI in HL-2A Tokamak
EX/P7-31	Y. B. Dong	China	Experimental Study of Disruption Mitigation Using Supersonic Molecular Beam and Massive Gas Injection on HL-2A and J-TEXT
EX/P7-32	J. Cheng	China	Dynamics of High-Intermediate-High Confinement Transitions on the HL-2A Tokamak
EX/P7-33	D. Kong	China	The Observation of Pedestal Turbulence Contributing Inward Particle and Heat Flux on the Edge of HL-2A Tokamak
EX/P7-34	G. Krashevskaya	Russian Federation	Plasma Confinement by Magnetic Field with Convex-Concave Field Lines
EX/P7-35	P. Khorshid		Calculation of Magnetic Field Perturbation Using Saddle Coils and Helical Windings Based on IR-T1 Tokamak
EX/P7-36	T. Kobayashi	Japan	Edge Plasma Dynamics during L-H Transition in the JFT-2M Tokamak

FRI

Id	Presenter		Title
TH/P7-37	Y. Suzuki	Japan	3D Plasma Response to Resonant External Magnetic Perturbation and its Impact on Fast Ion Confinement in JT-60SA Plasmas
TH/P7-38	M. Nakata	Japan	Gyrokinetic Analysis of Turbulent Heat and Particle Transport on JT-60U Plasmas
TH/P7-39	A. Bierwage	Japan	Multi-Time-Scale Energetic Particle Dynamics in JT-60U Simulated with MHD Activity, Sources and Collisions
EX/P7-40	K. Zhao	China	Plasma Flows and Fluctuations with Resonant Magnetic Perturbations on the Edge Plasmas of the J-TEXT Tokamak
EX/P7-41	H. Tanaka	Japan	Observation of Intermittent Plasma Ejection from a Highly Overdense Spherical Tokamak Plasma Maintained by Electron Bernstein Wave Heating and Current Drive in LATE
EX/P7-44	J. H. Severo	Brazil	Investigation of Co-Current Rotation at Plasma Edge in the TCABR
EX/P7-45	V. Moiseenko	Ukraine	Features of Regular Discharges in Uragan-3M Torsatron
FIP/P7-1	K. Kim	Korea, Republic of	Availability Considerations in the Design of K-DEMO
FIP/P7-2	K. Kim	Korea, Republic of	Physics and Engineering Assessments of the K-DEMO Magnet Configuration
FIP/P7-4	K. Im	Korea, Republic of	Design Concept of K-DEMO In-Vessel Components
FIP/P7-5	I. Jenkins	UK	The Impact on Tritium Breeding Ratio of Neutral Beam Port Location in DEMO
FIP/P7-6	B. Saoutic	France	DEMO Reactor Design by the New Modular System Code SYCOMORE
FIP/P7-7	A. Fasoli	Switzerland	TCV Heating and In-Vessel Upgrades for Addressing DEMO Physics Issues
FIP/P7-8	F. P. Orsitto	Italy	Diagnostics and Control for Steady State and Pulsed Tokamak DEMO
FIP/P7-9	V. Sergeev	Russian Federation	Design of Divertor and First Wall for DEMO-FNS
FIP/P7-10	D. Ivanov	Russian Federation	Superconducting Magnet for Russian Fusion Neutron Source DEMO-TIN
FNS/P7-11	A. Y. Dnestrovskij	Russian Federation	Integrated Modelling of DEMO-FNS Current Ramp-up Scenario and Steady State Regime

Id	Presenter		Title
FIP/P7-12	C. Day	Germany	The Operational Window for Divertor Detachment in a Fusion Reactor – A Physics-Technology Integrated Approach
FIP/P7-13	A. Spitsyn	Russian Federation	Concept of Fuel Cycle for a Fusion Neutron Source
FIP/P7-14	I. Kirillov	Russian Federation	Lead–Lithium Ceramic Breeder Blanket for Russian Thermonuclear Reactor DEMO-S
FIP/P7-15	K. Gi	Japan	Conceptual Design Study of the Large Size and Low Magnetic Field Superconducting Spherical Tokamak Power Plant
FIP/P7-16	T. Goto	Japan	Integrated Physics Analysis of Plasma Operation Control Scenario of Helical Reactor FFHR-d1
FIP/P7-17	R. Imazawa	Japan	Multi-Parameter Measurement Using Finite Electron Temperature Effect on Laser Polarimetry for Burning Plasma Reactor
FIP/P7-18	B. LaBombard	USA	ADX: a High Field, High Power Density, Advanced Divertor Test Facility
FIP/P7-19	V. Menon	India	Physics Design and Analysis Code SPECTRE for Tokamak Based Fusion Reactors
FNS/P7-20	U. Fischer	Germany	Advanced Computational Approaches and Tools for High-Fidelity Nuclear Analyses of Fusion Facilities
FIP/P7-21	JC. Vallet	France	Progress of the CEA Contributions to the Broader Approach Projects
FNS/P7-22	P. Goncharov	Russian Federation	Spectra of Neutrons from a Beam-Driven Fusion Source
FIP/P7-23	A. Shimkevich	Russian Federation	The Concept of Hybrid Reactor-Tokamak with Molten-Salt Thorium Blanket for Producing 233U out of Neutron Field
FIP/P7-24	B. Kuteev	Russian Federation	Development of DEMO-FNS Tokamak for Fusion and Hybrid Technologies
FNS/P7-25	A. Zhirkin	Russian Federation	The Neutronics Analysis of Blankets for the Hybrid Fusion Neutron Source
FNS/P7-27	T. Simonen	USA	Optimization of a Gas Dynamic Trap Neutron Source
MPT/P7-28	T. Sizyuk	USA	Plasma Facing Material Alternatives to Tungsten
MPT/P7-29	N. Ohno	Japan	Contributions of Linear Plasma Devices to PMI Research

FRI

Friday, October 17, 2014

Id	Presenter		Title
FIP/P7-30	G. Kulikov	Russian Federation	Fusion Hybrid with Thorium Blanket: on its Innovative Potential at Fuel Cycle of Nuclear Reactors
MPT/P7-31	V. Chernov	Russian Federation	Microstructure and Mechanical Properties of V-Me(Cr, W)-Zr-C Alloys as a Function of their Thermochemical Treatment Modes
MPT/P7-32	P. Zheng	China	Recent Progresses on Vanadium Alloys for Fusion Application in China
MPT/P7-33	A. Sivak	Russian Federation	Energetic, Crystallographic and Diffusion Characteristics of Hydrogen Isotopes in Iron
MPT/P7-34	M. Tsventoukh	Russian Federation	Unipolar Arcing at Advanced Fine-Structured Materials
MPT/P7-36	D. Kato	Japan	Super-Saturated Hydrogen Effects on Radiation Damages in Tungsten under High-Flux Divertor Plasma Irradiation
MPT/P7-37	V. Koidan	Russian Federation	Production of Radiation-Damaged Tungsten and its Study in High Flux Deuterium Plasma
MPT/P7-38	M. Oyaidzu	Japan	Anodic Polarization Study on F82H Steel in Tritiated Water
MPT/P7-40	V. Gribkov	Russian Federation	Experimental Results on the Irradiation of a Number of the Nuclear Fusion Relevant Materials at the Dense Plasma Focus "Bora" Device
MPT/P7-41	T. Troev	Bulgaria	Computational Study of Defects in Fusion Materials Containing Helium
MPT/P7-42	M. Chernyshova	Poland	Interaction of Hot Plasma and Fast Ion Streams with Materials under Tests in the Dense Plasma Focus Devices and Some Results of the Irradiation
MPT/P7-43	V. Gribkov	Russian Federation	Physical Processes Taking Place in the Dense Plasma Focus Devices at the Interaction of Hot Plasma and Fast Ion Streams with Materials under Tests and some Results of the Irradiation

Lunch Break (12:30 – 14:00)

Chair: E. Joffrin	(France)		<i>Plenary Hall: Blue 1–5 (14:00 – 16:10)</i>
Time Id	Presenter		Title
14:00 EX/9-1	A. Sips	European Commis- sion	Progress in Preparing Scenarios for ITER Operation
14:20 EX/9-2	I. M. Ferreira Nunes	Portugal	Compatibility of High Performance Operation with JET ILW
14:40 EX/9-3	C. Challis	UK	Improved Confinement in JET High Beta Plasmas with an ITER-like Wall
15:00 PPC/2-1	K. Nagaoka	Japan	Integrated Discharge Scenario for High-Temperature Helical Plasma on LHD
15:20 EX/9-4	J. Schweinzer	Germany	Development of the Q=10 Scenario for ITER on ASDEX Upgrade (AUG)
15:40 EX/9-5	G. Xu	China	A Long-Pulse H-Mode Regime with a New Coherent Mode Providing Continuous Transport across Pedestal in EAST

EX/9 and PPC/2: Operational Scenarios

PDF Link: Discussion

Coffee Break (16:10 – 16:40)

EX/10 and TH/7: Chair: D. Campb	0	•	PDF Link: Discussion Plenary Hall: Blue 1–5 (16:40 – 18:45)
Time Id	Presenter		Title
16:40 EX/10-1	W. W. Heidbrink	USA	Alfvén Eigenmodes Can Limit Access to High Fusion Gain, Steady-State Tokamak Operation
17:00 TH/7-1	Y. Todo	Japan	Multi-Phase Simulation of Alfvén Eigenmodes and Fast Ion Distribution Flattening in DIII-D Experiment
17:20 EX/10-2	M. Van Zeeland	USA	Fast Ion Transport during Applied 3D Magnetic Perturbations on DIII-D
17:40 TH/7-2	Z. Lin	USA	Radial Localization of Alfvén Eigenmodes and Zonal Field Generation
18:00 EX/10-3	M. Osakabe	Japan	Indication of Bulk-Ion Heating by Energetic Particle Driven Geodesic Acoustic Modes on LHD
18:20 EX/10-4	W. W. Heidbrink	USA	Effects of MHD Instabilities on Neutral Beam Current Drive

FRI

	Poster Sessi	on: P8		Poster Room: Green 8&9 (14:00 – 18:45)
	Id	Presenter		Title
	EX/7-1	A. Kallenbach	Germany	Partial Detachment of High Power Discharges in ASDEX Upgrade
	EX/7-2	M. Wischmeier	Germany	Impurity Seeding on JET to Achieve Power Plant like Divertor Conditions
	EX/7-3	H. Kasahara	Japan	Progress of High-Performance Steady-State Plasma and Critical PWI Issue in LHD
	EX/7-4	A. W. Leonard	USA	Developing Physics Basis for the Radiative Snowflake Divertor at DIII-D
TCIT	EX/8-1	H. Park	Korea, Republic of	Simultaneous Measurement of the ELMs at Both High and Low Field Sides and ELM Dynamics in ELM Crash-Free Period in KSTAR
	EX/11-1	U. Stroth	Germany	Experimental Turbulence Studies for Gyro-Kinetic Code Validation Using Advanced Microwave Diagnostics
	EX/11-2Ra	A. Gurchenko	Russian Federation	The Isotope Effect in GAM – Turbulence Interplay and Anomalous Transport in Tokamak
	EX/11-2Rb	V. Vershkov	Russian Federation	Density Fluctuations as an Intrinsic Mechanism to Keep Self-Consistent Shape of Pressure Profile
	EX/11-3	J. Dong	China	Mechanism of Low-Intermediate-High Confinement Transitions in Tokamaks
	EX/11-4	L. Schmitz	USA	First Direct Evidence of Turbulence-Driven Ion Flow Triggering the L- to H-Mode Transition
	FIP/3-1	A. Dinklage	Germany	The Initial Programme of Wendelstein 7-X on the Way to a HELIAS Fusion Power Plant
	FIP/3-2	E. Azizov	Russian Federation	Status of Upgrading Project of Tokamak T-15
	FIP/3-4Ra	N. Asakura	Japan	Physics and Engineering Studies of the Advanced Divertor for a Fusion Reactor
	FIP/3-5Ra	K. Feng	China	Current Status of Chinese Solid Tritium Breeder TBM
	FIP/1-4Ra	P. Bruzzone	Switzerland	Summary of the Test Results of ITER Conductors in SULTAN

Id	Presenter		Title
PPC/1-1	E. Kolemen	USA	Burning Plasma Relevant Control Development: Advanced Magnetic Divertor Configurations, Divertor Detachment and Burn Control
TH/6-1Ra	G. Huijsmans	ITER	Non-Linear MHD Simulations for ITER
TH/6-1Rb	M. Becoulet	France	Non-Linear MHD Modelling of Edge Localized Modes and their Interaction with Resonant Magnetic Perturbations in Rotating Plasmas
TH/6-2	K. Ichiguchi	Japan	Three-Dimensional MHD Analysis of Heliotron Plasma with RMP
TH/8-1	G. Park	Korea, Republic of	A 3D Nonlinear Simulation Study of the $L \rightarrow H$ Transition Criterion
TH/P8-1	S. Krashenin- nikov	USA	Plasma-Material Interaction Issues in Magnetic Fusion Devices
EX/P8-2	YS. Na	Korea, Republic of	Investigation of Toroidal Rotation Reversal in KSTAR Ohmic Plasmas
EX/P8-4	J. Kim	Korea <i>,</i> Republic of	Disruption Threshold of Error-Field-Induced Locked Mode under $n = 1$ and $n = 2$ Mixed Non-Axisymmetric Fields
EX/P8-5	YS. Park	USA	Plasma Rotation Alteration by Non-Axisymmetric Magnetic Fields, Resistive MHD Stability Analysis, and High Normalized Beta Plasmas Exceeding the Ideal Stability Limit in KSTAR
EX/P8-6	WН. Ко	Korea, Republic of	Change of the Momentum Profiles Driven by the Sawtooth Crashes and its Effect on the LH Transition in KSTAR
EX/P8-7	J. Seol	Korea, Republic of	Study of Type III ELMs in the KSTAR Tokamak
EX/P8-8	H. Lee	Korea, Republic of	Experimental Study of the Magnetic Braking Torque by Non-Axisymmetric Magnetic Perturbations in Different Plasma Collisionality Regimes on KSTAR
EX/P8-9	H. Lee	Korea <i>,</i> Republic of	Pedestal Characteristics during the Edge Localized Mode Mitigation by Super-Sonic Molecular Beam Injection on KSTAR
EX/P8-10	SH. Hong	Korea, Republic of	In-Vessel Dust Velocity Correlated with the Toroidal Rotation of the Plasma

	Id	Presenter		Title
	EX/P8-11	SH. Hahn	Korea, Republic of	L-H Transitions Triggered by SMBI: Experiment and Theory
	EX/P8-12	H. K. Park	Korea, Republic of	Helical Modes Induced by Localized Current Perturbations in Sawtoothing KSTAR Plasmas
	EX/P8-13	W. Lee	Korea, Republic of	Measurement of Apparent Poloidal Rotation of Ion-Scale Turbulence with the KSTAR Microwave Imaging Reflectometer
	EX/P8-14	S. G. Lee	Korea, Republic of	Toroidal Rotation and Momentum Transport Studies in KSTAR Plasmas
FRI	EX/P8-15	H. K. Park	Korea, Republic of	Accurate Estimation of Tearing Mode Stability Parameters in the KSTAR Using High-Resolution 2-D ECEI Diagnostic
	PPC/P8-16	YS. Na	Korea, Republic of	On Ohmic Breakdown Physics in a Tokamak
	PPC/P8-17	SH. Hahn	Korea, Republic of	Improvements in the Fast Vertical Control Systems in KSTAR, EAST, NSTX, and NSTX-U
	EX/P8-18	Y. Xu	China	Coupling between Intrinsic Rotation and Turbulence-Driven Residual Stress in the TEXTOR Tokamak
	ICC/P8-19	Y. An	Korea, Republic of	Low Loop Voltage Start-up Using Trapped Particle Configuration in Versatile Experiment Spherical Torus (VEST)
	FIP/P8-1	Z. Xu	China	Experimental Base of Innovation S-Channel for Fusion LM Blanket
	FIP/P8-2	F. Hernandez Gonzalez	Germany	Experimental Results and Validation of Thermo-Mechanical Models Used for the PREMUX Test Campaign, as Part of the Roadmap towards an Out-of-Pile Testing of a Full Scale HCPB Breeder Unit Mock-up
	FIP/P8-3	E. Platacis	Latvia	MHD-PbLi Facility for Experiments at Real Blanket Relevant Thermo-Hydraulic Conditions
	FIP/P8-4	L. V. Boccaccini	Germany	European DEMO Breeding Blanket Design and Development Strategy in a Roadmap to the Realisation of Fusion Energy
	MPT/P8-5	A. Zarins	Latvia	High-Temperature Radiolysis of Modified Lithium Orthosilicate Pebbles with Additions of Titania
	MPT/P8-6	Y. Feng	China	Development of Functional Materials for CN TBM

Id	Presenter		Title
MPT/P8-7	P. Wang	China	R&D Status of Reduced Activation Ferritic/Martensitic Steel for CN TBM
FIP/P8-8	S. Varoutis	Germany	Simulation of Neutral Gas Flow in the JET Subdivertor and Comparison with Experimental Results
FIP/P8-9	S. McIntosh	UK	Engineering Feasibility of the Double Decker Divertor
FIP/P8-10	Y. Nakashima	Japan	Development of Divertor Simulation Research in the GAMMA 10/PDX Tandem Mirror
FIP/P8-11	K. Hoshino	Japan	Studies of Impurity Seeding and Divertor Power Handling in Fusion Reactor
FIP/P8-12	B. Chektybayev	Kazakhstan	New Visible Wide Angle Viewing System for KTM Based on Multielement Image Fiber Bundle
MPT/P8-13	I. Tazhibayeva	Kazakhstan	Results of KTM Lithium Divertor Model Testing on the Tokamak KTM and Future Plans
MPT/P8-15	A. Novokhatsky	Russian Federation	Testing of Mock-ups for a Full Tungsten Divertor on Globus-M Tokamak
FIP/P8-17	V. Bykov	Germany	Advanced Structural Analysis of Wendelstein 7-X Magnet System Weight Supports
FIP/P8-18	Y. Kamada	Japan	JT-60SA Superconducting Magnet System
FIP/P8-19	T. Andreeva	Germany	Final Assessment of Wendelstein 7-X Magnetic Field Perturbations Caused by Construction Asymmetries
FIP/P8-20	P. Decool	France	Progress of CEA Contributions to the JT-60SA TF Coil Procurements
FIP/P8-21	N. Yanagi	Japan	Design and Development of High-Temperature Superconducting Magnet System with Joint-Winding for the Helical Fusion Reactor
FIP/P8-22	E. Gaio	Italy	Protection of Superconducting Magnets in Fusion Experiments: the New Technological Solution for JT-60SA
FIP/P8-23	M. Salvador	Mexico	Design of Toroidal Coils Testing Bench: Advances in the Mexican Tokamak "T"
FIP/P8-24	D. Sutherland	USA	The Dynomak: an Advanced Fusion Reactor Concept with Imposed-Dynamo Current Drive and Next-Generation Nuclear Power Technologies

Id	Presenter		Title
FIP/P8-25	V. Minaev	Russian Federation	Globus-M2 Design Peculiarities and Status of the Tokamak Upgrade
FIP/P8-26	R. Martin	UK	MAST Upgrade – Construction Status and Early Research Plans
FIP/P8-27	L. Sugiyama	Italy	Perspectives for the High Field Approach in Fusion Research and Advances within the Ignitor Program
FIP/P8-28	M. Emoto	Japan	Development and Successful Operation of the Enhanced-Interlink System of Experiment Data and Numerical Simulation in LHD
FIP/P8-29	A. Sushkov	Russian Federation	Engineering Aspects and Physical Research Program of the Modernized T-15 Tokamak
FIP/P8-30	S. A. Sabbagh	USA	Progress toward Commissioning and Plasma Operation in NSTX-U
FIP/P8-31	T. Akiyama	Japan	Conceptual Design of High Resolution and Reliable Density Measurement System on Helical Reactor FFHR-d1 and Demonstration on LHD
FIP/P8-32	H. B. Xu	China	Preliminary Test Results of GDC Electrode with Gap Insulation on SWIP Test Bed

	FNS/1 and MPT/1: Next Step Fusion Nuclear TechnologyPDF Link: DiscussionChair: G. Federici (European Commission)Plenary Hall: Blue 1–5 (08:30 – 10:15)						
Time	Id	Presenter		Title			
8:30	FNS/1-1	L. El-Guebaly	USA	Configuration Studies for an ST-Based Fusion Nuclear Science Facility			
8:50	FNS/1-2Ra	J. Knaster	Japan	The Accomplishment of the Engineering Design Activities of IFMIF/EVEDA: the European-Japanese Project Towards a Li(d,xn) Fusion Relevant Neutron Source			
9:10	MPT/1-2	X. Liu	China	Overview of Fusion Reactor Materials Study at SWIP			
9:30	MPT/1-3	A. M. Ito	Japan	Molecular Dynamics and Density Functional Simulations of Tungsten Nanostructure Formation by Helium Plasma Irradiation			
9:50	MPT/1-4	A. Hasegawa	Japan	Neutron Irradiation Effects on Grain-Refined W and W-Alloys			

Coffee Break (10:15 – 10:45)

Chair: Y. I	Kishimoto	o (Japan)		Plenary Hall: Blue 1–5 (10:45 – 12:30)
Time Id	Р	Presenter		Title
10:50 EX/	'11-1 L	J. Stroth	Germany	Experimental Turbulence Studies for Gyro-Kinetic Code Validation Using Advanced Microwave Diagnostics
11:10 EX/	'11 -2R a A		Russian Federation	The Isotope Effect in GAM – Turbulence Interplay and Anomalous Transport in Tokamak
EX,	′11 -2 Rb			Density Fluctuations as an Intrinsic Mechanism to Keep Self-Consistent Shape of Pressure Profile
11:30 EX/	′11-3 J.	. Dong	China	Mechanism of Low-Intermediate-High Confinement Transitions in Tokamaks
11:50 EX/	'11-4 L	Schmitz	USA	First Direct Evidence of Turbulence-Driven Ion Flow Triggering the L- to H-Mode Transition
12:10 TH	/8-1 0		Korea, Republic of	A 3D Nonlinear Simulation Study of the $L \rightarrow H$ Transition Criterion

EX/11 and TH/8: Edge Turbulence

PDF Link: Discussion

Lunch Break (12:30 – 14:00)

S/1: Summary

Chair: A. Becoulet (France)			Plenary Hall: Blue 1–5 (14:00 – 15:40)
Time Id	Presenter		Title
14:00	M. Kikuchi	IAEA	Nuclear Fusion Award Speeches
14:30 <mark>S/1-1</mark>	C. Hidalgo	Spain	Summary EX/C, EX/D, PPC
15:00 S/1-2	A. Sen	India	Summary EX/S, EX/W, ICC

Coffee Break (15:40 – 16:10)

S/2: Summary

Chair: Y. Kamada (Japan)

Plenary Hall: Blue 1–5 (16:10–17:40)

Presenter		Title	
A. Fukuyama	Japan	Summary Theory	
S. Jacquemot	France	Summary IFE	
B. Kuteev	Russian Federation	Summary FIP, FNS, MPT, SEE	
IAEA Representative	IAEA	Closing	
	A. Fukuyama S. Jacquemot B. Kuteev IAEA	A. Fukuyama Japan S. Jacquemot France B. Kuteev Russian Federation IAEA IAEA	A. FukuyamaJapanSummary TheoryS. JacquemotFranceSummary IFEB. KuteevRussian FederationSummary FIP, FNS, MPT, SEEIAEAIAEAClosing

Contents

Conference Secretariat	1
FEC Programme Committee	4
List of Contributions	5
Explanation of Abbreviations	5
Floor Plan: Park Inn Pribaltiyskaya	6
Conference Timetable	7
Programme Sunday, October 12, 2014 Monday, October 13, 2014 Tuesday, October 14, 2014 Wednesday, October 15, 2014 Thursday, October 16, 2014 Friday, October 17, 2014 Saturday, October 18, 2014	8 9 13 22 34 47 61
O: Opening 1 O/3 E. P. Velikhov Igor Kurchatov and the Russian Fusion Program 1	105 106
OV/1-1 L. Askinazi Fusion Research in Ioffe Institute 1 OV/1-2 O. Motojima The ITER Project Construction Status 1	
OV/1-3 F. Romanelli Overview of the JET Results 1 OV/1-4 R. J. Buttery DIII-D Research to Address Key Challenges for ITER and Fusion Energy 1	
 OV/2-1 A. Krasilnikov Progress with the ITER Project Activity in Russia 1 OV/2-2 H. Zohm Recent ASDEX Upgrade Research in Support of ITER and DEMO . 1 OV/2-3 K. Ida 	112
Overview of Transport and MHD Stability Study and Impact of Magnetic Field Topology in the Large Helical Device	114

OV/2-4 I. Chapman
Overview of MAST Results
OV/2-5 E. Marmar
Alcator C-Mod: Research in Support of ITER and Steps Beyond 116
OV/3-1 H. Azechi
Fast Ignition Realization EXperiment (FIREX) and Prospect to Iner-
tial Fusion Energy in Japan
OV/3-2 P. Barabaschi
Status of JT-60SA Project
OV/3-3 B. Wan
Advance of H-Mode Physics for Long-Pulse Operation on EAST 119
OV/3-4 SW. Yoon
Overview of KSTAR Results in 2013 Campaign
OV/4-1 M. Xu
Overview of HL-2A Recent Experiments
OV/4-2 S. Coda
The Science Program of the TCV Tokamak: Exploring Fusion Reac-
tor and Power Plant Concepts
OV/4-3 S. Kaye
Overview of Recent Physics Results from NSTX
OV/4-4 M. Kobayashi
3D Effects of Edge Magnetic Field Configuration on Divertor/SOL
Transport and Optimization Possibilities for a Future Reactor 124
OV/4-5 J. Sánchez
Transport, Stability and Plasma Control Studies in the TJ-II Stellarator 125
OV/5-1 P. Terry
Overview of Gyrokinetic Studies on Electromagnetic Turbulence . 126
OV/5-2 M. E. Puiatti
Overview of the RFX-Mod Contribution to the International Fusion
Science Program
OV/5-3 J. Sarff
Overview of Results from the MST Reversed Field Pinch Experiment128
OV/5-4 G. Pucella
Overview of the FTU Results
OV/5-5 S. Pradhan
First Experiments in SST-1
OV/P-01 N. Nakajima
Overview of DEMO Activities of IFERC Project in BA Activities 131
OV/P-02 G. Zhuang
Overview of the Recent Research on the J-TEXT Tokamak 132
OV/P-03 V. Gusev
Review of Globus-M Spherical Tokamak Results

OV/P-04 M. Gryaznevich
Contribution to Fusion Research from IAEA Coordinated Research
Projects and Joint Experiments
EX: Magnetic Confinement Experiments 135
EX/1-1 R. Nazikian
Recent Advances in the Understanding and Optimization of RMP
ELM Suppression for ITER
EX/1-2 A. Kirk
Effect of Resonant Magnetic Perturbations on Low Collisionality
Discharges in MAST and a Comparison with ASDEX Upgrade 137
EX/1-3 T. E. Evans
Comparative Studies of Edge Magnetic Islands and Stochastic Lay-
ers in DIII-D and LHD 138
EX/1-4 S. A. Sabbagh
Physical Characteristics of Neoclassical Toroidal Viscosity in Toka-
maks for Rotation Control and the Evaluation of Plasma Response 139
EX/1-5 Y. Jeon
Successful ELM Suppressions in a Wide Range of q_{95} Using Low n RMPs in KSTAR and its Understanding as a Secondary Effect of RMP140
EX/2-1 S. Inagaki
Dynamic Method to Study Turbulence and Turbulence Transport . 141
EX/2-2 G. R. McKee
Turbulence Behavior and Transport Response Approaching Burning
Plasma Relevant Parameters
EX/2-3 D. Ernst
Controlling H-Mode Particle Transport with Modulated Electron
Heating in DIII-D and Alcator C-Mod via TEM Turbulence 143
EX/3-1 E. Wolfrum
Overview of Recent Pedestal Studies at ASDEX Upgrade 144
EX/3-2 A. Diallo
Edge Instability Limiting the Pedestal Growth on Alcator C–Mod
Experiment and Modeling 145
EX/3-3 C. Maggi
Pedestal Confinement and Stability in JET-ILW ELMy H-Mode Sce-
narios
EX/4-1 G. Matthews
Melting of Tungsten by ELM Heat Loads in the JET Divertor 147
EX/4-2 M. Goniche
Near-Field Physics of Lower-Hybrid Wave Coupling to Long-Pulse, High Temperature Plasmas in Tore Supra

EX/4-3 A. Kreter
Fuel Retention and Erosion of Metallic Plasma-Facing Materials
under the Influence of Plasma Impurities
EX/5-1 R. Granetz
An ITPA Joint Experiment to Study Runaway Electron Generation
and Suppression
EX/5-2 C. Reux
Runaway Electron Generation with the ITER-like Wall and Effi-
ciency of Massive Gas Injection at JET
EX/5-3 R. L. Tanna
Novel Approaches for Mitigating Runaway Electrons and Plasma
Disruptions in Tokamak ADITYA
EX/6-1 M. Valisa
Heavy Impurity Transport in the Core of JET Plasmas 153
EX/6-2 M. Yoshida
Response of Ion and Electron Temperatures, Electron Density and
Toroidal Rotation to Electron Cyclotron Heating in JT-60U 154
EX/6-3 Y. Shi
Toroidal Rotation Profile Structure in L- and H-Mode KSTAR Plasmas155
EX/6-4 X. Ji
Interaction between Neoclassical Tearing Modes and Non-Local
Transport in HL-2A
EX/7-1 A. Kallenbach
Partial Detachment of High Power Discharges in ASDEX Upgrade 157
EX/7-2 C. Lowry
Impurity Seeding on JET to Achieve Power Plant like Divertor
Conditions
EX/7-3 H. Kasahara
Progress of High-Performance Steady-State Plasma and Critical
PWI Issue in LHD
EX/7-4 V. Soukhanovskii
Developing Physics Basis for the Radiative Snowflake Divertor at
DIII-D
EX/8-1 H. Park
Simultaneous Measurement of the ELMs at Both High and Low
Field Sides and ELM Dynamics in ELM Crash-Free Period in KSTAR161
EX/9-1 A. Sips
Progress in Preparing Scenarios for ITER Operation 162
EX/9-2 I. M. Ferreira Nunes
Compatibility of High Performance Operation with JET ILW 163 EX/9-3 C. Challis
Improved Confinement in JET High Beta Plasmas with an ITER-like Wall 164
vvan

EX/9-4 J. Schweinzer
Development of the Q=10 Scenario for ITER on ASDEX Upgrade
(AUG) 165
EX/9-5 G. Xu
A Long-Pulse H-Mode Regime with a New Coherent Mode Provid-
ing Continuous Transport across Pedestal in EAST
EX/10-1 W. W. Heidbrink
Alfvén Eigenmodes Can Limit Access to High Fusion Gain, Steady-
State Tokamak Operation
EX/10-2 M. Van Zeeland
Fast Ion Transport during Applied 3D Magnetic Perturbations on
DIII-D
EX/10-3 M. Osakabe
Indication of Bulk-Ion Heating by Energetic Particle Driven Geodesic
Acoustic Modes on LHD
EX/10-4 M. Podestá
Effects of MHD Instabilities on Neutral Beam Current Drive 170
EX/11-1 U. Stroth
Experimental Turbulence Studies for Gyro-Kinetic Code Validation
Using Advanced Microwave Diagnostics
EX/11-2Ra A. Gurchenko
The Isotope Effect in GAM – Turbulence Interplay and Anomalous
Transport in Tokamak
EX/11-2Rb V. Vershkov
Density Fluctuations as an Intrinsic Mechanism to Keep Self-Consistent
Shape of Pressure Profile
EX/11-3 J. Dong
Mechanism of Low-Intermediate-High Confinement Transitions in
Tokamaks
EX/11-4 L. Schmitz
First Direct Evidence of Turbulence-Driven Ion Flow Triggering the
L- to H-Mode Transition
EX/P1-18 A. Biancalani
Global Gyrokinetic Modeling of Geodesic Acoustic Modes and
Shear Alfvén Instabilities in ASDEX Upgrade
EX/P1-19 E. Viezzer
Radial Electric Field and Poloidal Impurity Asymmetries in the
Pedestal of ASDEX Upgrade: Quantitative Comparisons between
Experiment and Theory 177
EX/P1-20 B. Geiger
Experimental Quantification of the Impact of Large and Small Scale
Instabilities on Confined Fast Ions in ASDEX Upgrade 178

EX/P1-21 T. Tala
Identification of Intrinsic Torques in ASDEX Upgrade H-Mode Plas-
mas
EX/P1-22 M. García-Muñoz
Fast-Ion Response to Externally Applied 3D Magnetic Perturbations
in ASDEX Upgrade H-Mode Plasmas
EX/P1-23 W. Suttrop
Studies of Magnetic Perturbations in High-Confinement Mode Plas- mas in ASDEX Upgrade
EX/P1-24 D. Mazon
W Impurity Poloidal Assymmetries Observed at ASDEX Upgrade Using Soft-X-Ray Tomography Reconstruction
EX/P1-25 G. Birkenmeier
Filament Transport in the SOL of ASDEX Upgrade
EX/P1-27 A. Herrmann
Solid Tungsten Divertor-III for ASDEX Upgrade and Contributions
to ITER
EX/P1-28 V. Rozhdestvensky
Nonthermal Microwave Emission Features under the Plasma Ohmic
Heating and Lower Hybrid Current Drive in the FT-2 Tokamak \therefore 185
EX/P1-29 S. Lashkul
Impact of Isotopic Effect on Density Limit and LHCD Efficiency in
the FT-2 Experiments
EX/P1-30 A. Altukhov
Poloidal Inhomogeneity of Turbulence in the FT-2 Tokamak by
Radial Correlation Doppler Reflectometry and Full-f Gyrokinetic
Modeling
EX/P1-32 V. Bulanin
Geodesic Acoustic Mode Investigation in the Spherical Globus-M Tokamak Using a Multi-Diagnostic Approach
EX/P1-33 N. Bakharev
Fast Particle Behavior in Globus-M
EX/P1-36 I. Takagi Determination of the System Function for the Particle Circulation
Process Using Perturbation Technique in QUEST
EX/P1-37 K. Hanada
Investigation of Progression from Low to High Hydrogen Recycling
during Long Duration Discharges on a Spherical Tokamak, QUEST 191
EX/P1-38 H. Idei
Fully Non-Inductive Current Drive Experiments Using 28 GHz and
8.2 GHz Electron Cyclotron Waves in QUEST

EX/P1-39 K. Mishra
Self Organization of High β_p Plasma Equilibrium with an Inboard
Poloidal Null Sustained by Fully Non-Inductive Current Drive in
QUEST
EX/P1-40 M. Spolaore
Turbulent Électromagnetic Filaments in Toroidal Plasma Edge 194
EX/P1-41 R. Lorenzini
The Isotope Effect in the RFX-Mod Experiment
EX/P1-42 G. Spizzo
Density Limit Studies in the Tokamak and the Reversed-Field Pinch 196
EX/P1-43 S. Neudatchin
Study of ITB Formation, Electron Heat and Density Flux Structure
in New ECRH/ECCD Experiments at T-10 Tokamak
EX/P1-44 L. Klyuchnikov
Impurities Removal during Central ECR Heating in T-10 198
EX/P1-45 A. Melnikov
Study of GAM Radial Structure and Properties in OH and ECRH
Plasmas in the T-10 Tokamak 199
EX/P1-46 N. Ivanov
Magnetic Island and Plasma Rotation under External Resonant
Magnetic Perturbation in T-10 Tokamak
EX/P1-47 S. Mirnov
Experimental Investigation of the System of Vertical and Longitudi-
nal Lithium Limiters as a Prototype of Plasma Facing Components
of a Steady State Tokamak-Reactor on T-11M Tokamak 201
EX/P1-48 A. Shcherbak
Investigation of a Phenomenology of the Improved Confinement
Regime in T-11M Tokamak
EX/P1-49 A. Vertkov
Development of Lithium CPS Based Limiters for Realization of a
Concept of Closed Lithium Circulation Loop in Tokamak 203
EX/P1-50 I. Roy
The Auxiliary Heating and Current Drive Systems on The Tokamak
T-15 Upgrade
EX/P1-51 M. Inomoto
Generation of Energetic Electrons by Magnetic Reconnection with
Presence of High Guide Field 205
EX/P2-20 F. Turco
Impact of NBI-Injected Fast Ions in the Stabilization of the Resistive
Wall Mode in High- β_N Plasmas
EX/P2-21 D. Orlov
Suppression of Type-I ELMs with Incomplete I-Coil Set on DIII-D \therefore 207

EX/P2-22 N. W. Eidietis
Measurement of Radiated Power Asymmetry during Disruption
Mitigation on the DIII-D Tokamak
EX/P2-24 D. Battaglia
Full-f Neoclassical Simulations toward a Predictive Model for H-
Mode Pedestal Ion Energy, Particle and Momentum Transport 209
EX/P2-26 T. W. Petrie
Applying the Radiating Divertor Approach to Innovative Tokamak
Divertor Concepts
EX/P2-27 D. L. Rudakov
Reduction of Net Erosion of High-Z PFC Materials in DIII-D Diver-
tor Due to Re-Deposition and Low-Z Coating
EX/P2-28 C. Paz-Soldan
The Single Dominant Mode Picture of Non-Axisymmetric Field
Sensitivity and its Implications for ITER Geometric Tolerances 212
EX/P2-29 S. Smith
Electron Temperature Critical Gradient and Transport Stiffness 213
EX/P2-30 S. Mordijck
Momentum and Particle Transport Across the ITG-TEM Turbulence
Regimes in DIII-D H-Mode Plasmas
EX/P2-39 X. Gong
Development of Fully Noninductive Scenario at High Bootstrap
Current Fraction for Steady State Tokamak Operation on DIII-D
and EAST
EX/P2-40 K. Razumova
Heat Transport and Enhancement Confinement Regimes in Toka-
mak as a Result of Plasma Self-organization
EX/P2-41 P. Martin
Extreme Low-Edge Safety Factor Tokamak Scenarios via Active
Control of Three-Dimensional Magnetic Field on RFX and DIII-D . 217
EX/P2-42 M. Okabayashi
Avoidance of Tearing Mode Locking and Disruption with Electro-
Magnetic Torque Introduced by Feedback-Based Mode Rotation
Control in DIII-D and RFX-Mod
EX/P2-46 G. Mazzitelli
Thermal Loads on FTU Actively Cooled Liquid Lithium Limiter 219
EX/P2-47 C. Sozzi
Experiments on Magneto-Hydrodynamics Instabilities with ECH/ECCD
in FTU Using a Minimal Real-Time Control System
EX/P2-48 D. Carnevale
Runaway Electron Control in FTU

EX/P2-49 F. Causa
Cherenkov Emission Provides Detailed Picture of Non-Thermal Electron Dynamics in the Presence of Magnetic Islands
EX/P2-50 B. Esposito
On the Measurement of the Threshold Electric Field for Runaway Electron Generation in FTU 223
EX/P2-51 G. Granucci
Experiments and Modelling on FTU Tokamak for EC Assisted Plasma Start-up Studies in ITER-like Configuration
EX/P2-52 C. Mazzotta Peaked Density Profiles Due to Neon Injection on FTU 225
EX/P2-54 S. Nowak
(N)TM Onset by Central EC Power Deposition in FTU and TCV
Tokamaks
EX/P3-3 X. Zhang
High Power ICRF Systems and Heating Experiments in EAST 227
EX/P3-4 G. Calabrò
EAST Snowflake Experiment: Scenario Development and Edge
Simulations
EX/P3-5 B. Lyu
Core Plasma Rotation Characteristics of RF-Heated H-Mode Dis-
charges on EAST
EX/P3-6 L. Xiang
Investigation of Argon Seeding in Different Divertor Configurations
in EAST and Corresponding SOLPS 5.0 Modeling
EX/P3-7 G. Li
Studies of Impact of Edge Current Profiles, Plasma Shaping, Non-
linearity on Edge Localized Modes with BOUT++ Code
EX/P3-8 Y. Liang
ELM Mitigation by Lower Hybrid Waves in EAST
EX/P3-9 X. Gao
Study of Pedestal Turbulence on EAST Tokamak
EX/P3-10 L. Wang
Progress in Active Control of Divertor Power Load in the EAST
Superconducting Tokamak
EX/P3-11 B. Ding
Investigation of LHW-Plasma Coupling and Current Drive Related
to H-Mode Experiments in EAST
EX/P3-12 Y. Xu
The Latest Development of EAST Neutral Beam Injector 236
. ,

EX/P3-14 R. Reichle
Redefinition of the ITER Requirements and Diagnostics for Erosion,
Deposition, Dust and Tritium Measurements Accounting for the
Change to Tungsten Divertor
EX/P3-16 M. Wischmeier
Advancing Power Exhaust Studies from Present to Future Tokamak
Devices
EX/P3-17 G. Hogeweij
Impact of W on Scenario Simulations for ITER
EX/P3-18 M. Lehnen
Status of R&D for ITER Disruption Loads, Disruption Mitigation
and Runaway Electron Avoidance
EX/P3-47 M. Jakubowski
Influence of Magnetic Perturbations on Particle Pump-out in Mag-
netic Fusion Devices
EX/P3-48 D. Douai
Experimental and Modelling Results on Wall Conditioning for ITER
Operation
EX/P3-49 B. Chapman
Micro- and Macro-Instability, and Large Density and Beta in Im-
proved Confinement MST RFP Plasmas
EX/P3-50 M. Nornberg
Predator-Prey Time Dynamics and Locking Control of Spontaneous
Helical States in the RFP
EX/P3-52 S. Masamune
Attainment of High Electron Poloidal β in Axisymmetric State and
Two Routes to Self-Organized Helical State in Low-Aspect-Ratio RFP245
EX/P3-54 N. Kirneva
High Density Regime in Ohmic TCV Discharges with Positive and
Negative Triangularity
EX/P3-55 A. Merle
From Edge Non-Stiffness to Improved IN-Mode: a New Perspective
on Global Tokamak Radial Transport
EX/P3-56 B. Duval
Progress in Snowflake Divertor Studies on TCV
EX/P3-57 L. Porte
Multi-Diagnostic Study of Core Turbulence and Geodesic Acoustic
Modes in the TCV Tokamak
EX/P3-59 I. Furno
Basic Investigations of Turbulence and Interactions with Plasma and
Suprathermal Ions in the TORPEX Device with Open and Closed
Field Lines

EX/P4-1 G. Verdoolaege	
A New Methodology for Scaling Laws with Arbitrary Error Distri-	
butions: Case Study for the H-Mode Power Threshold	251
EX/P4-20 P. Brunsell	
Resistive Wall Mode Studies Utilizing External Magnetic Perturba-	
tions	252
EX/P4-21 P. Bagryansky	
Last Achievements in the Experiments with ECR Heating in the	
Gas Dynamic Trap	253
EX/P4-22 S. Hussain	
First Plasma Formation in Glass Spherical Tokamak (GLAST)	254
EX/P4-23 A. Burdakov	
Status of GOL-3 Multiple Mirror Trap Experiments	255
EX/P4-24 B. Blackwell	
Structure and Scaling of Fluctuations in the MHD Range in the	
H-1NF HELIAC	256
EX/P4-25 G. Navratil	
Active and Passive Experiments to Control the Helical Boundary of	
Wall-Stabilized Tokamak Plasma	257
EX/P4-26 S. Ohshima	
Observation of a Toroidally Symmetrical Electric Field Fluctuation	
with Radially Elongated Structure in Heliotron J	258
EX/P4-27 S. Yamamoto	
External Control of Energetic-Ion-Driven MHD Instabilities by ECH/E	CCD
in Heliotron J Plasmas	259
EX/P4-28 S. Kobayashi	
Parallel Flow Dynamics and Comparison with Neoclassical Trans-	
port Analysis in NBI Plasmas of Heliotron J	260
EX/P4-29 T. Mizuuchi	
A New Operation Regime for High-Density Plasma in Heliotron J .	261
EX/P4-30 M. Nagata	
Non-Inductive Solenoid-Less Plasma Current Start-up on HIST	
Using Transient Coaxial Helicity Injection	262
EX/P4-33 Y. Yu	
Observation of Zonal Flows in Core Plasma with Collective Scatter-	
ing Density Fluctuation Measurement	263
EX/P4-34 S. Sharapov	
Instabilities and Transport of Fast Ions on MAST	264
EX/P4-35 J. Hillesheim	
Cross-Polarization Doppler Backscattering Measurements and Mi-	
crotearing at the Top of the MAST H-Mode Pedestal	265
EX/P4-36 M. Valovic	
Pellet Fuelling of Plasmas Including ELM Mitigation in MAST	266

EX/P4-37 J. Harrison
Improved Understanding of Edge Plasma Dynamics Through Visi-
ble Imaging on MAST
EX/P4-38 A. Field
Influence of Flow Shear on the Structure of Ion-Scale Turbulence in
MAST
EX/P4-41 M. Martinez
Analysis of Ion Energy Spectrum and Spikes in ECRH TJ-II Plasmas, with Fixed and Variable Magnetic Configuration
EX/P4-43 B. Zurro
Studying the Impurity Charge Dependence of Impurity Confine- ment in ECR Heated TJ-II Stellarator Plasmas
EX/P4-45 F. Castejón
Stable Plasmas in Theoretically Mercier-Unstable TJ-II Configurations271
EX/P4-46 Á. Cappa
Influence of ECR Heating on NBI-Driven Alfvén Eigenmodes in the TJ-II Stellarator
EX/P4-47 T. Estrada
Limit Cycle Oscillations at the L-I-H Transition in TJ-II Plasmas:
Triggering, Temporal Ordering and Radial Propagation 273
EX/P5-18 M. Halitovs
Analysis of Tritium in Divertor Materials
EX/P5-20 A. B. Kukushkin
Theoretical Model of ITER High Resolution H-Alpha Spectroscopy
for a Strong Divertor Stray Light and Validation against JET-ILW Experiments
EX/P5-21 T. Wauters
ICRF Discharge Production for Ion Cyclotron Wall Conditioning on
JET
EX/P5-22 E. A. Lerche
ICRH for Mitigation of Core Impurity Accumulation in JET-ILW 277
EX/P5-23 V. V. Plyusnin
Parameters of Runaway Electrons in JET
EX/P5-24 E. Delabie
Overview and Interpretation of L-H Threshold Experiments on JET
with the ITER-like Wall
EX/P5-25 C. Giroud
Towards Baseline Operation Integrating ITER-Relevant Core and
Edge Plasma within the Constraint of the ITER-like Wall at JET 280
EX/P5-26 S. Brezinsek
Beryllium Migration in JET ITER-like Wall Plasmas

EX/P5-27 T. Loarer
Plasma Isotopic Change over Experiments in JET under Carbon and
ITER-like Wall Conditions
EX/P5-28 G. Kurskiev
A Study of Core Thomson Scattering Measurements in ITER Using
a Multi-Laser Approach
EX/P5-29 E. de la Luna
Comparative Study of High Triangularity H-Mode Plasma Perfor-
mance in JET with Be/W Wall and CFC Wall
EX/P5-30 M. Lennholm
Real-Time Control of ELM and Sawtooth Frequencies: Similarities
and Differences
EX/P5-31 M. Rubel
An Overview of Erosion-Deposition Pattern in JET with ITER-like
Wall
EX/P5-32 K. Schmid
WallDYN Simulations of Global Impurity Migration and Fuel Re-
tention in JET and Extrapolations to ITER
EX/P5-33 S. Gerasimov
JET Asymmetrical Disruptions
EX/P5-38 R. Sabot
Discriminating the Trapped Electron Mode Contribution in Density
,
Discriminating the Trapped Electron Mode Contribution in Density Fluctuation Spectra and Turbulent Transport
Discriminating the Trapped Electron Mode Contribution in Density Fluctuation Spectra and Turbulent Transport
Discriminating the Trapped Electron Mode Contribution in Density Fluctuation Spectra and Turbulent Transport
Discriminating the Trapped Electron Mode Contribution in Density Fluctuation Spectra and Turbulent Transport
Discriminating the Trapped Electron Mode Contribution in Density Fluctuation Spectra and Turbulent Transport
Discriminating the Trapped Electron Mode Contribution in Density Fluctuation Spectra and Turbulent Transport
Discriminating the Trapped Electron Mode Contribution in Density Fluctuation Spectra and Turbulent Transport
Discriminating the Trapped Electron Mode Contribution in Density Fluctuation Spectra and Turbulent Transport
Discriminating the Trapped Electron Mode Contribution in Density Fluctuation Spectra and Turbulent Transport
Discriminating the Trapped Electron Mode Contribution in Density Fluctuation Spectra and Turbulent Transport289EX/P5-39P. Jacquet Maximization of ICRF Power by SOL Density Tailoring with Local Gas Injection290EX/P5-40E. Joffrin Impact of Divertor Geometry on ITER Scenarios Performance in the JET Metallic Wall291EX/P5-46O. Mitarai Plasma Current Start-up without Central Solenoid in the Iron Core STOR-M Tokamak292EX/P5-48E. Tsitrone
Discriminating the Trapped Electron Mode Contribution in Density Fluctuation Spectra and Turbulent Transport
Discriminating the Trapped Electron Mode Contribution in Density Fluctuation Spectra and Turbulent Transport289EX/P5-39P. Jacquet Maximization of ICRF Power by SOL Density Tailoring with Local Gas Injection290EX/P5-40E. Joffrin Impact of Divertor Geometry on ITER Scenarios Performance in the JET Metallic Wall291EX/P5-46O. Mitarai Plasma Current Start-up without Central Solenoid in the Iron Core STOR-M Tokamak292EX/P5-48E. Tsitrone
Discriminating the Trapped Electron Mode Contribution in Density Fluctuation Spectra and Turbulent Transport
Discriminating the Trapped Electron Mode Contribution in Density Fluctuation Spectra and Turbulent Transport
Discriminating the Trapped Electron Mode Contribution in Density Fluctuation Spectra and Turbulent Transport289EX/P5-39P. Jacquet Maximization of ICRF Power by SOL Density Tailoring with Local Gas Injection290EX/P5-40E. Joffrin Impact of Divertor Geometry on ITER Scenarios Performance in the JET Metallic Wall291EX/P5-46O. Mitarai Plasma Current Start-up without Central Solenoid in the Iron Core
Discriminating the Trapped Electron Mode Contribution in Density Fluctuation Spectra and Turbulent Transport
Discriminating the Trapped Electron Mode Contribution in Density Fluctuation Spectra and Turbulent Transport289EX/P5-39P. Jacquet Maximization of ICRF Power by SOL Density Tailoring with Local Gas Injection290EX/P5-40E. Joffrin

EX/P6-19 T. Golfinopoulos
New Insights into Short-Wavelength, Coherent Edge Fluctuations
on Alcator C-Mod
EX/P6-20 L. F. Delgado-Aparicio
Destabilization of Internal Kink by Suprathermal Electron Pressure
Driven by Lower Hybrid Current Drive (LHCD)
EX/P6-21 D. Whyte
New In-Situ Measurements for Plasma Material Interaction Studies
in Alcator C-Mod
EX/P6-22 A. Hubbard
Multi-Device Studies of Pedestal Physics and Confinement in the
I-Mode Regime
EX/P6-25 K. Mukai
Development of Impurity Seeding and Radiation Enhancement at
Helical Divertor in LHD
EX/P6-26 N. Ohno
Plasma Structure Change and Intermittent Fluctuation near Mag-
netic Island X-Point under Detached Plasma Condition in LHD 301
EX/P6-27 M. Yokoyama
Comprehensive Understandings of Energy Confinement in LHD
Plasmas through Extensive Application of the Integrated Transport
Analysis Suite
EX/P6-28 I. Murakami
Development of Quantitative Atomic Modeling for Tungsten Trans-
port Study Using LHD Plasma with Tungsten Pellet Injection 303
EX/P6-29 S. Ohdachi
Pressure Driven MHD Instabilities in Intrinsic and Externally En-
hanced Magnetic Stochastic Region of LHD
EX/P6-30 M. Yoshinuma
Abrupt Reversal of Convective Flow of Carbon Impurity during
Impurity-Hole Formation on LHD
EX/P6-31 K. Fujii
Study of Neutral Hydrogen Transport in LHD Core Plasmas Based
on High Dynamic-Range Balmer-Alpha Spectroscopy 306
EX/P6-32 S. Sudo
Study of Transport Characteristics of Multiple Impurities Depend-
ing on the Impurity Source Location in LHD
EX/P6-33 M. Shoji
Studies of Dust Transport in Long Pulse Discharges in the Large
Helical Device
EX/P6-34 T. Shimozuma
Optimization of High Harmonic ECRH Scenario to Extend a Heat-
ing Plasma Parameter Range in LHD

EX/P6-35 Y. Narushima
Experimental Observation of Plasma Response to Resonant Mag-
netic Perturbation and its Hysteresis in LHD
EX/P6-36 X. Du
Interaction between Resistive Interchange Mode and Helically Trapped Energetic Ions and its Effects on the Energetic Ions and Bulk Plas- mas in LHD
EX/P6-37 S. Sakakibara
Characteristics of MHD Instabilities Limiting Beta Value in LHD 312
EX/P6-43 Y. Ren
Experimental Observation of Nonlocal Electron Thermal Transport in NSTX RF-Heated L-Mode Plasmas
EX/P6-45 E. Fredrickson
Parametric Dependence of Fast-Ion Transport Events on the Na- tional Spherical Tokamak Experiment
EX/P6-53 JW. Ahn
Impact of 3D Fields on Divertor Detachment in NSTX and DIII-D $$. 315
EX/P6-54 R. Maingi The Role of Lithium Conditioning in Achieving High Performance, Long Pulse H-Mode Discharges in the NSTX and EAST Devices 316
EX/P6-56 Y. Tan
Study of the Alfvén Wave Coupling in the SUNIST Spherical Tokamak317
EX/P6-57 A. Tukachinsky
Alfvén Oscillations in the TUMAN-3M Tokamak Ohmic Regime 318
EX/P6-58 V. Kornev
Effect of Horizontal Displacement on Fast Ion Confinement in TUMAN-3M
EX/P6-59 A. Belokurov
GAM Evolution and LH-Transition in the TUMAN-3M Tokamak . 320
EX/P7-16 S. Kulkarni
Recent ICRH-Wall Conditioning, Second Harmonic Heating and
Disruption Mitigation Experiments Using ICRH System in Tokamak
ADITYA 321
EX/P7-17 P. Dhyani
Disruption Control Using Biased Electrode in Aditya Tokamak 322
EX/P7-18 Y. Liu
L-H Transition Triggered by Fishbone Mode in the NBI Heated HL-2A Plasmas
EX/P7-19 Y. Xu
Neoclassical Tearing Modes Triggered by Intrinsic Error Field in the HL-2A Tokamak

EX/P7-20 D. Yu
Evolution of the Ion Temperature in Pedestal during the ELM Mitigation by SMBI325
EX/P7-21 M. Jiang
The Observation of Synchronous Oscillation prior to Disruption inthe HL-2A Tokamak326
EX/P7-22 L. Nie
Comparison of ELM-Filament Mitigation between Supersonic Molec- ular Beam Injection and Pellet Injection in the HL-2A Tokamak 327
EX/P7-23 W. Zhong
The Role of Edge Plasma Instabilities in Dynamical Evolution of Pedestal in the HL-2A Tokamak
EX/P7-24 Y. Zhang
Measurements of Fast-Ion Losses Induced by MHD Instabilities Using Scintillator-Based Probe in the HL-2A Tokamak
EX/P7-25 L. Yu
Transition and Interaction of Low-Frequency MHD Modes duringNeutral Beam Injection on HL-2A330
EX/P7-26 Z. Cui
Study of Carbon Transport in the Scrape-off Layer of HL-2A with Impurity Sources Located at Limiter, Baffle and Divertor 331
EX/P7-27 W. Chen
Characterization and Nonlinear Interaction of Shear Alfvén Waves in the Presence of Strong Tearing Modes in Tokamak Plasmas 332
EX/P7-31 Y. B. Dong
Experimental Study of Disruption Mitigation Using Supersonic Molecular Beam and Massive Gas Injection on HL-2A and J-TEXT . 333
EX/P7-32 J. Cheng
Dynamics of High-Intermediate-High Confinement Transitions on the HL-2A Tokamak
EX/P7-33 D. Kong
The Observation of Pedestal Turbulence Contributing Inward Parti-
cle and Heat Flux on the Edge of HL-2A Tokamak
EX/P7-34 G. Krashevskaya
Plasma Confinement by Magnetic Field with Convex-Concave Field
Lines
EX/P7-35 P. Khorshid
Calculation of Magnetic Field Perturbation Using Saddle Coils and
Helical Windings Based on IR-T1 Tokamak
EX/P7-36 T. Kobayashi
Edge Plasma Dynamics during L-H Transition in the JFT-2M Tokamak338

EX/P7-40 K. Zhao
Plasma Flows and Fluctuations with Resonant Magnetic Perturba-
tions on the Edge Plasmas of the J-TEXT Tokamak
EX/P7-41 H. Tanaka
Observation of Intermittent Plasma Ejection from a Highly Over-
dense Spherical Tokamak Plasma Maintained by Electron Bernstein
Wave Heating and Current Drive in LATE
EX/P7-44 J. H. Severo
Investigation of Co-Current Rotation at Plasma Edge in the TCABR 341
EX/P7-45 V. Moiseenko
Features of Regular Discharges in Uragan-3M Torsatron 342
EX/P8-2 D. Na
Investigation of Toroidal Rotation Reversal in KSTAR Ohmic Plasmas343
EX/P8-4 J. Kim
Disruption Threshold of Error-Field-Induced Locked Mode under
n = 1 and $n = 2$ Mixed Non-Axisymmetric Fields
EX/P8-5 YS. Park
Plasma Rotation Alteration by Non-Axisymmetric Magnetic Fields,
Resistive MHD Stability Analysis, and High Normalized Beta Plas-
mas Exceeding the Ideal Stability Limit in KSTAR
ЕХ/Р8-6 WH. Ко
Change of the Momentum Profiles Driven by the Sawtooth Crashes
and its Effect on the LH Transition in KSTAR
EX/P8-7 J. Seol
Study of Type III ELMs in the KSTAR Tokamak
EX/P8-8 H. Lee
Experimental Study of the Magnetic Braking Torque by Non-Axisymmetric
Magnetic Perturbations in Different Plasma Collisionality Regimes
on KSTAR
EX/P8-9 H. Lee
Pedestal Characteristics during the Edge Localized Mode Mitigation
by Super-Sonic Molecular Beam Injection on KSTAR
EX/P8-10 SH. Hong
In-Vessel Dust Velocity Correlated with the Toroidal Rotation of the
Plasma
EX/P8-11 SH. Hahn
L-H Transitions Triggered by SMBI: Experiment and Theory 351
EX/P8-12 G. Yun
Helical Modes Induced by Localized Current Perturbations in Saw-
toothing KSTAR Plasmas
EX/P8-13 W. Lee
Measurement of Apparent Poloidal Rotation of Ion-Scale Turbu-
lence with the KSTAR Microwave Imaging Reflectometer 353

EX/P8-14 S. G. Lee	
Toroidal Rotation and Momentum Transport Studies in KSTAR Plasmas	354
EX/P8-15 H. K. Park	
Accurate Estimation of Tearing Mode Stability Parameters in the KSTAR Using High-Resolution 2-D ECEI Diagnostic	355
EX/P8-18 Y. Xu	
Coupling between Intrinsic Rotation and Turbulence-Driven Resid- ual Stress in the TEXTOR Tokamak	356
TH: Magnetic Confinement Theory and Modelling	357
TH/1-1 S. Maeyama	
Multi-Scale ITG/TEM/ETG Turbulence Simulations with Real Mass	
Ratio and β Value	358
TH/1-2 P. Helander	
Advances in Stellarator Gyrokinetics	359
TH/2-1 V. Rozhansky	
Understanding of Impurity Poloidal Distribution in Edge Pedestal	200
by Modeling	360
TH/2-2 P. B. Snyder	
Super H-mode: Theoretical Prediction and Initial Observations of a New High Performance Regime for Tokamak Operation	361
TH/2-3 C. Chang	501
Gyrokinetic Study of Edge Blobs and Divertor Heat-Load Footprint	362
TH/3-2 P. Ricci	502
First-Principle Theory-Based Scaling of the SOL Width in Limited	
Tokamak Plasmas, Experimental Validation, and Implications for	
the ITER Start-up	363
TH/3-3 L. Aho-Mantila	
Assessment of Scrape-off Layer Simulations with Drifts against	
L-Mode Experiments in ASDEX Upgrade and JET	364
TH/4-1 V. A. Izzo	
The Role of MHD in 3D Aspects of Massive Gas Injection for Dis-	
ruption Mitigation	365
TH/4-2 A. Popov	
The Low Threshold Parametric Decay Instabilities Leading to Anoma-	
lous Absorption at ECRH in Toroidal Devices	366
TH/5-1 M. Honda	
Integrated Modeling of Toroidal Rotation with the 3D Non-Local	
Drift-Kinetic Code and Boundary Models for JT-60U Analyses and Prodictive Simulations	267
Predictive Simulations	507

TH/5-2 J. Garcia
Core Microturbulence and Edge MHD Interplay and Stabilization
by Fast Ions in Tokamak Confined Plasmas
TH/6-1Ra G. Huijsmans
Non-Linear MHD Simulations for ITER
TH/6-1Rb M. Becoulet
Non-Linear MHD Modelling of Edge Localized Modes and their
Interaction with Resonant Magnetic Perturbations in Rotating Plasmas370
TH/6-2 K. Ichiguchi
Three-Dimensional MHD Analysis of Heliotron Plasma with RMP 371
TH/7-1 Y. Todo
Multi-Phase Simulation of Alfvén Eigenmodes and Fast Ion Distri-
bution Flattening in DIII-D Experiment
TH/7-2 Z. Lin
Radial Localization of Alfvén Eigenmodes and Zonal Field Generation373
TH/8-1 G. Park
A 3D Nonlinear Simulation Study of the L \rightarrow H Transition Criterion 374
TH/P1-2 N. Gorelenkov
Developing and Validating Predictive Models for Fast Ion Relax-
ation in Burning Plasmas
TH/P1-3 S. K. Tiwari
Current Drive by Electron Temperature Gradient Turbulence in
Tokamak Pedestal Region
TH/P1-5 JK. Park
Computation of Resistive Instabilities in Tokamaks with Full Toroidal
Geometry and Coupling Using DCON
TH/P1-7 M. Rajkovic
Quantifying Self-Organization in Magnetically Confined Fusion
Plasmas
TH/P1-8 R. Farengo
Redistribution of Energetic Particles Due to Internal Kink Modes . 379
TH/P1-9 M. Malkov
From Micro to Macro: L-H Transition Dynamics and Power Thresh-
old Scaling
TH/P1-11 KC. Shaing
Transport Theory for Energetic Alpha Particles and Superbananas
in Tokamak Fusion Reactors with Broken Symmetry
TH/P1-12 H. Wang
Simulation Study of a New Kind of Energetic Particle Driven Geodesic
Acoustic Mode
TH/P1-13 L. Sugiyama
Nonlinear and Toroidal Mode Coupling Effects on $m = 1$, $n = 1$
Instabilities

TH/P1-14 G. Giruzzi
Modelling of Pulsed and Steady-State DEMO Scenarios
TH/P1-15 R. Singh
On Anomalous Dissipation and Relaxation in ELMs
TH/P1-16 T. Rafiq
Comparison of Simulated and Experimental Temperature, Density
and Toroidal Rotation Profiles in Tokamak Plasmas
TH/P1-17 I. Katanuma
A Flute Instability under the $E \times B$ Shear Flow in an Open System 387
TH/P1-31 M. K. Islam
Analysis of Plasma Behavior in the Localized Non-Axisymmetric B
Region of the GAMMA 10 Tandem Mirror
TH/P1-34 V. Dyachenko
The First Lower Hybrid Current Drive Experiments in the Spherical
Tokamak Globus-M 389
TH/P1-35 I. Senichenkov
Integrated Modeling of the Globus-M Tokamak Plasma
TH/P1-52 M. Leconte
Feedback of a Neoclassical Tearing Mode on Drift Wave – Zonal
Flow Turbulence
TH/P2-1 C. Pan
The Combining Effect of the Inductive Electric Field and the Lower
Hybrid Waves on the Impurity Ions Toroidal Rotation in the Lower
Hybrid Current Drive Tokamak Plasmas
TH/P2-2 A. Y. Aydemir
ELM Pacing with Periodic Plasma Column Displacements 393
TH/P2-5 Z. Gao
Frequency and Damping Rate of the Geodesic Acoustic Mode in
Collisional Plasmas
TH/P2-6 M. Schneller
Study of Nonlinear Fast Particle Transport and Losses in the Pres-
ence of Alfvén Waves
TH/P2-7 F. Jenko
Can Gyrokinetics Really Describe Transport in L-Mode Core Plasmas?396
TH/P2-9 T. Rhee A Reduced Model of ELM Mitigation by SMBI and Pellet Injection 397
0 ,
TH/P2-10 A. Kuley Nonlinear Particle Simulation of Radio Frequency Waves in Fusion
Plasmas
TH/P2-11 V. Pastukhov
Influence of Boundary Conditions on Turbulent Transport and
Plasma Energy Confinement Time Evolution in Tokamaks with
Additional Heating: Simulations for T-10 and T-15 Tokamaks 399
reactional reacting. Ontotations for 1-10 and 1-15 tokaniaks 577

TH/P2-12 N. Miyato
Nonlocal Transport from Edge to Core in Tokamak Plasmas 400
ТН/Р2-13 Н. Не
Fishbone Modes in Plasmas with Dual Neutral Beam Injection Heating401
TH/P2-14 Y. Kosuga
Progress on Transport Modeling by Trapped Ion Resonance Driven
Turbulence
TH/P2-15 N. Aiba
MHD Instability Excited by Interplay between Resistive Wall Mode
and Stable MHD Modes in Rotating Tokamak Plasmas 403
TH/P2-16 H. R. Strauss
Toroidal Rotation Produced by Disruptions and ELMs 404
TH/P2-38 R. Pinsker
Off-Axis Current Drive with High Harmonic Fast Waves for DIII-D 405
TH/P2-44 Y. Xiao
Gyrokinetic Simulation of Microturbulence in EAST Tokamak and
DIII-D Tokamak
TH/P2-45 T. Xia
Fluid Simulation of Particle and Heat Fluxes during Burst of ELMs
on EAST and DIII-D
TH/P3-13 X. Gong
Theoretical Analysis of the ICRH Antenna's Impedance Matching
for ELMy Plasmas on EAST 408
TH/P3-23 Y. Gott
Asymmetry Current in ICRF Heating ITER Plasmas
TH/P3-24 F. Köchl
Modelling of Transitions Between L- and H-Mode Including W
Behaviour in ITER Scenarios
TH/P3-25 P. Rodrigues
A Systematic Approach to the Linear-Stability Assessment of Alfvén
Eigenmodes in the Presence of Fusion-Born Alpha Particles for
ITER-like Equilibria
TH/P3-28 K. McClements
Fast Particle-Driven Ion Cyclotron Emission (ICE) in Tokamak Plas-
mas and the Case for an ICE Diagnostic in ITER
TH/P3-29 R. Dux
Influence of a Tungsten Divertor on the Performance of ITER H-
Mode Plasmas
TH/P3-30 T. Kurki-Suonio
ITER Energetic Particle Confinement in the Presence of ELM Control
Coils and European TBMs
Integrated Modelling of ITER Disruption Mitigation
megrated modeling of HER Disruption mugation 415

TH/P3-32 P. Minashin
Effect of Multi-Pass Absorption of Electron Cyclotron Heating Wave
on Initial Stage of Discharge in ITER-like Tokamak
TH/P3-34 M. T. Kotschenreuther
X-Divertors in ITER — Without any Hardware Changes or Addi-
tions — and in Current Machines, and DEMO Reactors 417
TH/P3-35 V. Leonov
Simulation of the Pre-Thermal Quench Stage of Disruptions at Mas- sive Gas Injection and Projections for ITER
TH/P3-36 V. Vdovin
Off-Axis Current Generation by Helicons and LH Waves in Core
of Modern Tokamaks and Reactors FNSF-AT, ITER, DEMO and
by Alfvén Waves in Pedestal Plasmas. Scenarios, Modeling and
Antennae
TH/P3-37 V. Nesenevich
On the Possibility of Alpha-Particle Confinement Study in ITER by
NPA Measurements of Knock-on Ion Tails
TH/P3-38 P. Aleynikov
Kinetic Modelling of Runaway Electrons and their Mitigation in ITER421
TH/P3-39 M. Isaev
Alfvén Eigenmode Evolution in ITER Steady-State Scenario 422
TH/P3-40 B. Bazylev
Modelling of Melt Damage of Tungsten Armour under Multiple
Transients Expected in ITER and Validations against JET-ILW Ex-
periments
TH/P3-41 F. Imbeaux
TH/P3-41 F. Imbeaux Design and First Applications of the ITER Integrated Modelling &
TH/P3-41 F. Imbeaux Design and First Applications of the ITER Integrated Modelling & Analysis Suite
TH/P3-41 F. Imbeaux Design and First Applications of the ITER Integrated Modelling & Analysis Suite
 TH/P3-41 F. Imbeaux Design and First Applications of the ITER Integrated Modelling & Analysis Suite TH/P3-42 E. M. Bass Fusion Alpha Loss in ITER with Local Marginal Stability to Alfvén
 TH/P3-41 F. Imbeaux Design and First Applications of the ITER Integrated Modelling & Analysis Suite 424 TH/P3-42 E. M. Bass Fusion Alpha Loss in ITER with Local Marginal Stability to Alfvén Eigenmodes 425
 TH/P3-41 F. Imbeaux Design and First Applications of the ITER Integrated Modelling & Analysis Suite 424 TH/P3-42 E. M. Bass Fusion Alpha Loss in ITER with Local Marginal Stability to Alfvén Eigenmodes Eigenmodes H/P3-43 J. R. Martin-Solis
 TH/P3-41 F. Imbeaux Design and First Applications of the ITER Integrated Modelling & Analysis Suite Analysis Suite 424 TH/P3-42 E. M. Bass Fusion Alpha Loss in ITER with Local Marginal Stability to Alfvén Eigenmodes Eigenmodes Eigenmodes Formation and Termination of Runaway Beams in Tokamak Disrup-
 TH/P3-41 F. Imbeaux Design and First Applications of the ITER Integrated Modelling & Analysis Suite Analysis Suite 424 TH/P3-42 E. M. Bass Fusion Alpha Loss in ITER with Local Marginal Stability to Alfvén Eigenmodes Eigenmodes Eigenmodes Formation and Termination of Runaway Beams in Tokamak Disruptions and Implications for ITER 426
 TH/P3-41 F. Imbeaux Design and First Applications of the ITER Integrated Modelling & Analysis Suite
 TH/P3-41 F. Imbeaux Design and First Applications of the ITER Integrated Modelling & Analysis Suite Analysis Suite 424 TH/P3-42 E. M. Bass Fusion Alpha Loss in ITER with Local Marginal Stability to Alfvén Eigenmodes Eigenmodes 425 TH/P3-43 J. R. Martin-Solis Formation and Termination of Runaway Beams in Tokamak Disruptions and Implications for ITER TH/P3-44 Y. Liu Modelling Toroidal Rotation Damping in ITER Due to External 3D
TH/P3-41F. ImbeauxDesign and First Applications of the ITER Integrated Modelling & Analysis Suite424TH/P3-42E. M. BassFusion Alpha Loss in ITER with Local Marginal Stability to Alfvén Eigenmodes425TH/P3-43J. R. Martin-Solis Formation and Termination of Runaway Beams in Tokamak Disrup- tions and Implications for ITER426TH/P3-44Y. Liu Modelling Toroidal Rotation Damping in ITER Due to External 3D Fields427
 TH/P3-41 F. Imbeaux Design and First Applications of the ITER Integrated Modelling & Analysis Suite Analysis Suite 424 TH/P3-42 E. M. Bass Fusion Alpha Loss in ITER with Local Marginal Stability to Alfvén Eigenmodes 425 TH/P3-43 J. R. Martin-Solis Formation and Termination of Runaway Beams in Tokamak Disruptions and Implications for ITER TH/P3-44 Y. Liu Modelling Toroidal Rotation Damping in ITER Due to External 3D Fields Fields 427
 TH/P3-41 F. Imbeaux Design and First Applications of the ITER Integrated Modelling & Analysis Suite Analysis Suite 424 TH/P3-42 E. M. Bass Fusion Alpha Loss in ITER with Local Marginal Stability to Alfvén Eigenmodes Eigenmodes Formation and Termination of Runaway Beams in Tokamak Disruptions and Implications for ITER TH/P3-44 Y. Liu Modelling Toroidal Rotation Damping in ITER Due to External 3D Fields Fields Fazgorski Integrated Core-SOL-Divertor Modelling for ITER Including Im-
 TH/P3-41 F. Imbeaux Design and First Applications of the ITER Integrated Modelling & Analysis Suite Analysis Suite 424 TH/P3-42 E. M. Bass Fusion Alpha Loss in ITER with Local Marginal Stability to Alfvén Eigenmodes Eigenmodes Formation and Termination of Runaway Beams in Tokamak Disruptions and Implications for ITER TH/P3-44 Y. Liu Modelling Toroidal Rotation Damping in ITER Due to External 3D Fields Fields Fazagorski Integrated Core-SOL-Divertor Modelling for ITER Including Impurity: Effect of Tungsten on Fusion Performance in H-Mode and
 TH/P3-41 F. Imbeaux Design and First Applications of the ITER Integrated Modelling & Analysis Suite
 TH/P3-41 F. Imbeaux Design and First Applications of the ITER Integrated Modelling & Analysis Suite Analysis Suite 424 TH/P3-42 E. M. Bass Fusion Alpha Loss in ITER with Local Marginal Stability to Alfvén Eigenmodes Eigenmodes Formation and Termination of Runaway Beams in Tokamak Disruptions and Implications for ITER TH/P3-44 Y. Liu Modelling Toroidal Rotation Damping in ITER Due to External 3D Fields <li< td=""></li<>

TH/P4-3 O. Agullo
Remote Generation of NTM Precursors by Interchange Turbulence 430
TH/P4-4 Y. Sarazin
Understanding Momentum Transport in Tokamak Plasmas 431
TH/P4-6 K. Dyabilin
The Interpretation of the Tokamak Self-Consistent Pressure Profiles 432
TH/P4-7 A. Reiman
A Cross-Benchmarking and Validation Initiative for Tokamak 3D
Equilibrium Calculations
TH/P4-9 A. Sadykov
Numerical Code "TOKSCEN" for Modeling of Plasma Evolution in
Tokamak
TH/P4-10 C. Bourdelle
L to H Mode Transition: Parametric Dependencies of the Tempera-
ture Threshold
TH/P4-11 I. Holod
Global Gyrokinetic Simulations of Electromagnetic Instabilities in
Tokamak Plasmas
TH/P4-13 R. Paccagnella
Progresses in 3D Nonlinear Numerical Simulation of Tokamak Dis-
ruptions
TH/P4-14 N. Bertelli
Full Wave Simulations for Fast Wave Heating and Power Losses in
the Scrape-off Layer of Tokamak Plasmas
TH/P4-15 D. Chandra
Modeling and Analytic Study of Plasma Flows on Tearing Mode
Stability
TH/P4-16 Z. Guo
Turbulent Elasticity and the Physics of Time Delay
TH/P4-17 I. Ivanova-Stanik
Influence of the Divertor Plate Material on the Plasma Performance
in DEMO
TH/P4-39 M. J. Hole
Advanced Equilibrium Models for Anisotropy, Flow and Chaotic
Fields
TH/P4-40 S. Saarelma
Understanding the MAST H-Mode Pedestal Through Experiments
and Modelling
TH/P4-49 O. Mishchenko
Global gyrokinetic particle-in-cell simulations of Alfvénic modes . 444
TH/P5-4 D. Morozov Thermal Equilibrium and Density Limit in Tokamak-Reactor 445
memiai Equilibrium and Density Limit in Tokamak-Reactor 445

TH/P5-6 T. Kiviniemi
Gyrokinetic Simulation of Phenomenology of GAMs 446
TH/P5-7 C. Castaldo
Advances in Modeling of Nonlinear Effects in LHCD Experiments 447
TH/P5-8 K. Imadera
Global Profile Relaxation Coupled with $E \times B$ Staircase in Toroidal
Flux-Driven ITG Turbulence
TH/P5-9 G. Hao
Finite Toroidal Flow Generated by Resistive Wall Tearing Modes in
a Toroidal Plasma
TH/P5-10 S. Guo
Progress in Theoretical Studies of Resistive Wall Modes for RFP
plasmas and Comparison with Tokamaks
TH/P5-12 G. M. Staebler
Limit Cycle Oscillations and L/H Transitions from Two Dimen-
sional Mean Field Momentum Transport Equations
TH/P5-13 A. Matsuyama
Simulation of Energy-Dependent Stochastic Transport Induced by
Low-Order MHD Instabilities for Runaway Electron Mitigation 452
TH/P5-14 N. Kasuya
Numerical Diagnostics of Non-Diffusive Transport Process by Use
of Turbulence Diagnostic Simulator
TH/P5-17 H. Miura
Two-Fluid Effects on Pressure-Driven Modes in a Heliotron Device 454
TH/P5-34 A. E. Järvinen
Comparison of H-Mode Plasmas in JET-ILW and JET-C with and
without Nitrogen Seeding
•
Steps in Validating Scrape-off Layer Simulations of Detached Plas- mas in the JET ITER-like Wall Configuration
TH/P5-36 A. Skovoroda
Long-Lived Ribbon Structure in JET Tokamak as a Manifestation of
a Force-Free Magneto-Current Island
TH/P5-37 S. Moradi
Core Micro-Instability Analysis of JET Hybrid and Baseline Dis-
charges with Carbon Wall
TH/P5-50 H. Bufferand
Numerical Modeling for Divertor Design and in Support to the
WEST Project
TH/P6-1 P. Cahyna
Modelling of Spatial Structure of Divertor Power Loads Caused by
Edge-Localized Modes Mitigated by Magnetic Perturbations 460

TH/P6-2 U. Daybelge Rotation Instability of Neoclassical Plasma Near Magnetic Separatrix461
TH/P6-4 A. Fukuyama
Kinetic Integrated Modeling of Burning Start-up Phase in Tokamaks 462
TH/P6-8 T. Onjun
Analysis of ITB and ETB Formations in Tokamak Plasma Using
Bifurcation Concept
TH/P6-9 L. Colas
Self-Consistent Modeling of Radio-Frequency Sheaths: Comparison with Tore Supra Measurements and Predictability for Future Machines464
TH/P6-10 S. Yi
How Turbulence Spreading Decouples the Flux from the Local Gradient: a Nonlinear Gyrokinetic Simulation Study
TH/P6-11 O. Meneghini
Integrated Modeling of Tokamak Experiments with OMFIT 466
TH/P6-12 J. Shiraishi
Extension of Kinetic-Magnetohydrodynamic Model to Include Toroidal
Rotation Shear Effect and its Application to Stability Analysis of Resistive Wall Modes
TH/P6-14 J. Zhu
Theoretical and Simulation Studies on the Wave and Particle Dy-
namics Associated with Alfvén Eigenmodes in Tokamak Plasmas $$. 468
TH/P6-15 W. Tang
New Physics Insights on Size-Scaling of Confinement Enabled by Computing at Extreme Scale
TH/P6-16 Z. Qiu
Nonlinear Excitation of Kinetic Geodesic Acoustic Modes by Drift
Waves in Nonuniform Plasmas
TH/P6-24 K. C. Lee
Analysis of Radial Electric Field Formation by Asymmetry of Neu-
tral Beam Injection on KSTAR and NSTX Based on the Gyro-Center
Shift
TH/P6-38 S. Murakami
Integrated Heat Transport Simulation of High Ion Temperature
Plasma of LHD 472
TH/P6-39 G. Kawamura
Transport Simulation Analysis of Peripheral Plasma with the Open and the Closed LHD Divertor
TH/P6-40 A. Ishizawa
Electromagnetic Gyrokinetic Analysis of Turbulent Transport in
Finite-beta LHD Plasmas

TH/P6-49 R. W. Harvey
NBI and HHFW Fast Ion Temporal Dynamics Modeling with CQL3D-
Hybrid-FOW in NSTX Discharges
TH/P6-50 E. Meier
Modeling Divertor Concepts for Spherical Tokamaks NSTX, NSTX-
U, and ST-FNSF
TH/P6-52 D. Russell
Modelling the Effect of Lithium on SOL Dynamics and the SOL
Heat Flux Width Observed in NSTX
TH/P6-55 R. Raman
Transient CHI Plasma Start-up Simulations and Projections to NSTX-U478
TH/P6-60 J. Ongena
Verification of the Simulated Radiated Power of the ICRH Antenna
Design for Wendelstein 7-X with Experimental Results Using a
Quarter Scale Mock-up Antenna
TH/P7-1 D. P. Brennan
Energetic Particle Driven $n = 1$ MHD Instabilities in Tokamaks
with Weakly Reversed Shear
TH/P7-2 K. Hallatschek
Evolution and System Dependent Properties of Zonal Flows and
GAMs in Tokamaks and Planet Atmospheres
TH/P7-4 L. Zheng
Finite Larmor Radius Effects on Low- n Magnetohydrodynamic
Modes at H-Mode Pedestal with Plasma Rotation
TH/P7-5 L. Chôné
Mechanisms and Dynamics of the External Transport Barrier For-
mation in Nonlinear Plasma Edge Simulations
TH/P7-6 C. Di Troia
Bayesian Derivation of Plasma Equilibrium Distribution Function
for Tokamak Scenarios
TH/P7-7 P. H. Diamond
A New Theory of Scale Selection: What Determines the Avalanche
Scale?
TH/P7-8 Y. Homma
Kinetic Modeling of Classical and Neo-Classical Transport for High-
Z Impurities in Fusion SOL/Divertor Plasmas Using Binary Colli-
sion Method
TH/P7-9 M. Nunami
Reduced Model for Gyrokinetic Turbulent Transport in Helical
Plasmas
TH/P7-10 B. Coppi
Open Theoretical Issues and Solutions for Fusion Relevant Physics
Regimes

TH/P7-13 W. A. Cooper	
Equilibrium and Fast Particle Confinement in 3D Tokamaks with	
Toroidal Rotation	489
TH/P7-14 V. Pustovitov	
Energy Principle for the Fast Resistive Wall Modes in Tokamaks	490
TH/P7-15 M. Lesur	
Chirping Alfvén Eigenmodes Drive Convective and Diffusive Trans-	
port	491
TH/P7-30 Z. Wang	
Simulations and Validations of Transport during Fueling by SMBI	
in HL-2A Tokamak	492
TH/P7-37 Y. Suzuki	
3D Plasma Response to Resonant External Magnetic Perturbation	
and its Impact on Fast Ion Confinement in JT-60SA Plasmas	493
TH/P7-38 M. Nakata	
Gyrokinetic Analysis of Turbulent Heat and Particle Transport on	
JT-60U Plasmas	494
TH/P7-39 A. Bierwage	
Multi-Time-Scale Energetic Particle Dynamics in JT-60U Simulated	
with MHD Activity, Sources and Collisions	495
TH/P8-1 S. Krasheninnikov	
Plasma-Material Interaction Issues in Magnetic Fusion Devices	496
	107
FIP: Fusion Engineering, Integration and Power Plant Design	497
FIP: Fusion Engineering, Integration and Power Plant Design FIP/1-1 Y. Seki	497
FIP: Fusion Engineering, Integration and Power Plant Design FIP/1-1 Y. Seki Development of Tungsten Monoblock Technology for ITER Full-	
FIP: Fusion Engineering, Integration and Power Plant Design FIP/1-1 Y. Seki Development of Tungsten Monoblock Technology for ITER Full- Tungsten Divertor in Japan	497 498
 FIP: Fusion Engineering, Integration and Power Plant Design FIP/1-1 Y. Seki Development of Tungsten Monoblock Technology for ITER Full- Tungsten Divertor in Japan FIP/1-2 J. P. Gunn 	498
 FIP: Fusion Engineering, Integration and Power Plant Design FIP/1-1 Y. Seki Development of Tungsten Monoblock Technology for ITER Full- Tungsten Divertor in Japan FIP/1-2 J. P. Gunn Surface Heat Loads on Tungsten Monoblocks in the ITER Divertor 	
 FIP: Fusion Engineering, Integration and Power Plant Design FIP/1-1 Y. Seki Development of Tungsten Monoblock Technology for ITER Full- Tungsten Divertor in Japan FIP/1-2 J. P. Gunn Surface Heat Loads on Tungsten Monoblocks in the ITER Divertor FIP/1-3 N. Koizumi 	498
 FIP: Fusion Engineering, Integration and Power Plant Design FIP/1-1 Y. Seki Development of Tungsten Monoblock Technology for ITER Full-Tungsten Divertor in Japan FIP/1-2 J. P. Gunn Surface Heat Loads on Tungsten Monoblocks in the ITER Divertor FIP/1-3 N. Koizumi Full-Scale Trial Results to Qualify Optimized Manufacturing Plan 	498 499
 FIP: Fusion Engineering, Integration and Power Plant Design FIP/1-1 Y. Seki Development of Tungsten Monoblock Technology for ITER Full- Tungsten Divertor in Japan FIP/1-2 J. P. Gunn Surface Heat Loads on Tungsten Monoblocks in the ITER Divertor FIP/1-3 N. Koizumi Full-Scale Trial Results to Qualify Optimized Manufacturing Plan for ITER Toroidal Field Coil Winding Pack in Japan 	498 499
 FIP: Fusion Engineering, Integration and Power Plant Design FIP/1-1 Y. Seki Development of Tungsten Monoblock Technology for ITER Full- Tungsten Divertor in Japan FIP/1-2 J. P. Gunn Surface Heat Loads on Tungsten Monoblocks in the ITER Divertor FIP/1-3 N. Koizumi Full-Scale Trial Results to Qualify Optimized Manufacturing Plan for ITER Toroidal Field Coil Winding Pack in Japan FIP/1-4Ra B. Stepanov 	498 499 500
 FIP: Fusion Engineering, Integration and Power Plant Design FIP/1-1 Y. Seki Development of Tungsten Monoblock Technology for ITER Full- Tungsten Divertor in Japan FIP/1-2 J. P. Gunn Surface Heat Loads on Tungsten Monoblocks in the ITER Divertor FIP/1-3 N. Koizumi Full-Scale Trial Results to Qualify Optimized Manufacturing Plan for ITER Toroidal Field Coil Winding Pack in Japan FIP/1-4Ra B. Stepanov Summary of the Test Results of ITER Conductors in SULTAN 	498 499 500
 FIP: Fusion Engineering, Integration and Power Plant Design FIP/1-1 Y. Seki Development of Tungsten Monoblock Technology for ITER Full- Tungsten Divertor in Japan FIP/1-2 J. P. Gunn Surface Heat Loads on Tungsten Monoblocks in the ITER Divertor FIP/1-3 N. Koizumi Full-Scale Trial Results to Qualify Optimized Manufacturing Plan for ITER Toroidal Field Coil Winding Pack in Japan FIP/1-4Ra B. Stepanov Summary of the Test Results of ITER Conductors in SULTAN FIP/1-4Rb V. Vysotsky 	498 499 500
 FIP: Fusion Engineering, Integration and Power Plant Design FIP/1-1 Y. Seki Development of Tungsten Monoblock Technology for ITER Full- Tungsten Divertor in Japan FIP/1-2 J. P. Gunn Surface Heat Loads on Tungsten Monoblocks in the ITER Divertor FIP/1-3 N. Koizumi Full-Scale Trial Results to Qualify Optimized Manufacturing Plan for ITER Toroidal Field Coil Winding Pack in Japan FIP/1-4Ra B. Stepanov Summary of the Test Results of ITER Conductors in SULTAN FIP/1-4Rb V. Vysotsky Research, Development and Production of ITER Toroidal Field Con- 	498 499 500 501
 FIP: Fusion Engineering, Integration and Power Plant Design FIP/1-1 Y. Seki Development of Tungsten Monoblock Technology for ITER Full- Tungsten Divertor in Japan FIP/1-2 J. P. Gunn Surface Heat Loads on Tungsten Monoblocks in the ITER Divertor FIP/1-3 N. Koizumi Full-Scale Trial Results to Qualify Optimized Manufacturing Plan for ITER Toroidal Field Coil Winding Pack in Japan FIP/1-4Ra B. Stepanov Summary of the Test Results of ITER Conductors in SULTAN FIP/1-4Rb V. Vysotsky Research, Development and Production of ITER Toroidal Field Con- ductors and Poloidal Field Cables in Russia 	498 499 500 501
 FIP: Fusion Engineering, Integration and Power Plant Design FIP/1-1 Y. Seki Development of Tungsten Monoblock Technology for ITER Full- Tungsten Divertor in Japan FIP/1-2 J. P. Gunn Surface Heat Loads on Tungsten Monoblocks in the ITER Divertor FIP/1-3 N. Koizumi Full-Scale Trial Results to Qualify Optimized Manufacturing Plan for ITER Toroidal Field Coil Winding Pack in Japan FIP/1-4Ra B. Stepanov Summary of the Test Results of ITER Conductors in SULTAN FIP/1-4Rb V. Vysotsky Research, Development and Production of ITER Toroidal Field Con- ductors and Poloidal Field Cables in Russia FIP/1-5 A. Encheva 	498 499 500 501
 FIP: Fusion Engineering, Integration and Power Plant Design FIP/1-1 Y. Seki Development of Tungsten Monoblock Technology for ITER Full- Tungsten Divertor in Japan FIP/1-2 J. P. Gunn Surface Heat Loads on Tungsten Monoblocks in the ITER Divertor FIP/1-3 N. Koizumi Full-Scale Trial Results to Qualify Optimized Manufacturing Plan for ITER Toroidal Field Coil Winding Pack in Japan FIP/1-4Ra B. Stepanov Summary of the Test Results of ITER Conductors in SULTAN FIP/1-4Rb V. Vysotsky Research, Development and Production of ITER Toroidal Field Con- ductors and Poloidal Field Cables in Russia 	498499500501502
 FIP: Fusion Engineering, Integration and Power Plant Design FIP/1-1 Y. Seki Development of Tungsten Monoblock Technology for ITER Full-Tungsten Divertor in Japan FIP/1-2 J. P. Gunn Surface Heat Loads on Tungsten Monoblocks in the ITER Divertor FIP/1-3 N. Koizumi Full-Scale Trial Results to Qualify Optimized Manufacturing Plan for ITER Toroidal Field Coil Winding Pack in Japan FIP/1-4Ra B. Stepanov Summary of the Test Results of ITER Conductors in SULTAN FIP/1-4Rb V. Vysotsky Research, Development and Production of ITER Toroidal Field Conductors and Poloidal Field Cables in Russia FIP/1-5 A. Encheva Overview of the Design Development, Prototype Manufacturing and Procurement of the ITER In-Vessel Coils 	498499500501502
 FIP: Fusion Engineering, Integration and Power Plant Design FIP/1-1 Y. Seki Development of Tungsten Monoblock Technology for ITER Full-Tungsten Divertor in Japan FIP/1-2 J. P. Gunn Surface Heat Loads on Tungsten Monoblocks in the ITER Divertor FIP/1-3 N. Koizumi Full-Scale Trial Results to Qualify Optimized Manufacturing Plan for ITER Toroidal Field Coil Winding Pack in Japan FIP/1-4Ra B. Stepanov Summary of the Test Results of ITER Conductors in SULTAN FIP/1-4Rb V. Vysotsky Research, Development and Production of ITER Toroidal Field Conductors and Poloidal Field Cables in Russia FIP/1-5 A. Encheva Overview of the Design Development, Prototype Manufacturing and Procurement of the ITER In-Vessel Coils FIP/1-6Ra C. Sborchia 	498499500501502
 FIP: Fusion Engineering, Integration and Power Plant Design FIP/1-1 Y. Seki Development of Tungsten Monoblock Technology for ITER Full-Tungsten Divertor in Japan FIP/1-2 J. P. Gunn Surface Heat Loads on Tungsten Monoblocks in the ITER Divertor FIP/1-3 N. Koizumi Full-Scale Trial Results to Qualify Optimized Manufacturing Plan for ITER Toroidal Field Coil Winding Pack in Japan FIP/1-4Ra B. Stepanov Summary of the Test Results of ITER Conductors in SULTAN FIP/1-4Rb V. Vysotsky Research, Development and Production of ITER Toroidal Field Conductors and Poloidal Field Cables in Russia FIP/1-5 A. Encheva Overview of the Design Development, Prototype Manufacturing and Procurement of the ITER In-Vessel Coils 	 498 499 500 501 502 503

FIP/1-6Rb HJ. Ahn
Manufacturing Design and Progress of the First Sector for ITER
Vacuum Vessel
FIP/2-1 L. R. Baylor
Disruption Mitigation System Developments and Design for ITER . 506
FIP/2-2Ra Y. Oda
Prototype Development of the ITER EC System with 170 GHz Gy-
rotron
FIP/2-2Rb T. Kobayashi
Development of Dual Frequency Gyrotron and Launcher for the
JT-60SA ECH/ECCD System
FIP/2-2Rc T. Imai
Development of Over 1 MW and Multi-Frequency Gyrotrons for
Fusion
FIP/2-3 S. Wukitch
ICRF Actuator Development at Alcator C-Mod
FIP/2-4 A. Masiello
Progress Status of the Activities in EU for the Development of the
ITER Neutral Beam Injector and Test Facility 511
FIP/2-5Ra H. Tobari
Development of DC Ultra-High Voltage Insulation Technology for
ITER NBI
FIP/2-5Rb A. Kojima
Progress in Long Pulse Production of Powerful Negative Ion Beams
for JT-60SA and ITER
FIP/3-1 A. Dinklage
The Initial Programme of Wendelstein 7-X on the Way to a HELIAS
Fusion Power Plant
FIP/3-2 E. Azizov
Status of Upgrading Project of Tokamak T-15
FIP/3-3 R. Kemp
DEMO Design Point Studies
FIP/3-4Ra N. Asakura
Physics and Engineering Studies of the Advanced Divertor for a
Fusion Reactor
FIP/3-4Rb Y. Sakamoto
DEMO Concept Development and Assessment of Relevant Tech-
nologies
FIP/3-5Ra K. Feng
Current Status of Chinese Solid Tritium Breeder TBM 519
FIP/3-6 K. Kim
Design Concept of K-DEMO for Near-Term Implementation 520

FIP/P4-1 Y. Zhai
Multi-Physics Engineering Analysis for an Integrated Design of ITER Diagnostic First Wall and Diagnostic Shield Module 521
FIP/P4-2 L. Hu
Progress on the ITER Diagnostic-Radial X-Ray Camera
FIP/P4-3 A. Garcia Carrasco Comprehensive First Mirror Test for ITER at JET with ITER-like Wall523
FIP/P4-4 D. Gin
Gamma-Ray Spectrometer in the ITER NPA System
FIP/P4-5 Y. Kawano Overview of ITPA R&D Activities for Optimization of ITER Diag- nostic Performance
FIP/P4-6 A. Litnovsky
Studies of Protection and Recovery Techniques of Diagnostic Mirrors for ITER
FIP/P4-7 I. Bolshakova
Experimental Evaluation of Long-Term and Stable Magnetic Sensors Operation in ITER-Relevant Conditions
FIP/P4-9 I. Ricapito
Tritium Transport Modelling: First Achievements on ITER Test Blanket Systems Simulation and Perspectives for DEMO Breeding Blanket
FIP/P4-10 J. Chen
Behaviors of ITER EHF FW under High Heat Flux for Mock-ups Manufactured by HIP Joining Technology
FIP/P4-12 W. Chung
Design Finalization and R&D Activities before the Start of Manu- facture of ITER Thermal Shield
FIP/P4-13 MS. Ha
Current Status of Final Design and R&D for ITER Blanket Shield Block in Korea
FIP/P4-15 N. Takeda
R&D Status on Remote Handling Technology for ITER Blanket Maintenance
FIP/P4-20 A. Labusov
Structural Analysis of the ITER Coil Power Supply System 533
FIP/P4-21 Y. Nunoya
Advance in Japanese Superconductor for ITER
FIP/P4-24 Y. Wang Preparation for Preliminary Design of ITER GDC

FIP/P4-25 V. Rozov
Hybrid Integral-Differential Simulator of EM Force Interactions /
Scenario-Assessment Tool with Pre-Computed Influence Matrix in
Applications to ITER
FIP/P4-26 V. Belyakov
Development of Predictive Simulator to Model Electromagnetic
Transients for ITER Application
FIP/P5-1 L. Savoldi Richard
Design Studies towards the Geometrical Optimization of the Thermal-
Hydraulic Performance of Cylindrical Hypervapotron-Type Collec-
tors for Gyrotrons
FIP/P5-3 T. Seki
ICRF Heating Experiment Using the Faraday Shield Less Antenna
and New High Power Antenna in LHD
FIP/P5-4 P. Khvostenko
ICRF System on Tokamak T-15
FIP/P5-5 A. Tribendis
Helicons Current Drive System in Tokamak T-15
FIP/2-4Rc V. Toigo
Progress in the Realization of the PRIMA Neutral Beam Test Facility 542
FIP/P7-1 T. Brown
Availability Considerations in the Design of K-DEMO 543 FIP/P7-2 G. Neilson
Physics and Engineering Assessments of the K-DEMO Magnet
Configuration
FIP/P7-4 K. Im
Design Concept of K-DEMO In-Vessel Components
FIP/P7-5 I. Jenkins
The Impact on Tritium Breeding Ratio of Neutral Beam Port Loca-
tion in DEMO
FIP/P7-6 B. Saoutic
DEMO Reactor Design by the New Modular System Code SYCO-
MORE
FIP/P7-7 A. Fasoli
TCV Heating and In-Vessel Upgrades for Addressing DEMO Physics
Issues
FIP/P7-8 F. P. Orsitto
Diagnostics and Control for Steady State and Pulsed Tokamak DEMO549
FIP/P7-9 V. Sergeev
Design of Divertor and First Wall for DEMO-FNS
FIP/P7-10 D. Ivanov
Superconducting Magnet for Russian Fusion Neutron Source DEMO-
TIN

FIP/P7-12 C. Day
The Operational Window for Divertor Detachment in a Fusion Reactor – A Physics-Technology Integrated Approach
FIP/P7-13 A. Spitsyn
Concept of Fuel Cycle for a Fusion Neutron Source
FIP/P7-14 I. Kirillov
Lead–Lithium Ceramic Breeder Blanket for Russian Thermonuclear
Reactor DEMO-S
FIP/P7-15 K. Gi
Conceptual Design Study of the Large Size and Low Magnetic Field
Superconducting Spherical Tokamak Power Plant
FIP/P7-16 T. Goto
Integrated Physics Analysis of Plasma Operation Control Scenario
of Helical Reactor FFHR-d1
FIP/P7-17 R. Imazawa
Multi-Parameter Measurement Using Finite Electron Temperature
Effect on Laser Polarimetry for Burning Plasma Reactor 557
FIP/P7-18 B. LaBombard
ADX: a High Field, High Power Density, Advanced Divertor Test
Facility
FIP/P7-19 V. Menon
Physics Design and Analysis Code SPECTRE for Tokamak Based
Fusion Reactors
FIP/P7-21 JC. Vallet
Progress of the CEA Contributions to the Broader Approach Projects 560
FIP/P7-23 A. Shimkevich
The Concept of Hybrid Reactor-Tokamak with Molten-Salt Thorium
Blanket for Producing 233U out of Neutron Field
FIP/P7-24 B. Kuteev
Development of DEMO-FNS Tokamak for Fusion and Hybrid Tech-
nologies
FIP/P7-30 A. Shmelev
Fusion Hybrid with Thorium Blanket: on its Innovative Potential at
Fuel Cycle of Nuclear Reactors 563
FIP/P8-1 Z. Xu
Experimental Base of Innovation S-Channel for Fusion LM Blanket 564
FIP/P8-2 F. Hernandez Gonzalez
Experimental Results and Validation of Thermo-Mechanical Models
Used for the PREMUX Test Campaign, as Part of the Roadmap
towards an Out-of-Pile Testing of a Full Scale HCPB Breeder Unit
Mock-up

FIP/P8-3 E. Platacis
MHD-PbLi Facility for Experiments at Real Blanket Relevant Thermo-
Hydraulic Conditions
FIP/P8-4 L. V. Boccaccini
European DEMO Breeding Blanket Design and Development Strat-
egy in a Roadmap to the Realisation of Fusion Energy
FIP/P8-8 S. Varoutis
Simulation of Neutral Gas Flow in the JET Subdivertor and Com-
parison with Experimental Results
FIP/P8-9 S. McIntosh
Engineering Feasibility of the Double Decker Divertor
FIP/P8-10 Y. Nakashima
Development of Divertor Simulation Research in the GAMMA
10/PDX Tandem Mirror
FIP/P8-11 K. Hoshino
Studies of Impurity Seeding and Divertor Power Handling in Fu-
sion Reactor
FIP/P8-12 B. Chektybayev
New Visible Wide Angle Viewing System for KTM Based on Multi-
element Image Fiber Bundle
FIP/P8-17 K. Egorov
Advanced Structural Analysis of Wendelstein 7-X Magnet System
Weight Supports
FIP/P8-18 Y. Koide
JT-60SA Superconducting Magnet System
FIP/P8-19 T. Andreeva
Final Assessment of Wendelstein 7-X Magnetic Field Perturbations
Caused by Construction Asymmetries
Progress of CEA Contributions to the JT-60SA TF Coil Procurements 576
FIP/P8-21 N. Yanagi
Design and Development of High-Temperature Superconducting
Magnet System with Joint-Winding for the Helical Fusion Reactor . 577
FIP/P8-22 E. Gaio
Protection of Superconducting Magnets in Fusion Experiments: the
New Technological Solution for JT-60SA
FIP/P8-23 M. Salvador
Design of Toroidal Coils Testing Bench: Advances in the Mexican
Tokamak "T"
FIP/P8-24 D. Sutherland
The Dynomak: an Advanced Fusion Reactor Concept with Imposed-
Dynamo Current Drive and Next-Generation Nuclear Power Tech-
nologies

FIP/P8-25 V. Minaev	
Globus-M2 Design Peculiarities and Status of the Tokamak Upgrade 58	1
FIP/P8-26 R. Martin	
MAST Upgrade – Construction Status and Early Research Plans 582	2
FIP/P8-27 B. Coppi	
Perspectives for the High Field Approach in Fusion Research and	
Advances within the Ignitor Program	3
FIP/P8-28 M. Emoto	
Development and Successful Operation of the Enhanced-Interlink	
System of Experiment Data and Numerical Simulation in LHD 584	4
FIP/P8-29 A. Sushkov	
Engineering Aspects and Physical Research Program of the Mod-	
ernized T-15 Tokamak 58	5
FIP/P8-30 M. Ono	
Progress toward Commissioning and Plasma Operation in NSTX-U 586	6
FIP/P8-31 T. Akiyama	
Conceptual Design of High Resolution and Reliable Density Mea-	
surement System on Helical Reactor FFHR-d1 and Demonstration	
on LHD	7
FIP/P8-32 H. B. Xu	
Preliminary Test Results of GDC Electrode with Gap Insulation on	
SWIP Test Bed	Q
	0
	-
FNS: Fusion Nuclear Physics and Technology 589	-
FNS: Fusion Nuclear Physics and Technology589FNS/1-1J. Menard	9
FNS: Fusion Nuclear Physics and Technology 589 FNS/1-1 J. Menard Configuration Studies for an ST-Based Fusion Nuclear Science Facility 590	9
 FNS: Fusion Nuclear Physics and Technology FNS/1-1 J. Menard Configuration Studies for an ST-Based Fusion Nuclear Science Facility590 FNS/1-2Ra J. Knaster 	9 0
FNS: Fusion Nuclear Physics and Technology 589 FNS/1-1 J. Menard Configuration Studies for an ST-Based Fusion Nuclear Science Facility590 FNS/1-2Ra J. Knaster The Accomplishment of the Engineering Design Activities of IFMIF/EVEI	9 0
FNS: Fusion Nuclear Physics and Technology 589 FNS/1-1 J. Menard 590 Configuration Studies for an ST-Based Fusion Nuclear Science Facility 590 FNS/1-2Ra J. Knaster 581 The Accomplishment of the Engineering Design Activities of IFMIF/EVEI 582 the European-Japanese Project Towards a Li(d,xn) Fusion Relevant 583	9 0 DA:
FNS: Fusion Nuclear Physics and Technology 589 FNS/1-1 J. Menard 590 Configuration Studies for an ST-Based Fusion Nuclear Science Facility 590 FNS/1-2Ra J. Knaster 590 The Accomplishment of the Engineering Design Activities of IFMIF/EVED 590 the European-Japanese Project Towards a Li(d,xn) Fusion Relevant 590 Neutron Source 590	9 0 DA:
FNS: Fusion Nuclear Physics and Technology 589 FNS/1-1 J. Menard 590 Configuration Studies for an ST-Based Fusion Nuclear Science Facility 590 FNS/1-2Ra J. Knaster 7 The Accomplishment of the Engineering Design Activities of IFMIF/EVEI 7 the European-Japanese Project Towards a Li(d,xn) Fusion Relevant 592 FNS/P4-27 A. Serikov	9 0 DA: 1
FNS: Fusion Nuclear Physics and Technology 589 FNS/1-1 J. Menard 590 Configuration Studies for an ST-Based Fusion Nuclear Science Facility 590 FNS/1-2Ra J. Knaster 590 The Accomplishment of the Engineering Design Activities of IFMIF/EVEI 591 the European-Japanese Project Towards a Li(d,xn) Fusion Relevant 592 FNS/P4-27 A. Serikov 592 Neutronic Analyses for ITER Diagnostic Port Plugs 592	9 0 DA: 1
FNS: Fusion Nuclear Physics and Technology 58 FNS/1-1 J. Menard 590 Configuration Studies for an ST-Based Fusion Nuclear Science Facility 590 FNS/1-2Ra J. Knaster 7 The Accomplishment of the Engineering Design Activities of IFMIF/EVEI 7 the European-Japanese Project Towards a Li(d,xn) Fusion Relevant 592 FNS/P4-27 A. Serikov 592 FNS/P7-11 A. Y. Dnestrovskij 592	9 0 DA: 1
FNS: Fusion Nuclear Physics and Technology 58 FNS/1-1 J. Menard 59 Configuration Studies for an ST-Based Fusion Nuclear Science Facility 59 FNS/1-2Ra J. Knaster 59 The Accomplishment of the Engineering Design Activities of IFMIF/EVEI 59 the European-Japanese Project Towards a Li(d,xn) Fusion Relevant 59 FNS/P4-27 A. Serikov 59 FNS/P7-11 A. Y. Dnestrovskij 59 Integrated Modelling of DEMO-FNS Current Ramp-up Scenario 59	9 0 DA: 1 2
FNS: Fusion Nuclear Physics and Technology 589 FNS/1-1 J. Menard Configuration Studies for an ST-Based Fusion Nuclear Science Facility 590 FNS/1-2Ra J. Knaster The Accomplishment of the Engineering Design Activities of IFMIF/EVEI the European-Japanese Project Towards a Li(d,xn) Fusion Relevant Neutron Source 592 FNS/P4-27 A. Serikov Neutronic Analyses for ITER Diagnostic Port Plugs 592 FNS/P7-11 A. Y. Dnestrovskij Integrated Modelling of DEMO-FNS Current Ramp-up Scenario and Steady State Regime 592	9 0 DA: 1 2
FNS: Fusion Nuclear Physics and Technology 589 FNS/1-1 J. Menard Configuration Studies for an ST-Based Fusion Nuclear Science Facility590 FNS/1-2Ra J. Knaster The Accomplishment of the Engineering Design Activities of IFMIF/EVEI the European-Japanese Project Towards a Li(d,xn) Fusion Relevant Neutron Source 592 FNS/P4-27 A. Serikov Neutronic Analyses for ITER Diagnostic Port Plugs 592 FNS/P7-11 A. Y. Dnestrovskij Integrated Modelling of DEMO-FNS Current Ramp-up Scenario and Steady State Regime 592 FNS/P7-20 U. Fischer	9 0 DA: 1 2
FNS: Fusion Nuclear Physics and Technology 589 FNS/1-1 J. Menard Configuration Studies for an ST-Based Fusion Nuclear Science Facility590 FNS/1-2Ra J. Knaster The Accomplishment of the Engineering Design Activities of IFMIF/EVEI the European-Japanese Project Towards a Li(d,xn) Fusion Relevant Neutron Source	9 0 DA: 1 2 3
FNS: Fusion Nuclear Physics and Technology 589 FNS/1-1 J. Menard Configuration Studies for an ST-Based Fusion Nuclear Science Facility590 FNS/1-2Ra J. Knaster The Accomplishment of the Engineering Design Activities of IFMIF/EVEI the European-Japanese Project Towards a Li(d,xn) Fusion Relevant Neutron Source 592 FNS/P4-27 A. Serikov Neutronic Analyses for ITER Diagnostic Port Plugs 592 FNS/P7-11 A. Y. Dnestrovskij Integrated Modelling of DEMO-FNS Current Ramp-up Scenario and Steady State Regime 592 FNS/P7-20 U. Fischer	9 0 DA: 1 2 3
FNS: Fusion Nuclear Physics and Technology 58 FNS/1-1 J. Menard Configuration Studies for an ST-Based Fusion Nuclear Science Facility590 FNS/1-2Ra J. Knaster The Accomplishment of the Engineering Design Activities of IFMIF/EVEI the European-Japanese Project Towards a Li(d,xn) Fusion Relevant Neutron Source Neutron Source 59 FNS/P4-27 A. Serikov Neutronic Analyses for ITER Diagnostic Port Plugs 592 FNS/P7-11 A. Y. Dnestrovskij Integrated Modelling of DEMO-FNS Current Ramp-up Scenario 592 FNS/P7-20 U. Fischer Advanced Computational Approaches and Tools for High-Fidelity 594 FNS/P7-22 P. Goncharov	9 0 DA: 1 2 3 4
FNS: Fusion Nuclear Physics and Technology 58 FNS/1-1 J. Menard Configuration Studies for an ST-Based Fusion Nuclear Science Facility 590 FNS/1-2Ra J. Knaster The Accomplishment of the Engineering Design Activities of IFMIF/EVEI the European-Japanese Project Towards a Li(d,xn) Fusion Relevant Neutron Source 592 FNS/P4-27 A. Serikov Neutronic Analyses for ITER Diagnostic Port Plugs 592 FNS/P7-11 A. Y. Dnestrovskij Integrated Modelling of DEMO-FNS Current Ramp-up Scenario and Steady State Regime 592 FNS/P7-20 U. Fischer Advanced Computational Approaches and Tools for High-Fidelity Nuclear Analyses of Fusion Facilities 594	9 0 DA: 1 2 3 4
FNS: Fusion Nuclear Physics and Technology 589 FNS/1-1 J. Menard Configuration Studies for an ST-Based Fusion Nuclear Science Facility590 FNS/1-2Ra J. Knaster The Accomplishment of the Engineering Design Activities of IFMIF/EVEI the European-Japanese Project Towards a Li(d,xn) Fusion Relevant Neutron Source 591 FNS/P4-27 A. Serikov Neutronic Analyses for ITER Diagnostic Port Plugs 592 FNS/P7-11 A. Y. Dnestrovskij Integrated Modelling of DEMO-FNS Current Ramp-up Scenario and Steady State Regime 593 FNS/P7-20 U. Fischer Advanced Computational Approaches and Tools for High-Fidelity 594 FNS/P7-22 P. Goncharov 594 FNS/P7-25 A. Zhirkin 594	9 0 DA: 1 2 3 4
FNS: Fusion Nuclear Physics and Technology58FNS/1-1J. MenardConfiguration Studies for an ST-Based Fusion Nuclear Science Facility590FNS/1-2RaJ. KnasterThe Accomplishment of the Engineering Design Activities of IFMIF/EVEIthe European-Japanese Project Towards a Li(d,xn) Fusion RelevantS97FNS/P4-27A. SerikovS97FNS/P4-27A. SerikovS97FNS/P7-11A. Y. DnestrovskijIntegrated Modelling of DEMO-FNS Current Ramp-up Scenarioand Steady State Regime593FNS/P7-20U. FischerAdvanced Computational Approaches and Tools for High-FidelityNuclear Analyses of Fusion Facilities594FNS/P7-22P. GoncharovSpectra of Neutrons from a Beam-Driven Fusion Source595	9 0 DA: 1 2 3 4 5

FNS/P7-27 T. Simonen	
Optimization of a Gas Dynamic Trap Neutron Source	597
ICC: Innovative Confinement Concepts	599
ICC/P4-31 B. Victor	
Progress on HIT-SI and Imposed Dynamo Current Drive	600
ICC/P4-48 S. Inoue	
Numerical Study of Energy Transfer Mechanism of Magnetic Re- connection/Torus Plasma Merging under High Toroidal Magnetic Field	601
ICC/P5-1 V. Ilgisonis	
Tokamak with an Ergodic Central Area	602
ICC/P5-41 V. Svidzinski	
Plasma Confinement by Pressure of Rotating Magnetic Field in Toroidal Device	603
ICC/P5-43 T. Asai	000
Control of Spontaneous Rotation in a Field-Reversed Configuration by Double-Sided Magnetized Plasmoid Injection	604
ICC/P8-19 Y. An	
Low Loop Voltage Start-up Using Trapped Particle Configuration in Versatile Experiment Spherical Torus (VEST)	605
IFE: Inertial Fusion Experiments and Theory	607
IFE/1-1 C. Li	
Effects of Ion Diffusion on Fusion Burn at the Shock Flash in Inertial-Confinement Fusion Implosions	608
IFE/1-2 S. Fujioka	
Experimental Platform for Efficient Heating of Fusion Fuel with Fast-Ignition Scheme	609
IFE/1-3 F. Beg	
Effect of Pre-Plasma on Intense Electron Beam Generation by Rela- tivistic Laser Radiation	610
IFE/1-4 E. Koresheva	
Conception of a Cryogenic Target Factory for IFE	611
IFE/1-5 H. J. Kong	
A High-Energy and Highly Repetitive fs/ps Laser Using Optical Parametric Chirped-Pulse Amplification with a ns Beam Combined Pumping Laser for Fast Ignition	612
IFE/P6-2 Z. Zhang	
Energy Transport by MeV Hot Electrons in Fast Ignition Plasma Driven with LFEX PW Laser	613

IFE/P6-3 H. Shiraga	
Fast Ignition Experiments and Intense Hard-X-Ray Harsh Environ-	
ment	614
Plasma Mirror technology on a PW, multi-kJ class Laser to reduce	
the pre-formed plasma for application to Fast Ignition research	615
IFE/P6-5 T. Johzaki	
Control of Electron Beam Using Strong Magnetic Field for Efficient Core Heating in Fast Ignition	616
IFE/P6-6 H. Nagatomo	
Computational Study of Magnetic Field Compression by Laser	
Driven Implosion	617
IFE/P6-7 M. Murakami	
High Compression of Matter by Hyperspherical Shock Waves for	(10
Application to Impact Ignition	618
IFE/P6-8 A. Sid	
Stabilization Effect of Weibel Modes in Relativistic Laser Fusion Plasma	610
IFE/P6-9 Y. Mori	017
1000 Times Enhancement of Fusion Reaction in Relation to Fast-Ion	
Heating Induced by a Direct-Irradiating Fast-Ignition Scheme	620
IFE/P6-10 Y. Nishimura	020
Counter Implosion of 500 μm Diameter CD Shell and Fast Heating	
of its Core Plasma by Tailored DPSSL-Pumped Laser	621
IFE/P6-11 R. Hanayama	
1Hz Pellets Injection and Laser Synchronous System for Continuous	
Laser Confinement Fusion and Neutron Generation	622
IFE/P6-12 T. Sekine	
Conceptual Design of kilo-Joule Laser Driver for Inertial Fusion	
Mini-Reactor CANDY	623
IFE/P6-13 M. Wölz	
Increasing Laser Power Density towards IFE Requirements: High- Power Laser Diode Bars	624
IFE/P6-16 M. Shmatov	
The Perspectives of the Use of the Advanced Fuels for Power Pro-	
duction	625
MPT: Materials Physics and Technology	627
MPT/1-2 X. Liu	
Overview of Fusion Reactor Materials Study at SWIP	628
MPT/1-3 A. M. Ito	
Molecular Dynamics and Density Functional Simulations of Tung- sten Nanostructure Formation by Helium Plasma Irradiation	629

MPT/1-4 A. Hasegawa
Neutron Irradiation Effects on Grain-Refined W and W-Alloys 630
MPT/P4-8 A. Razdobarin
RF Discharge for In-Situ Mirror Surface Recovery in ITER 631
MPT/P4-17 L. Begrambekov
Protecting B_4C Coating for ITER Divertor Tiles. Deposition, Opera-
tion, Removal of Erosion Products
MPT/P4-23 S. Wikman
Experimental Assessment of Erosion Corrosion Parameters of Cop-
per Alloys and Copper to Steel Joints at ITER Operational Conditions633
MPT/P5-2 W. Osei-Mensah
Radiation Responses for a Stainless Steel Composite as a Neutral
Beam Injector Guard Wall of ITER
MPT/P7-28 J. Brooks
Plasma Facing Material Alternatives to Tungsten 635
MPT/P7-29 R. Doerner
Contributions of Linear Plasma Devices to PMI Research 636
MPT/P7-31 V. Chernov
Microstructure and Mechanical Properties of V-Me(Cr, W)-Zr-C
Alloys as a Function of their Thermochemical Treatment Modes \therefore 637
MPT/P7-32 P. Zheng
Recent Progresses on Vanadium Alloys for Fusion Application in
China
MPT/P7-33 A. Sivak
Energetic, Crystallographic and Diffusion Characteristics of Hydro-
gen Isotopes in Iron
MPT/P7-34 M. Tsventoukh
Unipolar Arcing at Advanced Fine-Structured Materials 640
MPT/P7-36 D. Kato
Super-Saturated Hydrogen Effects on Radiation Damages in Tung-
sten under High-Flux Divertor Plasma Irradiation
MPT/P7-37 V. Koidan
Production of Radiation-Damaged Tungsten and its Study in High
Flux Deuterium Plasma
MPT/P7-38 M. Oyaidzu
Anodic Polarization Study on F82H Steel in Tritiated Water 643
MPT/P7-40 A. Cicuttin
Experimental Results on the Irradiation of a Number of the Nuclear
Fusion Relevant Materials at the Dense Plasma Focus "Bora" Device 644
MPT/P7-41 T. Troev
Computational Study of Defects in Fusion Materials Containing
Helium

MPT/P7-42 M. Chernyshova	
Interaction of Hot Plasma and Fast Ion Streams with Materials	
under Tests in the Dense Plasma Focus Devices and Some Results	
of the Irradiation	646
MPT/P7-43 V. Gribkov	
Physical Processes Taking Place in the Dense Plasma Focus Devices	
at the Interaction of Hot Plasma and Fast Ion Streams with Materials	
under Tests and some Results of the Irradiation	647
MPT/P8-5 A. Zarins	
High-Temperature Radiolysis of Modified Lithium Orthosilicate	
Pebbles with Additions of Titania	648
MPT/P8-6 Y. Feng	
Development of Functional Materials for CN TBM	649
MPT/P8-7 P. Wang	
R&D Status of Reduced Activation Ferritic/Martensitic Steel for	
CN TBM	650
MPT/P8-13 I. Tazhibayeva	
Results of KTM Lithium Divertor Model Testing on the Tokamak	
KTM and Future Plans	651
MPT/P8-15 A. Novokhatsky	
Testing of Mock-ups for a Full Tungsten Divertor on Globus-M	
Tokamak	652
Tokamak	
Tokamak	652 653
Tokamak	
Tokamak	653
Tokamak	653
Tokamak	653
Tokamak	653 654
Tokamak	653 654
Tokamak	653 654 655
Tokamak	653 654 655
Tokamak	653 654 655
Tokamak	653 654 655 656
Tokamak	653 654 655 656
 Tokamak	653 654 655 656
 Tokamak	653654655656657
 Tokamak	653654655656657
 Tokamak	653654655656657
 Tokamak	653654655656657658

PPC/P2-34 T. C. Luce	
Expanding the Physics Basis of the Baseline Q=10 Scenario toward	
ITER Conditions	660
PPC/P2-35 J. Ferron	
High Internal Inductance for Steady-State Operation in ITER and a	
Reactor	661
PPC/P2-36 C. C. Petty	
Achieving Steady-State Conditions in High-Beta Hybrid Scenario	
in DIII-D	662
PPC/P2-37 W. M. Solomon	
Advancing the Physics Basis of Quiescent H-Mode Through Explo-	
ration of ITER Relevant High Density Operation	663
PPC/P3-2 A. R. Polevoi	
Assessment of Operational Space for Long-Pulse Scenarios in ITER	664
PPC/P3-19 C. Kessel	
Examination of the Entry to Burn and Burn Control for the ITER 15	
MA Baseline and Other Scenarios	665
PPC/P3-20 A. Mineev	
Study of ITER First Plasma Initiation Using a 3D Electromagnetic	
Model	666
PPC/P3-21 Y. Gribov	
Plasma Vertical Stabilization in ITER	667
PPC/P3-22 M. Romanelli	
Evaluation of Fuelling Requirements and Transient Density Behav-	
ior in ITER Scenarios	668
PPC/P4-19 R. Wenninger	
Advances in the Physics Basis for the European DEMO Design	669
PPC/P5-42 D. Moreau	
Combined Magnetic and Kinetic Control of Advanced Tokamak	
Steady State Scenarios based on Semi-Empirical Modeling	670
PPC/P6-46 HS. Kim	
Development of Real Time Multiple Control Algorithm for Inte-	
grated Control of Plasma Profiles and Neoclassical Tearing Mode	671
PPC/P8-16 MG. Yoo	
On Ohmic Breakdown Physics in a Tokamak	672
PPC/P8-17 D. Mueller	
Improvements in the Fast Vertical Control Systems in KSTAR, EAST,	
NSTX, and NSTX-U	673
CEE. Safaty Environmental and Economic Across of Eucline	675
SEE: Safety, Environmental and Economic Aspects of Fusion SEE/P5-6 R. Hiwatari	675
Control Requirement of Tokamak Fusion Power Plant for Power	\overline{C}
Generation in Grid System	0/0

SEE/P5-8 E. Mukhin	
	677
SEE/P5-9 H. S. Tho	
Formation of the Business Ecosystem of the Big Science in Korea:	
Focus on Nuclear Fusion and Accelerator Devices	678
SEE/P5-10 M. Nakamura	
Analysis of Accident Scenarios of a Water-Cooled Tokamak DEMO	679
SEE/P5-12 J. Herb	
Review of the Safety Concept for Fusion Reactor Concepts and	
Transferability of the Nuclear Fission Regulation to Potential Fusion	
Power Plants	680
SEE/P5-13 M. Ni	
Tritium Safety Assessment for Fusion Reactor Based on Fuel Cycle	
and Environmental Dispersion Modelling	681
SEE/P5-15 D. Chen	
Physics Design and Economic Assessment of a Long-Pulsed Fusion	
Power Plant	682
י וי יו יוו סי חסת	603
	683
PD/P3-1 M. Nishiura	
Improved beta (local $\beta > 1$) and density in electron cyclotron reso-	(04
nance heating on the RT-1 magnetosphere plasma	684
PD/P3-2 A. Bishaev	(0 5
Plasma Confinement in the Trimix-3M Multipole Galatea Trap	685
PD/P3-3 M. Kozintseva	
Magnetic System of Multipole Trap–Galatea on the Basis of Levitat-	(0)
ing Quadrupole	686
PD/P4-1 A. Livshits	
Short Way Separation of D/T from He with Superpermeable Mem-	
branes in the Post-ITER Devices	687
PD/P5-1 S. Medvedev	
Negative Triangularity Tokamak: Stability Limits and Perspectives	(00
as Fusion Energy System	688
PD/P5-3 G. L. Jackson	
Enhanced Pedestal Performance in DIII-D Elm-free H-modes with	(00
Lithium Injection	689
PD/P5-4 D. Hatch	(00
, , , , , , , , , , , , , , , , , , ,	690
PD/P5-5 Y. Ono	
Plasmoid Ejection Mechanism in Dynamic Divertor Experiment	(01
and Simulation	691

PD/P6-1 S. Ryzhkov
Innovative Concept of the Compression and Heating of the Plasma
Targets in the Scheme for Magneto-Inertial Fusion
PD/P6-3 A. Sunahara
Direct heating of imploded plasma by fast-ions in the fast ignition
scheme
PD/P6-4 R. De Angelis
Overview of the results of the ABC facility at ENEA-Frascati 69
PD/P7-1 K. Kim
Design Concept of K-DEMO for Near-Term Implementation 69
S: Summary 69
S/1-1 C. Hidalgo
Summary EX/C, EX/D, PPC
S/1-2 A. Sen
Summary EX/S, EX/W, ICC
S/2-1 A. Fukuyama
Summary Theory
S/2-2 S. Jacquemot
Summary IFE
S/2-3 B. Kuteev
Summary FIP, FNS, MPT, SEE
Index: Indices 70

0

Opening

105



O/3

Slides Preprint

Igor Kurchatov and the Russian Fusion Program

E. P. Velikhov¹

¹National Research Centre "Kurchatov Institute", Moscow, Russian Federation

Corresponding Author: E. P. Velikhov, Velikhov_EP@nrcki.ru

The 110th anniversary of Academician Igor Kurchatov was celebrated a year ago. Kurchatov belongs to the pleiad of greatest Russian scientists. His research and managerial activity determined further development of Nuclear Energy and Controlled Fusion both in Russia and in the world.

In 1951 Kurchatov recognized the fundamental significance of high temperature plasma research performed by Igor Tamm and Andrei Sakharov and suggested the Government of USSR to use fusion neutrons for 239 Pu and 233 U breeding from 238 U and 232 Th as well as tritium breeding from ⁶Li. His historic letter initiated plasma research in devices with straight magnetic field, mirror machines and in toroidal magnetic configurations with plasma current, later named 'tokamaks'. Kurchatov clearly understood that building a magnetic fusion reactor was impossible without a deep knowledge of high temperature plasma physics. He appointed Academician Lev Artsimovich as the leader of the national fusion program and Academician Mikhail Leontovich as the leader of theoretical research.

A national Fusion Program for the period from 2014 to 2030 has been formulated in Russia taking into account the present status of fusion research, results of ITER design and construction activity, trends in development of Nuclear Energy and prospects of Fusion Energy. The program includes two main directions of research and development:

- 1. active participation in the ITER project and supporting it by theoretical research and experimental activity on national facilities;
- 2. implementation of magnetic fusion achievements and innovative nuclear technologies for faster development of global Atomic Energy via supplementing it by Fusion-Fission Hybrid Systems (FFHS) capable of extending fissile recourses, improving safety, ecology and nonproliferation regime.

The R&D program for hybrid systems and enabling technologies will be realized with the following milestones:

- 1. Design and construction of the demonstration fusion neutron source DEMO-FNS on the basis of a superconducting tokamak for tests of hybrid blankets and nuclear technologies by 2023;
- 2. Design and construction of the Pilot Hybrid Plant (PHP) by 2030.

Overviews



Fusion Research in Ioffe Institute

L. Askinazi¹, Globus-M Team¹, FT-2 Team¹, TUMAN-3M Team¹, and Diagnostic and Theory groups¹

¹ *Ioffe Physical-Technical Institute of the Russian Academy of Science, St. Petersburg, Russian Federation* Corresponding Author: L. Askinazi, leonid.askinazi@mail.ioffe.ru

Overview of the activities of the Plasma Physics Division at the Ioffe Institute in support of fusion program is presented. Experiments on LHCD (100 kW, 2.5 GHz) at the Globus-M tokamak (R = 0.36 m, a = 0.24 m, $B_{tor} = 0.4$ T, $I_{pl} = 200$ kA) with poloidally oriented grill resulted in RF driven current of up to 40 kA, in agreement with the theory predictions. At the FT-2 tokamak $(R = 0.56 \text{ m}, a = 0.08 \text{ m}, B_{tor} = 2.3 \text{ T}, I_{pl} = 30 \text{ kA})$ experiments with traditional toroidally oriented grill revealed no dependence of LHCD density limit on H/D ratio in spite of three times different LH resonance densities. Microwave Doppler Reflectometry (DR) at the Globus-M, and DR and Heavy Ion Beam Probe measurements at the tokamak TUMAN-3M (R = 0.53 m, a = 0.24 m, $B_{tor} = 1.0$ T, $I_{pl} = 190$ kA) demonstrated GAM suppression at the L-H transition. Observations at the FT-2 using Doppler Enhanced Scattering showed that GAM amplitude is anti-correlated both spatially and temporally with electron thermal diffusivity. For the first time turbulence amplitude modulation at GAM frequency was found both experimentally and in global gyrokinetic modeling. A model of L-H transition is proposed based on this effect. The loss mechanisms of energetic ions' (EI) were investigated in the NBI experiments on Globus-M and TUMAN-3M: orbit losses, sawtooth triggered redistribution of EIs and Alfvénic mode excitation. Non-conservation of adiabatic invariant of EI in small aspect ratio configuration was found numerically to play a role in EI losses. Empirical scaling of 2.5 MeV DD neutron rate for the two devices shows strong dependence on toroidal field $B_{tor}^{1.29}$ and plasma current $I_{pl}^{1,34}$; this justifies B_{tor} and I_{pl} increase by a factor of 2.5 in proposed upgrade of Globus-M. Bursts of ~ 1 MHz Alfvénic type oscillations correlating with sawtooth crashes were observed in OH at the TUMAN-3M. Possibility of low threshold parametric excitation of Bernstein and upper hybrid waves trapped in drift-wave eddies resulting in anomalous absorption in ECRH experiments in toroidal plasmas was discovered theoretically. A novel method of radial correlation Doppler reflectometry is shown to be capable of measuring the turbulence wave-number spectrum in realistic 2D geometry. Progress in design and fabrication of three diagnostics for ITER developed in Ioffe institute is reported: Neutral Particle Analysis, Divertor Thomson Scattering and Gamma Spectroscopy.

Slides

Paper

The ITER Project Construction Status

O. Motojima¹

¹ITER Organization, Saint Paul lez Durance, France

Corresponding Author: O. Motojima, osamu.motojima@iter.org

The ITER Project has visibly made its transition to the construction phase in the two years since the last Fusion Energy Conference in San Diego. By mid-February 2014 commitments to in-kind procurement are approaching 89.6 percentage of the total credit value and 70.7 percentage (99 out of 140) in the number of Procurement Arrangements. Construction is accelerating and the appearance of the site is changing on a daily basis. Vigorous efforts are underway to mitigate some remaining organizational problems, including the alignment of the ITER Organization (IO) and seven Domestic Agencies (DAs), minimizing any possible delay factor. The seven Parties are well committed to the construction of ITER. The ITER project has gone beyond the turning point. This fact should be understood and shared. We only can go forward together.

The total progress being made is so enormous that it is impossible to do justice to everything in a single presentation. Therefore, the buildings, the core tokamak and some of the balance of plant will be reported on here. Most ancillary systems ranging from heating and current drive systems, diagnostics and fuelling systems to remote handling and the hot cell facility are in an advanced state of design. Their status will have to be reported at another time. The same is true of both the integration and assembly efforts.



Overview of the JET Results

F. Romanelli¹

¹JET-EFDA, Culham Science Centre, Abingdon, UK

Corresponding Author: F. Romanelli, francesco.romanelli@jet.efda.org

The European fusion programme is moving into the phase of implementation of its Roadmap. In this context, the JET programme has focused on consolidation of ITER design choices and preparation for ITER operation, with a specific emphasis given to the Bulk Tungsten Melt Experiment that has been crucial for the final decision on the material choice for the day-one tungsten divertor in ITER. In the first JET campaigns with the ITER-like Wall (ILW) fuel retention and material migration studies were a high priority. Now the focus of JET experiments has shifted towards integrated scenario development with the goal of addressing issues such as plasma-facing component (PFC) heat loads and W impurity accumulation in conjunction with high performance. In particular, during the last year, the importance of the magnetic geometry in the divertor area, strike point location and divertor pumping were established as key aspects for achieving good H-mode confinement, in combination with avoiding tungsten accumulation using ICRH. Moreover, significant effort was devoted to the use of impurity seeding to produce core-divertor compatible reference scenarios at good confinement which are essential for ITER, as well as high radiative scenarios which are required for DEMO. ITER-relevant conditions for steady-state operation have been achieved for over 7 s at 2.5 MA/2.7 T and 21 MW input power with $H_{98}(y,2) = 0.85$ and low divertor target power loads and partial detachment between ELMs. In parallel, post-mortem analyses of the PFCs retrieved from the first ILW campaigns have confirmed the previously reported low fuel retention obtained by gas balance. These studies show that the reduced material erosion and migration leads to reduced trapping of fuel in deposited Be layers which have less incorporated fuel in comparison with Carbon layers. In addition, the pattern of deposition within the divertor has changed significantly with the ILW in comparison with JET carbon wall campaigns due to the much-reduced level of chemical erosion. Transport to remote areas is almost absent, with the only significant Be deposits $(15 \,\mu m)$ found on the apron of the inner divertor.

This work was supported by EURATOM and carried out within the framework of the European Fusion Development Agreement. The views and opinions expressed herein do not necessarily reflect those of the European Commission.

R. J. Buttery¹

¹General Atomics, San Diego, CA, USA

Corresponding Author: R. J. Buttery, buttery@fusion.gat.com

The DIII-D tokamak has addressed key challenges in preparation for ITER and the next generation of fusion devices. The robustness of RMP-ELM suppression was demonstrated using as few of 5 of the usual 12 coils. QH mode was extended to 80% Greenwald density fraction, establishing its viability for ITER. Disruption mitigation led to relatively symmetric non-localized heat loads, while vertical displacement events were better ameliorated by earlier mitigation. Real time ray tracing and spectral mode identification techniques enabled more efficient tearing mode control. Promising candidates for steady state (SS) fusion were demonstrated, with a fully non-inductive hybrid scenario, a sustained high l_i scenario for ITER's SS goal, a high q_{min} scenario with high β_N potential, and an 80% bootstrap scenario for EAST. Innovative boundary solutions were implemented with good performance achieved using a radiative divertor in ITER baseline and SS scenarios, and adapting snowflake divertor to the SS to further reduce heat flux. New divertor Thomson scattering enabled real time dual detachment/core density control, and characterized detachment in 2D. Scrape off layer (SOL) profiles exhibited a critical gradient behavior consistent with ideal ballooning limits, while increasing connection length broadened the SOL and lowered divertor heat flux, highlighting the importance of cross-field transport. Low Z gas injection was found to help prevent erosion of high Z plasma facing surfaces. Underpinning this, DIII-D continued to expand the scientific basis of fusion for projection and optimization of future devices. Transport studies characterized turbulence in electron heated regimes to constrain predictive models of burning plasmas, and showed how long wavelength turbulence rises, with transitions from ITG to TEM increasing particle transport and density peaking. Fast ion transport due to Alfvénic modes was found consistent with a critical gradient model, while 3D fields led to losses even over a single fast ion orbit. H-mode pedestal structure measurements highlighted the need for kinetic effects in full f simulations, while optimization of the pedestal exploited a predicted valley of improved stability to raise performance.

Work supported in part by the US DOE under DE-FC02-04ER54698, DE-FG02-89ER54297, and DE-AC02-09CH11466.

OV/1-4



Progress with the ITER Project Activity in Russia

A. Krasilnikov¹

¹Institution at Project center "ITER", Russian Federation

Corresponding Author: A. Krasilnikov, a.krasilnikov@iterrf.ru

Russian obligations in the ITER project consist of the development, manufacture, installation, and commissioning at the ITER site of 25 systems. At this stage Institution "Project center ITER" has signed with the ITER Organization 18 procurement arrangements for manufacture and supply of the equipment for ITER. Manufacture of the corresponding systems and development of another seven systems is progressing according to the ITER construction schedule. Nine unit lengths of Nb3Sn toroidal field conductor and nine unit lengths of NbTi poloidal field cables were supplied to European Union in 2013-2014 according to schedule. "Vezuvi-11M" gyrotron was tested in bench in NRC "Kurchatov institute" where all required by ITER parameters (frequency 170 GHz, power 1 MW, duration 1000 s, and efficiency 52%) were reached in combination. Twelve European and six Japanese mockups of divertor were tested in Efremov institute at thermal loads of 20 MW/m². Technology of Russian Beryllium manufacture for ITER first wall was developed in collaboration between Bochvar institute (technology developer) and JSC "Bazalt" with participation of Efremov institute. It was proposed to install gamma-spectrometer behind the NPA at the same line of sight as NPA. Such combination of NPA and gamma-spectrometer will provide additional possibilities to increase accuracy of D/T ratio measurements and fast ion behaviour studies. In collaboration with Institution "Project center ITER" the NPA complex was added by diamond spectrometer of fast atoms that also will increase possibilities of fast ions studies. Results of analysis demonstrate essential increase of high field side reflectometry by adding low field side antenna to provide refractometry measurements. The prototypes of monocrystal Molybdenum mirror were manufactured for hydrogen line and charge exchange recombination spectroscopy. The prototypes of U-235 and U-238 fission chambers and compact diamond neutron spectrometers were developed and tested. The prototypes of spectrometers for CXRS are manufactured and tested.

Slides

Paper

Recent ASDEX Upgrade Research in Support of ITER and DEMO

H. Zohm¹

¹*Max-Planck-Institut für Plasmaphysik, Garching, Germany* Corresponding Author: H. Zohm, hartmut.zohm@ipp.mpg.de

Research on ASDEX Upgrade is programmatically focused on resolving physics questions that are key to the successful operation of ITER as well as informing design choices for a future DEMO reactor. From 2014 on, a significant part of the ASDEX Upgrade programme is run under the EUROfusion MST programme.

Using the flexible set of in-vessel helical perturbation coils, penetration of 3D fields into the plasma is studied by analysing its impact on the edge plasma in L-mode discharges or examining the interaction with rotating core MHD modes. ELM mitigation by 3D fields at high collisionality allows access to very small, high frequency ELMs at edge temperatures and pressure gradients higher than in the usual small ELM regime at high density. This cannot be described by the usual peeling-ballooning model for ELM stability which, in general, is shown to be inadequate to explain the whole variety of type I ELM observations. The study of the impact of a full metal first wall on plasma operation and performance continues to be a major research topic. Comparison with JET has confirmed many of our results. Characterisation of the ITER Q = 10 scenario (standard H-mode at $q_{95} = 3$ and $\beta_N = 1.8$) revealed that, with full metal wall, confinement quality is marginal for reaching H = 1. In this scenario, type I ELMs are large and first attempts using helical fields or pellets showed limited success in mitigation. With higher β_N , confinement regularly exceeds H = 1. These findings suggest that the optimum operational point for ITER Q = 10 might be at higher q_{95} and β_N , evolving towards the 'improved H-mode' regime under study in ASDEX Upgrade.

Concerning research for DEMO, a major emphasis is put on the exhaust problem. Record values of P_{sep}/R exceeding 7 MW/m (total power up to 23 MW) with simultaneous time averaged peak target power load < 5 MW/m² have been demonstrated under partially detached conditions using feedback controlled N-seeding. Complete detachment at high input power P > 10 MW was achieved and extensive modelling helps to clarify the mechanisms behind the experimentally observed high density zone in the divertor plasma as well as the stable X-point radiation. Using double feedback on N and Ar impurity seeding, a value of $P_{rad,core}/P_{tot} \approx 70\%$ as will be needed for DEMO was demonstrated at very good plasma performance. Finally, we will report on operational experience with two rings of tiles consisting of ferritic steel on the high field side heat shield to analyse the implications of a possible use of bare EUROFER wall panels on DEMO and the use of newly installed rings of solid W tiles in the outer divertor strike zones.

All these studies are accompanied by progress in the understanding of the underlying fusion plasma physics, which is essential to obtain true predictive capability, and will be discussed in the contribution.

This project has received funding from the EURATOM research and training programme 2014–2018.



Overview of Transport and MHD Stability Study and Impact of Magnetic Field Topology in the Large Helical Device

K. Ida 1

¹National Institute for Fusion Science, Toki, Japan

Corresponding Author: K. Ida, ida@nifs.ac.jp

The progress of physics understanding and concurrent parameter extension since the last IAEA-FEC 2012 [1] in the Large Helical Device is overviewed. Recently the plasma with high ion and electron temperature ($T_i(0) \sim T_e(0) \sim 6$ keV) is obtained by the combination of 1) a reduction of wall recycling and neutrals by Helium ICRF discharges and 2) optimization of carbon pellet injection and on-axis ECH. The temperature regime obtained is significantly extended. The stochastic magnetic field in the plasma core which causes flattening of the temperature and the plasma flow can be eliminated by the control of the magnetic shear by NBCD and ECCD and a high central ion temperature ($T_i(0) \sim 8$ keV) discharge is achieved by overcoming the core temperature flattening frequently observed in the plasma with an ion-ITB. After the formation of the ion-ITB, the residual stress switches the sign from the counter- to the co-direction and results in a large toroidal flow in the co-direction [2]. On the other hand, the radial convective velocity of the carbon impurity (V_c) also changes sign from inward to outward and this reversal of convection causes the extremely hollow impurity profile (called impurity hole). A stochastization of the magnetic field affects the MHD instability driven by a pressure gradient. This is an interesting topic because the stochastization of the magnetic field is also a key issue in the resonant magnetic perturbation (RMP) experiment for edge localized mode (ELM) suppression. When the stochastization of the magnetic field is enhanced by a RMP, the pressure driven mode is suppressed even without a change in the pressure gradient itself. In LHD, a low mode (n/m = 1/1) magnetic island exists near the plasma periphery and the width of the magnetic island can be controlled by the RMP. By injecting hydrogen pellets into the O-point of the magnetic island, a significant peaked pressure profile inside the magnetic island is produced for a relatively long time, which is similar to the phenomena of a "snake" in a tokamak. Inside the LCFS, the stochastization causes the damping of flows, while it enhances the $E \times B$ flow due to the electron loss to the wall along the magnetic field.

References

[1] O.Kaneko, et al., Nucl. Fusion 53 (2013) 104015.

[2] K.Ida, et al., Phys. Rev. Lett. 111 (2013) 055001.

Slides

Paper

Overview of MAST Results

I. Chapman¹

¹CCFE Fusion Association, Culham Science Centre, Abingdon, UK

Corresponding Author: I. Chapman, ian.chapman@ccfe.ac.uk

MAST addresses key issues for ITER and DEMO. Mitigation of ELMs with resonant magnetic perturbations (RMPs) with n = 2, 3, 4, 6 has been demonstrated: at higher and lower collisionality; for the first ELM; during the current ramp-up; when a sub-set of in-vessel coils fail; and with rotating n = 3RMPs. Fields with n = 4, 6 cause less braking whilst the power to access H-mode is less with n = 4than n = 3, 6. Refuelling with gas or pellets gives plasmas with mitigated ELMs and reduced peak heat flux whilst less than 10% drop in stored energy. The 3D structure of the post-pellet plasmoid has been imaged, with increased fluctuations during pellet ablation. A synergy exists between pellet-fuelling and RMPs, since mitigated ELMs remove fewer particles. JOREK and CAS3D stability codes show that 3D deformations influence peeling-ballooning stability. ELM precursors strikingly observed with Doppler-backscattering (DBS) and beam emission spectroscopy (BES) are consistent with gyrokinetic simulations of micro-tearing modes (MTMs) in the pedestal. Global gyrokinetic runs show kinetic ballooning modes mediate the pedestal width, whilst nonlinear simulations suggest that MTMs carry significant electron heat flux. A scan in β at the L-H transition shows that pedestal height scales strongly with core pressure. The observed tilt of low-k turbulent vortices increases with flow shear, due to a decrease in poloidal wave number. Fast ion redistribution by fast particle modes depends on density, and access to a quiescent domain with 'classical' fast ion transport is found above a critical density. Highly efficient electron Bernstein wave (EBW) current drive (1 A/W) has been achieved in solenoid-free start-up. A new proton detector has characterised escaping fusion products. Langmuir probes and a high-speed camera suggest filaments play a role in particle transport in the private flux region whilst coherence imaging has measured scrape-off layer (SOL) flows. BOUT++ simulations show that fluxes due to filaments are strongly dependent on resistivity and magnetic geometry of the SOL, with higher radial fluxes at higher resistivity. MAST Upgrade is due to operate in 2015 to support ITER preparation and importantly to operate with a Super-X divertor to test extended leg concepts for particle and power exhaust.

This work was part-funded by the RCUK Energy Programme and the EU Horizon 2020 programme



0V

Alcator C-Mod: Research in Support of ITER and Steps Beyond

E. Marmar¹

Alcator C-Mod Team

¹Massachusetts Institute of Technology, Cambridge, MA, USA

Corresponding Author: E. Marmar, marmar@psfc.mit.edu

Alcator C-Mod studies high-field, high-performance diverted plasmas in support of ITER and steps beyond, focussing on RF and microwave tools for heating and current drive, with all metal high-Z plasma-facing components. Stability analysis of pedestals in the I-mode regime finds that pressures are well below the peeling-ballooning limit, as well as expected kinetic ballooning mode thresholds, likely explaining the generally observed lack of ELMs. Experiments using a new fieldaligned ICRF antenna, which is rotated to align with the total local magnetic field, show dramatic reductions high-Z metallic impurity generation, and reduced core contanimation. This antenna also shows improvement in load-tolerance, particularly through edge transients. Implementation of novel "mirror-probe" electronics has enabled simultaneous measurements of T_{e} , n_e and ϕ with 1 μ s time response using a single probe tip. Studies with this setup connected to a fast-scanning probe have revealed important properties of the Quasi-Coherent-Mode (QCM) which regulates edge particle transport in EDA H-mode. An Accelerator-based In-situ Material Surveillance diagnostic has been deployed, and the first between-shot measurements of surface evolution on areas of the inner-wall and above the divertor strike point have been made. Boron surface evolution and deuterium retention have been successfully tracked through a series of tokamak and wall-conditioning experiments. We have observed strong suppression of boundary turbulence and significant E improvement by injecting LH power into high-density H-modes, with H-factor increases up to 30%. An advanced lower hybrid RF (LHRF) actuator component has been implemented in the Integrated Plasma Simulator, and used to simulate modification of sawteeth via LHCD. Gyrokinetic simulations of TEM turbulence find a factor of two nonlinear upshift of the TEM critical density gradient, in close quantitative agreement with experiments. Upgrades which are ready for construction and operation in 2015 include: an actively heated (900 K) advanced tungsten DEMO-like outer divertor; an off-midplane LH launcher to test theories of improved penetration, absorption and current drive at high density, combined with LH source power upgrades to 4 MW; and a second magnetic field-aligned ICRF antenna.

Poster Session OVP, Monday, OV/2-5

Work supported by US Department of Energy

Fast Ignition Realization EXperiment (FIREX) and Prospect to Inertial Fusion Energy in Japan

H. Azechi¹, T. Endo², Y. Fujimoto¹, S. Fujioka¹, R. Hanayama³, K. Ishii³, A. Iwamoto⁴,
T. Jitsuno¹, T. Johzaki², J. Kaneko⁵, Y. Kitagawa³, R. Kodama¹, M. Koga⁶, J. Kawanaka¹,
H. Kan⁷, T. Kawashima⁷, K. Mima³, N. Miyanaga¹, Y. Mori³, M. Murakami¹, Y. Nakata¹,
H. Nagatomo¹, K. Nagai⁸, M. Nakai¹, S. Nakayama³, T. Nakazato¹, H. Nishimura¹,
Y. Nishimura³, T. Norimatsu¹, T. Ozaki⁴, H. Sakagami⁴, N. Sato⁷, Y. Sakawa¹,
N. Sarukura¹, T. Sekine⁷, K. Shigemori¹, T. Shimizu¹, H. Shiraga¹, A. Sunahara¹,
T. Taguchi⁹, K. Tsubakimoto¹, R. Tsuji¹⁰, and H. Yoshida¹¹

¹Institute of Laser Engineering, Osaka University, Osaka, Japan
²Graduate School of Engineering, Hiroshima University, Higashi-Hiroshima, Japan
³Graduate School for the Creation of New Photonics Industries, Hamamatsu, Shizuoka, Japan
⁴National Institute for Fusion Science, Toki, Japan
⁵Graduate School of Engineering, Hokkaido University, Japan
⁶University of Hyogo, Himeji, Japan
⁷Hamamatsu Photonics, K.K., Japan
⁸Tokyo Institute of Technology, Tokyo, Japan
⁹Setsunan University, Neyagawa, Japan
¹⁰Graduate School of Engineering, Ibaraki University, Japan

Corresponding Author: H. Azechi, azechi@ile.osaka-u.ac.jp

Fast ignition has high potential to ignite a fusion fuel with only about one tenth of laser energy necessary for the central ignition. One of the most advanced fast ignition programs is the Fast Ignition Realization Experiment (FIREX). The goal of its first phase is to demonstrate ignition temperature of 5 keV, followed by the second phase to demonstrate ignition-and-burn. Relativistic fast electrons as the energy carrier, however, unfavorably diverge at high laser intensities necessary for significant heating. This difficulty is overcome by kilo-Tesla magnetic field collimating fast electrons towards a compressed fuel. Such super-strong field has been created with a capacitor-coil target driven by a high power laser, and subsequent collimation has also been demonstrated, suggesting that one can achieve ignition temperature at the laser energy available in FIREX. Repetitive creation of fast ignition plasmas has been demonstrated together with the technology development of high-efficient rep lasers and pellet injection, tracking, and beam steering.





Status of JT-60SA Project

P. Barabaschi¹, Y. Kamada², and S. Ishida²

¹F4E: Fusion for Energy, Barcelona, Spain ²Japan Atomic Energy Agency, Naka, Japan

Corresponding Author: P. Barabaschi, pietro.barabaschi@f4e.europa.eu

In 2009, after a complex start-up phase due to the necessity to carry out a re-baselining effort to fit in the original budget while aiming to retain the machine mission, performance, and experimental flexibility, detailed design of the project was begun. In 2012, with the majority of time-critical industrial contracts in place, it was possible to establish a credible time plan, and now the project is progressing towards the first plasma in March 2019. After focussed R&D and qualification tests, the procurement of the major components and plant are now well underway. In the meantime the disassembly of the JT-60U machine has been completed in 2012. The assembly of JT-60SA started in January 2013 with the installation of the cryostat base, the first item delivered from Europe, and continued in February 2014 with the installation of the three lower superconducting equilibrium field coils. Winding of the TF coils winding packs started in July 2013 in EU. A cold test facility for the TF coils has been installed at the CEA Centre in Saclay. The first TF coil will start tests in 2015. The manufacture of the EF4, EF5, and EF6 coils has been completed. All Vacuum Vessel sectors will be completed by April 2014 and their assembly will soon commence. The manufacturing of the cryostat vessel body has now begun, with final delivery planned in 2017. Contracts for all Magnet Power Supplies are placed, fabrication ongoing with the one for the Quench Protection System completed and their installation to commence in 2014. On-site installation of the cryogenic system will be completed in 2015, and it will be operational late in 2016. The dual frequency 110 and 138 GHz gyrotron has made significant progress towards allowing EC heating (ECH) and current drive (ECCD) under a wide range of plasma parameters. Oscillations of 1 MW for 10 s were successful at both frequencies in a world first for a dual-frequency gyrotron by optimizing electron pitch factor using a triode electron gun. On the N-NB system, the pulse duration and the current density of the negative ion source have been successfully improved from 30 s at 80 A/m² in the previous operation to 100 s at 120–130 A/m². The paper will give an overview of the present status of the engineering design, manufacturing and assembly of the JT-60SA machine.

Slides

Paper

Advance of H-Mode Physics for Long-Pulse Operation on EAST

B. Wan¹, J. Li¹, H. Guo¹, Y. Liang², G. Xu¹, X. Gong¹, and A. M. Garofalo³

¹Institute of Plasma Physics, Chinese Academy of Sciences, Hefei, China ²Forschungszentrum Jülich, Jülich, Germany ³General Atomics, San Diego, CA, USA

Corresponding Author: B. Wan, bnwan@ipp.ac.cn

Since the last IAEA-FEC, significant progress has been made on EAST on both physics and technology fronts towards the long-pulse operation of high-confinement plasma regimes. EAST has been upgraded with more than 25 MW of CW heating and current drive power, along with 70 diagnostics, two internal cryopumps, an ITER-like W monoblock top divertor and resonant magnetic perturbation coils, which will enable EAST to investigate long-pulse H-mode operation with dominant electron heating and low torque input, which will be facing challenges on some of critical issues on ITER. New information has been obtained on the physics of L-H transition. Remarkable efforts have been made in mitigating type-I ELMs in a stationary state H-mode plasma with multi-pulses of supersonic molecular beam injection (SMBI), LHCD, lithium granule and deuterium pellet injection, as well as RMPs, thus potentially offering a valuable means of heat-flux control for next-step long-pulse fusion devices. Long-pulse H-mode discharges with $H_{98}(y, 2) \sim 1$ have been obtained either with ELM mitigation or in a small ELMy regime accompanied by a new electrostatic edge coherent mode, which appears in the steep-gradient pedestal region and plays a dominant role in driving heat and particles outwards. High peak heat load on the divertor due to type I ELMs, is reduced either by SMBI or LHCD. We find that ELM mitigation with SMBI is due to enhanced particle transport in the pedestal, correlated with large-scale turbulence and strongly anti-correlated with small-scale turbulence, while LHCD induces edge plasma ergodization, broadening the heat deposition footprint. Challenges and progresses on plasma control, effective H&CD, plasma-wall interactions under long-pulse, high-heat flux and high-Z metal wall conditions will also be presented.



Overview of KSTAR Results in 2013 Campaign

S.-W. Yoon¹, J.-G. Kwak¹, Y.-S. Bae¹, S. G. Lee¹, B.-H. Park¹, and Y.-K. Oh¹

¹National Fusion Research Institute, Daejeon, Korea, Republic of

Corresponding Author: S.-W. Yoon, swyoon@nfri.re.kr

Since the initial long-pulse H-mode operation in 2012, the H-mode has been sustained longer and the operational regime of plasma parameters has been significantly extended in KSTAR tokamak. The progress in long-pulse operation is mainly due both to the increased NBI heating power of PNBI ~ 3.5 MW and the advance in the shaping control which is not trivial with slow superconducting coils. In 2013 campaign, the duration of H-mode phase has been extended up to 25 s with 0.5 MA of plasma current and 3 MW of PNBI and, in the coming campaign as main operational goal, it is expected to be extended up to more than 30 s using 5 MW of PNBI. In addition, in 2014 campaign, the long-pulse operation will be in accordance with ITER requirement, i.e., in ITER similar shape, low safety factor and normalized β (\sim 2.0).

ELM suppression is discovered in wide range of coil configuration and the suppression window in the safety factor q_{95} has extended from 6.5 to 3.9 depending on the configuration, i.e., $q_{95} \sim 6.5$ for n = 1, $q_{95} \sim 5.0$ for the mixed n = 1 & n = 2, and $q_{95} \sim 4.0$ for n = 2 indicating the strong impact of resonant component on ELM suppression. Significant progress has been on the investigation of the underlying mechanism on RMP suppression using measurements of pedestal fluctuations and modeling of plasma response especially for n = 1 case where field penetration is global and full response modeling is required including the sielding effect of toroidal rotation.

Since the initial 2 segment measurements in 2012, detailed evaluation of error field (EF) has been performed by 4 segment compass scan by measuring maximum current in middle internal coils for each quadrant. In agreement with the previous measurements, the measured level of intrinsic error field is at order of 10^{-5} at the magnetic axis, which is an order of magnitude lower than other tokamaks. Strong focus is on the extended identification of detailed pattern of n = 1 error field utilizing the full poloidal sets of internal coils and its impact on the operational boundary is investigated especially for q_{95} range below three where effect of error field is critical due to the locked mode and MHD activities.

Including above topics, the presentation will address the recent results on rotation and transport physics, newly installed diagnostics, MHD activities and the future plan.

OV/4-1

Slides

Paper

Overview of HL-2A Recent Experiments

M. Xu¹, X. Duan¹, J. Dong¹, X. Ding¹, L. Yan¹, Y. Liu¹, X. Song¹, Y. Huang¹, X. Zou²,
Q. Yang¹, D. Liu¹, J. Rao¹, W. Xuan¹, L. Chen¹, W. Mao¹, Q. Wang¹, Q. Li¹, Z. Cao¹, J. Cao¹,
G. Lei¹, J. Zhang¹, X. Li¹, Y. Xu¹, J. Cheng¹, W. Chen¹, L. Yu¹, W. Zhong¹, D. Yu¹, Z. Shi¹,
C. Chen¹, D. Kong³, M. Isobe⁴, S. Morita⁴, Z. Cui¹, X. Ji¹, Y. B. Dong¹, W. Deng¹, B. Feng¹,
W. Hong¹, C. Cui¹, M. Huang¹, G. Li¹, H. Li¹, Q. Li¹, C. Liu¹, J. Peng¹, Y. Wang¹, B. Li¹,
L. Yao¹, L. Yao¹, B. Yuan¹, J. Zhou¹, Y. Zhou¹, C. Yu³, and Y. Liu¹

¹Southwestern Institute of Physics, Chengdu, Sichuan, China
 ²CEA-IRFM, Saint Paul lez Durance, France
 ³University of Science and Technology of China, Anhui, China
 ⁴National Institute for Fusion Science, Toki, Japan

Corresponding Author: M. Xu, minxu@swip.ac.cn

Xu

Since the last IAEA-FEC, experiments on HL-2A tokamak have been dedicated to address the physics on L-H transition, energetic-particles (EPs) and shear Alfvén waves (SAWs), ELM mitigation, disruption mitigation, edge impurity transport and other MHD related activities. In particular, significant progress has been made in the following areas:

- (i) For the first time in experiments, it was found that the phase between normalized radial electric field and the envelope of density fluctuations reverses during the intermediate phase (I-phase) in comparison to the usual predator-prey regime as the plasma approaches H-mode during the L-I-H confinement transition;
- (ii) The frequency up- and down-sweeping reverse shear Alfvén eigenmodes (RSAEs) were observed in NBI plasmas with $q_{min} \sim 1$. By using kinetic AE code (KAEC) simulation, it has been confirmed that the down-sweeping modes are kinetic RSAEs, and the up-sweeping modes are RSAEs that exist in the ideal or kinetic MHD limit;
- (iii) The transition and interaction among low-frequency MHD modes have been observed during NBI, which suggests profound interaction existing among fishbone mode, long-live mode (LLM) and tearing mode (TM);
- (iv) With SMBI a runaway electron plateau was observed at a rather low toroidal magnetic field. In addition, progresses have also been made in the analysis of the loss of energetic-ions, the ELM mitigation induced by supersonic molecular beam injection (SMBI), and the onset of neoclassical tearing mode (NTM) during nonlocal effect with SMBI, etc.

All these experiments benefited from several newly installed diagnostics, such as Motional Stark Effect (MSE), Charge Exchange Recombination Spectroscopy (CXRS) and a scintillator-based lost fast-ion probe (SLIP), and the upgrade of ECRH heating power to 5 MW.



The Science Program of the TCV Tokamak: Exploring Fusion Reactor and Power Plant Concepts

S. Coda¹

¹Ecole Polytechnique Fédérale de Lausanne, CRPP, Lausanne, Switzerland

Corresponding Author: S. Coda, stefano.coda@epfl.ch

TCV is acquiring a new 1 MW neutral beam and 2 MW additional third-harmonic ECRH to expand its operational range. Its existing shaping and ECRH launching versatility was amply exploited in an eclectic 2013 campaign. A new high-confinement mode (IN-mode) was found with an edge barrier in density but not in temperature. Density limits close to the Greenwald value were reached — at reduced confinement — by sawtooth regularization with ECRH. The edge gradients were found to be regimedependent and to govern the scaling of confinement with current. A new theory predicting a toroidal rotation component at the plasma edge, driven by inhomogeneous transport and geodesic curvature, was tested with promising results. The L-H threshold power was measured to be 15-20% higher in both H and He than D, to increase with the length of the outer separatrix, and to be independent of the current ramp rate. Core turbulence was found to decrease from positive to negative edge triangularity deep into the core, consistent with global confinement increase. The geodesic-acoustic mode was studied with multiple diagnostics, and its axisymmetry was confirmed by a full toroidal mapping of its magnetic component. The heat flux profile decay length and heat load profile on the wall were documented as functions of plasma shape in limited plasmas. In the snowflake (SF) divertor configuration we have documented the heat flux profiles on all four strike points. SF simulations with the 3D EMC3-Eirene code, including the physics of the secondary separatrix, underestimate the flux to the secondary strike points, possibly resulting from steady-state $E \times B$ drifts. With neon injection, radiation in a SF was 15% higher than in a conventional divertor. The novel triple-X and X-divertor configurations were achieved transiently in TCV. A new sub-ms real-time equilibrium reconstruction code was used in ECRH control of NTMs and in a prototype shape controller. The detection of visible light from the plasma boundary was also successfully used in a position-control algorithm. A new bangbang controller improved stability against vertical displacements. The RAPTOR real-time transport simulator was applied to current density profile control experiments with ECCD. Shot-by-shot internal inductance optimization was demonstrated by iterative learning control of the current reference trace.



OV/4-3

Overview of Recent Physics Results from NSTX

S. Kaye¹, S. A. Sabbagh²

¹Princeton Plasma Physics Laboratory, Princeton, NJ, USA ²Columbia University, New York, USA

Corresponding Author: S. Kaye, kaye@pppl.gov

NSTX is currently being upgraded to operate at twice the toroidal field and plasma current (up to 1 T and 2 MA), with a second, more tangentially aimed neutral beam for current and rotation control, allowing for pulse lengths up to 5 s. Recent NSTX physics analyses have addressed topics that will allow NSTX-U to achieve the research goals critical to a Fusion Nuclear Science Facility. These goals include accessing low collisionality and high β , producing stable, 100% non-inductive operation and assessing Plasma Material Interface (PMI) solutions to handle the high heat loads expected in the nextstep devices. Including rotation and kinetic resonances, which depend on collisionality, is necessary for predicting experimental stability thresholds of fast growing Ideal Wall and Resistive Wall Modes. Non-linear gyrokinetic simulations have been performed to study transport of heat, particles and momentum in the core plasma, and its dependence on collisionality and profile shapes. These studies include coupling between low- and high-k turbulence, the effect of rotation and non-local transport. PMI studies have focused on the effect of ELMs and 3D fields on plasma detachment and heat flux handling. DEGAS-2 has been used to study the dependence of gas penetration on SOL temperatures and densities for the MGI system being implemented on the Upgrade. Studies of lithium evaporation on graphite surfaces indicate that lithium increases oxygen surface concentrations on graphite, and deuterium-oxygen affinity, which increases deuterium pumping and reduces recycling. Source studies showed that the low lithium level observed in the core of lithium-coated wall NSTX plasmas was due to both high retention of lithium in the divertor as well as large neoclassical diffusivity. Noninductive operation and current profile control in NSTX-U will be facilitated by Coaxial Helicity Injection as well as RF and NB heating. CHI studies using NIMROD indicate that the reconnection process is consistent with the 2D Sweet-Parker theory. Full wave AORSA simulations show that RF power losses in the SOL increase significantly for both NSTX and NSTX-U when the launched waves propagate in the SOL. TAE avalanches can affect NB driven current through energy loss and redistribution of fast ions. Upgrade construction is moving on schedule with first operation of NSTX-U planned for Autumn 2014.

NO



3D Effects of Edge Magnetic Field Configuration on Divertor/SOL Transport and Optimization Possibilities for a Future Reactor

M. Kobayashi¹, K. Ida¹, Y. Feng², O. Schmitz³, T. E. Evans⁴, H. Frerichs⁵, Y. Liang³,
 P. Ghendrih⁶, G. Ciraolo⁶, A. Bader⁵, H. Guo⁷, F. Tabares⁸, D. Tafalla⁸, D. Reiter³, Z. Cui⁹,
 Y. Xu⁹, U. Wenzel², N. Asakura¹⁰, N. Ohno¹¹, S. Morita¹, S. Masuzaki¹, B. Peterson¹,
 K. Itoh¹, and H. Yamada¹

¹National Institute for Fusion Science, Toki, Japan
 ²Max-Planck-Institut für Plasmaphysik, Garching, Germany
 ³Forschungszentrum Jülich, Jülich, Germany
 ⁴General Atomics, San Diego, CA, USA
 ⁵University of Wisconsin-Madison, Madison, WI, USA
 ⁶CEA-IRFM, Saint Paul lez Durance, France
 ⁷Institute of Plasma Physics, Chinese Academy of Sciences, Hefei, China
 ⁸The National Fusion Laboratory, CIEMAT, Madrid, Spain
 ⁹Southwestern Institute of Physics, Chengdu, Sichuan, China
 ¹⁰Japan Atomic Energy Agency, Naka, Japan
 ¹¹University of Nagoya, Nagoya, Japan

Corresponding Author: M. Kobayashi, kobayashi.masahiro@lhd.nifs.ac.jp

This paper overviews recent progress on the experimental identification and physics interpretation of 3D effects of magnetic field geometry/topology on divertor transport in helical devices and tolamaks with RMP. The 3D effects are elucidated as a consequence of competition between transports parallel (\parallel) and perpendicular to magnetic field, in open field lines cut by divertor plates or in magnetic islands. The competition process has strong impacts on divertor functions, density regime, impurity screening, and detachment stability. Based on experiments and numerical simulations, key parameters (indicated with [] below) governing the transport process are discussed suggesting demanding issues to be addressed for divertor optimization in future reactors.

The divertor density regime, which is known for strong up- and down-stream coupling, highrecycling regime in 2D axi-symmetric configurations, is affected by the 3D configuration. In W7-AS, LHD, TEXTOR-DED and HSX, the dependency is weakened. This is due to enhanced loss of \parallel momentum or of \parallel -conduction energy. The dependency is functions of magnetic geometry parameters, [field line connection length], [poloidal wave length of RMP] and $[B_r/B_t]$.

Impurity screening is observed in Tore Supra, LHD, TEXTOR-DED with edge stochastization, and in W7-AS/X, TJ-II with island divertor. The enhanced outward particle flux due to $[B_r]$ provides the screening via friction force exerted on impurity. It is also found that suppression of ion thermal force, in the case of small $[B_r/B_t] \sim 10^{-4}$, is responsible for the screening. The systematic study in TEXTOR-DED and LHD has shown that [a thicker stochastic region] provides better screening effects.

In W7-AS and LHD, the larger [edge island width] leads to detachment stabilization. This is due to capturing of radiation with the islands and to the decoupling of edge and core plasmas in terms of core fueling of plasma/impurity. In TEXTOR-DED, [rotating RMP] fields result in density limit extension, avoiding MARFE onset. This is caused by spreading of recycling region, preventing edge cooling localization by recycling neutral/impurity.

Systematic understandings of the 3D effects of edge magnetic field based on the key parameters shown above will offer new perspectives on divertor optimization for future reactors, which are not available in 2D axi-symmetric configuration.

ΟV

Slides

Paper

Transport, Stability and Plasma Control Studies in the TJ-II Stellarator

J. Sánchez¹

¹The National Fusion Laboratory, CIEMAT, Madrid, Spain

Corresponding Author: J. Sánchez, joaquin.sanchez@ciemat.es

Recent improvements in TJ-II plasma diagnostics and operation have led to a better understanding of transport, stability and plasma control in fusion plasmas.

Impurity transport: Observations of asymmetries in impurity parallel flows in TJ-II ion-root plasmas have been interpreted as an indication of the compressible variation of the impurity flow field and hence of in-surface impurity density asymmetries. In addition, first-time observations of electrostatic potential variations within the same magnetic flux surfaces are presented which are reproduced by neoclassical Monte-Carlo calculations. The dependence of impurity confinement time has been also studied as a function of charge and mass.

Momentum transport and isotope physics: TJ-II has provided evidence that three-dimensional magnetic structures convey significant impact on plasma confinement and L-H transitions. Recent observations on the temporal ordering of the limit cycle oscillations at the L-I-H transition show the leading role of the plasma turbulence. Comparative studies in tokamaks and stellarators have provided direct experimental evidence of the importance of multi-scale physics for unravelling the physics of the isotope effect on transport.

Power exhaust physics: Novel solutions for plasma facing components based on the use of liquid metals like Li and alloys have been developed on TJ-II. The TJ-II programme on liquid metals addresses fundamental issues like the self-screening effect of liquid lithium driven by evaporation to protect plasma-facing components against heat loads and tritium inventory control, using Li-liquid limiters (LLL) recently installed.

Plasma stability studies: Experiments with magnetic well scan on TJ-II suggest that stability calculations, as those presently used in the optimization criteria of stellarators, might miss some stabilization mechanisms.

Fast particle control: The TJ-II results show that, upon moderate off-axis ECH power application, the continuous character of the Alfvén eigenmode (AEs) changes significantly and starts displaying frequency chirping. This result shows that ECH can be a tool for AE control that, if confirmed, could become ITER and reactor-relevant.

Overview of Gyrokinetic Studies on Electromagnetic Turbulence

P. Terry¹, M. J. Pueschel¹, D. Carmody¹, J. Sarff¹, and G. Whelan¹

¹University of Wisconsin-Madison, Madison, WI, USA

Corresponding Author: P. Terry, pwterry@wisc.edu

Recent results on electromagnetic turbulence from gyrokinetic studies in different magnetic configurations are overviewed, showing the characteristics of electromagnetic turbulence and transport in situations where it is both expected and unexpected, and showing how it is affected by equilibrium magnetic field scale lengths. Ballooning parity ion temperature gradient (ITG) turbulence is found to produce magnetic stochasticity and electron thermal transport through nonlinear excitation of linearly stable tearing parity modes. The process is governed by nonlinear three-wave coupling between the ITG mode, the zonal flow, and the damped tearing parity mode. A significant electron thermal flux scales as β^2 , consistent with magnetic flutter. Above a critical β known as the nonzonal transition, the magnetic fluctuations disable zonal flows by allowing electron streaming that effectively shorts zonal potential between flux surfaces. This leads to a regime of very high transport levels. A consideration of the residual flow in the presence of magnetic flutter confirms the disabling effect on zonal flows. Tearing parity microtearing modes become unstable in the magnetic geometry of spherical tokamaks and the RFP. They yield a growth rate in NSTX that requires finite collisionality, large β , and is favored by increasing magnetic shear and decreasing safety factor. In the RFP, a new branch of microtearing with finite growth rate at vanishing collisionality is shown from analytic theory to require the electron ∇B /curvature drift resonance. However, when experimental MST RFP discharges are modeled gyrokinetically, the turbulence is remarkably electrostatic, showing trapped electron mode turbulence, large zonal flows, and a large Dimits shift. Analysis of the effect of the RFP's shorter equilibrium magnetic field scale lengths shows that it increases the gradient thresholds for instability of trapped electron modes, ITG and microtearing. The stronger magnetic shear increases the β threshold for kinetic ballooning mode (KBM) instability. This in turn increases the thresholds for magnetic activity, including the nonzonal transition.

Slides

Paper

Overview of the RFX-Mod Contribution to the International Fusion Science Program

M. E. Puiatti¹, L. Marrelli¹, and P. Martin¹

¹Consorzio RFX, Associazione Euratom-ENEA sulla Fusione, Padova, Italy Corresponding Author: M. E. Puiatti, mariaester.puiatti@igi.cnr.it

The RFX-mod device can be operated both as a Reversed Field Pinch (RFP), where advanced regimes featuring helical shape develop, and as a Tokamak. Due to its flexibility, RFX-mod is contributing to the solution of key issues in the roadmap to ITER and DEMO, including 3D nonlinear MHD modeling, MHD instability control, internal transport barriers, edge transport and turbulence, isotopic effect, high density limit.

In RFP configuration, in the last two years advancements in the understanding of the self-organized helical states, featuring strong electron transport barriers, have been achieved; the role of microtearing modes in driving the residual transport at the barrier has been investigated experimentally and by gyrokinetic simulations. First experiments with deuterium as filling gas showed increased temperature and confinement time. New results on fast ion confinement and on the isotope effect on edge transport and turbulence are reported. RFX-mod contributed to the general issue of the high density limit physics, showing that in the RFP the limit is related to a toroidal particle accumulation due to the onset of a convective cell. The experimental program was accompanied by substantial progress in the theoretical activity: 3D nonlinear visco-resistive MHD and non-local transport modelling have been advanced; resistive wall and fast particle modes have been studied by a toroidal MHD kinetic hybrid stability code.

In Tokamak configuration, q(a) regimes down to q(a) = 1.2 have been pioneered, with (2, 1)Tearing Mode (TM) mitigated and (2, 1) RWM stabilized: the control of such modes can be obtained both by poloidal and radial sensors with proper control algorithm. Progress has been made in the avoidance of disruptions due to the locking of the (2, 1) TM. External 3D fields have been applied to study a variety of physical issues: effect of magnetic perturbations on sawtooth control, plasma flow, runaway electron decorrelation. Probes combining electrostatic and magnetic measurements have been inserted to characterize turbulence and flow pattern at the edge.



Overview of Results from the MST Reversed Field Pinch Experiment

J. Sarff¹, A. Almagri¹, J. Anderson¹, F. Auriemma², M. Borchardt¹, B. Breizman³, D. Brower⁴, S. Cappello², W. Cappechi¹, D. Carmody¹, K. Caspary¹, B. Chapman¹, D. Craig⁵, V. Davydenko⁶, P. Deichuli⁶, D. Demers⁷, J. Duff¹, D. Den Hartog¹, W. Ding⁴, S. Eilerman¹, A. Falkowski¹, P. Fimognari⁷, C. Forest¹, P. Franz², M. Galante¹, J. Goetz¹, R. Harvey⁸, D. Holly¹, P. Innocente², A. Ivanov⁶, J. Koliner¹, S. Kumar¹, J. D. Lee¹, M. Li³, L. Lin⁴, D. Liu⁹, R. Lorenzini², E. Martines², K. McCollam¹, M. McGarry¹, V. Mirnov¹, B. Momo², L. Morton¹, S. Munaretto¹, M. Nornberg¹, P. Nonn¹, S. Oliva¹, E. Parke¹, P. Piovesan², S. Polosatkin⁶, M. J. Pueschel¹, M. E. Puiatti², J. Reusch¹, J. Sauppe¹, A. Seltzman¹, C. Sovinec¹, D. Spong¹⁰, M. Spolaore², H. Stephens¹¹, N. Stupishin⁶, D. Terranova², M. Thomas¹, J. Titus¹², J. Trianna¹, P. Terry¹, J. Waksman¹, G. Whelan¹, P. Zanca², and L. Zheng³

¹University of Wisconsin-Madison, Madison, WI, USA
 ²Consorzio RFX, Associazione Euratom-ENEA sulla Fusione, Padova, Italy
 ³University of Texas at Austin, Austin, TX, USA
 ⁴University of California Los Angeles, CA, USA
 ⁵Wheaton College, Wheaton, USA
 ⁶Budker Institute of Nuclear Physics, Novosibirsk, Russian Federation
 ⁷Xantho Technologies, LLC, Madison, Wisconsin, USA
 ⁸CompX, Del Mar, California, USA
 ⁹University of California Irvine, CA, USA
 ¹⁰Oak Ridge National Laboratory, Oak Ridge, TN, USA
 ¹¹Pierce College, Los Angeles, CA, USA

¹²Florida A&M University, Tallahassee, FL, USA

Corresponding Author: J. Sarff, jssarff@wisc.edu

This overview of results from the MST reversed field pinch program summarizes physics important for the advancement of the RFP as well as for improved understanding of toroidal magnetic confinement in general. Topics include energetic particle effects, 3D helical equilibria, β and density limit studies, microturbulence, ion heating, and magnetic self-organization physics. With neutral beam injection, several bursty energetic particle (EP) modes are observed. The profiles of the magnetic and density fluctuations associated with these EP-modes are measured using an FIR interferometerpolarimeter. Equilibrium reconstructions of the quasi-single-helicity 3D helical state are provided by the V3FIT code that now incorporates several of MST's advanced diagnostics. A predator-prey theoretical model based on sheared flow and/or magnetic field has been developed that captures key QSH dynamics. Upgraded pellet injection permits study of density and β limits over MST's full range of operation, and an MST-record line-average density of 0.9×10^{20} /m³ ($n/n_G = 1.4$) has been obtained. Plasma β exhibits saturation at $\beta_{tot} \leq 20\%$ for a wide range of density, $0.2 < n/n_G < 1.6$. Gyrokinetic simulations (GENE) based on experimental toroidal equilibrium reconstructions predict unstable trapped electron modes. Nonlinear simulations show that the "Dimits shift" is large and persists at finite β . Experimentally, small-scale density fluctuations are detected in improved confinement plasmas. Impurity ion temperature measurements reveal a charge-to-mass-ratio dependence in the rapid heating that occurs during a sawtooth crash. Also, a toroidal asymmetry in the ion temperature is measured, correlated with 3D magnetic structure associated with tearing modes. Magnetic self-organization studies include measurements and modeling of the dynamo emf in standard RFP operation as well as with an applied ac inductive electric field to investigate the dynamics of oscillating field current drive (OFCD). Extended MHD computation for standard RFP conditions using NIMROD predicts dynamical coupling of current and plasma flow relaxation. The dynamo emf has also been measured when OFCD is applied, strengthening the understanding of and possibility for steady-state current sustainment using inductive current drive.



Slides

Paper

Overview of the FTU Results

G. Pucella¹, FTU Team¹

¹Associazione EURATOM-ENEA Unitá Tecnica Fusione, Frascati, Italy

Corresponding Author: G. Pucella, gianluca.pucella@enea.it

Since the 2012 IAEA-FEC Conference, FTU operations have been largely devoted to runaway electrons (RE) generation and control, to the exploitation of the 140 GHz EC system and to liquid metal limiter elements. Experiments on RE have shown that the measured threshold electric field is larger than predicted by collisional theory and can be justified considering synchrotron radiation losses. A new RE control algorithm was developed and tested in presence of a RE current plateau, which minimizes the interactions with plasma-facing components and safely quenches the discharges. The experimental sessions with 140 GHz EC system have been mainly devoted to experiments on real time control of MHD instabilities using the new EC launcher with fast steering capability. Experiments with EC power modulation have confirmed the possibility to lock the sawtooth period to the EC period, with EC injection inside the q = 1 surface, while experiments with central EC injection have shown the onset of 3/2 and 2/1 modes. EC assisted breakdown experiments have been focussed on ITER start-up issues, exploring the polarization conversion at reflection from inner wall and the capability to assure plasma start-up even in presence of a large stray magnetic field. A new actively Cooled Lithium Limiter (CLL) has been installed and tested. The CLL was inserted close to the last closed magnetic surface, without any damage to the limiter surface, and first elongated FTU plasmas with EC additional heating were obtained with the new CLL. Reciprocating Langmuir probes were used to measure the heat flux e-folding length in the scrape-off layer, with the plasma kept to lay on the internal limiter to resemble the ITER start-up phase. Density peaking and controlled MHD activity driven by Neon injection were investigated at different plasma parameters, and a full real-time algorithm for disruption prediction, based on MHD activity signals from Mirnov coils, was developed exploiting a large database of disruptions. New diagnostics were successfully installed and tested, as a gamma camera for RE studies and a diamond probe to detect Cherenkov radiation produced by fast electrons. Laser Induced Breakdown Spectroscopy measurements were performed under vacuum, so demonstrating the possibility to provide useful information on the fuel retention in present and future tokamaks, such as ITER.



Pradhan



ΛO

First Experiments in SST-1

S. Pradhan¹, Z. Khan¹, V. L. Tanna¹, A. N. Sharma¹, K. J. Doshi¹, U. Prasad¹, H. Masand¹, A. Kumar¹, K. B. Patel¹, M. K. Bhandarkar¹, J. R. Dhongde¹, B. K. Shukla¹, I. A. Mansuri¹, A. Varadarajulu¹, Y. S. Khristi¹, P. Biswas¹, C. N. Gupta¹, D. K. Sharma¹, R. Srinivasan¹, M. Kumar¹, R. Manchanda¹, S. P. Pandya¹, P. K. Atrey¹, Y. S. Joisa¹, K. Tahiliani¹, S. K. Pathak¹, P. K. Sharma¹, P. J. Patel¹, S. Kulkarni¹, D. Raju¹, H. S. Patel¹, P. Santra¹, T. J. Parekh¹, Y. Paravastu¹, F. S. Pathan¹, P. K. Chauhan¹, D. C. Raval¹, M. S. Khan¹, J. K. Tank¹, P. N. Panchal¹, R. N. Panchal¹, R. J. Patel¹, S. George¹, P. Semwal¹, P. Gupta¹, G. I. Mahesuria¹, D. P. Sonara¹, K. R. Dhanani¹, S. P. Jayswal¹, M. Sharma¹, J. C. Patel¹, F. Varmora¹, D. J. Patel¹, G. L. N. Srikant¹, D. R. Christian¹, A. Garg¹, N. Bairagi¹, G. R. Babu¹, A. G. Panchal¹, M. M. Vora¹, A. K. Singh¹, R. Sharma¹, H. D. Nimavat¹, P. R. Shah¹, H. H. Chudasama¹, T. Y. Raval¹, A. L. Sharma¹, A. Ojha¹, B. R. Parghi¹, M. Banaudha¹, A. R. Makwana¹, A. Das¹, and D. Bora¹

¹Institute for Plasma Research, Bhat, Gandhinagar, India

Corresponding Author: S. Pradhan, pradhan@ipr.res.in

Steady State Superconducting Tokamak (SST-1) has been commissioned after the successful experimental and engineering validations of its critical sub-systems. During the 'engineering validation phase' of SST-1; the cryostat was demonstrated to be leak tight to superconducting magnets system operations in all operational scenarios, the 80 K thermal shield was demonstrated to be uniformly cooled without regions of 'thermal run away and hot spots', the superconducting Toroidal Field (TF) magnets were demonstrated to be cooled to their nominal operational conditions and charged up to 1.5 T of field at the major radius, the assembled SST-1 machine shell was demonstrated to be a graded, stress-strain optimized and distributed thermo-mechanical device and the integrated vacuum vessel was demonstrated to be UHV compatible, etc. Subsequently, 'field error components' in SST-1 were measured to be acceptable towards plasma discharges. A successful break-down was obtained in SST-1 in June 2013 assisted with electron cyclotron pre-ionization in second harmonic mode, thus marking the 'First Plasma' in SST-1 and arrival of SST-1 into the league of contemporary steady state devices as well.

Subsequent to the first plasma, both physical experiments and boosting of engineering parameters in SST-1 have begun. A successful plasma start-up with $E \sim 0.4$ V/m, plasma current in excess of 50 kA for 100 ms assisted with ECH pre-ionization in second harmonic at a field of 0.75 T have been achieved. Lengthening the plasma pulse duration with LHCD, plasma current boosting up with ECH assisted pre-ionization in fundamental mode at 1.5 T apart from advance plasma physics experiments are presently being attempted in SST-1. In parallel, SST-1 has demonstrated in unique fashion pure cold gas cooling based nominal operations of its vapour cooled TF current leads up to 4650 A corresponding to 1.5 T of field in the plasma major radius. SST-1 has also achieved the distinction of being the only superconducting Tokamak in the world where the cable-in-conduit-conductor (CICC) based TF magnets are operated with helium cooling in Two-Phase mode during the plasma discharges up to 2.0 T of field at the plasma major radius.

Preprint

Overview of DEMO Activities of IFERC Project in BA Activities

N. Nakajima¹

¹International Fusion Energy Research Centre, Rokkasho, Japan

Corresponding Author: N. Nakajima, noriyoshi.nakajima@iferc.org

In order to complement ITER and contribute to an early realization of the DEMO reactor, International Fusion Energy Research Centre (IFERC) implements DEMO Design and Research and Development activities. The design basis for DEMO and the sensitivity to underlying physics and technology assumptions has been reviewed through a three-year collaboration. At this point, the plasma major radius and net electricity have been found to vary in a range of 8–9 m and 0.3–0.5 GW, respectively. The tentative target is to set the start points of DEMO1 (pulsed) and DEMO2 (steady state) with low fusion power (≤ 2 GW) for compatibility with divertor power handling. So far, DEMO1 with a major radius (R_p) of 9 m, net electricity $(P_{e,net})$ of 0.5 GW and pulse length of about 2 hours, and DEMO2 with $R_p \sim 8$ m and $P_{e,net} = 0.3-0.5$ GW have been proposed. Comparative studies on the remote maintenance methods are ongoing, and the modeling and event selection for the safety analysis of upper bounding sequences is in progress. Research and Development of common components for DEMO blanket have been performed in five task areas; 1) a long-term exposure test of organic compounds into tritium water for up to two years have been carried by JA without serious effects, and analysis of JET tile will be implemented under EU/JA collaboration in 2014, 2) the impact of heat treatment conditions on RAFM (Reduced Martensite Ferric Material) [F84H] steel properties and assessment of irradiation correlation are examined by JA, and the fabrication technology of RAFM [Eurofer] has been studied by EU, 3) using rotating electrode method apparatus, a series of trial tests for pebbles of beryllide for advanced neutron multiplier is carried out by JA to optimize the fabrication conditions, and EU proceeds with the fabrication of Be-Ti rods by hot extrusion of milled material in steel jackets and the characterization of the beryllides, 4) fabrication and the test of advanced tritium breeder pebbles, such as Li_2TiO_3 with excess Li are implemented by JA, and EU proceeds with production and characterization of Lithium orthosilicate pebbles with secondary phase of 20, 25, and 30 mol% lithium metaltitanate, and 5) EU/JA collaboration activities have progressed in the studies of characterization of electrical resistivity, He and H permeability and radiation damage effects of SiC_f/SiC composites progress.

Paper

Overview of the Recent Research on the J-TEXT Tokamak

G. Zhuang¹, K. Gentle², P. H. Diamond³, J. Chen¹, B. Rao¹, L. Wang¹, K. Zhao¹, S. Han³, Y. Shi³, Y. Ding¹, Z. Chen¹, X. Hu¹, Z. Wang¹, Z. Yang¹, and Z. Chen¹

¹Huazhong University of Science and Technology, Hubei, China
 ²University of Texas at Austin, Austin, TX, USA
 ³National Fusion Research Institute, Daejeon, Korea, Republic of

Corresponding Author: G. Zhuang, ge.zhuang@mail.hust.edu.cn

The experimental research over last two years on the J-TEXT tokamak is summarized, the most significant results including observation of core magnetic and density perturbations associated with sawtooth events and tearing instabilities by a high-performance polarimeter-interferometer (POLARIS), investigation of a rotating helical magnetic field perturbation on tearing modes, studies of resonant magnetic perturbations (RMP) on non-local transport, plasma flows and fluctuations. The POLARIS system has time response up to 1 s, phase resolution < 0.1o and spatial resolution ~ 3 cm. Temporal evolution of the safety factor profile, current density profile and electron density profile are obtained during sawtooth crash events and tearing instabilities as well as disruptions. The effects of RMPs in Ohmic plasmas are directly observed by polarimeter for the first time. Particle transport due to the sawtooth crashes is analyzed. Recovery between crashes implies an inward pinch velocity extending to the center. The J-TEXT RMP system can generate a rotating helical field perturbation with a rotation frequency up to 10 kHz, and dominant resonant modes of m/n = 2/1, 3/1 or 1/1. It is found that tearing modes can be easily locked and then rotate together with a rotating RMP. During the mode locking and unlocking, instead of amplifying the island, the RMP can suppress the island width. Further numerical studies extend the understanding of the experimental observations. The effects of RMPs on plasma flows and fluctuations are studied. Both toroidal rotation velocity and radial electric field increase with RMP coil current when the RMP current is no more than 5 kA. When the RMP current reaches 6 kA, the toroidal velocity profile becomes flatten. Both LFZF and GAM are also damped by strong RMPs. The effects of RMPs on non-local transport in J-TEXT have been studied by using horizontal SMBI and a static RMP. At relatively low density, nonlocal phenomena are easily achieved with SMBI injection, while the rotation response to the SMBI injection is reversed for strong RMPs. SMBI without an RMP makes a change of toroidal rotation in the counter-current direction. We discovered a turbulent acceleration term for parallel rotation which has different physics from the residual stress, and is thus a new candidate mechanism for the origin of spontaneous rotation.

OV-P

Paper

Review of Globus-M Spherical Tokamak Results

V. Gusev¹, N. Bakharev¹, B. Ber¹, E. Bondarchuk², V. Bulanin³, A. Bykov³, F. Chernyshev¹, E. Demina⁴, V. Dyachenko¹, P. Goncharov³, A. Gorodetsky⁵, E. Gusakov¹,
A. Iblyaminova¹, M. Irzak¹, E. Kaveeva³, S. Khitrov¹, M. Khokhlov², N. Khromov¹, S. Krasnov², G. Kurskiev¹, A. Labusov², S. Lepikhov¹, N. Litunovsky², I. Mazul²,
A. Melnik¹, V. Mikov⁶, V. Minaev¹, I. Miroshnikov³, E. Mukhin¹, A. Novokhatsky¹,
M. Patrov¹, A. Petrov³, Y. Petrov¹, V. Rozhansky³, N. Sakharov¹, A. Saveliev¹,
I. Senichenkov³, V. Sergeev³, P. Shchegolev¹, O. Shcherbinin¹, V. Tanchuk², S. Tolstyakov¹,
V. Varfolomeev¹, E. Vekshina³, A. Voronin¹, S. Voskoboinikov³, F. Wagner⁷, A. Yashin³,
G. Zadvitskiy³, A. Zakharov⁵, R. Zalavutdinov⁵, and E. Zhilin⁸

 ¹Ioffe Physical-Technical Institute of the Russian Academy of Science, St. Petersburg, Russian Federation
 ²D. V. Efremov Institute of Electrophysical Apparatus, St. Petersburg, Russian Federation
 ³St. Petersburg State Polytechnical University, St. Petersburg, Russian Federation
 ⁴A. A. Baikov Institute of Metallurgy and Material Sciences, RAS, Moscow, Russian Federation
 ⁵A. N. Frumkin Institute of Physical Chemistry and Electrochemistry, RAS, Moscow, Russian Federation
 ⁶Joint-Stock Company "INTEHMASH", St. Petersburg, Russian Federation
 ⁷Max-Planck-Institut für Plasmaphysik, Garching, Germany
 ⁸Ioffe Fusion Technology Ltd., St. Petersburg, Russian Federation

Corresponding Author: V. Gusev, vasily.gusev@mail.ioffe.ru

First experiments on noninductive current drive (CD) using lower hybrid waves at 2.45 GHz are described. Waves were launched by a 10 waveguide grill with 120° phase shift between neighboring waveguides. The experimental conditions for a poloidal slowing-down scheme are described. The CD efficiency is found to be somewhat less than for standard tokamak lower hybrid CD. Geodesic acoustic modes (GAM) have been discovered in Globus-M with the help of two Doppler reflectometers. GAMs are localized 2–3 cm inside the separatrix. The GAM frequency agrees with theory whereas the density oscillations is found to have mainly an n = 0, m = 0 spatial structure. Fast particle confinement during neutral beam injection has been studied and numerically simulated. Alfvén instabilities excited by fast particles were detected by a toroidal Mirnov probe array. Their excitation conditions are discussed and the dynamics of fast ion losses induced by Alfvén eigenmodes is presented. Unlike for conventional tokamaks, no isotopic effect on confinement has been observed in ohmic discharges comparing similar D and H plasmas. Plasma transport was modelled self consistently from the magnetic axis to the material wall. SOL parameters are compared with experimental results. For plasma-wall interaction studies a specific divertor target consisting of an a-priori damaged tungsten tiles was prepared. The damage was induced by an electron beam or by a plasma gun jet. The damage factor was equivalent to the damage produced by 100-1000 ELM events in ITER. The first results show a strongly nonuniform temperature field formation on the damaged targets after plasma disruptions. A preliminary explanation is that the initial damage gives rise to a layer with low thermal conductivity right under the surface. We will finish explaining specific engineering design issues of the next step Globus-M2 (1 T, 500 MA) and describe the status of component manufacture.



OV/P-04

Contribution to Fusion Research from IAEA Coordinated Research Projects and Joint Experiments

M. Gryaznevich^{1,2,3}, G. Van Oost⁴, J. Stöckel⁵, B. Kuteev⁶, and R. Kamendje⁷

¹Tokamak Energy Ltd, Abingdon, UK
 ²Technical University of Denmark, Roskilde, Denmark
 ³Imperial College, London, UK
 ⁴Ghent University, Ghent, Belgium
 ⁵Institute of Plasma Physics AS CR v.v.i., Prague, Czech Republic
 ⁶National Research Centre "Kurchatov Institute", Moscow, Russian Federation
 ⁷International Atomic Energy Agency, Vienna, Austria

Corresponding Author: M. Gryaznevich, mgryaz@gmail.com

IAEA Coordinated Research Projects (CRP) on "Utilisation of a Network of Small Magnetic Confinement Fusion Devices for Mainstream Fusion Research" and "Conceptual development of steady-state compact fusion neutron sources" continue to contribute to the mainstream Fusion Research. These CRPs join participants from 18 IAEA member states, who perform experiments and present results of individual and coordinated research and results of IAEA Joint Experiments (JE) at Research Coordinating Meetings, International Conferences and in publications. These activities also create platform for building long term relationships between scientists from developing and developed countries in fusion science and technology.

The objective of the CRP "Conceptual development of steady-state compact fusion neutron sources" (CFNS) is to support the research on the development of steady-state compact fusion neutron sources for scientific, technological and nuclear energy applications. This research provides concepts and conceptual designs for low and high power CFNS; determines operational domains with optimized plasma performance and aimed on the development of a scientific and technological basis and comprehensive safety analysis for the proposed CFNS.

The objective of the CRP "Utilization of a Network of Small Magnetic Confinement Fusion Devices for Mainstream Fusion Research" is to streamline results of studies on small fusion devices to mainstream fusion research by establishing a network of cooperation enabling coordinated investigations relevant to physics, diagnostics and technology issues of next fusion devices such as ITER and DEMO. Six IAEA JEs have been carried out. In the recent JEs, studies have been extended from characterization of plasma turbulence and correlation between the occurrence of transport barriers, improved confinement with electrostatic turbulence, to characterization of the plasma pedestal in ohmic and NB heated H-mode discharges, NBI-induced Alfvén Eigenmodes, studies of microwave emission, relation between halo currents and Ip 3D asymmetries during disruptions, evaluation of parallel electron power flux density using Langmuir and Ball-pen probes, RF pre-ionisation and investigation of the use of high-temperature superconductors in tokamak magnets.

Outputs of these activities will be overviewed and results of the recent JEs will be presented in detail.

ΕХ

Magnetic Confinement Experiments

135



Recent Advances in the Understanding and Optimization of RMP ELM Suppression for ITER

R. Nazikian¹, J. D. Callen², X. Chen³, J. S. deGrassie⁴, T. E. Evans⁴, N. M. Ferraro⁴, B. Grierson¹, J. D. King³, E. Kolemen¹, G. J. Kramer¹, M. Lanctot⁴, R. Maingi⁵, G. R. McKee², S. Mordijck⁶, R. A. Moyer⁷, D. Orlov⁷, T. H. Osborne⁴, C. Paz-Soldan³, M. W. Shafer⁵, S. P. Smith⁴, P. B. Snyder⁴, W. M. Solomon¹, E. A. Unterberg⁵, M. A. Van Zeeland⁴, J. G. Watkins⁸, *M. R. Wade*⁴, and A. Wingen⁵

¹Princeton Plasma Physics Laboratory, Princeton, NJ, USA
 ²University of Wisconsin-Madison, Madison, WI, USA
 ³Oak Ridge Institute for Science Eduction, Oak Ridge, TN, USA
 ⁴General Atomics, San Diego, CA, USA
 ⁵Oak Ridge National Laboratory, Oak Ridge, TN, USA
 ⁶College of William and Mary, Williamsburg, VA, USA
 ⁷University of California San Diego, CA, USA
 ⁸Sandia National Laboratories, Livermore, CA, USA

Corresponding Author: R. Nazikian, rnazikia@pppl.gov

Recent experiments with applied Resonant Magnetic Perturbations (RMPs) in low-collisionality ITER Similar Shape (ISS) plasmas on DIII-D have advanced the understanding of and increased confidence in obtaining ELM suppression in the ITER standard operating regime. ELM suppression is obtained with a reduced coil set (5--11 coils) on DIII-D, demonstrating the effectiveness of mixed harmonics (n = 1, 2, 3) with a partial coil set and mitigating the risk of reduced coil availability on ITER. Recent advances in linear two-fluid MHD simulations indicate that resonant field penetration and amplification at the top of the pedestal is ubiquitous in these ISS plasmas, together with resonant field screening and kink amplification in the steep pressure gradient region. Measurements with the X-ray imaging camera reveal new information on the plasma response to 3D fields. There is good agreement between X-ray imaging and M3D-C1 simulation in the steep pressure gradient region of the pedestal, validating theoretical predictions of resonant screening and a dominant edge-kink response. While direct imaging of islands in ELM suppressed plasmas remains elusive, measurements with the newly upgraded magnetic sensors are suggestive of partially screened fields at the top of the pedestal, consistent with M3D-C1 simulations. Indirect evidence of island formation and resonant field penetration is also provided by the observed flattening of the electron pressure profile at the top of the pedestal and concomitant shrinkage of the pedestal width when the RMP is applied. In addition, the flutter model of electron transport also predicts an electron thermal diffusivity "hill" at the top of the pedestal that is comparable to experimental values when the resonant field amplification at the top of the pedestal is included in the calculation. Optimization of the pedestal pressure is an important issue for ELM suppression in ITER given that a reduction in the pedestal pressure is commonly observed in ISS plasmas with applied RMPs. Recent experiments demonstrate that the pedestal pressure can be maintained at the level before the onset of the RMP if the effect of density pumpout is counteracted with density feedback.

This work was supported by the US Department of Energy under DE-AC02-09CH11466, DE-FG02-92ER54139, DE-FC02-04ER54698, DE-SC0007880, DE-FG02-07ER54917, and DE-AC05-00OR22725

Effect of Resonant Magnetic Perturbations on Low Collisionality Discharges in MAST and a Comparison with ASDEX Upgrade

A. Kirk¹, I. Chapman², Y. Liu², W. Suttrop³, P. Cahyna⁴, T. Eich³, M. Jakubowski³, S. Saarelma², R. Scannell², J. Harrison², A. Thornton², and M. Valovic²

¹JET-EFDA, Culham Science Centre, Abingdon, UK ²CCFE Fusion Association, Culham Science Centre, Abingdon, UK ³Max-Planck-Institut für Plasmaphysik, Garching, Germany ⁴Institute of Plasma Physics AS CR v.v.i., Prague, Czech Republic

Corresponding Author: A. Kirk, andrew.kirk@ccfe.ac.uk

The application of Resonant Magnetic Perturbations (RMPs) is foreseen as a mechanism to ameliorate the effects of ELMs on the ITER divertor. Various aspects of RMP operation crucial to ITER have been demonstrated on MAST such as mitigating the first ELM after the L-H transition, sustaining ELM mitigation during both the current ramp-up and in the event of failure of a sub-set of the in-vessel coils and applying a slowly rotating n = 3 RMP, which sustains ELM mitigation while rotating the pattern of the strike point splitting. Although ELM suppression has not been observed on MAST, ELM mitigation has been achieved using RMPs with toroidal mode number of n = 2, 3, 4 and 6 over a wide region of operational space, with considerable overlap with the regions where suppression of type-I ELMs is observed in other machines. The effect that the choice of toroidal mode number on the effectiveness of the mitigation has been investigated and shows that n = 3 or 4 is optimal. The ELM mitigation phase is typically associated with a drop in plasma density and overall stored energy. By carefully adjusting the refuelling, either by gas or pellet fuelling, to counteract the drop in density it has been possible to produce plasmas with mitigated ELMs, reduced peak divertor heat flux and with minimal degradation in pedestal height and confined energy.

Above a threshold value in the applied perturbation field (b_{res}^r) there is a linear increase in normalised ELM frequency $(f_{\rm ELM})$ with b_{res}^r . Experimentally it has been found that both the lobes produced near the X-point and the mid-plane corrugations also increase linearly with the size of b_{res}^r . These deformations to the plasma boundary have been replicated by modelling, which shows that they can strongly influence the peeling-ballooning stability boundary and hence lead to an increase in $f_{\rm ELM}$.

Mitigation of type I ELMs has also been achieved on ASDEX Upgrade at mid-low collisionalities, using RMPs with n = 1 and 2. In a large number of cases an increase of f_{ELM} with b_{res}^{τ} is also observed. However, unlike in MAST, there are some cases where this is not the case. This presentation will compare and contrast the results from the two devices with an aim of increasing our understanding and ability to extrapolate to future devices.

This work was part-funded by the RCUK Energy Programme and by Horizon 2020 programme.

Poster Session P3, Wednesday, EX/1-2

137

ЕΧ





Comparative Studies of Edge Magnetic Islands and Stochastic Layers in DIII-D and LHD

T. E. Evans¹, K. Ida², S. Ohdachi², K. Tanaka², M. Shafer³, S. Inagaki⁴, M. Austin⁵, Y. Suzuki², and E. A. Unterberg³

¹General Atomics, San Diego, CA, USA ²National Institute for Fusion Science, Toki, Japan ³Oak Ridge National Laboratory, Oak Ridge, TN, USA ⁴Kyushu University, Kasuga, Japan ⁵University of Texas at Austin, Austin, TX, USA

Corresponding Author: T. E. Evans, evans@fusion.gat.com

Joint experiments on the DIII-D tokamak and the LHD stellarator/heliotron have resulted in the discovered of spontaneous heat transport bifurcations across the O-point of an applied m/n = 2/1 magnetic islands in DIII-D and enhanced particle transport relative to heat transport in edge m/n = 1/1 LHD islands. The DIII-D results suggest that the heat transport bifurcations are due to islands transitioning from smooth flux surfaces to partially stochastic layers. Alternatively, measurements of the particle and heat transport inside edge static magnetic islands in LHD plasmas show an enhancement of the particle flux relative to the heat flux. The DIII-D results suggest that externally applied static 3D magnetic fields can produce a dynamic evolution of the magnetic topology in the LHD results show that edge magnetic islands preferentially increase the particle flux relative to the heat flux for reasons that have yet to be clarified.

Static magnetic islands and stochastic layers have been observed in low- β L-mode plasmas but not in diverted H-mode plasmas yet. In order to understand the physics of non-axisymmetrically perturbed high- β fusion H-mode plasmas, such as the mechanisms involved in edge localized mode (ELM) suppression with resonant magnetic perturbation (RMP) fields, it is necessary to determine if islands and stochastic layers exists and whether they are static or evolve in time due to the plasma response. Measurements in DIII-D show spontaneous transitions of the magnetic field on rational surfaces due to the plasma response. For example, flat spots in the T_e profile associated with m/n = 2/1, 3/1 and 4/1 islands are seen to appear and disappear as the discharge evolves suggesting either a time varying screening of the field by the plasma or a nonlinear coupling of the 2/1, 3/1 and 4/1 islands. In this contribution we discuss the measurements made in DIII-D along with transport results due to pellets injected into static islands in LHD and their implications for understaning the plasma response to 3D fields in H-mode plasmas.

This work was supported in part by the US Department of Energy under DE-FC02-04ER54698, DE-AC05-00OR22725, DE-FG03-97ER54415, and the NIFS budget code NIFS11ULHH021.



Physical Characteristics of Neoclassical Toroidal Viscosity in Tokamaks for Rotation Control and the Evaluation of Plasma Response

S. A. Sabbagh¹, R. E. Bell², T. E. Evans³, N. M. Ferraro³, I. R. Goumiri⁴, Y. Jeon⁵, W.-H. Ko⁵, Y.-S. Park¹, K. Shaing⁶, Y. Sun⁷, J. W. Berkery¹, D. Gates², S. P. Gerhardt², S.-H. Hahn⁵, S. C. Jardin², C. W. Rowley⁴, and K. Tritz⁸

¹Columbia University, New York, USA
 ²Princeton Plasma Physics Laboratory, Princeton, NJ, USA
 ³General Atomics, San Diego, CA, USA
 ⁴Princeton University, Princeton, NJ, USA
 ⁵National Fusion Research Institute, Daejeon, Korea, Republic of
 ⁶National Cheng Kung University, Tainan, Taiwan, China
 ⁷Institute of Plasma Physics, Chinese Academy of Sciences, Hefei, China
 ⁸Johns Hopkins University, Baltimore, MD, USA

Corresponding Author: S. A. Sabbagh, sabbagh@pppl.gov

Favorable use of low magnitude ($\delta B/B \sim O(10^{-3})$) three-dimensional (3D) magnetic fields in tokamaks includes mitigation of ELMs and Alfvénic modes, and alteration of the plasma rotation profile to strongly affect the stability of NTMs and RWMs. However, in ITER, these fields can significantly reduce the fusion gain, Q, by increasing alpha particle transport. These effects have been theoretically addressed using neoclassical toroidal viscosity (NTV) theory [1]. NTV magnitude and profile that determines the critical 3D applied field level for Q reduction, or for rotation feedback control, depends on the field spectrum, plasma collisionality, and plasma response to the field. The present work focuses on these critical questions with new analysis of results from NSTX and KSTAR. Experimental angular momentum alteration is directly compared to theoretical NTV torque density profiles, T_{NTV} , created by a range of applied 3D field spectra and plasma parameters in NSTX including configurations with dominant n = 2 and n = 3 field components. Large radial variations of T_{NTV} are found in ideal MHD models when the flux surface displacement is derived using an assumption of a fully penetrated δB . In contrast, experimentally measured T_{NTV} does not show strong torque localization. NSTX experiments yield a computed displacement ~ 0.3 cm, smaller than the ion banana width, and averaging T_{NTV} over the banana width more closely matches the measured dL/dt profile. Results from a model-based rotation controller designed using NTV from applied 3D fields as an actuator for instability control are shown. A favorable observation for rotation control, clearly illustrated by KSTAR experiments, is the lack of hysteresis of the rotation when altered by non-resonant NTV. These experiments also show the theoretical scaling of T_{NTV} with δB^2 and ion temperature $\sim T_i^{2.5}$. Due to this strong dependence of the T_{NTV} profile on δB , the T_{NTV} measurements significantly constrain the allowable field amplification. Plasma response models being tested against experiment include the fully-penetrated δB model, and various physics models in the M3D-C1 resistive MHD code. Analysis shows that the M3D-C1 single-fluid model produces a flux surface-averaged $|\delta B|$ consistent with the measured T_{NTV} .

References

[1] K.C. Shaing and C.T. Hsu, Nucl. Fusion 54 (2014) 033012.



Successful ELM Suppressions in a Wide Range of q_{95} Using Low *n* RMPs in KSTAR and its Understanding as a Secondary Effect of RMP

Y. Jeon¹, J.-K. Park², T. E. Evans³, G. Park¹, Y.-C. Ghim⁴, H. Han¹, W.-H. Ko¹, Y.-U. Nam¹, K. D. Lee¹, S. G. Lee¹, J. G. Bak¹, S.-W. Yoon¹, Y.-K. Oh¹, and J.-G. Kwak¹

¹National Fusion Research Institute, Daejeon, Korea, Republic of
 ²Princeton Plasma Physics Laboratory, Princeton, NJ, USA
 ³General Atomics, San Diego, CA, USA
 ⁴Korea Advanced Institute of Science and Technology, Daejeon, Korea, Republic of

Corresponding Author: Y. Jeon, ymjeon@nfri.re.kr

As the most plausible technique to control the edge localized modes (ELMs) of high confinement mode (h-mode) plasmas, which is critical for ITER and beyond, non-axisymmetric resonant magnetic perturbations (RMPs) have been actively investigated in KSTAR. Since the first success of ELM suppression using n = 1 RMPs in 2011 [1], our effort has been devoted to extend the operation regime of ELM control for both external magnetic configurations and plasma parameters. As results, it shows a possibility that the ELM-suppression can be achieved in a wide range of q_{95} (= 3.5–6.5) if the RMP field is configured properly. Several unique features of RMP-driven ELM-suppression are found, by which the physics mechanisms of ELM suppression and mitigation can be explicitly distinguished. These are a long time delay (a secondary effect) and an improved confinement (transport bifurcation). Furthermore, a persistent, rapidly repeating bursty event, localized in the plasma edge, is observed and suggested as a key player in the underlying physics mechanism of RMP-driven ELM-suppression.

References

[1] Y.M. Jeon et al., Phys. Rev. Lett. 109, 035004 (2012).

Dynamic Method to Study Turbulence and Turbulence Transport

S. Inagaki¹, K. Ida², S. Itoh³, K. Itoh², T. Tokuzawa², N. Tamura², S. Kubo², T. Shimozuma², K. Tanaka², H. Tsuchiya², Y. Nagayama², T. Kobayashi¹, M. Sasaki³, N. Kasuya¹, A. Fujisawa³, Y. Kosuga³, K. Kamiya⁴, H. Yamada², and A. Komori²

¹Kyushu University, Kasuga, Japan
 ²National Institute for Fusion Science, Toki, Japan
 ³Institute for Applied Mechanics, Kyushu University, Kasuga, Japan
 ⁴Japan Atomic Energy Agency, Naka, Japan

Corresponding Author: S. Inagaki, inagaki@riam.kyushu-u.ac.jp

Here we developed research methods of plasma turbulence transport associated with the nonlocal features. The ECH modulation experiment and the higher harmonic analysis of the heat wave indicated: (i) propagation of the change of T_e at the time of switch-off/on of ECH power is about 5 times faster than that of perturbation itself, (ii) propagation of the higher (7th) harmonic of the T_e perturbation is 5 times faster than prediction by the diffusive model. New bi-spectral analysis of fluctuations demonstrated a non-linear coupling of micro-fluctuations at different radial locations. These results are beneficial for control of plasma dynamics in future fusion reactors.

ЕΧ





Turbulence Behavior and Transport Response Approaching Burning Plasma Relevant Parameters

G. R. McKee¹, C. Holland², Z. Yan¹, E. J. Doyle³, T. C. Luce⁴, A. Marinoni⁵, C. C. Petty⁴, T. Rhodes³, L. Schmitz³, W. M. Solomon⁶, B. J. Tobias⁶, G. Wang³, and L. Zeng³

¹University of Wisconsin-Madison, Madison, WI, USA
 ²University of California San Diego, CA, USA
 ³University of California Los Angeles, CA, USA
 ⁴General Atomics, San Diego, CA, USA
 ⁵Massachusetts Institute of Technology, Cambridge, MA, USA
 ⁶Princeton Plasma Physics Laboratory, Princeton, NJ, USA

Corresponding Author: G. R. McKee, mckee@fusion.gat.com

Multi-scale turbulence properties are significantly altered and typically exhibit increased amplitude in high- β inductive plasmas as parameters approach those anticipated in burning plasmas. These increases, observed with multiple fluctuation diagnostics in high performance H-mode plasmas on DIII-D, explain the consequent local transport and global energy time confinement response. Burning plasmas will exhibit equilibrated ion and electron temperatures, low average injected torque and toroidal rotation, as well as low ρ^* , low ν^* and low q_{95} . Increased fluctuation amplitudes are observed as a result of reducing core toroidal rotation (and consequent $E \times B$ shear) and increasing T_e/T_i . Density and temperature fluctuation measurements were obtained over a broad wavenumber and radial range, and provide a basis for quantitative comparisons with nonlinear simulations to test turbulent transport models. The energy confinement time is reduced by about 40% as the toroidal rotation is decreased by nearly a factor of three, while core turbulence increases in matched advancedinductive plasmas ($\beta \approx 2.7, q_{95} = 5.1$). Density, electron and ion temperature profiles, as well as relevant dimensionless parameters (β , ρ^* , q_{95} , T_e/T_i , and ν^*) were maintained nearly fixed. Lowwavenumber (ion gyroradius scale) density fluctuations near mid-radius show significant amplitude reduction along with a slight reduction in radial correlation length at high rotation, while fluctuations in the outer region of the plasma, $\rho > 0.6$, exhibit little change in amplitude. In related experiments, low-k density fluctuations are observed to increase over the radial range $0.3 < \rho < 0.8$ as the T_e/T_i ratio is raised by 25% towards unity via application of 3.5 MW of off-axis electron cyclotron heating. The spatial correlation properties are modified, suggesting a change in the dominant underlying instability driving the observed turbulence. Transport likewise increases in all channels while the energy confinement time is reduced by 30%. Initial modeling with TGLF shows significant changes to linear growth rates and saturated turbulence levels as T_e/T_i is increased.

This work was supported by the US Department of Energy under DE-FG02-08ER54999, DE-FG02-89ER53296, DE-FG02-07ER54917, DE-FG02-08ERA54984, DE-FC02-04ER54698, DE-FG02-04ER54235 and DE-AC02-09CH11466.

Controlling H-Mode Particle Transport with Modulated Electron Heating in DIII-D and Alcator C-Mod via TEM Turbulence

D. Ernst¹, K. H. Burrell², W. Guttenfelder³, T. L. Rhodes⁴, L. Schmitz⁴, A. Dimits⁵,
E. J. Doyle⁴, B. Grierson³, M. Greenwald¹, C. Holland⁶, N. C. Luhmann, Jr.⁷, G. R. McKee⁸,
T. Munsat⁹, R. Perkins³, C. C. Petty², J. C. Rost¹, B. J. Tobias³, D. Truong⁸, G. Wang⁴,
S. Zemedkun⁹, and L. Zeng⁴

¹Massachusetts Institute of Technology, Cambridge, MA, USA
 ²General Atomics, San Diego, CA, USA
 ³Princeton Plasma Physics Laboratory, Princeton, NJ, USA
 ⁴University of California Los Angeles, CA, USA
 ⁵Lawrence Livermore National Laboratory, Livermore, CA, USA
 ⁶University of California San Diego, CA, USA
 ⁷University of California Davis, CA, USA
 ⁸University of Wisconsin-Madison, Madison, WI, USA
 ⁹University of Colorado, Boulder, Colorado, USA

Corresponding Author: D. Ernst, dernst@psfc.mit.edu

This work develops a quantitative understanding of the mechanisms for increased particle transport with electron heating in (quiescent) H-mode plasmas. Our DIII-D experiments demonstrate that H-mode core particle transport and density peaking can be locally controlled by modulated electron cyclotron heating (ECH). GYRO simulations show density gradient driven trapped electron modes (TEM) are the only unstable drift modes in the inner half-radius. Transport driven by TEMs increases strongly with electron temperature, reducing the density gradient during ECH. Thus α heating could reduce density peaking, self-regulating fusion power. The DIII-D experiments complement Alcator C-Mod experiments which controlled H-mode core particle transport with modulated minority ICRF heating. High-resolution profile reflectometer density profiles and local fluctuation measurements were obtained in DIII-D. Core density fluctuations intensify during electron heating in both C-Mod and DIII-D at TEM wavelengths. Several hundred GS2 nonlinear TEM simulations for Alcator C-Mod reproduce measured core density fluctuation levels using a new synthetic diagnostic, while matching inferred energy fluxes. A nonlinear upshift in the TEM critical density gradient, associated with zonal flow dominated states, increases strongly with collisionality. In the C-Mod experiments, the density gradient is clamped by this nonlinear TEM critical density gradient. The DIII-D experiments test our predicted strong collisionality variation of the TEM nonlinear upshift at an order of magnitude lower collisionality, while allowing T_e/T_i to nearly double during ECH, tripling the TEM growth rate. Intermittent, quasi-coherent DBS fluctuations near $\rho \sim 0.33$ grow stronger with ECH, with adjacent toroidal mode numbers characteristic of TEMs, accompanied by broadband turbulence. Density fluctuations from beam emission spectroscopy near $\rho \sim 0.7$ strongly increase. Core carbon density and metallic line intensities are modulated by ECH, consistent with TEM expectations. Finally, profile stiffness tests were performed via gas puff modulation that varied the density gradient as well as collisionality.

Supported by the U.S. Department of Energy under DE-FC02-08ER54966, DE-FC02-04ER54698, DE-AC02-09CH11466, DE-FG02-08ER54984, DE-FG02-07ER54917, DE-FG02-99ER54531, DE-FG02-89ER53296, DE-FG02-08ER54999, and DE-FC02-99ER54512.

ЕΧ



Overview of Recent Pedestal Studies at ASDEX Upgrade

E. Wolfrum¹, A. Burckhart¹, M. G. Dunne¹, P. A. Schneider¹, M. Willensdorfer¹, E. Fable¹, R. Fischer¹, D. Hatch², F. Jenko¹, B. Kurzan¹, *E. Viezzer*¹, S. K. Rathgeber¹, and P. Manz³

¹Max-Planck-Institut für Plasmaphysik, Garching, Germany
 ²University of Texas at Austin, Austin, TX, USA
 ³Physik-Department E28, Technische Universität München, Garching, Germany

Corresponding Author: E. Wolfrum, e.wolfrum@ipp.mpg.de

Extensive studies have shown that the pedestal E_r profile in H-mode and asymmetric density and flow profiles of impurity ions are consistent with neoclassical predictions. While the ions set the background flow profile and their transport properties can be described by neoclassical modelling, the mechanisms which determine the electron density and temperature profiles are more varied. A detailed study of the density build-up after the L-H transition can be modelled with the reduction in the diffusion coefficient in the ETB to a level of around $\sim 0.04 \text{ m}^2/\text{s}$, while the question of whether a particle pinch is present has not been resolved. The density level which is reached in H-mode after the L-H transition is directly proportional to the neutral gas level in the divertor just before the L-H transition The ELM cycle is characterised by different phases of recovery, in which ∇T_e and ∇n_e recover on different time scales. The final pressure gradient remains saturated until the next ELM occurs. To test the peeling-ballooning (PB) model, with experimental data, high quality edge current density profiles are derived from magnetic equilibrium reconstructions using internal pressure constraints as well as external magnetic and scrape-off layer current measurements. The ideal linear MHD code suite ILSA/MISHKA was used to determine the stability limit in the different phases of the ELM cycle. While the position of the operational point stays constant in pressure gradient-current density space, the stability limit moves closer until the ELM crash occurs, because more poloidal harmonics become unstable in a wider pedestal. However, the final ELM trigger condition cannot be determined by linear MHD stability alone. The same data has also been used as input for gyrokinetic simulations with GENE in order to determine the dominant type of turbulence. In the phase just before the ELM crash, the gyrokinetic analysis shows robustly unstable MTMs at the top of the pedestal as well as unstable KBMs in the whole pedestal region. The linear behavior of ∇T_e vs. T_e in real space for a wide data base of pre-ELM pedestals also indicates that a local mode (e.g., the KBM) rather than a global mode limits the T_e gradient. Results of velocimetry analysis of ECEI data demonstrate the existence of MTMs at the pedestal top.

EX/3-2

Slides

Paper

Edge Instability Limiting the Pedestal Growth on Alcator C-Mod Experiment and Modeling

A. Diallo¹, J. Hughes², M. Greenwald², B. LaBombard², E. M. Davis², S. G. Baek²,
 C. Theiler², P. B. Snyder³, J. Canik⁴, J. Walk², T. Golfinopoulos², J. Terry², M. Churchill²,
 A. Hubbard², M. Porkolab², L. F. Delgado-Aparicio¹, A. Pankin⁵, M. Reinke⁶, and
 A. White²

¹Princeton Plasma Physics Laboratory, Princeton, NJ, USA
²Massachusetts Institute of Technology, Plasma Science & Fusion Center, Cambridge, MA, USA
³General Atomics, San Diego, CA, USA
⁴Oak Ridge National Laboratory, Oak Ridge, TN, USA
⁵Tech-X Corporation, Colorado, USA
⁶University of York, Heslington, UK

Corresponding Author: A. Diallo, adiallo@pppl.gov

Improvement in global confinement and fusion performance are found to be correlated with the pressure at the top of the edge barrier ("pedestal height") both in experiments and theory. Performance predictions for future devices such as ITER rely on experimental validations of the hypothesis in the predictive models. To date, the leading model for pedestal structure prediction is EPED. This model uses both the peeling ballooning theory to limit the pedestal height and relies on the onset of the kinetic ballooning mode (KBM) to constrain the pedestal gradient. This paper presents detailed measurements on an edge instability limiting the pedestal temperature after edge-localized-modes (ELM) on Alcator-Mod. Using a suite edge diagnostics and a magnetic probe placed near the separatrix, this instability was corroborated using gyrokinetic calculations in the edge. The edge pedestal was determined to be ballooning unstable. In addition to the identification of the instability, the paper will also assess the levels of transport produced by this instability.

Work supported by U.S. DoE contracts DE-FC02-99ER54512 and DE-AC02-09CH11466.



Pedestal Confinement and Stability in JET-ILW ELMy H-Mode Scenarios

C. Maggi¹, S. Saarelma², M. Beurskens², L. Frassinetti³, L. Matthew⁴, C. Challis⁵, I. Chapman², D. L. L. Elena⁶, F. Joanne², C. Giroud², J. Hobirk¹, E. Joffrin⁷, P. Lomas², C. Lowry⁸, G. Maddison², J. Mailloux², I. M. Ferreira Nunes⁹, F. Rimini², J. Simpson², A. Sips¹⁰, and H. Urano¹¹

¹Max-Planck-Institut für Plasmaphysik, Garching, Germany
 ²CCFE Fusion Association, Culham Science Centre, Abingdon, UK
 ³KTH Royal Institute of Technology, Stockholm, Sweden
 ⁴University of York, Heslington, UK
 ⁵JET-EFDA, Culham Science Centre, Abingdon, UK
 ⁶The National Fusion Laboratory, CIEMAT, Madrid, Spain
 ⁷CEA-IRFM, Saint Paul lez Durance, France
 ⁸European Commission, Brussels, Belgium
 ⁹Institute of Plasmas and Nuclear Fusion, Association EURATOM/IST, Lisbon, Portugal
 ¹CCFE Fusion Association, Culham Science Centre, Abingdon, UK
 ¹⁰JET-EFDA, Culham Science Centre, Abingdon, UK

Corresponding Author: C. Maggi, costanza.maggi@ipp.mpg.de

The pedestal confinement of JET-ILW H-modes is presented and their stability investigated in the framework of P-B stability and the predictive code EPED. The changes in wall composition from C to Be/W point to the possible role of neutral recycling, low-Z impurities and scrape-off-layer physics in pedestal stability, highlighting the need for refinement of models predicting the pedestal height. Local linear gyro-kinetic analysis of JET pedestals finds them stable against KBMs due to the large bootstrap current. p_{PED} increases rapidly with power and the pressure gradient is in agreement with limits set by finite-*n* P-B instabilities both at high and low β . In low- δ , low- β H-modes the energy confinement is reduced due to higher deuterium fuelling than in JET-C, to avoid high W influxes into the core plasma. Changes in deuterium recycling from JET-C to JET-ILW may also play a role in cooling the pedestal. When the effective recycling is reduced, good confinement can be recovered and the operation point is at the P-B stability boundary. In high- δ , low- β H-modes a further degradation in energy confinement is observed compared to JET-C, due to reduced $p_{\rm PED}$. The pedestal structure at the end of the ELM cycle varies from narrow and steep at low fuelling to wide and shallow at high fuelling, challenging the EPED model, which does not predict a variation in pedestal width at fixed p_{PED} . At low β , plasma shaping does not affect pedestal confinement. This is consistent with the P-B model, predicting little or no improvement in p_{PED} with δ at high collisionality, due to reduction in edge bootstrap current. In high- β hybrid H-modes p_{PED} is 30% higher than at low δ , increasing more rapidly with power. The reduction in energy confinement of low- β , high δ H-modes can be compensated by nitrogen seeding. The P-B stability at the end of the ELM cycle is resumed, with the increase in p_{PED} being due to broadening of the pedestal pressure width at constant gradient. The mechanism underlying this improvement in pedestal stability with nitrogen seeding is not yet understood and challenges current predictive pedestal models.

This work was supported by EURATOM and carried out within the framework of the European Fusion Development Agreement. The views and opinions expressed herein do not necessarily reflect those of the European Commission.

Preprint Slides

G. Matthews¹, G. Arnoux², J. W. Coenen³, B. Bazylev⁴, R. Dejarnac⁵, and R. Pitts⁶

¹JET-EFDA, Culham Science Centre, Abingdon, UK
 ²CCFE Fusion Association, Culham Science Centre, Abingdon, UK
 ³Forschungszentrum Jülich, Jülich, Germany
 ⁴Karlsruhe Institute of Technology, Germany
 ⁵Institute of Plasma Physics AS CR v.v.i., Prague, Czech Republic
 ⁶ITER Organization, Saint Paul lez Durance, France

Corresponding Author: G. Matthews, guy.matthews@ccfe.ac.uk

Our priority for the 2013 JET campaigns was to provide relevant data for the ITER decision on whether to initially install a full tungsten divertor rather than a design with carbon at the strike points. A key element of this was an experiment using a specially modified divertor module which was used to study the characteristics and impact of ELM induced melting of bulk tungsten on JET operation — JET is currently the only machine with ELMs large enough to perform such experiments. A series of discharges at 3 MA plasma current and 23 MW of input power were used and resulted in parallel power densities of $\sim 3 \, {\rm GW/m^2}$ during ELMs and $\sim 0.5 \, {\rm GW/m^2}$ between ELMs. A $\sim 2 \, {\rm mm}$ vertical step in a not normally used part of the divertor was exposed to this heat load for up to 1.5 s.

Melting was achieved in series of seven identical discharges and the depth of material moved or removed on each pulse was very reproducible, at least an order of magnitude less than would be expected from bulk tungsten melting and equivalent to $sim10 \ \mu m$ per ELM. Tungsten droplets formed and migrated along the exposed edge to the private region driven by $j \times B$ forces. The impact on main plasma was negligible with no disruptions. Small spikes in spectroscopic tungsten signals were observed and suggest occasional ejection of droplets with effective radii of at least 80 $\ \mu m$. The JET results provided very positive support for the ITER decision to start with an all-W divertor and provide a valuable benchmark for the transient induced melt layer models used by ITER. Significant progress has been made in reproducing the thermal and melt behaviour seen in JET using the MEMOS code.

This work, part-funded by the European Communities under the contract of Association between EURATOM/CCFE was carried out within the framework of the European Fusion Development Agreement. The views and opinions expressed herein do not necessarily reflect those of the European Commission or those of the European Commission or of the ITER Organization. This work was also part-funded by the RCUK Energy Programme under grant EP/I501045.

This work was supported by EURATOM and carried out within the framework of the European Fusion Development Agreement. The views and opinions expressed herein do not necessarily reflect those of the European Commission.

EX/4-1

Near-Field Physics of Lower-Hybrid Wave Coupling to Long-Pulse, High Temperature Plasmas in Tore Supra

M. Goniche¹, C. Klepper², E. H. Martin³, J. Hillairet¹, R. C. Isler², L. Colas¹, C. Bottereau¹, A. Ekedahl¹, J. Harris², D. L. Hillis², S. Panayotis¹, B. Pégourié¹, P. Lotte¹, and G. Colledani¹

> ¹CEA-IRFM, Saint Paul lez Durance, France ²Oak Ridge National Laboratory, Oak Ridge, TN, USA ³North Carolina State University, USA

Corresponding Author: M. Goniche, marc.goniche@cea.fr

Interaction of radio-frequency waves with the edge plasma of tokamaks from which the wave is launched is now well recognized for waves in the Ion Cyclotron Range of Frequency (ICRF) but also in the range of Lower Hybrid Current Drive (LHCD) frequencies. A dynamic Stark spectroscopic measurement was carried out near a Tore Supra LHCD antenna, demonstrating that indeed the electric field oscillating at 3.7 GHz, in the range of 1-2 kV/cm for high power (1-4 MW/antenna) experiments, could be measured with a reasonable accuracy in the vicinity of the antenna. The spectroscopic sightline was provided by an endoscope viewing a region around the left-hand side of the antenna, including the lateral protection limiter (LPL). $D-\beta$ spectral line profiles were measured and the data were fitted to an all orders spectral line profile model. The spatial region from which the light is mostly collected near the antenna, determined from simulation, has a typical radial extension of 6 cm from the LPL.

Experimental spectral profile of the D- β line fits very well the simulated profile only when a radial polarization of the electric field is considered, as expected when the slow wave penetrates more dense plasmas. This measurement has been performed on numerous Tore Supra pulses with power launched by the LHCD antenna varying between 0.1 MW and 3 MW. It is found a good quantitative agreement between measured and modeled ERF (from full-wave coupling modelling) as long as the power launched by the upper modules (half of the total power) exceeds 0.5 MW. Noticeably, when the most outer waveguides are switched off, the measured field does not vary significantly as would be expected from the model. This unexpected result is thought to be the consequence of the bending of the rays during the propagation, with those originating from the outer waveguides evading the main emission region.

ЕΧ

Preprint Slides

Fuel Retention and Erosion of Metallic Plasma-Facing Materials under the Influence of Plasma Impurities

A. Kreter¹, L. Buzi¹, G. De Temmerman², T. Dittmar¹, R. Doerner³, C. Linsmeier¹, D. Nishijima³, M. Reinhart¹, and B. Unterberg¹

¹Forschungszentrum Jülich, Jülich, Germany ²FOM Institute DIFFER, Association EURATOM-FOM, Nieuwegein, The Netherlands ³University of California San Diego, CA, USA

Corresponding Author: A. Kreter, a.kreter@fz-juelich.de

The fuel retention and the lifetime of plasma-facing components are critical factors potentially limiting the availability of a magnetic fusion reactor. It is necessary to test how plasma-facing materials perform with respect to hydrogen retention and erosion under the realistic mixed species plasma conditions including impurities like helium and argon. This contribution summarizes the experimental studies on the linear plasma devices PSI-2, Magnum-PSI, and PISCES-B. Both plasma-facing materials foreseeing for ITER, tungsten and beryllium, were investigated. Aluminium was tested as a potential surrogate for toxic beryllium for plasma-material interaction studies. The fraction of helium or argon added to deuterium plasma was in a range of \sim 1–10%. Typical exposure parameters were an electron density of $\sim 10^{18}$ - 10^{19} m⁻³ for PSI-2 and PISCES-B and $\sim 10^{19}$ - 10^{20} m⁻³ for Magnum-PSI, an electron temperature of ~10 eV, an ion flux to the target of ~ 10^{22} – 10^{23} m⁻²s⁻¹ for PSI-2 and PISCES-B and $\sim 10^{23}$ – 10^{24} m⁻²s⁻¹ for Magnum-PSI, an incident ion energy of \sim 10–100 eV and a sample temperature of 400-1000 K. In pure deuterium plasmas the deuterium retention was higher at the lower flux for sample temperatures of 530 and 630 K. At 870 K, the deuterium retention was found to be higher at the high flux. Blisters of about 40–50 nm size were formed in the high flux exposures, while no blistering was observed at the low flux. The influence of helium and argon on the deuterium retention in tungsten was investigated in PSI-2. For a sample temperature of 380 K and a fluence of 10^{26} m⁻², the retention dropped by a factor of three to 1×10^{20} m⁻² when 5% helium was added to deuterium plasma. The addition of argon did not significantly affect the total deuterium retention. A comparison of beryllium and aluminium with respect to the deuterium retention and erosion properties was performed in PISCES-B and PSI-2. In general, aluminium exhibited similar phenomena to beryllium with respect to the evolution of the surface morphology and sputtering when exposed to deuterium and mixed deuterium-argon and deuterium-helium plasmas. However, the TDS characteristics of the aluminium targets indicated different deuterium retention mechanisms than in beryllium.

An ITPA Joint Experiment to Study Runaway Electron Generation and Suppression

R. Granetz¹, B. Esposito², J. Kim³, H. R. Koslowski⁴, M. Lehnen⁵, J. R. Martin-Solis⁶, C. Paz-Soldan⁷, T.-N. Rhee³, P. de Vries⁵, J. Wesley⁷, and L. Zeng⁸

¹Massachusetts Institute of Technology, Plasma Science & Fusion Center, Cambridge, MA, USA ²Associazione EURATOM-ENEA Unitá Tecnica Fusione, Frascati, Italy ³National Fusion Research Institute, Daejeon, Korea, Republic of ⁴Forschungszentrum Jülich, Jülich, Germany ⁵ITER Organization, Saint Paul lez Durance, France ⁶Universidad Carlos III de Madrid, Madrid, Spain ⁷General Atomics, San Diego, CA, USA ⁸Institute of Plasma Physics, Chinese Academy of Sciences, Hefei, China

Corresponding Author: R. Granetz, granetz@mit.edu

Results from an ITPA joint study of the threshold conditions for runaway electron (RE) generation suggest that suppression of RE's during disruptions on ITER could be less demanding than currently envisioned. In this study of quiescent, non-disrupting discharges, it is found that generating and maintaining measurable RE's is more difficult than predicted by collisional damping only, indicating that additional loss mechanisms may play a significant role in the dynamics of RE formation and decay. If this result also holds true during disruptions, which seems likely, then mitigation of RE's would not require fueling to the extremely high 'Rosenbluth' density. A study to compare empirical RE threshold conditions to Connor-Hastie (C-H) is being carried out by the ITPA MHD group. In order to obtain well-documented, reproducible results, the study is concentrating on RE's produced during quiescent, flattop conditions, when V_{loop} and n_e can be accurately measured. RE threshold data from a number of tokamaks (DIII-D, TEXTOR, FTU, KSTAR, C-MOD, JET so far), indicate that E-fields well in excess of C-H, or conversely, densities well below C-H are required for the detection of RE's, implying that other loss mechanisms in addition to collisional drag may be playing an important role. An alternative to the threshold method, involving the characterisation of the RE growth and decay rates at different densities after the RE's have formed, also supports the finding that other loss mechanisms in addition to collisional drag are playing an important role. Clear opportunities for involvement by the theory community will be stressed, including understanding the nature of non-collisional RE energy and particle loss mechanisms, and how these would scale from the quiescent flattop conditions in this study to the disruption conditions in ITER.

Paper

Slides

EX/5-2

Runaway Electron Generation with the ITER-like Wall and Efficiency of Massive Gas Injection at JET

C. Reux¹, V. V. Plyusnin², R. Koslowski³, B. Alper⁴, D. Alves², B. Bazylev⁵, E. Belonohy⁴, S. Brezinsek³, J. Decker¹, S. Devaux⁴, P. Drewelow⁶, P. de Vries⁷, A. Fil¹, S. Gerasimov⁴, L. Giacomelli⁴, I. Lupelli⁴, S. Jachmich⁸, V. Kiptily⁴, U. Kruezi⁴, M. Lehnen⁷, A. Manzanares⁹, J. Mlynář¹⁰, E. Nardon¹, E. Nilsson¹, V. Riccardo⁴, F. Saint-Laurent¹, and C. Sozzi¹¹

¹CEA-IRFM, Saint Paul lez Durance, France ²Institute of Plasmas and Nuclear Fusion, Association EURATOM/IST, Lisbon, Portugal ³Forschungszentrum Jülich, Jülich, Germany ⁴JET-EFDA, Culham Science Centre, Abingdon, UK ⁵Karlsruhe Institute of Technology, Germany ⁶Max-Planck-Institut für Plasmaphysik, Greifswald, Germany ⁷ITER Organization, Saint Paul lez Durance, France ⁸Laboratory for Plasma Physics, ERM/KMS, Brussels, Belgium ⁹The National Fusion Laboratory, CIEMAT, Madrid, Spain ¹⁰Institute of Plasma Physics AS CR v.v.i., Prague, Czech Republic ¹¹Istituto di Fisica del Plasma CNR, Euratom-ENEA-CNR Association, Milano, Italy

Corresponding Author: C. Reux, cedric.reux@cea.fr

Disruptions are a major concern for next generation tokamaks, including ITER. These MHD instabilities lead to the loss of the plasma thermal energy and current on the millisecond timescale. Large electric fields created by the plasma current quench can accelerate several MA of runaway electrons (RE) up to 20 MeV. The influence of the full-metal IET ITER-Like Wall (IET-ILW) on RE is thus a key question for future all-metal PFC machines. Experiments at JET have shown that even though RE are very rare in spontaneous disruptions, they can still be generated during disruptions with fast current quenches induced by argon massive gas injections. The operational domain where runaways appear under those conditions is similar to what it was in carbon wall (JET-C). Hard X-ray spectra show energies up to 10 MeV. Although the boundary location is similar, the runaway generation might be larger in JET-ILW than JET-C inside the domain with higher currents in JET-ILW with like-tolike plasma parameters. Temperatures of up to 900°C have been observed on PFC following beam impact. Disruptions can also generate excessive heat loads on plasma facing components (PFC) and electromagnetic forces in the machine structures due to halo and eddy currents. Massive Gas Injection (MGI) is presently one of the most promising techniques to mitigate both these effects by radiating away the plasma energy. However, the fraction of energy radiated by MGI at high plasma thermal content as well as the radiation peaking are key questions to ensure good extrapolability of the method to larger tokamaks. Recent experiments at JET-ILW have confirmed that the fraction of the total energy radiated decreases with increasing thermal energy content down to 70% for 10%/90% D₂/Ar mixtures. Injections on plasmas with or without a locked mode already present also show different radiation peaking pattern. This suggests that toroidal asymmetries might be strong in case of injections in an already developing disruption.



Novel Approaches for Mitigating Runaway Electrons and Plasma Disruptions in Tokamak ADITYA

R. L. Tanna¹, J. Ghosh¹, P. Chattopadhyay¹, P. Dhyani¹, J. Raval¹, S. Purohit¹, S. Joisa¹, C. Rao¹, V. Panchal¹, D. Raju¹, K. Jadeja¹, S. Bhatt¹, C. Gupta¹, C. Chavda¹, S. Kulkarni¹, B. Shukla¹, E. V. Praveenlal¹, A. Amardas¹, P. Atrey¹, U. Dhobi¹, R. Manchanda¹, N. Ramaiya¹, N. Patel¹, M. B. Chowdhuri¹, S. K. Jha¹, R. Jha¹, A. Sen¹, Y. C. Saxena¹, and D. Bora¹

¹Institute for Plasma Research, Bhat, Gandhinagar, India

Corresponding Author: R. L. Tanna, rakesh@ipr.res.in

ADITYA tokamak is engaged in carrying out several dedicated experiments on runaway mitigation, disruption control, etc., which are of utmost importance for the successful operation of large size tokamaks, such as ITER. Runaway electron generation and mitigation remains challenging topic in the present tokamak research, as these high-energetic electrons can cause severe damage to the vacuum vessel of any tokamak if left uncontrolled. An innovative mechanism has been developed in ADITYA tokamak to mitigate the runaway electrons before they can gain high energies. A localized vertical magnetic field perturbation is applied at one toroidal location to extract runaway electrons. During the start-up phase, ~ 260 G of perturbation field caused significant reduction in initial runaway electron energies. The applied local vertical field perturbation acts like an error field for the high energetic runaway electrons.

Disruptions: rapid events in which large fractions of the plasma thermal energy is lost, must be avoided for successful operation of a fusion reactor. Disruptions, induced by hydrogen gas puffing, are successfully mitigated by two innovative techniques in the ADITYA tokamak. These experiments led to better understanding of the disruption control mechanisms and also can be thought of as one of options for disruption control in ITER. We have demonstrated that (1) a bias electrode placed inside the LCFS of ADITYA tokamak can mitigate disruptions and (2) applying an ICRH pulse with power ~ 50 to 70 kW can also mitigate the disruption successfully. In both the cases the physical mechanism seems to be the control of MHD modes with induced poloidal rotation of edge plasma due to the generated radial electric fields. Real time control of disruptions from ADITYA tokamak, a significant types of spontaneous and deliberately-triggered disruptions from ADITYA tokamak, a significant contribution has been made to the international disruption database (ITPA). Apart from these several other experiments regarding low loop voltage start-up and current ramp-up have been carried out using ECRH and ICRH. The details of experimental results along with data analysis procedures and plausible mechanisms of different events will be presented in this paper.



Heavy Impurity Transport in the Core of JET Plasmas

M. Valisa¹, C. Angioni², P. Mantica³, T. Pütterich², M. Baruzzo¹, P. da Silva Aresta Belo⁴,
 E. A. Belli⁵, F. Casson⁶, I. Coffey⁷, P. Drewelow⁸, C. Giroud⁶, N. Hawkes⁶, T. Hender⁶,
 T. Koskela⁹, E. Lerche¹⁰, L. Lauro Taroni⁶, C. Maggi², J. Mlynář¹¹, M. O'Mullane¹²,
 M. E. Puiatti¹, M. Reinke¹³, and M. Romanelli⁶

¹Consorzio RFX, Associazione Euratom-ENEA sulla Fusione, Padova, Italy
 ²Max-Planck-Institut für Plasmaphysik, Garching, Germany
 ³Istituto di Fisica del Plasma CNR, Euratom-ENEA-CNR Association, Milano, Italy
 ⁴JET-EFDA, Culham Science Centre, Abingdon, UK
 ⁵General Atomics, San Diego, CA, USA
 ⁶CCFE Fusion Association, Culham Science Centre, Abingdon, UK
 ⁷Queen's University, Belfast, UK
 ⁸Max-Planck-Institut für Plasmaphysik, Greifswald, Germany
 ⁹Aalto University, Espoo, Finland
 ¹⁰Laboratory for Plasma Physics, ERM/KMS, Brussels, Belgium
 ¹¹Institute of Plasma Physics AS CR v.v.i., Prague, Czech Republic
 ¹²Department of Physics, University of Strathclyde, Glasgow UK
 ¹³University of York, Heslington, UK

Corresponding Author: M. Valisa, valisa@igi.cnr.it

In the context of the investigations on JET of the effects of an ITER-like wall on the plasma performance, this contribution presents a comprehensive picture of the W transport in the core of JET H-mode plasmas with up to 2.5 MA of plasma current, based on a successful agreement between experiment, interpretative simulations and theoretical predictions. The main outcome is that W is particularly sensitive to neoclassical transport, which is affected by any type of poloidal asymmetry and in particular largely enhanced by centrifugal effects. In presence of peaked density profiles and insufficiently peaked ion temperature profiles, the neoclassic inward pinch leads to W accumulation in the core and in extreme cases to a premature discharge termination. Only around mid-radius, turbulent outward convection competes with neoclassical transport. MHD activity may hamper or speed up the accumulation process depending on circumstances. The path towards W accumulation is described in details for a representative 2 MA hybrid discharge in which the W behavior follows closely the evolution of the electron density profile. Neoclassical and linear gyro-kinetic calculations of W transport closely reproduce both a 2D interpretive W density diagnostics based on the tomographic inversions of SXR signals and the interpretive simulations of a 1D impurity transport code (JETTO/SANCO). Ion Cyclotron Resonance Heating in the plasma center flattens the electron density profile and peaks the ion temperature profile and represents a means to reverse the neoclassical convection. Evidence of such flow reversal has been obtained by injecting Mo and analyzing the transient behavior of the impurity, which allows the deconvolution of convective and diffusive transport terms. This confirms analogous results of impurity out-flushing by central ICRH found in other experiments and in JET plasmas with carbon wall.

This work was supported by EURATOM and carried out within the framework of the European Fusion Development Agreement. The views and opinions expressed herein do not necessarily reflect those of the European Commission.



gyrokinetic (GK) calculations.

ΕX

Response of Ion and Electron Temperatures, Electron Density and Toroidal Rotation to Electron Cyclotron Heating in JT-60U

M. Yoshida¹, M. Honda¹, M. Nakata¹, H. Urano¹, T. Kobayashi¹, N. Miyato¹, H. Takenaga¹, S. Ide¹, and Y. Kamada¹

¹ Japan Atomic Energy Agency, Naka, Japan

Corresponding Author: M. Yoshida, yoshida.maiko@jaea.go.jp

Temporal and spatial responses of the electron and ion temperatures (T_e and T_i), the electron density (n_e), and the toroidal rotation velocity ($V\varphi$) with electron cyclotron heating (ECH) have been clarified for the first time with fast measurements in positive shear (PS) H-mode plasmas, weak shear (WS) plasmas with internal transport barriers (ITBs) and reversed shear (RS) plasmas with ITBs on JT-60U. We have found that: (i) Ion temperature inside the steep T_i gradient decreases with ECH after the T_e increase in PS and WS plasmas. The T_i reduction can be avoided with a large $V\varphi$ shear ($dV\varphi/dr$) that easily forms in RS plasmas. (ii) Electron density with peaked n_e profile decreases with ECH after the T_e increase. (iii) Counter intrinsic rotation is generated after the T_e increase and increases with the T_e increase. Time scale of the $V\varphi$ change is much longer than that of the T_e increase. The observations in the n_{e_r} T_i and $V\varphi$ in PS plasmas are consistently explained by theoretical models and

EX/6-3

Toroidal Rotation Profile Structure in L- and H-Mode KSTAR Plasmas

Y. Shi¹, S. Ko¹, J. Kwon¹, W.-H. Ko¹, P. H. Diamond^{1,2}, S. Yi¹, K. Ida³, K.-D. Lee¹, J. Jeong¹, S.-H. Seo¹, S.-H. Hahn¹, S. Yoon¹, S. G. Lee¹, Y.-S. Bae¹, M. Bitter⁴, K. Hill⁴, and G. Yun⁵

 ¹National Fusion Research Institute, Daejeon, Korea, Republic of ²University of California San Diego, CA, USA ³National Institute for Fusion Science, Toki, Japan ⁴Princeton Plasma Physics Laboratory, Princeton, NJ, USA
 ⁵Pohang University of Science and Technology (POSTECH), Korea, Republic of

Corresponding Author: Y. Shi, yjshi@nfri.re.kr

We report the results of L- and H-mode toroidal rotation experiments in KSTAR. Both NBI and ECH with varying resonance conditions were used for the heating mix and turbulence population control. The experimental results show that ECH causes a counter-current rotation increment both in L- and H-mode plasmas. In the H-mode case, the rotation profiles are flattened by on-axis ECH with a clear pivot point inside the pedestal and on-axis ECH can produce larger counter-current rotation than the off-axis ECH. There is no pivot point observed in rotation profiles for ECH in L-mode plasma. These KSTAR results suggest that toroidal rotation profiles are determined by an interplay of i) a co-current NBI torque; ii) a pedestal intrinsic torque, which is notable in H-mode plasma and insignificant in L-mode plasma; iii) a core intrinsic torque, which can become counter-current with ECH. We hypothesize here that the change of the core intrinsic torque with ECH is due to a transition from a state of ITG turbulence to CTEM turbulence, and thus a change in the sign of the turbulencedriven residual stress. For H-mode plasma, linear gyrokinetic analyses suggest that the steepening of ∇T_e and density peaking are two important mechanism for ITG \rightarrow TEM transition. For L-mode plasmas, gyrokinetic analyses indicate that off-axis ECH causes the excitation of TEM at r/a = 0.5, while on-axis ECH can excite TEM at core region only (r/a = 0.25). TEM at r/a = 0.5 is stronger than TEM at r/a = 0.25 within the framework of linear growth rate. This stronger TEM excitation in the off-axis ECH can be understood as a consequence of increased trapped particle population as the ECH resonance location moves to radially outward direction. The momentum transport coefficients, i.e., diffusivity and convection velocity were investigated with modulation ECH experiments in KSTAR. An inward pinch was found with the perturbation method. More detailed gyrokinetic analysis of micro-instabilities will be presented for varying ECH deposition locations and target plasmas. Also, we will perform nonlinear gyrokinetic simulations to calculate T_e fluctuation spectra and compare them with ECEI fluctuation measurements. Combining transport analysis and the nonlinear simulations, we will identify the role of the non-diffusive stress component in the formation of global rotation profile.



Interaction between Neoclassical Tearing Modes and Non-Local Transport in HL-2A

X. Ji¹, Y. Liu¹, Q. Yang¹, Z. Shi¹, B. Feng¹, L. Wei², Z. Wang², M. Jiang¹, Y. Xu¹, T. Sun¹, Y. B. Dong¹, W. Deng¹, and B. Yuan¹

¹Southwestern Institute of Physics, Chengdu, Sichuan, China ²Dalian University of Technology, Liaoning, China

Corresponding Author: X. Ji, jixq@swip.ac.cn

Scaling laws for the prediction of neoclassical tearing modes (NTMs) onset in next generation fusion devices such as ITER have been carried out. However, it is difficult to extrapolate current island width thresholds for the NTM onset to ITER due to the uncertainty physics behind the threshold mechanisms. And some events can also influence the mode onset, such as the large sawtooth period and pellet injection. In the HL-2A tokamak, NTMs driven unstable by the transient perturbation of local electron temperature induced by non-local transport (NLT) phenomenon have been observed in low- β plasmas for the first time. In HL-2A, the onset of m/n = 3/2 NTMs during NLT phenomenon induced by supersonic molecular beam injection (SMBI) has been observed in low- β plasmas with electron cyclotron resonance heating (ECRH). The inversion surface of electron temperature perturbation (δ Te) due to NLT effect is near the q = 3/2 surface, which is determined by the peak of 3/2 mode amplitudes measured by the ECE diagnostics. Compared with 3/2 NTMs triggered by sawtooth activities in HL-2A, the transient perturbation of local T_e gradient induced by non-local effect plays a crucial role on changing NTM threshold, which dramatically reduces the critical β -onset of 3/2 NTMs. In spontaneous 3/2 NTMs without detected core and edge MHD instabilities are observed during strong NLT effect. After the onset of NTM during NLT phenomenon induced by SMBI, additional molecular beam pulses are injected to study the interaction of magnetic islands with NLT effect. The non-local effect still exists with the small 3/2 island, island width $w3/2/a \sim 0.06$. In the case of large 2/1magnetic islands, $w2/1/a \sim 0.15$, the effect of NLT is almost suppressed. By the way, the collapse of the central electron temperature with an increase in the edge electron temperature is observed.



Slides

Paper

Partial Detachment of High Power Discharges in ASDEX Upgrade

A. Kallenbach¹, M. Bernert¹, L. Casali¹, L. Giannone¹, M. Maraschek¹, S. Potzel¹, F. Reimold¹, J. Schweinzer¹, and G. Tardini¹

¹Max-Planck-Institut für Plasmaphysik, Garching, Germany

Corresponding Author: A. Kallenbach, arne.kallenbach@ipp.mpg.de

To ensure a sufficient divertor lifetime ITER and a future DEMO reactor will operate under at least partial detachment (PD). PD is defined as a significant reduction of heat flux and pressure along field lines between mid-plane and divertor target for the first few power decay lengths in the scrapeoff layer. For PD conditions in ASDEX Upgrade (AUG) the peak heatflux in the divertor is below 5 MW/m². Strong divertor radiation will be required to achieve PD at reactor relevant power fluxes $P_{sep}/R = 15$ MW/m, given by the condition $P_{sep}/P_{LH} > 1.5-2$ for the achievement of good H-mode performance. While ITER can accept only low core radiation levels, the high core power flux in DEMO has to be removed to a large extent by core radiation for the avoidance of divertor power overload. Partial detachment in high power AUG discharges is achieved by double feedback of core and divertor radiation with Ar or Kr as core radiating species and N as divertor radiator. A high neutral divertor pressure is generally required to achieve PD, which is invoked by the combination of radiative losses and momentum loss processes like charge exchange and recombination. So far AUG has achieved 50% of the foreseen ITER performance in terms of P_{sep}/R under PD conditions and up to 70% core main chamber radiated power fraction. The total heating power was up to 23 MW in these experiments. A further enhancement is expected due to a recent optimization of power supplies, enabling a higher maximum heating power, and a switch for reducing the cryo pumping speed, enabling a higher divertor neutral pressure.

The paper will report recent achievements, describe technical solutions for PD control and address the rise in pedestal and core electron density, which is routinely observed under PD conditions in AUG.

Impurity Seeding on JET to Achieve Power Plant like Divertor Conditions

C. Lowry¹, M. Wischmeier², A. Huber³, C. Maggi², K. McCormick², M. Reinke⁴, P. Drewelow², S. Brezinsek⁵, L. Aho-Mantila⁶, G. Arnoux⁷, A. Sips⁸, A. Meigs⁸, G. Sergienko³, M. F. Nave⁹, S. Devaux⁸, S. Marsen², and M. Stamp⁸

¹European Commission, Brussels, Belgium
 ²Max-Planck-Institut für Plasmaphysik, Garching, Germany
 ³Institute of Energy and Climate Research, Forschungszentrum Jülich, Jülich, Germany
 ⁴Oak Ridge Institute for Science Eduction, Oak Ridge, TN, USA
 ⁵Forschungszentrum Jülich, Jülich, Germany
 ⁶VTT Technical Research Centre of Finland, Finland
 ⁷CCFE Fusion Association, Culham Science Centre, Abingdon, UK
 ⁸JET-EFDA, Culham Science Centre, Abingdon, UK

⁹Institute of Plasmas and Nuclear Fusion, Association EURATOM/IST, Lisbon, Portugal

Corresponding Author: C. Lowry, christopher.lowry@jet.efda.org

Power exhaust is recognised to be one of the major challenges to achieving power generation by magnetically confined thermonuclear fusion. In order to reduce the power density conducted to the divertor targets to a level that can be tolerated by available technologies it will be necessary to radiate close to 100% of the exhaust power. Although it is foreseen that a significant fraction of this radiation will be from within the separatrix, H-mode confinement requires the threshold power to be radiated from the scrape-off layer and divertor. Such high radiation levels necessarily require detachment of the divertor plasma, a regime which to present has not been convincingly modelled by state of the art boundary codes. It is therefore essential that relevant experimental results are used to justify the existence and practicality of such a solution. The main challenges and uncertainties of a highly radiating solution are: whether the required edge radiation levels and distribution can be achieved, along with acceptable core dilution; understanding the exact requirements to achieve H-mode confinement; and establishing the overall thermal stability. JET with its all-metal wall and the absence of an intrinsic edge and divertor radiator is particularly suited to investigating these issues, and targeted experiments began in 2013. At varying input power levels feed-forward impurity seeding of neon, nitrogen, and argon, has been used in moderately fuelled low triangularity vertical target configuration plasmas to push to the maximum achievable radiation levels. At present, only up to 75% radiated power fraction has been achieved for nitrogen seeded plasmas with ~ 20 MW of input power. It has not yet been determined whether this is the limit, but the increase in radiation fraction becomes an increasingly weak function of the seeding rate as the rate increases. Slightly lower maximum radiation levels were achieved with neon and argon (63% and 70%), and the details of the radiation distribution and its dynamics were markedly different. The results of these experiments and the implications for a power plant will be discussed in this paper.

This work was supported by EURATOM and carried out within the framework of the European Fusion Development Agreement. The views and opinions expressed herein do not necessarily reflect those of the European Commission.

EX/7-3

Slides

Paper

Progress of High-Performance Steady-State Plasma and Critical PWI Issue in LHD

H. Kasahara¹, Y. Yoshimura¹, K. Nagasaki², M. Tokitani¹, N. Ashikawa¹, Y. Ueda³, G. Motojima¹, M. Shoji¹, T. Seki¹, K. Saito¹, R. Seki¹, S. Kamio¹, G. Nomura¹, S. Kubo¹, T. Shimozuma¹, H. Igami¹, H. Takahashi¹, S. Ito¹, S. Masuzaki¹, H. Tanaka¹, J. Miyazawa¹, H. Tsuchiya¹, N. Tamura¹, K. Tanaka¹, T. Tokuzawa¹, and T. Mutoh¹

¹National Institute for Fusion Science, Toki, Japan ²Institute of Advanced Energy, Kyoto University, Kyoto, Japan ³Osaka University, Osaka, Japan

Corresponding Author: H. Kasahara, kasahara.hiroshi@lhd.nifs.ac.jp

An ultra-long-pulse plasma with a duration time of 48 min, a line-averaged electron density of 1.2×10^{19} m⁻³, and electron and ion temperatures (T_e , T_i) of 2 keV has been achieved by the averaged heating power ($P_{\rm ECH+ICH}$) of 1.2 MW for helium plasma. The heating energy injected into plasma reached 3.36 GJ, which is a new world record in toroidal plasmas. Three types of ICRF antennas were installed at different toroidal sections in order to avoid local hot spots around each ICRF antenna. In the ultra-long pulse plasma, the spike frequency of the line intensity for the carbon spectrum began to increase after 600 s, and the divertor temperature was almost saturated at 460°C. Many flashes are observed with a monitor TV camera which views mostly outside of LCFS and the divertor region. Both the frequency and intensity are increased as the discharge time goes on, which suggest that large sizes of carbon mixed-material layers on divertor region (domes and divertor plates) are ejected into the plasma.

A large amount of mixed-material layers, consisting mainly of carbon (> 90%) and iron impurities, are formed over a wide surface area of the plasma facing surface (PFS). Carbon impurity originally from the divertor region and iron impurity from the first wall by physical sputtering are deposited on the PFS. Comparing the mixed-material layers on divertor region with deposition layer on the stainless steel specimen installed at the equivalent position of the first wall surface with the expose time of ~ 1000 s for steady-state discharges, these composition were consistent with each other. Since such layers are hard and brittle, deposition layers are easily removed as a flake. Plasma termination may be caused by exfoliation of the mixed-material layers.

The mixed-material deposition layer can easily retain helium particles, and these trapped particles are released even below 400 K. The amount of trapped particles in it is proportional to the thickness of the mixed-material layers. Since such amount of He trapped particles was 100 times as large as that of plasma and neutral particles in the vacuum vessel, the release of He could not be negligible in wall-temperature increasing phase. Control of the growth rate of mixed-material layers will be critical issue in steady-state devices and long-term plasma operation such as a fusion reactor.



Developing Physics Basis for the Radiative Snowflake Divertor at DIII-D

V. Soukhanovskii¹, S. L. Allen¹, M. E. Fenstermacher¹, D. Hill¹, C. J. Lasnier¹, M. A. Makowski¹, A. G. McLean¹, W. H. Meyer¹, D. Ryutov¹, E. Kolemen², R. Groebner³, A. W. Hyatt³, *A. W. Leonard*³, T. H. Osborne³, T. W. Petrie³, J. A. Boedo⁴, and

J. G. Watkins⁵

¹Lawrence Livermore National Laboratory, Livermore, CA, USA
 ²Princeton Plasma Physics Laboratory, Princeton, NJ, USA
 ³General Atomics, San Diego, CA, USA
 ⁴University of California San Diego, CA, USA
 ⁵Sandia National Laboratories, Livermore, CA, USA

Corresponding Author: V. Soukhanovskii, vlad@llnl.gov

Recent DIII-D results using the snowflake (SF) divertor configuration demonstrate that the SF geometry enables significant manipulation of divertor heat transport for power spreading in attached and radiative divertor regimes, between and during edge localized modes (ELMs), while maintaining good H-mode confinement. Enhanced heat transport through the low poloidal field null-point region and divertor legs resulting in increased scrape-off layer (SOL) width and heat flux spreading over additional strike points (SPs) were observed. Direct measurements of divertor null-region poloidal β , using a unique DIII-D divertor Thomson scattering diagnostic, support the theoretically proposed mechanism of additional heat redistribution between strike points due to fast convection, especially efficient during ELMs. The measured divertor $\beta_p \sim 50\text{--}100$ was about 2–3 orders of magnitude higher the midplane β_p , and the high- β region was broader in the SF configuration. During an ELM, the β_p was increased up to an order of magnitude. Type I ELM heat transport was significantly affected by the SF divertor geometry. While the pealing-ballooning mode stability in the H-mode discharges was not significantly affected, the ELM frequency and size were changed by 10%-20%. The stored energy lost per ELM was reduced. In gas-seeded radiative regimes, SF geometry led to a significant reduction of peak heat fluxes between and during ELMs, while maintaining good H-mode performance. The results complement the initial NSTX and DIII-D SF divertor studies and contribute to the physics basis of the SF divertor as a promising concept for high power density tokamaks.

This work was performed under the auspices of the US Department of Energy by LLNL under DE-AC52-07NA27344.

EX/8-1

Slides

Paper

Simultaneous Measurement of the ELMs at Both High and Low Field Sides and ELM Dynamics in ELM Crash-Free Period in KSTAR

H. Park¹, M. Choi², M. Kim², J. Lee², W. Lee², J. Lee², G. Yun², Y. Jeon³, S. Lee³, S. Yoon³, C. Domier⁴, N. C. Luhmann, Jr.⁴, and X. Xu⁵

¹Ulsan National Institute of Science and Technology, Korea, Republic of
 ²Pohang University of Science and Technology (POSTECH), Korea, Republic of
 ³National Fusion Research Institute, Daejeon, Korea, Republic of
 ⁴University of California Davis, CA, USA
 ⁵Lawrence Livermore National Laboratory, Livermore, CA, USA

Corresponding Author: H. Park, hyeonpark@unist.ac.kr

Following successful characterization of the growth, saturation and bursting process of the Edge Localized Mode (ELM) by a 2D/3D Electron Cyclotron Emission Imaging (ECEI) system in KSTAR H-mode plasmas, the observed mode structure is verified via synthetic image reconstruction based on the BOUT++ code. In successive KSTAR campaigns, a wide range of toroidal mode numbers (~ 4 < n <~ 16) of the ELMs have enabled the establishment of the relationship between the poloidal and toroidal mode numbers (m, n) through the local magnetic shear (safety factor - q) (< m >= nq). ELM dynamics observed simultaneously at both high and low field sides revealed necessity of the Pfirsh-Schlüter flow, shear suppression of high n modes and inconsistency in mode numbers suggested further study. In KSTAR campaigns, Magnetic Perturbation (MP) coils with n = 1 and n = 2 structures successfully suppressed the ELMs. In the ELM suppressed period, persisting mode structures accompanied with weak bursting behaviours were observed.

Progress in Preparing Scenarios for ITER Operation

A. Sips^{1,2}, G. Giruzzi³, S. Ide⁴, C. Kessel⁵, T. C. Luce⁶, J. Snipes⁷, and J. Stober⁸

¹JET-EFDA, Culham Science Centre, Abingdon, UK
 ²European Commission, Brussels, Belgium
 ³CEA-IRFM, Saint Paul lez Durance, France
 ⁴Japan Atomic Energy Agency, Naka, Japan
 ⁵Princeton Plasma Physics Laboratory, Princeton, NJ, USA
 ⁶General Atomics, San Diego, CA, USA
 ⁷ITER Organization, Saint Paul lez Durance, France
 ⁸Max-Planck-Institut für Plasmaphysik, Garching, Germany

Corresponding Author: A. Sips, george.sips@jet.efda.org

In recent years, dedicated experiments and coordinated scenario simulations, initiated by the Integrated Operation Scenarios Topical Group of the ITPA, have significantly advanced the preparation of ITER operation. This contribution will review the progress made.

Plasma formation studies report robust plasma breakdown in devices with metal walls over a wide range of conditions, while other experiments use an inclined EC launch angle at plasma formation to mimic the conditions in ITER. For H-modes at $q_{95} \sim 3$ many experiments have demonstrated operation with scaled parameters for the ITER baseline scenario at $n_e/n_{GW} \sim 0.85$. Most experiments, however, obtain stable discharges at $H_{98}(y, 2) \sim 1.0$ only for $\beta_N = 2.0$ –2.2. During the current rise, a range of plasma inductance (li(3)) can be obtained from 0.65 to 1.0, with the lowest values obtained in H-mode operation. For the rampdown, the plasma should stay diverted and maintain H-mode. For an ohmic rampdown a reduction of the elongation from 1.85 to 1.4 would minimise the increase in plasma inductance from 0.8 to 1.3–1.4.

Simulations show that the proposed rampup and rampdown schemes developed since 2007 are compatible with the present ITER design for the poloidal field coils. ITER scenario preparation in hydrogen and helium requires high input power (> 50 MW). H-mode operation in helium may be possible at input powers above 35 MW at a toroidal field of 2.65 T, for studying H-modes and ELM mitigation. In hydrogen, H-mode operation is expected to be marginal, even at 2.65 T with 60 MW of input power. For a hybrid scenario at 12 MA the code simulations give a range for Q = 6.5–8.3, using 30 MW NBI and 20 MW ICRH. For non-inductive operation at 7–9 MA the simulation results show more variation. At high edge pedestal pressure ($T_{ped} \sim 7$ keV) the codes predict Q = 3.3–3.8 using 33 MW NB, 20 MW EC, and 20 MW IC. Simulations using a lower edge pedestal temperature (~ 3 keV) but improved core confinement obtain Q = 5–6.5, when ECCD is concentrated at mid-radius and ~ 20 MW off-axis current drive (ECCD or LHCD) is added.

This work was supported by EURATOM and carried out within the framework of the European Fusion Development Agreement. The views and opinions expressed herein do not necessarily reflect those of the European Commission.



ЕΧ

Compatibility of High Performance Operation with JET ILW

I. M. Ferreira Nunes¹, P. Lomas², M. Baruzzo³, M. Beurskens², C. Challis², L. Frassinetti⁴, J. Hobirk⁵, E. Joffrin⁶, C. Lowry⁷, F. Rimini², A. Sips⁸, and I. Voitsekhovitch²

¹Institute of Plasmas and Nuclear Fusion, Association EURATOM/IST, Lisbon, Portugal ²CCFE Fusion Association, Culham Science Centre, Abingdon, UK ³Associazione EURATOM-ENEA Unitá Tecnica Fusione, Frascati, Italy ⁴KTH Royal Institute of Technology, Stockholm, Sweden ⁵Max-Planck-Institut für Plasmaphysik, Garching, Germany ⁶CEA-IRFM, Saint Paul lez Durance, France ⁷European Commission, Brussels, Belgium ⁸JET-EFDA, Culham Science Centre, Abingdon, UK

Corresponding Author: I. M. Ferreira Nunes, isabel.nunes@jet.efda.org

As reported in the FEC 2012, operation with a Be/W wall at JET has had an impact on plasma confinement and scenario development relative to the carbon wall. The main differences observed were a degradation of confinement for low β_N scenarios (typically $H_{98} \sim 0.8$) and W accumulation in the plasma core at low fuelling gas. In order to develop high performance plasmas in DD and ultimately in DT, subsequent effort has been focused on understanding and improving the energy confinement, control of W accumulation in the core and robustness of the scenarios against disruptions. To achieve high performance, a high- β_N scenario with $H_{98} \sim 1.3$, safety factor of 3.6–4, $\beta_N > 2.5$ and tailored q profile and a low β_N scenario, $H_{98} \sim 1$, safety factor of 2.6–3, $\beta_N \sim 1.8$ –2 with fully diffused current profile are being developed. These scenarios operate at plasma currents up to 4.5 MA and toroidal magnetic fields up to 3.8 T. Both scenarios achieve similar values of neutron yield, although the high β_N scenario achieves it at lower plasma current values in quasi-stationary plasmas. To improve confinement whilst controlling the W accumulation, gas fuelling, ICRH for central heating, position of the strike points and increase of additional power are used. Divertor heat load control is obtained by either sweeping the strike points or by impurity injection. Cooling by N_2 has been demonstrated and scenarios with Ne or Ar injection are being developed. Disruption forces are approximately a factor two larger than with a JET-C wall and the use of massive gas injection has proven effective in mitigating forces and avoiding melting. The confinement studies will be extended to high plasma current and performance in terms of edge pedestal parameters, β_N and power above the power threshold for the L-H transition and compared to previous results in JET-C and previous ρ^* scaling. Extrapolations to DT will be presented.

This work was supported by EURATOM and carried out within the framework of the European Fusion Development Agreement. IST activities also received financial support from "Fundação para a Ciência e Tecnologia" through project Pest-OE/SADG/LA0010/2013. The views and opinions expressed herein do not necessarily reflect those of the European Commission.



Improved Confinement in JET High Beta Plasmas with an **ITER-like Wall**

C. Challis¹, J. Garcia², M. Beurskens¹, P. Buratti³, L. Frassinetti⁴, C. Giroud¹, N. Hawkes¹, J. Hobirk⁵, E. Joffrin², D. Keeling¹, D. King¹, C. Marchetto³, J. Mailloux¹, D. McDonald⁶, I. M. Ferreira Nunes⁷, G. Pucella³, S. Saarelma¹, and J. Simpson¹

> ¹CCFE Fusion Association, Culham Science Centre, Abingdon, UK ²CEA-IRFM, Saint Paul lez Durance, France ³Associazione EURATOM-ENEA Unitá Tecnica Fusione, Frascati, Italy ⁴VR, Fusion Plasma Physics, KTH Royal Institute of Technology, Stockholm, Sweden ⁵Max-Planck-Institut für Plasmaphysik, Garching, Germany ⁶EFDA CSU Garching, Germany

⁷Institute of Plasmas and Nuclear Fusion, Association EURATOM/IST, Lisbon, Portugal

Corresponding Author: C. Challis, clive.challis@ccfe.ac.uk

The replacement of the JET carbon wall (C-wall) by a Be/W ITER-like wall (ILW) has affected plasma confinement by the direct effect of wall materials on key plasma parameters and by the impact of operational techniques necessary to avoid damage to plasma facing components. To investigate the effect of changing wall materials on energy confinement scaling, experiments have been performed with both the C-wall and ILW to vary the heating power over a wide range with two different plasma shapes, spanning the β_N domain between the ITER baseline ELMy H-mode (β_N less than 2) and hybrid plasmas (β_N up to 3). With the ILW the power degradation of thermal energy confinement was found to be weak; much weaker than the IPB98(y, 2) scaling. This is consistent with the observation of higher H_{98} in the hybrid domain (typically 1.2–1.3 at β_N close to 3) compared with baseline plasmas (typically 0.7–1.0 with $\beta_N = 1.5$ –2.0) seen in the wider JET database. This weak power degradation of confinement, which was also seen in the C-wall experiments at low triangularity, is mainly due to increased edge pedestal pressure and core density peaking at high power. By contrast, the high triangularity C-wall plasmas exhibited elevated H_{98} over a wide power range with strong, IPB98(y, 2)like, power degradation. This strong power degradation of confinement appears to be linked to an increase in the source of neutral particles from the wall as the power increased. The loss of the improved confinement domain at low power with the ILW may be partly due to operational factors such as higher gas fuelling and increased distance between the outer divertor strike-point and the cryopump. But plasma radiation from the plasma core was also higher with the ILW, and other experiments with nitrogen seeding suggest that plasma composition may also play a role. The results presented in this paper show that the choice of wall materials can strongly affect core plasma performance, even changing confinement scalings that are relied upon for extrapolation to future devices.

This work was part-funded by the RCUK Energy Programme and by EURATOM and carried out within the framework of the European Fusion Development Agreement. The views and opinions expressed herein do not necessarily reflect those of the European Commission

ΕX

Slides

Paper

Development of the Q=10 Scenario for ITER on ASDEX Upgrade (AUG)

J. Schweinzer¹, V. Bobkov¹, R. Dux¹, A. Kallenbach¹, P. Lang¹, T. Pütterich¹, F. Ryter¹, J. Stober¹, and H. Zohm¹

¹*Max-Planck-Institut für Plasmaphysik, Garching, Germany*

Corresponding Author: J. Schweinzer, josef.schweinzer@ipp.mpg.de

In ITER, H-mode operation at 15 MA and q = 3 is planned to achieve 500 MW fusion power at Q = 10 in D-T-mixtures. This so-called ITER baseline (BL) scenario is characterized by normalized parameters for plasma density $f_{GW} = 0.85$, energy confinement H = 1 and $\beta_N = 1.8$. A high triangularity shape has been identified to be best suited to combine high density operation with good H-mode confinement.

Demonstration of this scenario in AUG requires central wave-heating to avoid core tungsten impurity accumulation. This boundary condition limits the possible values for plasma-current and magnetic field to two practical combinations for q = 3 plasmas on AUG: (i) operation at 1.1 MA/1.8 T using ECRH in X3 mode and (ii) 1.2 MA/2 T using ICRH from two antennas with boron-coated protection limiter tiles. Such AUG discharges have been explored and stationary behaviour has been obtained. Normalized parameters for confinement and density come simultaneously close to the target values of 1 and 0.85, respectively, as long as β_N stays at values 20% above the ITER target of 1.8. However, in the fully shaped flattop ELM-frequencies of 10–25 Hz are typical as well as ELM-energies of 100–200 kJ which cause significant losses of 15–25% of the stored energy. The observed large ELMs are intolerable in view of ITER. Therefore, three methods for ELM mitigation were tried: (i) ELM pace making with pellets of different mass and frequency injected from the HFS, (ii) application of magnetic perturbation coils and (iii) nitrogen seeding. Although these methods have been successfully applied to other AUG scenarios, so far, none of these three methods led to a breakthrough in the ITER BL demonstration discharges. Since the operation at q = 3 and $\beta_N < 2$ turned out to be difficult in particular with respect to the ELM behaviour, the idea came up to explore H-modes at lower plasma current and higher safety factor which still fulfill the requirement of Q = 10.

This paper will discuss the present status of ITER BL demonstration plasmas on AUG based on the 2012/13 data and will include the latest results of the 2014 AUG campaign which will focus on the extension of the operational space of ELM mitigation techniques as well as on a slight shift of the scenario's operational point towards a potential less 'difficult corner' at 20% lower plasma-current and thus higher safety-factor.

ΕX

A Long-Pulse H-Mode Regime with a New Coherent Mode Providing Continuous Transport across Pedestal in EAST

G. Xu¹, H. Wang¹, S. Ding¹, B. Wan¹, H. Guo¹, X. Xu², E. Wang², R. Bravenec³, Y. Xiao⁴, and J. Li¹

¹Institute of Plasma Physics, Chinese Academy of Sciences, Hefei, China
 ²Lawrence Livermore National Laboratory, Livermore, CA, USA
 ³Fourth State Research, Austin, TX, USA
 ⁴Institute for Fusion Theory and Simulation, Zhejiang University, China

Corresponding Author: G. Xu, gsxu@ipp.ac.cn

A long-pulse H-mode regime with a record pulse length over 30 s has been achieved in the EAST superconducting tokamak, sustained by RF heating and current drive with advanced lithium wall coating, exhibiting a good global confinement quality with $H_{98}(y, 2) \sim 0.9$. The H-mode plasmas are either ELM-free or mixed with irregular small ELMs. A new electrostatic edge coherent mode (ECM) is present continuously throughout the long-pulse H-mode discharges in the steep-gradient pedestal region, near the local electron diamagnetic frequency (20-90 kHz), propagating in the electron diamagnetic drift direction in the plasma frame. A significant fraction of the particle and heat exhaust across the pedestal is driven by the ECM, as demonstrated, for the first time, by direct probing the ECM-driven radial fluxes inside the separatrix using a new diamond-coated reciprocating probe array, which is essential for achieving steady state without large ELMs. In addition, the 2D structures of the ECM were examined with a unique, newly developed dual gas puff imaging (GPI) system, which has two view areas, up-down symmetrically about the midplane, showing strongly tilted ballooning mode structure and a poloidal wavelength of ~ 8 cm, corresponding to a poloidal mode number m > 50 and a toroidal mode number n = 16–19. The ECM is a predominantly electrostatic mode with rather small magnetic component, $\delta B/B_p \sim 1 \times 10^{-4}$, as detected by small magnetic coils mounted on the reciprocating probe at the ECM location. Simulations have been performed using GYRO eigenvalue solver and GS2 initial value code in a flux tube domain near the peak gradient region of the EAST pedestal, which indicate that the dissipative trapped electron mode (DTEM) is the dominant mode with characteristics consistent with those of the ECM. Preliminary results from GTC simulation also indicate that TEM is the most unstable mode under these circumstances. In addition, the ECM has been observed with the central-line-averaged density, $n_e = 1.9-5 \times 10^{19} \text{ m}^{-3}$ $(n_e/n_{GW} = 0.28$ -0.7) in the experiments, corresponding to a collisionality, $\nu_e^* = 0.5$ -5, evaluated at the top of pedestal, which is the same collisionality range where DTEM is active. These results may open a new avenue towards steady-state H-mode operations with a stationary pedestal as maintained by benign electrostatic microinstabilities rather than large ELMs.

166

EX/10-1

Preprint Slides

Alfvén Eigenmodes Can Limit Access to High Fusion Gain, Steady-State Tokamak Operation

W. W. Heidbrink¹, J. Ferron², C. T. Holcomb³, M. Podestá⁴, and M. Van Zeeland²

¹University of California Irvine, CA, USA ²General Atomics, San Diego, CA, USA ³Lawrence Livermore National Laboratory, Livermore, CA, USA ⁴Princeton Plasma Physics Laboratory, Princeton, NJ, USA

Corresponding Author: W. W. Heidbrink, heidbrink@fusion.gat.com

Experiments on the DIII-D tokamak show that Alfvén eigenmode (AE) activity degrades fast-ion confinement in many high β_N , high q_{min} , steady-state scenario discharges (β_N is the normalized plasma pressure and q_{min} is the minimum value of the safety factor). An extensive set of diagnostics measure degraded fast-ion confinement: neutron detectors, fast-ion D_{α} (FIDA) spectrometers, neutralparticle analyzers, and fast-ion pressure and current profiles inferred from the equilibrium. All fast-ion diagnostics that are sensitive to the co-passing population exhibit reductions relative to classical predictions. The increased fast-ion transport in discharges with strong AE activity accounts quantitatively for the previously observed [1] reduction in global confinement with increasing q_{min} ; however, not all high q_{min} discharges show appreciable degradation. In current ramp plasmas, stochastic transport by multiple resonances with many small-amplitude AEs causes "stiff" fast-ion transport; as a result, the achieved fast-ion profile is insensitive to the beam-deposition profile [2]. We postulate that a similar process often occurs in steady-state scenario plasmas. Initial linear stability calculations predict unstable toroidal AEs for these conditions; comparisons with critical-gradient models are underway. If AE degradation of fast-ion confinement can be avoided, modeling indicates that a discharge scenario with $q_{min} > 2$ can provide the MHD stability and bootstrap fraction required for high fusion gain, steady-state operation. The broad current and pressure profiles consistent with elevated q_{min} enable stable operation at reactor-relevant $\beta_N \sim 5$. One-dimensional modeling shows that these conditions are attainable in DIII-D using practical neutral-beam and electron-cyclotron current drive sources and that a self-consistent fully noninductive scenario exists. The challenge in future work is to incorporate calculations of AE-induced transport into the analysis.

This work was supported by the US Department of Energy under SC-G903402 and DE-FC02-04ER54698.

References

[1] J.R. Ferron, et al., Phys. Plasmas 20, 092504 (2013).

[2] W.W. Heidbrink, et al., Nucl. Fusion 53, 093006 (2013).



Fast Ion Transport during Applied 3D Magnetic Perturbations on DIII-D

M. Van Zeeland¹, N. M. Ferraro¹, W. W. Heidbrink², G. J. Kramer³, D. C. Pace¹, S. L. Allen⁴, X. Chen², T. E. Evans¹, B. Grierson³, M. García-Muñoz⁵, J. Hanson⁶, M. J. Lanctot¹, L. Lao¹, C. J. Lasnier⁴, R. Moyer⁷, R. Nazikian³, D. M. Orlov⁷, and J.-K. Park³

> ¹General Atomics, San Diego, CA, USA ²University of California Irvine, CA, USA ³Princeton Plasma Physics Laboratory, Princeton, NJ, USA ⁴Lawrence Livermore National Laboratory, Livermore, CA, USA ⁵Max-Planck-Institut für Plasmaphysik, Garching, Germany ⁶Columbia University, New York, USA ⁷University of California San Diego, CA, USA

Corresponding Author: M. Van Zeeland, vanzeeland@fusion.gat.com

Pitch angle and energy resolved measurements as well as wide field-of-view infrared imaging show fast ion losses correlated with applied 3D fields in DIII-D plasmas. In L-mode discharges with slowly rotating n = 2 magnetic perturbations, 3D field induced fast ion loss signals from separate scintillator detectors (FILDs), near and well below the plasma midplane, are observed to decay within one poloidal transit time after beam turn-off indicating they are predominantly prompt loss orbits. Beam deposition and full orbit modeling of these losses, both to the FILDs and wall, using M3D-C1 calculations of the perturbed kinetic profiles and fields reproduce many features of the measured losses. In particular, the predicted phase of the modulated loss signal with respect to the I-coil currents is in close agreement with FILD measurements as is the relative amplitudes of the modulated losses for the different beams used. Measurements and modeling indicate total prompt loss to the wall increases with application of the n = 2 perturbations by up to 7%, in these discharges, with the exact level depending on the phase of the applied 3D field. Modeling also shows negligible impact on the overall confined fast ion profile in these discharges, however, it is found that localized regions of velocity space can resonate with the applied fields leading to large changes in toroidal canonical angular momentum — something potentially useful as an EP control tool. Initial application of these tools to RMP ELM suppressed H-mode plasmas show that the applied fields induce a large loss of fast ions (10%-20% of injection rate for half-energy beam ions) from the edge of the plasma and that the magnitude of the loss depends significantly on the model of the perturbed magnetic field. Calculations including the plasma response to the non-axisymmetric fields show up to a factor of two enhancement of the losses relative to those with vacuum n = 3 fields alone.

This work was supported in part by the US Department of Energy under DE-FC02-04ER54698, SC-G903402, DE-AC02-09CH11466, DE-AC52-07NA27344, DE-FG0204ER54761, and DE-FG02-07ER54917.

ЕΧ

Preprint Slides

Indication of Bulk-Ion Heating by Energetic Particle Driven Geodesic Acoustic Modes on LHD

M. Osakabe¹, T. Ido¹, K. Ogawa¹, A. Shimizu¹, M. Yokoyama¹, R. Seki¹, C. Suzuki¹, M. Isobe¹, K. Toi¹, D. Spong², K. Nagaoka¹, Y. Takeiri¹, H. Igami¹, T. Seki¹, and K. Nagasaki³

> ¹National Institute for Fusion Science, Toki, Japan ²Oak Ridge National Laboratory, Oak Ridge, TN, USA ³Institute of Advanced Energy, Kyoto University, Kyoto, Japan

Corresponding Author: M. Osakabe, osa@nifs.ac.jp

Heating of bulk-ions by waves excited by energetic particles, such as fusion born alphas, was pointed out in the past theoretically [1], but none of the experimental results related on this phenomena was reported. This is the first report of experimental results indicating the increases of ion temperatures with Energetic-particle driven Geodesic Acoustic Mode (EGAM) excitation.

On the Large Helical Device (LHD), ion temperature increase, which was evaluated from the low energy neutral spectra, was observed with excitation of the EGAM for the first time. This phenomenon was observed when the high energy Neutral Beam (NB) of ~ 170 keV was injected into very low density plasmas below $\sim 1 \times 10^{18}$ m⁻³ sustained by Electron Cyclotron Heating (ECH). In IAEA-FEC 2012, the excitation of the instability and its identification as GAM were reported. In this report several possible mechanisms to explain this phenomenon were discussed, i.e., (1) change of measured ion spectra due to the orbit topology change, (2) increase of classical ion heating power by energetic particles, (3) enhancement of energy confinement properties and (4) enhanced ion heating by the EGAM. Among them, it was found that the enhanced ion heating by the mode activity was the most probable mechanism for this phenomenon. In addition to the analyses, increase of effective ion temperatures was correlated with the time integrated power of the mode amplitude. These analysis suggests the existence of a new energy channel of bulk-ion heating by energetic particles through the EGAM [2].

References

[1] N. J. Fisch and M. C. Herrmann, Nucl. Fusion 34 (1994) 1541.

[2] M. Sasaki, K. Itoh, and S. Itoh, Plasma Phys. and Control. Fusion 53 (2011) 085017.



Effects of MHD Instabilities on Neutral Beam Current Drive

M. Podestá¹, M. Gorelenkova¹, R. B. White¹, D. Darrow¹, E. Fredrickson¹, S. Gerhardt¹, and *W. W. Heidbrink*²

¹Princeton Plasma Physics Laboratory, Princeton, NJ, USA ²University of California Irvine, CA, USA

Corresponding Author: M. Podestá, mpodesta@pppl.gov

Neutral beam injection (NBI) is one of the primary tools foreseen for heating, current drive (CD) and *q*-profile control in future fusion reactors such as ITER and a Fusion Nuclear Science Facility. However, fast ions from NBI may also provide the drive for energetic particle-driven instabilities (e.g., Alfvénic modes — AEs), which in turn redistribute fast ions in both space and energy, thus affecting the control capabilities and overall efficiency of NB-driven current. Based on experiments on the NSTX tokamak, the effects of AEs and other low-frequency MHD instabilities on NB current drive efficiency are investigated. It is found that instabilities do indeed reduce the NB-driven current density over most of the plasma radius by up to 50%. Experimental results are then used to benchmark numerical tools to simulate NB-CD in the presence of instabilities. A new fast ion transport model, which accounts for particle's transport in phase space as required for resonant AE perturbations, is developed for the tokamak transport code TRANSP and utilized to obtain consistent simulations of NB-CD. Predictions for the NSTX-Upgrade device, which features a new set of off-axis NB injectors, are finally discussed for projected scenarios with different levels of MHD activity.



Slides

Paper

Experimental Turbulence Studies for Gyro-Kinetic Code Validation Using Advanced Microwave Diagnostics

U. Stroth¹

¹*Max-Planck-Institut für Plasmaphysik, Garching, Germany* Corresponding Author: U. Stroth, stroth@ipp.mpg.de

Turbulent transport remains one of the most important and challenging topics in fusion research. Scientific understanding of the related physical processes can only be enhanced through a close comparison of numerical simulations with experimental data. Microwave-based diagnostics represent almost the sole experimental approach capable of capturing plasma parameter fluctuations with the required spatio-temporal resolution. This contribution reports on an extensive international effort undertaken on the devices ASDEX Upgrade, TCV, Tore-Supra and W7-X to measure simultaneously a large spectrum of fluctuation parameters to achieve a comprehensive comparison with theoretical models and advanced numerical turbulence simulations. An overview is given of the work, which is coordinated by the Virtual Institute on Plasma Dynamical Processes and Turbulence Studies using Advanced Microwave Diagnostics including first results and advanced hardware developments relevant for reflectometry on future devices such as ITER and DEMO.

In the present campaign a full suite of new reflectometers is available on ASDEX Upgrade. The paper summarises the results achieved: Scale-resolved radial turbulence levels in H-mode discharges were measured and compared to GENE simulations in the transition range from ion-temperature-gradient to trapped-electron-mode turbulence. A correlation Doppler reflectometer is used for measuring the GAM structure in discharges where poloidal flow damping was varied by means of variations of the shape of the poloidal plasma cross-section and the isotope mass; results are compared with NEMORB simulations. A 2D correlation reflectometer is used to investigate the spatial structure of turbulent fluctuations and to address questions related to turbulence anisotropy and systematic eddy tilting in the flow-shear layers at the plasma edge. The aspects of turbulence spreading and non-local transport in response of local changes in density and temperature gradients are studied during phases with L-H transitions and power modulation by means of radial correlation measurements and an ultra-fast reflectometer, capable of scanning a large radial sector of the plasma within less than 2 μ s. Furthermore, reflectometery solutions using advanced hard-ware components without moving parts will be presented, for monitoring plasmas in the harsh environment of fusion reactors.

The Isotope Effect in GAM – Turbulence Interplay and Anomalous Transport in Tokamak

A. Gurchenko¹, E. Gusakov¹, A. Altukhov¹, L. Esipov¹, D. Kouprienko¹, M. Kantor¹, S. Lashkul¹, S. Leerink², P. Niskala², and A. Perevalov¹

¹Ioffe Physical-Technical Institute of the Russian Academy of Science, St. Petersburg, Russian Federation ²Aalto University, Espoo, Finland

Corresponding Author: A. Gurchenko, temp777ab@mail.ru

The interaction between large-scale mean $E \times B$ flows, geodesic acoustic modes (GAM) and small-scale drift-wave turbulence has been an important area of experimental research for anomalous transport of energy and particles in toroidal plasmas during the last decade utilizing more and more sophisticated tools. In this paper, results of investigation of the interplay of GAMs and broadband drift wave turbulence of different spatial scales performed in the FT-2 tokamak by the enhanced scattering (ES), Doppler reflectometry and standard reflectometry as well as by global gyrokinetic modeling are presented.

The turbulence and GAMs local properties were investigated in hydrogen and deuterium regimes. A number of important effects indicating the role of turbulence in GAM excitation, GAMs role in transport phenomena and the mechanism GAMs control the turbulence and transport are presented and discussed. A systematically larger level of GAMs amplitude in deuterium regime in comparison with hydrogen accompanied by smaller level of the electron thermal diffusivity became the striking example of the isotope effect. The weak influence of the GAM intermittency was observed both in H and D regimes in the small-scale turbulence radial wave number spectra obtained by correlative ES diagnostic. On contrary, a strong modulation of the large-scale turbulence level at the GAM frequency was found for the first time by cross-method utilizing both ES and reflectometry techniques. The modulation of the total reflectometric power and corresponding turbulence level by GAM was observed in the GAM frequency is also studied using the FT-2 global gyrokinetic modeling by ELMFIRE code.

ΕX

Density Fluctuations as an Intrinsic Mechanism to Keep Self-Consistent Shape of Pressure Profile

Paper

Slides

EX/11-2Rb

V. Vershkov¹, D. Shelukhin¹, G. Subbotin¹, A. Y. Dnestrovskij¹, A. Danilov¹, E. Gorbunov¹, D. Sergeev¹, S. Krylov¹, T. Myalton¹, D. Ryjakov¹, Y. Skosyrev¹, V. Trukhin¹, V. Chistiakov¹, and G. Okulov¹

¹National Research Centre "Kurchatov Institute", Moscow, Russian Federation Corresponding Author: V. Vershkov, v.vershkov@fc.iterru.ru

The paper presents new insight into previous and new experimental data of the turbulent density fluctuations behavior in T-10 OH and ECRH discharges. The experiments showed existence of the same maximal peaked pressure profile in both OH and ECRH tokamak plasmas as well as strong deterioration of particle confinement after plasma reach this profile (fast density decay in OH, "density pump out" in ECRH). Maximal peaking could be achieved either by flat density and peaked temperature or vice versa. Minimal turbulence level does not depend on heating power and observed when pressure profile is slightly wider than the extreme one. The density fluctuations did not significantly contribute to the heat transport but determined particle fluxes to maintain the pressure profile.



Mechanism of Low-Intermediate-High Confinement Transitions in Tokamaks

J. Dong¹, J. Cheng¹, L. Yan¹, Z. He¹, K. Itoh², H. Xie³, Y. Xiao³, K. Zhao¹, W. Hong¹, Z. Huang¹, L. Nie¹, S. Itoh⁴, W. Zhong¹, D. Yu¹, X. Ji¹, Y. Huang¹, X. Song¹, Q. Yang¹, X. Ding¹, X. Zou⁵, X. Duan¹, and Y. Liu¹

¹Southwestern Institute of Physics, Chengdu, Sichuan, China
 ²National Institute for Fusion Science, Toki, Japan
 ³Institute for Fusion Theory and Simulation, Zhejiang University, China
 ⁴Institute for Applied Mechanics, Kyushu University, Kasuga, Japan
 ⁵CEA-IRFM, Saint Paul lez Durance, France

Corresponding Author: J. Dong, jiaqi@swip.ac.cn

Understanding the physics mechanism of low-high (L-H) confinement transitions in toroidal plasmas is essential for ensuring heating power requirements for future fusion reactors. Early experiments show that plasma may enter an intermediate phase (I-phase) with limit cycle oscillations (LCOs) of plasma parameters and pass through a slow L-H transition if heating power is close to the H-mode threshold. The triggering mechanism and conditions for L-I and I-H transitions are foci in the H-mode physics studies. Two theoretical models of LCOs were proposed and shown consistent with recent experimental observations, respectively. Here, we first report a discovery of two types of LCOs (type-Y and type-J, respectively) on HL-2A tokamak, which provides an opportunity to advance our understanding of LCO physics, and then discuss the L-I-H transition triggering mechanisms and conditions. The dynamics of the two types of LCOs observed in the experiment are analyzed in detail. Two loops of zonal flow versus turbulence and turbulence versus pressure gradient are proposed for the two types of LCOs. The conditions for the observed I-H transitions are identified to be (1) the I-phase has type-J LCOs, (2) the plasma pressure gradient scale length L_{pe} is less than a critical value (1.7 cm, here) and the $E \times B$ flow shearing rate is higher than a critical value (10⁶ s⁻¹, here), and (3) the growth rate of the diamagnetic drift flow γ_{DD} is equal to or higher than the ion-ion collision frequency ν_{ii} . Detailed observations, revealing L-I-H transition mechanism, will be presented.

ЕΧ

Preprint Slides

First Direct Evidence of Turbulence-Driven Ion Flow Triggering the L- to H-Mode Transition

L. Schmitz¹, B. Grierson², L. Zeng¹, J. A. Boedo¹, T. L. Rhodes¹, Z. Yan³, G. R. McKee³, D. Eldon⁴, C. Chrystal⁴, P. H. Diamond⁴, W. A. Peebles¹, G. Tynan⁴, R. Groebner⁵, K. H. Burrell⁵, C. C. Petty⁵, E. J. Doyle¹, and G. Wang¹

> ¹University of California Los Angeles, CA, USA ²Princeton Plasma Physics Laboratory, Princeton, NJ, USA ³University of Wisconsin-Madison, Madison, WI, USA ⁴University of California San Diego, CA, USA ⁵General Atomics, San Diego, CA, USA

Corresponding Author: L. Schmitz, lschmitz@ucla.edu

Developing a physics-based model of the L-H transition is critical for confidently extrapolating the auxiliary heating requirements for ITER from the existing empirical L-H transition power threshold scaling. For the first time, it is shown here that the initial turbulence collapse preceding the L-H transition is caused by turbulence-generated (positive) $E \times B$ flow opposing the equilibrium (L-mode) edge plasma $E \times B$ flow related to the edge pressure gradient. Recent main ion CER measurements in Helium plasmas provide strong evidence of concomitant turbulence-driven main ion poloidal flow $\nu_i \Theta$. Near the power threshold, the transition dynamics is substantially expanded/slowed via limit cycle oscillations (LCO) between the turbulence intensity and the $E \times B$ velocity, allowing profile and flow measurements with unprecedented spatial and temporal resolution. During the LCO, $\nu_i \Theta$ lags the density fluctuation level \tilde{n} , consistent with energy transfer from the turbulence spectrum via the perpendicular Reynolds stress. As the LCO evolves, the periodic reduction of edge turbulence and transport subsequently enables a periodic increase in the edge pressure gradient and equilibrium $E \times B$ flow, reducing the LCO frequency and eventually securing the transition to H-mode.

A two-predator, one prey model, similar to a previously developed model [1] but in contrast retaining opposite polarity of the turbulence-driven and pressure-gradient-driven $E \times B$ flow, captures essential aspects of the transition dynamics, including the phasing of \tilde{n} , $\nu_i \Theta$ and $vE \times B$. The interpretation advanced here explains several unresolved experimental observations, including the counter-clockwise (\tilde{n} , E_r) limit cycle observed in the outer shear layer in DIII-D, and JFT-2M (consistent only with positive $E \times B$ flow drive). A positive electric field transient concomitant with initial turbulence suppression, has been demonstrated across a range in plasma density, heating power, and q_{95} , during "fast" L-H transitions and during extended LCO transitions. The evolution of turbulence-driven and pressure-gradient driven flow is shown to depend on plasma density and q_{95} ; implications for the density/collisionality scaling of the L-H transition power threshold will be discussed.

This work was supported by the US DOE under DE-FG0208ER54984, DE-FG03-01ER54615 and DE-FC02-04ER54698.

References

[1] Miki, Diamond, Phys. Plasmas 19, 092306 (2012).

Global Gyrokinetic Modeling of Geodesic Acoustic Modes and Shear Alfvén Instabilities in ASDEX Upgrade

A. Biancalani¹, A. Bottino¹, P. Lauber¹, D. Zarzoso¹, G. Conway¹, X. Wang¹, P. Simon¹, B. Scott¹, C. Di Troia², S. Briguglio², G. Vlad², and F. Zonca²

¹Max-Planck-Institut für Plasmaphysik, Garching, Germany ²Associazione EURATOM-ENEA Unitá Tecnica Fusione, Frascati, Italy

Corresponding Author: A. Biancalani, biancalani@ipp.mpg.de

In this work, we investigate theoretically the dynamics of global instabilities observed in AS-DEX Upgrade (AUG) by means of collisionless numerical simulations. We focus in particular on geodesic acoustic modes (GAM) and shear Alfvén instabilities. The numerical tools we use are the codes NEMORB (nonlinear global gyrokinetic PIC), LIGKA (linear global gyrokinetic) and XHMGC (nonlinear global hybrid). In the first part of this work, results of axisymmetric simulations of GAMs with gyrokinetic codes NEMORB and LIGKA with AUG equilibrium profiles are shown. In the second part, we show results of axisymmetric electromagnetic simulations with NEMORB and LIGKA in the presence of an EP population. Finally, in the third part, we show results of single-*n* (with *n* the toroidal mode number) numerical simulations of shear Alfvén instabilities with NEMORB, LIGKA and XHMGC. Comparisons with analytical theory and experimental data are also shown, for each case of interest.



Radial Electric Field and Poloidal Impurity Asymmetries in the Pedestal of ASDEX Upgrade: Quantitative Comparisons between Experiment and Theory

E. Viezzer¹, T. Pütterich¹, E. Fable¹, A. Bergmann¹, R. Dux¹, R. McDermott¹, C. Angioni¹, M. Cavedon¹, R. M. Churchill², M. G. Dunne¹, B. Lipschultz³, U. Stroth¹, E. Wolfrum¹, and ASDEX Upgrade Team¹

¹Max-Planck-Institut für Plasmaphysik, Garching, Germany ²Massachusetts Institute of Technology, Plasma Science & Fusion Center, Cambridge, MA, USA ³University of York, Heslington, UK

Corresponding Author: E. Viezzer, eleonora.viezzer@ipp.mpg.de

The formation of the H-mode transport barrier is strongly connected to the existence of a sheared plasma flow perpendicular to the magnetic field caused by a local radial electric field E_r . The strong gradients in E_r and the associated $E \times B$ velocity shear play a fundamental role in edge turbulence suppression, transport barrier formation and the transition to the H-mode. This contribution describes the nature and structure of the E_r well and its connection to H-mode confinement and discusses the impact of poloidal impurity asymmetries on the pedestal.

A detailed analysis of the edge E_r and kinetic profiles revealed that in H-mode E_r and the main ion pressure gradient term, $\nabla p_i/en_i$, are identical within the uncertainties. This relation corresponds to the cancellation of the poloidal components of the ion diamagnetic and $E \times B$ drifts and suggests that in the pedestal the perpendicular main ion flow is close to zero. This result is confirmed by direct measurements of the main ion temperature, density and flow velocities in helium plasmas. The main ion poloidal rotation exhibits very small values at the plasma edge, as expected from neoclassical theory. The edge poloidal flow measurements of both main ions and impurities have been compared to a hierarchy of neoclassical models. In all cases, the measurements are found to be in quantitative agreement with neoclassical theory demonstrating that in the pedestal the E_r well is sustained by the gradients of the main ion species.

New charge exchange measurements at ASDEX Upgrade reveal the existence of a poloidal asymmetry in the flow pattern at the pedestal. The flow asymmetry can be explained by an excess of impurity density at the high-field side following the postulate of divergence-free flows on a flux surface. Comparison of the measured flows to theoretical predictions based on the parallel momentum balance reveals the nature of the parallel impurity dynamics. The key features of the experimental data including the shape of the rotation profiles and the poloidal impurity density asymmetry are reproduced quantitatively for the first time. The impact of these findings with respect to impurity transport at the plasma edge are presented.

This project has received funding from the EURATOM research and training programme 2014–2018.



EX/P1-20

Experimental Quantification of the Impact of Large and Small Scale Instabilities on Confined Fast Ions in ASDEX Upgrade

B. Geiger¹, I. Classen², M. García-Muñoz¹, C. Hopf¹, P. Lauber¹, S. Nielsen³, M. Reich¹, F. Ryter¹, P. A. Schneider¹, M. Schneiller¹, G. Tardini¹, M. Weiland¹, and M. Salewski³

¹Max-Planck-Institut für Plasmaphysik, Garching, Germany ²FOM Institute DIFFER, Association EURATOM-FOM, Nieuwegein, The Netherlands ³Technical University of Denmark, Roskilde, Denmark

Corresponding Author: B. Geiger, benedikt.geiger@ipp.mpg.de

The transport of fast, suprathermal ions as generated by neutral beam injection (NBI) is an important topic in fusion research. In unperturbed plasmas the fast-ion transport is expected to be neoclassical, i.e., dominated by collisions, while an anomalous transport is observed in the presence of instabilities. This anomalous fast-ion redistribution must be investigated in detail because it may limit the heating and current drive performance in future fusion devices and could even damage the first wall. At the ASDEX Upgrade tokamak, fast ions are generated by up to eight different NBI sources and their distribution function can be measured by a comprehensive set of diagnostics: A multi-view fast-ion D-alpha (FIDA) spectroscopy diagnostic, neutral particle analyzers, neutron measurements and fast-ion loss detectors (FILD) permit studies in velocity space and real space. A reduction of the central fast-ion density of up to 50% has been measured in experiments with strong sawtooth activity. Outside the q = 1 surface, a corresponding increase is observed while the FILDs show no significant fast-ion redistribution to unconfined orbits. Simulations that assume flux aligned transport can explain the radial shape of this measured internal fast-ion redistribution well, but they underestimate its magnitude which could be explained by $E \times B$ drifts. Measurements during strong activity of reversed shear Alfvén eigenmodes (RSAE) show significant differences to neoclassical predictions. The observed radial fast-ion profiles are strongly flattened and broadened compared to the predictions. Non-linear simulations of the RSAE-induced fast-ion transport using the HAGIS/LIGKA code will be compared with the experimental data. In MHD-quiescent plasmas, a clear change of the radial fast-ion profiles is measured when replacing on-axis NBI with off-axis NBI. Neoclassical predictions are in very good agreement with this observation while simulations that assume an anomalous transport of $0.5 \text{ m}^2/\text{s}$ do not fit the experimental data. This is, however, in contradiction with previous off-axis NBI current drive experiments that related the absence of a measurable fast-ion driven current to a turbulence-induced fast-ion redistribution. New off-axis NBI current drive experiments are, hence, being conducted to resolve this contradiction and the results of this investigation will be discussed.

Preprint

Identification of Intrinsic Torques in ASDEX Upgrade H-Mode Plasmas

T. Tala¹, R. McDermott², A. Salmi¹, C. Angioni², T. Odstrcil², T. Pütterich², F. Ryter², W. Solomon³, G. Tardini², and E. Viezzer²

¹VTT Technical Research Centre of Finland, Finland ²Max-Planck-Institut für Plasmaphysik, Garching, Germany ³General Atomics, San Diego, CA, USA

Corresponding Author: T. Tala, tuomas.tala@vtt.fi

Tala

Previous work performed has amassed a substantial database of intrinsic rotation measurements in various tokamak devices. However, as our understanding of momentum transport has evolved, it has become clear that a reliable prediction of the rotation in future devices requires a more complete momentum transport model and a more fundamental understanding of the mechanisms driving the intrinsic rotation. Initial estimates from this database project a large intrinsic velocity (~ 300 km/s) for ITER. The next step in intrinsic rotation studies is to characterize the "intrinsic torque" associated with its generation. The primary goal of this paper is to clarify whether or not the edge localized intrinsic torque scales with the pedestal strength on the ASDEX-Upgrade tokamak. In the q-profile scan resulting effectively in a pedestal strength scan (factor of 2–3 variation in pedestal top values of T_i , T_e and n_e), the integrated intrinsic torque profiles show clearly that the intrinsic torque increases with increasing plasma current on the outer half of the plasma radius. All the cases at different currents have in common that the intrinsic torque has a rather broad profile with the main contribution coming from outside r/a = 0.4 which is somewhat different from what has been observed previously on DIII-D where the intrinsic torque is more pronouncedly peaked at the edge. In the ECRH power scan, the intrinsic torque during the low ECRH power phase is in the co-current direction and increases toward the plasma edge. In the high power ECRH phase, however, a negative (counter-current) torque source is present from the centre of the plasma up to mid radius consistent with previous work on AUG. The ECRH power deposition is centrally located. In addition to the counter intrinsic torque, the rotation modulation data cannot be explained by any other mechanism than outward convection at r/a < 0.4. The first intrinsic torque experiments on AUG show that co-torque is driven in the outer part of the plasma radius and that counter-torques can develop in the inner half radius when sufficient ECRH is applied to alter the heat transport and the local plasma turbulence.

EX/P1-22

Fast-Ion Response to Externally Applied 3D Magnetic Perturbations in ASDEX Upgrade H-Mode Plasmas

M. García-Muñoz¹, S. Äkäslompolo², R. Akers³, P. de Marne⁴, M. G. Dunne⁴, N. M. Ferraro⁵, S. Fietz⁴, J. Galdon¹, J. Garcia-Lopez¹, B. Geiger⁴, A. Herrmann⁴, M. Hoelzl⁴, M. C. Jimenez-Ramos¹, N. Lazanyi⁶, Y. Liu⁷, M. Nocente⁸, D. Pace⁵, K. Shinohara⁹, W. Suttrop⁴, M. Van Zeeland⁵, E. Strumberger⁴, and E. Wolfrum⁴

¹University of Seville, Spain
 ²Aalto University, Espoo, Finland
 ³CCFE Fusion Association, Culham Science Centre, Abingdon, UK
 ⁴Max-Planck-Institut für Plasmaphysik, Garching, Germany
 ⁵General Atomics, San Diego, CA, USA
 ⁶Budapest University, Association EURATOM, Budapest, Hungary
 ⁷JET-EFDA, Culham Science Centre, Abingdon, UK
 ⁸University of Milano-Bicocca, Italy
 ⁹Japan Atomic Energy Agency, Naka, Japan

Corresponding Author: M. García-Muñoz, manuel.garcia-munoz@ipp.mpg.de

The fast-ion response to externally applied 3D Magnetic Perturbations (MPs) has been investigated on ASDEX Upgrade (AUG) in H-mode plasmas with a wide range of collisionalities / densities and MP spectra. MPs have little effect on kinetic profiles, including fast-ions, in high collisionality plasmas with mitigated ELMs while a strong plasma (including fast-ions) response is observed in H-mode regimes with low collisionality/density and low q_{95} .

Multiple, absolutely calibrated, fast-ion loss detectors (FILDs) located at different toroidal and poloidal positions measure significant changes in escaping ion phase-space when MPs are applied. Fast-ion losses can be up to an order of magnitude larger with MPs than the nominal NBI prompt losses measured without MPs. The application of the 3D fields is followed by a rapid rise (within ms) of the associated fast-ion losses while the measured fast-ion losses exhibit a slow decay, ~ 100 ms, down to the nominal NBI prompt loss level, after the MP coils are switched off. The heat load associated to the MP induced fast-ion losses have been measured with infrared cameras imaging the divertor as well as FILD and the surrounding first wall. The measured heat load can be up to six times larger with MPs than without MPs. The impact the 3D fields have on the confined fast-ions have been monitored by means of Fast-Ion D-Alpha (FIDA) spectroscopy. FIDA measures an enhancement of the fast-ion content in plasma with a visible impact on the gradients of the fast-ion profiles when RMPs are applied and density pump-out is observed. A strong fast-ion response is typically accompanied by an apparent displacement of the outboard separatrix, 1–3 cm, as measured by Beam Emission Spectroscopy (BES) that modifies significantly the NBI deposition profile. The accurate fast-ion measurements presented here are used to test models of 3D fields using full orbit simulations. The perturbed equilibria are calculated in vacuum, using the 3D free boundary VMEC/NEMEC code as well as including the plasma response with the M3D-C1, MARS-F, and JOREK codes.



Studies of Magnetic Perturbations in High-Confinement Mode Plasmas in ASDEX Upgrade

W. Suttrop¹, L. Barrera Orte¹, R. Fischer¹, S. Fietz¹, J. C. Fuchs¹, R. McDermott¹, S. Rathgeber¹, E. Viezzer¹, and E. Wolfrum¹

¹Max-Planck-Institut für Plasmaphysik, Garching, Germany

Corresponding Author: W. Suttrop, wolfgang.suttrop@ipp.mpg.de

ASDEX Upgrade is equipped with two rows of in-vessel saddle coils for magnetic perturbations with toroidal mode numbers up to n = 4. A reliable ELM mitigation regime has been found in which large type-I ELMs are suppressed, and replaced by a small form of ELMs with significantly reduced energy loss from the plasma and heat load to the divertor. This regime is accessible at high pedestal plasma density, typically $n_{e,ped} > 65\% n_{GW}$, and high pedestal collisionality, $\nu^* > 1.2$. The access conditions to this regime are studied in more detail in experiments with gas fueling ramps and coil current ramps.

The effect of magnetic perturbations on H-mode plasmas with low pedestal collisionality, $\nu^* < 0.5$, is studied in discharges without gas puff fueling. Accumulation of tungsten impurities, which can occur if eroded material from the fully tungsten-cladded wall penetrates into the plasma and is transported radially inward there, is avoided by strong central wave heating and large wall clearance.

With neutral beam injection in opposite direction to the plasma current (counter-injection), complete ELM suppression is obtained during brief periods, reminiscent of Quiescent H-mode (QH) plasmas. However, the Edge Harmonic Oscillation (EHO) characteristic for QH plasmas is not observed.

With co-injection, a systematic study has been undertaken to vary the conditions for penetration of the perturbation field into the plasma core: 1) Field-alignment of the magnetic perturbation (resonant or non-resonant perturbation), 2) Variation of plasma rotation and hence, perpendicular electron fluid flow velocity. For conditions with minimal field shielding, i.e., non-resonant field and vanishing perpendicular electron flow, significant rotation braking is caused by $J \times B$ torque from the m/n = 1/1sawtooth pre-cursor, as demonstrated by a perturbation coil current modulation experiment. Under the same conditions, $J \times B$ torque from rotating neo-classical tearing modes is observed. In plasmas with small field shielding, a reduction of type-I ELM losses is often observed, along with a reduction of pedestal density (often dubbed "pump-out"). Further experimentation in the near future aims to diagnose the field perturbation using rotating magnetic perturbations and to study parameter dependencies of perturbation effects in these scenarios.



EX/P1-24

W Impurity Poloidal Assymmetries Observed at ASDEX Upgrade Using Soft-X-Ray Tomography Reconstruction

D. Mazon¹, C. Angioni², T. Pütterich², D. Vezinet², M. Sertoli², E. A. Belli³, R. Bilato², F. Casson⁴, T. Odstrcil², V. Bobkov², R. Dux², A. Gude², R. Guirlet¹, V. Igochine², P. Malard¹, and A. Kallenbach²

¹CEA-IRFM, Saint Paul lez Durance, France
 ²Max-Planck-Institut für Plasmaphysik, Garching, Germany
 ³General Atomics, San Diego, CA, USA
 ⁴CCFE Fusion Association, Culham Science Centre, Abingdon, UK

Corresponding Author: D. Mazon, didier.mazon@cea.fr

Many tokamaks are nowadays equipped with metallic walls. The positive effect of such modification compared to the previous carbon walls is a strong reduction of the tokamak wall erosion and tritium retention. But the drawback is a production and potential accumulation of heavy impurities in the plasma core which can cause high radiation losses and even trigger radiative collapses often leading to disruptions. Poloidal inhomogeneities of impurity distribution have a significant impact on radial impurity transport [1]. Understanding of the mechanisms leading to inhomogeneous impurity distribution is thus useful knowledge for the control of heavy impurity transport and hopefully accumulation avoidance. Poloidal asymmetries due to centrifugal effects or/and other sources of an equilibrium poloidal electric field in the core plasma, as those generated by minority Ion Cyclotron Resonance Heating (ICRH), are usually negligible in experimental impurity transport analysis on low-medium Z impurities. Such assumptions are not always valid for medium-high Z impurities.

Poloidal asymmetries such as those generated indirectly by minority ICRH heating or Neutral Beam Injection (NBI) have been observed and analyzed, using SXR tomographic reconstructions, during recent ASDEX Upgrade experimental campaigns. Trace injections of tungsten have been triggered by Laser Blow Off (LBO) ablation in different scenarios with fixed plasma current. Scans in NBI and ICRH power (H-minority heating scheme) and deposition location (change in frequency and/or toroidal field) have been performed in order to study their effects on Low Field Side (LFS) – High Field Side (HFS) asymmetries. Analysis of the obtained results is presented, focusing in particular on the effects of each actuator. Centrifugal effects have been recently implemented in the code GKW [2] for the description of turbulent impurity transport. The Hinton–Wong neoclassical theory in the presence of rotation, implemented in the NEO code, [3], can describe the impact of rotational effect on neoclassical transport. These new theoretical tools with the RF asymmetries now being implemented allow complete transport modeling of poloidal asymmetries.

References

- [1] F.J. Casson et al., Phys. Plasmas 17, 102305 (2010).
- [2] C. Angioni et al., Phys. Plasmas 19, 122311 (2012).
- [3] E. Belli et al., Plasma Phys. Cont. Fusion 54 015015 (2012).



Filament Transport in the SOL of ASDEX Upgrade

G. Birkenmeier¹, P. Manz¹, D. Carralero¹, F. Laggner², M. Bernert¹, T. Kobayashi³, G. Fuchert⁴, K. Krieger¹, F. Reimold¹, K. Schmid¹, M. Willensdorfer¹, E. Wolfrum¹, and U. Stroth¹

¹Max-Planck-Institut für Plasmaphysik, Garching, Germany
 ²Institute for Applied Physics, Vienna University, Austria
 ³Research Center for Plasma Turbulence, Kyushu University, Kasuga, Japan
 ⁴Institut Jean Lamour, Université de Lorraine, CNRS, Nancy, France

Corresponding Author: G. Birkenmeier, gregor.birkenmeier@ipp.mpg.de

At the edge of fusion plasmas, intermittently expelled density filaments, so-called blobs [1], are propagating through the scrape-off layer (SOL) perpendicular to the magnetic field. Due to its higher density and temperature compared with the background SOL plasma, they can lead to a significant degradation of plasma facing components in the main chamber. Since this degradation is critical for the first wall in future fusion devices, an understanding of the generation and the propagation of blobs is needed. Therefore, the dynamics of blob filaments is investigated in the SOL of ASDEX Upgrade by means of Lithium beam emission spectroscopy (Li-BES) [2], Langmuir probes, and gas puff imaging. This way, the density, velocity, lifetime, frequency and size of the blobs perpendicular to the magnetic field are determined. A comparison of the measurements with a recently developed analytical blob model based on a drift-interchange-Alfvén fluid model [3] indicates an influence of a finite ion temperature on the blob dynamics which has typically been neglected in other blob models. The blob dynamics agree well with the sheath-connected regime at lower plasma densities, and inertial effects play only a minor role [4]. At higher densities, a transition into another regime with large blob amplitudes and increased transport is found [5]. This points to a prominent role of blob transport at higher Greenwald fractions and has implications for the gross erosion of wall material in reactor relevant operation scenarios with a detached divertor near the density limit.

References

[1] D. A. D'Ippolito, J. R. Myra, and S. J. Zweben, Phys. Plasmas 18, 060501 (2011).

[2] M. Willensdorfer et al., Plasma Phys. Control. Fusion 56, 025008 (2014).

[3] P. Manz et al., Phys. Plasmas 20, 102307 (2013).

[4] G. Birkenmeier *et al.*, Proceedings of the 40th EPS Conference on Plasma Physics 2013, Espoo, Finland.

[5] D. Carralero et al., Proceedings of the 40th EPS Conference on Plasma Physics 2013, Espoo, Finland.

Solid Tungsten Divertor-III for ASDEX Upgrade and Contributions to ITER

A. Herrmann¹, H. Greuner¹, and K. Krieger¹

¹Max-Planck-Institut für Plasmaphysik, Garching, Germany

Corresponding Author: A. Herrmann, alh@ipp.mpg.de

AUG became a full tungsten experiment in 2007. At this time all plasma facing components have been coated with tungsten. To overcome the disadvantages of the coating — i.e., delamination of thick coatings, fast erosion of thin coatings in particular in the high heat load regime — we started to prepare a new outer divertor with solid tungsten at the outer strike line in 2010. The Div-III design was verified by extensive FEM calculations and high heat load testing of the target and its clamping structure in the test facility GLADIS. The Div-III concept was approved early in 2012 and the new divertor Div-III was installed in 2013.

The redesign of the outer divertor geometry was a chance to increase the pumping efficiency in the lower divertor by increasing the gap between divertor and vessel. This increases the conductance between roof baffle and cryo-pump that is located behind the outer divertor. We expect that this results in a lower collisionality in the outer scrape-off layer and consequently in a better overlap between AUG, JET, and ITER SOL parameters. To keep the option for operation with high SOL densities, a by-pass valve was placed into the cryo-pump allowing to operate AUG with full or 1/3 of the pumping speed. Safe divertor operation and heat removal becomes more and more significant for future fusion devices. This requires the development of "tools" for divertor heat load control and to optimize divertor technology and geometry. Whereas the heat load receiving capability of target concepts can be tested in high heat load test facilities such as GLADIS in Garching, the target behaviour under plasma conditions has to be investigated in a fusion experiment. Here, the new divertor manipulator, DIM-II, offers a bunch of possibilities. DIM-II allows retracting a two target wide part of the divertor into a target exchange box without venting AUG. Different "front ends" can be installed and exposed to the plasma. At present, front ends for probe exposition, gas puffing, electrical probes and actively cooled prototype targets are under construction. The installation of solid tungsten, the control of the pumping speed and the flexibility for divertor modifications on a weekly base is a unique feature of AUG and offers together with the extended set of diagnostics the possibility to investigate dedicated questions for a future divertor design.



Nonthermal Microwave Emission Features under the Plasma Ohmic Heating and Lower Hybrid Current Drive in the FT-2 Tokamak

V. Rozhdestvensky¹, S. Lashkul¹, V. Dyachenko¹, S. Krikunov¹, L. Esipov¹, A. Altukhov¹, D. Kuprienko¹, A. Stepanov¹, and A. Shevelev¹

¹*Ioffe Physical-Technical Institute of the Russian Academy of Science, St. Petersburg, Russian Federation* Corresponding Author: V. Rozhdestvensky, roz35@mail.ru

Results of studying the abnormal microwave emission (ME) arising under ohmic heating (OH) of the moderately dense plasma and generation of the low-hybrid current drive (LHCD) in the FT-2 tokamak are presented. The ME appearance is due to the "fan" instability development and the substantial local magnetic ripples existence. It was found that the ME arises continuously during OH in the frequency range 10-40 GHz and is accompanied by short, "gaint" flashes, which are greatly larger than the pedestal and have the narrow frequency spectrum. The synchrotron emission (SE) growth and less intensive flashes appear also in the range 57–75 GHz. As known they arise under the maser amplification of SE during interaction of AE with harmonics of magnetic ripples in the electron cyclotron autoresonance. Owing to the non-linear transformation of excited electron plasma waves into electromagnetic ones collective emission, CE, appears. It becomes possible the maser amplification of both SE and CE. The less intensive ME flashes arise apparently in the SE maser amplification only. The "gaint" flashes may be initiated under suitable conditions by transition of the maser-amplifier into the self-excitation regime, when the short powerful flashes of low-frequency coherent ME are generated. The plasma HF-pumping at the low-hybrid frequencies during the quasistationary OH stage provides the effective LHCD. The first high fast electron heating from 300 eV up to 550 eV at $P_{hf} = 90$ kW was registered in this regime together with the radiation losses growth due to the SE intensity increase in the 53–156 GHz range. It was accompanied by short ME spikes of the maser nature observed in the more narrow frequency range 53–78 GHz. The such ones were observed earlier under the plasma OH. It is possible this additional electron heating is due to the SE and spikes of ME absorbtion in the black plasma layers.



Impact of Isotopic Effect on Density Limit and LHCD Efficiency in the FT-2 Experiments

S. Lashkul¹, A. Altukhov¹, A. Gurchenko¹, E. Gusakov¹, V. Dyachenko¹, L. Esipov¹, M. Irzak¹, M. Kantor¹, D. Kouprienko¹, A. Saveliev¹, S. Shatalin², and A. Stepanov¹

¹ Ioffe Physical-Technical Institute of the Russian Academy of Science, St. Petersburg, Russian Federation ² St. Petersburg State Polytechnical University, St. Petersburg, Russian Federation

Corresponding Author: S. Lashkul, serguey.lashkul@mail.ioffe.ru

Current drive by lower hybrid waves (LHCD) is the most effective method to keep the plasma current, but it is feasible only at the plasma density not exceeding some density limit n_{DL} . In the present work the main attention is paid to investigation of this effect on the FT-2 (R = 0.55 m, a = 0.08 m, $B_T \leq 3$ T, $I_p = 19-40$ kA, $f_0 = 920$ MHz) tokamak. The dependence of LHCD efficiency on isotopic plasma content (hydrogen/deuterium) is studied. On the FT-2 tokamak, where a large experience has been accumulated in the area of plasma-LH wave interaction observation, the longcontinued experimental run on LHCD efficiency study has been realized. Characteristic features of such experiment are strong influence of the isotope plasma composition on the LH resonance density n_{LH} . For hydrogen plasma $n_{LH} \sim 3.5 \times 10^{13}$ cm⁻³, while for deuterium $n_{LH} \sim 10^{14}$ cm⁻³. The suppression of the LHCD and beginning of the interaction of LH waves with ions is controlled by the hydrogen/deuterium plasma density rise. In the hot hydrogen plasma ($T_e(r = 0 \text{ cm}) \approx 700 \text{ eV}$) the density limit n_{DL} of LHCD is approximately equal to the resonance value n_{LH} at which the interaction of the LH wave with the electron component is replaced by direct absorption by plasma ions $(n_{LH} \approx n_{LC} = 3.5 \times 10^{13} \text{ cm}^{-3}$ is the point of linear conversion). In the hot deuterium plasma one could expect an increase of n_{DL} because of a much higher value of $n_{LH} \ge n_{LC} \approx 10^{14} \text{ cm}^{-3}$. However it appeared that the observed density limit for LHCD generation $n_{DL} \approx 3.5-4 \times 10^{13}$ cm⁻³ is not determined by n_{LC} . Role of parametric instabilities in CD switch-off is considered in both cases. The cooling of the plasma column and density rise could lead to a reduction of the threshold for the parametric decay of f_0 and result in the earlier suppression of LHCD. In both cases the LHCD was inversely proportional to the density, which corresponds to the theoretical predictions. In order to analyze the experimentally observed effects the GRILL3D and FRTC codes have been used. The important role of the synergetic effect caused by the interaction of different spectral components of the excited RF waves was revealed. Next step of LHCD modeling is devoted to a dynamic modeling of LHCD plasma shots at rather low plasma densities $\langle n_e \rangle = 0.5 - 2 \times 10^{13}$ cm⁻³, when role of runaway electrons is significant at the FT-2 conditions.

Preprint

Poloidal Inhomogeneity of Turbulence in the FT-2 Tokamak by Radial Correlation Doppler Reflectometry and Full-f Gyrokinetic Modeling

A. Altukhov¹, A. Gurchenko¹, E. Gusakov¹, S. Leerink², L. Esipov¹, M. Irzak¹, M. Kantor¹, D. Kouprienko¹, S. Lashkul¹, A. Stepanov¹, and N. Teplova¹

¹Ioffe Physical-Technical Institute of the Russian Academy of Science, St. Petersburg, Russian Federation ²Aalto University, Espoo, Finland

Corresponding Author: A. Altukhov, a.altuhov@mail.ioffe.ru

The drift-wave turbulence responsible for anomalous transport of energy and particles in tokamak plasma is widely studied nowadays both experimentally and in theory. An interesting and important prediction of the numerical approach based on full-f gyrokinetic modeling is statistical inhomogeneity of trapped-electron-mode turbulence typical for ohmic discharge. Though the radial variation of the mean turbulence characteristics is well known to the experimental community the data on their poloidal dependence are rare. In this paper we address the problem using radial correlation reflectometry (RCR) technique utilizing simultaneous microwave plasma probing at different frequencies in the presence of a cut off and based on correlation analysis of backscattering signals. Oblique plasma probing as a method to cope with contribution of small angle scattering off long scale turbulence component have been justified recently. It was proved that the radial correlation Doppler reflectometry (RCDR) version of the diagnostic provides a way for determination of the turbulence radial wave number spectra and its detailed investigation. Following this approach the RCDR scheme in the 50-75 GHz frequency range from high magnetic field side have been assembled and detailed measurements in different poloidal octants were performed in FT-2 ohmic hydrogen and deuterium discharges. The turbulence parameters were measured at variable incidence angle (+10-30 degrees) corresponding to different turbulence poloidal wave numbers ($6-16 \text{ cm}^{-1}$) and frequency changing from 50 kHz to 400 kHz. The cut-off layer minor radius was varied in the range from 3 to 6 cm. Both frequency resolved and integrated RCDR CCFs were determined. The correlation length corresponding to the frequency averaged CCF is smaller than that, obtained in the Doppler shift frequency thus leading to its underestimation. A new antennae set from low field side and interferometer antennae are utilized for other poloidal octants. As a result of measurements using these antennae the variation of radial correlation length from 0.25 cm to 0.45 cm when moving from high-field side to low-field side of the torus was demonstrated in agreement to the results of gyrokinetic modeling performed with ELMFIRE code. A well pronounced excess of the turbulence correlation length in deuterium over its value in hydrogen discharges was shown.



EX/P1-32

Geodesic Acoustic Mode Investigation in the Spherical Globus-M Tokamak Using a Multi-Diagnostic Approach

V. Bulanin¹, V. Gusev², A. Iblyaminova², N. Khromov², G. Kurskiev², V. Minaev², M. Patrov², A. Petrov¹, Y. Petrov², N. Sakharov², P. Shchegolev², S. Tolstyakov², V. Varfolomeev², F. Wagner³, and A. Yashin¹

¹St. Petersburg State Polytechnical University, St. Petersburg, Russian Federation ²Ioffe Physical-Technical Institute of the Russian Academy of Science, St. Petersburg, Russian Federation ³Max-Planck-Institut für Plasmaphysik, Greifswald, Germany

Corresponding Author: V. Bulanin, v.bulanin@spbstu.ru

Owing to the active researches of intermediate regime which is known as limit cycle oscillation (LCO) regime, it is important to investigate oscillations of velocity of zonal flows, plasma density and magnetic field simultaneously. The geodesic acoustic mode (GAM) investigations using multidiagnostic were carried out on the spherical tokamak Globus-M (R = 0.36 m, a = 0.24 m, $I_p = 150$ kA, $B_T = 0.3$ T). Variation of GAM intensity showed features of LCO regime. The key implement for researches was a method of Doppler microwave backscattering, or Doppler reflectometry (DR). The diagnostic consisted of two Doppler reflectometers, which were apart in poloidal direction. Oscillations of plasma density emission, which were detected at different lines of sight. Structure of magnetic field perturbation has been investigated using poloidal and toroidal Mirnov probe arrays. Correlation analysis shown that the structure of $E \times B$ velocity oscillations had corresponded to n = 0, m = 0. The main structure of density fluctuations at GAM frequency had n = 0, m = 0 mode numbers. Besides the n = 0, m = 1 component is also presented. The mode structure for magnetic field disturbance was established. To interpret an origin of plasma density global perturbation at GAM frequency plausible model was suggested.



Fast Particle Behavior in Globus-M

N. Bakharev¹, F. Chernyshev¹, P. Goncharov², V. Gusev¹, A. Iblyaminova¹, V. Kornev¹, G. Kurskiev¹, A. Melnik¹, V. Minaev¹, M. Mironov¹, M. Patrov¹, Y. Petrov¹, N. Sakharov¹, P. Shchegolev¹, S. Tolstyakov¹, and G. Zadvitskiy²

¹Ioffe Physical-Technical Institute of the Russian Academy of Science, St. Petersburg, Russian Federation ²St. Petersburg State Polytechnical University, St. Petersburg, Russian Federation

Corresponding Author: N. Bakharev, bakharev@mail.ioffe.ru

Behavior of the fast particle population, arising during 20–30 keV hydrogen and deuterium neutral beam injection in the hydrogen and deuterium plasmas, is investigated. Experiments revealed large fast ion losses. Experimental results are confirmed by different types of modeling: simulation with the NUBEAM module, solution of Boltzmann kinetic equation with Landau collision term, and full 3D fast ion tracking algorithm. Dynamics of the energetic particle losses during the sawtooth oscillations and Alfvén eigenmodes is investigated. Losses induced by these instabilities may exceed 25%. A way to decrease fast ion losses in present conditions is shown. Modeling for the Globus-M2 tokamak is performed. Simulations predict essential improvement in the fast ion confinement.

Determination of the System Function for the Particle Circulation Process Using Perturbation Technique in QUEST

I. Takagi¹, A. Kuzmin²

¹Kyoto University, Kyoto, Japan ²Kyushu University, Kasuga, Japan

Corresponding Author: I. Takagi, takagi@nucleng.kyuoto-u.ac.jp

A new approach to realize steady state tokamak operation SSTO has been demonstrated in QUEST with all metal wall baked at 100°C. Using particle flux perturbations driven by particle source H_2 and plasma-wall interaction PWI the system functions of processes of retention and release into/from the wall are determined both in time and frequency domains. The system function for the particle circulation has been determined by perturbation technique and independent measurement of partial pressure and permeation flux. The temporal evolution of system function, especially very low frequency component, must be controlled in order to sustain the steady-state discharge.



Investigation of Progression from Low to High Hydrogen Recycling during Long Duration Discharges on a Spherical Tokamak, QUEST

K. Hanada¹, N. Yoshida¹, H. Zushi¹, K. Nakamura¹, A. Fujisawa¹, H. Idei¹, Y. Nagashima¹, H. Watanabe¹, M. Hasegawa¹, S. Kawasaki¹, H. Nakashima¹, A. Higashijima¹, O. Watanabe¹, Y. Takase², A. Fukuyama³, O. Mitarai⁴, and M. Peng⁵

¹Institute for Applied Mechanics, Kyushu University, Kasuga, Japan
 ²University of Tokyo, Japan
 ³Kyoto University, Kyoto, Japan
 ⁴School of Industrial Engineering, Tokai University, Japan
 ⁵Oak Ridge National Laboratory, Oak Ridge, TN, USA

Corresponding Author: K. Hanada, hanada@triam.kyushu-u.ac.jp

Progression from low (LR) to high recycling (HR) was observed in full non-inductive long duration discharges up to five minutes on QUEST. Transitional repetitive behavior between LR and HR was induced by periodic gas puffing and the period to recover to LR, τ_{rec} , was gradually prolonged. The period, τ_{rec} normalized by gas rate has a linear relation to time-integrated H_{α} . As the prolongation of τ_{rec} was also induced by higher gas rate even in the start-up phase, the value of τ_{rec} is an index of the amount of recycled hydrogen. The experimental observation indicates hydrogen recycling rate is dominantly depending on hydrogen fluence to the wall. To understand the dependence, deuterium storing capability of the specimen exposed to QUEST plasmas during an experimental campaign was investigated by implantation of deuterium molecule ions of 1 keV and subsequent thermal desorption spectrum (TDS) as a post-mortem analysis. The important desorption in the obtained TDSs appeared around 420 and 470 K, and these peaks can be reconstructed by a model including diffusion, recombination, trapping, and plasma induced desorption. The model calculation was applied to the QUEST long duration discharges and shows that recycling ratio has a clear dependence on fluence and the fluence in the QUEST long duration discharges is sufficient to make a saturation in recycling ratio of unity. These results indicate that hydrogen recycling has the capability to provide a clear effect on plasma in long duration discharges and the progression is driven by enhanced hydrogen recycling with high fluence to the wall.



Fully Non-Inductive Current Drive Experiments Using 28 GHz and 8.2 GHz Electron Cyclotron Waves in QUEST

H. Idei¹, T. Kariya², T. Imai², O. Watanabe¹, and K. Hanada¹

¹Institute for Applied Mechanics, Kyushu University, Kasuga, Japan ²University of Tsukuba, Tsukuba, Ibaraki, Japan

Corresponding Author: H. Idei, idei@triam.kyushu-u.ac.jp

28 GHz Electron Cyclotron Current Drive (ECCD) effect was clearly observed in Ohmically heated plasmas with feedback regulation of center solenoid coil current in 2nd harmonic inboard off-axis heating scenario. In non-inductive current drive experiments only by the 28 GHz injection, 54 kA plasma current was sustained for 0.9 s. Higher plasma current of 66 kA was non-inductively obtained by slow ramp-up of vertical field using the 28 GHz ECH/ECCD. Non-inductive high-density and current plasma start-up, which is a key issue for fusion reactor design, has been demonstrated using 2nd harmonic ECH/ECCD. Density jump across 8.2 GHz cutoff density was observed in superposed 28 GHz and 8.2 GHz injections. The 50 kA plasmas were sustained by the 8.2 GHz injection into the 28 GHz target plasma if the stable plasma shaping was obtained.



Self Organization of High β_p Plasma Equilibrium with an Inboard Poloidal Null Sustained by Fully Non-Inductive Current Drive in QUEST

K. Mishra¹, H. Zushi¹, H. Idei², M. Hasegawa¹, and T. Onchi¹

¹Kyushu University, Kasuga, Japan ²Institute for Applied Mechanics, Kyushu University, Kasuga, Japan

Corresponding Author: K. Mishra, mishra@triam.kyushu-u.ac.jp

There is a considerable interest in operating tokamak at high value of β_p , but maximum attainable β_n is limited by a equilibrium limit with appearance of a null point at the inboard side. Such configuration is realized transiently earlier by Electron Cyclotron Waves, but in QUEST such equilibrium is stably produced in steady state and its equilibrium properties are investigated. In QUEST, successful production of high β_p plasma ($\beta_p > 1$) and its long pulse sustainment by fully non-inductive (NI) current drive with the help of a modest power (< 100 kW) ECW is demonstrated. High β_p plasma is formed by confining energetic electrons produced by multiple resonant EC interaction in a high magnetic mirror configuration and high $B_z/B_t > 0.1$. We found that (i) high β_p plasma is naturally self organized to form a stable natural Inboard Poloidal field Null (IPN) equilibrium, (ii) a critical β_p , which defines the transition boundary from Inboard Limiter (IL) to IPN equilibrium, and (iii) a new feature of plasma self organization to enhance its negative triangular shape to sustain high β_p . With high β_p formation, plasma naturally self organizes to reduce the elongation as first observed in TFTR, which is also observed in the present case. However, we found a new self organization feature, where plasma shape adjusts itself to becomes more negatively triangular. This new feature overcompensates the diminution of β_p due to the reduction in elongation. A simple analytic solution of Grad-Shafranov equation is applied to investigate such aspect. The model supports this facet which, predicts higher β_p at larger negative triangularity. The boundary flux surfaces generated through the model agree well with the measurements. The model is also in agreement with the critical β_p for IL to IPN transition, which is very well matched with the measurements. This result shows a relatively simple method to produce and sustain high β_p plasma close to the equilibrium limit in a stable configuration exploiting its self organization property.



Turbulent Electromagnetic Filaments in Toroidal Plasma Edge

M. Spolaore¹

¹Consorzio RFX, Associazione Euratom-ENEA sulla Fusione, Padova, Italy Corresponding Author: M. Spolaore, monica.spolaore@igi.cnr.it

E Corres Fi featur

EX/P1-40

Filament or blob structures have been observed in all magnetic configurations with very similar features despite the difference in the magnetic geometry: theory and experiments suggest they exhibit a radial convective motion across the SOL, and the interest in blob dynamics is further motivated by their interaction with first wall and divertor. Despite their different generation mechanism, turbulent structures and Edge Localized Mode (ELM) filaments share some common physical features, as the localization in the cross-field plane and the associated parallel current, with a convective radial velocity component somehow related to their dimension.

Electromagnetic effects on filament structures deserve particular interest, among the others for the implication they could have for ELM, related for instance to their dynamics in the transition region between closed and open field lines or to the possibility, at high β regimes, of causing line bending which could enhance the interaction of blobs with the first wall. Electromagnetic features of turbulent filaments, emerging from turbulent background, will be shown in four different magnetic configurations: the stellarator TJ-II, the Reversed Field Pinch RFX-mod, a device that can be operated also as a ohmic tokamak, and the Simple Magnetized Torus TORPEX. In all cases, direct measurements of both field-aligned current density and vorticity were performed inside the filament. Despite the great specific differences, the inter-machine comparison revealed a clear dependence of the filament vorticity upon the local time-averaged $E \times B$ flow shear. Furthermore the wide range of local β that was explored through the four mentioned configurations allows concluding that this parameter plays a fundamental role in the appearance of the electromagnetic features of filaments, suggesting an underlying common physics.

The RFX-mod experiment versatility is exploited also from the point of view of the active control of the edge magnetic topology focusing on the filament interaction with local magnetic island. High frequency fluctuations, characterizing electrostatic and magnetic filament features, have been observed to be affected by the island proximity. This observation hints at the challenging possibility of active control of filaments and their related transport by modulating the local magnetic topology.



The Isotope Effect in the RFX-Mod Experiment

R. Lorenzini¹

¹Consorzio RFX, Associazione Euratom-ENEA sulla Fusione, Padova, Italy

Corresponding Author: R. Lorenzini, rita.lorenzini@igi.cnr.it

The isotope effect, namely the dependence of plasma confinement on the mass M_i of majority ion, is a well known property of tokamak configuration. Increasing M_i leads to an improvement of energy, particle and momentum confinement in all regimes of tokamak plasmas. Besides, M_i influences also many MHD roperties, e.g., increasing the period of plasma instabilities. However, in stellarators the confinement properties are independent of M_i . Despite a strong research effort, an explanation of the isotope effect in tokamaks is still lacking. During the past year the Reversed Field Pinch (RFP) device RFX-mod started to operate using Deuterium (D), besides Hydrogen (H), as filling gas. In this paper we present first results on the comparison among Hydrogen and Deuterium plasmas of RFX-mod, offering the opportunity of studying the isotope effect physics from a new perspective. First analyses of Deuterium plasmas show clearly the presence of an isotope effect also in RFP configuration. The plasma properties change with M_i in a way which reminds what happens in tokamaks. The electron temperature in D plasmas is about 20% higher than in H ones. This increase is essentially due to the steepening of T_e gradient in the external region of plasma (r/a > 0.7), while gradients in the plasma core does not undergo a significant modification. Discharges with similar plasma parameters are characterized by influxes of majority ion 30% lower in D plasmas than in H ones. Interestingly no significant difference is seen in the impurity influxes.

The mass M_i influences also the MHD properties of plasmas. At high current ($I_p > 1$ MA) the plasma is in the Quasi Single Helicity (QSH) state where a single MHD instability, the dominant one, overcomes the others, the so-called 'secondary' modes. The QSH phases are transiently interrupted by burst of MHD activity, the Dynamo Relaxation Events (DRE). The duration of QSH phases increases by a factor ~ 1.5 changing the main gas from H to D, resulting in a longer time interval among DREs responsible of QSH collapse. The energy of secondary modes during QSH is about 20% lower in D. Since the amplitude of dominant mode does not exhibit a significant variation, QSH are purer in D than in H. Furthermore the comparison among D and H plasmas shows that the current profile in D plasmas is more peaked than in H.



EX/P1-42

Density Limit Studies in the Tokamak and the Reversed-Field Pinch

G. Spizzo¹, G. Pucella², O. Tudisco², and M. Zuin¹

¹Consorzio RFX, Associazione Euratom-ENEA sulla Fusione, Padova, Italy ²Associazione EURATOM-ENEA Unitá Tecnica Fusione, Frascati, Italy

Corresponding Author: G. Spizzo, gianluca.spizzo@igi.cnr.it

Both in the tokamak and the reversed-field pinch (RFP), new finds show that the high density limit, which often disrupts tokamak discharges and slowly terminates RFP ones, is not governed by a unique, theoretically well-determined physical phenomenon, but by a combination of complicated mechanisms involving two-fluid effects, electrostatic plasma response to magnetic islands and plasmawall interaction. In this paper we will show that the description in terms of the unique "Greenwald density" $n_G = I_p / p_i a^2$ should be reinterpreted in terms of edge critical density, and related to the amplitude of the equilibrium magnetic field, the resonance of islands next to the edge, and input power. Recent results in FTU point out that in discharges with a variable density peaking the lineaveraged central density scales as $n_0 \sim B^{1.5}$, which is a scaling with the magnetic field. The usual Greenwald-like scaling $n_{edge} = 0.35 n_G$ holds for the edge density. The density limit depends also on the input power: recent experiments in the RFX-mod RFP with a lithized wall show that the central density increases linearly with the ohmic input power and that larger densities can be accessed, for the same input power, with better wall conditioning. An important point to raise is the role of the thermal instabilities in setting the environment for the development of the density limit: in both machines, FTU and RFX, the density limit is associated with the appearance of the multifaceted asymmetric radiation from the edge (MARFE), which is triggered by MHD activity (m/n = 2/1 in FTU and 0/1in RFX). In the RFX case, the MARFE is also linked to a well-defined flow pattern. In fact, the 0/1island, which resonates at q = 0 in the RFP edge (r/a = 0.9), is destabilized at high density, and generates an electrostatic response in the form of a convective cell, with the same 0/1 symmetry. The toroidal flow reverses direction along the toroidal angle, with the formation of two null points of v_{ϕ} (or, equivalently, radial electric field E_r): a source and a stagnation point, with the latter corresponding to the toroidally localized MARFE. The association between flow patterns and MARFE can be tested in FTU, by investigating the effect of ERCH on the MARFE and the density peaking. Initial results, on FTU as well as in ASDEX, indeed show a dependence of the disruption phenomenology on the ECRH.

Study of ITB Formation, Electron Heat and Density Flux Structure in New ECRH/ECCD Experiments at T-10 Tokamak

S. Neudatchin¹, A. Borshegovskii¹, S. Maltzev¹, T. Mualton¹, N. Mustafin¹, D. Sergeev¹, and D. Shelukhin¹

¹National Research Centre "Kurchatov Institute", Moscow, Russian Federation Corresponding Author: S. Neudatchin, sneudat@yandex.ru

In the present report, we focus at the analysis of four transport processes in T-10. First, we analyze inward electron heat pulse propagation (HPP) created by switch-on of additional off-axis ECRH on a sawteeth-free background sustained by off-axis ECRH. The presence of slow and diffusive inward HPP with "dynamic" hi-e value close to power balance value shows that the so-called "heat pinch" is either absent or very small. Second, analysis of sawtooth density oscillations in the regimes with central ECRH and in the experiments with ECCD current drive to damp the sawteeth oscillations (PECRH < 0.7 MW), shows that the electron pinch velocity value is close to the neoclassical one in the plasma centre. Under PECRH ≥ 1.5 MW, n_e profiles become hollow (or fully flat within the errorbars) at r/a < 0.5 and we observe sawteeth density oscillations with inverted phase (rise at $r = \pm 4$ cm and decay at $r = \pm 12$ cm). The decay of n_e in the centre between the crashes is explained by the presence of the outward electron convective velocity with $V_p \approx 0.3$ m/s at r/a = 0.35. Third, a set of experiments with programmed plasma motion allows us to analyze fine detail of T_e profile with ECE measurements. No signs of clear ITB at the q = 1 surface have been observed so far (PECRH up to 0.9 MW). In several shots, the existence of a narrow ITB with a 0.5 cm width and a doubled T_e gradient can be suggested within the errorbars. Finally, a new type of ITB created by sawtooth oscillations almost damped by off-axis ECCD has been found. A sawteeth crash causes the rise of T_e outside r_s and heat pulse does not propagate outside during 15 ms. The value of χ_e becomes 2.5 times lower compared with the L-mode scaling. The experiments with various values of current generation and reflectometer measurements are under the way.

EX/P1-43



EX/P1-44

Impurities Removal during Central ECR Heating in T-10

L. Klyuchnikov¹, V. Krupin¹, K. Korobov¹, A. Nemets¹, A. Borshegovskii¹, A. Y. Dnestrovskij¹, A. Gorbunov¹, V. Korolev¹, S. Krylov¹, N. Naumenko², V. Nikulin¹, I. Roy¹, G. Tilinin¹, and S. Tugarinov¹

> ¹Institute of Tokamak Physics, National Research Centre "Kurchatov Institute", Moscow, Russian Federation ²B.I. Stepanov Institute of physics NASB, Minsk, Belarus

Corresponding Author: L. Klyuchnikov, lklyuchnikov@list.ru

Experiments on impurities removal with central ECR heating on T-10 were carried out with various plasma parameters. CXRS and $Z_{\rm eff}$ measurements show removal of carbon nuclei from plasma during central ECRH. There is a complex of high-power gyrotrons for ECRH experiments on T-10. Spectroscopic diagnostics of T-10 allows measurement of the carbon concentration by CXRS diagnostics and the effective ion charge (Z_{eff}) radial distribution from bremstrahlung intensity with subtraction of background molecular linear spectra. Radial distribution of C⁺⁵ passive line intensity was measured simultaneously with CXRS measurements. This linear radiation allows to estimate ionization flux from C^{+5} into C^{+6} ions for calculation of C^{+6} particle confinement time $\tau_{particle}$: Value of $\tau_{particle}$ can be successfully defined only for impurities with relatively high Z (like carbon) due to the ionization flux into the nuclei in toroidal and poloidal coordinates for carbon impurity is homogeneous in T-10 conditions. Carbon confinement time in OH regimes rises with increasing of line averaged electron density and decreasing of plasma current. In ECR heated regimes with PECR=1 MW one observes sharp decrease of carbon confinement time to a value $\tau_{particle} \approx 23$ ms, which is almost the same for various plasma parameters within the error limits. The most contrast fall of $\tau_{particle}$ is observed at high plasma densities when one observes sharp decrease of total carbon concentration during central ECRH, although carbon ionization flux in ECR regimes is about twice higher than in OH plasma.

Work was carried out by "Rosatom" 13.05.2013 No. H.4x.44.90.13.1101



Study of GAM Radial Structure and Properties in OH and ECRH Plasmas in the T-10 Tokamak

A. Melnikov¹, S. Lysenko¹, L. Eliseev¹, S. Perfilov¹, S. Grashin¹, R. Solomatin¹, L. Krupnik², and V. Zenin¹

¹National Research Centre "Kurchatov Institute", Moscow, Russian Federation ²NNC 'Kharkov Institute of Physics and Technology', Kharkov, Ukraine

Corresponding Author: A. Melnikov, melnikov_07@yahoo.com

Zonal flows and their high-frequency counterpart, the Geodesic Acoustic Modes (GAMs) are considered as a possible mechanism of the plasma turbulence self-regulation. The paper presents the results of the systematic study of GAM properties in the T-10 tokamak with heavy ion beam probe (HIBP) in the core and with multipin Langmuir probes in the edge. It was shown that GAM has radially homogeneous structure of the global eigenmode. The radial distribution of GAM frequency f_{GAM} is almost uniform, in spite of the temperature dependence on the radius. However, f_{GAM} grows with the radially averaged electron temperature approximately as $\sqrt{T_e}$. The GAM amplitude also shows a tendency to be almost constant over the whole observed radial area in the plasma. The typical amplitude of GAM potential oscillations is \sim 20–80 Volts on the background of steady state values of potential up to -1 kV. GAMs are more pronounced during ECRH, when they have the main peak at 22–27 kHz and the higher frequency satellite peak at 25–30 kHz. GAM characteristics and limits of GAM existence were investigated as functions of density, magnetic field, safety factor, and ECRH power. It was found that GAMs are suppressed with the density increase. The phase shift between the oscillations of potential and density was about $\pi/2$. The poloidal mode number for GAM associated potential perturbation is estimated as m = 0 for the whole observed radial interval. The constancy of the GAM frequency with radius is in agreement with recent theoretical findings, which predicts that global GAM (GGAM) can exist in typical tokamak discharges with positive magnetic shear and monotonic temperature profiles. Eigenfrequency of GGAM is constant over the radius in contrast with frequency of GAM continuum.

Magnetic Island and Plasma Rotation under External Resonant Magnetic Perturbation in T-10 Tokamak

N. Ivanov¹, L. Eliseev¹, A. Kakurin¹, A. Melnikov¹, S. Perfilov¹, and V. Soloviev¹

¹National Research Centre "Kurchatov Institute", Moscow, Russian Federation Corresponding Author: N. Ivanov, <u>ivanov_nv@nrcki.ru</u>

The experimental comparison of the m = 2 mode and plasma rotation velocities at the q = 2magnetic surface in a range of the mode amplitudes is presented in this paper. The phase velocity of the mode rotation is measured with a set of poloidal magnetic field sensors located at the inner side of the vacuum vessel wall. The plasma rotation velocity at the q = 2 magnetic surface in the direction of the mode phase velocity is measured with the heavy ion beam diagnostics. In the presence of a static RMP the rotation is irregular that appears as cyclical variations of the mode and plasma instantaneous velocities. The period of these variations is equal to the period of the mode oscillations. In each period the velocities depend on the angular shift between the mode and RMP. A non-monotonic dependence of the mode rotation irregularity on the mode amplitude is observed. The rotation irregularity increases in both cases of sufficiently big and small amplitudes. In the case of big mode amplitude the rotation irregularity of the mode coincides with the rotation irregularity of the resonant plasma layer. On the contrary, the observed rise of the mode rotation irregularity in the case of sufficiently small mode amplitude is not followed by an increase of the rotation irregularity of the resonant plasma layer. It means that a decoupling between the mode and plasma rotations is observed for small islands. The experimental results are simulated with the TEAR code based on the two-fluid MHD approximation. The effects of plasma resistivity, viscosity, RMP, and the current induced in the resistive vacuum vessel are taken into account. The calculated irregularities of the mode and plasma rotation depend on the mode amplitude similar to the experimental data. For large islands, the rotation irregularity is attributed to variations of the electromagnetic torque applied to the resonant layer. For small islands, the deviations of the mode rotation velocity from the plasma velocity take place due to the effect of finite plasma resistivity.



Experimental Investigation of the System of Vertical and Longitudinal Lithium Limiters as a Prototype of Plasma Facing Components of a Steady State Tokamak-Reactor on T-11M Tokamak

S. Mirnov¹, I. Lyublinski², V. Lazarev¹, A. Belov¹, N. Djigailo¹, S. Dzhurik¹, S. Kravchuk¹, V. Nesterenko¹, A. Scherbak¹, A. Vertkov², and M. Zharkov²

¹Troitsk Institute for Innovation & Fusion Research, Moscow region, Russian Federation ²JSC "Red Star", Moscow, Russian Federation

Corresponding Author: S. Mirnov, mirnov@triniti.ru

During operation on the tokamak T-11M it was achieved almost complete (up to 80%) closing of lithium circulation circuit between the edge of hot (106 K) plasma and the chamber wall. Lithium, emitted by the vertical capillary Li limiter during operations of T-11M has been collected by the cryogenic target and removed outside the tokamak vacuum chamber without disturbing of tokamak operation cycle, what is a key requirement for use of lithium in a steady state tokamak-reactor. In T-11M it was tested a new functional model of the prototype of closed lithium circuit for the protection of chamber wall by a simultaneous using of the vertical lithium limiter T-11M as an emitter of lithium and new longitudinal lithium limiter as its collector. Such technological scheme can be suggested for the steady state fusion neutron source (FNS) on the tokamak basis.

Investigation of a Phenomenology of the Improved Confinement Regime in T-11M Tokamak

A. Shcherbak¹, S. Mirnov¹, V. Lazarev¹, A. Panov¹, and A. Alekseev¹

¹Troitsk Institute for Innovation & Fusion Research, Moscow region, Russian Federation Corresponding Author: A. Shcherbak, romashkovo_n@mail.ru

Regimes of discharge of improved plasma confinement were found in the experiments with a vertical lithium limiter on T-11M tokamak, which was manifested in spontaneous growth of the electron density up to the limit Greenwald and above. Previously, such modes arising after chamber lithization were observed in the tokamak FTU. The analysis of data obtained in T-11M has showed that this regime of improved confinement is differed from the ordinary mode (L-mode) by the sharp profile of the plasma density $N_e(r)$, relatively high values of $N_e(0)$ in the center and ordinary density values $N_e(a)$ in the edge of plasma, as if there is an internal transport barrier in the center. Another visible difference of this mode from L-mode is a significant increase of soft X-ray power from the center, while maintaining or even reducing $Z_{\text{eff}}(0)$. In the central region of plasma the lifetime of particles is increased by approximately twice. The energy lifetime is increased by 30–40%. Major differences of the regime of improved confinement from remarkable limiter H-mode observed in T-11M, for example, after boronization are peaking of the density profile, absence of active ELMs, and collection of impurities in the plasma center. An analogy of such regimes is carried out with previously detected on the Alcator C-Mode I-mode.



Development of Lithium CPS Based Limiters for Realization of a Concept of Closed Lithium Circulation Loop in Tokamak

A. Vertkov¹, I. Lyublinski¹, M. Zharkov¹, S. Mirnov², V. Lazarev², and A. Szherbak²

¹JSC "Red Star", Moscow, Russian Federation

²Troitsk Institute for Innovation & Fusion Research, Moscow region, Russian Federation

Corresponding Author: A. Vertkov, avertkov@yandex.ru

Development of commercially attractive project of a tokamak based fusion neutron source, intended for the progress in fusion power reactor and fission technology, requires the possibility of plasma facing elements (PFE) to steady-state operation under extremely high power loads. Cooling of tokamak boundary plasma owing to radiation of none fully stripped lithium ions is considered as a promising way for PFE protection. It may be effectively realized when the main part of lithium ions are involved in the closed circuit of migration between plasma and PFE surface. Such power exhaust process may be implemented with the use of in-vessel lithium device based on lithium capillary-pore system (CPS) as plasma-facing material. CPS ensures the PFE self-regeneration during steady-state operation, provides the returning of collected and condensed lithium to emitting zone that prevents lithium accumulation outside the plasma interaction area. Several types of limiters based on lithium CPS with different ratio of emitting/collecting area and collectors for T-11M tokamak have been developed, created and tested with the aim of experimental substantiation for the concept of lithium closed circulation loop, investigation of lithium behavior in tokamak plasma and estimation of lithium CPS stability under high power flux. Design and main experimental test results are presented and discussed for horizontal, vertical, longitudinal lithium limiters and also for devices of lithium collection and extraction from the tokamak chamber; ring-type collector, cryogenic target.

The Auxiliary Heating and Current Drive Systems on The Tokamak T-15 Upgrade

I. Roy¹, I. Anashkin¹, A. Barsukov¹, V. Dyachenko², E. Gusakov², M. Irzak², S. Khitrov², P. Khvostenko¹, A. Panasenkov¹, A. Saveliev², A. Sidorov², O. Shcherbinin², and G. Tilinin¹

> ¹Institute of Tokamak Physics, National Research Centre "Kurchatov Institute", Moscow, Russian Federation

²*Ioffe Physical-Technical Institute of the Russian Academy of Science, St. Petersburg, Russian Federation* Corresponding Author: I. Roy, roy_in@nrcki.ru

The auxiliary Heating and Current Drive systems of the T-15 upgrade tokamak are presented. The NBI system will consist of three hydrogen NB injectors 6 MW total power at pulse duration up to 30 s. The ECRH and CD system will consist of seven gyrotrons 6 MW total RF launched power at pulse duration up to 30 s. The LHH and CD system will be able to launch 4 MW RF power with 30 s duration.



Generation of Energetic Electrons by Magnetic Reconnection with Presence of High Guide Field

M. Inomoto¹, T. G. Watanabe¹, K. Yamasaki¹, S. Kamio², T. Yamada³, A. Wang¹, X. Guo¹, T. Ushiki¹, H. Ishikawa¹, H. Nakamata¹, H. Itagaki¹, A. Kuwahata¹, B. Gao¹, and R. Yanai¹

¹University of Tokyo, Japan ²National Institute for Fusion Science, Toki, Japan ³Kyushu University, Kasuga, Japan

Corresponding Author: M. Inomoto, inomoto@k.u-tokyo.ac.jp

Magnetic reconnection allows highly-conducting plasma to change its magnetic topology in nuclear fusion plasmas, such as sawtooth crash, internal reconnection event, and so on. Recent theoretical and numerical works revealed that the presence of guide field (GF) greatly changes the collisionless reconnection in a qualitative way. One of the essential changes is that electrons are efficiently accelerated near the X-point to achieve high kinetic energy. Those fast electrons then cause secondary modification on reconnection structure, sometimes involving excitation of waves by electron beam instability. In this paper, we report some evidences of accelerated electrons in the UTST device, which provides well-controlled reconnection condition with toroidal GF 20 times higher than the reconnection field.

During the non-steady reconnection process in the UTST, a sharp ring-shape emission was found near the X-point. Toroidally accelerated electrons by reconnection electric field are supposed to ionize singly charged carbon impurities in the middle phase of reconnection. The SXR from the X-point region was observed simultaneously with the reconnection electric field. Generation of electron high energy tail up to 300 eV was confirmed by comparison of SXR signals through various filters. The SXR emission showed almost linear increasing trend with the toroidal GF when it exceeds the threshold value of $GF \sim 0.12$ T, suggesting that the number of accelerated electrons is determined by the duration of electrons remaining near the X-point. As a consequence, highly-efficient electron acceleration takes place in the magnetic reconnection with high GF even though the released magnetic energy was not very large. In contrast, the ion flow acceleration was observed only in the cases with reconnection electric field higher than 100 V/m. Thus, in the high GF case, the released magnetic energy is mainly converted to the kinetic energy of bulk ions, which then is converted to thermal energy; however, some electrons are effectively accelerated by the reconnection electric field to form a high energy tail. The accelerated fast electrons could excite low frequency modes near the reconnection region, which may cause bad influences on confinement property of tokamak plasmas.



EX/P2-20

Impact of NBI-Injected Fast Ions in the Stabilization of the Resistive Wall Mode in High- β_N Plasmas

F. Turco¹, J. Hanson¹, G. A. Navratil¹, M. J. Lanctot², and A. D. Turnbull²

¹Columbia University, New York, USA ²General Atomics, San Diego, CA, USA

Corresponding Author: F. Turco, turcof@fusion.gat.com

Modeling results, obtained with the full kinetic MARS-K code [1] for a set of DIII-D experimental equilibria, predict that the absence of fast beam generated ions in ITER will lead to a plasma response $\sim 40\%$ higher than in the present NBI-sustained H-mode plasmas. It has been postulated that the presence of fast ions may have a stabilizing effect on the RWM that would account for its observed stability, specifically in the DIII-D tokamak (the fast-ion generating Neutral Beam Injection system is the main heating system DIII-D plasmas). These dependencies may extrapolate unfavourably to machines with significantly smaller fractions of fast ions such as ITER. Elevated plasma response values will likely cause the potential onset of a resistive wall mode (RWM) instability. If the RWM is destabilized, operation above the no-wall limit will likely require a set of coils and a feedback system capable of detecting and stabilizing the external kink instability on the wall-time scale (~ 2.5 ms in DIII-D). Active MHD spectroscopy can be used to indicate the approach to pressure driven MHD limits. This technique can define when the RWM feedback is needed and ultimately help to avoid disruptions. The MHD spectroscopy system reacts differently in the case of current driven instabilities. The plasma response amplitude in these cases remains low up to $\sim 93\%$ of the limit, showing an abrupt increase only in the last $\sim 5\%$ of the current ramp, making it much less effective as a warning system. However, new modelling shows that the mode structure of the current driven RWM is very close to that of the pressure driven case, as measured in DIII-D plasmas with $q_{edge} \sim 2$ and modelled with the MARS-F and MARS-K codes. These equilibria, which show a hard disruptive limit when q_{edqe} crosses 2, were used to develop an RWM feedback system that allowed crossing the q = 2 limit and sustain the plasma at $q \sim 1.9$ for ~ 400 wall times [2].

Work supported in part by the US DOE under DE-FG02-04ER54761, DE-AC02-09CH11466 and DE-FC02-04ER54698.

References

[1] Y. Liu, Phys. Plasmas 15, 092505 (2008).

[2] J.M. Hanson, *et al.*, Bulletin of the American Physical Society, Division of Plasma Physics 58, TI2.00003 (2013).



Suppression of Type-I ELMs with Incomplete I-Coil Set on DIII-D

D. Orlov¹, T. E. Evans², R. Moyer¹, R. Maingi³, R. Nazikian⁴, N. M. Ferraro², A. Wingen³, M. E. Fenstermacher⁵, and C. Paz-Soldan⁶

¹University of California San Diego, CA, USA
 ²General Atomics, San Diego, CA, USA
 ³Oak Ridge National Laboratory, Oak Ridge, TN, USA
 ⁴Princeton Plasma Physics Laboratory, Princeton, NJ, USA
 ⁵Lawrence Livermore National Laboratory, Livermore, CA, USA
 ⁶Oak Ridge Institute for Science Eduction, Oak Ridge, TN, USA

Corresponding Author: D. Orlov, orlov@fusion.gat.com

Recent experiments on DIII-D have demonstrated the ability to suppress edge localized modes (ELMs) using edge-resonant magnetic perturbations (RMPs) produced by an incomplete I-coil set in ITER similar shape plasmas with low pedestal electron collisionality. Robust ELM suppression has been reproducibly obtained on DIII-D using a wide range of toroidal RMP modes during experiments in which various non-axisymmetric coil loops were turned off pseudo-randomly. RMP ELM suppression was achieved on DIII-D with 11, 10, 9, 7, and 5 out of 12 I-coils. In these experiments, using fine I-coil current steps we determined the I-coil current amplitude threshold for RMP ELM suppression in each I-coil configuration. The suppression current threshold showed almost no dependence on the number of the active I-coils will likely be able to meet the ELM suppression criterion in case of multiple coil failures.

The experimental results confirmed the previous modeling work predictions [1, 2] that ITER ELM coils would be able to meet the ITER coil design criterion even with 19 of 27 loops by adjusting the coil currents within the allowed range of current amplitudes. In the DIII-D experiments, while the dominant n = 3 harmonic was reduced due to an overall decrease in the amount of the perturbation, the sidebands assisted in maintaining necessary value of the island overlap region resulting in sufficient level of stochastization of the plasma pedestal region that is believed to be needed for RMP ELM suppression. This was also confirmed in the linear two-fluid plasma response modeling with M3D-C1. The effect of non-purity of the perturbation spectrum on ELM suppression may lead to new ELM suppression strategies and better understanding of the suppression mechanisms. Sustained RMP ELM suppression with only 7 of 12 I-coils was demonstrated on DIII-D. As the ELM suppression was achieved at constant I-coil current, high pedestal electron toroidal rotation and constant pedestal electron density were maintained for the duration of the ELM suppression phase, as well as good plasma confinement.

This work was supported in part by the US DOE under DE-FG02-07ER54917 and DE-FC02-04ER54698.

References

[1] D.M. Orlov, et al., Fusion Eng. Design 87 (2012) 1536.

[2] T.E. Evans, et al., Nucl. Fusion 53 (2013) 093029.



EX/P2-22

Measurement of Radiated Power Asymmetry during Disruption Mitigation on the DIII-D Tokamak

N. W. Eidietis¹, N. Commaux², R. Granetz³, E. M. Hollmann⁴, D. A. Humphreys¹, V. A. Izzo⁴, C. J. Lasnier⁵, R. Moyer⁴, C. Paz-Soldan², E. J. Strait¹, and R. Raman⁶

¹General Atomics, San Diego, CA, USA
 ²Oak Ridge National Laboratory, Oak Ridge, TN, USA
 ³Massachusetts Institute of Technology, Cambridge, MA, USA
 ⁴University of California San Diego, CA, USA
 ⁵Lawrence Livermore National Laboratory, Livermore, CA, USA
 ⁶University of Washington, Seattle, WA, USA

Corresponding Author: N. W. Eidietis, eidietis@fusion.gat.com

Experiments have been undertaken on the DIII-D tokamak to examine the magnitude and causes of radiated power asymmetries during disruption mitigation. In order to mitigate the most deleterious effects of disruptions, massive quantities of radiating impurities can be injected into the pre-disruptive plasma to pre-emptively radiate away the stored thermal and magnetic energy. However, toroidal and poloidal asymmetries in the radiation pattern could still result in localized melting of ITER's Be first wall. Measurements of the toroidal asymmetry in radiated power during disruption mitigation by massive gas injection (MGI) on the DIII-D tokamak indicate that the asymmetry during the thermal quench (TQ) and current quench (CQ) is largely insensitive to the number or location of injection sites [1]. Moreover, the observed absolute values of asymmetry during the TQ and CQ are well below those expected to be problematic for ITER. Infra-red imaging of the MGI valve location and surrounding wall indicates no highly localized, preferential heating of the injector location relative to the surrounding sector of wall, providing confidence that localized melting of the injector site in ITER is unlikely. Modification of the observed magnitude of the toroidal asymmetry during the TQ by application of a large n = 1 error field supports recent modeling results that indicate large n = 1 MHD during the TQ is the root cause of the radiation asymmetry [1, 2]. Further work examines the poloidal radiation asymmetries resulting from massive impurity injection and the effect of spatially distributed impurity injectors upon those asymmetries. In addition, the radiation asymmetries observed during MGI are compared to those observed during shattered pellet injection [3].

This work was supported in part by the US Department of Energy under DE-FC02-04ER54698, DE-AC05-00OR22725, DE-FG02-07ER54917, DE-AC52-07NA27344, and DE-AC05-00OR23100.

References

- [1] N. Commaux, et al., submitted to Phys. Plasmas.
- [2] V.A. Izzo, Phys. Plasmas 20, 056107 (2013).
- [3] N. Commaux, et al., Nucl. Fusion 50, 112001 (2010).

Full-f Neoclassical Simulations toward a Predictive Model for H-Mode Pedestal Ion Energy, Particle and Momentum Transport

D. Battaglia¹, J. A. Boedo², K. H. Burrell³, C.-S. Chang¹, J. Canik⁴, J. S. deGrassie³, S. Gerhardt¹, B. Grierson¹, R. Groebner³, R. Maingi⁴, and *S. Smith*³

¹Princeton Plasma Physics Laboratory, Princeton, NJ, USA
 ²University of California San Diego, CA, USA
 ³General Atomics, San Diego, CA, USA
 ⁴Oak Ridge National Laboratory, Oak Ridge, TN, USA

Corresponding Author: D. Battaglia, dbattagl@pppl.gov

Optimization and control of the H-mode pedestal and scrape-off layer (SOL) for burning plasma devices such as ITER requires a predictive model for the transport of particles, energy and momentum from the top of the pedestal to the first wall. The transport simulation code XGC0 leverages highperformance computing to rigorously compute the full-f multi-species (D⁺, C^{6+} , e^-) flux-driven neoclassical transport with self-consistent neutral recycling and model-based anomalous transport in the H-mode pedestal and SOL. Net particle transport and electron thermal transport is anomalous, while ion thermal and momentum transport is predominately neoclassical in the steep-gradient region of the pedestal. The separate transport mechanisms resolves the decoupling of energy and particle transport often observed in the evolution of the H-mode barrier or in regimes with enhanced particle transport from an edge mode, such as QH-mode or I-mode. It is shown that the radial electric field (E_r) in the pedestal is the root solution that balances ion orbit loss of high-energy counter- I_p ions against a pinch of colder ions. Neoclassical effects lead to non-Maxwellian ion energy distributions that manifest as intrinsic co- I_p parallel flows, T_i anisotropy ($T_{\theta} \neq T_{\phi}$) and non-monotonic Z_{eff} profiles, especially at low collisionality. These effects are quantitatively demonstrated through comparisons of XGC0 simulations to a low-collisionality QH-mode pedestal and a zero-torque intrinsically rotating ECH-heated discharge on DIII-D. EPH-mode on NSTX is a stationary ELM-free regime that has a double barrier in the ion thermal transport and a single barrier in the particle transport. XGC0 simulations indicate that the enhanced thermal ion confinement occurs when the parallel rotational shear length is on the order of ion orbit, improving the confinement of tail ions and reinforcing the rotational shear. The neoclassical origin of E_r results in a predictable connection between the $E \times B$ flow shear and magnetic geometry that can be leveraged to control the requirements for the L-H transition. For example, experiment and simulation demonstrate that a lower edge T_i is required to enter H-mode as the X-point increases to a low-triangularity shape on NSTX.

This work was supported by the US Department of Energy under DE-AC02-09CH11466, DE-FG02-07ER54917, DE-FC02-04ER54698, and DE-AC05-00OR22725.

Preprint

Applying the Radiating Divertor Approach to Innovative Tokamak Divertor Concepts

T. W. Petrie¹, S. L. Allen², J. Canik³, M. E. Fenstermacher², J. Ferron¹, R. Groebner¹, C. T. Holcomb², A. W. Hyatt¹, E. Kolemen⁴, R. J. La Haye¹, C. J. Lasnier², A. W. Leonard¹, T. C. Luce¹, A. G. McLean², R. Maingi³, R. Moyer⁵, W. M. Solomon⁴, V. Soukhanovskii², F. Turco⁶, and J. G. Watkins⁷

¹General Atomics, San Diego, CA, USA
 ²Lawrence Livermore National Laboratory, Livermore, CA, USA
 ³Oak Ridge National Laboratory, Oak Ridge, TN, USA
 ⁴Princeton Plasma Physics Laboratory, Princeton, NJ, USA
 ⁵University of California San Diego, CA, USA
 ⁶Columbia University, New York, USA
 ⁷Sandia National Laboratories, Livermore, CA, USA

Corresponding Author: T. W. Petrie, petrie@fusion.gat.com

Results are reported and interpretation made of recent experiments on DIII-D that assess the effectiveness of three innovative tokamak divertor concepts under radiating divertor (RD) conditions: (1) high performance standard double-null divertor (DND) plasmas, (2) high performance double-null "snowflake" (SF-DN) plasmas, and (3) single-null H-mode plasmas with different parallel connection lengths between their X-points and outer divertor targets (L||-XPT). In general, all three concepts are attractive, with reduced heat flux and good H-mode confinement. Significant reductions in peak divertor heat flux (q_{\perp}, P) of more than 50% and 85% at the outer and inner targets, respectively, were observed in DND plasmas under neon/deuterium-based RD conditions, and high performance metrics were maintained, e.g., $\beta_N \simeq 3.0$ and $H_{98}(y,2) \simeq 1.35$. Under these RD conditions, < 20% of the input power ($\approx 10-13$ MW) was radiated in the core, while > 40% outside the main plasma. Impurity injection from poloidal locations other than the private flux region opposite the $B \times \nabla B$ drift direction produced high levels of fuel dilution. High performance SF-DN plasmas mirrored the DND results under similar RD conditions. While the heat flux profiles at the inner target of the SF-DN and DND plasmas behaved similarly under comparable RD conditions, q_{\perp} , P at its outer divertor target of the SF-DN cases was generally about a factor of two lower. Impurity build up in the main plasma, however, was 15%-20% higher in the SF-DN, due in part to difficulty in pumping the broad density profile under the outer divertor leg of the SF-DN. Plasmas with longer L_{||}-XPT had lower $q \perp$, P than those with the shorter L \parallel -XPT. SOLPS modeling has indicated that cross-field transport between the X-point and the divertor target resulted in broadened heat flux profiles and reduced $q \perp$, P. Under similar RD conditions, the longer L||-XPT cases maintained lower $q \perp$, P by at least 50%. Partial detachment at the outer divertor under RD conditions occurred at lower \tilde{n}_e in the longer L \parallel -XPT cases. This study represents a first systematic step in examining three potential solutions to the excessive power loading expected in future generation high-powered tokamaks.

This work was supported in part by the US DOE under DE-FC02-04ER54698, DE-AC52-07NA27344, DE-AC05-00OR22725, DE-FG02-07ER54917, DE-FG02-04ER54541, and DE-AC04-94AL85000.

Preprint

Reduction of Net Erosion of High-Z PFC Materials in DIII-D Divertor Due to Re-Deposition and Low-Z Coating

D. L. Rudakov¹, P. C. Stangeby², W. R. Wampler³, J. Brooks⁴, C. P. Chrobak⁵, J. D. Elder², A. Hassanein⁴, A. W. Leonard⁵, A. G. McLean⁶, R. Moyer¹, T. Sizyuk⁴, J. G. Watkins³, and C. P. Wong⁵

¹University of California San Diego, CA, USA
 ²University of Toronto, Ontario, Canada
 ³Sandia National Laboratories, Livermore, CA, USA
 ⁴Purdue University, West Lafayette, IN, USA
 ⁵General Atomics, San Diego, CA, USA
 ⁶Lawrence Livermore National Laboratory, Livermore, CA, USA

Corresponding Author: D. L. Rudakov, rudakov@fusion.gat.com

We report a substantial reduction of net compared to gross erosion of a tungsten PFC surface observed in DIII-D divertor in good agreement with modeling, and suppression of molybdenum erosion by a local gas injection. A sample featuring a 1 mm and a 1 cm diameter 15–24 nm thick W films deposited on a Si substrate over a carbon inter-layer was exposed in the lower divertor of DIII-D using the Divertor Material Evaluation System (DiMES). The exposure was performed in lower single null L-mode deuterium plasma discharges near the attached outer strike point (OSP) for a total of ~16 s. The plasma density $n_e = 1.2 \times 10^{19} \text{ m}^{-3}$ and electron temperature $T_e = 32-35 \text{ eV}$ near OSP were measured by the divertor Langmuir probes. Net erosion was determined by comparing Rutherford backscattering (RBS) measurements of the W layer thickness on the 1 cm spot before and after the exposure, and gross erosion was estimated from similar measurements on the 1 mm spot. The measured net and gross erosion rates were 0.14 and 0.48 nm/s, respectively, giving net/gross erosion ratio of 0.29. REDEP/WBC modeling of this experiment yielded a very close ratio of 0.33. A second exposure of a sample with similar W coatings on a Mo inter-layer performed in similar geometry at similar T_e but ~ ×3 higher n_e yielded erosion rates about twice higher and net/gross erosion ratio of 0.38. Modeling of the second experiment is in progress. In another experiment, two Mo-coated Si samples 1 cm in diameter were exposed near attached OSP, first in L-mode for ~ 14 s, second in H-mode for ~ 7 s, with ¹³CH₄ gas injected ~ 12 cm upstream of the samples. Suppression of Mo erosion was evidenced in situ by the disappearance of MoI line radiation at 386.3 and 390.2 nm once the gas injection was turned on. Post-mortem RBS analysis found the erosion of Mo near the center of the samples being below the measurement resolution of 0.3 nm, corresponding to a rate of 0.02 nm/s. Compared to the previously measured erosion rates in L-mode of 0.4--0.7 nm/s this constitutes a reduction of more than 20. Carbon deposition was measured on both samples, corresponding to a rate of ~ 20 nm/s in L-mode and ~ 4 nm/s in H-mode. The ratio of ${}^{13}C/{}^{12}C$ carbon in the deposits was about 1.6 on both samples, indicating that the deposition was largely from the gas injection.

This work was supported by the US DOE under DE-FG02-07ER54917.



EX/P2-28

The Single Dominant Mode Picture of Non-Axisymmetric Field Sensitivity and its Implications for ITER Geometric Tolerances

C. Paz-Soldan¹, K. H. Burrell², R. J. Buttery², J. S. deGrassie², N. M. Ferraro², A. M. Garofalo², J. Hanson³, J. D. King⁴, R. J. La Haye², M. Lanctot², N. Logan⁵, J.-K. Park⁵, D. Shiraki⁴, W. M. Solomon⁵, E. J. Strait², and B. J. Tobias⁵

¹Oak Ridge Institute for Science Eduction, Oak Ridge, TN, USA
 ²General Atomics, San Diego, CA, USA
 ³Columbia University, New York, USA
 ⁴Oak Ridge National Laboratory, Oak Ridge, TN, USA
 ⁵Princeton Plasma Physics Laboratory, Princeton, NJ, USA

Corresponding Author: C. Paz-Soldan, paz-soldan@fusion.gat.com

Experiments at DIII-D have demonstrated that several key 3D field sensitivities are directly related to their coupling to the least-stable kink mode of the plasma, and concomitantly that the plasma is remarkably insensitive to fields which have no net coupling to this single dominant (kink) mode. Specifically, plasma rotation and error field (EF) penetration thresholds are nearly unchanged despite application of large amplitude probing fields with no kink coupling. The plasma sensitivity to 3D fields which have no kink coupling is of critical importance as this sets the true geometric tolerance of the tokamak — so long as it is equipped with at least a single row of EF correction coils (EFCCs) and its 3D field sources are well characterized, thus allowing the kink-coupling of the intrinsic EF to be nulled by the EFCCs. The observed weak sensitivity to the no kink coupling field challenges the stringent tolerance requirements currently enforced, as a strong performance recovery when using EFCCs is expected though it is not presently taken into account. The validity of the single dominant mode picture is determined experimentally by contrasting the plasma sensitivity to large-amplitude probing fields that have varying levels of coupling to the kink mode. Sensitivity to rotation braking is contrasted in both H- and L-mode plasmas, where for both scenarios, braking by n = 1 probing fields is reduced by nearly a factor of ten when the kink mode coupling is nulled. EF penetration is also contrasted with both H-mode and Ohmic plasmas. In both cases the penetration threshold is nearly unchanged (vs. a no-field baseline) when the probing field has no kink coupling, despite its large amplitude. The maintenance of the edge rotation due to the neoclassical toroidal viscosity (NTV) with n = 2 fields is also largest when coupling to the kink is maximized. A validated single dominant mode picture can also be applied to predicting optimal EFCC currents for any plasma scenario regardless of 3D field source. This is achieved by nulling the kink mode coupling of the intrinsic EF. Recent work shows that an exhaustive database of over 20 experimentally determined n = 1 optimal EFCC currents is consistent with nulling the n = 1 kink coupling of each plasma.

This work was supported by the US DOE under DE-AC05-06OR23100, DE-FC02-04ER54698, DE-AC02-09CH11466, and DE-FG02-04ER54761.



Electron Temperature Critical Gradient and Transport Stiffness

S. Smith¹, C. C. Petty¹, C. Holland², M. Austin³, T. Rhodes⁴, G. R. McKee⁵, D. Truong⁵, G. Wang⁴, and L. Zeng⁴

¹General Atomics, San Diego, CA, USA ²University of California San Diego, CA, USA ³University of Texas at Austin, Austin, TX, USA ⁴University of California Los Angeles, CA, USA ⁵University of Wisconsin-Madison, Madison, WI, USA

Corresponding Author: S. Smith, smithsp@fusion.gat.com

In a continuing effort to validate turbulent transport models, the electron heat flux has been probed as a function of electron temperature gradient on the DIII-D tokamak. In the scan of gradient, a critical electron temperature gradient has been found in the electron heat fluxes and stiffness at various radii in L-mode plasmas. The TGLF reduced turbulent transport model [1] and full gyrokinetic GYRO model [2] obtain the observed critical gradients and stiffnesses, but they do not predict the absolute level of transport at all radii. Here the stiffness is defined as the ratio of the heat pulse diffusivity (obtained by modulating 1 of the electron cyclotron heating gyrotrons) to the power balance diffusivity. For a regime where the heat flux is linearly proportional to the temperature gradient (with no offset), the stiffness is 1. There can be a critical gradient above which the flux is no longer proportional to the gradient; the stiffness will then jump above 1. Consistent with a critical gradient paradigm, the inferred stiffness at each radial location starts around 1 and jumps up above 1 at a critical gradient. The value of the critical gradient is observed to increase with radius in the plasma. The TGLF and GYRO predicted fluxes and stiffnesses exhibit a similar critical gradient; however there are conditions, such as when the experimentally inferred fluxes are large compared to gyrobohm fluxes, under which both codes underpredict the baseline level of transport. In addition to inferring the power balance and heat pulse diffusivities, the electron temperature fluctuations were measured at $\rho = 0.6$ using the Correlated Electron Cyclotron Emission diagnostic. Although the GYRO code does reasonably well at predicting the fluxes at this radius, it substantially underpredicts these electron temperature fluctuations, while still exhibiting a critical gradient similar to the measured fluctuations. This is a quandary because, in the past, predicted fluxes and fluctuations either both agree or disagree with experiment. The nature of the experiment-code discrepancies is prompting reevaluation of the range of wavenumbers used in GYRO simulations.

This work was supported by the US Department of Energy under DE-FC02-04ER54698.

References

[1] G.M. Staebler, J.E. Kinsey, and R.E. Waltz, Phys. Plasmas 14, 055909 (2007).. [2] J. Candy and R.E. Waltz, J. Comput. Phys. 186, 545 (2003).

EX/P2-30

Momentum and Particle Transport Across the ITG-TEM Turbulence Regimes in DIII-D H-Mode Plasmas

S. Mordijck¹, L. Schmitz², E. J. Doyle², C. Chrystal³, W.-H. Ko⁴, and C. C. Petty⁵

¹College of William and Mary, Williamsburg, VA, USA
 ²University of California Los Angeles, CA, USA
 ³University of California San Diego, CA, USA
 ⁴National Fusion Research Institute, Daejeon, Korea, Republic of
 ⁵General Atomics, San Diego, CA, USA

Corresponding Author: S. Mordijck, mordijck@fusion.gat.com

Turbulent particle transport and momentum transport have been shown to be closely connected theoretically as well as experimentally. In DIII-D H-mode plasmas we study the changes in particle and momentum transport across the linear ITG-TEM stability regime as well as studying the changes in particle transport as a function of the rotation profile. Counter to previous experimental [1], we do not find a correlation between normalized rotational shear (u') and density peaking $[\max(a/L_n)]$ and only a weak dependence of core T_e/T_i on density peaking. The density profiles do not become more peaked when we vary u' from, by changing the momentum injection with the neutral beams. However, there is a correlation between the radius where, the maximum peak in the density scale length occurs and the radius at which the plasma transitions from ITG to TEM. We find that the intermediate density fluctuations increase in the core of the co- and balanced-injected experiments and decrease outside mid-radius when compared with the counter-injected experiment. Together with a strong reduction in $E \times B$ shear outside mid-radius, this should result in a large increase in transport for the counter injected case. However, experimental perturbative D and ν transport coefficients show that the increase in D for the counter-injected experiment is fully countered with an even stronger increase in ν . In order to further study the role of turbulence in determining particle and momentum transport, we compare experiments in which we vary the heating from dominantly NBI-heated to ECH while keeping the injected momentum constant. We find that the ECH plasmas have a slightly more peaked density profile, but the overall density is strongly reduced. The rotation profiles for the ECH plasmas are more flat, but no rotation reversal is observed even though the plasmas transition from ITG to TEM close to mid-radius. The NBI heated plasmas all exhibit a rotational "well" in the pedestal area, which is not observed in the ECH heated plasmas and results in an overall lower core rotation. When adding a gas puff in the ECH heated plasma, we observe the return of the rotational well and the overall reduction of the core rotation at higher density.

This work supported by the US DOE under DE-SC0007880, DE-FG02-08ER54984, and DE-FC02-04ER54698.

References

[1] C. Angioni et al., Nucl. Fusion 51 (2011) 023006.



Development of Fully Noninductive Scenario at High Bootstrap Current Fraction for Steady State Tokamak Operation on DIII-D and EAST

X. Gong¹, B. Wan¹, J. Li¹, and A. M. Garofalo²

¹Institute of Plasma Physics, Chinese Academy of Sciences, Hefei, China ²General Atomics, San Diego, CA, USA

Corresponding Author: X. Gong, xz_gong@ipp.ac.cn

A main goal for EAST is to investigate an approach to fully noninductive long-pulse operation based on high bootstrap fraction under fusion relevant conditions. Building on results of previous DIII-D experiments, first joint experiments on DIII-D have developed a fully noninductive plasma scenario with EAST-similar plasma cross section shape, plasma current formation consistent with the superconductive coils on EAST, and values of plasma current, toroidal field, and heating power consistent with the new EAST capabilities. These EAST demonstration discharges on DIII-D have achieved and sustained fully noninductive conditions at $f_{BS} \ge 80\%$, $\beta_N \ge 3.0$, $\beta_T \sim 2.0\%$, and $f_{\text{Greenwald}} \ge 90\%$. Data supports that an ITB observed at large minor radius ($\rho \sim 0.7$) can be consistent with steady-state operation. Excellent energy confinement and high normalized pressure $(\beta_N > 3)$ were maintained even with the low NBI torque (~ 3 Nm) expected on EAST. ELM dynamics appear as a limiting instability toward stationary sustainment of even higher performance. These fully noninductive high bootstrap discharges need to pursue integration of ELM control on both of DIII-D and EAST. The experimental conditions on DIII-D have been used to simulate possible advanced steady-state scenarios for EAST, and the first experimental tests of these scenarios on EAST will be presented. Simulations using PTRANSP with the CDBM transport model show that such DIII-D scenarios are accessible on EAST for 0.5 MA steady-state plasma at $\beta_N \sim 2.4$ and with bootstrap current fraction of 65% by utilizing half of the total EAST H&CD capabilities planned for 2014. A weak core magnetic shear similar to the DIII-D scenario and with ITB footprint at $\rho \sim 0.6$ is achieved in the simulations. The scenario demonstrated on DIII-D and predicted for EAST could be extended to durations much longer than the current relaxation time and even the wall equilibration time using the expected EAST capabilities in the upcoming campaign, prior to the IAEA conference. Success of this endeavor will be a significant progress toward the goal of fusion energy.

This work was supported in part by the US Department of Energy under DE-FC02-04ER54698, DE-AC52-07N27344, and DE-AC02-09CH11466, and the National Magnetic Confinement Fusion Science Program of China under No. 2011GB101000.



Heat Transport and Enhancement Confinement Regimes in Tokamak as a Result of Plasma Self-organization

K. Razumova¹, N. Timchenko¹, and K. Dyabilin¹

¹National Research Centre "Kurchatov Institute", Moscow, Russian Federation Corresponding Author: K. Razumova, razumova_ka@nrcki.ru

Based on hypotheses about self-organization and pressure profile shape conservation in tokamak plasma, the turbulent heat transport processes are analyzed. The mechanism of internal transport barriers formation in regions without low number rational magnetic surfaces is suggested. The stronger pressure profile distortions from the self-consistent profile bring to the lower mode number excitation, increasing the heat flux. It is shown that the specific feature of the energy turbulent transport by low modes is the possibility of the internal transport barriers formation. The nontraditional explanation for H mode and regimes with the improved confinement ("advanced tokamak") is suggested.

Work is supported by ROSATOM contract No. H.4x.44.90.13.1101.



Extreme Low-Edge Safety Factor Tokamak Scenarios via Active Control of Three-Dimensional Magnetic Field on RFX and DIII-D

P. Martin¹, M. Baruzzo¹, J. Bialek², T. Bolzonella¹, D. Bonfiglio¹, R. Cavazzana¹, N. M. Ferraro³, A. M. Garofalo³, J. Hanson⁴, A. Hyatt³, G. L. Jackson³, J. King⁵, R. J. La Haye³, M. Lanctot³, L. Marrelli¹, G. A. Navratil⁴, M. Okabayashi², K. E. J. Olofsson⁴, R. Paccagnella¹, C. Paz-Soldan⁵, P. Piovesan¹, C. Piron¹, L. Piron¹, D. Shiraki⁴, E. J. Strait³, D. Terranova¹, F. Turco⁴, A. Turnbull³, P. Zanca¹, and B. Zaniol¹

¹Consorzio RFX, Associazione Euratom-ENEA sulla Fusione, Padova, Italy ²Princeton Plasma Physics Laboratory, Princeton, NJ, USA ³General Atomics, San Diego, CA, USA ⁴Columbia University, New York, USA ⁵Oak Ridge National Laboratory, Oak Ridge, TN, USA

Corresponding Author: P. Martin, piero.martin@igi.cnr.it

High current, stable tokamak plasmas with edge safety factor below or around 2 are attractive for magnetic fusion due to favourable high fusion gain and higher confinement. But they have long been considered inaccessible in modern devices owing to the unforgiving MHD instabilities. Even in tokamaks with a resistive wall, the onset of an n = 1 resistive wall mode leads to a disruptive limit at edge safety factor $q_{edge} = 2$ (for limiter plasmas) and $q_{95} \approx 2$ (diverted plasmas). This paper reports how for the first time two very different tokamaks, a large MA-class shaped device like DIII-D and a high aspect ratio circular experiment like RFX-mod, have robustly overcome the edge safety factor = 2 limit by active control of plasma stability and demonstrate that operation below 2 is possible for hundreds of resistive wall times. In addition these experiments reveal a new tool to control sawtooth frequency and amplitude, a result that has the potential of extending the tokamak operating space even further by avoiding deleterious giant sawteeth. The application of 3D fields with a strong n = 1 component that couples to the m = 1, n = 1 internal kink is found to significantly reduce the sawtooth amplitude and increase their frequency, demonstrating the benefits of this helical state. Experimental results have been compared with theory and numerical models. The experimental stability limit has been identified in DIII-D limiter plasmas as $q_{edqe} = 2.08 \pm 0.011$, slightly higher than the external kink mode limit $q_{edge} = 2.0$ predicted by ideal MHD analysis (DCON). In both devices the approach to the stability limit is characterized by the onset of an n = 1, m = 2 mode and growth rate of the order of τ_{wall} , consistent with ideal MHD predictions. RFX-mod shows that at $q_{edge} < 2.0$ the growth rate of the uncontrolled modes decreases as q_{edge} is lowered towards 1.5, i.e., indicating stability improvement as $q_{edge} = 1.5$ is approached from above. This is consistent with external kink mode stability expected from ideal MHD theory at $q_{edge} < 2.0$: a peak in the external kink growth rate is expected near, but below $q_{edge} = 2.0$, followed by a decrease in the growth rate. Sawtooth destabilization via applied magnetic perturbation is explained with the nonlinear MHD PIXIE3D code as a purely nonlinear effect, and not simply a modification of the (1, 1) kink linear stability.



EX/P2-42

Avoidance of Tearing Mode Locking and Disruption with Electro-Magnetic Torque Introduced by Feedback-Based Mode Rotation Control in DIII-D and RFX-Mod

M. Okabayashi¹, P. Zanca², E. J. Strait³, A. M. Garofalo³, J. Hanson⁴, Y. In⁵, R. J. La Haye³, *L. Marrelli*², P. Martin², P. Piovesan², C. Piron², L. Piron², D. Shiraki⁶, and F. A. Volpe⁴

¹Princeton Plasma Physics Laboratory, Princeton, NJ, USA
²Consorzio RFX, Associazione Euratom-ENEA sulla Fusione, Padova, Italy
³General Atomics, San Diego, CA, USA
⁴Columbia University, New York, USA
⁵FAR-TECH, San Diego, USA
⁶Oak Ridge National Laboratory, Oak Ridge, TN, USA

Corresponding Author: M. Okabayashi, mokabaya@pppl.gov

Disruptions caused by tearing modes (TM) are considered to be one of the most critical roadblocks to achieving safe steady state operation of tokamak fusion reactors. Here, a new scheme to avoid such disruptions is proposed by utilizing the electromagnetic (EM) torque produced with 3D coils that are available in many present tokamaks. In this scheme, the EM torque to the modes is created by a toroidal phase shift between the externally-applied field and the excited TM fields, compensating the mode momentum loss due to the interaction with the resistive wall and error field. Fine control of torque balance is provided by a feedback scheme. Experimentally, we have explored this in DIII-D, a non-circular divertor configuration with 3D coils inside the wall, and made comparisons to the performance in RFX-mod (operated as a tokamak), a circular limiter device with active feedback coils outside the wall using a slightly different, independently developed technique.

In high- β poloidal discharges in DIII-D, by applying sufficiently high gain, a large amplitude m/n = 2/1 TM propagating initially with the plasma rotation was successfully slowed down in a controlled manner to very low frequency, i.e., of the order of the inverse of resistive wall time τ_{ω} , and sustained over several seconds. Upon termination of feedback, the mode became locked leading to disruption. The controllability of torque balance was illustrated by rotating the mode forward or backward with varying feedback phase shift. In RFX-mod the controllability of mode rotation has been demonstrated at moderate plasma density $(n/n_G < 0.5$ where n_G is the Greenwald limit) and low q(a) (q(a) < 2.5), using pure real gains with no added phase shift. Here the key element for sustaining a mode at slow rotation frequency, $\sim 1/\tau_{\omega}$, is the minimization of coil-sideband pollution. Theoretical models developed independently for both devices showed that experiment observations are consistent with common understanding.

The achievements in both devices showed that this approach is robust, suggesting that the application to ITER would expand the horizon of its operational regime. The 3D coils currently under consideration for ELM suppression would be well suited to this purpose.

This work was supported by the US Department of Energy under DE-AC02-09CH11466, DE-FC02-04ER54609, DE-FG02-08ER85195, and DE-FG02-04ER54761.



G. Mazzitelli¹, M. L. Apicella¹, G. Apruzzese¹, F. Crescenzi¹, F. Iannone¹, G. Maddaluno¹, V. Pericoli Ridolfini², S. Roccella¹, M. Reale¹, B. Viola¹, I. Lyublinski³, and A. Vertkov³

¹Associazione EURATOM-ENEA Unitá Tecnica Fusione, Frascati, Italy ²Consorzio CREATE, Naples, Italy ³JSC "Red Star", Moscow, Russian Federation

Corresponding Author: G. Mazzitelli, giuseppe.mazzitelli@enea.it

Power load on the divertor is one of the main problems to be solved for steady state operation on the future reactors and liquid metals (Li, Ga, Sn) could be a viable solution for the target materials. Since 2006 experiments by using a Capillary Porous System (CPS) Liquid Lithium Limiter (LLL) were successfully performed on FTU indicating a good capability of the system to sustain power loads. In order to prevent the overheating of the liquid Li surface and the consequent strong Li evaporation for $T > 500^{\circ}$ C, an advanced version of LLL has been realized and installed on FTU by using the same vertical bottom port of the previous limiter. This new system, named Cooled Lithium Limiter (CLL), has been optimized to demonstrate the lithium limiter capability to sustain thermal loads as high as 10 MW/m² with up to 5 s of plasma discharge duration. CLL includes an actively cooled system with water circulation at high pressure and is characterized by: 1) the small thickness of the Li CPS meshes (of W) placed in direct contact with the cooling tube (of Mo) and 2) the double role of water circulation at the temperature of about 200°C, for heating lithium up to the melting point and for the heat removal during the plasma discharges. The heat load on the CLL is evaluated by different means: a fast infrared camera observing the whole limiter, the temperature measurements of inlet and outlet water as detected by the thermocouples and the measurements of the electron temperature and density by Langmuir probes placed on the CLL. Thermal loads analysis is performed by applying ANSYS code that has been adapted to the real CPS geometry and to the active cooling conditions of the new limiter. As first step, CLL has been tested in the FTU scrape-off layer to identify the best plasma conditions for a good uniformity of the thermal load by using the intensity of the Li and D atom emission at 670.8 nm and 656.3 nm to control Li production. The first experiments analyzed so far and simulated by ANSYS code, point out that heat loads as high as $2-3 \text{ MW/m}^2$ for 1.5 s have been withstood without problems. Analysis is in progress for plasma discharges with CLL inserted deeper in the FTU scrape-off layer and close to the LCMS. In this paper the heat load measurements and their analysis will be reported and discussed to provide a clear understanding of CLL behavior under plasma discharges.



EX/P2-47

Paper

Experiments on Magneto-Hydrodynamics Instabilities with ECH/ECCD in FTU Using a Minimal Real-Time Control System

C. Sozzi¹, C. Galperti¹, E. Alessi¹, S. Nowak¹, G. Apruzzese², F. Belli², W. Bin¹, L. Boncagni², A. Botrugno², A. Bruschi¹, P. Buratti², G. Calabrò², B. Esposito², L. Figini¹, S. Garavaglia¹, G. Granucci¹, L. A. Grosso², C. Marchetto¹, M. Marinucci², D. Marocco², C. Mazzotta², V. Mellera¹, D. Minelli¹, M. Mosconi³, A. Moro¹, V. Piergotti², G. Pucella², G. Ramogida², A. Romano², and O. Tudisco²

¹Istituto di Fisica del Plasma CNR, Euratom-ENEA-CNR Association, Milano, Italy ²Associazione EURATOM-ENEA Unitá Tecnica Fusione, Frascati, Italy ³Dipartimento di Energetica, Politecnico di Milano, Italy

Corresponding Author: C. Sozzi, sozzi@ifp.cnr.it

Experiments of magneto-hydrodynamic (MHD) instability control using injection of Electron Cyclotron Waves (ECW) are being performed in the FTU tokamak at toroidal field of 5.3 T, plasma current of 0.5 MA, line averaged density of 0.6×10^{20} m⁻³. The control system is based on only three real time key items: an equilibrium estimator (EQUIFAST) based on a statistical regression, a MHD instability marker (SVDH) using a 3D array of pick-up coils and the fast ECW launcher. One beam of 0.33 MW, 140 GHz, max pulse duration of 0.5 s has been used for heating in the Ordinary Mode polarization (OM1) with perpendicular toroidal injection and nearly on axis EC resonance. The EC absorption volume has been controlled by the poloidal steering of the launcher. The MHD activity (m, n = 2, 1 or 3, 2 modes) has been deliberately induced either by Neon impurity injection or by a density ramp hitting the density limit. No diagnostics providing the radial localization of the instabilities have been used. This is given a-posteriori through the evaluation of the effectiveness of the stabilization. When the ECW power is switched on, the instability amplitude shows a marked sensitivity to the position of the absorption volume with an increase or decrease of its growth rate. A significant reduction of the MHD amplitude has been obtained during the ECW injection phase. However, the continued cooling by Neon recycling that originates the instabilities does not allow their complete suppression at least at this ECW power level. The MHD control loop has been modified for the density limit experiments. The automatic search of the steering angle producing the fastest instability reduction has been introduced, based on the evaluation of the time derivative of the MHD amplitude. Once such angle is reached the controller holds the position until the SVDH signal crosses the switching off threshold. This control criterion has led to the suppression of the instabilities, even if the ECW injection is in some cases accompanied by a density pump-out reducing the density below the onset threshold. These experiments are the first attempt of feedback control of the ECW launcher in FTU for MHD control purposes. The control tools used are essential and based on a minimal set of diagnostics. Such experimental condition mimics the situation of a fusion reactor where reduced diagnostics capabilities are expected.



Runaway Electron Control in FTU

D. Carnevale¹, B. Esposito², L. Boncagni², S. Galeani¹, M. Sassano¹, F. Belli²,
 C. Cianfarani², E. Giovannozzi², G. Granucci³, D. Marocco², G. Maddaluno², S. Podda²,
 G. Pucella², M. Riva², O. Tudisco², and V. Vitale²

¹Università Roma Tor Vergata, Dipartimento di Ing. Civile ed Ing. Informatica, Italy ²Associazione EURATOM-ENEA Unitá Tecnica Fusione, Frascati, Italy ³Istituto Di Fisica Del Plasma - CNR, Italy

Corresponding Author: D. Carnevale, daniele.carnevale@uniroma2.it

Runaway electrons (RE) are highly energetic electrons that might gain energy up to 20–30 MeV (FTU). Runway electron beam can be harmful for plasma facing components: its low pitch angle allows the deposition of a high amount of energy on small areas yielding serious and deep damages of the vessel structure. For Tokamakas such as ITER, RE beams current should be around 11–13 MA and an impact with the vessel would irreparably damage the machine. We have proposed a new tool in the FTU plasma control system (PCS) for position and I_p ramp-down control of disruption-generated runaway electrons and first experimental results are discussed.

The RE hybrid control algorithm switches among three phases: 1) in the I_p pre-quench phase the currents in the poloidal coils used for the radial control of the plasma are optimized by a dedicated algorithm called Current Allocator; 2) when the I_p quench is detected (on-line) the system performs actions to improve the radial control in case of formation of a RE plateau; 3) at the onset of the RE plateau, which is detected on-line by dedicated algorithms, the I_p is ramped down and the RE beam position is controlled, by means of real-time (RT) diagnostic signals (magnetics, neutrons), in such a way to minimize the interactions with the plasma facing components and safely shut down the discharge. This algorithm was tested in dedicated low density plasma discharges in which a significant RE population is generated during the I_p flat top and Ne gas is injected to induce a disruption: the rapid variation of the resistivity and the increased loop voltage at the disruption accelerate the pre-existing RE population and lead, in some cases, to the formation of a RE current plateau. The effectiveness of the RE hybrid control algorithm in this phase will be discussed as well as the possible improvements including code portability to other devices.



EX/P2-49

Cherenkov Emission Provides Detailed Picture of Non-Thermal Electron Dynamics in the Presence of Magnetic Islands

F. Causa¹, G. Pucella¹, P. Buratti¹, E. Giovannozzi¹, B. Esposito¹, L. Jakubowski², K. Malinowski², M. Rabinski², M. J. Sadowski², and J. Zebrowski²

> ¹Associazione EURATOM-ENEA Unitá Tecnica Fusione, Frascati, Italy ²National Centre for Nuclear Research (NCBJ), Świerk, Poland

Corresponding Author: F. Causa, federica.causa@enea.it

In the 2013 experimental campaign a novel optical diagnostic system, based on the Cherenkov effect, was installed on FTU, in collaboration with the NCBJ group (IPPLM Association) to study the dynamics of non-thermal electrons in the presence of magnetic islands. Data from the Cherenkov probe was correlated with data from several other diagnostics, including ECE, neutron and gamma detector, Mirnov coils, soft X-ray cameras, demonstrating that the modulation of the Cherenkov signal is due to the rotation of the magnetic island. An aspect of interest under investigation is the internal structure of the peaks of the Cherenkov signal, with sub-peak full-width at half maximum of the order of 10 μ s, and approximately 20 μ s sub-peak separation. This level of detail opens up new possibilities for the investigation of fast electrons dynamics in the presence of high-amplitude magnetic islands. The study will present the analysis of the experimental data focusing on the identification of the magnetic island position and geometry during tearing mode instabilities. This work is in the initial phase; future work is planned to enable energy discrimination of the incoming electrons (for example through the implementation of a multi-channel probe), as well as an increase of the spatial information (by installing a second probe).

On the Measurement of the Threshold Electric Field for Runaway Electron Generation in FTU

B. Esposito¹, J. R. Martin-Solis², Z. Popovic², G. Artaserse¹, F. Belli¹, A. Botrugno¹,
C. Cianfarani¹, V. Cocilovo¹, D. Marocco¹, C. Mazzotta¹, L. Panaccione¹, S. Podda¹,
G. Ramogida¹, M. Riva¹, A. Romano¹, and O. Tudisco¹

¹Associazione EURATOM-ENEA Unitá Tecnica Fusione, Frascati, Italy ²Universidad Carlos III de Madrid, Madrid, Spain

Corresponding Author: B. Esposito, basilio.esposito@enea.it

The determination of the threshold density value to be achieved by means of massive gas injection for runaway electron (RE) suppression in ITER relies on the relativistic collisional theory of RE generation which predicts that, below a critical electric field (E_R), no runaway electrons can be generated. No account of additional loss mechanisms, that may reduce the critical density, is usually made in the above treatment.

Past experiments by means of electron-cyclotron-resonance heating in the flat-top phase of FTU discharges had shown that runaway suppression is found to occur at electric fields substantially larger than those predicted by the relativistic collisional theory of runaway generation. This was found to be consistent with an increase of E_R due to the electron synchrotron radiation losses, which lead to a new electric field threshold ($E_{R,rad}$).

The main aim of this work is to verify whether the earlier finding that synchrotron radiation losses play a role in runaway generation is also confirmed in FTU discharges with no additional heating. Recent experiments in FTU have systematically investigated the conditions for RE generation in stationary and reproducible conditions (flat top of ohmic discharges) for a wide range of plasma parameter values: toroidal magnetic field ($B_t = 3-7.2$ T), plasma current ($I_p = 0.35-0.5$ MA) and Z_{eff} (1.5–15).

The threshold electric field for RE generation was measured using feedforward gas programming to obtain a decreasing electron density until RE are generated. The results indicate that the measured threshold electric field is larger by a factor 5–10 than expected according to the purely collisional theory and is very close to the new threshold calculated including synchrotron radiation losses ($\sim 2E_{R,rad}$).



EX/P2-51

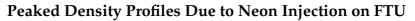
Experiments and Modelling on FTU Tokamak for EC Assisted Plasma Start-up Studies in ITER-like Configuration

G. Granucci¹, D. Ricci¹, S. Garavaglia¹, L. Figini¹, W. Bin¹, D. Farina¹, C. Sozzi¹, A. Moro¹, M. Cavinato², G. Artaserse³, G. Calabrò³, G. Ramogida³, and O. Tudisco³

¹Istituto di Fisica del Plasma CNR, Euratom-ENEA-CNR Association, Milano, Italy ²F4E: Fusion for Energy, Barcelona, Spain ³Associazione EURATOM-ENEA Unitá Tecnica Fusione, Frascati, Italy

Corresponding Author: G. Granucci, granucci@ifp.cnr.it

The intrinsic limited toroidal electric field (0.3 V/m for ITER) in devices with superconducting poloidal coils (ITER, JT-60SA, DEMO) requires an additional heating, like Electron Cyclotron (EC) waves, to initiate plasma current and to sustain it during the burn-through phase. The circular full metallic FTU tokamak, equipped with an ECRH system (140 GHz, 0.5 s, up to 1.6 MW), has contributed in the past to a wide documented study on the possible configuration and perspective of EC assisted plasma breakdown, performing experiments focused on low electric field start-up with perpendicular injection of EC power. Afterwards a new experimental and modelling activity, addressing the study of assisted plasma start-up in a configuration close to ITER one (magnetic field, wave oblique injection and polarization) realized on FTU, has been initiated and presented. These new experiments have been supported by a 0-D code, BKD0, developed to model the FTU plasma start-up and linked to a beam tracing code to computing, in a consistent way, EC absorption. The FTU results demonstrate the role of polarization conversion with oblique injection at the inner wall reflection, confirmed by a faster plasma current ramp up (from 3.5 to 8.6 MA/s), when the waves reflects on the inner vessel surface. This effect is related to the higher temperature reached as a result of the better power absorption of extraordinary polarized waves generated at reflection, guaranteeing a wider operational window in term of filling pressure and toroidal electric field. Dedicated experiments showed also the capability of EC power to sustain plasma start-up even in presence of strong vertical magnetic field (10 mT), with a null outside the vacuum vessel. These results assume more and more importance considering that the first plasma in ITER will be likely obtained at half field (2.5 T), where the influence of stray field is doubled. The 0-D BKD0 code, developed and applied to FTU data to reproduce the ITER relevant configurations at half and full toroidal magnetic field, has been used to determine operational window of sustained breakdown as a function of toroidal electric field and filling pressure. Experimental results are in agreement with the BKD0 simulations, supporting the use of the code to predict start-up also in future tokamaks, like ITER and JT60SA.



C. Mazzotta¹, G. Artaserse¹, A. Botrugno¹, R. Cesario¹, B. Esposito¹, L. Gabellieri¹, M. Marinucci¹, D. Marocco¹, G. Pucella¹, C. Sozzi², and O. Tudisco¹

¹Associazione EURATOM-ENEA Unitá Tecnica Fusione, Frascati, Italy ²Istituto di Fisica del Plasma CNR, Euratom-ENEA-CNR Association, Milano, Italy

Corresponding Author: C. Mazzotta, cristina.mazzotta@enea.it

The density profile peaking produced by Ne-gas puffing was studied in in different L-mode plasma scenarios during recent experimental campaigns on FTU. In fact an stable radiative edge seeded with light impurities has beneficial effects and provokes density peaking without any undesirable central impurity accumulation [1,2]; on the other hand, a too large amount of impurities can lead to a disruptive MHD activity. In order to maintain the positive effect of the edge radiation it is important to fix the conditions of a strong increase of particle confinement while minimizing the amount of impurities needed. On FTU the Ne injection causes a spontaneous increase of the line average density by a factor 2 in the absence of Deuterium gas puffing. A Ne doped discharge is compared with a complementary one that reaches the same density by D gas puffing in the absence of Neon injection. The comparison shows a more peaked density for the Ne doped discharge. A qualitative estimate from UV spectroscopy measurements indicates that the density behavior cannot be attributed simply to the stripped electrons from the puffed Ne, but a modification of particle transport should be invoked in order to explain the spontaneous rise and the higher peaking. The recent experiments were devoted to characterize the plasma response to Ne injection at different densities and plasma currents. The principal results are: i) if density before the Ne puff is increased, the same injected impurity amount induces an abrupt density increase that rapidly ends in a disruption; ii) as the plasma current rises a less steep increase of the density is observed, and more D gas is necessary to obtain the same MHD activity that leads to the disruption. Finally, the observed density peaking is analyzed in terms of electron diffusion coefficients D and pinch velocity U. In the framework of a simple particle transport model [3], the presence of an inward pinch is confirmed. A micro-stability analysis will be performed to investigate the role of the ion and electron gradient driven modes on particle transport.

References

[1] G. Telesca et al., Nucl. Fusion 40 1845 (2000).

- [2] A. Messiaen et al., Phys. Rev. Lett. 77 2487 (1996).
- [3] V. Zanza et al., Nucl. Fusion 36 825 (1996).

EX/P2-52



EX/P2-54

(N)TM Onset by Central EC Power Deposition in FTU and TCV Tokamaks

S. Nowak¹, P. Buratti², O. Sauter³, E. Lazzaro¹, G. Pucella², D. Testa³, W. Bin¹, G. Canal³, B. Duval³, L. Federspiel³, C. Galperti¹, S. Garavaglia¹, G. Granucci¹, A. Karpushov³, D. Kim³, A. Moro¹, H. Reimerdes³, J. Rossel³, C. Sozzi⁴, A. Tuccillo², O. Tudisco², and D. Wagner³

¹CNR, Italy

²Associazione EURATOM-ENEA Unitá Tecnica Fusione, Frascati, Italy
 ³Ecole Polytechnique Fédérale de Lausanne, CRPP, Lausanne, Switzerland
 ⁴Istituto di Fisica del Plasma CNR, Euratom-ENEA-CNR Association, Milano, Italy

Corresponding Author: S. Nowak, nowak@ifp.cnr.it

The onset of both the conventional and neoclassical tearing modes (N)TMs remains an important issue for the fusion plasma operations. The understanding of the (N)TM onset driven by on-axis EC action, far from the mode locations, is a field still not well understood for the MHD instability control. Comparison of the responses from different devices with comparable size and operation parameters can give clear information about the main mechanisms leading to the mode destabilization. In L-mode the effects of central electron cyclotron heating (ECH) and current drive (ECCD) on the presence of (N)TMs have been investigated in TCV without explicit triggers as sawteeth and in FTU with the presence of latent MHD activity. In TCV two possible concomitant driving mechanisms for these instabilities, due to the on-axis EC power, have been associated to the change of plasma current density profile and of mode stability parameter upstream of the resonant location q = m/n and to the change in sign of the local difference between the toroidal plasma and the (N)TM velocity due to the EC torque, allowing the destabilizing action of the ion polarization current. In FTU the former mechanism has been related to both the mode onset and the amplification of a mode that was present in a marginally stable state. A scaling for the onset and amplification of (N)TM will be given and discussed taking into account geometrical and operational parameters. Investigation of the plasma current density evolution will be done using the current diffusion equation in transport codes as JETTO and ASTRA in order to calculate the stability parameter changes and compare this dynamics in FTU and TCV.

High Power ICRF Systems and Heating Experiments in EAST

X. Zhang¹, Y. Zhao¹, L. Lu², B. Wan¹, X. Gong¹, Y. Mao¹, Y. Lin³, J. Li¹, L. Hu¹, Y. Song¹, R. Kumazawa⁴, S. Wukitch³, J.-M. Noterdaeme⁵, F. Braun⁵, and H. Kasahara⁴

¹Institute of Plasma Physics, Chinese Academy of Sciences, Hefei, China
 ²CEA-IRFM, Saint Paul lez Durance, France
 ³Massachusetts Institute of Technology, Plasma Science & Fusion Center, Cambridge, MA, USA
 ⁴National Institute for Fusion Science, Toki, Japan
 ⁵Max-Planck-Institut für Plasmaphysik, Garching, Germany

Corresponding Author: X. Zhang, xjzhang@ipp.ac.cn

The ICRF system of 12.0 MW has been developed for EAST. To support the long pulse operation over 1000 s, the ICRF heating system is upgraded with active cooling, especially for ICRF antenna systems. The ICRF system of 6.0 MW has been operating in the 2012 experimental campaign. A new 6.0 MW system has been successfully commissioned at full power on water dummy load. In the upcoming campaign, the ICRF system is capable of delivering more than 10 MW of rf power to the plasma. The relevant experimental results from the upcoming campaign will be given.

Heating power modulation experiments using ion cyclotron resonance heating (ICRH) in the Hydrogen minority scheme have been performed in the 2012 campaign of the EAST. The power deposition profile in the ion cyclotron range of frequencies (ICRF) has been investigated experimentally. The D (H) minority heating scheme provides a dominant localized ion heating. In this scheme, electron heating occurs only through collisions with the minority ion tail. The results shows that the peak of the experimental power deposition profile is always occurred around to $\omega = \omega_{cH}$. The global energy confinement time was calculated in the ICRF modulation experiment, and compared with the scaling law, ITER-89. It was found that the calculated results coincided with ITER scaling law. The global energy confinement time decreases by a factor of 2 approximately from that in Ohmic plasmas with the ICRF heating power increases up to 1.6 MW. The heating efficiency was somewhat lower than expected. The effect on the sawtooth period was demonstrated in the experiments analyzed in this paper.

EX/P3-3



EAST Snowflake Experiment: Scenario Development and Edge Simulations

G. Calabro¹, S. Chen², Y. Guo², Z. Luo², R. Albanese³, R. Ambrosino¹, F. Crisanti¹, G. De Tommasi¹, E. Giovannozzi¹, S. Mastrostefano¹, A. Pironti¹, V. Pericoli Ridolfini¹, G. Ramogida¹, A. Tuccillo¹, F. Villone³, and B. Viola¹

¹Associazione EURATOM-ENEA Unitá Tecnica Fusione, Frascati, Italy ²Institute of Plasma Physics, Chinese Academy of Sciences, Hefei, China ³CREATE/ENEA/Euratom Association, Università di Napoli, Naples, Italy

Corresponding Author: G. Calabrò, calabro@frascati.enea.it

Snow Flake Divertor (SFD) configuration has been proposed as one valid way to reduce the plasmawall interaction. For technological reasons, SFD configuration is difficult to realize and control in real experiments, especially for a tokamak like EAST that does not have dedicated divertor coils designed to locally shape the magnetic field topology. For this reason, Quasi-SFD (QSF) static equilibrium configurations (where two poloidal field $B_n = 0$ points are close enough to produce a large region with poloidal field close to zero in the divertor region) have been studied by using EFIT and FIXFREE equilibrium codes. The tokamak simulation code (TSC), a numerical model of the axisymmetric tokamak plasma and the associated control systems, has been then used to model the EAST QSF scenario (300 kA/1.8 T). During the simulation, iso-flux control scheme is used to control plasma shape, and the poloidal field (PF) coils current is limited to be smaller than 15% of the actual allowed technical limits. TSC outputs will be preliminary used to set the plasma control system (PCS) operating during the experiments. CREATE-NL tools has been used to linearize the configuration, in order to increase the QSF to higher plasma current, and a dedicated control algorithm will be developed to use magnetic topology as a control actuator of the local radiation in presence of impurities seeding. The analysis of vertical stability growth rates of QSF configurations with 2D and 3D models is ongoing. Preliminary results on the comparison of edge simulations between the standard divertor (SD) and SFD will be also presented. First QSF experiment will be performed during next EAST restart.



Core Plasma Rotation Characteristics of RF-Heated H-Mode Discharges on EAST

B. Lyu¹, F. Wang¹, Y. Li¹, J. Fu¹, Y. Shen¹, X. Zhang¹, M. Wang¹, M. Bitter², K. Hill², S. G. Lee³, H. Zhang¹, Y. Xiong¹, Y. Shi³, and B. Wan¹

¹Institute of Plasma Physics, Chinese Academy of Sciences, Hefei, China ²Princeton Plasma Physics Laboratory, Princeton, NJ, USA ³National Fusion Research Institute, Daejeon, Korea, Republic of

Corresponding Author: B. Lyu, blu@ipp.ac.cn

Lyu

Access to high-confinement plasmas on the EAST tokamak was readily achieved through LHCD, ICRF, or their combined application along with improved wall conditioning and wave-plasma coupling capabilities. Using a tangentially viewing X-ray crystal spectrometer, core plasma rotation profiles and their temporal evolutions were obtained. This paper presented typical plasma rotation behaviors for non-stationary and stationary H-mode discharges generated with concurrent LHCD and ICRF heating. A substantial increase of the co-current core rotation was observed at L-H transitions. For unsteady discharges with multiple L-H and H-L transitions, central rotation velocity varied as the plasma entered and left the H-mode phase. For stationary ELMy H-mode discharges, the rotation increases at an L-H transition and core plasma rotation profile remains very stable during the entire H-mode phase, although the occurrence of ELMs tended to slow down the core rotation. Changes of the steady-state core rotation at L-H transitions were found to be dependent on the plasma parameters for different ELM types. A linear relation between the rotation and stored energy, similar to the Rice scaling was obtained for both ELM-free and ELMy H-mode discharges; and for ELMy-free discharges the slope was by a factor of 1.75 steeper.

This work was supported by National Magnetic Confinement Fusion Science Program of China (No. 2011GB101004, 2011GB107001 and 2013BG112004), National Science Foundation of China (No. 11175208, 11305212 and 11375235) and JSPS-NRF-NSFC A3 Foresight Program in the field of Plasma Physics (No. 11261140328).

Preprint

Investigation of Argon Seeding in Different Divertor Configurations in EAST and Corresponding SOLPS 5.0 Modeling

L. Xiang¹, H. Guo¹, M. Wischmeier¹, L. Wang¹, Z. Wu¹, Y. Duan¹, H. Wang¹, and Y. Chen¹

¹Institute of Plasma Physics, Chinese Academy of Sciences, Hefei, China Corresponding Author: L. Xiang, <u>lyxiang@ipp.ac.cn</u>

Introducing external impurities into plasma provides an effective means to reduce divertor power load for present and future fusion devices [1]. Dedicated argon (Ar) seeding experiments focusing on the effects of the plasma configuration and seeding position have been carried out in EAST, with the corresponding simulations using SOLPS 5.0 code package being also ongoing.

The double null (DN) divertor configuration is found to have a cooler divertor plasma before Ar seeding comparing to lower single null (LSN), as expected [2]. When Ar is seeded, the parallel heat flux to the lower divertor, measured by target Langmuir probes, exhibits a slightly more dramatic decrease in the case of DN configuration than in LSN configuration. At the outer midplane, the measurements by reciprocating probe reveal that the electron temperature and density are higher in DN configuration than in LSN configuration after Ar seeding. This indicates a greater gradient of temperature along the field line in DN case, which is beneficial for reducing divertor power load. In addition, the plasma stored energy Wdia increase with Ar seeding in DN case, meaning the confinement is improved.

Comparisons have also been made between Ar puffing into the divertor volume in LSN configuration and into main chamber in USN configuration. The radiation in the latter case increases by 42.6% together with a significant increase in $Z_{\rm eff}$, while in both cases the plasma stored energy almost stays unchanged. Though electron temperature and density at midplane is higher, the parallel heat flux at divertor plate is lower in USN case. However, after Ar seeding no decrease in parallel heat flux to upper outer divertor plate is seen in this case. At inner plate only the peak value of parallel heat flux reduces by 13%. It is evident that Ar can readily penetrate into the core when it is puffed into the main chamber volume, but does not affect the heat flux to the divertor very much in this case. We will include cases of different Ar puff locations as well as cases of Ar seeding in different plasma configurations in the SOLPS simulation to compare with present and further experiment results.

References

[1] ITER Physics Basis 1999, Nucl. Fusion 39, 2208, (1999).

[2] S.C. Liu et al., Phys. Plasmas 21, 022509, (2014).

Studies of Impact of Edge Current Profiles, Plasma Shaping, Nonlinearity on Edge Localized Modes with BOUT++ Code

G. Li¹, Z. Liu¹, X. Xu², T. Xia¹, X. Gao¹, P. B. Snyder³, S. Ding¹, J. Li¹, S. Liu¹, C. Ma⁴, L. Shao¹, A. Turnbull³, and P. Xi⁴

¹Institute of Plasma Physics, Chinese Academy of Sciences, Hefei, China ²Lawrence Livermore National Laboratory, Livermore, CA, USA ³General Atomics, San Diego, CA, USA ⁴Peking University, Beijing, China

Corresponding Author: G. Li, ligq@ipp.ac.cn

This work extends previous BOUT++ work to systematically study the edge current driven kink mode, the effect of plasma shaping on the ELMs, to benchmark with other codes, and to validate the BOUT++ nonlinear ELM simulation on EAST tokamak experiments. A sequences of equilibrium with different edge current is generated with the CORSICA code, by keeping total current and pressure profile fixed. With the edge current increasing, the dominant modes are changed from high-n ballooning modes to low-n kink modes. We found the edge current provides stabilizing effects on high-n ballooning modes, but not always provides the destabilizing effect on edge kink mode. We benchmarked BOUT++ linear results with GATO and ELITE codes. It is shown that the vacuum model has important effect on the edge kink mode calculation. The resistivity vacuum has destabilizing effect on both the kink modes and ballooning mode. Nonlinear calculation shows that with the edge current increasing, the linear growth rate of the ELM size decreases. However, at the final saturated stage after the nonlinear evolution, the ELM size increases with the edge current. We studied the role the plasma geometry, by choosing the circular, elongated, and shaped with X-point equilibrium. The shaped plasma and the X-point geometry has stabilizing effect on the ELMs. We benchmarked those calculation with other codes. 3D ELMs nonlinear simulation on EAST tokamak has first been studied, based on the discharge #41019. The result shows that there are four phases during one ELM crash, which gives us a vivid dynamic process of the ELM crash. We also prove the exactness of the nonlinear simulation by comparing the results of experiment and simulation, including the energy loss and speed of the ELM effluxes. The experimental energy loss of ELM crash is consistent with the nonlinear simulation within same order of magnitude. The speed of the simulated ELM effluxes is comparable with the experimental data by Gas Puffing Image (GPI) diagnosis, and the ELM crashes start at the outer mid-plane.

EX/P3-7



EX/P3-8

ELM Mitigation by Lower Hybrid Waves in EAST

Y. Liang¹, J. Li², B. Wan², X. Gong², H. Guo², G. Xu², Y. Sun², M. Rack¹, P. Denner¹,
L. Zeng², K. Gan², E. Gauthier³, L. Wang², B. Ding², L. Hu², H. Wang², X. Zou³, Y. Wang²,
B. Shen², J. Hu², F. Liu², Y. Jie², J. Qian², R. Chen², S. Zhang², T. Zhang², Z. Wu²,
M. Wang², T. Shi², J. Shan², N. Yan⁴, B. Lv², and U. Samm¹

¹Forschungszentrum Jülich, Jülich, Germany
 ²Institute of Plasma Physics, Chinese Academy of Sciences, Hefei, China
 ³CEA-IRFM, Saint Paul lez Durance, France
 ⁴Association EURATOM/DTU Physics, Roskilde, Denmark

Corresponding Author: Y. Liang, y.liang@fz-juelich.de

ELM mitigation has been observed on the Experimental Advanced Superconducting Tokamak (EAST) when lower hybrid waves (LHWs) are applied to H-mode plasmas sustained mainly with ion cyclotron resonant heating (ICRH). This has been demonstrated to be due to the formation of helical current filaments (HCFs) flowing along field lines in the scrape-off layer induced by LHWs. Because of the geometric effect of the LHW antenna, the perturbation fields induced by the HCFs are dominated by the n = 1 components, where n is the toroidal mode number. In comparison to previous RMP ELM mitigation experiments, using a set of fixed in-vessel coils, ELM mitigation with LHWs on EAST is achieved with a wider range of q_{95} . This is because the HCFs induced by the LHWs flow along the magnetic field lines in the SOL, thus the helicity of the HCFs always closely fits the pitch of the edge field lines whatever the value of the plasma edge safety factor.

Splitting of the outer divertor strike point during LHWs has been observed similar to previous observations with RMPs. The change in edge magnetic topology has been qualitatively modelled by including the HCFs in a field line tracing code. The results show a strong modification of the plasma edge topology dependent on the edge safety factor as well as the amplitude of currents flowing in these filaments. This can qualitatively explain the experimental observations of SP splitting.



Study of Pedestal Turbulence on EAST Tokamak

X. Gao¹, H. Qu¹, T. Zhang¹, Z. Liu¹, Y. Yang¹, Q. Zang¹, X. Han¹, S. Zhang¹, Y. Gao¹, and Y. Wang¹

¹Institute of Plasma Physics, Chinese Academy of Sciences, Hefei, China

Corresponding Author: X. Gao, xgao@ipp.ac.cn

Pedestal turbulence was studied by a microwave reflectometry on EAST tokamak. The characteristics of edge pedestal turbulence during L-I-H transition, ELM-free H-mode phase, and inter-ELM phase have been studied on EAST recently. 1) An edge spatial structure of density fluctuation and its dithering temporal evolution is observed on EAST tokamak during the L-H transition phase. 2) A coherent mode and/or a multi-harmonic mode often appears during the ELM-free phase before the first ELM on EAST tokamak. Analysis shows that there is a critical density for two modes on EAST. 3) In plasma with type-III ELMs, a precursor mode before ELM is usually observed. The frequency of the precursor was born about 150 kHz and gradually decreased up to the ELM. The mode amplitude increases or shows saturation before ELM. In the plasma with compound ELMs composed of high and low frequency ELMs, the precursor was also available before the high frequency ELM while the harmonic oscillations with frequencies of 20, 40, and 60 kHz appears before the low frequency ELM.

This work was supported by National Magnetic Confinement Fusion Program of China (No. 2014GB106000 and 2014GB106003) and the National Natural Science Foundation of China (No. 11275234, 11305215, 11321092).



Progress in Active Control of Divertor Power Load in the EAST Superconducting Tokamak

L. Wang¹, J. Hu¹, H. Guo¹, J. Li¹, B. Wan¹, G. Xu¹, X. Zou², Y. Liang³, A. Loarte⁴, D. Mansfield⁵, I. Vinyar⁶, C. Li¹, Z. Sun¹, Y. Chen¹, J. Li¹, K. Gan¹, L. Xiang¹, S. Liu¹, H. Wang¹, X. Gong¹, G. Luo¹, and L. Hu¹

¹Institute of Plasma Physics, Chinese Academy of Sciences, Hefei, China
 ²CEA-IRFM, Saint Paul lez Durance, France
 ³Forschungszentrum Jülich, Jülich, Germany
 ⁴ITER Organization, Saint Paul lez Durance, France
 ⁵Princeton Plasma Physics Laboratory, Princeton, NJ, USA
 ⁶PELIN, LLC, 27A, Gzhatskaya, St. Petersburg, Russian Federation

Corresponding Author: L. Wang, wliang@ipp.ac.cn

Divertor power and particle exhaust is a critical issue facing the operation of next-step fusion devices such as ITER and DEMO. Active control of excessive heat and particle fluxes under high power steady-state plasma conditions has become a frontier hotspot in magnetic confinement fusion development. Significant progress has been made in controlling transient and stationary divertor heat fluxes in the Experimental Advanced Superconducting Tokamak (EAST) since the last IAEA-FEC, using many innovative techniques such as deuterium/lithium (D_2/Li) pellet injection, Supersonic Molecular Beam Injection (SMBI), and integration of radiative divertor scenario with three-dimensional (3D) magnetic topology change induced by lower hybrid current drive (LHCD). We find that the injection of solid D_2 pellets can directly induce divertor plasma detachment in the RF-heated plasmas, significantly reducing steady-state heat fluxes on the divertor target plates. Plasma detachment can be modulated periodically by multi-pellet injection. Furthermore, D₂ pellet injection tends to trigger compound ELMs in H-modes, mitigating transient heat fluxes, compared to the standard Type I ELMs. In addition, Li granule injection has been demonstrated, for the first time in tokamaks, to be effective at triggering small ELMs with near 100% efficiency, thus providing a novel means for divertor power load control. ELM mitigation with SMBI has also been successfully achieved in EAST, significantly reducing the amplitude and increasing the frequency of ELMs. With multi-pulse SMBI, we demonstrated for the first time that the stationary divertor heat footprint can be actively modified by transferring heat from the outer strike point to the striated heat flux area in the far scrape-off layer, which is induced by LHCD. Similar results have been observed with divertor argon seeding. This provides an additional knob for the control of the stationary divertor power load, beyond or in addition to the achievement of highly radiating divertor conditions, which may be of great interest for future fusion devices such as ITER.

Investigation of LHW-Plasma Coupling and Current Drive Related to H-Mode Experiments in EAST

B. Ding¹, L. Zhang¹, M. Li¹, Y. Yang¹, W. Wei¹, Y. Li¹, S. Wang¹, M. Wang¹, H. Xu¹, G. Xu¹, L. Zhao¹, H. Hu¹, H. Jia¹, M. Cheng¹, Y. Yang¹, L. Liu¹, H. Zhao², Y. Peysson³, J. Decker³, M. Goniche³, L. Amicucci⁴, R. Cesario⁴, A. A. Tuccillo⁴, S. G. Baek⁵, R. R. Parker⁵, P. Bonoli⁵, C. Yang¹, H. Liu¹, G. Li¹, J. Shan¹, F. Liu¹, Y. Zhap¹, X. Gong¹, L. Hu¹, X. Gao¹, H. Guo¹, B. Wan¹, and J. Li¹

¹Institute of Plasma Physics, Chinese Academy of Sciences, Hefei, China
 ²University of Science and Technology, Anhui, China
 ³CEA-IRFM, Saint Paul lez Durance, France
 ⁴Associazione EURATOM-ENEA Unitá Tecnica Fusione, Frascati, Italy
 ⁵Massachusetts Institute of Technology, Cambridge, MA, USA

Corresponding Author: B. Ding, bjding@ipp.ac.cn

LHW-plasma coupling and high density are two important issues in achieving LHCD H-mode plasma in EAST. Firstly, effects of LHW on the density at the grill mouth are investigated by a Langmuir probe installed in the top of the LHW antenna. Results show that the measured density with anti-clockwise B_t is lower than those with clockwise B_t , suggesting the asymmetric density behaviour in SOL. Simulation with a diffusive-convective model suggest that such asymmetry is mainly due to $E \times B$ drift. Secondly, high density experiments with LHCD are further analyzed by means of simulation, showing that parametric instability (PI), collision absorption (CA) in edge region, and density fluctuation could be responsible for the low current drive (CD) efficiency at high density. i) Frequencies and growth rates of coupled modes could be identified near the antenna and the LCFS. Modelling results show that the line broadening of the operating LH frequency and the downshifted sidebands, observed during the experiments, could be produced by PI effects driven by ion-sound and ion-cyclotron (IC) quasimodes, respectively, near the plasma edge in the low field side. The growth rates are larger in the case of poor lithiation, consistently with the observed reduced CD efficiency. Simulations also show that the growth rate peak of the IC sideband occurs near the LCFS, and, in case of poor lithiation, has a smaller frequency shift from the pump, in agreement with the RF probe spectra. ii) The fraction of LH power calculated with GENRAY code indicates that more LHW power is absorbed in SOL by collision in the case of poor lithiation, whether at low density or high density, making some contribution to the low CD efficiency in this case. iii) Modification of spectrum due to density fluctuation makes the power deposition and driven current profile predicted by C3PO/LUKE ray-tracing and Fokker-Planck move inward, but the total value of driven current decreases (30%). This may partly explain the small CD efficiency in the case of SMBI. In addition, CD efficiency with considering bootstrap current and hot electrical conductivity has been investigated in EAST H mode. Results show the efficiency maximum locates at $n_e \sim 2.2 \times 10^{19} \text{ m}^{-3}$, above which the efficiency drops significantly with density increase, nearly consistent with the above HXR emission. Further study will be continued.

EX/P3-12

The Latest Development of EAST Neutral Beam Injector

Y. Xu¹, C. Hu¹, Y. Xie¹, S. Liu¹, Z. Liu¹, P. Sheng¹, Y. Xie¹, and L. Liang¹

¹Institute of Plasma Physics, Chinese Academy of Sciences, Hefei, China

Corresponding Author: Y. Xu, yjxu@ipp.ac.cn

As the first full superconducting non-circular cross section tokamak in the world, EAST is used to explore the forefront physics and engineering issues on the construction of tokamak fusion reactor. Neutral beam injection has been recognized as one of the most effective means for plasma heating. According to the research plan of the EAST physics experiment, two sets of neutral beam injector (4–8 MW, 10–100 s) will be built and operational in 2014. The paper presents the development of EAST neutral beam injector and the latest experiment results obtained on the test-stand about long pulse beam extraction and high power beam extraction, those results show that all targets reach or almost reach the design targets. All these will lay a solid foundation for the achievement of plasma heating and current drive for EAST in 2014.

Redefinition of the ITER Requirements and Diagnostics for Erosion, Deposition, Dust and Tritium Measurements Accounting for the Change to Tungsten Divertor

R. Reichle¹, P. Andrew¹, R. Barnsley¹, L. Bertalot¹, G. Jagannathan¹, S. Lisgo¹, R. Pitts¹, P. Shigin¹, W. Shu¹, G. Vayakis¹, and M. Walsh¹

¹ITER Organization, Saint Paul lez Durance, France

Corresponding Author: R. Reichle, roger.reichle@iter.org

Dust and tritium inventories in the vacuum vessel have upper limits in ITER. Erosion, migration and re-deposition of wall material and co-deposition of fuel material are closely linked to the these inventories. The related suite of diagnostic and the respective set of plasma-wall-interaction physics related measurement requirements is now redefined as a whole because the decision to change from carbon to tungsten as divertor target material has been taken and the construction schedule requires developing the diagnostic concepts. This paper presents the result of this redefiniton.



EX/P3-16

Advancing Power Exhaust Studies from Present to Future Tokamak Devices

M. Wischmeier¹, L. Aho-Mantila², B. Matthias¹, T. Eich¹, A. Kallenbach¹, D. Carralero¹, D. Coster¹, T. Lunt¹, H. W. Müller¹, S. Potzel¹, A. Scarabosio¹, S. Bernhard¹, and F. Reimold¹

> ¹Max-Planck-Institut für Plasmaphysik, Garching, Germany ²VTT Technical Research Centre of Finland, Finland

Corresponding Author: M. Wischmeier, marco.wischmeier@ipp.mpg.de

Power exhaust is a crucial issue for future fusion devices such as ITER and DEMO. A device like DEMO despite being of a similar geometrical size of ITER will need to accommodate an about 3 to 4 times higher thermal power, aggravating the issue of power exhaust. ASDEX Upgrade with its fully tungsten covered wall, high ratio of heating power to major radius and extensive edge and SOL diagnostics is well suited for studying most aspects of power exhaust. Limiting the total power flux to the divertor target plates is only possible in the detached regime. Despite its crucial importance for safe operation of future larger devices the understanding of the processes leading to divertor detachment is incomplete.

The paper summarizes the efforts undertaken in gradually advancing the understanding of power exhaust in a variety of conditions: It presents how the H-mode density limit is controlled by a fuelling limit and an enhanced loss of power at the plasma edge. The power fall off length in the divertor is determined by the volumetric dissipation in the divertor connected to the recycling of neutrals and consequently to the divertor geometry. Experiments with nitrogen as seeding impurity for L-mode and H-mode are used for validating the SOLPS code package. In such studies the activation of drift terms in the numerical model is crucial for minimizing the differences to the experimental data. The movement of the radiation in the divertor under varying conditions is explained and maximum radiation is reached with stable radiation in the vicinity of the X-point. A phase of strong fluctuating radiation for strongest discrepancy between the numerical and experimental results. Studies on the snowflake as an alternative divertor geometry solution using the EMC3-EIRENE code are also presented.



Impact of W on Scenario Simulations for ITER

G. Hogeweij¹, V. Leonov², J. Schweinzer³, A. Sips⁴, C. Angioni³, G. Calabrò⁵, R. Dux³, A. Kallenbach³, E. Lerche⁶, C. Maggi³, and T. Pütterich³

¹FOM Institute DIFFER, Association EURATOM-FOM, Nieuwegein, The Netherlands ²National Research Centre "Kurchatov Institute", Moscow, Russian Federation ³Max-Planck-Institut für Plasmaphysik, Garching, Germany ⁴JET-EFDA, Culham Science Centre, Abingdon, UK ⁵Associazione EURATOM-ENEA Unitá Tecnica Fusione, Frascati, Italy ⁶Laboratory for Plasma Physics, ERM/KMS, Brussels, Belgium

Corresponding Author: G. Hogeweij, g.m.d.hogeweij@differ.nl

AUG and JET, the largest present devices with high-Z PFC components, have identified requirements for stable H-mode operation, i.e., to keep heavy impurity concentrations sufficiently low, to avoid central accumulation, radiative collapses and disruptions. Limitations in the operational space which can be accessed in H-mode have been identified, e.g., (i) the need of operating at sufficiently high levels of gas puff, impeding access to low density regimes at low gas puff levels; (ii) central electron heating and/or frequent sawteeth may be needed to avoid W core accumulation. This paper starts with a short review of experimental results on erosion sources, edge (pedestal) transport, and core W transport. Then implications for ITER are discussed, concentrating on the effect of core W accumulation on the discharge evolution. In different ways the critical W concentration in ITER was assessed, i.e., the maximal tolerable level without significantly perturbing the evolution of li, or the q and T_e profiles.

First, impurity transport (both neoclassical and anomalous) was modelled with the ZIMPUR code, in combination with ASTRA for the description of the bulk plasma parameters evolution with a scaling based transport model. The calculated critical W concentration is $\sim 7 \times 10^{-5}$ for the inductive scenario, and a factor 2–3 lower for the hybrid and steady state scenarios.

Second, the current ramp-up phase in JET, AUG, and ITER was modelled with the CRONOS suite of codes for different W concentrations. For ITER the expected plasma parameters for the baseline ITER ramp-up were used; for JET and AUG the experimental data (T_e , n_e , Z_{eff}) were taken. The Bohm-gyroBohm model for thermal transport was used, and n_W/n_e profiles were assumed either flat or of the same (peaked) shape as measured in JET. The effects of flat and peaked W profiles are very different. The modelling results are in excellent agreement with experimental findings. As maximum tolerable W concentrations have now been calculated for different ITER scenarios, future work can concentrate on further quantify these limitations, using current understanding of neo-classical and anomalous W transport.

This work was supported by EURATOM and carried out within the framework of the European Fusion Development Agreement. The views and opinions expressed herein do not necessarily reflect those of the European Commission.

Status of R&D for ITER Disruption Loads, Disruption Mitigation and Runaway Electron Avoidance

M. Lehnen¹, *D. Campbell*¹, K. Aleynikova¹, P. Aleynikov¹, P. de Vries¹, Y. Gribov¹, G. Huijsmans¹, M. Kocan¹, S. Maruyama¹, A. Loarte¹, R. Pitts¹, and J. Snipes¹

¹ITER Organization, Saint Paul lez Durance, France

Corresponding Author: M. Lehnen, michael.lehnen@iter.org

The energy stored during a burning plasma pulse in ITER will significantly exceed that in present devices. Rapid release of this energy during a disruption has the potential to cause surface melting of plasma-facing components (PFCs) and will cause high electromagnetic loads, in some cases close to the design limits. Heat load specifications for ITER, which enter, for example, in the design process for blanket modules and full-W divertor, are based on empirical data on footprint broadening, deposition time and confinement degradation prior to the thermal quench. Runaway electrons (RE) can cause localized high energy deposition and, under some circumstances, up to 300 MJ of magnetic energy could be converted to RE kinetic energy. Electromagnetic loads are quantified in terms of halo current and current quench time, for which a broad database exists. However, understanding the origin of current asymmetries, which can be particularly challenging for the mechanical structures, remains an open issue.

To ensure the required lifetime of PFCs, therefore, reliable disruption prediction will be required to allow action for disruption avoidance or, as a last resort, to trigger the disruption mitigation system (DMS). Three systems are under consideration for the ITER DMS: massive gas injection (MGI), shattered pellet injection (SPI) and Be injection as a back-up option. MGI experiments have shown that electromagnetic and thermal load mitigation is feasible. However, it remains to be confirmed for the latter that 90% radiation efficiency, as envisaged for ITER, can be reliably achieved. RE mitigation remains an open issue. Several options like densification, position control, and destabilization of MHD during RE formation have been tested in recent years and their applicability was shown to be — if at all — limited for ITER. However, more recent experiments indicate that lower densities than predicted by the present theory can already suppress RE formation. Another promising effect is pitch-angle scattering on high-Z impurities, resulting in RE energy dissipation by synchrotron radiation. Simulations including this effect are in qualitative agreement with experimental observations. Overall, achieving mitigation of all disruption loads in ITER is challenging and will need a careful choice of injection technique, injected species, amount of material, and injection timing.



Influence of Magnetic Perturbations on Particle Pump-out in Magnetic Fusion Devices

M. Jakubowski¹, T. E. Evans², A. Kirk³, G. R. McKee⁴, O. Schmitz⁵, W. Suttrop¹, K. Tanaka⁶, J. Canik⁷, A. Dinklage¹, C. Hidalgo⁸, and Y. Jeon⁹

¹Max-Planck-Institut für Plasmaphysik, Garching, Germany
 ²General Atomics, San Diego, CA, USA
 ³JET-EFDA, Culham Science Centre, Abingdon, UK
 ⁴University of Wisconsin-Madison, Madison, WI, USA
 ⁵Forschungszentrum Jülich, Jülich, Germany
 ⁶National Institute for Fusion Science, Toki, Japan
 ⁷Oak Ridge National Laboratory, Oak Ridge, TN, USA
 ⁸The National Fusion Laboratory, CIEMAT, Madrid, Spain
 ⁹National Fusion Research Institute, Daejeon, Korea, Republic of

Corresponding Author: M. Jakubowski, marcin.jakubowski@ipp.mpg.de

Control of Type-I Edge Localized Modes (ELMs) is an important task for next step fusion devices like ITER. Following the results obtained on DIII-D resonant magnetic perturbations (RMPs) became a very popular tool to control plasma exhaust in tokamaks like ASDEX-Upgrade, MAST, KSTAR, and probably ITER. RMPs produce a stochastic boundary which reduces the pressure gradients in the pedestal region allowing the suppression or mitigation of ELMs while keeping the outward transport enhanced. The density reduction in the pedestal area is a large contributor to reducing the pressure gradient below the peeling-ballooning stability limit. There were already several attempts both experimentally and theoretically to understand the interaction of magnetic perturbation with L-mode and H-mode plasmas, this work is aimed to summarize recent experimental results from ASDEX-Upgrade, DIII-D, KSTAR, MAST, NSTX, LHD, and TEXTOR with resonant and non-resonant magnetic perturbations. In L-mode plasmas the influence on the edge and core plasma is typically more pronounced, when comparing to H-mode plasmas, what is attributed to much better coupling of non-axisymmetric perturbation with the plasma equilibrium. Recent MAST results show that the largest degree of pump-out coincides with the best alignment of the external field to the equilibrium field, which agrees with findings from TEXTOR. During H-mode discharges numerous experiments report changes in transport during phases where type I ELMs are mitigated (JET, DIII-D) or suppressed (ASDEX Upgrade, DIII-D, KSTAR) by external perturbations. As observed in ASDEX Upgrade, DIII-D, and LHD the pump-out seems to depend on pedestal collisionality and density. Additionally on ASDEX-Upgrade depending on the spectrum of the magnetic perturbation one gets either reduction (for a non-resonant case) or increase (for a resonant case) of pedestal and central electron densities. This cannot be explained with increased frequency of mitigated ELMs as the particle losses per event decrease with ELM frequency as reported on ASDEX Upgrade, MAST, and LHD.



Experimental and Modelling Results on Wall Conditioning for ITER Operation

D. Douai¹, D. Kogut¹, M. Baldwin², S. Brezinsek³, R. Doerner², G. Hagelaar⁴, S.-H. Hong⁵, P. Lomas⁶, A. Lyssoivan⁷, I. M. Ferreira Nunes⁸, R. Pitts⁹, V. Rohde¹⁰, T. Schwarz-Selinger¹⁰, P. de Vries⁹, and T. Wauters⁷

¹CEA-IRFM, Saint Paul lez Durance, France
 ²University of California San Diego, CA, USA
 ³Forschungszentrum Jülich, Jülich, Germany
 ⁴Laboratoire Plasma et Conversion d'Energie - UMR5213, Toulouse, France
 ⁵National Fusion Research Institute, Daejeon, Korea, Republic of
 ⁶JET-EFDA, Culham Science Centre, Abingdon, UK
 ⁷Laboratory for Plasma Physics, ERM/KMS, Brussels, Belgium
 ⁸Institute of Plasmas and Nuclear Fusion, Association EURATOM/IST, Lisbon, Portugal
 ⁹ITER Organization, Saint Paul lez Durance, France
 ¹⁰Max-Planck-Institut für Plasmaphysik, Garching, Germany
 Corresponding Author: D. Douai, david.douai@cea.fr

Wall conditioning will be required in ITER to control fuel and impurity recycling and to improve plasma performance and reproducibility. In the nuclear phase, wall conditioning will also contribute to the control of the tritium (T) inventory within the fuelling cycle. This paper reviews experimental and modelling research activities on wall conditioning in preparation of ITER operation.

Baking and Glow Discharge Conditioning (GDC), the primary wall conditioning techniques that ITER will use for cleaning, have been in particular studied in JET-ILW, providing results of particular relevance to ITER operation. The use of Be as PFC material lead to significant reduced needs for wall conditioning after the initial plasma restart, following baking at 200°C and D2-GDC, dramatically contrasting with restart and operation in JET-C with CFC-dominated walls. A novel 2D multi-fluid model has been developed and benchmarked against experimental data, with the aim to assess uniformity and wall coverage with the ITER glow discharge system currently re-designed. We present benchmarking results either from a small laboratory chamber or from large toroidal machines and show that H2-GDC in ITER will be fairly homogeneous in terms of electron density and temperature and toroidal distribution of the ion fluxes to the wall, determining the rate of cleaning. The efficiency of isotopic exchange with GDC or Ion Cyclotron Wall Conditioning (ICWC) for Tritium removal has been assessed in various devices, in particular JET-ILW and ASDEX-Upgrade. A 1D model of isotope exchange in Be has been developed. The model includes processes like hydrogen implantation, trapping to the ion-induced trap sites, detrapping to a solute (mobile) state, diffusion in Be and recombination to molecular form at the surface. Calculated hydrogen depth profiles are compared with those obtained on the linear plasma device PISCES-B. Extrapolation to the ITER, from a database on fuel removal efficiency of isotopic exchange experiments with Ion Cyclotron Wall Conditioning on current tokamaks, in particular JET-ILW and ASDEX-Upgrade, indicates that up to 0.4 gT could be removed between pulses, whereas the estimated T-retention lies between 0.14 and 0.5 gT per 400 s long ITER D:T shots.

EX-P

Preprint

Micro- and Macro-Instability, and Large Density and Beta in Improved Confinement MST RFP Plasmas

B. Chapman¹, J. Anderson¹, D. Brower², W. Capecchi¹, D. Carmody¹, K. Caspary¹, S. Combs³, D. Den Hartog¹, W. Ding², J. Duff¹, F. Ebrahimi⁴, L. Lin², L. Morton¹, E. Parke¹, M. J. Pueschel¹, J. Sarff¹, P. Terry¹, and W. Young¹

¹University of Wisconsin-Madison, Madison, WI, USA
 ²University of California Los Angeles, CA, USA
 ³Oak Ridge National Laboratory, Oak Ridge, TN, USA
 ⁴Princeton University, Princeton, NJ, USA

Corresponding Author: B. Chapman, bchapman@wisc.edu

In MST plasmas where inductive current profile control routinely produces tokamak-like confinement with enhanced density and temperature gradients, a far-forward-collective-scattering diagnostic reveals a broadband reduction of density fluctuations, with as much as a 100-fold drop in amplitude. This drop is precipitated largely by the reduction of current-gradient-driven tearing modes. However, in the region where thermal gradients are largest, there is a localized peak in the density fluctuation power spectrum. The source of these fluctuations is not established, but gyrokinetic modeling with the GENE code suggests the trapped electron mode, driven by the local density gradient. These plasmas, whose density is well below the Greenwald limit, routinely exhibit a large total β (average plasma pressure normalized to the total edge field pressure) of about 15 percent, but this β is limited only by the finite Ohmic heating power. With the goal of trying to establish the limits on density and β in these plasmas, frozen deuterium pellets were injected to increase the density and the Ohmic heating power. This has resulted in an RFP-record density of 1.6 times the Greenwald limit, but the upper limit on the density in these plasmas still has yet to be established. Over a broad range of density, from well below to well above the Greenwald limit, the total β is routinely enhanced. And now, with the addition of NBI, the total β has reached an RFP record of about 28% (with toroidal $\beta \sim 115\%$), and it appears that this represents a soft limit on β . Magnetic fluctuations increase as the density increases, leading to increased energy transport, and these discharges do not exhibit premature terminations. According to MHD modeling with the NIMROD code, both pressure-driven tearing and interchange modes can be linearly unstable in these plasmas, unlike the discharges at lower β . These instabilities can contribute to the enhancement of magnetic fluctuations. This soft β limit phenomenology is similar to that observed in some stellarators.



EX/P3-50

Predator-Prey Time Dynamics and Locking Control of Spontaneous Helical States in the RFP

M. Nornberg¹, F. Auriemma², D. Brower³, M. Cianciosa⁴, B. Chapman¹, W. Ding³, J. Duff¹, P. Franz², J. Goetz¹, J. Hanson⁴, D. Den Hartog¹, D. Holly¹, P. Innocente², J. Koliner¹, L. Lin³, M. McGarry¹, L. Morton¹, S. Munaretto¹, E. Parke¹, J. Sarff¹, D. Terranova², P. Terry¹, and G. Whelan¹

¹University of Wisconsin-Madison, Madison, WI, USA ²Consorzio RFX, Associazione Euratom-ENEA sulla Fusione, Padova, Italy ³University of California Los Angeles, CA, USA ⁴Auburn University, Auburn, AL, USA

Corresponding Author: M. Nornberg, mdnornberg@wisc.edu

Reversed Field Pinch (RFP) plasmas tend toward self-organized behavior depending on the nonlinear coupling between mutually interacting tearing modes. In multiple helicity plasmas one or more linearly unstable tearing modes may drive energy into stable modes through this coupling. In contrast, at high current and low density plasmas tend towards a state with a single dominant core mode. Although secondary modes are present, their amplitudes are reduced in this Quasi-Single Helicity (QSH) state. Recent work on modeling the shear-suppression mechanism has produced a predator-prey model of the QSH dynamics that reproduces the observed time dynamic behavior, in particular the increased persistence of the QSH state with increased plasma current. To diagnose these plasmas, we have established an error field control mechanism that locks the structure to a particular helical phase, to the advantage of the advanced diagnostic set on MST. With this diagnostic set, we have obtained evidence of helical structure in electron temperature, density, and impurity temperature.



Attainment of High Electron Poloidal β in Axisymmetric State and Two Routes to Self-Organized Helical State in Low-Aspect-Ratio RFP

S. Masamune¹, A. Sanpei¹, H. Tanaka¹, K. Nishimura¹, R. Ueba¹, G. Ishii¹, R. Kodera¹, H. Himura¹, N. Mizuguchi², K. Ichiguchi², T. Akiyama², K. Kawahata², D. Den Hartog³, R. Paccagnella⁴, and H. Koguchi⁵

¹ Kyoto Institute of Technology, Kyoto, Japan
 ²National Institute for Fusion Science, Toki, Japan
 ³ University of Wisconsin-Madison, Madison, WI, USA
 ⁴ Consorzio RFX, Associazione Euratom-ENEA sulla Fusione, Padova, Italy
 ⁵ AIST, Tsukuba, Japan

Corresponding Author: S. Masamune, masamune@kit.ac.jp

Improvement of plasma performance has been advanced in the low-aspect-ratio (low-A) reversed field pinch (RFP) RELAX, whose main objectives include exploring the low-A RFP configuration. In axisymmetric RFP states in deep-reversal region, it is found that central electron poloidal β , $\beta_p (= p_{e0}/(B_{pa}^2/(2\mu_0)))$, which almost equals the electron β in the RFP, has reached to 5–10%. Feedback control using saddle coil array is applied to stabilize a single resistive wall mode (RWM). As a result, fine tuning of the equilibrium becomes effective in achieving the resultant β_p of higher than 10%. The attained parameter region is close to where we expect sizable fraction of the bootstrap current which is characteristic to low-A RFP configuration. In shallow-reversal region characterized by relaxation to the quasi-single helicity (QSH) state, soft-X-ray (SXR) computed tomography (CT) technique has revealed helically deformed m/n = 1/4 structure of SXR emissivity profile. 3D MHD simulation using the MIPS code has shown two possible routes to the self-organized helical state depending on the initial equilibrium; one through core-resonant tearing mode, and the other through internally non-resonant kink mode. The self-organized helical structure agrees well with experimental results.

High Density Regime in Ohmic TCV Discharges with Positive and Negative Triangularity

N. Kirneva¹, S. Coda², O. Sauter², R. Behn², G. Canal², M. Chernikh³, B. Duval², A. Karpushov², B. Labit², A. Pochelon², L. Porte², B. Tal⁴, and V. Vuille²

¹National Research Centre "Kurchatov Institute", Moscow, Russian Federation
 ²Ecole Polytechnique Fédérale de Lausanne, CRPP, Lausanne, Switzerland
 ³National Research Centre "Kurchatov Institute", Moscow, Russian Federation
 ⁴Wigner Research Center, Association EURATOM, Budapest, Hungary

Corresponding Author: N. Kirneva, kirneva@gmail.com

Studies of high density plasmas approaching the Greenwald limit are timely and necessary in view of future reactor operation, both to gain a phenomenological understanding of their behavior and to validate and improve the theoretical treatment of their stability, confinement, and control, as well as the physics underlying the density limit process itself. One of the key features of the TCV tokamak is the possibility to change plasma shaping in a wide range of plasma elongation and triangularity. In previous TCV experiments it was shown that in both ohmic and ECRH L-mode discharges the plasma confinement time increases with plasma elongation and decreases with triangularity. In the present work the operational space of TCV has been extended to densities close to the Greenwald limit, and the evolution of the Ohmic confinement with the density increase has been investigated in limited discharges with positive and negative triangularity.

We find that the limit density value has the same increasing dependence on plasma current in both cases; however, the dependence is weaker than predicted by the Greenwald formula. The limit density approached the Greenwald limit only in the $\delta_{95} > 0$ case at low current. In discharges with $\delta_{95} < 0$ the value of the limit density appeared to be lower in the whole density range explored.

The increase in plasma density in both cases was found to be accompanied by a change in sawtooth behavior, namely an increase in the sawtooth period, a modification of the relaxation dynamics, and a reduction in regularity (variable period and amplitude); this was then followed by the disappearance of sawtooth oscillations altogether. Energy and particle confinement are also affected by the density increase. In discharges with $\delta_{95} > 0$ a transition from linear to saturated ohmic confinement is observed at a line-averaged density $(4-4.5) \times 10^{19} \text{ m}^{-3}$, and the start of the sawtooth-free phase is followed by a decrease in the energy confinement ine. In the $\delta_{95} < 0$ case the confinement behavior was found to be strongly dependent on plasma current: at high I_p ($q_{95} \sim 3$) the density dependence of τ_E is similar to the $\delta_{95} > 0$ case, whereas at low current ($q_{95} \sim 0.5$) a pronounced confinement degradation with density is observed. The possible role of MHD activity and the effect of the gas-puffing rate will be discussed.

From Edge Non-Stiffness to Improved IN-Mode: a New Perspective on Global Tokamak Radial Transport

A. Merle¹, O. Sauter¹, A. Karpushov¹, S. Brunner¹, D. Kim¹, G. Merlo¹, and R. Behn¹

¹Ecole Polytechnique Fédérale de Lausanne, CRPP, Lausanne, Switzerland Corresponding Author: A. Merle, antoine.merle@epfl.ch

Dedicated experiments have been performed on the TCV tokamak to compare the inverse scale lengths of the main plasma region with the one observed in the edge region in standard L-mode plasmas. The main plasma region is known to be characterized by a central region with relatively flat profiles, influenced by the sawtooth activity, and a stiff region where the inverse scalelength is relatively independent on the heat flux. TCV has demonstrated recently that the edge region, inside the last closed flux surface, is not stiff and is key to understanding global confinement properties [1]. It is shown that the inverse scale length in this region increases with increasing I_p , increasing P_{ECH} , increasing density and with a change of the plasma triangularity from positive to negative. The role of this non-stiff edge region is also key to understanding the saturation of the ohmic confinement at high density [1]. In these experiments, the ion transport is seen to be essentially neoclassical and the dependence of T_i profiles with I_p will be discussed as well. A new improved L-mode, called the IN-mode, has been obtained on TCV with global confinement time scaling near H-mode values, $H_{98}(y,2) = 0.9$. This mode will be discussed in detail and compared with the edge non-stiffness discussed above. On TCV, the edge T_e does not show a steep gradient, but the edge density is maintained high, hence the name IN-mode. This high edge density is favourable for keeping high T_i values and good global confinement. The IN-mode has been obtained over a wide range of q_{95} and density values, thanks to either a short transition into H-mode or a high gas puffing rate applied directly after break-down and sustained during the I_p ramp-up. Indications are that low l_i are sustained in this way. Core and edge transport properties of these L-mode plasmas are studied in detail with ASTRA simulations [2] and help to better characterize the non-stiff edge properties. The evolution of the profiles up to the L- to H-mode transition is analyzed as well. In particular the role of the edge bootstrap current on the edge q profile is analyzed, with the bootstrap current building up thanks to the edge non-stiff region having steep gradients.

References

[1] O. Sauter et al., accepted in PoP.

[2] G.V. Pereverzev and P.N. Yushmanov, IPP Report, 2002.



Preprint

Progress in Snowflake Divertor Studies on TCV

B. Duval¹, H. Reimerdes¹, W. Vijvers¹, B. Labit¹, G. Canal¹, and T. Lunt²

¹Ecole Polytechnique Fédérale de Lausanne, CRPP, Lausanne, Switzerland ²Max-Planck-Institut für Plasmaphysik, Garching, Germany

Corresponding Author: B. Duval, basil.duval@epfl.ch

Dissipating the energy emitted from a fusion reactor remains critical to achieving a commercially viable design with acceptable machine lifetime. Using the extreme shaping capability of TCV together with an 'open-vessel' design, the Snowflake (SF) configuration divertor was first demonstrated on TCV. Although a nearly 'exact' SF configuration was obtained, most of this work concentrated on SF configurations with a clear separation between the X-points (which may however vary during ELMs). This paper reports on the range of experiments performed over the last years on TCV, designed to understand the processes involved in power distribution between the four legs of a SF-divertor configuration by comparing the geometrical characteristics with measured power depositions. To date, these experiments are mostly performed at relatively low power density and particle density where the distribution to the divertor is expected to be dominated by transport parallel to the magnetic field lines and should be consistent with present divertor theory. Initial analysis of L-mode discharges indicated an enhanced transport into the private flux region and a reduction of peak heat. This enhanced transport, although relatively small, cannot be explained by the modified field line geometry alone and likely requires an additional or enhanced cross-field transport channel. A first attempt to model the configuration by matching the power and particle profiles at the primary strike points was unable to explain the observed power to the secondary strike points. This work was extended to both the L-mode and H-mode plasma confinement regimes. During ELM activity, up to $\sim 20\%$ of the exhausted energy was redistributed to the additional SPs and the peak heat flux to the inner primary was SP reduced by a factor of 2--3. Further avenues for progress, including an upgrade to the diagnostic array with the installation of a reciprocating probe and improved IR cameras, are in hand and, using the experience gained with SF configurations, research on other divertor geometries is under consideration. The need to find a working solution for fusion reactor exhaust and these highly encouraging TCV results demonstrate that this work in alternative divertor concepts is providing vital experimental and theoretical research information.

Preprint

Multi-Diagnostic Study of Core Turbulence and Geodesic Acoustic Modes in the TCV Tokamak

L. Porte¹, S. Coda¹, C. de Meijere¹, Z. Huang¹, P. Hennequin², A. Krämer-Flecken³, L. Vermare², V. Vuille¹, S. Brunner¹, J. Dominski¹, F. Margairaz¹, G. Merlo¹, T. Vernay¹, and L. Villard¹

> ¹Ecole Polytechnique Fédérale de Lausanne, CRPP, Lausanne, Switzerland ²CNRS, LPP Ecole Polytechnique, France ³Forschungszentrum Jülich, Jülich, Germany

Corresponding Author: L. Porte, laurie.porte@epfl.ch

TCV is equipped with a suite of diagnostics capable of making fluctuation measurements of several plasma parameters. The suite has been used in a large variety of TCV discharges. Emphasis has been placed on the study of turbulence as a function of plasma shape and in particular of edge triangularity. Correlation ECE (CECE) measurements have shown that the relative electron temperature fluctuation amplitude decreases as edge triangularity goes from positive to negative (± 0.34). At the same time tangential phase contrast imaging (TPCI) measurements show an analogous reduction in the density fluctuation component deep into the plasma core ($\rho \sim 0.3$). Local, non-linear, flux tube, gyrokinetic simulations have reproduced the fluctuation reduction in the plasma edge but not in the core ($\rho < 0.7$). The geodesic acoustic mode (GAM) has been identified in TCV discharges through its toroidal symmetry and the linear scaling of its frequency with sound speed. It has been simultaneously detected in radiative temperature, electron density, magnetic field and plasma flow velocity measurements, appearing as a coherent mode in the 20-30 kHz range close to the plasma edge. The multiple diagnostic identification of the GAM has allowed its radial location and poloidal distribution and its propagation direction to be determined. The poloidal mode number of its magnetic component is predominantly 2 as predicted by theory. In some cases the GAM no longer appears as a single coherent mode but as a continuum with radially varying frequency. The transition from coherent to continuum nature has been observed in a discharge during the course of a current ramp. Global simulations with the PIC gyrokinetic code ORB5 have been performed to study the GAM characteristics. Results are in good, semi-quantitative agreement with experimental findings. Synthetic diagnostics are being developed to allow comparison of numerical simulations with experimental results. Prototype CECE and TPCI synthetic diagnostics have been developed as post processing modules for use with the GENE code and are planned for the ORB5 code. First comparisons with experimental data will be presented.

Basic Investigations of Turbulence and Interactions with Plasma and Suprathermal Ions in the TORPEX Device with Open and Closed Field Lines

I. Furno¹, F. Avino¹, A. Bovet¹, A. Fasoli¹, K. Gustafson¹, J. Loizu¹, P. Ricci¹, and C. Theiler¹

¹Ecole Polytechnique Fédérale de Lausanne, CRPP, Lausanne, Switzerland Corresponding Author: I. Furno, ivo.furno@epfl.ch

TORPEX is a flexible device dedicated to investigating basic plasma physics phenomena of importance for fusion. It can feature a simple magnetized toroidal (SMT) configuration with a dominant toroidal magnetic field and a small vertical field component, or accommodate closed field-line configurations using a current-carrying conductor suspended in the center of the chamber. This produces a poloidal magnetic field with a rotational transform, which, combined with vertical field coils, allows magnetic configurations of increasing complexity and of more direct relevance to confined plasma experiments. Among these are simple plasmas limited by the vessel on the low field side, single or double-null X-points, and even advanced divertor configurations like snowflakes. Using an extensive set of diagnostics, systematic studies of plasma instabilities, their development into turbulence and meso-scale structures, and their effects on both thermal and suprathermal plasma components are performed. The impact of the experimental results obtained on TORPEX is enlarged by their systematic application to model validation, performed using rigorous methodologies for quantitative experiment-theory comparisons.

In the past two years, we conducted investigations of supra-thermal ion-turbulence interaction, a basic issue for burning plasmas, on SMT plasmas. These investigations reveal that the transport of supra-thermal ions is generally non-diffusive and can be super- or sub-diffusive depending on two parameters: the suprathermal ion energy normalized to the electric temperature and the electric potential fluctuations normalized to the electron temperature. The orbit averaging mechanism predicted to reduce the effect of turbulence on the suprathermal ions in burning plasmas has been clearly identified, both for gyro- and drift-orbits.

To better mimic the SOL-edge magnetic geometry in tokamak, we have installed a new system that creates twisted field line configurations. First experiments are devoted to the characterization of the background plasma and fluctuation features in the presence of quasi circular-shaped flux surfaces. Measurements of toroidal and poloidal wave numbers indicate field aligned modes. Further studies are under way to compare the experimental measurements with the simulation results and assess the main instability driving mechanism.

A New Methodology for Scaling Laws with Arbitrary Error Distributions: Case Study for the H-Mode Power Threshold

G. Verdoolaege^{1,2}, J.-M. Noterdaeme^{3,2}

¹Laboratory for Plasma Physics, ERM/KMS, Brussels, Belgium ²Ghent University, Ghent, Belgium ³Max-Planck-Institut für Plasmaphysik, Garching, Germany

Corresponding Author: G. Verdoolaege, geert.verdoolaege@ugent.be

In regression analyses for deriving scaling laws in the context of fusion studies, usually standard regression methods have been applied, of which ordinary least squares (OLS) is the most popular. However, concerns have been raised with respect to several assumptions underlying OLS in its application to fusion data. We present a new regression method that allows arbitrary distribution models and regression laws, rendering the technique particularly useful in the context of fusion research. The method is based on probabilistic modeling of all variables involved in the scaling expression, using adequate probability density functions (PDFs) and a natural similarity measure between them (geodesic distance). We hence obtain an optimization-based generalization of OLS regression, which we term geodesic least squares (GLS). The key advantage over existing methods is that, while still requiring a proposal for the deterministic and stochastic parts of the regression model, the dependence on that particular model is greatly reduced, allowing much more flexibility for estimating the model parameters that best fit the data. We demonstrate this important quality by means of a synthetic data set and by estimating the scaling law for the power threshold for the L-to-H transition in tokamaks, using data from the multi-machine ITPA database. The GLS technique indeed displays a greatly reduced susceptibility to data outliers and model misspecification. Furthermore, the prediction of the power threshold for ITER is higher than that obtained with OLS on the same database. Future work will address application of the method to various regression problems in fusion, particularly in cases with substantial and possibly non-Gaussian error bars.

Resistive Wall Mode Studies Utilizing External Magnetic Perturbations

P. Brunsell¹, L. Frassinetti¹, F. Volpe², K. E. J. Olofsson², R. Fridström¹, and C. A. Setiadi¹

¹KTH Royal Institute of Technology, Stockholm, Sweden ²Columbia University, New York, USA

Corresponding Author: P. Brunsell, per.brunsell@ee.kth.se

Experimental methods for resistive wall modes studies utilizing external magnetic perturbations have been developed in the reversed field pinch experiment EXTRAP T2R. This work describes experimental techniques that employ external magnetic perturbations to estimate the resistive wall magnetic diffusion times for non-axisymmetric fields, to asses the machine error field and to extract resistive wall mode dynamics. The techniques are experimentally implemented in the EXTRAP T2R reserved-field pinch. The extension of the techniques to the tokamak configuration is discussed.

A method based on the application of rotating external fields has been developed for the estimation of the wall diffusion times for non-axisymmetric fields. The method provides the estimate of the wall diffusion time for each Fourier harmonic. This technique intrinsically incorporates the effects of three-dimensional structures such as shell gaps.

A machine error field assessment technique utilizing externally applied controlled magnetic perturbations has been developed. The method is based on the generation of stable or marginally stable external RWMs, and sustaining their rotation by means of a rotating external magnetic perturbation. Due to the machine error field, the RWMs rotate non-uniformly and are modulated in amplitude. This behavior is utilized to infer the amplitude and the toroidal phase of the corresponding error field harmonic. The technique is tested against externally applied, as well as intrinsic machine error fields.

Resistive wall mode dynamics is extracted from a set of experiments using randomized low amplitude external magnetic perturbations. Stable and unstable non-resonant modes are accurately identified. Previous work on this method at EXTRAP T2R using a 2×32 sensor array were suggestive of RWM spectrum spatial under-sampling, potentially leading to aliasing of mode numbers. This work presents new results with a 2×64 sensor array that is dense enough to avoid the aliasing problem. The RWM growth rate spectrum obtained from the generically estimated linear time-invariant system compares well to the ideal MHD model calculation. Using an extended sensor array of 2×64 coils, the method has provided the first generic and simultaneous measurement of the full RWM dispersion relation in reversed field pinch plasma.

Last Achievements in the Experiments with ECR Heating in the Gas Dynamic Trap

P. Bagryansky¹, A. Ivanov¹, A. Lizunov¹, Y. Kovalenko¹, V. Maximov¹, S. Murakhtin¹, V. Prikhodko¹, V. Savkin¹, E. Soldatkina¹, A. Solomakhin¹, D. Yakovlev², and K. Zaytsev¹

¹Budker Institute of Nuclear Physics, Novosibirsk, Russian Federation ²Novosibirsk State University, Novosibirsk, Russian Federation

Corresponding Author: P. Bagryansky, p.a.bagryansky@inp.nsk.su

Axially symmetric magnetic mirror device, Gas-Dynamic Trap (GDT, Budker Institute, Novosibirsk) has recently demonstrated a tangible increase of the electron temperature with application of ECR heating. According to Thomson scattering data, the electron temperature exceeding 0.4 keV has been achieved thus demonstrating twofold increase. Additionally to standard device operation with 5 MW neutral beams, a newly installed electron cyclotron resonance heating (ECRH) system was employed (54.5 GHz, 0.4 MW). The reported increase of the electron temperature along with previous experiments, which demonstrated plasma confinement with β as high as 60%, provide a firm basis for extrapolating to a fusion-relevant high-flux neutron source based on GDT.



First Plasma Formation in Glass Spherical Tokamak (GLAST)

S. Hussain¹, G. M. Vorobyov²

¹National Tokamak Fusion Program (NTFP), Pakistan ²St. Petersburg University, St. Petersburg, Russian Federation

Corresponding Author: S. Hussain, shahid92_pk@yahoo.com

GLAST is a small spherical tokamak having vacuum vessel of dielectric material (Pyrex glass) with aspect ratio of 1.67, $B_T = 0.4$ T and a discharge time of 10 ms. This device is indigenously developed in Pakistan and is designed to study the breakdown avalanche, plasma startup, and current formation using inductive and non-inductive processes in the presence of dielectric walls of the vessel having no issues of the eddy currents.

As a starting point, we have studied the preionization, the transition from pre-ionization to breakdown avalanche and then to the plasma current column formation. We first obtained the pre-ionization using ECR and then build up plasma current by central solenoid and with small vertical magnetic field.

A 1.5 kW, 2.45 GHz magnetron microwave system with a pulse of 5 ms has been used to facilitate the startup of plasma current on GLAST spherical tokamak. The applied toroidal field was so adjusted for the ECR layer to form at the inboard side close to the central pipe. The width and the intensity of resonance layer were optimized by changing the gas pressure, orientation of the waveguide and relative delay between TF and microwave pulse. A high speed camera was used for these studies.

Two pairs of vertical field coils were used in series with the central solenoid to generate null magnetic flux inside the vessel at the center of the resonance layer (R = 6 cm). The ohmic heating system and the TF coil system were fired with suitable relative delays in the presence of pulsed microwave. A plasma current of about 2 kA was produced for about 0.5 ms. A small vertical field was then added with the help of three pairs of coil systems without changing other operating parameters. We were succeeded to enhance the plasma current with the maxima at 5 kA by scanning the field in both directions and also by varying the current through the vertical coil system. The optimum values of the vertical magnetic field were experimentally determined and found to be between 40–50 G.

The direction of plasma current was changed with changing the direction of vertical field provided an evidence of plasma current by vertical field drift effect. The diagnostic systems such as Rogowski coil, flux loop, fast photo-diode, spectrometers and a high speed camera were used to record the signatures of plasma current and also to estimate some plasma parameters.

Preprint

Status of GOL-3 Multiple Mirror Trap Experiments

A. Burdakov¹

¹Budker Institute of Nuclear Physics, Novosibirsk, Russian Federation

Corresponding Author: A. Burdakov, a.v.burdakov@inp.nsk.su

The GOL-3 Multiple Mirror Trap is an 11 m long solenoid with an axially-periodical (corrugated) magnetic field. In the basic operation regime, the solenoid consists of 52 magnetic corrugation cells with $B_{max}/B_{min} = 4.8/3.2$ T. Deuterium plasma of $10^{20}-10^{22}$ m⁻³ density is heated up to ~ 2 keV ion temperatures (at ~ 10^{21} m⁻³ density and $\tau_E \sim 1$ ms) by a high power relativistic electron beam. The new source of intense long-pulse electron beam with a plasma cathode was developed at BINP for the experiments on a quasi-stationary beam injection in GOL-3. The injector was installed in the end tank of GOL-3 multiple mirror trap, and tested to produce 20 MW, 100 keV electron beam with a sub-ms pulse duration. The new data will be presented including that on electron beam transport, on the plasma stabilization by controlled both the radial current profile and the plasma potential.

Structure and Scaling of Fluctuations in the MHD Range in the H-1NF HELIAC

B. Blackwell¹, S. Haskey¹, J. Howard¹, D. Pretty¹, A. Thorman¹, J. Bertram¹, M. J. Hole¹, A. Koenies², C. Nuehrenberg², and R. Dewar¹

¹Australian National University, Canberra, Australia ²Max-Planck-Institut für Plasmaphysik, Greifswald, Germany

Corresponding Author: B. Blackwell, boyd.blackwell@anu.edu.au

The H-1 flexible heliac with its wide range of magnetic configurations is an ideal device for studying instabilities in the low to mid Alfvénic range — low to hundreds of kHz, in H/He RF-produced plasma around 0.5 T. More than 80 magnetic probes in three arrays, and several optical imaging diagnostics provide data on poloidal, helical, and radial mode structures. Sensitive multichannel interferometry, framing cameras synchronised with the mode, and gas puff illumination techniques provide density fluctuation data in two dimensions. The vast data set acquired shows very clear dependences on transform and density, made possible by the low shear and precise control of configuration. Electron density fluctuation profiles from a new, high sensitivity 21 chord interferometer, will be compared with tomographically inverted fluctuation mode structures from synchronously acquired images of CII impurity line emission. Mode structure and dispersion data are compared with predictions of several codes, notably CAS3D, and CONTI, and show both Alfvénic GAE-like and/or acoustic-like (BAE) behaviour in different regimes. Scaling with magnetic field and mass density will be compared with expectations for Alfvénic and GAM and other modes.

Active and Passive Experiments to Control the Helical Boundary of Wall-Stabilized Tokamak Plasma

G. Navratil¹, S. Angelini¹, J. Bialek¹, P. Byrne¹, P. Hughes¹, J. Levesque¹, M. Mauel¹, Q. Peng¹, D. Rhodes¹, and C. Stoafer¹

¹Columbia University, New York, USA

Corresponding Author: G. Navratil, navratil@columbia.edu

We report high-resolution detection of the time-evolving, three-dimensional (3D) magnetic structure of wall-stabilized tokamak discharges in the HBT-EP device [1]. The time-evolution of unstable and saturated wall-stabilized external kink modes are studied in detail with and without applying magnetic perturbations with non-axisymmetric control coils [2,3]. Naturally occuring external kinks are composed of independent helical modes that are seen to modulate each other in time[4]. For limited discharges produced with a rapid plasma current ramp, strong multimode kink behavior is excited whenever modes resonate with the edge safety factor, q(a), m/n = 3/1 and 6/2. In contrast, when the plasma boundary is diverted, we show for the first time that kink mode dynamics becomes dominated by a single mode in agreement with expectations from ideal MHD [1]. We observed the dynamic, multimode structure of plasmas with a distributed array of more than 200 magnetic sensors [5], with high-speed videography of the plasma-wall interactions, and with soft X-ray detectors. Naturally occuring external kinks and resistive wall modes (RWM) are excited with plasma current ramps, and we find the kink mode amplitude and dynamics depends strongly on the position of the adjustable wall and on the application of magnetic feedback [6]. Additionally, experiments are underway with a newly installed adjustable ferritic wall [1] that will enable systematic investigations of multimode kink dynamics as the separation between the ferritic wall and the plasma changes, and will also allow first tests of active control of the ferritic resistive wall mode (FRWM) using high-speed, multiple-input, multiple-output control [7]. Initial experiments with rapidly rotating external kink modes show wall stabilization in the presence of a close ferromagnetic wall ($r/a \sim 1.07$). Future experiments with slower plasma rotation are expected to see reduced wall stabilization due to ferritic effects.

References

[1] D.A. Maurer, et al., Phys. Plasmas 19, 056123 (2012).

- [2] D. Shiraki, et al., Phys. Plasmas 20, 102503 (2013).
- [3] N. Rath, et al., Plasma Phys. Control. Fusion 55, 084003 (2013).

[4] J.P. Levesque, et al., Nuclear Fusion 53, 073037 (2013).

- [5] D. Shiraki, et al., Rev. Sci. Instrum 84, 063502 (2013).
- [6] N. Rath, et al., Nuclear Fusion 53, 073052 (2013).
- [7] N. Rath, et al., Fusion Eng. Des. 87, 1895 (2012).

EX/P4-25





EX/P4-26

Observation of a Toroidally Symmetrical Electric Field Fluctuation with Radially Elongated Structure in Heliotron J

S. Ohshima¹, S. Kobayashi², S. Yamamoto², K. Nagasaki², T. Mizuuchi², H. Okada², T. Minami², S. Kado², K. Hashimoto³, K. Kasajima³, H. Lee⁴, L. Zang³, N. Kenmochi³, S. Konoshima², and F. Sano²

¹Kyoto University, Kyoto, Japan

²Institute of Advanced Energy, Kyoło University, Kyoło, Japan ³Graduate School of Energy Science, Kyoło University, Kyoło, Japan ⁴Korea Advanced Institute of Science and Technology, Daejeon, Korea, Republic of

Corresponding Author: S. Ohshima, ohshima@iae.kyoto-u.ac.jp

An electric field fluctuation with radially elongated structure is found inside the last closed flux surface (LCFS) in a medium sized helical device, Heliotron J. The experiment is conducted in lowdensity ECH plasma discharges with line averaged density $n_e \sim 0.3 \times 10^{19} \text{ m}^{-3}$ and the edge plasma parameters of $T_e \sim 50$ eV and $n_e \sim 0.4 \times 10^{18}$ m⁻³ at LCFS. Multiple Langmuir probes installed at different toroidal/poloidal sections of Heliotron J reveal a high correlation between floating potential signals measured with the probes is observed in the low frequency range less than 4 kHz, which implies the fluctuation has a symmetric structure in the toroidal direction. The fluctuation has electrostatic characteristics but is not accompanied by density perturbation. These characteristics are quite similar to those of zonal flows, however, its radial wavelength is, unlike those in other devices, comparatively large. The electric field fluctuation generates the velocity shear synchronized with the fluctuation around LCFS since the fluctuation amplitude sharply increases inside LCFS. The maximum shearing rate of the velocity shear is about 1.5×10^5 s⁻¹ at just inside LCFS, which is comparable to that observed in other devices for turbulence decorrelation. Cross-bicoherence analysis shows that nonlinear coupling between the radial and poloidal electric field fluctuations exists in the low frequency range, which implies that the fluctuation with meso-scale structure might be driven by the Reynolds stress.

External Control of Energetic-Ion-Driven MHD Instabilities by ECH/ECCD in Heliotron J Plasmas

S. Yamamoto¹, K. Nagasaki¹, S. Kobayashi¹, S. Ohshima¹, T. Mizuuchi¹, H. Okada¹, T. Minami¹, S. Kado¹, Y. Nakamura², F. Volpe³, K. Nagaoka⁴, S. Konoshima¹, N. Shi¹, L. Zang², N. Kenmochi², and F. Sano¹

¹Institute of Advanced Energy, Kyoto University, Kyoto, Japan
²Graduate School of Energy Science, Kyoto University, Kyoto, Japan
³Columbia University, New York, USA
⁴National Institute for Fusion Science, Toki, Japan

Corresponding Author: S. Yamamoto, yamamoto.satoshi.6n@kyoto-u.ac.jp

Energetic-ion-driven MHD instabilities such as Alfvén eigenmodes (AEs) and energetic particle modes (EPMs) have been studied in NBI-heated Heliotron J plasmas. We clarified the characteristics of the observed EPMs such as mode structure and observation region. We demonstrated that EPMs could be controlled by means of both positive and negative magnetic shear induced by electron cyclotron (EC) driven plasma current in Heliotron J plasmas.

Parallel Flow Dynamics and Comparison with Neoclassical Transport Analysis in NBI Plasmas of Heliotron J

S. Kobayashi¹, H. Lee², K. Nishioka³, Y. Nakamura³, S. Nishimura⁴, T. Mizuuchi¹, S. Kado¹, K. Nagasaki¹, H. Okada¹, T. Minami¹, S. Yamamoto¹, S. Ohshima⁵, M. Yokoyama⁴, S. Murakami⁶, K. Watanabe⁴, R. Seki⁴, N. Kenmochi³, S. Konoshima¹, and F. Sano¹

¹Institute of Advanced Energy, Kyoto University, Kyoto, Japan
²Korea Advanced Institute of Science and Technology, Daejeon, Korea, Republic of ³Graduate School of Energy Science, Kyoto University, Kyoto, Japan ⁴National Institute for Fusion Science, Toki, Japan ⁵Kyoto University, Kyoto, Japan

⁶Departement of Nuclear Engineering, Kyoto University, Kyoto, Japan

Corresponding Author: S. Kobayashi, kobayashi@iae.kyoto-u.ac.jp

This paper describes the parallel flow dynamics experimentally obtained in NBI plasmas of Heliotron J and its comparison with neoclassical transport analysis. In this study, two magnetic configurations with different magnetic ripple strength (gamma), core gamma of 0.031 m^{-1} for the standard and 0.073 m⁻¹ for the high ripple configurations, have been adopted to investigate the effect of gamma on the parallel flow velocity. The experiments were carried out in the plateau regime. In the configuration having a high gamma strength, the parallel flow velocity of carbon at the core region is measured to be 2–3 times smaller than that in the standard ripple case. The dependence of the flow velocity on gamma shows that the damping force by the neoclassical (NC) parallel viscosity is much higher in the high gamma case. On the other hand, in the region of r/a > 0.6, the flow velocity was measured to be around 2-4 km/s for both the co- and counter-NBI plasmas. It was also observed that the flow velocity of r/a > 0.6 was not so sensitive to gamma. Since a Fokker-Planck analysis expects that the external torque is small in the region of r/a > 0.6, the insensitivity of parallel flow both to the NBI direction and gamma implies a spontaneous flow. The measurement results are compared with a NC transport calculation based on the Sugama-Nishimura method with taking the external NBI force into account. The numerical analysis estimates the flow velocity by solving the parallel force balance for multi-species (electron, deuterium, and carbon ions) which includes the collisional interactions between the species. The experimentally observed flow velocity in the core region is consistent with that predicted based on the NC prediction. However, some discrepancy is seen between the two outside the core region. The deviation of the effective parallel viscosity calculated by the experimental result from the NC prediction increases with radius. This indicates some damping mechanisms, viscosity by turbulence or neutral, should be taken into account to interpret the deviation.

A New Operation Regime for High-Density Plasma in Heliotron J

T. Mizuuchi¹, S. Kobayashi¹, F. Sano¹, K. Nagasaki¹, H. Okada¹, T. Minami¹, S. Kado¹,
S. Yamamoto¹, S. Ohshima¹, N. Shi¹, S. Konoshima¹, H. Lee², L. Zang², H. Fukushima²,
Y. Nagae², N. Kenmochi², T. Harada², K. Kasajima², M. Maruyama², N. Noguchi²,
T. Sano², Y. Nakamura², Y. Nakashima³, N. Nishino⁴, K. Mukai⁵, R. Seki⁵, Y. Suzuki⁵,
K. Tanaka⁵, K. Watanabe⁵, M. Yokoyama⁵, and S. Murakami⁶

¹Institute of Advanced Energy, Kyoto University, Kyoto, Japan
 ²Kyoto University, Kyoto, Japan
 ³University of Tsukuba, Tsukuba, Ibaraki, Japan
 ⁴Graduate School of Engineering, Hiroshima University, Higashi-Hiroshima, Japan
 ⁵National Institute for Fusion Science, Toki, Japan
 ⁶Departement of Nuclear Engineering, Kyoto University, Kyoto, Japan

Corresponding Author: T. Mizuuchi, mizuuchi@iae.kyoto-u.ac.jp

With careful control of a short pulse high-intensity gas fueling (HIGP) scenario in a novel magnetic configuration with a lower toroidicity in Heliotron J, high-density ($n_e \sim 10^{20} \text{ m}^{-3}$) NBI plasma is realized with an improved confinement mode in the edge. A condition of low neutral density attained by the fueling cut-off after HIGP and suppression of the edge turbulence opens a new high-density operation window in Heliotron J.



EX/P4-30

Non-Inductive Solenoid-Less Plasma Current Start-up on HIST Using Transient Coaxial Helicity Injection

M. Nagata¹

¹University of Hyogo, Himeji, Japan

Corresponding Author: M. Nagata, nagata@eng.u-hyogo.ac.jp

An advantage of the Spherical Torus (ST) is the low aspect ratio and so elimination of a central solenoid coil is required for attractive high- β fusion reactors based on the ST concept. Thus alternate methods for the plasma start-up that do not rely on the central solenoid are necessary for the viability of the ST concept. The non-inductive current drive by the CHI had been demonstrated for spheromaks (SSPX) and ST plasmas (HIST [1], HIT-II, NSTX). While this method offers the potential for steady-state current drive, it was found that this approach could not produce the enough amount of the closed flux because it relies on non-axisymmetric magnetic activity to drive current on closed flux region. Unlike the steady-state CHI (edge current drive) where dynamo activity is required to relax the current inward, in transient CHI (T-CHI) only axisymmetric reconnection during plasmoid ejection process from the injector is believed to be adequate for generating a high quality closed flux. The transient CHI without requiring for dynamo is a promising candidate for the non-inductive plasma start-up. So far, the T-CHI method has been successfully applied to NSTX for the start-up followed by inductive ramp-up. This coupled discharge has now achieved plasma currents larger than 1 MA [2]. Understanding the physics of the flux closure during T-CHI still remains as a key issue, which is the primary purpose of this paper. Internal magnetic field measurements in a smaller machine make it possible to confirm the generation of closed flux surfaces. Recently, we have for the first time examined the T-CHI method on HIST (R = 0.30 m, a = 0.24 m, A = 1.25) [3]. In this experiment, T-CHI has generated toroidal currents up to ~ 30 kA under the condition of the presence of closed flux. One of main results is to verify the flux closure after plasmoid ejection by using internal magnetic probes. We have found that the closed poloidal flux increases proportionally with the toroidal current as increasing the injection voltage across the inner and outer gun electrodes. The plasmoid injection and reconnection time of ~ 0.025 ms is much faster than the resistive time scale.

References

- [1] M. Nagata et al., 24th IAEA Fusion Energy Conference, ICC/1-1Rb (2012).
- [2] R. Raman et al., Phys. Rev. Lett., 104, 095003 (2010).
- [3] M. Nagata et al., Phys. Plasmas 10, 2932 (2003).

Observation of Zonal Flows in Core Plasma with Collective Scattering Density Fluctuation Measurement

Y. Yu¹, T. Lan¹, Y. Li², H. Shen¹, A. Liu¹, J. Xie¹, C. Yu¹, W. Liu¹, M. Ye¹, W. Zhang², A. Ti², and J. Li²

¹University of Science and Technology, Anhui, China ²Institute of Plasma Physics, Chinese Academy of Sciences, Hefei, China

Corresponding Author: Y. Yu, yuyi@ustc.edu.cn

In this paper, we extend the indirect approach using Instantaneous Frequency Method (IFM) on the density fluctuations measured by the CO_2 laser collective scattering67 diagnostics in HT-7 tokamak to estimate the velocities of plasma poloidal rotation. The error analysis shows that the estimated poloidal rotation velocities are very reliable with high signal-to-noise ratio. A coherent mode is observed in the fluctuations of poloidal velocities with the mode frequency from 10 kHz to 20 kHz. It is identified as geodesic acoustic mode (GAM) zonal flow with poloidal symmetry (m = 0) and its mode frequency coinciding with the theoretical expected GAM frequency, which is decided by the local plasma temperature. In the meantime, the envelope analysis is carried out on the high frequency density fluctuations. In addition, the phase shift between the GAM radial electric field and the envelope of density fluctuations is proved to be radians. These results strongly recommended that the envelope modulation on the density fluctuation only reflects the shearing effect by the GAM. The results confirm that the envelope modulation in the high frequency density fluctuations only comes from the shearing by GAM.



EX/P4-34

Instabilities and Transport of Fast Ions on MAST

S. Sharapov¹, K. McClements¹, R. Akers¹, N. Ben Ayed¹, W. U. Boeglin², M. Cecconello³,
G. Cunningham¹, O. Jones¹, M. Fitzgerald¹, E. Fredrickson⁴, J. Harrison¹, J. Hillesheim¹,
D. Keeling¹, I. Klimek³, M. K. Lilley⁵, R. Nyqvist⁶, J. Oliver⁷, and R. V. Perez²

¹CCFE Fusion Association, Culham Science Centre, Abingdon, UK
 ²Florida International University, FL, USA
 ³Uppsala University, Sweden
 ⁴Princeton Plasma Physics Laboratory, Princeton, NJ, USA
 ⁵Imperial College, London, UK
 ⁶Chalmers University of Technology, Göteborg, Sweden
 ⁷Bristol University, UK

Corresponding Author: S. Sharapov, sergei.sharapov@ccfe.ac.uk

A systematic and significant recent effort in diagnosing energetic ion driven instabilities and related transport of the energetic ions on MAST is setting a stage for new understanding of such instabilities relevant to the next-step burning plasma experiment. The fast ion-driven Alfvénic instabilities are detected on MAST in the frequency range up to ~ 5 MHz with magnetic coils and with Doppler backscattering system. The fast ion population on MAST is represented by D NBI injected at $E_b \approx 60-70$ keV, and it is studied with a four-channel neutron camera and energetic proton detector measuring the two branches of the beam-thermal DD fusion reactions, and fast ion $D\alpha$ emission produced by beam ions. The instabilities driven by the beam are seen over a wide frequency range: i) fishbones at 10–50 kHz, ii) TAE at 50–150 kHz, Alfvén cyclotron instabilities at 400 kHz–3.8 MHz. Special attention was paid on MAST to establishing the link to NSTX data on beam-driven "avalanches" consisting of several coupled TAEs with strong downward frequency sweep and higher amplitudes than un-coupled TAEs. Based on measurements from the neutron camera, as well as the FIDA and proton detector measurements, the effects of fast ion-driven instabilities on the beam profile are assessed, and modelling is performed with the HAGIS code. A search for plasma scenario minimising the effect of fast ion-driven instabilities on the beam radial profile was performed by scanning plasma density. Together, these studies aim at providing the data base to design experiments on MAST-Upgrade with its higher B_T and off-axis beams, which will test extensively theories and models used for ITER and DEMO.

This work was part-funded by the RCUK Energy Programme and by EURATOM and carried out within the framework of European Fusion Development Agreement. The views and opinions expressed herein do not necessarily reflect those of the European Commission

Preprint

Cross-Polarization Doppler Backscattering Measurements and Microtearing at the Top of the MAST H-Mode Pedestal

J. Hillesheim¹, N. Crocker², D. Dickinson¹, A. Kirk¹, H. Meyer³, W. Peebles², C. Roach¹, R. Scannell³, and S. Saarelma³

¹JET-EFDA, Culham Science Centre, Abingdon, UK ²University of California Los Angeles, CA, USA ³CCFE Fusion Association, Culham Science Centre, Abingdon, UK

Corresponding Author: J. Hillesheim, jon.hillesheim@ccfe.ac.uk

Microtearing modes (MTMs) have been predicted to be unstable at the top of the H-mode pedestal in MAST plasmas [1], playing a role in determining pedestal transport between Edge Localized Modes (ELMs), and therefore of pedestal structure and ELM stability. This is a deepening of the understanding embodied by the widely applied model EPED [2], which relies only on Kinetic Ballooning Mode (KBM) stability to account for inter-ELM transport. We present a novel diagnostic technique, combining Doppler Backscattering (DBS) and cross-polarization scattering. This has enabled measurements sensitive to local, internal magnetic field fluctuations at the radial location and wavenumber range where MTMs have been predicted to be unstable in MAST.

Doppler backscattering is a diagnostic technique which is typically used to measure intermediate and high wavenumber density fluctuations and their lab frame propagation velocity. Two 8-channel DBS systems and a flexible quasi-optical system with 2D steering and a rotatable polarizer were installed at MAST in 2013, which enabled either standard or cross-polarization scattering. Results show a significant level of magnetic field fluctuations at the top of the pedestal, with a different temporal evolution than density fluctuations, at locations and wavenumbers where microtearing modes are predicted to be unstable.

This work was part-funded by the RCUK Energy Programme [grant number EP/I501045], the European Union's Horizon 2020 programme, and the US Department of Energy under DE-FG02-99ER54527. The views and opinions expressed herein do not necessarily reflect those of the European Commission.

References

[1] Dickinson et al., Phys. Rev. Lett. 108, 135002 (2012).

[2] Snyder et al., Nucl. Fusion 51, 103016 (2011).



EX/P4-36

Pellet Fuelling of Plasmas Including ELM Mitigation in MAST

M. Valovic¹, L. Garzotti¹, C. Gurl¹, A. Kirk¹, G. Motojima², D. Dunai³, A. Field¹, A. Patel¹, and C. Roach¹

¹JET-EFDA, Culham Science Centre, Abingdon, UK ²National Institute for Fusion Science, Toki, Japan ³Wigner Research Center, Association EURATOM, Budapest, Hungary

Corresponding Author: M. Valovic, martin.valovic@ccfe.ac.uk

Pellet fuelling is studied using top-high field side pellet injection into NBI heated H-mode plasmas, in both single and double null configurations. ELMs are mitigated by external magnetic perturbation coils (RMPs). Pellet-triggered Thomson scattering, visible bremsstrahlung imaging, fibrescope combined with a fast camera and BES diagnostics are used to study various aspects of pellet fuelling process. The ratio of intensities of the Balmer line and the continuum is used to produce 2D images of the density and temperature of the pellet cloud. The pellet cloud has a size ~ 5 cm with no strong elongation along the magnetic field lines. Interaction of pellet fuelling with the ELM mitigation has been tested in MAST using RMPs. In the majority of cases the fuelling pellet is followed by an ELM, either promptly during the pellet lifetime or with a small delay. Unfavourable cases exist with postpellet compound ELMs which promptly remove all pellet material. There are however favourable examples with conventional post pellet ELMs allowing longer pellet retention times. In these cases the size of the post-pellet ELM is correlated with the size of the pre-pellet ELM suggesting that the post-pellet ELM loss is controlled by RMPs, though some correlation with pellet size exists. Profiles of electron density loss during post-pellet ELMs show a characteristic shape extending up to $r/a \sim 0.7$. This area encompasses the region of inverted density gradient raising the question about the character of core particle transport during the post-pellet ELM. To elucidate this mechanism of particle loss, BES data have been analysed. To assess post-pellet inter-ELM particle transport, a micro-stability survey is performed using the linear gyrokinetic GS2 code. It is shown that in the region of large inverted density gradient caused by the pellet ITG and ETG modes can be stabilised. In this region TEMs are also stable due to the stabilising effect of opposing electron diamagnetic and precession drift velocities. In the outer zone, where dn/dr < 0, ITG modes are also stabilised but they are replaced by TEMs and micro-tearing modes.

This work was funded by the RCUK Energy Programme under grant EP/I501045 and by the European Union's Horizon 2020 research and innovation programme. The views and opinions expressed herein do not necessarily reflect those of the European Commission.

Preprint

Improved Understanding of Edge Plasma Dynamics Through Visible Imaging on MAST

J. Harrison¹, S. Silburn², B. Dudson³, G. Fishpool¹, H. Frerichs⁴, J. Howard⁵, A. Kirk¹, R. Sharples², and P. Tamain⁶

¹CCFE Fusion Association, Culham Science Centre, Abingdon, UK ²University of Durham, Durham, UK ³University of York, Heslington, UK ⁴University of Wisconsin-Madison, Madison, WI, USA ⁵Australian National University, Canberra, Australia ⁶CEA-IRFM, Saint Paul lez Durance, France

Corresponding Author: J. Harrison, james.harrison@ccfe.ac.uk

Diagnostics imaging spectral line emission at visible wavelengths are widely used in the fusion community to gather a wealth of information about plasma conditions and transport processes particularly in the cooler regions of the scrape-off layer (SOL). Visible imaging diagnostics have been used extensively on MAST to diagnose the plasma boundary as the open vacuum vessel and divertor design offer significant access for wide-angle camera views. These diagnostics have provided insight into filamentary cross-field transport processes in the SOL and divertor, distortion of the magnetic topology by application of resonant magnetic perturbations (RMPs) and imaging of the flow of impurity species. High-speed imaging (> 100 kHz) of the divertor is providing insight into the effects of an X-point on the propagation of filaments in the common flux region from upstream to divertor strike points in L-mode and H-mode confinement regimes. There is evidence for the existence of filaments in the private flux region of the inner divertor leg, emerging near the X-point and moving toward the inner divertor target. Fast imaging has been used to study filament motion upstream in the main chamber across the whole poloidal cross-section of the region between the X-points. Fast imaging of ELMs both upstream and in the divertor show these transients propagate through the SOL in the main chamber and show the propagation of the heat pulse to plasma-facing surfaces. A wide-angle coherence imaging diagnostic has been developed for use on MAST to image impurity flows in the SOL with up to 1 kHz time resolution and 1–2 mm spatial resolution. Flows of C^{1+} , C^{2+} and He¹⁺ impurity charge states have been measured in the divertor and main chamber. Notable first results from this new diagnostic include observations of the poloidal position of stagnation point moving in response to vertical shifts of the plasma away from a balanced double-null magnetic configuration. These measurements are in broad agreement with interpretive modelling results. Moreover coherence imaging has provided the first measurements of impurity flows with X-point lobe structures due to RMPs. These data support EMC3-EIRENE code predictions that the ion flow velocity within the lobes differs from the unperturbed SOL.

This work was part-funded by the RCUK Energy Programme and by Horizon 2020 programme.

Influence of Flow Shear on the Structure of Ion-Scale Turbulence in MAST

A. Field¹, N. Crocker², D. Dunai³, M. Fox⁴, Y.-C. Ghim⁵, E. Highcock⁴, J. Hillesheim⁶, F. Parra⁴, T. Peebles², C. Roach⁶, A. Schekochihin⁴, and F. van Wyk⁴

¹CCFE Fusion Association, Culham Science Centre, Abingdon, UK
 ²University of California Los Angeles, CA, USA
 ³Wigner Research Center, Association EURATOM, Budapest, Hungary
 ⁴Rudolf Peierls Centre for Theoretical Physics, University of Oxford, Oxford, UK
 ⁵Korea Advanced Institute of Science and Technology, Daejeon, Korea, Republic of
 ⁶JET-EFDA, Culham Science Centre, Abingdon, UK

Corresponding Author: A. Field, anthony.field@ccfe.ac.uk

In support of our goal to develop a predictive capability for turbulent transport close to threshold, a 2D BES diagnostic has been used to study the structure and dynamics of the ion-scale turbulence in MAST. Our previous work has shown this turbulence to be critically balanced, i.e., exhibiting a balance of linear timescales. Here, this work is extended to study the influence of flow shear on the radial and poloidal structure of the turbulence. The resulting eddy 'tilt' is found to increase with the product of the shearing rate and correlation time, while the poloidal wavenumber decreases and the radial correlation length unexpectedly remains quite constant. These observations are consistent with a concomitant decrease of the turbulent ion heat flux.

Local, non-linear, gyro-kinetic simulations using GS2 for the periphery of an L-mode plasma, in which the flow shear is varied while holding other gradients fixed, show that the turbulent heat flux reduces sharply close to the experimental shearing rate. Furthermore, turbulence is excited even below the ion temperature gradient required for linear instability, indicating that this turbulence is sub-critical. For comparison with observations, the simulated density turbulence is processed using a 'synthetic' BES diagnostic and subsequently analysed with similar correlation techniques to those used for the experimental data. Initial results exhibit a similar increase of the eddy tilt with flow shear to that found experimentally.

Work is also underway to determine the properties of ion-scale zonal flows from the BES and other turbulence data. Such zonal flows are due to radially localized potential fluctuations, constant on a flux surface, which are believed to play an important role in the turbulent dynamics, particularly under conditions close to marginality. Initial results from L-mode plasmas indicate significant power in perpendicular velocity fluctuations at frequencies below 2 kHz, which is also observed in data from a Doppler Back-Scattering (DBS) reflectometry system. Detection of significant coherence between these toroidally displaced measurements is also required to confirm whether the observed velocity fluctuations are due to zonal flows.

This work was part funded by STFC, the RCUK Energy Programme, the European Union's Horizon 2020 Programme, the US DOE DE-FG02-99ER54527 and HAS.

Analysis of Ion Energy Spectrum and Spikes in ECRH TJ-II Plasmas, with Fixed and Variable Magnetic Configuration

M. Martinez¹, B. Zurro¹, A. Baciero¹, D. Jiménez-Rey¹, and V. Tribaldos²

¹The National Fusion Laboratory, CIEMAT, Madrid, Spain ²Universidad Carlos III de Madrid, Madrid, Spain

Corresponding Author: M. Martinez, marcos.martinez@externos.ciemat.es

During ECR heating microwave power is coupled to the electrons whereas ions are only heated through, usually weak, collisional coupling because of the cut-off density limitation. However, contrary to what is expected, significant suprathermal ions have been observed in TJ-II ECRH plasmas by either spectrometry of H_{α} emission [1] and by means of a luminescent probe capable of detecting those suprathermal ions as they escape from the confined plasma [2, 3], with very high sensitivity.

The TJ-II luminescent detector used in counting mode and with energy discrimination [4] has allowed observing changes and spikes in the energy distribution of suprathermal ions, which can be associated with changes in the plasma parameters. The increase of the luminescent detector count (spikes) around certain energies is always observed during ECRH operation and never detected during NBI heating. The ion suprathermal population and its energies are found to strongly depend on whether the ECRH power deposition is on or off-axis. Also, a change of the shape of suprathermal ion distribution function is found when the magnetic field configuration is varied during the discharge. In the present work a detailed analysis is presented on the ion energy spectrum in ECRH plasmas, for fixed and changing magnetic field configuration.

References

[1] D. Rapisarda, B. Zurro, V. Tribaldos, A. Baciero, *et al.*, Plasma Phys. Controlled Fusion 49, 309 (2007).

[2] D. Jiménez-Rey, B. Zurro, J. Guasp et al., Rev. Sci. Instrum. 79, 093511 (2008).

[3] B. Zurro, A. Baciero, V. Tribaldos et al., Nuclear Fusion 53, 083017 (2013).

[4] B. Zurro, A. Baciero et al., Rev. Sci. Instrum. 83, 10, 10D306 (2012).



EX/P4-43

Studying the Impurity Charge Dependence of Impurity Confinement in ECR Heated TJ-II Stellarator Plasmas

B. Zurro¹, E. M. Hollmann², A. Baciero¹, M. A. Ochando¹, K. J. McCarthy¹, F. Medina¹, J. L. Velasco¹, I. Pastor¹, D. Baião³, E. de la Cal¹, and D. Rapisarda¹

¹The National Fusion Laboratory, CIEMAT, Madrid, Spain ²University of California San Diego, CA, USA ³Institute of Plasmas and Nuclear Fusion, Association EURATOM/IST, Lisbon, Portugal

Corresponding Author: B. Zurro, b.zurro@ciemat.es

Impurity confinement time has been studied as a function of charge and mass of the impurity ions by using laser blow-off injection of trace impurities into electron cyclotron heated discharges of the TJ-II heliac. Impurities ranging from low-Z (LiF) to high-Z (W) are injected. The experiment has been carried out at constant density ($5 \times 10^{19} \text{ m}^{-3}$), injected power (500 kW) and magnetic configuration. A lower impurity confinement time ($\sim 5 \text{ ms}$) in the plasma core as compared with the plasma edge ($\sim 10 \text{ ms}$) is revealed from soft X-ray analysis and tomographic reconstruction of signals from a fast bolometer array. A dependence of impurity confinement with charge seems to be the most probable explanation of the results obtained; this is supported by the analysis of spectrally resolved data in the VUV range. The results seem qualitatively consistent with the dependence of impurity neoclassical transport on the background radial electric field. The results obtained will be discussed in the context of other stellarator and tokamak experiments on trace impurity transport.

Stable Plasmas in Theoretically Mercier-Unstable TJ-II Configurations

F. Castejón¹, A. Aguilera¹, A. López-Fraguas¹, C. Hidalgo¹, T. Estrada¹, M. A. Ochando¹, I. Pastor¹, and E. de la Cal¹

¹The National Fusion Laboratory, CIEMAT, Madrid, Spain

Corresponding Author: F. Castejón, francisco.castejon@ciemat.es

Stable plasmas in Mercier unstable magnetic configurations are obtained in TJ-II, which is unexpected according to the MHD stability theory. The most feasible explanation is that the plasma tends to self-organize in the unstable regions avoiding the instabilities. This result is relevant for new stellarator design, since the magnetic well is strongly related to the plasma shape, created by complex coils. Relaxing the Mercier stability criterion allows one to build simpler coils, which is easier and cheaper. Moreover, these stellarator results can help to understand the role of triangularity and elongation in tokamaks, since these quantities are related to magnetic well.

Stability Mercier criterion takes into account magnetic well, shear, plasma current and geodesic curvature. Since TJ-II is an almost shearless stellarator, the Mercier stability is governed by the magnetic well and the curvature. Taking advantage of TJ-II flexibility we have varied the magnetic configuration keeping almost constant the rotational transform profile while varying the magnetic well. The heating method was NBI in order to have nonnegligible β . The experimental results show that we get confined plasmas even in Mercier unstable configurations. The confinement time, normalized to the plasma volume, is similar in all the configurations, once the radiated power is substracted. It is also shown that the shear layer moves accordingly to the position of the theoretical LCFS as the magnetic well scan is performed, showing that the plasma edge confinement is not severely affected. The plasma turbulence presents changes as the scan is performed, as shown by both the probe and fast cameras, with an increase of fluctuations as the magnetic well is decreased. The Doppler reflectometer does not show significant changes either on the turbulence amplitude or on the spectrum at radial positions of $r/a \approx 0.4$ -0.6. The resonance (n = 8, m = 5) is located in the edge: the Thomson scattering measurements show a flattening of pressure profiles in the positions close to the rational in some cases without magnetic well, showing that the pressure profile reacts to the destabilization of the mode. The non-linear evolution of the modes could lead to self stabilization phenomena in stellarators, which could explain that plasmas are well confined even in Mercier-unstable configurations.



EX/P4-46

Influence of ECR Heating on NBI-Driven Alfvén Eigenmodes in the TJ-II Stellarator

Á. Cappa¹, F. Castejón¹, T. Estrada¹, J. M. Fontdecaba¹, M. Liniers¹, and E. Ascasíbar¹

¹The National Fusion Laboratory, CIEMAT, Madrid, Spain

Corresponding Author: Á. Cappa, alvaro.cappa@ciemat.es

Controlling the amplitude of Alfvén Eigenmodes (AE) in fusion plasmas is an open issue with paramount relevance for ITER and beyond, because the fast-ion losses associated to these modes might be deleterious for plasma performance as well as destructive for the plasma facing components. Experiments in TJ-II have demonstrated a clear effect of the ECRH application on the NBI driven AE activity. Moderate values of ECH power produce the onset of a chirping mode whose amplitude is strongly dependent on plasma density and on the power and the launching direction of the injected ECRH waves. When the power of a second gyrotron is added the chirping mode amplitude is reduced and, depending on the density conditions, it may even be suppressed. CNPA measurements show that ECRH power enhances the detected steady neutral flux. Dependence on plasma density: experiments are restricted to a range of low plasma densities, in which the ECRH impact on the AEs is observable in TJ-II. The amplitude of the bursting AE rises with increasing density for moderate ECRH values but appears to be independent of plasma density in the mitigated AE state resulting from switching-on a second gyrotron. Dependence on power deposition location and magnetic configuration: rotational transform as well as ECRH launching direction scans have been carried out. The main finding is a clear relation between the ECRH effect and the power deposition location. For a given magnetic configuration, strong chirping occurs for specific deposition locations that depend on the magnetic configuration. Dependence on ECRH power: for a given magnetic configuration and low plasma density, a clear reduction of the chirping mode amplitude occurs when ECRH power is decreased. Moreover, the quasi-periodic character of the chirping repetition frequency is progressively lost. For slightly higher plasma densities the mode amplitude becomes weakly dependent on power and no regular repetition frequency is observed. Dependence of the AE amplitude on NBI parameters: in the absence of external ECH perturbation, the NBI parameters can be varied to explore the mode properties. Using the TJ-II Doppler reflectometer, the density fluctuations amplitude at the AE frequency has been measured. The result shows that the mode amplitude depends weakly on neutral beam energy while it increases notably with the beam current.

Limit Cycle Oscillations at the L-I-H Transition in TJ-II Plasmas: Triggering, Temporal Ordering and Radial Propagation

T. Estrada¹, C. Hidalgo¹, E. Blanco¹, and E. Ascasíbar¹

¹The National Fusion Laboratory, CIEMAT, Madrid, Spain

Corresponding Author: T. Estrada, teresa.estrada@ciemat.es

The spatiotemporal evolution of the interaction between turbulence and flows has been studied close to the L-H transition threshold conditions in the edge of TJ-II plasmas. As in other devices the temporal dynamics of the interaction displays limit cycle oscillations (LCO) with a characteristic predator-prey relationship between flows and turbulence. Recently, some controversial results arise: two types of LCO are found in HL-2A showing opposite temporal ordering. The first type is the standard predator-prey model where the turbulence increase leads the zonal flow generation that suppresses the former. In the second type, the $E \times B$ flow grows first causing the reduction of the fluctuations. The later points to the pressure gradient as a candidate for maintaining the oscillations and eventually inducing the transition to the H-mode. At TJ-II, the turbulence-flow front is found to propagate radially outwards at the onset of the LCO and in some particular cases, after a short time interval without oscillations, a reversal in the front propagation velocity is observed. Associated to this velocity reversal, a change in the temporal ordering of the LCO is measured. However, the change in the temporal ordering is not related to an intrinsic change in the nature of the LCO. In both cases the turbulence increase leads the process and produces an increase in the $E \times B$ flow shear. TJ-II findings indicate that, in addition to the role of turbulence driven zonal-flow and pressure gradients, radial propagation mechanisms play an important role on the LCO dynamics. Dedicated experiments have been carried out to investigate the physical mechanisms triggering the onset and radial propagation of the LCO. At TJ-II the LCO are preferentially observed close to the transition threshold conditions at specific magnetic configurations having a low order rational close to the plasma edge. Preceding the onset of the oscillations, high frequency modes are often observed accompanying a low frequency MHD mode. These high frequency modes resemble those found in FTU plasmas interpreted as Alfvén modes nonlinearly coupled with a magnetic island. The mechanism by which the magnetic island is easing the onset of the LCO may be related to local changes in the radial electric field and/or in the turbulence that propagate towards the plasma edge driving the plasma to the threshold conditions.

Preprint

Analysis of Tritium in Divertor Materials

M. Halitovs¹, G. Kizane¹, L. Avotina¹, and B. Lescinskis¹

¹University of Latvia, Riga, Latvia

Corresponding Author: M. Halitovs, mihails.halitovs@lu.lv

The accumulation of tritium in fusion devices, especially divertor region, has always been a major difficulty. The 15–25 μ m tungsten W coating with Mo or Rh interlayers for carbon fibre composite (CFC) material is proposed as the latest upgrade for pure CFC divertor tiles used before. Coating should decrease the sputtering of plasma facing materials, accumulation of tritium on the surface and in the bulk of divertor materials. To analyse the efficiency of W coating the series of experiments were conducted evaluating the effect of W coating on reducing surface and bulk tritium accumulation. Samples from JET fusion device MkII-HD and MkII-HD ILW divertor configurations were analysed particularly floor tiles 4 and 6 and lower outer divertor circle tiles 7. To determine the total amount and location of tritium were used full combustion and liquid scintillation counting methods. For floor tiles 4 with applying W coating, surface tritium activity reduced by a factor of 20, also reducing bulk tritium activity by more than 4 times. As a result of less divertor material erosion and further tritium accumulation in erosion materials, bulk activity is also diminished. W coating on floor tiles 6 reduces the total amount of tritium collected, yet the effect is much less significant than for tile 4 being under more frequent plasma interaction during fusion. Bulk activity remains almost the same for samples of this tile. It can be concluded that kinetic collision-like tritium access through the surface of divertor tiles is much less influent for the bulk activity. Tritium bulk activity levels are most likely driven by diffusion processes. The reducing effect of W coating is even smaller for tile 7 samples. While coating slightly decreases the tritium surface activity, the bulk activity remains similar to previously described tiles.



Theoretical Model of ITER High Resolution H-Alpha Spectroscopy for a Strong Divertor Stray Light and Validation against JET-ILW Experiments

A. B. Kukushkin¹, V. Neverov¹, M. Stamp², A. Alekseev¹, S. Brezinsek³, A. Gorshkov¹,
 M. von Hellermann⁴, M. Kadomtsev¹, V. Kotov³, A. S. Kukushkin⁴, M. Levashova¹,
 S. Lisgo⁴, V. Lisitsa¹, V. Shurygin¹, E. Veshchev⁴, D. Vukolov¹, and K. Vukolov¹

¹National Research Centre "Kurchatov Institute", Moscow, Russian Federation ²JET-EFDA, Culham Science Centre, Abingdon, UK ³Forschungszentrum Jülich, Jülich, Germany ⁴ITER Organization, Saint Paul lez Durance, France

Corresponding Author: A. B. Kukushkin, kukushkin_ab@nrcki.ru

Theoretical model suggested for ITER H-alpha High-Resolution Spectroscopy (HRS) is validated against recent JET ITER-like wall (ILW) experiments. The model assumes reconstruction of neutral hydrogen isotopes density in the SOL, and evaluation of the recycling flux from the main chamber first wall, via solving a multi-parametric inverse problem with allowance for i) strong divertor stray light (DSL) on the in-vessel lines-of-sight (LoS), ii) substantial deviation of neutral atom velocity distribution function from a Maxwellian in the SOL, iii) data for direct observation of divertor. The developed "synthetic" Balmer-alpha diagnostic is tested on the example of data from the SOLPS4.3 (B2-EIRENE) code predictive modeling of the flat-top of Q = 10 inductive operation of ITER. The JET-ILW HRS data on resolving the power at deuterium spectral line D-alpha with direct observation of the divertor from the top and with observation of the inner wall along tangential and radial LoS from equatorial ports are analyzed. These data allow the evaluation of the DSL spectrum and the signal-to-background ratio for D-alpha light emitted from the far SOL and divertor in JET ILW. The results support the expectation of a strong impact of the DSL upon the H-alpha (and Visible Light) Spectroscopy Diagnostic in ITER.

This work is supported by the RF State Corporation ROSATOM and EURATOM, and carried out within the framework of the European Fusion Development Agreement. The views and opinions expressed herein do not necessarily reflect those of the European Commission and ITER Organization.



EX/P5-21

ICRF Discharge Production for Ion Cyclotron Wall Conditioning on JET

T. Wauters¹, A. Lyssoivan¹, D. Douai², S. Brezinsek³, E. Belohony⁴, T. Blackman⁵, V. Bobkov⁴, K. Crombé¹, E. Delabie⁶, D. Aleksander⁷, M. Graham⁵, D. Hartmann⁸, E. Joffrin², D. Kogut², E. A. Lerche¹, T. Loarer², P. Lomas⁵, A. Manzanares⁹, M.-L. Mayoral¹⁰, I. Monakhov⁵, J.-M. Noterdaeme⁴, M. Oberkofler⁴, *J. Ongena*¹, V. P. Philipps³, V. V. Plyusnin¹¹, G. Sergienko³, M. Tripský¹, and D. Van Eester¹

¹Laboratory for Plasma Physics, ERM/KMS, Brussels, Belgium
 ²CEA-IRFM, Saint Paul lez Durance, France
 ³Forschungszentrum Jülich, Jülich, Germany
 ⁴Max-Planck-Institut für Plasmaphysik, Garching, Germany
 ⁵JET-EFDA, Culham Science Centre, Abingdon, UK
 ⁶FOM Institute DIFFER, Association EURATOM-FOM, Nieuwegein, The Netherlands
 ⁷Jožef Stefan Institute, 1000 Ljubljana, Slovenia
 ⁸Max-Planck-Institut für Plasmaphysik, Greifswald, Germany
 ⁹The National Fusion Laboratory, CIEMAT, Madrid, Spain
 ¹⁰CCFE Fusion Association, Culham Science Centre, Abingdon, UK
 ¹¹Institute of Plasmas and Nuclear Fusion, Association EURATOM/IST, Lisbon, Portugal
 Corresponding Author: T. Wauters, t.wauters@fz-juelich.de

Discharge wall conditioning is an effective tool to improve plasma performance by i) reducing the generation of plasma impurities liberated from the wall and ii) controlling the recycling of hydrogenic fluxes. On ITER discharge wall conditioning will be employed as well for iii) mitigating the tritium inventory build-up, for which one relies mostly on the removal of tritium-rich co-deposited layers. Ion cyclotron wall conditioning (ICWC) is a well-studied discharge wall conditioning technique having the advantage over Glow Discharge Conditioning (GDC) that it is applicable in the presence of magnetic fields. The ICWC mode of operation is included in the functional requirements of the ITER ion cyclotron resonance heating and current drive system, and is envisaged for use between ITER plasma pulses, in the presence of the toroidal magnetic field. Ion Cyclotron Range of Frequencies (ICRF) plasma production employing ICRH&CD antennas designed for Fast Waves excitation is studied extensively on JET in the frame of fuel removal experiments by isotopic exchange aiming at the development of ICWC scenarios for ITER. This contribution presents an overview of these ICWC experiments with focus on i) establishing safe and reliable operation of the ICRF antennas in plasma production mode at ITER full field (JET 3.3 T, 25 MHz) and half field scenario (JET 1.65 T, 25 MHz) and ii) achieving high conditioning efficacy in isotopic exchange scenarios. The experimental results are complemented by modeling results using the recently upgraded 1D (along major radius) transport code Tomator1D for ICRF plasma production in a torus in presence of a toroidal magnetic field, the Monte Carlo code RFdinity1D simulating ICRF discharge initiation at $\omega_{pe} < \omega$, and a 1D full wave RF code, together providing insight on ICRF plasma production physics as well as on ICRF plasma parameters which are outside measurement limits of JET density and temperature diagnostics.

This work was supported by EURATOM and carried out within the framework of the European Fusion Development Agreement. The views and opinions expressed herein do not necessarily reflect those of the European Commission.

ICRH for Mitigation of Core Impurity Accumulation in JET-ILW

E. A. Lerche^{1,3}, M. Goniche², P. Jacquet³, D. Van Eester¹, V. Bobkov⁴, L. Colas², I. Monakhov³, C. Noble³, T. Blackman³, F. Rimini³, S. Brezinsek⁵, A. Czarnecka⁶, K. Crombé¹, C. Challis⁷, D. Remi², N. Fedorczak², C. Giroud³, J. Graves⁸, J. Hobirk⁴, E. Joffrin², V. Kiptily³, M. Lennholm³, P. Lomas³, C. Maggi⁴, L. Aho-Mantila⁹, P. Mantica¹⁰, G. Matthews⁷, M.-L. Mayoral³, J. Mlynář¹¹, P. Monier-Garbet², M. F. Nave¹² I. M. Ferreira Nunes¹², V. Petrzilka¹¹, T. Pütterich⁴, M. Reich⁴, A. Shaw³, A. Sips⁷, M. Tsalas¹³, and M. Valisa⁸

¹Laboratory for Plasma Physics, ERM/KMS, Brussels, Belgium
 ²CEA-IRFM, Saint Paul lez Durance, France
 ³CCFE Fusion Association, Culham Science Centre, Abingdon, UK
 ⁴Max-Planck-Institut für Plasmaphysik, Garching, Germany
 ⁵Forschungszentrum Jülich, Jülich, Germany
 ⁶Institute of Plasma Physics and Laser Microfusion, Warsaw, Poland
 ⁷JET-EFDA, Culham Science Centre, Abingdon, UK
 ⁸Ecole Polytechnique Fédérale de Lausanne, CRPP, Lausanne, Switzerland
 ⁹VTT Technical Research Centre of Finland, Finland
 ¹⁰Associazione EURATOM-ENEA Unitá Tecnica Fusione, Frascati, Italy
 ¹¹Institute of Plasma Physics AS CR v.v.i., Prague, Czech Republic
 ¹²Institute of Plasmas and Nuclear Fusion, Association EURATOM/IST, Lisbon, Portugal
 ¹³FOM Institute DIFFER, Association EURATOM-FOM, Nieuwegein, The Netherlands

Corresponding Author: E. A. Lerche, ealerche@msn.com

Since 2011 JET has been operating with a full-metal ITER-like wall (ILW), with most of the main chamber plasma facing components made from beryllium (Be) and featuring a bulk tungsten (W) divertor [1, 2]. In H-modes with PNBI> 15 MW of neutral beam injection (NBI), accumulation of heavy impurities (in particular W) has become a concern, since aside from degrading the plasma performance it can — in some cases — lead to radiative collapse of the discharges. One efficient way of avoiding this deleterious central impurity accumulation is to provide a localized heat source to the plasma core, since the resulting peaked temperature profiles have a favourable impact on the transport of the high-Z impurities in this region. The main results concerning the use of ICRH for core impurity mitigation in high power H-mode discharges in JET-ILW will be discussed. It will be shown that the ICRH scenario has to be optimized for core electron heating (low minority concentration, central absorption) and that a minimum RF power (~ 4 MW) is needed for achieving sufficiently peaked temperature profiles ($T_{e0} > 5$ keV) in typical JET H-mode plasmas ($n_{e0} = 7-9 \times 10^{19}$ /m³) for effective core impurity mitigation to take place. In these conditions, the W concentration profiles as inferred from soft X-ray tomography are hollow, as opposed to the NBI only heated H-modes, which show a strongly peaked W profile in the plasma centre (r/a < 0.2). Aside from assisting the high performance H-mode baseline development and from being routinely used to provide a smooth H-L transition for reliable discharge termination, ICRH has also proven to be essential for achieving steady state nitrogen seeded H-mode discharges in JET-ILW [3].

This work was supported by EURATOM and carried out within the framework of the EFDA. The views and opinions expressed herein do not necessarily reflect those of the European Commission.

References

- [1] G. Matthews et al., Phys. Scr. 2011 (2011) 014001.
- [2] S. Brezinsek et al., Abs. PSI2014, Karazawa, Japan.
- [3] C. Giroud et al., this conference.

Paper



EX/P5-23

Poster: Session P5, Thursday 8:30

Parameters of Runaway Electrons in JET

V. V. Plyusnin¹, C. Reux², V. Kiptily³, A. Shevelev⁴, J. Mlynář⁵, M. Lehnen⁶, P. de Vries⁶,
E. Khilkevitch⁴, A. Huber⁷, G. Sergienko⁷, R. Pereira¹, A. Fernandes¹, B. Alper³, D. Alves¹,
U. Kruezi³, S. Jachmich⁸, M. Brix³, A. Boboc³, V. Riccardo³, L. Giacomelli³, C. Sozzi⁹,
S. Gerasimov¹⁰, E. de la Luna¹¹, G. Matthews³, A. Manzanares¹¹, and F. Saint-Laurent²

 ¹Institute of Plasmas and Nuclear Fusion, Association EURATOM/IST, Lisbon, Portugal ²CEA-IRFM, Saint Paul lez Durance, France ³JET-EFDA, Culham Science Centre, Abingdon, UK
 ⁴Ioffe Physical-Technical Institute of the Russian Academy of Science, St. Petersburg, Russian Federation ⁵Institute of Plasma Physics AS CR v.v.i., Prague, Czech Republic ⁶ITER Organization, Saint Paul lez Durance, France ⁷Forschungszentrum Jülich, Jülich, Germany ⁸Laboratory for Plasma Physics, ERM/KMS, Brussels, Belgium ⁹Istituto di Fisica del Plasma CNR, Euratom-ENEA-CNR Association, Milano, Italy ¹⁰CCFE Fusion Association, Culham Science Centre, Abingdon, UK ¹¹The National Fusion Laboratory, CIEMAT, Madrid, Spain

Corresponding Author: V. V. Plyusnin, vladislav.plyusnin@ipfn.ist.utl.pt

The database on runaway electrons (RE) collected in JET with plasma facing components based on carbon-fibre composite tiles (JET-C) has been updated by recent results of experiments on disruptions and RE generation in JET with full-metal ITER-like wall (JET-ILW). Unlike the first operations of JET-ILW, which did not reveal the probability of runaway electron generation, new experiments with Massive Gas Injection (MGI) did. In these studies the runaway generation process has been mapped on following JET operation parameters — toroidal magnetic fields, pre-disruption plasma densities and on fractions of argon used at MGI in mixture with deuterium (10–100%) — for future RE suppression experiments. New results on runaway generation boundary to the lower magnetic fields (up to 1 T) was found. RE current (up to 150 kA) has been measured already at 1.2 T. Temporal and spatial dynamics of RE beams have been studied using measured hard and soft X-ray emissions during RE stage. Energy spectra of RE have been measured. Data is used to contribute into the enhancement of the model of RE generation in the presence of spatial dynamics of current carrying channel and to the analysis of the interaction of RE beams with plasma facing components.

This work was supported by EURATOM and carried out within the framework of the European Fusion Development Agreement and of the Contract of Association between the EURATOM and Instituto Superior Tecnico and has also received financial support from Fundação para a Ciência e Tecnologia (FCT), Portugal. The views and opinions expressed herein do not necessarily reflect those of the European Commission or the ITER Organization.



Overview and Interpretation of L-H Threshold Experiments on JET with the ITER-like Wall

E. Delabie¹, C. Maggi², H. Meyer³, T. M. Biewer⁴, C. Bourdelle⁵, M. Brix⁶, I. S. Carvalho⁷, M. Clever⁸, P. Drewelow⁹, N. Hawkes⁶, J. Hillesheim⁶, A. Meigs⁶, L. Meneses⁷, F. Rimini⁶, P. Siren¹⁰, E. Solano¹¹, and M. Stamp⁶

¹FOM Institute DIFFER, Association EURATOM-FOM, Nieuwegein, The Netherlands
 ²Max-Planck-Institut für Plasmaphysik, Garching, Germany
 ³CCFE Fusion Association, Culham Science Centre, Abingdon, UK
 ⁴Oak Ridge National Laboratory, Oak Ridge, TN, USA
 ⁵CEA-IRFM, Saint Paul lez Durance, France
 ⁶JET-EFDA, Culham Science Centre, Abingdon, UK
 ⁷Institute of Plasmas and Nuclear Fusion, Association EURATOM/IST, Lisbon, Portugal
 ⁸Forschungszentrum Jülich, Jülich, Germany
 ⁹Max-Planck-Institut für Plasmaphysik, Greifswald, Germany

¹⁰VTT Technical Research Centre of Finland, Finland
 ¹¹The National Fusion Laboratory, CIEMAT, Madrid, Spain

Corresponding Author: E. Delabie, e.g.delabie@differ.nl

The expected threshold power (P_{th}) required to access H-mode operation on ITER is extrapolated from a multi-machine scaling that is strongly weighted to a dataset of JET carbon wall discharges. To assess differences in P_{th} due to the change to a Be/W-wall, a series of experiments has been conducted at JET to measure P_{th} as function of plasma density for different B_t/I_p [1]. At medium to high density a reduction in the threshold power of 30% is found, favourable for ITER. At lower density P_{th} exhibits a minimum, not observed with the current divertor in the C-wall. The density at the minimum in P_{th} scales as $B_t^{(4/5)}$.

The radial electric field has been reconstructed from the force balance equation before the L-H transition in the low and high density branch, but no trend has yet been found. Subsequent experiments have focussed on the effect of the impurity composition and the divertor configuration. Nitrogen seeding around the minimum in P_{th} increases the threshold to similar values as in the C-wall. P_{th} decreases with increasing lower triangularity and increases with increasing upper triangularity. Operation with strike points on the vertical targets strongly increases P_{th} and leads to a loss of the minimum.

Two mechanisms are being explored to explain the observations. The first is proposed in [2], in which the most unstable modes in the high density branch are identified in gyrokinetic simulations as resistive ballooning modes which are destabilized by increasing $Z_{\rm eff}$, in agreement with the observations. A second possibility is related to changes in the recycling and radiation. Plasmas in the high density branch are partially detached but re-attach during the heating ramp. This often leads to an oscillatory (sawtooth triggered) behaviour known as divertor oscillations. Near the minimum in P_{th} , oscillatory L-H transitions are commonly observed. They share many characteristics with the divertor oscillations, but have a short H-mode phase. These observations suggest a link between the divertor regime and the two qualitatively very different branches of the L-H transition.

This work was supported by EURATOM and carried out within the framework of EFDA. The views and opinions expressed herein do not necessarily reflect those of the European Commission.

References

[1] C. F. Maggi et al., Nucl. Fus. 54 (2014) 023007.

[2] C. Bourdelle et al., Nucl. Fus. 54 (2014) 022001.

EX/P5-25

Paper

Towards Baseline Operation Integrating ITER-Relevant Core and Edge Plasma within the Constraint of the ITER-like Wall at JET

C. Giroud¹, S. Jachmich², P. Jacquet¹, A. E. Järvinen³, E. Lerche², F. Rimini¹,
L. Aho-Mantila⁴, I. Balboa¹, P. Belo¹, M. Beurskens¹, S. Brezinsek⁵, G. Cunningham¹,
E. Delabie⁶, S. Devaux¹, L. Frassinetti⁷, A. Figueiredo⁸, A. Huber⁵, J. Hillesheim⁹,
L. Garzotti¹, M. Goniche⁹, M. Groth³, P. Lomas¹, G. Maddison¹, S. Marsen¹⁰,
G. Matthews¹, S. Menmuir⁷, G. van Rooij⁶, S. Saarelma¹, and M. Stamp⁵

¹CCFE Fusion Association, Culham Science Centre, Abingdon, UK
 ²Laboratory for Plasma Physics, ERM/KMS, Brussels, Belgium
 ³Aalto University, Espoo, Finland
 ⁴VTT Technical Research Centre of Finland, Finland
 ⁵Forschungszentrum Jülich, Jülich, Germany
 ⁶FOM Institute DIFFER, Association EURATOM-FOM, Nieuwegein, The Netherlands
 ⁷KTH Royal Institute of Technology, Stockholm, Sweden
 ⁸Institute of Plasmas and Nuclear Fusion, Association EURATOM/IST, Lisbon, Portugal
 ⁹CEA-IRFM, Saint Paul lez Durance, France
 ¹⁰Max-Planck-Institut für Plasmaphysik, Greifswald, Germany

Corresponding Author: C. Giroud, carine.giroud@ccfe.ac.uk

The reference scenario for achieving Q = 10 in ITER is an integrated type-I ELMy H-mode scenario that combines good core plasma performance of $H_{98}(y,2) \sim 1$, $\beta_N \sim 1.8$, $\langle n \rangle / n_{GW} \sim 0.85$, and high fuel purity ($Z_{\rm eff}$ 1.6), together with edge parameters compatible with the Be/W Plasma Facing Components (PFCs) in stationary conditions for $t_{stat} \sim 400$ s (i.e., 100 times the energy confinement time τ_E). With extrinsic impurity radiation, the power flowing through the separatrix can be reduced such that only 5% reaches the divertor target plate between ELMs. Previously, it was reported that the fuelled JET ELMy H-mode plasmas with $I_p = 2.5$ MA, $B_T = 2.7$ T, $q_{95} \sim 3.3$, $P_{nbi} \sim 18$ MW, at high triangularity ($\delta \sim 0.4$) had a pedestal pressure reduced by 40% with the change of PFCs from carbon (JET-C) to Be/W (JET-ILW). In these plasmas with horizontal target divertor geometry, N-seeding partially recovered the pedestal pressure loss. Good plasma performance, close the ITER requirements, was achieved but plasma conditions were not stationary $(t_{stat}/\tau_E \sim 6)$ due to the loss of sawtooth activity. Here, new experiments are reported where higher ICRH heating power was used to control the plasma core. This paper shows how the operational space for the integrated scenario has been expanded to: i) stationary plasma conditions, ii) at lower $\langle n \rangle > /n_{GW}$, and iii) plasmas with different divertor geometries. The increased pedestal pressure in JET-ILW with N-seeding is confirmed to be dependent on plasma triangularity and effect is strongest for high-delta plasma (40%) than for low-delta plasmas (15%). Plasmas with vertical target divertor geometry provide better control of the pedestal density and W contamination of the confined plasma than with a horizontal target configuration whilst maintaining good core performance of high-delta N-seeded plasmas. Stationary ELMy H-mode were obtained achieving plasma conditions of $H_{98}(y, 2) \sim 0.85$, $\beta_N \sim 1.6$, $\langle n \rangle / n_{GW} \sim 0.85$, $Z_{\text{eff}} \sim 1.6$, $f_{rad} \sim 0.55, P_{RF} \sim 3$ MW with low divertor target power load and partial detachment between ELMs for 7 s — an increase of t_{stat}/τ_E from previous value of ~ 6 to ~ 28.

This work was part-funded by the RCUK Energy Programme and by EURATOM and carried out within the framework of the EFDA. The views and opinions expressed herein do not necessarily reflect those of the European Commission.



Beryllium Migration in JET ITER-like Wall Plasmas

S. Brezinsek¹, V. P. Philipps¹, G. Matthews², M. Rubel³, D. Borodin¹, K. Schmid⁴, A. Widdowson⁵, M. Mayer⁴, M. Stamp⁵, J. Likonen⁶, A. Baron-Wiechec⁵, P. Coad⁵, A. Garcia-Carasco³, K. Heinola⁵, A. Kirschner¹, S. Krat⁴, C. Linsmeier¹, B. Lipschultz⁷, and P. Petersson³

> ¹Forschungszentrum Jülich, Jülich, Germany ²JET-EFDA, Culham Science Centre, Abingdon, UK ³KTH Royal Institute of Technology, Stockholm, Sweden ⁴Max-Planck-Institut für Plasmaphysik, Garching, Germany ⁵CCFE Fusion Association, Culham Science Centre, Abingdon, UK ⁶TEKES

⁷University of York, Heslington, UK

Corresponding Author: S. Brezinsek, s.brezinsek@fz-juelich.de

The understanding of material migration is a key issue for a successful and safe operation of ITER. JET is used as test bed to investigate the process cycle which is connected the lifetime of first wall components by erosion and the safety due to long-term retention. Divertor configuration: The current understanding of Be migration the JET-ILW can be described as follows: neutral Be and BeD from physical and chemical assisted physical sputtering by CX neutrals and residual plasma flux at the recessed wall enters the plasma, is dissociated, ionised and transported by SOL-flows towards the inner divertor where significant deposition takes place. The amount of Be eroded at the first wall and the amount of Be deposited in the inner divertor are almost comparable (~12–15 g). The primary impurity source in JET-ILW is by a factor 5.3 reduced in comparison with JET-C resulting in a lower divertor material deposition by more than an order of magnitude. Within the divertor, Be performs much less re-erosion and transport steps than C due to an energetic threshold for Be sputtering and inhibits by this the transport to the divertor floor and to remote areas at the pump-duct. The low migration is also consistent with low fuel inventory and dust production.

Limiter configuration: Be gross erosion yield was determined by spectroscopy between 0.03 (E = 35 eV) and above 1 caused by self-sputtering (E = 200 eV). Chemical assisted physical sputtering via BeD has been identified to contribute to the effective Be yield, i.e., at E = 75 eV about 1/3 enhanced erosion with respect to bare physical sputtering. An effective Be gross yield of 10% is representative for limiter plasmas in the initial campaign. This is equivalent to an average erosion rate of 4.1×10^{18} Be/s or 1.5 g Be sputtered from one midplane tile. The corresponding net erosion rate amounts 2.3×10^{18} Be/s. This is equivalent to 0.8 g Be revealing a factor two between net and gross erosion. The primary impurity source in limiter configuration in JET-ILW is only 25% above the JET-C case. The main fraction of eroded Be stays within the main chamber and only a small part of Be escapes geometrically from the main chamber into the divertor.

This work was supported by EURATOM and carried out within the framework of the EFDA. The views and opinions expressed herein do not necessarily reflect those of the European Commission.



Plasma Isotopic Change over Experiments in JET under Carbon and ITER-like Wall Conditions

T. Loarer¹, S. Brezinsek², V. P. Philipps², and D. Douai¹

¹CEA-IRFM, Saint Paul lez Durance, France ²Forschungszentrum Jülich, Jülich, Germany

Corresponding Author: T. Loarer, thierry.loarer@cea.fr

In ITER, isotopic exchange by deuterium could be envisaged as a method for minimising the tritium inventory in the vessel. In JET ITER-Like Wall (JET-ILW) an isotopic plasma wall changeover experiment has been carried out to determine the amount of particle accessible by changing the plasma from H to D. The results of this series are presented and discussed in this paper. Starting with a wall devoid of D₂ and preloaded in H₂, change over experiments from H₂ to D₂ has been carried out in JET-ILW. Thirteen repetitive pulses have been performed under conditions of: $I_p = 2.0$ MA, $B_T = 2.4$ T, $\langle n \rangle_e = 4.5 \times 10^{19}$ m⁻³, a gas injection of 6.0×10^{21} D/s and 0.5 MW of ICRH. During the plateau phase, the strike points were moved from vertical to horizontal divertor targets. The gas balance analysis integrated over the experimental session shows that the total amount of H removed from the wall is in the range of $1-3 \times 10^{22}$ H. The H concentration is shown to be lower than 10% in the plasma after four pulses and below 4.5% after 13 pulses. These results are compared with the T-D change over experiments performed during the DT campaign in JET-C which exhibits an amount of T removed from the wall of 2×10^{23} T with 10% of T concentration after 10 discharges. Finally, evaluation of isotopic plasma wall changeover as a method for minimising the fuel inventory in full metallic devices like JET-ILW and ITER is discussed.

This work was supported by EURATOM and carried out within the framework of the European Fusion Development Agreement. The views and opinions expressed herein do not necessarily reflect those of the European Commission.

A Study of Core Thomson Scattering Measurements in ITER Using a Multi-Laser Approach

G. Kurskiev¹, S. Petr², P. Andrew³, M. Bassan³, I. Bukreev¹, P. Chernakov¹, M. Kochergin¹, A. B. Kukushkin², S. Masyukevich¹, E. Mukhin¹, A. Razdobarin¹, D. Samsonov¹, V. Semenov¹, and S. Tolstyakov¹

¹Ioffe Physical-Technical Institute of the Russian Academy of Science, St. Petersburg, Russian Federation ²National Research Centre "Kurchatov Institute", Moscow, Russian Federation ³ITER Organization, Saint Paul lez Durance, France

Corresponding Author: G. Kurskiev, gleb.kurskiev@gmail.com

The electron component is the main channel for anomalous power loss, and the main indicator of transient processes in the tokamak plasma, thus electron temperature and density profiles mainly define the operational mode of the machine. All these things impose high requirements on precision, spatial and temporal resolution of the Thomson Scattering (TS) measurements. Future tokamak-reactors will be equipped with high power heating complexes including neutral beam injection, electron, and ion cyclotron resonance heating (ERCH and ICRH) providing the temperatures as high as 40 keV both for electrons and ions. Pronounced relativistic effects in the TS spectra are expected in such plasma, and the complexity of TS measurement interpretation in tokamak reactors is associated with the deviation of electron velocity distribution (EVD) from a Maxwellian that can take place under a strong ECRH/ECCD. The ill-posed inverse problem of reconstructing the EVD parameters from the measured TS spectra can be solved by assuming moderate anisotropy of the EVD in electron pitch angles in the thermal and weakly/moderate super-thermal energy range and giving more freedom for a strongly non-Maxwellian, more energetic component of the super-thermal EVD.

The second problem is concerned with restrictions on the spectral window for TS spectra measurements. The blue boundary is determined by the possible strong background line radiation of Be (< 550 nm). In addition, the range shorter than 450 nm is forbidden because of glass darkness due to intensive neutron/gamma irradiation effects and W and He lines. Thus, high temperature measurements are impossible for 1064 nm probing wavelength since the TS signal in the frame of the operational window weakly depends on T_e . The analyses of the expected errors demonstrate that the proposed multiple probing wavelengths of Nd:YAG lasers, 1320 nm, 1064 nm, and 946 nm allow covering a wide electron temperature range 0.5–40 keV.

Such an approach is essential in the presence of inaccessible optical components on the large fusion machines where spectral characteristics may change with time, posing a problem for the calibration of the TS diagnostic. In this paper, a particular example of the ITER core plasma TS system design is considered, and a comparative analysis of conservative and advanced approaches is given.



EX/P5-29

Comparative Study of High Triangularity H-Mode Plasma Performance in JET with Be/W Wall and CFC Wall

E. de la Luna¹, P. Lomas², S. Saarelma², V. Parail², I. M. Ferreira Nunes³, M. Beurskens², M. Groth⁴, A. Loarte⁵, M. F. Nave³, G. Saibene⁶, A. Sips⁷, H. Urano⁸, F. Rimini², E. Solano¹, and R. Sartori⁶

¹The National Fusion Laboratory, CIEMAT, Madrid, Spain ²CCFE Fusion Association, Culham Science Centre, Abingdon, UK ³Institute of Plasmas and Nuclear Fusion, Association EURATOM/IST, Lisbon, Portugal ⁴Aalto University, Espoo, Finland ⁵ITER Organization, Saint Paul lez Durance, France ⁶F4E: Fusion for Energy, Barcelona, Spain ⁷JET-EFDA, Culham Science Centre, Abingdon, UK

⁸ Japan Atomic Energy Agency, Naka, Japan

Corresponding Author: E. de la Luna, elena.delaluna@ciemat.es

The ITER Q = 10 baseline scenario requires good confinement ($H_{98} \approx 1$) at sufficiently high density ($\ge 0.85 \times n_{GW}$, where n_{GW} is the Greenwald density). In JET-C (with CFC plasma facing components), raising the plasma triangularity (averaged triangularity > 0.4) was the only way found to increase the plasma density near the Greenwald density while maintaining good confinement $(H_{98} > 0.9)$. The situation in JET with the new ITER-like wall (ILW) is somewhat different. Whilst the confinement degradation with gas fuelling appeared to be compatible with that measured in JET-C, the positive influence of triangularity on confinement has not been yet recovered. High triangularity H-mode plasmas in JET-ILW exhibit lower β_N (< 1.5) and lower pedestal pressure (mainly pedestal temperature) compared to JET-C with similar input power and D fuelling levels, and the confinement is strongly reduced to values close to those measured in the type III ELM regime in JET-C ($H_{98} < 0.8$). The lower pedestal temperature measured in JET-ILW appears to be linked to the high recycling conditions at which the experiments were conducted, with signs of inter-ELM divertor detachment. In order to shed some light on the mechanism responsible for this unexpected result, systematic comparisons of an extended database of JET-C and JET-ILW discharges have been carried out. Experiments in JET-C show the key role played by the pedestal temperature in the access to good confinement at high density. This is consistent with peeling-ballooning stability predictions, where the increased pedestal stability resulting from plasma shaping disappears at low edge currents (low pedestal temperature, high collisionality). The studies presented here focus on specific aspects of the highly shaped plasmas in JET-ILW, such as the impact of β_N in the edge stability at high triangularity, the different ELM dynamics seen in JET-C and JET-ILW, the increased plasma-wall interaction on the top of the vacuum vessel and the link between ELM frequency, W source and W accumulation which is particularly relevant for high triangularity plasmas where low ELM frequencies are expected.

This work was supported by EURATOM and carried out within the framework of the European Fusion Development agreement. The views and opinions expressed herein do not necessarily reflect those of the European Commission.



Real-Time Control of ELM and Sawtooth Frequencies: Similarities and Differences

M. Lennholm¹, D. Frigione², J. Graves³, P. S. Beaumont⁴, T. Blackman⁴, I. S. Carvalho⁵,
 I. Chapman⁴, R. Dumont⁶, R. Felton⁴, L. Garzotti⁴, M. Goniche⁶, A. Goodyear⁴, D. Grist⁴,
 S. Jachmich⁷, T. Johnson⁸, P. Lang⁹, E. Lerche⁷, E. de la Luna¹⁰, I. Monakhov⁴, R. Mooney⁴,
 J. Morris⁴, M. F. Nave⁵, M. Reich⁹, F. G. Rimini⁴, A. Sips¹, H. Sheikh⁴, C. Sozzi¹¹, and
 M. Tsalas¹²
 JET-EFDA Contributors
 ¹European Commission, Brussels, Belgium
 ²Associazione EURATOM-ENEA Unitá Tecnica Fusione, Frascati, Italy
 ³Ecole Polytechnique Fédérale de Lausanne, CRPP, Lausanne, Switzerland
 ⁴CCFE Fusion Association, Culham Science Centre, Abingdon, UK

⁵Institute of Plasmas and Nuclear Fusion, Association EURATOM/IST, Lisbon, Portugal ⁶CEA-IRFM, Saint Paul lez Durance, France

⁷Laboratory for Plasma Physics, ERM/KMS, Brussels, Belgium

⁸KTH Royal Institute of Technology, Stockholm, Sweden

⁹Max-Planck-Institut für Plasmaphysik, Garching, Germany

¹⁰The National Fusion Laboratory, CIEMAT, Madrid, Spain

¹¹Istituto di Fisica del Plasma CNR, Euratom-ENEA-CNR Association, Milano, Italy

¹²FOM Institute DIFFER, Association EURATOM-FOM, Nieuwegein, The Netherlands

Corresponding Author: M. Lennholm, morten.lennholm@jet.efda.org

ELMs and Sawteeth, located in different parts of the plasma, are similar from a control engineering point of view. Both manifest themselves through quiescent periods interrupted by periodic collapses. For both, large collapses, following long quiescent periods, have detrimental effects while short periods are associated with decreased confinement. It is of interest to implement control systems to maintain the collapse frequency in the desired range. Two control strategies can be considered. In pacing control, exemplified by pellet ELM triggering, the plasma is perturbed periodically at the desired frequency. Continuous control schemes, exemplified by ECRH or ICRH control of sawteeth, modify the underlying plasma parameters which determine the collapse frequency. Both pacing and continuous control techniques have been developed on JET, using pellet and gas injection for ELM frequency control and ICRH for sawtooth control. Avoidance of tungsten accumulation has become a major challenge following the installation of the all metal 'ITER like wall' on JET and sawteeth and ELMs play an important role by expelling tungsten from the core and edge of the plasma respectively. Control of tungsten has therefore been added to divertor heat load reduction, NTM avoidance and helium ash removal as reasons for requiring ELM and sawtooth control. JET experiments have, for the first time, established feedback control of the ELM frequency, via real time variation of the injected gas flow. Using this controller in conjunction with pellet injection allows the ELM frequency to be kept as required despite variations in pellet ELM triggering efficiency. JET Sawtooth control experiments have, for the first time, demonstrated that low field side ICRH, as foreseen for ITER, can shorten sawteeth lengthened by central fast ions. The development of ELM and sawtooth control could be key to achieve stable high performance JET discharges with minimal tungsten content. Integrated control of a range of mutually coupled plasma instabilities and properties, including ELMs and sawteeth will be required in future tokamaks and gaining such experience on current tokamaks is essential.

This work, supported by EURATOM, was carried out in the framework of the European Fusion Development Agreement. The views and opinions expressed herein do not necessarily reflect those of the European Commission.



EX/P5-31

An Overview of Erosion-Deposition Pattern in JET with ITER-like Wall

M. Rubel¹, A. Widdowson², E. Alves³, C. Ayres², A. Baron-Wiechec², *S. Brezinsek*⁴, P. Coad², K. Heinola⁵, D. Ivanova¹, J. Likonen⁶, G. Matthews², and P. Petersson¹

¹KTH Royal Institute of Technology, Stockholm, Sweden
 ²CCFE Fusion Association, Culham Science Centre, Abingdon, UK
 ³Institute of Plasmas and Nuclear Fusion, Association EURATOM/IST, Lisbon, Portugal
 ⁴Forschungszentrum Jülich, Jülich, Germany
 ⁵University of Helsinki, Finland
 ⁶VTT Technical Research Centre of Finland, Finland

Corresponding Author: M. Rubel, rubel@kth.se

Since August 2011 the JET tokamak has been operated with the ITER-Like Wall (JET-ILW): beryllium in the main chamber and tungsten in the divertor, i.e., the material configuration decided for ITER. Material erosion and fuel inventory studies are priorities of the JET-ILW programme. A large number of diagnostic tools was developed and installed to elucidate the overall material migration scenario. They are based either on transport tracers (limiter and divertor tiles) or on deposition monitors (wall probes). Following results have been obtained after the first ILW operation. Beryllium limiters and upper dump plates: The central part of inner wall limiters in the mid-plane zone was identified as the main erosion area of Be: up to 80 μ m. The sides of limiters are covered by deposits up to 50 μ m thick. On all types of Be tiles there are regions of shallow melting and arcing. The deuterium content is in the range from 0.02×10^{18} cm $^{-2}$ in the eroded to 4.5×10^{18} cm $^{-2}$ level in the deposits. Divertor: The deposition pattern is not uniform. The deposition is found mainly in the inner divertor with maximum at the top of the divertor: Be-rich layers up to 15 μ m thick. Remote areas in the divertor: The maximum thickness of deposits does not exceed 1 μ m which is nearly three orders of magnitude less than measured in some deposits in JET carbon walls.

Ex-situ analyses of components have shown that the overall fuel inventory in JET-ILW is low, both absolute (below 5×10^{18} cm⁻²) and relative: Be/D concentration ratio > 10 in thick deposits. The absolute amount of carbon in co-deposits is low. This result is consistent with spectroscopy data. The lack of a major carbon source reduces transport and corresponding fuel accumulation in shadowed areas. No flaking deposits were detected. The amount of dust retrieved during the shut-down was below 2 g. The results clearly indicate a significant reduction of fuel retention and dust formation in a metal-wall machine in comparison to the operation with carbon walls.

This work was supported by EURATOM and carried out within the framework of the European Fusion Development Agreement. The views and opinions expressed herein do not necessarily reflect those of the European Commission.

WallDYN Simulations of Global Impurity Migration and Fuel Retention in JET and Extrapolations to ITER

K. Schmid¹, K. Krieger¹, S. Lisgo², and S. Brezinsek³

¹Max-Planck-Institut für Plasmaphysik, Garching, Germany ²ITER Organization, Saint Paul lez Durance, France ³JET-EFDA, Culham Science Centre, Abingdon, UK

Corresponding Author: K. Schmid, klaus.schmid@ipp.mpg.de

The migration of first wall material due to erosion, plasma transport and re-deposition is one of the key challenges in current and future fusion devices. To predict erosion/re-deposition patterns and to understand the underlying principal processes, the global simulation code WallDYN was developed that couples the evolution of the first wall surface composition to plasma impurity transport. To benchmark the WallDYN model, it was applied to the JET ITER-Like Wall experiment (JET-ILW), which mimics the ITER first wall material configuration and is thus an ideal environment to validate the predictive significance of WallDYN calculations for ITER application. WallDYN simulations were performed for L-mode and H-mode plasma scenarios used in global retention studies both during the JET-ILW campaigns and previous JET-Carbon (JET-C) campaigns. The WallDYN calculations show good qualitative agreement with the Be deposition patterns determined from JET-ILW post-campaign wall tile analysis, with no Be layer growth on the W divertor targets but strong Be deposition on the inner divertor baffle and the lower part of the main wall limiters. A comparison of the calculated retention results for C and Be first wall configurations with the experimental results even shows a quantitative agreement when long term outgassing is taken into account. Applying the same model and process physics as for the JET calculations, the impurity migration and resulting fuel species co-deposition in ITER for different wall configurations and background plasmas was calculated. The simulations show that wall configurations including C feature on average a 10 and 100 times higher retention rate than wall configuration only containing Be and W. For C containing configurations only 100 to 700 full 400 s ITER discharges would be possible before hitting the 700 g T-limit. In contrast for Be and W only configurations, between 3000 and 20000 full 400 s ITER discharges are possible. Independent on the wall material configuration, the different background plasmas result in a factor \sim 10 variation in co-deposition despite similar total wall fluxes. These strong variations show that a simple wall flux scaling is not enough for predicting retention in ITER for various plasma conditions. Still, for the current ITER material choice (Be wall and W divertor) co-deposition will not limit the ITER operation.



EX/P5-33

JET Asymmetrical Disruptions

S. Gerasimov¹, R. Albanese², M. Baruzzo³, T. Hender¹, G. Rubinacci², M. Tsalas⁴, F. Villone², and L. Zakharov⁵

¹CCFE Fusion Association, Culham Science Centre, Abingdon, UK
 ²CREATE/ENEA/Euratom Association, Università di Napoli, Naples, Italy
 ³Consorzio RFX, Associazione Euratom-ENEA sulla Fusione, Padova, Italy
 ⁴FOM Institute DIFFER, Association EURATOM-FOM, Nieuwegein, The Netherlands
 ⁵Princeton Plasma Physics Laboratory, Princeton, NJ, USA

Corresponding Author: S. Gerasimov, sergei.gerasimov@ccfe.ac.uk

Asymmetrical disruptions may occur during ITER operations. It is possible that they may be accompanied by large sideways forces and by toroidal rotation. This is of particular concern because resonance with the natural frequencies of the vacuum vessel and in-vessel components could lead to the high dynamic amplification of the forces. Roughly half of all JET disruptions have toroidally asymmetric halo currents, i.e., they have asymmetric currents that flow partly inside the plasma and partly inside the surrounding wall. The presented analysis covers 1634 JET disruptions from 2005 up to 2014, with both C-wall and ITER like wall. The unique magnetic diagnostics at JET, namely a full set of poloidal coils and saddle loops recorded from four toroidally orthogonal locations and two poloidal in-vessel loops recorded from two toroidally opposite locations, allow for a comprehensive analysis of asymmetrical disruptions with a large scale database. The observed 3D structures (asymmetries) usually rotate toroidally. Various types of rotation were identified on JET: nearly uniform multi-turn rotations, trapped (or locked) toroidal rotations, reversal rotations and others. The observed rotation of the I_p asymmetry is in the range from -5 turns to +10 turns, where rotation is most commonly seen in the electron drift direction. A 3D JET vessel model is being developed to calculate the asymmetrical vessel poloidal current by using the measured poloidal voltages. The phase correlation between the toroidal and poloidal vessel current asymmetries will allow the deduction of the relationship between toroidal and poloidal components of the asymmetrical vessel currents during disruptions on JET. The JET study on the 3D effects during the I_p current quench provides unique experimental data that can help to improve the understanding of disruptions and to develop robust models, which could be used to predict the loads at future machines like ITER.

This work, part-funded by the European Communities under the contract of Association between EURATOM/CCFE was carried out within the framework of the European Fusion Development Agreement. The views and opinions expressed herein do not necessarily reflect those of the European Commission. This work was also part-funded by the RCUK Energy Programme under grant EP/I501045.



Discriminating the Trapped Electron Mode Contribution in Density Fluctuation Spectra and Turbulent Transport

R. Sabot¹, H. Arnichand¹, S. Hacquin¹, A. Krämer-Flecken², X. Garbet¹, C. Bourdelle¹, J. Citrin¹, J.-C. Giacalone¹, G. Hornung¹, C. Bottereau¹, F. Clairet¹, G. Falchetto¹, and J. Bernardo³

¹CEA-IRFM, Saint Paul lez Durance, France ²Forschungszentrum Jülich, Jülich, Germany ³Institute of Plasmas and Nuclear Fusion, Association EURATOM/IST, Lisbon, Portugal Corresponding Author: R. Sabot, roland.sabot@cea.fr

Core turbulence in tokamak plasmas is driven by two main instabilities: Ion Temperature Gradient (ITG) and Trapped Electron Modes (TEM). Experimental identification is challenging because both instabilities are unstable in the limit of long wavelengths. Analysis of Tore Supra and Textor discharges suggest a link between the onset of quasicoherent modes, a broad secondary peak on the reflectometry signal, and the destabilization of TEM. First studied on T-10 and Textor Tokamak, its wavelength is lower than the inverse of the ion Larmor radius. It was termed quasi-coherent due to marked poloidal and toroidal correlation. On Tore Supra and Textor, this extra peak which is centred between 40–120 kHz with a bandwidth of few tens kilohertz, could be observed from the edge to the core on the low field side; stabilized on the high field side, its amplitude is damped at the top of the machine. All these characteristics point to a link with drift wave instabilities.

In ohmic plasmas in Tore Supra and Textor, quasi-coherent modes are detected only in Low Ohmic Confinement (LOC) regime. They are stabilized at LOC SOC transition and they disappear in the Saturated Ohmic Confinement (SOC) regime where one expects TEM stabilization. Perpendicular velocity measurements made from the top of TEXTOR by correlation reflectometry show that QC modes rotate 300 m/s faster in the electron diamagnetic direction than density fluctuations at lower frequency. In Tore Supra, quasi-Coherent modes destabilization by Electron Cyclotron Resonance Heating has also been observed. Quasi-coherent mode amplitude increases during the ECRH phase. Moreover, they are observed only in region where quasilinear simulations predict TEM to play an important role. Thus both in terms of amplitude and radial localization, quasi-coherent mode observations coincide with the excitation of TEM instabilities. Although the nature of these modes is still under investigation, these observations support a link between quasi-coherent mode and an enhanced electron transport due to TEM destabilization.



Maximization of ICRF Power by SOL Density Tailoring with Local Gas Injection

P. Jacquet¹, M. Goniche², V. Bobkov³, E. Lerche⁴, L. Colas², J. Hosea⁵, S. Moriyama⁶, R. Pinsker⁷, S. Wang⁸, H. Faugel³, I. Monakhov¹, J.-M. Noterdaeme³, V. Petrzilka⁹, R. Pitts¹⁰, A. Shaw¹, I. Stepanov³, A. Sips¹¹, D. Van Eester⁴, S. Wukitch¹², and X. Zhang¹³

¹CCFE Fusion Association, Culham Science Centre, Abingdon, UK ²CEA-IRFM, Saint Paul lez Durance, France ³Max-Planck-Institut für Plasmaphysik, Garching, Germany

⁴Laboratory for Plasma Physics, ERM/KMS, Brussels, Belgium

⁵Princeton Plasma Physics Laboratory, Princeton, NJ, USA

⁶Japan Atomic Energy Agency, Naka, Japan

⁷General Atomics, San Diego, CA, USA ⁸Korea Atomic Energy Research Institute, Daejeon, Korea, Republic of

⁹Institute of Plasma Physics AS CR v.v.i., Prague, Czech Republic

¹⁰ITER Organization, Saint Paul lez Durance, France

¹¹JET-EFDA, Culham Science Centre, Abingdon, UK

¹²Massachusetts Institute of Technology, Plasma Science & Fusion Center, Cambridge, MA, USA

¹³Institute of Plasma Physics, Chinese Academy of Sciences, Hefei, China

Corresponding Author: P. Jacquet, philippe.jacquet@ccfe.ac.uk

Experiments have been performed under the coordination of the ITPA on several tokamaks, including ASDEX Upgrade (AUG), JET, and DIII-D, to characterise the increased ICRF antenna loading achieved by optimising the position of gas injection relative to the RF antennas. On DIII-D, AUG, and JET (with the C-wall and recently the ITER-Like Wall) a 50% increase in the antenna loading was observed when injecting deuterium in ELMy H-mode plasmas using mid-plane inlets close to the powered antennas and, in the case of JET, with smaller improvement when using inlets located at the top of the machine. The gas injection rate required ($\sim 0.7 \times 10^{22}$ el/s in AUG, $\sim 1.5 \times 10^{22}$ el/s in JET) is compatible with good plasma energy confinement and no degradation of confinement was observed when using the mid-plane or top inlets instead of divertor valves. Optimized gas injection was also found to be beneficial for reducing tungsten (W) sputtering yield at the AUG antenna limiters. On JET, a reduction of the plasma W content is also observed when using mid-plane or top gas inlets during ICRF heating. Electron density measurements in the scrape-off layer (SOL) at the outer mid-plane were made on AUG, JET, and DIII-D. On all machines an increase in the SOL density was measured when puffing gas from the mid-plane and from the top in the casae of JET. With nearby midplane inlets, the antenna loading increase is however higher than the predictions based on antenna coupling analysis using the SOL electron density measured at distant toroidal locations, pointing towards toroidal asymmetries in the SOL density. Modelling the specific effects of divertor/top/mid-plane injection on the outer mid-plane density is being carried out using EDGE2D for JET; preliminary simulations indeed indicate that outer mid-plane gas injection maximizes the density increase in front of the antennas. The extrapolation of these experimental results and modelling to ITER will be discussed and the requirements for further modelling highlighted.

This work was part-funded by the RCUK Energy Programme and by EURATOM and carried out within the framework of the EFDA. The views and opinions expressed herein do not necessarily reflect those of the European Commission.



Impact of Divertor Geometry on ITER Scenarios Performance in the JET Metallic Wall

E. Joffrin¹, J. Garcia¹, P. Tamain¹, P. Buratti², C. Challis³, M. Groth⁴, L. Frassinetti⁵, F. Köchl⁶, E. de la Luna⁷, C. Giroud⁸, T. Loarer¹, I. M. Ferreira Nunes⁹, G. Matthews³, A. Sips³, and H. Weisen³

¹CEA-IRFM, Saint Paul lez Durance, France
 ²Associazione EURATOM-ENEA Unitá Tecnica Fusione, Frascati, Italy
 ³JET-EFDA, Culham Science Centre, Abingdon, UK
 ⁴Aalto University, Espoo, Finland
 ⁵KTH Royal Institute of Technology, Stockholm, Sweden
 ⁶Institute of Atomic and Subatomic Physics, TU-Vienna, Vienna, Austria
 ⁷The National Fusion Laboratory, CIEMAT, Madrid, Spain
 ⁸CCFE Fusion Association, Culham Science Centre, Abingdon, UK
 ⁹Institute of Plasmas and Nuclear Fusion, Association EURATOM/IST, Lisbon, Portugal

Corresponding Author: E. Joffrin, emmanuel.joffrin@cea.fr

The transition from a full carbon wall to tungsten components in the divertor and beryllium components plasma facing components in JET has been an essential step in 2011 for demonstrating the compatibility of ITER scenario with a metallic environment. Specific exploration of the divertor geometry have been conducted in JET in 2013 to identify the divertor conditions showing the optimum confinement and thermal neutron rate for both the baseline scenario ($\beta_N = 2$) and the hybrid scenario ($\beta_N = 3$). The global confinement in the baseline scenario (2.5 MA/2.75 T) is maximised when the strike points are located in the divertor corner close to the pumping throat where pumping is maximised. It is the lowest when the strike points are located on the vertical target which is also the ITER divertor configuration. The height of the density pedestal drops by a factor of 2 when the outboard pumping gorge is located in the private flux region, suggesting a change in the effective particle source. The electron temperature profile changes are small, however for discharge run in the divertor corner the pedestal and core ion temperature profile is increased by typically 30%. Record neutron rate pulses have been achieved in the hybrid scenario with low triangularity at 2.35 T/2 MAs $\beta_N \sim 3.2$ and $H_{98}(y, 2) \sim 1.4$ with the outer strike point located in the pumping throats in comparison to similar discharges with the strike point away from the divertor corner.

This work was supported by EURATOM and carried out within the framework of the European Fusion Development Agreement. The views and opinions expressed herein do not necessarily reflect those of the European Commission.



EX/P5-46

Plasma Current Start-up without Central Solenoid in the Iron Core STOR-M Tokamak

O. Mitarai¹, G. Tomney², E. Lewis², D. McColl², C. Xiao², and A. Hirose²

¹Tokai University, Tokyo, Japan ²University of Saskatchewan, Canada

Corresponding Author: O. Mitarai, omitarai@ktmail.tokai-u.jp

Plasma current start-up in the iron core STOR-M tokamak (R = 0.46 m, a = 0.12 m and $B_t = 0.6$ T) without the central solenoid (CS-less) has been demonstrated. The plasma current can be maintained during the iron core saturation phase. In particular, effects of the turn number of the outer OH coils (N = 4 or N = 6) on the CS-less discharges have been compared. The plasma current start-up is reproducible due to a wide null field region in the absence of bias OH coil current for both cases. For the N = 4 case, the plasma current is ~10 kA, and the plasma current can be sustained after the additional 3rd capacitor bank is applied near the iron core saturation phase. Slow transition from the unsaturated to partially saturated phase has been observed in the iron core tokamak. For the N = 6 case, the plasma current is increased up to 18 kA for the same fast bank voltage. It has also been noticed that the main discharge is shortened from 35 ms to 20 ms. After the 3rd bank is applied at 18 ms when the magnetizing current was 0.5 kA, the plasma current quickly reached a constant value and then terminated shortly. Although more optimization is needed to prolong the plasma current driven by the 3rd bank, the magnetizing current is smaller due to stronger coupling between OH coils and the iron core. Therefore, the transition time from the unsaturated to saturated phase is shorter, adding slightly more difficulties to the plasma corrent and optimization.

The experimental results suggest a feasible operation scenario in a future ST. A reliable plasma current start-up can initiated by the outer OH coils with an iron core and the current can be further ramped up to a steady state value by additional heating power and vertical field coils after iron core saturation. A smaller turn number may be beneficial to achieve smoother transition from the unsaturated to saturated iron core phase.



Preparing ITER Tungsten Divertor Operation in Tore Supra: Physics Basis for the WEST Project

E. Tsitrone¹, C. Bourdelle¹, J. Bucalossi¹, R. Guirlet¹, J.-F. Artaud¹, V. Basiuk¹,
M. Becoulet¹, H. Bufferand¹, G. Ciraolo¹, Y. Corre¹, J. Decker¹, G. Dif-Pradalier¹,
R. Dumont¹, A. Ekedahl¹, N. Fedorczak¹, C. Fenzi¹, M. Firdaouss¹, J. Garcia¹,
P. Ghendrih¹, G. Giruzzi¹, C. Grisolia¹, A. Grosman¹, P. Hennequin², F. Imbeaux¹,
I. Ivanova-Stanik³, P. Maget¹, Y. Marandet⁴, O. Meyer¹, M. Missirlian¹, E. Nardon¹,
B. Pégourié¹, M. Schneider¹, and R. Zagorski³

¹CEA-IRFM, Saint Paul lez Durance, France
 ²CNRS, LPP Ecole Polytechnique, France
 ³Institute of Plasma Physics and Laser Microfusion, Warsaw, Poland
 ⁴PIIM, CNRS, Aix-Marseille Université, Marseille, France

Corresponding Author: E. Tsitrone, emmanuelle.tsitrone@cea.fr

Power exhaust is one of the main challenges for next step fusion devices. The WEST project (Tungsten (W) Environment in Steady State Tokamak) is targeted at paving the way for the ITER divertor procurement and operation. It consists of implementing a divertor configuration and installing an ITER like actively cooled tungsten divertor in Tore Supra, taking full benefit of its unique long pulse capability. This paper describes the physics studies developed to prepare the scientific exploitation of WEST. WEST provides an integrated platform for testing the ITER divertor components under combined heat and particle loads in a tokamak environment and allows extending plasma scenarios over relevant plasma wall equilibrium timescale (~minutes).

Three classes of plasma scenario are foreseen. A standard scenario at medium power (12 MW) will be the workhorse for testing the ITER like PFCs and demonstrating integrated H mode long pulse operation. For the study of plasma wall interactions at high particle fluence, a scenario up to 1000 s is foreseen. Finally, a high power scenario at 15 MW will be developed for 30 s high performance discharges. Ongoing work includes integrated modelling of the three classes of plasma scenario, studies for RF heating, assessment of power loads and particle fluence on the WEST divertor, and estimate of the tungsten plasma contamination. For the three scenarios foreseen, ITER relevant heat fluxes (in the range 10–20 MW/m²) are expected on the WEST ITER like divertor. From preliminary estimates, reaching ITER relevant fluence (~ 10^{27} D/m²) for plasma wall interaction studies would require a few days of operation.

The RF heating will ensure dominant electron heating. The penetration of LH heating is seen to be challenging for high pedestal plasma density. The ICRH frequency can be tuned, and is optimized to provide central heating. In scenarios with significant LH current drive, a reversed q profile is obtained, likely accompanied by an Internal Transport Barrier. Results from COREDIV indicate tungsten core concentrations similar to those obtained for ASDEX Upgrade simulations. The above simulations are consolidated by experimental results: a WEST-like configuration has been performed in ASDEX Upgrade, showing that high power H-mode operation is possible in a full tungsten environment with the shallow divertor geometry foreseen for WEST.



EX/P5-49

Non-Inductive Plasma Start-up Experiments on the TST-2 Spherical Tokamak Using Waves in the Lower-Hybrid Frequency Range

Y. Takase¹, T. Wakatsuki¹, T. Shinya¹, A. Ejiri¹, H. Furui¹, J. Hiratsuka¹, K. Imamura¹, T. Inada¹, H. Kakuda¹, H. Kasahara², R. Kumazawa¹, C. Moeller³, T. Mutoh², Y. Nagashima⁴, K. Nakamura¹, A. Nakanishi¹, T. Ohsako¹, K. Saito², T. Sakamoto¹, T. Seki², M. Sonehara¹, H. Togashi¹, S. Tsuda¹, and T. Yamaguchi¹

¹University of Tokyo, Japan ²National Institute for Fusion Science, Toki, Japan ³General Atomics, San Diego, CA, USA ⁴Kyushu University, Kasuga, Japan

Corresponding Author: Y. Takase, takase@k.u-tokyo.ac.jp

Although the spherical tokamak (ST) has the attractiveness of good stability at high β , it is presently considered impractical to realize a compact ST fusion reactor unless the central solenoid can be eliminated. Non-inductive plasma current start-up and sustainment by waves in the lower-hybrid (LH) frequency range (200 MHz) have been studied on the TST-2 spherical tokamak (major radius $R_0 =$ 0.38 m, minor radius a = 0.25 m, toroidal magnetic field $B_t = 0.3$ T, plasma current $I_p = 0.14$ MA) using three types of antenna: 11-element inductively-coupled combline (ICC) antenna, dielectric loaded 4-waveguide array (GRILL) antenna, and 13-element capacitively-coupled combline (CCC) antenna. The maximum plasma currents of 15 kA, 10 kA and 12 kA were achieved, respectively. The GRILL antenna was used to determine the optimum range of parallel index of refraction, $1 < n_{para} < 5$. The highest current drive figure of merit, $\eta_{CD} = n_e I_p R_0 / P_{RF}$ where n_e is the electron density and P_{RF} is the injected RF power, was achieved by CCC. This antenna has the advantage of exciting a uni-directional LH wave with high directionality and a sharp n_{para} spectrum. Up to about 3 kA, the plasma current can be sustained even when waves were excited in the anti-current-drive direction. At higher I_p , current is carried by high energy electrons accelerated by waves. Both X-ray response to P_{RF} modulation and orbit calculations indicate significant orbit losses of high energy electrons, especially those created near the plasma edge. The efficiency of current drive should improve by reducing prompt orbit losses. Operation at higher B_t moves the wave damping region to the plasma core by improving wave accessibility, whereas higher I_p reduces the orbit width and higher n_e prevents electrons to be accelerated to too high energy. However, since a density limit above which the current drive efficiency deteriorates is observed experimentally, the density must be kept below this limit. It is found experimentally that the injection of ECH power is useful to prevent the density from increasing too much. In addition, a further improvement of the n_{para} spectrum of the LH wave excited by the CCC antenna should be possible by reducing the electron density in front of the antenna.

High Density LHRF Experiments in Alcator C-Mod and Implications for Reactor Scale Devices

R. R. Parker¹, S. G. Baek¹, P. Bonoli¹, M. Churchill¹, J. Hughes¹, *B. LaBombard*¹, M. Reinke¹, J. Rice¹, S. Shiraiwa¹, T. Christian¹, J. Terry¹, G. Wallace¹, and D. Whyte¹

¹Massachusetts Institute of Technology, Plasma Science & Fusion Center, Cambridge, MA, USA Corresponding Author: R. R. Parker, parker@psfc.mit.edu

Parametric Decay Instabilities (PDI) have been linked to the sudden loss of superthermal electrons and current drive efficiency as the density is increased above a critical density n_{crit} in lower hybrid current drive experiments in Alcator C-Mod. Spectral peaks occur at multiples of the ion cyclotron frequency near the inner wall. As the density is increased to n_{crit} , the sidebands become strong with energy content comparable to that in the spectrum around f_0 and pump depletion sets in. The onset and character of the PDI are consistent with solutions of the PDI dispersion relation $\epsilon \epsilon_1 + (1 + \chi_i)\chi_e \mu^2 = 0$ where the coupling constant μ^2 depends linearly on the square of the parallel and perpendicular components of the pump electric field. The results show that the observed PDI are associated with excitation of ion cyclotron quasi-modes ($\omega \approx n\omega_{ci}$) which are found to be dominant over ion sound quasi-modes ($\omega \approx k_{\parallel} v_{ti}$). In both experiment and calculation strong excitation occurs for $\omega/\omega_{LH} \ge$ 4. Even with $n \approx n_{crit}$, the data show that the pump propagates to the inner wall with modest attenuation. This implies that the absorption of the pump is weak during the first pass from the LH antenna to the inner wall and suggests that stronger first-pass absorption should restore the current drive efficiency observed at lower density. Operating at higher T_e and locating the launcher off mid-plane can improve single pass absorption. An off-midplane "bi-junction" launcher has been designed for C-Mod and is planned to be installed in the near future. When combined with the present mid-plane launcher the total available power will be increased from 1 to 2 MW. Simulations indicate that even with full absorption of the pump at the inner wall, e.g., by PDI, ~ 150 kA can be driven at $n = 1.4 \times 10^{20}$ m⁻³. Injecting LH power into higher density H-mode plasmas has a profound effect on the edge and SOL turbulence, decreasing the density-fluctuation power significantly. In many of these discharges, increases in confinement are observed after the LH power is applied. In this case strong PDI occur at the cyclotron frequency and harmonics corresponding to the field near the launcher. Application of LHCD to reactor scale devices will be discussed, including advantages of launching from the inner wall.

This work supported in part by: US Department of Energy, DE-FC02-99ER54512

Preprint

New Insights into Short-Wavelength, Coherent Edge Fluctuations on Alcator C-Mod

T. Golfinopoulos¹, B. LaBombard¹, R. R. Parker¹, W. Burke¹, J. Terry¹, D. Brunner¹, E. M. Davis¹, R. Granetz², M. Greenwald², J. Hughes¹, J. Irby¹, R. Leccacorvi¹, E. Marmar¹, W. Parkin¹, M. Porkolab², R. Vieira¹, and S. M. Wolfe¹

¹Massachusetts Institute of Technology, Plasma Science & Fusion Center, Cambridge, MA, USA ²Massachusetts Institute of Technology, Cambridge, MA, USA

Corresponding Author: T. Golfinopoulos, golfit@mit.edu

Two new research tools — a Mirror Langmuir Probe (MLP) and a "Shoelace" antenna — have diagnosed and actively perturbed fluctuations in the Alcator C-Mod tokamak edge plasma. Both tools elucidate the physics associated with the Quasi-Coherent Mode (QCM, $k_p \sim 1.5$ /cm, $f \sim 50-200$ kHz), the edge fluctuation responsible for the increased particle flux which sustains the steady-state Enhanced D_{α} H-mode. The MLP has characterized the QCM with unprecedented detail, showing it to be primarily a drift wave, with curvature also playing an important role. In addition, the Shoelace antenna actively probes these fluctuations at a specific k_p (1.5/cm) within a broad (45–300 kHz) frequency range.

The MLP provides electron density (n_e) , temperature, and potential (φ) measurements at a ~ 1 MHz rate, and scans across the scrape-off layer to just inside the last closed flux surface (LCFS). Recent experiments using the MLP to investigate the QCM have placed the mode within a ~ 3 mm layer which spans the LCFS, in a region of stationary drift where the shear vanishes from the combined diamagnetic and $E \times B$ flows. The mode rotates in the electron diamagnetic drift (EDD) direction in both the lab and plasma frames. The probe has revealed that the QCM frequency band is well-described by the drift-wave dispersion relation. Moreover, the MLP has shown that φ lags n_e by ~ 16 degrees, indicative of drift-wave behavior. MLP and B_p coil measurements also show a significant interchange component in the mode drive.

Complementing this diagnosis of the QCM, the Shoelace antenna drives edge fluctuations directly. Its winding imposes $k_p = 1.5$ /cm, matching the QCM, and it is driven at arbitrary frequency from 45–300 kHz, with the capacity to lock in real time to a fluctuation signal. Cross-coherence between the antenna current and fluctuation diagnostics (phase contrast imaging, Mirnov coils, and polarimetry) shows that the antenna produces a coherent B_p excitation throughout the discharge, and a coherent n_e response after the transition to H-mode, starting prior to the onset of an intrinsic QCM. The driven mode is roughly field-aligned, with phase velocity pointing in the EDD direction, and is guided by field lines. The response is resonant at the QCM frequency, with a weak damping rate, $\gamma/\omega \sim 5$ -10%. Experiments in 2014 will determine whether the antenna also drives transport like the QCM.



Destabilization of Internal Kink by Suprathermal Electron Pressure Driven by Lower Hybrid Current Drive (LHCD)

L. F. Delgado-Aparicio¹, S. Shiraiwa², L. E. Sugiyama³, R. Granetz², J. Irby³, R. R. Parker³, S. G. Baek², I. Faust², G. Wallace², R. Mumgaard², S. Scott¹, D. Gates¹, N. Gorelenkov¹, N. Bertelli¹, C. Gao², M. Greenwald², A. Hubbard², J. Hughes², E. Marmar², P. Phillips⁴, M. Reinke⁵, J. Rice², W. Rowan⁴, R. Wilson¹, S. M. Wolfe², and S. Wukitch²

¹ Princeton Plasma Physics Laboratory, Princeton, NJ, USA
 ² Massachusetts Institute of Technology, Plasma Science & Fusion Center, Cambridge, MA, USA
 ³ Massachusetts Institute of Technology, Cambridge, MA, USA
 ⁴ University of Texas at Austin, Austin, TX, USA
 ⁵ Oak Ridge Institute for Science Eduction, Oak Ridge, TN, USA

Corresponding Author: L. F. Delgado-Aparicio, ldelgado@pppl.gov

Understanding the stability and behavior of 3D helical modes in the core of an axisymmetric toroidal configuration remains one of the challenges of fusion research [1–3]. A new type of periodic fishbone-like instability with a (1, 1) internal kink-like structure [3] has been observed in Alcator C-Mod tokamak during the development of advanced non-inductive scenarios using radio frequency lower hybrid current-drive (LHCD). For the first time, measurements at high spatial and temporal resolution directly connect changes in the fast LH-generated electrons to the mode onset, saturation, and damping. Its radial profile has the characteristic Bessel function form of the cylindrical or lowest order toroidal 1/1 kink eigenfunction [3]. Suprathermal electron energies are measured directly using the downshift of electron gyrofrequency due to relativistic effects and correlate with the mode. The results suggest that the mode is destabilized by the nonresonant suprathermal electron pressure contribution to the central β instead of the wave-particle resonance of traditional fishbones [3]. The independence of the fast electron pressure from the thermal pressure that drives the conventional internal kink also explains its varied co-existence with the sawtooth crash and precursor oscillations.

This work was performed under US DoE contracts including DE-FC02-99ER54512 and others at MIT and DE-AC02-09CH11466 at PPPL.

References

- [1] L. Delgado-Aparicio, et al., Phys. Rev. Lett., 110, 065006, (2013).
- [2] L. Delgado-Aparicio, et al., Nucl. Fusion, 53, 043019, (2013).
- [3] L. Delgado-Aparicio, et al., Phys. Rev. Lett., submitted, (2014).

New In-Situ Measurements for Plasma Material Interaction Studies in Alcator C-Mod

D. Whyte¹, H. Barnard¹, Z. Hartwig¹, B. Sorbom¹, D. Terry¹, R. Lanza¹, and P. Stahle¹

¹Massachusetts Institute of Technology, Plasma Science & Fusion Center, Cambridge, MA, USA Corresponding Author: D. Whyte, whyte@psfc.mit.edu

Accelerator-based In-situ Material Surveillance (AIMS) is a novel technique for providing in-situ 2D maps of the properties of plasma-facing surfaces in fusion devices, and has been successfully prototyped on the Alcator C-Mod tokamak. AIMS adapts ion-beam analysis, the leading ex-situ material diagnostic tool, to the tokamak environment in order to provide quantitative non-destructive probing of surface properties. A high-current compact accelerator injects an ~MeV deuteron ion beam into the tokamak in-between discharges. The beam is magnetically steered, toroidally and poloidally, to different plasma-facing surfaces by steady-state low magnitude tokamak B fields. The deuterons induce nuclear reactions in surface isotopes producing ~MeV penetrating gammas and neutrons. Measured gamma and neutron spectra are interpreted to provide quantitative assessment of the surface isotopes. Thus, AIMS provides, for the first time, 2D mapping of surface quantities that are time-resolved during plasma operations. The first AIMS experiments on Alcator C-Mod have studied boron film thickness and deuterium retention. AIMS provides good quantitative agreement with ex-situ analysis of boron thickness taken after the C-Mod campaign. Boronization has a clear effect on increasing the boron at the inner divertor but much less at the center-post location, likely due to outboard radial transport caused by $E \times B$ drift away from the EC resonance during boronization. The deuterium retention is strongly affected by the boron layer formation, but much less by plasma-cleaning techniques. Near the inner midplane, the boron deposits ~200 nm in 18 I-mode LSN diverted shots, and then becomes a location of net erosion for the following inner-wall limited shots. The measured high boron net erosion/deposition rates, combined with their complex temporal and spatial evolution, indicate the necessity for in-situ surface measurements such as AIMS.



Multi-Device Studies of Pedestal Physics and Confinement in the I-Mode Regime

A. Hubbard¹, T. Osborne², F. Ryter³, X. Gao⁴, J. Ko⁵, R. M. Churchill¹, I. Cziegler⁶,
M. E. Fenstermacher², S. Gerhardt⁷, P. Gohil², J. Hughes¹, Z. Liu⁴, A. Loarte⁸, R. Maingi⁷,
L. Barrera Orte³, R. Fischer³, P. Manz³, A. Marinoni¹, R. McDermott³, G. R. McKee⁹,
E. Marmar¹, J. Rice¹, L. Schmitz¹⁰, C. Theiler¹, E. Viezzer³, J. Walk¹, D. Whyte¹, A. White¹,
S. M. Wolfe¹, E. Wolfrum³, Z. Yan⁹, T. Zhang⁴, and T. Happel³

¹Massachusetts Institute of Technology, Plasma Science & Fusion Center, Cambridge, MA, USA
 ²General Atomics, San Diego, CA, USA
 ³Max-Planck-Institut für Plasmaphysik, Garching, Germany
 ⁴Institute of Plasma Physics, Chinese Academy of Sciences, Hefei, China
 ⁵National Fusion Research Institute, Daejeon, Korea, Republic of
 ⁶University of California San Diego, CA, USA
 ⁷Princeton Plasma Physics Laboratory, Princeton, NJ, USA
 ⁸ITER Organization, Saint Paul lez Durance, France
 ⁹University of Wisconsin-Madison, Madison, WI, USA
 ¹⁰University of California Los Angeles, CA, USA

Corresponding Author: A. Hubbard, hubbard@psfc.mit.edu

I-Mode is a promising ELM-suppressed regime that combines H-mode-like energy confinement with L-mode-like particle and impurity transport. Key to its potential extrapolation to ITER and reactor regimes is the scaling of accessibility conditions and performance. The multi-machine experiments reported here, supported by the Pedestal and Edge Physics as well as Transport and Confinement ITPA groups, are the start of such studies. The regime has been most extensively studied on Alcator C-Mod but has also been explored for several years on ASDEX Upgrade. More recently, I-mode has been observed on DIII-D. Experiments on EAST and KSTAR are planned in 2014. Observations on the different devices share some general characteristics, but also reveal some differences. In all devices, the I-mode is generally obtained under conditions for which the H-mode power threshold is high (e.g., unfavorable $B \times \nabla B$ drift). ICRH, NBI, and ECH have each been used successfully. The key defining feature of the regime is the appearance of an edge temperature pedestal, similar to that in H-mode, while the edge density profile remains unchanged from L-mode. Particle and thermal transport are thus decoupled. The increase in T_{ped} is accompanied by improvement in energy confinement. In the best cases, confinement exceeds $H_{98}(y, 2)$, and can be maintained in stationary conditions for the duration of heating. The height of the temperature pedestal which can be obtained without transition to H-mode varies; in some conditions and devices confinement improvement is more modest. Understanding the conditions both for L-I and I-H mode transitions is thus critical.

Fluctuations in the pedestal region, and in the core plasma, also change at the transition to Imode. Here there are some differences in observations on different devices. We will present the observed features of I-modes on each device. Pedestal profiles and parameters will be compared both in absolute parameters, which now span a very wide range, and in dimensionless parameters. Dimensionless identity experiments have been carried out between C-Mod and ASDEX Upgrade. Pedestal stability analysis has been conducted which explains the observed lack of ELMs. The transition power thresholds and normalized confinement properties will also be compared, and implications of these multi-device studies for extrapolation to ITER and DEMO discussed.



Development of Impurity Seeding and Radiation Enhancement at Helical Divertor in LHD

K. Mukai¹, S. Masuzaki¹, B. Peterson¹, T. Akiyama¹, M. Kobayashi¹, H. Tanaka¹, S. Pandya², R. Sano², G. Motojima¹, N. Ohno³, T. Morisaki¹, C. Suzuki¹, J. Miyazawa¹, and N. Tamura¹

¹National Institute for Fusion Science, Toki, Japan ²Graduate University for Advanced Studies, Hayama, Japan ³University of Nagoya, Nagoya, Japan

Corresponding Author: K. Mukai, mukai.kiyofumi@lhd.nifs.ac.jp

Reduction of heat and particle loads to the divertor is crucial to the realization of a fusion reactor. Divertor detachment is a favorable mode of operation for this purpose. In this study, impurity seeding was conducted in the Large Helical Device (LHD) using neon (Ne) puffing. Enhanced radiation loss and reduction of the divertor heat load were observed without significant changes in stored energy and line averaged density. In LHD, the radiated power fraction against the heating power, $P_{rad}/P_{heating}$, where P_{rad} and $P_{heating}$ are the total radiation power and the heating power, respectively, is limited up to around 30% in hydrogen plasmas even for high density plasma just below the radiative collapse $(n_{e,bar} > 1 \times 10^{20} \text{ m}^{-3})$, where $n_{e,bar}$ is the line averaged density. With Ne seeding, the ratio could be raised to 30–53% in spite of the much lower density ($n_{e,bar} \sim 1.3-5.5 \times 10^{19} \text{ m}^{-3}$). The energy confinement parameter is defined as $W_p/(P_{heating}^{-0.61} n_{e,bar}^{0.54})$ based on the ISS04 scaling, where W_p is the plasma stored energy, and the normalized energy confinement parameter is defined as the ratio between during the radiation enhancement and that just before the Ne seeding. The confinement degradation during detachment remains less than 20% over the operation regime in this study. $P_{rad}/P_{heating}$ is limited by the radiative collapse of the plasma, and the achieved fraction with impurity seeding is 53% during relatively low density discharges ($n_{e,bar}$ just before the seeding ~ 1.3×10^{19} m⁻³), while in hydrogen plasmas before the seeding, the fraction is up to around 15% regardless of $n_{e,bar}$. $P_{rad}/P_{heating}$ during the seeding decreased with increasing density. At high density ($n_{e,bar}$ > 4×10^{19} m⁻³), the radiated power fraction is less than 40%. Radiation profile measurement with an InfraRed Imaging Video Bolometer (IRVB) was conducted during Ne seeding in relatively high density plasmas in this study ($n_{e,bar}$ 4 × 10¹⁹ m⁻³). The localized supplemental radiation was observed along the helical divertor X-point (HDX). Since the radiation enhancement is localized in the SOL during the Ne seeding, and the degradation of the plasma confinement is relatively small. On the other hand, in hydrogen plasmas just before the radiative collapse, the radiation enhanced region is localized on the inboard side and does not follow the HDX.



Plasma Structure Change and Intermittent Fluctuation near Magnetic Island X-Point under Detached Plasma Condition in LHD

N. Ohno¹, H. Tanaka², S. Masuzaki², M. Kobayashi², T. Akiyama², T. Morisaki², Y. Narushima², G. Motojima², and Y. Tsuji¹

¹University of Nagoya, Nagoya, Japan ²National Institute for Fusion Science, Toki, Japan

Corresponding Author: N. Ohno, ohno@ees.nagoya-u.ac.jp

Recent study in the Large Helical Device (LHD) indicated that applying resonant magnetic perturbation (RMP) field is able to keep highly-radiating zone near the magnetic island X-point inside the ergodic region and particle flux onto the divertor plate is reduced accompanied by stable plasma detachment [1]. However, it is not clear yet where the particle flux starts to decrease in the RMP assisted plasma detachment experimentally. In addition, recent studies in several magnetic confinement devices implied that intermittent cross-field transport would be enhanced in the detached divertor [2 - 4].

We have investigated plasma structure change and plasma fluctuation property near helical divertor X-point and on divertor plate by using a fast scanning Langmuir probe and a probe array embedded on a divertor plate in the RMP assisted detached plasmas in LHD. When the RMP induced magnetic island X-point (n/m = 1/1) is located near the helical divertor X-point, the reduction of particle flux accompanied by the plasma detachment occurred near the helical divertor X-point (n/m = 2/10), which leads to the reduction of the particle flux at the strike point on the divertor plate. We also found that when the divetor plasma turned to be the detached condition, the enhanced plasma fluctuations were confirmed between the helical divertor X-point and ergodic region, which exhibited a dynamic behavior having a large amount of positive-spike components with highly intermittent property.

References

M. Kobayashi et al., Nucl. Fusion 53 (2013) 093032.

[2] B. L. Stansfield et al., J. Nucl. Mater. 241-243 (1997) 739.

[3] N. Ohno et al., J. Plasma Fusion Res. 80 (2004) 275.

[4] H. Tanaka et al., Phys. Plasmas 17 (2010) 102509.



Comprehensive Understandings of Energy Confinement in LHD Plasmas through Extensive Application of the Integrated Transport Analysis Suite

M. Yokoyama¹, R. Seki¹, C. Suzuki¹, K. Ida¹, M. Osakabe¹, S. Murakami², S. Satake¹, and H. Yamada¹

¹National Institute for Fusion Science, Toki, Japan ²Departement of Nuclear Engineering, Kyoto University, Kyoto, Japan

Corresponding Author: M. Yokoyama, yokoyama@lhd.nifs.ac.jp

The integrated transport analysis suite, TASK3D-a, has enhanced energy transport analyses in LHD. It has elucidated the systematic dependence of ion and electron energy confinement on a wide variation of plasma parameters, and the fitting expressions for ion and electron heat diffusivities with local plasma parameters. Conventionally, scaling laws for the global energy confinement time (τ_E) have been one of the approaches to systematically understand the energy confinement, and then also to design and predict future devices. However, recent extensive application of TASK3D-a to a wide-ranging LHD experiment database has provided a breakthrough to improve this situation; from scaling laws for τ_E to fitting expressions for ion and electron heat diffusivity. NBI-heated high ion-temperature plasmas and medium-to-high density plasmas have been mainly analyzed. The general tendency is recognized to be that the normalized ion (electron) heat diffusivity increases (decreases) as the temperature ratio, T_e/T_i , is increased.

Accumulation of TASK3D-a analyses results has led to the attempt at deducing functional fittings for χ_e and χ_i with local parameters. This approach has remarkable advantages such as the fitting can be performed separately for ions and electrons, and gradients of profiles can be taken into account. Thus, it is much more relevant to interpret the physics mechanism of the energy confinement than the conventional scaling approach for τ_E . Moreover, such deduced fitting functions for heat diffusivities can be directly implemented into the predictive modelling, so that the transport model assumption (like a Gyro-Bohm) is no longer required. These attempts have been on-going through multivariate nonlinear regression analysis by assuming the predictor variables such as the normalized collision frequency, T_e/T_i , and normalized scale lengths of temperature gradient. So far, the fitting expressions for ion and electron heat diffusivities have been successfully obtained.

These results are significant in terms of deducing comprehensive understandings of energy confinement based on "big data" which are created through a close-link between TASK3D-a and the LHD experiment. This approach should be applicable to any other fusion experiments.



Development of Quantitative Atomic Modeling for Tungsten Transport Study Using LHD Plasma with Tungsten Pellet Injection

I. Murakami¹, H. A. Sakaue¹, C. Suzuki¹, D. Kato¹, M. Goto¹, N. Tamura¹, S. Sudo¹, and S. Morita¹

¹National Institute for Fusion Science, Toki, Japan Corresponding Author: I. Murakami, <u>murakami, izumi@nifs.ac.jp</u>

Quantitative tungsten study with reliable atomic modeling is important for successful achievement of ITER and fusion reactors. We have developed tungsten atomic modeling for understanding the tungsten behavior in fusion plasmas. The modeling is applied to the analysis of tungsten spectra observed from currentless plasmas of the Large Helical Device (LHD) with tungsten pellet injection. We found that extreme ultraviolet (EUV) lines of W^{24+} to W^{33+} ions are very sensitive to electron temperature (T_e) and useful to examine the tungsten behavior in edge plasmas. Based on the first quantitative analysis of measured spatial profile of W^{44+} ion, the tungsten concentration is determined to be $n(W^{44+})/n_e = 1.4 \times 10^{-4}$ and the total radiation loss is estimated as ~ 4 MW, of which the value is roughly half the total NBI power.



Pressure Driven MHD Instabilities in Intrinsic and Externally Enhanced Magnetic Stochastic Region of LHD

S. Ohdachi¹, Y. Suzuki¹, H. Tsuchiya¹, and K. Watanabe¹

¹National Institute for Fusion Science, Toki, Japan

Corresponding Author: S. Ohdachi, ohdachi@nifs.ac.jp

ĽΧ-.

MHD activities in the region where the magnetic flux surfaces are disturbed by the externally applied field are now extensively studied in the context of the physics of ELM mitigation. Magnetic stochasticity plays important role as well in the high- β experiment of the Large Helical Device (LHD), where topologically similar magnetic stochastic region is formed naturally outside the last closed flux surface (LCFS). Characteristic of the MHD instabilities within the stochastic region of LHD is studied. It is noted that pressure-driven modes are always unstable in peripheral region of the LHD because the peripheral region stays in the magnetic hill. The plasma expands from the LCFS in high- β experiments. There appear MHD instabilities with amplitude of 10^{-4} of the toroidal magnetic field. From the mode number of activities (poloidal / toroidal mode number m/n = 2/3, 1/2, 2/4), the location of corresponding rational surface is near the LCFS or certainly outside the LCFS and is consistent with fluctuation measurements. Parameter dependence of the saturation level is then examined for evaluation of impact of MHD activities. The saturation level increases with the increase of the pressure gradient. Degree of stochasticity is an important factor to affect the saturation level. Since the thickness of the stochastic region and the degree of stochasticity is increased with the increase of plasma β , the stochasticity becomes more important in high- β conditions. In order to study the dependence on the stochasticity exclusively, experiments with the resonant magnetic field perturbation (RMP) with m/n = 1/1 is made. While the magnetic island is formed around the $\iota = 1$ surface, the stochasticity outside the nested region is enhanced. Amplitude of m/n = 2/3 and 2/4 modes are reduced by this RMP field when the normalized RMP coil current exceeds 0.3 kA/T. Since the local pressure gradient and the local plasma parameters are not changed by the RMP, this reduction is thus caused by the change of the magnetic field structure itself. Local flow velocity or the flow velocity shear can also affect the MHD stability. However, in the present LHD experiment, change in the velocity is small at the mode rational surface. Stochastisation of the magnetic field found to be an effective tool to suppress the MHD activities without causing degradation of the pressure gradient.

Abrupt Reversal of Convective Flow of Carbon Impurity during Impurity-Hole Formation on LHD

M. Yoshinuma¹, K. Ida¹, K. Nagaoka¹, M. Osakabe¹, H. Takahashi¹, H. Nakano¹, and K. Tanaka¹

¹National Institute for Fusion Science, Toki, Japan

Corresponding Author: M. Yoshinuma, yoshinuma@nifs.ac.jp

An extremely hollow carbon impurity profile (impurity-hole) has been observed associated with increase of ion temperature gradient in the discharges with ion-ITB on LHD. Simultaneous achievement of the impurity-hole and ion-ITB is favorable feature in nuclear fusion plasma, where both good energy confinement and ash exhaust are required. The impurity-hole is characterized as small diffusion and large outward convection of impurities [1]. The outward convection observed in experiment contradicts to the prediction of neoclassical impurity transport and the convection velocity becomes larger as the magnetic axis shifted outward and the ion charge of Z is increased [2]. In this paper, the dynamic behaviors of the convection velocity of carbon impurity during the formation of impurity-hole are described.

1) The dynamic impurity transport analysis shows that the abrupt (time scale of 30 ms) reversal of turbulent-driven convection flow of carbon impurity from inward to outward takes place at the formation.

2) The reversal starts at the position where the ion temperature gradient becomes steep and propagates toward the core and edge in the time scale of 100 ms while the ion temperature increases in the time scale of 300 ms.

References

[1] M.Yoshinuma, et al., Nucl. Fusion 49 (2009) 062002.

[2] K.Ida, et al., Phys. Plasmas 16 (2009) 056111.

EX-P



Study of Neutral Hydrogen Transport in LHD Core Plasmas Based on High Dynamic-Range Balmer-Alpha Spectroscopy

K. Fujii¹, M. Goto², and S. Morita²

¹Kyoto University, Kyoto, Japan

²National Institute for Fusion Science, Toki, Japan

Corresponding Author: K. Fujii, fujii@me.kyoto-u.ac.jp

The radial distribution of the neutral hydrogen atom density $(n_{\rm H})$ and pressure $(P_{\rm H})$ in the Large Helical Device (LHD) is studied. The $n_{\rm H}$ distribution is determined from a detailed analysis of the intensity-calibrated Balmer-alpha line profile while the $P_{\rm H}$ distribution is obtained with a simple one-dimensional analytical model. We have for the first time determined $n_{\rm H}$ at the center of a fusion-oriented plasma, which is approximately three orders smaller than that at the edge. On the contrary, $P_{\rm H}$ changes only a factor of 10 from the edge to core regions. The central $n_{\rm H}$ has a tendency to become smaller as the line-averaged electron density is increased.

Preprint

Study of Transport Characteristics of Multiple Impurities Depending on the Impurity Source Location in LHD

S. Sudo¹, N. Tamura¹, K. Tanaka¹, S. Muto¹, C. Suzuki¹, H. Funaba¹, J. Miyazawa¹, M. Yokoyama¹, M. Yoshinuma¹, K. Ida¹, R. Yasuhara¹, I. Yamada¹, and H. Yamada¹

¹National Institute for Fusion Science, Toki, Japan

Corresponding Author: S. Sudo, sudo@nifs.ac.jp

By injecting tracers into the LHD plasma with a tracer-encapsulated solid pellet (TESPEL) method, we found that the impurity source location is essential for determining the impurity transport property. The impurity transport for three different locations of impurity source are studied by i) thick-shell-type TESPEL (thickness of $\sim 240 \ \mu$ m), ii) thin-shell-type TESPEL (thickness of $\sim 75 \ \mu$ m) and iii) Ar gas puffing. As a result, a new property of the impurity behavior was revealed owing to the advantage of the direct and local deposition of the multiple tracers (V, Mn, and Co) by TESPEL in the plasma as follows. 1) In the plateau regime ($n_e = 3-4 \times 10^{19} \text{ m}^{-3}$), the tracers deposited in the plasma flow away faster than the case of the Pfirsch Schlueter (PS) regime ($n_e = 5-7 \times 10^{19} \text{ m}^{-3}$), while the intrinsic impurities can enter easily into the plasma core. 2) In the PS regime, the tracers deposited in the plasma are kept for a long time, while the impurities coming from the outside of the plasma are prevented from entering into the plasma core. This is confirmed with the Ar gas puffing as a simulator for intrinsic impurities. In case ii), the tracer penetration depth becomes shallower (around $\rho = 0.85$) than the case i) (around $\rho = 0.75$). The tracers deposited in this location have still the same feature as the case i). The Ar Li- and Be-like emissions mainly coming from the plasma periphery are observed in the both regimes. The ratio of the emission intensity of the PS versus the plateau regime is compared with the calculation by the STRAHL code, and it indicates that Ar particles reach up to the region of $\rho = 0.87$ -0.93 in the PS regime. Thus, the layer discriminating the impurity behavior is identified as the region of $\rho = 0.9$. The dominant friction force against the thermal force in the scrape-off layer works as the outflow mechanism of the impurity in case of the PS regime, as the ratio of the friction force versus the thermal force is proportional to $n_e^{-2.5} \sim 3$ in the plasma periphery. The method and the present results will contribute to the future impurity transport study in the edge region of the fusion plasma.



Studies of Dust Transport in Long Pulse Discharges in the Large Helical Device

M. Shoji¹, M. Tokitani¹, H. Kasahara¹, T. Seki¹, K. Saito¹, S. Kamio¹, R. Seki¹, Y. Tanaka², A. Pigarov³, R. Smirnov³, G. Kawamura¹, S. Masuzaki¹, Y. Uesugi³, and T. Mutoh¹

¹National Institute for Fusion Science, Toki, Japan ²Kanazawa University, Ishikawa, Japan ³University of California San Diego, CA, USA

Corresponding Author: M. Shoji, shoji@lhd.nifs.ac.jp

Dust transport study in magnetic plasma confinement devices has been attracting attention because it is concerned that dusts influence main plasma performances in nuclear fusion reactors. Exfoliated dusts consisting of accumulated impurity deposition layers can enter the main plasma to enhance impurity radiation. The Large Helical Device (LHD) is a unique test stand for studying the dust effects because of the performance of steady-state operations with saturated wall conditions which are equivalent to situation in nuclear fusion reactors. Many incandescent dusts have been observed in ICRF heated long pulse discharges. Spectrometers have detected frequent spikes of iron emission induced by the dusts. Stereoscopic observations of the three-dimensional trajectories of the dusts using a fast framing camera show that the dusts exist in the peripheral plasma and do not penetrate into the main plasma for high heating power, while dust penetration were observed for low heating power. A dust transport simulation code (DUSTT) was applied to investigate observations of the dust trajectories. It can calculate the time evolution of the force, heat, mass, and charge balance of dusts in plasmas. The original DUSTT code is optimized to axisymmetric plasma configurations such as Tokamaks. Thus, the code was modified and implemented in a three-dimensional, neutral particle transport code (EIRENE), which enables the analysis of dust transport in non-axisymmetric plasma configuration like a LHD. The LHD peripheral plasma is mainly composed of two magnetic structures: divertor legs and ergodic layers. The simulation shows that the peripheral plasma has two functions for preventing the dusts from the penetration. One is sweeping on the divertor legs by the plasma flow (mainly by ion drag force), and another one is evaporation on the ergodic layers by the effect of the heat load due to the high peripheral plasma temperature. It explains the observations in the long pulse discharges for the high and low ICRF heating power in LHD, showing that the dusts are swept off and are evaporated in the peripheral plasma for the high heating power. It indicates that penetration of dusts, which size is in the range collected in the present devices, into the main plasma will be controlled in nuclear fusion reactors because of the evaporation of dusts by the high temperature peripheral plasma.



Optimization of High Harmonic ECRH Scenario to Extend a Heating Plasma Parameter Range in LHD

T. Shimozuma¹, H. Igami¹, S. Kubo¹, Y. Yoshimura¹, H. Takahashi¹, M. Osakabe¹, T. Mutoh¹, M. Nishiura², H. Idei³, K. Nagasaki⁴, N. Marushchenko⁵, and Y. Turkin⁵

¹National Institute for Fusion Science, Toki, Japan
 ²Graduate School of Frontier Science, University of Tokyo, Japan
 ³Institute for Applied Mechanics, Kyushu University, Kasuga, Japan
 ⁴Institute of Advanced Energy, Kyoto University, Kyoto, Japan
 ⁵Max-Planck-Institut für Plasmaphysik, Garching, Germany

Corresponding Author: T. Shimozuma, shimozuma.takashi@lhd.nifs.ac.jp

High harmonic Electron Cyclotron Resonance Heating (ECRH) is potential means of extending plasma density and β -value ranges of fusion-relevant plasmas. Instead of the normally used fundamental ordinary (O1) and the second harmonic extraordinary (X2) modes, sufficient absorption can be expected using even O2 and X3 mode heating scenarios, when the temperature and density of a target plasma are high and the injection and/or magnetic field configurations are optimized. The cut-off densities of O2 and X3 mode wave propagation are twice and four-thirds of the X2 mode cut-off density, respectively. Moreover, the resonant magnetic field strength of the X3 mode becomes two-thirds of the field for the X2 mode.

We investigated the optimized condition of both the EC wave injection and the magnetic field configuration in the Large Helical Device (LHD). Firstly, in the case of O2 mode injection with a frequency of 77 GHz and with the optimized injection angle, about 30–40% absorption could be kept beyond the cut-off density of X2 mode, which is 3.7×10^{19} m⁻³. Secondly, in X3 mode heating experiment, the stepwise power injection from three gyrotrons pushed up the electron temperature, leading to the absorption improvement and achieving more than 40% absorption efficiency. Superposed stepwise injection from three gyrotrons with a total of 3 MW increased the central electron temperature to about 3.5 times of the initial target plasma temperature of 0.6 keV. This clearly shows that the temperature increase improves the absorption rate of the subsequent injection. Thirdly, for both cases, the ray-tracing (TRAVIS) code analyses show fairly good agreement with the plasma-parameter dependences of the absorption rates experimentally obtained.

Experimental results and ray tracing analyses show also that the O2 and X3 mode ECRH can be expected as methods with sufficient absorption, when the EC beam is injected 1) along the ECR layer over a long distance in the injection case from the upper-port antenna (U-antenna case) and 2) through the saddle point of the magnetic field strength between two ECR layers in the injection case from the outer-port antenna (O-antenna case) in LHD. The high harmonic ECRH is expected to have a potential to extend the heating regime utilizing optimized injection condition and magnetic configurations with a long-distance resonance.



Experimental Observation of Plasma Response to Resonant Magnetic Perturbation and its Hysteresis in LHD

Y. Narushima¹, S. Sakakibara¹, S. Ohdachi¹, Y. Suzuki¹, K. Watanabe¹, S. Nishimura¹, M. Furukawa², Y. Takemura¹, K. Ida¹, M. Yoshinuma¹, and I. Yamada¹

¹National Institute for Fusion Science, Toki, Japan ²Tottori University, Tottori, Japan

Corresponding Author: Y. Narushima, narusima@lhd.nifs.ac.jp

EX/P6-35

Dynamics of magnetic islands in helical plasmas has been studied by means of an externally imposed resonant magnetic perturbation (RMP) to clarify its effect on the MHD stability and confinement in the Large Helical Device (LHD) plasmas. It has been reported that spontaneous healing and growth of magnetic islands can be clearly separated on the space of plasma β , collisionality, and poloidal flow. The dependence on the magnetic configuration has been also reported, in which the ramping-up RMP is likely to penetrate for the low magnetic shear and mitigated magnetic hill. This study clarifies configuration effect on healing/growth transition of magnetic islands for the first time. Dynamical response of island has been investigated for various magnetic configurations with different magnetic axis position ranging $R_{ax} = 3.55 - 3.80$ m. To clarify the effect originated from magnetic configuration, plasma parameters are kept approximately constant during the discharge. In case the RMP is ramped up during the discharge, the magnetic island shows healing at the beginning of the discharge. At that period, the plasma response field compensates the RMP field to shield it. When the RMP reaches a threshold, it penetrates into the plasma and makes the magnetic island. On the other hand, in case the RMP is ramped down during the discharge, the RMP initially penetrates into the plasma and makes the magnetic island. When the decreasing RMP reaches a threshold, it is shielded and the magnetic island disappears. It is observed that thresholds of the amplitude of RMP for the healing/growth transition of magnetic island depend on magnetic axis position R_{ax} . The RMP threshold increases as the magnetic axis position R_{ax} increases. Furthermore, it was found that the threshold of RMP for healing is smaller than that for growth, which means hysteresis in the critical RMP at a healing/growth transition. The magnetic island response to RMP and its hysteresis have been identified in LHD. The experimental observation shows 1) the threshold of RMP increases with the R_{ax} of the magnetic configuration, and 2) the hysteresis is seen in the critical RMP at a healing/growth transition.



Interaction between Resistive Interchange Mode and Helically Trapped Energetic Ions and its Effects on the Energetic Ions and Bulk Plasmas in LHD

X. Du¹, K. Toi², M. Osakabe², S. Ohdachi², K. Ida², K. Tanaka², T. Ido², M. Yoshinuma², K. Ogawa², M. Isobe², K. Nagaoka², T. Ozaki², S. Sakakibara², R. Seki², A. Shimizu², and Y. Suzuki²

¹The Graduate University for Advanced Studies, Japan ²National Institute for Fusion Science, Toki, Japan

Corresponding Author: X. Du, du.xiaodi@lhd.nifs.ac.jp

Bursting resistive interchange modes destabilized by a characteristic motion of helically trapped energetic ions are for the first time observed in a helical plasma and induce large negative radial electric field near the edge, which indicates non-ambipolar losses of the fast ions by the modes. The burst modes also induce a clear change of toroidal plasma rotation and micro-turbulence suppression accompanying transient confinement improvement.



Characteristics of MHD Instabilities Limiting Beta Value in LHD

S. Sakakibara¹, Y. Takemura¹, K. Watanabe¹, Y. Suzuki¹, S. Ohdachi¹, Y. Narushima¹, K. Ida¹, K. Tanaka¹, H. Yamada¹, and I. Yamada¹

¹National Institute for Fusion Science, Toki, Japan

Corresponding Author: S. Sakakibara, sakakis@lhd.nifs.ac.jp

Effects of low-n MHD instabilities on plasma performance have been assessed in the regime where an achieved β value is regulated by instabilities. In stellarators and heliotrons, interchange instability driven by pressure gradient is most concerned to impose the limit of the achievable β value. Previous experiments in LHD show that high β plasma with more than 5% was successfully achieved in the moderately unstable regime where violated instabilities are benign and does not result in harmful consequence like disruption. The resistive interchange modes were dominantly observed in the all β range because of magnetic hill in periphery, and it was verified that the amplitudes of modes were suppressed by an increment of the magnetic Reynolds number, S, which is favorable in fusion reactor regime with high electron temperature, T_e . However, since the growth rate of the ideal interchange mode is independent of S, verification of the significance of the ideal stability boundary is still major problem to be solved in helical devices. Here we focus on the effect of the mode on the confinement property in the regime where the destabilization of the ideal interchange mode is predicted by linear theory. The unstable regime of an ideal interchange mode is characterized by enhanced magnetic hill and reduced magnetic shear. The magnetic hill was enhanced by shifting the magnetic axis position to the inward, whereas the magnetic shear was reduced by increasing the plasma aspect ratio and/or plasma current. In the enhanced magnetic hill configuration, the rotating m/n = 2/1 mode appears and the amplitude is increased with deceleration of the mode rotation, which forms the flattening structure of pressure profile around the m/n = 2/1 resonance. After the stop of the rotation, the profile flattening is extended to the core region, which drops the central β by more than 30%. In the reduced magnetic shear configuration, m/n = 1/1 mode also decreases the central β by about 60% after the rotation stops as well as m/n = 2/1 mode. Both experiments give us the following key results: i) low-*n* modes are significantly destabilized in the ideal-unstable configurations and lead to degradation of central β by at most 60%, and ii) the degree of their damages strongly depends on the mode rotation velocity.



Experimental Observation of Nonlocal Electron Thermal Transport in NSTX RF-Heated L-Mode Plasmas

Y. Ren¹, B. P. LeBlanc¹, W. Guttenfelder¹, S. Kaye¹, E. Mazzucato¹, *K. C. Lee*², C. W. Domier³, R. E. Bell¹, and H. Yuh⁴

¹Princeton Plasma Physics Laboratory, Princeton, NJ, USA
²National Fusion Research Institute, Daejeon, Korea, Republic of ³University of California Davis, CA, USA
⁴Nova Photonics, Inc., Princeton, NJ, USA

Corresponding Author: Y. Ren, yren@pppl.gov

Understanding electron thermal transport is crucial for improving and predicting the confinement performance of future devices, e.g., FNSF and ITER. The observations of nonlocal electron thermal transport in tokamaks and stellarators challenge the standard local model of turbulence and transport. Here, we report the first observation of nonlocal electron thermal transport in a set of NSTX RF-heated L-mode plasmas with $B_T = 5.5$ kG, $I_p = 300$ kA and RF heating power of about 1 MW. We observed that electron-scale turbulence spectral power (measured with a high-k collective microwave scattering system) is reduced by almost an order of magnitude immediately after the RF heating are not exactly synchronized, and the drop in the turbulence spectral power has a time delay of about 1 ms relative to the RF cessation. The correlation and time delay between the reduction of turbulence and RF cessation indicate a causal relation between the measured turbulence and heat flux. Local linear gyrokinetic stability analyses show that ion and electron-scale instabilities are robustly unstable in these plasmas and are far from marginal stability. Thus linear stability is unlikely able to explain the observed reduction in electron-scale turbulence at the RF cessation.

Parametric Dependence of Fast-Ion Transport Events on the National Spherical Tokamak Experiment

E. Fredrickson¹, N. N. Gorelenkov¹, M. Podestá¹, S. P. Gerhardt¹, R. E. Bell¹, A. Diallo¹, B. LeBlanc¹, and A. Bortolon²

¹Princeton Plasma Physics Laboratory, Princeton, NJ, USA ²University of Tennessee, Knoxville, TN, USA

Corresponding Author: E. Fredrickson, efredrickson@pppl.gov

Neutral-beam heated tokamak plasmas commonly have more than one third of the plasma kinetic energy in the non-thermal energetic beam ion population. This population of fast ions heats the plasma, provides some of the current drive, and can affect the stability (positively or negatively) of magneto-hydrodynamic instabilities. This population of energetic ions is not in thermodynamic equilibrium, thus there is free-energy available to drive instabilities, which, of course, leads to redistribution of the fast ion population. Understanding under what conditions beam-driven instabilities arise, and the extent of the resulting perturbation to the fast ion population, is important for predicting and eventually demonstrating non-inductive current ramp-up and sustainment in NSTX-U, as well as the performance of future fusion plasma experiments such as ITER. This paper presents an empirical approach towards understanding the stability boundaries for some common energetic-ion-driven instabilities seen on NSTX.

Impact of 3D Fields on Divertor Detachment in NSTX and DIII-D

J.-W. Ahn¹, R. Bell², A. Briesmeister¹, J. Canik¹, A. Diallo², T. E. Evans³, N. M. Ferraro³, S. Gerhardt², B. Grierson², T. K. Gray¹, S. Kaye², M. J. Lanctot³, B. LeBlanc², J. Lore¹, R. Maingi¹, A. G. McLean⁴, D. Orlov⁵, T. Osborne³, *T. W. Petrie*³, A. L. Roquemore², F. Scotti², O. Schmitz⁶, M. Shafer¹, V. Soukhanovskii⁴, E. A. Unterberg¹, and A. Wingen¹

¹Oak Ridge National Laboratory, Oak Ridge, TN, USA
 ²Princeton Plasma Physics Laboratory, Princeton, NJ, USA
 ³General Atomics, San Diego, CA, USA
 ⁴Lawrence Livermore National Laboratory, Livermore, CA, USA
 ⁵University of California San Diego, CA, USA
 ⁶University of Wisconsin-Madison, Madison, WI, USA

Corresponding Author: J.-W. Ahn, jahn@pppl.gov

Increasing input power and plasma current in present and future tokamaks naturally leads to more serious divertor and first wall heat flux problem, both for the steady state and the transient ELM heat deposition. Therefore, ELM control using the 3D fields and peak heat flux reduction with divertor detachment must be compatible.

A large amount of deuterium (D2) gas is puffed into the lower divertor area in NSTX, for naturally ELMy H-mode plasmas, to produce partially detached divertor condition. 0.2 kA n = 3 error field correction was applied as a baseline, followed by super-position of the n = 3 perturbation field (-0.5 kA) for the second half of the gas puff period. Two divertor gas puff rates were tested; low ($\sim 7 \times 10^{21}$ D/s) and high gas puff ($\sim 1.1 \times 10^{22}$ D/s). After the detachment onset by gas puff, the peak heat flux is reduced by $\sim 70\%$ compared to those in the attached regime. However, it is seen that the profile becomes peaked again in the low gas puff case after 3D fields were applied to the detached plasma, i.e., the divertor plasma re-attached, while it remains detached in the high gas puff case. Therefore, the 3D fields can re-attach weakly detached plasma but this can be avoided by enhancing detachment with higher gas puff.

A similar experiment was carried out at DIII-D to investigate the impact of n = 3 3D fields by I-coils on divertor detachment, which was established by upstream D2 gas puffs. A 4 kA coil current, with both even and odd parities, was applied to high density ($n_e > 7 \times 10^{19}$ m⁻³ and $v_e^* > 1$) H-mode discharges. It was found that the plasma did not respond to the applied 3D fields, i.e., there was no striation observed either in the heat or particle flux profile, although the pedestal collisionality was high enough compared to the value reported necessary ($v_e^* > 0.5$) to achieve heat flux striations in a previous study. Field line tracing using TRIP3D-MAFOT with and without the use of data from M3D-C1 shows that plasma response can significantly alter the pattern of striations by implementing 3D edge transport calculation by EMC3-Eirene. Characterization of 3D field spectra and shape parameters regarding their impact on detachment conditions, along with comparison of results from NSTX and DIII-D, will be presented.

This work was supported by US DOE.

The Role of Lithium Conditioning in Achieving High Performance, Long Pulse H-Mode Discharges in the NSTX and EAST Devices

R. Maingi¹, D. Mansfield¹, X. Gong², Z. Sun², M. Bell¹, Y. Duan², H. Guo², J. Hu², R. Kaita¹, S. Kaye¹, H. Kugel¹, J. Li², V. Soukhanovskii³, B. Wan², and *G. Xu²*

¹Princeton Plasma Physics Laboratory, Princeton, NJ, USA
 ²Institute of Plasma Physics, Chinese Academy of Sciences, Hefei, China
 ³Lawrence Livermore National Laboratory, Livermore, CA, USA

Corresponding Author: R. Maingi, rmaingi@pppl.gov

The role lithium wall conditioning plays in the achievement of high performance, long pulse discharges in NSTX and EAST is documented. Common observations include a reduction in hydrogenic recycling, confinement enhancement, and the elimination of ELMs. The plasma confinement and pulse length in both devices improve with increasing lithium conditioning. In NSTX, the impurity accumulation which occurred when natural ELMs were suppressed by lithium conditioning, was ameliorated by triggering controlled ELMs, e.g., with pulsed 3D fields. In EAST, active lithium conditioning during discharges has overcome this problem, producing an ELM-free H-mode with controlled density and impurities.

In NSTX, analysis was done on lithium scans with high δ and κ , more prototypical of the shapes envisioned for NSTX-U. The improvements in pulse length, reduction in recycling, and elimination of ELMs in these highly shaped discharges reflect those with lower shaping. The edge density and pressure gradients were reduced in the outermost 5% of the profile in both the high and intermediate shapes, which is critical for the edge stability improvement. Moreover, while the pressure gradient was reduced, the pedestal broadened, increasing the pressure at the pedestal top and overall performance.

In EAST, the extensive lithium wall conditioning routinely applied via evaporators prior to a run day was integral to the 32 s long H-mode pulse lengths. However, during the course of a run day, the efficacy of the lithium coating can decline, and thus conditioning during discharged by injecting lithium powder into the edge plasma has been investigated. As in NSTX, large ELMs were eliminated, in this case with real time lithium injection. Although the radiated power and edge soft–X-ray emission were moderately higher in the discharges with active conditioning, these and the line-averaged electron density remained relatively constant in time, in contrast to the NSTX observations which showed secular rises in these quantities with large lithium doses.

In summary, the results from both devices demonstrate several common benefits of lithium conditioning. The new observation on EAST of a quasi-steady discharge devoid of large ELMs improves the prospects for the applicability of lithium conditioning for future devices, removing one of the obstacles to progress in NSTX experiments.



Study of the Alfvén Wave Coupling in the SUNIST Spherical Tokamak

Y. Tan¹, Y. Liu¹, and Z. Gao¹

¹Tsinghua University, Beijing, China

Corresponding Author: Y. Tan, tanyi@sunist.org

Tan

The coupling between Alfvén waves and plasmas are studied before applying high power rf waves to drive current in the SUNIST spherical tokamak (R/a: 0.3 m/0.23 m; $B_{T0} = 0.15$ T; $I_P = 30-70$ kA; $n_e \sim 10^{19}$ m⁻³; pulse length: 10–25 ms). The impedance of antennas reflects the coupling and can be easily obtained from the rf voltage across and the rf current through the antennas since the frequencies of the waves are low. The evolution of wave coupling in typical discharges confirms that the coupling heavily depends on the electron density and the plasma shape. The impedance of the antennas without BN limiters as a function of frequency qualitatively agrees with the 1D MHD calculation results of mixed n = 1/-1 and m = 1/-1 modes. However, the dependence of the impedance of antennas with BN limiters on toroidal field is much weaker. The Alfvén continuum is obtained by continuously scanning the toroidal field.

Alfvén Oscillations in the TUMAN-3M Tokamak Ohmic Regime

A. Tukachinsky¹, S. Lebedev¹, L. Askinazi¹, V. Kornev¹, and M. Vildjunas¹

¹*Ioffe Physical-Technical Institute of the Russian Academy of Science, St. Petersburg, Russian Federation* Corresponding Author: A. Tukachinsky, a.tukachinsky@mail.ioffe.ru

The bursts of high frequency (~ 1 Hz) oscillations have been registered by magnetic probes in experiments carried out on the TUMAN-3M tokamak. The line averaged plasma density was $n_e < 2.5 \times 10^{19} \text{ m}^{-3}$ and $B_T \sim 0.7$ –1 T, the regimes were both ohmic and NBI-heated. The gaps in oscillation spectra between high and low frequency parts of the spectra were observed under conditions mentioned above. The frequency in the higher part of the spectrum followed the dependence of Alfvén wave velocity VA on magnetic field strength and plasma density. This dependence allows identifying the high frequency waves as Alfvén waves. When n_e was increased, the gap disappeared because oscillation frequency decreased and entered the region of high level noise. The Alfvén wave identification became difficult. The neutral beam injection did not effect noticeably the Alfvén oscillations.

Alfvén waves are usually excited by fast ions in tokamak experiments [1, 2], but in ohmic regimes fast ions are practically absent. The high frequency oscillations (electron fishbones) produced by fast electrons were also observed in ECRH and LHCD experiments [3]. The bursts of oscillations observed in the TUMAN-3M experiments were excited in OH regimes at the moments of internal disruptions, sawteeth, when fast reconnection led to fast change in magnetic field geometry and its magnitude. Fast magnetic field oscillations were observed during internal (gongs [4]) and minor [5] disruptions. However, in those papers the possibility of the Alfvén wave generation was not considered. At some moments oscillations looked as beats of waves with close frequencies, reflecting the spectrum width.

The Alfvén mode localized in the plasma core has been apparently observed. In the plasma center the ratio $\Delta B/B$ is small (when $r \rightarrow 0$ then $\Delta B/B \rightarrow 0$) and the so called "gap mode" does not necessarily exist. For this mode frequency should be $f \approx VA/4\pi Rq$. In our experiments the observed frequency was $f \approx VA/2\pi R$, so for $q \ge 1$ the mode was apparently not a gap mode.

References

[1] K.L. Wong, Plasma Phys. Control. Fusion 1999 41 R1.

[2] D. Curran, Ph. Lauber, P.J. Mc Carthy et al., Plasma Phys. Control. Fusion 2012, 055001.

[3] F. Zonca *et al.*, Nuclear Fusion 2007, 47,1588 [4] P.A. Duperrex, A. Pochelon, *et al.*, Nuclear Fusion, (1992) 32, 7, 1161

[5] P. Savruhin et al., EX/P4-34, 24 IAEA FEC Conference, 2012



Effect of Horizontal Displacement on Fast Ion Confinement in TUMAN-3M

V. Kornev¹, L. Askinazi¹, S. Lebedev¹, A. Melnikov², V. Rozhdestvensky¹, N. Zhubr¹, F. Chernyshev¹, S. Krikunov¹, D. Razumenko¹, A. Tukachinsky¹, and M. Vildjunas¹

¹Ioffe Physical-Technical Institute of the Russian Academy of Science, St. Petersburg, Russian Federation ²National Research Centre "Kurchatov Institute", Moscow, Russian Federation

Corresponding Author: V. Kornev, vladimir.kornev@mail.ioffe.ru

The investigation of the behavior of fast ion (FI) is among the most important directions of research in the field of magnetic plasma confinement. Study the FI confinement in compact tokamak with relatively low toroidal magnetic field is topical in view of the increasing interest in developing neutron sources based on the nuclear fusion reactions. Capture efficiency of FI and thermalization one was studied in present experimental series by mean of neutron rate measurement. The temporal evolution and the absolute magnitude of the neutron emission were detected by He3 gas discharge detector. Regression analysis of the experimental data with available plasma and heating beam parameters in TUMAN-3M tokamak gives dependence of neutron rate on engineering parameters. The empirical scaling expression indicates expected strong dependence of neutron emission rate on toroidal magnetic field and beam energy. Results of experimental study of influence of plasma position along major radius on the efficiency of plasma heating and fast ions confinement are presented. Plasma shift inwards along the major axis led to the increase of the electron temperature from 300 eV to 400 eV and results in 20% increase in neutron emission rate. Increase of neutron rate indicates on improvement of fast ion confinement.



GAM Evolution and LH-Transition in the TUMAN-3M Tokamak

A. Belokurov¹, L. Askinazi¹, A. Komarov², V. Kornev¹, L. Krupnik², S. Lebedev¹, A. Smirnov¹, A. Tukachinsky¹, M. Vildjunas¹, and N. Zhubr¹

¹ Ioffe Physical-Technical Institute of the Russian Academy of Science, St. Petersburg, Russian Federation ²NNC 'Kharkov Institute of Physics and Technology', Kharkov, Ukraine

Corresponding Author: A. Belokurov, belokurov@mail.ioffe.ru

Geodesic acoustic mode (GAM) is a specific mode of low-frequency oscillations in toroidal plasma, which does not participate in radial transport directly, although affects anomalous transport through control of turbulence level [1]. GAM-induced shear of radial electric field is not constant in time, therefore possibility of LH-transition initiating in this case is to be studied. GAM were experimentally studied in TUMAN-3M tokamak by means of heavy ion beam probe [2] and Doppler reflectometry. Oscillations were detected before ohmic LH-transition and disappeared in H-mode. There was also detected an interrelation between GAM and ambient turbulence. To understand if GAM can hinder or facilitate the transition, there was designed a simple model of LH-transition under the effect of GAMinduced radial electric field, based on TUMAN-3M tokamak geometry and basic plasma parameters. Simulation of spatial and temporal evolution of plasma density profile was carried out. Radial electric field was disturbed by oscillations, which structure, frequency and localization area corresponded to GAM in TUMAN-3M tokamak. Diffusion coefficient was taken in a form $D = k(\omega(r,t))D_0(r)$, with radial electric field shear dependent factor $k(\omega)$, similar to one proposed in [3] and spatial dependent part $D_0(r)$. Simulation results show possibility of LH-transition, initiated by a spaceand time-localized GAM burst, if GAM parameters, such as amplitude, frequency, wavelength, and burst duration are within certain limits, which are related to each other and also depend on plasma

parameters, primarily ion temperature. If GAM parameters are within those limits (e.g., amplitude is higher than a certain threshold), LH-transition occurs and system stays in H-mode after the GAM burst. Comparison of modeling with experimental observation of GAM in TUMAN-3M tokamak shows that experimental GAM parameters are within the limits, which define possibility of GAM-induced LH-transition.

References

[1] K. Itoh, S.-I. Itoh, et al., Phys. Plasmas 13, 055502 (2006).

[2] L.G. Askinazi et al., JTP Letters 38, 6 (2012).

[3] G.M. Staebler, Plasma Phys. Control. Fusion 40 (1998) 569-580



Recent ICRH-Wall Conditioning, Second Harmonic Heating and Disruption Mitigation Experiments Using ICRH System in Tokamak ADITYA

S. Kulkarni¹, S. Kumar¹, Y. Srinivas¹, A. Varia¹, R. Joshi¹, H. Jadav¹, M. Parihar¹,
B. Kadia¹, K. Parmar¹, G. Ashok¹, J. Ghosh¹, R. Yadav¹, K. Jadeja¹, R. Tanna¹, S. Bhatt¹,
C. Gupta¹, A. Kumar¹, S. Gupta¹, S. Banerjee¹, U. Dhobi¹, S. Pathak¹, E. V. Praveenlal¹,
J. Raval¹, S. Joisa¹, R. Manchanda¹, N. Ramaiya¹, N. Patel¹, M. Gupta¹, S. Pandya¹,
K. Mahavar¹, R. Jha¹, S. Jha¹, J. Thomas¹, A. Kumar¹, P. Chattopadhyay¹, P. Atrey¹,
A. Das¹, P. Kaw¹, D. Bora¹, and M. B. Chowdhuri¹

¹Institute for Plasma Research, Bhat, Gandhinagar, India

Corresponding Author: S. Kulkarni, kulkarni@ipr.res.in

ADITYA is a medium size tokamak with major radius 0.75 m and minor radius of 0.25 m, with toroidal magnetic field up to 1.5 T and has circular plasma in hydrogen gas. The diagnostics used in ICRH experiments are Langmuir probes, visible camera, spectroscopy, soft X-ray and hard X-ray detection techniques, diamagnetic loop, heterodyne on-line density measurements, Thompson scattering, Neutral particle analyzer, Limiter thermography, Residual Gas Analyzer(RGA), microwave diagnostics along with normal machine diagnostics like loop voltage, position, and plasma current measurements. The indigenously developed ICRH system is installed on ADITYA having 1 MW RF generator in the frequency range of 20–40 MHz, transmission line with matching system, vacuum interface, and fast wave poloidal type antenna with Faraday shield.

Here we report the recent experiments carried out on tokamak ADITYA using the developed ICRH system of 1 MW at 24.8 MHz frequency. The experiments are carried out to have plasma heating at second harmonic, disruption mitigation and also wall conditioning in presence of toroidal magnetic field. The wall conditioning experiments are carried out in presence of toroidal magnetic field under resonant (0.75 T), non-resonant (0.45 T) conditions as well as with 20% He gas in a hydrogen plasma (0.45 T). All three sets are found more effective in releasing wall impurities like water and methane as half an order (~ 5) of initial vacuum condition. As per data, the resonant ICWC is more effective to reduce carbon impurity and non-resonant ICWC is more effective to reduce oxygen impurity from vessel. The heating experiments at second harmonic are carried out using RF pulses of different magnitudes (5–100 ms) at different RF powers (40–200 kW) in plasma duration of 100 ms. The soft X-ray data shows an electron temperature rise from 250 eV to maximum of 500 eV.

In order to carry out mitigation of disruptions induced by hydrogen gas puff, ICRH system was used in both fixed and real time feedback mode. In an attempt to control the disruptions in real time the gas-puff induced H intensity increase is used as a precursor for the disruption and mitigation is successfully carried out.



EX/P7-17

Disruption Control Using Biased Electrode in Aditya Tokamak

P. Dhyani¹, J. Ghosh¹, P. Chattopadhyay¹, R. Tanna¹, D. Raju¹, S. Joisa¹, A. K. Chattopadhyay¹, D. Basu¹, N. Ramaiya¹, S. Kumar¹, K. Sathyanarayana¹, S. Bhatt¹, P. Atrey¹, C. Gupta¹, C. Rao¹, R. Jha¹, Y. Saxena¹, and R. Pal²

> ¹Institute for Plasma Research, Bhat, Gandhinagar, India ²Saha Institute of Nuclear Physics, Kolkata, India

Corresponding Author: P. Dhyani, pravesh@ipr.res.in

Improvement in tokamak plasma confinement using biased electrodes observed in many tokamaks is a well-established phenomenon. In this paper we show that very use of the same biased electrode can mitigate the disruptions in tokamak plasmas through stabilization of magnetohydrodynamics (MHD) modes. Disruption induced in ADITYA tokamak by H₂ gas puffing is successfully mitigated by applying the positive bias voltage to the electrode placed in the LCFS prior to the gas injection. Sheared ($E_r \times B_{\phi}$) rotation of the plasma generated by biasing leads to substantial reduction in growth of MHD modes (m/n = 3/1, 2/1) and avoids disruptions through prevention of mode locking.

Preprint

L-H Transition Triggered by Fishbone Mode in the NBI Heated HL-2A Plasmas

Y. Liu¹, W. Zhong¹, Z. Shi¹, Y. Xu¹, M. Isobe², Y. Zhang¹, W. Deng¹, and X. Ji¹

¹Southwestern Institute of Physics, Chengdu, Sichuan, China ²National Institute for Fusion Science, Toki, Japan

Corresponding Author: Y. Liu, yiliu@swip.ac.cn

Liu

The L-H transition physics is one of the most important subjects for realizing a controlled nuclear fusion. In this paper, we present new results to show the nature of L-H transition and related mechanisms that trigger its onset. A novel feature, i.e., the coupling between the fishbone mode and the edge transport during NBI heated discharges, is found. Some of the results are similar to the fishbone-triggering on internal transport barrier while others are unique and appear to be pertinent to edge transport barrier. In some discharges a burst of a large fishbone is followed immediately by an L-H transition or shortly followed by an edge localized mode (ELM). Furthermore, an I-phase triggered by 'persistent EPMs' or sawtooth is also observed.

The measurement of edge plasma poloidal rotation, using reflectometry, has been performed to elucidate the correlation between the nonlinear evolution of fishbone instability and the edge radial electric field. It was found that a sudden increase in the plasma poloidal rotation happened immediately after the onset of each fishbone and ultimately the last fishbone triggered the transition to I-phase when the poloidal rotation velocity reaches 2 km/s. Thus, the enhancement in plasma poloidal rotations and results in the transition. Further experimental results suggest that the fishbone could provide a locally enhanced shear in the plasma flow by fast ion redistribution and/or heat propagation, and act as a trigger for the L-H or L-I transition.

We present evidence showing that EPMs can affect bulk plasma confinement through flow generation and kinetic effects. The finding of triggering phenomena by fishbone activities should be emphasized since the resultant shear of electric field in a future burning plasma could reach a sufficiently large level to reduce the turbulence transport. This gives us a hope that the alpha-particle losses induced by the alpha-particle driven MHD instabilities in a burning plasma may cause a sudden change of the plasma confinement by resultant structured electric field.



EX/P7-19

Neoclassical Tearing Modes Triggered by Intrinsic Error Field in the HL-2A Tokamak

Y. Xu¹, Q. Yang¹, X. Ji¹, T. Sun¹, W. Zhong¹, Y. B. Dong¹, F. Xia¹, A. Sun¹, M. Jiang¹, and L. Wei²

> ¹Southwestern Institute of Physics, Chengdu, Sichuan, China ²Dalian University of Technology, Liaoning, China

Corresponding Author: Y. Xu, xuyuan@swip.ac.cn

Extrinsic magnetohydrodynamic (MHD) events such as sawtooth crash, fishbone or edge localized mode (ELM) instabilities are often required to provide the seed islands for triggering neoclassical tearing mode (NTM). However, the spontaneous onset NTM (m/n = 3/2) without any detectable extrinsic MHD events has been observed in the HL-2A tokamak. The intrinsic error field is considered as an alternative mechanism to provide the seed island for generating the NTM.

The spontaneous onset NTM on HL-2A was realized with PECRH = 1.7 MW and co-current PNBI = 0.8 MW in an L-mode discharge. From the time-frequency spectrogram, the initial frequency of NTM is almost zero and its frequency rises around 13 kHz, the mode existent time coincides with the NBI duration. This is different from the seed island for the NTM is formed by toroidal coupling with the 2/1 tearing mode in the ELMy free H-mode. The same oscillations appear in the β_N and frequency spectrogram of the NTM. The amplitude of the magnetic field corresponding to the 3/2NTM decreases gradually during the ramping up phase of the mode frequency. And then it keeps almost invariant until the disappearance of this mode. The NTM propagates in the ion diamagnetic drift direction. In addition, the frequency of the 3/1 mode with a frequency of about 6 kHz exists during most ECRH phase. This mode has similar characteristics with the edge harmonic mode (EHO), propagating poloidally in the direction of the electron diamagnetic drift and toroidally in the co-current and NBI direction. All the observations suggest that there is no direct interaction between the EHO and NTM. The error field in HL-2A mainly originates from the installation error of various coils. The 3/1 mode frequency is much larger than the error field one so that there is no clear interaction between them. The initial frequency close to zero for the 3/2 NTM should be related to the error field. Here bootstrap current fraction is estimated as ~ 15% when $\beta_N = 1$. Although n = 2 error field is small, it is enough to provide the seed island for the NTM. Thus, the intrinsic error field is a suitable candidate for triggering the NTM on HL-2A.



Evolution of the Ion Temperature in Pedestal during the ELM Mitigation by SMBI

D. Yu¹, C. Chen¹, Y. Wei¹, W. Zhong¹, Z. Shi¹, J. Cheng¹, M. Jiang¹, K. Zhao¹, Y. Zhou¹, Y. Huang¹, Y. Liu¹, L. Yan¹, Q. Yang¹, and X. Duan¹

¹Southwestern Institute of Physics, Chengdu, Sichuan, China

Corresponding Author: D. Yu, yudl@swip.ac.cn

Yu

To study the mechanism of the ELM mitigation by SMBI, a high spatial and temporal resolution charge exchange recombination spectroscopy (CXRS) has been developed. This paper presents the first observation of the evolutions of ion temperature and its gradient in the pedestal measured with CXRS. It is found that the gradient of the ion temperature and the pedestal size both decrease around one third during ELM mitigation. In addition, it is observed that at least 20% decrement of T_i has to be attained in order to achieve a noticeable ELM frequency change. In shot 22536, around 2.5×10^{19} deuterium molecules are injected and the plasma density increases from 2.8 to 3.1×10^{19} m⁻³. The ion temperature and plasma toroidal rotation velocity decrease from 276 eV and 30 km/s to 81 eV and 13 km/s, respectively; the ELM frequency measured from D_{α} signals increases from ~140 to ~1200 Hz. As for the ETB of ion temperature, its height decreases but its structure sustains during the ELM mitigation phase.

To assess the cooling effect of the SMBI in detail, edge ion temperatures of 24 shots and 33 SMBI pulses are analyzed. The averaged ion temperature at the pedestal top decreases from 216 eV to 108 eV; whereas it decreases from 89 eV to 58 eV at the pedestal bottom, indicating the ion temperature decreases more at the pedestal top than that at the pedestal bottom. This cooling effect results in the ion temperature gradient decreasing from 45 eV/cm to 26 eV/cm. Furthermore, the averaged pedestal width decreases from 2.9 cm to 2 cm.

The ELM frequency can be increased significantly by SMBI. However, no ELM frequency change can be observed when the injected inventory is small. By increasing the SMBI pulse duration from 1.5 ms to 3 ms (the pressure keeps constant as 2 MPa) in shot 22497, the injected inventory is doubled. The first two SMBI pulses result in the relative decrement of T_i around ~ 20%, and the influence on the D_{α} and its frequency is ignorable. However, the ELM frequency increases significantly when the last two SMBI pulses are injected, as the relative decrements of T_i are 35% and 37%, respectively. It seems that the ELM frequency keeps no change when the decrement of T_i is equal or less than 20%. And the increment of ELM frequency increases exponentially with $\delta T_i/T_i$. The trend indicates that the decrement of $\delta T_i/T_i$ of ~20% is the critical value.



EX/P7-21

The Observation of Synchronous Oscillation prior to Disruption in the HL-2A Tokamak

M. Jiang¹, D. Hu², X. G. Wang², Z. Shi¹, Y. B. Dong¹, Y. Zhang¹, X. Ji¹, J. X. Li¹, Y. Liu¹, Q. W. Yang¹, and X. Duan¹

¹Southwestern Institute of Physics, Chengdu, Sichuan, China ²Peking University, Beijing, China

Corresponding Author: M. Jiang, jiangm@swip.ac.cn

Recently, a class of distinctive MHD activities before the onset of disruption has been identified on HL-2A density limit and radiation induced disruptive discharges, where the higher radiation level is generally considered as the consequence of high electron density or excessive boundary fueling. This precursor mode is named here according to its phenomenological behavior as the Synchronous Oscillation prior to Disruption (SOD), which is characterized by the synchronous oscillations between electron cyclotron emission (ECE) signal, the core soft X-ray signal, Mirnov probe signal, and H_{α} line radiation signal in the divertor. Although the frequency of this behavior will decrease as the plasma evolves towards the onset of thermal quench, the oscillations of SOD has a strong correlation with the following thermal quench. This long time-scale behavior makes it suitable to be incorporated as a part of disruption prediction, avoidance and mitigation scheme. Furthermore, these characteristics of SOD also enable us to look deeper into the physics behind those phenomenological behaviors, thus provide us a clearer understanding about density limit and radiation induced disruptions.

It is found that a 2/1 mode and its higher order harmonics are dominant during the SOD activities. The frequency of this 2/1 mode would maintain above 2 kHz for several ten milliseconds or even longer before beginning to slow down. The ultimate mode locking will always trigger the onset of thermal quench. It should be noted that the frequency of this 2/1 mode corresponds to the toroidal rotation frequency at the plasma edge, suggesting that MHD modes locating at the plasma edge might be responsible for those activities. For most SOD discharges, it has been observed that most plasma current is contracted within the q = 2 rational surface. The analysis of perturbation structure implies that resistive kink mode and its higher order harmonics, rather than the overlapping of a few major islands, triggered the disruption.

Comparison of ELM-Filament Mitigation between Supersonic Molecular Beam Injection and Pellet Injection in the HL-2A Tokamak

L. Nie¹, J. Cheng¹, Y. Huang¹, Y. Xu¹, D. Yu¹, W. Zhong¹, J. Dong¹, X. Ding¹, X. Duan¹, M. Xu¹, L. Yan¹, L. Yao¹, B. Feng¹, K. Zhao¹, J. Gao¹, C. Chen¹, Z. Huang¹, H. Xu¹, G. Zhu¹, D. Liu¹, D. Kong², X. Ji¹, Z. Feng¹, C. Liu¹, K. Yao¹, J. Shang¹, and Q. Yang¹

> ²Institute of Plasma Physics, Chinese Academy of Sciences, Hefei, China ¹Southwestern Institute of Physics, Chengdu, Sichuan, China

Corresponding Author: L. Nie, nielin@swip.ac.cn

Nie

It is widely accepted that the transient heat flux carried by edge localized mode-filaments (ELMfilaments) can dramatically erode divertor materials, increase impurities and recycling. Thus, it is an extremely challenge to decompose heat flux originating from core plasma. In this paper, the statistical characteristics of ELM-filament within mitigation by the Supersonic Molecular Beam Injection (SMBI) and Pellet Injection (PI) have been studied. In these experiments, we use four-tip probe to measure the temporal evolution of floating potential, electron temperature, and density. The injection depths are about 1-2 cm and 15-18 cm inside LCFS by the SMBI and the PI, respectively. It is found that ELM amplitude reduces and its frequency increases after SMBI/PI. We extract ELM filament structure on the basis of threshold $\delta n_e/\sigma$, where σ is the standard deviation of δn_e . In both mitigations, larger amplitude filament burst rate decrease significantly, implies that the larger amplitude filaments are suppressed. The divertor ion-electron collisionality, and the long-range correlation are also calculated, respectively. In both ELM-mitigations, we observe that the ion-electron collisionality increases after SMBI/PI, while the long-range correlation decreases significantly. This phenomenon is in good agreement with the theory prediction that collisionality affects the parallel correlation. The particle and heat fluxes are estimated, respectively. Taking the heat fluxes for example, it is found that the transient heat fluxes decrease 50%-60% after SMBI and 40%-50% after PI. This is a direct evidence for the transient heat flux suppression. The average heat flux decreases from 1.2 kW/m^2 to 0.4 kW/m^2 after SMBI, meanwhile the thermal radiation increase, implies that there is another energy loss channel by thermal radiation, in addition to the energy loss carried by filaments. But after PI, the thermal radiation does not increase, the average heat flux only change from 1.2 kW/m² to 1.1 kW/m², almost retaining.



EX/P7-23

The Role of Edge Plasma Instabilities in Dynamical Evolution of Pedestal in the HL-2A Tokamak

W. Zhong¹, X. Zou², Z. Shi¹, X. Duan¹, Y. Xu¹, M. Xu¹, W. Chen¹, M. Jiang¹, Z. Liu¹, J. Cheng¹, X. Ji¹, Y. Zhou¹, D. Yu¹, J. Li¹, L. Yu¹, Y. Xu¹, J. Gao¹, J. Dong¹, X. Ding¹, Y. Liu¹, L. Yan¹, Q. Yang¹, and Y. Liu¹

¹Southwestern Institute of Physics, Chengdu, Sichuan, China ²CEA-IRFM, Saint Paul lez Durance, France

Corresponding Author: W. Zhong, zhongwl@swip.ac.cn

Pedestal behaviors play a key role in determining the global energy confinement of tokamak plasmas, and fusion reaction efficiency of burning plasmas. It is essential to understand the mechanism of the pedestal formation and evolution for optimizing plasma performance and improving accuracy of predictive models. Thus it is important experimentally to track the swift evolution of the pedestal parameters and underlying instabilities in the narrow and steep gradient region. In HL-2A, the characteristics of the edge plasma instabilities and their effects on the dynamical evolution of pedestal have been investigated. Firstly, quasi-coherent modes have been observed in density fluctuations. The dominant mode with frequencies in the range of (50–100) kHz appears during the ELM-free period prior to the first ELM. By analyzing the pedestal density gradient, we found that there is a threshold for the excitation of the mode. This mode can also be observed during inter-ELMs. Experimental results show that the modes are excited after the ELM crash and terminated before the onset of the next ELM. The radial wave-number of the mode is estimated from the data measured by two radially separated reflectometers. The wave-number spectrum shows that the mode is radially propagating inward. The toroidal mode number of the edge mode is n = 7 deduced from Mirnov signals. The corresponding poloidal mode number is about m = 21 according to the local safety factor. A statistic method is applied to evaluate the relationship between the amplitude of the pedestal mode and the pedestal electron density gradient during ELM cycle. The result indicates that the modes are excited at about 40% of normalized interval before the ELM onset. During and after the ELM event, the modes disappear. It seems that the presence of the modes is linked to a relatively larger density gradient. In addition, the results made by a gyrokinetic simulation show that a Kinetic Peeling Ballooning Mode (KPBM) is localized in pedestal region, which has similar features to our observation. Thus, the edge mode in HL-2A is very likely a KPBM mode, and which may play a significant role in determining the dynamics of a pedestal.



Measurements of Fast-Ion Losses Induced by MHD Instabilities Using Scintillator-Based Probe in the HL-2A Tokamak

Y. Zhang¹, Y. Liu¹, M. Isobe², X. Luo³, W. Chen¹, X. Ding¹, G. Yuan¹, J. Yang¹, X. Song¹, X. Li¹, Q. Yang¹, and X. Duan¹

¹Southwestern Institute of Physics, Chengdu, Sichuan, China ²National Institute for Fusion Science, Toki, Japan ³Sichuan University, Sichuan, China

Corresponding Author: Y. Zhang, zhangyp@swip.ac.cn

Understanding and controlling the confinement of fast ion populations is increasing in importance as we approach self-ignited devices. MHD instabilities in magnetically confined plasmas can often be driven by a population of fast ions. In contrast, these instabilities can often lead to the anomalous loss of fast ions. Therefore, numerous efforts have been dedicated to studying the fast ion transport and the interplay of fast ions and MHD modes.

In the 2013 HL-2A experimental campaign, the loss of neutral beam ions induced by MHD instabilities has been measured with a new scintillator-based lost fast-ion probe (SLIP). A single luminous spot appears on the scintillator plate when NBI source turn-on. The spot is consistent with loss at a single energy and pitch angle and it is interpreted as the prompt loss of beam ions. The position and size of this spot is steady during the whole NBI heating. Another luminous spot can be seen on the scintillator plate during TM. Moreover, the spot becomes brighter with the TM becomes stronger. Along with the disappearance of the TM, the spot dims and then vanishes. The position of the second spot in the scintillator plate is located in the region with lower energy and lower pitch angle, in contrast to the first spot. The energy and pitch angle of the lost fast ions induced by TM are 30 keV and 60°, respectively. The time evolution of the images of fast-ion losses due to long-lived mode (LLM) and sawtooth was also measured during a discharge. The energy and pitch angle of the lost fast ions induced by LLM are 25 keV and 67°, respectively. Compared to the spots due to TM and LLM, the spot induced by sawtooth has a broad range of energies and pitch angles. The energy of the sawtooth-induced lost fast-ions ranges from 25 keV to 35 keV, and the pitch angle ranges from 65° to 75°. The brightness of the luminous spot due to LLM is significantly weaker than the brightness of the spot due to sawtooth, which imply that the deteriorated effect of sawtooth on the confinement of fast ions is obviously stronger than the effect of LLM. There may be some interactions between MHD modes and fast ions, which causing the fast ion losses with the wide range of energy and pitch angle.



Yu

Transition and Interaction of Low-Frequency MHD Modes during Neutral Beam Injection on HL-2A

L. Yu¹, W. Chen¹, X. Ding¹, X. Ji¹, Z. Shi¹, J. Li¹, Y. Zhou¹, Y. Li¹, W. Li¹, B. Feng¹, Y. Huang¹, X. Song¹, J. Cao¹, J. Rao¹, J. Dong¹, Y. Liu¹, L. Yan¹, Q. Yang¹, and X. Duan¹

¹Southwestern Institute of Physics, Chengdu, Sichuan, China

Corresponding Author: L. Yu, yulm@swip.ac.cn

Fishbone instability not only can lead to loss of energetic particles, but also can trigger other low-frequency MHD modes, such as tearing mode/neoclassical tearing mode (TM/NTM) and the long-lived mode (LLM), then to effect the confinement of the fusion plasma. Meanwhile, the TM/NTM is a very important MHD mode, which can cause serious confinement degeneration and will be the principal limit on performance in large tokamaks, like ITER. It is also found that the LLM can lead to confinement degradation and flatten the toroidal rotation. The obvious reduction of plasma stored energy can be observed usually in the presence of such perturbation. It has been found that fishbone instabilities as seed magnetic island can trigger the 2/1 and 3/2 NTMs on ASDEX-U and NSTX. Recently, simulations according to the discharge parameters and equilibrium on NSTX and MAST have been done, and the results are in agreement with experiment phenomena. The low-frequency MHD modes, such as fishbone, LLM and TM/NTM modes had been identified on HL-2A. In this paper we will present the new experimental results about transition and nonlinear interaction of these low-frequency MHD modes.

The transition from fishbone to LLM has been observed, and the fishbone triggering TMs has been presented during NBI on HL-2A. It is found that the LLM localizes at r = 4.5 cm, but the two TMs occur at r = 16.3 cm and r = 21.5 cm. The frequencies of fishbone and its harmonic decrease from $f \sim 30-10$ kHz and $f \sim 60-20$ kHz, respectively, during t = 655.5-657.5 ms. And the two TMs, with initial frequencies about $f \sim 10$ and $f \sim 20$ kHz, follow fishbone and its harmonic at $t \approx 657.5$ ms. And the two TM frequencies drop from $f \sim 10-1.5$ kHz and $f \sim 20-3$ kHz, respectively, during t = 657.5-660 ms. At last, the two TM frequencies keep as $f \sim 5$ kHz and $f \sim 10$ kHz. Note that the mode numbers of two TMs are m/n = 2/1 and 3/2, respectively.

The nonlinear couplings of LLM and TMs are observed by the multi-channel ECE signals. It is observed that the 1/1 LLM and 2/1 TM provide the same frequencies, with $f \sim 5$ kHz, but they localize at different radial position during t = 661.0-667.0 ms. And the matching conditions are satisfied between two TMs and LLM, i.e., $f_{TM1} + f_{LLM} = f_{TM2}$ and $n_{TM1} + n_{LLM} = n_{TM2}$, indicating that one of the TMs may be induced by the coupling between the other two modes through the wave–wave nonlinear interaction.

330

Study of Carbon Transport in the Scrape-off Layer of HL-2A with Impurity Sources Located at Limiter, Baffle and Divertor

Z. Cui¹, S. Morita², M. Kobayashi², X. Ding¹, X. Ji¹, J. Cheng¹, P. Sun¹, C. Dong¹, H. Zhou¹, W. Hong¹, Z. Shi¹, Y. Li¹, B. Fu¹, P. Lu¹, L. Yan¹, Q. Yang¹, Y. Xu¹, and X. Duan¹

¹Southwestern Institute of Physics, Chengdu, Sichuan, China ²National Institute for Fusion Science, Toki, Japan

Corresponding Author: Z. Cui, cuizy@swip.ac.cn

Impurity transport in the scrape-off layer (SOL) has been studied for the ohmic heating plasma based on a space-resolved vacuum ultraviolet spectroscopy of which the intensity is absolutely calibrated with bremsstrahlung continuum in the HL-2A divertor tokamak. The radial profiles of carbon emissions of CIII (977 Å: 2s2 1S0-2s2p 1P1) and CIV (1548 Å: 2s 2S-2p 2P) as well as the ratio of CIV to CIII are used to investigate the edge impurity transport with relation to the source locations and the sputtering characteristics. The experimental results show that impurity profiles in the SOL have been clearly changed against different source locations: the profiles of CIV and CIII become flat for the dominant divertor source, but they become peaked for the dominant baffle source. Furthermore, in low electron density condition ($n_e < 2.6 \times 10^{13}$ cm⁻³) the normalized intensities of CIV and CIII by the line-averaged electron density, CIV/n_e and CIII/n_e , decrease with the increase of density. The ratios of CIV to CIII increase with n_e . On the other hand, in the moderate density conditions $(n_e > 2.6 \times 10^{13} \text{ cm}^{-3})$ the values of CIV/ n_e and CIII/ n_e become saturated. The ratios of CIV to CIII gradually decrease with density. The observations have been analyzed with the EMC3-EIRENE simulation code. The calculated profiles are fairly in a good agreement with the observations, i.e., peaked profile for the baffle source and flat profile for the divertor source. The reason why the impurity profile is sensitive to the configuration is due to the screening efficiency depending on the source location. An enhanced physical sputtering is also suggested by the simulations to explain the observations on the electron density dependence of the carbon ions transport in the SOL region.

Paper

Characterization and Nonlinear Interaction of Shear Alfvén Waves in the Presence of Strong Tearing Modes in Tokamak Plasmas

W. Chen¹, Z. Qiu², X. Ding¹, L. Yu¹, H. S. Xie², X. Ji¹, J. Li¹, Y. G. Li¹, W. Zhong¹, Y. Zhang¹, J. Cao¹, X. Song¹, S. Song¹, M. Xu¹, Q. Yang¹, Y. Liu¹, L. W. Yan¹, X. Duan¹, Z. Shi¹, and J. Dong¹

> ¹Southwestern Institute of Physics, Chengdu, Sichuan, China ²Zhejiang University, Zhejiang, China

Corresponding Author: W. Chen, chenw@swip.ac.cn

Shear Alfvén waves (SAWs) are very common in magnetized plasmas both in space and laboratory. In present-day fusion and future burning plasmas, SAWs are easily excited by fast particles and energetic alpha particles produced by nuclear fusion reactions. SAWs can cause the loss and redistribution of energetic particles which can affect plasma performance or damage the plasma wall. The physics of SAWs is an intriguing but complex area of research. Meanwhile, it is important of studying axi-symmetry mode and nonlinear mode coupling. The axi-symmetry mode such as zonal flows(ZFs) and geodesic acoustic mode (GAM) is associated with the plasma turbulence and confinement. The role of nonlinear mode coupling is generally important in determining the mode excitation, saturation or damping. The SAWs can interact nonlinearly, and lone wave packets can suffer decay instabilities including the parametric and modulational those, where the pump decays into a daughter SAW, ion acoustic wave or ZFs.

In the paper, we will report the excitation and generation of the AEs and two kind axi-symmetry magnetic activities in the presence of strong tearing modes (TMs) during NBI on HL-2A, and present that there exists the intense nonlinear interactions between AEs and low-frequency MHD modes, and develop a theory to explain this experimental phenomenon. Detailedly, in the presence of large magnetic island, the TAEs or BAEs are driven by the energetic-particles. The AEs then are modulated by the strong TMs, resulting in the subsequent generation of Alfvénic sidebands including the co-/counter-propagating AEs, and two kind axi-symmetry magnetic activities with n = 0 have been observed in the presence of strong tearing modes. One kind has been identified, and belongs to EGAM. The density fluctuations induced by EGAM are firstly measured by microwave Doppler reflectometers. Another kind is found for the first time, its frequency IB is in the range of TAE frequency. The Fourier bicoherence analysis suggests these axi-symmetry modes are generated by the nonlinear mode coupling via the decay process between AEs and low-frequency MHD modes. The experimental results indicate that the nonlinear mode coupling is one of mechanisms of the energy cascade in energetic-particle turbulence or Alfvén turbulence.



Experimental Study of Disruption Mitigation Using Supersonic Molecular Beam and Massive Gas Injection on HL-2A and J-TEXT

Y. B. Dong¹, Y. Zhang¹, Z. Chen², L. Zeng³, C. Chen¹, H. Zhuang³, J. Gao¹, Y. Luo², Y. Liu¹, Y. Xu¹, and G. Zhuang²

¹Southwestern Institute of Physics, Chengdu, Sichuan, China
²Huazhong University of Science and Technology, Hubei, China
³Max-Planck-Institut für Plasmaphysik, Garching, Germany

Corresponding Author: Y. B. Dong, caroldyb@swip.ac.cn

In tokamak experiments, including JET, JT-60U, Tore Supra, and TEXTOR, it has been shown that the runaway electron (RE) generation occurs usually above a threshold at $B_t \approx 2$ T independent on machine size. Recently, disruption mitigation experiments with SMBI and MGI have been carried out in the HL-2A and J-TEXT tokamaks to study various injection scenarios and gas jet penetration. The improved SMBI system has been developed at HL-2A with a larger orifice (0.5 mm of diameter), a quite shorter opening time (0.2 ms), and its maximum throughput is up to 1.0×10^{21} (10 ms, 50 bar). The SMBI was triggered by a negative voltage spike in the loop voltage signal prior to the thermal quench. In the SMBI mitigation experiments at HL-2A, the RE plateau is achieved even at $B_t = 1.3$ T, much lower than the B_t threshold observed in other tokamaks. Both Ne and Ar gases could create runaway electron at $B_t = 1.3$ T. In addition, a fast massive gas injection valve has been constructed and tested on the J-TEXT tokamak, whose shortest opening time is about 0.25 ms and maximum gas capacity is 1.0×10^{24} . In J-TEXT disruption mitigation experiments, after injecting Ar to induce disruption, both B_t threshold and electron density threshold of the RE plateau generation are observed in J-TEXT. The threshold of B_t is 1.2 T, similar to that found in HL-2A. The RE plateau is easier to obtain at lower electron densities. This might be understood by hot tail RE generation.



Dynamics of High-Intermediate-High Confinement Transitions on the HL-2A Tokamak

J. Cheng¹, J. Dong¹, L. Yan¹, K. Itoh², Z. Huang¹, K. Zhao¹, W. Hong¹, L. Yao¹, C. Chen¹, B. Feng¹, L. Nie¹, S. Itoh³, D. Yu¹, X. Ji¹, W. Zhong¹, X. Song¹, Q. Yang¹, X. Ding¹, Y. Xu¹, X. Zou⁴, X. Duan¹, and Y. Liu¹

¹Southwestern Institute of Physics, Chengdu, Sichuan, China
 ²National Institute for Fusion Science, Toki, Japan
 ³Institute for Applied Mechanics, Kyushu University, Kasuga, Japan
 ⁴CEA-IRFM, Saint Paul lez Durance, France

Corresponding Author: J. Cheng, chengj@swip.ac.cn

It is essential to understand L-H transition mechanisms to provide a predictable power threshold for a successful operation in fusion reactors. Early theoretical and experimental studies have shown that plasma may pass an intermediate phase (I-phase) when the heating power gradually increases, approaching the H-mode power threshold. This extended time scale provides opportunity to study the L-H transition mechanism. Recently, this phenomenon accompanying with limit cycle oscillations was studied using a Langmiur probe array on the HL-2A in detail. Here, we report extended observations of dynamics in high-intermediate-high (H-I-H) confinement transitions on this device. The H-I transition was stimulated by the supersonic molecular beam injection (SMBI) with gas pressure ~ 2.5 MPa and pulse width ~ 2.0 ms. The Lissajous diagram between the normalized radial electric field X = $e\rho_{\theta}|E_{r}|/T_{e}$ and the envelope of density fluctuations in the I-phase shows that all cycles rotate in the counterclockwise (CCW) direction, which means that the increase of the turbulence causes the reduction of radial electric field while the increase of the radial electric field induces decrease of turbulence. It seems that once the system enters such CCW LCO state the plasma may be able to enter a positive feedback loop which triggers the I-H transition. Another interesting finding is a coherent mode with 11.7 kHz appearing just prior to the I-H transition (lasting about 1.0 ms). The mode numbers of the magnetic fluctuations are identified to be m/n = 3/1. It was found that the amplitude of magnetic fluctuations rapidly increases while that of LCOs significantly reduces. This contrast indicates that there is a possible interaction between the coherent mode and the turbulence, which is also favorable for the I-H transition. Detailed results will be presented.

Preprint

The Observation of Pedestal Turbulence Contributing Inward Particle and Heat Flux on the Edge of HL-2A Tokamak

D. Kong¹, A. Liu², T. Lan², H. Shen², L. Yan³, J. Cheng³, M. Xu³, J. Dong³, W. Hong³, S. Zhang⁴, T. Zhang⁴, X. Gao¹, W. Ding⁵, X. Sun², J. Xie², H. Li², W. Liu², and C. Yu²

¹Institute of Plasma Physics, Chinese Academy of Sciences, Hefei, China
 ²University of Science and Technology, Anhui, China
 ³Southwestern Institute of Physics, Chengdu, Sichuan, China
 ⁴Max-Planck-Institut für Plasmaphysik, Garching, Germany
 ⁵University of California Los Angeles, CA, USA

Corresponding Author: D. Kong, dfkong@ipp.ac.cn

The theoretical and experimental results indicate that the total confinement of the core plasma in a fusion device relies on the structure of pedestal on the edge, and the pedestal turbulence plays an essential role on the pedestal structure. The pedestal turbulence have been studied by using the Langmuir probe arrays on the edge of HL-2A tokamak. The probe arrays were performed about 1 cm inside the separatrix with the NBI heating power of 0.7 MW and ECRH power of 1 MW, some kind of low frequency (20–80 kHz) pedestal turbulence (shorted for LFT) with large amplitude has been observed during the construction and recovery of pedestal on HL-2A. The LFT begins to excite with the increasing of local electron density and temperature. Amplitude of LFT is large, about ~ 250 V in the potential field, while the corresponding magnetic fluctuations of LFT is weak. The abnormal particle and heat flux contributed by LFT have also been measured by four-tip probe. The result shows that the LFT contributed inward particle and total heat flux during the construction and recover of the pedestal on HL-2A. Those results may indicate a physical mechanism of the construction of the pedestal after the L-H mode transition, as well as the recovery of pedestal between ELMs.



Plasma Confinement by Magnetic Field with Convex-Concave Field Lines

G. Krashevskaya¹, M. Tsventoukh²

¹National Research Nuclear University MEPhI, Moscow, Russian Federation ²P. N. Lebedev Physical Institute, RAS, Moscow, Russian Federation

Corresponding Author: G. Krashevskaya, krashevskaya-gv@mail.ru

It has been found that the plasma confinement by magnetic field of alternating-sign curvature — with convex-concave field lines — results in a strong stabilizing action against convective (flute-interchange) perturbations [1]. For simple combinations of mirrors and cups the calculations give a strongly, centrally peaked stable plasma pressure profiles instead of a shallow ones [1, 2]. The pressure peaking arises at the minimum of the second adiabatic invariant J that takes place at the 'middle' of a tandem mirror–cusp transverse cross-section. The peaking arises for various plasma anisotropy, e.g., for the distribution function with 'empty loss cones', as well for the opposite case, that with a longitudinal velocity prevailing. The magnetic configurations with peaking include, e.g., axially symmetric mirrors equipped with outer divertors and inner field reversing rings (cusps, internal rings, high- β cells) and closed multimirror traps. Such a methodic gives a promising tool for the magnetic confinement systems optimization. It can be applied in various fusion applications, like fusion-fission hybrid systems, as well as for intense plasma and particle sources, like multiply-charged ion sources.

The question is whether the required conditions for the experimental obtaining of the pressure peaking are limited by large enough alternating-sign magnetic field line curvature and low plasma-collisionality. This has been addressed to a compact magnetic confinement system with reverse-dipole configuration and ECR-discharge at low pressure [3].

This device has been modified by adding of external magnetic field to create the field lines of alternating-sign curvature. The electrostatic and magnetic probe techniques have been improved to investigate the plasma parameters spatial distribution and to find out whether the peaking can be experimentally observed in such a conditions.

References

[1] M.M. Tsventoukh 2014 Nucl. Fusion 54 022004.

[2] M.M. Tsventoukh 2011 Nucl. Fusion 51 112002.

[3] G.V. Krashevskaya et al., 2012 Proc. VIII Int. Workshop MICROWAVE DISCHARGES:

FUNDAMENTALS AND APPLICATIONS, Zvenigorod, Sept. 10–14, 2012. Ed. Yu.A. Lebedev. Moscow 2012, pp 101–104.



Calculation of Magnetic Field Perturbation Using Saddle Coils and Helical Windings Based on IR-T1 Tokamak

P. Khorshid¹, M. Broumand², Y. Adltalab¹, E. Abizimoghadam¹, and M. Ghoranneviss²

¹Dept. of Physics, Islamic Azad University, Mashhad, Iran, Islamic Republic of

²Plasma Physics Research Center, Islamic Azad University, Tehran, Iran, Islamic Republic of Corresponding Author: P. Khorshid, pkhorshid@gmail.com

The effect of externally applied resonant helical magnetic fields (RHFs) and a set of saddle coils on plasma column were calculated. The magnetic field of saddle coils compared with magnetic field of the helical winding coil on IR-T1 tokamak in a simulation method. The equation of helical windings that they mounted on vacuum chamber in a spiral modes (L = 2, n = 1) and (L = 3, n = 1), where L represents the number of toroidal rounds, and n represents the direction of the poloidal round, using Green function has been calculated. The coordinate system defined on a torus and an electric current applied to create a magnetic field and the magnetic field of resonant helical magnetic field disorders of the confinement were calculated in the whole space. The results shown that the magnetic resonance field in the absence of plasma flow on the direction of the magnetic field confining the plasma column is performed, it was observed that the resultant structure for L = 2 is symmetric in 180 degrees but in the L = 3 is less symmetric. Also, it was observed that the intensity of perturbed magnetic field in the edge of plasma column for L = 3 is higher, so that it could conclude that RHF application may effect mostly on edge magnetohydrodynamics behavior. The shape and structure of the Saddle coils has been defined toroidally and then poloidally configuration. The resulting simulation code is used to predict the position and structure of saddle coil that has same magnetic field generation with respect to helical winding.



EX/P7-36

Edge Plasma Dynamics during L-H Transition in the JFT-2M Tokamak

T. Kobayashi¹, K. Itoh², T. Ido², K. Kamiya³, S. Itoh⁴, Y. Miura³, Y. Nagashima¹, A. Fujisawa¹, S. Inagaki¹, K. Ida², and K. Hoshino³

¹ Kyushu University, Kasuga, Japan
 ²National Institute for Fusion Science, Toki, Japan
 ³Japan Atomic Energy Agency, Naka, Japan
 ⁴Institute for Applied Mechanics, Kyushu University, Kasuga, Japan

Corresponding Author: T. Kobayashi, kobayashi@riam.kyushu-u.ac.jp

This is the first report of the spatiotemporal dynamics of edge plasma during L-H transition, which is based on the direct measurement of radial electric field, density gradient and turbulence intensity in the JFT-2M tokamak. The observations with fine spatial- and time- resolutions provide quantitatively clear views of the L-H transition, which enable us to discuss detailed physical mechanism, as follows: i) At the L-H transition, an abrupt increase [time scale of $O(100 \ \mu s)$] of strong mean radial electric field (which is localized in radius with FWHM~ 7 mm) leads the increase of density gradient and reduction of turbulence intensity. Reynolds stress force remains too small to drive the abrupt increase of the radial electric field. ii) Rapid inward propagation of the turbulence suppression that makes front is observed at the transition. This might be linked to the fast core-edge coupling seen in global improvement of confinement after the H-mode transition.



Plasma Flows and Fluctuations with Resonant Magnetic Perturbations on the Edge Plasmas of the J-TEXT Tokamak

K. Zhao¹, Y. Shi², S. Hahn², P. H. Diamond², Y. Sun¹, H. Liu¹, Z. Chen¹, Y. Ding¹, Z. Chen¹, J. Cheng³, L. Nie³, M. Leconte², J. Bark², Z. Cheng¹, L. Gao¹, X. Zhang¹, Z. Yang¹, N. Wang¹, L. Wang¹, L. Yan³, J. Dong³, and G. Zhuang¹

> ¹*Huazhong University of Science and Technology, Hubei, China* ²*National Fusion Research Institute, Daejeon, Korea, Republic of* ³*Southwestern Institute of Physics, Chengdu, Sichuan, China*

Corresponding Author: K. Zhao, kjzhao@swip.ac.cn

Plasma flows and fluctuations are studied with resonant magnetic perturbations (RMPs) using Langmuir probe arrays on the edge plasmas of the J-TEXT tokamak. The toroidal velocity near the last closed flux surface (LCFS) tends to increase at first with increasing RMP current. When the RMP current reaches 6 kA, the toroidal velocities increase (inside the LCFS) and decease (outside the LCFS). The effects of RMPs on toroidal rotations suggest that the intrinsic rotation is driven with RMPs. The absolute amplitude of the radial electric field E_r near the LCFS also increases at first with RMP, then significantly decreases at 6 kA. A narrow zone (NZ) is detected in the edge plasmas. In the NZ, the E_r sign is changed from negative to positive, and the electron temperature, and turbulence and zonal flow intensity all drop. Significantly, the profile of poloidal and toroidal turbulent stresses is also changed in the NZ. The occurrence of the NZ results in the formation of a new shear layer in the edge plasma. The results suggest that the NZ formation occurs due to the magnetic island overlap near the rational flux surface of q = 3, due to 3/1 RMP coils. The measurements of turbulent stresses and E_r are consistent with that the intrinsic rotation can be driven with RMPs. Both Low frequency zonal flows (LFZFs) and geodesic acoustic modes (GAMs) are damped by strong RMPs.

Observation of Intermittent Plasma Ejection from a Highly Overdense Spherical Tokamak Plasma Maintained by Electron Bernstein Wave Heating and Current Drive in LATE

H. Tanaka¹, M. Uchida¹, T. Maekawa¹, K. Kuroda¹, C. Ikeda¹, T. Shigemura¹, K. Nagao¹, and M. Wada¹

¹Kyoto University, Kyoto, Japan

Corresponding Author: H. Tanaka, h-tanaka@energy.kyoto-u.ac.jp

Non-inductive start-up of spherical tokamak (ST) is an important issue to realize compact and economical fusion reactors. In the Low Aspect ratio Torus Experiment (LATE) device, non-inductive start-up and formation of ST by electron Bernstein (EB) waves in a highly overdense regime has been explored. By injection of a 2.45 GHz microwave power of ~60 kW, the plasma current I_p is ramped up to ~12 kA and the electron density increases up to ~t7 times the plasma cutoff density. Such a highly overdense ST plasma is produced by improved polarization adjustment for EB mode-conversion in the first propagation band. However, when I_p exceeds ~10 kA, I_p and the density become saturated. Intermittent plasma ejections across the last closed flux surface (LCFS) have been observed for the first time. Repetition of large ejection events causes saturation and gradual decrease of density and plasma current.



Investigation of Co-Current Rotation at Plasma Edge in the TCABR

J. H. Severo¹, G. Ronchi¹, R. M. O. Galvao¹, I. C. Nascimento¹, Z. O. Guimaraes-Filho¹, Y. K. Kuznetsov¹, M. F. Nave², F. do Nascimento¹, and M. Tendler³

¹Plasma Physics Laboratory, Institute of Physics, University of São Paulo, Brazil
²Institute of Plasmas and Nuclear Fusion, Association EURATOM/IST, Lisbon, Portugal
³KTH Royal Institute of Technology, Stockholm, Sweden

Corresponding Author: J. H. Severo, jhsevero@if.usp.br

Poloidal and toroidal plasma rotation play an important role on particle and energy confinement and on the stabilization of magnetohydrodynamic instabilities, depending on the rotation intensity. In the TCABR tokamak, the intrinsic toroidal rotation in ohmic discharges is normally sheared, with counter-current in the core and co-current rotation at plasma edge. The origin of co-current rotation may be related to a radial friction force between neutral particles and ions/electrons during gas injection. This radial force in the presence of a poloidal component of the magnetic field accelerates plasma in the toroidal direction. If the speed of neutral particles is much larger than the diffusion velocity of ions and electrons, the friction force is in radial direction (outward), which produces co-current rotation.

In turbulent plasmas, electrons and ions can diffuse in radial direction with equal velocity due the ambipolar diffusion. In the TCABR tokamak the velocity of neutral particles is of order of 10^3 m/s, while the ions and electrons diffusion velocity is about 10 m/s, which produces an outward radial friction force. We suspect that in small machines, where the electron temperature at plasma edge is of order of 10 eV, neutral gas can penetrate into the plasma column for a short time before being ionized. These neutral particles will produce co-rotation. A rough estimate for ionization time at the plasma edge in TCABR is 0.1 ms, for electron temperature and density around 10 eV and 10^{18} m⁻³, respectively. For this characteristic ionization time, a neutral particle can penetrate 10 cm inside the plasma.

To investigate this mechanism, we are carrying out an experimental program for measuring the toroidal rotation at plasma edge for different poloidal positions of gas injection, i.e., top, outboard, and inboard, at the same poloidal cross-section and always in the radial direction. We have observed increase of co-current rotation at radial position r/a = 0.94 during gas injection at all poloidal positions.

The next phase of the experimental campaign will focus on gas injection in the toroidal and poloidal directions. In the paper we will present a comprehensive report on the experimental results and will discuss a model to describe the correlation of intrinsic co-current rotation at plasma edge with the position of gas injection.



EX/P7-45

Features of Regular Discharges in Uragan-3M Torsatron

V. Moiseenko¹, A. Lozin¹, M. Kozulya¹, A. Shapoval¹, V. Bondarenko¹, R. Pavlichenko¹, Y. Mironov¹, V. Konovalov¹, A. Kulaga¹, V. Romanov¹, N. Zamanov¹, V. Voitsenya¹, and I. Garkusha¹

¹Institute of Plasma Physics of NSC KIPT, Kharkiv, Ukraine

Corresponding Author: V. Moiseenko, moiseenk@mail.ru

The Uragan-3M device is equipped with two antennas which are fed by RF power with the frequency below ion cyclotron. The frame antenna was used for pre-ionization and the three-half turn (THT) antenna makes plasma heating. In this experimental series, the radial profiles of CV and H_{α} line intensity and the second cyclotron harmonic emission are measured using a pulse-by-pulse technique. The results of these measurements and Biot-Savart calculations could be explained by existence of a small central area with relatively good plasma confinement surrounded by a zone where the confinement is poor. If so, the relatively low average electron temperature and high RF power needed to sustain plasma are the consequences.





Investigation of Toroidal Rotation Reversal in KSTAR Ohmic Plasmas

D. Na¹, Y.-S. Na¹, S.-M. Yang¹, H.-S. Kim¹, T. S. Hahm¹, H. Jhang², S. G. Lee², W.-H. Ko², R. McDermott³, C. Angioni³, and W. Lee⁴

¹Seoul National University, Seoul, Korea, Republic of
 ²National Fusion Research Institute, Daejeon, Korea, Republic of
 ³Max-Planck-Institut für Plasmaphysik, Garching, Germany
 ⁴University of California San Diego, CA, USA

Corresponding Author: D. Na, mania0020@snu.ac.kr

A reversal of the intrinsic toroidal rotation at the core region has been observed in Ohmic plasmas of various tokamaks as confinement characteristics changes from the low density linear Ohmic confinement (LOC) regime to the saturated Ohmic confinement (SOC) regime. On the other hand, dedicated experiments on KSTAR in search of this phenomenon have not exhibited any toroidal rotation reversal to date, while similar behaviours in the core toroidal rotation dependency on density have been observed across the confinement regime transition from LOC to SOC. We characterise common features of results from KSTAR by recognising that the toroidal rotation at normalised radius around 0.6, so-called the anchor point, acts as an effective boundary value affecting the core rotation value. We found that the toroidal rotation at the anchor point plays an important role to the core rotation reversal which exhibits strong correlation with the plasma current. Momentum transport modelling considering diffusion, pinch, and residual stress reveals that the core toroidal rotation reversal, for KSTAR plasma conditions, could occur even without sign-flip of the residual stress appearing during the Ohmic confinement transition.

Disruption Threshold of Error-Field-Induced Locked Mode under n = 1 and n = 2 Mixed Non-Axisymmetric Fields

J. Kim¹, Y. In¹, J. Seol¹, G. Kim², G. Yun², J. Kim³, J. Bak¹, J. Yoo³, J. Park⁴, Y. Park⁵, and S. A. Sabbagh⁵

¹National Fusion Research Institute, Daejeon, Korea, Republic of ²Pohang University of Science and Technology (POSTECH), Korea, Republic of ³University of Science and Technology, Anhui, China ⁴Princeton Plasma Physics Laboratory, Princeton, NJ, USA ⁵Columbia University, New York, USA

Corresponding Author: J. Kim, jayhyunkim@nfri.re.kr

During 2013 KSTAR campaign, we conducted mixed non-axisymmetric (NA) field experiments to investigate the effect of overlap between differently aligned NA fields by the field error correction coils. Locking and error field (EF) penetration were induced by the torque imbalance between the intrinsic rotation and external magnetic braking. Further increase of the n = 1 EF resulted in minor disruption. As anticipated by the magnetic braking effect, the stronger n = 2 NA field case exhibited earlier EF penetration and locking. On the contrary to the locking phenomena, subsequent minor disruption was delayed and even avoided by the stronger n = 2 NA field. The delay or avoidance of minor disruption has a dependence on the pitch of the n = 2 NA field. Analysis of the locked mode amplitude revealed that the n = 2 NA field started to hinder the growth of n = 1 locked mode when the mode amplitude reached certain level. The starting level of the hindrance appears to rely on the n = 2 NA field strength. More interestingly, the fast growth was recovered just before minor disruption. It seems that there exists 2nd threshold of EF penetration related to the disruption phenomena like 1st threshold in the locking phenomena. Nevertheless, the pure n = 1 field case without n = 2 field did not show clear change of the growth rate after locking and just exhibited gradual increase of the locked mode towards the minor disruption.



Plasma Rotation Alteration by Non-Axisymmetric Magnetic Fields, Resistive MHD Stability Analysis, and High Normalized Beta Plasmas Exceeding the Ideal Stability Limit in KSTAR

Y.-S. Park¹, S. A. Sabbagh¹, W.-H. Ko², Y. Jeon², J. G. Bak², J. W. Berkery¹, J. Bialek¹, M. Choi³, S.-H. Hahn², J. Kim², J.-G. Kwak², S. G. Lee², Y.-K. Oh², H. K. Park⁴, S.-W. Yoon², K.-I. You², and G. Yun³

¹Columbia University, New York, USA
 ²National Fusion Research Institute, Daejeon, Korea, Republic of
 ³Pohang University of Science and Technology (POSTECH), Korea, Republic of
 ⁴Ulsan National Institute of Science and Technology, Korea, Republic of

Corresponding Author: Y.-S. Park, ypark@pppl.gov

H-mode plasma operation of KSTAR has been expanded to reach the ideal MHD no-wall β limit. The closest approach to this limit has achieved high normalized β , β_N , up to 2.8 while reducing plasma internal inductance, l_i , to near 0.7 exceeding the computed n = 1 ideal no-wall limit. The ratio of β_N/l_i , has reached 4 and the maximum plasma stored energy has exceeded 0.5 MJ. As a method to access the ITER-relevant low plasma rotation regime, non-resonant alteration of the rotation profile by non-axisymmetric magnetic fields has been demonstrated, enabling a study of the underlying neoclassical toroidal viscosity (NTV) physics. Non-axisymmetric field spectra were applied using invessel control coils (IVCCs) with varied n = 2 field spectra (by different combinations of upper/lower and middle IVCCs), electron cyclotron heating, and supersonic molecular beam injection to alter the plasma rotation profile in high- β H-mode plasmas and analyze their distinct effects on the rotation. The rotation profile was significantly altered with rotation reduced by more than 60% using the full range of techniques used as measured by several diagnostics without tearing activity or mode locking. To investigate the physical aspects of the measured rotation braking by NTV, changes in the steady-state rotation profiles are analytically examined by using the toroidal momentum balance equation in order to isolate the effect of the NTV. The NTV scaling with δB^2 shows good agreement with the measured profile change. The NTV coefficient scales as $T_i^{2.27}$, in general agreement with the low collisionality $(1/\nu)$ regime scaling of NTV theory. Determination of the classical tearing stability index, Δ' , is a crucial foundation for analysis at high- β . The 2/1 tearing stability in KSTAR is first quantified by using Δ' calculated from the PEST-3 code. The stability calculation is examined for a 2/1 mode residing at low β where pressure driven effects are expected to be small. The mode evolution is well described by the calculated Δ' . The robustness of the calculations is tested by varying the q_0 constraint which results in a modest change in Δ' , however, the systematic change in sign of Δ' remains consistent with the measured mode behavior. The stability calculations using the M3D-C1 code show qualitative agreement with Δ' from PEST-3.



EX/P8-6

Change of the Momentum Profiles Driven by the Sawtooth Crashes and its Effect on the LH Transition in KSTAR

W.-H. Ko¹, K. Lee¹, J. Lee¹, S. Yoon¹, G. Yun², J. Bak¹, H. Lee¹, K. Ida¹, Y. Jeon¹, Y. Oh¹, J. Kwak¹, P. H. Diamond³, and J. Kwon¹

> ¹National Fusion Research Institute, Daejeon, Korea, Republic of ²Pohang University of Science and Technology (POSTECH), Korea, Republic of ³University of California San Diego, CA, USA

Corresponding Author: W.-H. Ko, whko@nfri.re.kr

This paper describes the change of the rotation profiles driven by the sawtooth crashes and its effect on the LH trasition in KSTAR. After sawtooth crashes, the basic features of a slowly rising central electron temperature (T_e) followed by a rapid drop in temperature have been frequently observed on many tokamaks and the rise of the central toroidal rotation and ion temperature (T_i) have been measured in KSTAR tokamak. The fluctuation of the core T_i and rotation correlated with sawtooth in T_e profile from ECE in KSTAR.

The sawtooth oscillation in the T_e of both core and edge region was shown and electron temperature slightly increase independent of sawtooth growth because of transition in KSTAR. The neutral beam power was insufficient to suppress sawtooth and it can trigger an L-H transition at substantially lower threshold power than what is required without sawtooth. The sawtooth duration has been extended to double and it so called 'double sawtooth' and the double sawtooth is synchronized of LH transition on sawteeth cycle as shown in TCV. It is investigated for sawtooth to play an important role in an LH transition on KSTAR.

The heat and momentum fluxes are changed before and after the sawtooth crash during LH transition. The transition enables the observation of the heat and momentum fluxes changed because of the edge transport barrier. This indicates that it is important to consider the power flow to the edge plasma due to a sawtooth crash.

The sawtooth dynamics in detail was described comprehensively by 2D ECE imaging analysis during the sawtooth crash and LH transition. The sawtooth dynamics and its physics will be further investigated including the transition by assessing dependencies on q and core density profile from Thomson Scattering and fast particle population and new experimental results will be included here.

Preprint

Study of Type III ELMs in the KSTAR Tokamak

J. Seol², Y.-U. Nam², H. Lee², A. Aydemir², J. Kim¹, Y.-C. Ghim¹, S. G. Lee¹, B.-H. Park¹, and J.-G. Kwak¹

¹National Fusion Research Institute, Daejeon, Korea, Republic of ²University of Texas at Austin, Austin, TX, USA

Corresponding Author: J. Seol, jseol@nfri.re.kr

In this paper, we report the characteristics of Type III ELM in KSTAR mostly focusing on the Type III ELM regime after L-H transition. In the KSTAR tokamak, Type III ELMs are frequently observed after the transition from L-mode to H-mode. The repetition frequency of the Type III ELMs is 200–1000 Hz. As the edge plasma pressure increases, ELM-free regime occurs, which is followed by Type I ELM regime. Type III ELM regime at the L-H transition occurs regardless of the input powers. A magnetic precursor oscillation observed before the Type III ELM crash in the low field side midplane while ELM bursts are observed in all toroidal and poloidal Mirnov coils. In this study, we perform the MHD stability analysis of the plasma edge with considering the density perturbation.

EX/P8-8

Paper

Experimental Study of the Magnetic Braking Torque by Non-Axisymmetric Magnetic Perturbations in Different Plasma Collisionality Regimes on KSTAR

H. Lee¹, J. Seol¹, S. G. Lee¹, J. Yoo², L. Terzolo¹, J. Kim¹, H. Han¹, K. You¹, and J.-G. Kwak¹

¹National Fusion Research Institute, Daejeon, Korea, Republic of ²University of Science and Technology, Anhui, China

Corresponding Author: H. Lee, jdfm@nfri.re.kr

Although tokamaks confine plasmas with an axisymmetric toroidal magnetic field, there is always a slight non-axisymmetric magnetic perturbations (NAMPs) resulted from the misalignment of the toroidal magnetic field coils or ripple error fields due to the finite number of toroidal magnetic field coils. NAMPs can also appear due to MHD activities (internal kink modes, tearing modes, etc.) or external magnetic perturbations such as resonant magnetic fields (RMPs), which can be applied for either active control or suppression of the edge localized modes (ELMs) in H-mode plasmas. It is well known from several tokamak experiments that the application of NAMPs or MHD activities can significantly slow down the plasma rotation. Strong braking of the toroidal rotation by the externally applied n = 1 nonresonant magnetic perturbations has been frequently observed in the KSTAR tokamak. Recent experiments in the KSTAR tokamak have shown that n = 2 non-resonant magnetic perturbations can also damp the toroidal rotation. In this paper, a comprehensive investigation of the several experiments dedicated on the toroidal rotation braking by the external magnetic perturbations is carried out. The braking torque due to the magnetic perturbations are determined from the momentum transport equation with the measured toroidal rotation profiles by the charge exchange spectroscopy and X-ray imaging crystal spectroscopy diagnostics of high temporal resolution up to 10 ms. The neoclassical toroidal viscosity theory is considered to explain the magnetic braking of the toroidal rotation. The dependencies of the magnetic braking torque on the plasma collisionality and rotation are also discussed.

EX–P

Pedestal Characteristics during the Edge Localized Mode Mitigation by Super-Sonic Molecular Beam Injection on KSTAR

H. Lee¹, S.-H. Hahn², W.-H. Ko², J. Lee², S.-W. Yoon², H. Han², J.-W. Juhn³, H. Lee², S. H. Lee¹, J. Hong¹, J. Jang¹, J. S. Park¹, and W. Choe¹

¹Korea Advanced Institute of Science and Technology, Daejeon, Korea, Republic of ²National Fusion Research Institute, Daejeon, Korea, Republic of ³Seoul National University, Seoul, Korea, Republic of

Corresponding Author: H. Lee, leehy0816@kaist.ac.kr

This paper describes the pedestal characteristics during the Edge Localized Mode (ELM) mitigation by Super-sonic Molecular Beam Injection (SMBI) on KSTAR. After SMBI, whose pressure and duration time are 1 MPa and 8 ms, respectively, the reductions in both amplitude and time interval of D_{α} signals indicate the mitigation of type I-like ELM by SMBI. Despite the cold neutral gas injected by SMBI, the stored energy (W_p) did not change by the injection event. The fractional changes in electron density $(\delta n_e/n_e)$ and stored energy $(\delta W_p/W_p)$ by a single ELM burst and the change in H factor are small after SMBI. The ELM frequency ($f_{\rm ELM}$) was increased by a factor of 2–3 due to SMBI, on the other hand, the change in $f_{\rm ELM}$ owing to the increase in the line-averaged electron density is only 8–15%. The influence time, which is the time length of ELM mitigation, was about 300 ms.

During the mitigated ELM phase by SMBI, both pedestal electron density gradient (∇n_e^{ped}) and the pedestal electron temperature (T_e^{ped}) were reduced. As a result, the pedestal electron pressure (P_e^{ped}) and its gradient were decreased by about 50%. According to a diffusive, bi-stable cellular automata model, the key mechanism of ELM mitigation is that the controlled relaxation of the ∇P_e^{ped} changes large ELMs to small ELMs. This prediction is qualitatively consistent with the experimental result and it suggests that the modification of pedestal profiles by SMBI is closely related to the ELM mitigation.

Paper



In-Vessel Dust Velocity Correlated with the Toroidal Rotation of the Plasma

S.-H. Hong¹, K.-R. Kim², and W.-H. Ko¹

¹National Fusion Research Institute, Daejeon, Korea, Republic of ²University of Science and Technology, Anhui, China

Corresponding Author: S.-H. Hong, sukhhong@nfri.re.kr

We present the in-vessel dust velocity distribution and its correlation with toroidal rotation of plasma. Main diagnostic for the dust monitoring is visible CCD cameras and toroidal rotation of plasma is measured by charge exchange spectroscopy (CES). A total of 4129 dust trajectories (1237 in 2010 campaign, 1821 in 2011 campaign, 1071 in 2012 campaign) were analyzed. The dust velocity distributions in three campaigns are well described by lognormal distribution function, and they are in a broad range from 7 to 461 m/s with the peaks at 30 m/s (2010), 34 m/s (2011), and at 46 m/s (2012). This is related to the increase of NBI input power level, since most of KSTAR plasmas are NBI driven ones. As the NBI input power increases (Ohmic, L-, and H-mode), the peak velocity and the high velocity tail increase. It is found that the dust velocity is strongly correlated with normalized stored energy (ω/I_p), similar to the Rice scaling.

Preprint

L-H Transitions Triggered by SMBI: Experiment and Theory

S.-H. Hahn¹, P. Gohil², P. H. Diamond³, and J. Kwon¹

¹National Fusion Research Institute, Daejeon, Korea, Republic of ²General Atomics, San Diego, CA, USA ³University of California San Diego, CA, USA

Corresponding Author: S.-H. Hahn, hahn76@nfri.re.kr

Recent understanding of the L-H transition phenomena developed a possible explanation that a gas-induced density profile change can trigger a "Stimulated edge transport barrier (ETB)" state, which can be used to reduce the required power threshold relative to the known power threshold scalings for standard fueling.

Experimental investigations on these stimulated transitions were carried in KSTAR using an SMBI (supersonic molecular beam injection) system. Available edge profile measurements show that the SMBI drives a localized edge density increase, accompanied by strong edge cooling. The density gradient driven by SMBI is not as steep as what is seen in the H-mode, but formed gradient is sustainable because it can alter the edge required to enhance the particle confinement. Behavior induced by an SMBI strongly depends on the baseline density of the plasma at the moment of injection. The known density rollover, $n_{min} = 2.0 \times 10^{19}$ m⁻³ for KSTAR1, seems to play a role as an important parameter.

The non-trivial "stimulated ETB" occurs only on the higher branch of P_{thr} vs n_e in KSTAR. A reproducible gas-stimulated ETB state occurs for a certain amount of SMBI particles with 30–50% reductions in the total absorbed power ($P_{abs} = P_{inj} - dW/dt - P_{rad}$). These stimulated transitions are always limited in duration, but the transition state is sustained by repeated injections in the experiment.

A spatial-temporal evolution of the edge electron density/temperature is also obtained by KSTAR Thomson scattering during the SMBI-stimulated ETB period. During that period, it is observed that the edge density level decreases steadily, hence the corresponding electron pressure becomes lower. The electron temperature, however, does not change much after the stimulated ETB is achieved (t > 6.52 s).

A reduced model of the L \rightarrow H transition has been used to study injection-stimulated transitions. Results demonstrate: 1) shallow injection is optimal, and superior to strong puffing, 2) transient improved confinement states can be maintained by repetitive injection, 3) the principle means of accessing enhanced confinement is via stronger edge $E \times B$ shear, 4) in contrast to standard transitions, a burst of zonal flow growth does not lead stimulated transition events. Ongoing work is concerned with detailed comparison with experiment.



Helical Modes Induced by Localized Current Perturbations in Sawtoothing KSTAR Plasmas

G. Yun¹, G.-H. Choe¹, A. Bierwage², Y.-U. Nam¹, M. Choi¹, W. Lee¹, *H. K. Park*³, S. Yoon⁴, C. Domier⁵, and N. C. Luhmann, Jr.⁵

 ¹Pohang University of Science and Technology (POSTECH), Korea, Republic of ²Japan Atomic Energy Agency, Naka, Japan
 ³Ulsan National Institute of Science and Technology, Korea, Republic of ⁴National Fusion Research Institute, Daejeon, Korea, Republic of ⁵University of California Davis, CA, USA

Corresponding Author: G. Yun, gunsu@postech.ac.kr

A variety of helical structures such as dual or multiple flux tubes, distinct from the normal m = 1 internal kink, are commonly observed in sawtoothing plasmas in the KSTAR tokamak assisted by electron cyclotron heating (ECH). Detailed 2D and quasi-3D images have shown that the dual flux tubes have m/n = 1/1 helicity, co-rotate around the magnetic axis, and later merge into a single m = 1 mode prior to the crash. Similar evolution is observed for the cases of triple or more flux tubes, where the mode helicity is ambiguous. A strong correlation has been found between the ECH position and the mode structure. A reduced MHD simulation code with a heuristic current source model has been developed to understand this correlation.

Work supported by NRF Korea under grant no. NRF-2009-0082507 and U.S. DoE under contract No. DE-FG-02-99ER54531.



Measurement of Apparent Poloidal Rotation of Ion-Scale Turbulence with the KSTAR Microwave Imaging Reflectometer

W. Lee¹, J.-E. Leem¹, G. Yun¹, H. K. Park², Y.-C. Ghim³, Y.-U. Nam⁴, W.-H. Ko⁴, J. H. Jeong⁴, Y.-S. Bae⁴, Y.-S. Park⁵, C. W. Domier⁶, and N. C. Luhmann, Jr.⁶

 ¹Pohang University of Science and Technology (POSTECH), Korea, Republic of ²Ulsan National Institute of Science and Technology, Korea, Republic of ³Korea Advanced Institute of Science and Technology, Daejeon, Korea, Republic of ⁴National Fusion Research Institute, Daejeon, Korea, Republic of ⁵Columbia University, New York, USA ⁶University of California Davis, CA, USA

Corresponding Author: W. Lee, woochanglee@postech.ac.kr

Mean apparent poloidal rotations of ion-scale density fluctuations in the laboratory frame were observed with the microwave imaging reflectometer (MIR) system in KSTAR ohmic and neutral beam (NB) heated L-mode plasmas. The estimated apparent poloidal velocities are 1-2 km/s at $r/a \sim 0.5$ in the electron diamagnetic direction for ohmic plasmas, and 8–10 km/s at $r/a \sim 0.6$ and 5–6 km/s at $r/a \sim 0.7$ in the ion diamagnetic direction for NB heated L-mode plasmas. For NB heated L-mode plasmas, the apparent poloidal velocities often deviate from the poloidally projected toroidal velocities of carbon ions and the difference is 2–3 km/s. Possible sources of the measured difference are under investigation including difference in toroidal velocity between the carbon and main deuterium ions.



EX/P8-14

Toroidal Rotation and Momentum Transport Studies in KSTAR Plasmas

S. G. Lee¹, J. W. Yoo², J. Seol¹, H. Lee¹, L. Terzolo¹, Y. S. Kim¹, M. Bitter³, and K. Hill³

¹National Fusion Research Institute, Daejeon, Korea, Republic of ²University of Science & Technology, Daejeon, Korea, Republic of ³Princeton Plasma Physics Laboratory, Princeton, NJ, USA

Corresponding Author: S. G. Lee, sglee@nfri.re.kr

An investigation of toroidal rotation and momentum transport was carried out at KSTAR. The impurity toroidal rotation has been observed in the core region from the Doppler shift of helium-like argon X-ray line with various plasma discharges including a pure ohmic heating and neutral beam injection (NBI). In the ohmic plasmas, the direction and magnitude of the core rotation strongly depends on the initial plasma conditions during the plasma current ramp-up phase, and the measured ion thermal Mach number is proportional to the normalized plasma pressure. In the NBI heated plasmas, the core toroidal rotation is proportional to the ion temperature up to ~ 2.5 keV, and then it is saturated to ~ 250 km/s with the ion temperature up to 4 keV. This observation is under consideration with the NUBEAM simulations focusing on the effects of the beam energy and momentum transport. This paper will describe the experimental results of the toroidal rotation and momentum transport studies in the KSTAR device.



Accurate Estimation of Tearing Mode Stability Parameters in the KSTAR Using High-Resolution 2-D ECEI Diagnostic

H. K. Park¹, M. Choi², G. Yun², W. Lee², Y.-S. Park³, S. A. Sabbagh³, K. Gibson⁴, C. Bowman⁴, C. Domier⁵, N. C. Luhmann, Jr.⁵, B. Jun-Gyo⁶, and S. G. Lee⁶

¹Ulsan National Institute of Science and Technology, Korea, Republic of
 ²Pohang University of Science and Technology (POSTECH), Korea, Republic of
 ³Columbia University, New York, USA
 ⁴University of York, Heslington, UK
 ⁵University of California Davis, CA, USA
 ⁶National Fusion Research Institute, Daejeon, Korea, Republic of

Corresponding Author: H. K. Park, hyeonpark@unist.ac.kr

An accurate method to estimate the tearing mode stability parameters, i.e., the classical stability index (Δ') and the critical width for pressure flattening (w_c), has been developed based on electron cyclotron emission imaging (ECEI) diagnostic in the KSTAR. The measured ECE images of tearing modes are compared with synthetic images reconstructed from the tearing mode T_e model for the estimation. A good agreement between the measurement and model has been obtained, and an accuracy of the estimation result is improved with the 2D high-resolution ECE images contrast to the 1D data result. The observed tearing mode is found to be classically stable ($r_s \Delta' = -1.633 \pm 1.265$) but have a non-negligible neoclassical drive from the bootstrap current loss ($w_c/w \sim 0.2$).

Xu

Coupling between Intrinsic Rotation and Turbulence-Driven Residual Stress in the TEXTOR Tokamak

Y. Xu¹, C. Hidalgo², I. Shesterikov³, M. Berte³, P. Dumortier³, M. Van Schoor³, M. Vergote³, A. Krämer-Flecken⁴, and R. Koslowski⁵

¹Southwestern Institute of Physics, Chengdu, Sichuan, China
 ²The National Fusion Laboratory, CIEMAT, Madrid, Spain
 ³Laboratory for Plasma Physics, ERM/KMS, Brussels, Belgium
 ⁴Institute of Energy and Climate Research, Forschungszentrum Jülich, Jülich, Germany
 ⁵Forschungszentrum Jülich, Jülich, Germany

Corresponding Author: Y. Xu, xuyh@swip.ac.cn

Direct measurements of residual stress (force) have been executed at the edge of the TEXTOR tokamak using multi-tip Langmuir and Mach probes, together with counter-current NBI torque to balance the existing toroidal rotation. Substantial residual stress and force have been observed at the plasma boundary, confirming the existence of a finite residual stress as possible mechanisms to drive the intrinsic toroidal rotation. In low-density discharges, the residual stress displays a quasi-linear dependence on the local pressure gradient, consistent with theoretical predictions. At high-density shots the residual stress and torque are strongly suppressed. The results show close correlation between the residual stress and the $E_r \times B$ flow shear rate, suggesting a minimum threshold of the $E_r \times B$ flow shear required for the $k \parallel$ symmetry breaking. These findings provide the first experimental evidence of the role of $E_r \times B$ sheared flows in the development of residual stresses and intrinsic rotation.

Magnetic Confinement Theory and Modelling



Multi-Scale ITG/TEM/ETG Turbulence Simulations with Real Mass Ratio and β Value

S. Maeyama¹, Y. Idomura¹, M. Nakata¹, M. Yagi¹, and N. Miyato¹

¹Japan Atomic Energy Agency, Naka, Japan

Corresponding Author: S. Maeyama, maeyama.shinya@jaea.go.jp

Understanding electron heat transport is one of the critical issues in ITER. Although electron temperature gradient (ETG) driven turbulence has been regarded as a candidate of electron heat transport, recent multi-scale plasma turbulence simulations have reported that ion-scale instabilities such as ion temperature gradient modes (ITGs) and trapped electron modes (TEMs) dominate heat transport not only of ions but also of electrons. However, their simulations are limited to the reduced ion-to-electron mass ratios and electrostatic ($\beta = 0$) approximation, the following points are not yet clarified: (i) Are ETGs negligible even with the real mass ratio, where ion and electron scales are separated by a factor of the square root of the ion-to-electron mass ratio (m_i/m_2)^{1/2} ~ 43 if $T_i = T_e$? (ii) Does ion-scale turbulence dominate heat transport even with the real β value, where electromagnetic (finite- β) effects stabilize ITGs but not ETGs? To resolve these issues, we have carried out multi-scale plasma turbulence simulations employing the real mass ratio and β value, which is first realized by developing massively parallel finite-difference/spectral methods for the electromagnetic gyrokinetic simulation code GKV.

Our study reveals real-mass-ratio and real- β effects on multi-scale turbulence: (i) Ion-scale turbulence eliminates electron-scale turbulence and dominates electron heat transport even when employing the real mass ratio and β value. (ii) When growth rates of ITGs are reduced by the finite- β effects, full-spectrum analyses of multi-scale turbulence are essentially required. The results suggest that the simulations resolving only ion scales give good estimates only if ion-scale modes are highly unstable. On the other hand, in high- β regimes where ion-scale modes are stabilized, proper treatments of the contributions of electron scales are important for evaluating transport levels and modeling turbulent transport.

Helander

TH/1-2

Slides

Paper

Advances in Stellarator Gyrokinetics

P. Helander¹, F. Jenko¹, R. Kleiber¹, G. G. Plunk¹, J. H. E. Proll¹, J. Riemann¹, and P. Xanthopoulos¹

¹Max-Planck-Institut für Plasmaphysik, Garching, Germany

Corresponding Author: P. Helander, per.helander@ipp.mpg.de

We summarise a number of recent advances in gyrokinetic theory and simulations of microinstabilities and turbulence in stellarators, and compare with tokamaks.

Trapped-electron modes (TEMs) can be very different in different types of devices, because these instabilities are excited by trapped electrons in regions of unfavourable magnetic curvature. Tokamaks and stellarators are fundamentally different in the sense that the regions of trapping and bad curvature overlap in tokamaks but need not do so in stellarators. In particular, quasi-isodynamic stellarators can have the property that the bounce-averaged curvature is favourable for the great majority of all trapped particles. Analytical theory suggests that TEMs are then stable in large parts of parameter space, and this prediction is confirmed by GENE simulations, which show that these modes are more stable the more the regions of bad curvature and magnetic trapping are separated from each other. As predicted by analytical theory, the electrons are far less destabilising in the stellarator. Not only is the growth rate lower, but the most unstable mode has a shorter perpendicular wavelength, which could result in less transport.

Linear simulations of linear ITG modes in W7-X and LHD geometry using the EUTERPE show that the growth rate is similar in these two devices and that the mode structure is affected by details in the magnetic geometry. GENE simulations of saturated turbulence show that the density fluctuations are much less evenly distributed over the flux surface than in typical tokamaks. Instead of covering the entire outboard side of the torus, the turbulence is localised to narrow bands in regions of bad magnetic curvature. Possibly as a consequence of this localisation, the transport scaling is more sensitive to the normalised gyroradius and becomes stiffer when this parameter is small. This happens although these simulations are local in the radial direction, and the situation is different from that in tokamaks, where flux-tube simulations yield the same results as simulations of entire flux surfaces.



Understanding of Impurity Poloidal Distribution in Edge Pedestal by Modeling

V. Rozhansky¹, E. Kaveeva¹, I. Veselova¹, S. Voskoboinikov¹, D. Coster², E. Fable², T. Pütterich², and E. Viezzer²

¹St. Petersburg State Polytechnical University, St. Petersburg, Russian Federation ²Max-Planck-Institut für Plasmaphysik, Garching, Germany

Corresponding Author: V. Rozhansky, rozhansky@mail.ru

Modeling of the impurities distribution in the pedestal region of ASDEX-Upgrade H-mode shot was done using the B2SOLPS5.2 transport code. Strong LFS-HFS asymmetry of B⁺⁵ density and strong decoupling between parallel velocity distribution of the impurities and the main ions was obtained in qualitative agreement with the experimental observations [1]. Similar asymmetry was obtained earlier in the modeling of He ions distribution in the MAST H-mode by the same code [2]. It is demonstrated that the observed phenomena could be understood by the impact of neoclassical effects in the presence of strong density gradients in the barrier region. Obtained results are completely different from the predictions of the standard neoclassical theory. In particular the role of the poloidal drift and parallel thermal force are important. The physical mechanisms can also explain observed phenomena on C-Mod. The poloidal LFS-HFS asymmetry of impurities changes their radial transport so the standard neoclassical for impurities should be revisited in the edge barrier region.

References

[1] E. Viezzer et al., PPCF 55 (2013) 124037.

[2] V. Rozhansky et al., Proc.37th EPS Conf. on Contr. Fus. and Plasma Phys. v. 34A (2010) P2.190.

Super H-mode: Theoretical Prediction and Initial Observations of a New High Performance Regime for Tokamak Operation

P. B. Snyder¹, E. A. Belli¹, K. H. Burrell¹, J. Candy¹, A. M. Garofalo¹, R. Groebner¹, A. W. Leonard¹, R. Nazikian², T. H. Osborne¹, W. M. Solomon², and H. R. Wilson³

¹General Atomics, San Diego, CA, USA ²Princeton Plasma Physics Laboratory, Princeton, NJ, USA ³University of York, Heslington, UK

Corresponding Author: P. B. Snyder, snyder@fusion.gat.com

A new "Super H-mode" regime is predicted at very high pedestal pressure, enabling pedestal height and predicted fusion performance substantially higher than for H-mode operation. This new regime exists due to a bifurcation of the pedestal solution that occurs in strongly shaped plasmas above a critical density. The Super H-mode regime is predicted to be accessible, and to increase fusion performance, for ITER, as well as for DEMO designs with strong shaping. An initial set of experiments on DIII-D has identified the predicted pedestal pressure bifurcation, and finds pedestal height and width, and their variation with density, in good agreement with theoretical predictions.

The pressure at the top of the edge transport barrier (or "pedestal height") strongly impacts global confinement and fusion performance, with fusion power production expected to scale with the square of the pedestal height. The EPED model predicts the H-mode pedestal height and width based upon two fundamental and calculable constraints: 1) onset of non-local peeling-ballooning (P-B) modes at low to intermediate mode number, 2) onset of nearly local kinetic ballooning modes (KBM) at high mode number. EPED has been extensively tested against experiment, finding agreement to $\sim 20\%$ in both dedicated experiments and broad statistical comparisons. EPED predicts strong dependence of the pedestal height on poloidal field (B_p) , toroidal field (B_t) and plasma shape. An important dependence on density derives primarily from the dependence of the bootstrap current on collisionality. For strongly shaped plasmas, a bifurcation into Super H-Mode and H-mode branches is predicted above a critical density. Recent experiments on DIII-D have successfully tested the predicted density dependence at both high and low density, including observations of the predicted bifurcation and access to the Super H-mode regime. Super H-mode access is also predicted for ITER, and extensive sets of predictions and optimizations will be presented for ITER at a range of densities and plasma currents. We note that collisionality is impacted by impurities as well as density, and present scenarios for improving performance of ITER and existing devices by introducing low-Z impurities.

This work was supported in part by the US DOE under DE-FG02-95ER54309, DE-FG02-92ER54141 and DE-FC02-06ER54873.

TH/2-2



Gyrokinetic Study of Edge Blobs and Divertor Heat-Load Footprint

C. Chang¹, J. A. Boedo², R. Hager¹, S.-H. Ku¹, J. Lang¹, R. Maingi¹, D. Stotler¹, S. Zweben¹, and *S. Parker*³

¹Princeton Plasma Physics Laboratory, Princeton, NJ, USA ²University of California San Diego, CA, USA ³University of Colorado, Boulder, Colorado, USA

Corresponding Author: C. Chang, cschang@pppl.gov

For a better understanding of the complicated physics of the inter-related "intermittent plasma objects (blobs)" and divertor heat-load footprint, the full-function gyrokinetic PIC code XGC1 has been used in realistic diverted geometry. Neoclassical and turbulence physics are simulated together selfconsistently in the presence of Monte Carlo neutral particles. Blobs are modeled here as electrostatic nonlinear turbulence phenomenon. It is found that the "blobs" are generated, together with the "holes," around the steep density gradient region. XGC1 reasserts the previous findings [1] that blobs move out convectively into the scrape-off layer, while the holes move inward toward plasma core. The blob/hole generation, shape and dynamics are strongly related to the poloidal $E_r \times B$ shearing. In a DIII-D H-mode plasma (#096333) with $B_0 = 2.1$ T, the median radial size of the density blobs in the scrape-off layer is only about 1 cm. The L-mode type large "blobs" occur only at the tail of PDF. While the blobs move out radially, they are carried toward the outer divertor plate by strong $VE \times B$ $(\gg > V_r)$ in H-mode, consistently with experimental observation [2]. The measured radial width of the total heat load, mapped to the outer midplane, is only ≈ 4.4 mm. This width is much less than the median radial size of the intermittent plasma objects (~ 1 cm). It is rather closer to the local banana width (~ 2.7 mm), yielding approximately the $1/I_p$ -type scaling found from our previous pure neoclassical simulation [3] or a heuristic neoclassical argument Goldston. However, it also shows some spreading by the turbulence. The presentation will be extended to ITER plasma edge, where the ion banana width at separatrix becomes negligible compared to the meso-scale blob size, to report on the limit in the $1/I_p$ scaling by the intermittent turbulence. Also, detailed XGC1 study of the blob dynamics show that the blobs and their dynamics interact more strongly with presheath than with the Debye sheath. Similarities and differences with results from existing models will be presented. Comprehensive experimental validation on multiple tokamaks (DIII-D, NSTX, C-Mod, JET, etc) will also be presented.

References

- [1] D. D'Ippolito et al., Phys. Plasmas 18 (2011) 060501.
- [2] J. Boedo et al., Phys. Plasmas 10 (2003) 1670.
- [3] Report on DOE FES Joint Facilities Research Milestone 2010 on Heat-Load Width, Appendix H.

Ricci

Slides

Paper

First-Principle Theory-Based Scaling of the SOL Width in Limited Tokamak Plasmas, Experimental Validation, and Implications for the ITER Start-up

P. Ricci¹, F. Halpern¹, L. Joaquim¹, S. Jolliet¹, A. Mosetto¹, F. Riva¹, W. Christoph¹, A. Fasoli¹, I. Furno¹, B. Labit¹, F. Nespoli¹, C. Theiler², G. Arnoux³, J. P. Gunn⁴, J. Horacek⁵, M. Kocan⁶, B. LaBombard⁷, and C. Silva⁸

¹Ecole Polytechnique Fédérale de Lausanne, CRPP, Lausanne, Switzerland

²Massachusetts Institute of Technology, Plasma Science & Fusion Center, Cambridge, MA, USA

³CCFE Fusion Association, Culham Science Centre, Abingdon, UK

⁴CEA-IRFM, Saint Paul lez Durance, France

⁵Institute of Plasma Physics AS CR v.v.i., Prague, Czech Republic

⁶Max-Planck-Institut für Plasmaphysik, Garching, Germany

⁷Massachusetts Institute of Technology, Plasma Science & Fusion Center, Cambridge, MA, USA

⁸Institute of Plasmas and Nuclear Fusion, Association EURATOM/IST, Lisbon, Portugal

Corresponding Author: P. Ricci, paolo.ricci@epfl.ch

The steady-state heat load onto the plasma facing components of tokamak devices depends on the SOL width, which results from a balance between plasma outflowing from the core region, turbulent transport, and losses to the divertor or limiter. Understanding even the simplest SOL configurations, like circular limited plasmas, is a stepping-stone towards more complicated configurations, with important implications for the ITER start-up and ramp-down phases. Here we present a first-principle based scaling for the characteristic SOL pressure scale length in circular, limited tokamaks that has been obtained by evaluating the balance between parallel losses at the limiter and non-linearly saturated resistive ballooning mode turbulence driving anomalous perpendicular transport. It is found that the SOL width increases with the tokamak major radius, the safety factor, and the density, while it decreases with the toroidal magnetic field and the plasma temperature. The scaling is benchmarked against the flux-driven non-linear turbulence simulations that have been carried out with the GBS code. This code solves the drift-reduced Braginskii equations and evolves self-consistently plasma equilibrium and fluctuations, as the result of the interplay between the plasma injected by a source, which mimics the plasma outflow from the tokamak core, the turbulent transport and the plasma losses to the vessel. GBS has been subject to a verification and validation procedure unparalleled in plasma physics. The theoretical scaling reveals good agreement with experimental data obtained in a number of tokamaks, including TCV, Alcator C-MOD, COMPASS, JET, and Tore Supra.



Assessment of Scrape-off Layer Simulations with Drifts against L-Mode Experiments in ASDEX Upgrade and JET

L. Aho-Mantila¹, G. Conway², H. W. Müller², S. Müller², S. Potzel², D. Coster², M. Wischmeier², A. Meigs³, and M. Stamp³

> ¹VTT Technical Research Centre of Finland, Finland ²Max-Planck-Institut für Plasmaphysik, Garching, Germany ³JET-EFDA, Culham Science Centre, Abingdon, UK

Corresponding Author: L. Aho-Mantila, leena.aho-mantila@vtt.fi

Recent results of validating scrape-off layer simulations with drifts are summarized, based on detailed comparisons between 2D SOLPS5.0 fluid code solutions and L-mode experiments in the full-metal devices ASDEX Upgrade and JET. The effects of drifts in various divertor power exhaust scenarios are analysed in extensively characterized discharges, in which the levels of deuterium fuelling, seeding of N impurities, and magnetic field direction are varied. In-out asymmetries in the plasma conditions are observed throughout the divertor legs when the ion ∇B drift is towards the divertor, and these asymmetries are observed to reduce with the field reversal. In the modelling, the effects of the various drift terms are analysed in comparison to the geometrical effects, and a pronounced role of the $E \times B$ drifts is identified in the resulting asymmetries. At the lowest densities, the simulations with fully activated drift terms reproduce the Balmer line emission and radiation in the JET divertor, several poloidally distributed temperature profile measurements in ASDEX Upgrade, as well as a high-density region in the inner divertor of ASDEX Upgrade. In conditions with strong power dissipation, the modelling captures the incremental effects of impurities on the divertor radiation, but high levels of fuelling and seeding lead to discrepancies between the modelled and measured target conditions. At low levels of fuelling and impurity radiation, the simulations tend to underestimate the strong scrape-off layer flows measured in forward field in ASDEX Upgrade, although a satisfactory agreement is obtained with measurements of the scrape-off layer radial electric field.

This work was supported by EURATOM and carried out within the framework of the European Fusion Development Agreement. The views and opinions expressed herein do not necessarily reflect those of the European Commission.

TH/4-1

Slides

Paper

The Role of MHD in 3D Aspects of Massive Gas Injection for Disruption Mitigation

V. A. Izzo¹, P. Parks², N. Commaux³, N. W. Eidietis², R. Granetz⁴, E. M. Hollmann¹, G. Huijsmans⁵, D. Humphreys², C. Lasnier⁶, A. Loarte⁵, R. Moyer¹, C. Paz-Soldan⁷, T. Strait², and R. Raman⁸

¹University of California San Diego, CA, USA
 ²General Atomics, San Diego, CA, USA
 ³Oak Ridge National Laboratory, Oak Ridge, TN, USA
 ⁴Massachusetts Institute of Technology, Cambridge, MA, USA
 ⁵ITER Organization, Saint Paul lez Durance, France
 ⁶Lawrence Livermore National Laboratory, Livermore, CA, USA
 ⁷Oak Ridge Institute for Science Eduction, Oak Ridge, TN, USA
 ⁸University of Washington, Seattle, WA, USA

Corresponding Author: V. A. Izzo, izzo@fusion.gat.com

Massive gas injection (MGI) is a leading candidate technology for disruption mitigation in ITER, and recent modeling has suggested that MHD modes play a critical role in determining the distribution of radiated power during an MGI shutdown. NIMROD 3D MHD simulations of MGI in both ITER and DIII-D reveal how the distribution of gas jets and the n = 1 mode interact to determine the localization of radiated power, and the likelihood of wall-melting on ITER. Various combinations of the four ports allocated for the ITER disruption mitigation system (DMS) are modeled, along with a range of gas quantities and species to determine the optimal scenario for ITER. The midplane port interacts with the plasma very differently than the upper ports due to the difference in minor radius. Use of the midplane port improves the radiated energy fraction with no detrimental effect on the radiation toroidal peaking. In DIII-D, dedicated experiments were performed to understand the effect of the n = 1 mode phase on the distribution of radiated power. By varying the phase of applied n = 1 fields, the radiation toroidal peaking during MGI was altered. Simulations of MGI in DIII-D with external n = 1 fields are carried out and compared to the experiments to better understand this effect and its implications for optimizing radiation symmetry.

This work was supported in part by the US Department of Energy under DE-FAG02-95ER54309, DE-FC02-04ER54698, DE-AC05-00OR22725, and DE-AC52-07NA27344.

The Low Threshold Parametric Decay Instabilities Leading to Anomalous Absorption at ECRH in Toroidal Devices

A. Popov¹, E. Gusakov¹, A. Saveliev¹, and E. Sysoeva¹

¹*Ioffe Physical-Technical Institute of the Russian Academy of Science, St. Petersburg, Russian Federation* Corresponding Author: A. Popov, a.popov@mail.ioffe.ru

In the paper the universal scenarios of the low-threshold parametric decay instabilities (PDIs), explaining the anomalous phenomena being already observed [1, 2] and potentially important for the energy budget in the future ECRH experiments, are treated. We investigate the scenario of a low-threshold absorptive PDI [3] based on the parametric excitation of the electron Bernstein wave 3D trapped in the drift wave eddies, filaments or blobs possessing density maximum and aligned with the magnetic field. The nonlinear excitation of this wave and the heavily damped low frequency oscillations manifests itself as the low-threshold absolute PDI resulting in anomalous absorption of the part of the microwave power by ions and electrons. In particular, this instability can be responsible for fast ion production often observed in 2nd harmonic ECRH experiments in toroidal plasmas [1]. We consider the anomalous backscattering reported in [2] as a secondary nonlinear process, which accompanies a primary low-threshold PDI [4]. The effect of the parametric decay of the 2nd harmonic extraordinary (X)-mode wave into two short wave-length upper hybrid (UH) plasmons, propagating in opposite directions, is considered. The radial localization of both the UH plasmons can be achieved in a vicinity of the density profile local maximum corresponding to either the discharge axis for the peaked profile, or the O-point of the magnetic island, or the presence of a blob. On the other hand, when the UH plasmons propagate oppositely and the pump microwave beam has the finite size, the absolute two-plasmon PDI of the X wave is possible, the power threshold of which, being derived explicitly, is two orders of magnitude smaller than the one derived in the case of a monotonous density profile. The estimations of the threshold for the ordinary wave parametric decay into the 2D trapped UH plasmon and an ion Bernstein wave for the projected ITER conditions are presented as well.

References

- [1] D. Rapisarda et al., Plasma Phys. Control. Fusion 49, 309 (2007).
- [2] S.K. Nielsen et al., Plasma Phys. Control. Fusion 55, 115003 (2013).
- [3] E.Gusakov, A.Popov, A. Saveliev, Plasma Phys. Control. Fusion 56, 015010 (2014).
- [4] E. Gusakov, A. Popov, EPJ Web of Conferences 32, 01007 (2012).

Slides

Paper

Integrated Modeling of Toroidal Rotation with the 3D Non-Local Drift-Kinetic Code and Boundary Models for JT-60U Analyses and Predictive Simulations

M. Honda¹, S. Satake², Y. Suzuki², M. Yoshida¹, N. Hayashi¹, K. Kamiya¹, A. Matsuyama¹, K. Shinohara¹, G. Matsunaga¹, M. Nakata¹, S. Ide¹, and H. Urano¹

¹Japan Atomic Energy Agency, Naka, Japan ²National Institute for Fusion Science, Toki, Japan

Corresponding Author: M. Honda, honda.mitsuru@jaea.go.jp

The integrated framework for toroidal momentum transport is developed, which self-consistently calculates the neoclassical toroidal viscosity (NTV), the radial electric field E_r and the resultant toroidal rotation together with the scrape-off-layer (SOL) physics-based boundary model. The coupling of TOPICS, VMEC, and FORTEC-3D makes it possible to calculate the NTV due to the non-axisymmetric perturbed magnetic field in the actual geometry. It is found that the NTV significantly influences toroidal rotation profile to the boundary rotation necessitates the boundary condition modeling. Owing to the high-resolution measurement in the JT-60U edge region, E_r is found to be rather insensitive at the separatrix. Focusing on E_r , the boundary model of toroidal momentum can be developed in conjunction with the SOL/divertor plasma code. This modeling realizes self-consistent predictive simulations for operation scenario development in JT-60SA and ITER.



Core Microturbulence and Edge MHD Interplay and Stabilization by Fast Ions in Tokamak Confined Plasmas

J. Garcia¹, J. Citrin², T. Goerler³, N. Hayashi⁴, F. Jenko³, P. Maget¹, P. Mantica⁵, M. J. Pueschel⁶, D. Told³, C. Bourdelle¹, R. Dumont¹, G. Giruzzi¹, W. Haverkort⁷, G. Hogeweij², S. Ide⁴, T. Johnson⁸, and H. Urano⁴

¹CEA-IRFM, Saint Paul lez Durance, France
 ²FOM Institute DIFFER, Association EURATOM-FOM, Nieuwegein, The Netherlands
 ³Max-Planck-Institut für Plasmaphysik, Garching, Germany
 ⁴Japan Atomic Energy Agency, Naka, Japan
 ⁵Associazione EURATOM-ENEA Unitá Tecnica Fusione, Frascati, Italy
 ⁶University of Wisconsin-Madison, Madison, WI, USA

⁷Centrum Wiskunde & Informatica (CWI), Amsterdam, The Netherlands

⁸VR, Fusion Plasma Physics, KTH Royal Institute of Technology, Stockholm, Sweden

Corresponding Author: J. Garcia, jeronimo.garcia@cea.fr

Extensive linear and non-linear gyrokinetic simulations, including kinetic electrons, collisions, flow shear, realistic geometry, electromagnetic effects, impurities, as well as perpendicular and parallel magnetic fluctuations, and linear MHD analyses performed respectively with the GENE and MISHKA codes, have shown for the first time that the large population of fast ions found in the plasma core under particular heating conditions has a strong impact on core microturbulence and edge MHD. In particular, nonlinear electromagnetic stabilization of Ion Temperature Gradient (ITG) turbulence can be very much enhanced by fast ion pressure gradients. These results can explain the improved ion energy confinement regime observed in L-mode ion heat transport studies at the JET tokamak which manifests itself as a reduction of the ion temperature stiffness and which, until now had not been reproduced by nonlinear gyrokinetic simulations. The same effect has been shown to be important in high- β hybrid scenarios from JET and JT-60U with a large population of fast ions. Up to 4 times of lower ion heat flux for the same R/LT_i is obtained in these plasmas when the fast ions contribution is taken into account. This can explain the higher core ion temperature gradients obtained in these regimes as the flow shear is found to play a much weaker role. In addition to the core transport stabilization, the fast ions have been seen to favorably impact edge transport. The high core total pressure achieved due to fast ions modifies the Shafranov-shift leading to a pedestal pressure which can increase by 10% when the extra core pressure is taken into account. Therefore, a virtuous circle starts in these plasmas when the fast ions increase the total core pressure without increasing the turbulence drive, even reducing the ITG microturbulence. This leads to an improved edge pedestal pressure by means of the increased Shafranov-shift in a manner unachievable by simple thermal pressure, which is strongly limited by microturbulence.

This work was supported by EURATOM and carried out within the framework of the European Fusion Development Agreement. The views and opinions expressed herein do not necessarily reflect those of the European Commission.

Huijsmans

TH/6-1Ra

Preprint Slides

Non-Linear MHD Simulations for ITER

G. Huijsmans¹, F. Liu¹, S. Futatani², A. Loarte¹, F. Köchl³, M. Hoelzl⁴, A. M. Garofalo⁵, and E. Nardon⁶

¹ITER Organization, Saint Paul lez Durance, France
 ²Ecole Centrale de Lyon, France
 ³Institute of Atomic and Subatomic Physics, TU-Vienna, Vienna, Austria
 ⁴Max-Planck-Institut für Plasmaphysik, Garching, Germany
 ⁵General Atomics, San Diego, CA, USA
 ⁶CEA-IRFM, Saint Paul lez Durance, France

Corresponding Author: G. Huijsmans, guido.huijsmans@iter.org

Validation of MHD models and MHD simulations on current experiments is needed to provide a physics basis for the application of these models to ITER. This paper describes the progress made towards validation in the area of the stability of the H-mode edge pedestal and ELM control.

ELM control: pellet pacing: The injection of pellets is one of the methods foreseen to control ELM energy losses and power fluxes in ITER. Previous non-linear MHD simulations using the JOREK code of pacing pellets in DIII-D have shown that the minimum pellet size for an ELM trigger is correlated with the 3D pressure perturbation created by the pellet. This has been extended to the simulation of pacing pellets injected in JET. The simulation domain including the divertor allows simulation of a full pellet triggered ELM cycle. The simulated ELM size is found to depend on the pedestal properties of the target plasma. The divertor heat load shows an n = 1 asymmetry for low field side injection (as observed experimentally). The paper will discuss the dependence of the power deposition asymmetry on the injection geometry and the consequences for ITER.

ELM control: QH-mode: Recently, DIII-D has made significant progress in the development of ELM free QH mode plasmas in an ITER relevant regime, using the RMP coils to control the rotation profile. To develop the physics basis for ITER, non-linear MHD simulations of DIII-D QH-mode plasmas have been performed. The JOREK code has been coupled with the STARWALL code for the resistive wall, vacuum and coils contributions. The influence of the rotation and rotation shear on the stability and saturation of the kink mode will be investigated and compared with DIII-D experiments.

SOL MHD stability: Observations of the SOL heat flux width of the inter-ELM scrape-off layer (SOL) for low density H-modes, show an inverse dependence on the poloidal field. Extrapolating to ITER results in a narrow SOL width of ~ 1 mm. The MHD stability limits of the pedestal and SOL pressure profile have been analysed to evaluate whether MHD limits could prevent such narrow profiles. ITER scenarios with narrow SOL widths are found to be stable to infinite-*n* ballooning modes. The ballooning stability in the pedestal shows a higher (by $\sim 40\%$) stability limit in the SOL compared to the pedestal. This indicates that the narrow SOL are consistent with MHD stability limits in ITER.

Non-Linear MHD Modelling of Edge Localized Modes and their Interaction with Resonant Magnetic Perturbations in Rotating Plasmas

M. Becoulet¹, F. Orain¹, J. Morales¹, X. Garbet¹, G. Dif-Pradalier¹, C. Passeron¹, G. Latu¹,
 E. Nardon¹, A. Fil¹, V. Grandgirard¹, G. Huijsmans², S. Pamela³, A. Kirk⁴, M. Hoelzl⁵,
 E. Franck⁵, E. Sonnendrucker⁵, B. Nkonga⁶, and P. Cahyna⁷

¹CEA-IRFM, Saint Paul lez Durance, France
 ²ITER Organization, Saint Paul lez Durance, France
 ³CCFE Fusion Association, Culham Science Centre, Abingdon, UK
 ⁴JET-EFDA, Culham Science Centre, Abingdon, UK
 ⁵Max-Planck-Institut für Plasmaphysik, Garching, Germany
 ⁶Nice University, France

⁷Institute of Plasma Physics AS CR v.v.i., Prague, Czech Republic

Corresponding Author: M. Becoulet, marina.becoulet@cea.fr

The intensive experimental and theoretical study of Edge Localized Modes (ELMs) and methods for their control has a great importance for ITER. The application of small external Resonant Magnetic Perturbations (RMPs) has been demonstrated to be efficient in ELM suppression/mitigation in present day tokamaks. RMPs are foreseen as one of the promising methods of ELM control in ITER. In the present work the dynamics of the full ELM cycle including both the linear and non-linear stages of the crash and the possible explanation of the mechanism of ELM mitigation by RMPs are presented based on the results of the multi-harmonics non-linear resistive MHD modeling using the JOREK code. These simulations are performed in the realistic tokamak geometry with the X-point and the Scrape-Off-Layer (SOL) with relevant plasma flows: toroidal rotation, the bi-fluid diamagnetic effects, and neoclassical poloidal friction. The introduction of flows in the modelling demonstrated a large number of new features in the physics of ELMs and their interaction with RMPs compared to previous results.

The novelty of the present work consists firstly in the demonstration of non-linear MHD simulations with the diamagnetic effects the multi-cycle ELMy regimes. Secondly, the ELMs rotation on the linear stage (precursors) and on the non-linear stage (ELM filaments) were modeled. Finally for the first time ELMs mitigation by RMPs was demonstrated for realistic JET-like parameters. The peak power reaching the divertor is found to be reduced by a factor of ten by RMPs. Mitigated ELMs represent small relaxations due to the non-linearly driven modes coupled to the imposed n = 2 RMPs. The divertor footprints of the mitigated ELMs exhibit structures created by n = 2 RMPs, however, slightly modulating them due to the presence of other harmonics, feature observed in experiments.

TH/6-2

Slides

Paper

Three-Dimensional MHD Analysis of Heliotron Plasma with RMP

K. Ichiguchi¹, Y. Suzuki¹, M. Sato¹, Y. Todo¹, S. Sakakibara¹, S. Ohdachi¹, Y. Narushima¹, and B. Carreras²

¹National Institute for Fusion Science, Toki, Japan ²BACV Solutions Inc., Oak Ridge, TN, USA

Corresponding Author: K. Ichiguchi, ichiguch@nifs.ac.jp

In the recent study of magnetically confined fusion plasmas, resonant magnetic perturbations (RMPs) are studied from the viewpoint of the magnetohydrodynamics (MHD) stability against pressure driven modes, because RMPs can locally change the pressure gradient. Particularly, in heliotrons, since pressure driven modes are the most dangerous, the change of the pressure gradient can directly influence the global stability. Here, the interaction between pressure driven modes and magnetic islands generated by an RMP is numerically analyzed in a Large Helical Device (LHD) configuration with a high aspect ratio and magnetic hill. For the MHD analysis of the RMP effects, an equilibrium with a pressure profile consistent with the disturbed magnetic surfaces is necessary. To obtain such an equilibrium, we utilize the HINT2 code, which finds a three-dimensional (3D) equilibrium without any assumption of the existence of nested surfaces. A horizontally uniform RMP is applied and an m = 1/n = 1 magnetic island is generated in the equilibrium. The pressure profile is deformed so that the gradient is smaller at the O-point than at the X-point. Next, the plasma dynamics is examined with the MIPS code, which solves the full 3D MHD equations by following the time evolution. In this LHD configuration, a typical interchange mode is the most unstable instability in the case without the RMP. On the other hand, in the case with the RMP, because of the poloidal asymmetry of the equilibrium pressure a ballooning type mode is the most unstable, with the mode structure localized around the X-point. The mode can utilize the driving force most effectively by being localized around the steepest pressure gradient point. In the nonlinear evolution of the mode, the pressure starts to collapse around the X-point, and then, the collapse spreads to the core region. Therefore, the phase of the mode structure in the poloidal and the toroidal directions is fixed to that of the island. Such fixed phase is observed in the LHD experiments with a natural error field that works as an RMP. Further analysis for a wide range of parameters will allow us to understand further the RMP effects on the pressure driven modes.



Todo

Multi-Phase Simulation of Alfvén Eigenmodes and Fast Ion **Distribution Flattening in DIII-D Experiment**

Y. Todo¹, M. Van Zeeland², A. Bierwage³, and W. W. Heidbrink⁴

¹National Institute for Fusion Science, Toki, Japan ²General Atomics, San Diego, CA, USA ³Japan Atomic Energy Agency, Naka, Japan ⁴University of California Irvine, CA, USA

Corresponding Author: Y. Todo, todo@nifs.ac.jp

This paper presents the first simulation that predicts both nonlinear saturation amplitude of Alfvén eigenmodes (AE modes) and fast ion transport that are close to measured values in experiment. This simulation enables us to predict the alpha particle distribution and the AE modes activity, which is one of the major concerns for burning plasmas such as ITER. A multi-phase simulation [1], which is a combination of classical simulation and hybrid simulation for energetic particles interacting with a magnetohydrodynamic (MHD) fluid, is employed in this work. The classical simulation follows energetic particle orbits in the equilibrium magnetic field without MHD perturbations. The hybrid simulation code MEGA is extended with realistic beam deposition profile, collisions (slowing down, pitch angle scattering, and energy diffusion), and losses, and is used for both the classical and hybrid phases. The simulation is applied to DIII-D discharge #142111 where the fast ion spatial profile is significantly flattened due to multiple AE modes [2]. Temperature fluctuations due to two of the dominant toroidal Alfvén eigenmodes (TAE modes) in the simulation results are compared in detail with the electron cyclotron emission (ECE) measurement in the experiment. It is demonstrated that the temperature fluctuation profile and the phase profile are in very good agreement with the measurement, and the amplitude is also in agreement within a range of 40%. The fast ion pressure profile flattening observed in the experiment is also successfully reproduced.

References

[1] Y. Todo et al., submitted to Nucl. Fusion.

[2] M.A. Van Zeeland et al., 2012 Nucl. Fusion 52 094023.

TH/7-2

Slides

Paper

Radial Localization of Alfvén Eigenmodes and Zonal Field Generation

Z. Lin¹

¹University of California Irvine, CA, USA

Corresponding Author: Z. Lin, zhihongl@uci.edu

In the well-accepted and widely-exercised paradigm, the Alfvén eigenmode (AE) growth rate can be calculated from a perturbative energetic particle (EP) contribution to a fixed mode structure and real frequency given by MHD properties of thermal plasmas. However, our studies show that accurate prediction of the AE growth rate requires non-perturbative, self-consistent simulations to calculate the true mode structures. GTC gyrokinetic particle simulations of DIII-D discharge #142111 near 525 ms find a radial localization of the toroidal Alfvén eigenmode (TAE) due to the the modification of the MHD mode structure, i.e., non-perturbative EP contribution. The EP-driven TAE has a radial mode width much smaller than that predicted by the MHD code NOVA. The TAE radial position peaks at and moves with the location of the strongest EP pressure gradients. Experimental data confirms that the eigenfunction drifts quickly outward in the radial direction. The EP contribution also breaks the radial symmetry of the ballooning mode structure and induces a dependence of the TAE frequency on the toroidal mode number, in excellent agreement with the experimental measurements. The radial localization could have profound implications on the EP transport.

GTC nonlinear simulation of the TAE in DIII-D discharge #142111 near 525 ms finds that zonal fields are driven by TAE mode coupling (passive generation). The collisionless skin-depth effects suppress the modulational instability. The growth rate of the zonal fields is twice of the TAE growth rate, consistent with earlier MHD-gyrokinetic hybrid simulations. A threshold of the TAE amplitude for driving the zonal fields is also observed. The effects of the zonal fields on the TAE nonlinear saturation are weak. GTC nonlinear simulations of β -induced Alfvén eigenmode (BAE) show that the mode frequency has a fast chirping associated with the oscillation of the mode amplitude. Localized zonal fields with a negative value around the mode rational surface are generated by BAE. In the weakly driven case, the zonal fields with a strong geodesic acoustic mode (GAM) component have weak effects on the BAE evolution. In the strongly driven case, the zonal fields are dominated by a more significant zero frequency component and have stronger effects on the BAE dynamics.



A 3D Nonlinear Simulation Study of the L \rightarrow H Transition Criterion

G. Park¹, S. S. Kim¹, T. Rhee¹, H. Jhang¹, M. Leconte¹, P. H. Diamond¹, and X. Xu³

 ¹National Fusion Research Institute, Daejeon, Korea, Republic of ²University of California San Diego, CA, USA
 ³Lawrence Livermore National Laboratory, Livermore, CA, USA

Corresponding Author: G. Park, gypark@nfri.re.kr

High confinement mode (H-mode) is essential as a baseline operating scenario in ITER. In order to develop a predictive model of the power threshold for access to H-mode in ITER, it is essential to understand first the underlying mechanism that triggers the transition. It is widely accepted that edge transport barrier (ETB) formation in H-mode is due to the suppression of turbulence by $E \times B$ flow shear. In several recent experiments, turbulence-driven flows were suggested as a trigger for the L \rightarrow H transition. In this paper, a 3D fluid simulation model of the L \rightarrow H transition is presented. Specifically, we report the results of 3D flux-driven simulations of resistive ballooning modes (RBM) turbulence with neoclassical flow damping effect in the edge of a tokamak. It is found that ETB forms naturally due to mean shear feedback through evolving pressure gradient once input power exceeds a threshold value. We show that 1) the transition to ETB is triggered by the turbulence-driven flow via a limit cycle oscillation (LCO) of turbulence intensity and $E \times B$ flow shear; 2) the correct transition criterion (threshold) is given by $R_T > 1$ (R_T : normalized Reynolds power defined as a ratio of the Reynolds power to the rate of energy input into the turbulence), instead of the conventional mean shear criterion, i.e., $E \times B$ flow shearing rate larger than linear growth rate; 3) neoclassical poloidal rotation damping effect significantly affects the transition process. A slow power ramp-down simulation is also performed to study $H \rightarrow L$ back transition and hysteresis phenomena. Detailed results will be presented.



Paper

Developing and Validating Predictive Models for Fast Ion Relaxation in Burning Plasmas

N. Gorelenkov¹, *W. W. Heidbrink*², J. Lestz¹, M. Podestá¹, M. Van Zeeland³, and R. White¹

¹Princeton Plasma Physics Laboratory, Princeton, NJ, USA ²University of California Irvine, CA, USA ³General Atomics, San Diego, CA, USA

Corresponding Author: N. Gorelenkov, ngorelen@pppl.gov

The performance of the burning plasmas is limited by the confinement of super-Alfvénic fusion products, alpha particles, resonating with the Alfvénic eigenmodes (AEs). Two techniques are developed to evaluate the AE induced fast ion relaxation. Both rely on linear instability theory and are confirmed by experiments. The first is the reduced quasilinear technique or critical gradient model (CGM) where marginally unstable (or critical) gradient of fast ion pressure is due to unstable AEs. It allows the reconstruction of fast ion pressure profile and computed their losses. The second technique is called hybrid that is also based on NOVA-K linear stability computations of TAE (or RSAE) mode structures and growth rates. AE amplitudes are computed from the nonlinear theory perturbatively and used in the numerical runs. With the help of the guiding center code ORBIT the hybrid model relaxes the fast particle profiles. We apply these models for NSTX and DIII-D plasmas with the neutral beam injections for validations. Both methods are relatively fast ways to predict the fast ion profiles in burning plasmas and can be used for predictive modeling prior to building experimental devices such as ITER.



TH/P1-3

Current Drive by Electron Temperature Gradient Turbulence in Tokamak Pedestal Region

S. K. Tiwari¹, P. Kaw¹, R. Singh¹, and P. H. Diamond²

¹Institute for Plasma Research, Bhat, Gandhinagar, India ²National Fusion Research Institute, Daejeon, Korea, Republic of ²University of California San Diego, CA, USA

Corresponding Author: S. K. Tiwari, sanatkrtiwari86@gmail.com

Cor HH turł

In this paper, the quasilinear version of the current evolution equation in the presence of ETG turbulence in the tokamak pedestal region is written down. It has been shown that the current drive has to fight the conventional resistive dissipation mechanism as well as new dissipation mechanisms, such as a turbulence driven hyper-resistivity coefficient associated with the ETG turbulence. It is likely that the ETG turbulence tends to saturate at amplitudes much larger than what the mixing length theory would predict, primarily because of nonlinear radial streamer like mechanisms, which encourage big radial steps across the magnetic fields and give appropriate and reasonable magnitudes of the cross field transport due to this instability. We have used these saturated ETG turbulence levels to estimate the magnitudes of the spontaneous source of toroidal current injection as well as the anomalous hyper resistivity coefficient. These estimates of turbulence driven current are compared with the background bootstrap current in the pedestal region. It is concluded that significant modification of the equilibrium currents as well as current profiles may arise in the pedestal region as a consequence of the turbulent injection of current in the basic pedestal plasma.

Preprint

Computation of Resistive Instabilities in Tokamaks with Full **Toroidal Geometry and Coupling Using DCON**

J.-K. Park¹, A. H. Glasser², Z. R. Wang¹, and Y. Liu³

¹Princeton Plasma Physics Laboratory, Princeton, NJ, USA ²University of Washington, Seattle, WA, USA ³JET-EFDA, Culham Science Centre, Abingdon, UK

Corresponding Author: J.-K. Park, jpark@pppl.gov

Precise determination of resistive instabilities is an outstanding issue in tokamaks, remaining unsatisfactory for a long time despite its importance for advanced plasma control. This paper presents the first successful computation of such resistive instabilities including full mode coupling and multiple singular surfaces, by upgrading DCON [1] with a resonant-Galerkin method [2] using improved basis functions such as Hermite cubics and high-order Frobenius power series. Incorporating the resistive layer model of Glasser-Greene-Johnson (GGJ) [3] and matching the inner-layer solutions into full outer-layer solutions in DCON, a complete picture of resistive instabilities in tokamaks can be obtained and studied. Excellent quantitative agreement with the MARS-F code [4], for both growth rate and outer-layer solutions, has been achieved. Convergence is also a distinguished property in DCON as tested with challenging NSTX equilibria with strong shaping, high- β , and multiple rational surfaces up to 10. Another important advantage in DCON is the separation of the inner-layer from the outer-layer regions, which will allow us to extend inner-layer model efficiently to more advanced fluid equations including drift kinetic effects and to perform more precise calculations of non-ideal stability and 3D perturbed equilibria in the future.

This research was supported by U.S. DOE contracts #DE-AC02-09CH11466.

References

[1] A. H. Glasser and M. S. Chance, Bull. Am. Phys. Soc. 42, 1848 (1997).

[2] A. Pletzer and R. L. Dewar, J. Plasma Physics 45, 427 (1991).

[3] A. H. Glasser, J. M. Greene, and J. L. Johnson, Phys. Fluids 18, 7 (1975).

[4] Y. Liu et al., Phys. Plasmas 19, 172509 (2012).



TH/P1-7

Quantifying Self-Organization in Magnetically Confined Fusion Plasmas

M. Rajkovic¹, M. Milovanovic², T. Watanabe³, and M. Skoric⁴

¹University of Belgrade, Institute of Nuclear Sciences Vinca, Serbia ²Mathematical Institute of the Serbian Academy of Sciences and Arts, Serbia ³University of Nagoya, Nagoya, Japan ⁴National Institute for Fusion Science, Toki, Japan

Corresponding Author: M. Rajkovic, milanr@vin.bg.ac.rs

Plasma self-organization is the frontier research area in plasma physics and its understanding is extremely important for the construction of innovative fusion configurations. Emergence, an outcome of self-organization, implies the appearance of certain large scale structures, forms or patterns, formed from a large number of simple interactions of smaller parts of the system. Motivated by these requirements, we have developed a framework (mathematical and computational), which, at the same time, makes choice of the optimal wavelet for analysis of data, enables optimal prediction of the dynamics, quantifies stages of self-organization and removes the effects of noise, when required. It also includes the role of scales in the process. A spatiotemporal data of the gyrokinetic Vlasov simulation results for the ion temperature gradient turbulence, where the standard and the inwardshifted configurations of the Large helical Device are considered in this study. Although fluctuations of the electrostatic potential for zonal flows exhibit spatiotemporal chaos in both configurations, we show that self-organization is different in the two cases. Specifically, we show that complexity is more intense in the standard configuration, however the increase in time of complexity is higher in the inward-shifted configuration implying faster relaxation. These results are shown to be consistent with the results of the analysis of the spatiotemporal chaotic dynamics in the two configurations. We illustrate how this method may be used to test various confinement configurations in order to achieve the optimal self-organization under given circumstances. We also analyze the ion-saturation current measurements of three different confinement regimes, namely the L-mode, the H-mode and the dithering H-mode, in the scrape-off layer of several devices. We show how self-organization in each of the regimes may be compared and also how changes in configuration may be predicted. Finally, we discuss the versatility of the method and other potential uses in the realm of fusion plasmas.

Preprint

Redistribution of Energetic Particles Due to Internal Kink Modes

R. Farengo¹, H. Ferrari¹, P. Garcia-Martinez², L. Lampugnani², M.-C. Firpo³, E. Wahb³, and A. Lischitz⁴

> ¹Comision Nacional de Energia Atomica, Argentina ²CONICET, Argentina ³Ecole Polytechnique, France ⁴Laboratoire d'Optique Appliquée, France

Corresponding Author: R. Farengo, farengo@cab.cnea.gov.ar

The internal kink modes associated with sawtooth oscillations can produce a redistribution of the energetic particles population, thus modifying the power deposition profile and increasing particle losses and wall loading. We study the effect of internal kink modes on the confinement of alpha particles and neutral beam ions by following the trajectories of a large number of particles in the total electric and magnetic fields, sum of the equilibrium plus the perturbation. The equilibrium is a simple analytical solution of the Grad-Shafranov equation with ITER like parameters and q_{axis} less than 1. To calculate the perturbed fields we use the experimental information regarding the space and time dependence of the displacement eigenfunctions corresponding to the modes condsidered and ideal MHD. A redistribution parameter is introduced to quantify the displacement of the particles from their initial flux surface. The effect of the (1, 1), (2, 2), and (2, 1) modes is studied for different particle energies and mode frequency and amplitude. The results show, that for energies below 1 MeV, the redistribution can have a strong dependence on the particle energy and mode frequency.



TH/P1-9

From Micro to Macro: L-H Transition Dynamics and Power Threshold Scaling

M. Malkov¹, P. H. Diamond¹, K. Miki², and G. Tynan¹

¹University of California San Diego, CA, USA ²Japan Atomic Energy Agency, Naka, Japan

Corresponding Author: M. Malkov, mmalkov@ucsd.edu

It is believed that L-H transition occurs via coupling of turbulence to low frequency shear flows by Reynolds work. As a consequence, turbulence and turbulent transport collapse, enabling the growth of diamagnetic electric field shear and the transition. This work focuses on the missing link between microscopics and macroscopics, and its critical role in power threshold scaling. The major goal is the understanding of the observed occurrence of a minimum in the power threshold. We pursued a model which separates electron and ion temperature evolution by extending a recent 1D, five-field model which captures the transition layer evolution well, but does not have this capability. In the new model, density appears as an electron-ion coupling parameter, as well as in ZF damping. We propose and examine the explanation that: i) the initial trend of decrease in the power threshold is due to stronger collisional electron-ion coupling which enables the development of stronger diamagnetic electric field. This scaling trend reflects the role of the mean shear in locking-in of the transition, ii) the subsequent increase in the threshold is due to the increase in damping of shear flows with ion collisionality. This scaling trend reflects the role of the turbulence generated shear flow as a trigger mechanism. Our studies reveal a clear power threshold minimum in density scans ran for a fixed, electron dominated heating mix, but an even more distinct minimum is predicted for the fixed density when scanning the ion to total heating ratio. Here we see that the power threshold minimum appears as an interplay of electron-ion coupling. In addition to the basic scaling trends, model studies reveal: a) the threshold power increases for off-axis electron heat deposition. This follows from the fact that electron-ion coupling is reduced in this instance, b) a minimum power is predicted for a heating mix scan as well as for a density scan. This points towards the possibility of a global minimum in the threshold power in terms of a number of relevant parameters, c) no clear threshold minimum is predicted by this model for pure ion heat deposition. Ongoing work is concerned with quantifying the strength of hysteresis in terms of multiple macroscopic parameters and with relating this to observed back-transition shear flow and turbulence dynamics.



Paper

Transport Theory for Energetic Alpha Particles and Superbananas in Tokamak Fusion Reactors with Broken Symmetry

K.-C. Shaing¹, M. Schlutt¹

¹University of Wisconsin-Madison, Madison, WI, USA

Corresponding Author: K.-C. Shaing, kshaing@wisc.edu

Error fields or magnetohydrodynamic (MHD) activities break toroidal symmetry in real tokamak fusion reactors, e.g., ITER. It has been shown in a comprehensive theory for neoclassical toroidal plasma viscosity for tokamaks that broken symmetry enhances particle, momentum, and energy transport. The enhanced energy transport increases with increasing energy. Because fusion-born alpha particles have energy significantly higher than that of fuel ions, the enhanced energy loss for alpha particles can be an issue for reactors if their energy transport loss rate is faster than the slowing down rate. In that case, the fusion energy gain factor *Q* will be significantly impacted. To quantify the tolerable magnitude for the error fields or MHD activities, transport theory for energetic alpha particles is developed. The theory is a generalization of the theory for neoclassical toroidal plasma viscosity. The superbanana plateau and superbanana regimes are the most relevant regimes for fusion-born alpha particles. The transport theory for energetic alpha particles developed is extended to the limit where the slowing down operator dominates and to allow for the finite value of the radial electric field.

Simulation Study of a New Kind of Energetic Particle Driven Geodesic Acoustic Mode

H. Wang¹, Y. Todo¹, and M. Osakabe¹

¹National Institute for Fusion Science, Toki, Japan

Corresponding Author: H. Wang, wanghao@nifs.ac.jp

A new kind of energetic particle driven geodesic acoustic mode (EGAM), which has weak bulk plasma temperature dependence of frequency, has been found in the Large Helical Device (LHD) experiments. In this work, the new kind of EGAM is investigated with a hybrid simulation code for energetic particles and magnetohydrodynamics (MHD). It is demonstrated that the new EGAM in the simulation results has weak bulk plasma temperature dependence of frequency, which is in contrast to the traditional EGAM whose frequency is proportional to the square root of bulk plasma temperature. Three conditions are found to be important for the transition from the traditional EGAM to the new EGAM: 1) energetic particle pressure substantially higher than the bulk plasma pressure, 2) charge exchange time (τ_{cx}) sufficiently shorter than the slowing down time (τ_s) to create a bump-on-tail type distribution, and 3) bulk plasma density is low enough. The energetic-particle distribution function is characterized by the $\tau_s = 8$ s and $\tau_{cx} < 1$ s. The energetic ion inertia term is added into the MHD momentum equation to simulate with energetic particle density comparable to the bulk plasma density. In addition, a Gaussian-type pitch angle distribution is assumed for the energetic ions. Linear growth properties of the new EGAM are investigated. It is found that the new EGAM frequency increases as the central value of the Gaussian pitch angle distribution decreases, where smaller pitch angle variable corresponds to higher parallel velocity and higher transit frequency. This indicates that the frequency of new EGAM is significantly affected by the energetic particle transit frequency, and the new EGAM is a kind of energetic particle mode (EPM) whose frequency is determined by the energetic particles. Furthermore, the frequency depends on energetic particle β value (β_h) and τ_{cx} . Growth rate of new EGAM increases as β_h increases similarly with other energetic particle driven instabilities, but the frequency increases as β_h increases. For higher β_h , the effect of energetic particles is enhanced to make the frequency closer to the energetic-particle transit frequency. Moreover, shorter τ_{cx} causes higher growth rate and frequency, because more particles exist in the high-energy region of phase space.



Paper

Nonlinear and Toroidal Mode Coupling Effects on m = 1, n = 1Instabilities

L. Sugiyama¹, L. F. Delgado-Aparicio²

¹Massachusetts Institute of Technology, Cambridge, MA, USA ²Princeton Plasma Physics Laboratory, Princeton, NJ, USA

Corresponding Author: L. Sugiyama, sugiyama@mit.edu

Instabilities with poloidal and toroidal mode numbers m/n = 1/1 remain an important concern for fusion in toroidal plasmas. Sawtooth crashes can periodically reduce the central plasma pressure and fusion rate or trigger more dangerous instabilities. Recent experimental results [1–3] have identified new types of 1/1 modes around and inside the q = 1 magnetic surface. Nonlinear full MHD numerical simulations with M3D and their analysis [1, 2, 4, 5] demonstrate that these modes are dynamic and strongly influenced by toroidal and nonlinear mode coupling, effects that have been ignored in most nonlinear theories. As in experiment, multiple 1/1 structures can appear simultaneously around and inside q = 1. They include long-lived 1/1 helical density concentrations or "snakes" and a variety of internal kink like modes. Background plasma toroidal rotation is important; 1/1 modes tend to rotate coherently with the plasma. Some snakes, such as those due to heavy impurity ions, can form around q = 1 without a magnetic island. The states tend to minimize the free energy, since the 1/1 helical temperature develops opposite sign to the helical density, reducing the non-axisymmetric pressure. Snakes can coexist with and partially stabilize periodic sawtooth crashes inside q < 1.

At low resistivity, the 1/1 resistive internal kink and sawtooth crash are shaped by terms in the momentum balance that are higher order in inverse aspect ratio, even at small $r_1/R_o = 1/10$. The narrow Sweet-arker-like reconnection layer of reduced MHD rarely develops. Instead, a fast crash phase driven by toroidal nonlinearity, enhanced by these terms, matches experimental crash times and the observed temperature redistribution. The crash does not follow the Kadomtsev sawtooth model because the density is not tightly tied to the magnetic field lines. The higher order terms and mode coupling can affect other instabilities, such as m > 1 magnetic islands and plasma edge instabilities.

Work supported by the US DOE Office of Fusion Energy Sciences and SciDAC programs.

References

- [1] L. Delgado-Aparicio, L. Sugiyama, et al., Phys. Rev. Letters 110, (2013) 65006.
- [2] L. Delgado-Aparicio, L. Sugiyama, et al., Nucl. Fusion 53, (2013) 043019.
- [3] L. Delgado-Aparicio, et al., submitted to Phys. Rev. Letters (2014).
- [4] L.E. Sugiyama, Phys. Plasmas 20, 032504 (2013).
- [5] L.E. Sugiyama, Phys. Plasmas, to appear (2014).



TH/P1-14

Modelling of Pulsed and Steady-State DEMO Scenarios

G. Giruzzi¹, J.-F. Artaud¹, I. Ivanova-Stanik², R. Kemp³, R. Zagorski², M. Baruzzo³, T. Bolzonella⁴, E. Fable⁵, L. Garzotti³, D. King³, R. Stankiewicz², W. Stepniewski², P. Vincenzi⁴, and D. Ward³

¹CEA-IRFM, Saint Paul lez Durance, France
 ²Institute of Plasma Physics and Laser Microfusion, Warsaw, Poland
 ³JET-EFDA, Culham Science Centre, Abingdon, UK
 ⁴Consorzio RFX, Associazione Euratom-ENEA sulla Fusione, Padova, Italy
 ⁵Max-Planck-Institut für Plasmaphysik, Garching, Germany

Corresponding Author: G. Giruzzi, gerardo.giruzzi@cea.fr

An intensive programme has been started in the EU, aiming at a more and more refined selection of the DEMO design. The general strategy adopted consists in developing two DEMO concepts in parallel: a pulsed tokamak, characterised by rather conventional physics and technology assumptions (DEMO1) and a steady-state tokamak, with moderately advanced physics and technology assumptions (DEMO2). The physics assessment part of this programme involves three main steps: i) the analysis of the general physics guidelines of a tokamak DEMO; ii) the search for optimum working points, performed by means of systems codes, i.e., 0-D codes combining both physics and technology constraints; iii) space and time dependent simulations of plasma scenarios, performed by means of integrated modelling codes with various levels of assumptions. In this last area of work, a coordinated effort has been undertaken at the EU level, as an EFDA Task Agreement during 2012 and 2013. The general goal of this Task was the analysis of working points produced by the systems code PROCESS for both DEMO1 and DEMO2 by means of various integrated modelling codes. Iterations between systems codes and scenario modelling should eventually converge to the definition of optimum working points that are consistent with the physics guidelines. The main results of this work on scenario modelling are reported here. The computational tools used for these studies are:

- The 0.5-D integrated modelling code METIS,
- The coupled core-edge code COREDIV,
- The 1.5-D integrated modelling codes ASTRA, JINTRAC and CRONOS.

Starting from the 0-D outputs of the PROCESS code for both DEMO1 and DEMO2 working points, the following steps have been performed:

- test of the consistency of the PROCESS working points by exploratory runs of METIS. Iterations with PROCESS in order to improve the working points,
- assessment of density and temperature profiles consistent with the reference working points and with first-principle particle transport models (TGLF, GLF23), by ASTRA,
- assessment of impurity and radiation profiles consistent with the reference working points and with suitable impurity transport assumptions by COREDIV,
- global scenario assessment by 1.5-D simulations with JINTRAC and CRONOS,
- sensitivity analysis for variations of selected plasma and machine parameters and of transport models (by METIS, ASTRA, COREDIV).



Paper

On Anomalous Dissipation and Relaxation in ELMs

R. Singh^{1,2}, P. H. Diamond^{1,3}, P. Xi⁴, and X. Xu⁵

 ¹National Fusion Research Institute, Daejeon, Korea, Republic of ²Institute for Plasma Research, Bhat, Gandhinagar, India ³University of California San Diego, CA, USA ⁴Peking University, Beijing, China ⁵Lawrence Livermore National Laboratory, Livermore, CA, USA

Corresponding Author: R. Singh, rsingh129@yahoo.co.in

We present a new dynamical model of pedestal ELM phenomena based upon the multi-scale interaction between low-n MHD ballooning mode and short scale ETG turbulence. ELM dynamics are determined by the few basics process results from multi scale interaction. These includes: generation of hyper resistivity in coupled ballooning mode — ETG turbulence; excitation of hyper resistive BM near ideal MHD threshold; regulation of via feedback loop between hyper resistive and ETG mode; formation of steep current and pressure gradients between primary resonances by process of gradient pinching. It is argued that gradient pinching, which occurs as primary modes grow, will destabilize dissipative convective cells throughout the pedestal. In particular, these cells will be driven in the region between the primary helicity. This ensemble of BMs and dissipative BMs will result in fast relaxation throughout the region of the pedestal.

Comparison of Simulated and Experimental Temperature, Density and Toroidal Rotation Profiles in Tokamak Plasmas

T. Rafiq¹, A. Kritz¹, A. Pankin², X. Yuan³, G. M. Staebler⁴, and R. Budny⁵

¹Lehigh University, Bethlehem, PA, USA
 ²Tech-X Corporation, Colorado, USA
 ³Princeton Plasma Physics Laboratory, Princeton, NJ, USA
 ⁴General Atomics, San Diego, CA, USA
 ⁵Princeton University, Princeton, NJ, USA

Corresponding Author: T. Rafiq, rafiq@lehigh.edu

The predictive TRANSPort and integrated modeling code, PTRANSP, is used to compute temperature, electron density, plasma current density, toroidal rotation velocity and radial electric field profiles. The predictive TRANSPort and integrated modeling code, PTRANSP, is used to compute temperature, electron density, plasma current density, toroidal rotation velocity and radial electric field profiles. The anomalous transport model, the Multi-Mode anomalous transport model, MMM7.1 [1], or the Trapped Gyro-Landau Fluid model, TGLF [2, 3], is used along with the new numerical transport solver, PT-SOLVER [4], in carrying out the simulations. PT-SOLVER is a modular, parallel, and multi-regional solver particularly suited for stiff turbulent anomalous transport models such as MMM7.1 and TGLF. The MMM7.1 and TGLF models are used to compute the anomalous transport driven by the electron and ion temperature gradient modes, trapped electron mode, and kinetic and resistive ballooning modes. The neoclassical transport is calculated using the Chang-Hinton model. Neutral beam heating and current drive are obtained using the NTCC NUBEAM module and ion cyclotron heating and current drive are obtained using the full wave TORIC module. The evolution of the current density and magnetic-q profiles is computed by advancing the magnetic diffusion equation. The self-consistent evolution of the equilibrium is computed using the toroidal equilibrium code TEQ. The results are presented for a variety of discharges in order to illustrate the extent to which the MMM7.1 and TGLF transport models yield profiles that are consistent with experimental tokamak data. The comparison is quantified by calculating the RMS deviations and Offsets, and the plasma parameter dependencies of the anomalous transport resulting from the use of MMM7.1 and TGLF models are illustrated.

This research is supported by the U.S. Department of Energy.

References

[1] T. Rafiq, A.H. Kritz, J. Weiland, A.Y. Pankin, L. Luo, Phys. Plasmas 20, 032506 (2013).

[2] G.M. Staebler, J.E. Kinsey, and R.E. Waltz, Phys. Plasmas 14, 055909 (2007).

[3] J.E. Kinsey, G.M. Staebler, and R.E. Waltz, Phys. Plasmas 15, 055908 (2008).

[4] R.V. Budny, X. Yuan, S. Jardin, *et al.*, 24th IAEA Fusion Energy Conference (FEC2012), San Diego, USA (2012).



Paper

A Flute Instability under the $E \times B$ Shear Flow in an Open System

I. Katanuma¹, S. Kato¹, Y. Okuyama¹, S. Sato¹, and R. Kubota¹

¹University of Tsukuba, Tsukuba, Ibaraki, Japan

Corresponding Author: I. Katanuma, katanuma@prc.tsukuba.ac.jp

A flute mode is the most dangerous instability in an open system such as the GAMMA10 tandem mirror. So how to stabilize the flute instability is an important problem. This paper studies the stabilizing effects of the $E \times B$ shear flow on a flute instability in the Cartesian geometry by the particle simulation and in the GAMMA10 magnetic field by the reduced MHD simulation. The particle 💾 simulation uses the (2 and 1/2) dimensional electrostatic implicit code with 128×128 meshes. Ions (electrons) are distributed to have the step functional density profile in x and the ions (electrons) flow in the y-direction with the $E \times B$ drift shear as an initial condition. The gravitational acceleration force g is applied in the x-direction. It was found that the flute mode was always unstable to the step functional density profile in x, where conducting boundary condition in x and the periodic boundary condition in y were adopted. The shear flow can excite the Kelvin-Helmholtz (K-H) instability which is stable in the uniform shear flow. A flute instability was transformed into a K-H instability after linearly growing phase. Whether the system is unstable to a flute mode depends on whether the excited K-H mode has an enough power of collapsing the system. It was newly found the suppression condition of plasma collapse (or the stability condition of secondary instability) with discontinuous density step under the uniform shear flow. The flute instability under the shear flow in GAMMA10 was investigated by using the reduced MHD code. Here the centrifugal acceleration of ions resulting from a magnetic field line curvature is included in the radial dependence of magnetic field line specific volume in the code. The shear flow is inputted initially by the equilibrium dynamic plasma vorticity and the resultant electrostatic potential. The reduced MHD simulation adopts the smooth radial pressure profile as an initial condition with uniform azimuthal shear flow. It was found that the linear growth rate of a flute instability was decreased by the $E \times B$ shear flow, so that the linear stability analysis was applicable in the smooth pressure radial profile. The reduced MHD simulation found that the flute instability was stabilized by the $E \times B$ shear flow in the linear phase. So it was newly determined the stability condition of the flute instability by the $E \times B$ uniform shear flow in GAMMA10.



Analysis of Plasma Behavior in the Localized Non-Axisymmetric B Region of the GAMMA 10 Tandem Mirror

M. K. Islam¹, Y. Nakashima², and K. Yatsu²

¹Bangladesh Atomic Energy Commission, Bangladesh ²University of Tsukuba, Tsukuba, Ibaraki, Japan

Corresponding Author: M. K. Islam, khairulislam@yahoo.com

Ion current in ion drift direction as well as the plasma shift in that direction in the localized non-axisymmetric magnetic field region of the anchor cell of the GAMMA 10 tandem mirror were measured. In addition, electron current perpendicular to the ion drift direction was found in this region. To understand these plasma behaviors, relevant kinetic properties of plasma particles are analyzed numerically. Numerical analysis indicates that the ion drift due to the nonaxisymmetric magnetic field and electron displacement due to small angle Coulomb scattering during passing through drifted ions are the possible candidates of the observed plasma phenomenon.



Paper

The First Lower Hybrid Current Drive Experiments in the Spherical Tokamak Globus-M

V. Dyachenko¹, E. Gusakov¹, M. Irzak¹, A. Saveliev¹, V. Gusev¹, Y. Petrov¹, O. Shcherbinin¹, V. Varfolomeev¹, N. Khromov¹, S. Khitrov¹, A. Voronin¹, and N. Sakharov¹

¹Ioffe Physical-Technical Institute of the Russian Academy of Science, St. Petersburg, Russian Federation Corresponding Author: V. Dyachenko, v.dyachenko@mail.ioffe.ru

The development of quasi-stationary methods of non-inductive current drive in plasmas of spherical tokamaks is extremely important for their using in thermonuclear devices. Specific properties of spherical tokamaks provide the possibilities the current drive by the waves of intermediate frequency range slowed down in poloidal direction. This approach, developed theoretically in the Ioffe Physical-Technical Institute and described in [1], is used now in LHCD experiments on the low aspect ratio tokamak Globus-M (R = 0.36 m, $a_0 = 0.24$ m, $B_0 = 0.4$ T, $I_p = 0.2$ MA, elongation ~ 1.8, triangularity (0.4–0.5), $n_0 = (3-5) \times 10^{19}$ m⁻³, $n_b = 1 \times 10^{17}$ m⁻³, $T_{e0} = 400$ –800 eV). The grill consists of 10 waveguides with inner cross-section 90 × 10 mm. The waveguides are oriented so that the electric RF fields on the fundamental waveguide mode TE₁₀ were co-directed with poloidal direction in the tokamak. Numerical simulation confirms the quite good efficiency of current drive. The first experimental results are presented for input power level of 100 kW (2.45 GHz). The value of generated current is estimated by the drop of loop voltage as 20–40 kA.

References

[1] E.Z. Gusakov, V.V. Dyachenko et al., PPCF, 52, (2010), 075018.



Integrated Modeling of the Globus-M Tokamak Plasma

I. Senichenkov¹, E. Kaveeva¹, A. Gogoleva¹, E. Vekshina¹, G. Zadvitskiy¹, P. Molchanov¹, V. Rozhansky¹, S. Voskoboinikov¹, N. Khromov², S. Lepikhov², and V. Gusev²

¹St. Petersburg State Polytechnical University, St. Petersburg, Russian Federation ²Ioffe Physical-Technical Institute of the Russian Academy of Science, St. Petersburg, Russian Federation Corresponding Author: I. Senichenkov, i.senichenkov@spbstu.ru

In the present paper the results of integrated modeling of Globus-M tokamak plasma with the help of recently coupled core transport code ASTRA and edge transport code B2SOLPS are presented. In the modeling taken into account are the neoclassical transport, auxiliary heating and current drive by the NBI, 2D drift fluxes, currents and electric field in the edge plasma in a real geometry of magnetic flux surfaces and first wall constructions of a spherical tokamak. It is demonstrated that the modeling results are in a satisfactory agreement with laser and probe measurements and fast neutral particle analyzer and neutron analyzer signals for various plasma current values both in ohmically heated and NBI-heated discharges. The dependence of the scrape-off layer structure and the heat loads to the divertor targets on the plasma current and the discharge power is investigated. It is found that the heat flux decay length agrees with a predictions of the scaling [1] stemming from a large multi-machine experimental database. Thus this scaling passed through the tests versus experimental data from a small spherical tokamak with small magnetic field, plasma current and power, and the database is expanded correspondingly.

References

[1] T. Eich et al., Phys. Rev. Lett., 107, 215001 (2011).

Preprint

Feedback of a Neoclassical Tearing Mode on Drift Wave - Zonal Flow Turbulence

M. Leconte¹, P. H. Diamond^{1,2}, and D.-K. Oh¹

¹National Fusion Research Institute, Daejeon, Korea, Republic of ²University of California San Diego, CA, USA

Corresponding Author: M. Leconte, mleconte@nfri.re.kr

We study the feedback loop of a spontaneous magnetic perturbation (neoclassical tearing mode) on a background of drift wave — Zonal Flows, in the framework of a 1D predator-prey model for the evolution of turbulence intensity I(x,t), Zonal Flow energy U(x,t), electron temperature gradient T(x) and island-width. A modified Rutherford equation describes the magnetic island dynamics. The magnetic island is driven by the neoclassical bootstrap current, and acts to damp turbulence-driven Zonal Flows, while turbulence also affects the island-chain evolution by flattening the temperature profile, thus depleting the bootstrap current.

A critical issue in fusion devices is what determines the threshold island width, set by a competition between parallel heat conduction along tilted field lines v.s. perpendicular diffusion across field lines. Since perpendicular heat diffusion is mostly turbulent, the threshold island width is determined by turbulence. As turbulence is regulated by Zonal Flows, this threshold is ultimately tied to Zonal Flow intensity and thus Zonal Flow damping. As the island grows, Zonal Flows are strongly (but locally) damped and turbulence remains un-quenched in the vicinity of the island. In effect, they are two plasma regions divided by the island separatrix: Outside of the magnetic island, the plasma is ZF-dominated, whereas inside the island, the plasma is pushed back to a saturated turbulence regime (L-mode-like regime). Turbulence spreading across the island-separatrix occurs at quasi-periodic intervals and triggers temperature profile collapse, due to turbulent heat diffusion. Our results suggest that the threshold island-width is modulated by the microturbulence at the Limit-Cycle Oscillation frequency of the predator-prey system. Hence, the threshold island-width is ultimately set by ZF damping.

TH/P2-1

The Combining Effect of the Inductive Electric Field and the Lower Hybrid Waves on the Impurity Ions Toroidal Rotation in the Lower Hybrid Current Drive Tokamak Plasmas

C. Pan¹, S. Wang²

¹Institute of Plasma Physics, Chinese Academy of Sciences, Hefei, China ²University of Science and Technology, Anhui, China

Corresponding Author: C. Pan, ckpan@ipp.ac.cn

Plasma rotation in tokamaks driven by the lower-hybrid-waves (LHW) was firstly reported by the Alcator C-Mod team and also observed in the EAST tokamaks. The LHW injection can induce both coand counter-current directed changes in toroidal rotation. The direct momentum absorption of the LHW induces the impurity ions to rotate in the counter-current direction. The inductive electric field decreases due to the drop of the loop voltage during the lower hybrid current drive. The inductive electric field in tokamaks has considerable effect on the impurity ions rotation and causes the impurity ions to rotate in the counter-current direction. The rotation and causes the impurity ions to rotate in the counter-current direction. The rotation of the impurity ions is usually measured in the experiments. The resulting rotation velocity of the impurity ions should be determined by the combining effect of the inductive electric field and the LHW. For the higher current case, the effect of the inductive electric field is negligible. For the lower current case, the effect of the inductive electric field can not be neglected.



ELM Pacing with Periodic Plasma Column Displacements

A. Y. Aydemir¹, H. Han¹, J. Kim¹, J. Y. Kim¹, O. J. Kwon², H. Lee¹, B. Park¹, and J. Seol¹

¹National Fusion Research Institute, Daejeon, Korea, Republic of ²Department of Physics, Daegu University, Gyeongbuk, Korea, Republic of

Corresponding Author: A. Y. Aydemir, aydemir@nfri.re.kr

Although ELM control by RMP's has been successfully demonstrated on a number of tokamaks, whether this method will be successful in all anticipated ITER operational scenarios is not clear. Thus, there is a recognized need to investigate other approaches to reducing transient heat and particles loads due to ELM's on PFC's in ITER. A low-cost technique that may not require dedicated equipment is the ELM-pacing with periodic vertical displacement (or "jogging") of the plasma. Since its first demonstration on the TCV tokamak, vertical jogging has been shown to be an effective mitigation scheme on ASDEX, JET, and other devices. More recently, KSTAR has demonstrated ELM control and mitigation using a number of different techniques, including vertical jogs of the plasma.

However, a general understanding of the physics consistent with all experimental observations is still missing. On TCV, ELM triggering by vertical jogs is attributed to increased edge currents induced by the plasma displacement away from the X-point. On ASDEX, however, ELM's are triggered when the plasma is moving towards the X-point, with a decrease in the edge currents. The peeling-ballooning stability boundary sensitively depends on the parallel current and pressure profiles at the edge, both of which are affected by plasma displacements. In particular, the current is modified both inductively and through induced changes in the pressure gradient. The inductive component seems to play a dominant role in the TCV results, consistent with the fast time-scale of the "kicks." Results from other tokamaks are in qualitative agreement with the assumption that the changes in the pressure gradient, either directly (at the ballooning boundary) or indirectly through its effect on the bootstrap current (at the peeling boundary), play a more significant role in triggering ELM's. A more quantitative comparison with experimental results and possible implications of this method for ELM-mitigation in ITER await detailed stability calculations.



TH/P2-5

Frequency and Damping Rate of the Geodesic Acoustic Mode in **Collisional Plasmas**

Z. Gao¹, Y. Li¹

¹Tsinghua University, Beijing, China

Corresponding Author: Z. Gao, gaozhe@tsinghua.edu.cn

The frequency and damping rate are two most fundamental properties of the GAM. The collisional effect could be important in the plasma edge. In our work [1], where a number conservation Krook collisional operator was used in the gyrokinetic model, it was found that the damping rate of the GAM is non-monotonic as the collision rate increases. At low ion collision rate the damping rate increases linearly with the collision rate; while as the ion collision rate is higher than v_{ti}/R , the damping rate decays with an increasing collision rate. At the same time, as the collision rate increases, the GAM frequency decreases. However, it is noted that the number-conserving Krook collision operator is rather approximate. It is of interest to investigate the eigen-frequency of the GAM using more accurate operators and thereby find which properties of a collision operator are important for the dynamics of the GAM.

In this work four different ion collision operators, including (a) a Krook operator with number conservation only, (b) a Krook operator with number and energy conservation, (c) a Lorentz operator which conserves number and energy automatically and (d) a Lorentz operator with an energy-dependent collision rate, are employed in a drift-kinetic model to investigate the collisional effect on the GAM frequency and damping rate. Comparison between different collision operators is performed as well. For operator (a), the result is the same as previously. For operator (b), the damping rate is only one ninth of that from (a). For operator (c), the damping rate approximates to that from (a) at low collisionality but give a lower damping rate than that from (b) and (a) at high collisionality. The result from operator (d) is close to that from (c). Due to finite collisional damping, the GAM frequency decreases. At very high collisionality, the GAM frequency approaches to v_{ti}/R for operator (a) but to $\sqrt{(5/3)v_{ti}/R}$ for the other three operators. The result shows that both density and energy conservation of the collision operator are important for determining the GAM frequency and damping rate. The absence of energy conservation induces the overestimation of collisional effect at high collisionality.

Work supported by NSFC, under Grant Nos. 10990214, 11075092, 11261140327 and 11325524, MOST of China, under Grant No. 2013GB112001.

References

[1] Z. Gao, Phys. Plasmas 20, 032501 (2013).



Study of Nonlinear Fast Particle Transport and Losses in the Presence of Alfvén Waves

M. Schneller¹, P. Lauber¹, W. Xin¹, S. Briguglio², G. Benedikt¹, M. García-Muñoz³, M. Weiland¹, and R. Bilato¹

> ¹Max-Planck-Institut für Plasmaphysik, Garching, Germany ²Associazione EURATOM-ENEA Unitá Tecnica Fusione, Frascati, Italy ³University of Seville, Spain

Corresponding Author: M. Schneller, mirjam@ipp.mpg.de

A nonlinear hybrid model is used to study energetic particle transport and losses in realistic CAMAK — particularly ASDEX Upgrade — multi-mode scenarios. The second data and the scenarios are also be a second data and the scenarios are also b TOKAMAK — particularly ASDEX Upgrade — multi-mode scenarios. The model consists of the vacuum-extended version of the drift kinetic HAGIS code. As crucial new elements of a realistic scenario, the perturbation structures, frequencies and damping rates are taken as obtained from the gyrokinetic eigenvalue solver LIGKA.

In the view of ITER, where in certain scenarios, a "sea" of small-amplitude perturbations is likely, realistic multi-mode simulations will be carried out in the near-stability regime. This requires the use of the newly implemented non-local damping via accounting for a parallel electric field. The crucial question is, if the interaction between the sea of perturbations with the EPs will drive linearly stable or weakly unstable modes such that particle losses occur in a domino effect. Which of the modes are driven unstable in the simulation and their amplitudes can then be compared with the dominant modes measured in present-day experiments such as ASDEX Upgrade.

Moving further above the stability threshold, it is not only important to account for the correct damping mechanisms. Also, the radial wave structure is very sensitive to the EP distribution function and is expected to evolve, as the distribution function changes. Although the nonlinear wave-particle interaction is calculated self-consistently within the HAGIS-LIGKA model, at the present status, other nonlinearities such as the evolution of wave structure and damping rate are not included yet. Before extending the model in this direction, the expected effect of the radial wave structure evolution is investigated, both with a numerical approach as well as with the help of experimental observation. Concerning the numerical study, HAGIS-LIGKA results are compared to those of a different hybrid code, HMGC, which already contains wave structure evolution. For that comparison, a new phase space diagnostic technique is developed for both codes, the so called Hamiltonian Mapping Technique. From the experimental side, next to Alfvénic modes, fishbones offer a good opportunity to model frequency and amplitude evolution according to experimental observation and compare the occurring transport in phase space.

Can Gyrokinetics Really Describe Transport in L-Mode Core Plasmas?

F. Jenko¹, J. Citrin², T. Goerler¹, D. Told¹, J. Abiteboul¹, A. Banon Navarro¹, C. Bourdelle³, R. Bravenec⁴, F. Casson⁵, H. Doerk¹, R. Dumont³, E. Fable¹, J. Garcia³, W. Haverkort², D. Hogeweij², N. Howard⁶, T. Johnson⁷, P. Mantica⁸, M. J. Pueschel⁹, and A. White⁶

¹Max-Planck-Institut für Plasmaphysik, Garching, Germany
 ²FOM Institute DIFFER, Association EURATOM-FOM, Nieuwegein, The Netherlands
 ³CEA-IRFM, Saint Paul lez Durance, France
 ⁴Fourth State Research, Austin, TX, USA
 ⁵CCFE Fusion Association, Culham Science Centre, Abingdon, UK
 ⁶Massachusetts Institute of Technology, Cambridge, MA, USA

⁷KTH Royal Institute of Technology, Stockholm, Sweden

⁸Associazione EURATOM-ENEA Unitá Tecnica Fusione, Frascati, Italy

⁹University of Wisconsin-Madison, Madison, WI, USA

Corresponding Author: F. Jenko, fsj@ipp.mpg.de

The common view in fusion theory is that nonlinear gyrokinetics constitutes a reliable firstprinciples approach to describe turbulent transport in MCF devices. Surprisingly, however, two recent findings challenged this notion. First, the experimental ion heat fluxes in the outer core of certain DIII-D L-mode discharges were underpredicted by GK simulations by almost an order of magnitude. This finding has been dubbed the "shortfall problem" and has triggered extensive theoretical efforts on an international level. Second, a careful analysis of some L-mode discharges in the JET tokamak revealed a significant reduction of ion temperature profile stiffness in the presence of strong NBI [1]. This was first attributed to a combination of high toroidal flow shear and low magnetic shear. However, nonlinear GK simulations failed to confirm this suspicion, overpredicting the observed fluxes by up to an order of magnitude. This finding could be called the "excess problem" and is as severe as the shortfall problem described above. The main goal of the present contribution is to revisit both of these problems and substantiate or refute them. At stake is the plasma theory community's confidence to devise a predictive transport capability for devices like ITER or DEMO on the basis of nonlinear GK. Via careful studies with the GENE code (using about 30 million CPUh), both of these challenges could be met successfully. While the transport levels in outer-core L-mode discharges of DIII-D, C-Mod, and ASDEX Upgrade [2] can be reproduced within the experimental error bars, the observed ion temperature stiffness reduction in JET can be explained in terms of nonlinear electromagnetic effects in the presence of fast ions [3]. Thus, a number of ideas about possible elements missing in the present theoretical description or even a possible breakdown of GK are identified as premature. Meanwhile, these studies highlight the fact that the search for adequate minimal models of turbulent plasma transport under various experimental circumstances is highly non-trivial.

This work was supported by EURATOM and carried out within the framework of the European Fusion Development Agreement. The views and opinions expressed herein do not necessarily reflect those of the European Commission.

References

M. Mantica, PRL 107, 135004 (2011).
 D. Told, PoP 20, 122312 (2013).
 J. Citrin, PRL 111, 155001 (2013).



A Reduced Model of ELM Mitigation by SMBI and Pellet Injection

T. Rhee¹, J. M. Kwon¹, P. H. Diamond^{1,2}, S.-H. Hahn¹, and S. Yi¹

¹National Fusion Research Institute, Daejeon, Korea, Republic of ²University of California San Diego, CA, USA

Corresponding Author: T. Rhee, trhee@nfri.re.kr

The importance and urgency of ELM control for ITER urge to develop tractable reduced model to understand ELM mitigation experiments because first principle models of ELMs have not been developed due to terrific complexities of ELM-related physics. In this work, we present such an effort particularly focused on ELM mitigation experiment by supersonic molecular beam injection (SMBI) and pellet injection (PI). We employs cellular automata model (CA) including key physical elements for transport (i.e., turbulent transport, its suppression by diamagnetic shear flow, and MHD limit) in the H-mode pedestal and expand it to include the SMBI and PI. A finding is that extended CA model can capture many essential features of the experiments, and both SMBI and pellet injection can be seen as different regions of a continuous spectrum of experiments with varying amounts and penetration depths of injected material. Shallow and small injection (SMBI) can mitigate large ELMs by triggering more frequent, yet smaller scale ejection events. With larger and deeper deposition of material, injection forces the formation of pedestal pressure profiles which trigger large ELMs. Therefore, repetitive deep injection emerges as ELM pacing.

Nonlinear Particle Simulation of Radio Frequency Waves in Fusion Plasmas

A. Kuley¹, J. Bao², Z. Wang¹, Z. Lin¹, Z. Lu³, and F. Wessel⁴

¹University of California Irvine, CA, USA ²Peking University, Beijing, China ³University of California San Diego, CA, USA ⁴Trialpha Energy, Foothill Ranch, California, USA

Corresponding Author: A. Kuley, akuley@uci.edu

Nonlinear global particle in cell simulation model in toroidal geometry has been developed for the first time to provide a first principle tool to study the radio frequency (RF) nonlinear interactions with plasmas. In this model, ions are considered as fully kinetic ion (FKi) particles using the Vlasov equation and electrons are treated as guiding centers using the drift kinetic (DKe) equation. FKi/DKe is suitable for the intermediate frequency range, between electron and ion cyclotron frequencies. This model has been successfully implemented in the gyrokinetic toroidal code (GTC) using realistic toroidal geometry with real electron-to-ion mass ratio. To verify this simulation model, we first use an artificial antenna to verify the linear mode structure and frequencies of electrostatic normal modes including ion plasma oscillation, ion Bernstein wave, lower hybrid wave, and electromagnetic modes and fast wave and slow wave in the cylindrical geometry. We then verify the linear propagation of lower hybrid waves in cylindrical and toroidal geometry. Because of the poloidal symmetry in the cylindrical geometry, the wave packet forms a standing wave in the radial direction. However, in the toroidal geometry, the waves propagate as two counter propagating waves in the poloidal direction due to the poloidal asymmetry of the magnetic field. The wave packet propagates faster in high field side compare to the low field side. This feature has been verified by the Wentzel-Kramers-Brillouin (WKB) solution. The nonlinear GTC simulation of the lower hybrid wave shows that the amplitude of the electrostatic potential is oscillatory due to the trapping of resonant electrons by the electric field of the lower hybrid wave. The nonlinear bounce frequencies have been verified with the analytic results. For comparison, in linear simulation the lower hybrid wave decays exponentially due to linear Landau damping.

Preprint

Influence of Boundary Conditions on Turbulent Transport and Plasma Energy Confinement Time Evolution in Tokamaks with Additional Heating: Simulations for T-10 and T-15 Tokamaks

V. Pastukhov¹, A. Y. Dnestrovskij¹, D. Smirnov¹, and N. Chudin¹

¹National Research Centre "Kurchatov Institute", Moscow, Russian Federation Corresponding Author: V. Pastukhov, pastukhov_vp@nrcki.ru

Temporal evolution of anomalous transport and global plasma energy confinement time is studied Temporal evolution of anomalous transport and global plasma energy confinement time is studied in simulations of plasma turbulence in tokamaks with additional plasma heating. The simulations have shown that external boundary conditions with the specially chosen power dependence of best fluxes shown that external boundary conditions with the specially chosen power dependence of heat fluxes on the local time-dependent values of plasma density and temperatures at the boundary of plasma core with SOL region can provide the evolution of the plasma confinement time to the known steady state plasma confinement scalings. Such boundary conditions can be interpreted as the corresponding power scaling for an effective plasma confinement time in SOL. The first set of simulation runs were performed for conditions of experimental shots at T-10 tokamak using CONTRA-C code (cylindrical geometry). The second set of simulations were performed both for T-10 experimental shots and for expected T-15 conditions using transport code ASTRA with special turbulent block CONTRA-A (toroidal geometry with non-circular plasma cross-section). Both codes are based on adiabatically reduced MHD-like equations of turbulent convection.

Nonlocal Transport from Edge to Core in Tokamak Plasmas

N. Miyato¹, M. Yagi¹, A. Matsuyama¹, and T. Takizuka²

¹Japan Atomic Energy Agency, Naka, Japan ²Osaka University, Osaka, Japan

Corresponding Author: N. Miyato, miyato.naoaki@jaea.go.jp

A nonlocal response of plasma to edge density sources, which has been sometimes observed in toroidally magnetic confinement plasmas, is found in global fluid simulations. In the 4-field reduced MHD model, a toroidally-elongated particle source is applied in the edge region after saturation of the resistive ballooning mode turbulence is attained. The nonlocal transport appears at the location far from the edge source. The detailed process of the nonlocal transport is revealed for the first time. Both nonlinear and toroidal couplings between axisymmetric Fourier modes are responsible for the nonlocal transport. Especially (m, n) = (1, 0) and (-1, 0) modes play an essential role to produce the nonlocal transport, where m and n are poloidal and toroidal mode numbers, respectively. In the RMHD simulation only the resistive ballooning modes are unstable at the edge and no turbulence exists in the core region where the nonlocal response appears. The (1,0) pressure perturbation is an ingredient of the geodesic acoustic mode (GAM) oscillation of zonal flows (ZFs) and can be driven by drift wave turbulence such as ion temperature gradient (ITG) driven turbulence in toroidal plasmas. Therefore, it is interesting to investigate what happens in the nonlocal transport observed in the RMHD simulation if the ITG turbulence exists in the core. In order to study effects of edge density source on the ITG-ZF/GAM behavior, the global ITG turbulence code has been modified, in which the edge density source is implemented as a sink or cold pulse in the temperature equation. It is found in electrostatic ITG turbulence simulations that strong GAM oscillation is excited in an inner region than the sink location when the sink is imposed to simulate the cold pulse propagation. After investigating the above simulations in detail, we will perform simulations including both density source and temperature sink by extending the codes further.



L-P

Fishbone Modes in Plasmas with Dual Neutral Beam Injection Heating

H. He¹, J. Dong¹, K. Zhao¹, H. Jiang², and Z. He¹

¹Southwestern Institute of Physics, Chengdu, Sichuan, China ²Fujian University of Technology, China

Corresponding Author: H. He, hehd@swip.ac.cn

Neutral beam injection (NBI) is one of the important methods to heat plasmas in current tokamaks. However, fishbone instability induced by fast ions during NBI experiment is the main source for resulting in fast ion loss. Generally speaking, the density gradient of fast ions is the primary driving force to destabilize the fishbone modes. Therefore, it is possible to reduce the instability by eliminating the density gradient of the fast ions, employing dual neutral beam injection (DNBI) scheme in tokamak plasmas. The DNBI refers to two NBI lines heating plasma with one at the magnetic axis and the other (called off-axis NBI) at another radial position. With such tangential DNBI, a radial density profile of fast ions can be formed from superposition of dual Gaussian distributions. The dispersion equation for the fishbone instability is numerically solved for a density profile of fast ions of DNBI. A slowing down distribution with Gaussian pitch angle profile is used for each NBI. The dependences of the real frequency and growth rate of the fishbone modes on the parameters such as β of hot ions (ratio of fast ions pressure/magnetic pressure), Δ (the distance between the axis and deposition position one of the off-axis NBI) and χ (ratio of the on-axis NBI intensity and the off-axis one) are investigated in detail. The results show that the density distribution of fast ions from DNBI can bring about a stable window in the radial direction where the fishbone mode cannot be excited by fast ions. The width of the stable window increases linearly with radius increasing of magnetic flux surface of safety factor q = 1. Besides, the width of the stable window increases with decreasing of density profile index of fast ions and keeps constant for large enough density profile index. The growth rates of fishbone modes dramatically decrease with the ratio of DNBI intensity and the critical β values of fast ions increase with increasing of the ratio. The fishbone instabilities can be avoided with DNBI and may be an effective method to prevent fast ion loss resulted from fishbone modes.



Progress on Transport Modeling by Trapped Ion Resonance Driven Turbulence

Y. Kosuga¹, S. Itoh¹, P. H. Diamond^{2,3}, K. Itoh², and M. Lesur²

¹Institute for Applied Mechanics, Kyushu University, Kasuga, Japan ²National Fusion Research Institute, Daejeon, Korea, Republic of ³University of California San Diego, CA, USA

Corresponding Author: Y. Kosuga, kosuga@riam.kyushu-u.ac.jp

Corres Pr the col

Predictive modeling of turbulent transport is essential to the success of ITER and DEMO. Due to the collisionless nature of fusion plasmas, turbulence with strong wave-particle interaction — such as collisionless trapped electron or ion modes (CTEM/CTIM) or energetic particle (EP) modes can develop in fusion plasmas. However, transport caused by these turbulence cannot be described by the conventional quasilinear transport analysis. This is since the precession resonance allows a long correlation time between resonant trapped particles and fluctuations to produce a group of correlated resonant trapped particles, called granulations. In the presence of granulations, transport is not determined by quasilinear diffusion, but by Lenard-Balescu flux with Fokker-Planck drag. In this paper, we report progress on the modeling of turbulent transport caused by trapped ion granulations. In the first part of the work, we present application of transport caused by trapped ion granulations to the problem of toroidal momentum transport. In this part, we show that residual stress, which is a part of momentum flux that is not proportional to the velocity or velocity shear, can arise from momentum flux carried by trapped ion granulations. We discuss that this process can be viewed as a conversion of poloidal and toroidal momentum via trapped ion granulations. As an application to tokamak phenoemenology, we consider plasmas at L-H transiton, where poloidal $E \times B$ flows are accelerated. This acceleration can be converted to toroidal acceleration via the mechanism presented here. For typical parameters at the top of the pedestal of medium size tokamaks, we quantitatively find that this process can accelerate toroidal flows up to thermal Mach number ~ 0.1 . In the second part of the work, we discuss the feedback mechanism from macroscopic flows to microscopic turbulence with trapped ion granulations. We discuss extension of Biglari-Diamond-Terry mechanism of turbulence suppression by shear flows to the problem of turbulence with degree of freedom in velocity space, in order to account for the effect on trapped ion granulations. We show that energy dependent trapped ion precession enters decorrelation process, in addition to conventional $E \times B$ scattering and shearing.



MHD Instability Excited by Interplay between Resistive Wall Mode and Stable MHD Modes in Rotating Tokamak Plasmas

N. Aiba¹, M. Hirota², A. Matsuyama¹, J. Shiraishi¹, and A. Bierwage¹

¹Japan Atomic Energy Agency, Naka, Japan ²Tohoku University, Sendai, Japan

Corresponding Author: N. Aiba, aiba.nobuyuki@jaea.go.jp

A mechanism exciting magnetohydrodinamic (MHD) instabilities in rotating tokamak plasmas is found numerically for the first time. This mechanism is the interplay between a resistive wall mode (RWM) and a stable MHD mode. When a plasma has a discrete stable MHD eigenmode, the RWM can be destabilized when the plasma rotation frequency is close to the real frequency of the stable eigenmode. In a cylindrical plasma, such a destabilizing mechanism can be observed as the result of the interplay between RWM and a stable external kink mode. In a tokamak plasma, it is found that not only an external kink mode but also Alfvén eigenmodes can be the counterpart of this interplay. It is numerically demonstrated that this mechanism can overcome the continuum damping leading to the destabilization of RWM in a realistic tokamak plasma. These results indicate that understanding of the stable MHD modes is important for robust stabilization of RWM. The destabilization can be avoided by optimization of the safety factor profile. This optimization is indispensable in the design of steady state high- β tokamaks such as JT-60SA, DEMO and future tokamak reactors.

Toroidal Rotation Produced by Disruptions and ELMs

H. R. Strauss¹, R. Paccagnella², L. Sugiyama³, J. Breslau⁴, and S. Jardin⁴

¹HRS Fusion, West Orange, NJ, USA

²Consorzio RFX, Associazione Euratom-ENEA sulla Fusione, Padova, Italy ³Massachusetts Institute of Technology, Cambridge, MA, USA ⁴Princeton Plasma Physics Laboratory, Princeton, NJ, USA

Corresponding Author: H. R. Strauss, hank@hrsfusion.com

In several experiments, including JET [1], Alcator C-Mod [2], and NSTX [3], it was observed that disruptions were accompanied by toroidal rotation. There is a concern that there may be a resonance between rotating toroidal perturbations and the resonant frequencies of the ITER vacuum vessel, causing enhanced damage. We present MHD simulations with M3D [4] of ITER, JET, and DIII-D, as well as theory, demonstrating that asymmetric vertical displacement event (AVDE) disruptions and ELMs can produce toroidal rotation. Net toroidal rotation requires three conditions [5].

- 1 The poloidal magnetic field penetrates the wall, which is a condition that the plasma can transmit torque to the wall.
- 2 Rotation requires vertical asymmetry, which can be produced by a VDE. Simulations and theory indicate that the magnitude of the rotation is a stong function of VDE displacement.
- 3 Rotation requires MHD turbulence. In disruption simulations, the thermal quench and rotation generation occur at the same time, and are caused by toroidally varying MHD perturbations. The rotation persists into the current quench.

This work was supported in part by the US DOE, ITER, and F4E.

References

- [1] S. N. Gerasimov, et al., Proc. of EPS 37th Conference on Plasma Physics, Dublin, Ireland (2010).
- [2] R. S. Granetz, et al., Nucl. Fusion 36, 545 (1996).
- [3] S. P. Gerhardt, et al., Nucl. Fusion 52 063005 (2012).
- [4] W. Park, E. Belova, G. Y. Fu, X. Tang, H. R. Strauss, L. E. Sugiyama, Phys. Plasmas 6 1796 (1999).
- [5] H. Strauss, L. Sugiyama, R. Paccagnella, J. Breslau, S. Jardin, Nucl. Fusion, in press (2014).

Preprint

Off-Axis Current Drive with High Harmonic Fast Waves for DIII-D

R. Pinsker¹, R. Prater¹, C. Moeller¹, M. Porkolab², O. Meneghini³, and V. Vdovin⁴

¹General Atomics, San Diego, CA, USA ²Massachusetts Institute of Technology, Cambridge, MA, USA ³Oak Ridge National Laboratory, Oak Ridge, TN, USA ⁴National Research Centre "Kurchatov Institute", Moscow, Russian Federation

Corresponding Author: R. Pinsker, pinsker@fusion.gat.com

responding Author: R. Pinsker, pinsker@fusion.gat.com Modeling shows that fast waves at very high ion cyclotron harmonics (also called "whistlers" or "helicons") can drive current efficiently in the mid-radius region of a high- β tokamak plasma, as is required to sustain steady-state high performance discharges in a DEMO-like configuration. DIII-D has developed discharges with high electron β and high electron temperature so that full first-pass damping of the waves is expected to take place off-axis. We show that in a specific existing high- β DIII-D target discharge, 0.5 GHz fast waves at launched $n_{\parallel} \sim$ 3–4 would drive a noninductive current of 60 kA/MW at $\rho = 0.55$, where the electron density is $\sim 5 \times 10^{19}$ m⁻³ and the electron temperature is ~ 3 keV. With complete first-pass absorption, loss processes (mode conversion, far-field sheath formation, etc.) associated with weak single-pass damping are minimized. The calculated current drive efficiency is 2 to 4 times higher than that of off-axis neutral beams or electron cyclotron current drive using the present DIII-D systems. Strong, radially localized absorption on electrons can be obtained only for local values of β_e exceeding 1.8%. At lower values, the waves propagate to smaller minor radius before being absorbed. Varying the launched value of n_{\parallel} shows that the driven current hardly changes in either magnitude or in radial location in the range of $2.8 < n_{\parallel} < 4.2$, for reasons that are understood from examination of the ray data. We have identified an appropriate launching structure to excite a well-defined and toroidally directional wave spectrum — the traveling wave antenna known as the "comb-line". This structure permits the use of a large number of radiating elements in a phased array with feeds only at the ends of the wide, all-metallic antenna. The key parameter determining the necessary width of the array is the radial distance from the antenna surface to the location in the plasma edge where the rays begin to propagate. To determine this distance at the poloidal location of the proposed antenna, DIII-D will test a low-power prototype comb-line at that location to ascertain the needed width of the high-power antenna. We plan to perform the low power experiments in 2015 and proceed to experiments at the 1 MW level at 0.5 GHz in 2016.

This work was supported by the US Department of Energy under DE-FC02-04ER54698.



Gyrokinetic Simulation of Microturbulence in EAST Tokamak and DIII-D Tokamak

Y. Xiao¹, T. Zhang¹, and C. Zhao¹

¹Institute for Fusion Theory and Simulation, Zhejiang University, China

Corresponding Author: Y. Xiao, yxiao@zju.edu.cn

The new capabilities in the gyrokinetic simulation code GTC enable it to simulate the turbulent transport in real tokamak experiments. We apply these capabilities to simulate one ITG turbulence case for DIII-D tokamak and one TEM turbulence case for EAST tokamak with real experimental profiles and equilibrium magnetic field. For DIII-D case, the radial heat diffusivity profile simulated by GTC is highly consistent with that by GYRO. For the EAST case, we find that the collisional effect is very important in successfully explaining the low mode frequency and large wavelength for the electron coherent mode (ECM) observed in the EAST pedestal.

Fluid Simulation of Particle and Heat Fluxes during Burst of **ELMs on EAST and DIII-D**

T. Xia¹, X. Xu², G. Li¹, and M. E. Fenstermacher²

¹Institute of Plasma Physics, Chinese Academy of Sciences, Hefei, China ²Lawrence Livermore National Laboratory, Livermore, CA, USA

Corresponding Author: T. Xia, xiaty@ipp.ac.cn

In this paper we report the simulations of the evolution of the particle and heat flux during the burst of ELMs in realistic discharges on DIII-D and EAST tokamaks. A set of six-field two-fluid equations based on the Braginskii equations with non-ideal physics effects is found to simulate pedestal collapse under the BOUT++ framework [1]. In general studies with shifted-circular geometry, the analysis of radial transport coefficients indicates that the ELM size is mainly determined by the energy loss at the crash phase. The typical values for transport coefficients in the saturation phase after ELM crashes are $D_r \sim 200 \text{ m}^2/\text{s}$, $\chi_{ir} \sim \chi_{er} \sim 40 \text{ m}^2/\text{s}$. The DIII-D ELMy H-mode discharge #144382 is a lower single-null, small ELM crash event detected with multiple fast acquisition data chords in the pedestal, scrape-off layer (SOL) and divertor [2]. The measured density, temperatures and electric field profiles inside the separatrix are used in our simulation. The ELMs of this discharge is destabilized by the resistive-ballooning modes according to the linear analyzes. In order to consider the kinetic modification of parallel transport in SOL, the sheath limit of the flux limited expression are applied for the parallel thermal conduction. The energy loss during our simulation is around 18 kJ, which is close to the experiment measured value 17 kJ. The collapse width of the electron density profile is the same as the measurements. The peak amplitude of heat flux distributions on divertor targets in our simulation is 700 W/cm² at 0.28 ms after ELM crash, compared to the measured value 500 W/cm². The radial heat flux distributions indicate that this ELM is convective dominant. For EAST ELMy H-mode discharge #38300 [3], which is close to double null geometry, the measured profiles of density and temperatures inside the separatrix are used in our simulation. This discharge is ideal peeling-ballooning unstable. The power loss of the simulation is around 0.7 MW, which is the typical value of EAST discharges with LHCD. The dependency of the direction of toroidal magnetic field on the asymmetric distribution of particle fluxes on upper and lower divertor targets will be reported in this paper.

References

Xia

[1] Nuclear Fusion, 53, 073009 (2013).

[2] M.E. Fenstermacher, et al., 40th EPS, P4.104.

[3] PPCF., 55, 125008 (2013).

Theoretical Analysis of the ICRH Antenna's Impedance Matching for ELMy Plasmas on EAST

X. Gong¹, D. Du², Z. Wang², J. Yu², and P. Zheng²

¹Southwestern Institute of Physics, Chengdu, Sichuan, China ²University of South China, Hengyang, China

Corresponding Author: X. Gong, gongxueyu0508@126.com

A well-optimized design of an ion cyclotron resonance heating (ICRH) antenna is very important for steady-state plasma heating with high radio frequency (RF) power of several tens of megawatts. However, a sharp decrease in the coupling RF power because of impedance mismatch of ICRH system is an issue that must be resolved for present-day fusion reactors and International Thermonuclear Experimental Reactor. This paper has theoretically analyzed the ICRH antenna's impedance matching for ELMy plasmas on experimental advanced superconducting tokamak (EAST) by the transmission line theory. The results indicate that judicious choice of the optimal feeder location is found useful for adjustable capacitors' tolerance to the variations of the antenna input impedance during edge-localized mode (ELM) discharge, which is expected to be good for the design of ICRH antenna system and for real-time feedback control during ELM discharge on EAST.

Preprint

Asymmetry Current in ICRF Heating ITER Plasmas

Y. Gott¹, E. Yurchenko¹

¹National Research Centre "Kurchatov Institute", Moscow, Russian Federation

Corresponding Author: Y. Gott, gott_yv@nrcki.ru

The possibilities of using transverse ICRF heating tokamak plasma minorities for toroidal current driving is investigated in this paper. Three ways of this heating utilization are proposed. Firstly, such heating gives possibility to drive the seed current near magnetic axis, secondly, it can be used for safety current profile adjusting (the negative shear producing) due to synchronous heating of two types of minorities — hydrogen and helium ions, and, thirdly, it can be used for non-inductive asymmetry toroidal current drive in plasma cross-section. Unlike to the isotropic heating when the ratio between amount of trapped and untrapped particles is conserved, during the transverse heating almost all particles become trapped and precisely trapped particles drive toroidal current due to asymmetry ion motion in and against inductive current direction. For the asymmetry current calculation theoretical distribution function of the minority proposed by T.H. Stics and distribution function measured in JET tokamak were used. Fulfilled estimations show that the transverse ICRF heating hydrogen minority up to energy in several MeV that is possible to have the toroidal current in the mega-amperes range.



TH/P3-24

Modelling of Transitions Between L- and H-Mode Including W Behaviour in ITER Scenarios

F. Köchl¹, A. Loarte², V. Parail³, A. S. Kukushkin², A. Polevoi², G. Saibene⁴, and R. Sartori⁴

¹Institute of Atomic and Subatomic Physics, TU-Vienna, Vienna, Austria
 ²ITER Organization, Saint Paul lez Durance, France
 ³CCFE Fusion Association, Culham Science Centre, Abingdon, UK
 ⁴F4E: Fusion for Energy, Barcelona, Spain

Corresponding Author: F. Köchl, florian.koechl@ccfe.ac.uk

The dynamics of the access to and exit from high QDT regimes in the H-mode confinement regime in ITER is expected to be qualitatively different to present experiments: neutral fuelling is much less effective, $P_{sep}/P_{L-H} < 2.0$ even in stationary QDT~ 10 burning conditions, the density evolution determines not only P_{L-H} but also P_{α} which in turn affects dW_{th}/dt after a transition, and plasma position control may be challenging in case of an unexpected back transition to L-mode. In addition, the presence of W may impose additional operational constraints due to possible core accumulation and increased radiation during transients (possibility of a sudden return to L-mode confinement, plasma-wall contact and/or a disruption). To determine under which conditions the plasma evolution to/from H-mode can be optimised, and to assess the problem of possible core W accumulation, modelling studies have been carried out with the JINTRAC suite of codes, simulating the core and core+SOL plasma evolution for the entire period of density evolution following transitions to /from H-mode in the ITER 15 MA/5.3 T and 7.5 MA/2.65 T scenarios.

Simulation scans for the L-H transition have been performed with varying target waveforms for the density evolution, applying a feedback on pellet fuelling. Depending on boundary and operational conditions, limits for the density ramp rate and/or a delay time before the application of increased fuelling could be established. Below these limits, the plasma remains in dithering conditions with $P_{sep} \sim P_{L-H}$ for a long while before it enters a good quality H-mode regime at $P_{sep} > P_{L-H}$, leading to increased flux consumption and a significantly reduced burn duration. In extreme cases, the plasma never reaches high performance H-mode and returns back to L-mode. The back transition to L-mode has also been assessed. The fast reduction in core energy would cause P_{sep} to remain close to P_{L-H} . The plasma would then not immediately reach L-mode but stay in H-mode for a while, followed by a dithering phase before the ETB completely disappears. The energy loss could become accelerated though by an immediate transition to dithering mode, e.g., after a strong MHD event. Subsequent W accumulation could then lead to an immediate transition to L-mode and a disruption.



A Systematic Approach to the Linear-Stability Assessment of Alfvén Eigenmodes in the Presence of Fusion-Born Alpha Particles for ITER-like Equilibria

P. Rodrigues¹, A. Figueiredo¹, J. Ferreira¹, R. Coelho¹, F. Nabais¹, D. Borba¹, N. F. Loureiro¹, H. J. C. Oliver², and S. Sharapov³

¹Institute of Plasmas and Nuclear Fusion, Association EURATOM/IST, Lisbon, Portugal ²HH Wills Physics Laboratory, University of Bristol, Bristol, UK ³CCFE Fusion Association, Culham Science Centre, Abingdon, UK

Corresponding Author: P. Rodrigues, par@ipfn.ist.utl.pt

A systematic approach to assess the linear stability of Alfvén eigenmodes in the presence of fusion-born alpha particles is described. Because experimental results for ITER are not available yet, there is no guidance about which Alfvén eigenmodes will interact more intensively with the fast-particle population. Therefore, the number of modes that need to be considered in stability assessments becomes quite large and care must be exercised when choosing the numeric tools to work with, which must be fast and efficient. In the presented approach, the eigenmodes are first found after an intensive scan of a suitable frequency range, performed within reasonable bounds for the toroidal and poloidal mode numbers. Each solution found is then tested to find if its discretization over the radial grid in use is adequate. Finally, the interaction between the identified eigenmodes and the alpha-particle population is evaluated with the drift-kinetic code CASTOR-K, in order to assess their growth rates and hence their linear stability. The described approach enables one to single out the most unstable eigenmodes in a given scenario, which can then be handled with more specialized tools. This ability eases the task of evaluating alpha-particle interactions with Alfvén eigenmodes, either for ITER scenarios or for any other scenario planning.



TH/P3-28

Fast Particle-Driven Ion Cyclotron Emission (ICE) in Tokamak Plasmas and the Case for an ICE Diagnostic in ITER

K. McClements¹, R. Dendy¹, L. Carbajal², S. Chapman², J. Cook², R. D'Inca³, B. Harvey⁴, B. Heidbrink⁵, and S. Pinches⁶

¹CCFE Fusion Association, Culham Science Centre, Abingdon, UK
 ²University of Warwick, Coventry, UK
 ³Max-Planck-Institut für Plasmaphysik, Garching, Germany
 ⁴CompX, Del Mar, California, USA
 ⁵University of California Irvine, CA, USA
 ⁶ITER Organization, Saint Paul lez Durance, France

Corresponding Author: K. McClements, k.g.mcclements@ccfe.ac.uk

Fast particle-driven waves in the ion cyclotron frequency range (ion cyclotron emission or ICE) have provided a valuable diagnostic of confined and escaping fast ions in many tokamaks. This is a passive, noninvasive diagnostic that would be compatible with the high radiation environment of DT plasmas in ITER, and could provide important information on fusion alpha-particles and beam ions in that device. In JET ICE from confined fusion products scaled linearly with fusion reaction rate over six orders of magnitude [1] and provided evidence that alpha-particle confinement was close to classical [2]. In TFTR ICE was observed from super-Alfvénic alpha-particles in the plasma edge [3]. The intensity of beam-driven ICE in DIII-D is more strongly correlated with drops in neutron rate during fishbone excitation than signals from more direct beam ion loss diagnostics [4]. In ASDEX Upgrade ICE is produced by both super-Alfvénic DD fusion products and sub-Alfvénic D beam ions [5]. The magnetoacoustic cyclotron instability (MCI), driven by the resonant interaction of population-inverted energetic ions with fast Alfvén waves, provides a credible explanation for ICE. One-dimensional PIC and hybrid simulations have been used to explore the nonlinear stage of the MCI [6,7], thereby providing a more exact comparison with measured ICE spectra and opening the prospect of exploiting ICE more fully as a fast ion diagnostic. For realistic values of fast ion concentration, the nonlinearlysaturated ICE spectrum closely resembles the measured spectrum. The PIC/hybrid approach should soon make it possible to simulate the nonlinear physics of ICE in full toroidal geometry. Emission has been observed at a wide range of poloidal locations, and so there is flexibility in the requirements of an ICE detector. Such a detector could be implemented in ITER by installing a toroidal loop or adding a detection capability to the ICRH antennae.

This work was part-funded by the RCUK Energy Programme and by the European Union's Horizon 2020 programme.

References

- [1] G.A. Cottrell et al., NF 33 (1993) 1365.
- [2] K.G. McClements et al., . PRL 82 (1999) 2099.
- [3] S.J. Zweben et al., NF 40 (2000) 91.
- [4] W.W. Heidbrink et al., PP&CF 53 (2011) 085028.
- [5] R. D'Inca et al., Proc. 38th EPS Conf. Plasma Phys., P1.053 (2011).
- [6] L. Carbajal et al., PoP 21 (2014) 012106.
- [7] J.W.S. Cook et al., PP&CF 55 (2013) 065003.

Preprint

Influence of a Tungsten Divertor on the Performance of ITER H-Mode Plasmas

R. Dux¹, A. Loarte², A. S. Kukushkin², E. Fable¹, D. Coster¹, and A. Chankin¹

¹Max-Planck-Institut für Plasmaphysik, Garching, Germany ²ITER Organization, Saint Paul lez Durance, France

Corresponding Author: R. Dux, ralph.dux@ipp.mpg.de

The effect of a tungsten divertor on the performance of H-mode plasmas in ITER has been investigated by combining scrape-off layer transport calculations performed with SOLPS with core transport simulations using the ASTRA code, which was coupled to the impurity transport code STRAHL. The penetration of W into the central plasma mainly depends on two mechanisms: prompt re-deposition of W to the target and the radial transport in the edge transport barrier (ETB) during and between ELMs. Within an ELM, the transport of W is strongly enhanced and concomitantly, the physical sputtering of W at the divertor target strongly increases.

Monte Carlo simulations of prompt W re-deposition, which included the effects of multiple W ionisation and electric field force on the ions in the magnetic pre-sheath, were carried out for ITER controlled ELM conditions. It was found that W re-deposition causes a significant (factor 10000) reduction in the net W erosion. The avalanche effect, where W self-sputtering could lead to a runaway process of increasing W sputtering, can be ruled out. Thus, the SOLPS simulations found that controlled ELMs conditions present very little danger of plasma contamination with sputtered W.

Between ELMs, it can be assumed that the W-transport in the ETB is due to neoclassical transport which was studied for a large range of pedestal profiles. The radial convection velocity of W was found to be outward directed for the major part of the tested profiles. This is due to a combination of high pedestal temperatures and high separatrix densities making the outward directed temperature screening term to be the predominant contribution of the convection. The high densities at the separatrix are needed to control the power exhaust and the sputtering in the divertor and the high pedestal temperatures are expected to be achieved to meet the fusion performance objectives.

Combined ASTRA+STRAHL transport simulations in presence of ELMs of varying frequencies have been carried out. Both neoclassical and ad-hoc anomalous transport models have been included to simulate the evolution of the W profile in the pedestal region. When using the sources as calculated with SOLPS, there was no influence on the total plasma radiation. Even for the most pessimistic case of no redeposition, ELM frequencies in the range 10–30 Hz lead still to tolerable W concentrations.



ITER Energetic Particle Confinement in the Presence of ELM Control Coils and European TBMs

T. Kurki-Suonio¹, E. Hirvijoki¹, S. Sipilä¹, M. Gagliardi², S. Äkäslompolo¹, T. Koskela¹, O. Asunta¹, K. Särkimäki¹, and A. Snicker¹

> ¹Aalto University, Espoo, Finland ²F4E: Fusion for Energy, Barcelona, Spain

Corresponding Author: T. Kurki-Suonio, taina.kurki-suonio@aalto.fi

TH/P3-30

The new physics introduced by ITER operation, of which there is very little prior experience, is related to the very energetic (3.5 MeV) alpha particles produced in large quantities in fusion reactions. These particles not only constitute a massive energy source inside the plasma, but also present a potential hazard to the material structures that provide the containment of the burning plasma. In addition, the negative neutral beam injection (NBI) produces 1 MeV deuterons and the application of ICRH produces minority ions in multi-MeV range, both of which have to be well confined to ensure successful operation of ITER.

Since energetic ions are very sensitive to the details of the magnetic field, in this contribution the field was calculated in unprecedented detail, including all the known magnetic perturbations such as ferritic inserts, TBMs, and ELM Control Coils (ECC). The FEM solver COMSOL was used to first calculate the magnetization of the ferromagnetic components due to plasma current and currents flowing in the field coils. The perturbation field due to the magnetization was then calculated and added to the unperturbed field integrated from the coils using the Biot-Savart law.

The cases reported here correspond to the 15 MA standard H-mode operation and the 9 MA advanced scenario in ITER. Both thermonuclear fusion alphas and NBI ions from ITER heating beams are addressed. Both species are simulated using the Monte Carlo orbit-following code ASCOT in the full 3D magnetic configuration given by the COMSOL calculations. The first wall also has full 3D features. The ferritic components are found not to jeopardize the integrity of the first wall, but the application of ECC needs further attention, in particular for the potential resonance amplification.



Integrated Modelling of ITER Disruption Mitigation

S. Konovalov¹, P. Aleynikov², K. Aleynikova¹, Y. Gribov², M. Lehnen², G. Huijsmans², V. Leonov¹, V. Lukash¹, R. Khayrutdinov¹, A. Ivanov³, S. Medvedev³, and V. Zhogolev¹

> ¹National Research Centre "Kurchatov Institute", Moscow, Russian Federation ²ITER Organization, Saint Paul lez Durance, France ³Keldysh Institute of Applied Mathematics, RAS, Moscow, Russian Federation

Corresponding Author: S. Konovalov, konovalov_sv@nrcki.ru

Feasibility of the ITER disruption mitigation system (DMS) to a) mitigate heat loads on the divertor target plates and plasma facing components during the thermal quench (TQ) phase of the disruption; Feasibility of the ITER disruption mitigation system (DMS) to a) mitigate heat loads on the divertor b) reduce electromagnetic forces on the vacuum vessel during current quench; and c) avoid or control the runaway electron (RE) generation are studied in the present report. Complex variety of physical phenomena comprising disruption of a tokamak discharge requires integrated modeling approach. The well-validated DINA code [1] is used as an integrating core module for disruption simulator development. Whenever possible the DINA results are verified by ASTRA code [2] simulations. Impurity charge state dynamics, radiation and transport are calculated by the ZIMPUR code [3]. Newly developed gas flow model allows accurate accounting for the technical specifications of MGI system foreseen for ITER DMS. RE generation, evolution, and suppression are simulated with use of Monte-Carlo solver for RE kinetic equation integrated with DINA code.

Full disruption scenarios from "prediction" of expected disruption, till complete termination of the plasma current are simulated to determine operation domain for the ITER DMS based on MGI. It is shown that optimization of MGI parameters (geometry, gas mix content and quantities) allows to draw consistent scenario of mitigated disruption with use of two-component MGI system. The first one is aimed on the TQ heat load mitigation, while the second one provides safe plasma current termination without excessive forces on the construction and suppression of REs beams if they appeared.

References

[1] Khayrutdinov, R.R. and Lukash, V.E., J. of Comp. Physics, 109, (1993) 193.

[2] Pereversev, G.V., Yushmanov, P.N., Preprint IPP 5/98, Garching. Germany (2002).

[3] Leonov, V.M., Zhogolev, V.E., Plasma Phys. Control. Fusion, 47 (2005) 903.



Effect of Multi-Pass Absorption of Electron Cyclotron Heating Wave on Initial Stage of Discharge in ITER-like Tokamak

P. Minashin¹, R. Khayrutdinov², A. B. Kukushkin¹, and V. Lukash¹

 $^1 National \ Research \ Centre \ ``Kurchatov \ Institute'', \ Moscow, \ Russian \ Federation$ ²Troitsk Institute for Innovation & Fusion Research, Moscow region, Russian Federation

Corresponding Author: P. Minashin, t32amephi@gmail.com

A model is suggested for calculating the efficiency of multi-pass absorption of EC heating wave in tokamaks at initial stage of discharge, and the effect on the start-up in ITER-like tokamak is analyzed. The single-pass absorption of injected EC wave is evaluated with the scaling obtained using the OGRAY code. The model for subsequent multi-pass absorption, after first reflection of the EC wave from the wall of vacuum chamber, assumes isotropy and uniformity of the respective EC radiation intensity in plasma. The model modifies the CYNEQ code approach developed for the plasma-produced EC radiation transport at high EC harmonics and verified in the benchmarking with other codes. We consider the following case: a) multiple reflection of injected EC wave (O-mode) from the wall; b) polarization scrambling in wall reflections; c) full single-pass absorption of the X-mode. Our parametric analysis for typical electron temperature and density at initial stage of discharge in ITERlike tokamak shows strong dependence of multi-pass absorption efficiency on the O-X conversion in wall reflections. The multi-pass absorption model is incorporated in the 1D simulations of plasma start-up with the DINA code that enables us to extend the results of previous simulations with the single-pass absorption model.

Preprint

X-Divertors in ITER — Without any Hardware Changes or Additions — and in Current Machines, and DEMO Reactors

M. T. Kotschenreuther¹, P. Valanju¹

¹University of Texas at Austin, Austin, TX, USA

Corresponding Author: M. T. Kotschenreuther, mtk@austin.utexas.edu

We show that X-Divertors (XD), that mainly expand magnetic flux near the SOL peak heat flux strike point on the divertor plates, can be created for ITER, many existing tokamaks (e.g., SST-1, EAST, AUG, ...), and future Reactors (KDEMO, ARIES) without modifying their Poloidal Field (PF) coil sets (or adding internal coils). For ITER, KDEMO, SST-1, and EAST, we will present sequences of XDs, starting from their SDs, in which the flux expansions on the divertor plates increases smoothly. All these XDs (including ITER) can be made without adding any internal PF coils, with all currents in existing PF coils under their maximum limits, have nearly the same strike points as the SD cases so no modifications of their divertors or pumping will be needed, and have core plasma shapes that maintain the specified conformity with their given first walls. Further, because XDs preferentially expand flux near the SOL strike point, they are expected to increase stability of detached plasmas, thus allowing a possible way to overcome "shadowing" issues arising from lower angles of field line incidence. Note that the incidence angle at higher flux expansions at SOL strike points can only be reduced by increased major radius of the Super X-Divertor (SXD). The demonstration of these XDs opens the possibility that they could be tested and, then, used to assist in high-power operation on ITER. Some further issues need examination, e.g., full time-dependent plasma startup and operation scenarios, vertical stability, etc. The SOLPS code will be used to gauge the effects of XDs on SOL, and possibly plasma detachment.



Simulation of the Pre-Thermal Quench Stage of Disruptions at **Massive Gas Injection and Projections for ITER**

V. Leonov¹, S. Konovalov¹, M. Lehnen², and V. Zhogolev¹

¹National Research Centre "Kurchatov Institute", Moscow, Russian Federation ²ITER Organization, Saint Paul lez Durance, France

Corresponding Author: V. Leonov, leonov_vm@nrcki.ru

During disruption mitigation by massive gas injection (MGI) the thermal energy is expected to be radiated with high efficiency in order to prevent excessive heat loads to first wall and divertor PFCs. The energy loss will take place in two phases: a) the so-called pre-thermal quench phase that lasts from the arrival of the first gas to the onset of increased transport due to MHD activity during b) the second phase the thermal quench (TQ). Quantification of the duration of the pre-TQ phase is essential for the design of the ITER disruption mitigation system (DMS). The DMS has to be designed such that the impurity amount accumulated during pre-TQ stage should be sufficient for re-radiation of more than 90% of heat flux at subsequent TQ phase of ITER disruption.

The modelling with the code ASTRA together with ZIMPUR impurity transport and radiation code allows the description of the cooling process at the plasma edge, including the penetration of impurities and the shrinking of the current channel. Newly developed model for the gas flow at the end of delivery tube of MGI system well reproduce experimentally measured evolution. The validation of the simulation approach on available experimental data has demonstrated its ability to produce quantitative estimations of the pre-TQ stage duration and of the accumulated in the plasma amounts of Ar and deuterium under MGI.

The comparison of the simulation results with experiment will allow the identification of how the pre-TQ duration scales with plasma minor and major radius, plasma current, thermal energy, plasma density, and temperature profiles on which an extrapolation to ITER can be based. Simulation results of the pre-TQ stage in reference ITER scenarios are presented. The ability of the ITER MGI systems to provide injection of necessary impurity amount during pre-TQ stage are discussed.

Preprint

Off-Axis Current Generation by Helicons and LH Waves in Core of Modern Tokamaks and Reactors FNSF-AT, ITER, DEMO and by Alfvén Waves in Pedestal Plasmas. Scenarios, Modeling and Antennae

V. Vdovin¹

¹National Research Centre "Kurchatov Institute", Moscow, Russian Federation Corresponding Author: V. Vdovin, vdovin_vl@nrcki.ru

The Innovative concept and 3D full wave code modeling Off-axis current drive by RF waves in large scale tokamaks, reactors FNSF-AT, ITER, and DEMO for steady state operation with high efficiency is proposed. The scheme uses the helicons radiation (fast magnetosonic waves at high (20-40) IC frequency harmonics) at frequencies of 500–1000 MHz, propagating in the outer regions of the plasmas with a rotational transform [1]. Modeling with full wave three-dimensional codes PSTELION and STELEC2 showed flexible control of the current profile in DIII-D, T-15, and KSTAR and reactor plasmas of ITER, FNSF-AT, and DEMO, using multiple frequencies, the positions of the antennae and toroidal waves slow down. Commercially available klystrons of MW/tube range, CW working, are promising for commercial stationary fusion reactors. The compact antennae of waveguide type in Traveling Wave regime are proposed, and the example of possible RF system for today's tokamaks and proposed for russian FNSF-AT project is given. For spherical tokamaks the Helicons excitation scheme does not provide efficient Off-axis CD profile tayloring flexibility due to strong coupling of helicons with O-mode, also through the boundary conditions in low aspect machines, and intrinsic large amount of trapped electrons, as will be shown by STELION modeling for the NSTX tokamak. Alfvén Resonance Heating/CD method for ELMs and EHO control pedestal plasma is proposed. New possibility is to control the plasma current in pedestal being an essential element in peeling and ballooning mode stability. We propose to use the Alfvén resonance scheme based on well known shear Alfvén wave relation for frequencies well below of ion cyclotron ones: $\omega = K/VA$. The slow waves and KAW are absorbed mainly by the electrons in pedestal area. Respectively, with properly toroidally phased antenna the SLOW/KAW waves highly efficiently (similar to LH) drive non inductive current to be exploited for ELMs and EHOs control in tokamaks. The antenna with ICRF-like poloidal loops or RMP coils arrays excites the near fields which penetrate into plasma. Thus exploration of Alfvén Resonance scenario to low frequencies from megaherz to tenth kHz evidences the importance of KAW excitation in tokamak pedestal area, with possible influence on MHD unstable modes like ELMs and EHO.

References

[1] Vdovin V. Plas Phys. Rep Vol.39 (2013), N2 95.

On the Possibility of Alpha-Particle Confinement Study in ITER by NPA Measurements of Knock-on Ion Tails

V. Nesenevich¹, V. Afanasyev¹, P. Goncharov², M. Mironov¹, M. Petrov¹, and S. Petrov¹

¹ Ioffe Physical-Technical Institute of the Russian Academy of Science, St. Petersburg, Russian Federation ² St. Petersburg State Polytechnical University, St. Petersburg, Russian Federation

Corresponding Author: V. Nesenevich, vnesenevich@npd.ioffe.ru

One of the issues of the neutral particle diagnostics on ITER is to measure the distribution functions of the fast deuterium (D) and tritium (T) ions in MeV energy range. High energy tails in D,T-ion energy distributions (so-called knock-on ions) appear as a result of the close elastic collisions between the thermal fuel ions and the fusion alpha particles. The knock-on ion density depends directly on the density and energy distribution of the alpha particles. Therefore measurements of the neutralized knock-on D,T-ion fluxes escaping the plasma volume can provide information on the alpha particle confinement in DT-plasma. This report presents results of the numerical simulation for the neutralized fast D,T-ion fluxes in case of ITER fusion plasma and considers measurements of these fluxes in respect to neutral particle diagnostics and its capabilities on ITER.



Kinetic Modelling of Runaway Electrons and their Mitigation in ITER

P. Aleynikov¹, K. Aleynikova², B. Breizman³, G. Huijsmans¹, S. Konovalov², S. Putvinski⁴, and V. Zhogolev²

¹ITER Organization, Saint Paul lez Durance, France ²National Research Centre "Kurchatov Institute", Moscow, Russian Federation ³University of Texas at Austin, Austin, TX, USA ⁴Trialpha Energy, Foothill Ranch, California, USA

Corresponding Author: P. Aleynikov, pavel.aleynikov@iter.org

Runaway electrons (RE) can be generated during plasma disruptions in ITER. A large portion of the toroidal current can then be carried by RE, so that a substantial fraction of the magnetic energy would be associated with the RE current. The uncontrolled loss of such REs in ITER needs to be avoided to minimize the detrimental effects from disruptions. This calls for an adequate means to control or suppress a RE beams in ITER. Massive Gas Injection (MGI) has been successfully employed to mitigate disruptions in present tokamaks, and is therefore considered to be an essential component of the envisioned ITER Disruption Mitigation System (DMS). Recent experiments has shown, that MGI of high-Z impurities (Ar, Ne,...) into a RE beam leads to a fast current decay.

In the present work, the ITER MGI target parameters are assessed taking into account the interaction of REs with high-Z nuclei. The 2D Fokker-Planck equation is solved, which describes the kinetics of REs, coupled to an electric field evolution model. Enhanced scattering of REs on high-Z impurities was shown to modify the RE distribution function, resulting in the broadening of the velocity distribution as well as a decrease in the average kinetic energy of REs.

As an alternative mechanism of enhanced scattering or stopping REs, the possible excitations of kinetic instabilities (whistlers or magnetized waves) are considered. It was shown, that an instability window for whistlers exists within possible ITER disruptions parameters. Simulations of RE suppression by MGI revealed that both the RE current and kinetic energy can be successfully dissipated by the injection of a moderate amount of a noble gas, well below ITER technical limitations.



Alfvén Eigenmode Evolution in ITER Steady-State Scenario

M. Isaev¹, P. Aleynikov², S. Konovalov¹, and S. Medvedev³

¹National Research Centre "Kurchatov Institute", Moscow, Russian Federation ²ITER Organization, Saint Paul lez Durance, France ³Keldysh Institute of Applied Mathematics, RAS, Moscow, Russian Federation

Corresponding Author: M. Isaev, isaev@nfi.kiae.ru

Alfvén eigenmode instability analysis in ITER steady-state plasma scenarios with reversed magnetic shear was performed with the NOVA and TAEFL codes [1]. In our work for this scenario we explore the stability of Alfvén eigenmodes with the KINX code [2]. Both isotropic fusion alphas and beam ions contribute into the mode drive. Fast particle dynamics, linear growth rate, mode amplitude evolution and the wave nonlinear saturation level are computed with the VENUS+df [3] orbit following code. Anisotropic beam particle distribution is computed from realistic geometry of ITER NBI. Calculation results give the estimations of the Alfvén stability linear growth rates and nonlinear saturation level of the mode amplitude for ITER steady state scenario.

References

[1] M.A. Van Zeeland et al., Nucl. Fusion 52 (2012) 094023.

[2] L. Degtyarev et al., Comp. Phys. Comm., 103 (1997) 10.

[3] W.A. Cooper *et al.*, Plasma Phys. Contr. Fus. 53 (2011) 024001.

Modelling of Melt Damage of Tungsten Armour under Multiple Transients Expected in ITER and Validations against JET-ILW Experiments

B. Bazylev¹, G. Arnoux², J. W. Coenen³, M. Clever³, J. Coffey⁴, Y. Corre⁵, R. Dejarnac⁶, S. Devaux², E. Gauthier⁵, J. Horacek⁶, T. Hirai⁵, S. Jachmich⁷, M. Knaup³, K. Krieger⁸, S. Marsen⁹, G. Matthews², A. Meigs², P. Mertens³, R. Pitts⁵, T. Pütterich⁸, M. Stamp², G. Sergienko³, P. Tamain⁵, and V. Thompson²

 ¹Karlsruhe Institute of Technology, Germany
 ²JET-EFDA, Culham Science Centre, Abingdon, UK
 ³Forschungszentrum Jülich, Jülich, Germany
 ⁴Astrophysics Research Centre, School of Mathematics and Physics, Queen's University, Belfast, UK
 ⁵CEA-IRFM, Saint Paul lez Durance, France
 ⁶Institute of Plasma Physics AS CR v.v.i., Prague, Czech Republic
 ⁷Laboratory for Plasma Physics, ERM/KMS, Brussels, Belgium
 ⁸Max-Planck-Institut für Plasmaphysik, Garching, Germany
 ⁹Max-Planck-Institut für Plasmaphysik, Greifswald, Germany

Corresponding Author: B. Bazylev, boris.bazylev@kit.edu

The ITER Organization has recently decided to install a full-tungsten (W) divertor from the start of operations. One of the key issues with such a strategy is the possibility of W melting and melt splashing during transients, which can lead to modifications of surface topology and which may lead to higher disruption frequency or compromise subsequent plasma operation. Although every effort will be made to avoid leading edges, ITER plasma stored energies are sufficient that transients can drive shallow melting on the top surfaces of components.

A new experiment has now been performed on JET-ILW in the ITER-Like Wall (ILW) environment, in which a deliberately misaligned W element (lamella) in the outer divertor has been used to perform controlled ELM transient melting experiments for the first time in a tokamak. This paper reports on the application of the 3D MEMOS code to modeling of these experiments. Input heat loads are obtained from experimental data, notably high resolution IR camera thermography. Importantly, the code indicates that that shielding by the evaporated tungsten prevents bulk melting between ELMs. Encouragingly, the simulations are also able to quantitatively reproduce the dimensions of the damaged area observed by high resolution photography after the first pulse in which melting was achieved. MEMOS simulations on the consequences of multiple mitigated major disruptions (MD), mitigated vertical displacement events (VDE) and major disruptions expected in ITER on damage of tungsten castellated armour have been performed for several scenarios of impact conditions specified by IO.

This work, supported by the European Communities under the EFDA Task Agreement between EURATOM and Karlsruhe Institute of Technology (KIT) and contract between IO and KIT, was carried out within the framework of the European Fusion Development Agreement. The views and opinions expressed herein do not necessarily reflect those of the European Commission or of the ITER Organization.



TH/P3-41

Design and First Applications of the ITER Integrated Modelling & Analysis Suite

F. Imbeaux¹, S. Pinches², J. Lister³, Y. Buravand¹, T. Casper², B. Duval³, B. Guillerminet¹, M. Hosokawa², W. Houlberg², P. Huynh¹, S.-H. Kim², G. Manduchi⁴, M. Owsiak⁵, B. Palak⁵, M. Plociennik⁵, G. Rouault⁶, O. Sauter³, and P. Strand⁷

¹CEA-IRFM, Saint Paul lez Durance, France
 ²ITER Organization, Saint Paul lez Durance, France
 ³Ecole Polytechnique Fédérale de Lausanne, CRPP, Lausanne, Switzerland
 ⁴Consorzio RFX, Associazione Euratom-ENEA sulla Fusione, Padova, Italy
 ⁵PSNC, Poznan, Poland
 ⁶CORYS T.E.S.S., Grenoble, France
 ⁷Chalmers University of Technology, Göteborg, Sweden

Corresponding Author: F. Imbeaux, frederic.imbeaux@cea.fr

The ITER Integrated Modelling & Analysis Suite (IMAS) will support both plasma operation and research activities on the ITER tokamak experiment. The IMAS will be accessible to all ITER Members as a key tool for the scientific exploitation of ITER. It will allow collective development of Integrated Modelling tools, by sharing data, code components and, ultimately, workflows based on coupling together various code components. Its design started in 2011 and a first prototype of the IMAS infrastructure has already been implemented at the ITER Organization (IO). The purpose of this paper is to describe the essential features of the IMAS design, the implemented prototype, as well as the first physics applications which have been developed under the IMAS infrastructure. The IMAS infrastructure is based on a standardized data model that covers experimental and simulated data with the same representation. The standard data model is device-generic and can be used to describe data from existing experiments. Since the data model will progressively cover a large number of areas (plasma, diagnostics, actuators, other tokamak subsystems, ...) and will be developed by many contributors, a set of data model design rules and guidelines have been established to ensure consistency and homogeneity of the data model. Physics components, once interfaced to the data model, can be coupled into an Integrated Modelling workflow orchestrated by a workflow engine. A first implementation of all these infrastructure elements has been carried out and is described in this paper. First applications have been integrated under the prototype IMAS infrastructure to allow their performance to be tested and to demonstrate the expected functionalities of the infrastructure. Transport solvers with free boundary equilibrium capabilities have been integrated to the IMAS infrastructure, namely CORSICA and DINA. ITER pulse simulations have been carried out by coupling the Plasma Control System (PCS), which in ITER has a dedicated and distinct simulation platform based on the Simulink® software, to the physics solvers. This has required the development of an original co-simulation technique between the plasma and plant simulator (under IMAS) and the dedicated PCS simulator. First results of full tokamak simulations under the IMAS infrastructure will be described in the paper.

Preprint

Fusion Alpha Loss in ITER with Local Marginal Stability to Alfvén Eigenmodes

E. M. Bass¹, R. E. Waltz²

¹University of California San Diego, CA, USA ²General Atomics, San Diego, CA, USA

Corresponding Author: E. M. Bass, bassem@fusion.gat.com

A simple 1D radial transport code predicting the fusion alpha density profiles in an ITER burning plasma unstable to Alfvén eigenmodes (AEs) is illustrated. With the local AE thresholds exceeded only in the mid-core in the baseline case, we find only moderate mid-core flattening of the alpha density (and heating) profile and negligible alpha heating loss. Neglecting "ripple loss," only microturbulent low energy alpha transport remains at the edge for this baseline case, so escaping alpha particles are best described as very hot helium. Edge energy loss in the alpha channel is then 1000 times smaller than in the thermal channels. This work extends earlier work of [1] treating the fusion alpha transport from high-*n* micro-turbulence to include marginal stability (or "stiff") transport from alpha driven low-*n* Alfvén eigenmodes. The local alpha density gradient AE thresholds are provided by physically realistic linear gyrokinetic GYRO code calculations. The transported alpha profiles. The baseline thermal plasma (and hence fusion alpha source) profiles are taken from [2] (ITER performance projection). The distinction between the alpha particle and the much smaller alpha energy microturbulent transport loss is emphasized. Any high-energy alpha losses would both reduce needed plasma heating and increase the risk of material damage to plasma-facing surfaces. We predict no such losses in this baseline case.

This work was supported by the US Department of Energy under DE-FG02-95ER54309 and DE-FC02-08ER54977.

References

[1] C. Angioni, A.G. Peters, et al., Nucl. Fusion 49, 055013 (2009).

[2] J.E. Kinsey, G.M. Staebler, R.E. Waltz, and J. Candy, Nucl. Fusion 51, 083001 (2011).



Formation and Termination of Runaway Beams in Tokamak Disruptions and Implications for ITER

J. R. Martin-Solis¹, A. Loarte², E. Hollmann³, B. Esposito⁴, M. Lehnen², and V. Riccardo⁵

¹Universidad Carlos III de Madrid, Madrid, Spain
 ²ITER Organization, Saint Paul lez Durance, France
 ³University of California San Diego, CA, USA
 ⁴Associazione EURATOM-ENEA Unitá Tecnica Fusione, Frascati, Italy
 ⁵JET-EFDA, Culham Science Centre, Abingdon, UK

Corresponding Author: J. R. Martin-Solis, solis@fis.uc3m.es

Large runaway electron (RE) currents could be formed during the current quench (CQ) phase of ITER disruptions. Although the main interest of studying REs is related to their final deposition on the plasma facing components (PFCs), much less attention has been paid to their termination phase, when the current and the REs are lost. During this phase, conversion of magnetic energy of the runaway plasma into runaway kinetic energy can occur which can increase substantially the energy fluxes deposited by the REs on the PFCs. In this work, an inter-machine comparison for various devices (JET, DIII, and FTU) has been performed which, together with simple 0D modeling of the termination phase, has allowed to identify the physical processes determining the magnetic into kinetic energy conversion. It is predicted that, in ITER, for fast RE losses below 1 ms, it is essentially the plateau runaway kinetic energy that will be deposited on the PFCs. For long enough RE losses, the avalanche generation of runaways will play an important role, increasing the energy deposited by the REs onto the PFCs, and energies up to 300 MJ for a plateau RE current of 10 MA are predicted. With the aim of improving our understanding of the physics underlying the runaway heat loads onto the PFCs in ITER disruptions, an integrated analysis in which the results of the modeling of the disruption CQ and runaway formation provide the basic inputs for the termination phase of the disruption, is carried out for selected ITER scenarios. This is done by means of simplified models, but retaining the essential physical processes, including the effect of the main runaway generation mechanisms expected in ITER, effects associated with current profile shape during the formation and termination of the runaway current, as well as, in the case of high impurity content, corrections to the runaway dynamics to account for the collisions of the REs with the partially stripped impurity ions. The ultimate goal is to provide a guidance for the most severe foreseen ITER scenarios as well as for the most suitable schemes for the minimization of the effects of runaway impact on the ITER first wall.

This work was supported by EURATOM and carried out within the framework of the European Fusion Development Agreement. The views and opinions expressed herein do not necessarily reflect those of the European Commission.



Modelling Toroidal Rotation Damping in ITER Due to External 3D Fields

Y. Liu¹, R. Akers², I. Chapman², Y. Gribov³, G. Hao⁴, G. Huijsmans³, A. Kirk¹, A. Loarte³, S. Pinches³, M. Reinke⁵, D. Ryan⁶, and Z. Wang⁷

¹JET-EFDA, Culham Science Centre, Abingdon, UK
 ²CCFE Fusion Association, Culham Science Centre, Abingdon, UK
 ³ITER Organization, Saint Paul lez Durance, France
 ⁴Southwestern Institute of Physics, Chengdu, Sichuan, China
 ⁵Oak Ridge Institute for Science Eduction, Oak Ridge, TN, USA
 ⁶University of York, Heslington, UK
 ⁷Princeton Plasma Physics Laboratory, Princeton, NJ, USA

Corresponding Author: Y. Liu, yueqiang.liu@ccfe.ac.uk

Liu

Three-dimensional external magnetic field perturbations, can either be intentionally applied such as in the experiments of mitigating edge localised modes (ELM) using resonant magnetic perturbations (RMP), or be un-intentionally generated such as the intrinsic error fields (EF). One crucial consequence of applying these (nearly) static 3D fields is the plasma flow damping.

In this work, we model the toroidal rotation damping in ITER plasmas using the recently developed MARS-Q code. This code solves the n = 0 toroidal momentum balance equation together with the single fluid MHD equations describing the plasma response to external 3D fields. The code includes the momentum diffusion and pinch terms, as well as various momentum sink/source terms (torques) that contribute to the momentum balance and consequently determine the time evolution of the flow profile and its amplitude. We include the resonant electromagnetic $J \times B$ torque, the neoclassical toroidal viscous (NTV) torque, the $(v, \nabla)v$ type of Reynolds stress torque associated with the plasma inertia, the torque source due to neutral beam injection (NBI), the torque due to energetic particle losses in the 3D fields, as well as the torque source associated with the intrinsic rotation. Both the RMP field and the intrinsic error field are considered, with somewhat different toroidal spectra: n = 3 and 4 for the former and n = 1 and 2 for the latter.

For an ITER 15 MA plasma with the pedestal temperature of 4.5 kA, that we have modeled, preliminary results from the MARS-Q runs show a minor damping of the plasma flow with 30 kAt RMP coil current in the n = 4 configuration. On the other hand, the plasma rotation at the edge is fully damped with 45 kAt current after about 40 ms of applying the n = 4 RMP field. A further increase of the coil current to 60 kAt leads to a quicker damping of the edge flow (~ 20 ms). Similar simulations with the n = 3 coil configuration at 45 kAt current also show edge rotation braking. The modelling suggests that the primary damping comes from the NTV torque.



TH/P3-45

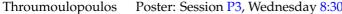
Integrated Core-SOL-Divertor Modelling for ITER Including Impurity: Effect of Tungsten on Fusion Performance in H-Mode and Hybrid Scenario

R. Zagorski¹, I. Voitsekhovitch², I. Ivanova-Stanik¹, F. Köchl³, J. Citrin⁴, E. Fable⁵, J. Garcia⁶, L. Garzotti², J. Hobirk⁵, D. Hogeweij⁴, E. Joffrin⁶, X. Litaudon⁶, A. Polevoi⁶, and G. Telesca⁷

¹Institute of Plasma Physics and Laser Microfusion, Warsaw, Poland
 ²JET-EFDA, Culham Science Centre, Abingdon, UK
 ³Institute of Atomic and Subatomic Physics, TU-Vienna, Vienna, Austria
 ⁴FOM Institute DIFFER, Association EURATOM-FOM, Nieuwegein, The Netherlands
 ⁵Max-Planck-Institut für Plasmaphysik, Garching, Germany
 ⁶CEA-IRFM, Saint Paul lez Durance, France
 ⁷Ghent University, Ghent, Belgium

Corresponding Author: R. Zagorski, roman.zagorski@ipplm.pl

Different plasma performance (energy confinement, discharge duration) has been generally observed in operationally close JET discharges with carbon (C) and ITER-like wall (ILW). Presence of tungsten (W) in ILW discharges is one of the major changes introduced with the wall replacement which may partly explain the differences observed at JET and have an impact on ITER operation. Effect of W on ITER H-mode and hybrid fusion performance is analysed here via integrated core-SOL-divertor modelling performed with ASTRA and JETTO (theory-based core simulations for main species) and COREDIV (impurities and core-SOL-divertor integration) codes used iteratively. Be, He, W and Ne impurities are simulated self-consistently with main plasma species. Core toroidal rotation velocity is also predicted, which is another novelty of this work. The core thermal and particle transport is simulated with the GLF23 transport model which has been extensively validated on a number of H-mode plasmas and hybrid scenarios (HS) in various tokamaks. Here, this model is tested in self-consistent simulations of temperatures, density and toroidal rotation velocity in JET HS. The correlation of the $E \times B$ shear amplification factor α_E with Mach number has been found in these simulations. The α_E and Prandtl number validated on JET are projected to ITER. The COREDIV model has been successfully benchmarked with the JET H-mode discharges and advanced scenarios. Modelling results show that the core-SOL-divertor coupling in ITER plasmas is very strong in presence of W impurity and it affects the operational domains for considered scenarios. The long-pulse H-mode scenario analysed in the density range $n = (8.3-11.9) \times 10^{19} \text{ m}^{-3}$ has narrow operational window limited by the tolerable power to divertor (achieved due to optimised neon gas puff and marginally sustained H-mode under given modelling assumptions. The consequences of strong core-SOL-divertor coupling for low density H-mode and hybrid operation where the improvement in fusion performance due to a good core confinement is counteracted by large W production and core radiation are investigated. Sensitivity studies will be presented showing under what conditions the core-SOL-divertor coupling is reduced allowing high H-mode and hybrid performance.



On the Equilibrium and Stability of ITER Relevant Plasmas with Flow

G. N. Throumoulopoulos¹, A. Kuiroukidis², and H. Tasso³

¹University of Ioannina, Greece ²Technological Education Institute of Serres, Serres, Greece ³Max-Planck-Institut für Plasmaphysik, Garching, Germany

Corresponding Author: G. N. Throumoulopoulos, gthroum@cc.uoi.gr

We present recent results on steady states of translational symmetric and axisymmetric ITER relevant plasmas with incompressible sheared flow in connection with a generalized Grad-Shafranov equation and on their stability [1-2]. The presentation includes equilibria either with monotonically increasing safety factor profiles pertinent to the L-H transition or with reversed magnetic shear. Linear and nonlinear solutions of the generalized Grad-Shafranov equation including nonparallel flows of plasmas surrounded by a diverted boundary are constructed analytically, quasi analytically and numerically. It turns out that the electric field makes the safety factor flatter and increases the magnitude and shear of the toroidal velocity in qualitative agreement with experimental evidence on the formation of Internal Transport Barriers in tokamaks, thus indicating a stabilizing effect of the electric field. For parallel flows the linear stability is examined by applying a sufficient condition [3]. In this case one equilibrium corresponding to the H-state is potentially stable in the sense that the stability condition is satisfied in an appreciable part of the plasma while another solution corresponding to the L-state does not satisfy the condition. In the majority of the equilibria considered stabilization is caused by the variation of the magnetic field in the direction perpendicular to the magnetic surfaces (related to the magnetic shear) in conjunction with the sheared flow, depends on the plasma shaping and is sensitive to the up-down asymmetry.

References

[1] G. N. Throumoulopoulos, H. Tasso, Phys. Plasmas 19, 014504 (2012).

[2] A.P. Kuiroukidis and G. N. Throumoulopoulos, Phys. Plasmas 19, 022508 (2012); J. Plasma Phys. 79, 257 (2013); J. Plasma Phys. 80, 27 (2014); Phys. Plasmas 21, 032509 (2014).

[3] G. N. Throumoulopoulos and H. Tasso, Phys. Plasmas 14, 122104 (2007).

TH/P3-46





Remote Generation of NTM Precursors by Interchange Turbulence

O. Agullo¹, A. Poyé², M. Muraglia¹, S. Benakadda¹, N. Dubuit¹, X. Garbet³, A. Sen⁴, and M. Yagi⁵

¹Aix-Marseille Université, Marseille, France
 ²CeLIA, University Bordeaux, France
 ³CEA-IRFM, Saint Paul lez Durance, France
 ⁴Institute for Plasma Research, Bhat, Gandhinagar, India
 ⁵Japan Atomic Energy Agency, Naka, Japan

Corresponding Author: O. Agullo, olivier.agullo@univ-amu.fr

Nonlinear 3D simulations are performed. A RMHD model describing the simultaneous evolution of the interchange turbulence and the tearing instability is used. We show that, through nonlinear generation of radially extended modes, turbulence generated at the plasma edge can lead to the formation of seed islands in the vicinity of the q = 2 surface. The special role of the zonal flow in that context is explicited.

Understanding Momentum Transport in Tokamak Plasmas

Y. Sarazin¹, J. Abiteboul², G. Dif-Pradalier¹, B. McMillan³, C. Bourdelle¹,
T. Cartier-Michaud¹, P. Cottier¹, D. Estève¹, X. Garbet¹, J.-B. Girardo¹, V. Grandgirard¹,
P. Ghendrih¹, F. Hariri⁴, G. Latu¹, D. Newman⁵, C. Norscini¹, C. Passeron¹,
J. Reynolds-Barredo⁶, R. Sanchez⁶, F. Spineanu⁷, M. Vlad⁷, and L. Villard⁴

¹CEA-IRFM, Saint Paul lez Durance, France
 ²Max-Planck-Institut für Plasmaphysik, Garching, Germany
 ³University of Warwick, Coventry, UK
 ⁴Ecole Polytechnique Fédérale de Lausanne, CRPP, Lausanne, Switzerland
 ⁵Department of Physics, University of Alaska, Fairbanks, AK, USA
 ⁶Universidad Carlos III de Madrid, Madrid, Spain
 ⁷National Institute of Laser, Plasma and Radiation Physics, Bucharest, Romania

Corresponding Author: Y. Sarazin, yanick.sarazin@cea.fr

Toroidal rotation is generally thought to be beneficial for tokamak performance: it stabilizes deleterious MHD modes and its shear may contribute to turbulence saturation. Conversely, large rotation can trigger PVG (Parallel Velocity Gradient) turbulence and increase the transport. In most present tokamaks, toroidal rotation is largely controlled by external means, mainly by neutral beam injection. In ITER, the injected torque is not expected to lead to significant toroidal Mach numbers. There are alternative mechanisms leading to plasma spin-up. First, symmetry breaking can generate toroidal rotation, leading to intrinsic rotation self-generated by turbulence. Second, scrape-off layer flows may also drive rotation in the plasma core through boundary condition effects. Indeed, they can reach large parallel Mach numbers due to plasma-surface interaction.

These issues and their impact on energy confinement are addressed by means of gyrokinetic simulations of Ion Temperature Gradient driven turbulence (adiabatic electrons) with the GYSELA and NEMORB codes. No scale separation is assumed between equilibrium and fluctuations. Mean profiles self-consistently adjust to sources of heat and toroidal momentum. Without injected torque, the Reynolds' stress efficiently generates toroidal rotation. Momentum and heat dynamics exhibit similar characteristics, both transported by the same large-scale avalanche-like events. Five main results are obtained: i) a finite volume source of toroidal momentum directed in the counter-current direction is found to counter-balance the plasma intrinsic rotation due to turbulence; ii) a finite and poloidally asymmetric prescribed toroidal rotation at the outer edge, minicking the expected scrape-off layer flow, impacts the whole core rotation profile; iii) in each case, those simulations with the largest toroidal rotations exhibit the smallest energy confinement times, as a result of both the onset of the PVG instability, and of an erosion of the $E \times B$ staircase; iv) for small aspect ratios typical of Spherical Tokamaks, a strong toroidal flow is generated due to a spontaneous symmetry breaking; v) the toroidal rotation modifies the statistical characteristics of turbulent transport, as quantified with diagnostics imported from the theory of non-Markovian stochastic systems.





TH/P4-6

The Interpretation of the Tokamak Self-Consistent Pressure Profiles

K. Dyabilin¹, K. Razumova¹

¹National Research Centre "Kurchatov Institute", Moscow, Russian Federation Corresponding Author: K. Dyabilin, dyabilin_ks@nrcki.ru

The phenomenon of a pressure profiles self-consistency in tokamak plasmas is interpreted in the framework of a "thermodynamic" approach, used successfully in complex non-equilibrium systems studies. Plasma is considered as the self-organized system and self-consistent solutions correspond to the minimum of the free energy. The solutions for the self-consistent pressure profiles are in accordance with experiments. The deduced energy confinement scaling law is in a good agreement with the empirical so called IPB98(y, 2) scaling. Basing on the Smoluchowski linear relaxation equation, the dynamic of the system in the vicinity of the free energy minimum is analyzed. The important features of the dynamics, such as inward energy pinch and density pump-out effect, are deduced in the analysis.

Authors gratefully acknowledge L.A. Maksimov and V.S. Mukhovatov for helpful comments. Work is supported by ROSATOM contract No H.4x.44.90.13.1101.

A Cross-Benchmarking and Validation Initiative for Tokamak 3D Equilibrium Calculations

A. Reiman¹, A. Turnbull², *T. E. Evans*², E. Lazarus³, J. Breslau¹, J. Canik³, A. Cerfon⁴, C.-S. Chang¹, N. M. Ferraro², R. Hager¹, J. King², M. Lanctot², S. Lazerson¹, Y. Liu⁵, G. McFadden⁶, D. Monticello¹, J.-K. Park¹, C. Sovinec⁷, Y. Suzuki⁸, F. Turco⁹, and P. Zhu⁷

¹Princeton Plasma Physics Laboratory, Princeton, NJ, USA
 ²General Atomics, San Diego, CA, USA
 ³Oak Ridge National Laboratory, Oak Ridge, TN, USA
 ⁴New York University, New York, NY, USA
 ⁵JET-EFDA, Culham Science Centre, Abingdon, UK
 ⁶NIST, Gaithersburg, MD, USA
 ⁷University of Wisconsin-Madison, Madison, WI, USA
 ⁸National Institute for Fusion Science, Toki, Japan
 ⁹Columbia University, New York, USA

Corresponding Author: A. Reiman, reiman@pppl.gov

We are pursuing a cross-benchmarking and validation initiative for tokamak 3D equilibrium calculations, with 11 codes participating: the linearized tokamak equilibrium codes IPEC and MARS-F, the time-dependent extended MHD codes M3D-C1, M3D, and NIMROD, the gyrokinetic code XGC, as well as the stellarator codes VMEC, NSTAB, PIES, HINT, and SPEC. A full day of dedicated experiments on the DIII-D tokamak for the purpose of generating data for validation has been scheduled for May. The data will allow us to do validation simultaneously with cross-benchmarking. Initial crossbenchmarking calculations are finding a disagreement between the VMEC stellarator equilibrium code and the tokamak linearized 3D equilibrium codes IPEC and MARS-F. Investigation of the source of the disagreement has led to new insights into the domain of validity of linearized 3D equilibrium codes and of the VMEC code. The initial case being studied is DIII-D shot number 142603, which was part of a campaign to study ELM suppression using externally imposed nonaxisymmetric fields. We are working with stellarator-symmetric equilibria to allow us to do cross-benchmarking between stellarator and tokamak codes. One approach to understanding the differences between the VMEC and linearized solutions has been to compare the solutions of the two codes for simple model equilibria. For a large aspect ratio plasma with a circular boundary perturbed by a single m = 2, n = 1 harmonic, there is a large localized current near the rational surface. The IPEC solution readily captures this feature, but the VMEC code requires an impractically large number of radial grid surfaces to arrive at a reasonable approximation to it, leading to a substantially altered global solution when VMEC is run with even the highest radial resolutions that are normally used in VMEC calculations. On the other hand, it has been found that the approximation used in the linearized equilibrium codes can break down at surprisingly small perturbation amplitudes due to the overlap of the calculated perturbed flux surfaces. The MARS-F and IPEC linearized equilibrium codes assume nested flux surfaces. For the linearized equilibrium solutions for shot 142603, roughly everything outside of the q = 3.5 surface satisfies the overlap condition, despite the fact that the perturbation amplitude, $\delta B/B$, is of order 0.001 at the plasma boundary.



TH/P4-9

Numerical Code "TOKSCEN" for Modeling of Plasma Evolution in Tokamak

A. Sadykov¹, D. Sychugov², G. Shapovalov¹, M. Skakov¹, B. Chektybayev¹, and N. Gasilov³

¹Institute of Atomic Energy, National Nuclear Center, Kazakhstan ²Moscow State University, Russian Federation ³Baskent University, Ankara, Turkey

Corresponding Author: A. Sadykov, sadykov_a@nnc.kz

The description of the code TOKSCEN (TOKamak SCENario) for modeling of plasma evolution will be presented in the report. The modeling bases on numerical solving of Grad-Shafranov equation of plasma equilibrium and circuit equations for eddy currents for every time step. Circuit equations for eddy currents are solved in matrix form using technique of matrix inversion. Plasma current distribution proposed to be given. The code has the possibility to calculate increment of vertical instability for every time step of the plasma evolution.



L to H Mode Transition: Parametric Dependencies of the Temperature Threshold

C. Bourdelle¹, N. Fedorczak¹, A. Loarte², F. Militello³, C. Maggi⁴, G. Dif-Pradalier¹, X. Garbet¹, and J. Citrin⁵

¹CEA-IRFM, Saint Paul lez Durance, France ²ITER Organization, Saint Paul lez Durance, France ³JET-EFDA, Culham Science Centre, Abingdon, UK ⁴Max-Planck-Institut für Plasmaphysik, Garching, Germany ⁵FOM Institute DIFFER, Association EURATOM-FOM, Nieuwegein, The Netherlands

Corresponding Author: C. Bourdelle, clarisse.bourdelle@cea.fr

On a global scale, the L to H mode transition happens above a critical power threshold. On a local scale, a critical temperature threshold (T_{th}) is often reported to characterize the transition. The parametric dependencies of this local criterion are easier to be compared to theoretical approaches based on local mechanisms. Such a comparison is presented here. The L to H mode transition is modelled by a ratio of two times, one characterizing the turbulence and one characterizing the mean radial electric field shear ($E \times B$ shear). The assumption made is that the transition in H mode occurs when the shorter of the two times is the one characterizing the $E \times B$ shear. The $E \times B$ shear is estimated by a value at the LCFS depending on the temperature gradient and a more inner value where the poloidal velocity is given by the neoclassical theory. The background turbulence results from a competition between Ion Temperature Gradient and Trapped Electron Modes at low collisionality and Resistive Ballooning Modes at higher collisionality which is modelled analytically thanks to fluid limit formulations. The ratio of the analytically derived growth rate and $E \times B$ shearing rate is a function of the temperature as well as other factors. By changing a parameter (*B*, density, etc.) a critical value of this ratio is reached for a different temperature. The resulting T_{th} dependences are coherent with the dependences of the power threshold with respect to B; it explains the existence of a minimum in density and its shift towards larger value in case of lower $Z_{\rm eff}$ as observed in JET-ILW.

This work was supported by EURATOM and carried out within the framework of the European Fusion Development Agreement. The views and opinions expressed herein do not necessarily reflect those of the European Commission.

Global Gyrokinetic Simulations of Electromagnetic Instabilities in Tokamak Plasmas

I. Holod¹, D. Fulton¹, and D. Liu²

¹University of California Irvine, CA, USA ²College of Physical Science and Technology, Sichuan University, China

Corresponding Author: I. Holod, iholod@uci.edu

Plasma confinement and stability can be significantly affected by large scale electromagnetic processes, while the last ones can be triggered by microscopic wave-particle interactions. Thus non-perturbative treatment of kinetic effects is needed for fully self-consistent description of tokamak plasmas. In this work we present recent progress in gyrokinetic simulation of electromagnetic instabilities excited at plasma edge region, using global gyrokinetic particle-in-cell code GTC. We also demonstrate new extended GTC capabilities allowing simulation of tearing and internal kink modes.

Gyrokinetic simulations of plasma edge region have been done using realistic DIII-D equilibrium and profiles. The electrostatic simulations in the middle of the pedestal recover instability with a mode structure peaked at $\theta = \pm \pi/2$ rotating in the electron diamagnetic direction. As β_e increases, the electromagnetic simulations recover unstable mode with similar mode structure, but rotating in the ion diamagnetic direction, which is similar to kinetic-ballooning mode.

The fluid-kinetic hybrid electron model used in GTC has been extended to include a parallel force balance equation, which permits magnetic perturbations with even (tearing) parity. Extension of the simulation radial domain to the magnetic axis allows simulations of the internal kink mode. Linear behavior of both resistive and collisionless tearing mode, as well as kink mode is verified in a cylindrical geometry.

Work is supported by U.S. DOE theory grant DE-SC0010416, and DOE SciDAC GSEP Center.



Progresses in 3D Nonlinear Numerical Simulation of Tokamak Disruptions

R. Paccagnella¹, H. Strauss², J. Breslau³, Y. Vadim¹, L. Sugiyama⁴, and S. C. Jardin³

¹Consorzio RFX, Associazione Euratom-ENEA sulla Fusione, Padova, Italy ²HRS Fusion, West Orange, NJ, USA ³Princeton Plasma Physics Laboratory, Princeton, NJ, USA ⁴Massachusetts Institute of Technology, Cambridge, MA, USA

Corresponding Author: R. Paccagnella, roberto.paccagnella@igi.cnr.it

In this paper numerical simulations of tokamak disruptions in the framework of 3D single fluid visco-resistive magnetohydrodynamics (MHD) in full toroidal geometry are presented. The progresses achieved in the last few years by employing the M3D code will be summarized and reviewed. Similarities and differences between simulations and the experimental behavior in existing devices will be also outlined.

New simulations relevant for the ITER device will be presented. In particular the problem of the mode and halo current slow rotations during the current quench phase will be addressed for its implications to the stresses transmitted on the ITER mechanical structure that could be possibly amplified by resonant effects.

Moreover, open critical issues, such as the Lundquist number or wall penetration time scaling of the simulations to ranges of values fully relevant for the ITER device, the necessity or not of a detailed simulation of the thermal quench phase and the correctness and relevance of various normal velocity boundary conditions will be addressed. New directions in disruptions simulations and also, if possible, new strategies for disruptions control and mitigation will be also discussed.



Full Wave Simulations for Fast Wave Heating and Power Losses in the Scrape-off Layer of Tokamak Plasmas

N. Bertelli¹, E. F. Jaeger², J. C. Hosea¹, C. K. Phillips¹, L. Berry³, P. Bonoli⁴, S. Gerhardt¹, D. Green³, B. LeBlanc¹, R. Perkins¹, *R. I. Pinsker⁵*, R. Prater⁵, P. M. Ryan³, G. Taylor¹, E. J. Valeo¹, J. R. Wilson¹, and J. C. Wright⁴

¹Princeton Plasma Physics Laboratory, Princeton, NJ, USA
 ²XCEL Engineering Inc., USA
 ³Oak Ridge National Laboratory, Oak Ridge, TN, USA
 ⁴Massachusetts Institute of Technology, Cambridge, MA, USA
 ⁵General Atomics, San Diego, CA, USA

Corresponding Author: N. Bertelli, nbertell@pppl.gov

Because fast waves in the ion cyclotron range of frequency (ICRF) have been used successfully to sustain and control the plasma performance, they will play an important role in the ITER experiment. Recent experimental studies of high harmonic fast wave (HHFW) heating on the National Spherical Torus eXperiment (NSTX) have shown that substantial HHFW power loss (up to 60% of the coupled HHFW power can be lost) can occur along the open field lines in the scrape-off layer (SOL). This paper examines the power loss by using the full wave code AORSA, in which the edge plasma beyond the last closed flux surface (LCFS) is included in the solution domain. A collisional damping parameter is used as a proxy to represent the real, and most likely nonlinear, damping processes, and it is applied to specific NSTX discharges in order to predict the effects and possible causes of this power loss. Full wave simulations demonstrate a direct correlation between the location of the fast wave cut-off layer, the large amplitude of the RF fields in the scrape-off region, and the power losses in the SOL (driven by the RF field) observed in the NSTX experiments. A strong transition to higher SOL power losses has been found when the FW cut-off is moved away from in front of the antenna by increasing the edge density. When evanescent waves become propagating waves in the SOL, due to higher density in front of the antenna, the power losses start to increase significantly, commensurate with the amplitude of the RF field found in the SOL. This same behavior is also confirmed by 3D AORSA results where the full antenna spectrum is reconstructed. Moreover, the 3D simulations show that the absorbed power in the SOL is largest near the LCFS and near the front of the antenna, as experimentally observed. Numerical simulations for "conventional" tokamaks with higher aspect ratios, such as DIII-D, are also performed showing similar behavior found in NSTX and NSTX-U. A prediction for the NSTX-U experiment is also presented indicating a favorable condition for the experiment due to a wider evanescent region in edge density.

This work is supported by U.S. DOE Contract # DE-AC02-09CH11466



Modeling and Analytic Study of Plasma Flows on Tearing Mode Stability

D. Chandra¹, A. Thyagaraja^{2,3}, C. Ham⁴, T. C. Hender⁴, J. R. Hastie⁴, J. W. Connor⁴, A. Sen¹, and P. Kaw¹

¹Institute for Plasma Research, Bhat, Gandhinagar, India ²Astrophysics Group, University of Bristol, Bristol, UK ³CCFE Fusion Association, Culham Science Centre, Abingdon, UK ⁴JET-EFDA, Culham Science Centre, Abingdon, UK

Corresponding Author: D. Chandra, debasischandra@gmail.com

Neoclassical tearing modes (NTMs) can severely degrade plasma confinement and thus prevent the achievement of high values of β in ITER. Recent experimental observations from some tokamaks indicate that equilibrium sheared-toroidal flows have a beneficial influence on NTMs: thus, an increase in the equilibrium flow [with shear] leads to an increase of the NTM excitation threshold and also decreases the size of the saturated island size. In the present work, motivated by such considerations, we examine effects of flow shear on the stability of tearing modes. We have used a cylindrical model computation using the CUTIE code and asymptotic analysis to study the (2, 1) mode stability in the presence of sub-Alfvénic toroidal and poloidal sheared flows. Sheared toroidal flows appear to have a destabilizing effect, whilst moderate poloidal flows tend to be stabilizing. We have derived scalings and associated symmetries involving both resistivity and viscosity. The model equations will next be enlarged to include two fluid and poloidal flow effects to study their influence on the tearing growth rate. The final phase of CUTIE studies will involve nonlinear simulations to study the scaling of the island size with the size and sign of flow shear. In contrast to the cylindrical results, our simulations with the toroidal MHD code, NEAR, for a toroidal flow show stabilizing effects on the evolution of a single (2, 1) tearing mode both in the linear stage as well as in the nonlinear saturated state. The principal component of this stabilizing effect is identified as arising due to a flow induced 'Shafranov'-like shift in the profiles of the equilibrium current (q profile) and the pressure profile. This results in a stabilizing change in the stability index Δ' . Other stabilizing effects arise from poloidal flow, toroidal geometry, toroidal mode coupling and viscosity contributions. A quantitative assessment of their relative contributions is currently in progress.



Turbulent Elasticity and the Physics of Time Delay

Z. Guo¹, P. H. Diamond^{1,2}, Y. Kosuga³, and O. Gurcan⁴

¹National Fusion Research Institute, Daejeon, Korea, Republic of ²University of California San Diego, CA, USA ³Institute for Advanced Study, Kyushu University, Kasuga, Japan ⁴LPP/Ecole Polytechnique/CNRS, France

Corresponding Author: Z. Guo, guozhipku@gmail.com

We present a theory of turbulent elasticity — a novel property of drift wave-zonal flow (DW-ZF) turbulence — which follows from the time delay in the response of DWs to ZF. In this work, we: 1) predict and calculate a generic time delay (i.e., a new time scale!) from dynamical first principle; 2) predict zonal shearing wave pattern, in contrast to the dipolar shear layers commonly assumed; 3) calculate the threshold for the onset of limit-cycle-oscillations in the basic predator-prey feedback system, which governs the DW-ZF turbulence. This new insight provides a natural framework for understanding temporally periodic ZF structures in the Dimits shift regime and in the transition from low-confined mode to high-confined mode.



Influence of the Divertor Plate Material on the Plasma Performance in DEMO

I. Ivanova-Stanik¹, R. Zagorski¹

¹Institute of Plasma Physics and Laser Microfusion, Warsaw, Poland Corresponding Author: I. Ivanova-Stanik, irena.ivanova-stanik@ifpilm.pl

One of the most challenging issues of fusion research is the development of DEMO scenario which satisfy simultaneously the requirement of sufficiently high power amplification with the needs for sustainable power exhaust. Independently of the plasma facing materials in DEMO impurity seeding seems to be an unavoidable element of operation to protect the divertor from excessive heat loads.

The presented approach is based on integrated numerical modelling of DEMO discharges using the COREDIV code, which self-consistently solves 1D radial transport equations of plasma and impurities in the core region and 2D multi-fluid transport in the SOL. The model is self-consistent with respect to both the effects of impurities on the alpha-power level and the interaction between seeded and intrinsic impurities. This interaction leads to a significant change in the intrinsic impurity fluxes and energy power balance, and it is found to be essential for a correct evaluation of the average power to the target plates. The code has been successfully benchmarked with a number of JET ILW and ASDEX-U discharges.

Calculations are performed for DEMO inductive scenario, characterised by rather conventional physics and technology assumptions. Preliminary results show significant difference in the reactor performance for different plate materials. It has been found that the fusion performance in the terms of fusion factor Q is quite similar for W and Mo plates, whereas it is slightly reduced for Ni target. It is mostly related to the stronger dilution effect in the case of Ni impurity. Second important finding is that for Ni divertor, even without seeding, the divertor heat load is at the acceptable level. In the case of W and Mo seeding is always required to reduce power load to the target plates. With tungsten divertor, most of the radiation comes from the core, whereas in the case of Mo and in particular for Ni targets the power crossing the separatrix is well above the PLH threshold. It should be noted that for Ni target the radiation fraction is always large (> 0.85%) independent on the level of seeding. For all targets however, the core radiation (line+bremsstrahlung+synchrotron) remains the main energy loss channel.



TH/P4-39

Advanced Equilibrium Models for Anisotropy, Flow and Chaotic Fields

M. J. Hole¹, M. Fitzgerald¹, G. Dennis¹, G. von Nessi¹, R. Dewar¹, S. Hudson², and Z. Qu¹

¹Australian National University, Canberra, Australia ²Princeton Plasma Physics Laboratory, Princeton, NJ, USA

Corresponding Author: M. J. Hole, matthew.hole@anu.edu.au

The purpose of this topical review [1] is to present the state of the art in diagnosis, interpretation and modelling of waves, particles and the magnetic configuration in fusion plasmas. A focus of the review, detailed in this abstract, is the physics and validation of magnetic configuration, which underpins all confinement, stability and transport physics. As the effect of fast particles become important enough to modify the macroscopic variables of the plasma, the macroscopic fluid equations for equilibrium need to be modified to encapsulate the effects of pressure anisotropy, particle and heat flow. A recent advance has been the development of EFIT TENSOR [2], to solve tokamak equilibrium problem with toroidal flow and anisotropy. EFIT TENSOR solves MHD equations with a bi-Maxwellian closure model neglecting poloidal rotation. The code is a modification of the existing force balance solver EFIT++. We show that for sufficiently anisotropic plasma, the parallel transport model can be compared against measured current profiles, providing a novel measure of heat flow from equilibrium constraints. A companion code, HELENA-ATF, has been written to enable physics studies with anisotropy and flow, and provide a finely converged equilibrium solution for ongoing stability physics studies. We have identified the different components of the toroidal current, and examined the impact of the widely applied p^* approximation to anisotropy. This study shows that an isotropic reconstruction can infer a correct p^* , only by getting an incorrect toroidal flux function.

We also report on progress in the modelling of fully 3D (nontoroidally axis-symmetric) fields with a new physics model, Multiple Relaxed region MHD, a generalisation of Taylor's theory, in which the plasma is partitioned into a finite number of nested regions that independently undergo Taylor relaxation. This approach has had recent success in modelling the spontaneous formation of single helical axis and double helical axis states in the reverse field pinch [3]. Finally, we report on developments of a force balance validation framework based on Bayesian inference [4].

References

[1] M. J. Hole and M. Fitzgerald, accepted, Plasma Phys. Con. Fus.

- [2] M. Fitzgerald et al., Nuc. Fus. 53, 113040, 2013.
- [3] G. Dennis et al., Phys. Rev. Lett. 111, 055003, 2013.
- [4] G.T. von Nessi, et al., J. Phys. A: Math. Theor. 46, 185501, 2013.

Understanding the MAST H-Mode Pedestal Through Experiments and Modelling

S. Saarelma¹, A. Bottino², I. Chapman¹, N. Crocker³, A. Diallo⁴, D. Dunai⁵, D. Dickinson⁶, J. Hillesheim¹, A. Kirk⁷, B. McMillan⁸, C. Roach⁷, R. Scannell¹, J. Simpson¹, and T. Peebles³

¹CCFE Fusion Association, Culham Science Centre, Abingdon, UK
 ²Max-Planck-Institut für Plasmaphysik, Garching, Germany
 ³University of California Los Angeles, CA, USA
 ⁴Princeton Plasma Physics Laboratory, Princeton, NJ, USA
 ⁵Wigner Research Center, Association EURATOM, Budapest, Hungary
 ⁶University of York, Heslington, UK
 ⁷JET-EFDA, Culham Science Centre, Abingdon, UK
 ⁸University of Warwick, Coventry, UK

Corresponding Author: S. Saarelma, samuli.saarelma@ccfe.ac.uk

The global plasma confinement in H-mode is connected with the pedestal performance making it essential to understand the pedestal dynamics. Recent experiments in MAST combined with modelling have given us insight on the processes governing the pedestal.

A growing mode (n = 40, radial extent of 2 cm) rotating in the counter direction is observed using Beam Emission Spectroscopy (BES) in MAST H-mode pedestal top just before an ELM crash. The mode locks the edge rotation shear triggering the filamentary structures to exit plasma as ELMs. Local linear gyro-kinetic modelling finds unstable micro-tearing modes at this region. In the steep pedestal region, where the assumptions of local gyro-kinetic simulations become challenged, we find in a global simulation that the global effects have stabilising kinetic ballooning modes there.

Increasing the global β_p by 20% at the LH-transition leads to a doubling of the electron pressure pedestal height before the first ELM. The MHD stability modelling shows that increased ρ_e can be explained by pedestal stability improvement due to the larger Shafranov shift combined with increased concentration of impurities. In single-null experiments with varying plasma current we find that the pedestal width in flux space scales inversely with the plasma current.

This work was funded by the RCUK Energy Programme under grant EP/I501045.



Global gyrokinetic particle-in-cell simulations of Alfvénic modes

O. Mishchenko¹, R. Kleiber¹, M. Cole¹, A. Koenies¹, R. Hatzky¹, A. Zocco¹, T. Feher¹, and M. Borchardt¹

¹Max-Planck-Institut für Plasmaphysik, Garching, Germany

Corresponding Author: O. Mishchenko, ami@ipp.mpg.de

We give an overview of recent developments in electromagnetic simulations based on the gyrokinetic particle-in-cell codes GYGLES and EUTERPE. The code GYGLES is a linear global (full radius, full flux surface) gyrokinetic particle-in-cell code that is able to simulate up to three kinetic species (ions, electrons, fast ions). It solves the field equations for the electrostatic and parallel vector potentials. The code EUTERPE is an extension of the GYGLES code which permits nonlinear and non-axisymmetric (stellarator) simulations based on numerical (VMEC) equilibria. Both codes have been applied to simulate Alfvénic instabilities in plasmas of fusion interest. Global Alfvén Eigenmodes, Toroidal Alfvén Eigenmodes (TAE), their interaction with fast particles and the Alfvénic continuum, and modification of TAE instabilities into Energetic Particle Modes (EPM) have been successfully considered with the GYGLES code. Recently, the gyrokinetic internal m = 1 kink mode and m = 1reconnecting mode have been simulated with GYGLES in screw pinch geometry. The EUTERPE code contains a hierarchical collection of numerical tools of increasing complexity, including a simple perturbative scheme (CKA-EUTERPE), based on the reduced-MHD eigenvalue solver CKA; the more advanced hybrid self-consistent fluid-electron gyrokinetic-ion model; and the most comprehensive, but also most computationally expensive, fully-gyrokinetic model. The perturbative CKA-EUTERPE tool has been implemented in stellarator geometry (Wendelstein 7-X and HELIAS reactor) to study the interaction of fast particles with Alfvén Eigenmodes. The fluid-electron gyrokinetic-ion hybrid model has been extensively used to simulate internal kink modes and fishbones in tokamak geometry. The fully-gyrokinetic electromagnetic model of the EUTERPE code has been verified using the International Tokamak Physics Activity (ITPA) benchmark and further improvements of the cancellation scheme have been considered.

Preprint

Thermal Equilibrium and Density Limit in Tokamak-Reactor

D. Morozov¹, S. Vafin¹, and A. Mavrin¹

¹National Research Centre "Kurchatov Institute", Moscow, Russian Federation

Corresponding Author: D. Morozov, dmitry.morozov.41@mail.ru

The problem of thermal equilibrium and density limit in contemporary tokamaks has been discussed by many authors. As it is well known a part of disruptions is related to the radiation collapse [1, 2]. However, the influence of the fusion energy production has not yet been investigated. The problem for a tokamak-reactor is analyzed in the present paper. The empirical Greenwald criterion $n_c \sim I$ [3] determining the critical plasma density may be exceeded in tokamaks with an auxiliary heating. Here I is the total toroidal current. An auxiliary heating increases the value of n_c by factor 1.5 and more [1, 4-6]. One may expect that the fusion power also can increase the critical plasma density. The thermal balance in tokamaks plasmas is discussed in the present paper. The critical density is defined by the equality of the heating power (auxiliary plus fusion) and the radiation losses at the edge. The influence of the fusion power input as well as the auxiliary heating on the critical density is studied. The simplified analytic model and the numerical one are presented both. The analytic model is based on some simplifying assumptions. The auxiliary heating as well as the fusion one is assumed to be localized at the center of the plasma column. It is shown that the fusion input for D-T mixture increases the critical density in comparison with the critical density in pure deuterium plasmas. The reason is as follows. The fusion reaction rate is proportional to the value of n^2 , and, it rises together with the temperature. Hence, the critical density rises up increasing the fusion output drastically. Numerical results confirm the analytical ones qualitatively.

This work was partially supported by the grant No. 3328.2014.2 of President of Russian Federation for Leading Scientific Schools.

References

[1] Wesson, J.A. et al., 1989 Nucl. Fusion 29 641.

[2] De Vries, P.C. et al., 2011 Nucl. Fusion 51 053018.

[3] Greenwald, M., Terry, J.L., Wolf, S.M. et al., Nucl. Fusion, (1988) 28, 2199.

[4] Alikaev, V.V., Bagdasarov, A.A. *et al.*, Proc. of 17th EPS Conf. on Plasma Phys. and Contr. Fus., Amsterdam (1991) v. 14B., Pt. III, 1080.

[5] Stabler A., McCormic, K., et al., Nucl. Fusion, (1992) 32, 1585.

[6] Petric, T.W., Kellman, A.G., Mahdavi, M.A., Nucl. Fusion, ((1993) 33, 929.



TH/P5-6

Gyrokinetic Simulation of Phenomenology of GAMs

T. Kiviniemi¹, P. Niskala¹, S. Leerink¹, J. Heikkinen¹, and T. Korpilo¹

¹Aalto University, Espoo, Finland

Corresponding Author: T. Kiviniemi, timo.kiviniemi@aalto.fi

The global full-f nonlinear gyrokinetic code ELMFIRE is used for simulating geodesic acoustic modes (GAMs) over a wide range of parameters. For radial wavelength of GAMs, the agreement between analytic value and simulation results is shown to be good for low collisional regime which is not the case with high collisionality. The isotope scan considering hydrogen, deuterium, tritium, and helium was done changing the isotope while keeping all the other parameters fixed. The speed of the radial GAM propagation is shown decrease and radial wavelength is shown to increase as a function of mass. Results are compared to analytic estimates and experimental measurements at the FT–2 and Textor tokamaks.

Preprint

Advances in Modeling of Nonlinear Effects in LHCD **Experiments**

C. Castaldo¹, F. Napoli², S. Ceccuzzi¹, R. Cesario¹, and G. Schettini²

¹Associazione EURATOM-ENEA Unitá Tecnica Fusione, Frascati, Italy ²Univerita' degli Studi Roma Tre, Italy

Corresponding Author: C. Castaldo, carmine.castaldo@enea.it

The concept of lower hybrid current drive (LHCD) in fusion reactors has been recently supported by the experimental evidence that lower hybrid wave power can penetrate at reactor-relevant plasma density. The control of plasma-wave nonlinear interactions occurring at the plasma edge allowed to overcome the density limit observed in previous LHCD experiments. Suitable antenna designs, optimised spectra and operating conditions for efficient current drive in fusion reactors should be based on an accurate modeling of the nonlinear effects. The main nonlinear effect involved in LHCD experiments is the parametric decay of the launched 'pump' waves into LH sidebands. The latter emerge from the thermal noise and are amplified by parametric instabilities (PI) involving ion-acoustic quasi-modes. We propose, here, a full-wave analysis of the nonlinear interactions, considering full LH spectra. We include the effects of the collisions and introduce an accurate modeling of the LH waves produced by the thermal noise. The new modeling significantly improves the standard approach to treat PI in inhomogeneous plasmas, which is based on the eikonal approximation and is limited to 4-wave interactions in collisionless plasmas. We derived from the Maxwell-Boltzmann system, utilising the perturbation theory, the coupled nonlinear equations for the electric field in the high frequency (LH waves) and low frequency (ion-acoustic quasi-modes) ranges. Numerical solutions have been obtained by an iterative method. The frequency spectra of the LH waves calculated for typical LH experimental scenarios confirmed the broadening effect measured by the RF probes. The new model also confirms the result of the standard PI theory that the broadening of the LH frequency spectra is reduced by increasing the density gradient and the electron temperature. In addition, we have found that the nonlinear effects are reduced by increasing the mass/charge ratio of the plasma ions. This suggests a possible, beneficial effect of the lithization, considering that single ionization of Li atoms is expected in the peripheral plasma region where PI occur. The relevant results are discussed and compared with the measured RF spectra in LHCD experiments performed in the FTU tokamak.



TH/P5-8

Global Profile Relaxation Coupled with $E \times B$ Staircase in Toroidal Flux-Driven ITG Turbulence

K. Imadera¹, Y. Kishimoto¹, O. Kevin¹, T. Kobiki¹, and J. Li¹

¹Graduate School of Energy Science, Kyoto University, Kyoto, Japan

Corresponding Author: K. Imadera, imadera@center.iae.kyoto-u.ac.jp

By means of a newly developed 5D toroidal global gyrokinetic code with heat source/sink, we investigated the nonlocal characteristics of flux-driven ITG turbulence to clarify the underlying mechanism of avalanches, profile resilience and their dynamic responses in toroidal system. We found that the turbulent transport and associated profile relaxation are dominated by two processes. One is the fast-scale intermittent bursts resulting from the instantaneous formation of radially extended potential vortices, whose size ranges from meso to even macro-scale ($\sim L_T$) across the $E \times B$ staircase. Such potential structures are considered to trigger the nonGaussian PDF (probability density function) tails of turbulent heat flux, which becomes longer as heat input power increases. The other is the slowscale radial convection of temperature corrugation coupled with the meso-scale $E \times B$ staircase, which propagates from half-minor radius to edge. Ascribed to these events with long correlation lengths, a self-organized resilient profile keeping the exponential function form is found to be established even in the presence of mean flows. We also investigated the dynamic response of such transport processes by step-up/down switching test for heat input power, P_{in} . A hysteresis nature in the gradient-flux relation is found to be observed, which originates from a time delay of the $E \times B$ staircase to the step-up/down event. We further found that the partition of the mean flow energy to that of the total fluctuation, i.e., $\eta = E^{\text{mean}}/(E^{\text{mean}} + E^{\text{turb}})$ is proportional to $P_{in}^{-1/2}$ in a quasi-steady state. This suggests that stronger intermittent bursts due to high input power lead to weaker mean flow level, which is considered to be a reason that the profile can keep the function form even in high input power regime, while typical scale length L_T weakly depends on P_{in} .



Finite Toroidal Flow Generated by Resistive Wall Tearing Modes in a Toroidal Plasma

G. Hao¹, Y. Liu², A. Wang¹, Y. Xu¹, M. Xu¹, Y. Sun³, H. Qu¹, X. Peng¹, J. Xu¹, Z. Wang¹, and X. Qiu¹

¹Southwestern Institute of Physics, Chengdu, Sichuan, China
 ²JET-EFDA, Culham Science Centre, Abingdon, UK
 ³Institute of Plasma Physics, Chinese Academy of Sciences, Hefei, China

Corresponding Author: G. Hao, haogz@swip.ac.cn

Hao

The toroidal plasma flow, and/or flow shear, plays a critical role in affecting the macroscopic magnetohydrodynamic (MHD) instabilities (e.g., the resistive wall mode, the tearing mode, etc.) as well as the plasma confinement. A finite toroidal plasma rotation generated without external momentum input is very important for ITER, since its momentum input is expected to be small in relation to the plasma volume. In this work, it is shown that an intrinsic steady-state toroidal rotation can be generated by the neoclassical toroidal viscous (NTV) torque, which results from an unstable tearing mode (TM) in tokamak. The preliminary results show that a toroidal rotation of 17 krad/s (28 km/s) can be reached in the HL2A-like plasma. At the initial state (t = 0), the plasma is static. The steady state solution is achieved in about 46 ms, during which the initially unstable TM reaches saturation due to the nonlinear coupling to the self-generated plasma flow. The above results indicate that a TM may give considerable contribution to the generation of the plasma flow in the absence of the external momentum input. In addition, the achieved steady-state rotation (both amplitude and the rotation profile) is insensitive to the given initial perturbation amplitude (as long as it is small), the ion/electron temperature ratio, and the distance between the resistive wall and plasma surface. On the other hand, the saturated rotation amplitude is significantly increased with increasing the plasma resistivity. We also find that the saturated rotation is much slower than that of the NTV theory predicted off-set rotation, which is comparable in magnitude to the ion diamagnetic flow speed.



TH/P5-10

Progress in Theoretical Studies of Resistive Wall Modes for RFP plasmas and Comparison with Tokamaks

S. Guo¹, X. Y. Xu¹, Y. Q. Liu², M. Baruzzo¹, T. Bolzonella¹, Z. R. Wang³, S. Cappello¹, M. Veranda¹, D. Bonfiglio¹, and D. Escande¹

¹Consorzio RFX, Associazione Euratom-ENEA sulla Fusione, Padova, Italy ³Princeton Plasma Physics Laboratory, Princeton, NJ, USA ²CCFE Fusion Association, Culham Science Centre, Abingdon, UK

Corresponding Author: S. Guo, shichong.guo@igi.cnr.it

Recent results of the theoretic studies on Resistive Wall Modes (RWM) in Reversed Field Pinch (RFP) plasmas are reported. Different features of RWM instabilities between RFP and tokamak are investigated in order to provide in-depth understanding on RWM physics. The toroidal MHD-kinetic hybrid stability code MARS-K [1] was applied to the studies, taking into account the full kinetic effects of the thermal particles and the isotropic/anisotropic Energetic Particles (EP). A brief summary on the characteristics of RWMs in RFP configuration are presented. Especially, due to the different mechanisms of the kinetic damping, the stabilization of RWMs in RFPs requires a plasma rotation at least in the range of the ion acoustic frequency; whereas only very slow, even vanishing rotation is required for stabilizing the pressure driven RWMs in the tokamak plasmas.

The shaped cross section of the RFP plasmas leads to a lower ideal wall β limit than that of the circular one; and does not bring an appreciable benefit in kinetic damping on RWMs. The physics mechanism leading to the conclusion is provided by the analysis. The energetic particle effects on RWMs in RFP plasmas are also investigated. Furthermore, a non-resonant fishbone-like mode (FLM) in RFP plasmas is predicted. The FLM instability is an external kink mode, which can be driven by the resonance of the precession drift of the trapped EPs under certain condition, even for a RFP with an ideal wall. The kinetic effect of thermal particles plays a stabilizing role on FLMs in RFPs. Different features of FLM instabilities in RFP and tokamak plasmas are discussed. 3D magnetic perturbation of RWMs can induce neoclassical toroidal viscosity (NTV) in RFP plasmas. The preliminary results will be presented and discussed. Example of the experimental study on RWM in RFX-mod, correlated to the theory, will be presented. In a complementary way, the possibility to exploit the internally nonresonant kink instability to build up 3D RFP helical state is studied by means of the 3D nonlinear MHD visco-resistive codes SpeCyl and PIXIE3D [2].

References

[1] Y.Q. Liu, et al., PoP 15, 112503 (2008).

[2] S. Cappello, et al., Proc 24th IAEA FEC (2012).



Limit Cycle Oscillations and L/H Transitions from Two **Dimensional Mean Field Momentum Transport Equations**

G. M. Staebler¹

¹General Atomics, San Diego, CA, USA

Corresponding Author: G. M. Staebler, staebler@fusion.gat.com

The two dimensional momentum transport of the mean field (i.e., low frequency compared to the turbulence) $E \times B$ toroidal and ion poloidal velocities are modeled with both collisional and turbulent contributions to the transport equations. The radial and temporal evolution of the edge barrier is modeled. It will be shown that there are both normal one-step L/H transitions to suppressed turbulence and newly discovered limit cycle oscillations, from this two dimensional system, without the aid of oscillations from turbulent zonal flows. The results of the new model will be compared with recent high resolution measurements of L/H transitions and limit cycle oscillations, or dithering transitions, which have given unprecedented detail of the dynamics and spatial structure of the plasma velocities and turbulence. The properties that govern which type of transition occurs in the 2D momentum equations are the collisional poloidal velocity damping force and the Reynolds force (radial derivative of the Reynolds stress). Over a range of $E \times B$ velocity shear, the effective momentum diffusivity due to the turbulence is negative, which provides the drive for the instability. The linear stability of the two dimensional momentum equations admits purely growing and finite frequency instabilities. Nonlinear gyro-kinetic turbulence simulations are shown to have a zonal electric field energy that is a fraction of the total electric field energy of the turbulence as the mean field $E \times B$ velocity shear is increased. The L-mode is a state of high turbulence and zonal electric field energy and the H-mode has suppressed turbulence and zonal flow electric field energy. The new momentum transport modeling has a low mean field $E \times B$ velocity in the L-mode and a poloidal velocity that departs from the neoclassical value due to the high momentum transport driven by the turbulence. In the H-mode barrier region, the modeling gives mean field $E \times B$ and ion poloidal velocities that approach neoclassical levels. These properties compare well with the measured radial structure of the L- and H-mode plasmas.

This work was supported by the US Department of Energy under DE-FG02-95ER54309 and DE-AC02-09CH11466.

Simulation of Energy-Dependent Stochastic Transport Induced by Low-Order MHD Instabilities for Runaway Electron Mitigation

A. Matsuyama¹, M. Yagi¹, Y. Ishii¹, N. Aiba¹, and Y. Kagei¹

¹ Japan Atomic Energy Agency, Naka, Japan

Corresponding Author: A. Matsuyama, matsuyama.akinobu@jaea.go.jp

Corres Tc ITER. mecha

To extend the capability of RE mitigation is an urgent issue towards the safety operation of ITER. We investigate the RE losses induced by low-order MHD instabilities and clarify a dominant mechanism for determining the energy dependence of the onset of RE orbit stochasticity. This is due to that for highly relativistic REs, sideband resonance of the orbit shift with macroscopic modes is much stronger than what is expected for nonrelativistic particles. We demonstrate that the sideband resonance can cause both the enhancement and the suppression of orbit stochasticity at high energy relevant to the Dreicer-generated REs, depending not only on perturbation amplitudes but also on phase differences between the modes. We also report the development of a new 3D guiding-centre code for simulating the RE generation during major disruptions. To study the RE mitigation scenarios, we have developed, for the first time, a guiding-centre Monte-Carlo code including the RE generation process, which extends an original 3D guiding-centre orbit code ETC-Rel to include the RE source model as well as collisions and radiations. It also takes into account time-evolving loop voltage in a self-consistent way with generated RE current. Different energy spectra between existing tokamaks and ITER indicate that the RE control strategies must be based on detailed understanding of energy dependence of the RE transport. While Dreicer-generated seed REs tend to accelerate towards high energy, secondary REs that develop slowly on the timescale of current quench are dominant in ITER. Consequently, the effectiveness of the RE control by inducing the prompt loss will depends on the energy dependence of the onset of RE orbit stochasticity that is explained in this paper.



Numerical Diagnostics of Non-Diffusive Transport Process by Use of Turbulence Diagnostic Simulator

N. Kasuya¹, M. Sasaki¹, S. Inagaki¹, K. Itoh², M. Yagi³, and S. Itoh⁴

¹Kyushu University, Kasuga, Japan
 ²National Institute for Fusion Science, Toki, Japan
 ³Japan Atomic Energy Agency, Naka, Japan
 ⁴Institute for Applied Mechanics, Kyushu University, Kasuga, Japan

Corresponding Author: N. Kasuya, kasuya@riam.kyushu-u.ac.jp

Hysteresis in the flux-gradient relation (similar to what has been revealed by the dynamical response to the heating modulation [1]) is found in the global nonlinear turbulence simulation for the first time. Here we report i) the abrupt increase of the heat flux after the gradual change of the flux and pressure gradient on the onset of the additional heating, and ii) the simultaneous response of the flux associated with the radial width of fluctuations and their nonlinear couplings, which spreads the pressure response from core to edge with a speed of ten times faster than the diffusion velocity. The nonlinear simulation demonstrated the counter-clockwise hysteresis in the flux-gradient relation contrary to the experimental observation. This result implies the possibility that variety of hysteresis responses will be observed in fusion plasmas, and it is necessary to extend the approach from local to global nonlinear simulations with new degrees of freedom.

References

[1] S. Inagaki, et al., Nucl. Fusion 53 (2013) 113006.



Two-Fluid Effects on Pressure-Driven Modes in a Heliotron Device

H. Miura¹, R. Goto², T. Hatori², A. Ito¹, and M. Sato¹

¹National Institute for Fusion Science, Toki, Japan ²Graduate University of Advanced Studies, Kanagawa, Japan

Corresponding Author: H. Miura, miura.hideaki@nifs.ac.jp

Two-fluid effects on pressure-driven unstable modes are studied numerically to understand physics in linear and nonlinear evolution of them in a heliotron device. Full 3D simulations show that the introduction of the two-fluid term can bring about the deterioration of the stabilizing effect of the parallel heat conduction through generation of large magnetic perturbations, to lead to a saturation profile worse than that in single-fluid MHD. Possible contributions of the gyro-viscosity to the saturation of the modes are also shown based on the complementary 2D simulations.

Two-fluid effects in simulations of the Large Helical Device are studied by the use of the MINOS code for the initial equilibrium of $R_{ax} = 3.6$ m and $\beta_0 = 5\%$. Both the two-fluid MHD and the singlefluid MHD equations are solved in the helical-toroidal coordinate for the fully toroidal system. It is shown that the two-fluid term can enhance the perturbation spontaneously, and change the constitution of dominant Fourier coefficients in the exponential growth. Many of the Fourier coefficients in the two-fluid MHD acquire larger amplitudes than those in the single fluid MHD simulation, either because their exponential growth is not stabilized by the parallel heat conduction or because they acquire large amplitude spontaneously by the two-fluid effects. The deterioration is also closely related with the nonlinearity of the two-fluid term which causes energy transfer from a large to a small scale and broadens the energy spectrum distribution. Our 3D simulations as well as the complementary 2D simulations show that the two-fluid MHD plasma acquires larger amplitudes and wider distribution of the spectrum than the single-fluid MHD plasma. Especially, it is shown that the two-fluid effects broaden the spectrum through the nonlinear energy transfer and the gyro-viscosity does not necessarily suppress the high wave number region sufficiently. Thus, the two-fluid term can cause a strong magnetic field perturbation by the large amplitudes as well as by the wider spectrum, weakening the stabilizing by effect of the parallel heat conduction in the nonlinear stage.



Comparison of H-Mode Plasmas in JET-ILW and JET-C with and without Nitrogen Seeding

A. E. Järvinen¹, M. Groth¹, P. da Silva Aresta Belo², S. Brezinsek³, M. Beurskens⁴,
G. Corrigan⁵, S. Devaux⁶, C. Giroud⁴, T. Eich⁶, D. Harting⁵, A. Huber³, S. Jachmich⁷,
K. Lawson⁵, M. Lehnen³, B. Lipschultz⁸, G. Maddison⁵, S. Marsen⁶, A. Meigs⁵,
D. Moulton¹, B. Sieglin⁶, M. Stamp⁵, S. Wiesen³, and G. Matthews⁵

¹Aalto University, Espoo, Finland

 ²Institute of Plasmas and Nuclear Fusion, Association EURATOM/IST, Lisbon, Portugal ³Forschungszentrum Jülich, Jülich, Germany
 ⁴CCFE Fusion Association, Culham Science Centre, Abingdon, UK ⁵JET-EFDA, Culham Science Centre, Abingdon, UK
 ⁶Max-Planck-Institut für Plasmaphysik, Garching, Germany
 ⁷Laboratory for Plasma Physics, ERM/KMS, Brussels, Belgium ⁸University of York, Heslington, UK

Corresponding Author: A. E. Järvinen, aaro.jarvinen@aalto.fi

In high confinement mode plasmas with edge localized modes in JET [1], the fluid edge code EDGE2D/EIRENE predicts transition to nitrogen induced detachment at the low-field side target plate when more than 40% of the power crossing the separatrix is radiated. This is observed both in the ITER-like wall and in the previous carbon wall environments and is consistent with experimental observations. When the carbon wall is replaced with the ITER-like wall, a factor of two reduction in the divertor radiated power and 60% increase in the power deposited to the outer plate is predicted by EDGE2D/EIRENE for unseeded plasmas consistent with the experiments. This observation is attributed to the higher radiative potential of carbon compared to beryllium in the simulated divertor conditions. At the radiation levels required for detachment, EDGE2D/EIRENE shows that nitrogen is radiating 80% of the total divertor radiation with the ITER-like wall with beryllium contributing less than a few %. With the carbon wall, nitrogen radiation contribution is around 65% with carbon providing 20% of the total radiation. When the divertor radiation levels in the ITER-like wall simulations due to nitrogen injection reach the predicted carbon wall levels, the outer divertor temperatures and total plasma currents are the same within 10% between the two materials configurations through the following nitrogen injection scan. Therefore, the lower intrinsic divertor radiation with the ITER-like wall is compensated by stronger nitrogen radiation contribution in the simulations leading to detachment at similar total divertor radiation fractions, as well as to very similar outer plate conditions, as is predicted in the full carbon environment. The neutral deuterium flux crossing the separatrix in the carbon wall simulations exceed those in the ITER-like wall simulations by 5–10%, due to a factor of 2 higher molecular fractions in the recycling fluxes emitted from carbon surfaces.

This work was supported by EURATOM and carried out within the framework of the European Fusion Development Agreement. The views and opinions expressed herein do not necessarily reflect those of the European Commission.

References

[1] C. Giroud, et al., Nucl. Fusion 53 (2013) 113025.



TH/P5-35

Steps in Validating Scrape-off Layer Simulations of Detached Plasmas in the JET ITER-like Wall Configuration

M. Groth¹, M. Clever², K. Lawson³, A. Meigs³, M. Stamp³, J. Svensson⁴, P. Belo⁵,
S. Brezinsek², M. Brix³, J. W. Coenen², G. Corrigan³, T. Eich⁴, C. Giroud³, D. Harting³,
A. Huber², S. Jachmich⁶, K. Uron³, M. Lehnen⁷, C. Lowry⁸, C. Maggi⁴, S. Marsen⁴,
G. Sergienko², B. Sieglin⁴, G. van Rooij⁹, and S. Wiesen²

¹ Aalto University, Espoo, Finland
 ² Forschungszentrum Jülich, Jülich, Germany
 ³ JET-EFDA, Culham Science Centre, Abingdon, UK
 ⁴ Max-Planck-Institut für Plasmaphysik, Garching, Germany
 ⁵ Institute of Plasmas and Nuclear Fusion, Association EURATOM/IST, Lisbon, Portugal
 ⁶ Laboratory for Plasma Physics, ERM/KMS, Brussels, Belgium
 ⁷ ITER Organization, Saint Paul lez Durance, France
 ⁸ European Commission, Brussels, Belgium
 ⁹ FOM Institute DIFFER, Association EURATOM-FOM, Nieuwegein, The Netherlands

Corresponding Author: M. Groth, mathias.groth@aalto.fi

Further steps have been taken in validating predictions of detached divertor simulations with the edge fluid code EDGE2D coupled to the neutral Monte-Carlo code EIRENE for JET low confinement mode plasmas in the ITER-like wall configuration. Fully detached and strongly recombining divertor plasmas close to the density limit were characterized experimentally by bolometry, spectroscopy, and plasma imaging. The absence of carbon as a primary radiator and carbon chemistry in the sputtering processes greatly simplified the assessment of the role of deuterium in removing momentum and power from the plasma to achieve detachment.

Predictions of the line-integrated bolometer signals confirmed the previous observation and consistently show a factor of 2 to 3 lower power levels than measured, consistent with the previously reported power deficit. Inclusion of cross-field drifts due to $E \times B$ and $B \times \nabla B$ raises the power from the high field side divertor by 50%. Assuming full coverage of the tungsten divertor with beryllium further raises the total power by another 50%. However, assessment of the components of power radiated from the divertor in these plasmas showed that deuterium atomic and molecular line radiation accounts for more than 90% of the radiation, with radiative recombination becoming important ($\sim 30\%$) at high density. Emission from beryllium, tungsten, oxygen, and carbon are measured to be insignificant in these plasmas, while BeD molecules may produce significant radiation. While predictions of the Balmer-alpha line intensities across the low field side divertor leg fall short by factors of 2 to 4 when the divertor plasma is detached, the simulations reproduce line emission from high-*n* Balmer transitions (10–2, 11–2), which indicate that recombination is a significant process in the low field side divertor plasma at plasma temperatures of or below 1 eV in front of the target plate. The predicted two-dimensional profiles of Balmer-alpha line emission in the divertor show the emission being extended into the divertor plasma both on the high field and low field side, while the measurements reveal more localised emission at the strike points.

This work was supported by EURATOM and carried out within the framework of the European Fusion Development Agreement. The views and opinions expressed herein do not necessarily reflect those of the European Commission.

Preprint

Long-Lived Ribbon Structure in JET Tokamak as a Manifestation of a Force-Free Magneto-Current Island

A. Skovoroda¹, E. Sorokina¹

¹National Research Centre "Kurchatov Institute", Moscow, Russian Federation Corresponding Author: A. Skovoroda, skovorod@nfi.kiae.ru

Magnetic and current structures arising due to resonant perturbations of an equilibrium currentcarrying magnetic configuration are analyzed using the Hamiltonian formalism. Special attention is paid to axisymmetric tokamak and pinch configurations. It is shown that, due to the very different dependencies of the magnetic and current rotational transforms on the plasma pressure, the resonances (islands) of the magnetic field may not coincide with those of the current. The perturbed force-free equilibrium of a cylindrical pinch in which the field and current islands overlap is analyzed. The longlived ribbon structures observed in the JET tokamak are explained as a manifestation of a force-free magneto-current island.



Core Micro-Instability Analysis of JET Hybrid and Baseline Discharges with Carbon Wall

S. Moradi 1

¹*Ecole Polytechnique, France*

Corresponding Author: S. Moradi, sara.moradi@lpp.polytechnique.fr

In recent years there has been an increasing worldwide effort in the development of the so-called hybrid or improved H-mode scenarios as a hybrid between an AT and a baseline plasma. In these scenarios, by optimising the current density profile, an enhanced normalised confinement can be achieved, as compared to the ITER baseline scenario, the ELMy H-mode. During the 2008–2009 experimental campaigns at the IET, a remarkable improvement in the normalised confinement was achieved in hybrid scenarios $H_{98}(y, 2) \sim 1.3-1.4$ in both high ($\delta = 0.4$) and low ($\delta = 0.2$) triangularity plasmas [1]. However, the underlying physics basis for the observed increased normalized confinement remain somewhat unclear, making the hybrid plasmas an interesting choice for modelling and trying to explain the underlying mechanisms responsible for their deviation from the "known" H-mode confinement. Therefore, in this work we investigate the core micro-instability characteristics of hybrid and baseline plasmas in a selected set of JET plasmas with carbon wall through local linear and nonlinear gyro-kinetic simulations with the GYRO code [2]. We find that a good core confinement due to strong stabilisation of the micro-turbulence driven transport can be expected in the hybrid plasmas due to the stabilising effect of the fast ion pressure that is more effective at the low magnetic shear of the hybrid discharges. While parallel velocity gradient destabilization is important for the inner core, at outer radii the hybrid plasmas may benefit from a strong quench of the turbulence transport by $E \times B$ rotation shear.

References

[1] M.N. A Beurskens et al., Nucl. Fusion, 53, 013001 (2013).

[2] J. Candy and E. Belli, General Atomics Report, GA-A26818 (2011).

Numerical Modeling for Divertor Design and in Support to the WEST Project

H. Bufferand¹, *G. Ciraolo*¹, Y. Marandet², J. Bucalossi¹, P. Ghendrih¹, P. Tamain¹, R. Leybros³, N. Fedorczak¹, F. Schwander⁴, and E. Serre⁵

¹CEA-IRFM, Saint Paul lez Durance, France
 ²PIIM, CNRS, Aix-Marseille Université, Marseille, France
 ³M2P2, Aix-Marseille Université, Marseille, France
 ⁴Aix-Marseille Université, Marseille, France
 ⁵CNRS, France

Corresponding Author: H. Bufferand, hugo.bufferand@cea.fr

Operating a fusion reactor requires handling high heat loads on the divertor plasma facing components. In support of the ITER divertor strategy, the WEST project on Tore Supra aims at studying tungsten monoblocks behaviour when submitted to heat flux, and high plasma fluence, representative of ITER conditions during long pulses. A considerable simulation effort is dedicated to properly estimate the power load on the materials and understand diverted plasma specificities in term of impurity screening. In this context we report recent results from the SOLEDGE2D plasma transport code coupled with the MonteCarlo EIRENE code for neutral transport. Complex and realistic geometries can be handled by SOLEDGE thanks to the penalization technique allowing us to properly taking into account the interaction between the plasma and the multiplicity of objects located in the vessel. Thanks to these specific numerical capabilities, we can address the synergy between plasma transport and geometry of plasma facing components on, for example, neutral recirculation or impurity contamination, with a good insight on the influence of divertor, including the secondary X-point effect, and baffle geometries. In the perspective of the WEST operation, simulations are performed to address reference operational domain of the tokamak. We present simulations results for the different plasma density regimes obtained in the divertor region, from the low density sheath limited regime to the high recycling regime up to the detachment for higher plasma density. Moreover, we report investigation on supersonic parallel flows. We demonstrate that supersonic parallel flows into the divertor volume are ubiquitous at low density and governed by the divertor magnetic geometry. As density is increased subsonic divertor plasmas are recovered. On detachment, we show that the change in the geometry of the particle source can also drive a transition to a supersonic regime. The comprehensive theoretical analysis is completed by simulations for the WEST geometry. Such results are essential in assessing the divertor performance and when interpreting measurements and experimental evidence.



TH/P6-1

Modelling of Spatial Structure of Divertor Power Loads Caused by Edge-Localized Modes Mitigated by Magnetic Perturbations

P. Cahyna¹, M. Becoulet², G. Huijsmans³, A. Kirk⁴, E. Nardon², F. Orain², S. Pamela⁴, R. Panek¹, and A. Thornton⁴

¹Institute of Plasma Physics AS CR v.v.i., Prague, Czech Republic ²CEA-IRFM, Saint Paul lez Durance, France ³ITER Organization, Saint Paul lez Durance, France ⁴JET-EFDA, Culham Science Centre, Abingdon, UK

Corresponding Author: P. Cahyna, cahyna@ipp.cas.cz

Resonant magnetic perturbations (RMPs) can mitigate the edge-localized modes (ELMs), i.e., cause a change of the ELM character towards smaller energy loss and higher frequency. During mitigation a change of the spatial structure of ELM loads on divertor was observed on DIII-D and MAST: the power is deposited predominantly in the footprint structures formed by the magnetic perturbation. In the present contribution we develop a theory explaining this effect, based on the idea that part of the ELM losses is caused by parallel transport in the homoclinic tagle formed by the magnetic perturbation of the ELM. The modified tangle resulting from the combination of the ELM perturbation and the applied RMP has the expected property of bringing open field lines in the same areas as the tangle from the RMP alone. We show that this explanation is consistent with features of the mitigated ELMs on MAST.

We in addition validated our theory by an analysis of simulations of mitigated ELMs using the code JOREK. We produced detailed laminar plots of field lines on the divertor in the JOREK runs with an ELM, an applied RMP, and an ELM mitigated by the presence of the RMP. The results for an ELM clearly show a high-*n* rotating footprint structure appearing during the nonlinear stage of the ELM, which is not present in the precursor stage of the ELM. The results for an *n* = 2 RMP from the ELM control coils show the expected n = 2 footprint structure. The results for the mitigated ELM show a similar structure, modulated by a higher n perturbation of the ELM, consistent with our theory.

Rotation Instability of Neoclassical Plasma Near Magnetic Separatrix

U. Daybelge¹, C. Yarim¹

¹Istanbul Technical University, Istanbul, Turkey

Corresponding Author: U. Daybelge, daybelge@itu.edu.tr

Plasma rotation plays a central role in magnetic confinement of toroidal plasmas, as it can reduce turbulence and enhance transport. In turn rotation can be generated both intrinsically by microturbulence via Reynolds stress, and by external momentum sources, such as, for example, neutral beam injection (NBI). By assuming a collisional plasma with steep gradients at the edge region of an axisymmetric tokamak with large aspect ratio, we investigated the rotation of the plasma and its stability criteria through a numerical analysis in the context of neoclassical transport theory. The governing equations of temperature, density, and poloidal and toroidal velocities were obtained previously by reducing the Braginskii equations with Mikhailowskii-Tsypin corrections. This system of equations can be cast into a generic reaction-diffusion form. Under various types of BCs to be found in the medium, and inputs like NBI, Pellet Injection or Loop Voltage, we studied the selection of wave trains, the symmetry-breaking bifurcations, responsible for the emergence of spatiotemporal patterns, that are stationary or oscillatory in space and time. In our simulations the interaction of wave and Turing instabilities were also considered, as the rise of Turing type of patterns requires the diffusivities in the individual equations to be of different order, as is the case in our equations.

Kinetic Integrated Modeling of Burning Start-up Phase in Tokamaks

A. Fukuyama¹, H. Nuga², and S. Murakami³

¹Kyoto University, Kyoto, Japan
 ²University of Tsukuba, Tsukuba, Ibaraki, Japan
 ³Departement of Nuclear Engineering, Kyoto University, Kyoto, Japan

Corresponding Author: A. Fukuyama, fukuyama@nucleng.kyoto-u.ac.jp

ener mod

In order to self-consistently describe the start-up phase of burning plasmas in the presence of energetic particles, we have developed a kinetic integrated tokamak modeling code TASK3G. This modeling is based on the behavior of the momentum distribution function of each particle species. The time evolution of the momentum distribution function is described by an advanced Fokker-Planck component TASK/FP. The burning start-up of ITER plasmas with multi-scheme heating and current drive is studied including radial transport and fusion reaction rate calculated from the momentum distribution function. The dependence on heating scheme, heating power and start timing has been studied and the optimum condition for the reduction of heating power is discussed.



Analysis of ITB and ETB Formations in Tokamak Plasma Using Bifurcation Concept

T. Onjun¹, B. Chatthong¹, R. Picha², and N. Poolyarat³

¹Sirindhorn International Institute of Technology, Pathum Thani, Thailand ²Thailand Institute of Nuclear Technology, Bangkok, Thailand ³Thammasat University, Pathum Thani, Thailand

Corresponding Author: T. Onjun, thawatchai@siit.tu.ac.th

The formation of transport barriers, including both ETB (edge transport barrier) and ITB (internal transport barrier), in tokamak plasma is investigated using bifurcation concept. A set of heat and particle transport equations with both neoclassical and anomalous effects is used to represent the plasma in slab geometry. The neoclassical coefficients are assumed to be constant, while the anomalous coefficients, taking effect only above critical gradients, are assumed to be locally driven by gradients of pressure and density. The transport suppression is assumed to occur only in the anomalous channel with flow shear and magnetic shear as suppression mechanisms. The flow shear, presented in term of coupling pressure and density gradients, is assumed to nonlinearly suppress the transport, whereas the magnetic shear plays a more complicated role in the suppression of the transport and reduction of the flow shear strength. Both transport equations are analytically and numerically solved for local plasma gradients in order to examine ETB and ITB formations. It is found that the results exhibit bifurcation nature when mapped onto fluxes versus gradients space in which abrupt jumps in the gradients can be observed at both transport barrier locations. ETB appears to form only if the critical flux is reached regardless of the magnetic shear profile, while ITB formation is possible only with a reversed magnetic shear profile. In addition, with a suitable magnetic shear profile, the minimum flux criterion is not needed for ITB formation, though the abrupt jumps in the gradients become smoother at lower flux. ITB location and width are also found to be correlated to the nature of *q*-profile. In particular, the location is in the vicinity of where *q*-profile reverses its direction and the width appears to be inversely proportional to its curvature.

Self-Consistent Modeling of Radio-Frequency Sheaths: Comparison with Tore Supra Measurements and Predictability for Future Machines

L. Colas¹, J. P. Gunn¹, J. Hillairet¹, X. Litaudon¹, J. Jacquot², D. Milanesio³, L. Lu¹, J.-M. Bernard¹, S. Carpentier⁴, Y. Corre¹, F. Durodie⁵, E. Faudot⁶, M. Firdaouss¹, M. Goniche¹, W. Helou¹, S. Heuraux⁶, M. Kubic¹, P. U. Lamalle¹, R. Maggiora³, and R. A. Pitts¹

¹CEA-IRFM, Saint Paul lez Durance, France
 ²Max-Planck-Institut für Plasmaphysik, Garching, Germany
 ³Polytechnic University of Turin, Turin, Italy
 ⁴EIRL S. Carpentier-Couchana, Meyrargues, France
 ⁵Laboratory for Plasma Physics, ERM/KMS, Brussels, Belgium
 ⁶Institut Jean Lamour, Université de Lorraine, CNRS, Nancy, France

Corresponding Author: L. Colas, laurent.colas@cea.fr

In magnetic Fusion devices, nonlinear wave-plasma interactions in the plasma edge often set operational limits for Radio-Frequency (RF) heating systems, due to impurity production or excessive heat loads. Understanding these interactions is key for reliable high-power Ion Cyclotron (IC) wave launch over long pulses in all-metal devices. Edge IC losses are attributed to a Direct Current (DC) biasing of the Scrape-Off Layer (SOL) plasma by RF sheath rectification. This paper presents a first step towards self-consistent modelling of RF wave penetration and the edge plasma DC biasing. A wave equation propagates the Slow magnetosonic mode from a map of the parallel RF electric field imposed at the outer boundary of the simulation domain. The local DC plasma potential VDC is governed by the continuity equation for DC currents in presence of anisotropic DC conductivity. The RF and DC modules are coupled by nonlinear RF and DC sheath boundary conditions at the lateral boundaries of the simulation domain. The code is implemented with COMSOL, presently in two dimensions (radial/toroidal), with boundaries either parallel or normal to the confinement magnetic field. This approach could reproduce qualitative observations about heat loads and probe potentials measured in the vicinity of Tore Supra antennas that were hardly compatible with earlier models. For example asymmetric strap excitation led to left/right sheath asymmetry between the two extremities of the same field lines. Biasing of the free SOL has to rely on VDC diffusion from the private SOL due to the transport of DC current. This mechanism is qualitatively consistent with DC current flows measured in the vicinity of active antennas. The relative simplicity of the present model, its sensitivity to SOL parameters (density, temperature) and the large uncertainty on SOL transport coefficients make quantitative RF-sheath predictions challenging. Poloidal distributions of sheath potentials and relative comparisons between antennas look more robust for predictive assessment. This was assessed by comparing two Faraday screen types on Tore Supra and was subsequently applied to estimate sheath effects for the ITER antenna with different strap phasings. Finally a roadmap is proposed for testing the present model further against existing experiments, and for improving it towards full-wave propagation and shaped walls.

How Turbulence Spreading Decouples the Flux from the Local Gradient: a Nonlinear Gyrokinetic Simulation Study

S. Yi¹, J. Kwon¹, and P. H. Diamond^{1,2}

¹National Fusion Research Institute, Daejeon, Korea, Republic of ²University of California San Diego, CA, USA

Corresponding Author: S. Yi, vism@nfri.re.kr

Understanding and prediction of turbulent transport are crucial to achieving improved confinement states in advanced magnetic fusion reactors. However, conventional transport models based on the local saturation paradigm fail to explain many experimental phenomena, e.g., the broken gyro-Bohm scaling, the stiffness of ion temperature profile etc. Nonlinear turbulence spreading in inhomogeneous plasma turbulence can explain the discrepancies [1] by decoupling local turbulence intensity, and thus turbulent flux, from the local gradient. In this contribution, we report on a gyrokinetic simulation study of turbulence spreading, especially focusing on its effects on ion heat transport under conditions of variable magnetic shear and external toroidal rotation shear. These are known to be critical to controlling ion heat transport in experiments [2]. Our key findings from the simulations are two: 1) nonlinear turbulence spreading is enhanced at low magnetic shear, and 2) ion heat transport is more effectively reduced by the suppression of turbulence spreading due to external rotation shear in low magnetic shear region. Sheared toroidal rotation is more effective on the decorrelation of turbulence in the low magnetic shear region. Our result is consistent with the findings of recent stiffness control experiments [2], where the combination of low magnetic shear and external rotation shear was shown to be effective in controlling T_i -profile stiffness. As turbulence spreading is very likely an important contributor to the ion heat transport dynamics in experiments, our novel findings suggest a new interpretation of de-stiffening.

References

[1] T.S. Hahm, et al., Plasma Phys. Control. Fusion 46, A323 (2004).

[2] P. Mantica, et al., Phys. Rev. Lett. 107, 135005 (2011).

L-P

Paper



TH/P6-11

Integrated Modeling of Tokamak Experiments with OMFIT

O. Meneghini¹, S. Smith², E. A. Belli², G. Falchetto³, N. M. Ferraro², B. Grierson⁴, J. Candy², V. S. Chan², C. Holland⁵, O. Izacard⁵, H. St John², T. Osborne², L. Lao², G. Li⁶, R. Prater², Q. Ren⁶, P. B. Snyder², G. M. Staebler², and A. Turnbull²

¹Oak Ridge National Laboratory, Oak Ridge, TN, USA
 ²General Atomics, San Diego, CA, USA
 ³CEA-IRFM, Saint Paul lez Durance, France
 ⁴Princeton Plasma Physics Laboratory, Princeton, NJ, USA
 ⁵University of California San Diego, CA, USA
 ⁶Institute of Plasma Physics, Chinese Academy of Sciences, Hefei, China

Corresponding Author: O. Meneghini, meneghini@fusion.gat.com

One Modeling Framework for Integrated Tasks (OMFIT) is a comprehensive integrated modeling framework developed to facilitate the interpretation of today experiments, enable theory validation, and support the design of next step devices. OMFIT is unique in its underlying data structure and grassroots approach. After only two years since the beginning of the project, the framework is now routinely used for frontline scientific research, and has an expanding collection of supported physics codes and workflows, which is driven by a growing number of users. OMFIT streamlined and increased the scientific throughput of a series of DIII-D experimental data analyses that are tedious, time-consuming, hard to track and error-prone if done manually. These include kinetic plasma equilibrium reconstruction, core and edge stability surveys, and critical-gradient transport studies. The effects on kinetic equilibrium reconstructions of using an exact neoclassical bootstrap current calculation or the approximate Sauter formula were evaluated. Magnetic flutter and neoclassical toroidal viscosity were shown to well describe the effect of resonant magnetic perturbations (RMPs) on edge transport and rotation. A neural-network approach was developed to perform nonlinear multivariate regression of transport fluxes as a function of local dimensionless plasma parameters, and showed excellent quantitative agreement with the DIII-D measurements. The numerical efficiency of the method makes it an ideal candidate for real-time transport simulations.

Concerning predictive transport simulations, OMFIT made possible the design of a workflow that can efficiently find the self-consistent equilibrium and transport solutions by taking advantage of the time-scale separation between transport and current evolution. We found that the feedback between the transport fluxes and plasma equilibrium strongly affects the resulting kinetic profiles and can significantly improve the agreement with the experiments. This technique was validated on DIII-D data used to design baseline and advanced tokamak operational scenarios for both DIII-D and FNSF. Future work in this area of research will focus on including the EPED model in the workflow so to take into account the interplay between edge stability and core transport.

Work supported in part by US DOE under DE-FG02-95ER54698

Extension of Kinetic-Magnetohydrodynamic Model to Include Toroidal Rotation Shear Effect and its Application to Stability Analysis of Resistive Wall Modes

J. Shiraishi¹, N. Miyato¹, G. Matsunaga¹, M. Honda¹, N. Hayashi¹, and S. Ide¹

¹ Japan Atomic Energy Agency, Naka, Japan

Corresponding Author: J. Shiraishi, shiraishi.junya@jaea.go.jp

Extension of the kinetic-magnetohydrodynamic model is presented to include toroidal rotation shear effect for the first time. The sheared rotation is introduced through generalization of the guiding center Lagrangian, yielding two additional terms in a quadratic form of mode-particle resonance. These two terms are overlooked in conventional models. The new model is applied to stability analysis of resistive wall modes (RWMs) successfully. Numerical results show that the rotation shear reduces RWM growth rates further, which is consistent with experimental results.



TH/P6-14

Theoretical and Simulation Studies on the Wave and Particle Dynamics Associated with Alfvén Eigenmodes in Tokamak Plasmas

J. Zhu¹, Z. Ma¹, G. Fu², L. Yu³, W. Chen⁴, X. Zhang³, Z. Sheng¹, Z. Qiu¹, L. Chen¹, and F. Zonca⁵

¹IFTS, Zhejiang University, Zhejiang, China
 ²Princeton Plasma Physics Laboratory, Princeton, NJ, USA
 ³East China University of Science and Technology, China
 ⁴Southwestern Institute of Physics, Chengdu, Sichuan, China
 ⁵Associazione EURATOM-ENEA Unitá Tecnica Fusione, Frascati, Italy

Corresponding Author: J. Zhu, zwma@zju.edu.cn

In this work, we present analytical and simulation results of the wave and energetic particle (EP) dynamics associated with Alfvén Eigenmodes (AE) in tokamak fusion plasmas. It is found that i) both the nonlinear saturation and the wave-frequency chirping dynamics of toroidal Alfvén eigenmodes (TAE) depend crucially on the EP velocity anisotropy, and exhibits features of wave-EP phase/resonance locking; ii) the finite frequency geodesic acoustic modes (GAMs) could be spontaneously excited by TAEs and could, consequently, leading to effective saturation of TAEs; and iii) both kinetic effects associated with short perpendicular wavelengths and current gradient term play crucial roles in the existence of downward frequency sweeping reverse shear Alfvén eigenmodes (RSAEs) in consistence with HL-2A experimental observations.

Preprint

New Physics Insights on Size-Scaling of Confinement Enabled by Computing at Extreme Scale

W. Tang^{1,2}

¹Princeton University, Princeton, NJ, USA ²Princeton Plasma Physics Laboratory, Princeton, NJ, USA

Corresponding Author: W. Tang, wtang@pppl.gov

The extreme scale plasma turbulence studies described in this paper have helped produce new results on confinement scaling in magnetic fusion systems through the deployment of novel algorithms able to deal with the formidable computational challenges associated with powerful, world-class supercomputers characterized by much lower memory than in the past. Nonlinear particle-in-cell simulations carried out on leadership class supercomputers have produced results that help accelerate progress in the understanding of plasma turbulence. In particular, the long time behavior of turbulent transport in ITER-scale plasmas is studied using simulations with unprecedented phase-space resolution to address the reliability and realism of the well-established picture of "rho-star size scaling" of confinement in tokamaks and the associated physics question of if and how turbulent transport changes with the size of laboratory plasmas up to the ITER scale.

The current generally supported picture is that size-scaling follows an evolution from a "Bohm-like" trend where the confinement degrades with increasing system size, to a "Gyro-Bohm-like" trend where the confinement for JET-sized plasmas begins to "plateau" and then exhibits no further confinement degradation as the system size further increases toward ITER-sized plasmas [1, 2]. A number of physics papers over the past decade have proposed theories — such as turbulence spreading — to account for this transition to Gyro-Bohm scaling with plasma size for large systems [3, 4]. The main point in this paper is that this key decade-long fusion physics picture of the rho-star "rollover" trend associated with the toroidal ion temperature gradient instability should be re-examined by modern supercomputing-enabled simulation studies which are now capable of being carried out with much higher phase-space resolution and duration. Associated new results will be presented.

References

[1] Z. Lin, S. Ethier, T. S. Hahm, and W. M. Tang, Phys. Rev. Lett. 88, 195004 (2002).

[2] B. F. McMillan, et al., Phys. Rev. Lett. 105, 155001 (2010).

[3] Z. Lin and T. S. Hahm, Phys. Plasmas 11, 1099-1108 (2004).

[4] O. D. Gurcan, P. H. Diamond, T. S. Hahm, and Z. Lin, Phys. Plasmas 12, 032303 (2005).



Nonlinear Excitation of Kinetic Geodesic Acoustic Modes by Drift Waves in Nonuniform Plasmas

Z. Qiu¹, *L.* Chen¹, and F. Zonca²

¹Zhejiang University, Zhejiang, China ²Associazione EURATOM-ENEA Unitá Tecnica Fusione, Frascati, Italy

Corresponding Author: Z. Qiu, zqiu@zju.edu.cn

is Th

In this work, nonlinear excitation of geodesic acoustic modes (GAM) by drift wave (DW) turbulence is investigated, taking into account effects of finite kinetic dispersiveness and system nonuniformities. The nonlinear equations describing nonlinear parametric decay of DW into GAM and DW lower sideband are derived using nonlinear gyrokinetic theory. The corresponding governing equations are solved both analytically and numerically to investigate the effects of finite kinetic dispersiveness and system nonuniformities on the parametric decay process, such as nonuniform diamagnetic frequency, finite radial envelope and DW pump and GAM continuum. It is found that the parametric decay process is a convective instability for typical tokamak parameters when finite group velocities associated with kinetic dispersiveness and finite radial envelope are taken into account. When, however, nonuniformity of diamagnetic frequency is taken into account, the parametric decay process becomes, time asymptotically, a quasi-exponentially growing absolute instability. The nonuniformity of GAM continuum, meanwhile, causes radial symmetry breaking between outward and inward propagating modes, but the qualitative picture remains the same.



Analysis of Radial Electric Field Formation by Asymmetry of Neutral Beam Injection on KSTAR and NSTX Based on the Gyro-Center Shift

K. C. Lee¹, S. G. Lee¹, Y.-U. Nam¹, L. Tezolo¹, H. Han¹, W. Lee², J. Leem², S. Zoletnik³, M. Lampert³, B. P. LeBlanc⁴, and R. Bell⁴

¹National Fusion Research Institute, Daejeon, Korea, Republic of
 ²Pohang University of Science and Technology (POSTECH), Korea, Republic of
 ³Wigner Research Center, Association EURATOM, Budapest, Hungary
 ⁴Princeton Plasma Physics Laboratory, Princeton, NJ, USA

Corresponding Author: K. C. Lee, kclee@nfri.re.kr

An analysis of radial electric field formation in the core region of tokamak is developed based on the gyro-center shift (GCS) theory and its calculation is compared with experimental measurements on KSTAR and NSTX. The GCS theory suggests the radial electric field formation by the perpendicular component of neutral beam injection (NBI) momentum input [1]. Most of induced $E \times B$ drift is balanced with the parallel rotation so that the plasma rotation is purely toroidal but there are regions where the induced radial electric field generates poloidal rotation since the neutral beam is injected into the same flux tube with different pitch angles when it propagates into inboard side and outboard side. The poloidal rotation measurements from beam emission spectroscopy (BES) and microwave imaging reflectometer (MIR) for the edge region and X-ray imaging crystal spectrometer (XICS) for the core region with analysis using NUBEAM code will be presented on KSTAR. The profile measurement of poloidal velocity by charge exchange recombination spectroscopy (CHERS) on NSTX is also compared with the calculation based on GCS theory.

References

Lee

[1] Lee, K. C., Plasma Phys. Control. Fusion 51 065023 (2009).



TH/P6-38

Integrated Heat Transport Simulation of High Ion Temperature Plasma of LHD

S. Murakami¹, H. Yamaguchi¹, A. Sakai¹, K. Nagaoka², H. Takahashi², H. Nakano², M. Osakabe², K. Ida², M. Yoshinuma², M. Yokoyama², A. Wakasa¹, and A. Fukuyama³

¹Departement of Nuclear Engineering, Kyoto University, Kyoto, Japan ²National Institute for Fusion Science, Toki, Japan ³Kyoto University, Kyoto, Japan

Corresponding Author: S. Murakami, murakami@nucleng.kyoto-u.ac.jp

High ion temperature, T_i , experiments have been performed applying the tangential and perpendicular NBI heating systems in LHD. The high T_i plasma up to 7.3 keV has been obtained during the decay phase of the density after rapid increase due to a carbon pellet injection. Simple heat transport analysis of these high T_i plasma has been done but the rapid change of density effect on the NBI heat deposition and the multi-ion species effects on the heat transport is not treated accurately. In order to analyze the transport property of the time evolving plasma, we have to use NBI heat deposition analysis code including the effect of plasma time evolution. Also the plasma contains sufficient impurities due to the He gas puff and C pellet injection and the heat transport simulation should take care the multi-ion species. In this paper we study the high T_i plasma with C pellet injection of LHD applying the integrated simulation code, TASK3D+GNET-TD. The NBI heat deposition profile of time evolving plasma is evaluated by GNET-TD extending the 5D drift kinetic equation solver GNET. The heat transport of multi-ion species plasma (e, H, He, C) is studied by the integrated transport simulation code, TASK3D. It is found that an achievement of high ion temperature plasma is attributed to the 1) increase of heating power per ion due to the temporal increase of effective charge, 2) reduction of effective neoclassical transport with impurities, 3) reduction of turbulence transport. The reduction of turbulence transport is most significant contribution to achieve the high ion temperature and the reduction of the turbulent transport from the L-mode plasma (normal hydrogen plasma) is evaluated to be a factor about five by using integrated heat transport simulation code.

Transport Simulation Analysis of Peripheral Plasma with the Open and the Closed LHD Divertor

G. Kawamura¹, Y. Feng², M. Kobayashi¹, M. Shoji¹, T. Morisaki¹, and S. Masuzaki¹

¹National Institute for Fusion Science, Toki, Japan ²Max-Planck-Institut für Plasmaphysik, Garching, Germany

Corresponding Author: G. Kawamura, kawamura.gakushi@nifs.ac.jp

Transport of plasma, neutral, and impurities in peripheral regions is closely linked to the configuration of the device. The divertor configuration of LHD (Large Helical Device) has been modified to the closed one to control neutral transport and achieve effective pumping. In order to make comparisons of the open and the closed LHD divertor, a new calculation mesh covering the ergodic, the divertor-leg and the vacuum regions has been developed for three-dimensional transport code EMC3-EIRENE. This paper presents simulation analysis of transport and validation with experimental measurements.

A series of simulations with the both divertor configurations was carried out with the electron density from 1×10^{19} to 8×10^{19} m⁻³ at the last closed flux surface (LCFS) and a fixed heating power of 8 MW to simulate a density-buildup in a discharge. The typical electron temperature on the divertor plates decreases from 40 eV to less than 5 eV during the density scan. The simulations involve plasma-wall interactions such as hydrogen recycling and impurity generation.

An influence of the change from the open to the closed configuration is observed as increase of the plasma source. The source increases mainly in the legs in low-density discharges and in the ergodic region in high-density discharges. The electron temperature on the divertor plates becomes low in the case of the closed configuration because of the large plasma source. The increase of plasma source and difference of neutral transport cause increase of neutral density under the dome structure by a factor of ten in the closed configuration. The ratio of the pressure between the both configurations and its dependence on the electron density at the LCFS are in good agreement with measurements.

Transport of carbon sputtered from the plasma-wetted surfaces with a fixed sputtering yield was simulated. The increase of plasma-neutral interaction enhances particle flux onto the surface, and hence the number of sputtered carbon increases in the case of the closed configuration. The amount of carbon ions in the leg increases during the density buildup regardless of the configurations but reduction of carbon accumulation in ergodic region, i.e., impurity screening, is observed when the electron density is high. The impurity transport is significantly affected by parallel flow in the ergodic region with long flux tubes.



TH/P6-40

Electromagnetic Gyrokinetic Analysis of Turbulent Transport in Finite-beta LHD Plasmas

A. Ishizawa¹, T.-H. Watanabe², H. Sugama¹, K. Tanaka¹, and N. Nakajima¹

¹National Institute for Fusion Science, Toki, Japan ²University of Nagoya, Nagoya, Japan

Corresponding Author: A. Ishizawa, ishizawa@nifs.ac.jp

Turbulent transport in finite- β Large Helical Device (LHD) plasmas is investigated by means of electromagnetic gyrokinetic simulations. It is found that i) the ITG mode growth rate decreases with increasing β , and the kinetic ballooning mode (KBM) becomes a dominant instability for local β values larger than 2–3% in typical LHD configurations, ii) shearing between oppositely inclined convection cells newly found in the LHD configuration leads to saturation of the KBM instability which is hardly saturated in flux tube simulations of finite- β tokamaks because of weak zonal flow generation, and iii) the efficiency of KBM turbulence in the transport is much smaller than that of ITG turbulence.

Whereas in low- β torus plasmas the zonal flow shear acts to regulate ITG driven turbulence, it has often been observed by gyrokinetic simulations that instabilities continue to grow without reaching a physically relevant level of saturation at finite- β tokamaks. The corresponding problem in finite- β helical plasmas is an open question, and we have revealed a new saturation mechanism.

The finite- β turbulence is saturated by the new saturation mechanism that is the nonlinear interactions of oppositely inclined convection cells through mutual shearing, even when the zonal flow is weak. The new mechanism may also cause saturation of turbulence in finite- β tokamaks in the presence of three-dimensionality such as toroidal ripples and resonant magnetic perturbation (RMP).

Preprint

NBI and HHFW Fast Ion Temporal Dynamics Modeling with CQL3D-Hybrid-FOW in NSTX Discharges

R. W. Harvey¹, Y. Petrov¹, D. Liu², W. W. Heidbrink², G. Taylor³, and P. Bonoli⁴

¹CompX, Del Mar, California, USA ²University of California Irvine, CA, USA ³Princeton Plasma Physics Laboratory, Princeton, NJ, USA ⁴Massachusetts Institute of Technology, Cambridge, MA, USA

Corresponding Author: R. W. Harvey, rwharvey@compxco.com

The CQL3D Fokker-Planck code [1] has been upgraded to include physics of finite-orbit-width (FOW) guiding-center orbits [2, 3], as compared with the previous zero-orbit-width (ZOW) model, and a recent first-order orbit calculation [2]. The Fast Ion Diagnostic FIDA [4, 5] signal resulting from neutral beam (NBI) and high harmonic fast wave (HHFW) RF power injected into the NSTX spherical tokamak can now be modeled quite accurately using ion distributions from the CQL3D-Hybrid-FOW code, a rapidly executing variant that includes FOW+gyro-orbit losses to the plasma edge, FOW effects on NBI injection and HHFW diffusion, but does not include neoclassical radial diffusion. Accurate, prompt FI losses are a key feature of the marked modeling improvement relative to previous ZOW results. By comparing NBI-only and NBI+HHFW shots, independent confirmation of the usual 35% edge loss of HHFW in NSTX is obtained. Further, HHFW prompt losses from the plasma core are shown to be $3 \times a$ slarge (> 25% total) as the NBI-only case. Limited neoclassical radial diffusion calculations show an increase of the FI distribution at large plasma radius, consistent with the near edge signal from the FIDA [5]. The modulated NBI and time-dependent background plasma variations are accounted for, also giving temporal neutron variation in approximate agreement with NSTX observations.

Supported by USDOE grants DE-SC0006614, DE-FG02-04ER54744, and DE-FC02-01ER54649, and DE-AC05-00R22725.

References

[1] R.W. Harvey and M. McCoy, http://www.compxco.com/cql3d.html.

- [2] R.W. Harvey, Yu. Petrov, et al., EPS, Strasbourg, France (2011).
- [3] Yu. Petrov and R.W. Harvey, Proc. of IAEA FEC, San Diego (2012).



Modeling Divertor Concepts for Spherical Tokamaks NSTX, NSTX-U, and ST-FNSF

E. Meier¹, V. Soukhanovskii¹, R. Bell², A. Diallo², S. Gerhardt², R. Kaita², B. LeBlanc², A. G. McLean¹, J. Menard², M. Podestá², T. Rognlien¹, F. Scotti², and A. W. Leonard³

> ¹Lawrence Livermore National Laboratory, Livermore, CA, USA ²Princeton Plasma Physics Laboratory, Princeton, NJ, USA ³General Atomics, San Diego, CA, USA

Corresponding Author: E. Meier, meier23@llnl.gov

TH/P6-50

As magnetic confinement fusion research progresses toward the reactor scale, increasingly intense power exhaust threatens the integrity of plasma facing components. The compact nature, i.e., small major radius (R), of the spherical tokamak (ST) presents an economically attractive path to fusion commercialization, but magnifies the power exhaust challenge, because the plasma-wetted area is proportional to R. To address this challenge, experimentally constrained divertor modeling in the National Spherical Torus Experiment (NSTX) is extrapolated to investigate divertor concepts for future ST devices. Analysis is conducted with the multi-fluid edge transport code, UEDGE. Modeling of NSTX snowflake divertor experiments demonstrates an ability to capture observed physics behavior, including partial detachment and several-fold heat flux reduction. Increased plasma-wetted area in the snowflake enhances neutral gas power loss to the outer divertor targets, enabling the partially detached state. NSTX Upgrade (NSTX-U) analysis shows that heat flux can be mitigated (to $< 10 \text{ MW/m}^2$, i.e., within present technological limits) using impurity seeding in both snowflake and standard divertor configurations. For a notional Spherical-Tokamak-based Fusion Nuclear Science Facility (ST-FNSF), divertor concepts are identified that provide heat flux mitigation ($< 10 \text{ MW/m}^2$) in updown-symmetric double-null magnetic geometries with 40 MW input power and 100%-recycling metal targets. This research provides guidance for upcoming experiments and a basis for continued development of predictive capability for divertor performance in STs.

Research supported by US DOE Contracts DE-AC52-07NA27344 and DE-AC02-09CH11466.

Preprint

Modelling the Effect of Lithium on SOL Dynamics and the SOL Heat Flux Width Observed in NSTX

D. Russell¹, D. D'Ippolito¹, J. Myra¹, J. Canik², T. K. Gray², and S. Zweben³

¹Lodestar Research Corporation, USA ²Oak Ridge National Laboratory, Oak Ridge, TN, USA ³Princeton Plasma Physics Laboratory, Princeton, NJ, USA

Corresponding Author: D. Russell, dave@lodestar.com

The effect of lithium wall coatings on scrape-off-layer (SOL) turbulence is modeled with the Lodestar SOLT code to explore the implications for the SOL heat flux width on NSTX of experimentally observed, Li-induced changes in the pedestal profiles. The connection is important because pedestal profiles impact the overall fusion performance of ITER and future machines while the SOL heat flux width impacts the survivability of divertor target plates. The SOLT code used in the modeling has been expanded recently to include ion temperature evolution and ion diamagnetic drift effects. This work focuses on two NSTX shots: pre- and post-Li deposition. The simulation density and energy profiles are constrained, inside the last closed flux surface only, to match those measured in the two experiments, and the resulting drift-interchange-driven turbulence is explored. The effect of Li enters the simulation only through the profile constraint: Li modifies the experimental density and temperature profiles, and these profiles affect the simulation SOL turbulence. The power entering the SOL (P_{SOL}) measured in the experiments is matched in the simulations by adjusting "free" dissipation parameters (e.g., diffusion coefficients) that are not measured directly in the experiments. At power-matching, a) the heat flux SOL width (λ_a) is smaller in the post-Li case, as observed experimentally, and b) density fluctuation amplitudes are reduced, post-Li, also as observed. The instabilities and saturation mechanisms that underlie the SOLT model equilibria are discussed.

Work supported by USDOE grants DE-FG02-97ER54392 and DE-FG02-02ER54678.



TH/P6-55

Transient CHI Plasma Start-up Simulations and Projections to NSTX-U

R. Raman¹, F. Ebrahimi², S. C. Jardin², T. Jarboe¹, J. Menard², D. Mueller², *B. Nelson*¹, and M. Ono²

¹University of Washington, Seattle, WA, USA ²Princeton Plasma Physics Laboratory, Princeton, NJ, USA

Corresponding Author: R. Raman, raman@aa.washington.edu

Transient Coaxial Helicity Injection (CHI) in the National Spherical Torus Experiment (NSTX) has generated toroidal current on closed flux surfaces without the use of the central solenoid. When induction from the solenoid was added, CHI initiated discharges in NSTX achieved 1 MA of plasma current using 65% of the solenoid flux of standard induction-only discharges. CHI is incorporated into the NSTX-U machine design, to be used for the start-up phase of a full non-inductive current ramp-up scenario. The objective for first two years of CHI research on NSTX-U is to re-establish transient CHI start-up in the new vessel geometry, and to generate 400 kA of closed-flux start-up current. In support of these planned experiments, the TSC code has been used to develop transient CHI start-up scenarios using the full NSTX-U vessel geometry, implemented during the past year. We have also used the resistive MHD code NIMROD, to understand the mechanisms that lead to the generation of closed flux plasma in a transient CHI discharge. These simulations show that the new machine capabilities on NSTX-U significantly enhance CHI-startup capability. Simulations have also confirmed the role of the magnitude of the injector flux, the importance of a narrow flux foot print width, and rapid time scales required for reducing the injector voltage and (current) in increasing the magnitude of the closed flux fraction [1]. What is particularly noteworthy is that the NIMROD simulations suggest that the reconnection mechanisms for transient CHI appear to be very similar to 2D Sweet-Parker type reconnection, and 3D effects do not seem to be important.

This work is supported by US DOE contracts DE-FG02-99ER54519, DOE-FG02-12ER55115, and DE-AC02-09CH11466.

References

[1] F. Ebrahimi, et al., submitted to Phys. Plasmas.

Preprint

Verification of the Simulated Radiated Power of the ICRH Antenna Design for Wendelstein 7-X with Experimental Results Using a Quarter Scale Mock-up Antenna

J. Ongena¹, A. Messiaen¹, A. Krivska¹, F. Louche¹, B. Schweer¹, M. Vervier¹, M. Van Schoor¹, V. Borsuk², O. Neubauer², R. Wolf³, D. Hartmann⁴, and D. Birus⁴

¹Laboratory for Plasma Physics, ERM/KMS, Brussels, Belgium
 ²Forschungszentrum Jülich, Jülich, Germany
 ³Max-Planck-Institut für Plasmaphysik, Garching, Germany
 ⁴Max-Planck-Institut für Plasmaphysik, Greifswald, Germany

Corresponding Author: J. Ongena, j.ongena@fz-juelich.de

An ICRH antenna consisting of two poloidal straps is now under design for W7-X in a collaboration between IEK-4/FZJ and LPP/ERM-KMS. The two straps are on one side connected to a tuning capacitor and grounded to the antenna box at the other end. To reduce the voltage in the feeding transmission lines and matching system, a pre-matching has been implemented by connecting the RF transmission lines at an intermediate position on each strap. This paper describes the optimization of this design to maximize coupling to the plasma using modern simulation codes (MWS, TOPICA) and its experimental validation obtained using a reduced scale mock-up, loaded with salted water and a ferroelectric dielectric to mimick the plasma.

Energetic Particle Driven n = 1 MHD Instabilities in Tokamaks with Weakly Reversed Shear

D. P. Brennan¹, J. M. Finn², M. R. Halfmoon³, A. D. Turnbull⁴, and R. White⁵

¹Princeton University, Princeton, NJ, USA
 ²Los Alamos National Laboratory, Los Alamos, NM, USA
 ³University of Tulsa, OK, USA
 ⁴General Atomics, San Diego, CA, USA
 ⁵Princeton Plasma Physics Laboratory, Princeton, NJ, USA

Corresponding Author: D. P. Brennan, dylanb@princeton.edu

Recent simulation results have indicated that in experiments with weakly reversed magnetic shear and the minimum in safety factor q just above unity, energetic particles in a slowing down distribution can drive two important MHD modes unstable, one a nonresonant, dominantly 1/1 mode localized within the minimum in q, and the other a resonant, dominantly 2/1 mode, which can cause a disruption of the discharge. These discharges tend to have a long steady state with high confinement, and are therefore a candidate operational scenario for burning plasma experiments. The delta-f kinetic-MHD model in the 3D extended MHD code NIMROD is used to perform a simulation study of energetic particle effects on these two instabilities. The analysis makes use of model equilibria relevant to the DIII-D and NSTX experiments, where related instabilities are observed.

Experimentally, during steady state operation, a benign nonlinearly saturated m/n = 1/1 structure is observed, in qualitative agreement with the computed mode in key physical respects. At slightly higher β_N the 2/1 mode is found unstable and terminates the discharge. To explain the physics of the driven instabilities we examine their theoretical origins in simplified configurations, including an analysis of the mode-particle resonances.

We use the Orbit code to analyze these resonances between the particles and the mode, in both the ideal MHD stable and particle driven cases. Ideal MHD eigenfunctions have a fixed phase of the instability with radius, which is the usual basis on which to study mode-particle interaction, while the nonideal MHD eigenfunctions with particle interaction effects can have phase variation in the radial direction. The Orbit code has thus been modified to account for this phase variation. The details of the resonant interaction in the simulations is clarified by this analysis, in that the perturbations generate islands in the phase space of particle orbits, the structure of which sheds light on the physics of the interaction.

Preprint

Evolution and System Dependent Properties of Zonal Flows and GAMs in Tokamaks and Planet Atmospheres

K. Hallatschek¹, A. Kammel¹

¹Max-Planck-Institut für Plasmaphysik, Garching, Germany

Corresponding Author: K. Hallatschek, klaus.hallatschek@ipp.mpg.de

We have studied the evolution of the zonal flows (ZF) in first principles two-fluid and gyrokinetic turbulence simulations, while artificially controlling the starting conditions or time dependence of the flows to find the rules governing the flow evolution, the preferred, stable and unstable states, and the influence of inhomogeneities, i.e., the effects of the boundary conditions and of radially varying plasma 📕 parameters and other non-Boussinesq effects. Thus a robust functional describing the parallel and perpendicular Reynolds stresses has been determined, which inserted into a 1D momentum balance equation is able to reproduce the evolution of the self-consistent radial ZF pattern from noise to the stationary state. Thereby a qualitative difference was discovered between toroidal ion temperature gradient (ITG) turbulence and sheared cylinder resistive drift wave (DW) turbulence induced flows. While in the ITG case, the wavelength of the flow pattern is fixed independent of the initialization, the DW turbulence maintains the period of any initialized pattern while enforcing a square wave shearing rate profile. In a way, the DW-ZF system can be regarded as a digital storage medium with two admissible flow shear states, while the ITG-ZF system has no memory.

For the GAMs, the deterministic part of the turbulence dramatically changes the dispersion relation, resulting in orders of magnitude higher radial drift speeds and determines the preferred GAM wavenumber. This can lead to bursting GAM and turbulence activity, which depends on the sign of the ∇B drift with respect to the closest X-point.

A comparative study of rotating planetary (Jovian) turbulence using the novel NAN (Navier Stokes, anelastic turbulence) code incorporating the associated density contrasts, shows that here ZFs are being generated similarly by a Reynolds stress based self amplification, control turbulence (bursting and profile modulation is observed) and interact with the turbulence modes through wave kinetic effects. The contrast between these notions and the ones in the geophysical framework, which focus on the transport and stretching of vorticity (not momentum as by Reynolds stress) will be reviewed in the contribution.



TH/P7-4

Finite Larmor Radius Effects on Low-*n* Magnetohydrodynamic Modes at H-Mode Pedestal with Plasma Rotation

L. Zheng¹, M. T. Kotschenreuther¹, and P. Valanju¹

¹University of Texas at Austin, Austin, TX, USA

Corresponding Author: L. Zheng, lzheng@mail.utexas.edu

Finite Larmor radius effects (FLR) on the low-*n* MHD modes at high-mode (H-mode) pedestal are investigated in this paper with the inclusion of bootstrap current for equilibrium and rotation effects for stability. When bootstrap current is taken into account, a safety-factor reversal or plateau can be generated at the pedestal. We have shown that the modes of infernal type (or fat interchange modes) can prevail at the safety-factor reversal or plateau region and such a type of modes exhibits the typical features of the so-called edge hormonic oscillations (EHOs) at the QH-mode discharges. There is a physical ground for us to consider the FLR effects. We note that the diamagnetic frequency (ω_*) is directly proportional to pressure gradient and inversely proportional to density. This leads ω_* to become big and vary dramatically at the pedestal, where the infernal modes tend to develop. The AEGIS code is extended to include the FLR effects using the steep pressure gradient ordering. The JET H-mode discharges are reconstructed numerically using the VMEC code, with bootstrap current taken into account. Generally speaking, the FLR effects are stabilizing for infernal modes. Our results show that the FLR effects depend sensitively on the safe factor value (q_s) at the safety-factor reversal or plateau region. The FLR effects are weaker, when q_s is larger than an integer; while stronger, when q_s is smaller or less larger than an integer. We also found that the FLR effects also depend sensitively on the rotation direction. The FLR stabilization in the co-rotation case (for sheared rotation) is stronger than in the counter rotation case with respect to the ion diamagnetic drift direction. We have studied n = 1, 2, and 3 cases and found that with the FLR drift effects being taken into account the frequency-multiplying rule $\omega = n\Omega_s$ are still roughly held. However, we found that in the higher mode number case the wave-particle resonance effects need to be considered. We are also applying the AEGIS-K code to study the MHD modes at the plasma edge fully kinetically. Our investigation on low-n MHD modes at H-mode pedestal is relevant to ITER as well.



Mechanisms and Dynamics of the External Transport Barrier Formation in Nonlinear Plasma Edge Simulations

L. Chôné¹, *P. Beyer*², Y. Sarazin¹, G. Fuhr², and S. Benkadda²

¹CEA-IRFM, Saint Paul lez Durance, France ²Aix-Marseille Université, Marseille, France

Corresponding Author: L. Chôné, laurent.chone@univ-amu.fr

Theoretical understanding of the low to high confinement (L-H) transition in magnetic fusion devices such as ITER still remains unresolved, causing significant uncertainties on the power requirements for entering the H-mode. In particular, turbulence is known to be stabilised by sheared $E \times B$ flows, but the mechanism generating the flows in an H-mode is not clearly identified yet.

In this work, spontaneous stabilisation of turbulence leading to generation of a transport barrier is achieved in flux-driven 3D edge turbulence simulation with an extended fluid model accounting for collisional relaxation of the flow towards force balance. The transition to this state of improved confinement occurs with an input power threshold. Above this threshold, a strong equilibrium shear flow governed by force balance stabilises the turbulence, causing a steepening of the pressure gradient close to the last closed flux surface. The dynamics of the barrier onset is characterised by a complex interplay between the equilibrium flow and zonal-flows when the threshold is marginally crossed, which is reminiscent of the I-phase observed in experiments.

Performing simulations over several confinement times with a reduced 1D model reveals a regime of relaxations of the barrier at constant input power. This regime is found slightly above the power threshold, and disappears when increasing further the input power. In this regime, the barrier collapses quasi-periodically, and each relaxation is associated with a burst of turbulent flux. Simulations have shown that the relaxations become less frequent when the injected power is increased, a behaviour reminiscent of type-III ELMs.



TH/P7-6

Bayesian Derivation of Plasma Equilibrium Distribution Function for Tokamak Scenarios

C. Di Troia¹

¹Associazione EURATOM-ENEA Unitá Tecnica Fusione, Frascati, Italy Corresponding Author: C. Di Troia, claudio.ditroia@enea.it

A parametric distribution function has been proposed as equilibrium distribution function (EDF) for charged particles in fusion plasmas, representing, e.g., supra-thermal particle distribution produced by additional external heating sources in tokamak experiments. This EDF describes an equilibrium because it exclusively depends on constants of motion (COMs). Assuming an axisymmetric system with no equilibrium electric field, the EDF depends on the toroidal canonical momentum P_{φ} , the kinetic energy w and the generalized pitch angle $\lambda = \mu/w$ where μ is the magnetic moment. For a given equilibrium magnetic field these COMs are suitably expressed in guiding center (GC) coordinates. COMs are useful variables for describing and classifying GC orbits, as shown in this work for the general case. It is shown that, by varying the EDF control parameters, it can represent anisotropic equilibria for Neutral Beam Injection, Ion Cyclotron, and Electron Cyclotron Resonance Heating scenarios. Moreover it can also represent isotropic equilibria for Slowing-Down alpha particles and core thermal plasma populations.

The purpose of the work is to present the derivation of the EDF from first principles and general hypothesis. The present derivation is probabilistic and makes use of the Bayes Theorem. The joint probability to find a GC in a specific state is obtained from Bayesian inference. The posterior probability density function (pdf) is proportional to the product of the prior pdf (e.g., the population described by a Maxwellian) multiplied by the conditional pdf which is the product of Birnbaum-Saunders pdf, concerning the magnetic moment, multiplied by a Gaussian pdf, describing the GC velocity. The bayesian argument, used in the present derivation, allows us to describe how far from the prior pdf (e.g. Maxwellian) the plasma is, based on the information obtained from magnetic moment and GC velocity pdf.



A New Theory of Scale Selection: What Determines the Avalanche Scale?

P. H. Diamond¹, Y. Kosuga², Z. Guo³, and O. Gurcan⁴

¹University of California San Diego, CA, USA ²Institute for Advanced Study, Kyushu University, Kasuga, Japan ³National Fusion Research Institute, Daejeon, Korea, Republic of ⁴LPP/Ecole Polytechnique/CNRS, France

Corresponding Author: P. H. Diamond, pdiamond@ucsd.edu

A novel theory to describe the formation of shear flow patterns and avalanches by radially propagating heat flux waves is presented. A model for heat avalanche dynamics is extended to include a finite delay time between the instantaneous heat flux and the mean flux, based on an analogy between heat avalanche dynamics and traffic flow dynamics. The response time introduced here is an analogue of the drivers' response time in traffic dynamics. The microscopic foundation for the time delay is the time for mixing the phase space density. The inclusion of the finite response time changes the model equation for avalanche dynamics from Burgers equation to a nonlinear telegraph equation. Based on the telegraph equation, the formation of heat flux jams is predicted. The growth rate and typical interval of jams are calculated. The connection of the jam interval to the typical step size of the shear flow staircase is discussed. The separation between shear flow layers is calculated and constitutes the effective outer scale of the avalanche distribution.



Kinetic Modeling of Classical and Neo-Classical Transport for High-Z Impurities in Fusion SOL/Divertor Plasmas Using Binary Collision Method

Y. Homma¹, Y. Sawada¹, S. Yamoto¹, and A. Hatayama¹

¹Keio University, Tokyo, Japan

Corresponding Author: Y. Homma, yuki.homma@ppl.appi.keio.ac.jp

Cor Scra

TH/P7-8

Effects of the classical and neo-classical impurity transport across the magnetic *B*-field in the Scrape-Off Layer (SOL) of fusion plasmas, have been studied with a new kinetic model using Binary Collision method (BCM). Our model is able to simulate the following two effects, which have been theoretically predicted but neglected in all the existing kinetic impurity transport simulations in the SOL/Divertor plasmas; 1) the inward pinch (IWP) due to density gradient of background plasmas and 2) the temperature screening effect (TSE, outward transport) caused by temperature gradient. The IWP and TSE, which are proportional to the impurity charge *Z*, become more important for high-Z impurities such as tungsten. Under typical parameters of fusion SOL/Divertor plasma, the simulated IWP and TSE flow have shown non-negligible magnitudes (several meters per second) compared with the anomalous diffusive flow.

Preprint

Reduced Model for Gyrokinetic Turbulent Transport in Helical Plasmas

M. Nunami¹, H. Sugama¹, and T.-H. Watanabe²

¹National Institute for Fusion Science, Toki, Japan ²University of Nagoya, Nagoya, Japan

Corresponding Author: M. Nunami, nunami.masanori@nifs.ac.jp

A reduced model for turbulent transport driven by micro-instabilities such as ion temperature gradient (ITG) modes is constructed based on nonlinear and linear gyrokinetic plasma turbulence simulations performed under a wide range of conditions for the local plasma parameters and different field configurations of helical systems. It is shown that the ion heat diffusivity has a functional dependence on the amplitudes of turbulent fluctuations and zonal flows in the nonlinear simulations.

On the other hand, the amplitudes of turbulent fluctuations and zonal flows obtained from the nonlinear simulations are well correlated with linear gyrokinetic simulation results on the ITG instability and zonal flows. Based on these properties, the reduced model for the ion heat transport in helical plasmas is constructed by combination of the linear growth rates of the instability, the linear response functions of the zonal flow potentials, and elaborate nonlinear gyrokinetic simulations. The model involves a similarity with the conventional mixing length ansatz but with explicit introduction of the zonal flow contribution. It is confirmed that the model is in good agreement with nonlinear gyrokinetic simulation results including the cases of the high ion temperature plasmas in the Large Helical Device experiment.

Since the present model is represented in terms of only linear calculation results, the computational cost of the model, i.e., the elapsed time, is extremely smaller than that of the nonlinear turbulence simulations (the ratio is less than 5%). Therefore, the model can be applied to an integrated transport code or survey of the transport levels in a wide range of multiple parameters corresponding to various experimental conditions. The basic idea of the model is also applied to tokamak configurations including the both species of ions and electrons, although detailed values of the coefficients in the model function may be altered.



Open Theoretical Issues and Solutions for Fusion Relevant Physics Regimes

B. Coppi¹, T. Zhou¹, B. Basu¹, P. Montag¹, *L. Sugiyama*¹, and P. Buratti²

¹Massachusetts Institute of Technology, Cambridge, MA, USA ²Associazione EURATOM-ENEA Unitá Tecnica Fusione, Frascati, Italy

Corresponding Author: B. Coppi, coppi@mit.edu

New features [1] of the Quasi Coherent Mode (QCM) have been observed in the EDA H-Regime and our theoretical model indicates that: i) the relevant resistive mode driving factor is the edge sharp plasma pressure gradient; ii) a novel mode topology is involved as the usual "disconnected mode approximation" cannot be applied given that the rotational transform $\iota(\psi) = 1/q(\psi) = 0$ on the LCMS around which the mode is localized; iii) the mode ballooning (poloidally) is related to the limited region [2] around the equatorial plane where the pitch of the magnetic field is about constant. Modes producing reconnection in low collisionality regimes have been observed to have a phase velocity in the direction of the ion diamagnetic velocity [3] contrary to the well accepted drift-tearing mode theory [4]. Then two theoretical lines leading to a mode with this phase velocity direction have been pursued: i) a theory based on the simultaneous effects of classical transport coefficients (plasma resistivity, longitudinal thermal conductivity and transverse ion viscosity) ii) an analysis [5] introducing a "mode inductivity" [6] to represent the electromagnetic coupling of the current channels inside the reconnection layer to other outside it. The "spontaneous rotation" of axisymmetric plasmas is confirmed to be related [7], to the excitation of modes involving the extraction of angular momentum from the plasma column and the recoil of the background plasma in the opposite direction. The features of the drift-tearing mode [4], of the ion-drift reconnecting mode [3] and of m = 1 internal modes, that are responsible for the "generation" of the experimentally observed angular momentum within the plasma column, are identified. Velocity profiles reproducing the observations are obtained from the angular momentum balance equation [7] with sources associated with both the internal electrostatic and electromagnetic modes.

References

- [1] B. Labombard, Bull. Am. Phys. Soc. 58, (2013) 367.
- [2] L. Sugiyama, Phys. Plasmas 17, (2010) 062505.
- [3] P. Buratti, B. Coppi, G. Pucella, et al., Bull. Am. Phys. Soc. 58, (2013) 142.
- [4] B. Coppi, Phys. Fluids 8, (1965) 2273.
- [5] B. Coppi and T. Zhou, MIT-LNS Report HEP 13/09 Cambridge, MA (2013).
- [6] B. Coppi, Bull. Am. Phys. Soc. 45, (2000) 366.
- [7] B. Coppi, 2000 IAEA Int. Fus. En. Conf., (Vienna, 2000); Nucl. Fusion 42, (2002) 1.



Equilibrium and Fast Particle Confinement in 3D Tokamaks with Toroidal Rotation

W. A. Cooper¹, D. Brunetti¹, J. Faustin¹, J. Graves¹, D. Pfefferle¹, M. Raghunathan¹, O. Sauter¹, T.-M. Tran¹, I. Chapman², and N. Aiba³

¹Ecole Polytechnique Fédérale de Lausanne, CRPP, Lausanne, Switzerland ²CCFE Fusion Association, Culham Science Centre, Abingdon, UK ³Japan Atomic Energy Agency, Naka, Japan

Corresponding Author: W. A. Cooper, wilfred.cooper@epfl.ch

A Magnetohydrodynamic (MHD) equilibrium model to treat plasma rotation approximately in three-dimensional (3D) tokamak geometry with nested flux surfaces is explored. For this purpose, we assume in 3D that the velocity is purely toroidal in (R, ϕ, Z) cylindrical coordinates. Furthermore, we impose that the toroidal angular rotation frequency is constant on each flux surface. Isothermal conditions are invoked so the temperature is also constant on a flux surface. The MHD force balance relation contains an extra term absent in the axisymmetric limit that causes problems to obtain a closed analytic formulation. However, experimental observations provide us with a guide to progress further. Specifically, the measurements on MAST with Long-Lived Modes (LLM) indicate that the toroidal rotation becomes rigid in the core of the plasma where the 3D deformation is large, but sheared flow survives in the outer region which essentially retains axisymmetric properties. Under these conditions, the term in question vanishes. Then, the rigourous energy functional that describes MHD toroidal flow in the axiymmetric limit becomes applicable in this case. The 3D VMEC equilibrium solver has been adapted to numerically investigate the approximate toroidal rotation model we have derived. We concentrate our applications on the simulation of MAST LLMs. We have successfully computed bifurcated solutions of the MHD equilibrium state with a helical core deformation in the presence of toroidal flow with an angular rotation frequence that is flat in the core (nearly rigid) and sheared at the edge. The centrifugal force has the effect of diminishing the helical distortion of the pressure compared with that of the magnetic geometry. The magnitude of the deformation is most sensitive to details of the safety factor q-profile, mainly the proximity of q_{min} to unity and the radial location of q_{min} in the simulations with weak reversed magnetic shear that we have performed. Fast particle confinement is investigated with the guiding centre orbit code VENUS. In the presence of toroidal flow, the drift orbit equations depend on the electrostatic potential φ_E associated with the rotation and quasineutrality. When the equilibrium state has 3D deformations, geometrical terms appear from the evaluation of Ohm's Law that considerably complicate the description of fast particle confinement.



Energy Principle for the Fast Resistive Wall Modes in Tokamaks

V. Pustovitov¹, A. Galyuzov²

¹National Research Centre "Kurchatov Institute", Moscow, Russian Federation ²Moscow Institute of Physics and Technology, Dolgoprudny, Moscow Region, Russian Federation Corresponding Author: V. Pustovitov, pustovit@nfi.kiae.ru

The paper is devoted to theoretical issues in the problem of plasma stability in the toroidal fusion systems with a resistive wall. The basis of the existing stability theory is the standard energy principle [1] derived within the ideal magnetohydrodynamics (MHD) model. A part of that generally accepted approach is the condition that the Poynting vector vanishes at the plasma-facing surface of the toroidal vacuum vessel (simply called wall). In other words, the standard stability theory treats the wall as an ideal conductor preventing the energy flux outside. Ideal plasma with an ideal wall constitute a conservative system. In reality, the system is dissipative at least because of the wall resistivity. In experiments with pulse duration longer than the resistive wall time, this is manifested in excitation of the resistive wall modes (RWMs) in the regions stable according to predictions of the ideal MHD with an ideal wall. Here the energy principle is modified by incorporating the dissipation due to the wall resistivity. Mathematically, the difference from the classical task is that tangential component of the perturbed electric field is now nonzero at the wall. Physically, this means the outward flux of energy (absent in the standard energy principle). This flux can be found by calculating the full energy balance in the outer region or estimated with substitution of proper trial functions. The latter is an element of the variational approaches. Here it is applied by using a proper ansatz for the perturbation in the plasma-wall vacuum gap and in the wall, suitable for the modes faster than conventional RWMs. Accuracy of this method is discussed and asymptotic relations are considered. One of them is the modified energy principle allowing estimates of the growth rates of the fast RWMs. These are, for example, the precursors of more violent and much faster ideal MHD modes. The proposed method is a natural extension of the classical energy principle and contains it in the asymptotic limit. Theoretical and experimental applications of the results are also discussed.

References

[1] I.B. Bernstein et al., Proc. Roy. Soc. London A 244, 17 (1958).



Chirping Alfvén Eigenmodes Drive Convective and Diffusive Transport

M. Lesur¹, P. H. Diamond^{2,3}, Y. Kosuga¹, S. Itoh⁴, and K. Itoh⁵

 ¹Kyushu University, Kasuga, Japan
 ²National Fusion Research Institute, Daejeon, Korea, Republic of ³University of California San Diego, CA, USA
 ⁴Institute for Applied Mechanics, Kyushu University, Kasuga, Japan
 ⁵National Institute for Fusion Science, Toki, Japan

Corresponding Author: M. Lesur, maxime.lesur@polytechnique.org

A major concern in burning plasmas is that high energy ions can excite plasma instabilities in the frequency range of Alfvén eigenmodes, which significantly enhance their transport. We focus on the Toroidal Alfvén Eigenmode (TAE). In many TAE experiments, the mode frequency is observed to split into two branches that sweep upwardly and downwardly. This nonlinear frequency sweeping (chirping) is due to the dynamics of phase-space structures, known as holes. Holes are vortex-like (BGK-like) structures in phase-space, with a depletion of density. Holes are formed by electrostatic self-trapping. Simulations of the Berk-Breizman extension of the bump-on-tail model reproduce many features of chirping TAEs, in a regime of quasi-periodically repetitive bursts. In this paper, we analyse data of TAE experiments on MAST based on simulations of the Berk-Breizman model. We report on the impacts of phase-space structures on particle transport. We show that this nonlinearity induces collective transport, which exceeds the quasilinear estimate in unstable plasmas, and a new convective (drag) term. It is well known that the conventional wave-coherent response yields diffusive transport. In contrast, phase-space structures are wave-incoherent, and introduce convective transport. Indeed, trapped particles are convected along with phase-space structures. The flux-gradient relation confirms the existence of a strong convective flux. Phase-space structures also contribute to diffusive transport. This is despite the absence of turbulence, since we consider a single mode. In other words, the observed transport contradicts quasi-linear theory, which predicts no transport at all. Phase-space structure-driven transport thus dominates for isolated single modes. In addition, our simulations suggest the possibility of strong turbulent flux (energy exchange) in linearly-stable plasmas. These results impact resonance-driven modes in general, and TAE-driven transport in tokamaks with strong neutral beam injection in particular.



Simulations and Validations of Transport during Fueling by SMBI in HL-2A Tokamak

Z. Wang¹, X. Xu², T. Xia³, D. Yu¹, G. Zheng¹, J. Huang⁴, S. Chen⁴, W. Zhong¹, J. Dong¹, A. Sun¹, M. Xu¹, Z. Shi¹, T. Sun⁴, and L. Yao¹

¹Southwestern Institute of Physics, Chengdu, Sichuan, China
 ²Lawrence Livermore National Laboratory, Livermore, CA, USA
 ³Institute of Plasma Physics, Chinese Academy of Sciences, Hefei, China
 ⁴Sichuan University, Sichuan, China

Corresponding Author: Z. Wang, zhwang@swip.ac.cn

Plasma fueling with higher efficiency and deeper injection is crucial to enable fusion power performance requirements at high density for next generation devices such as ITER. In BOUT++ code framework, a new module (named trans-neut) has been developed to deal with neutrals and plasmas transport during fueling of supersonic molecular beam injection (SMBI) or gas puffing(GP). It modifies the BOUT++ code of boundary plasma turbulence to study the dynamics of neutrals transport and their interactions with plasma during fueling. Results of calculations have been done for the realistic divertor geometry of the HL-2A tokamak. A seven-field fluid model coupling plasma density, heat, and momentum transport equations together with neutral density and momentum transport equations for both molecules and atoms has been developed. Collisional interactions between molecules, atoms, and plasma have been included such as dissociation, ionization, recombination and charge-exchange reactions. During SMBI, neutral molecules and atoms propagate inwards continuously across the separatrix and penetrate about 4 cm inside the separatrix where the propagating front of molecules stagnates due to the total molecule dissociation rate balancing with the molecule injection rate. Both positive and negative parallel ion velocities are driven near SMBI region due to parallel pressure gradient, which provides convection for parallel plasma density transport. The poloidal propagation of plasma density blobs (i.e., source) and ion temperature holes (i.e., sink) has been observed. The simulations of mean profiles variations during SMBI have been compared and validated with HL-2A experiment results which are consistent qualitatively well with each other.



3D Plasma Response to Resonant External Magnetic Perturbation and its Impact on Fast Ion Confinement in JT-60SA Plasmas

Y. Suzuki¹, G. Matsunaga², M. Honda², H. Urano², K. Shinohara², and S. Ide²

¹National Institute for Fusion Science, Toki, Japan ² Japan Atomic Energy Agency, Naka, Japan

Corresponding Author: Y. Suzuki, suzuki.yasuhiro@lhd.nifs.ac.jp

The reduction of the heat load on divertors caused by Edge Localized Modes (ELMs) is a key issue in ITER. Large energy flux of Type-I ELMs is expected to cause melting of the tungsten divertors in ITER. One of the methods to control ELMs is an application of Resonant Magnetic Perturbation (RMP) fields; in fact, mitigation or suppression of ELMs by RMPs are observed in many tokamak experiments. However, those results are not verified in the steady state operation. Therefore, to extrapolate those results to ITER, RMPs experiments in the JT-60SA tokamak are critical and urgent issues. In the JT-60SA experiments, Error Field Correction Coils (EFCCs) will be utilized as RMP coils. For this reason, we have qualitatively and quantitatively studied the magnetic field topology with superposed RMPs by EFCCs to develop scenarios of RMPs experiment in the JT-60SA. In the operational aspects, how much the EFCC current to stochastize the magnetic field structure is necessary since EFCCs must be used for the error field correction and the capacity of EFCC power supplies is limited.

We have modeled RMPs of n = 3 and found that the current of EFCCs ($I_{\rm EFCC}$) higher than 10 kA can stochastize the magnetic field in the edge region under the vacuum approximation without including plasma responses. To evaluate an effect of plasma responses, the 3D MHD equilibrium is calculated by the HINT2 code resulting in significant changes of the magnetic topology. Namely, magnetic islands in the plasma core evolve but the stochasticity of magnetic field lines in the edge region decreases. To recover the same stochasticity in the vacuum approximation with $I_{\rm EECC}$ of 10 kA, current higher than 30 kA is necessary for the 3D plasma responses. Thus, the 3D plasma response can shield RMPs. Moreover, fast ion losses directly depend on the magnetic topology. 3D Monte Carlo simulations are performed with RMPs and the loss behavior is significantly changed by the 3D plasma response.



Gyrokinetic Analysis of Turbulent Heat and Particle Transport on JT-60U Plasmas

M. Nakata¹, M. Honda¹, M. Yoshida¹, H. Urano¹, S. Maeyama¹, M. Nunami², and T. Watanabe³

¹Japan Atomic Energy Agency, Naka, Japan ²National Institute for Fusion Science, Toki, Japan ³University of Nagoya, Nagoya, Japan

Corresponding Author: M. Nakata, nakata.motoki@jaea.go.jp

First-principle based gyrokinetic simulation is a powerful method for investigating turbulent transport in fusion plasmas. Since a local limit condition [(plasma size)/(ion gyroradius) $\gg 300$] is well satisfied in ITER and DEMO reactors, quantitative evaluations for the prediction capability of local gyrokinetic simulations are crucially urgent and important issues. This paper presents the first and brand-new results on the first-principle based turbulence simulation study on JT-60U tokamak plasmas [cf. (plasma size)/(ion gyroradius) ~ 500 for L-mode] by using a multi-species electromagnetic gyrokinetic code GKV with realistic MHD equilibria, towards ITER and DEMO. The inclusion of fully gyrokinetic ions and electrons beyond the conventional adiabatic approximation reveals a transition of dominant micro-instability from ITGs (inner core region) to TEMs (outer core region) depending on radial positions, and the resultant turbulent heat and particle transport levels are examined quantitatively. New findings in this study are summarized: i) GKV simulations successfully reproduce experimental results on ITG/TEM driven ion and electron heat transport in the core region. Possible physical mechanisms on the so-called "transport shortfall" in the outer core region are examined in view of zonal flow dynamics. Additionally, ii) different nonlinear dependence of ion-scale zonal flows on the heat and particle transport levels is newly identified, i.e., weaker impact on the electron heat and particle transport compared to the ion heat one. These findings on the quantitative agreement among turbulence simulations and experimental results, and on the nonlinear dependence on zonal flows in the transport levels contribute significant progress in improving the prediction capability of gyrokinetic simulations and in constructing a more credible transport model for ITER and DEMO.

Preprint

Multi-Time-Scale Energetic Particle Dynamics in JT-60U Simulated with MHD Activity, Sources and Collisions

A. Bierwage¹, K. Shinohara¹, Y. Todo², and M. Yagi¹

¹ Japan Atomic Energy Agency, Naka, Japan ²National Institute for Fusion Science, Toki, Japan

Corresponding Author: A. Bierwage, bierwage.andreas@jaea.go.jp

The dynamics of Alfvén waves and fast ions in JT-60U plasmas driven by powerful Negative-ionbased Neutral Beams (N-NB) are studied for the first time using long-time simulations, which include N-NB sources, collisions, MHD and wave-particle interactions self-consistently. The simulations are able to reproduce experimentally observed bursts of MHD activity, which chirp down and up in the frequency range 40-60 kHz and occur at intervals 5-15 ms. The underlying modes are identified as resonant wave-packets known as Energetic Particle Modes (EPM) with dominant toroidal mode number n = 1. The EPM bursts modify the fast ion distribution significantly, which means that selfconsistent simulations as performed here are needed for accurately computing fusion rates, heating and current drive. The successful reproduction of chirping bursty modes in JT-60U validates the new tools for predictive simulations of future experiments, such as JT-60SA and ITER. On the physics side, the self-consistent simulations enable us to study the important meso-time-scale dynamics that connect slow and fast processes. For instance, it is found that the large Larmor radius of N-NB ions together with resistive dissipation play a key role for the intermittency of the bursts. The JT-60U plasmas studied are also subject to Abrupt Large Events (ALE), which are characterized by short intense magnetic fluctuation signals and subsequent drops in the plasma core neutron rates. Efforts are underway to reproduce these relaxation events with the long-time simulations in order to unravel the underlying physical processes, such as the trigger mechanism. The self-consistent simulations are complemented with conventional simulations, where the plasma response is probed starting from a suitable initial condition. It is shown that EPMs with toroidal mode numbers n > 1 may be excited by particles that have energies about 100–200 keV below the N-NB ion birth energy (400 keV). The ALE period is comparable to the time needed for a particles to slow down into that energy range, which indicates that n > 1 modes are important for ALEs. Furthermore, EPMs are subject to convective amplification and different harmonics interact via scattering of resonant particles. These nonlinear effects may play a role for triggering relaxation events, like ALEs. Further analyses are in progress and will be reported at the conference.



TH/P8-1

Plasma-Material Interaction Issues in Magnetic Fusion Devices

S. Krasheninnikov¹, J. Guterl¹, A. Pigarov¹, R. Smirnov¹, W. Lee¹, E. Marenkov², and A. Pisarev²

¹University of California San Diego, CA, USA ²National Research Nuclear University MEPhI, Moscow, Russian Federation

Corresponding Author: S. Krasheninnikov, skrash@mae.ucsd.edu

The processes involving plasma-material interactions in magnetic fusion devices are very multifaceted and include a wide spectrum of phenomena ranging from plasma recycling and transport of hydrogen species in the wall material to the modification of wall properties, surface morphology, and dust formation which, being ejected from the wall, can have crucial impact on plasma performance. Here we present the results of our studies of some issues related to the plasma-material interactions: i) modeling of the role of the first wall outgassing on H-mode pedestal re-healing after the ELM crashes in DIII-D; ii) transport of hydrogen (H) species in co-deposits; iii) hydrogen outgassing from tungsten (W) surface; iv) an impact of W dust on ITER plasma performance.

We demonstrate that: i) re-healing of particle content in H-mode pedestal after ELM crash in DIII-D is completely determined by the outgassing of divertor plates; ii) transport of H in co-deposits, which are characterized by continues spectrum of traps, depending on the regime, can be described either by nonlinear or fractional diffusion equations; iii) Molecular dynamic (MD) simulations of H desorption from W surface show that the Tersoff potential for H-W interactions overestimates three-body interactions at tungsten surface and should be adjusted to reproduce experimental features of hydrogen desorption as molecules; iv) Modeling of W dust injection into ITER shows that it can result in pronounced impact on both core and edge plasma performance and W concentration at $\Psi_{norm} = 0.95$ reaches potentially dangerous level ~ 10^{-5} for the dust mass injection rate ~ 1 mg/s.

Fusion Engineering, Integration and Power Plant Design



Development of Tungsten Monoblock Technology for ITER Full-Tungsten Divertor in Japan

Y. Seki¹, K. Ezato¹, S. Suzuki¹, K. Yokoyama¹, K. Mohri¹, T. Hirai², F. Escourbiac², and V. Kuznetsov³

¹Japan Atomic Energy Agency, Naka, Japan ²ITER Organization, Saint Paul lez Durance, France ³D. V. Efremov Institute of Electrophysical Apparatus, St. Petersburg, Russian Federation

Corresponding Author: Y. Seki, seki.yohji@jaea.go.jp

Through R&D for a plasma facing unit (PFU) of a full-tungsten (W) ITER divertor, Japan Atomic Energy Agency (JAEA) succeeded in demonstrating the durability of the W divertor which endured a repetitive heat load of 20 MW per sqare meter without macroscopic cracks of all W armors. At the beginning of this activity, the bonding technology armor to heat sink was one of the most important key issues in a manufacturing process. JAEA improved the bonding process of the W divertor mock-ups. At first the bonding between the W armor and the copper interlayer (Cu) is performed by using several technologies, such as "Direct casting of Cu" or "Diffusion bonding" or "HIP bonding". Then the brazing between the Cu and the cooling pipe is done. Then the rejection rate due to those bonding processes has been significantly reduced. As a performance test for the bonding and a heat removal capability, the high heat flux testing was carried out for six small-scale mock-ups for the R&D of the full-W ITER divertor. Moreover, a W part of four full-scale prototype PFUs were also tested. In the tests, all of the W monoblocks endured the repetitive heat load of 10 MW per sqare meter for 5,000 cycles and 20 MW per sqare meter for 1,000 cycles without the macroscopic crack, which strongly encourages the realization of the full-W divertor target from the start of the operation in ITER. This paper presents the latest R&D activities on the full-W ITER divertor in JAEA.



Slides

Paper

Surface Heat Loads on Tungsten Monoblocks in the ITER Divertor

J. P. Gunn¹, S. Carpentier-Chouchana², R. Dejarnac³, F. Escourbiac⁴, T. Hirai⁴, M. Kocan⁴, V. Komarov⁴, M. Komm³, A. Kukushkin⁴, R. Pitts⁴, and Z. Wei⁵

¹CEA-IRFM, Saint Paul lez Durance, France
 ²EIRL S. Carpentier-Chouchana, Meyrargues, France
 ³Max-Planck-Institut für Plasmaphysik, Garching, Germany
 ⁴ITER Organization, Saint Paul lez Durance, France
 ⁵Southwestern Institute of Physics, Chengdu, Sichuan, China

Corresponding Author: J. P. Gunn, jamie.gunn@cea.fr

ITER will begin operation with a full W divertor consisting of solid W monoblocks (MB) bonded to CuCrZr water-carrying cooling tubes. We seek to predict heat flux distributions on MBs comparing three models: optical calculations, ion orbit calculations, and PIC. The consequences of five design aspects are analyzed in terms of available models:

- 1. Divertor target tilting to shadow leading edges at inter-cassette gaps leads to increased local power flux and total power to wetted MBs, as well as to reduced margin against surface melting during fast transients, due to the increased *B*-field angle (the total power to each target is the same, but it is distributed among fewer MBs).
- 2. Within a single tilted target, chamfering foreseen to protect leading edges of the MBs against misalignments also leads to increased local power flux due to the increased *B*-field angle, but that is exactly compensated by a reduction of the wetted area, thus the total power to individual MBs is conserved. ANSYS thermal simulations predict additional heating of MB trailing edges due to nonuniform heat flux deposition.
- 3. Relative misalignments between plasma-facing units (PFU) play a critical role in the total power incident on a single MB. A MB on a PFU that is radially misaligned by 0.3 mm on a tilted target [cf. point (1)] will collect a total convected plasma power that is 50% higher than a perfectly aligned MB on an untilted target. If that power were spread uniformly over the top surface of the MB, it would be equivalent to a power flux that is 50% higher than the specified limits. There is no shaping solution that can remedy this problem.
- 4. Due to their large Larmor radii, ions released from the pedestal during ELMs can strike magnetically shadowed poloidal edges. The fraction of ELM parallel power flux that penetrates into gaps is independent of ion temperature over the range 0.5 keV $< T_i < 5$ keV. According to the ion orbit model, energetic ELMs can cause leading edge melting.
- 5. Unintuitive focusing of power onto the edges of toroidal gaps due to finite Larmor radius and sheath electric fields causes overheating. According to the ion orbit model, this can cause toroidal edge temperatures to attain the W recrystallization range for steady state loads, and melting of toroidal edges for both slow and fast transient loads.

Full-Scale Trial Results to Qualify Optimized Manufacturing Plan for ITER Toroidal Field Coil Winding Pack in Japan

N. Koizumi¹, M. Nakahira¹, K. Matsui¹, T. Hemmi¹, H. Kajitani¹, M. Iguchi¹, and T. Sakurai¹

¹ Japan Atomic Energy Agency, Naka, Japan

Corresponding Author: N. Koizumi, koizumi.norikiyo@jaea.go.jp

A heat-treated Nb3Sn cable-in-conduit conductor (CICC) must be inserted into a groove of a radial plate (RP), which is designed to maintain the mechanical and electrical reliability of the insulation of ITER Toroidal Field (TF) coil during its 20 years' operation. The difference between heat-treated conductor length and RP groove length must be controlled with accuracy of $\pm 0.05\%$. JAEA developed high accuracy winding system and procedure with the order of $\pm 0.01\%$ in wound conductor length and performed full-scale winding trials. The target tolerance of $\pm 0.01\%$ was achieved. In addition, very complicate procedure of RP insertion between upper and lower windings (pancakes), which consist of unit length conductor, is also qualified by using full-scale dummy conductor winding and trial insertion of wound dummy conductor into RP groove was performed, too. Furthermore, proto double-pancake (DP) was successfully heat-treated. These results justify validity of optimized manufacturing plan and allow us to start TF coil winding pack (WP) manufacture.

FIP/1-4Ra

Preprint Slides

Summary of the Test Results of ITER Conductors in SULTAN

B. Stepanov¹, *P. Bruzzone*¹, K. Sedlak¹, N. Mitchell², A. Devred², A. Vostner², Y. Nunoya³, V. Tronza⁴, S.-H. Park⁵, T. Boutboul⁶, N. Martovetsky⁷, and W. Yu⁸

¹Ecole Polytechnique Fédérale de Lausanne, CRPP, Lausanne, Switzerland
 ²ITER Organization, Saint Paul lez Durance, France
 ³Japan Atomic Energy Agency, Naka, Japan
 ⁴ITER Russian Federation, Moscow, Russian Federation
 ⁵National Fusion Research Institute, Daejeon, Korea, Republic of
 ⁶F4E: Fusion for Energy, Barcelona, Spain
 ⁷Oak Ridge National Laboratory, Oak Ridge, TN, USA
 ⁸Institute of Plasma Physics, Chinese Academy of Sciences, Hefei, China

Corresponding Author: B. Stepanov, boris.stepanov@psi.ch

After completing the qualification tests of the ITER cable-in-conduit conductors (CICC), the series manufacture tests are running in the SULTAN test facility at PSI, Villigen, Switzerland, with target completion date in 2015. The key test for the conductor samples is the current sharing temperature, T_{cs} , at the nominal operating field and current, i.e., the maximum temperature at which the conductors operate before developing an electric field of 10 μ V/m. All the TF samples fulfilled the ITER requirement of $T_{cs} \ge 5.8$ K after 1000 load cycles. The T_{cs} results have a broad scattering among the suppliers, from 5.8 K up to 6.6 K.

The assembly of the Nb₃Sn based CICC samples (for TF and CS coils) is carried out at CRPP. The NbTi CICC samples (for PF, CC, and bus bars) are assembled at the suppliers, with a U-bend replacing the bottom joint. The poor performance of some Main Busbar (MB) conductor samples, caused by poor sample assembly, triggered the effort to assemble a MB sample at CRPP with solder filled terminations and a bottom joint. The superior test results of the MB-CRPP sample, closely matching the performance assessment carried out using 3D field distribution and *n*-index behaviour was a successful achievement of the last year of operation.

According to the Procurement Arrangement for the ITER coils, the winding companies must qualify the joint and termination manufacture by SULTAN samples. The first joint sample tested in SULTAN was a TF joint from EU, followed by a Correction Coil (CC) joint sample from China. Other joint samples are being assembled in USA (Central Solenoid), in Russia (PF1), and in China (PF6).

All the ITER coils use the "twin box" design for joints, except the Central Solenoid. At the first test in SULTAN of a twin-box TF joint sample in 2013, an unexpected resistance increase was observed after an accidental dump of the SULTAN field, causing a large field transient parallel to the joint contact surface, with large eddy currents and electromagnetic loads at the pressure-contact between strand bundle and copper plate of the twin box. The resistance requirement for the TF joint was still fulfilled after the dump. The impact of transient field on resistance and stability was investigated at an additional test campaign of the TF joint sample, with intentional dumps of the SULTAN field.

Research, Development and Production of ITER Toroidal Field Conductors and Poloidal Field Cables in Russia

V. Vysotsky¹, K. Shutov¹, A. Taran¹, I. Chensky¹, L. Potanina¹, and G. Svalov¹

¹Russian Scientific R&D Cable Institute, Russian Federation

Corresponding Author: V. Vysotsky, vysotsky@ieee.org

Russian Federation is the initiator and active participant in development and building of International Thermonuclear Experimental Reactor (ITER). The major element of ITER is its huge superconducting magnet. Special superconducting cables and conductors had to be developed to satisfy very strict demands for such conductors. A lot of Research and Development (R&D) works have been performed in Russia to create our own production of superconductors, cables, and conductors. Russian Scientific R&D Cable Institute (known by Russian abbreviation as VNIIKP) has been participating in ITER project since 1993 both at the early stage of R&D and at the following stage of Engineering Design Activity (EDA). Tests of several short samples at Sultan test facility were crowned by successful testing of Toroidal Field (TF) and Poloidal Field (PF) insert coils performed in Japan in 2001 and 2008 correspondingly. After many R&D works bow VNIIKP is actively implementing the final production and delivery stage of cables and conductors. By 2009 the new and modern technological complex has been accomplished to produce PF cables for both the Russian Federation (RF) and European parts and TF conductors for RF part. The complex includes several productions such as chemical technology line, cabling facility, and jacketing line. In this review we present a short history of VNIIKP participation in ITER and our current achievements, including some R&D results. The technology used and our production line are described in some details.

Slides

Paper

Overview of the Design Development, Prototype Manufacturing and Procurement of the ITER In-Vessel Coils

A. Encheva¹, C. H. Choi¹, C. Sborchia¹, R. LeBarbier¹, B. Macklin¹, and E. Popova¹

¹ITER Organization, Saint Paul lez Durance, France

Corresponding Author: A. Encheva, anna.encheva@iter.org

ITER is incorporating two types of In-Vessel Coils (IVCs): ELM Coils to mitigate Edge Localized Modes and VS Coils to provide Vertical Stabilization of the plasma. Strong coupling with the plasma is required in order that the ELM and VS Coils can meet their performance requirements. Accordingly, the IVCs are mounted on the Vacuum Vessel (VV) inner wall, in close proximity to the plasma, just behind the Blanket Shield Modules (BSM). Fitting the coil systems in between the BSM and the VV leads to difficult integration with diagnostics and cooling water manifolds. This location results in a radiation and temperature environment that is severe necessitating new solutions for material selection, as well as challenging thermo-mechanical analyses and design solutions. Due to high radiation environment, mineral insulated copper conductors enclosed in a steel conduit have been selected.

The project is being led and managed by the ITER Organization in close collaboration with the Chinese Academy of Sciences (ASIPP) in Hefei, China, and with the Princeton Plasma Physics Laboratory (PPPL) in Princeton NJ, USA. Prototype manufacturing has been completed by ASIPP. The aim was to develop suitable manufacturing procedures and techniques necessary to fabricate the ELM and VS Coils, and to qualify electrical and mechanical test procedures to meet the acceptance criteria. An extensive set of analyses to evaluate the effects of the high temperatures and electromagnetic loads on the In-Vessel Coils has been carried out at PPPL. The design of the IVCs has been finalized, and it takes into account the results from the prototype manufacturing.

The procurement of the IVCs and their conductors will be done via direct call-for-tenders from the ITER Organization and preparation has already started. It is expected that the first call-for-tender will be launched in mid-2014 and the contract signed in early 2015.

This paper will give an overview of the detailed design and prototype manufacturing, procurement and schedule for the In-Vessel Coils.



Progress in the Design and Manufacture of High Vacuum Components for ITER

C. Sborchia¹, H. Hahn², A. Alekseev¹, V. Barabash¹, A. Bayon³, A. Bhardwaj⁴, C. H. Choi¹, B. Doshi¹, S. Fabritsiev⁵, B. Giraud¹, G. Gupta⁴, P. Jucker³, H.-S. Kim⁶, E. Kuzmin⁵, R. Pathak⁴, J. Raval⁴, J. Reich¹, J. W. Sa¹, P. Savrukhin⁷, I. Sekachev¹, Y. Utin¹, P. Vertongen¹, G. Vitupier¹, and C. Zhou¹

> ¹ITER Organization, Saint Paul lez Durance, France ²National Fusion Research Institute, Daejeon, Korea, Republic of ³F4E: Fusion for Energy, Barcelona, Spain ⁴ITER India, India

⁵D. V. Efremov Institute of Electrophysical Apparatus, St. Petersburg, Russian Federation ⁶National Fusion Research Institute, Daejeon, Korea, Republic of ⁷National Research Centre "Kurchatov Institute", Moscow, Russian Federation

Corresponding Author: C. Sborchia, carlo.sborchia@iter.org

ITER is a large experimental tokamak device being built to demonstrate the feasibility of fusion power. The main scope of this paper is to report the status of the design and manufacturing activities of two major ITER components, the ITER Vacuum Vessel (VV) and the Cryostat. Both components will provide the necessary high-vacuum required in the case of the VV for plasma operation and confinement and to allow for cooldown of the superconducting magnets to cryogenic temperature (Cryostat).

The design of the two systems has been developed by the ITER Organization (IO) with the support of many R&D activities carried out by the Parties and is almost complete. Procurement Arrangements (PAs) with four Domestic Agencies (DAs) have been signed to develop the manufacturing design and manufacture the components of these systems. Some detailed design on specific components still needs to be completed.

Manufacturing contracts have been placed in 2010–2012 with many preparation and qualification activities. The production of the full-scale VV sectors and cryostat sections has started in the four DAs with the procurement of base materials and manufacture of mock-ups or full-scale components. Realistic manufacturing schedules are being consolidated and the presently expected completion dates will also be reported in this paper.

FIP/1-6Rb

Preprint Slides

Manufacturing Design and Progress of the First Sector for ITER Vacuum Vessel

H.-J. Ahn¹, G. H. Kim¹, G. H. Hong¹, H.-S. Kim¹, C. K. Park¹, S. W. Jin¹, H.-G. Lee¹, K.-J. Jung¹, J. S. Lee², T. S. Kim², B. R. Roh², J. W. Sa³, Y. Utin³, C. Jun³, and C. H. Choi³

¹National Fusion Research Institute, Daejeon, Korea, Republic of ²Hyundai Heavy Industries, Ulsan, Korea, Republic of ³ITER Organization, Saint Paul lez Durance, France

Corresponding Author: H.-J. Ahn, hjahn@nfri.re.kr

The ITER Vacuum Vessel (VV) is a torus shaped double wall structure and consists of nine sectors and several ports. Main functions of the VV are to provide high vacuum for plasma operation and to protect radioactive contamination as the first safety barrier. Korea Domestic Agency (KODA) has responsibility for procuring of two sectors including the first sector which will be delivered before others. KODA contracted with Hyundai Heavy Industries Co., Ltd (HHI) to product the VV sectors and major ports.

The design and fabrication of the VV as nuclear equipment shall be complied with the RCC-MR code and regulations of nuclear pressure equipment in France (ESPN). The manufacturing design has been developed to fabricate the main vessel and port structures in accordance with the design requirements. All manufacturing sequences including welding methods are also established to meet the demanding tolerance and inspection requirement. The manufacturing design of Korean sectors has special design concepts to minimize welding distortion such as self-sustaining support ribs and cup-and-cone type segment joints. Several mock-ups have been constructed to verify and develop the manufacturing design and procedures. Qualifications for welding, forming and NDE have been conducted to verify related procedures according to the requirement.

For fabrication of the VV sectors and ports, 3,000 tons of plates and forgings had been produced by European steel companies and delivered to HHI. Four poloidal segments (PS) for the first sector are being fabricated simultaneously in HHI factory. All inner shells were cut, bent and machined for welding. Welding and NDE of inner shells for PS2 and PS4 are finished. To reduce schedule delay, machining of forging blocks are on-going in parallel. Some of machined blocks are welded on the inner shell by TIG and electron beam welding.



Disruption Mitigation System Developments and Design for ITER

L. R. Baylor¹, S. Combs¹, *S. Maruyama*², D. Rasmussen¹, S. Meitner¹, C. Barbier¹, N. Ericson¹, P. Fisher¹, M. Lyttle¹, G. Kiss², J. Wilgen¹, and S. Smith¹

¹Oak Ridge National Laboratory, Oak Ridge, TN, USA ²ITER Organization, Saint Paul lez Durance, France

Corresponding Author: L. R. Baylor, baylorlr@ornl.gov

Disruptions present a challenge for ITER to withstand the intense heat flux, the large forces from halo currents, and the potential first wall damage from multi-MeV runaway electrons. Injecting large quantities of material into the plasma when a disruption is detected will reduce the plasma energy and increase its resistivity and electron density to mitigate these effects and thus a system with this capability is needed for maintaining successful operation of ITER. A disruption mitigation system is under design for ITER to inject sufficient material deeply into the plasma for a rapid shutdown and runaway electron collisional suppression. Here we present progress on the development and design of both a shattered pellet injector that produces large solid cryogenic pellets to provide reliable deep penetration of material [1] and a fast opening high flow rate gas valve for massive gas injection.

The shattered pellet injector utilizes a multi-barrel pipe-gun type device that forms large cryogenic pellets in-situ in the barrels. The pellets are accelerated by a high pressure gas burst and are shattered when they impinge on a bend guide tube in the port plug shield block that is optimized to produce a spray of solid fragments mixed with gas and liquid at speeds approaching the sound speed of the propellant gas. A prototype injector has been fabricated and tested with deuterium pellets of 16 mm size for thermal mitigation and is being upgraded to test and characterize 25 mm size D_2 and neon pellets for runaway electron suppression.

A fast opening high flow rate gas valve for massive gas injection has been designed for use in the ITER environment, which requires a novel eddy current flyer plate design and large diameter tritium compatible seat material as compared to earlier DMV designs by Juelich [2]. Modeling of the gas flows from the valves through guiding tubes gives a response time for the MGI design to be less than desired unless the valves are mounted within port plugs. Implications of the design with respect to response time and reliability are discussed.

References

- [1] N. Commaux, et al., Nucl. Fusion 50 (2010) 112001.
- [2] S.A. Bozhenkov, et al., Rev. Sci. Instrum. 78 (2007) 033503.

FIP/2-2Ra

Prototype Development of the ITER EC System with 170 GHz Gyrotron

Y. Oda¹, K. Kajiwara¹, R. Ikeda¹, K. Ohshima¹, K. Hayashi¹, K. Takahashi¹, K. Sakamoto¹, D. Purohit², F. Gandini², T. Omori², C. Darbos², and M. Henderson²

> ¹Japan Atomic Energy Agency, Naka, Japan ²ITER Organization, Saint Paul lez Durance, France

Corresponding Author: Y. Oda, oda.yasuhisa@jaea.go.jp

To study the operational performance of ITER EC heating and current drive system (H&CD), a mock-up of the ITER mm wave system has been assembled using the high power long gyrotron test stand in JAEA. The prototype system is composed of the primary parts of the EC H&CD system, including: 170 GHz gyrotron, power supply, transmission line (TL) and mock-up of equatorial launcher (EL) and control system. The gyrotron power was transmitted via the precise aligned TL (40 m) with 7 miter bends to the EL achieving a 91% of HE11 mode purity. The experiments were realized using a mock-up of the conceptual EC control system based on the ITER Plant Control Design Handbook (PCDH). The system has achieved CW 5 kHz power switching, which demonstrates the compatibility for MHD control of ITER plasma. The modulation was achieved using a novel configuration of the electron beam acceleration power supply. In the experiment, stable 5 kHz of power modulation was demonstrated with minimized spurious frequency excitation at the ramp-up phase of each pulse, which satisfied the ITER criteria. The JAEA test stand is a flexible system with its center piece a frequency-step-tunable gyrotron at 170 GHz, 137 GHz, or 104 GHz. The output beam is radiated to the identical direction from the output window for each frequency, consequently the power was transmitted to the end of the TL at these three frequencies.





Development of Dual Frequency Gyrotron and Launcher for the JT-60SA ECH/ECCD System

T. Kobayashi¹, S. Moriyama¹, K. Yokokura¹, M. Sawahata¹, M. Terakado¹, S. Hiranai¹, K. Wada¹, Y. Sato¹, J. Hinata¹, K. Hoshino¹, A. Isayama¹, M. Saigusa², K. Kajiwara¹, Y. Oda¹, R. Ikeda¹, K. Takahashi¹, and K. Sakamoto¹

¹Japan Atomic Energy Agency, Naka, Japan ²Ibaraki University, Japan

Corresponding Author: T. Kobayashi, kobayashi.takayuki@jaea.go.jp

The development of a gyrotron and launcher operated at two frequencies, 110 GHz and 138 GHz, has made a significant progress toward electron cyclotron heating (ECH) and current drive (ECCD) in JT-60SA. High-power, long-pulse gyrotrons are required for the JT-60SA ECH/ECCD system which has the total injection power of 7 MW and the pulse duration of 100 s using 9 gyrotrons. The wave frequency in the original specification is 110 GHz, which is effective for off-axis ECH/ECCD to sustain a high- β plasma at the toroidal field of 1.7 T. On the other hand, the higher frequency waves at 130–140 GHz enables ECH/ECCD in the core plasma region at the maximum toroidal field of 2.3 T in JT-60SA. However, a dual frequency gyrotron that can generate the target output power and pulse length (1 MW for 100 s) was not developed since it requires high oscillation efficiency to obtain high power and low diffraction loss to achieve long pulse, simultaneously. In 2011, we started to develop a new dual frequency gyrotron (110 GHz, 138 GHz) equipped with a triode type electron gun to obtain high oscillation efficiency. High-power, long-pulse operations of the dual frequency gyrotron have been carried out since the last IAEA FEC. Developments of an ECH launcher with high reliability based on a linear-motion antenna concept and a polarizer with optimized groove depth, width, and period for dual frequency operation are also in progress. Main results are as follows: i) Oscillations of 1 MW for 10 s were successful at both frequencies for the first time in the world as a dual-frequency gyrotron by optimizing electron pitch factor using the triode electron gun; ii) Low diffraction loss and cavity Ohmic loss enabling 1 MW for 100 s and 1.5-2 MW for several seconds were experimentally confirmed, and a 100 MJ oscillation was achieved (0.51 MW, 198 s, 110 GHz), so far; iii) An oscillation at 82 GHz was also successful as an additional frequency showing the possibility of the use of fundamental harmonic waves; iv) Launcher optics design toward dual-frequency operations showed little difference in the poloidal beam width for these frequencies; v) Prototype tests of a wide-band twister polarizer at both low power (< 1 mW) and high power (~ 0.25 MW, 3 s) showed promising results.

Imai

FIP/2-2Rc

Slides

Paper

Development of Over 1 MW and Multi-Frequency Gyrotrons for Fusion

T. Imai¹, T. Kariya¹, R. Minami¹, T. Numakura¹, T. Eguchi¹, T. Kato¹, Y. Endo¹, M. Ichimura¹, T. Shimozuma², S. Kubo², H. Takahashi², Y. Yoshimura², H. Igami², S. Ito², T. Mutoh², K. Sakamoto³, H. Idei⁴, H. Zushi⁴, K. Nagasaki⁵, F. Sano⁵, M. Ono⁶, and Y. Mitsunaka⁷

¹University of Tsukuba, Tsukuba, Ibaraki, Japan
 ²National Institute for Fusion Science, Toki, Japan
 ³Japan Atomic Energy Agency, Naka, Japan
 ⁴Kyushu University, Kasuga, Japan
 ⁵Kyoto University, Kyoto, Japan
 ⁶Princeton Plasma Physics Laboratory, Princeton, NJ, USA
 ⁷Toshiba Electron Tubes and Devices Co. Ltd. (TETD), Tochigi, Japan

Corresponding Author: T. Imai, imai@prc.tsukuba.ac.jp

EC (Electron Cyclotron) scheme is quite promising tool for heating and current drive (H&CD) and plasma control for present and future devices up to DEMO and Commercial reactors. Development of gyrotron is a key to open this promising door. Multi-MW and multi-frequency technologies are major issues to challenge for robust and cost effective reactor heating system. In the University of Tsukuba, gyrotrons of wide range of frequencies from 14 GHz to 300 GHz have been developed for this purpose in collaboration with JAEA, NIFS, and TETD. Over-1 MW dual frequency gyrotron of new frequency range (14-35 GHz), where the reduction of diffraction loss and cathode optimization are quite important, has been developed for EC/EBW H&CD for GAMMA 10/PDX, QUEST, Heliotron J and NSTX-U. Output power of 1.25 MW at 28 GHz and estimated oscillation power of 1.2 MW at 35.45 GHz from the same tube have been achieved with a cathode angle improvement. This is the first demonstration of an over 1 MW dual-frequency operations in lower frequency, which contributes to the technology of wide band multi-frequency/multi-MW tube for DEMO EC/EBW H&CD. The output power of 600 kW for 2 s at 28 GHz was also demonstrated. It is applied to the QUEST and has resulted higher EC-driven current than ever. Further, in the joint program of NIFS and Tsukuba for LHD ECH gyrotrons, a new frequency of 154 GHz has been successfully developed with a TE(28,8) cavity, which delivered 1.16 MW for 1 s, 0.3 MW in CW (30 minutes), and a total power of 4.4 MW to LHD plasma with another three 77 GHz tubes, which extended the LHD plasma to high T_e region. All these gyrotron performances are new records in each frequency range.



ICRF Actuator Development at Alcator C-Mod

S. Wukitch¹, Y. Lin¹, S. Shiraiwa¹, A. Hubbard¹, B. LaBombard¹, B. Lipschultz², D. Miller¹, M. Reinke³, and J. Terry¹

¹Massachusetts Institute of Technology, Plasma Science & Fusion Center, Cambridge, MA, USA ²University of York, Heslington, UK ³Oak Ridge Institute for Science Eduction, Oak Ridge, TN, USA

Corresponding Author: S. Wukitch, wukitch@psfc.mit.edu

Future fusion reactors will present more severe constraints on ion cyclotron range of frequency (ICRF) heating and current drive actuators than ITER. Reliably coupling power to the plasma despite load variations is critical. In addition, ICRF interaction with the edge plasma, particularly impurity contamination and enhanced localized heat loads, is challenging. We report on progress developing an ICRF actuator with favorable scaling towards reactors. Using a field aligned (FA) antenna, we have found that the FA antenna loading is similar to TA antennas but the FA antenna reflection coefficient has significantly reduced variation, thus it is inherently load tolerant. We speculate the variation in reflection coefficient is a result of slow wave coupling of neighboring straps and field alignment significantly reduces this coupling.

The underlying physics of RF plasma edge interaction is thought to be linked to RF electric fields parallel to the magnetic field, E_{\parallel} . One source of RF E_{\parallel} is from the antenna itself and can minimize integrated E_{\parallel} through geometry. Experiments comparing a field aligned (FA) and a toriodally aligned (TA) antenna have demonstrated that FA antenna has significantly reduced impurity contamination compared to TA antennas. The impurity sources measured at the antenna are nearly eliminated for the FA antenna. This is an important milestone since this is the first demonstration that an ICRF antenna is reduced to a level similar to that observed for identical discharges heated by the TA antenna and the FA antenna is not powered. The estimated energy deposited is 0.4% of the total injected energy and marks the first time an ICRF antenna has achieved the target level for the ITER design, 0.625% of 20 MW.

One path to increase antenna power density is to use materials with high strength and high melting temperature. Furthermore copper will be restricted to thin coatings in a reactor due to material swelling and poor strength at high temperature. We have found that the higher strength materials have higher breakdown voltage compared to copper. Highly polished molybdenum and tungsten breakdown field is 40% higher than copper. The latest results and analysis will be presented.



FIP/2-4

Progress Status of the Activities in EU for the Development of the ITER Neutral Beam Injector and Test Facility

A. Masiello¹, G. Agarici¹, D. Boilson², T. Bonicelli¹, H. Decamps², U. Fantz³, P. Franzen³, J. Graceffa², B. Heinemann³, R. Hemsworth², D. Marcuzzi⁴, F. Paolucci¹, M. Simon¹, V. Toigo⁴, and P. Zaccaria⁴

> ¹F4E: Fusion for Energy, Barcelona, Spain ²ITER Organization, Saint Paul lez Durance, France ³Max-Planck-Institut für Plasmaphysik, Garching, Germany ⁴Consorzio RFX, Associazione Euratom-ENEA sulla Fusione, Padova, Italy

Corresponding Author: A. Masiello, antonio.masiello@f4e.europa.eu

The development of the Neutral beam system for ITER has been progressing well thanks to the start of the operations of the ELISE (Extraction from a Large Ion Source Experiment) at the Max Planck Institute for Plasma Physics in Garching, Germany, and to the big effort devoted to the establishment of the ITER Neutral Beam (NB) Test Facility in Padua, Italy. This paper presents the main experimental results of ELISE, the status of the manufacturing activities for the components of the NB test facility and the progress made in the design of the mechanical components and in that of auxiliary and power supplies systems.

Development of DC Ultra-High Voltage Insulation Technology for ITER NBI

H. Tobari¹, M. Hanada¹, K. Watanabe¹, M. Kashiwagi¹, M. Dairaku¹, H. Yamanaka¹, T. Maejima¹, N. Umeda¹, N. Seki¹, H. Abe¹, Y. Terunuma¹, D. Shiina¹, T. Kondo¹, S. Tanaka², M. Kadowaki², K. Yamaguchi², H. Decamps³, M. Kuriyama³, J. Graceffa³, L. Svennson³, R. Hemsworth³, and D. Boilson³

¹Japan Atomic Energy Agency, Naka, Japan ²Hitachi, Ltd., Japan ³ITER Organization, Saint Paul lez Durance, France

Corresponding Author: H. Tobari, tobari.hiroyuki@jaea.go.jp

In the ITER NBI for plasma heating and current drive, a 1 MeV, 40 A deuterium negative ion (D⁻) beam is designed to be accelerated for 3600 s. The beam energy and the pulse duration of the D⁻ beam are 2–5.5 times higher and 360 times longer than those in the negative-ion-based NBIs on LHD and JT-60U, respectively. Thus, to realize higher voltage and longer pulse duration, the generation, transmission and insulation of DC ultra-high voltage are critical issues for the ITER NBI. In addition, the high-current busbar, cooling water and gas pipes at -200 kV – 1 MV potential are simultaneously transmitted through the HV bushing from the gas-insulated transmission line in the PS to the beam source (BS) to minimize the installation space. Those are significant differences from that in existing N-NB systems. Especially, a DC 1 MV insulating transformer for feeding an electric power from the ground to 1 MV potential is one of most challenging components. For stable power transmission through the HV bushing, 1 MV vacuum insulation and a stiffness to withstand the maximum pressure difference of 0.9 MPa in a limited space are required. Japan Atomic Energy Agency (JAEA) is in charge of the procurement of these high voltage parts of the 1 MV PS and the HV bushing. As for the insulating transformer, a DC long pulse insulation structure and a composite bushing for the isolation of the high-voltage to the air have been newly developed. The mockup transformer successfully demonstrated a stable insulation of DC -1.2 MV for 3600 s. The HV bushing serves as the terminal of the HV transmission line. It is made in five 200 kV stages and a two-stage mockup has been developed, and stable voltage holding at 480 kV for 3600 s was demonstrated. These R&D results fulfill the ITER requirement, which allows the realization of the PS and HV bushing for the ITER NBI.

FIP/2-5Rb

Slides

Paper

Progress in Long Pulse Production of Powerful Negative Ion **Beams for JT-60SA and ITER**

A. Kojima¹, N. Umeda¹, M. Hanada¹, M. Yoshida¹, M. Kashiwagi¹, H. Tobari¹, K. Watanabe¹, N. Akino¹, M. Komata¹, K. Mogaki¹, S. Sasaki¹, N. Seki¹, S. Nemoto¹, T. Shimizu¹, Y. Endo¹, K. Ohasa¹, M. Dairaku¹, H. Yamanaka¹, and L. Grisham²

> ¹ Japan Atomic Energy Agency, Naka, Japan ²Princeton Plasma Physics Laboratory, Princeton, NJ, USA

Corresponding Author: A. Kojima, kojima.atsushi@jaea.go.jp

The long pulse generation of the powerful negative ion beams of 500 keV, 22 A (130 A/m^2) and 1 MeV, 40 A (200 A/m²) is the essential challenge to realize the negative-ion-based neutral beam injectors (NBIs) for JT-60SA and ITER, where 10 MW D0 beam for 100 s and a 16.5 MW for 3600 s are designed, respectively. In Japan Atomic Energy Agency (JAEA), after the achievements of the beam current density and energy required for JT-60SA and ITER with a short pulse duration, the target of R&D is focused on the extension of the pulse duration in JT-60 negative ion source and the MeV accelerator.

Significant progress in the extension of pulse duration of the powerful negative ion beams has been made to realize the neutral beams injectors for JT-60SA and ITER. The pulse duration and the current density of the JT-60 negative ion source has been successfully improved from 30 s at 80 A/m^2 in the previous operation to 100 s at 120–130 A/m², which satisfy the rated values for JT-60SA. This progress has been achieved by controlling the negative ion production via the surface temperature of the plasma grid. The pulse duration of the MeV class negative ion beams for ITER has been also extended by more than an order of magnitude in the MeV accelerator. A long pulse acceleration of 8.7 s has been achieved at 880 keV, 130 A/m^2 by improving the cooling capability of the extraction grid where the aperture displacement for the beamlet steering is also modified, so there is no limitation to increase the power density and the pulse duration. This is the longest pulse duration of the MeV-class negative ion beams in the world.



The Initial Programme of Wendelstein 7-X on the Way to a HELIAS Fusion Power Plant

A. Dinklage¹, TW7-X Team¹

¹Max-Planck-Institut für Plasmaphysik, Garching, Germany

Corresponding Author: A. Dinklage, dinklage@ipp.mpg.de

The stellarator concept offers a possible alternative to a tokamak Fusion Power Plant (FPP). One of the missions of the EU Roadmap to the realisation of fusion energy is to develop the stellarator line to maturity. World-wide efforts on different stellarator lines cover a substantial range of candidate magnetic configurations; the EU programme focuses on the optimized, helical advanced stellarator (HELIAS) line. Wendelstein 7-X (W7-X) is the first fully optimized stellarator to proof the concept of physics-based, optimized shaping of the magnetic field structure to get to plasma performances projectable to fusion in upscaled devices.

To demonstrate reactor potential, W7-X needs to operate reliably at high-power and high-density quasi-continuously with a viable divertor concept. At the same time, basic science issues of 3D plasmas will advance plasma physics. The key for the physics program is steady-state heat and particle exhaust by qualified divertor operation with actively cooled plasma facing components. However, to develop steady-state scenarios aggressively but to avoid technical risks from water cooling, the initial operation phase of W7-X will begin with carbon limiter discharges later replaced by an inertially cooled test divertor for the development of high-performance operation.

Initially, the discharge lengths will be limited to 5–10 s at maximum anticipated heating powers. Critical for later high-performance operation, the development of discharge scenarios at high densities with full density control is one leading objective to develop reliable divertor operation schemes. Fuelling schemes, e.g., with pellets, will be qualified to avoid central density depletion due to thermodiffusion. Furthermore, the behavior of impurities as well as the potential occurrence of edge localized modes will be investigated. Basic issues relevant to FPPs such as the impact of stellarator optimization on turbulent transport and improved confinement modes are part of the plan. The very beginning of the exploitation of W7-X will be a technical demonstration of ECH plasma break-down, X2-heated plasmas and measurements of vacuum flux-surfaces. In this phase, neoclassical electron heat transport will be investigated. The physics plan to steady-state operation in the initial phase of W7-X and the underlying strategy with regard to a HELIAS stellarator FPP will be outlined.



Slides

Paper

Status of Upgrading Project of Tokamak T-15

E. Azizov¹, P. Khvostenko¹, V. Belyakov², E. Bondarchuk², O. Filatov², V. Krylov², A. Melnikov¹, A. Mineev², M. Sokolov¹, and A. Sushkov¹

¹National Research Centre "Kurchatov Institute", Moscow, Russian Federation ²D. V. Efremov Institute of Electrophysical Apparatus, St. Petersburg, Russian Federation

Corresponding Author: E. Azizov, azizov_ea@nrcki.ru

Status of T-15 upgrade tokamak is presented. T-15 upgrade tokamak has the following parameters: R = 1.48 m, a = 0.67 m, B = 2.0 T, $I_{pl} = 2.0$ MA. Poloidal system is capable of realizing the divertor both with single null and double null magnetic configuration and plasma shape with elongation $k_{95} = 1.7$ –1.9 and triangularity delta 0.3–0.4. Installation will equipped with the auxiliary plasma heating and current drive ($P_{aux} = 15$ –20 MW) systems. One of the main tasks of experimental study program on T-15 upgrade tokamak is the obtaining of physical and technological data for fusion neutron source creation. The design of electromagnetic system and vacuum chamber and also the modernization of engineering systems are described. Time schedule of T-15 upgrade tokamak assembling is presented. Physical start-up of the T-15 upgrade tokamak is outlined in 2016.



DEMO Design Point Studies

R. Kemp¹, D. Ward¹, G. Federici², R. Wenninger², and J. Morris³

¹JET-EFDA, Culham Science Centre, Abingdon, UK ²EFDA, Garching, Germany ³CCFE Fusion Association, Culham Science Centre, Abingdon, UK

Corresponding Author: R. Kemp, richard.kemp@ccfe.ac.uk

To allow coherent conceptual design activities, and later engineering design activities, for a demonstration fusion power plant (DEMO), a self-consistent design point must first be developed. The DEMO design point is a set of parameters characterising the key features of a DEMO power plant on which evaluation of different systems can be based with confidence that there are no significant conflicts between those systems. System codes representing the full plant by capturing the interactions between (usually relatively simple) models of all the important plant subsystems are used to identify design points based on assumptions about plasma performance and technology. The purpose of using a systems code is to identify potential solution spaces without having to carry out complex analysis at every point.

The EU DEMO strategy currently considers two possible operating scenarios: a conservative pulsed design, using near-ITER technology and plasma performance, termed DEMO1; and an optimistic, higher-performance, steady-state option (DEMO2). This contribution presents the work being carried out to develop these design points, including development of the systems code models. The process involves an iteration between the systems code PROCESS and more detailed analysis such as integrated scenario modelling with transport codes. The results of the detailed modelling are used to refine the assumptions and thus the design space of available solutions, within which the design points can be re-optimised. The target performance parameters for each DEMO option and the current device parameters in each case are also presented, and we discuss the sensitivity study work that has been carried out to assess the robustness of each design and justify the choice of variables. In each case the variables are subject to change as more DEMO-relevant models and experimental data become available and technological knowledge improves. However, these operating points are intended to provide a well-justified and stable foundation on which to base wider design evaluation work.

This work was funded by the RCUK Energy Programme and the European Communities under the contract of Association between EURATOM and CCFE, and by the European Union's Horizon 2020 research and innovation programme. The views and opinions expressed herein do not necessarily reflect those of the European Commission.



Paper

Slides

Physics and Engineering Studies of the Advanced Divertor for a Fusion Reactor

N. Asakura¹, K. Hoshino¹, H. Utoh¹, K. Shinya², N. Ohno³, Y. Someya¹, S. Tokunaga¹, K. Shimizu¹, K. Tobita¹, M. Kobayashi⁴, and H. Tanaka⁴

¹Japan Atomic Energy Agency, Naka, Japan
 ²Toshiba Nuclear Engineering Services Co., Japan
 ³University of Nagoya, Nagoya, Japan
 ⁴National Institute for Fusion Science, Toki, Japan

Corresponding Author: N. Asakura, asakura.nobuyuki@jaea.go.jp

Magnetic configurations of advanced divertor, i.e., super-X (SXD) and snowflake, were recently proposed, and the concepts have been demonstrated in experiments. For the application to the DEMO reactor, engineering design as well as the plasma performance should be determined. A short super-X divertor (short-SXD) is proposed as a new option for DEMO divertor, where field line length from the divertor null to the outer target was largely increased (more than two times) in a similar size of conventional divertor. Physics and engineering design studies of a fusion reactor with the short-SXD installed at the outer divertor have progressed. Minimal number of the divertor coils (1 or 2) were installed inside the toroidal field coil, i.e., interlink-winding (interlink). Arrangement of the poloidal field coils (totaling 8 or 9) and their currents were determined, taking into account of the engineering design such as vacuum vessel and the neutron shield structures, and maintenance scenario of the divertor and blankets. Divertor plasma simulation (SONIC) showed that large radiation region is produced between the super-X null and the target, and the plasma temperature becomes low (1–2 eV) both at the inner and outer divertors, i.e., fully detached plasma was obtained efficiently.



DEMO Concept Development and Assessment of Relevant Technologies

Y. Sakamoto¹, K. Tobita¹, H. Utoh¹, N. Asakura¹, Y. Someya¹, K. Hoshino¹, M. Nakamura¹, and S. Tokunaga¹

¹ Japan Atomic Energy Agency, Naka, Japan

Corresponding Author: Y. Sakamoto, sakamoto.yoshiteru@jaea.go.jp

Recent development of a DEMO concept with a medium size (major radius of \sim 8.2 m) and a lower fusion power (\sim 1.5 GW) is presented together with assessment of relevant technologies. The maximum toroidal field is evaluated at \sim 1.3 T, which is nearly independent on strand materials (Nb₃Sn or Nb₃Al) unlike a compact DEMO, while the increase of the allowable design stress has a large impact on that. The divertor simulation study indicates that the tolerable level of divertor heat flux ($\sim 5 \text{ MW/m}^2$) is foreseeable for the medium size DEMO, and the design study of short super-X divertor as an option is progressing to efficiently obtain the fully detached plasma. The assessment of various maintenance schemes indicates that the vertical port maintenance scheme provides advantages in easy handling, the layout of poloidal coils, the size of toroidal coils, and separate maintenance of the in-vessel components. Finally, the study of the waste management suggests that the ratio of radioactive waste to be disposed of in shallow land burial can be increased thanks to the lower fusion power.



FIP/3-5Ra

Current Status of Chinese Solid Tritium Breeder TBM

K. Feng¹

¹Southwestern Institute of Physics, Chengdu, Sichuan, China

Corresponding Author: K. Feng, fengkm@swip.ac.cn

China had promised to test its TBM modules during different ITER operation phase and have signed the CN HCCB TBMA with ITER IO recently. Related design and R&D activities for each TBM modules with auxiliary systems and interface with ITER facility were introduced. The preliminary conceptual design of CN HCCB TBM has been completed while the design optimization is in progress. Basic characteristics and main design parameters and technical characteristics of CN HCCB TBM are introduced briefly.

The neutron multiplier Be pebbles of kg-scale are fabricated by the Rotating Electrode Processing (REP). Be alloy are prepared by powder metallurgical (PM) methods. Be pebbles of diameters 0.5 mm and 1.0 mm as the neutron multiplier are fabricated. Related performance test is ongoing. The fabrication of pebble bed container and performance experiment of breeder pebble bed has being started. The lithium orthosilicate, Li4SiO4 pebbles with lithium 80% enriched in ⁶Li as tritium breeding materials of HCCB TBM have been fabricated at laboratory level by melt-spraying method. Chinese Low-activated Ferritic/martensitic steel, CLF-1, as TBM structural materials is developing from laboratory scale towards industrially level. The structure material CLF-1 of ton-scale was recently produced by vacuum induction melting and electro-slag re-melting method. The mock-up fabrication and component tests by using the CLF-1 steel for Chinese test blanket module have being developed. Recent status on the fabrication technology development of CN HCCB TBM module was also reported.

Chinese HCCB TBM will be tested in Port #2 of ITER test ports with the India LLCB TBM simultaneously. Two TBMs and its associated ancillary systems will be integrated on same Port as well as interfaced with ITER buildings and sub-systems. The design and fabrication of related ancillary system with ITER facility are being performed.



Design Concept of K-DEMO for Near-Term Implementation

K. Kim¹, H.-S. Kim¹, S. Oh¹, K. Im¹, Y. Lee¹, J. Yeom¹, J. Park¹, C. Lee¹, G.-S. Lee¹, G. Neilson², C. Kessel², T. Brown², P. Titus², and Y. Zhai²

¹National Fusion Research Institute, Daejeon, Korea, Republic of ²Princeton Plasma Physics Laboratory, Princeton, NJ, USA

Corresponding Author: K. Kim, kkeeman@nfri.re.kr

Korean Fusion Energy Development Promotion Law (FEDPL) was enacted in 2007 to promote a long-term cooperative fusion research and development among participating industries, universities, and research institutes. As a following step, a conceptual design study for a steady-state Korean fusion demonstration reactor (K-DEMO) has been initiated in 2012. The conceptual design activity will continue to the end of 2021 and the construction is planned to be completed by the end of 2037.

One special concept discussed of K-DEMO is a two-staged development plan. At first, K-DEMO is designed not only to demonstrate a net electricity generation ($Q_{eng} > 1$) and a self-sustained tritium cycle (Tritium breeding ratio, TBR > 1.05), but also to be used as a component test facility. Then, at its second stage, a major upgrade is carried out by replacing in-vessel components in order to show a net electric generation on the order of 500 MWe. After the thorough 0D system analysis, the major radius and minor radius are chosen to be 6.8 m and 2.1 m, respectively, considering practical engineering feasibilities. In order to minimize the deflection of wave and maximize the efficiency, a top launch high frequency (> 200 GHz) electron cyclotron current drive (ECCD) system is the main candidate for the current profile control and off-axis current drive of K-DEMO. For matching the high frequency ECCD, a high magnetic field is required and it can be achieved by using high performance Nb₃Sn-based superconducting conductor currently being used in accelerator magnet area and the peak magnetic field is approaching to 16 T with the magnetic field at the plasma center above 7 T. Pressurized water is the most prominent choice for the main coolant of K-DEMO when considering balance of plant development details. Considering the plasma performance and the peak heat flux in the divertor system, a double-null divertor system becomes the reference choice of K-DEMO. For a high availability operation, K-DEMO incorporates a vertical maintenance design.

A design concept and radial builds for K-DEMO considering a vertical maintenance scheme are presented together with preliminary design parameters.

Multi-Physics Engineering Analysis for an Integrated Design of ITER Diagnostic First Wall and Diagnostic Shield Module

Y. Zhai¹, D. Loesser¹, M. Smith¹, V. Udintsev², T. Giacomin², D. Johnson¹, A. Khodak¹, W. Wang¹, R. Feder¹, and J. Klabacha¹

¹Princeton Plasma Physics Laboratory, Princeton, NJ, USA ²ITER Organization, Saint Paul lez Durance, France

Corresponding Author: Y. Zhai, yzhai@pppl.gov

ITER diagnostic first walls (DFWs) and diagnostic shield modules (DSMs) are designed to protect diagnostic instrument and components from plasma facing environment and provide structural support of diagnostic systems under high thermal and electromagnetic loads while allowing for diagnostic access to the plasma. The design of DFWs and DSMs are largely driven by 1) plasma radiation and nuclear heating during normal operation; 2) EM loads during plasma disruptions. A multi-physics engineering analysis methodology has been developed at PPPL and the analysis protocol was used for an integrated design of ITER DFW and DSM. The analysis was performed to identify stress and deformation issues for single and combined load cases following the ITER SDC-IC rules required for design by analysis.

Two major issues driving the mechanical design of DFWs are identified as the result of the multiphysics analysis: 1) Thermal fatigue strain range on the first wall panel during normal operation is the design driver for the first wall thickness; a 5 mm thick first wall panel was selected based on the < 0.3% equivalent strain range limit for 30,000 thermal cycles. The stress due to pressure on the first wall is a small fraction of the stress due to combined loads, which provides the ESPN exemption. 2) Stress on the DFW attachment tabs under EM disruption loads drives tab geometry optimization and bolt selection. A force-deflection interface matrix at the three DFW tabs is defined to identify stiffness requirements on the DSM based on tab stress and deflection margins.

To validate feasibility of DSM configuration as the result of interface stiffness requirement, several disruption load-related issues need to be addressed since they may significantly alter the load distribution and its associate dynamic amplification among DFW, DSM and the PP structure. Our study showed that the DSM design configuration has a significant impact on the interface load transfer and thus affects the design of DFW attachment scheme. Dynamic amplification on displacement and interface reaction moment under transient disruption loads also depends on the DSM configuration. Moreover, transient effect of the electrical contact between DSMs and PP structure during disruptions increases the net disruption loads on the full EPP structure by 10–20%.

Paper

Progress on the ITER Diagnostic-Radial X-Ray Camera

L. Hu¹, K. Chen¹, Y. Chen¹, J. Shen¹, S. Li¹, X. Sheng¹, L. Niu¹, Y. Chen¹, and J. Zhao¹

¹Institute of Plasma Physics, Chinese Academy of Sciences, Hefei, China

Corresponding Author: L. Hu, lqhu@ipp.ac.cn

The Radial X-ray Camera (RXC) is designed to measure the poloidal profile of the plasma X-ray emission with high spatial and temporal resolution. The primary role of the RXC diagnostic is to measure low (m, n) MHD modes, sawteeth, lock modes, disruption precursors and L-H transition indicators. RXC also provides supplementary measurements of plasma position, radiative power, runaway electrons, impurity content, etc. [1, 2]. The camera consists of two subsystems, i.e., in-port and ex-port cameras which view the outer and core region respectively through vertical slots in the diagnostics shield module (DSM) of an equatorial port plug [1]. At present, detailed camera design is in progress and focuses on internal camera whose structure is much more complicated than that of external camera. Double-tube (inner and outer tube) structure, dove groove, two-half structure, cooling and shielding are designed. The design facilitates the machining and maintenance. The structure analysis results showed that in the worst case, even the maximum stress was still less than allowable stress. Through optimizing layout of shielding, apertures and light path, good balance between shielding and the signal noise ratio has been obtained. The camera neutronics analysis result indicated that the detectors can be operated during the whole D-D phase without detector replacement. Simulation of the camera measurement indicated that the camera satisfy the measurement requirement specified in the procurement arrangement. In order to measure background noise and accommodate detector position error, the concepts of blind channel and overlap channels have been implemented in the design. Since the beryllium window is a critical component of RXC which plays the role of vacuum sealing and light filtering, two set of Be windows with good pressure-resistant performance have been designed and tested. The electronics and data acquisition (DAQ) and I&C (Instrumentation and Control) group have also made good progress. The test results of different circuit scheme showed maximum noise level can be less than 10 nA. Besides, the DAQ and I&C people have fixed hardware scheme for camera DAQ and plant I&C.

References

- [1] Donné A. J. H., et al., Chapter 7: Diagnostics. Nuclear fusion, 47(2007) S337.
- [2] Annex B_55 E7_Radial X Ray Camera (ITER_D_97RVCA v1.2).



Pa<u>pe</u>r

Comprehensive First Mirror Test for ITER at JET with ITER-like Wall

A. Garcia Carrasco¹, M. Rubel¹, P. Petersson¹, D. Ivanova¹, A. Widdowson², J. Likonen³, and L. Marot^{4,5}

¹KTH Royal Institute of Technology, Stockholm, Sweden
 ²JET-EFDA, Culham Science Centre, Abingdon, UK
 ³VTT Technical Research Centre of Finland, Finland
 ⁴Ecole Polytechnique Fédérale de Lausanne, CRPP, Lausanne, Switzerland
 ⁵Department of Physics, University of Basel, Basel, Switzerland

Corresponding Author: A. Garcia Carrasco, alvarogc@kth.se

Windows and first mirrors are essential plasma-facing components in all optical spectroscopy and imaging systems used for plasma diagnosis in a reactor-class machine. To recognize the extent of changes in the mirror performance a thorough First Mirror Test (FMT) has been carried out at the JET tokamak. The major goal is to assess the optical performance, and — by surface analyses — to determine causes of reflectivity changes. Up to date, FMT has been the most comprehensive study program of mirror behaviour in fusion environments. This paper summarises recent results from JET-ILW and provides a brief comparison to the operation with carbon walls (JET-C). Twenty mirrors were exposed in JET-ILW for 18.9 h with 13.1 h of X-point operation. Divertor: Reflectivity of divertor mirrors was degraded by 50-85% because of the deposit formation: 60-600 nm thick layers (in JET-C carbon deposits over 20 μ m were formed). Be is the main element inco-deposits, the others are: D, C, N, O, inconel components, and traces of W. Main Chamber Wall: The majority of Mo mirrors (7 out of 8) from the main wall retained high total reflectivity, i.e., the decrease was below 5%. The surface region (15–30 nm) of wall mirrors contained only light impurities. The results obtained so far for the main chamber mirrors allow some optimism regarding the reliability of diagnostics in ITER. To ensure the best possible predictions the FMT is continued in JET with the increased heating power. There is no doubt, however, that in ITER long-term exposure and off-normal events may change properties of the mirrors. A practical solution for maintaining high mirror performance in the main chamber diagnostics may be based on a periodic evaporation of a fresh Mo layer on the mirror surface. This approach can be applied in-situ and it is more realistic than photonic cleaning, protective filters, local plasma or gas puff, or other methods critically assessed in Ref. [1].

This work was supported by EURATOM and carried out within the framework of the European Fusion Development Agreement. The views and opinions expressed herein do not necessarily reflect those of the European Commission.

References

[1] Rubel, M. et al., J. Nucl. Mater., 390-391 1066 (2009).



FIP/P4-4

Gamma-Ray Spectrometer in the ITER NPA System

 D. Gin¹, I. Chugunov¹, A. Shevelev¹, E. Khilkevitch¹, M. Petrov¹, S. Petrov¹,
 V. Afanasyev¹, M. Mironov¹, V. Naidenov¹, D. Doinikov¹, A. Pasternak¹, I. Polunovskii¹, and J.-M. Drevon²

¹Ioffe Physical-Technical Institute of the Russian Academy of Science, St. Petersburg, Russian Federation ²ITER Organization, Saint Paul lez Durance, France

Corresponding Author: D. Gin, pipha@mail.ru

Gamma-ray Spectrometer (GRS) is as a part of the diagnostic system built around neutral particle analyzer (NPA). Viewing the same plasma area in the equatorial plane as the rest components of the system, GRS can significantly improve its diagnostic abilities. Line integrated diagnostic of gamma-ray emission over this area can support NPA data on the following key ITER measurements (parameters) [1]:

11: Fuel ratio in plasma core (020: n_d/n_t core);

28: Ion temperature profile (064: Core T_i);

30: Confined alphas and fast ions (069: Alpha Energy Spectrum)

with time resolution of up to 100 ms each. Also detailed data on fast ions velocity distribution functions and some other parameters not mentioned in [1] can be obtained. Finally, application of GRS in NPA system could support tomographic measurements provided by Vertical and Radial Gamma ray Spectrometers.

GRS consists of high resolution germanium (HPGe) and scintillation LaBr₃ detectors installed inside a neutron dump of NPA system. Direct neutron fluxes suppressed with LiH attenuator. This report is dedicated to the latest developments of the gamma ray diagnostic techniques. Monte Carlo calculations of neutron and gamma-ray fluxes in EQ11 Port Cell and in the places of allocation of gamma-detectors have been carried out. Gamma and neutrons emissions in the tokamak for different scenario were modelled and spectra calculated. Latest diagnostic justification and development results also includes new processing codes implementations which are capable of real-time processing of LaBr₃ signal with count-rates up to 10^7 s^{-1} , tritium production in LiH attenuator studies and others — to be discussed in details in the report.

The work was supported by contract No. 05-12 between "Technoexan, Ltd" and Institution "Project Center ITER" and No. 02-12 between Ioffe Institute and Institution "Project Center ITER".

References

[1] Costley, A.E., et al., SRD-55, 2012.

Preprint

Overview of ITPA R&D Activities for Optimization of ITER Diagnostic Performance

Y. Kawano¹, S. Zoletnik², G. Vayakis³, and H. K. Park⁴

¹Japan Atomic Energy Agency, Naka, Japan
 ²Institute for Particle and Nuclear Physics, Budapest, Hungary
 ³ITER Organization, Saint Paul lez Durance, France
 ⁴Ulsan National Institute of Science and Technology, Korea, Republic of

Corresponding Author: Y. Kawano, kawano.yasunori@jaea.go.jp

In this paper, highlighted progress of the Topical Group activity is overviewed. International Tokamak Physics Activity (ITPA) Topical Group on Diagnostics has been conducting the R&D activities for supporting the optimization of ITER diagnostic performance. For diagnostics of escaping α particles, assessment of several measurement techniques have been carried out, especially, feasibility test of activation probe technique has progressed under a multi machine joint experiment. For mitigation of degradation effects for plasma facing first mirrors, development of cleaning techniques for beryllium proxy impurities deposited on mirrors has progressed by the use of plasma discharges. Characteristics of wall reflected stray-lights have been investigated towards to mitigate their impact on optical diagnostics.



Studies of Protection and Recovery Techniques of Diagnostic Mirrors for ITER

A. Litnovsky¹, M. Matveeva¹, L. Buzi¹, Y. Krasikov¹, V. Kotov¹, A. Panin¹, D. Castano Bardawil¹, T. Akiyama², W. Biel¹, and C. Linsmeier¹

¹Forschungszentrum Jülich, Jülich, Germany ²National Institute for Fusion Science, Toki, Japan

Corresponding Author: A. Litnovsky, a.litnovsky@fz-juelich.de

Mirrors will be used in optical diagnostic systems of ITER to guide the light from plasma towards detectors and cameras. In the severe particle and radiation environment, the mirrors will be subjected to the erosion due to fast particles and to deposition of impurities from the plasma. These processes affect adversely the mirror reflectivity and therefore must be suppressed or mitigated at the maximum possible extent. The use of shutters and shaped diagnostic ducts for mirror protection represent the passive protection techniques. Among the active recovery techniques, in-situ cleaning of mirrors by the plasma is the most promising candidate option.

The first positive results of experiments and the predictive modeling envisage the successful suppression of deposition in the diagnostic tubes with fins trapping the impurities on their way towards the mirrors located in the end of these tubes. To benchmark the modeling predictions, cylindrical and cone-shaped diagnostic tubes were exposed in TEXTOR for about 140 hours of plasma operation. After exposure, a deposition ranging 50–150 nm was found on the mirrors located in the cylindrical tubes. No drastic suppression of deposition was observed in the cylindrical tubes with fins. At the same time, no detectable deposition was found on the mirrors located at the end of cone-shaped tubes outlining the advantages of the cone geometry.

Active cleaning by plasma sputtering was performed on molybdenum mirrors pre-coated with an aluminum film 100 nm thick. Aluminum was used as proxy of beryllium in these studies. Electroncyclotron resonance-generated plasmas were used for plasma exposures. The mirrors were biased to increase the effectiveness of plasma sputtering. During the exposure in helium plasma, the entire coating was sputtered within nine hours, leaving no trace of aluminum and leading to the full recovery of the specular reflectivity. Remarkably, the diffuse reflectivity of the mirror substrate did not increase in the wavelength range of 250–2500 nm demonstrating the complete recovery of the mirror surface by plasma sputtering of the coating without detrimental effects on the mirror itself. The analyses of passive and active mirror recovery efforts will be provided in the contribution.

Paper

Experimental Evaluation of Long-Term and Stable Magnetic Sensors Operation in ITER-Relevant Conditions

I. Bolshakova¹, S. Belyaev², V. Chekanov², V. Coccorese³, I. Duran⁴, S. Gerasimov³, N. Kargin⁵, R. Konopleva², Y. Kost⁶, O. Makido⁶, F. Shurygin⁶, A. Murari³, A. Quercia³, M. Strikhanov⁵, S. Timoshyn⁶, I. Vasilevskiy⁵, and A. Vinnichenko⁵

 ¹Lviv Polytechnic National University, Ukraine
 ²B. P. Konstantinov Petersburg Nuclear Physics Institute, St. Petersburg, Russian Federation ³JET-EFDA, Culham Science Centre, Abingdon, UK
 ⁴Institute of Plasma Physics AS CR v.v.i., Prague, Czech Republic
 ⁵National Research Nuclear University MEPhI, Moscow, Russian Federation
 ⁶Magnetic Sensor Laboratory, Lviv Polytechnic National University, Lviv, Ukraine

Corresponding Author: I. Bolshakova, inessa@mail.lviv.ua

Radiation resistant sensors and magnetic measuring instrumentation have been designed and its performance in the conditions of fusion reactors have been demonstrated, by the international research collaboration between researchers from different countries supported by STCU (Science and Technology Center in Ukraine) projects and funded from the EU, USA, Japan, and Canada. Created radiation-resistant semiconductor sensors of magnetic field have received an experimental evaluation during their testing in nuclear research reactors, and showed their performance under the conditions of neutron fluences several times higher than the maximum neutron fluence in steady-state sensor locations in ITER reactor ($> 10^{18} \text{ n/cm}^2$). 3D probes with Hall sensors have been successfully tested in European reactors TORE SUPRA and JET. Notably, long-term operation of sensor and equipment has been demonstrated over the period of five years (2009–2014) at JET.

Works targeting further increase in radiation resistance and measurement accuracy of magnetic measuring equipment with Hall sensors are currently underway, namely:

- New radiation modification methods of semiconductor sensors have been developed for their parameter stabilization in ITER-like neutron fluxes.
- Materials for sensors with new properties and high sensitivity to magnetic field have been created on the basis of nano-size InAs/i-GaAs heterostructures.
- High precision 3D magnetometers have been created to measure the spatial distribution of magnetic induction vector.

Conducted studies have confirmed the long-term operation of the developed magnetic measuring sensors in ITER-relevant conditions and promising qualities of these development products for DEMO.



FIP/P4-9

Tritium Transport Modelling: First Achievements on ITER Test Blanket Systems Simulation and Perspectives for DEMO Breeding Blanket

I. Ricapito¹, P. Calderoni¹, A. Ibarra², C. Moreno², Y. Poitevin¹, A. Rueda³, and J. Serna³

¹F4E: Fusion for Energy, Barcelona, Spain
 ²The National Fusion Laboratory, CIEMAT, Madrid, Spain
 ³Empresarios Agrupados, Madrid, Spain

Corresponding Author: I. Ricapito, italo.ricapito@f4e.europa.eu

The European TBM Programme will generate experimental data for development and validation of tritium transport simulation tools which are essential for predicting the tritium processing performance of a breeding blanket in DEMO or power reactor. In this ambit, two European TBS (Test Blanket Systems)will be tested in ITER under a wide range of operative conditions and neutron irradiation scenarios.

The modelling tool, developed in the frame of a contractual collaboration between F4E and CIEMAT/Empresarios Agrupados, is based on the customization of the EcosimPro simulation platform. It implements a 1D dynamic mathematical model, without including any multiphysics coupling effect (e.g., MHD, heat generation and temperature variation over the time, thermal-hydraulics etc.). The physics of tritium transport is comprehensive, as it fully takes into account the phenomena of tritium transport at gas-metal interface and at the liquid metal boundary layer. For any selected operating scenario and for a selected time window, the simulation tool gives an output consisting of: a) the amount of tritium permeated from the TBM breeding region into the main coolant; b) the amount of tritium solubilized inside the functional and structural materials of the TBM as well as in all TBS ancillary systems; c) the tritium permeated at the end of the TBS chain and sent to the ITER rooms; d) the percentage of tritium generated in the TBM per unit time.

The paper describes first the characteristics and main equations of the simulation tool. Then, it presents and discusses the preliminary simulation results covering a wide interval of TBS operating conditions and plasma irradiation scenarios isolated inductive pulses, back to back plasma pulses, long pulses. The test matrix has been arranged to make possible a check of the internal consistency of the code and, at the same time, to have a preliminary performance prediction of the two TBS in terms of tritium recovery capability and inventory distribution. Last but not least, the paper provides the main lines of development of tritium transport modelling from this preliminary phase up to the final one when the predictive capabilities have to be exploited at the maximum extent in support of the DEMO breeding blanket design.

Preprint

Behaviors of ITER EHF FW under High Heat Flux for Mock-ups Manufactured by HIP Joining Technology

J. Chen¹, F. Jin¹, P. Wang¹, J. Wu¹, L. Shen¹, X. Liu¹, D. Liu¹, X. Zhu¹, Z. Li¹, X. Duan¹, E. Niu², G. Alexander³, K. Vladimir³, and L. Bao⁴

¹Southwestern Institute of Physics, Chengdu, Sichuan, China
 ²ITER Chinese Domestic Agency, China
 ³D. V. Efremov Institute of Electrophysical Apparatus, St. Petersburg, Russian Federation
 ⁴ITER Organization, Saint Paul lez Durance, France

Corresponding Author: J. Chen, chenjm@swip.ac.cn

To withstand a surface heat load up to 4.7 MW/m² in a life time of 16000 cycles, the enhanced heat flux (EHF) ITER FW panel uses a hypervapotron (HVT) CuCrZr/316L(N) cooling channel and small Beryllium tiles. R&D has been carried out in China on manufacturing and testing of EHF FW mock-ups towards the final provision of series FW products for ITER. A hot iso-static pressing (HIP) technology was successfully developed and qualified to join the FW materials of Beryllium, CuCrZr alloy, and 316L(N) stainless steel (SS). Alternatively, an explosion bonding technology has qualified recently to provide bimetallic CuCrZr/SS plates. This technology provided enough margins for both tensile strength and grain size of the Copper alloy to ITER requirement.

Various small scale mock-ups have been manufactured to evaluate the size effect of Be tiles and the manufacturing variants for optimization. The mock-ups were tested in Efremov Research Institute at 4.7 MW/m^2 for 7500 cycles and 5.9 MW/m^2 for 1500 cycles. According to the test result, the maximum Be tile size shall be less than $16 \times 16 \text{ mm}^2$ while the $12 \times 12 \text{ mm}^2$ Be tile is acceptable. Post-HHFT examination showed cracks along Be/Cu interface in the Ti and Cu diffusion layers for the failed mock-up. The crack may initiated from coated pure Copper at the Be tile corner, where oxidization was observed and thermo-mechanical analysis showed higher stress than other areas. To improve the HHFT performance, the thickness of the compliant Cu layer should be optimized.

The acceptable Be tile is too small for manufacturing large scale FW panel. Possibility to use $51 \times 12 \text{ mm}^2$ Be tile by castellation was investigated. Mock-ups have been manufactured and the HHFT was done at 4.7 MW/m² for 16000 cycles. In addition, more mock-ups will be manufactured to evaluate the effect of artificial defects at Be/Cu interface for the purpose to establish an acceptance criteria for the future series products. At the same time, in parallel an EHF FW semi-prototype is being manufactured and will be qualified by HHFT in 2015. The semi-prototype is manufactured by a combination procedure of explosion bonding, HIP joining, laser welding, and TIG welding. Various R&D activities have been carried out and the technologies have been qualified according to the relevant ITER specification and standards.



Design Finalization and R&D Activities before the Start of Manufacture of ITER Thermal Shield

W. Chung¹, D. K. Kang¹, K. Nam¹, C. H. Noh¹, K. O. Kang¹, H.-J. Ahn¹, H.-G. Lee¹, K.-J. Jung¹, C. H. Harris², N. I. Her², C. H. Choi², and C. Sborchia²

¹National Fusion Research Institute, Daejeon, Korea, Republic of ²ITER Organization, Saint Paul lez Durance, France

Corresponding Author: W. Chung, whchung@nfri.re.kr

ITER Thermal Shield (TS) plays the role of reducing the heat load transferred by thermal radiation and conduction from warm components to the magnet structures that operate at 4.5 K. Thermal radiation to the magnet structures is minimized by cooling the TS at 80 K helium temperature and by providing the TS surfaces with low emissivity using silver coating.

Korea Domestic Agency (KODA) has performed the TS design with the collaboration of industries since 2007. The final design of TS main components was approved in October 2012. After the approval of the TS final design, fine tuning of the final design had been performed considering the interface with the adjacent components and the updated assembly schemes. The manifold pipes around the TS main components are to be installed in the tokamak to supply helium gas to the TS. The final design of the manifold was performed after the final design of the TS main components had been completed. The manufacturing drawing was approved in April 2014.

Full-scale mock-up of Vacuum Vessel Thermal Shield (VVTS) 10 degree sector was developed to prevent possible risks of manufacturing. All the manufacturing processes except the silver coating were tested and verified in the fabrication of mock-up. Pre-qualification tests were conducted to find proper processes for forming and welding. Welding joint shape between panel and flange was validated by the mock-up. Shell thickness change was measured after bending, forming and buffing processes. Sequential press-bending was successfully tested for the fabrication of complex VVTS ports. Bending jig for the 3D shape of cooling tube routing was also developed in detail and tested for the VVTS port cooling tube.

This paper shows the key results from final design and R&D of ITER TS performed by Korea before the start of manufacturing. The manufacturing of VVTS is now on-going and the first two 40 degree sectors of the VVTS will be manufactured until the end of 2015.

Paper



Current Status of Final Design and R&D for ITER Blanket Shield Block in Korea

M.-S. Ha¹, S.-W. Kim¹, H.-C. Jung¹, H.-S. Hwang¹, Y.-G. Heo², D.-H. Kim³, H.-J. Ahn¹, H.-G. Lee¹, and K.-J. Jung¹

¹National Fusion Research Institute, Daejeon, Korea, Republic of ²DNDE Inc., Busan, Korea, Republic of ³ITER Organization, Saint Paul lez Durance, France

Corresponding Author: M.-S. Ha, msha12@nfri.re.kr

The main function of the ITER blanket shield block (SB) is to provide nuclear shielding and support the first wall (FW) panel. It is required to accommodate all the components located on the vacuum vessel (in particular the in-vessel coils, blanket manifolds and the diagnostics). The conceptual, preliminary, and final design reviews (FDR) have been completed in the framework of Blanket Integrated Product Team (BIPT). Korea domestic agency (KODA) has been successfully completed not only the final design activities including thermo-hydraulic and thermo-mechanical analyses for SB02, 06, 08, and 16 but also the SB Full Scale Prototype (FSP) pre-qualification program prior to issuing of the procurement agreement.

SB #2 and #6 are located at in-board region of Tokamak. The pressure drop was less than 0.3 MPa, and fully satisfied the design criteria. The thermo-mechanical stresses were also allowable even though the peak stresses occurred at nearby radial slit end holes, and their fatigue lives were evaluated much more than 30,000 cycles. The SB #8 is one of the most difficult modules for design, since this module shall endure the severe thermal loading not only from nuclear heating but also from plasma heat flux at uncovered regions by the First Wall (FW). In order to resolve the design issue, the Neutral Beam (NB) shine-through module concept was applied for FW uncovered region, and it has been successfully verified as a possible design resolution. The SB #16 is located at out-board central region of Tokamak. This module is under much higher nuclear loading than other modules and is covered by an enhanced heat flux FW panel. In the early design stage, many cooling headers on front region were inserted to mitigate a peak stress nearby the access hole and radial slit end hole. However, the cooling headers on front region needed to be removed in order to reduce the risk from cover welding during manufacturing. Finally, a few cooling headers remained by the effort through several iterations to remove them and to optimize the cooling channels. The SB #8 FSP has been manufactured and tested in accordance with pre-qualification program based on the preliminary design, and related R&D activities were implemented to resolve the fabrication issues.

This paper provides the current status of final design and relevant R&D activities of the blanket shield block.



R&D Status on Remote Handling Technology for ITER Blanket Maintenance

N. Takeda¹

¹Japan Atomic Energy Agency, Naka, Japan

Corresponding Author: N. Takeda, takeda.nobukazu@jaea.go.jp

In ITER, the blanket must be replaced remotely for maintenance because of high radiation field. This study demonstrated two of three steps of blanket positioning process, a Virtual Reality (VR) system and final positioning because the other step, a robot vision system has been demonstrated in the previous study. Regarding the VR system, positioning accuracy of 46.7 mm was achieved. Regarding final positioning, the blanket module could be positioned without gaps and errors. As a result, feasibility of the positioning strategy for the blanket module has been verified.



Paper

Structural Analysis of the ITER Coil Power Supply System

A. Labusov¹, E. Privalova¹, M. Sukhanova¹, A. Arneman¹, N. Khrabrykh¹, V. Panov¹, S. Gavrilov¹, and S. Akulitsky¹

¹D. V. Efremov Institute of Electrophysical Apparatus, St. Petersburg, Russian Federation Corresponding Author: A. Labusov, labusov@sintez.niiefa.spb.su

The ITER Coil Power Supply and Distribution System (CPSS) serves for operation of the ITER tokamak magnet system. The CPSS is the complex system which consists of electrical equipment of different purpose and the busbar system used for electrical connection between this equipment and the coils of the magnet system. In accordance with the Procurement Arrangement the Russian Federation is responsible for design, manufacturing, delivery, installation, initial commissioning and corresponding tests of the CPSS components. The Efremov Institute is in charge of this activity. The compliance with structural design criteria is the common practice when designing the plant equipment. In contrast to other ITER subsystems no special structural codes are mandatory or specified for the busbar system.

This paper presents the approach used for mechanical analysis and strength assessment performed in the course of design, manufacturing and tests of one of the main CPSS component; the busbar system. Based on the proposed approach structural analysis of the busbar system of the ITER CPSS has been performed in support of design and manufacturing of the busbars, their connection zones (compensators, jumpers) and busbar supporting system.



Advance in Japanese Superconductor for ITER

Y. Nunoya¹, Y. Nabara¹, Y. Takahashi¹, T. Suwa¹, M. Oshikiri¹, F. Tsutsumi¹, J. Takamura¹, S. Chuheishi¹, and K. Shibutani¹

¹ Japan Atomic Energy Agency, Naka, Japan

Corresponding Author: Y. Nunoya, nunoya.yoshihiko@jaea.go.jp

Japan Atomic Energy Agency (JAEA) has been manufacturing superconductors for ITER Toroidal Filed (TF) coils and Center Solenoid (CS). Since CS will be operated in the pulse mode, development of conductor that has stable performance against cyclic electromagnetic force was necessary. Conductor with shorter twist pitch cable to yield higher cable stiffness was successfully developed and no degradation against cyclic electromagnetic force was observed in a full-size conductor test. This result allowed JAEA to start CS cable manufacturing in 2013 consequently. At the end of 2013, manufacturing of 91% of Japanese TF conductors was successfully completed. All superconducting strand for TF whose total length is 23,000 km has completed in six years. It was demonstrated that strand performance has maintained stable from the initial to the final production.

Paper

Preparation for Preliminary Design of ITER GDC

Y. Wang¹, M. Wang¹, H. Xu¹, L. J. Cai¹, T. Lin¹, Y. Lu¹, and W. Han¹

¹Southwestern Institute of Physics, Chengdu, Sichuan, China

Corresponding Author: Y. Wang, wangyq@swip.ac.cn

A DC Glow Discharge Cleaning (GDC) system is designed for ITER. The procurement arrangement of GDC was signed between ITER Organization and China Domestic Agency at the end of 2013. However, some critical engineering issues still need to be solved, such as gap insulation and shielding, ceramic spray on U-shape cooling pipe, design of cooling channel inside electrodes, structure, thermal, electromagnetic and seismic analysis.

The GDC electrode works as a shield plug during plasma operation, so water cooling is necessary. The cooling pipes of GDC are used to feed power to electrodes, thus all the components of GDC inside the vacuum vessel are on high potential. The glow discharge between the first walls, or the inner surface of vacuum vessel and the front of electrode is expected, but the one between rod and cooling pipes of electrode and other parts inside port plugs must be avoided. We plan to suppress the unexpected glow discharge by two means, gap insulation and ceramic insulation.

During GDC, the electrode front is impacted by accelerated electrons, so the electrode is heated. Because the cooling water for ITER GDC electrode is the backing water of tokamak ($240 \pm 10^{\circ}$ C at 4.4 ± 0.4 Mpa) which approaches its boiling point, the cooling of electrode during GDC is a big concern. Thus, a four-layer structure for cooling flumes in the head of electrode is designed. Fluid-structure interaction analysis results show that the heat load during GDC which is given in the load specification can be taken by the backing water, but the margin is limited.

The seven GDC electrodes are different from each other due to integration constrains of various diagnostics components in port plugs, so analysis and design for each electrode will be performed in preliminary design stage respectively. To find out experience of the analysis for the coming preliminary design, we perform electromagnetic, structure, thermal, and seismic analysis based on the GDC Configuration Management Modules (CMM) presented on the second GDC CDR. GDC is one of the systems which must be available before plasma operation. The preparation for the preliminary design of GDC makes the potential problems exposed as early as possible and guides the following design work of GDC.

FIP/P4-25

Paper

Hybrid Integral-Differential Simulator of EM Force Interactions / Scenario-Assessment Tool with Pre-Computed Influence Matrix in Applications to ITER

V. Rozov¹, A. Alekseev¹

¹ITER Organization, Saint Paul lez Durance, France

Corresponding Author: V. Rozov, vladimir.rozov@iter.org

A necessity to address a wide spectrum of engineering problems in ITER determined the need of efficient tools for modeling of the magnetic environment and force interactions between main components of the magnet system. The assessment of the operating window for the machine, determined by the electro-magnetic (EM) forces, and the check of feasibility of particular scenarios play an important role for ensuring the safety of exploitation. Such analysis-powered prevention of damages forms an element of the Machine Operations and Investments Protections strategy. The corresponding analysis is a necessary step in preparation to the commissioning, which finalizes the Construction phase. It shall be supported by the development of the efficient and robust simulators and multi-physics/multi-system integration of models. The developed numerical model of interactions in the ITER magnetic system, based on the use of pre-computed influence matrices, facilitated immediate and complete assessment and systematic specification of EM loads on magnets in all foreseen operating regimes, their maximum values, envelopes and the most critical scenarios. The common principles of interaction in typical bilateral configurations have been generalized for asymmetry conditions, inspired by the plasma and by the hardware, including asymmetric plasma event and magnetic system fault cases. The specification of loads is supported by the technology of functional approximation of nodal and distributed data by continuous patterns and analytical interpolants. The global model of interactions together with the "meshless" analytical format of output provides the source of self-consistent and transferable data on spatial distribution of the system of forces for assessments of structural performance of the components, assemblies and supporting structures. The used numerical model is fully parametrized, which makes it well suitable for multi-variant and sensitivity studies (positioning, off-normal events, asymmetry, etc.). The obtained results and matrices form a basis for a relatively simple and robust force

processor as a specialized module of a global simulator for diagnostic, operational instrumentation, monitoring and control, as well as a scenario assessment tool. The paper gives an overview of the model, applied technique, assessed problems and obtained qualitative and quantitative results.

Development of Predictive Simulator to Model Electromagnetic Transients for ITER Application

V. Belyakov¹, A. Alekseev¹, A. Belov¹, V. Kukhtin¹, E. Lamzin¹, S. Sychevsky¹, E. Gapionok¹, and A. Bazarov¹

¹D. V. Efremov Institute of Electrophysical Apparatus, St. Petersburg, Russian Federation Corresponding Author: V. Belyakov, belyakov@niiefa.spb.su

A vital part of the commissioning and testing plasma scenarios of the International Thermonuclear Experimental Reactor (ITER) is predictive simulations for the overall behaviour during operation. Due to the complexity of the facility and severe constraints related to its cost-efficiency and reliability, particular attention should be paid to ensure required performance. The use of dynamic simulators gives an opportunity to efficiently correlate a large number of parameter on various scenarios and provide general consistency of the reactor. The paper presents an attempt to proceed to a simulator for electromagnetic transients in ITER. The basic software tool is the code TYPHOON. The algorithms and mathematical techniques are described that are targeted to achieve parallelism in computations. Preprint

Design Studies towards the Geometrical Optimization of the Thermal-Hydraulic Performance of Cylindrical Hypervapotron-Type Collectors for Gyrotrons

L. Savoldi Richard¹, C. Bertani¹, F. Cau², F. Cismondi², G. Gantenbein³, S. Illy³, G. Monni¹, and **R. Zanino**¹

¹Polytechnic University of Turin, Turin, Italy
 ²F4E: Fusion for Energy, Barcelona, Spain
 ³Karlsruhe Institute of Technology, Germany

Corresponding Author: L. Savoldi Richard, laura.savoldi@polito.it

Gyrotrons are used in current and future fusion experiments to heat the plasma with microwaves in the electron cyclotron frequency range, as well as to drive with a noninductive mechanism a nonnegligible fraction of the plasma current. For example, in ITER, the Electron Cyclotron Heating and Current Drive system will be made of 24 gyrotrons, operating at 170 GHz with an output power of ~ 1 MW each.

The efficiency of the device is typically of the order of (at most) 50%, so that the rest of the power of the spent electron beam is lost to the inner surface of a hollow solid cylinder structure called the collector, typically cooled by water in forced flow. Several constraints characterize the collector design, e.g., the maximum allowable temperature, the minimum lifetime in terms of cycles related to fatigue, etc. Going towards the design and CW operation of higher power gyrotrons for the development of DEMO and future fusion devices, the issue of the heat load received by the collector walls, using solutions like the hypervapotron (HV) geometry, widely studied in recent years for the cooling of plasma facing components, are being considered, together with ad-hoc sweeping strategies of the electron along the collector surface (longitudinal, transverse, combined), to make the thermal load as uniform as possible.

Here we concentrate on the investigation of a HV-like structure in a different geometrical configuration — the hollow cylinder of the collector. We apply the StarCCM+ commercial CFD code to the analysis of the effect of different aspect ratios (AR) of the HV cavities on the heat exhaust capabilities of a model collector, computing a self-consistent estimate of the heat transfer coefficient between collector and coolant, that will have to be implemented in the structural analyses of the collector walls for the fatigue and collector life time assessment.

Starting from the deep cavities (AR \sim 3), adopted as first reference geometry, an optimum TH performance of the collector can be achieved with shallower (AR \sim 1) cavities, minimizing the maximum collector temperature. Also other possible geometrical configurations are considered, for instance zigzag structures, in order to assess the options for further improvements of the collector TH performance.

ICRF Heating Experiment Using the Faraday Shield Less Antenna and New High Power Antenna in LHD

T. Seki¹, T. Mutoh¹, K. Saito¹, H. Kasahara¹, R. Seki¹, S. Kamio¹, M. Osakabe¹, and K. Nagasaki²

¹National Institute for Fusion Science, Toki, Japan ²Institute of Advanced Energy, Kyoto University, Kyoto, Japan

Corresponding Author: T. Seki, seki@nifs.ac.jp

In ICRF heating experiments, impurity influx has been a serious problem from the early phase of fusion research. It was thought that the RF electric field parallel to the magnetic field line near the antenna caused the impurity influx, and Faraday Shield (FS) was thought to be necessary to shield out such an electric field. If the FS is possible to be removed, the design and the construction become much easier. It will have an impact on the designing of the antenna for the steady-state devices. On the other hand, high-power injection is an important subject in the reactor, which limits the number of the ports for the heating devices. The results presented in this research provide important guideline for the design of the ICRF antenna for future devices.

Some experiments without FS have been carried out in short pulse length in tokamak devices. The results were different from the device-to-device and high-power and long-pulse experiments have been awaited. Faraday Shield of one strap of ICRF antenna was removed in LHD. The loading resistance without FS antenna was increased twice or more than that of with FS antenna. It means the higher power can be injected from the FS less antenna when the same power is supplied from the transmitter. Behaviors of the impurities and radiation loss power were almost same. Heating efficiency is lower in the without FS antenna. The power, which is not contributed to the plasma heating, may cause harmful effect in the plasma periphery in high power and steady-state operation. However, there is no serious problem in LHD experiment so far.

Aiming at a high-power and steady-state heating, new antenna was installed in LHD. The strap is tilted and Faraday Shield is aligned to the magnetic field line (Field-Aligned). Impedance Transformer is incorporated between the antenna head and the vacuum feedthrough. Then, we named this antenna FAIT antenna. This is designed to increase the loading resistance and reduce the RF voltage of the transmission line and feedthrough. The loading resistance was compared with the existing antenna, which had the same structure at the antenna head. It was more than twice higher and higher power was easily injected in FAIT antenna. It means the impedance transformer is working well as we expected. FS less and FAIT antennas were used for high power and steady-state experiment without any problem.

Paper

ICRF System on Tokamak T-15

P. Khvostenko¹, *V. Vdovin*¹, and E. Azizov¹

¹National Research Centre "Kurchatov Institute", Moscow, Russian Federation

Corresponding Author: P. Khvostenko, khvostenko_pp@nrcki.ru

This system of ICRH/CD should provide RF heating and current drive in plasma of tokamak T-15. A total of 6 MW RF power in the plasma should be initially available from the IC system. ICRH and CD system consists of three in-port antennas, corresponding transmission lines, delivering RF energy from sources, matching system, and ancillary subsystems.

Functional requirements in physics Main heating schemes ICH system should be working on the second hydrogen harmonic at nominal $B_o = 2.0$ T (frequency of 60 MHz). Hydrogen minority ions scenario at fundamental harmonic near of 30 MHz is also forseen. This circuit also includes a scenario minority He-3 in order to heat bulk ions. The system must be capable of generating a current near the plasma axis. Minority current due to He-3 addition should be created on the outer magnetic surface q = 1 for the control of sawtooth period at nominal field $B_o = 2.0$ T (frequency ~ 40 MHz for the 2nd harmonic of He-3). The system conditions the chamber wall.

Functional technology requirements: Components RF sources should use the technologies available today; The reliability will be determined at the design stage; RF sources should be able to be effective, a quasi-continuous under high VSWR change to a maximum value equal to 2, for any phase of the reflection coefficient.

Functional Requirements treatment needed; Sources of RF power should match modes of operation: for plasma heating and current; conditioning of the chamber wall; Antennas conditioning; Testing of RF antennas.

ICH Antennae on T-15. ICRF complex has three antennas placed in adjacent horizontal ports. Each antenna consists of 2 poloidal current-carrying conductors, grounded in the center, transparent FS. The poloidal limiters are installed on both sides of the antenna to protect it. They are made of blocks CFC tiles. For option 30 s pulses antenna has water cooling, including Faraday screen and the vacuum chamber wall of the transmission line. FS is made from 625 inconel (or stainless steel SS316 L) tube coated C4B (back up is CTi). We are also considering advanced option of low impedance surface multi loop broad antenna with wave impedance near of 5 Ω , fed by strip lines in horizontal ports.

FIP–P

Preprint

Helicons Current Drive System in Tokamak T-15

A. Tribendis¹, V. Vdovin², E. Azizov², A. Krasilnikov³, and G. Kurkin¹

¹Budker Institute of Nuclear Physics, Novosibirsk, Russian Federation
²National Research Centre "Kurchatov Institute", Moscow, Russian Federation
³RosAtom ITERRF DA, Russian Federation

Corresponding Author: A. Tribendis, a.g.tribendis@inp.nsk.su

The innovative efficient current drive scheme in the tokamaks using the Helicons radiation has recently been proposed [1] to stabilize high normalised β strongly shaped reactor relevant plasmas. The scheme has shown broad current profile tailoring capabilities in modern tokamaks, reactors FNSF-AT, ITER, and DEMO, and uses reliable RF CW technique developed for large accelerators. This paper describes the conceptual design of RF systems for tokamak T-15 and proposal for JT-60AS in order to check the predictions [1] in the experiments, to analyse commercially available RF power sources and their efficiency, transmission RF energy lines, matching elements and RF energy launch into tokamak chamber.

In this paper we consider a new system for the scheme to maintain CW current by fast waves, at frequencies of 500–700 MHz, being lower of so-called Lower Hybrid (LH) frequency. In this frequency range there are commercially available CW klystrons of megawatt level, running stationary. The advantages of the scheme (partially tested at lower frequencies in tokamaks) are the use of electrically strong antennae of resonator/waveguide type and substantially greater coupling antenna-plasma (frequency 10 times greater of IC frequency).

Apart of impressive ITER project in final signing stage there is the bilateral NRC KI – DIII-D GA Agreement for joint testing of the proposed Innovative Off-axis CD scheme on operating tokamak DIII-D with its high electron β plasmas needed for helicons scenario. It appears that Russia can fulfill its ambitious 4 MW Helicons CD project on T-15 tokamak after pioneering 1 MW testing on DIII-D tokamak: of highly effective method of Off-axis current generation via a quasi-stationary fast waves (helicons), which provides a reliable way of CW operation in DEMO and fusion Power Plant, combining a clear physical mechanism and the developed technology for large accelerators in previous 40 years in the range of 350–1000 MHz. The T-15 Helicons system project will be presented by demonstration of Advanced Traveling Wave Antennae (TWA) to be used for Helicons excitation and 4 MW 509 MHz 1.2 MW klystron based RF complex with four TWA antennae, each fed by 1 MW waveguide transmission line (totally 4 lines), circulators etc.

References

[1] V. Vdovin, Plasma Physics Reports, vol. 39 (2013) #2, 125.



FIP/2-4Rc

Progress in the Realization of the PRIMA Neutral Beam Test Facility

V. Toigo¹, D. Boilson², T. Bonicelli³, M. Hanada⁴, and A. K. Chakraborty⁵

¹Consorzio RFX, Associazione Euratom-ENEA sulla Fusione, Padova, Italy ²ITER Organization, Saint Paul lez Durance, France ³F4E: Fusion for Energy, Barcelona, Spain ⁴ Japan Atomic Energy Agency, Naka, Japan ⁵Institute for Plasma Research, Bhat, Gandhinagar, India

Corresponding Author: V. Toigo, vanni.toigo@igi.cnr.it

In ITER, additional heating systems are provided to reach higher plasma temperature and to sustain fusion conditions; among them two Neutral Beam Injectors (NBI) will be installed, capable of producing high energy beams up to 1 MeV, to transfer to the plasma up to 16.7 MW and to operate for up to 1 hour.

Such a high NBI performance has never yet been reached. A research and development plan has been launched to minimize the risks of unsuccessful results of the ITER NBI operation; it involves the realization of a full scale test facility in which issues related to NB physics and technology will be studied and assessed in advance with respect to the ITER operation, in order to guarantee the full ITER performances by means of a dedicated R&D programme.

This test facility, called PRIMA, is under construction in Padova; it will host two experiments: SPIDER and MITICA, full scale prototypes of the ion source and of the whole injector, respectively. SPIDER will be a RadioFrequency (RF) ion source, based on the configuration adopted by IPP, with the same characteristics foreseen in ITER NBI but with beam energy limited to 100 keV. It can generate both Hydrogen and Deuterium Ions; the accelerator is equipped with provisions to filter electrons and it will allow the use of cesium to attain the high values of current density required in the ITER NB ion source. SPIDER is procured by F4E and INDA. MITICA is the full-scale prototype of the ITER injector, with a similar scheme and layout, provided with the same power supply system and also the control and protection systems are being designed according to the same rules and constraints as in ITER. MITICA is procured by F4E and JADA.

The paper will give a general overview of the test facility and will describe in detail the status of development of the SPIDER and MITICA projects and the last progress in the realization of the main components. A general plan of the realization and commissioning steps will be also given. The most important and critical issues regarding both physics and technology will be presented and the solutions identified or still under evaluations will be discussed.

Preprint

Availability Considerations in the Design of K-DEMO

T. Brown¹, C. Kessel¹, K. Kim², G. Neilson¹, J. S. Park², P. Titus¹, and K. Im²

¹Princeton Plasma Physics Laboratory, Princeton, NJ, USA ²National Fusion Research Institute, Daejeon, Korea, Republic of

Corresponding Author: T. Brown, tbrown@pppl.gov

A DEMO device has been considered the next step following ITER as a near-term prototypical reactor design that is tritium self-sufficient and produces a limited amount of net electricity. The machine maintenance approach and planned configuration concept plays a major role in establishing the design point. DEMO will also need to show that adequate operating availability can be achieved over a reasonable time period, as a last step before full-scale electricity production. The ability to operate with high availability and reliability plays a key ingredient in defining the DEMO configuration, fostering the need for rapid removal/replacement of limited-life in-vessel components. DEMO preconceptual studies are being carried out by China, EU, Japan, and South Korea (with US participation). The device designs span a range of maintenance approaches from full radial extraction of large invessel modules through all TF horizontal openings to vertical maintenance of segmented in-vessel components. Progress made on S. Korea's K-DEMO design will be provided with emphasis on the design choices identified to promote high availability and a review of how these design selections compare with the choices made on the Chinese, EU and Japan concepts.



FIP/P7-2

Physics and Engineering Assessments of the K-DEMO Magnet Configuration

G. Neilson¹, T. Brown¹, K. Im², C. Kessel¹, K. Kim², P. Titus¹, and Y. Zhai¹

¹Princeton Plasma Physics Laboratory, Princeton, NJ, USA ²National Fusion Research Institute, Daejeon, Korea, Republic of

Corresponding Author: G. Neilson, hneilson@pppl.gov

With ITER now under construction, increased attention is being paid to the roadmap from ITER to a fusion DEMO, including studies of next-step fusion facilities with nuclear missions. Among these, South Korea's K-DEMO is unique in its focus on a high toroidal magnetic field, large major radius, steady-state tokamak design for the core of a facility to test fusion nuclear components in Phase I and, after upgrades, produce 500 MW of electricity in Phase II. Innovative features of the K-DEMO magnet set include the use of two toroidal field (TF) coil winding packs, each of a different design, to reduce the amount of costly superconducting material in the low-field regions. Also, the configuration is constrained by maintenance considerations, leading to a magnet arrangement with large TF coils and widely-spaced poloidal field (PF) coils to accommodate removal of in-vessel components as large modules. A Princeton Plasma Physics Laboratory team has supported the pre-conceptual K-DEMO study with the following physics and engineering assessments of the magnet configuration: 1) design point and operating space assessment, 2) conductor assessment, and 3) structural assessment. It is found that a reference design point at 6.8 m major radius and 7.4 T toroidal field provides sufficient operating margins for the 500 MWe Phase II mission. An analysis of the electro-mechanical behavior of candidate cable-in-conduit conductors predicts 10-30% critical current degradation in the initial load cycle, and an additional degradation in the range of 5% with cyclic loading, supporting current design assumptions. A first-pass global analysis of the magnet system found out-of-plane deformations of the TF coil to be only ~ 1 cm, but the inner leg of the TF coil was found to be over-stressed by about 40%. An increase of 10 cm (25%) in the wall thickness in the wedged "nose" of the case was estimated to be sufficient to resolve the issue. Although the design evolution is still at an early stage, these assessments support the design point choices to date and the expectation that a feasible solution for the high-field K-DEMO magnet system can be found.

Design Concept of K-DEMO In-Vessel Components

K. Im¹, J. S. Park¹, S. Kwon¹, K. Kim¹, C. Kessel², T. Brown², and G. Neilson²

¹National Fusion Research Institute, Daejeon, Korea, Republic of ²Princeton Plasma Physics Laboratory, Princeton, NJ, USA

Corresponding Author: K. Im, khim@nfri.re.kr

As a way to realize a large-scale fusion energy, a DEMO device has been considered as a next step after the international ITER device. Pre-conceptual DEMO studies are being carried out by the international fusion community including China, EU, Japan, and Korea (with participation of the USA). Early in 2007 in Korea, Fusion Energy Development Promotion Law (FEDPL) was enacted to settle down the legal base of fusion energy development. As a following step, a pre-conceptual design study for the Korean fusion demonstration reactor (K-DEMO) has been initiated with the uniqueness of high magnetic field ($B_0 = 7.4$ T), R = 6.8 m, a = 2.1 m, and steady-state tokamak. K-DEMO tokamak plasma will be operated in double-null configuration with high elongation ($\kappa = 2$) and triangularity ($\delta = 0.625$). Pressurized water is used as coolant for in-vessel components.

Blanket modules are toroidally subdivided into 16 inboard modules and 32 outboard modules, in order to allow for vertical maintenance. Each blanket module consists of plasma-facing first wall, layers of breeding parts, shielding and manifolds. Vanadium is placed as interlaying material between tungsten first wall and RAFM structural material. K-DEMO blanket system adopts ceramic breeders using Li₄SiO₄ pebbles with beryllide as neutron multiplier to ensure better safety with water coolant. Layers of breeders and multipliers were optimized by MCNP simulations to achieve global TBR > 1.05. Material selection and thickness of shielding are optimized to maintain the nuclear heating to the superconducting magnets below allowables. Heat load on blanket first wall by core plasma radiation is maintained below $\sim 0.5 \text{ MW/m}^2$. Approximately 60% of plasma power is handled in divertor region. To maintain the target peak heat flux below 10 MW/m², $\sim 90\%$ of divertor plasma power should be radiated in divertor region with 10 degree of target tilting angle and a power decay length $\lambda_q \simeq 1.5$ mm as expected by recent result. Tungsten-based target is used with steel-based structural material carrying pressurized water coolant. In line with the blanket toroidal segmentation for vertical maintenance, upper and lower divertor modules are also subdivided into 32 toroidal modules, respectively.

The results of thermo-hydraulic and structural analyses are presented to support the developed design concepts.

Paper

The Impact on Tritium Breeding Ratio of Neutral Beam Port Location in DEMO

I. Jenkins¹, E. Surrey¹, and S. Zheng¹

¹CCFE Fusion Association, Culham Science Centre, Abingdon, UK

Corresponding Author: I. Jenkins, ian.jenkins@ccfe.ac.uk

The Tritium Breeding Ratio (TBR) is a critical quantity on DEMO as it will determine the continued availability of one the required fuels and thus strongly affect the viability of the device. The breeding blanket segments will be designed to cover as much of the inside of the vessel as feasible, excepting the divertor region. They must also take account of remote maintainability and allow necessary gaps for plasma heating systems and plasma diagnostics to function. The location and size of such ports on the reactor vessel may reduce the TBR by reducing the area of the blanket. In order to examine the sensitivity of the TBR with respect to the placement of Neutral Beam (NB) ports, modelling of Neutral Beam Current Drive (NBCD) has been undertaken in relevant plasma scenarios with reference to a model of a Helium Cooled Pebble Bed (HCPB) blanket. For the scenarios examined, it is shown that NBCD can equally well be deployed using ports at elevations up to 4 m above and below the mid-plane. Consequently, the effect of the ports required for NB on the available blanket area reduces the TBR in the model from 1.12 to 1.08 if they are located at the mid-plane, but only to 1.09 or 1.10 if the ports are located optimally above or below the mid-plane. This difference may become critical as other aspects of the design requiring ports, such as diagnostics, are integrated into the design as the value of TBR must, critically, exceed unity by a healthy margin.

This work was funded by the RCUK Energy Programme under grant EP/I501045 and the European Communities under the contract of Association between EURATOM and CCFE, and by the European Union's Horizon 2020 research and innovation programme. The views and opinions expressed herein do not necessarily reflect those of the European Commission.



DEMO Reactor Design by the New Modular System Code SYCOMORE

B. Saoutic¹, C. Reux¹, F. Imbeaux¹, J.-F. Artaud¹, P. Bernardi¹, G. Ciraolo¹, J. Bucalossi¹, J.-L. Duchateau¹, C. Fausser², D. Galassi¹, L. Di Gallo¹, P. Hertout¹, J.-C. Jaboulay³, A. Li Puma³, and L. Zani¹

¹CEA-IRFM, Saint Paul lez Durance, France ²CEA-DER, France ³CEA-DM2S, France

Corresponding Author: B. Saoutic, bernard.saoutic@cea.fr

Demonstration power plant is the next step for fusion energy following ITER. Key questions remain before a design is selected. Some of these questions can be addressed by simulation through system codes. System codes aim at modeling the whole plant with all its subsystems and identifying their interactions and their impact on the design choice. The SYCOMORE code is a modular system code developed to address key questions relevant for tokamak fusion reactor design. SYCOMORE is developed within the European Integrated Tokamak Modelling framework (ITM) and provides a global view of the plant, from technological elements to physics-oriented issues. It contains modules for plasma, divertor, blankets, shields, magnets, power conversion and global plant power balance. The modules are connected in a calculation chain to ensure self-consistency of the design.

The code has recently shown that increasing the minor radius of a reactor is much more beneficial from the net electric power output than increaser the major radius, even at similar plasma volumes. The major radius effect on confinement is a trade-off between larger plasma volume and lower plasma current due to fixed q_{95} . On the contrary, increasing the minor radius increases the plasma volume and keeps a high enough plasma current resulting in a linear increase of net electric output with the minor radius. Similarly, small minor radius (below 2.5 m for 9.4 m major radius R = 9.4 m) lead to high amounts of heating power required to compensate for thermal losses and subsequently high argon seeding fraction to protect the divertor and low fusion power. This shows the critical importance of the radial build on the reactor performances as well as the necessity to compute all subsystems sizes and characteristics in a self-consistent way.

Benchmark activities with international system codes are also led to confirm these results. They show a good general agreement with other international codes and highlight some critical differences in the way some physics or technological processes are treated (radiation power, shielding thickness, etc.).



FIP/P7-7

TCV Heating and In-Vessel Upgrades for Addressing DEMO Physics Issues

A. Fasoli¹

¹Ecole Polytechnique Fédérale de Lausanne, CRPP, Lausanne, Switzerland Corresponding Author: A. Fasoli, ambrogio.fasoli@epfl.ch

The TCV tokamak is characterized by the most extreme plasma shaping capability worldwide, the highest microwave EC power concentration in the plasma, and a large degree of flexibility in its heating and control schemes. TCV is presently undergoing major heating upgrades, installing a neutral beam for direct ion heating and increasing the EC power injected in X-mode at the third harmonic (X3). The injection of 1 MW 30 keV D beam will allow access to regimes with $T_i/T_e > 1$ and $\beta_N \sim 2.8$ in L- and H-mode, with densities compatible with X3 EC heating. A lower energy and power (20 keV, 0.5 MW) D NBI is suitable for lower densities with X2 EC heating and current drive. Tangential injection is necessary, due to beam access, shine through, and orbit losses. The modifications to the TCV vacuum vessel required for installing two ports, through which 1 MW of power can be injected, are presently under way. The neutral beam is under construction at Budker INP-Plasma (Russia), with energies of 20–35 keV and power up to 1 MW for 2 s.

The X3 upgrade consists of adding two dual-frequency gyrotrons (X2/X3, 126 GHz/84 GHz) with a total power at 126 GHz of 2 MW. The design of the new gyrotron will be carried out at CRPP with contributions from KIT, and will be based on the gyrotron (140 GHz/1 MW/CW) manufactured by Thales Electron Devices for the W7-X stellarator.

Further substantial improvements in the TCV infrastructure are under examination. Additional power in the dual frequency gyrotron systems is envisioned, to complete and maintain the heating capabilities in regimes of relevance for burning plasma conditions. Substantial diagnostic improvements would also be undertaken, in the areas of THz waves and of advanced imaging systems in the visible, infrared, and mm-wave ranges. An even more substantial modification would be the insertion of new in-vessel modular structures, generating a divertor aperture with variable closure to explore solutions to the crucial problem of the heat and particle exhaust, yet maintaining a good degree of flexibility. To be considered for DEMO, innovative solutions like the snowflake divertor need in fact to be proven viable in the presence of a closed divertor chamber, which allows for high neutral density in the divertor, and of an effective pumping system for particle control.



Diagnostics and Control for Steady State and Pulsed Tokamak DEMO

F. P. Orsitto¹, R. Villari¹, F. Moro¹, T. Todd², S. Lilley³, I. Jenkins³, R. Felton³, W. Biel⁴, A. Silva⁵, M. Scholz⁶, J. Rzadkiewicz⁷, I. Duran⁸, M. Tardocchi⁹, G. Gorini⁹, C. Morlock¹⁰, and G. Federici¹⁰

¹Associazione EURATOM-ENEA Unitá Tecnica Fusione, Frascati, Italy
 ²JET-EFDA, Culham Science Centre, Abingdon, UK
 ³CCFE Fusion Association, Culham Science Centre, Abingdon, UK
 ⁴Forschungszentrum Jülich, Jülich, Germany

⁵Institute of Plasmas and Nuclear Fusion, Association EURATOM/IST, Lisbon, Portugal

⁶Henryk Niewodniczański Institute of Nuclear Physics, PAN, Kraków, Poland

⁷National Centre for Nuclear Research (NCBJ), Świerk, Poland

⁸Institute of Plasma Physics AS CR v.v.i., Prague, Czech Republic

⁹Istituto di Fisica del Plasma CNR, Euratom-ENEA-CNR Association, Milano, Italy ¹⁰Eurofusion Project Management Unit, Boltzmannstr. 2, Garching, Germany

Corresponding Author: F. P. Orsitto, francesco.orsitto@enea.it

This paper reports work done for EFDA PPPT in 2013. It includes the constraints of neutron fluence and Tritium Breeding Ratio (TBR) on diagnostics installation; the technology readiness level of a minimum diagnostics set for control (including burn control); an extended set of diagnostics for control code training; results on diagnostics technology; burn and divertor control. Two DEMO devices (2 GW power) are considered: a long pulse inductive device (PLS) based on H-mode and a steady state (SS) fully noninductive device. The differences in parameters and operational constraints lead to different requirements for the diagnosis and control of the devices. The space available is limited by cost constraints regarding blanket thickness and Li^6 enrichment to achieve the necessary TBR > 1, so in DEMO only 3-5 m² can be available. The DEMO neutron wall loading on the first wall (FW) is 1.82 MW/m² corresponding to 20 dpa (displacement per atom) in 2 FPY (Full Power Year), \sim 7 times the ITER damage level on FW. The damage due to neutrons is maximum on the outboard equatorial side, and at a distance of 50 cm from the first wall (FW) is 0.5 dpa in 1 FPY for DEMO1, while the damage decreases to 5×10^{-3} dpa in 1 FPY at 100 cm from first wall. Calculations are performed for EUROFER. As consequence, using tungsten recrystalized mirrors (resistant to 3 dpa damage) is possible. So Microwave and IR (infrared) diagnostics are feasible on DEMO as well as direct line-ofsight techniques like neutronics and X-rays. These findings open up the possibility of polarimetry for plasma density and current control since steady-state DEMO needs additional control on current and pressure profiles. Both devices (PLS and SS) need burn control at high electron temperature and the MHD control on neoclassical tearing modes. The divertor control must be considered implying the measurements of radiated power fraction, plasma temperature, density, and composition. The extrapolation from ITER to DEMO is large but several promising techniques have been identified despite the nuclear and erosion-deposition problems.



FIP/P7-9

Design of Divertor and First Wall for DEMO-FNS

V. Sergeev¹, B. Kuteev², D. Glazunov³, P. Goncharov¹, V. G. Skokov¹, A. S. Bykov¹, A. V. Spitsyn², V. M. Timokhin¹, A. A. Gervash³, V. A. Rozhansky¹, Y. S. Shpanskii², A. A. Golikov², A. Y. Dnestrovskij², P. A. Molchanov¹, A. V. Klishchenko², I. V. Mazul³, and V. S. Petrov²

¹St. Petersburg State Polytechnical University, St. Petersburg, Russian Federation
 ²National Research Centre "Kurchatov Institute", Moscow, Russian Federation
 ³D. V. Efremov Institute of Electrophysical Apparatus, St. Petersburg, Russian Federation

Corresponding Author: V. Sergeev, v.sergeev@spbstu.ru

In this report we discuss key issues of design of the divertor and the first wall of DEMO-FNS. Parameters determining heat loads on the wall and on the divertor targets are similar to those of ITER. Therefore, technologies being developed for ITER project may be partly used in DEMO-FNS design.

As a result of analysis of modern solutions and a simple hybrid modelling, a double null close magnetic configuration was chosen with a long external leg and a V-shaped corner that are preferable for obtaining the detachment regime. The divertor has a modular design like in ITER. The number of divertor cassettes is equal to 48 = 3N, where N = 16 is the number of toroidal magnetic coils. Water cooled first wall of the tokamak is made of Be-CuCrZr-SS. It functions as a stabilizer of MHD instabilities.

Calculations of thermal loads on the wall and divertor plates done with a simple hybrid model were enhanced using a 1D code ASTRA for the core plasma, and a 2D code B2SOLPS5.2 for peripheral plasma. The calculations have shown that it is possible to organize the heat load distribution so that the heat flux density does not exceed 10 MW/m^2 on the divertor plates. Addition of a small amount of neon with no significant impact on the effective charge of the core plasma allows obtaining regimes of partial detachment or detached divertor plasmas.

Surfaces of wall and divertor plates are covered by beryllium tiles. In the project, the usage of liquid lithium on plasma facing components is foreseen. Circulation of lithium will contribute to a reduction of impurities in the plasma core, a reduction of heat flux through "non-coronal radiation" of lithium, and to protection of solid-state plasma facing components from radiation damages by fast alpha-particles.

New test bed experiments with a flat mockup of the first wall coated by beryllium tiles and cooled by water will be presented in the report, which were made on CEFEY-M facility. The temperature of the surface of a beryllium plates reached $280-300^{\circ}$ C at 5 MW/m^2 and $600-650^{\circ}$ C at 10.5 MW/m^2 . The mockup successfully sustained 1000 cyclic loads with the lower power and 100 cyclic loads with the higher power. None of the beryllium plates lost the thermal contact with the coolant. The design can be recommended for divertor plates to make a machine with mono-material plasma facing components.



Superconducting Magnet for Russian Fusion Neutron Source DEMO-TIN

D. Ivanov¹, I. Anashkin¹, and B. Kolbasov¹

¹National Research Centre "Kurchatov Institute", Moscow, Russian Federation Corresponding Author: D. Ivanov, denis.ivanov30@mail.ru

The presentation describes the conceptual design of the superconducting magnet (SC) of the fusion neutron source DEMO-TIN that is now under development in Russia and the estimations of the mechanical and electrical loads in it, its shielding, as well as cooling and other performances. The main parameters of that device are as follows: plasma major radius $R_0 = 2.5$ m, minor radius of the plasma column $a_{pl} = 1$ m, elongation k = 2.1, plasma current $I_{pl} = 5$ MA. The magnet should produce the toroidal field (TF) on the plasma axis $B_0 = 5$ T, and that in the coils $B_m = 12$ T. Coils outer dimensions are 9 m \times 5 m, their radial thickness is 0.5 m, inner bore radius for inductor $R_i = 0.5$ m. The shield thickness for protection against irradiation between the coils and the vacuum vessel is equal to 0.5 m. Therefore, the space for TF magnet legs comes out very small and the current density is $27 \text{ MA}/\text{m}^2$ which is considerably higher than in existing magnets. Magnet will use the Nb₃Sn wire produced at present for ITER magnet at Chepetsk engineering works in Russia. In principle, the fabrication of such magnet is possible, however, it has too small margins in estimated mechanical stresses in coil cases, in the number of wires for required current-carrying capacity, in the cross section of high-conductivity stabilizing material and in the proper cooling of magnet. Therefore, the application of high-temperature SC materials is strongly preferable for such magnet, although it requires more R&D for its design and fabrication. However, designing and testing of current-carrying cable, the model coil with it and then the prototype coil are necessary in all cases.

The Operational Window for Divertor Detachment in a Fusion Reactor – A Physics-Technology Integrated Approach

C. Day¹, Y. Igitkhanov¹, V. Hauer¹, and C. Gleason-Gonzalez¹

¹Karlsruhe Institute of Technology, Germany

Corresponding Author: C. Day, christian.day@kit.edu

The operational window of the divertor in a fusion reactor is mainly given by power handling requirements limited by the material properties, and He ash exhaust requirements limited by the effective pumping speed performance of the divertor vacuum system. Hence, the divertor has to reconcile key physics and technology functions in a sound way. This paper is presenting an integrated assessment of the operational window for an ITER-type divertor in the European pulsed DEMO1 scenario.

While the high recycling divertor regime may be acceptable for ITER, the high heat flux and the large incident ion fluxes seriously limit the lifetime of the divertor target. As a solution, the detached divertor regime is investigated here in view of DEMO. The expected detachment characteristics, such as the existence of a considerable electron pressure drop along the field lines in the scrape-off layer, and the compatibility of the decrease in plasma flux to the divertor plate with the observed increase of neutral pressure and hydrogen emission from the divertor region, are calculated in the light of an existing analytical and numerical model for plasma detachment. The detachment criterion defines very clearly operational limits that can be translated into requirements on the gas throughput and the exhaust vacuum system. In order to illustrate this interrelation, a quantitative analysis has been made for two torus exhaust vacuum system configurations in a DEMO reactor environment. One is based on scaled-up ITER style cryopumps, including their complex pumping speed dependence on pressure and gas species; the second is based on vapour diffusion pumps which have recently been introduced as reference for the European DEMO. In both cases, the geometry of an ITER type divertor is being used and Ar being utilized as radiative seeding gas, the window of divertor detachment operation is investigated depending on plasma and neutral gas densities. The analysis compares the two configurations and provides the number of pumps required for steady-state operation under detached conditions. The chosen approach is novel as such that it results in a pressure dependent pump albedo which takes into account that the neutrals are in collisional flow regime at various degrees of rarefaction. This concept represents a substantial improvement over the previously employed assumption of constant albedo.



Concept of Fuel Cycle for a Fusion Neutron Source

A. Spitsyn¹, B. Kuteev¹, A. Golubeva¹, S. Anan'ev¹, D. Cherkez¹, N. Bobyr¹, and A. Mednikov¹

¹National Research Centre "Kurchatov Institute", Moscow, Russian Federation Corresponding Author: A. Spitsyn, spitsyn_av@nrcki.ru

This report will describe conceptual design of the fusion DT fuel cycle for steady-state facility DEMO-FNS project in comparison with fuel cycle for FNS-ST and with engineering design of fuel cycle for T-15 tokamak which is considered as mockup of the fuel cycle without tritium. Project DEMO-FNS is developed for demonstration of fusion and hybrid technologies and it requires technologies with resource up to 5000 hours/year, remote maintenance, significant amount of tritium involved in the fuel cycle.

Optimization of the fuel cycle characteristics was aimed at integration of the blanket in the tokamak design, pumping systems, fuel feed systems and fueling of additional heating systems, water and gas detritiation waste, reduced flows and inventory of hydrogen isotopes and tritium in the fuel cycle sybsystems. Special attention was paid to safety issues. Distribution of hydrogen isotopes in technological systems and rooms, possibilities and consequences of explosions and fires at the facility, the maximum emissions of radiotoxicity in case of any accident were estimated.

In the concepts of the fuel cycles the following new provisions are used:

- noncomplete separation of D/T mixture and using equal shares of D and T;
- choice of turbomolecular pumps for a ~ 1 MW level facility and cryogenic pump for a higher than 10 MW facility;
- small fraction of fuel (0.5–5%) delivering to the hydrogen isotope separation system;

Studies confirm feasibility of the fuel cycles for the facilities considered. Tasks on technology life time, as well as problems of safety and licensing require a significant R&D program. Consistent implementation of the fuel cycles systems for T-15 and then for DEMO-FNS will provide the opportunity for fuel cycle of the next level facilities like pilot hybrid reactor and DEMO.

Lead–Lithium Ceramic Breeder Blanket for Russian Thermonuclear Reactor DEMO-S

I. Kirillov¹, D. Obukhov¹, and D. Pertsev¹

¹D. V. Efremov Institute of Electrophysical Apparatus, St. Petersburg, Russian Federation Corresponding Author: I. Kirillov, kirillir@sintez.niiefa.spb.su

Two blanket concepts were considered and found perspective in Russian design of demonstration thermonuclear reactor DEMO-S (1998–2000): ceramics helium cooled and lithium self-cooled, where lithium is used as tritium breeder and coolant. Indian specialists proposed in 2007 a concept of the lead–lithium ceramic breeder (LLCB) blanket for their DEMO reactor and a test module for International Thermonuclear Experimental Reactor ITER. Lead–lithium eutectic and ceramic are used for tritium breeding, eutectic is cooling also the breeding zone and helium is cooling the blanket first wall and module structure. Analysis of this concept for Russian DEMO-S reactor is made in the paper. Some advantages over helium cooled ceramic breeder and pure lead–lithium blankets are revealed, in particular higher value of tritium breeding ratio and longer service life. The conclusion on viability of LLCB blanket for DEMO reactor and RF interest in developing and testing in ITER of this blanket type is expressed.

Conceptual Design Study of the Large Size and Low Magnetic Field Superconducting Spherical Tokamak Power Plant

K. Gi¹, Y. Ono¹, M. Nakamura², Y. Someya², N. Aiba², H. Utoh², and K. Tobita²

¹University of Tokyo, Japan ²Japan Atomic Energy Agency, Naka, Japan

Corresponding Author: K. Gi, gi@ts.t.u-tokyo.ac.jp

A new conceptual design of the 3 GW-level, low-magnetic-field, superconducting spherical tokamak (ST) power plant was proposed as an attractive choice for tokamak fusion reactors. We reassessed a possibility of the ST as a power plant using the conservative reactor engineering constraints often used for the conventional tokamak reactor design for the first time. An extensive parameters scan which cover all range of feasible superconducting ST reactors was completed using the system code: TPC code by developing a new bootstrap current fraction (f_{BS}) scaling. The superconducting TF coils were designed by the SCONE code, where Nb₃Al is chosen as the superconducting material and the number of TF coils is set to be 12. The CS coils system is included in this design not only for position control of the steady-state ST plasma but also for flux supply for the plasma ramp-up. Five constraints: i) advanced plasma constraint, ii) blanket constraint, iii) beta limit constraint, iv) plasma confinement constraint, and v) divertor heat load constraint, were established for the purpose of determining the optimum operation point among more than 16 million operation points obtained in the above parameters scan. Using the five constraints, we obtained 2269 operation points for the ST reactors with 3 GW fusion output. Their COEs were evaluated using the classical cost model by CRIEPI, and they decisively depend on the f_{BS} values regardless to the aspect ratio. Compared with the estimated future energy COEs in Japan, cost-effective ST power plants can be designed if their COEs are smaller than 120 M/kWh (2013), corresponding to f_{BS} of 70–87%. A 2D self-consistent free-boundary MHD equilibrium and PF coils configuration of the ST plant was constructed by modifying the neutral beam injection (NBI) system and plasma profiles using the ACCOME code. Off-axis NBI enables the equilibrium to have low plasma inductance, hence high elongation and reversed shear of $q_{min} > 2$. The optimized low-field/large-size ST reactor design is based on moderate and realistic plasma and fusion engineering parameters such as its acceptable wall load, but it is still attractive due to economic competitiveness against existing energy sources in Japan.

This work was supported by a Grant-in-Aid for JSPS Fellows 24-1756.

Paper



Integrated Physics Analysis of Plasma Operation Control Scenario of Helical Reactor FFHR-d1

T. Goto¹, R. Sakamoto¹, J. Miyazawa¹, C. Suzuki¹, R. Seki¹, M. Yokoyama¹, and A. Sagara¹

¹National Institute for Fusion Science, Toki, Japan

Corresponding Author: T. Goto, goto.takuya@lhd.nifs.ac.jp

Plasma operation control scenario of the LHD-type helical reactor FFHR-d1 was examined using a 1D calculation code, which calculates temporal evolution of the plasma radial profile by solving a diffusion equation in cylindrical geometry using the model based on LHD experimental results. This study is the first 1D analysis of the plasma operation control scenario of helical reactors. It was found that direct feedback control of fusion power by the pellet fuelling, which was considered in the 0D analysis, was difficult because of the delayed response of the fusion power due to shallow pellet penetration in the case of the pellet injection velocity of 1.5 km/s, which is achievable without special technological development. In spite of the fusion power, line-averaged electron density was selected as a controlled parameter because it promptly responds after the pellet injection and there are several kinds of well-established diagnostics. It was confirmed that the line-averaged electron density can be controlled over a wide parameter range by manipulating the pellet injection timing. With a combination of the heating power control based on the measurement of the fusion power, the fusion power can be smoothly increased to the target value and stably sustained. Perturbation in the fusion power is less than 1%. Steady-state sustainment with a smaller fusion power is also achievable with adequate auxiliary heating. In addition, there is no principal physics restriction in the rate of change in the fusion power and then a plasma start-up at a slow rate (e.g., several hours to reach the steady state) is achievable. This high controllability with a small number of simple diagnostics attributes to characteristics of helical system with a net current-free plasma. It is desirable for the operation of peripheral equipment and power plant equipment and indicates another advantage of the helical system. This operation control scenario provides the design conditions of the plasma control system and contributes to the system design of FFHR-d1. Although consistency check with equilibrium, transport, heating profile and impurity effect over a whole time period is needed, the simple control method by the measurement of line-averaged electron density and fusion power is expected to have robustness against the change in the plasma property.



Multi-Parameter Measurement Using Finite Electron Temperature Effect on Laser Polarimetry for Burning Plasma Reactor

R. Imazawa¹, Y. Kawano¹, and K. Itami¹

¹ Japan Atomic Energy Agency, Naka, Japan

Corresponding Author: R. Imazawa, imazawa.ryota@jaea.go.jp

The authors have proposed a multi-parameter measurement system which identifies current density (j_{ϕ}) , total plasma current (I_p) , electron density (n_e) and electron temperature (T_e) from information of a laser polarimetry and a plasma boundary. This study carries out performance assessment of the multi-parameter measurement and proposes a new equilibrium solver suitable for the measurement. Laser wavelength, an injection laser layout and measurement errors were $57/119/171 \ \mu$ m, 15 viewing chords, 0.1 degree error on the Faraday effect measurement, and 0.6 degree error on the Cotton-Mouton effect measurement, respectively. A reference profile of j_{ϕ} was supposed to be ITER operation scenario 2 (an inductive scenario), and n_e and T_e at the magnetic axis were supposed to be 10^{20} m⁻³ and 30 keV, respectively. The reconstruction error of j_{ϕ} (I_p), n_e , and T_e were 3.8%, 3.9%, and 22%, respectively. When the reconstruction is carried out with the given information of a plasma boundary, a finite element method is usually applied to the equilibrium solver. However, it is difficult to make equilibrium reconstruction in real time by using the finite element method because of optimization of mesh generation and mapping the measurement data to a local non-dimensional coordinate. The new equilibrium solver for the first time applies meshless methods to a nonlinear problem of the Grad-Shafranov equation and can solve problems of applying the previous method to real-time plasma control. Modified meshless methods (RBF-MFS and Kansa's method) solved Grad-Shafranov equation ten to hundred times faster than the finite element method, to obtain a same accuracy. Since a laser polarimetry does not depend on time history and a plasma boundary can be detected by a time-history-independent diagnostics, the new reconstruction method including the new equilibrium solver is suitable for steady state operation (e.g., one year) to obtain multi-parameters (j_{ϕ}) I_p , n_e , and T_e) from a small number of diagnostics (e.g., a poloidal polarimeter and a reflectometer at least).



ADX: a High Field, High Power Density, Advanced Divertor Test Facility

B. LaBombard¹, E. Marmar¹, J. Irby¹, J. Terry¹, R. Vieira¹, D. Whyte¹, S. M. Wolfe¹,
S. Wukitch¹, W. Beck¹, P. Bonoli¹, J. Doody¹, R. Ellis², D. Ernst¹, C. Fiore¹, R. Granetz¹,
M. Greenwald¹, Z. Hartwig¹, A. Hubbard¹, J. Hughes¹, I. Hutchinson¹, C. Kessel²,
M. T. Kotschenreuther³, R. Leccacorvi¹, Y. Lin¹, B. Lipschultz⁴, S. Mahajan³, J. Minervini¹,
R. Nygren⁵, R. R. Parker¹, F. Poli², M. Porkolab¹, M. Reinke⁴, J. Rice¹, T. Rognlien⁶,
W. Rowan³, S. Shiraiwa¹, D. Terry¹, C. Theiler¹, P. Titus², M. Umansky¹, P. Valanju³,
G. Wallace¹, A. White¹, J. Wilson², and S. Zweben²

¹Massachusetts Institute of Technology, Plasma Science & Fusion Center, Cambridge, MA, USA ²Princeton Plasma Physics Laboratory, Princeton, NJ, USA

³University of Texas at Austin, Austin, TX, USA

⁴University of York, Heslington, UK

⁵Sandia National Laboratories, Livermore, CA, USA

⁶Lawrence Livermore National Laboratory, Livermore, CA, USA

Corresponding Author: B. LaBombard, labombard@psfc.mit.edu

The MIT Plasma Science and Fusion Center and collaborators are developing a concept for an advanced divertor experimental test facility (ADX) — a tokamak specifically designed to address critical gaps in the world fusion research program on the pathway to DEMO. This high field (6.5 T, 1.5 MA), high power density ($P/S \sim 1.5 \text{ MW/m}^2$) facility will test innovative divertor concepts for next-step DT fusion devices (FNSF, DEMO) at reactor-level boundary plasma pressures and parallel heat flux densities while producing reactor-relevant core plasma conditions. The experimental platform will also test advanced lower hybrid current drive (LHCD) and ion-cyclotron range of frequency (ICRF) actuators at the plasma densities and magnetic field strengths of a DEMO, with the unique ability to deploy launcher structures both on the low-magnetic-field side and the high-field side — a location where energetic plasma-material interactions can be more easily controlled and reduced. This innovative experiment will perform plasma science and technology R&D necessary to inform the conceptual development and accelerate the readiness-for-deployment of next generation DT fusion devices — in a timely manner, on a flexible, reconfigurable research platform.



Physics Design and Analysis Code SPECTRE for Tokamak Based Fusion Reactors

V. Menon¹, S. Radhakrishnan¹, P. K. Kaw¹, A. Sharma¹, C. Danani¹, U. Prasad¹, R. Pragash¹, S. Khirwadkar¹, R. Kumar¹, S. Pradhan¹, S. Deshpande¹, A. Das¹, and D. Bora¹

¹Institute for Plasma Research, Bhat, Gandhinagar, India

Corresponding Author: V. Menon, vinay289@gmail.com

SPECTRE is a 0-D physics code developed for Indian DEMO reactors. The code gives a set of operating points based on the ignition criteria and the radial build up is estimated by solving iteratively for the plasma temperature for a given fusion power and fusion gain (Q). The ratio of plasma density to Greenwald density is chosen so that the reactor operates within density limit while the β limit is checked after obtaining the consistent plasma parameters. The code takes pre-defined plasma shape parameters, aspect ratio, profile factors of temperature and density, edge safety factor. Engineering constraints like maximum allowable field at the TF inner leg, blanket, and shield thickness are also given depending upon the technological requirements.

The energy confinement for this study is based on IPB98(y, 2) scaling law. The helium fraction is estimated by balancing the net power coupled to plasma with transport losses by assuming the ratio of helium particle confinement time to global energy confinement time. The ratio of the ion temperature to electron temperature is estimated and given as an input to the code. The power balance includes losses like synchrotron, Bremsstrahlung, and impurity line radiation. The possible impurities depending upon the choice of plasma facing components are considered for estimating the line radiation. Line radiation from Tungsten and Beryllium are considered in the code from the impurity fractions. The plasma temperature is estimated by solving the power balance equation iteratively. Derived plasma parameters like P_{L-H} power threshold, bootstrap fraction, neutron wall load, loop voltage, and Divertor heat load are estimated.

Progress of the CEA Contributions to the Broader Approach Projects

J.-C. Vallet¹, S. Chel¹, R. Gondé¹, and F. Robin¹

¹CEA-IRFM, Saint Paul lez Durance, France

Corresponding Author: J.-C. Vallet, jean-claude.vallet@cea.fr

The Broader Approach Agreement (BA) to ITER was signed jointly by Europe and Japan, in February 2007, for a period of ten years. The BA comprises three projects: IFERC, the International Fusion Energy Research Center, including the Computational Simulation Center, CSC, IFMIF-EVEDA, Engineering Design and Validation of a 14 MeV neutron irradiation facility for material testing and STP, the ITER Satellite Tokamak Program, with the JT-60SA project. CEA is participating respectively for 85%, 33%, and 42% of the EU contribution to the three projects. The purpose of the BA is to support ITER operation and to contribute to DEMO design and studies.

For IFERC-CSC, CEA provided the "Helios" supercomputer, having a performance of 1.5 Petaflop/s peak (1.2 Petaflop/s Linpack). During the last period 2012–2013, the operation feedback exhibits an overall utilization exceeding 85% summarized in effective computation approaching 30 Mnodes-hours/y and in several hundreds of associated scientific publications.

The IFMIF/EVEDA project consists in Design and Validation Activities aiming at providing the IFMIF Intermediate Engineering Design, IIED which is now completed and in developing the Linear IFMIF Prototype Accelerator (LIPAc). The LIPAc injector, developed, built and tested at CEA is now being installed at Rokkasho. The prototype of the superconducting Half Wave Resonator (HWR) is now validated, and the Engineering Design for the SRF-LINAC proposed jointly by CEA and CIEMAT was approved.

For JT-60SA, CEA is responsible for procuring the full Cryogenic System, 9 of the 18 Toroidal Field Coils, TFC, (the other 9 by ENEA) and the whole Magnet Supporting Structures, the TFC Cold Test Facility, CTF, and the cold test performance, as well as 5 Superconducting Magnet Power Supplies. Since the last IAEA conference, specification and contractual phases have been ended. All the related industrial contracts were placed to European manufacturers well renowned in the fusion field. Industrial designs as well as industrial qualifications for manufacturing processes are now achieved and manufacturing are ongoing. At about three years to the end of the BA agreement, this report synthesizes progress and status of the CEA contributions which, at various degrees have entered the realization or operation phases and are still progressing or working well.

Preprint

The Concept of Hybrid Reactor-Tokamak with Molten-Salt Thorium Blanket for Producing 233U out of Neutron Field

A. Shimkevich¹, E. Azizov¹, P. Alekseev¹, G. Gladush¹, V. Dokuka¹, S. Subbotin¹, and R. Hayrutdinov¹

¹National Research Centre "Kurchatov Institute", Moscow, Russian Federation Corresponding Author: A. Shimkevich, shimkevich_al@nrcki.ru

A conceptual facility of tokamak and molten-salt thorium blanket with direct-contacted liquidmetal mass-exchanger which allows uninterrupted extracting protactinium from the blanket and accumulating it in a cascade salt trap separately from fission products. It is supposed to use only the outer blanken without placing near the central column of the tokamak toroidal coil protection from neutron irradiation. It will allow to have a sufficiently large volume of plasma at the moderate size of facility (R = 1.7 m, a = 0.77 m). Then, the central column of the toroidal tokamak coil can be made of copper and other parts of the electromagnetic system are the superconductor ones.

At the stage of induction input of the current, the plasma has diverter configuration and then, the plasma current increases to demanded value by means of neutral injection. Numerical calculations by a code of "DYNE" have shown that one can obtain a neutron flux with power of ~ 15 MW and its density in the blanket of ~ 0.2 MW/m² that will provide a rate of protactinium production in the salt composition, 0.7FLiNaK+0.3ThF₄, at the level of ~ 4 × 10⁻⁷ mol/s at the injection of double-weight hydrogen by power of 23 MW and ECR heating by power of 2.5 MW.

At the uninterrupted extraction of protactinium from the blanket with the same rate, such the facility can become attractive to industrial production of nuclear fuel (233 U) from thorium. For extraction of protactinium and others radio-nuclides (lanthanides) from the blanket, it is offered using a reduction extraction of these elements into the liquid-metal carrier (direct-contacting liquid salt) by management RedOx potential (Fermi level) of the salt composition, 0.7FLiNaK+0.3ThF₄.

Further, establishing Fermi level in the molten salt of a first cascade of salt trap (direct contacting the liquid-metal carrier only for protactinium oxidation allows desorbing only it from the liquid metal. In the second cascade of the trap with higher oxidation potential, one can extract the all radio-nuclides including lanthanides. At correct setup of the trap cascades, a protactinium portion in the second cascade will be 0.01% of the first one and a portion of other radio-nuclides in the first cascade will be four orders less than in the second one. Thus, one can organize effective producing ²³³U from thorium as a nuclear fuel for thermal reactors.



Development of DEMO-FNS Tokamak for Fusion and Hybrid Technologies

B. Kuteev¹, E. Azizov¹, P. Alexeev¹, V. Ignatiev¹, S. Subbotin¹, and V. Tsibulskiy¹

¹National Research Centre "Kurchatov Institute", Moscow, Russian Federation Corresponding Author: B. Kuteev, kuteev_bv@nrcki.ru

Limited resources of fissile nuclides, disposal of spent nuclear fuel and controlled nuclear fusion are the major system challenges on the path from contemporary to future large-scale Nuclear Energy (NE). Creation of fusion-fission hybrid systems in near-term outlook will definitely ensure success in solving these problems. This will provide involvement of practically unlimited resources of fertile isotopes (²³⁸U and ²³²Th) into the nuclear fuel cycle and realize that with substantially reduced radiotoxicity. In combination with ITER data on burning plasma physics, development of hybrid systems will make decisive input in progress of enabling technologies and materials needed for realization of the fast track strategy to Fusion Power Plant by 2050. Subjective tests show that the optimal power fraction of hybrids in the NE structure is less than 10%. The fusion power varies from 50 MW to a few GW in energy valuable hybrid systems.

Development of a fusion neutron source DEMO-FNS for demonstrating energy valuable hybrid technologies based on a conventional tokamak (CT) with the power of deuterium and tritium fusion up to 50 MW started in Kurchatov Institute in 2013. The design is aimed at steady state operation of the device providing the neutron flux ($\sim 0.2 \text{ MW/m}^2$) and the fluence ($\sim 2 \text{ MW \cdot y}$) with the blanket area ($\sim 100 \text{ m}^2$) sufficient to test materials and components in fusion spectra for DEMO program support and to develop hybrid technologies for transmutations, fissile nuclides production and energy generation.

The concept of DEMO-FNS has been formulated assuming amplification factor $Q \sim 1$, duty factor ~ 0.3 , electric power consumption < 200 MW, tritium consumption < 700 g/y, divertor loading < 10 MW/m², plasma current 5 MA, magnetic field 5 T, major radius 2.5 m, aspect ratio 2.5 and auxiliary heating power up to 36 MW, construction cost ~ 1 G\$. From safety point of view the device was considered as a radiation source with opportunity to become a subcritical nuclear facility with generated heat power less than 500 MW. Commercially available materials are considered in the design owing to reduced neutron loadings and fluencies compared with DEMO.

Preprint

Fusion Hybrid with Thorium Blanket: on its Innovative Potential at Fuel Cycle of Nuclear Reactors

A. Shmelev¹, *G. Kulikov*¹, E. Azizov², V. Kurnaev¹, G. Salahutdinov¹, E. Kulikov¹, and V. Apse¹

¹National Research Nuclear University MEPhI, Moscow, Russian Federation ²National Research Centre "Kurchatov Institute", Moscow, Russian Federation

Corresponding Author: A. Shmelev, shmelan@mail.ru

Technology of controlled thermonuclear fusion (CTF) is traditionally regarded as a practically inexhaustible energy source. However, development, mastering, broad deployment of fast breeder reactors and closure of nuclear fuel cycle (NFC) can also extend fuel base of nuclear power industry (NPI) up to practically unlimited scales. Under these conditions, it seems reasonable to introduce into a circle of the CTF-related studies the works directed towards solving some principal problems which can appear in a large-scale NPI in closed NFC. It was shown [1] that advanced nuclear fuel (231 Pa $^{-232}$ U- 233 U) can be generated in thorium blanket of hybrid thermonuclear reactor (HTR). The first challenge is a large scale of operations in NFC back-end that should be reduced by achieving substantially higher fuel burn-up in power nuclear reactors. As was shown in [1], the use of 231 Pa $^{-232}$ U- 233 U fuel in light-water reactor (LWR) opens a possibility of principle to reach very high (about 30% HM) or even ultra-high fuel burn-up. The second challenge is a potential unauthorized proliferation of fissionable materials. As is known, a certain remarkable quantity of 232 U being introduced into uranium fraction of nuclear fuel can produce a serious barrier against switching the fuel over to non-energy purposes.

Involvement of HTRs into NPI structure can substantially facilitate resolving these problems. If HTR will be involved into NPI structure, then main HTR mission consists not in energy generation but in production of nuclear fuel with a certain isotope composition.

The present paper analyzes some neutron-physical features in production of advanced nuclear fuels in thorium HTR blankets. The obtained results demonstrated that such a nuclear fuel may be characterized by very stable neutron-multiplying properties during full LWR operation cycle and by enhanced proliferation resistance too. The paper evaluates potential benefits from involvement of HTR with thorium blanket into the international closed NFC.

References

[1] E.G. Kulikov, G.G. Kulikov, E.F. Kryuchkov, A.N. Shmelev. Nucl. Phys. Eng., 4, pp. 291–299 (2013).

Experimental Base of Innovation S-Channel for Fusion LM Blanket

Z. Xu¹, C. Pan¹, X. Zhang¹, J. Chen¹, and X. Duan¹

¹Southwestern Institute of Physics, Chengdu, Sichuan, China

Corresponding Author: Z. Xu, xuzy@swip.ac.cn

MHD geometry sensibility phenomenon was accidentally measured while an experimental investigation of MHD effect was conducting of the flow channel inserts (FCI) for liquid metal (LM) blanket system. Though the geometry sensibility phenomenon (or called secondary flow MHD effect) is successfully used to understand FCI duct flow behaviors, but, up to now, it is very little about secondary flow knowledge. To understand secondary flow MHD effect and to try to reduce MHD pressure drop by this effect, four special design experiments are carried out at the liquid metal experimental loop upgrade facility in Southwestern Institute of Physics, China. The experimental results indicate that MHD pressure drop can be significantly reduced in the special designed ducts. And an innovation S-channel is addressed to reduce MHD pressure drop and to propel LM blanket MHD engineering feasibility key issue study forward.



Experimental Results and Validation of Thermo-Mechanical Models Used for the PREMUX Test Campaign, as Part of the Roadmap towards an Out-of-Pile Testing of a Full Scale HCPB **Breeder Unit Mock-up**

F. Hernandez Gonzalez¹, Y. Gan², M. Kamlah¹, and M. Kolb¹

¹Karlsruhe Institute of Technology, Germany ²School of Civil Engineering, University of Sydney, NSW, Australia

Corresponding Author: F. Hernandez Gonzalez, francisco.hernandez@kit.edu

PREMUX is a key experiment in the roadmap for a full-scale test of a Helium Cooled Pebble Bed Breeder Unit (HCPB BU) mock-up at the Karlsruhe Institute of Technology in Germany. This experiment reproduces a slice of the BU corresponding to the most thermally loaded region of the Li_4SiO_4 pebble bed in the BU. Li_4SiO_4 pebble bed in the BU.

The experiment has three main goals: 1) to serve as a test rig to validate the feasibility of a new heater concept designed for a future BU out-of-pile testing, 2) to be used as benchmark experiment to validate the different finite element codes used for the thermo-mechanical performance assessment of the BU, and 3) to evaluate the thermal conductivity of the Li_4SiO_4 pebble bed. Additional tests have been performed to evaluate the influence of the purge gas pressure in the temperature of the pebble bed and as a preliminary assessment of the robustness of the BU against variations of the coolant mass flow.

The paper aims at reporting the results from the experimental campaign in PREMUX and presents the thermal and thermo-mechanical finite element models implemented in ANSYS that are used for the assessment of the thermo-mechanical performance of the HCPB BU. A benchmarking exercise using the experimental results of PREMUX for the validation of these models is reported and discussed.

FIP/P8-3

Preprint

MHD-PbLi Facility for Experiments at Real Blanket Relevant Thermo-Hydraulic Conditions

E. Platacis¹, S. Ivanov², A. Shishko², and I. Bucinieks²

¹University of Latvia, Riga, Latvia ²Institute of Physics, University of Latvia, (IPUL), Riga, Latvia

Corresponding Author: E. Platacis, erik@sal.lv

The report describes and presents for the potential collaborators the MHD PbLi experimental facility at IPUL designed for liquid metal blanket related investigations. As the key element of the facility the cryogen-free magnet systems should be considered providing an up to 5 T field in a D = 30 cm and L = 100 cm bore. Since a water cooled heat shielding is installed working temperatures up to 500°C could be discussed. The experimental facility includes a SS316L made loop, an EM pump and flowmeter, pressure gauges with a direct electrical output, a system for measuring pressure drops along the channels, probes for registration of electric potential variations on the channel walls, a data sampling system and a processor minimizing the measuring errors, a system of thermal stabilization. In many relations the introduced MHD PbLi experimental facility at IPUL should be considered as a step forward compared with similar existing facilities. This experimental facility modification was used in experiments with the models of LLCB channel units typical to the Indian blanket concept.

European DEMO Breeding Blanket Design and Development Strategy in a Roadmap to the Realisation of Fusion Energy

L. V. Boccaccini¹, G. Aiello², A. Del Nevo³, P. Norajitra¹, D. Rapisarda⁴, and C. Bachmann⁵

¹Karlsruhe Institute of Technology, Germany
 ²CEA, DEN, Saclay, DM2S, SERMA, Gif-sur-Yvette, France
 ³ENEA CR Brasimone, Camugnano, Italy
 ⁴The National Fusion Laboratory, CIEMAT, Madrid, Spain
 ⁵EFDA, Garching, Germany

Corresponding Author: L. V. Boccaccini, lorenzo.boccaccini@kit.edu

The EU Fusion Roadmap foresees the development and construction of a DEMO reactor that will deliver several 100's of MW of net electrical power starting from 2050. Although the EU breeding blanket programme has a long history of more than 30 years, this ambitious goal presents a significant challenge. The breeding blanket however will require a significant development R&D to cope with the challenges posed by the DEMO environment. Although DEMO will not be an optimised machine and will not reach performances expected for a first generation of fusion reactors, the gap between ITER and DEMO will be significant. The lifetime neutron fluence of high energy neutrons will be about two orders of magnitude larger. This calls for a class of structural materials not foreseen in ITER, in particular ferritic martensitic steels able to ensure an adequate life time of the blanket reducing the impact of replacement time and hence increasing the plant availability. In addition, this new class of materials should provide reduced activation characteristics to minimise drastically the total amount of high-activated long-life wastes. The need to ensure tritium (T) self-sufficiency requires the integration in the blanket design of breeder and neutron multiplier materials, and to provide efficient systems to extract the T produced and confine it to prevent safety hazards of reactor personnel and population. The requirement of electricity production poses additional challenges to the blanket design and materials. Finally, safety and licensing requirements for a nuclear power plant will impact the selection of blanket design solutions, material choice and adopted technologies. In the present EU programme four breeding blanket concepts are under investigation for the possible use in an EU DEMO reactor according to the EU Fusion Roadmap. These blanket concepts are the two Helium cooled concepts tested in the European TBM Programme in ITER, a solid and a liquid breeder concepts, a water cooled PbLi concepts and a dual coolant He-PbLi concept. The adaptation of these blankets to the reference DEMO plant and the selection of the most suitable concept will be the work over the next seven years in the framework of the new EUROFusion Consortium.



FIP/P8-8

Simulation of Neutral Gas Flow in the JET Subdivertor and Comparison with Experimental Results

S. Varoutis¹, C. Gleason-Gonzalez¹, D. Moulton², U. Kruezi³, M. Groth², C. Day¹, and JET-EFDA Contributors³

¹Karlsruhe Institute of Technology, Germany ²Aalto University, Espoo, Finland ³JET-EFDA, Culham Science Centre, Abingdon, UK

Corresponding Author: S. Varoutis, stylianos.varoutis@kit.edu

Over the last few years much effort has been invested in modeling the complex geometry of divertor and subdivertor region in tokamak fusion reactors. The main goal is the investigation of the impact of neutral gas dynamics on the particle removal process, during operation. Depending on the plasma conditions, the neutral gas flow starts from viscous regime above the dome and close to divertor targets and then covers transitional and even free molecular regime in the subdivertor area. Consequently, a reliable estimate of the macroscopic parameters in such a complex system requires a tool to describe the flow in the whole range of the Knudsen number. Currently, the code, which is used in the JET activities on fluid edge plasma modeling, is the EDGE2D-EIRENE, where the EDGE2D part consists of a 2D plasma fluid code, while the EIRENE part consists of a 3D Monte-Carlo solver for neutrals, based on the BGK approximation. The standalone EIRENE code over the years has been proven to work sufficiently in neutral modelling, but no qualitative and quantitative comparison with a more complete neutral code has been performed. Consequently, the aim of this work is twofold. First, it is focused on the numerical simulation of the neutral gas flow and the calculation of overall quantities of practical interest, i.e., pressure, density, recirculation rates etc., inside the complex geometry of the JET subdivertor by applying and comparing the standalone EIRENE and the DSMC algorithms. Second, for validation purposes, both numerical approaches will be compared with existing JET ITER-Like Wall experimental data for the neutral gas pressure in the subdivertor. The pressure measurements were obtained with the KT5P gauge located at the end of the main vertical lower port of Octant 8. It is noted that the direct comparison between the two approaches will be performed for the case of a 2D toroidally symmetric simplified representation of subdivertor. The comparison will be focused on L-mode plasmas, which represent low, medium and high neutral gas divertor densities respectively. Based on the detailed comparison, deficits and advantages of each code will be outlined.

This work was supported by EURATOM and carried out within the framework of the European Fusion Development Agreement. The views and opinions expressed herein do not necessarily reflect those of the European Commission.



Engineering Feasibility of the Double Decker Divertor

S. McIntosh¹, D. Hancock², D. Taylor², W. Morris², E. Surrey², T. Todd², G. Cunningham², and G. Fishpool²

¹JET-EFDA, Culham Science Centre, Abingdon, UK ²CCFE Fusion Association, Culham Science Centre, Abingdon, UK

Corresponding Author: S. McIntosh, simon.mcintosh@ccfe.ac.uk

The term "double decker divertor" refers to a novel divertor concept in which the inboard leg of a single null poloidal field divertor is pulled around the interior of the vacuum vessel to allow it to be treated as an outboard leg. This topology reduces the inboard leg parallel heat flux by increasing the target radius, moving the plasma wall interaction to an area of lower magnetic field. Both divertor legs are pulled outwards in major radius to form a horizontal "double deck". The volume of each divertor leg is further increased by passing the divertor legs through regions of low poloidal field.

This class of strongly shaped field in the divertor region requires the placement of poloidal field coils within the toroidal field coil cage. A semi-monocoque structural design is proposed to hold six divertor coils within the toroidal field coils of a reactor. Vertical coil loads of up to 35 MN are transferred through a highly stressed EUROFER skin wrapped around radial spars cantilevered inwards from the external structure. A boundary of 0.8 m has been allowed around each coil for neutron shielding, thermal insulation and structural features.

A magnetic potential solver developed to provide a rapid indication of permissible positional errors, suggests a tolerance on maximum vertical displacement of ± 5 mm. A structural analysis of the radially symmetric cantilevers shows the design to be displacement limited with maximum equivalent stress of ~100 MPa in the 130 mm thick skin. This value lies below the ~400 MPa yield limit for unirradiated EUROFER at 500°C.

Comparison of the magnetic parameters of the inner leg in the double-decker and conventional divertor topologies is given. The double-decker shows significant potential improvements: placement of the inner leg target at an increased radius, R, reduces the magnitude of the magnetic field, |B|, at the target by a 30%, the SOL volume, V, is increased almost 4-fold and the 3D connection length, L3D, is increased almost 2-fold (taken from the equatorial low field side).

This work was funded by the RCUK Energy Programme under grant EP/I501045 and the European Communities under the contract of Association between EURATOM and CCFE. The views and opinions expressed herein do not necessarily reflect those of the European Commission.

FIP/P8-10

Paper

Development of Divertor Simulation Research in the GAMMA 10/PDX Tandem Mirror

Y. Nakashima¹, M. Sakamoto¹, M. Yoshikawa¹, K. Oki¹, H. Takeda¹, K. Ichimura¹, K. Hosoi¹, M. Hirata¹, M. Ichimura¹, R. Ikezoe¹, T. Imai¹, T. Kariya¹, I. Katanuma¹, J. Kohagura¹, R. Minami¹, T. Numakura¹, M. Iwamoto¹, Y. Hosoda¹, N. Asakura², M. Fukumoto², A. Hatayama³, Y. Hirooka⁴, S. Kado⁵, H. Kubo², S. Masuzaki⁴, H. Matsuura⁶, S. Nagata⁷, N. Nishino⁸, N. Ohno⁹, A. Sagara⁴, T. Shikama⁷, M. Shoji⁴,

A. Tonegawa¹⁰, and Y. Ueda⁶

¹University of Tsukuba, Tsukuba, Ibaraki, Japan
 ²Japan Atomic Energy Agency, Naka, Japan
 ³Keio University, Tokyo, Japan
 ⁴National Institute for Fusion Science, Toki, Japan
 ⁵Kyoto University, Kyoto, Japan
 ⁶Osaka University, Osaka, Japan
 ⁷Tohoku University, Sendai, Japan
 ⁸Graduate School of Engineering, Hiroshima University, Higashi-Hiroshima, Japan
 ⁹University of Nagoya, Nagoya, Japan
 ¹⁰Tokai University, Tokyo, Japan

Corresponding Author: Y. Nakashima, nakashma@prc.tsukuba.ac.jp

This paper presents the first achievement of detachment from high temperature plasma equivalent to the SOL plasma of tokamaks using a large tandem mirror device. In Plasma Research Center, University of Tsukuba, we have started divertor simulation experiments at the end-cell of GAMMA 10/PDX (E-divertor) in order to realize the divertor simulation closely resemble to actual divertor environment [1, 2].

The first experiment for realizing detached plasma state from the high-temperature plasmas has been performed using H₂ and noble gas injection in the divertor simulation experimental module (D-module) recently installed in the west end-cell of GAMMA 10/PDX. Here, the plasma with $n_e \sim 2 \times 10^{18} \text{ m}^{-3}$ and $T_{i\parallel} \sim 150 \text{ eV}$ was produced with two ICRF waves (RF1 and RF2) in the upstream region (central-cell). The highest electron density of $2.4 \times 10^{18} \text{ m}^{-3}$ was obtained by simultaneous injection of H₂ and Xe into D-module. The particle and heat fluxes on the V-shaped target plate mounted in D-module were measured and the dependence on the Ar plenum pressure was examined. As increasing the amount of injection gas, both particle and heat fluxes continuously decrease. It is also observed that the electron temperature is drastically reduced from few tens eV to $\sim 3 \text{ eV}$ due to the Ar injection. Furthermore, in the case with H₂ and Xe, the ion flux was almost fully suppressed at the V-shaped corner. At the same time, 2D image of H_α emission captured with the fast camera showed the clear detachment of emission zone from the target plate. Above results clearly show the evidence of plasma detachment in D-module.

Recently two antennas for additional ICRF heating (RF3) were installed in anchor cells in order to build up both particle and heat fluxes at the end-cell. A remarkable increase of the plasma density and end-loss ion flux is achieved during RF3. We evaluated the particle flux at the mirror exit by investigating correlation between particle flux determined from the probe measurements near the mirror throat and the end-loss ion current measured with end-loss ion energy analyzer (ELIEA). From this evaluation, the particle flux is estimated to be 1.7×10^{23} /m²s at the end-mirror exit.

References

[1] Y. Nakashima, et al., Fusion Eng. Design volume 85 issue 6 (2010) 956-962.

[2] Y. Nakashima, et al., Journal of Nuclear Materials 438 (2013) S738-S741.



Studies of Impurity Seeding and Divertor Power Handling in Fusion Reactor

K. Hoshino¹, N. Asakura¹, K. Shimizu¹, and S. Tokunaga¹

¹Japan Atomic Energy Agency, Naka, Japan

Corresponding Author: K. Hoshino, hoshino.kazuo@jaea.go.jp

The power handling in the divertor is one of the most crucial issues for a fusion reactor design. In the previous study of development of the power handling scenario for a compact DEMO reactor, SlimCS, further reduction of the target heat load was required even in the case where more than 90% of the exhausted power from the core plasma was radiated by the argon impurity gas seeding. In this paper, the impact of the impurity seeding and the machine specifications on the power handling in the fusion reactor divertor has been investigated by using an integrated divertor code SONIC. With decreasing the fusion power, the divertor plasma detachment is extended and the target heat load decreases. The SONIC simulation found the operational regime, i.e., the target heat load less than 6 MW/m² for a tungsten mono-block divertor with a ferritic steel water-cooling pipe, at the fusion power less than 2 GW. It is also found that the impurity radiation fraction on the exhausted power can be reduced to 80% at the fusion power of 2 GW in the case of a copper-alloy water-cooling tube.

New Visible Wide Angle Viewing System for KTM Based on Multielement Image Fiber Bundle

B. Chektybayev¹, G. Shapovalov¹, and A. Kolodeshnikov¹

¹Institute of Atomic Energy, National Nuclear Center, Kazakhstan Corresponding Author: B. Chektybayev, chektybaev@nnc.kz

In the paper is described new endoscopic visualization system of KTM tokamak which allows to observe plasma through the long equatorial port. System has been designed to observe processes inside plasma and the processes due to plasma-wall interactions. Design of KTM's visualization system based on special image fiber bundle and entrance wide angle objective lens, which allows to have image of large section of the vacuum chamber, both poloidal half cross section and divertor through the long enough equatorial port. System also consists of two video cameras: slow, and fast with image intensifier. In the design of the system had been used commercial available elements that allowed reduce cost and decrease time of the research and development. In the paper advantage and disadvantage of the system in comparison with conventional endoscopes based on a lens system, perspective of utilization this system on future tokamaks and future steady state fusion reactors are discussed.



Advanced Structural Analysis of Wendelstein 7-X Magnet System Weight Supports

K. Egorov¹, V. Bykov¹, J. Fellinger¹, F. Schauer¹, and M. Köppen¹

¹*Max-Planck-Institut für Plasmaphysik, Garching, Germany* Corresponding Author: K. Egorov, konstantin.egorov@ipp.mpg.de

The Wendelstein 7-X (W7-X) optimized stellarator is presently under final stage of assembly at the Max-Planck-Institut für Plasmaphysik in Greifswald. The goal of W7-X is to verify that the advanced stellarator magnetic confinement concept is a viable option for a fusion reactor. The coil system consisting of 70 superconducting coils of seven different types is supported by a massive central support structure (CSS), and thermally protected by the cryostat. The magnet system weight is borne by supports which are bolted to the cold CSS. The CSS is supported by 10 so-called cryo-legs that penetrate through the cryostat wall to the warm machine base. The design of the cryo-legs incorporates glass-reinforced plastic tubes to guarantee relatively small thermal conductivity for low heat flux to the cryostat. In order to ensure free thermal shrinkage of the magnet system and to reduce stresses in the cryo-legs, sliding and rotating bearings are used as interfaces to the machine base. The rods between the machine base and the warm ends of the cryo-legs prevent toroidal movements of the magnet system with respect to the torus axis, as well as a horizontal shift due to any non-symmetric loads.

During assembly of the W7-X magnet system some important measurement results have been collected and analyzed. In particular, the assembly of the magnet system introduced some imperfections in the vertical position of the cryo-legs causing considerable additional internal stresses which were not considered during the design stage. In addition, trim coils were installed at a later stage which were not planned originally when the magnet structure was designed. The loads induced by them are not cyclic symmetrical, therefore, the previously used method to analyze one magnet system module with periodical boundary conditions is not applicable. Consequently, a model of the complete magnet system including all five modules was created and analyzed with respect to the mentioned goal.

Fatigue analyses of the cryo-legs under the new cyclic loads applied on top of the approximately 100 t static weight has been performed in order to evaluate the life time. The paper presents the progress in structural analyses of the W7-X magnet system under the as-built conditions, loads due to the trim coil operation, and results of the weight support life cycle analysis.



Poster: Session P8, Friday 14:00

JT-60SA Superconducting Magnet System

Y. Koide¹, K. Yoshida¹, M. Wanner², P. Barabaschi², A. Cucchiaro³, S. Davis², P. Decool⁴,
E. Di Pietro², G. Disset⁴, L. Genini⁴, N. Hajnal², R. Heller⁵, A. Honda¹, Y. Ikeda¹,
Y. Kamada¹, Y. Kashiwa¹, K. Kizu¹, K. Kamiya¹, H. Murakami¹, F. Michel⁴,
J.-L. Marechal⁴, G. Phillips², G. Polli³, P. Rossi³, K. Shibanuma¹, V. Tomarchio²,
K. Tsuchiya¹, K. Usui¹, M. Verrecchia², and L. Zani⁴

¹ Japan Atomic Energy Agency, Naka, Japan
 ² F4E: Fusion for Energy, Barcelona, Spain
 ³ Associazione EURATOM-ENEA Unitá Tecnica Fusione, Frascati, Italy
 ⁴ CEA-IRFM, Saint Paul lez Durance, France
 ⁵ Karlsruhe Institute of Technology, Germany

Corresponding Author: Y. Koide, koide.yoshihiko@jaea.go.jp

The most distinctive feature of the superconducting magnet system for JT-60SA is the optimized coil structure in terms of the space utilization as well as the highly accurate coil manufacturing as follows, thus meeting the requirements for the steady-state tokamak research: A conceptually new outer inter-coil structure is introduced to the toroidal field coils to realize their slender shape, allowing large-bore diagnostic ports for detailed measurements; a method to minimize the manufacturing error of the equilibrium-field coils has been established, aiming at the precise plasma shape and position control; a compact butt joint has been successfully developed for the Central Solenoid, which allows to make the best use of the space for the Central Solenoid to extend the duration of the plasma pulse.

Final Assessment of Wendelstein 7-X Magnetic Field Perturbations Caused by Construction Asymmetries

T. Andreeva¹, V. Bykov¹, T. Bräuer¹, K. Egorov¹, M. Endler¹, J. Fellinger¹, J. Kißlinger², M. Köppen¹, and F. Schauer¹

¹Max-Planck-Institut für Plasmaphysik, Greifswald, Germany ²Max-Planck-Institut für Plasmaphysik, Garching, Germany

Corresponding Author: T. Andreeva, tamara.andreeva@ipp.mpg.de

Wendelstein 7-X, currently under construction at the Max-Planck-Institut für Plasmaphysik in Greifswald, Germany, is a continuation of the helical advanced stellarator line, with the final goal to demonstrate the reactor capability of modular stellarators. The magnet system of the machine consists of 50 nonplanar and 20 planar coils, which are arranged in five identical modules. If the symmetry of the five magnet system modules is violated, magnetic field perturbations occur which lead to uneven loads on the divertor targets and affect the plasma performance. Such perturbations are unavoidable due to manufacturing and assembly tolerances as well as due to coil deformations during the assembly process and machine operation.

In order to compensate for the impact of manufacturing and positioning errors, a step-by-step optimization of the Wendelstein 7-X module positioning on the machine base was performed. It helped to avoid error field accumulations during assembly and resulted in a significant reduction of the magnetic field perturbation as well as in saving assembly time concerning possible readjustments. In addition, finite element calculations were performed to evaluate the magnet system deformations during machine operation, caused by asymmetries of the magnet system structure and its supports. Corresponding magnetic field perturbations were assessed for cases where coils were deformed according to structural analysis results and also for random deformations. The sequential torus assembly procedure with removal of temporary supports after module positioning on the machine base also leads to nonsymmetrical coil deformations. This was simulated with finite element methods for all 70 coils. Results of this analysis complement the full overview of relevant sources of magnetic field perturbations in Wendelstein 7-X.

The paper summarizes all calculations performed for an evaluation of the Wendelstein 7-X magnetic field perturbations, shows a comparative analysis for different sources of error fields and demonstrates that the compromise between physical needs and engineering challenges can be successfully met with help of the installed Wendelstein 7-X compensation tools (trim coils).

Progress of CEA Contributions to the JT-60SA TF Coil Procurements

P. Decool¹, W. Abdel Maksoud², H. Cloez¹, G. Disset², L. Genini², G. Gros¹, G. Jiolat¹, J.-L. Marechal¹, S. Nicollet¹, F. Nunio², M. Nusbaum³, A. Torre¹, J.-C. Vallet¹, J. M. Verger¹, R. Gondé¹, H. Rocipon⁴, and A. Striebig⁵

¹CEA-IRFM, Saint Paul lez Durance, France
 ²CEA-IRFU, Gif-sur-Yvette, France
 ³Alstom Power Systems, F-90000 Belfort, France
 ⁴Alsyom, F-65000 Tarbes, France
 ⁵SDMS F-38160 Saint Romans, France

Corresponding Author: P. Decool, patrick.decool@cea.fr

In 2005, when the ITER site decision was made, the French Government decided to participate to the joint Europe-Japan implementation of the so-call "Broader Approach Activities" (BA) in support of the ITER project and DEMO activities. The BA comprises the ITER Satellite Tokamak Programme (STP) which consists in upgrading the JT-60U machine into the largest fully superconducting and actively cooled D shaped Tokamak JT-60SA before ITER, and in the participation to its scientific exploitation. The French commitments, in charge of CEA as Voluntary Contributor (VC), are described in the Agreement of Collaboration (AoC). This report synthetizes progress and status of the CEA contribution related to the Toroïdal Field Coils (TFC) procurement which is 9 of the 18 TFCs, the whole supporting structures and the TFC Cold Test Facility (CTF). These last two years, an extensive R&D program was defined and conducted, by CEA and industrial manufacturers to assess both specifications, manufacturing processes and tooling qualifications for the manufacturing of key components of the Toroidal Magnetic Field System of JT-60SA that are TF coils and their supporting structures. This program included the development of the TFC-CTF for performing the cryogenic test of the TFC. After successful achievement of qualification mock-ups, the green light to begin the winding of the first coils was given to the coils manufacturer. For the structures, after validation of the original design solutions, the industrial contracts were signed and the components production was started. For the CTF after conceptual design activities, the main components were ordered and delivered and their commissioning was started to be ready in time for the first coils cryogenic tests. All these activities and results as well as the present status of the related products are extensively described in this paper.



Design and Development of High-Temperature Superconducting Magnet System with Joint-Winding for the Helical Fusion Reactor

N. Yanagi¹, S. Ito², Y. Terazaki³, Y. Seino², K. Natsume¹, S. Hamaguchi¹, H. Tamura¹, J. Miyazawa¹, T. Mito¹, H. Hashizume², and A. Sagara¹

¹National Institute for Fusion Science, Toki, Japan ²Tohoku University, Sendai, Japan ³The Graduate University for Advanced Studies, Kanagawa, Japan

Corresponding Author: N. Yanagi, yanagi@lhd.nifs.ac.jp

Conceptual design studies of the LHD-type helical fusion reactor, FFHR-d1, are progressing steadfastly. The magnet system consists of a pair of helical coils (major radius 15.6 m) and two pairs of vertical field coils. A 3 GW fusion power generation requires a toroidal magnetic field of 4.7 T and the total stored magnetic energy reaches 160 GJ. A conductor current of 94 kA is needed at the maximum magnetic field of 12 T. We select the high-temperature superconducting (HTS) conductor as a plausible candidate owing to a number of advantages, such as high cryogenic stability and excellent mechanical rigidity. Simple stacking of YBCO tapes is proposed to fabricate a large-current capacity conductor with high mechanical strength. Formation of non-uniform current distribution among HTS tapes having no transposition and twisting is allowed due to the high cryogenic stability. An innovative winding method is proposed by connecting prefabricated half-helical-pitch HTS conductors, which drastically facilitates the in-situ fabrication process compared with a case of constructing a 50 m-diameter winding machine. A bridge-type mechanical lap joint is a viable technique having a staircase-like structure to make face-to-face connection of YBCO surfaces. The joint fabrication should be carried out by an industrial robot. The conductor has internal insulation around the copper jacket. The outer stainless-steel jacket is welded between neighboring conductors to secure mechanical rigidity of windings and to skip the vacuum pressure impregnation process that needs to raise the whole coil temperature to 150° C to fill gaps between windings by epoxy resin. The conductor surface is cooled by gas helium through cooling channels formed on the stainless-steel jacket. A large-scale HTS conductor sample with a 3 m length was fabricated using GdBCO tapes and successfully tested. The maximum current reached 100 kA at 5.3 T and 20 K. A numerical simulation, solving the magnetic field and current density profiles self-consistently among HTS tapes, shows good agreement between the measured and calculated critical currents under a wide range of magnetic fields and temperatures. The joint resistance was evaluated to be 2 n Ω , which assures that the Joule heating produced at 7,800 joints in the helical coils be cooled by < 5 MW of electricity in the cryoplant.

Protection of Superconducting Magnets in Fusion Experiments: the New Technological Solution for JT-60SA

E. Gaio¹, A. Maistrello¹, L. Novello², M. Matsukawa³, A. Ferro¹, K. Yamauchi³, and R. Piovan¹

¹Consorzio RFX, Associazione Euratom-ENEA sulla Fusione, Padova, Italy ²F4E: Fusion for Energy, Barcelona, Spain ³Japan Atomic Energy Agency, Naka, Japan

Corresponding Author: E. Gaio, elena.gaio@igi.cnr.it

JT-60SA satellite tokamak is an experimental device, presently under construction, equipped with superconducting Toroidal Field (TF) and Poloidal Field (PF) magnets, capable of confining high temperature plasmas (current up to 5.5 MA) for 100 s. The majority of the new power supplies are provided by Europe, and the Italian National Research Council (CNR), acting through Consorzio RFX, contributes in particular with two systems: the Quench Protection Circuits (QPC) for the superconducting (SC) magnets and the Power Supply System for RWM control. The function of QPCs is to conduct the coil current in normal operation and commutate it into a dump resistor in case of quench or other faults by means of a dc Circuit Breaker (CB). In JT-60SA, the total number of QPC units is 13: three for the TF circuit and ten for the PF circuits. The nominal currents to be interrupted and the maximum reapplied voltages are 25.7 kA and 2.8 kV for the TF QPCs and ± 20 kA and ± 5 kV for PF QPCs.

An R&D program has been carried out since 2007 to identify innovative solutions for the interruption of high dc current, able to improve the maintainability and availability of the protection systems for SC magnets. An advanced design was finally worked out for JT-60SA: it consists in a hybrid mechanical-static CB composed of a ByPass Switch (BPS) for conducting the continuous current, in parallel to a Static Circuit Breaker (SCB) based on Integrated Gate Commutated Thyristor (IGCT) for current interruption.

Dc circuit breakers based on this hybrid approach and at this level of power have never been realized before. Moreover, the JT-60SA QPC represents the first application of this technology for protection of SC magnets in fusion experiments. The contract for QPC procurement is now in a well advanced state: the final design was approved in 2011, the qualification of the full scale prototype was completed in 2012 and the manufacturing and routine testing of the units is being completed.

The paper will give an overview of the main R&D tasks for the development of this new technological approach, which has been developed for fusion experiments but can also be suitable for different applications. Then, the paper will describe in detail the progress and present status of the procurement of the JT-60SA QPCs, which are expected to be delivered in Japan within 2014.

Preprint

Design of Toroidal Coils Testing Bench: Advances in the Mexican Tokamak "T"

M. Salvador¹, J. Martinez², J. González¹, J. Morones³, S. Sanna⁴, J. Almaguer³, J. A. González¹, O. Muñoz¹, A. Nieto¹, O. Islas¹, U. Acosta¹, J. Arce¹, M. Chavez¹, V. Arredondo¹, G. Cavazos¹, M. Sanromán¹, C. Olivares³, C. Saldaña³, and C. Uder¹

¹Facultad de Ingeniería Mecánica y Eléctrica, Universidad Autónoma de Nuevo León, Mexico
²Comisión Federal de Electricidad, Monterrey, Nuevo León, Mexico
³Facultad de Ciencias Físico Matemáticas, Universidad Autónoma de Nuevo León, Mexico
⁴Dipartimento di Fisica "A. Volta", Università degli Studi di Pavia, Italy

Corresponding Author: M. Salvador, max.salvadorhr@uanl.edu.mx

The Fusion Research Group (GIF) of the Autonomous University of Nuevo Leon (UANL) presents its advances into the toroidal coil testing bench system, toward the reinforcement of the Tokamak Experimental Facility. This tokamak design has been beneficiated from the Mexican Public Education Secretary (UANL-EXB-156), is a D-shaped Tokamak with the next main characteristics: major radius R = 41 cm, minor radius a = 18.5 cm, aspect ratio A = 2.2162, safety factor q = 1.9552, plasma current $I_p = 277$ kA, toroidal field $B_t = 1.3$ T, electronic plasma density $n_e \approx 2-3 \times 10^{13}$ /cm³. The presented testing bench platform objective is to evaluate the general systems involved into our D-shaped coil.

The present work shows our D-shaped toroidal coil testing bench, in which we present the results about the final coil design and its electrical, control and storage systems which are used to input high currents on the testing bench, also we describe the mechanical case design and simulations, the thermal considerations for different test scenarios and the magnetic field produced by our toroidal coil design.

The Dynomak: an Advanced Fusion Reactor Concept with Imposed-Dynamo Current Drive and Next-Generation Nuclear **Power Technologies**

D. Sutherland¹, T. Jarboe¹, K. Morgan¹, G. Marklin¹, and N. Brian¹

¹University of Washington, Seattle, WA, USA

Corresponding Author: D. Sutherland, das1990@uw.edu

A high- β spheromak reactor concept called the dynomak has been designed with an overnight capital cost that is competitive with conventional power sources. This reactor concept utilizes recently discovered imposed-dynamo current drive (IDCD) and a molten salt (FLiBe) blanket system for first wall cooling, neutron moderation and tritium breeding. Currently available materials and ITER developed cryogenic pumping systems were implemented in this design from the basis of technological feasibility. A tritium breeding ratio (TBR) of greater than 1.1 has been calculated using a Monte Carlo N-Particle (MCNP5) neutron transport simulation. High temperature superconducting tapes (YBCO) were used for the equilibrium coil set, substantially reducing the recirculating power fraction when compared to previous spheromak reactor studies. Using zirconium hydride for neutron shielding, a limiting equilibrium coil lifetime of at least thirty full-power years has been achieved. The primary FLiBe loop was coupled to a supercritical carbon dioxide Brayton cycle due to attractive economics and high thermal efficiencies. With these advancements, an electrical output of 1000 MW from a thermal output of 2486 MW was achieved, yielding an overall plant efficiency of approximately 40%.

Preprint

Globus-M2 Design Peculiarities and Status of the Tokamak Upgrade

V. Minaev¹, V. Gusev¹, M. Patrov¹, N. Sakharov¹, V. Varfolomeev¹, E. Bondarchuk², A. Cherdakov², A. Kavin², M. Khokhlov², S. Krasnov², A. Labusov², V. Mikov³, V. Tanchuk², A. Voronova², and E. Zhilin⁴

¹Ioffe Physical-Technical Institute of the Russian Academy of Science, St. Petersburg, Russian Federation
 ²D. V. Efremov Institute of Electrophysical Apparatus, St. Petersburg, Russian Federation
 ³JSC INTEKHMASH, St. Petersburg, Russian Federation
 ⁴Ioffe Fusion Technology Ltd., St. Petersburg, Russian Federation

Corresponding Author: V. Minaev, vladimir.minaev@mail.ioffe.ru

The Globus-M spherical tokamak has demonstrated practically all of the project objectives. The main factor limiting further enhancement of plasma parameters, is the relatively low toroidal magnetic field. The increasing of the magnetic field up to 1.0 T together with the plasma current up to 0.5 MA will entail serious rise in loads on the magnetic system in the upgraded tokamak Globus-M2. Thereupon a review of the design was developed. The vacuum vessel remains the same in order to reduce project cost. Results of the complete 3D finite element model thermal and stress analysis are presented for the novel magnetic system. The mechanical strength was enhanced significantly. Radius of the toroidal field coil outer limb was enlarged slightly in order to reduce field ripples. The central column and the toroidal field coil joints were fully redesigned. As far as Globus-M2 poloidal field coil positions did not changed with respect to Globus-M, it allows keeping the full set of plasma magnetic configurations available in the existing machine. Final design of the tokamak upgrade is discussed in the report as well as current status of the work.

MAST Upgrade – Construction Status and Early Research Plans

R. Martin¹

¹CCFE Fusion Association, Culham Science Centre, Abingdon, UK Author: R. Martin, richard martin@ccfo.ac.uk

 $Corresponding \ Author: R. \ Martin, \ richard.martin@ccfe.ac.uk$

The Mega Amp Spherical Tokamak (MAST) is a centre piece of the UK fusion research programme. A MAST Upgrade programme is under way with three primary objectives: 1) To develop reactorrelevant advanced divertor concepts, in particular long leg and Super-X configurations; 2) Add to the knowledge base for ITER, by addressing important plasma physics questions and developing predictive models to help optimise performance of ITER; and 3) Explore the feasibility of using a spherical tokamak as the basis for a fusion Component Test Facility; looking at start-up, current drive, steady state behaviour, exhaust, plasma confinement, high- β operation and performance reliability. To deliver this capability the load assembly is being comprehensively upgraded. Most of the design has been completed and the project is now well into the manufacture and assembly phase. Many long lead time items have now been delivered including the new Divertor Field Power Supplies, the new Toroidal Field Power Supplies and a large number of the in-vessel coils.

Many new diagnostics are included in the upgrade; in particular magnetic diagnostics for real time plasma position and shape control, as well as post pulse equilibrium reconstruction. The divertor has extensive Langmuir probe coverage, bolometry arrays (and tomographic reconstruction), reciprocating probes (magnetic, Langmuir probe, RFEA detector heads), Thomson scattering, coherence imaging for divertor flows, imaging spectroscopy, and infrared imaging. The extensive and high resolution diagnostics presently on MAST will be retained and further diagnostics are intended.

Early research will focus on exhaust studies, specifically production and control of various divertor configurations, physics of perpendicular and parallel transport, detachment formation and stability. The programme will quickly expand to include advances in areas such as fast ion instabilities and core transport, building on earlier research on MAST. In particular MAST Upgrade retains a powerful capability to study pedestal and ELM physics. The closed divertor will lead to lower main chamber neutral densities; as a result quantifying divertor closure, H-mode access and density-limits will be an early priority.

This work was part-funded by the RCUK Energy Programme and by the European Union's Horizon 2020 programme.



Perspectives for the High Field Approach in Fusion Research and Advances within the Ignitor Program

B. Coppi¹, A. Airoldi², R. Albanese², M. Allegretti³, G. Ambrosino², G. Belforte³, F. Bombarda⁴, A. Bianchi⁵, E. Boggio-Sella², A. Cardinali⁴, G. Cenacchi², E. Costa⁶, A. D'Amico⁷, P. Detragiache⁴, G. De Tommasi², A. DeVellis⁴, G. Faelli⁸, A. Ferrari⁸, A. Frattolillo⁴, F. Giammanco⁹, G. Grasso¹⁰, M. Lazzaretti⁵, S. Mantovani⁸, L. Merriman¹¹, S. Migliori⁴, R. Napoli³, A. Perona⁹, G. Perona³, S. Pierattini⁴, A. Pironti², G. Ramogida⁴, G. Rubinacci², M. Sassi², A. Sestero⁴, *L. Sugiyama*¹¹, M. Tavani⁶, A. Tumino¹⁰, F. Villone², and L. Zucchi⁸

¹MIUR, Italy

²CREATE/ENEA/Euratom Association, Università di Napoli, Naples, Italy
 ³Polytechnic University of Turin, Turin, Italy
 ⁴Associazione EURATOM-ENEA Unitá Tecnica Fusione, Frascati, Italy
 ⁵ANSALDO Nucleare, Italy
 ⁶INAF, Italy
 ⁷Università di Roma, Italy
 ⁸CIFS, Italy
 ⁹Università di Pisa, Italy
 ¹⁰Columbus Superconductors, Italy
 ¹¹Massachusetts Institute of Technology, Cambridge, MA, USA

Corresponding Author: B. Coppi, coppi@psfc.mit.edu

The Ignitor Program maintains the objective of approaching D-T ignition conditions by incorporating systematically advances in high magnetic field technology and in experiments on high density well confined plasmas. Another objective is to chart the development of the high field line of experiments. Considering that a detailed machine design has been carried out [1], a subset of the areas to be covered is: 1) Numerical Simulations and Relevant Transport Theory. The machine parameters have been optimized so to allow a programed combination of Ohmic heating, alpha-particle heating and ICRH to approach ignition. A transport model [1] is formulated by which the effects of the (anomalous) current diffusion can be directly investigated and in which the threshold power to access H-mode confinement can be significantly reduced when $Z_{\rm eff}$ is low. 2) Plasma Disruptions and Sensors. In depth analyses have been carried out on the onset and development of disruptions and the adopted control system with favorable conclusions. A diagnostic system with innovative elements, such as a multipurpose Second-Harmonic-Interferometer and a sensoring function for the onset of disruption, has been devised. 3) Nonlinear feedback control simulations with 3D structures. A new tool (CarMa0NL [2]), describes the evolution of axisymmetric plasmas with three-dimensional conducting structures. An upgrade of CarMa0NL, including the position-shape-current integrated feedback controller has been used. 4) Superconducting components. The cables adopted for the largest poloidal field coils involve about 300 MgB₂ multi-filamentary strands (each) of 1 mm in diameter and a copper tube for the He-gas flow in the center with advanced design and electrical properties of these strands. 5) High Field Superconducting Experiments. An important incentive for the analysis of high field superconducting experiments is the realization that "hybrid" high fields magnets can be fabricated using two components: MgB₂ for the "low" field outer part and a high temperature superconductor for the high field inner part. The parameters of a superconducting compact machine capable of producing currents about 15 MA have been identified.

References

[1] B. Coppi, A. Airoldi, R. Albanese, et al., Nucl. Fus. 53, 104013 (2013).

[2] F. Villone et al., Pl. Phys. Cont. Fus. 55, 095008 (2013).



Development and Successful Operation of the Enhanced-Interlink System of Experiment Data and Numerical Simulation in LHD

M. Emoto¹, C. Suzuki¹, Y. Suzuki¹, M. Yokoyama¹, R. Seki¹, and K. Ida¹

¹National Institute for Fusion Science, Toki, Japan

Corresponding Author: M. Emoto, emoto.masahiko@nifs.ac.jp

The enhanced-interlink system of experiment data and numerical simulation has been developed, and successfully operated routinely in LHD. This system consists of analyzed diagnostic data, real-time coordinate mapping, and I/O to numerical simulation. It has enabled automated data handling and transfer between experiment and numerical simulation, to extensively perform experiment analyses. It can be considered as one of prototypes for seamless data-centric approach for integrating experiment data and numerical simulation/modellings in fusion experiment.

In large-scale fusion experiments and future reactors, it is crucial to establish reliable data-centric system to perform data acquisition from many actuators/diagnostics, and to issue signals for controlling plasma operation possibly along with relevant numerical analyses. In LHD, in order to systematically handle various data acquired by different diagnostics, Analyzed Data Server was setup, and it has been functionally extended. Now it has been successfully coupled to numerical simulation, TASK3D-a.

Numerical simulations for toroidal plasmas usually employ density and temperature profiles described in averaged minor radius or flux functions. Therefore the conversion (so-called mapping) from real coordinates to flux coordinate (or reff) is required to establish inter-linkage between experiment data and numerical simulation. For this purpose, three-dimensional equilibrium database using VMEC was established. Based on this database, the equilibrium mapping system called TSMAP (Thomson Scattering MAPping) was developed. It searches for the best-fitted equilibrium so as to minimize the discrepancy between inward and outward side of an electron temperature profile measured by the Thomson scattering system. In order to calculate the profiles on the flux coordinate automatically, an automatic calculation system, AutoAna, was developed. It provides the necessary data for numerical simulations soon after the experiment data is available.

Utilizing this system, experimental analyses by numerical simulations have been extensively progressed. The author believe this data-centric approach for integrating experiment data and numerical simulation and modellings contribute to not only LHD but other plasma fusion projects including DEMO reactor in the future.

Preprint

Engineering Aspects and Physical Research Program of the Modernized T-15 Tokamak

A. Sushkov¹, N. Kirneva¹, K. Korobov¹, V. Krupin¹, A. Melnikov¹, N. Mustafin¹, P. Savrukhin¹, and E. Shestakov¹

¹National Research Centre "Kurchatov Institute", Moscow, Russian Federation Corresponding Author: A. Sushkov, alexey-sushkov@yandex.ru

The project of the T-15 tokamak modernization is now starting to be implemented at the Kurchatov Institute. The main objectives of the research program of the modernized T-15 are: steady-state operation; real time plasma current and pressure control in order to increase β_N (Advanced Tokamak operation); analysis of T_e/T_i effect on the confinement properties; studies of the effects of Zonal flows on transport and confinement and the role of the radial electric field E_r in confinement; plasma turbulence studies; investigations of MHD effects and disruptions; plasma edge physics; liquid lithium wall experiments; divertor optimization and first wall materials investigations under reactor-like power load on the divertor plates. To meet this challenges the new device should be equipped with state-of-art diagnostics, real time plasma control, auxiliary heating and current drive systems. Therefore in the vacuum vessel design special attention was placed on the convenience for the diagnostics and heating systems. The paper will describe the design features and present construction status of the T-15 upgrade. The research program foreseen for the initial operation phase will be discussed.



Progress toward Commissioning and Plasma Operation in NSTX-U

M. Ono¹, C. James¹, D. Lawrence¹, S. Gerhardt¹, R. Kaita¹, J. Menard¹, E. Perry¹, T. Stevenson¹, S. Ronald¹, A. von Halle¹, M. Williams¹, N. Atnafu¹, W. Blanchard¹, M. Cropper¹, A. Diallo¹, D. Gates¹, R. Ellis¹, K. Erickson¹, P. Heitzenroeder¹, J. Hosea¹, R. Hatcher¹, S. Jurczynski¹, S. Kaye¹, G. Labik¹, J. Lawon¹, B. LeBlanc¹, R. Maingi², C. Neumeyer¹, R. Raman³, S. Raftopoulos¹, R. Ramakrishnan¹, L. Roquemore¹, S. A. Sabbagh⁴, H. Schneider¹, M. Smith¹, B. Stratten¹, V. Soukhanovskii⁵, G. Taylor¹, P. Titus¹, K. Tresemer¹, and A. Zolfaghari¹

¹Princeton Plasma Physics Laboratory, Princeton, NJ, USA ²Oak Ridge National Laboratory, Oak Ridge, TN, USA

³University of Washington, Seattle, WA, USA

⁵Lawrence Livermore National Laboratory, Livermore, CA, USA

Corresponding Author: M. Ono, mono@pppl.gov

The National Spherical Torus Experiment—Upgrade (NSTX-U) is the most powerful spherical torus facility being constructed at PPPL, Princeton, USA. The NSTX-U project has entered the last phase of construction, and preparation for plasma operations is now underway. The major mission of NSTX-U is to develop the physics basis for an ST-based Fusion Nuclear Science Facility (FNSF). The ST-based FNSF has the promise of achieving the high neutron fluence needed for reactor component testing with relatively modest tritium consumption. At the same time, the unique operating regimes of NSTX-U can contribute to several important issues in the physics of burning plasmas to optimize the performance of ITER. The NSTX-U program further aims to determine the attractiveness of the compact ST for addressing key research needs on the path toward a fusion demonstration power plant (DEMO). Enabled by key technology innovations, the upgrade will nearly double the toroidal magnetic field B_T , plasma current I_p , and NBI heating power compared to NSTX, and increase the TF flat top pulse length from 1 s to 6.5 s. The new center stack will provide $B_T = 1$ T at a major radius of $R_0 = 0.93$ m compared to 0.55 T at $R_0 = 0.85$ m in NSTX, and will enable a plasma current I_p of up to 2 MA for 5 s compared to the 1 MA for 1 s in NSTX. The anticipated plasma performance enhancement is a quadrupling of the plasma stored energy and at least doubling of the plasma confinement time, which would result in an order of magnitude increase in the fusion performance parameter $n\tau T$. With $\beta_T \sim 25\%$ at $B_T = 1$ T, the absolute average plasma pressure in NSTX-U could become comparable to that of present-day tokamaks. A much more tangential 2nd NBI system, with 2–3 times higher current drive efficiency compared to the 1st NBI system, is installed. NSTX-U is designed to attain the 100% noninductive operation needed for a compact FNSF design. With higher fields and heating powers, the NSTX-U plasma collisionality will be reduced by a factor of 3–6 to help explore the trend in transport towards the low collisionality FNSF regime. If the favorable trends observed on NSTX holds at low collisionality, high fusion neutron fluences could be achievable in very compact ST devices. NSTX-U first plasma is planned for November 2014, at which time the transition to plasma operation will occur.

⁴Columbia University, New York, USA



Conceptual Design of High Resolution and Reliable Density Measurement System on Helical Reactor FFHR-d1 and Demonstration on LHD

T. Akiyama¹, R. Yasuhara¹, M. Isobe¹, R. Sakamoto¹, T. Goto¹, K. Kawahata¹, K. Nakayama², S. Okajima², and A. Sagara¹

¹National Institute for Fusion Science, Toki, Japan ²Chubu University, Kasugai, Japan

Corresponding Author: T. Akiyama, takiyama@nifs.ac.jp

This paper describes a conceptual design of the density measurement system on the helical reactor FFHR-d1 based on its quantitative operation scenario. One of the important plasma parameters which is used for plasma control is the line averaged electron density on FFHR-d1. This is because the startup and the steady state plasma will be mainly operated by feedback control of the line averaged electron density. From recent quantitative investigations of operation scenario in FFHR-d1, the density resolution of the order of 10^{17} m⁻³ with a response time less than 10 ms is required. In addition to that, the density measurement has to meet the reactor design. As for the interferometer, the vibration isolation system, which is necessary for the usual interferometer, cannot be installed on FFHR-d1.

A possible system which can satisfy the requirements is a combination of a dispersion interferometer (DI) and a polarimeter. The DI is a special interferometer which can cancel the vibration components by itself. Hence the DI meets the reactor design and the immunity to the vibrations can also improve the density resolution. The DI can suppress failures of fringe counting "fringe jump", which lead to uncontrollability of the density, by fast sampling which reduces the phase shift less than one fringe between sampling intervals. Even when the fringe jump occurs, a polarimeter, which measures the Faraday rotation, can correct the fringe number of the DI. Although the density resolution of the polarimeter is not enough, there is no fringe jump. Hence the combination can increase the reliability of the density measurement. The appropriate wavelength of the laser source, vacuum windows, deposition mitigation for first mirrors are also investigated.

A prototype of the dispersion interferometer is installed on LHD, which can realize a demo relevant density plasma. The achieved density resolution is 2×10^{17} m⁻³ with a response time of 30 μ s. While the fringe jump occurs in the existing FIR interferometer in the case of repetitive pellet injected discharges, the DI can successfully measure without any jumps. In this way, the DI on LHD demonstrates the feasibility of the density measurement with the dispersion interferometer, which satisfies the requirements from FFHR-d1. This system is applicable not only to FFHR-d1 but also to other demo reactor designs.



Preliminary Test Results of GDC Electrode with Gap Insulation on SWIP Test Bed

H. B. Xu¹, M. X. Wang¹, Y. Wang¹, L. J. Cai¹, T. Lin¹, and L. Wan¹

¹Southwestern Institute of Physics, Chengdu, Sichuan, China

Corresponding Author: H. B. Xu, xuhb@swip.ac.cn

A DC glow discharge system is in preparation for ITER with primary aim to control impurities and particle recycling. On the current design stage, GDC electrode will be integrated into a Diagnostic Port Plug (DPP) as a part of the assembly. A Gap structure is used as electrical insulation among GDC electrode, DFW and DSM. Meanwhile, in order to avoid glow discharge generated by the cooling water pipes with high voltage in ITER vacuum vessel and the low pressure gas around, electrical shielding is necessary. Therefore, they need Faraday shielding to restrict the breakdown.

From prior test results and experiences, electrode with different gap structures ($\delta 1$ - $\delta 2$ - $\delta 3$) for electrical insulation is designed. Meanwhile, in this test, stainless steel net with area 60 × 100 mm² and a 1 × 1 mm² mesh size is fixed in surface of stainless case. The electrode is installed on SWIP GDC Test Bed. The test results are given in this paper.

The aim is to test on He/H_2 breakdown, discharge characteristics and heat load on electrode and to explore the feasibility and reliability of electrical insulation of the gap. The present work provide basis for design of ITER GDC in the future.

Fusion Nuclear Physics and Technology



Configuration Studies for an ST-Based Fusion Nuclear Science Facility

J. Menard¹, T. Brown¹, J. Canik², B. Covele³, *L. El-Guebaly*⁴, S. Gerhardt¹, S. Kaye¹, C. Kessel¹, M. T. Kotschenreuther³, S. Mahajan³, R. Maingi¹, L. Mynsberge⁴, C. Neumeyer¹, M. Ono¹, R. Raman⁵, S. A. Sabbagh⁶, V. Soukhanovskii⁷, P. Valanju³, R. Woolley¹, and A. Zolfaghari¹

¹Princeton Plasma Physics Laboratory, Princeton, NJ, USA
 ²Oak Ridge National Laboratory, Oak Ridge, TN, USA
 ³University of Texas at Austin, Austin, TX, USA
 ⁴University of Wisconsin-Madison, Madison, WI, USA
 ⁵University of Washington, Seattle, WA, USA
 ⁶Columbia University, New York, USA
 ⁷Lawrence Livermore National Laboratory, Livermore, CA, USA

Corresponding Author: J. Menard, jmenard@pppl.gov

A Fusion Nuclear Science Facility (FNSF) could play an important role in the development of fusion energy by providing the nuclear environment needed to develop fusion materials and components. The spherical tokamak (ST) is a leading candidate for an FNSF due to its potentially high neutron wall loading and modular configuration. A key consideration for the choice of FNSF configuration is the range of achievable missions as a function of device size. Possible missions include: providing high neutron flux (1–2 MW/m²) and fluence (3–6 MWy/m²), demonstrating tritium self-sufficiency (tritium breeding ratio $TBR \ge 1$), and demonstrating electrical self-sufficiency. All of these missions must also be compatible with a viable divertor, first-wall, and blanket solution. During the past two years, U.S. studies have, for the first time, developed ST-FNSF configurations simultaneously incorporating: 1) a blanket system capable of $TBR \sim 1$; 2) a poloidal field (PF) coil set supporting high elongation and triangularity for a range of li and normalized β values consistent with NSTX/NSTX-U previous and planned operation; 3) a long-legged Super-X divertor analogous to the planned MAST-U divertor which substantially reduces projected peak divertor heat-flux and has all outboard PF coils outside the vacuum chamber and as superconducting to reduce power consumption; and 4) a vertical maintenance scheme in which blanket structures and the centerstack (CS) can be removed independently. Progress in these ST-FNSF mission versus configuration studies including dependence on plasma major radius R_0 for a range $R_0 = 1-1.6$ m will be described. TRANSP and NUBEAM calculations of negative neutral beam heating and current drive scenarios will also be described.

The Accomplishment of the Engineering Design Activities of **IFMIF/EVEDA:** the European-Japanese Project Towards a Li(d,xn) Fusion Relevant Neutron Source

I. Knaster¹

¹IFMIF/EVEDA, Aomori, Japan

Corresponding Author: J. Knaster, juan.knaster@ifmif.org

The International Fusion Materials Irradiation Facility (IFMIF), presently in its Engineering Validation and Engineering Design Activities (EVEDA) phase under the frame of the Broader Approach Agreement between Europe and Japan, has accomplished on summer 2013, on schedule, its EDA phase with the release of the engineering design report of IFMIF plant, which is here described, compliant with our mandate. Many improvements of the design from former phases are implemented, relevantly a reduction of beam losses and operational costs thanks to the superconducting accelerator concept; the re-location of the quench tank outside the Test Cell with a reduction of tritium inventory and a simplification on its replacement in case of failure; the separation of the irradiation modules from the reliability and cost reduction; and the water cooling of the liner and biological shielding of the Test Cell, enhancing the efficiency and economy of the related and Cell, enhancing the efficiency and economy of the related sub-systems. In addition, maintenance strategy has been modified to allow a shorter yearly stop of the irradiation operations and a more careful management of the irradiated samples. The design of IFMIF plant is intimately linked with the EV activities carried out since the entry into force of IFMIF/EVEDA in June 2007. These last and their on-going accomplishment have been thoroughly described elsewhere [1], which combined with the present paper allows a clear understanding of the maturity of the European-Japanese international efforts. This released intermediate design report, which could be annexed if required concurrently with the accomplishment of the on-going EV activities, will allow taking decisions on its construction and/or serve the basis for a less ambitious facility in terms of dpa, aligned with the needs of our fusion community.

References

[1] J. Knaster et al., 2013 Nuclear Fusion 53 116001.



FNS/1-2Ra



Neutronic Analyses for ITER Diagnostic Port Plugs

A. Serikov¹, L. Bertalot², U. Fischer¹, B. Levesy², S. Pak², C. S. Pitcher², A. Suarez², and V. S. Udintsev²

¹Karlsruhe Institute of Technology, Germany ²ITER Organization, Saint Paul lez Durance, France

Corresponding Author: A. Serikov, arkady.serikov@kit.edu

The radiation shielding performance of two diagnostic port plugs of ITER, Equatorial and Upper Port Plugs (EPP and UPP) has been evaluated resulting in several proposals for shielding design improvements. These improvements were based on the comprehensive optimization of the shielding variants obtained with parametric analyses of the geometry and material composition of the port structures. The crucial parameter for the optimization was the value of Shut-Down Dose Rate (SDDR) in the EPP and UPP interspaces inside the ITER bioshield. The SDDR was minimized following the ALARA (As Low as Reasonably Achievable) principle taking into account the feasibility to implement the shielding options with the actual hardware in the vicinity of EPP and UPP. The port plugs are large structures which play the dual and opposite roles of providing access for the diagnostic systems while being vacuum-tight and ensuring that the vacuum vessel ports are adequately "plugged" to prevent the leakage of neutron and gamma radiation. The shielding performance of the plugs should be effective not only against the 14 MeV neutron irradiation from the D-T plasma and secondary gammas produced by neutron interaction with the structures during the ITER operation, but also against the decay gamma radiation emitted from the radioactive materials of ITER during its cooling time. For that reason, SDDR calculations were performed using the state-of-the-art methodology to provide reliable estimates of SDDR inside the port interspaces where personnel access is assumed after a cooling time of ~ 12 days with the target value of 100 μ Sv/h following the ALARA approach. The neutronic results presented in this paper can be useful for the development of a common approach for the shielding arrangement of ITER ports. These results can impact the design of the general-purpose port because the radiation environment at the ports is mostly related to the gap interfaces between the ports and components of ITER, such as blanket, manifolds, and vacuum vessel. Design solutions for an improved shielding have been elaborated taking into account the effect of radiation "cross-talks" between the ports, and introducing several types of gap labyrinths which can reduce the radiation streaming. Such design options have been proposed for implementation and their feasibility was checked at the level of port integration.



Integrated Modelling of DEMO-FNS Current Ramp-up Scenario and Steady State Regime

A. Y. Dnestrovskij¹, B. Kuteev¹, A. Bykov², A. Ivanov³, V. Lukash¹, S. Medvedev³, V. Sergeev², D. Sychugov⁴, and R. Khayrutdinov¹

¹National Research Centre "Kurchatov Institute", Moscow, Russian Federation
 ²St. Petersburg State Polytechnical University, St. Petersburg, Russian Federation
 ³Keldysh Institute of Applied Mathematics, RAS, Moscow, Russian Federation
 ⁴M.V. Lomonosov Moscow State University, Moscow, Russian Federation

Corresponding Author: A. Y. Dnestrovskij, dnestrov0@gmail.com

The approach to the integrated modelling of plasma regimes in the projected neutron source DEMO-FNS [1] based on different codes is developed. The integrated modelling allows eliminating uncertainties in external parameters for such tasks as plasma current ramp up, steady-state plasma consistency, plasma stability and heat load onto the wall and divertor plates. The following codes are employed for the integrated modelling

- 1. The ASTRA transport code [2] is used for adjustment of the steady-state regime parameters. The NUBEAM Monte Carlo code incorporated into the ASTRA code.
- 2. The DINA free boundary equilibrium and evolution code [3].
- 3. The SPIDER free boundary equilibrium and equilibrium reconstruction code [4] and KINX ideal MHD stability code [5].
- 4. The TOKAMEQ free boundary equilibrium code [6] and the TOKSTAB vertical displacement stability code [7].
- 5. The SOL-Onion-skin semi-analytic modelling code of self-consistent description of the core, edge and divertor plasmas based on the experimental scaling laws [8]. The uncertain parameters are verified by calculations of the main plasma profiles with the ASTRA code and of the edge and divertor plasma with the B2SOLPS5.2 [9] code.

The consistent steady state regime for the DEMO-FNS plasma and the plasma current ramp up scenario are developed as a result of integrated modelling approach. The design with the long-legged divertor is proposed. The copper insets are suggested for the suppression of the instability to vertical displacement.

References

[1] B.V.Kuteev et al., This conference.

- [2] G.V. Pereverzev, P.N. Yushmanov, (2002) MPIPP ID 282186 http://edoc.mpg.de/282186.
- [3] R.R. Khayrutdinov and V.E. Lukash. J. Comput. Physics, (1993), V. 109, p 193.
- [4] A.A. Ivanov et al., 2005 32nd EPS Conf. on Plasma Physics 29C (ECA) P-5.063.
- [5] L. Degtyarev et al., Comput. Phys. Comm. vol. 103, 10 (1997).
- [6] D.Yu. Sychugov, VANT, Termoyadernyi sintez 31 (4), (2008), 85 (in Russian).
- [7] D.Yu. Sychugov, VANT, Termoyadernyi sintez 33 (3), (2010), 46 (in Russian).
- [8] V.Yu. Sergeev et al., Plasma Physics Reports, 2012, Vol. 38, No. 7, pp. 521.
- [9] V. Rozhansky, et al., . Nuclear Fusion (2001) 41 387.



Advanced Computational Approaches and Tools for High-Fidelity Nuclear Analyses of Fusion Facilities

U. Fischer¹, K. Kondo¹, D. Leichtle¹, H. Liu¹, P. Pereslavtsev¹, A. Serikov¹, Y. Qiu¹, and B. Weinhorst¹

¹Karlsruhe Institute of Technology, Germany

Corresponding Author: U. Fischer, ulrich.fischer@kit.edu

The nuclear design and optimisation of fusion facilities and their components rely on the data provided by neutronic calculations. Suitable computational approaches, tools, and data, qualified and validated for design applications are required to enable reliable design analyses and ensure a sufficient prediction accuracy of the results. Recent efforts aim at extending the capabilities of the simulation tools for the provision of high-fidelity neutronic results on meshes generated on the basis of engineering CAD geometry models. Such meshes can be adapted to the requirements of subsequent thermal-hydraulic (TH) and structural mechanics (SM) calculations and can be also used for the results visualisation.

At the Karlsruhe Institute of Technology (KIT), Institute for Neutron Physics and Reactor Technology (INR), the development efforts lately focused on various computational schemes coupling, on the one hand, the MC radiation transport simulation to the CAD geometry, and, on the other hand, to high resolution activation calculations, TH/SM simulations and the visualisation of the results on the CAD geometry. The related development works have been mainly performed in the framework of the Power Plant Physics and Technology (PPPT) programme launched initially by the European Fusion Development Agreement (EFDA) and integrated now into the new Eurofusion projects.

This paper presents the recent progress achieved at KIT on i) the related development of a multiphysics coupling approach for neutronics, TH and SM analyses; ii) the extension and improvement of the conversion software tool McCad for the generation of MC geometry models from CAD geometry data; and iii) the further enhancement of a coupled programme system for the MC based calculations of high-resolution shut-down dose rate distributions. The paper includes application examples on ITER and DEMO showing the suitability of the tools for real design analyses.



Spectra of Neutrons from a Beam-Driven Fusion Source

P. Goncharov¹

¹St. Petersburg State Polytechnical University, St. Petersburg, Russian Federation

Corresponding Author: P. Goncharov, p.goncharov@spbstu.ru

A tokamak-based source of nuclear fusion neutrons, such as considered in some recent papers and program talks, employs injection of fast atom beams into plasma. Energy spectrum is one of the key characteristics of a neutron source. Distributions of electrically charged fusion products are also important to know since they contribute to plasma heating, if they are confined, and they influence the first wall, if they are lost from the plasma. Compared to thermonuclear fusion product spectra, the treatment of distributions of fusion products from a beam-heated plasma is much less complete in existing bibliography. The bibliography is not abundant for the case of non-Maxwellian velocity distributions of fuel nuclei. The results in early works show different shapes of neutron spectra for DT reaction. Spectra in more recent works differ from earlier ones. In addition to beam particle slowing down, suprathermal tails due to nuclear elastic scattering of fast ions are taken into consideration in some recent studies. The details of calculation of fuel nuclei distribution functions and particular numerical techniques to obtain the fusion product spectra are not discussed in those works. The purpose of this contribution is to describe a fast, easily reproducible semianalytical approach to calculate the distributions of fusion products in case of the presence of substantial suprathermal tails in fuel nuclei velocity distributions. Results for a variety of distributions of suprathermal fuel nuclei will be presented. Numerical techniques and a number of methods of verification of calculated fusion product spectra will be discussed.



The Neutronics Analysis of Blankets for the Hybrid Fusion Neutron Source

A. Zhirkin¹, B. Kuteev¹, M. Gurevich¹, and B. Chukbar¹

¹National Research Centre "Kurchatov Institute", Moscow, Russian Federation Corresponding Author: A. Zhirkin, aleksej-zhirkin@yandex.ru

In this work it is investigated the capabilities of hybrid fusion neutron source (FNS) blankets in reprocessing of spent nuclear fuel and generation of nuclides ²³³U, ²³⁹Pu, and tritium. The basic kinds of blankets are considered. There are the blanket with use of heavy water solutions of salts and oxides of uranium and thorium, solid-state, and molten salt blanket. The structure and geometrical parameters of blankets, moderator, and fertile materials are optimized to obtain the ultimate nuclear fuel yield at the least accumulation of radiation toxic wastes. The neutronics comparative analysis of the different blanket models is presented. In the result, the optimal FNS blanket models are chosen.



Optimization of a Gas Dynamic Trap Neutron Source

T. Simonen¹, A. Molvik², H. Du^{3,4}, and Y. Wu^{3,4}

¹University of California Berkeley, Berkeley, CA, USA ²Lawrence Livermore National Laboratory, Livermore, CA, USA, (Retired) ³Institute of Plasma Physics, Chinese Academy of Sciences, Hefei, China ⁴University of Science and Technology, Anhui, China

Corresponding Author: T. Simonen, simonen42@yahoo.com

Fusion development will require materials capable of withstanding the harsh bombardment of 14 MeV D-T neutron bombardment. The Gas Dynamic Trap (GDT) neutron source concept is aimed to test and qualify suitable materials and sub-components. In this paper we evaluate two ways to further increase the attractiveness of the neutron source suggested by the GDT team. First is the use of ECH power to reduce the neutral beam injection power required to heat and sustain the warm plasma. Second is the use of an additional coil on each end to reduce the power and particle end leakage. These two ideas will increase the electron temperature and thereby increase the neutron output. In addition, these ideas also reduce the gas throughput and thereby reduce the size of the tritium reprocessing system and reduce the number of neutral beam injectors subject to neutron exposure. We benchmark our ideas and modeling to GDT experiments as well as earlier experiments.

Innovative Confinement Concepts



Progress on HIT-SI and Imposed Dynamo Current Drive

B. Victor¹, T. Jarboe¹, C. Hansen¹, A. Hossack¹, G. Marklin¹, K. Morgan¹, B. Nelson¹, and D. Sutherland¹

¹University of Washington, Seattle, WA, USA

Corresponding Author: B. Victor, bvictor@uw.edu

Increasing the Imposed Dynamo Current Drive (IDCD) frequency up to 68.5 kHz on the HIT-SI experiment produced, for the first time, sustained spheromaks with high-pressure confinement (βgeq MHD β limit). Equilibrium profiles of the driven spheromak are stable to the n = 1 kink instability. The injectors drive the edge of the plasma to a high lambda (= $\mu_0 j/B$) with a low lambda region forming in the center. This produces a q profile that is stable to the ideal n = 1 kink mode for operations at all frequencies. Pressure confinement is achieved as the injector drive frequency is increased above the sound transit time ($\omega_{ini} > v_i/a$, where a is the minor radius). The high, Mercier unstable, β and stability to ideal kink modes indicate imposed fluctuations may be interrupting the growth of pressure driven modes keeping the instability local and preserving global confinement. Toroidal currents of 90 kA and current gains of nearly 4, a spheromak record, have been achieved. Computational advances include NIMROD simulations of a larger, hotter experiment showing closed flux for many injector cycles at $\delta B/B$ of approximately 6% and the validation of an extended MHD code capable of simulating the full HIT-SI geometry including injectors. If a larger machine can repeat this result at higher temperatures, this method could provide an economical path to fusion. Provided the method scales, power-efficient, steady-state sustainment of a plasma at the MHD- β limit is a major achievement for fusion research.

Numerical Study of Energy Transfer Mechanism of Magnetic Reconnection/Torus Plasma Merging under High Toroidal Magnetic Field

S. Inoue¹, Y. Ono¹, C. Z. Cheng¹, and R. Horiuchi²

¹University of Tokyo, Japan ²National Institute for Fusion Science, Toki, Japan

Corresponding Author: S. Inoue, inoue@ts.t.u-tokyo.ac.jp

The high-power reconnection heating has been studied in TS-3, TS-4, and MAST merging spherical tokamak (ST) experiments as a promising solenoid (CS)-free startup with significant heating. The magnetic reconnection plays an important role to ramp-up high temperature ST plasmas, which converts magnetic energies to plasma kinetic energies, increasing poloidal β value of produced main plasma. An important question is how the magnetic reconnection converts magnetic energy of two ST plasmas into thermal or kinetic energy of the produced ST and whether the high toroidal field decreases the conversion rate or not. We performed the first 2D PIC simulation [1] for reconnection region of two merging ST plasmas and found: 1) significant ion heating; and 2) its fast conversion from poloidal magnetic energy into ion kinetic energy under high toroidal field condition. We also found that the kinetic effects plays important role for its energy conversion. Electrons are accelerated by the reconnection electric field with existence of the toroidal field, forming the quadrupole structures of electrostatic (ES) potential. The electrostatic potential optimizes ion current profiles against new in-plane electromagnetic electric field, causing significant energy conversion from magnetic energy to ions kinetic energy. The physical origin of ES potential is parallel acceleration of electrons, indicating that the Hall MHD regime is not sufficient to describe the phenomena. Second, we scanned the toroidal field from 1/4 to 4 of the constant poloidal field in the simulation. We found that the peak ion temperature slightly increases with toroidal field. Finally, the TS-3 merging experiment also reveals that the ion temperature weakly depends on the toroidal field under the constant inflow condition. The series of numerical and experimental results agree well with the recent MAST experiment under collisionless and high toroidal field condition.

References

[1] H. Ohtani, et al., Plasma and Fusion Research, 4, 024 (2009).

Tokamak with an Ergodic Central Area

V. Ilgisonis¹, A. Skovoroda¹, and E. Sorokina¹

¹National Research Centre "Kurchatov Institute", Moscow, Russian Federation

Corresponding Author: V. Ilgisonis_vi@nrcki.ru

A possibility to organize in the center of a tokamak the large ergodic area surrounded by nested magnetic surfaces is discussed. The ergodicity of the area dense fulfilled by the magnetic field lines provides the constancy of plasma pressure that mostly removes some drift and current instability in the area. The surrounding magnetic surfaces commonly response for the plasma thermal insulation. The general Hamiltonian approach is used to show that such magnetic configuration can be realized either by external current windings or by the special profiling of plasma current. The charged particles trajectories in the ergodic area can be similar to the trajectories in the conventional tokamak.

Preprint

Plasma Confinement by Pressure of Rotating Magnetic Field in Toroidal Device

V. Svidzinski¹

¹FAR-TECH, San Diego, USA

Corresponding Author: V. Svidzinski, svidzinski@far-tech.com

A novel plasma confinement concept in which plasma is confined in a dynamic steady state by a pressure of rotating magnetic field in a toroidal geometry will be presented. The confining rotating magnetic field is created by AC currents driven by applying oscillating voltages to toroidal and poloidal gaps (insulated horizontal and vertical cuts) in the shell of the torus with 90 degrees phase shift between these voltages. The toroidal component of magnetic field is created by oscillating poloidal current in the shell and the poloidal component of the field is created by toroidal image current on the plasma surface. The confining rotating field is localized in the vacuum layer between the plasma and the toroidal shell, it penetrates plasma on a few skin depths. Plasma discharge is created by the inductive electric field when the gap voltages are applied or by a preionization pulse. Toroidal plasma equilibrium and stability in this concept are achieved due to the realized constraint of conservation of the amplitude of the oscillating magnetic flux through any section of the vacuum layer between the plasma and the conducting shell. The fast rotating magnetic field penetrates plasma and the conducting shell only on a few skin depths such that the magnetic flux is mostly localized in the layer between the plasma and the shell. Toroidal plasma equilibrium in this concept is modeled by: 1) calculating time evolution of plasma column in the torus when the oscillating voltages are applied to the gaps, and 2) by calculating the time averaged magnetic pressure on the plasma boundary due to these voltages. These 2D results will be presented along with the results of 3D modeling of equilibrium which includes realistic gaps. Plasma stability is analyzed in a simplified cylindrical geometry, demonstrating that plasma boundary is MHD stable under nonrestrictive conditions. Similar results, but somewhat modified by the toroidal effects, are expected in the toroidal geometry. Limitation on the plasma pressure is due to the RF power dissipation in the skin layer of the conducting shell such that a superconducting shell is required for operation at high plasma pressures. Possible application of this concept to efficient fusion reactor depends on availability of superconductors (for the shell material) which can operate in magnetic field 1 T in the MHz frequency range.



Control of Spontaneous Rotation in a Field-Reversed Configuration by Double-Sided Magnetized Plasmoid Injection

T. Asai¹, H. Itagaki², K. Masashi¹, L. Steinhauer³, J. Sekiguchi¹, T. Matsumoto¹, H. Sano¹, T. Takahashi^{1,4}, M. Inomoto², and Y. Narushima⁵

¹Nihon University, Japan
 ²University of Tokyo, Japan
 ³Trialpha Energy, Foothill Ranch, California, USA
 ⁴Gunma University, Maebashi, Japan
 ⁵National Institute for Fusion Science, Toki, Japan

Corresponding Author: T. Asai, asai.tomohiko@nihon-u.ac.jp

The mechanism and control of spontaneous toroidal spin-up of a field-reversed configuration (FRC) have been investigated on the Nihon University Compact Torus Experiment (NUCTE). The FRC has highly favorable technological features especially as a D-³He fusion reactor core, i.e., extremely high- β , linear device geometry, natural divertor and axial mobility, allowing separation of start-up and confinement functions. One of the critical issues of FRC study is to understand the toroidal spin-up which triggers the most dangerous global instability (the rotational instability) a centrifugally-driven interchange-like mode with toroidal mode number n = 2.

The radial profile of this self-generated toroidal flow has commonly been described as relaxing toward rigid rotation, i.e., toward uniform angular rotation frequency v_{θ}/r , with the driving torque acting from outside in. Surprisingly, detailed observation of toroidal flow revealed that, rather than tending toward rigid rotation, the profile showed slower rotation in the edge region, thus indicating the transmission of toroidal torque directly into the interior rather than by a diffusive "viscous" process. This suggests the action of the flux-loss spin-up mechanism.

Toroidal rotation eventually causes a destructive instability reflected by a deformation of the toroidal cross-section. In the experiments, plasmoid injection from each end by "magnetized coaxial plasma guns" (MCPG) has been conducted aiming to mitigate the spin-up. Each MCPG generates a spheromak-like plasmoid which travels axially to merge with the pre-existing FRC. The particle inventory of the plasmoids is less than 1/50 of the target FRC in these experiments. The toroidal fluxes of the two plasmoids are opposed so that the MCPGs add no net toroidal flux. Since the MCPG discharges form isolated plasmoids, the open field lines do not electrically connect the FRC core to the gun electrodes. Nevertheless, the injection has a dramatic effect to limit toroidal spin-up: it halts the rise of angular velocity and delays the onset of the n = 2 deformation from 25 to 35 μ s. This instability may also be suppressed through nonmagnetized plasmoid injection by end-on plasma guns. However, the possible refluxing effect by the magnetized plasmoid injection indicates an advantage of MCPG for both current drive and stabilization.

Low Loop Voltage Start-up Using Trapped Particle Configuration in Versatile Experiment Spherical Torus (VEST)

Y. An¹, H. Lee¹, J. Lee¹, J. Jo¹, J. Yang¹, J. Jo¹, Y. Kim¹, B. Jung¹, K. Chung¹, Y. Na¹, T. Hahm¹, and Y. Hwang¹

¹Seoul National University, Seoul, Korea, Republic of

Corresponding Author: Y. An, ayh1800@snu.ac.kr

The effect of the poloidal field structure on pre-ionization and start-up has been investigated with a special focus on the trapped particle configuration in VEST (Versatile Experiment Spherical Torus), a spherical torus recently built at Seoul National University. VEST is characterized by two partial solenoid coils installed at both vertical ends of a center stack, which is intended to be used for the double null merging start-up experiment. The pre-ionization using electron cyclotron heating (ECH) has been adopted for the reliable start-up in many tokamaks including spherical torus devices. ECH has been also utilized for the initial plasma start-up experiment of VEST and the radial profiles of plasma parameters are measured using triple Langmuir probe to investigate the effect of poloidal field structure on pre-ionization and start-up. It was found that the electron density increases larger than twofold with small amount of pressure driven current generated when trapped particle configuration is applied. It is also found that the higher plasma current can be achieved under trapped particle configuration with identical loop voltage compared with the case without trapped particle configuration. Up to 40 kA of plasma current could be generated under the trapped particle configuration with sufficiently lower volt-second than that required for the similar current level in field null configuration, which indicates that this kind of structure can be utilized for the saving of volt-second consumption. Experiment results under various magnetic field configurations with varying mirror ratio show that the poloidal field structure with high mirror ratio can result in more efficient plasma start-up with lower loop voltage or ECH power. This result can be utilized for optimal start-up scenario development of tokamaks requiring low loop voltage such as ITER or of spherical torus with limited volts-seconds.

Work supported by the National Research Foundation of Korea (NRF) grant funded by the Korea government (MSIP) (No. 2008-0061900)

Paper

Inertial Fusion Experiments and Theory

Effects of Ion Diffusion on Fusion Burn at the Shock Flash in Inertial-Confinement Fusion Implosions

C. Li¹, J. Frenje¹, M. Johnson¹, H. Rinderknecht¹, M. Rosenberg¹, F. Seguin¹, H. Sio¹, A. Zylstra¹, R. D. Petrasso¹, P. Amendt², C. Bellei², S. Wilks², R. Betti³, D. Meyerhofer³, J. Soures³, and D. Casey²

> ¹Massachusetts Institute of Technology, Cambridge, MA, USA ²Lawrence Livermore National Laboratory, Livermore, CA, USA ³Laboratory for Laser Energetics, Rochester, NY, USA

Corresponding Author: C. Li, li@psfc.mit.edu

Understanding the physics responsible to the disagreement between experimental results and numerical simulations are of fundamental importance to inertial-confinement fusion (ICF) implosions, and particularly to the ignition-scale layered implosions currently taking place at the National Ignition Facility (NIF). The plasma kinetic effects, which have been overlooked in the conventional single-spicesaveraged hydrodynamic codes, are attracting increasing attentions. It has been realized that such effects, including the ion diffusions, play important roles particularly in the early implosion phase and can potentially affect the dynamics in the later implosion phases. To quantitatively study the effects of ion diffusions at the early implosions, we have imploded a series of thin-glass shells filled with tritium-helium-3 (T^{3} He) gas or deuterium-tritium-helium-3 (DT^{3} He) gas. For the first time, spectra of multiple charged-fusion products from these implosions are obtained at the time of shock flash and used to infer stratification of ions with different electric charge states (Z), ion masses (m) and chargeto-mass ratios (Z/m). These experiments provide useful information to verify the recent theoretical work by Amendt et al., [1], on plasma diffusion crossing the shock front due to the thermodynamic gradients. While there are a number of diffusion sources, including the conventional concentration diffusion (due to concentration gradient), barodiffusion (due to pressure gradient), electrodiffusion (due to electric field), and thermodiffusion (due to temperature gradient), the preliminary analysis suggest that barodiffusion and electrodiffusion are the dominant sources in these implosions. These experiments provide new physical insight into the effects of the ion diffusion on species stratification in shocked/reshocked hot plasmas and have important implication to the ongoing experiments at the NIF.

References

608

[1] P.A. Amendt et al., Phys. Rev. Lett. 109, 075002 (2013).

Slides

Paper

Experimental Platform for Efficient Heating of Fusion Fuel with Fast-Ignition Scheme

S. Fujioka¹, Y. Arikawa¹, Z. Zhang², M. Alessio², T. Nagai², Y. Abe², K. Ishihara², K. Sadaoki², S. Sakata², M. Taga², T. Ikenouchi², H. Inoue², M. Utsugi², S. Hattori², T. Hosoda², S. H. Lee², A. Sunahara¹, T. Johzaki³, H. Sakagami⁴, T. Ozaki⁴, K. Mima⁵, T. Taguchi⁶, L. Giuffrida⁷, J. Santos⁷, J. Honrubia⁸, H. Sawada⁹, K. Shigemori², Y. Hironaka², T. Sano², Y. Fujimoto², K. Yamanoi², T. Norimatsu², K. Tsubakimoto², S. Tokita², Y. Nakata², J. Kawanaka², T. Jitsuno², N. Miyanaga², M. Nakai², H. Nishimura², H. Nagatomo², H. Shiraga², and H. Azechi²

 ¹Institute for Laser Technology, Suita, Osaka, Japan
 ²Institute of Laser Engineering, Osaka University, Osaka, Japan
 ³Graduate School of Engineering, Hiroshima University, Higashi-Hiroshima, Japan
 ⁴National Institute for Fusion Science, Toki, Japan
 ⁵Graduate School for the Creation of New Photonics Industries, Hamamatsu, Shizuoka, Japan
 ⁶Department of Electrical and Electronics Engineering, Setsunan University, Osaka, Japan
 ⁷University of Bordeaux, France
 ⁸Department of Applied Physics, School of Aerospace Engineering, University of Nevada, Reno, USA

Corresponding Author: S. Fujioka, sfujioka@ile.osaka-u.ac.jp

A series of experiments were carried out to evaluate energy coupling efficiency from a heating laser to a fuel core in the fast-ignition scheme of laser-driven inertial confinement fusion. Here we break down the efficiency, which is governed by enormous interactions and instabilities among intense laser, high-energy-density plasma, and relativistic electron beam (REB), into three measurable parameters: i) energy conversion efficiency from a laser to a REB, ii) probability of collision between the REB and a fusion fuel core, and iii) fraction of energy deposited in the fuel core from the REB. These three parameters were measured in the basic experiment under minic plasma circumstances of the integrated fast-ignition experiment. In the heating experiment, fusion neutron yield was measured to understand the heating mechanism by comparing the yield with a two-dimensional Fokker-Planck computation of the REB transport in the core plasma. The experimental results indicate that "unstoppable" and "diverging" problems of the REB must be solved for heating the fuel core efficiently with the REB. Guiding of the REB by > 1 kT magnetic field produced by a laser-driven capacitor-coil target is essential to overcome these difficulties.



Effect of Pre-Plasma on Intense Electron Beam Generation by Relativistic Laser Radiation

F. Beg¹, C. McGuffey¹, J. Peebles¹, A. Sorokovikova¹, B. Qiao¹, C. Jarrott¹, M. Donovan², T. Ditmire², M. Hegelich², C. Wagner², M. Martinez², G. Dyer², M. Wei³, H. McLean⁴, A. Meadows², E. McCary², V. Minello², and S. Krasheninnikov⁵

¹University of California San Diego, CA, USA
 ²University of Texas at Austin, Austin, TX, USA
 ³General Atomics, San Diego, CA, USA
 ⁴Lawrence Livermore National Laboratory, Livermore, CA, USA
 ⁵University of California San Diego, CA, USA

Corresponding Author: F. Beg, fbeg@ucsd.edu

Recent experiments [1, 2] and modeling [3, 4] have shown that the large-scale preplasma significantly affects the laser-plasma interaction (LPI) dynamics and the resultant fast electron energy distribution, where the fast electron energies are much higher than the ones predicted by ponderomotive scaling due to additional stochastic acceleration in the low density region. We have carried out comprehensive numerical simulations using the Large Scale Plasma (LSP) code to investigate the dynamics of LPI and fast electron source generation as a function of laser pulse length, and preplasma density scale length. We confirmed that the most energetic electrons are generated through the synergistic effects of the interaction of electrons with both electrostatic potential well in preplasma and laser radiation. We have performed 2D simulations showing both formation of deep electrostatic well and very energetic electrons with spectra similar to we obtained in 1D simulations. These effects were more prevalent for pulse durations longer than 1 ps. We also found filamentation of the laser field causing an increase of the radiation field intensity. However, this increase was insufficient to significantly alter the high-energy part of electron distribution. We have carried out experiments using the Texas Petawatt Laser to validate modeling predictions. In these experiments we used an artificial laser prepulse to create well-defined prepalsma. We used a proton beam produced from a second short-pulse laser to probe the electric field in the extended plasma and its correlation with fast electron energies. Both experimental results and comparison with numerical simulations will be presented at the meeting and its relevance to fast ignition inertial confinement fusion will be discussed.

The work has been supported by the Department of Energy under contract DE-NA0001858.

References

- [1] S. D. Baton et al., Phys. Plasmas 15, 042706 (2008).
- [2] T. Yabbuchi et al., Phys. Plasmas, 17, 060704 (2010).
- [3] B. S. Paradkar et al., Phys. Rev. E 83, 046401 (2011).
- [4] B. S. Paradkar et al., Phys. Plasma 19, 060703 (2012).

Preprint Slides

Conception of a Cryogenic Target Factory for IFE

E. Koresheva¹, I. Aleksandrova¹, E. Koshelev¹, B. Kuteev², A. Nikitenko¹, V. Nikolaev³, and I. Osipov³

¹P. N. Lebedev Physical Institute, RAS, Moscow, Russian Federation ²National Research Centre "Kurchatov Institute", Moscow, Russian Federation ³Power Efficiency Center INTER RAO UES, Moscow, Russian Federation

Corresponding Author: E. Koresheva, elena.koresheva@gmail.com

A central feature of an inertial fusion energy (IFE) power plant is a target that must be delivered to the target chamber center at a rate of about 1–15 Hz. A high rep-rate target supply system, which operates with moving free-standing targets (FST) is the culmination of a 25-year science-and-technology effort of the Lebedev Physical Institute (LPI) in collaboration with other Russian Institutes. This report provides an overview of our research activities towards realization of the FST target supply system for IFE including high rep-rate cryogenic target production, transport, and tracking:

- 1. Cryogenic target mass production: the FST layering method has been developed for rapid fuel layering via heat conductivity in moving free-standing targets. A batch mode is applied, and high cooling rates (q = 1-50 K/s) are maintained to form isotropic ultra-fine solid layers inside free-rolling targets. The total layering time is typically less than 15 s, which has a side benefit in the view of tritium inventory minimization. A spherically symmetric layer with a uniform thickness and acceptable surface quality have such a structure, which supports the fuel layer survivability under target injection and transport through the reaction chamber.
- 2. Cryogenic target transport:
 - Gravitational target transport was demonstrated at cryogenic temperatures, including the assembly of a couple "target and sabot". A design of the corresponding device was developed.
 - Electromagnetic target transport in the couple of "target and sabot" was demonstrated at cryogenic temperatures. A device for injecting the fusion cryogenic targets at the laser focus of a reaction chamber was developed.
 - Magnetic levitation transport. Our recent results (successfully made at T = 6-80 K) have shown that maglev transport systems based on using high-temperature superconductors (HTSC) is an excellent springboard for the development of IFE cryogenic target positioning and transport systems, including a new type of cryogenic target accelerators — a magnetic levitation accelerator.
- 3. Injected target tracking: Fourier holography was proposed and examined in the computer experiments for on-line characterization and tracking of a flying target.



A High-Energy and Highly Repetitive fs/ps Laser Using Optical Parametric Chirped-Pulse Amplification with a ns Beam Combined Pumping Laser for Fast Ignition

H. J. Kong¹, J. Oh¹, S. Park¹, S. Cha¹, J. S. Kim², K. Churn¹, and B. J. Lee³

¹Korea Advanced Institute of Science and Technology, Daejeon, Korea, Republic of ²Laser Spectronix, Seoul, Korea, Republic of ³Department of AGEE, HGU, Pohang, Korea, Republic of

Corresponding Author: H. J. Kong, hjkong@kaist.ac.kr

The authors propose the high-energy and high repetitive fs/ps laser system which uses the output beam of a coherent beam combination laser using stimulated Brillouin scattering phase conjugate mirrors (SBS-PCMs) as the pump beam of optical parametric chirped-pulse amplification (OPCPA). To verify the feasibility of the OPCPA system, the authors will utilize 4 kW (4×0.1 J @ 10 kHz/10 ns) Kumgang laser for the pump beam of the OPCPA. The authors expect that fast ignition can be realized with the coherent-beam combination laser for compression and the fs/ps laser using the OPCPA system for ignition.



Energy Transport by MeV Hot Electrons in Fast Ignition Plasma Driven with LFEX PW Laser

Z. Zhang¹, H. Nishimura¹, S. Fujioka¹, Y. Arikawa¹, M. Nakai¹, T. Ozaki², H. Chen³, J. Park³, G. J. Williams³, H. Shiraga¹, S. Kojima¹, M. Alessio¹, H. Nagatomo⁴, T. Johzaki⁵, A. Sunahara⁶, N. Miyanaga¹, J. Kawanaka¹, Y. Nakata¹, T. Jitsuno¹, and H. Azechi¹

¹Institute of Laser Engineering, Osaka University, Osaka, Japan ²National Institute for Fusion Science, Toki, Japan ³Lawrence Livermore National Laboratory, Livermore, CA, USA ⁴Osaka University, Osaka, Japan ⁵Graduate School of Engineering, Hiroshima University, Higashi-Hiroshima, Japan ⁶Institute for Laser Technology, Suita, Osaka, Japan

Corresponding Author: Z. Zhang, zhang-z@ile.osaka-u.ac.jp

The absolute energy transfer efficiency from laser to hot electrons in fast ignition plasma was estimated by applying quantitative high energy K_{α} X-ray spectroscopy. The absolute yield of Sn, Ta, and Au K_{α} lines were measured by a calibrated Laue spectrometer. The Laue spectrometer was developed to cover the high energy K_{α} lines from Mo ($K_{\alpha} = 17.48$ keV) to Au ($K_{\alpha} = 68.80$ keV). Absolute calibrations have been carried out for the crystal and detector separately by using precalibrated laser produced K_{α} sources and radiation isotopes. The hot electron propagation inside the solid target and K_{α} photon generation is simulated by Monte-Carlo. Considering the K_{α} photon number measured by the Laue spectrometer, the transfer efficiencies were estimated by comparing the experimental measurement and simulation results.

The transfer efficiencies from LFEX to target were estimated with planar and cone-guided geometries. Four types of cone were used: the standard Au cone with 7 μ m thickness; an open Au cone without tip; a W-shape Au cone with double Au layers; and a diamond like carbon (DLC) cone. The transfer efficiencies of LFEX laser to a guiding-cone was found to be much higher than the planar target case, and was quantified to be between 20% to 50%.



IFE/P6-3

Fast Ignition Experiments and Intense Hard-X-Ray Harsh Environment

H. Shiraga¹, Y. Arikawa¹, K. Mayuko², M. Nakai¹, T. Ozaki³, S. Fujioka¹, H. Nishimura¹, and H. Azechi¹

¹Institute of Laser Engineering, Osaka University, Osaka, Japan ²University of Hyogo, Himeji, Japan ³National Institute for Fusion Science, Toki, Japan

Corresponding Author: H. Shiraga, shiraga@ile.osaka-u.ac.jp

Fast ignition (FI) experiments have been performed at the Institute of Laser Engineering, Osaka University by using Gekko-XII laser for implosion and LFEX laser for fast heating of fuel targets. In FI experiment with intense heating laser irradiation (> 10^{19} W/cm²), most of heating laser energy is converted to that of hot electrons with energy ranging well up to several 10 MeV. Intense hard X-rays (or so-called " γ rays" in terms of the photon energy) are generated from hot electrons via Bremsstrahlung in the target material. Such high-energy photons are a real threat as intense background signals to the X-ray and neutron diagnostics. Neutrons generated via (γ , n) reactions taking place in and around the target chamber are also a threat to the neutron diagnostics. We found that FI experiments are in such a γ ray and neutron harsh environment, and evaluated those conditions which have never been experienced in conventional laser-plasma experiments. We have developed many new plasma diagnostics that are compatible with such a γ ray and neutron harsh environment. FI physics- and integrated-experiments have been successfully performed with those improved plasma diagnostics with much better accuracy than in the previous experiments even in such a γ ray and neutron harsh environment. These works are also useful as test pilot experiments for future experimental fusion reactors in which much more harsh environment is anticipated.



Plasma Mirror technology on a PW, multi-kJ class Laser to reduce the pre-formed plasma for application to Fast Ignition research.

A. Morace¹, H. Shiraga¹, M. Nakai¹, Y. Arikawa¹, H. Azechi¹, K. Kondo², H. Nishimura¹, and A. Sagisaka²

¹Institute of Laser Engineering, Osaka University, Osaka, Japan ²Japan Atomic Energy Agency, Naka, Japan

Corresponding Author: A. Morace, morace@ile.osaka-u.ac.jp

In the Fast Ignition scheme, the heating of the compressed Deuterium Tritium capsule is produced by a fast electron beam generated by an ultra-high intensity laser pulse, transporting the laser energy from the interaction region up to the compressed DT fuel and producing a one-sided hot spot, from which the thermonuclear burst propagates to the rest of the fuel. In order to achieve ignition, the fast electron average temperature is required to be within the 1–2 MeV range in order to efficiently deposit the energy in a small volume of the compressed core, while the typical fast electron spectrum, instead, presents a large amount of energy carried by high energy electrons (≥ 5 MeV). This large hot electron temperature is believed to be associated to the formation of a relatively long scale length preformed plasma, related to the presence of a pedestal preceding the main laser pulse. In this work we propose a method to further reduce the fast electron average energy by reducing the pre-plasma scale length, by implementing a Plasma Mirror (PM) device on LFEX laser.

The first test of the PM has been successfully performed at LFEX laser, a multi-PW class laser, capable in the current development state, to deliver up to 2 kJ of laser energy at 1 ω (1053 nm) in about 1.5 ps. The first stage of the experiment consisted in the characterization of the PM reflectivity versus laser energy fluence, using LFEX laser with a reduced pulse energy of ~ 1 J, giving equivalent condition for high power interaction. The fluence on the PM was varied by varying the distance between the PM and target chamber center (TCC), where the LFEX beams are focused. As theoretically expected, a reflectivity of ~ 50% is found for LFEX fluences above 40 J/cm².

The second stage of the experiment consisted in measuring the TNSA proton energy obtained focusing the LFEX beam after PM, for a LFEX pulse energy of about 300 J corresponding to 150 J on target and 1.5 ps pulse duration, on a thin 3 μ m Al foil, and a peak proton energy above 3 MeV has been obtained.

In conclusion, we confirmed and demonstrated that the Plasma Mirror Technology can be successfully implemented on LFEX laser, and work at pulse conditions relevant for the FIREX project at ILE, Osaka University.



Control of Electron Beam Using Strong Magnetic Field for Efficient Core Heating in Fast Ignition

T. Johzaki¹, T. Taguchi², S. Atsushi³, H. Nagatomo⁴, H. Sakagami⁵, K. Mima⁶, S. Fujioka⁴, and H. Shiraga⁴

 ¹Graduate School of Engineering, Hiroshima University, Higashi-Hiroshima, Japan
 ²Department of Electrical and Electronics Engineering, Setsunan University, Osaka, Japan
 ³Institute for Laser Technology, Suita, Osaka, Japan
 ⁴Institute of Laser Engineering, Osaka University, Osaka, Japan
 ⁵National Institute for Fusion Science, Toki, Japan
 ⁶Graduate School for the Creation of New Photonics Industries, Hamamatsu, Shizuoka, Japan

Corresponding Author: T. Johzaki, tjohzaki@hiroshima-u.ac.jp

One of the most crucial issues of fast ignition is efficient core heating by laser produced fast electron beam. The main factors in preventing efficient heating are: 1) too high fast-electron energy and 2) too large beam divergence. The fast electron energy could be controlled by eliminating pre-plasma generation and by using heating laser with shorter wavelength. With respect to the beam divergence, it is difficult to control the angular spread of fast electrons since laser-plasma interactions are the nonlinear phenomena. To control the electron beam, we propose the beam guiding using self-generated and externally applied magnetic fields. In the present paper, we demonstrate: 1) the suppression of the Weibel instability in the low density plasma close to the laser-plasma interaction region, and 2) a sufficient beam guiding performance in the dense region (propagation region from interaction region to the core) by applying kT-class external magnetic fields on the basis of the numerical simulations. It is found that a sufficient enhancement of core heating efficiency is expected from the both effects.



Computational Study of Magnetic Field Compression by Laser Driven Implosion

H. Nagatomo¹, T. Johzaki², A. Sunahara³, K. Mima⁴, H. Sakagami⁵, A. Nishiguchi⁶, T. Sano⁷, S. Fujioka⁷, H. Shiraga⁷, and H. Azechi⁷

¹Osaka University, Osaka, Japan
²Graduate School of Engineering, Hiroshima University, Higashi-Hiroshima, Japan
³Institute for Laser Technology, Suita, Osaka, Japan
⁴Graduate School for the Creation of New Photonics Industries, Hamamatsu, Shizuoka, Japan
⁵National Institute for Fusion Science, Toki, Japan
⁶Osaka Institute of Technology, Osaka, Japan
⁷Institute of Laser Engineering, Osaka University, Osaka, Japan

Corresponding Author: H. Nagatomo, naga@ile.osaka-u.ac.jp

A compression of external magnetic field by a laser driven implosion is studied using two dimensional radiation hydrodynamic simulation. The simulation results show that: i) it is possible to compress the magnetic field to be 10 kT (10^8 G), and ii) the strong magnetic field should affect the implosion dynamics because of the suppression of the electron heat flux which across strong magnetic field lines. This result suggest that a target and initial conditions for fast ignition with external magnetic field must be designed carefully not only for the control of the hot electron transport but also for the formation of high dense plasma.

High Compression of Matter by Hyperspherical Shock Waves for Application to Impact Ignition

M. Murakami¹, J. Sanz², and Y. Iwamoto³

¹Institute of Laser Engineering, Osaka University, Osaka, Japan ²ETSI Aeronauticos, Universidad Politecnica de Madrid, Spain ³Graduate School of Ehime University, Ehime, Japan

Corresponding Author: M. Murakami, murakami-m@ile.osaka-u.ac.jp

To achieve substantially high compression performance of the impact ignition, a novel compression scheme is proposed, in which hollow targets with specifically curved structures initially filled with uniform matter, are driven by converging shock waves. i) Its self-similar dynamics is analyzed in detail. ii) The dynamic behavior is demonstrated using two-dimensional hydrodynamic simulations. iii) A rigorous linear perturbation analysis is proposed, which gives a new dispersion relation with cut-off mode numbers as a function of the specific heat ratio, above which eigenmode perturbations are smeared out in the converging phase.

This study provides: 1) a new scheme achieving super-high compression via strong shock with the special geometries as another path to achieve high pressures via orthodox adiabatic compression; and 2) a rigorous perturbation analysis to give the new growth rates that are significantly different from the widely accepted prediction. These new knowledge is expected to be applied to "Impact Ignition" — an advanced scheme of ICF, in terms of the reshaped cone casing that works as igniter.



Stabilization Effect of Weibel Modes in Relativistic Laser Fusion Plasma

A. Sid¹, S. Belghit¹, and A. Ghezal²

¹PRIMALAB laboratory, University of Batna, Algeria ²COMENA, Algeria

Corresponding Author: A. Sid, a_sid@univ-batna.dz

In this work, the Weibel instability due to inverse bremsstrahlung (IB) absorption in laser fusion plasma has been investigated. The stabilization effect due to the coupling of the self-generated magnetic field by Weibel instability with the laser wave field is explicitly showed. In this study, the relativistic effects are taken into account where the basic equation is the relativistic Fokker-Planck (F-P) equation.

The main obtained result is that the coupling of self generated magnetic field with the laser wave causes a stabilizing effect of excited Weibel modes. We found a decrease in the spectral range of Weibel unstable modes. This decreasing is accompanied by a reduction of two orders in the growth rate of instability or even stabilization of these modes. It has been shown that the previous analysis of the Weibel instability due to IB have overestimated the values of the generated magnetic fields. Therefore, the generation of magnetic fields by the Weibel instability due to IB should not affect the experiences of inertial confinement fusion.

1000 Times Enhancement of Fusion Reaction in Relation to Fast-Ion Heating Induced by a Direct-Irradiating Fast-Ignition Scheme

Y. Mori¹, Y. Nishimura¹, R. Hanayama¹, K. Ishii¹, K. Fujita¹, S. Okihara¹, Y. Kitagawa¹, T. Sekine², N. Satoh², T. Kurita², M. Takagi², T. Watari², T. Kawashima², H. Kan², A. Sunahara³, Y. Sentoku⁴, O. Komeda⁵, N. Nakamura⁵, T. Kondo⁵, M. Fujine⁵, H. Azuma⁶, T. Motohiro⁶, T. Hioki⁶, M. Kakeno⁶, E. Miura⁷, Y. Arikawa⁸, T. Nagai⁸, Y. Abe⁸, T. Ozaki⁹, and A. Noda¹⁰

 ¹Graduate School for the Creation of New Photonics Industries, Hamamatsu, Shizuoka, Japan
 ²Hamamatsu Photonics, K.K., Japan
 ³Institute for Laser Technology, Suita, Osaka, Japan
 ⁴University of Nevada, Reno, USA
 ⁵TOYOTA Motor Corporation, Japan
 ⁶TOYOTA Central Research and Development Laboratories Inc., Japan
 ⁷National Institute of Advanced Industrial Science and Technology, Tokyo, Japan
 ⁸Institute of Laser Engineering, Osaka University, Osaka, Japan
 ⁹National Institute for Fusion Science, Toki, Japan
 ¹⁰Advanced Research Center for Beam Science, Institute for Chemical Research, Kyoto University, Japan

Corresponding Author: Y. Mori, ymori@gpi.ac.jp

For inertial confinement fusion, the high-density compression and core heating are essential processes. National Ignition Facility (NIF) is a promising candidate for the development of a fusion power plant. However, a self-ignition scheme, that is, to burn the core in implosion itself is not as straightforward as expected. A potential solution for this is the fast-ignition scheme, because this scheme can separate and optimize the process of fuel compression and its heating respectively. In this paper, we proposed and performed a new-scheme fast-ignition which includes direct ion heating of an imploded core. The Laser for Fast Ignition Experiment (LFEX) directly heated a pre-imploded core, enhancing D(d, n)³He–reaction neutron (DD neutron) yields by a factor of 1000 (5 × 10⁸ n/4 π sr) from that of pre- imploded core. This is the best ever obtained in fast-ignition scheme. Temperature of a part of the core increased by a factor of two, i.e., from 0.8 keV to 1.8 keV. The laser-driven hot electrons and fast ions contribute to the core heating. The thermal fusion neutron yield of $6.4 \times 10^7 \text{ n}/4\pi$ sr also breaks the previous record of 2×10^7 n/4 π sr. STAR ID hydro-code predicts that deuterons are related to beam fusion and carbons to thermal fusion, respectively. The proposed scheme here is a potential path to fast-ignite the core at high gain fusion. We would like to stress two points: 1) Not only hot electrons, but also energetic ions can fast ignite the core; 2) The neutron yield has increased as high as 1,000 times than that achieved before, which is a record of the fast ignition scheme.



Counter Implosion of 500 μ m Diameter CD Shell and Fast Heating of its Core Plasma by Tailored DPSSL-Pumped Laser

Y. Nishimura¹, Y. Mori¹, Y. Kitagawa¹, R. Hanayama¹, K. Ishii¹, S. Nakayama¹, T. Sekine², T. Kurita², N. Sato², T. Kawashima², H. Kan², O. Komeda², T. Kondo², M. Fujine², H. Azuma³, T. Hioki³, T. Kajino³, T. Motohiro³, S. Oshima³, A. Sunahara⁴, E. Miura⁵, and Y. Sentoku⁶

 ¹The Graduate School for the Creation of New Photonics Industries, Toyota Technical Development Corporation, Japan
 ²TOYOTA Motor Corporation, Japan
 ³TOYOTA Central Research and Development Laboratories Inc., Japan
 ⁴Institute for Laser Technology, Suita, Osaka, Japan
 ⁵National Institute of Advanced Industrial Science and Technology, Tokyo, Japan
 ⁶University of Nevada, Reno, USA

Corresponding Author: Y. Nishimura, yasuhiko2460@gpi.ac.jp

Laser fusion experiment extracts net energy from fuel on the National Ignition Facility (NIF) by using 1.8 MJ, 500 TW single shot laser. Following an effort of this scientific proof of ignition, engineering development needs to start on Inertial Fusion Energy (IFE) by using a repetitive fusion driver. To realize the IFE power plant, one key issue is a high-repetition-rate laser of kJ-class or greater. Others are the fuel fabrication and high-repetition injection, and ignition-high gain physics. And also, Power plant technology, such as innovative wall materials, will need to be developed. So, we are researching and developing to aiming at the early realization of a compact laser fusion experimental mini-reactor. In the latest results of our research, the basic experiment of the fast-ignition scheme with the counter-illumination was obtained a core overheating by Diode Pumped Solid State Laser (DPSSL) system in a small laboratory. For the purpose of high-repetitive implosion and heating of $500 \ \mu m$ in diameter shell targets, we, for the first time, developed a fast-ignition scheme tailored pulse DPSSL system. The tailored implosion beam consists of a preceding foot pulse "K" from KURE-1 (4.4 J, 1053 nm, 15.2 ns) and a main chirped pulse from HAMA (1.4 J, 800 nm, 300 ps). The heating beam "S" is a pulse-compressed beam "L" from HAMA (1.0 J, 800 nm, 192 fs). We divide each beam into two counter beams. The target is a deuterated polystyrene (CD) shell-target of 500 μ m in diameter and 7 μ m in thickness. Two counter tailored beams successfully imploded the shell to form a core plasma, which S-Beam heated and yielded DD neutrons of $10^4 \text{ n}/4\pi$ sr. The system works each 10 ms. STAR1D hydrocode well predicted the results. In this presentation, we will describe the tailored HAMA laser system for the shell implosion and heating and the preliminary results, as well as the simulations.



1Hz Pellets Injection and Laser Synchronous System for Continuous Laser Confinement Fusion and Neutron Generation

R. Hanayama¹, O. Komeda², Y. Nishimura¹, Y. Mori¹, K. Ishii¹, Y. Kitagawa¹, T. Sekine³, N. Satoh³, T. Kurita³, T. Kawashima³, H. Kan³, N. Nakamura², T. Kondo², M. Fujine², H. Azuma⁴, T. Motohiro⁴, T. Hioki⁴, M. Kakeno⁴, Y. Sentoku⁵, A. Sunahara⁶, and E. Miura⁷

 ¹Graduate School for the Creation of New Photonics Industries, Hamamatsu, Shizuoka, Japan
 ²TOYOTA Motor Corporation, Japan
 ³Hamamatsu Photonics, K.K., Japan
 ⁴TOYOTA Central Research and Development Laboratories Inc., Japan
 ⁵University of Nevada, Reno, USA
 ⁶Institute for Laser Technology, Suita, Osaka, Japan
 ⁷National Institute of Advanced Industrial Science and Technology, Tokyo, Japan

Corresponding Author: R. Hanayama, hanayama@gpi.ac.jp

We succeeded in injection of spherical deuterated polystyrene bead pellets at 1 Hz and symmetrical engagement and irradiation of them with two ultra-intense laser beams. i) This is the first demonstration of ultra-intense laser engagement of injected flying pellets. The laser intensity was high enough to produce a DD neutron yield of $9.5 \times 10^4/4\pi$ sr/shot. ii) We observed channel formation through the free-falling pellets, which might be the evidence to support a scheme for fast ignition. Deuterated polystyrene (CD) beads whose diameter is 1 mm are used as pellets. Each pellet free-falls to the laser focal point 18 cm below at 1 Hz. The signals from the two photodiodes above the focal point are sequentially sent to a laser controller, which forecasts the arrival time at the focal point and sends a shooting-request signal to the diode-pumped, ultra-intense laser HAMA appropriately. As soon as HAMA receives the signal, its two laser beams are emitted onto the injected pellet with an appropriate delay time. In experiments, up to 1,300 continuous injections were successfully demonstrated. Currently, pellets are successfully engaged by two counter laser beams at a probability of about 70%. The laser energy, pulse duration, wavelength, and the intensity were 0.63 J per beam, 104 fs, and 811 nm, 4.7×10^{18} W/cm², respectively. In 7% of engaged shot, neutron generation was observed. The maximum yield of produced neutrons is $9.5 \times 10^4/4\pi$ sr/shot, four times larger than that of single beam experiment, although the total laser energy is similar at 1.2 J. Moreover, the laser is found out to bore a straight channel with 10 μ m-diameter through a bead. One possible explanation about channel boring is as follows: Free-electrons generated by the pre-pulse and pedestal components of the laser pulse might work as a guiding wire for the fast-electrons generated by the main high intensity pulse using the guiding wire. The intense laser is expected to transport sufficient energy along the path from the focal point to the core. We conceived this idea of hole boring, as a means for obtaining a clean path from the focal point to the core. The hole boring observed in this experiment can be applied for the fast-ignition.

Preprint

Conceptual Design of kilo-Joule Laser Driver for Inertial Fusion Mini-Reactor CANDY

T. Sekine¹, T. Kurita¹, N. Satoh¹, T. Kawashima¹, H. Kan¹, Y. Mori², S. Nakayama², R. Hanayama², K. Ishii², Y. Kitagawa², O. Komeda³, T. Kondo³, M. Fujine³, H. Azuma⁴, T. Motohiro⁴, T. Hioki⁴, T. Kajino⁴, S. Oshima⁴, Y. Nishimura², Y. Sentoku⁵, A. Sunahara⁶, and E. Miura⁷

¹Hamamatsu Photonics, K.K., Japan ²Graduate School for the Creation of New Photonics Industries, Hamamatsu, Shizuoka, Japan ³TOYOTA Motor Corporation, Japan ⁴TOYOTA Central Research and Development Laboratories Inc., Japan ⁵University of Nevada, Reno, USA ⁶Institute for Laser Technology, Suita, Osaka, Japan ⁷National Institute of Advanced Industrial Science and Technology, Tokyo, Japan

Corresponding Author: T. Sekine, t-sekine@crl.hpk.co.jp

Development of a kilo-Joule class diode-pumped solid-state laser (kJ-DPSSL) as a beam line of Mega-Joule class driver is necessary for realization of inertial fusion energy. We conceptually designed a kJ-DPSSL for an inertial fusion mini-reactor CANDY. The CANDY is the kJ-DPSSL driven integrated fusion mini-reactor based on fast ignition scheme. The driver consists of two implosion laser drivers in 0.5- μ m wavelength and two heating laser drivers in 1- μ m wavelength. Each beam irradiates 1 kJpulse energy at 10 Hz repetition rate. The implosion beam has a temporary tailored pulse shape and the heating beam has 0.2 to 10 ps pulse duration. The implosion and heating beams coaxially counter-irradiate a fuel pellet. These key components which construct kJ-DPSSL driver have been technologically and economically assessed based on our fusion research. We have started construction of repetitive inertial fusion experimental system based on the 20-J-DPSSL. The DPSSL KURE-I (12 J in 527 nm with 10 ns at 1 Hz)-pumped HAMA laser (3.8 J in 800 nm with 100 fs at 1 Hz) is used for an inertial confinement fusion experiment as a feasibility study. Counter irradiation fusion driver consists of tailored-implosion pulses with heating ultra-intense pulses have been developed for optimization of fusion reaction. And physical studies about fast-heating and some technological developments of repetitive target injection have been achieved. These result indicate that development of the kJ-DPSSL dramatically progress study of reactor core physics, cryogenic pellet-injection and reactor wall. The assessment for feasible program has clarified the design criteria including the cost of diode, laser materials, and optics, as well as the lead time for the research, development and system construction.

Increasing Laser Power Density towards IFE Requirements: High-Power Laser Diode Bars

M. Wölz¹, A. Pietrzak¹, A. Kindsvater², J. Meusel², K. Stolberg², R. Hülsewede¹, and J. Sebastian¹

¹JENOPTIK Diode Lab GmbH, Berlin, Germany ²JENOPTIK Laser GmbH, Jena, Germany

Corresponding Author: M. Wölz, martin.woelz@jenoptik.com

The feasibility of inertial confinement fusion depends critically on the laser drivers. Advances in the light power density and the efficiency are still to be made. We present an overview of the fundamental limitations of laser diode arrays, which are used for pumping the solid state lasers, and show which steps the industry has taken so far in order to achieve the ambitious goals.

The pump power requirements of large-scale projects such as LIFE or HiPER are within reach of semiconductor laser diode assemblies. Pulsed light output powers per laser bars have been around 300 W per bar, as in the JENOPTIK 940 nm bars previously used for pumping the Yb:YAG slabs in the DiPOLE project. By redesigning the semiconductor laser structures the peak power is now increased to 500 W per bar for 808 nm, 880 nm and 940 nm pump wavelengths.

The second important aspect of high pump power densities is dense array packaging of the laser bars. To this end, a scalable QCW stack for conductive cooling is under development at JENOPTIK. Design-to-cost is a must if inertial fusion power plants are to become reality. The new diode array follows this rule: compared to the standard assembly, manufacturing is simplified by simultaneous solder joining of submounts and ceramics. At the same time, the stack is engineered for reliability by the choice of materials. We illustrate this assembly technique that paves the way to automation and further reduction in cost-per-Watt.

The construction of one inertial fusion power plant will require a number of semiconductor laser chips in excess of the current annual production by two orders of magnitude. This adds to the engineering task of improving the device characteristics a challenge to production. While the industry benefits from the recent boost in solid state lighting that acts as a technology driver, cooperation between manufacturers will be imperative, and to this end we present standardization efforts.

Preprint

The Perspectives of the Use of the Advanced Fuels for Power Production

M. Shmatov¹

¹Ioffe Physical-Technical Institute of the Russian Academy of Science, St. Petersburg, Russian Federation Corresponding Author: M. Shmatov, m.shmatov@mail.ioffe.ru

The use of the D-D fusion reactions for power production has been discussed for many years. The main advantage of the power plants employing these reactions consists in a lower amount of tritium involved in the process. Ignition of the D-D fusion reactions is a more difficult task compared to the ignition of the D-T fusion reaction. For power plants with the magnetic plasma confinement, the use of the D-D and D-³He fusion reactions in the observable future will probably be impossible or at least inexpedient [1]. Ignition of deuterium explosions by the fission explosions is the most technically simple approach to using the D-D fusion reactions for power production [2], but this approach seems to be politically unacceptable.

The problem of using microexplosions with physically important reactions of D-D fusion for power production was discussed rather widely. The compression of a fuel with small or zero average atomic fraction of tritium using laser or other driver with very high parameters, and, hence, very high cost is only one of the possible approaches. The most effective approaches are those in which the compression of such fuel is caused entirely or mostly by thermal radiation of one or several D-T microexplosions [3, 4]. For realization of these approaches, the driver with the parameters corresponding to ignition of D-T microexplosions with the yields of about 1 GJ or less will be sufficient [4].

The use the $p^{-11}B$ reaction for power production in the scenarios with heating the fuel by the picosecond duration, petawatt power laser pulses without its compression was proposed [5]. However, the use of this method for power production is impossible, because the transversal expansion of the plasma would result in the very low fuel burning efficiencies corresponding to the acceptable laser pulse energies and fusion yields.

References

[1] Stott P.E., Plasma Phys. Control. Fusion 47, 1305 (2005).

[2] Ivanov G.A. et al., Vzryvnaya Deiterievaya Energetika, Snezhinsk, RFYaTs - VNIITF (2004).

[3] Winterberg F., J. of Fusion Energy 2, 377 (1982).

[4] Shmatov M.L., Pis'ma v ZhTF 36, No. 8, 82 (2010) [Tech. Phys. Lett. 36, 386 (2010)].

[5] Hora H. et al., Energy Environ. Sci. 3, 479 (2010).

Materials Physics and Technology



Overview of Fusion Reactor Materials Study at SWIP

X. Liu¹, J. Chen¹

¹Southwestern Institute of Physics, Chengdu, Sichuan, China

Corresponding Author: X. Liu, xliu@swip.ac.cn

Development of materials is an important issue for the future nuclear fusion reactors. In this paper, the developments and main achievements of fusion reactor materials at Southwestern Institute of Physics (SWIP) are overviewed by focusing on the plasma facing materials and components (PFMs/PFCs), structural materials, and functional materials. For PFMs/PFCs, an ITER grade high purity tungsten and the CVD-W coating with a fast deposition rate up to 0.5 mm/h have been developed and characterized. High heat flux components fabricated by joining them with CuCrZr alloy have been developed, which can provide a simple and economics method for the construction of W first wall and divertor in the current fusion devices. For structural materials, two kinds of low activation materials are developed, one is a reduced activation ferritic/martensitic (RAFM) steel, named as CLF-1, aiming at the near team use, such as ITER-TBM and CFETR. The other one is V-4Cr-4Ti alloy, aiming at future applications in the next generation fusion reactors. Compared with other RAFM steels, such as Eurofer 97 or F82H, CLF-1 has similar chemical compositions, but N is selected as a controllable element and has slightly higher content, which induces higher tensile strength, in particular better high-temperature creep performances. As to vanadium alloys, a 30 kg engineering-scale ingot of V-4Cr-4Ti alloy has been prepared by melting, and mechanical alloying has been used for dispersion strengthening with different particles, such as Y₂O₃, TiC, SiC and Ti₃SiC₂. Preliminary results indicate the newly designed multi-component alloy V-4Cr-4Ti-1.5Y-0.3Ti₃Si- C_2 has the most efficient strengthening effect and the best thermal stability. In the case of functional materials, tritium breeder and neutron multiplier materials are developed for the fabrication of ITER-Chinese Helium Cooled Ceramic Breeder Test Blanket Module (CN HCCB TBM), and the potential application in CFETR. Moreover, some of the specialized facilities have been constructed at SWIP, a comprehensive capability for development, evaluation and testing of materials/components is being established.

Molecular Dynamics and Density Functional Simulations of Tungsten Nanostructure Formation by Helium Plasma Irradiation

A. M. Ito¹, A. Takayama¹, Y. Oda¹, T. Tamura², R. Kobayashi², T. Hattori², S. Ogata², N. Ohno³, S. Kajita³, M. Yajima³, Y. Noiri³, Y. Yoshimoto⁴, S. Saito⁵, S. Takamura⁶, T. Murashima⁷, M. Miyamoto⁸, and H. Nakamura¹

¹National Institute for Fusion Science, Toki, Japan
 ²Nagoya Institute of Technology, Aichi, Japan
 ³University of Nagoya, Nagoya, Japan
 ⁴Tottori University, Tottori, Japan
 ⁵Kushiro National College of Technology, Japan
 ⁶Aichi Institute of Technology, Japan
 ⁷Tohoku University, Sendai, Japan
 ⁸Shimane University, Japan

Corresponding Author: A. M. Ito, ito.atsushi@nifs.ac.jp

The tungsten nanostructure induced by helium plasma irradiation had been found by the experimental researches for the plasma facing materials in fusion reactors. For the generation of the tungsten nanostructure, it is concerned about the decrease of the maximum allowable heat load and the erosion by arcing on the surface. To clear these problem, we had researched on the formation mechanisms of the tungsten nanostructure by using molecular dynamics (MD), density functional theory (DFT), and other simulation methods.

The diffusion and agglomeration of helium in tungsten material were investigated by DFT calculation. As a result, the binding energy of helium atoms at interstitial site is about 1.5 eV comparable to that at mono-vacancy, about 2.5 eV [1]. This reason is that the electron density in the region around the interstitial site trapping a noble gas atom decreases and then this region also becomes new trap site for the other noble gas atoms [2]. The migration barrier energy of a helium atom in tungsten material is third part of that of a hydrogen atom. Moreover, the migration barrier energies of helium dimer and trimer at an interstitial site are much smaller than that of single helium atom. These facts imply that helium atoms can be spontaneously agglomerated at interstitial site.

The nanostructure formation on the surface was calculated by MD using developed high accuracy potential model [3]. According to our simulation result, the tungsten nanostructure formation proceeds as follows: The growth of helium bubbles generated the foam structure of tungsten which means nano-walls separating the helium bubbles. Simultaneously, the foam structure in the region close to the surface was lifted up by the helium bubble swelling in the bulk region. Strictly speaking, the foam structure created by the MD is not fuzzy fibered and then the MD is considered as early formation phase of tungsten nanostructure. We suggest that the foam structure changes to porous structures due to the bursting of helium bubbles and it can transform to the fuzzy structure by the surface diffusion.

References

[1] T. Tamura, R. Kobayashi, S. Ogata, A.M. Ito, Modelling Simul. Mater. Sci. Eng. 22 (2014) 015002.

[2] A. Takayama, A.M. Ito, S. Saito, et al., Jpn. J. Appl. Phys. 52 (2013) 01AL03.

[3] A.M. Ito, Y. Yoshimoto, S. Saito, et al., Phys. Scr. in Press.

629





Neutron Irradiation Effects on Grain-Refined W and W-Alloys

A. Hasegawa¹, M. Fukuda¹, T. Tanno², S. Nogami¹, K. Yabuuchi¹, T. Tanaka², and T. Muroga²

¹Tohoku University, Sendai, Japan ²Japan Atomic Energy Agency, Naka, Japan

Corresponding Author: A. Hasegawa, akira.hasegawa@qse.tohoku.ac.jp

Microstructural data of neutron irradiated W such as size and number density of voids and precipitates obtained by W up to 1.5 dpa irradiation in the temperature range of 400–800°C were compiled quantitatively. Nucleation and growth process of these defects were clarified and a qualitative prediction of the damage structure development and hardening of W in fusion reactor environments were made taking into account the solid transmutation effects for the first time. Irradiation behavior of grain-refined W-alloys, produced by K- or La-doping, was also examined. Expected radiation resistant W-alloys, by combined Re addition and the grain refining process, were fabricated and characterization of unirradiated state were performed.

RF Discharge for In-Situ Mirror Surface Recovery in ITER

A. Razdobarin¹, P. Andrew², V. Bukhovets³, I. Bukreev¹, P. Chernakov¹, A. Gorodetsky³, M. Kochergin¹, A. Koval¹, G. Kurskiev¹, F. Leipold², A. Litvinov¹, A. Markin³, S. Masyukevich¹, I. Miroshnikov⁴, E. Mukhin¹, R. Reichle², D. Samsonov¹, V. Semenov¹, S. Tolstyakov¹, M. Walsh², R. Zalavutdinov³, and A. Zakharov³

 ¹Ioffe Physical-Technical Institute of the Russian Academy of Science, St. Petersburg, Russian Federation
 ²ITER Organization, Saint Paul lez Durance, France
 ³A. N. Frumkin Institute of Physical Chemistry and Electrochemistry, RAS, Moscow, Russian Federation
 ⁴St. Petersburg State Polytechnical University, St. Petersburg, Russian Federation

Corresponding Author: A. Razdobarin, aleksey.razdobarin@mail.ioffe.ru

Plasma cleaning is considered as a most promising method for in-situ recovery the surface of diagnostic mirrors installed inside ITER vacuum chamber. The engineering and physical aspects of plasma cleaning technique, being developed for Thomson scattering system in the divertor, is presented with the focus on general issues common for all optical diagnostics in ITER.

The parameters of capacitively coupled RF discharge, designed for optical surface recovery in the divertor region, are measured as a function of applied power frequency in the range 80–400 MHz. To fix the ion maximal energy in the desirable range under fast variation of neutral gas pressure in ITER the remote control of the discharge is to be provided by the RF power variation. The deuterium ion energy depending on RF power and pressure were measured for 81.3 MHz power frequency. The experimental results on magnetic field influence on ion flux parameters are also discussed.

To estimate the efficiency of the suggested system the experiments of aluminum (as Be-proxy) film removal were performed in D_2 and D_2/O_2 glow discharge. The sputtering yield of Al was found to be 0.003 for D_2^+ ions with mean energy ~ 80 eV. It was shown that addition of 2% oxygen increases sputtering rate by 4 times. The impact of metal deposits on the performance of diagnostic mirrors is discussed. It was shown that metallic film with a thickness as low as a few nm may cause significant degradation of the diagnostic mirrors with transparent oxide coating.



Protecting B₄C Coating for ITER Divertor Tiles. Deposition, Operation, Removal of Erosion Products

L. Begrambekov¹, E. Azizov², O. Buzhinsky², V. Kurnaev¹, N. Klimov², and I. Mazul³

¹National Research Nuclear University MEPhI, Moscow, Russian Federation ²Troitsk Institute for Innovation & Fusion Research, Moscow region, Russian Federation ³D. V. Efremov Institute of Electrophysical Apparatus, St. Petersburg, Russian Federation

Corresponding Author: L. Begrambekov, lbb@plasma.mephi.ru

Tungsten is considered as the plasma facing material of the ITER divertor. High power density plasma irradiation of tungsten initiates the number of processes (see for instance [1, 2]) resulting in its accelerated destruction. Application of the in situ renewable protecting boron carbide (B_4C) coating was shown can keep tungsten tiles from plasma irradiation, and by this means prevent development of the above mentioned processes [3].

The report presents the first results of investigation of the important aspects of the B_4C coating application in ITER have not been investigated yet. Among them there are the regime and conditions of high adhesive plasma deposition of B_4C on tungsten; testing of B_4C coating ability to withstand the thermal cycling and high power density irradiation by plasma ions and electrons; the method of removal of the products of B_4C erosion from the vessel.

References

[1] V.A. Makhlaj, I.E. Garkusha, N.N. Arsenov, et al., J. of Nucl. Mat., 438 (2013) S233-236.

[2] G.Putnik, Th. Loewehoff, J. of Nucl. Mat., 438 (2013) S945-S948.

[3] O.I. Buzhinskij, V.G. Otroschenko, D.G. Whyte et al., J. of Nucl. Mat., 313-316 (2003) 214.

Experimental Assessment of Erosion Corrosion Parameters of Copper Alloys and Copper to Steel Joints at ITER Operational Conditions

S. Wikman¹, C. Gustafsson², J. Eskhult², and J. Oijerholm²

¹F4E: Fusion for Energy, Barcelona, Spain²Studsvik Nuclear AB, Studsvik, Sweden

Corresponding Author: S. Wikman, stefan.wikman@f4e.europa.eu

The ITER In-Vessel design includes coolant water interfaces with the copper alloy CuCrZr exposed to high water velocities. For reasons of structural integrity, the formation of activated corrosion products as well as the need for water purification, it is important to assess the erosion corrosion susceptibility of CuCrZr. In ITER, the materials will be subjected to different water chemistry conditions depending on whether the plasma is active or not. The present work, organized by F4E via a task agreement with ITER IO, was performed at Studsvik. Experimental studies at oxidizing conditions were recently finished, while a similar test at reducing condition is ongoing. Exposure of CuCrZr and CuCrZr/316L(N)-IG specimens was performed in two consecutive autoclaves, operating at different temperatures, where the specimens were subjected to impinging coolant water flow. Each campaign was divided into four exposure periods allowing for specimens to be taken out for intermediate inspections. The first test campaign was performed under oxidizing conditions in order to simulate operational conditions during plasma burn. Specimens weight were measured after each exposure period. Specimen surfaces and oxide cross sections were analyzed by HR-SEM after the final period after which erosion corrosion and release rates were calculated. The corrosion rates at oxidizing conditions were 25 and 37 μ m per year at 110°C and 150°C respectively. The rates were constant with exposure time. At 250°C the rate was much higher, 1600 μ m per year. Erosion corrosion rates recorded for CuCrZr under simulated ITER coolant water conditions are disturbingly high. For comparison it can be mentioned that corrosion rates of structural materials in LWR reactors generally are considerably lower than 1 μ m/year. The ongoing test campaign comprises exposure under reducing conditions representing nominal off-plasma operational condition. Although preliminary results indicate much lower corrosion rates, the effect of alternating corrosion potential may be destructive. Erosion corrosion of CuCrZr can thus potentially cause serious problems for the ITER coolant systems.



Radiation Responses for a Stainless Steel Composite as a Neutral Beam Injector Guard Wall of ITER

W. Osei-Mensah¹, J. Justice Fletcher², and J. Korbla Gbadago¹

¹Ghana Atomic Energy Commission, Legon-Accra, Ghana ²University of Ghana, Accra, Ghana

Corresponding Author: W. Osei-Mensah, entroppii@yahoo.com

Assessing the amount, type, and energy of radiation encountered requires knowledge of radiation source and the shielding effect of the type of material between the radiation source and the area of interest. The choice of elements in structural materials such as stainless-steel can reduce the radiation levels due to particle activation. The dose rate to workers and electrical components are managed from the material used for radiation shielding. This work analyses concrete-steel composites as a radiation material for the ITER neutral beam duct. Quantitative analysis of radiation effects in the vicinity of the Neutral Beam Injection (NBI) was carried out using MCNP5 simulation. The MCNP5 simulation is used to determine the gamma photon flux at a reference position outside the shield. The flux is the then used to calculate the dose rate for a reference position outside the composite shield.



Plasma Facing Material Alternatives to Tungsten

J. Brooks¹, L. El-Guebaly², A. Hassanein¹, and *T. Sizyuk*¹

¹Purdue University, West Lafayette, IN, USA ²University of Wisconsin-Madison, Madison, WI, USA

Corresponding Author: J. Brooks, brooksjn@purdue.edu

Tungsten is the leading high-Z candidate surface material for future tokamak divertor and first wall plasma facing components. There are good reasons for this choice including low activation, high melting point, good thermo-mechanical properties, low sputter erosion, and low tritium retention/codeposition. However, there are concerns about He, D-T, and neutron-induced microstructure integrity, fatigue, dust, and other issues, and a general major concern about relying on one material. To broaden the options for fusion development we identified and examined five potential alternative high-Z plasma facing materials: zirconium, niobium, molybdenum, hafnium, and tantalum. These can potentially serve as full-thickness structural materials, or thinner coating materials, depending on the plasma environment, hydride-formation, etc. We assessed these materials from three initial standpoints: neutron-induced activation, sputter erosion and redeposition, and plasma transient response. This initial analysis is encouraging, showing: 1) environmentally attractive activation and waste disposal for a commercial power plant divertor surface, using advanced recycling, 2) acceptable sputtering erosion and redeposition performance, similar to a tungsten divertor, and 3) concerns about the transient response of the alternative materials but not fundamentally different than concerns for tungsten. We identify future steps needed to advance the qualification of these materials.



Contributions of Linear Plasma Devices to PMI Research

R. Doerner¹, G. De Temmerman², and *N. Ohno*³

¹University of California San Diego, CA, USA ²FOM Institute DIFFER, Association EURATOM-FOM, Nieuwegein, The Netherlands ³University of Nagoya, Nagoya, Japan

Corresponding Author: R. Doerner, rdoerner@ucsd.edu

Linear plasma devices (LPDs), sometimes called divertor simulators, bridge the gap between single effect measurements (such as ion beam sputtering measurements, or electron beam high-heat flux tests) and more complicated toroidal plasma confinement facilities. LPDs offer the opportunity to investigate the synergy and coupling between the variety of processes taking place at the interface between a material object and an incident high-energy plasma. This submission describes benefits associated with performing plasma-based research using linear plasma devices and will describe some of the key contributions (both from a plasma physics and a material science viewpoint) of the research performed in these facilities. The benefits to interpretation of measurements made in existing toroidal confinement devices by data from LPDs will be highlighted. In addition, research in LPDs aimed at future DEMO-like devices is already underway and results describing the behavior of tungsten in this environment will be described. In recent years, linear plasma devices have evolved to increase their relevance to existing machines and future fusion devices, for example by coupling of advanced diagnostics and by improving machine capabilities. In addition, their contribution to the direct support of ITER research needs showcases their importance in fusion technology development. As a consequence, linear plasma devices contribute greatly to the advancement of plasma-material interactions as a field of scientific research, to technology development for next step facilities and to the testing of advanced materials as long term solutions for future fusion reactors.

Preprint

Microstructure and Mechanical Properties of V-Me(Cr, W)-Zr-C Alloys as a Function of their Thermochemical Treatment Modes

V. Chernov¹, M. Potapenko¹, V. Drobyshev¹, M. Kravtsova¹, A. Tyumentsev², S. Ovchinnikov², I. Ditenberg², Y. Pinzhin², A. Korotaev², and I. Smirnov²

¹A.A. Bochvar High-Technology Research Institute of Inorganic Materials, Moscow, Russian Federation ²V.D. Kuznetsov Siberian Physical-Technical Institute, Tomsk State University, Tomsk, Russian Federation

Corresponding Author: V. Chernov, chernovv@bochvar.ru

Nanostructured vanadium alloys of V-Me (Cr, W)-Zr-C system have good prospects as structural materials for a new generation of fusion and fission (fast) nuclear power reactors. The required properties of the alloys are achieved by methods of combined heat treatment, including conventional (traditional) thermomechanical treatment (TMT), as for the referenced V-4Ti-4Cr alloys (annealing at 1000°C for 1 h), and additional thermochemical treatment (TCT: oxygen saturation and internal oxidation).

Alloys V-8.75Cr-0.14W-1.17Zr-0.01C-0.02O-0.01N (wt.%, ingot weight is 0.9 kg, sheet thickness is 1 mm) and V-4.23Cr-7.56W-1.69Zr-0.02C-0.02O-0.01N (wt.%, ingot weight is 1.2 kg, sheet thickness is 1 mm) have been smelted. Methods have been developed and combined treatment (TMT + TCT) of alloys obtained has been performed (internal oxidation with a given level of bulk oxygen concentration determined, in turn, by the zirconium concentration), which provides the formation of nanoscale particles ZrO_2 of controlled dispersity in alloys, preservation of nanoscale heterophase structure up to the temperature 1300–1400°C, increase of recrystallization temperature up to 1400–1600°C.

Formation of such microstructure results in significant precipitate and substructure hardening and substantially (as compared to traditional TMT modes) improvement of the mechanical properties of the vanadium alloys throughout the whole range of temperatures up to 800°C. At the maximal hardening effects of the internally oxidized alloy specimens the value of elongation at room temperature remains high enough (about 12%). Obtained mechanical properties of the vanadium alloys by using the combined treatment are significantly higher than those achieved so far for the referenced alloy V-4Ti-4Cr.

High thermal stability of the specified nanoparticles and defect substructure indicates the prospects of using the proposed methods of combined treatment (TMT + TCT) to significantly improve the performance of not only short-term but also long-term high-temperature strength of new vanadium alloys. An important advantage of the combined method of the alloys treatment is the possibility of its implementation for semimanufacture articles or end-products (sheets, pipes, etc.) obtained from initially high technological (low strength and high ductility) vanadium alloys.



Recent Progresses on Vanadium Alloys for Fusion Application in China

P. Zheng¹, J. Chen¹, J. Zhao², C. Zhang³, R. Wei¹, X. Miao¹, S. Yang¹, H. Fu¹, Z. Xu¹, and X. Duan¹

¹Southwestern Institute of Physics, Chengdu, Sichuan, China
 ²Dalian University of Technology, Liaoning, China
 ³Institute of Modern Physics, Chinese Academy of Sciences, China

Corresponding Author: P. Zheng, zhengpf@swip.ac.cn

Vanadium alloys, especially those with the compositions of V-4Cr-4Ti, are attractive materials for fabricating self-cooled liquid lithium blanket in a fusion reactor. However, vanadium alloys are still not considered to be used in near term fusion reactors, because the issues relating to its high temperature deformation, neutron irradiation damage and so on are not sufficiently solved. Thus, the mechanical properties, irradiation resistance of this alloy should be improved further.

Vanadium researches for fusion applications in China are mainly carried out at Southwestern Institute of Physics (SWIP). Recently domestic collaborations with other partners have been broadened out to focus on: 1) the enhancement of V-4Cr-4Ti alloys via nano-particle dispersion strengthening; 2) 3D atomic probe tomography (APT) analysis of alloying elements in V matrix; 3) effects of H and He ion implantation on V and V-Ti alloy; and, 4) molding of point defects including H and He behaviors in pure V and V-alloys.

Remarkable progress has been achieved in the mechanical alloying of V-4Cr-4Ti material. Ti_3SiC_2 is proved to efficiently strengthen this alloy with higher thermal stability compared with the situation for other carbides such as TiC and SiC. Dissolution and distribution of the alloying elements and other defects characterized in 3D-APT is expected to benefit more understanding of mechanical alloying process for V-4Cr-4Ti and related impurity control. The most activities challenged the evolution of energetic particles, along with the vacancies caused by them, into the matrix of V and V-alloy. Simulated behaviors of interstitial impurities and substitutional atoms are investigated to explain possible change in mechanical properties of the alloy. Ion radiation hardening caused by H implantation has been found harder to be recovered than that caused by He and H/He implantation. Moreover, the addition of Ti reduces the irradiation hardening effectively.

Preprint

Energetic, Crystallographic and Diffusion Characteristics of Hydrogen Isotopes in Iron

A. Sivak¹, P. Sivak¹

¹National Research Centre "Kurchatov Institute", Moscow, Russian Federation Corresponding Author: A. Sivak, saidko@mail.ru

Energetic and crystallographic characteristics of various interstitial configurations of H atoms and their complexes with self-point defects (SIA: self-interstitial atom, vacancy) in bcc Fe have been calculated by molecular statics using Fe-H interatomic interaction potential developed by [1] (and modified here) and Fe-Fe matrix potential M07 developed by [2].

The most energetically favorable configuration of an interstitial H atom is tetrahedral configuration. The height of the energy barrier for H atom migration is 0.04 eV. H atom in the substitution position is unstable and shifts in the direction of the nearest octopore during the relaxation process staying at a distance of 0.024 nm from it. The resulting configuration has the highest binding energy of all the considered complexes "vacancy – H atom" (0.54 eV). The energy barriers for the jump of H atom from a vacancy to the nearest tetrapore and back are 0.47 eV and 0.05 eV, respectively. The binding energy of the most energetically favorable configuration of the considered complexes "SIA – H atom" equals 0.15 eV. The interaction energy of H atom with a SIA decreases with distance slower than in the case of interaction with a vacancy. The binding energy of H atom with an edge dislocation in $\langle 100 \rangle$ {001} slip system is 0.49 eV.

The binding energies of complexes "vacancy – nH atoms" ($n = 1, \dots, 15$) have been calculated. The binding energy of H atom with the complex decreases from 0.54 eV to 0.35 eV with increasing of n from 1 to 6. The value of binding energy decreases sharply to ~ 0.1 eV at n > 6. One vacancy can contain up to 6 H atoms. Adding of the seventh H atom leads to the expulsion of one of the other six H atoms from the vacancy.

The temperature dependences of hydrogen isotopes (H, D, T) diffusivities in Fe have been calculated for the temperature range 70–1100 K using molecular dynamics. The temperature dependencies for the diffusivities at temperatures higher than 300 K have a parabolic form. The diffusivities for the H, D, T isotopes are almost the same at room temperature. The isotope effect becomes stronger at higher temperature, e.g., ratios D^H/D^D D^H/D^T at 1100 K equal 1.2 and 1.3, respectively.

References

[1] A. Ramasubramaniam et al., Phys. Rev. B 79 (2009) 174101.

[2] L. Malerba et al., J. Nucl. Mat. 406 (2010) 19.



Unipolar Arcing at Advanced Fine-Structured Materials

M. Tsventoukh¹, G. Mesyats¹, and S. Barengolts¹

¹P. N. Lebedev Physical Institute, RAS, Moscow, Russian Federation

Corresponding Author: M. Tsventoukh, elley@list.ru

Novel approaches for the fusion devices first wall include materials with 'advanced' surface structures. The general idea is the creation of a specific layer (of a micron size) at the first-wall surface. Most promising are: liquid-metal at a capillary-porous structure [1, 2], and recently discovered tungsten 'fuzz' structure that consists of metal nanowires [3–5]. The advantages of these surfaces are a low sputtering yield, reducing of surface cracking etc. However, there is an undesirable feature, which is the promotion of self-sustained unipolar arcs that can be ignited more easily at such film-like surface [6, 7]. It has been found that the arcing is promoted by the pulsed action of ELM-plasma, and that arc cathode spot burn in the tungsten layer of a few-micron size [8, 9]. Vacuum arc investigations on film cathodes [10] strongly promotes the understanding of physics of whole 'vacuum discharge' [11–13].

The vacuum discharge implies a formation of plasma from the electrode material for a large current transfer. It consists of three stages: vacuum breakdown, vacuum spark, and, finally, vacuum arc. The basic feature of all these stages are an explosive electron emission (EEE) pulses and ectons that arise from microcenters at the cathode and are responsible for an electron emission current of a large density and large magnitude.

The model of unipolar arcing [7, 14–15] will be further improved with taking into account the ignition of the EEE pulses under the external action of plasma and power fluxes at a surface microstructure.

References

- [1] Hirooka et al., 2010 Nucl. Fusion 50 077001.
- [2] Mirnov et al., 2006 Plasma Phys. Control. Fusion 48 821.
- [3] Kajita et al., 2007 Nucl. Fusion 47 1358.
- [4] Doerner, Baldwin and Stangeby 2011 Nucl. Fusion 51 043001.
- [5] Wright et al., 2012 Nucl. Fusion 52 042003.
- [6] Kajita et al., 2009 Nucl. Fusion 49 032002.
- [7] Barengolts, Mesyats, Tsventoukh 2010 Nucl. Fusion 50 125004.
- [8] Herrmann 2009 J. Nucl. Mater. 390-391 747.
- [9] Rohde 2011 J. Nucl. Mater. 415 S46-S50.
- [10] Kesaev 1968 'Cathode Processes of Electrical Arc', Nauka, Moscow.
- [11] Mesyats and Proskurovsky 1989 Pulsed Electrical Discharge in Vacuum (Berlin: Springer Verlag).
- [12] Mesyats 2013 IEEE Trans. Plasma Sci. 41 676.
- [13] Anders 2008 Cathodic Arcs (Springer, NY).
- [14] Barengolts, Mesyats, Tsventoukh, 2008 JETP 107 1039.
- [15] Barengolts, Mesyats, Tsventoukh 2011 IEEE Trans. Plas. Sci. 39 1900.



Super-Saturated Hydrogen Effects on Radiation Damages in Tungsten under High-Flux Divertor Plasma Irradiation

D. Kato¹, H. Iwakiri², K. Morishita³, Y. Watanabe⁴, and T. Muroga¹

¹National Institute for Fusion Science, Toki, Japan ²University of Ryukyus, Okinawa, Japan ³Kyoto University, Kyoto, Japan ⁴Japan Atomic Energy Agency, Naka, Japan

Corresponding Author: D. Kato, kato.daiji@nifs.ac.jp

Tungsten is a prime candidate as divertor material of ITER and DEMO reactors which would be exposed to unprecedentedly high-flux plasmas as well as neutrons. Radiation defects such as vacancies and impurities inherent in the divertor plasmas will play primary roles in enhancement of tritium retention in the tungsten. In this paper, for a better characterization of the radiation damages in the tungsten under the divertor condition, we examine influences of super-saturated hydrogen on vacancies in the tungsten. The present first-principle calculations based on density functional theories (DFT) reveal unusual phenomena predicted at super-saturated hydrogen concentration as follows.

- 1. Strongly enhanced vacancy concentration with the super-saturated hydrogen is predicted by a thermodynamics model assuming multiple-hydrogen trapping in the vacancies. This is ascribed to strong lowering of vacancy formation energies by trapping many hydrogen atoms.
- The hydrogen trapping enhances vacancy clustering, also. Formation energies of di-vacancies are significantly lowered by trapping single hydrogen atoms. The calculated formation energies for the first nearest neighbor and the second nearest neighbor configurations almost coincide with an experimental value deduced from field ion microscopy.
- 3. DFT molecular dynamics revealed that hydrogen clusters can prevent a vacancy from recombining with the neighboring crowd ion-type self-interstitial-atom. This suggests that neutron damage effects will be increased in the presence of the hydrogen clusters.



Production of Radiation-Damaged Tungsten and its Study in High Flux Deuterium Plasma

V. Koidan¹, B. Khripunov¹, A. Ryazanov¹, V. Gureev¹, S. Kornienko¹, S. Latushkin¹, A. Muksunov¹, V. Petrov¹, E. Semenov¹, V. Stolyarova¹, V. Unezhev¹, L. Danelyan¹, V. Kulikauskas², and V. Zatekin²

> ¹National Research Centre "Kurchatov Institute", Moscow, Russian Federation ²Lomonosov University, Moscow, Russian Federation

Corresponding Author: V. Koidan, koidan_vs@nrcki.ru

Method of high-level radiation damage production in tungsten have been developed and studied on the facilities of the Kurchatov institute together with high flux plasma effect on the damaged material. The results of the experimental work for the last two years are presented in the paper. Radiation damage from DT neutrons is simulated with surrogate irradiations by high energy ions from accelerator. Tungsten W 99.95 wt % was irradiated by different ions species at a cyclotron: by helium ions He²⁺ at 3.5–4 MeV and by carbon ions C³⁺ at 10 MeV to the total fluence of $10^{21}-10^{23}$ ion/m². The samples have been obtained with primary displacements in the range 0.1–600 dpa that covers the whole range according to the fusion reactors including the ITER and DEMO projects. The task was to find out the dependence of the result of the plasma action on tungsten with the presence of radiation damage in it. Radiation swelling effect for both ion species has been exhibited in tungsten by evaluation of linear dimension changes with profilometer (0.5–0.8% in case of carbon ions). The irradiated samples were exposed to steady state deuterium plasma in the linear plasma device LENTA in the divertor and SOL simulated conditions. Erosion of the material surface as well as the surface and damaged layer microstructure changes have been studied in those condition. Important increase in deuterium retention in tungsten (by an order of magnitude) has been found at the depth of maximal damage. Implanted helium content in the surface layer has been measured by elastic nuclear backscattering.

The work was supported by RFBR grants: #11-08-01093-a, #13-08-00692-a.

References

- [2] A.I. Ryazanov, et al., Fus. Sci. & Technol., V.61, Nr. 2, FUSTE8 (2) 107-117 (2012).
- [3] V.S. Koidan, et al., IAEA FEC-23, 2010, CD Rep. FTP/3-3Rb.

^[1] B.I. Khripunov, et al., JNM, 390-391 (2009) 921-924.



Anodic Polarization Study on F82H Steel in Tritiated Water

M. Oyaidzu¹, K. Isobe¹, and T. Hayashi¹

¹Japan Atomic Energy Agency, Naka, Japan

Corresponding Author: M. Oyaidzu, oyaizu.makoto@jaea.go.jp

Since it is predicted from the previous studies that the effects of tritium on corrosion of F82H steel, one of Reduced Activation Ferritic Martensitic Steels, would be higher than that of SUS304 stainless steel, a corrosion behavior of F82H steel in tritiated water circumstance was studied by means of anodic polarization measurements, one of the electrochemical techniques, with changing the tritium concentration and dissolved oxygen concentration in 0.05 M sodium sulfate solution at 293 K. The experimental results indicate that the self-passivation of F82H steel induced by dissolved oxygen was inhibited in tritiated water solution at ambient temperature. If passivation of F82H steel would not proceed, the surface was kept corrosive and therefore the corrosion would be enhanced. Furthermore, when dissolved oxygen, which is necessary to make F82H steel self-passivated under the present experimental condition, coexisted with tritium, the corrosion of F82H steel became much less apt to be passivated: Even the electrochemical passivation was inhibited. Similar phenomenon has been investigated for SUS304 stainless steel, indicating that the key reaction was supposed to be elution of chromium during passivation by further oxidation induced by oxidative radiolysis products such as hydroxyl radical, super-oxide radical and so on. Therefore, it is indicated that the mechanism of the tritium effects on the passivation of F82H steel would be similar to or the same as that of SUS304 stainless steel, since the chromium plays an important role in the passivation of F82H steel as well as SUS304 stainless steel. It was found from the present results that the effects of tritium on corrosion of F82H steel would not be negligible problem to design the blanket and the other relevant components since radiochemical reactions are generally less susceptible to temperature.



Experimental Results on the Irradiation of a Number of the Nuclear Fusion Relevant Materials at the Dense Plasma Focus "Bora" Device

A. Cicuttin¹, V. Gribkov²

¹The Abdus Salam Interantional Centre for Theoretical Physics, Italy ²Institute of Plasma Physics and Laser Microfusion, Warsaw, Poland

Corresponding Author: A. Cicuttin, cicuttin@ictp.it

Samples of materials counted as perspective ones for use in the first-wall and construction elements in fusion reactors (W, Ti, Al, low-activated ferritic steel "Eurofer" and some alloys) were irradiated in the Dense Plasma Focus (DPF) device "Bora" having bank energy of ≤ 5 kJ. The device can generate powerful streams of hot dense ($T \sim 1 \text{ keV}$, $n \sim 10^{24} \text{ m}^{-3}$) deuterium plasma streams ($v \sim 10^5 \text{ m/s}$) and fast ($E \sim 0.1...1.0$ MeV) deuterons of power flux densities P up to 10^{10} and 10^{12} W/cm² correspondingly. A so-called "damage factor" $F = P \times \tau/2$ ensures an opportunity to simulate radiation loads (predictable for both reactors types) by the plasma and ion streams generated in DPF, which have namely those parameters as expected in the fusion reactor (FR) modules. Before and after irradiation we provided investigations of our samples by means of a number of analytical techniques. Among them we used optical and scanning electron microscopy to understand character and parameters of damageability of the surface layers of the samples. Atomic force microscopy was applied to measure roughness of the surface after irradiation. These characteristics are quite important for understanding of mechanisms and values of dust production in FR that may relate to tritium retention and emergency situations in FR facilities. We also applied two new techniques. For surface we elaborated the portable X-ray diffractometer that combines X-ray single photon detection with high spectroscopic and angular resolutions. A laser-based remote distance sensor allows positioning the material point of analysis with a precision of about 30 μ m. For bulk damageability investigations we applied an X-ray microCT system where X-rays were produced by a Hamamatsu microfocus source (150 kV, 500 µA, 5 µm minimum focal spot size). The detector was a Hamamatsu CMOS flat panel coupled to a fiber optic plate under the GOS scintillator. The reconstruction of 3D data was run with Cobra 7.4 and DIGIX CT software while VG Studio Max 2.1 and Amira 5.3 were used for segmentation and rendering. We also provided microhardness measurements. The report contains results of the investigations of modifications of the elemental contents, structure and properties of the materials.



Computational Study of Defects in Fusion Materials Containing Helium

T. Troev¹, V. Angelov¹

¹Bulgarian Academy of Sciences, Bulgaria

Corresponding Author: T. Troev, troev@inrne.bas.bg

The interaction of the intensive neutron fluxes with the first wall components of the fusion reactors result on serious structure damages in fusion materials. Atomic displacement cascades induce formation of point defects (i.e., vacancies, interstitial atoms, vacancy and interstitial clusters) and segregation of alloying elements, while nuclear transmutation reactions produce helium and hydrogen atoms. The measure for the radiation damage in the material microstructure is dpa. The development of models for the accumulation of radiation defects and transmutation products, including helium and hydrogen, in complex microstructures will be one of the priorities for the EU Materials Modelling programme for the Horizon 2020. Computational studies of atom cascades due to the 14 MeV neutrons passage in Fe and W targets have been performed by transport Monte Carlo codes MCNP/MCNPX and FLUKA. The purpose was to determine the dpa and percentage of the formed helium atoms in Fe and W samples. We plan also to compare the computational data from FLUKA and MCNPX.

The second part of the study has covered the positron lifetime computer simulations by TCDFT for 14 MeV neutrons in alpha-Fe and W samples, containing helium. The positron lifetimes calculated by TCDFT correlate with the magnitude of electron density of the sample.



Interaction of Hot Plasma and Fast Ion Streams with Materials under Tests in the Dense Plasma Focus Devices and Some Results of the Irradiation

M. Chernyshova¹, V. Gribkov^{1,2}, M. Kubkowska¹, M. Paduch¹, E. Kowalska-Strzeciwilk¹, R. Miklaszewski¹, E. Zielinska¹, E. Demina², V. Pimenov², M. Vilemova³, and J. Matejicek³

¹Institute of Plasma Physics and Laser Microfusion, Warsaw, Poland ²A. A. Baikov Institute of Metallurgy and Material Sciences, RAS, Moscow, Russian Federation ³Institute of Plasma Physics AS CR v.v.i., Prague, Czech Republic

Corresponding Author: M. Chernyshova, maryna.chernyshova@ipplm.pl

Dense Plasma Focus (DPF) devices PF-6 (6 kJ) and PF-1000 (1.2 MJ) placed at the IPPLM, Warsaw, Poland, are the main facilities that were employed for tests of perspective materials intended for use in future fusion reactors (FR) like ITER and NIF. Their discharge currents reach very high values up to 0.76 MA and almost 3.0 MA correspondingly that are the record figures for the facilities of their classes. Moreover these machines are equipped with a large number of contemporary and unique diagnostics that allow investigations of processes of irradiation of samples under tests with high temporal, spatial, angular and spectral resolution. During irradiation experiments a large number of parameters are monitored. Among them temporal and spatial evolution of primary (DPF pinch) plasma density, soft and hard X-ray and neutron radiations, angular and spatial distribution of these radiations types together with fast ions and relativistic electrons, as well as the same characteristics for secondary plasma, produced by these penetration radiations at the surface of a solid state target under irradiation. Subsequent analysis of the irradiated specimens includes a number of contemporary techniques that give an information of the irradiated materials' elementary contents, structure and properties. The report discuss results obtained at the irradiation of a number of materials (W, CFC, SiC, Ti, Al, low-activated ferritic steel "Eurofer" and a number of alloys) as well as its subsequent analytical examination with optical and electron scanning microscopy, distribution of elements on the sample's surface before and after irradiation, analysis of damageability of the samples depending on the irradiation parameters and so on.

Preprint

Physical Processes Taking Place in the Dense Plasma Focus Devices at the Interaction of Hot Plasma and Fast Ion Streams with Materials under Tests and some Results of the Irradiation

V. Gribkov¹

¹Institute of Plasma Physics and Laser Microfusion, Warsaw, Poland Corresponding Author: V. Gribkov, gribkovv@rambler.ru

Dense Plasma Focus device represents a source of powerful streams of penetrating radiations (hot plasma, fast electron and ion beams, X-ray and neutrons) of nanosecond-scale pulse durations. Power flux densities of the radiation types may reach in certain cases values up to 10^{13} W/cm². They are widely used at present time in more than thirty labs in the world in the field of radiation material science. Areas of their implementations are testing of the materials perspective for use in modern fusion reactors (FR) of both types, modification of surface layers with an aim of improvements of their properties, production of some nanometer structures on their surface, and so on. To use the above-mentioned device correctly in these applications it is important to understand mechanisms of generation of the above-mentioned radiations, their dynamics inside and outside of the pinch, and processes of interaction of these streams with targets. In this report the most important issues on the above matter will be discussed in relation to the cumulative hot plasma stream and the beam of fast ions with illustration of experimental results obtained at four DPF devices ranged in the limits of bank energies from 1 kJ to 1 MJ. Among them, mechanisms of a jet formation, a current abruption phenomenon, a super-Alfvén ion beam propagation inside and outside of DPF plasma, generation of secondary plasma and formation of shock waves in plasma and inside a solid state target, etc. Nanosecond time-resolved techniques (electric probes, laser interferometry, frame self-luminescent imaging, X-ray and neutron probes, etc.) give an opportunity to investigate the above-mentioned events and to observe the process of interaction of the radiation types with targets. After irradiation, the specimens are analyzed by contemporary instrumentation: optical and scanning electron microscopy, local X-ray spectral and structure analysis, atomic force microscopy, the portable X-ray diffractometer that combines X-ray single-photon detection with high spectroscopic and angular resolutions, an X-ray microCT system with Cobra 7.4 and DIGIX CT software, micro-hardness measurements, etc. A number of results in this area are presented.

High-Temperature Radiolysis of Modified Lithium Orthosilicate Pebbles with Additions of Titania

A. Zarins¹, G. Kizane¹, A. Supe¹, R. Knitter², M. Kolb², O. Leys², L. Baumane³, D. Conka¹, and O. Valtenbergs¹

¹University of Latvia, Riga, Latvia ²Karlsruhe Institute of Technology, Germany ³Latvian Institute of Organic Synthesis, Riga, Latvia

Corresponding Author: A. Zarins, arturs.zarins@lu.lv

In ITER (International Thermonuclear Experimental Reactor) several concepts of Test Blanket Modules (TBMs) will be tested and verified, because tritium breeding is a key issue in future burning plasma machines such as DEMO. The Helium Cooled Pebble Bed (HCPB) TBM, proposed by the European Union, will use lithium orthosilicate pebbles with 2.5 wt% excess of silica as reference tritium breeding ceramic. However, latest irradiation experiments showed that the reference pebbles may crack and form fragments under operation conditions as expected in the HCPB TBM. Therefore, it may be favorable to change the chemical composition of the reference pebbles and to replace the silica excess by titanium to obtain lithium metatitanate as a second phase. However, to develop a new chemical composition for the tritium breeding ceramic, it is a critical issue to understand high-temperature radiolysis, i.e., radiation-induced chemical processes, microstructural changes and phase transitions which will occur during irradiation at elevated temperature. Therefore, the aim of this research was to investigate the high-temperature radiolysis of the modified lithium orthosilicate pebbles with different contents of titanium for the first time. The high-temperature radiolysis was performed with accelerated electrons by a linear electron accelerator ELU-4 (E = 5 MeV) up to 5 GGy absorbed dose at 380–670 K in dry argon atmosphere. The formation of radiation-induced defects (RD) and radiolysis products (RP) was analyzed by electron spin resonance (ESR) spectroscopy. The phase transitions were detected by powder X-ray diffractometry (p-XRD) and Fourier transform infrared (FT-IR) spectroscopy. The microstructural changes were investigated by scanning electron microscopy (SEM). After irradiation of up to 5 GGy absorbed dose at 380–670 K, no major changes in the p-XRD patterns and FT-IR spectra of the modified lithium orthosilicate pebbles with additions of titanium were observed. Using ESR spectroscopy it has been determined that in the modified pebbles several paramagnetic species of RD and RP are formed and accumulated. The obtained results indicate that by replacing the excess of silica with equal amounts of titanium, the total concentration of paramagnetic RD and RP in the modified pebbles decreases.



Development of Functional Materials for CN TBM

Y. Feng¹, X. Wang¹, K. Feng¹, J. Zhang², and J. Hu³

¹Southwestern Institute of Physics, Chengdu, Sichuan, China ²Baoji Haibao Special Metal Materials Co. Ltd., China ³Kunming University of Science and Technology, China

Corresponding Author: Y. Feng, fengyj@swip.ac.cn

For the Chinese Helium Cooled Ceramic Breeder Test Blanket Module (CN HCCB TBM) design, the tritium breeder and the neutron multiplier are considered as two important functional materials to increase the tritium breeding ratio (TBR) performance. Lithium orthosilicate is selected as reference tritium breeder material, and beryllium is selected as neutron multiplier in the design. The main line of functional materials research and development is based on the use of the functional materials in the form of pebble beds. This paper will briefly introduce the current progress on Li₄SiO₄ pebbles and Beryllium pebbles.

The fabrication process for Lithium Orthosilicate pebbles by melt spraying method has been developed at SWIP. The morphology and surface appearance of the different pebble batches are very similar. Preliminary physical properties of pebbles were characterized. The effective thermal conductivity of Li₄SiO₄ pebble bed is measured using a hot wire method. The packing fraction was $\sim 60\%$ using 1.0 mm diameter pebbles for the single size pebble bed. Helium at atmospheric pressure was used as a filling gas. The effective conductivity was measured as a function of temperature. The experimental results showed that the effective thermal conductivity decreased with the increase of the average bed temperature. In the coming work, an independent adjustment of temperature and deformation experimental apparatus will be designed and built to investigate the thermal mechanical behavior of the beds.

The rotating electrode process (REP) has been adopted to produce beryllium pebbles for impurity control, sharp particle size distributions and mass production. The different size beryllium pebbles have been fabricated by controlling the arc current and velocity of the rotating electrode. The beryllium pebbles look almost perfectly spherical with a very smooth external surface. Preliminary characterizations of beryllium pebbles have been carried out. The plastic deformations of the pebbles have been measured and correlated with the applied loads. The tested sample is not separated into many parts up to 2000 N and only one big crack parallel to the compressive force direction is observed. It is observed that the fracture properties of the beryllium pebbles are not affected by pebble size.



R&D Status of Reduced Activation Ferritic/Martensitic Steel for CN TBM

P. Wang¹, J. Chen¹, S. Liu², and Z. Xu¹

¹Southwestern Institute of Physics, Chengdu, Sichuan, China ²Institute of Metal Research, Chinese Academy of Sciences, Shenyang, China

Corresponding Author: P. Wang, wangph@swip.ac.cn

To provide structural material support for the design and fabrication of Chinese Helium-Cooled Ceramic tritium Breeder test blanket module (CN HCCB TBM) as well as for China demonstration (DEMO), a kind of Reduced Activation Ferritic/Martensitic (RAFM) steel named CLF-1 has been developed at Southwestern Institute of Physics (SWIP) in China since 2003. With the cooperation among domestic institutes and factories, a lot of products have been produced, including 5 ton plates with different thickness from 2 mm to 35 mm, welding fillers and different size of tubes and pipes, which have totally fulfilled the needs for manufacturing small size mock-ups. Now a 1/3 size CN HCCB TBM has been successfully manufactured. Compared with other RAFM steels, the CLF-1 steel has similar physical properties and relatively higher tensile strength, especially the thermal creep properties. These advantages may be resulted from its fully martensitic microstructure with fine and dispersed tiny carbides. According to the structure design of CN HCCB TBM, a detailed R&D program on various joining technologies is undergoing to support the design. Both electron beam welding (EB) and tungsten inert gas welding (TIG) showed that preheating was not necessary but a post-welding heat treatment is essential for sound joint. Currently these joining technologies are being applied for different size plates and for the joining of plates and pipes to make the joining techniques applicable for TBM manufacturing. A neutron irradiation campaign has been started in the high flux engineering test reactor (HFETR) in China. In 2014 a target dose irradiation level will be about 1 dpa and the irradiation temperature is 300°C. The irradiation experiments are aiming to provide the basic irradiation database required for fusion blanket design, including the effects of neutron irradiation on the mechanical properties, microstructures and so on. A qualification program of CLF-1 steel has been started at SWIP. In future, larger scale ingots of CLF-1 steel larger than 5 tons will be produced to provide material for the material qualification and TBM manufacturing on the required scale. Various properties including more neutron irradiation properties will be measured to sufficient data for specifying the design criteria.



Results of KTM Lithium Divertor Model Testing on the Tokamak KTM and Future Plans

I. Tazhibayeva¹, G. Shapovalov¹, T. Kulsartov¹, Y. Ponkratov¹, I. Lyublinski², A. Vertkov², G. Mazzitelli³, E. Azizov⁴, and S. Mirnov⁵

¹Institute of Atomic Energy, National Nuclear Center, Kazakhstan ²JSC "Red Star", Moscow, Russian Federation ³Associazione EURATOM-ENEA Unitá Tecnica Fusione, Frascati, Italy ⁴National Research Centre "Kurchatov Institute", Moscow, Russian Federation ⁵Troitsk Institute for Innovation & Fusion Research, Moscow region, Russian Federation

Corresponding Author: I. Tazhibayeva, tazhibayeva@ntsc.kz

Research program of the lithium divertor module at tokamak KTM includes the following tasks: study of lithium behavior under tokamak's condition and lithium influence on vacuum conditions; study of the processes of plasma interaction with lithium surface; study of lithium influence on plasma parameters; and study of the shielding effects of receiving divertor surface due to re-emitting on lithium. Module of lithium divertor (MLD) on the base of capillary porous systems (CPS) of tokamak KTM (one of 24 tiles of standard graphite divertor) is a box-like element with a channel for coolant flow (eutectic alloy Na-K) and a tank for feeding the receiving surface with lithium. The planned energy flow on the lithium surface under nominal parameters of tokamak KTM (up to 10 MW/m^2) is a 700 kJ during 5 s discharge. Currently, the KTM facility can only be operated on the capacitors battery, since KTM standard power supply system is not fully connected, thus the decision was made to carry out two consecutive stages of the experiments with uncooled model of lithium divertor (first stage) and then with the cooled one. For the first stage an uncooled (autonomous) module of lithium divertor was used, surface temperature was stabilized by means of heat capacity of the structure with stainless steel-molybdenum heat accumulator; and heating up to the lithium melting point is realized by electric heater. Thermal-hydraulic tests of the Na-K cooled model of lithium divertor were conducted at the auxiliary test-bench, which was manufactured on the basis of standard transport-sluice device of tokamak KTM. Initial temperature of lithium surface (200°C) and its stabilization at the level of up to 550°C during plasma discharge was kept by the coolant flow; coolant temperature and circulation parameters were regulated by the external system for thermo-stabilization (STS). Tests with Na-K coolant proved operability of all the subsystems and elements of the thermo-stabilization systems during all the course of the tests under temperature range from 20 to 200°C. The main results of KTM tokamak experiments with uncooled and cooled MLD are presented in this paper. Future tasks were proposed for the next stage of the KTM "Lithium" Program.



Testing of Mock-ups for a Full Tungsten Divertor on Globus-M Tokamak

A. Novokhatsky¹, V. Gusev¹, B. Ber¹, A. Bykov², A. A. Gervash³, A. Gorodetsky⁴, S. Grigoriev³, E. Demina⁵, N. Khromov¹, V. Kuznetsov³, S. Lepikhov¹, N. Litunovsky³, A. Makhankov³, I. Mazul³, I. Miroshnikov², E. Mukhin¹, Y. Petrov¹, M. Prusakova⁵, N. Sakharov¹, V. Sergeev², V. Tanchuk³, S. Tolstyakov¹, A. Voronin¹, A. Zakharov⁴, and R. Zalavutdinov⁴

¹Ioffe Physical-Technical Institute of the Russian Academy of Science, St. Petersburg, Russian Federation ²St. Petersburg State Polytechnical University, St. Petersburg, Russian Federation

³D. V. Efremov Institute of Electrophysical Apparatus, St. Petersburg, Russian Federation

⁴A. N. Frumkin Institute of Physical Chemistry and Electrochemistry,

⁵A. A. Baikov Institute of Metallurgy and Material Sciences,

RAS, Moscow, Russian Federation

Corresponding Author: A. Novokhatsky, a.novokhatsky@mail.ioffe.ru

Current research is the first investigation of cyclic plasma-wall interaction with tungsten elements designed for ITER divertor on Globus-M tokamak. The experiment is focusing on surface morphology, chemical composition and structure of pre-melted (damaged) layers of tungsten after irradiation by electron beam and plasma jet. The irradiated by the electron beam and plasma jet ITER–like tungsten mock-ups, were installed at the outer strike point region of Globus-M lower divertor. Measurements of the SOL heat flux width in ohmic and NBI-heated shots of Globus-M with open divertor magnetic configuration ($I_p = 130-220$ kA, $B_t = 0.4$ T, $n_e = (2-3) \times 10^{19}$ m⁻³, $T_e = 400-700$ eV, PNBI = 600 kW) are presented. Results of the infrared camera and probes are compared together and with results of simulations by means of the B2SOLPS5.3 code.

RAS, Moscow, Russian Federation

Plasma Overall Performance and Control



Burning Plasma Relevant Control Development: Advanced Magnetic Divertor Configurations, Divertor Detachment and Burn Control

E. Kolemen¹, S. L. Allen², B. D. Bray³, M. E. Fenstermacher², R. Hawryluk¹, D. A. Humphreys³, A. W. Hyatt³, C. J. Lasnier², A. W. Leonard³, M. A. Makowski², A. G. McLean², R. Maingi⁴, R. Nazikian¹, T. W. Petrie³, V. Soukhanovskii², and E. A. Unterberg⁴

¹Princeton Plasma Physics Laboratory, Princeton, NJ, USA
 ²Lawrence Livermore National Laboratory, Livermore, CA, USA
 ³General Atomics, San Diego, CA, USA
 ⁴Oak Ridge National Laboratory, Oak Ridge, TN, USA

Corresponding Author: E. Kolemen, ekolemen@pppl.gov

Novel control schemes have been implemented at DIII-D to test and optimize heat-handling capabilities and burn regulation for advanced tokamaks. The topological instability of the snowflake (SF) configuration, which has a second-order null-point, motivated implementation of a control system to sustain the SF. We implemented the world's first real-time SF detection and control system on DIII-D in order to stabilize this configuration. The algorithm calculates the position of the two null-points in real-time by locally expanding the Grad-Shafranov equation and controls shaping coil currents to achieve and stabilize various snowflake configuration. SF divertor experiments achieved a 2.5 times increase in the flux expansion and a 2.5 reduction in peak heat flux for many energy confinement times without any adverse effect to core plasma such as confinement in advanced tokamak scenario with $\beta_N = 3.0$ and $H_{98}(y,2) \cong 1.35$. Also, a new detachment and radiation control algorithm was implemented at DIII-D. The algorithm uses divertor temperature measurements from real-time Thomson diagnostics and a line ratio measurement to compute the detachment level, and a real-time bolometer diagnostic to determine core and divertor radiation. The new system was used to test the feasibility of the envisioned ITER partial-detachment operation using divertor Thomson measurements on DIII-D. A dedicated partial detachment control was implemented to control the detachment front location using divertor temperature measurements from real-time Thomson diagnostics while minimizing the effect of the detachment on the core by fixing the core density independent of the detachment control. The control stabilized the detachment front fixed at the user defined distance between the strike point and the X-point throughout the shot. Finally, in a new approach to burn control, it was demonstrated that the simulated fusion power could be controlled by the application of non-axisymmetric fields using in-vessel coils. In DIII-D experiments, alpha-heating excursions were simulated with transient increases in neutral beam power. The burn control algorithm compensated the increased heating power by increasing the I-coil current, which reduced the energy confinement time and kept the stored energy (proxy for fusion power) constant.

This work was supported by the US DOE under DE-AC02-09CH11466.



Slides

Paper

Integrated Discharge Scenario for High-Temperature Helical Plasma on LHD

K. Nagaoka¹, H. Takahashi¹, S. Murakami², H. Nakano¹, Y. Takeiri¹, H. Tuchiya¹, M. Osakabe¹, K. Ida¹, M. Yokoyama¹, M. Yoshinuma¹, S. Morita¹, M. Goto¹, T. Oishi¹, N. Publant³, K. Fujii², K. Tanaka¹, N. Tamura¹, Y. Nakamura¹, T. Ido¹, A. Shimizu¹, S. Kubo¹, H. Igami¹, R. Seki¹, C. Suzuki¹, Y. Suzuki¹, K. Tsumori¹, K. Ikeda¹, M. Kisaki¹, Y. Yoshimura¹, T. Shimozuma¹, T. Seki¹, K. Saito¹, H. Kasahara¹, S. Kamio¹, T. Mutoh¹, O. Kaneko¹, H. Yamada¹, and A. Komori¹

¹National Institute for Fusion Science, Toki, Japan ²Kyoto University, Kyoto, Japan ³Princeton Plasma Physics Laboratory, Princeton, NJ, USA

Corresponding Author: K. Nagaoka, nagaoka@nifs.ac.jp

Study of high-temperature plasma is a key for realizing helical fusion reactor, because helical plasmas have good confinement properties in high density regime and a significant advantage in steady state operation. Recently, after the last IAEA-FEC 2012, discharge scenarios for high-temperature helical plasma have been developed in LHD.

An ion ITB was formed in neutral beam injected (NBI) plasmas with wall conditioning and carbon pellet injection. It was observed with a newly installed high-dynamic-range Balmer-alpha spectroscopy that the wall conditioning reduced the neutral density even in the core plasma. The ion heat transport in the ion ITB core is further improved due to reduction of charge exchange loss of fast ions. The carbon pellet injection also enhances the ion ITB formation and enlarges the width of ion ITB. Repetitive helium discharges with duration over 10 s were carried out more than 30 times with electron cyclotron heating (ICH) for wall recycling, and central ion temperature of 8 keV was achieved with enhanced ion ITB formation.

An ion ITB and an electron ITB were successfully combined with application of localized on-axis ECH to ion ITB with wall recycling and carbon pellet injection, and $T_{e0} \sim T_{i0} \sim 6$ keV were achieved. The width of ion ITB is larger than that of electron ITB. The scale length of temperature gradients for ion and electron, R/L_{T_i} and R/L_{T_e} , are over 10, indicating simultaneous improvement of ion and electron heat transports. The positive radial electric field was observed in the combined ITBs plasma, while the ion ITB in NBI plasma was formed with negative electric field. The ion temperature gradient at the barrier is observed to decrease with the local temperature ratio (T_e/T_i) . It is noted that the improvement of ion heat transport was attributable to the reduction of anomalous transport [1], and it does not depend so much on the radial electric field, but on the temperature ratio (T_e/T_i) . As a result of this dependence, the combination of the wide ion ITB and the narrow electron ITB is realized.

This study demonstrated that the profile control is a key to combine ion ITB and electron ITB and have a potential to improve the performance of helical plasmas.

References

[1] H. Takahashi et al., Nuclear Fusion. 53 (2013) 073034.



Real-Time Control of NTMs Using ECCD at ASDEX Upgrade

M. Reich¹, C. Raspon¹, and O. Sauter²

¹Max-Planck-Institut für Plasmaphysik, Garching, Germany ²Ecole Polytechnique Fédérale de Lausanne, CRPP, Lausanne, Switzerland

Corresponding Author: M. Reich, matthias.reich@ipp.mpg.de

In high performance plasmas, Neoclassical Tearing Modes (NTMs) are regularly observed at large β -values. NTMs reduce the achievable normalized β and degrade the fusion reactor performance which scales as β_N squared. A widely used method, also foreseen for ITER, for avoiding and controlling NTMs is the deposition of electron cyclotron current drive (ECCD) on the relevant rational surface. ASDEX Upgrade is making a large effort to develop, operate and evaluate an ECCD based, generic solution to MHD control, easily portable to new devices like ITER. A number of real-time diagnostics and intelligent controllers achieve precise control of ECCD deposition inside the O-point, thus minimizing the power required for NTM stabilization.

For robustly operating our feedback loop, proper integration into and coordination of several diagnostic systems with the discharge control system (DCS) was essential, hence a reliable framework was designed, developed and tested. The relevant cooperating diagnostic systems are "Equilibrium", "ECE/Mirnov" and "rt-TORBEAM" with "ECRH" as the main actuator, centrally coordinated by DCS at timescales faster than typical current diffusion times (AUG: $\tau \approx 150$ ms). All subsystems adhere to cycle times of 15 ms (rt-TORBEAM) or less than 5 ms (all others), such that the full control loop can be executed every 20 ms, making sophisticated experiments possible. Using the feedback loop, we can reliably target and — provided sufficient ECCD power is applied — stabilize NTMs triggered at β_N larger than 2. The system can target either 2/1 or 3/2 NTMs, whichever is detected to have the higher amplitude. The amplitude can also be used to refine the target by searching for the deposition location which minimizes the amplitude. To avoid a mode developing at all, preemptive stabilisation can be performed by tracking rational surfaces from a real-time equilibrium.

In our experiments we are developing and testing a variety of control strategies, to preempt and/or stabilize existing NTMs. We have started to integrate ECCD based control of other MHD instabilities, like sawteeth, into the control scheme, thus capitalizing on the generic approach of mapping all relevant information into the same reference coordinate system given by the real-time magnetic equilibrium. This strategy can directly be adopted by next step machines such as ITER.



Compatibility of Internal Transport Barrier with Steady-State Operation in the High Bootstrap Fraction Regime on DIII-D

A. M. Garofalo¹, X. Gong², C. T. Holcomb³, J. Qian², Q. Ren², W. M. Solomon⁴, M. Van Zeeland¹, B. Wan², G. Xu², O. Meneghini⁵, and G. M. Staebler¹

¹General Atomics, San Diego, CA, USA
 ²Institute of Plasma Physics, Chinese Academy of Sciences, Hefei, China
 ³Lawrence Livermore National Laboratory, Livermore, CA, USA
 ⁴Princeton Plasma Physics Laboratory, Princeton, NJ, USA
 ⁵Oak Ridge National Laboratory, Oak Ridge, TN, USA

Corresponding Author: A. M. Garofalo, garofalo@fusion.gat.com

A high bootstrap current fraction plasma regime is desirable for steady-state tokamak operation because it reduces the demands on external non-inductive current drive. Typically, this regime is characterized by high β_N and an internal transport barrier (ITB), leading to concerns about stability limits and profile control with reduced external input (power). Recent DIII-D research has increased confidence in the potential of the high bootstrap fraction approach for applicability to a steady-state fusion reactor. Fully noninductive plasmas have been sustained for long durations with large-radius ITBs, bootstrap fraction $\geq 80\%$, $\beta_N \geq 3$, $\beta_T \sim 1.5\%$, and with the ITBs and good confinement maintained even with low net torque from neutral beam injection (NBI). Building on earlier DIII-D work [1], the new experiments utilized an approach to fully noninductive operation based on removing the current drive by transformer induction. The plasmas exhibit excellent energy confinement quality, with $H_{98}(y, 2) \sim 1.5$. Similar confinement was obtained after reducing the NBI torque from ~ 6 Nm to < 3 Nm. The excellent confinement is associated with the formation of an ITB at large minor radius in all channels (n_e , T_e , T_i , rotation). The very broad bootstrap current profile is fairly well-aligned with the total current profile, explaining why the minimum safety factor is high and constant or slowly increasing, and the ITB is maintained at large minor radius for ~ 4 s, more than three times the current profile relaxation time, τ_{CR} estimated to be ~ 1 s. A further important result, providing evidence of dynamical stability, is that the ITB is maintained at large minor radius despite edge localized mode (ELM) perturbations, which become particularly large at the highest obtained $\beta_N \sim 3.5$. Stability analysis shows that this β_N value is close to the ideal wall MHD stability limit, because a large outer gap was used to reduce wall heating by prompt fast ion losses. However, detailed analysis shows that fast ion losses are anomalously high only during the β_N and density ramp-up phase. Future experiments will test an optimized outer gap waveform and methods of ELM control to enable a further increase of β_N and thus of the plasma current.

This work was supported in part by the US DOE under DE-FC02-04ER54698, DE-AC52-07NA27344, and DE-AC02-09CH11466.

References

[1] P.A Politzer, et al., Nucl. Fusion 45 (2005) 417.



Physics-Model-Based Control of the Plasma State Dynamics for the Development and Sustainment of Advanced Scenarios in DIII-D

J. E. Barton¹, M. D. Boyer¹, W. Shi¹, W. P. Wehner¹, E. Schuster¹, J. Ferron², M. L. Walker², D. A. Humphreys², T. C. Luce², B. G. Penaflor², and R. D. Johnson²

¹Lehigh University, Bethlehem, PA, USA ²General Atomics, San Diego, CA, USA

Corresponding Author: J. E. Barton, justin.barton@lehigh.edu

DIII-D experiment results are presented to demonstrate the potential of integrated physics-modelbased q-profile and β_N control for the systematic development and sustainment of advanced scenarios. Both simulations and experiments demonstrate improved control performance relative to unoptimized preprogrammed control, by utilizing a combined feedforward+feedback scheme. At the core of the control scheme is a nonlinear, physics-based, control-oriented model of the plasma dynamics valid for H-mode scenarios. A partial differential equation model of the *q*-profile dynamics is developed by combining the poloidal magnetic flux diffusion equation with physics-based models of the electron density and temperature profiles, the plasma resistivity and the noninductive current sources (both auxiliary and bootstrap). The plasma internal energy (related to β_N) dynamics are modeled by a volume-averaged energy balance equation. Firstly, a nonlinear, constrained optimization algorithm to design feedforward actuator trajectories is developed with the objective of numerically complementing the traditional trial-and-error experimental effort of advanced scenario planning. The goal of the optimization algorithm is to design actuator trajectories that steer the plasma to a target state (q-profile and β_N) at a predefined time during the discharge, such that the achieved state is stationary in time, subject to the plasma dynamics (described by the physics-based models) and plasma state and actuator constraints. Secondly, integrated feedback controllers are designed to track a target q-profile and β_N evolution with the goal of rejecting the effects of external plasma disturbances and adding robustness to the control scheme. The feedback controllers are synthesized by embedding both static and dynamic physics-based plasma response models into the control design and to be robust to uncertainties in the electron density, electron temperature, and plasma resistivity profiles. The algorithms use the heating and current-drive system and total plasma current as actuators to control the plasma dynamics. Finally, experimental and simulation results are presented to demonstrate the capabilities of the optimized actuator trajectories and feedback controllers to control the plasma dynamics in DIII-D advanced scenarios.

Work supported by US DOE (DE-SC0001334, DE-SC0010661 and DE-FC02-04ER54698).



Experimental Simulation of Burn Control Using DIII-D In-Vessel Coils

R. Hawryluk¹, N. W. Eidietis², B. Grierson¹, A. W. Hyatt², *E. Kolemen*¹, R. Nazikian¹, C. Paz-Soldan³, W. M. Solomon¹, and S. M. Wolfe⁴

¹Princeton Plasma Physics Laboratory, Princeton, NJ, USA
 ²General Atomics, San Diego, CA, USA
 ³Oak Ridge Institute for Science Eduction, Oak Ridge, TN, USA
 ⁴Massachusetts Institute of Technology, Cambridge, MA, USA

Corresponding Author: R. Hawryluk, rhawryluk@pppl.gov

A new approach has been developed to control fusion power by applying a non-axisymmetric magnetic field (n = 3) using the DIII-D in-vessel coils (I-coils) to modify the energy confinement time. This has potential advantages for a power plant due to the reduced power requirements relative to auxiliary heating and that it may enable the control of the plasma response more rapidly than with fueling or impurity influxes due to recycling of the fuel gas and impurities. In the relatively low collisionality DIII-D discharges, the application of non-axisymmetric magnetic fields results in a decrease in confinement time and density pump-out. The stored energy, which is used as a surrogate for fusion power, was controlled by the application of non-axisymmetric fields. The regulation of the stored energy by means of I-coil feedback yields comparable to or more stationary conditions than by the conventional approach of varying the neutral beam power. Transient increases in neutral beam power were used to simulate alpha-heating excursions. The feedback loop largely compensated the increased heating power by increasing the I-coil current, which reduced the energy confinement time. The accompanying increased particle transport in the pedestal was compensated by means of feedback control of the density at the top of the pedestal using the Thomson scattering system and fueling by means of the gas system. TRANSP was used to examine fast ion and profile effects in the interpretation of these results. These experiments demonstrated that it is possible to control the stored energy, which is a proxy for fusion power, by means of applying non-axisymmetric magnetic fields.

The work was supported by US DOE under DE-AC02-09CH11466, DE-FC02-99ER54512 and DE-FC02-04ER54698.

Preprint

Expanding the Physics Basis of the Baseline Q=10 Scenario toward ITER Conditions

 T. C. Luce¹, G. L. Jackson¹, T. W. Petrie¹, R. Pinsker¹, W. M. Solomon², F. Turco³, N. Commaux⁴, J. Ferron¹, A. M. Garofalo¹, B. Grierson², J. Hanson³, A. Hyatt¹, G. R. McKee⁵, R. J. La Haye¹, M. Lanctot¹, C. Paz-Soldan⁶, M. Porkolab⁷, T. L. Rhodes⁸, and G. Taylor²

¹General Atomics, San Diego, CA, USA
 ²Princeton Plasma Physics Laboratory, Princeton, NJ, USA
 ³Columbia University, New York, USA
 ⁴Oak Ridge National Laboratory, Oak Ridge, TN, USA
 ⁵University of Wisconsin-Madison, Madison, WI, USA
 ⁶Oak Ridge Institute for Science Eduction, Oak Ridge, TN, USA
 ⁷Massachusetts Institute of Technology, Cambridge, MA, USA

⁸University of California Los Angeles, CA, USA

Corresponding Author: T. C. Luce, luce@fusion.gat.com

Results obtained recently in DIII-D provide critical information for ITER baseline scenario operation. Much of the physics basis for ITER baseline scenario operation has been obtained in plasmas with significant fueling and applied torque from neutral beam injection (NBI). DIII-D has unique capabilities to extend this physics basis toward ITER conditions by applying neutral beam injection (NBI) with combinations of co- and counter-injection to reduce torque input, applying electron cyclotron heating (ECH) to reduce fueling and torque and to equilibrate the electron and ion temperatures, and exploring the effects of steady-state and transient divertor heat flux reduction with radiative divertor operation. All of these tools have been applied to plasmas with a boundary shape close to that of ITER to minimize systematic effects in projection of the results to ITER. The existence of stationary plasmas at nearly zero applied torque in DIII-D with sufficient normalized pressure and confinement for Q = 10 in ITER at 15 MA is a key validation of the baseline scenario. Sustained operation with normalized parameters sufficient for Q = 10 operation in ITER ($\beta_N = 1.9, H_{98} = 1.05, I_N = 1.41$) has been achieved with nearly zero external torque input from NBI ($T_{NB} = 0.3$ Nm) for more than four resistive relaxation times $(4\tau_R)$. Similar conditions with $P_{EC} > P_{NB}$ and $T_{NB} = 0.5$ Nm have been sustained for $> 3\tau_R$. Confinement at low torque is reduced relative to the standard co-NBI, but there is sufficient confinement margin in DIII-D so that the reduction brings the plasmas to $H_{98} \sim 1$. Application of ECH does not reduce the confinement quality of the plasmas relative to those with NBI only as long as plasmas at the same applied torque are compared. Radiative divertor operation is successful in reducing steady-state and transient heat flux to the divertor in DIII-D at low q_{95} and reduced torque without enhanced accumulation of the seed impurity used for radiation. The studies of the flux usage indicate sufficient flux should be available in ITER to meet the > 300 s operational requirement. However, the operational difficulties encountered with tearing mode stability at low applied torque suggest that a more diverse set of plasmas should be considered for the Q = 10 mission, due to the sensitivity of ITER to disruptions.

This work was supported by the US DOE under DE-FC02-04ER54698.



High Internal Inductance for Steady-State Operation in ITER and a Reactor

J. Ferron¹, C. T. Holcomb², T. C. Luce¹, J. M. Park³, E. Kolemen⁴, R. J. La Haye¹, W. M. Solomon⁴, and F. Turco⁵

¹General Atomics, San Diego, CA, USA ²Lawrence Livermore National Laboratory, Livermore, CA, USA ³Oak Ridge National Laboratory, Oak Ridge, TN, USA ⁴Princeton Plasma Physics Laboratory, Princeton, NJ, USA

Corresponding Author: J. Ferron, ferron@fusion.gat.com

Increased confinement and ideal stability limits at relatively high values of the internal inductance (l_i) have enabled an attractive scenario for steady-state tokamak operation to be demonstrated in DIII-D. The potential of the scenario was shown in high elongation and triangularity double-null divertor discharges in which $\beta_N > 4.5$ was achieved at $l_i \approx 1.3$. This high value of β_N just reached the ideal n = 1 kink stability limit calculated without the effect of a stabilizing vacuum vessel wall, with the ideal-wall limit still higher at $\beta_N > 5.5$. Confinement is above the H-mode level with $H_{98} \approx 1.8$. This type of discharge is a candidate for a reactor that could either operate stably at $\beta_N \approx 4$ without the requirement for a nearby conducting wall or $n \ge 1$ active stabilization coils, or at $\beta_N \approx 5$ with wall stabilization. With the high β_N and relatively high $q_{95} = 7$, the discharge in the experiment is overdriven with bootstrap current fraction $f_{BS} \approx 0.8$, noninductive current fraction $f_{NI} > 1$ and negative surface voltage. For ITER, operation at $l_i \approx 1$ is a promising option. Improved core confinement at high l_i could compensate for reduced H-mode pedestal confinement if a low pedestal height results from pedestal physics and/or ELM-stabilization using 3D fields. At $l_i \approx 1$, f_{BS} would be ≈ 0.5 with the remainder from external current driven efficiently near the axis. This scenario has been tested in the ITER shape in DIII-D at $q_{95} = 4.8$, so far reaching $f_{NI} = 0.7$ and $f_{BS} = 0.4$ at $\beta_N \approx 3.4$ with performance appropriate for the ITER Q = 5 mission, $H_{89}\beta_N/q_{95}^2 > 0.3$. High l_i discharges thus far take advantage of inductively driven current density near the axis as a partial substitute for externally-driven current. Studies with the FASTRAN transport code using the TGLF energy transport model explored how increased current drive power for DIII-D, 9 MW electron cyclotron current drive (ECCD) and 13 MW off-axis beam power, could be applied to maintain a stationary, fully noninductive high l_i discharge. Solutions are found at $\beta_N = 4$, $l_i = 1.07$, and $f_{BS} = 0.5$ calculated stable without a conducting wall with ECCD and neutral beam current drive near the axis and at $\beta_N = 5$ calculated to be stable with the vacuum vessel wall.

This work was supported by the US DOE under DE-FC02-04ER54698, DE-AC52-07NA27344, DE-AC05-00OR22725, DE-AC02-09CH11466, and DE-FG02-04E54761.



Achieving Steady-State Conditions in High-Beta Hybrid Scenario in DIII-D

C. C. Petty¹, F. Turco², C. T. Holcomb³, J. Kinsey¹, T. C. Luce¹, J. Ferron¹, E. J. Doyle⁴, A. M. Garofalo¹, A. Hyatt¹, and G. L. Jackson¹

¹General Atomics, San Diego, CA, USA
 ²Columbia University, New York, USA
 ³Lawrence Livermore National Laboratory, Livermore, CA, USA
 ⁴University of California Los Angeles, CA, USA

Corresponding Author: C. C. Petty, petty@fusion.gat.com

The natural attributes of the hybrid scenario, especially the anomalously broad current profile that suppresses sawteeth by maintaining the safety factor minimum (q_{min}) above unity, allows steady-state conditions with zero surface loop voltage to be achieved in 1 MA discharges in DIII-D with efficient central current drive and simultaneous high- β and high confinement. Steady-state hybrid plasmas can achieve $\beta_N = 3.6$ for the full duration of the NB pulse (> $1\tau_R$) without exciting the deleterious m/n = 2/1 tearing mode, corresponding to β_T up to 3.4%. The experimental β_N exceeds the DCONcalculated no-wall n = 1 stability limit by 20%. With central current drive, the surface loop voltage is driven down to zero for > $1\tau_R$ when the poloidal β is increased above 1.9 by raising the EC power to 3.05 MW and reducing I_P from 1.1 MA to 1.0 MA. High- β hybrids can have slightly more than 50% bootstrap current fraction despite $q_{min} \approx 1$; the other half of the plasma current is driven efficiently using central EC and NB current drive. Inside of the q = 3/2 surface the current profile is strongly overdriven, and time dependent TRANSP modeling shows that q_{min} should drop to ~ 0.8 by the end of the discharge. The fact that q_{min} remains above unity and sawteeth are suppressed shows that the hybrid scenario maintains an anomalously broad current profile even in the presence of strong central current drive. The thermal energy confinement time is excellent, with confinement factors of up to $H_{98}(y,2) = 1.6$ even during strong central EC heating. The experimental density and temperature profiles are well reproduced by the TGLF transport model, and measured changes in electron thermal transport, due to shape-induced pedestal changes or electron heating, parallel the predicted changes in the level of high-k turbulence. A zero-dimensional physics model demonstrates that attractive scenarios with $Q_{\rm fus} = 3.5$ --3.8 exist for steady-state operation in ITER and FNSF using central EC current drive, with higher $Q_{\rm fus}$ possible using higher efficiency NB current drive. Therefore, high- β hybrid plasmas with central current drive should be considered as an alternative method for achieving the fusion performance goals in steady-state scenarios in ITER and FNSF.

This work was supported in part by the US Department of Energy under DE-FC02-04ER54698, DE-FG02-04ER54761, DE-AC52-07N27344, and DE-FG02-08ER54984



Advancing the Physics Basis of Quiescent H-Mode Through Exploration of ITER Relevant High Density Operation

W. M. Solomon¹, K. H. Burrell², M. E. Fenstermacher³, A. M. Garofalo², B. Grierson¹, A. Loarte⁴, R. Nazikian¹, and P. B. Snyder²

¹Princeton Plasma Physics Laboratory, Princeton, NJ, USA
 ²General Atomics, San Diego, CA, USA
 ³Lawrence Livermore National Laboratory, Livermore, CA, USA
 ⁴ITER Organization, Saint Paul lez Durance, France

Corresponding Author: W. M. Solomon, solomon@fusion.gat.com

Recent experiments on DIII-D have overcome a long-standing limitation in accessing quiescent H-mode (QH-mode), a high confinement state of the plasma that does not exhibit the explosive instabilities associated with edge localized modes (ELMs). In the past, QH-mode was associated with low density operation, but has now been extended to high normalized densities compatible with operation envisioned for ITER. Through the use of strong shaping, QH-mode plasmas have been maintained at high densities, both absolute ($\tilde{n}_e > 7 \times 10^{19} \text{ m}^{-3}$) and normalized Greenwald fraction $\tilde{n}_e/n_G > 0.7$. In these plasmas, the pedestal can evolve to very high pressures and current as the density is increased, becoming comparable to some of the highest performance transient pedestals seen on DIII-D. Calculations of the pedestal height and width from the EPED model are quantitatively consistent with the experimental observed evolution with density. Such comparisons of the dependence of the maximum density threshold for QH-mode with plasma shape help validate the underlying theoretical peeling-ballooning models describing ELM stability. High density QH-mode operation with strong shaping has allowed stable access to a previously predicted regime of very high pedestal dubbed "Super H-mode". In general, QH-mode is found to achieve ELM-stable operation while maintaining adequate impurity exhaust, due to the enhanced impurity transport from an edge harmonic oscillation, thought to be a saturated kink-peeling mode driven by rotation shear. In addition, the impurity confinement time is not affected by rotation, even though the measured $E \times B$ shear is observed to increase at low toroidal rotation, resulting in reduced turbulence and increased energy confinement. Together with the simultaneous achievement of high- β , high confinement and low q_{95} for many energy confinement times, these results suggest QH-mode as a potentially attractive operating scenario for ITER's Q = 10 mission.

This work was supported by the US Department of Energy under DE-AC02-09CH11466 and DE-FC02-04ER54698.



Assessment of Operational Space for Long-Pulse Scenarios in ITER

A. R. Polevoi¹, A. Loarte¹, N. Hayashi², H. Kim³, S.-H. Kim¹, F. Köchl⁴, A. Kukushkin¹, V. M. Leonov⁵, S. Y. Medvedev⁶, M. Murakami⁷, Y.-S. Na³, A. Y. Pankin⁸, J. Park⁷, P. Snyder⁷, J. A. Snipes¹, and V. E. Zhogolev⁹

¹ITER Organization, Saint Paul lez Durance, France ²Japan Atomic Energy Agency, Naka, Japan ³Seoul National University, Seoul, Korea, Republic of ⁴Institute of Atomic and Subatomic Physics, TU-Vienna, Vienna, Austria ⁵National Research Centre "Kurchatov Institute", Moscow, Russian Federation ⁶Keldysh Institute of Applied Mathematics, RAS, Moscow, Russian Federation ⁷General Atomics, San Diego, CA, USA ⁸Tech-X Corporation, Colorado, USA ⁹National Research Centre "Kurchatov Institute", Moscow, Russian Federation Corresponding Author: A. R. Polevoi, alexei.polevoi@iter.org

Operational space (I_p, n) for long pulse scenarios $(t_{\text{burn}} \sim 1000 \text{ s}, Q > 5)$ foreseen in ITER was assessed by 1.5D core transport modelling with pedestal parameters predicted by the EPED1 code. The analyses include the majority of transport models (CDBM, GLF23, Bohm/GyroBohm (BgB), MMM7.1, MMM95, Weiland, Scaling-Based) presently used for interpretation of experiments and ITER predictions. The EPED1 code was modified to take into account boundary conditions predicted by SOLPS for ITER. In contrast with standard EPED1 assumptions the EPED1 with the SOLPS boundary conditions predicts no degradation of the pedestal pressure with density reduction. Reducing the plasma density to $n_e \sim 5-6 \times 10^{19} \text{ m}^{-3}$ leads to an increased plasma temperature (similar pedestal pressure) which reduces the loop voltage and increases the duration of the burn phase to $t_{\rm burn} \sim 1000 \, {\rm s}$ with Q > 5 for $I_p > 13$ MA at moderate normalised pressure, $\beta_N \sim 2$ in ITER. These ITER plasmas require the same level of additional heating power as the reference Q = 10 inductive scenario at 15 MA (33 MW NBI and 17-20 MW EC heating and current drive power). However, unlike the "hybrid" scenarios considered previously, these H-mode plasmas do not require specially shaped q profiles nor improved confinement in the core for the transport models considered in this study. Thus, these medium density H-mode plasma scenarios with $I_p > 13$ MA present an attractive alternative to hybrid scenarios to achieve ITER's long pulse Q > 5 and deserve further analysis and experimental demonstration in present tokamaks.

Examination of the Entry to Burn and Burn Control for the ITER 15 MA Baseline and Other Scenarios

C. Kessel¹, T. Casper², F. Felici³, S. Kim⁴, V. Leonov⁵, and *F. Köchl*⁶

¹ Princeton Plasma Physics Laboratory, Princeton, NJ, USA
 ²Lawrence Livermore National Laboratory, Livermore, CA, USA
 ³Eindhoven University of Technology, The Netherlands
 ⁴ITER Organization, Saint Paul lez Durance, France
 ⁵National Research Centre "Kurchatov Institute", Moscow, Russian Federation
 ⁶Institute of Atomic and Subatomic Physics, TU-Vienna, Vienna, Austria

Corresponding Author: C. Kessel, ckessel@pppl.gov

ITER will reach the burning regime $P_{\text{fusion}}/P_{\text{input}}$ of ~ 10 by operating in an ELMy H-mode. Control of the flattop burn phase is a critical demonstration for ITER, showing the simultaneous regulation of the plasma core fuel density, fusion power gain, and consistent divertor operation, under several constraints and perturbations. The ITPA-IOS group is doing time dependent integrated simulations (TSC/TRANSP, Corsica, CRONOS, ASTRA/ZIMPUR, RAPTOR) of the burn regime in ITER to understand impacts of physics uncertainties and to develop and test control strategies for the device. Entry to burn simulations are performed to examine the dependences on injected power, rate of rise of the density, argon impurity timing and amount, and feedback control. At SOF densities of $n_{20}(0) \sim 0.45$ showed marginal access for 43 MW of injected power, while 73 MW was capable of entering and sustaining an H-mode regardless of the density rise trajectory. Simulations examining early, medium, and late Ar injection showed that with 73 MW of input power the earlier injection did not hinder or significantly affect the entry to H-mode, while at 43 MW the timing and amount of Ar strongly affected the access. Simulations examined the impact of the multi-regime H-mode by considering type I ELMy H-mode for $P_{\rm net}/P_{\rm thr} \ge 1.3$ with $H_{98} = 1$, type III ELMy H-mode with $H_{98} = 0.8$ for $0.5 < P_{
m net}/P_{
m thr} < 1.3$, and hysteresis that maintains $H_{98} = 0.8$ until $P_{
m net}/P_{
m thr} < 0.5$ where H_{98} drops to 0.5 (L-mode). With 73 MW of input power, and 0.05 and 0.15% argon, fractions the plasma could enter type I H-mode and remain there, for 0.05%, while it dropped back to type III H-mode or lower, with lower energy confinement, at 0.15%. Simulations of a steady state scenario in flattop were conducted with simultaneous multi-variable feedback of the density by fueling, the fusion power by NB injection, power losses to the divertor by Ar impurity seeding, and the loop voltage with lower hybrid current drive power. Perturbations were introduced as an impurity burst at low and high levels, 0.7% and 2.0% to the electron density. The diagonal version of the controller could be used, and simulations of similar perturbations were examined at high Q, all showing good plasma controllability.

Work is partially supported by the US Department of Energy under DE-AC02-CH0911466



Study of ITER First Plasma Initiation Using a 3D Electromagnetic Model

A. Mineev¹, V. Belyakov¹, Y. Gribov², A. Kavin¹, K. Lobanov¹, A. Belov¹, E. Lamzin¹, and S. Sytchevsky¹

¹D. V. Efremov Institute of Electrophysical Apparatus, St. Petersburg, Russian Federation ²ITER Organization, Saint Paul lez Durance, France

Corresponding Author: A. Mineev, min-anat@mail.ru

The First Plasma operation is expected to be performed in ITER without blanket modules (with temporary limiters), with a toroidal magnetic field of 2.65 T at 6.2 m (half of the nominal value), starting from a partly charged central solenoid (producing half of the nominal poloidal magnetic flux). The First Plasma initiation will be more challenging in ITER than in present tokamaks. One reason is due to high stray magnetic fields caused by 1.5 MA of eddy currents induced in the vacuum vessel and by 70 MA of currents in the central solenoid (CS). Moreover, the First Plasma initiation is complicated by a low value of the toroidal electric field (0.3 V/m), by a high volume of the vacuum vessel (1700 m^3) and by a high content of impurities. On the other hand, several MW of ECRF heating will be available to assist plasma breakdown and burnthrough. Nevertheless, a carefully tuned poloidal field (PF) scenario will be essential to assure successful plasma initiation. The PF system should reduce the stray magnetic fields to about 2 mT in a large breakdown region with a minor radius of about 1.6 m and support a stable plasma equilibrium with increasing plasma current after the breakdown. Taking into account all of the above mentioned difficulties of plasma initiation in ITER, it is important to develop numerical tools to design a proper scenario of PF operation. So far, the design of scenarios of the PF system operation during plasma initiation and simulations of the plasma initiation were performed with the TRANSMAK code using 2D axisymmetric models of ITER conducting structures and 0D plasma transport model. In this paper, another approach is presented with first results of the design and simulation of PF scenarios of the First Plasma initiation using a 3D electromagnetic model developed on the basis of the TYPHOON codes. This model includes 3D conducting structures of the vacuum vessel and cryostat, the toroidal field (TF) coils, and the ferromagnetic inserts located between the shells of the vacuum vessel. The values of connection lengths confirm a good quality of the magnetic field null obtained using the 3D electromagnetic model: in the breakdown area with the effective minor radius 1.8 m the toroidally averaged components of the magnetic field is less than 2 mT and the connection length averaged over the boundary of this region is 2000 m.



Plasma Vertical Stabilization in ITER

Y. Gribov¹, A. Kavin², V. Lukash³, R. Khayrutdinov³, J. Snipes¹, and L. Zabeo¹

¹ITER Organization, Saint Paul lez Durance, France

²D. V. Efremov Institute of Electrophysical Apparatus, St. Petersburg, Russian Federation ³National Research Centre "Kurchatov Institute", Moscow, Russian Federation

Corresponding Author: Y. Gribov, yuri.gribov@iter.org

This paper describes the progress in analysis of the ITER plasma vertical stabilization (VS) system since its Design Review 2007–2008. Two indices characterising plasma vertical stabilization were studied. These are 1) the maximum value of plasma vertical displacement due to free drift that can be stopped by the VS system and 2) the maximum Root Mean Square value of low frequency noise in the dZ/dt "diagnostic" signal used in the VS feedback loop. The first VS index was calculated using the PET code for 15 MA high- $l_i \log$ - β plasmas. The second VS index was studied in the simulations of the most demanding for plasma magnetic control 15 MA scenarios having the fastest plasma current ramp-up with early X-point formation, the fastest plasma current ramp-down in divertor configuration and the H to L mode transition at the current flattop. The simulations were performed from the beginning of the central solenoid discharge till the end of plasma current ramp-down using the DINA code with feedback control of the plasma current, position and shape, taking into account engineering limits imposed on the coils, power supplies and plasma-wall gaps. The studies performed demonstrate that the VS in-vessel coils, adopted recently in the baseline design, increase of the VS controllability range by about a factor of 6 providing operating margins sufficient to achieve ITER's goals. PPC/P3-22

Paper

Evaluation of Fuelling Requirements and Transient Density Behavior in ITER Scenarios

M. Romanelli¹, V. Parail¹, A. Loarte², A. S. Kukushkin², G. Ambrosino³, M. Cavinato⁴, D. Harting¹, G. Corrigan¹, P. da Silva Aresta Belo¹, L. Garzotti¹, F. Köchl⁵, E. Militello Asp¹, and R. Sartori⁴

¹CCFE Fusion Association, Culham Science Centre, Abingdon, UK ²ITER Organization, Saint Paul lez Durance, France ³Università di Napoli Federico II, Italy ⁴F4E: Fusion for Energy, Barcelona, Spain ⁵Technical University Wien, Vienna, Austria

Corresponding Author: M. Romanelli, michele.romanelli@ccfe.ac.uk

ITER operation requires effective fuelling of the core-plasma for conditions in which neutral dynamics through the scrape-off layer is expected to affect significantly the efficiency of gas penetration. In order to assess fuelling requirements in transients as well as in stationary phases, integrated coreedge plasma modelling has been carried out for plasma conditions expected in the reference 15 MA Q = 10 scenario with emphasis on H-mode operation. The simulations follow the build-up of the H-mode scenario all the way through the L-mode phase, L-H transition, initial ELM free H-mode and the stationary ELMy H-mode phase with controlled ELMs. The JINTRAC suite of codes has been used for this analysis. As a first step the edge plasma has been modelled separately for a range of conditions with the EDGE2D/EIRENE code (included in the JINTRAC suite) and previous results obtained with SOLPS have been confirmed. Full plasma simulations have been carried out with JINTRAC in integrated mode with both the Bohm gyro Bohm core-transport model and GLF23 including two impurities species (Be and Ne). Simulations show that following the H-L transition for the 15 MA DT plasma fuelled by gas-fuelling only the plasma density increases initially on a very fast timescale. However, after this initial phase the pedestal density starts to evolve at a much slower rate due to the low value of particle transport diffusion in the pedestal (neoclassical) and decreasing edge transparency to neutrals and finally saturates at values of $n_e \sim (5-6) \times 10^{19} \text{ m}^{-3}$, even for the largest gas-fuelling rates achievable in ITER. Following the L-H transition the pedestal temperature raise rapidly until the edge stability limit is reached and ELMs are triggered. In correspondence of each ELM the density rise drops down significantly. This evolution is similar for DT H-mode plasmas in ITER over a large range of conditions suggesting that, within the uncertainties of the particle transport model, $n_e \sim (5-6) \times 10^{19} \text{ m}^{-3}$ is the highest plasma density achievable in H-mode with gas fuelling alone in ITER; thus allowing high n_e/n_{GW} operation by gas-fuelling only for the lowest plasma currents (5--7.5 MA). The achievement of high density H-modes for plasma currents above those requires pellet injection.

This work was funded jointly by the RCUK and ITER Task Agreement C19TD51FE.

Advances in the Physics Basis for the European DEMO Design

R. Wenninger^{1,7}, L. Aho-Mantila², C. Angioni¹, A. Fasoli³, J. Garcia⁴, G. Giruzzi⁴, F. Jenko¹, M. Wischmeier¹, H. Zohm¹, R. Albanese⁵, R. Ambrosino⁶, J.-F. Artaud⁷, M. Bernert¹, E. Fable¹, G. Federici⁷, P. Maget⁴, M. Mattei⁵, G. Ramogida⁶, B. Sieglin¹, and F. Villone⁵

¹Max-Planck-Institut für Plasmaphysik, Garching, Germany
 ²VTT Technical Research Centre of Finland, Finland
 ³Ecole Polytechnique Fédérale de Lausanne, CRPP, Lausanne, Switzerland
 ⁴CEA-IRFM, Saint Paul lez Durance, France
 ⁵CREATE/ENEA/Euratom Association, Università di Napoli, Naples, Italy
 ⁶Associazione EURATOM-ENEA Unitá Tecnica Fusione, Frascati, Italy
 ⁷EFDA, Garching, Germany

Corresponding Author: R. Wenninger, ronald.wenninger@ipp.mpg.de

In the European Fusion Roadmap ITER is followed by a Demonstration Fusion Power Reactor (DEMO), for which a conceptual design is now under development. The relevant physics knowledge need for the concept design analysis — referred to as DEMO Physics Basis — is incomplete. This contribution reports first results of a coherent effort to develop the DEMO Physics Basis, carried out by European experts. Based on an earlier assessment this program has been started in recent years and expanded in 2014 towards a more systematic and broader activity. To give an example, the vertical stability of a DEMO plasma has been investigated. Especially for typical ramp-down conditions critical growth rates have been found. Furthermore employing a realistic feedback control system, the required installed power to control the ramp-down plasma after an initial perturbation has been found to be out of the acceptable range. In order to quickly resolve this, it is planned to start already at this stage searching for a stable ramp-down trajectory. The program to develop the DEMO Physics Basis includes investigations in the areas of transport, MHD, fast particles, plasma wall interaction and disruptions. In this phase of the program it is essential to have an intense discussion with the international fusion science community on various aspects of DEMO modelling and extrapolation of experimental results to DEMO.



Combined Magnetic and Kinetic Control of Advanced Tokamak Steady State Scenarios based on Semi-Empirical Modeling

D. Moreau¹, J.-F. Artaud¹, J. Ferron², D. A. Humphreys², F. Liu¹, R. Prater², and M. L. Walker²

¹CEA-IRFM, Saint Paul lez Durance, France ²General Atomics, San Diego, CA, USA

Corresponding Author: D. Moreau, didier.moreau@cea.fr

This paper deals with combined magnetic and kinetic control for advanced tokamak (AT) operation, using the ARTAEMIS model-based approach, a method that relies on two-time-scale semi-empirical system identification and near-optimal control theory. It is applied here to the control of AT scenarios on DIII-D, in which the safety factor profile and the normalized pressure parameter, β_N , play a crucial role in governing plasma confinement and stability. A control-oriented state space model was identified from simulated data obtained using a rapidly converging plasma transport code, METIS, that includes an MHD equilibrium and current diffusion solver, and combines plasma transport non-linearity with 0D scaling laws and 1.5D ordinary differential equations [1]. A number of open-loop simulations were performed, in which four independent heating and current drive (H&CD) sources were randomly modulated around the typical values of a reference AT discharge on DIII-D: on-axis co-current neutral beam injection (NBI) power, off-axis co-current NBI power, electron cyclotron current drive power with an off-axis current deposition, and plasma surface loop voltage. Using these simulated data, a two-time-scale model was obtained for the coupled evolution of the poloidal flux profile and β_N , from which the controller was synthesized. The paper discusses the results of closed-loop nonlinear simulations, using this controller for steady state AT operation. These simulations are predictive of what would happen if DIII-D were able to run longer pulses, or in steady state devices such as EAST or Tore Supra/WEST. They were run with various sets of target profiles and controller settings, and with perturbations of the actuator values and plasma parameters. With feedforward plus feedback control the steady state target profiles and β_N parameter are satisfactorily tracked despite large disturbances applied to the feedforward powers and other plasma parameters. The effectiveness of the ARTAEMIS algorithm to simultaneously control the plasma poloidal flux profile, safety factor profile and β_N in steady state, fully noninductive AT discharges is thus demonstrated. Its robustness with respect to disturbances of the H&CD actuators and of plasma parameters such as the H-factor, plasma density and effective charge, is also shown.

References

[1] J.F. Artaud, et al., Nucl. Fusion 50 (2010) 04300.



Development of Real Time Multiple Control Algorithm for Integrated Control of Plasma Profiles and Neoclassical Tearing Mode

H.-S. Kim¹, S.-H. Kim², Y. Jeon³, K. Kim¹, M. H. Kim¹, and Y.-S. Na¹

 ¹Seoul National University, Seoul, Korea, Republic of ²ITER Organization, Saint Paul lez Durance, France
 ³National Fusion Research Institute, Daejeon, Korea, Republic of

Corresponding Author: H.-S. Kim, ftwalker.hyuns@gmail.com

Control of plasma profiles and magneto hydrodynamic (MHD) instabilities is essential to establish advanced operation scenarios, a promising approach towards DEMO. For the purpose of simultaneous control of these plasma profiles and MHD instabilities, an integrated real time control algorithm is developed in this work. The developed control algorithm deals with electron temperature (T_e) and safety factor (q) profiles for radial plasma profile control and the NTM for MHD instability control. Control of normalized β is also considered for a global performance control. We address the issue of the actuator sharing by avoiding conflict among each multiple control variables while maintaining a high performance plasma. The T_e and q profiles are controlled by using a new real time profile control approach which is applied to 2013 KSTAR experiments for its validation on control of T_e . For NTM control, the minimum growth rate seeking algorithm is adopted as an extremum seeking control. The normalized β is controlled using a classical Proportional-Integral-Derivative (PID) controller. Finally, all the control algorithms developed separately are combined into a multiple control algorithm. In this work, we employ a Multiple Model Multiple Controller Adaptive Controller which includes a supervisory control based on the Unfalsified Control principle and robust control techniques to synthesize the multiple controllers. In order to verify our approach, it is applied to KSTAR advanced operation scenarios developed using CRONOS by reflecting the planed KSTAR H/CD mix.



On Ohmic Breakdown Physics in a Tokamak

M.-G. Yoo¹, *Y.-S. Na*¹, J. Kim², Y. An¹, B. Jung¹, Y.-S. Hwang¹, S. B. Shim³, H. J. Lee³, and T. S. Hahm¹

¹Seoul National University, Seoul, Korea, Republic of ²National Fusion Research Institute, Daejeon, Korea, Republic of ³Pusan National University, Korea, Republic of

Corresponding Author: M.-G. Yoo, hope123@snu.ac.kr

The ohmic breakdown is the one of major methods to initiate the plasma in various devices. The electron avalanche, the main mechanism of the ohmic breakdown, is well described by traditional Townsend avalanche theory in the case of low pressure gas and simple slab geometry. The physical mechanism of the ohmic breakdown process in the tokamak, however, is not fully understood yet due to time-varying complex electromagnetic fields in toroidal geometry entirely different from the simple slab case. A deep understanding of the ohmic breakdown physics is essential to design robust and optimal breakdown scenarios in tokamak devices. Previous studies have focused on the qualities of the electromagnetic fields produced by external coil systems and by eddy currents induced in the vacuum vessel based on the Townsend avalanche theory. The avalanche phenomena during the breakdown, however, could be significantly affected by electric fields induced in the plasma due to space charge accumulated in the device. In this research, a PIC(Particle In Cell)-MCC(MonteCarlo Collision) code is developed to simulate the avalanche phenomena in the tokamak considering the space-charge effect and various atomic physics. The developed code is applied to the breakdown scenarios of tokamaks such as KSTAR and VEST tokamak. We found that the self-induced electric fields play crucial roles by decreasing the plasma density growth rate and by enhancing the perpendicular transport due to $E \times B$ drift. The space-charge effects newly observed in this research could be important clues to a deeper understanding of unresolved issues of the ohmic breakdown in the tokamak.

672



Improvements in the Fast Vertical Control Systems in KSTAR, EAST, NSTX, and NSTX-U

D. Mueller¹, N. W. Eidietis², D. Gates¹, S. Gerhardt¹, *S.-H. Hahn*³, E. Kolemen¹, J. Menard¹, Y.-S. Park⁴, S. A. Sabbagh⁴, S.-W. Yoon³, and B. Xiao⁵

¹Princeton Plasma Physics Laboratory, Princeton, NJ, USA
 ²General Atomics, San Diego, CA, USA
 ³National Fusion Research Institute, Daejeon, Korea, Republic of
 ⁴Columbia University, New York, USA
 ⁵Institute of Plasma Physics, Chinese Academy of Sciences, Hefei, China

Corresponding Author: D. Mueller, dmueller@pppl.gov

The realization of a wide variety of plasma shapes with varying plasma current density profiles places challenging demands on the vertical control system. In particular the bootstrap current scales quadratically with elongation at fixed normalized $\beta_N = \beta_T a B_T / I_p$ where I_p is the plasma current, B_T is the toroidal field, and $\beta_T = P/(B_T^2/2\mu_0)$ and P is the volume averaged plasma pressure. The plasma elongation is controlled by the action of coils that generally act to produce a field shape with an index of curvature that is closer to vertical instability as the elongation is increased. In devices such as KSTAR, EAST, and ITER, the superconducting coils are separated from the plasma by conducting structures that limit the plasma response time to changes in the coil currents. Fast control of the plasma vertical motion, essential for stable operation at high elongation and disruption avoidance, can be accomplished with coils internal to the vacuum vessel in these devices. Shape control systems in tokamaks are generally based upon equilibrium analysis that does not lend itself well to fast control and in particular cannot produce a reliable time derivative of the vertical position. The simple analysis of standard integrated magnetic signals to produce a vertical position (z) signal can be incapable of yielding a derivative term (dz/dt) that has sufficient signal-to-noise ratio to be adequate for control. Employing the difference of up-down symmetric un-integrated voltage loops can provide better signal to noise for dz/dt. The results of using the voltage loop-based sensors in the KSTAR and EAST fast vertical control system in their upcoming runs will be presented. In particular, the efficacy of employing these diagnostics in the fast control loop to achieve greater plasma elongation over a range of plasma internal inductance will be examined.

This research was supported by US DOE contract DE-AC02-09CH11466

Safety, Environmental and Economic Aspects of Fusion

SEE/P5-6

Paper

Control Requirement of Tokamak Fusion Power Plant for Power Generation in Grid System

R. Hiwatari¹, K. Okano², and K. Shinya³

¹Central Research Institute of Electric Power Industry, Japan ²Keio University, Tokyo, Japan ³Toshiba Nuclear Engineering Services Co., Japan

Corresponding Author: R. Hiwatari, hiwatari@criepi.denken.or.jp

There are several plant controls for a power plant in the electric grid system. Electric power supply from a fusion power plant (FPP) has to be also matched with the grid operation. Moreover, the grid system is now being renovated to a so-called smart-grid system, and the control functionality of a power plant in the grid system must be more sophisticated in several ten years. More functionality of FPP in the grid system, more valuable FPP will become to the grid operation. This paper discusses control requirements for FPP in the grid system. First, the development priority of plant operation controls for FPP is clarified, and control requirements on the core plasma and the primary and secondary cooling system are investigated.

The controls for commissioning (COM) and tripping to house load (THL) have to be investigated more carefully for the DEMO design. COM is a special control to carry out the final demonstration of electric supply and safe grid connection. THL is considered as a high development priority for FPP in order to re-supply power immediately after the accident of the grid system, because FPP generally requires a large ramp-up electric power from the grid system.

Operation flexibility for the plant control of COM and THL is investigated. When the fusion power increases, the plasma current profile is usually changed from the peaked to the flat or hollow one, because of increase of bootstrap current. As for plasma equilibrium, flux supply for the current rampup is restricted for a small fusion power operation, due to the peaked current profile and the maximum experienced magnetic field on CS coils. The position control of divertor strike points consistent with the plasma shape control is also critical issue. To fix the divertor strike points, the X-point and plasma shape are changed, and triangularity decreases from the rated value of 0.3 to about 0.2.

Next, several controls of the fusion power are assessed to find an operational space for COM and THL. The high confinement improvement factor is found to be required. The plasma current control is also found to prioritize for the fusion power control. From another viewpoint, the tritium ratio control is preferable for COM, because of reducing the initial tritium loading. Application of the turbine bypass in the secondary cooling system is also proposed for another control option of the electric output.



In-Situ Monitoring Hydrogen Isotope Retention in ITER First Wall

E. Mukhin¹, S. Tolstyakov¹, A. Smirnov², A. Bazhenov¹, P. Andrew³, R. Barnsley³,
I. Bukreev¹, P. Chernakov⁴, M. Kochergin¹, A. Koval¹, A. S. Kukushkin³, G. Kurskiev¹,
A. Litvinov¹, N. Litunovsky⁵, I. Mazul⁵, S. Masyukevich¹, I. Miroshnikov²,
A. Novohatsky¹, R. Pitts³, A. Razdobarin¹, A. Safronov¹, D. Samsonov¹, V. Semenov¹,
M. Shimada³, G. Vayakis³, and M. Wash³

¹Ioffe Physical-Technical Institute of the Russian Academy of Science, St. Petersburg, Russian Federation ²St. Petersburg State Polytechnical University, St. Petersburg, Russian Federation ³ITER Organization, Saint Paul lez Durance, France ⁴Spectral-Tech ZAO, St. Petersburg, Russian Federation ⁵D. V. Efremov Institute of Electrophysical Apparatus, St. Petersburg, Russian Federation

Corresponding Author: E. Mukhin, e.mukhin@mail.ioffe.ru

The routine operation of ITER leads to retention of a sufficient fraction of the tritium fuel. This requires an inventory of radioactive material which must be limited and monitored. As a nuclear device, ITER must limit in-vessel tritium retention to minimize the consequences of potential accidents during normal operation and maintenance as well as to reduce the potential for environmental contaminations. Even if safety is not a key issue, the economy of a fusion reactor ultimately depends on comparison of the tritium consumed by retention and by fusion.

A well-established way to extract the retained hydrogen is heating. The recently proposed in-situ technique for measuring hydrogen isotope retention in the tokamak first wall is based on the first wall local baking with the use of cw laser and analysis of thermally extracted gas components. The power density required to heat the tungsten ITER walls up to the $\sim 350^{\circ}$ C is of 0.1–0.4 kW/cm², depending on thickness and thermal conductivity of the deposited films. Two different methods are considered for detecting the quantity of released gas: 1) mass spectrometry and 2) atomic spectroscopy. Detection by mass spectrometry requires that the contribution to the torus pressure due to the heated spot is detected by a residual gas analyzer. To use instead atomic spectroscopy, it is necessary to locally concentrate the released gas. To accumulate the gas we propose to surround the heated target with a buffer gas (e.g., He, Ne or Ar) of 100 Pa pressure significantly exceeding that of hydrogen to be extracted. The extracted gas density and composition can be spectroscopically measured in locally generated plasma. Two local plasma sources, laser torch and ECR discharge, are discussed with the focus on their implementation in large fusion machines. To get absolute density from spectral line radiation without modeling of excited level populations, the intensity of hydrogen isotope lines has to be normalized to the radiation of known minor hydrogen additive.

Formation of the Business Ecosystem of the Big Science in Korea: Focus on Nuclear Fusion and Accelerator Devices

H. S. Tho¹, W. J. Choi¹, Y. B. Kim¹, and H. Chang¹

¹National Fusion Research Institute, Daejeon, Korea, Republic of

Corresponding Author: H. S. Tho, ths5001@nfri.re.kr

The importance of fundamental research for society and economic life has been underscored since the 1990's. In addition to scientific advancements, many "big science" institutes such as CERN also generate various types of economic and innovation benefits for their countries' economies. The direct and corollary financial effects generated by procurement activity have been investigated in several studies by CERN. However, in relation to nuclear fusion, this has not been studied thus far near as much in any country's fusion research institutes. Big science, referring to nuclear fusion and accelerators, shares the characteristics of requiring long-term and massive budget investments, human resources, and extreme technologies. In reality, such projects are often implemented through the formation of cooperative relations with small and medium businesses (SMBs) possessing outstanding technological capacities. On the other hand, the reality is that the entry of corporations into the business ecosystem of big science is not easy and that even those which have entered big science fail to find sales outlets for their developed technology following the supply of single items, thus leading to a situation in which their technological capacities lie idle. To enhance the ecosystem of Korean big science, we review the formation process of the business ecosystem of big science ecosystem in Korea.

Big science institutes are expected to play a critical role in the building of the technological competence of domestic industries, especially in developing countries. This study recommends a basis for more systemic cooperation between big science and industry, which would allow industry and new businesses based on new technology to work with and benefit from big science in a systematic manner, while also allowing big science to obtain the latest technologies and capable industrial partners at low cost. Consequently, the present study seeks to propose strategies for activating the business ecosystem of nuclear fusion and accelerators. It derives the four policy alternatives of approach, care, expansion, and infrastructure in accordance with the results of an empirical analysis to activate the business ecosystem of nuclear fusion and accelerators.



Analysis of Accident Scenarios of a Water-Cooled Tokamak DEMO

M. Nakamura¹, K. Ibano², K. Tobita¹, Y. Someya¹, H. Tanigawa¹, W. Gulden³, and Y. Ogawa²

¹Japan Atomic Energy Agency, Naka, Japan ³F4E: Fusion for Energy, Barcelona, Spain ²University of Tokyo, Japan

Corresponding Author: M. Nakamura, nakamura.makoto@jaea.go.jp

Safety of tokamak DEMO cooled by pressurized water has been studied for the first time. We have quantitatively assessed consequences of two types of accidents: ex-vessel and in-vessel loss-of-coolant accidents (LOCAs) of the first wall/blanket cooling channels. As for the former case, we have analyzed ex-vessel double-ended break of the cooling channel. The analysis result suggests that the reactor building has a mitigation function of tritium release to the environment against the ex-vessel LOCA. As for the latter case, we have analyzed multiple, double-ended outboard first wall cooling pipe break in the vacuum vessel of the whole perimeter in the toroidal direction. The analysis result suggests that the pressure in the vacuum vessel reaches the design value even though the pressure suppression system is in operation. Possible safety provision for such a major in-vessel LOCA is proposed.

Preprint SEE/P5-12

Review of the Safety Concept for Fusion Reactor Concepts and Transferability of the Nuclear Fission Regulation to Potential Fusion Power Plants

J. Herb¹, J. Raeder², A. Weller², R. Wolf², L. V. Boccaccini³, D. Carloni³, X. Z. Jin³, R. Stieglitz³, and C. Pistner⁴

¹Gesellschaft für Anlagen- und Reaktorsicherheit (GRS) mbH, Germany
 ²Max-Planck-Institut für Plasmaphysik, Garching, Germany
 ³Karlsruhe Institute of Technology, Germany
 ⁴Öko-Institut e.V. (Institute for Applied Ecology), Freiburg im Breisgau, Germany
 Corresponding Author: J. Herb, joachim.herb@grs.de

During the last decades a safety concept for fusion power plants (FPP) has been developed which is based on the defence-in-depth safety concept of installations with radioactive inventories, especially nuclear fission power plants. We present the main findings of a thorough literature study to reveal the current state of the fusion safety concept. The safety concept for FPPs like the concept for nuclear (fission) power plants (NPP) applies the concept of defence in depth. However, specific differences were identified between the implementations of the safety concepts due to the physical and technological characteristics of fusion and fission.

In safety concepts based on the concept of levels of defence, postulated initiating events (PIE) are identified and assigned to different levels of defence, covering the range from normal operation to very rare events. We also examine the transferability of the current German nuclear fission safety requirements to the concepts of FPPs and especially the transferability of the fundamental safety function "confinement of the radioactive materials", "cooling" and "reactivity control".

Like in a NPP, in a FPP measures and installations are foreseen to limit the consequences of PIEs to the radiological criteria of the applicable level of defence. Inherent physical principles, as well as passive and active safety systems are used for these measures and installations. Due to the current level of detail for the design of future FPP, the criteria for the measures and installations on the different levels of defence are not yet as detailed as for a fission power plant.

The safety analyses in the reviewed fusion literature have focused on plant-internal events. According to the current developments in the safety concepts of NPPs external hazards, e.g., earthquakes and flooding, or very rare human-induced hazards, e.g., the crash of a large airplane, have to be considered in safety analyses. These advanced requirements will also be applicable to future FPPs. Therefore, together with the development of more detailed plant concepts also events resulting from external hazards or very rare human-induced hazards have to be taken into account in more detail.

Paper

Tritium Safety Assessment for Fusion Reactor Based on Fuel Cycle and Environmental Dispersion Modelling

M. Ni¹, B. Nie¹, C. Lian¹, J. Jiang¹, and Y. Wu¹

¹Institute of Nuclear Energy Safety Technology, CAS, Anhui, China Corresponding Author: M. Ni, muyi.ni@fds.org.cn

The environment assessment of large inventory tritium in fusion reactor is an important issue before fusion energy can be considered for commercial use. In this paper, a new approach for assessing the radioactive consequences of tritium release under accident events has been developed. Firstly, the tritium fuel cycle in fusion reactor was simulated based on system dynamics method, and the tritium inventories in each subsystems were evaluated. And combined with FMEA (Failure Mode and Effects Analysis) of tritium plant, the potential tritium release source and its relevant probability were discussed in detail. Then, the processes of tritium atmosphere dispersion, dry and wet deposition, HT oxidation in air and soil, HTO reemission, HT/HTO/OBT transfer among the soil, plants, animals and human beings had been took into detailed consideration. Gaussian puff model and related corrections were introduced to calculate the accident emission and reemission, and a virtual point source method was utilized for HTO reemission modeling. Finally, an integral average of tritium concentration in atmosphere was used for dose assessment of the public. Using those models, a tritium safety assessment module of Tritium Analysis program for fusion System (TAS) was developed. A final discussion showed the improved accuracy and many advantages of this "fuel cycle – environment dispersion" coupling method for tritium safety assessment under accident events.



Physics Design and Economic Assessment of a Long-Pulsed Fusion Power Plant

D. Chen¹, W. Duan¹, Y. Hou¹, J. Jiang¹, and Y. Wu¹

¹Institute of Nuclear Energy Safety Technology, CAS, Anhui, China Corresponding Author: D. Chen, dehong.chen@fds.org.cn

A fusion power plant based on long-pulsed operated tokamak fusion reactor was proposed to avoid the issues of steady-state operation of noninductive current driven methods. The plasma current, excepting the bootstrap current, is only driven inductively to sustain several hours. The burning stage can be sustained by α heating and started by ohmic and radio frequency wave heating methods. Thus, the axillary heating methods was cut in order to save about 1/3 of gross electric power supply to them. With 0.8 of plant capability assumed, the capital cost and cost of electricity (COE) were assessed and minimized to search feasible physics designs with stable power balance and under feasible engineering conditions. The plasma equilibrium and charge evolution were analyzed with TSC (Tokamak Simulation Code) to verify the magnetic flux requirement and stability of self-sustained heating and inductive current driven. The COE was also compared with the case of steady-state operation with sensitivity analysis of duty ratio and efficiency of noninductive current driven methods. The results indicated that the feasibility of the periodic operated fusion reactor depends on its duty ratio and can be an alternative scenario for future demonstration reactor and fusion power plant.

Post-Deadline contributions



PD/P3-1

Improved beta (local $\beta > 1$) and density in electron cyclotron resonance heating on the RT-1 magnetosphere plasma

M. Nishiura¹, Z. Yoshida¹, H. Saitoh¹, Y. Yano¹, Y. Kawazura¹, T. Nogami¹, and M. Yamasaki¹

¹University of Tokyo, Japan

Corresponding Author: M. Nishiura, nishiura@ppl.k.u-tokyo.ac.jp

This study reports the recent progress in improved plasma parameters of the RT-1 device. Increased input power and the optimized polarization of electron cyclotron resonance heating (ECRH) with an 8.2 GHz klystron produced a significant increase in electron beta, which is evaluated by an equilibrium analysis of Grad-Shafranov equation. The peak value of the local electron beta β_e was found to exceed 1. In the high beta and high-density regime, the density limit was observed for H, D, and He plasmas. The line average density was close to the cutoff density for 8.2 GHz ECRH. A density limit exists even at the low beta region. This result indicates the density limit is caused by the cutoff density rather than the beta limit. From the analysis of interferometer data, the uphill diffusion produces a peaked density profile beyond the cutoff density.

Preprint

Plasma Confinement in the Trimix-3M Multipole Galatea Trap

A. Bishaev¹, G. Bugrov¹, M. Gavrikov², A. Desytskov¹, M. Kozintseva¹, T. Kolesnikova¹, B. Kopchenkov¹, V. Savel'ev², and M. Shapovalov¹

¹Moscow State Technical University of Radioengineering, Electronics and Automation, Moscow, Russian Federation

²Keldysh Institute of Applied Mathematics, RAS, Moscow, Russian Federation

Corresponding Author: A. Bishaev, bishaev@mirea.ru

Quasi-stationary plasma confinement with a high β value was implemented in the Trimix-3M multipole magnetic trap. In the trap, magnetic surfaces of complex cross-section delimit a closed toroidal region with zero magnetic field at its center. The lifetime of the plasma in the trap is ~ 1 ms and the average value of β is ~ 0.35. The Rogowski loop is used to measure the value of the toroidal current arising after the injection of a plasmoid through the magnetic crust of the Trimix-3M magnetic multipole trap. This current is due to plasma diamagnetism. A relation is established between the value of the diamagnetic current and the maximal plasma pressure realized on the separatrix of the magnetic field of the trap. It is thus shown that magnetic measurements in the multipole trap, for a known concentration value, allow us to determine the plasma temperature in the trap and the energy confinement time. Injection of a plasmoid is implemented through the magnetic crust of the trap. Both theory and experiment have shown that the depth of penetration of the plasmoid into a transverse magnetic field is proportional to the plasmoid energy and is inversely proportional to the magnetic pressure and the cross-section area of the plasmoid. This fact can be used to optimize the process of trapping a plasmoid.

Magnetic System of Multipole Trap–Galatea on the Basis of Levitating Quadrupole

M. Kozintseva¹, A. Bishaev¹, A. Bush¹, M. Gavrikov², A. Denis'uk¹, K. Kamentsev¹, T. Kolesnikova¹, V. Savelyev², and A. Sigov¹

¹Moscow State Technical University of Radioengineering, Electronics and Automation, Moscow, Russian Federation

²Keldysh Institute of Applied Mathematics, RAS, Moscow, Russian Federation

Corresponding Author: M. Kozintseva, kozintseva@mirea.ru

The possibility of the creation of the magnetic system of multipole trap-Galatea on the basis of the levitating quadrupole from the superconducting coils-rings is considered. Based upon the superconductor property to conserve the trapped magnetic flux the analytical dependence of the potential energy of the proposed configurations from the coordinates of the levitating coils and the deflection angle of their axis has been obtained. The calculations in Mathcad system have shown that under the definite values of the physical parameters (the trapped magnetic flux, dimensions and masses of coils, etc.) this dependence has local minimums, which correspond to the stable equilibrium states of levitating coils. For carrying out experiments with levitation several multiturn short-circuited coils-rings have been made from the high-temperature superconducting (HTSC) wire of the SCS4050-i-AP 2G HTS type. HTSC rings have been made also from the preliminary synthesized powder of HTSC phase YBa2Cu3Oy with the help of melt textured growth (MTG) method. Using the experimental data on the trapped magnetic fluxes for HTSC rings, their dimensions and masses, and also the parameters of the ordinary coil with the current, with the help of calculations of the pointed out dependence for the potential energy the search of the equilibrium states for the different cases has been carried out. Under the magnetic fluxes of the same polarity in coils, the stable levitating states of: 1) single HTSC ring both in the field of other HTSC ring and in the filed of the ordinary coil with the current; 2) two HTSC rings in the filed of the ordinary coil with the constant current are observed experimentally in positions corresponding to calculated values.

Preprint

Short Way Separation of D/T from He with Superpermeable Membranes in the Post-ITER Devices

A. Livshits¹, A. Yukhimchuk²

¹Bonch-Bruevich St. Petersburg State University of Telecommunications, St. Petersburg, Russian Federation ²All-Russia Research Institute of Experimental Physics, Sarov, Russian Federation

Corresponding Author: A. Livshits, livshits@sut.ru

Due to severe limitations on the content of He in the plasma, the exhaust of nuclear fusion reactor will mainly consist of unburned fuel, including expensive and radioactive tritium. If all this exhaust mixture is directed to the tritium plant for its separation from helium and other impurities (as planned in ITER), this leads to a significant tritium inventory in the vacuum pumps and processing systems.

To reduce the cost and improve the safety of nuclear fusion power plant it would be desirable to separate the major portion of D/T mixture from He in the immediate vicinity of the divertor output, compress it there and direct it back into the plasma by the shortest way passing the tritium plant.

The membranes superpermeable to suprathermal hydrogen particles can be applied for the realization of such "short way separation" scheme in future fusion machines and first of all in DEMO. Suprathermal hydrogen particles whose energy (kinetic, chemical or internal) exceeds ≈ 1 eV are able to pass through the superpermeable membrane (SPM) almost like an opening of the same area. SPM separates the permeating hydrogen from any impurities including He as well as automatically compresses it by orders of magnitude.

The combination of SPM with the plasma generation of suprathermal hydrogen appears to be most suitable technical solution. It would be reasonable to start the experiments with SPM coupled with plasma in favor of post-ITER devices including DEMO. Such experiments must be mainly purposed for modeling, testing and optimization of possible arrangements for the short way refueling in fusion machines.

PD/P5-1

Paper

Negative Triangularity Tokamak: Stability Limits and Perspectives as Fusion Energy System

S. Medvedev^{1,2}, M. Kikuchi³, L. Villard⁴, T. Takizuka⁵, P. Diamond⁶, H. Zushi⁷, K. Nagasaki⁸, X. Duan⁹, Y. Wu¹⁰, A. Ivanov¹, A. Martynov¹, Y. Poshekhonov¹, A. Fasoli⁴, and O. Sauter⁴

¹Keldysh Institute of Applied Mathematics, RAS, Moscow, Russian Federation
 ²National Research Nuclear University MEPhI, Moscow, Russian Federation
 ³Japan Atomic Energy Agency, Naka, Japan
 ⁴Ecole Polytechnique Fédérale de Lausanne, CRPP, Lausanne, Switzerland
 ⁵Osaka University, Osaka, Japan
 ⁶University of California San Diego, CA, USA
 ⁷Riam Kyushu University, Fukuoka, Japan
 ⁸Institute of Advanced Energy, Kyoto University, Kyoto, Japan
 ⁹Southwestern Institute of Physics, Chengdu, Sichuan, China
 ¹⁰Institute of Nuclear Energy Safety Technology, CAS, Anhui, China

Corresponding Author: S. Medvedev, medvedev@a5.kiam.ru

Fusion research has to solve the power handling toward fusion demonstration power reactor (DEMO). A tokamak plasma with strongly negative triangularity may offer such an opportunity as an innovative concept. The present paper discusses the edge stability, beta limits and power handling issues for the negative triangularity tokamaks. The edge MHD stability is the most crucial item for power handling in tokamak. The key design philosophy is to achieve a "soft-edge beta limit" instead of achieving the highest possible beta for the steady state operation with a high bootstrap current fraction. This may lead to a fundamental change to the direction of advanced tokamak research. That is why negative triangularity tokamak plasmas are subject to an increased interest both in existing experiments and in studies of core physics as well as power handling relevant to DEMO.

For the case of negative triangularity, the 2nd stability access is closed for ballooning modes. The destabilization of a whole range of fixed boundary medium- and low-*n* modes takes place for pedestal heights just above the values for which the Mercier criterion for localized modes is violated, implying possible changes in the ELM characteristics. While negative triangularity plasma has some favorable MHD property to ELMs, the beta limit is relatively low. Negative triangularity tokamak configurations with optimized pressure gradient profiles can be stable for normalized $\beta \sim 3$ at moderate elongation k = 1.5 and internal inductance value 0.9, even in the absence of the magnetic well.

Apart from the ELM mitigation, negative triangularity tokamaks feature other possibilities for power handling such as naturally increased separatrix wetted area and more flexible divertor configuration using PF coils inside the TF coil made of NbTi superconductor in the low field region. Negative triangularity experiments in TCV show a reduction in electron heat transport by a factor two compared with D-shaped configuration, which is partly explained by nonlinear gyrokinetic simulations. This configuration also allows the inboard ECRF launching to have higher density limit for the ECRF propagation and better pumping accessibility due to larger conductance. The SOL width may also be modified especially in the case of double null configuration with almost vertical magnetic surfaces at the LFS.



Paper

Enhanced Pedestal Performance in DIII-D Elm-free H-modes with Lithium Injection

G. L. Jackson¹, R. Maingi², J. A. Boedo³, A. R. Briesemeister⁴, J. S. deGrassie¹,
R. Groebner¹, A. W. Leonard¹, G. R. Mckee⁵, R. Moyer³, R. Nazikian², T. L. Rhodes⁶,
A. L. Roquemore², T. H. Osborne¹, P. B. Snyder¹, D. Mansfield², C. P. Chrobak¹,
B. A. Grierson², A. G. McLean⁷, Z. Yan⁵, S. L. Allen⁷, and D. Battaglia²

¹General Atomics, San Diego, CA, USA
 ²Princeton Plasma Physics Laboratory, Princeton, NJ, USA
 ³University of California San Diego, CA, USA
 ⁴Oak Ridge National Laboratory, Oak Ridge, TN, USA
 ⁵University of Wisconsin-Madison, Madison, WI, USA
 ⁶University of California Los Angeles, CA, USA
 ⁷Lawrence Livermore National Laboratory, Livermore, CA, USA

Corresponding Author: G. L. Jackson, jackson@fusion.gat.com

With lithium injection, an enhanced pedestal with ELM-free periods up to 350 ms has been observed, accompanied in the edge region by increased density fluctuations and reduced intrinsic impurity accumulation in the core plasma. The increase in pedestal width is rapid, usually occurring in a few ms and can expand by more than 100% during the ELM-free phases with lithium injection. This is accompanied by an increase of more than two times the edge pedestal electron pressure and confinement enhancements, $H_{98}(y, 2)$ up to 2.1 have been obtained.



PD/P5-4

Gyrokinetic study of ASDEX-Upgrade inter-ELM profile evolution

D. Hatch¹, F. Jenko², E. Wolfrum², E. Viezzer², M. Dunne², M. J. Pueschel³, D. Told², and H. Doerk²

¹University of Texas at Austin, Austin, TX, USA ²Max-Planck-Institut für Plasmaphysik, Garching, Germany ³University of Wisconsin-Madison, Madison, WI, USA

Corresponding Author: D. Hatch, drhatch@austin.utexas.edu

The gyrokinetic Gene code is used to study Inter-ELM H-mode pedestal profile evolution for an ASDEX-Upgrade discharge. Four main instabilities are observed during various inter-ELM phases—density gradient driven drift waves (DW), microtearing modes (MTM), kinetic ballooning modes (KBM), and electron temperature gradient (ETG) modes. DWs are the dominant pedestal instability during the early density-buildup phase. The drift waves are characterized by significant outward particle flux, and show no evidence of a large pinch mechanism. The electron temperature gradient achieves a critical value early in the ELM cycle, concurrent with the appearance of both MTMs and ETG modes. The nominal profiles are stable to KBMs, but moderate increases in β are sufficient to surpass the KBM threshold. Certain aspects of the dynamics support the premise of KBM-constrained pedestal evolution; the density and temperature profiles separately undergo large changes, but in a manner which keeps the pressure profile constant and near the KBM limit. Nonlinear simulations of DW turbulence and ETG turbulence are also described.

Preprint

Plasmoid Ejection Mechanism in Dynamic Divertor Experiment and Simulation

Y. Ono¹, S. Inoue¹, Y. Hayashi¹, C. Z. Cheng¹, and R. Horiuchi²

¹University of Tokyo, Japan ²National Institute for Fusion Science, Toki, Japan

Corresponding Author: Y. Ono, ono@k.u-tokyo.ac.jp

We have been developing a new type of divertor concept: "dynamic divertor" composed of periodic ejection of plasmoid from a core-plasma and its gas-puff cooling, to reduce significantly heat flux to divertor plates. Our TS-4 experiment and PIC simulation consistently solved the plasmoid formation and pinch-off mechanisms essential to the dynamic divertor operation. We found the acceleration dV/dt of plasmoid promotes its pinch-off from the core-plasma through fast reconnection and also that the external inflow flux controlled by the external coil current increases with the plasmoid size. In TS-4, the X-point region between the ST plasma and the divertor plate are formed by induction of two poloidal field (PF) coils. The corresponding plasmoid ejection was observed in 2-1/2D Full PIC simulation (PASMO) with 2×10^{10} particles in a domain of (x, y) = (512, 256) Debye length under uniform guide field ~ 4 reconnecting magnetic field. The maximum acceleration rate dV/dtof plasmoid occurs simultaneously with the maximum reconnection electric field E_t , indicating that the acceleration rate of plasmoid is directly connected with the reconnection time — the plasmoid pinch-off time like the coronal mass ejection in the solar flares. The plasmoid ejection from the current sheet reduces significantly its thermal and magnetic pressures, causing further thinning of the current sheet. When the current sheet is compressed thinner than the ion meandering length (ion gyro-radius), its effective resistivity tends to increase significantly, causing its anomalous dissipation and thus faster reconnection rate, both in TS-4 experiment and the PIC simulation. They agree in the normalized plasmoid ejection time ~ 5 Alfven time but E_t and dV/dt in the former is 70% and 50% of those in the latter, probably due to low downstream magnetic pressure in the slab model simulation. The PIC simulation also indicates that the heat flux from the core-plasma is transported along the separatrix field line and confined in the plasmoid. The field-aligned velocity component is essential to the plasma transport from the core-plasma to the plasmoid, which indirectly connects them for the gas-puff cooling.

Innovative Concept of the Compression and Heating of the Plasma Targets in the Scheme for Magneto-Inertial Fusion

S. Ryzhkov¹, V. Kuzenov¹, and P. Frolko¹

¹Bauman Moscow State Technical University, Moscow, Russian Federation Corresponding Author: S. Ryzhkov, svryzhkov@gmail.com

This paper presents a concept of dynamic plasma compression which unites a technique of megagauss magnetic field generation and methods of plasma confinement in a specially formed magnetic configuration. This concept is a determining one for the magneto-inertial (hybrid) approach to the controlled thermonuclear fusion. Comparing to the inertial confinement the main magneto-inertial fusion advantages are smaller values of plasma density and temperature, which are nevertheless sufficient for heating the target and thermonuclear reaction ignition. In this case magnetized plasma is initially created inside an axisymmetric magnetic trap and exposed to direct compression by means of laser beams (laser driver) and/or plasma jets (plasma liner).

Prospective high energy density systems such as different sources of neutrons and protons will be used in the near future to perform cutting-edge materials research, non-destructive analysis, medical isotope production, chemical waste disposal, personnel training, etc. The goal of the investigation is complex numerical research and optimization of the pulsed high-temperature processes in a dense magnetized plasma (target). Distinctive feature of this problem is the presence of initial seed fields (the imposed external pulse magnetic field) and compression of a magnetic flux by laser beams (laser driver) or plasma jets (plasma liner). An embedded magnetic field is compressed along with the target plasma to achieve magnetic insulation. The presence of the megagauss magnetic field strongly inhibits electron thermal conduction losses by several orders of magnitude. Modeling of magnetized plasma compressed by the laser beams and plasma jets is described. Theoretical estimation of MIF prospects as the target compressed by a pusher (laser Driver or plasma liner) for the achievement of fusion temperatures is done.



Paper

Direct heating of imploded plasma by fast-ions in the fast ignition scheme

A. Sunahara¹, T. Johzaki², H. Sakagami³, H. Nagatomo⁴, Y. Arikawa⁴, S. Fujioka⁴, H. Shiraga⁴, H. Azechi⁴, K. Mima⁵, Y. Mori⁵, and Y. Kitagawa⁵

 ¹Institute for Laser Technology, Suita, Osaka, Japan
 ²Graduate School of Engineering, Hiroshima University, Higashi-Hiroshima, Japan
 ³National Institute for Fusion Science, Toki, Japan
 ⁴Institute of Laser Engineering, Osaka University, Osaka, Japan
 ⁵Graduate School for the Creation of New Photonics Industries, Hamamatsu, Shizuoka, Japan

Corresponding Author: A. Sunahara, suna@ile.osaka-u.ac.jp

In the conventional fast ignition scheme of inertial confinement fusion (ICF), the heating laser energy is transferred to energetic fast electrons towards the imploded plasma core and heats it while the high dense core is maintained. We propose direct heating of the imploded core by the ultra-intense laser in the fast-ignition scheme. When the high pressure of imploded core plasma breaks the tip of the cone up, the heating laser directly irradiates the imploded plasma expanding into cone and generates the fast-ions as well as the fast-electrons. Both fast-ions and electrons are generated and they contribute to the heating of the imploded core plasma simultaneously. In order to estimate the temperature scaling of the core heated by fast-ions and electrons in this scheme, we investigated the conversion efficiency and the kinetic energy of generated energetic particles. Then, we calculated the transport of particles in the imploded core. We obtained the calculated results that the core temperature reached beyond 5 keV for the laser intensity of 10^{21} W/cm², in which the core peak temperature was obviously larger than that with electron heating only for the same laser condition. Also, we conducted a preliminary experiment in this scheme by using 1 kJ 1.5 ps ultra-intense heating laser (LFEX) and Gekko XII laser system at Osaka University. To confirm that the heating laser directly irradiates the imploded core plasma, we use the tip-less DLC cone attached CD shell target. We had three shots with different LFEX injection timing, -200 ps to +200 ps from maximum compression of the implodedcore. We observed increasing neutron yields of $2-3 \times 10^6$, compared to the yields of $1-3 \times 10^5$ without heating laser.

PD/P6-4

Overview of the results of the ABC facility at ENEA-Frascati

R. De Angelis¹, F. Consoli¹, P. Andreoli¹, G. Cristofari¹, G. Di Giorgio¹, M. Cipriani¹,
F. Ingenito¹, A. Y. Gus'kov², A. Rupasov², M. Calamosca³, A. Bonasera⁴, M. Barbarino⁴,
M. Kalal⁵, D. Giulietti⁶, A. Curcio⁶, C. Verona⁷, and G. Verona Rinati⁷

 ¹Associazione EURATOM-ENEA Unitá Tecnica Fusione, Frascati, Italy
 ²P. N. Lebedev Physical Institute, RAS, Moscow, Russian Federation
 ³ENEA, Istituto di radioprotezione, Bologna, Italy
 ⁴INFN-LNS, Catania, Italy
 ⁵Faculty of Nuclear Sciences and Physical Engineering, Czech Technical University, Prague, Czech Republic
 ⁶Dipartimento di Fisica "E. Fermi", Università di Pisa, Pisa, Italy
 ⁷Dipartimento di Ingegneria Industriale, Università di Tor Vergata, Rome, Italy

Corresponding Author: R. De Angelis, riccardo.deangelis@enea.it

The laboratory for inertial confinement fusion is dedicated to the study of laser produced plasmas in the two-beam laser facility ABC, which can deliver up to 200 J in pulses of 3 ns duration. The system is suitable for irradiating planar targets at $I = 10^{14--15}$ W \cdot cm⁻². This paper summarizes the main research programs brought forward in the last year.

Theoretical and experimental investigations have been dedicated to the study of porous absorbers and to the measurements of their homogenizing properties. The efficiency with which the laser energy is absorbed and transmitted after conversion to a shock wave in the plasma is measured by the volumes of craters left on the metal holders. Shadowgraphic images and time resolved interferometry are used to study the density behavior. Numerical simulation of the hydrodynamic stability of the plasma are also under study with the Multi2D code [4].

The possibility of producing the proton Boron fusion reaction $p + {}^{11}\text{B} \rightarrow 3\alpha$ in a laser produced plasma are also studied at laser intensities up to $10^{15} \text{ W} \cdot \text{cm}^{-2}$. The tracks observed on CR 39 detectors are compared with numerical prediction in order to define if they are α particles originating from *p*B fusion reactions.

The emission of electromagnetic waves in the radiofrequency-microwave range has been observed in many experiments of laser-plasma interaction. The spectral range of these waves can reach several gigahertz and can be of very high intensity, representing a source of noise and a possible limitation on the use of some detectors. In this work we describe the measurements of this electromagnetic pulse, under different conditions of laser-plasma interaction and for different kind of targets[5].

References

[1] S.Yu. Gus'kov et al., JETP 81, 296 (1995).

[2] S.Yu. Gus'kov et al., Laser Part. Beams 17, 287 (1999).

[3] R. De Angelis et al., Proceedings of the IFSA conference 2013–Nara.

[4] R. Ramis, J. Meyer-ter-Vehn, J. Ramirez, Computer Physics Communications, **180**, 6, June 2009, pp 977–994.

[5] Proceedings of ICFTD 2013, Frascati, Rome.

Preprint

Design Concept of K-DEMO for Near-Term Implementation

K. Kim¹

¹National Fusion Research Institute, Daejeon, Korea, Republic of

Corresponding Author: K. Kim, kkeeman@nfri.re.kr

Korean Fusion Energy Development Promotion Law (FEDPL) was enacted in 2007 to promote a long-term cooperative fusion research and development among participating industries, universities and research institutes. As a following step, a conceptual design study for a steady-state Korean fusion demonstration reactor (K-DEMO) has been initiated in 2012. The conceptual design activity will continue to the end of 2021 and the finish of the construction is planned to be completed by the end of 2037.

One special concept discussed of K-DEMO is a two-staged development plan. At first, K-DEMO is designed not only to demonstrate a net electricity generation ($Q_{eng} > 1$) and a self-sustained tritium cycle (Tritium breeding ratio, TBR>1.05), but also to be used as a component test facility. Then, at its second stage, a major upgrade is carried out by replacing in-vessel components in order to show a net electric generation on the order of 500 MWe. After the thorough 0-D system analysis, the major radius and minor radius are chosen to be 6.8 m and 2.1 m, respectively, considering practical engineering feasibilities. In order to minimize the deflection of wave and maximize the efficiency, a top launch high frequency (> 200 GHz) electron cyclotron current drive (ECCD) system is the main candidate for the current profile control and off-axis current drive of K-DEMO. For matching the high frequency ECCD, a high magnetic field is required and it can be achieved by using high performance Nb3Sn-based superconducting conductor currently being used in accelerator magnet area and the peak magnetic field is approaching to 16 T with the magnetic field at the plasma center above 7 T. Pressurized water is the most prominent choice for the main coolant of K-DEMO when considering balance of plant development details. Considering the plasma performance and the peak heat flux in the divertor system, a double-null divertor system becomes the reference choice of K-DEMO. For a high availability operation, K-DEMO incorporates a vertical maintenance design.

A design concept and radial builds for K-DEMO considering a vertical maintenance scheme are presented together with preliminary design parameters.

Summary



Summary EX/C, EX/D, PPC

C. Hidalgo¹

¹The National Fusion Laboratory, CIEMAT, Madrid, Spain Corresponding Author: C. Hidalgo, carlos.hidalgo@ciemat.es Summary EX/C, EX/D, PPC.

S/1-2

Summary EX/S, EX/W, ICC

A. Sen¹

¹Institute for Plasma Research, Bhat, Gandhinagar, India Corresponding Author: A. Sen, senabhijit@gmail.com Summary EX/S, EX/W, ICC.

Summary Theory

A. Fukuyama¹

¹Kyoto University, Kyoto, Japan

Corresponding Author: A. Fukuyama, fukuyama@nucleng.kyoto-u.ac.jp Summary Theory.

Preprint Slides

6

Summary IFE

S. Jacquemot¹

¹LULI, France

Corresponding Author: S. Jacquemot, sylvie.jacquemot@polytechnique.fr Summary IFE.



Summary FIP, FNS, MPT, SEE

B. Kuteev¹

¹National Research Centre "Kurchatov Institute", Moscow, Russian Federation Corresponding Author: B. Kuteev, kuteev@nfi.kiae.ru Summary FIP, FNS, MPT, SEE.

Indices

Index by contribution number

EX/1-1136	EX/P1-30 187	EX/P3-49 243
EX/1-2137	EX/P1-32 188	EX/P3-5 229
EX/1-3138	EX/P1-33 189	EX/P3-50 244
EX/1-4139	EX/P1-36 190	EX/P3-52 245
EX/1-5140	EX/P1-37 191	EX/P3-54 246
EX/10-1167	EX/P1-38 192	EX/P3-55 247
EX/10-2	EX/P1-39 193	EX/P3-56 248
EX/10-3169	EX/P1-40 194	EX/P3-57 249
EX/10-4170	EX/P1-41 195	EX/P3-59 250
	EX/P1-42 196	EX/P3-6 230
EX/11-1171		
EX/11-2Ra 172	EX/P1-43 197	EX/P3-7231
EX/11-2Rb 173	EX/P1-44 198	EX/P3-8 232
EX/11-3174	EX/P1-45 199	EX/P3-9 233
EX/11-4175	EX/P1-46 200	EX/P4-1251
EX/2-1141	EX/P1-47 201	EX/P4-20 252
EX/2-2142	EX/P1-48 202	EX/P4-21 253
EX/2-3143	EX/P1-49 203	EX/P4-22 254
EX/3-1144	EX/P1-50 204	EX/P4-23 255
EX/3-2145	EX/P1-51 205	EX/P4-24 256
EX/3-3146	EX/P2-20 206	EX/P4-25 257
EX/4-1147	EX/P2-21 207	EX/P4-26 258
EX/4-2148	EX/P2-22 208	EX/P4-27 259
EX/4-3149	EX/P2-24 209	EX/P4-28 260
EX/5-1150	EX/P2-26 210	EX/P4-29 261
EX/5-2151	EX/P2-27 211	EX/P4-30
EX/5-2151 EX/5-3152	EX/P2-28 212	EX/P4-33
	EX/P2-29 213	
EX/6-1153		EX/P4-34
EX/6-2154	EX/P2-30 214	EX/P4-35 265
EX/6-3155	EX/P2-39 215	EX/P4-36
EX/6-4156	EX/P2-40 216	EX/P4-37 267
EX/7-1157	EX/P2-41 217	EX/P4-38 268
EX/7-2158	EX/P2-42 218	EX/P4-41 269
EX/7-3159	EX/P2-46 219	EX/P4-43 270
EX/7-4160	EX/P2-47 220	EX/P4-45 271
EX/8-1161	EX/P2-48 221	EX/P4-46 272
EX/9-1162	EX/P2-49 222	EX/P4-47 273
EX/9-2163	EX/P2-50 223	EX/P5-18 274
EX/9-3164	EX/P2-51 224	EX/P5-20 275
EX/9-4165	EX/P2-52 225	EX/P5-21 276
EX/9-5166	EX/P2-54 226	EX/P5-22 277
EX/P1-18 176	EX/P3-10 234	EX/P5-23 278
EX/P1-19 177	EX/P3-11 235	EX/P5-24 279
EX/P1-20 178	EX/P3-12 236	EX/P5-25
EX/P1-21 179	EX/P3-14 237	EX/P5-26
EX/P1-22	EX/P3-16	EX/P5-27 282
EX/P1-23 181		EX/P5-28
	EX/P3-17 239	
EX/P1-24 182	EX/P3-18	EX/P5-29 284
EX/P1-25 183	EX/P3-3227	EX/P5-30 285
EX/P1-27 184	EX/P3-4 228	EX/P5-31 286
EX/P1-28	EX/P3-47 241	EX/P5-32
EX/P1-29 186	EX/P3-48 242	EX/P5-33 288

EX/P5-38 289
EX/P5-39 290
EX/P5-40 291
EX/P5-46 292
EX/P5-48 293
EX/P5-49 294
EX/P6-17 295
EX/P6-19 296
EX/P6-20 297
EX/P6-21 298
EX/P6-22 299
EX/P6-25 300
EX/P6-26 301
EX/P6-27 302
EX/P6-28 303
EX/P6-29 304
EX/P6-30 305
EX/P6-31 306
EX/P6-33 308
EX/P6-34 309
EX/P6-35 310
EX/P6-36 311
EX/P6-37 312
EX/P6-43 313
EX/P6-53 315
EX/P6-54 316
EX/P6-56 317
EX/P6-57 318
EX/P6-58 319
EX/P6-59 320
,
EX/P7-17 322
EX/P7-18 323
EX/P7-19 324
EX/P7-20 325
EX/P7-21 326
EX/P7-22 327
EX/P7-23 328
EX/P7-24 329
EX/P7-25 330
EX/P7-26 331
EX/P7-27 332
EX/P7-31 333
EX/P7-32 334
EX/P7-33 335
EX/P7-34 336
EX/P7-35 337
EX/P7-36 338
EX/P7-40 339
EX/P7-41 340
EX/P7-44
EX/P7-45 342

EX/P8-10 35 EX/P8-11 35 EX/P8-12 35 EX/P8-13 35 EX/P8-14 35 EX/P8-15 35 EX/P8-18 35 EX/P8-2 34 EX/P8-5 34 EX/P8-6 34 EX/P8-8 34	123456345678
EX/P8-9 34 FIP/1-1 49 FIP/1-2 49 FIP/1-3 50 FIP/1-4Ra 50 FIP/1-4Rb 50 FIP/1-4Rb 50 FIP/1-6Ra 50 FIP/1-6Rb 50 FIP/2-1 50 FIP/2-2Ra 50 FIP/2-2Rb 50 FIP/2-2Rc 50 FIP/2-3 51 FIP/2-4 51 FIP/2-4Rc 54	890123456789012
FIP/2-5Ra 51 FIP/2-5Rb 51 FIP/3-1 51 FIP/3-2 51 FIP/3-3 51 FIP/3-4Ra 51 FIP/3-4Rb 51 FIP/3-5Ra 51 FIP/3-6 52 FIP/P4-1 52 FIP/P4-10 52 FIP/P4-13 53 FIP/P4-13 53 FIP/P4-15 53 FIP/P4-2 52	23456789019012
FIP/P4-2 52 FIP/P4-20 53 FIP/P4-21 53 FIP/P4-24 53 FIP/P4-25 53 FIP/P4-26 53 FIP/P4-3 52 FIP/P4-4 52 FIP/P4-5 52 FIP/P4-6 52	34567345

FIP/P4-7 527
FIP/P4-9528
FIP/P5-1538
FIP/P5-3539
FIP/P5-4540
FIP/P5-5541
FIP/P7-1543
FIP/P7-10551
FIP/P7-12552
FIP/P7-13553
FIP/P7-14554
FIP/P7-15555
FIP/P7-16556
FIP/P7-17557
FIP/P7-18558
FIP/P7-19559
FIP/P7-2544
FIP/P7-21
FIP/P7-23561
FIP/P7-24562
FID / D7 20
FIP/P7-30
FIP/P7-4545
FIP/P7-5
FIP/P7-6
FIP/P7-7548
FIP/P7-8549
FIP/P7-9550
FIP/P8-1
FIP/P8-10570
FIP/P8-11571
FIP/P8-12572
FIP/P8-17573
FIP/P8-18574
FIP/P8-19575
FIP/P8-2565
FIP/P8-20576
FIP/P8-21577
FIP/P8-22578
FIP/P8-23579
FIP/P8-24580
FIP/P8-25581
FIP/P8-26582
FIP/P8-27583
FIP/P8-28584
FIP/P8-29585
FIP/P8-3566
FIP/P8-30586
FIP/P8-31
FIP/P8-32588
FIP/P8-4
FIP/P8-8
FIP/P8-9569
FNS/1-1 590
FNS/1-2Ra591
1 + 10/1 + 4100 + 10000 + 10000 + 10000 + 10000 + 1000 + 1000 + 1000 + 1000 + 1000 +

705

Index

FNS/P4-27592
FNS/14-27
FNS/P7-11593
FNS/P7-20594
FNS/P7-22595
ENIC / DF OF
FNS/P7-25596
FNS/P7-27597
ICC/P4-31 600
ICC/P4-48 601
ICC/P5-1 602 ICC/P5-41 603
ICC/P5-41 603
ICC/P5-43 604
ICC/13-45
ICC/P8-19 605
IFE/1-1608
IFE/1-2609
IFE/1-3 610
IFE/1-4 611
IFE/1-5 612
IFE/P6-10621
IFE/P6-11622
IFE/P6-12623
IFE/P6-13624
IFE/P6-16625
IFE/P6-2613
HE/102
IFE/P6-3614
IFE/P6-4615
IFE/P6-5616
IFE/P6-6617
IFE/P6-7618
IEF / DC (10)
IFE/P6-8619
IFE/P6-9620
MPT/1-2628
MPT/1-3629
MPT/1-4
MPT/P4-17 632
MPT/P4-23 633
MPT/P4-8631
MPT/P5-2 634
MPT/P7-29 636
MPT/P7-31 637
MPT/P7-32 638
MPT/P7-33 639
MPT/P7-34 640
MPT/P7-36 641
MPT/P7-37 642
MPT/P7-38 643
MPT/P7-40 644
MPT/P7-41 645
MPT/P7-42 646
MPT/P7-43 647
MPT/P8-13 651
MDT /D0 1E
MPT/P8-15 652

MPT/P8-5 648
MPT/P8-6 649
MPT/P8-7 650
O/3106
OV/1-1 108
OV/1-2109
OV/1-3 110
OV/1-4 111
OV/2-1 112
OV/2-2 113
OV/2-3 114
OV/2-4 115
OV/2-5 116
OV/3-1 117
OV/3-2118
OV/3-3 119
OV/3-4 120
OV/4-1 121
OV/4-2122
OV/5-2 127
OV/5-3 128
OV/5-4 129
OV/5-5 130
OV/P-01131
OV/P-02132
OV/P-03133
OV/P-04134
PD/P3-1 684
PD/P3-2 685
PD/P3-3 686
PD/P4-1 687
PD/P5-1 688
PD/P5-3 689
PD/P5-4 690
PD/P5-5 691
PD/P6-1 692
PD/P6-3 693
PD/P6-4 694
PD/P7-1 695
PPC/1-1 654
PPC/2-1 655
PPC/P1-26
PPC/P2-31
PPC/P2-32
PPC/P2-33
PPC /P2-34 660
PPC/P2-34660 PPC/P2-35661
PPC/P2-36

PPC/P2-37663
PPC/P3-19665
PPC/P3-2664
PPC/P3-20
PPC/P3-21
PPC/P3-22668
PPC/P4-19669
PPC/P5-42670
PPC/P6-46671
PPC/P8-16672
PPC/P8-17673
S/1-1
S/1-2699
S/2-1700
S/2-2701
S/2-3702
S/2-3
SEE/P5-12 680
SEE/P5-13 681
SEE/P5-15 682
SEE/P5-6 676
SEE/P5-8 677
SEE/P5-9 678
TH/1-1358
TH/1-2359
TH/2-1
TH/2-2
TH/2-3
TH/3-2
TH/3-3364
TH/4-1
TH/4-2
TH/5-1
TH/5-2368
TH/6-1Ra
TH/6-1Rb370
TH/6-2
TH/7-1
TH/7-2373
TH/8-1
TH/P1-11 381
TH/P1-12
TH/P1-13
TH/P1-14
TH/P1-15
TH/P1-16
TH/P1-17 387
TH/P1-2 375
TH/P1-3 376
TH/P1-31
TH/P1-34 389
TH/P1-35
111/11-00

TH/P1-5377
TH/P1-52
TH/P1-7
TH/P1-8379
TH/P1-9
TH/P2-1
TH/P2-10
TH/P2-11
TH/P2-12
TH/P2-13 401
TH/P2-14
TH/P2-15403
TH/P2-16404
TH/P2-2
TH/P2-38405
TH/P2-44406
TH/P2-45407
TH/P2-5
TH/P2-6
TH/P2-7
TH/P2-9
TH/P3-13408
TH/P3-23409
TH/P3-24410
TH/P3-25 411
TH/P3-28412
TH/P3-29413
TH/P3-30414
TH/P3-31 415
TH/P3-32416
TH/P3-34 417
TH/P3-35418
TH/P3-36419
TH/P3-37 420
TH/P3-38 421
TH/P3-39422
TH/P3-40

TH/P3-41424
TH/P3-42425
TH/P3-43426
TH/P3-44 427
TH/P3-45
TH/P3-46
TH/P4-10
TH/P4-11
TH/P4-13 437
TH/P4-14
TH/P4-15439
TH/P4-16440
TH/P4-17 441
TH/P4-3 430
TH/P4-39
TH/P4-4 431
TH/P4-40 443
TH/P4-49 444
TH/P4-6 432
TH/P4-7 433
TH/P4-9 435
TH/P5-10 450
TH/P5-12 451
TH/P5-13 452
TH/P5-14
TH/P5-17 454
TH/P5-34
TH/P5-35
TH/P5-36 457
TH/P5-37 458
TH/P5-4445
TH/P5-50459
TH/P5-6 446
TH/P5-7 447
TH/P5-8 448
TH/P5-9449
TH/P6-1460

TH/P6-10465
TH/P6-11466
TH/P6-12467
TH/P6-14468
TH/P6-15469
TH/P6-16470
TH/P6-2 461
TH/P6-24 471
TH/P6-38472
TH/P6-39473
TH/P6-4
TH/P6-40
TH/P6-49475
TH/P6-50476
TH/P6-52477
TH/P6-55478
TH/P6-60479
TH/P6-8463
TH/P6-9464
TH/P7-1
TH/P7-10
TH/P7-13489
TH/P7-14490
TH/P7-15491
TH/P7-2 481
TH/P7-30492
TH/P7-37493
TH/P7-38494
TH/P7-39495
TH/P7-4
TH/P7-5483
ТН/Р7-6 484
TH/P7-7 485
TH/P7-8486
TH/P7-9 487
TH/P8-1 496

Index by Author

— A —	
Abdel Maksoud, W	57(
Abe, H.	
Abe, Y	
Abiteboul, J	
Abizimoghadam, E	32'
Acosta, U	
Adltalab, Y.	
Afanasyev, V	
Agarici, G	
Aguilera, A	
Agullo, O	
Ahn, HJ.	29 505 5 30 53
Ahn, JW	31
Aho-Mantila, L. 28, 36, 1	158 238 277 280 36 4
669	100, 200, 277, 200, 004
Aiba, N	19, 403 , 452, 489, 55
Aiello, G.	
Airoldi, A	
Äkäslompolo, S	
Akers, R	180, 264, 42
Akino, N	
Akiyama, T 60, 2	245.300.301.526.58
Akulitsky, S	
Albanese, R	
Aleksander, D	
Aleksandrova, I	
Alekseev, A.	202, 275, 504, 536, 53
Alekseev, P	
Alessi, E	
Alessio, M	
Alexander, G	
Alexeev, P	
Aleynikov, P	.25, 240, 415, 421, 422
Aleynikova, K	
Allegretti, M.	
Allen, S. L	
Almagri, A	
Almaguer, J.	
Alper, B	
Altukhov, A	.15, 172, 185, 186, 18
Alves, D	
Alves, E	
Amardas, A	
Ambrosino, G	
Ambrosino, R	
Amendt, P	
Amicucci, L	
An, Y	
Anan'ev, S	
Anashkin, I	

Anderson, J	128, 243
Andreeva, T	
Andreoli, P	
Andrew, P 237, 283,	631,677
Angelini, S	
Angelov, V	645
Angioni, C 153, 177, 179, 182, 239,	343, 669
Apicella, M. L.	219
Apruzzese, G	219, 220
Apse, V	563
Arce, J	579
Arikawa, Y609, 613–615,	620, 693
Arneman, A	533
Arnichand, H.	289
Arnoux, G147, 158,	363, 423
Arredondo, V	579
Artaserse, G.	223-225
Artaud, JF 293, 384, 547,	669,670
Asai, T	. 38, 604
Asakura, N 56, 124, 517, 518,	
Ascasíbar, E	272, 273
ASDEX Upgrade Team,	
Ashikawa, N.	159
Ashok, G	
ASHOK, G	321
Askinazi, L	318-320
	318–320 414
Askinazi, L	318–320 414 586
Askinazi, L 9, 11, 108, Asunta, O	318–320 414 586 321, 322
Askinazi, L	318–320 414 586 321, 322 130
Askinazi, L 9, 11, 108, Asunta, O	318–320 586 321, 322 130 616
Askinazi, L 9, 11, 108, Asunta, O	318–320 414 586 321, 322 130 616 128, 244
Askinazi, L 9, 11, 108, Asunta, O	318–320 414 586 321, 322 130 616 128, 244 138, 213
Askinazi, L 9, 11, 108, Asunta, O	318–320 414 586 321, 322 130 616 128, 244 138, 213 250
Askinazi, L 9, 11, 108, Asunta, O	318–320 414 586 321, 322 130 616 128, 244 138, 213 250 274
Askinazi, L 9, 11, 108, Asunta, O	318–320 414 586 321, 322 130 616 128, 244 138, 213 250 274 347
Askinazi, L. 9, 11, 108, Asunta, O. Atnafu, N. Atrey, P. 152, Atrey, P. K. Atsushi, S. Austin, M. Auriemma, F. Austin, M. Avino, F. Avotina, L. Aydemir, A. Aydemir, A. Y. Y.	318–320 414 586 321, 322 130 616 128, 244 138, 213 250 274 347 347
Askinazi, L 9, 11, 108, Asunta, O	318–320 414 586 321, 322 130 616 128, 244 138, 213 250 274 347 . 18, 393 286 617, 693
Askinazi, L 9, 11, 108, Asunta, O	318–320 414 586 321, 322 130 616 128, 244 138, 213 250 274 347 . 18, 393 286 617, 693
Askinazi, L 9, 11, 108, Asunta, O	318–320 414 586 321, 322 130 616 128, 244 138, 213 250 274 347 3566 3566 3566 3566 3566 3566 3566
Askinazi, L 9, 11, 108, Asunta, O	318–320 414 586 321, 322 130 616 128, 244 138, 213 250 274 347 3566 3566 3566 3566 3566 3566 3566

B —

Babu, G. R	
Bachmann, C	
Baciero, A	
Bader, A	124
Bae, YS	120, 155, 353
Baek, S. G	. 145, 235, 295, 297
Bagryansky, P	
Baião, D	

Bairagi, N	130
Bak, J	14, 346
Bak, J. G	40, 345
Bakharev, N	
Balboa, I.	
Baldwin, M.	242
Banaudha, M	
Banerjee, S.	
Banon Navarro, A	396
Bao, J.	
Bao, L	
Barabaschi, P	
Barabash, V.	504
Barbarino, M	
Barbier, C	506
Bark, J	
Barnard, H.	
Barnsley, R 23	
Baron-Wiechec, A	31, 286
Barrera Orte, L18	
Barsukov, A	204
Barton, J. E Baruzzo, M153, 163, 217, 288, 38	L <mark>9, 65</mark> 8
Baruzzo, M 153, 163, 217, 288, 38	34, 450
Basiuk, V	293
Bass, E. M	25, 425
Bassan, M.	
Basu, B	488
Basu, D	. 322
Battaglia, D20	
Baumane, L.	
Baylor, L. R.	29.506
Bayon, A.	
Bazarov, A.	
Bazhenov, A	
Bazylev, B 25, 147, 15	51 422
Beaumont, P. S	
Beck, W.	
Becoulet, M	70 460
Beg, F	
Deg, F.	
Begrambekov, L.	
Behn, R	
Belforte, G.	
Belghit, S	
Bell, M.	
Bell, R	
Bell, R. E 139, 31	
Bellei, C	608
Belli, E. A153, 182, 36	61, 466
Belli, F 220, 22	21, 223
Belo, P	30, 456
Belohony, E.	276
Belokurov, A	15, 320
Belonohy, E.	

Belov, A	201,	537,	666
Belyaev, S.			
Belyakov, V.	33, 515,	537,	666
Ben Ayed, N.			264
Benakadda, S			430
Benedikt, G.			395
Benkadda, S			
Ber, B			
Bergmann, A			177
Berkery, J. W		139,	345
Bernard, JM			464
Bernardi, P			547
Bernardo, J			289
Bernert, M.			
Bernhard, S.			
Berry, L			438
Bertalot, L		237.	592
Bertani, C			
Berte, M			
Bertelli, N.			
Bertram, J.			256
Betti, R			
Beurskens, M146, 163, 1	164.280.	284	455
Beyer, P		. 50.	483
Bhandarkar, M. K.			
Bhardwaj, A			
Bhatt, S			
Bialek, J.		257.	345
Biancalani, A.		. 14.	176
Bianchi, A		,	583
Biel, W			
Bierwage, A 52 , 3	352.372.	403.	495
Biewer, T. M			
Bilato, R			
Bin, W			
Birkenmeier, G		.15.	183
Birus, D			479
Bishaev, A.		685.	686
Biswas, P.			130
Bitter, M.			
Blackman, T			
Blackwell, B		. 30, 3	256
Blanchard, W			
Blanco, E.			
Bobkov, V165, 1	182, 276,	277,	290
Boboc, A			
Bobyr, N.			
Boccaccini, L. V		567.	680
Boedo, J. A160, 1	175, 209	362.	689
Boeglin, W. U.			
Boggio-Sella, E			583
Boilson, D		512	542
Bolshakova, I.		. 32.	527
Bolzonella, T			

Bombarda, F	583
Bonasera, A	694
Boncagni, L	221
Bondarchuk, E 133, 515,	581
Bondarenko, V	342
Bonfiglio, D 217,	450
Bonicelli, T	542
Bonoli, P 235, 295, 438, 475,	558
Bora, D	
Borba, D.	
Borchardt, M 128,	
Borodin, D.	
Borshegovskii, A 197,	
Borsuk, V.	479
Bortolon, A.	314
Botrugno, A	225
Bottereau, C	289
Bottino, A	431
435	101,
Boutboul, T	501
Bovet, A.	
Bowman, C.	
Boyer, M. D.	
Bräuer, T.	
Braun, F	
Bravenec, R	
Bray, B. D	
Breizman, B	
Brennan, D. P	
Breeler I 404 422	400
Breslau, J404, 433, Brezinsek, S37, 151, 158, 242, 275–277,	437
281 , 282, 286, 287, 455, 456	200,
	500
Brian, N.	
Briesemeister, A. R.	
Briesmeister, A	315
Briguglio, S	395
Brooks, J	
Broumand, M.	
Brower, D	244
Brown, T	590
Brunetti, D	
Brunner, D.	
Brunner, S	
Brunsell, P	252
Bruschi, A	
Bruzzone, P	501
Bucalossi, J	547
Bucinieks, I.	
Budny, R	386
Bufferand, H 293,	459
Bugrov, G Bukhovets, V	685

Bukreev, I	
Bulanin, V	
Buratti, P	. 164, 220, 222, 226, 291, 488
Buravand, Y	
Burckhart, A	
Burdakov, A	
Burke, W	
Burrell, K. H	.143, 175, 209, 212, 361, 663
Buttery, R. J	
Buzhinsky, O	
Buzi, L	
Bykov, A	
	59 , <i>573</i> , 575

— C —

Cahyna, P42,	137 370	460
Cai, L. J		
Calabrò, G 23, 220,		
Calamosca, M		
Calderoni, P.		
Callen, J. D.		
Campbell, D.	24	240
Canal, G.		
Candy, J.		
Canik, J 145, 209, 210, 241, 315,	433 477	590
Cao, J		
Cao, Z		
Capecchi, W		
Сарра, А́	31	272
Cappechi, W.		
Cappello, S.		
Carbajal, L.	,	
Cardinali, A		
Carloni, D		
Carmody, D		
Carnevale, D		
Carpentier, S		
Carpentier-Chouchana, S		
Carralero, D		
Carreras, B.		
Cartier-Michaud, T		
Carvalho, I. S.		
Casali, L.		
Casey, D		
Caspary, K		
Casper, T		
Casson, F		
Castaldo, C	36,	447
Castano Bardawil, D		
Castejón, F	. 31, 271,	272

Cau, F	
Causa, F	222
Cavazos, G	
Cavazzana, R.	
Cavedon, M.	
Cavinato, M	
Cecconello, M	
Ceccuzzi, S.	
Cenacchi, G.	
Cerfon, A.	
Cesario, R	100
Clesario, R	
Chakraborty, A. K.	542
	201
Challis, C 48 , 55 , 146, 163, 164 , 277,	291
Chan, V. S.	466
Chandra, D	439
Chang, C	362
Chang, CS209,	
Chang, H.	
Chankin, A	
Chapman, B 12 , 18 , 26 , <i>128</i> , 243 ,	
Chapman, I.10, 11, 115, 137, 146, 285, 427,	443,
489	
Chapman, S.	412
Chatthong, B	463
Chattopadhyay, A. K.	322
Chattopadhyay, P 152, 321,	322
Chauhan, P. K.	130
Chavda, C.	152
Chavez, M.	
Chekanov, V	
Chektybayev, B	572
Chel, S.	
Chen, C121, 325, 327, 333,	334
Chen, D	687
Chen, H	
Chen, J	
Chen, K	522
Chen, L	170
Chen, R	470
Chen, S	492
Chen, W 51, 121, 328–330, 332,	
Chen, X	
Chen, Y 230, 234,	
Chen, Z 132, 333,	
Cheng, C. Z601,	691
Cheng, J 51 , 121, 174, 325, 327, 328, 331,	334,
335, 339	
Cheng, M	235
Cheng, Z	
Chensky, I	502
Cherdakov, A.	581
Cherkez, D	553
Chernakov, P	

Chernikh, M	
Chernov, V54,	
Chernyshev, F	319
Chernyshova, M54,	646
Chistiakov, V	173
Choe, GH.	
Choe, W	
Choi, C. H	530
Choi, M	355
Choi, W. J	
Chôné, L	
Chowdhuri, M. B	
Christian, D. R.	
Christian, T.	
Christoph, W	
Chrobak, C. P	689
Chrystal, C175,	214
Chudasama, H. H	130
Chudin, N	399
Chugunov, I	
Chuheishi, S	534
Chukbar, B	
Chung, K	605
Chung, W	530
Churchill, M145,	
Churchill, R. M 177,	299
Churn, K.	
Cianciosa, M.	
Cianfarani, C	
Cicuttin, A.	644
Cipriani, M.	694
Ciraolo, G	547
Cismondi, F	
Citrin, J	425
Clairet, F	
Classen, I.	178
Clever, M	
Cloez, H.	
Coad, P	286
Coccorese, V	
Cocilovo, V	223
Coda, S 11, 17, 122, 246,	249
Coelho, R	
Coenen, J. W 147, 423,	456
Coffey, I.	153
Coffey, J	423
Colas, L	464
Cole, M.	444
Colledani, G.	
Combs, S	
Commaux, N	
Conka, D	
Connor, J. W.	
Consoli, F.	
Consoli, 1	074

Conway, G	176, 364
Cook, J	
Cooper, W. A	
Соррі, В	
Corre, Y.	
Corrigan, G.	
Costa, E	
Coster, D 2	
Cottier, P	
Covele, B	
Craig, D	
Crescenzi, F.	
Crisanti, F	
Cristofari, G	
Crocker, N.	265, 268, 443
Crombé, K	
Cropper, M	
Cucchiaro, A	
Cui, C	
Cui, Z	51, 121, 124, 331
Cunningham, G	264, 280, 569
Curcio, A	
Czarnecka, A	
Cziegler, I	

— D —

da Silva Aresta Belo, P.	
Dairaku, M	
D'Amico, A	
Danani, C	
Danelyan, L	
Danilov, A	
Darbos, C	
Darrow, D	
Das, A	
Davis, E. M	
Davis, S	
Davydenko, V	
Day, C	
Daybelge, U	
de la Cal, E	
de la Luna, E	37 , 278, 284 , 285, 291
de Marne, P	
de Meijere, C	
De Temmerman, G	
De Tommasi, G	
de Vries, P	.150, 151, 240, 242, 278
De Angelis, R	
Decamps, H	
Decker, J	151, 235, 293
Decool, P	59 , 574, 576
deGrassie, J. S	136, 209, 212, 689
Deichuli, P	

Dejarnac, R	499
Del Nevo, A	.567
Delabie, E 37, 276, 279,	280
Delgado-Aparicio, L. F 145, 297 ,	383
Demers, D.	128
Demina, E	652
Den Hartog D 128 243-	-245
Dendy, R	412
Deng, W 121, 156,	222
Denig, W	525
Denis uk, A	000
Denner, P	
Dennis, G	
Deshpande, S	
Desytskov, A	685
Detragiache, P	583
Devaux, S	455
DeVellis, A	583
Devred, A	501
Dewar, R	442
Dhanani, K. R	130
Dhobi, U 152,	321
Dhongde, J. R	130
Dhyani, P 50 , 152,	322
Di Gallo, L	547
Di Giorgio, G	
Di Pietro, E	574
Di Troia, C	1974
Diagnostic and Theory groups	109
Diagnostic and Theory groups,	108
Diagnostic and Theory groups, Diallo, A 145 , 314, 315, 443, 476,	108 586
Diagnostic and Theory groups, Diallo, A 145 , 314, 315, 443, 476,	108 586
Diagnostic and Theory groups, Diallo, A 145 , 314, 315, 443, 476,	108 586
Diagnostic and Theory groups, Diallo, A 145 , 314, 315, 443, 476, Diamond, P Diamond, P. H.132, 155, 175, 339, 346, 351, 376, 380, 385, 391, 397, 402, 440	108 586
Diagnostic and Theory groups, Diallo, A	108 586 688 374,
Diagnostic and Theory groups, Diallo, A 145 , 314, 315, 443, 476, Diamond, P Diamond, P. H.132, 155, 175, 339, 346, 351, 376, 380, 385, 391, 397, 402, 440 465, 485 , 491 Dickinson, D	108 586 688 374,), 443
Diagnostic and Theory groups, Diallo, A	108 586 688 374,), 443 435
Diagnostic and Theory groups, Diallo, A 145 , 314, 315, 443, 476, Diamond, P Diamond, P. H.132, 155, 175, 339, 346, 351, 376, 380, 385, 391, 397, 402, 440 465, 485 , 491 Dickinson, D	108 586 688 374,), 443 435
Diagnostic and Theory groups, Diallo, A	108 586 688 374,), 443 435 143 412
Diagnostic and Theory groups, Diallo, A 145 , 314, 315, 443, 476, Diamond, P. H. 132, 155, 175, 339, 346, 351, 376, 380, 385, 391, 397, 402, 440 465, 485 , 491 Dickinson, D	108 586 688 374,), 443 435 143 412 235
Diagnostic and Theory groups, Diallo, A 145 , 314, 315, 443, 476, Diamond, P. H. 132, 155, 175, 339, 346, 351, 376, 380, 385, 391, 397, 402, 440 465, 485 , 491 Dickinson, D	108 586 688 374,), 443 435 143 412 235
Diagnostic and Theory groups, Diallo, A 145 , 314, 315, 443, 476, Diamond, P. H.132, 155, 175, 339, 346, 351, 376, 380, 385, 391, 397, 402, 440 465, 485 , 491 Dickinson, D	108 586 688 374,), 443 435 143 412 235 231 335
Diagnostic and Theory groups, Diallo, A 145 , 314, 315, 443, 476, Diamond, P. H.132, 155, 175, 339, 346, 351, 376, 380, 385, 391, 397, 402, 440 465, 485 , 491 Dickinson, D	108 586 688 374,), 443 435 143 412 235 231 335
Diagnostic and Theory groups, Diallo, A 145 , 314, 315, 443, 476, Diamond, P Diamond, P. H.132, 155, 175, 339, 346, 351, 376, 380, 385, 391, 397, 402, 440 465, 485 , 491 Dickinson, D	108 586 688 374,), 443 435 143 412 235 231 335 334
Diagnostic and Theory groups, Diallo, A 145, 314, 315, 443, 476, Diamond, P Diamond, P. H.132, 155, 175, 339, 346, 351, 376, 380, 385, 391, 397, 402, 440 465, 485, 491 Dickinson, D	108 586 688 374,), 443 412 235 231 335 334 339
Diagnostic and Theory groups, Diallo, A	108 586 688 374,), 443 435 143 412 235 231 335 334 339 514
Diagnostic and Theory groups, Diallo, A	108 586 688 374,), 443 435 143 412 235 231 335 334 339 514 477
Diagnostic and Theory groups, Diallo, A	108 586 688 374,), 443 435 143 412 235 231 335 334 339 514 477 576
Diagnostic and Theory groups, Diallo, A	108 586 688 374,), 443 435 143 412 235 231 335 334 339 514 477 576 637
Diagnostic and Theory groups, Diallo, A	108 586 688 374,), 443 435 143 412 235 231 334 339 514 477 576 637 610
Diagnostic and Theory groups, Diallo, A	108 586 688 374,), 443 435 143 412 235 231 334 339 514 477 576 637 610 149
Diagnostic and Theory groups, Diallo, A	108 586 688 374,), 443 435 143 412 231 335 334 339 514 477 576 637 610 149 201
Diagnostic and Theory groups, Diallo, A	108 586 688 374,), 443 435 143 412 235 231 335 334 339 514 477 576 637 610 149 201 593
Diagnostic and Theory groups, Diallo, A	108 586 688 374,), 443 435 143 412 235 231 335 334 477 576 637 610 149 201 593 341
Diagnostic and Theory groups, Diallo, A	108 586 688 374,), 443 435 143 412 235 231 335 334 477 576 637 610 149 201 593 341 690
Diagnostic and Theory groups, Diallo, A	108 586 688 374,), 443 435 143 412 235 231 335 334 477 576 637 610 149 201 593 341 690 636

Dokuka, V	561
Domier, C161, 352, 3	355
Domier, C. W	353
Dominski, J 2	
Dong, C	331
Dong, J.56, 62, 121, 174, 327, 328, 330, 332, 3	34,
335, 339, 401, 492	
Dong, Y. B 51, 121, 156, 324, 326, 3	333
Donovan, M	
Doody, J	558
Doshi, B	504
Doshi, K. J 1	30
Douai, D	282
Doyle, E. J 142, 143, 175, 214, 6	662
Drevon, JM.	524
Drewelow, P	279
Drobyshev, V	537
Du, D	
Du, H	597
Du, X	
Duan, W	582
Duan, X. 121, 174, 325-332, 334, 529, 564, 6	38,
688	
Duan, Y	316
Dubuit, N4	30
Duchateau, JL	547
Dudson, B	267
Duff, J 128, 243, 2	244
Dumont, R 285, 293, 368, 3	396
Dumortier, P	
Dunai, D	43
Dunne, M	590
Dunne, M. G 144, 177, 1	80
Duran, I	
Durodie, F4	64
Duval, B 26, 226, 246, 248, 4	
Dux, R24, 165, 177, 182, 239, 4	13
Dyabilin, K	32
Dyachenko, V15, 133, 185, 186, 204, 3	889
Dyer, G	
Dzhurik, S 2	
— E —	
Ebrahimi, F	78

Ebrahimi, F	
Egorov, K	573 , 575
Eguchi, T	
Eich, T	137, 238, 455, 456
Eidietis, N. W	. 19, 208, 365, 659, 673
Eilerman, S	
Ejiri, A	
Ekedahl, A	
El-Guebaly, L	49, 61, 590, 635
Elder, J. D	
Eldon, D	

Elena, D. L. L.	
Eliseev, L	
Ellis, R	
Emoto, M	
Encheva, A	
Endler, M.	
Endo, T	117
Endo, Y	509, 513
Erickson, K	
Ericson, N	
Ernst, D 2	2, 35, 143, 558
Escande, D	
Escourbiac, F.	498, 499
Esipov, L	. 172, 185–187
Eskhult, J.	
Esposito, B 21, 150, 220-222	2, 223 , 225, 426
Estève, D	
Estrada, T31	, 271, 272, 273
Evans, T. E 13, 23, 29, 124, 136	, 138 , 139, 140,
168, 207, 241, 315, 43	
Ezato, K	

— F —

Fable, E 144, 177, 360,	, 384, 396, 413, 428, 669
Fabritsiev, S.	
Faelli, G	
Falchetto, G	
Falkowski, A	
Fantz, U	
Farengo, R	
Farina, D	
Fasoli, A52,	, 250, 363, 548 , 669, 688
Faudot, E	
Faugel, H	
Fausser, C	
Faust, I	
Faustin, J	
Feder, R	
Federici, G.	
Federspiel, L	
Fedorczak, N	277, 293, 435, 459
Feher, T	
Felici, F	
Fellinger, J	
Felton, R	
Feng, B	121, 156, 327, 330, 334
Feng, K	56, 519, 649
Feng, Y	58, 124, 473, 649
Feng, Z	
Fenstermacher, M. E	160, 207, 210, 299, 407,
654, 663	
Fenzi, C	
Fernandes, A	
Ferrari, A	

Ferrari, H)
Ferraro, N. M. 136, 139, 168, 180, 207, 212, 217	,
315, 433, 466	
Ferreira Nunes, I. M. 48, 55, 146, 163, 164, 242	,
277, 284, 291	
Ferreira, J	L
Ferro, A	
Ferron, J 20, 167, 210, 658, 660, 661, 662, 670	
Field, A	
Fietz, S	
Figini, L	
Figueiredo, A	с
Fil, A	
Filatov, O	
Finognari, P	, ,
Finn, J. M	
Fiore, C	
Firdaouss, M	
Firpo, MC	
Fischer, R	
Fischer, U	
Fisher, P506	
Fishpool, G	
Fitzgerald, M	
Fontdecaba, J. M 272	
Forest, C	3
Fox, M	3
Franck, E	
Franz, P128, 244	Ł
Franzen, P	L
Frassinetti, L 146, 163, 164, 252, 280, 291	L
Frattolillo, A	3
Fredrickson, E 44, 170, 264, 314	Ŀ
Frenje, J	
Frerichs, H 124, 267	
Fridström, R 252	,
Frigione, D	
Frolko, P	
FT-2 Team,	Į.
FTU Team,	
Fu, B	
Fu, G	2
Fu, H	2
Fu, J	
Fuchert, G	,
Fuchs, J. C	
Fuhr, G) -
Fujii, K	
Fujimoto, Y	
Fujine, M	5
Fujioka, S 34 , 42 , 117, 609 , 613, 614, 616, 617 693	
Fujisawa, A	3
Fujita, K)

Fukuda, M	
Fukumoto, M	
Fukushima, H	
Fukuyama, A	42, 63, 191, 462, 472, 700
Fulton, D	
Funaba, H	
Furno, I	
Furui, H	
Furukawa, M	
Futatani, S	

— G —

Gabellieri, L	225
Gagliardi, M	
Gaio, E	
Galante, M	
Galassi, D	
Galdon, J	
Galeani, S	221
Galperti, C 220,	226
Galvao, R. M. O	341
Galyuzov, A	
Gan, K	234
Gan, Y	565
Gandini, F	507
Gantenbein, G	
Gao, B	205
Gao, C	297
Gao, J	333
Gao, L	339
Gao, X	
Gao, Y	
Gao, Z	394
Gapionok, E	
Garavaglia, S220, 224,	226
Garbet, X 289, 370, 430, 431,	435
Garcia Carrasco, A32,	523
Garcia, J.40, 49, 164, 291, 293, 368, 396, 428,	
Garcia-Carasco, A	
Garcia-Lopez, J	
Garcia-Martinez, P	379
García-Muñoz, M 15 , 168, 178, 180 ,	
Garg, A	
Garkusha, I	
Garofalo, A. M 19, 20 , 119, 212, 215, 217,	218,
361, 369, 657 , 660, 662, <i>663</i>	
Garzotti, L266, 280, 285, 384, 428,	668
Gasilov, N	434
Gates, D	673
Gauthier, E	
Gavrikov, M685,	
Gavrilov, S	533
Geiger, B15, 178,	180

Genini, L	576
Genni, L	100
Gentle, K	132
George, S.	130
Gerasimov, S	527
Gerhardt, S 170, 209, 299, 315, 438, 476,	586
	500,
590, 673	
Gerhardt, S. P	314
Gervash, A. A	652
Ghendrih, P 124, 293, 431,	459
Ghezal, A.	
Ghim, YC 140, 268, 347,	
Ghoranneviss, M	
Ghosh, J152, 321,	322
Gi, K	
Giacalone, JC.	
Giacomelli, L	278
Giacomin, T	
Giammanco, F	.583
Giannone, L	
Gibson, K.	
Gin, D	555
Giovannozzi, E	
Girardo, JB	.431
Giraud, B	504
Giroud, C. 37, 146, 153, 164, 277, 280, 291,	455
456	1 55,
Giruzzi, G 14, 162, 293, 368, 384,	669
Giuffrida, L	609
Giulietti, D	694
Giulietti, D Gladush, G	694 .561
Giulietti, D Gladush, G Glasser, A. H.	694 561 377
Giulietti, D Gladush, G Glasser, A. H Glazunov, D	694 .561 .377 .550
Giulietti, D Gladush, G Glasser, A. H Glazunov, D Gleason-Gonzalez, C	694 561 377 550 568
Giulietti, D Gladush, G Glasser, A. H Glazunov, D Gleason-Gonzalez, C	694 561 377 550 568 108
Giulietti, D Gladush, G Glasser, A. H Glazunov, D Gleason-Gonzalez, C	694 561 377 550 568 108
Giulietti, D Gladush, G Glasser, A. H Glazunov, D Gleason-Gonzalez, C	694 .561 377 .550 568 108 396
Giulietti, D Gladush, G Glasser, A. H Glazunov, D Gleason-Gonzalez, C	694 561 377 550 568 108 396 244
Giulietti, D Gladush, G Glasser, A. H Glazunov, D Gleason-Gonzalez, C Globus-M Team, Goerler, T	694 .561 377 .550 568 108 396 244 .390
Giulietti, D Gladush, G Glasser, A. H. Glazunov, D. Gleason-Gonzalez, C	694 .561 377 .550 568 108 396 244 .390 351
Giulietti, D Gladush, G Glasser, A. H. Glazunov, D. Gleason-Gonzalez, C	694 561 377 550 568 108 396 244 390 351 296
Giulietti, D Gladush, G Glasser, A. H. Glazunov, D. Gleason-Gonzalez, C	694 561 377 550 568 108 396 244 390 351 296
Giulietti, D Gladush, G Glasser, A. H. Glazunov, D. Gleason-Gonzalez, C. Globus-M Team, Goerler, T. Goerler, T. Gogoleva, A. Gobil, P. Golfinopoulos, T. Golikov, A. A.	694 .561 377 .550 568 108 396 244 .390 351 296 550
Giulietti, D Gladush, G Glasser, A. H. Glazunov, D. Gleason-Gonzalez, C. Globus-M Team, Goerler, T. Goerler, T. Gogoleva, A. Gobil, P. Golfinopoulos, T. Golikov, A. A.	694 .561 377 .550 568 108 396 244 .390 351 296 550
Giulietti, D Gladush, G Glasser, A. H Glazunov, D Gleason-Gonzalez, C Globus-M Team, Goerler, T	694 .561 377 .550 568 108 396 244 .390 351 296 550 553 595
Giulietti, D Gladush, G Glasser, A. H Glazunov, D Gleason-Gonzalez, C Gobus-M Team, Goerler, T	694 561 377 550 568 108 396 244 390 351 296 550 553 595 576
Giulietti, D Gladush, G Glasser, A. H Glazunov, D Gleason-Gonzalez, C Goerler, T	694 561 377 550 568 108 396 244 390 351 296 550 553 595 576
Giulietti, D Gladush, G Glasser, A. H Glazunov, D Gleason-Gonzalez, C Gobus-M Team, Goerler, T	694 561 377 550 568 108 396 244 390 351 296 550 553 595 576 235,
Giulietti, D Gladush, G Glasser, A. H Glazunov, D Gleason-Gonzalez, C Gobus-M Team, Goerler, T	694 561 377 550 568 108 396 244 390 351 296 550 553 595 576 235,
Giulietti, D Gladush, G Glasser, A. H Glazunov, D Gleason-Gonzalez, C Golobus-M Team, Goerler, T	694 561 377 550 568 108 396 244 390 351 296 550 553 595 576 235,
Giulietti, D Gladush, G Glasser, A. H Glazunov, D Gleason-Gonzalez, C Goerler, T Goerler, T Gogoleva, A Gohil, P Gohil, P Golfinopoulos, T Golikov, A. A Golubeva, A Goncharov, P Goncharov, P Gondé, R Gong, X 316, 408, 657 Goniche, M.28, 35, 148, 235, 277, 280, 285, 464	694 561 377 550 568 396 244 390 351 296 550 555 555 576 235, 290,
Giulietti, D Gladush, G Glasser, A. H Glazunov, D Gleason-Gonzalez, C Golobus-M Team, Goerler, T Goorler, T Gogoleva, A Gohil, P Golfinopoulos, T Golikov, A. A Golubeva, A Goncharov, P Goncharov, P Gondé, R Gondé, R Gong, X 316, 408, 657 Goniche, M.28, 35, 148, 235, 277, 280, 285, 464 González, J	694 561 377 550 568 396 244 390 351 296 550 553 595 576 235, 290, 579
Giulietti, D	694 561 377 550 568 396 244 390 351 296 550 553 595 576 235, 290, 579 579
Giulietti, D Gladush, G Glasser, A. H Glazunov, D Gleason-Gonzalez, C Golobus-M Team, Goerler, T Goorler, T Gogoleva, A Gohil, P Golfinopoulos, T Golikov, A. A Golubeva, A Goncharov, P Goncharov, P Gondé, R Gondé, R Gong, X 316, 408, 657 Goniche, M.28, 35, 148, 235, 277, 280, 285, 464 González, J	694 561 377 550 568 396 244 390 351 296 550 553 595 576 235, 290, 579 579
Giulietti, D	694 561 377 550 568 396 244 390 351 296 553 595 576 235, 290, 579 579 285
Giulietti, D Gladush, G Glasser, A. H. Glazunov, D. Gleason-Gonzalez, C. Goerler, T. Goerler, T. Goorler, T. Goorler, T. Goorler, T. Golikov, A. Golinopoulos, T. Golikov, A. Golubeva, A. Golubeva, A. Goncharov, P. Soncharov, P. Gondé, R. Gondé, R. Gondé, R. Gondé, R. Gondé, S. Gondé, S.	694 561 377 550 568 396 244 390 351 296 550 553 595 576 235, 290, 579 579 285 198
Giulietti, D	694 561 377 550 568 396 244 390 351 296 550 553 595 576 235, 290, 579 579 285 198 173
Giulietti, D Gladush, G Glasser, A. H. Glazunov, D. Gleason-Gonzalez, C. Goerler, T. Goerler, T. Goorler, T. Goorler, T. Goorler, T. Golikov, A. Golinopoulos, T. Golikov, A. Golubeva, A. Golubeva, A. Goncharov, P. Soncharov, P. Gondé, R. Gondé, R. Gondé, R. Gondé, R. Gondé, S. Gondé, S.	694 561 377 550 568 108 396 244 390 351 296 550 553 595 576 235, 290, 579 579 285 198 173 375

Gorelenkova, M	170
Gorini, G	
Gorodetsky, A133, 631,	652
Gorshkov, A.	275
Goto, M	655
Goto, R	454
Goto, T	587
Gott, Y	
Goumiri, I. R.	
Graceffa, J	512
Graham, M	276
Grandgirard, V	431
Granetz, R 34, 48, 150, 208, 296, 297, 365,	558
Granucci, G	226
Grashin, S	
Grasso, G.	
Graves, J	
Gray, T. K	477
Green, D.	438
Greenwald, M 143, 145, 296, 297,	558
Greuner, H	
Gribkov, V	
Gribov, Y	047 667
Grierson, B 136, 143, 168, 175, 209, 315, 4	
659, 660, 663	±00,
Grierson, B. A	680
Grigoriev, S.	
Grisham, L	
Grisolia, C.	
Grist, D	
Groebner, R 160, 175, 209, 210, 361,	
Gros, G.	
Grosman, A.	
Grosso, L. A.	220
Groth, M	568
Gryaznevich, M12,	
Gude, A	
Guillerminet, B.	424
Guimaraes-Filho, Z. O	
Guirlet, R	293
Gulden, W	679
Gunn, J. P 10 , 29 , 363, 464,	499
Guo, H119, 124, 166, 230, 232, 234, 235,	316
Guo, S	
Guo, X	205
Guo, Y	
Guo, Z 30, 440,	485
Gupta, C 152, 321,	322
Gupta, C. N	130
Gupta, G	504
Gupta, M	321
Gupta, P	130
Gupta, S	321
Gurcan, O	

Gurchenko, A56, 17	2, 186, 187
Gureev, V.	642
Gurevich, M.	596
Gurl, C	
Gus'kov, A. Y	
Gusakov, E 133, 172, 186, 187, 20	4,366,389
Gusev, V 12, 133, 188, 189, 389, 39	0,581,652
Gustafson, K	
Gustafsson, C	33 , 633
Guterl, J	
Guttenfelder, W	143, 313

— н —

Ha, MS.	531
Hacquin, S	289
Hagelaar, G.	242
Hager, R	433
Hahm, T	605
Hahm, T. S	672
Hahn, H	
Hahn, S	
Hahn, SH.58, 139, 155, 345, 349, 351, 397,	673
Hajnal, N.	
Halfmoon, M. R.	480
Halitovs, M	
Hallatschek, K50,	481
Halpern, F.	
Ham, C	439
Hamaguchi, S.	577
Han, H140, 348, 349, 393,	471
Han, S	
Han, W	535
Han, X	
Hanada, K 16, 191,	192
Hanada, M	
Hanayama, R46, 117, 620, 621, 622,	
Hancock, D.	569
Hansen, C	600
Hanson, J 168, 206, 212, 217, 218, 244,	660
Hao, G	449
Happel, T	299
Harada, T	
Hariri, F	431
Harris, C. H.	530
Harris, J	
Harrison, J	267
Harting, D 455, 456,	
Hartmann, D	
Hartwig, Z	558
Harvey, B	412
Harvey, R	128
Harvey, R. W 44,	475
Hasegawa, A	630
Hasegawa, M191,	193

Hashimoto, K	. 258
Hashizume, H	
Haskey, S.	
Hassanein, A	
Hastie, J. R.	
Hatayama, A	
Hatch, D	
Hatcher, R.	
Hatori, T.	
Hattori, S.	
Hattori, T.	
Hatzky, R.	
Hauer, V.	
Haverkort, W	
Hawkes, N	, 279
Hawryluk, K 654	. 659
Hayashi, K.	. 507
Hayashi, N	, 664
Hayashi, T.	
Hayashi, Y.	
Hayrutdinov, R	
He, H 19	
He, Z174	, 401
Hegelich, M	
Heidbrink, B	. 412
Heidbrink, W. W. 14, 48, 55, 167, 168, 170,	372
<i>375,</i> 475	
Heikkinen, J.	.446
Heinemann, B	
Heinola, K	286
Heinola, K	286 .586
Heinola, K	286 .586
Heinola, K	286 586 359 574
Heinola, K. 281 Heitzenroeder, P. 100 Helander, P. 22, 36	286 586 359 574
Heinola, K	286 586 359 574 464
Heinola, K	286 586 359 574 464 500
Heinola, K	286 586 359 574 464 500 512
Heinola, K.	286 586 359 574 464 500 512 288
Heinola, K.	286 586 359 574 464 500 512 288 439
Heinola, K.	286 586 359 574 464 500 512 288 439 507
Heinola, K.	286 586 359 574 464 500 512 288 439 507 293
Heinola, K. 281 Heitzenroeder, P. 22, 36 Heller, R. 22, 36 Helou, W. 4 Henmi, T. 4 Hender, T. 511 Hender, T. 153 Hender, T. C. 4 Hennequin, P. 249 Heo, YG. 249	286 586 359 574 464 500 512 288 439 507 293 531
Heinola, K. 281 Heitzenroeder, P. 22, 36 Heller, R. 22, 36 Helou, W. 1 Henmi, T. 1 Hemsworth, R. 511 Hender, T. 153 Hender, T. C. 1 Hennequin, P. 249 Heo, Y-G. 1 Her, N. I. 1	286 586 359 574 464 500 512 288 439 507 293 .531 530
Heinola, K. 281 Heitzenroeder, P. 22, 36 Heller, R. 22, 36 Helou, W. 4 Henmi, T. 4 Hender, T. 511 Hender, T. 153 Hender, T. C. 4 Hender, T. C. 4 Hennequin, P. 249 Heo, YG. 4 Her, N. I. 39	. 286 . 586 . 359 . 574 . 464 . 500 . 512 . 288 . 439 . 507 . 293 . 531 . 530 . 680
Heinola, K. 281 Heitzenroeder, P. 22, 36 Heller, R. 22, 36 Helou, W. Henmi, T. Hensworth, R. 511 Hender, T. 153 Hender, T. C. 153 Henderson, M. 400 Hennequin, P. 249 Heo, YG. 410 Her, N. I. 39 Hernandez Gonzalez, F. 58	. 286 .586 . 359 .574 .464 .500 .512 .288 439 .507 .293 .531 .530 .530 . 680 . 565
Heinola, K. 281 Heitzenroeder, P. 22, 36 Heller, R. 22, 36 Helou, W. 12, 36 Helou, W. 13, 14 Henmi, T. 153 Hender, T. C. 153 Hender, T. C. 153 Hender, T. C. 14 Hender, T. C. 153 Hender, T. C. 14 Hender, T. C. 153 Hennequin, P. 249 Heo, YG. 150 Her, N. I. 39 Hernandez Gonzalez, F. 58 Herrmann, A. 15, 180	. 2866 .5866 . 359 .5744 .4644 .5000 .5122 .2888 .439 .5077 .2933 .5311 .5300 . 6800 . 565 . 184
Heinola, K. 281 Heitzenroeder, P. 22, 36 Heller, R. 22, 36 Helou, W. 151 Henmi, T. 153 Hender, T. C. 153 Hender, T. C. 153 Hender, T. C. 164 Hennequin, P. 249 Heo, YG. 167 Her, N. I. 167 Herb, J. 39 Hernandez Gonzalez, F. 58 Herrmann, A. 15, 180 Hertout, P. 150	. 2866 .5866 . 359 . 5744 . 4644 . 5000 . 5122 . 2888 . 4399 . 5077 . 2933 . 5311 . 5300 . 6800 . 5655 . 184 . 547
Heinola, K. 281 Heitzenroeder, P. 22, 36 Heller, R. 22, 36 Helou, W. 151 Hemmi, T. 153 Hender, T. 153 Hender, T. C. 153 Henderson, M. 160 Hernequin, P. 249 Heo, YG. 39 Hernandez Gonzalez, F. 58 Herrmann, A. 15, 180 Hertout, P. 140 Heuraux, S. 150	. 286 .586 . 359 .574 .464 .500 .512 .288 439 .507 .293 .531 .530 . 680 . 565 . 184 .547 .464
Heinola, K. 281 Heitzenroeder, P. 22, 36 Heller, R. 22, 36 Helou, W. 4 Hemmi, T. 4 Hemmir, T. 153 Hender, T. 153 Hender, T. C. 153 Hender, T. C. 4 Hennequin, P. 249 Heo, YG. 39 Hernandez Gonzalez, F. 58 Herrmann, A. 15, 180 Hertout, P. 45, 15, 180 Heuraux, S. 43, 241, 271, 273, 356	. 286 . 586 . 359 . 574 . 464 . 500 . 512 . 288 . 439 . 507 . 293 . 507 . 293 . 531 . 530 . 680 . 680 . 565 . 184 . 547 . 464 . 698
Heinola, K. 281 Heitzenroeder, P. 22, 36 Helander, P. 22, 36 Heller, R. 151 Henwi, T. 153 Hender, T. 153 Her, N. I. 164 Herr, N. I. 150 Herrmann, A. 151 Herruman, A. 151 Heuraux, S. 110 Hidalgo, C. 63, 241, 271, 273, 356 Higashijima, A. 110	. 286 . 586 . 359 . 574 . 464 . 500 . 512 . 288 . 439 . 507 . 293 . 531 . 530 . 531 . 530 . 680 . 565 . 184 . 547 . 464 . 547 . 464 . 547 . 464 . 500 . 574 . 500 . 574 . 574 . 500 . 574 . 574 . 500 . 574 . 574 . 500 . 512 . 507 . 507 . 507 . 507 . 507 . 507 . 507 . 500 . 512 . 507 . 507
Heinola, K.	. 286 . 586 . 359 . 574 . 464 . 500 . 512 . 288 . 439 . 507 . 293 . 531 . 530 . 565 . 184 . 547 . 464 . 698 . 191 . 268
Heinola, K.	. 286 . 586 . 359 . 574 . 464 . 500 . 512 . 288 . 439 . 507 . 293 . 531 . 530 . 565 . 184 . 547 . 464 . 698 . 191 . 268
Heinola, K. 281 Heitzenroeder, P. 22, 36 Heller, R. 122, 36 Heller, R. 151 Helou, W. 153 Hender, T. 153 Hender, T. C. 153 Hender, T. C. 153 Hender, T. C. 164 Hennequin, P. 249 Heo, YG. 19 Herb, J. 39 Hernandez Gonzalez, F. 58 Herrmann, A. 15, 180 Hertout, P. 180 Heidalgo, C. 63, 241, 271, 273, 356 Highscok, E. 111, D. Hill, D. 155, 229	2866 5866 3599 5744 5000 5122 2888 4399 5077 2933 5301 5300 6800 565 184 5477 4644 6988 1911 2688 1600
Heinola, K.	2866 5866 3599 5744 5000 5122 2888 4399 5077 2933 5301 5300 6800 565 184 5477 4644 6988 1911 2688 1600

Hillis, D. L	
Hinata, I	
Hioki T	
Hirai T	
Hirateuka I	
Hironaka V	
Hirooka V	
Hiroso A	
Hiwatari, K	
Hobirk, J	146, 163, 164, 277, 428
Hoelzl, M	
Hogeweij, G	
Holcomb, C. T	167, 210, 657, 661, 662
Hole, M. J	31 , 256, 442
	142, 143, 213, 466
Honda, A	
Honda, M4	10, 49, 154, 367 , 467, 493, 494
Honda, M4 Hong, G. H	10, 49, 154, 367, 467, 493, 494
Honda, M4 Hong, G. H Hong, J	10 , 49 , 154, 367 , 467, 493, 494
Honda, M 4 Hong, G. H Hong, J Hong, SH	10 , 49 , 154, 367 , 467, 493, 494
Honda, M 4 Hong, G. H Hong, J Hong, SH	10 , 49 , 154, 367 , 467, 493, 494
Honda, M 4 Hong, G. H Hong, J Hong, SH Hong, W	10 , 49 , 154, 367 , 467, 493, 494 505 349 57, 242, 350 121, 174, 331, 334, 335
Honda, M 4 Hong, G. H Hong, J Hong, SH Hong, W Honrubia, J	10 , 49 , 154, 367 , 467, 493, 494
Honda, M 4 Hong, G. H Hong, J Hong, SH Hong, W Honrubia, J Hopf, C	10 , 49 , 154, 367 , 467, 493, 494
Honda, M 4 Hong, G. H Hong, J Hong, SH Hong, W Honrubia, J Hopf, C Horacek, J	10 , 49 , 154, 367 , 467, 493, 494
Honda, M 4 Hong, G. H Hong, J Hong, SH Hong, W Honrubia, J Hopf, C Horacek, J	10, 49, 154, 367, 467, 493, 494
Honda, M 4 Hong, G. H Hong, J Hong, SH Hong, W Honrubia, J Hopf, C Horacek, J Horiuchi, R Hornung, G	10 , 49 , 154, 367 , 467, 493, 494 505 349 57, 242, 350 121, 174, 331, 334, 335 609 178 363, 423 601, 691
Honda, M 4 Hong, G. H Hong, J Hong, SH Hong, W Honrubia, J Hopf, C Horacek, J Horiuchi, R Hornung, G Hosea, J	40, 49, 154, 367, 467, 493, 494 505 349 57, 242, 350 121, 174, 331, 334, 335 609 178 363, 423 601, 691 289 290, 586
Honda, M 4 Hong, G. H Hong, J Hong, SH Honrubia, J Honrubia, J Horf, C Horacek, J Horiuchi, R Hornung, G Hosea, J	10 , 49 , 154, 367 , 467, 493, 494 505 349 57, 242, 350 121, 174, 331, 334, 335 609 178 363, 423 601, 691 289 290, 586 438
Honda, M 4 Hong, G. H Hong, J Hong, SH Honrubia, J Honrubia, J Horf, C Horiacek, J Horiuchi, R Hornung, G Hosea, J Hoshino, K	40, 49, 154, 367, 467, 493, 494 505 349 57, 242, 350 121, 174, 331, 334, 335 609 178 363, 423 601, 691 289 290, 586 438 59, 338, 508, 517, 518, 571
Honda, M 4 Hong, G. H Hong, J Hong, SH Honrubia, J Horrubia, J Horruchi, R Horiuchi, R Hornung, G Hosea, J. C Hosbino, K	40, 49, 154, 367, 467, 493, 494 505 349 57, 242, 350 121, 174, 331, 334, 335 609 178 363, 423 601, 691 289 290, 586 438 59, 338, 508, 517, 518, 571 609
Honda, M 4 Hong, G. H Hong, J Hong, SH Honrubia, J Honrubia, J Horf, C Horiuchi, R Horiuchi, R Hornung, G Hosea, J Hosoda, T Hosoda, Y	40, 49, 154, 367, 467, 493, 494 505 349 57, 242, 350 121, 174, 331, 334, 335 609 178 363, 423 601, 691 289 290, 586 438 59, 338, 508, 517, 518, 571 609 57, 242, 350
Honda, M 4 Hong, G. H Hong, J Hong, SH Honrubia, J Hopf, C Horiacek, J Horiacek, J Horinung, G Hosea, J. C Hosoda, T Hosoda, Y Hosoi, K	40, 49, 154, 367, 467, 493, 494 505 349 57, 242, 350 121, 174, 331, 334, 335 609 178 363, 423 601, 691 289 290, 586 438 59, 338, 508, 517, 518, 571 609 570 570
Honda, M 4 Hong, G. H Hong, J Hong, SH Honrubia, J Hopf, C Horiacek, J Horiacek, J Horinung, G Hosea, J. C Hosoda, T Hosoda, Y Hosoi, K Hosoi, K	40, 49, 154, 367, 467, 493, 494 505 349 57, 242, 350 121, 174, 331, 334, 335 609 178 363, 423 601, 691 290, 586 438 59, 338, 508, 517, 518, 571 570 424
Honda, M 4 Hong, G. H Hong, J Hong, SH Honrubia, J Hopf, C Horiacek, J Horiacek, J Horinung, G Horsea, J. C Hosoda, T Hosoda, Y Hosoi, K Hossoi, K Hossack, A	40, 49, 154, 367, 467, 493, 494 505 349 57, 242, 350 121, 174, 331, 334, 335 609 178 363, 423 601, 691 289 290, 586 438 59, 338, 508, 517, 518, 571 570 424 600
Honda, M 4 Hong, G. H Hong, J Hong, SH Honrubia, J Hopf, C Horacek, J Horacek, J Horacek, J Horacek, J Hosea, J. C Hosoda, T Hosoda, Y Hosoda, X Hossock, M Hossack, A	40, 49, 154, 367, 467, 493, 494 505 349 57, 242, 350 121, 174, 331, 334, 335 609 178 363, 423 601, 691 290, 586 438 59, 338, 508, 517, 518, 571 570 424 600 601 602 603 604 605 607 570 600 601 602 603 604 605 606 607 608 609 600 601 602 603 604 605 606 607 608 609 601 602 603 604 605 606 607 608 608
Honda, M 4 Hong, G. H Hong, J Hong, SH Hong, W Horrubia, J Horf, C Horacek, J Horacek, J Horacek, J Hosea, J. C Hosea, J. C Hosea, J. C Hosoda, T Hosoda, T Hosoda, Y Hosokawa, M Hosokawa, M Hosokawa, A Houlberg, W	40, 49, 154, 367, 467, 493, 494 505 349 .57, 242, 350 .121, 174, 331, 334, 335 .601 .601, 691 .290, 586 .438 .59, 338, 508, 517, 518, 571 .505 .57, 242, 350 .121, 174, 331, 334, 335 .601, 691 .289 .290, 586 .438 .59, 338, 508, 517, 518, 571 .602 .570 .524 .600 .622 .602 .624 .600 .624 .600 .622 .623 .624 .624 .625 .626 .622 .623 .624 .624 .625 .626 .627 .628 .629 .629 .6200 .621 .622 .621
Honda, M 4 Hong, G. H Hong, J Hong, SH Honrubia, J Horrubia, J Horruchi, A Horacek, J Horacek, J Hosea, J. C Hosea, J. C Hosoda, T Hosoda, T Hosoda, Y Hosoda, Y Hosokawa, M Hosokawa, M Hou, Y Houblerg, W	
Honda, M 4 Hong, G. H Hong, J Hong, SH Hong, W Horrubia, J Horrubia, J Horacek, J Horacek, J Horiuchi, R Horiuchi, R Hosea, J. C Hosea, J. C Hosoda, T Hosoda, T Hosoda, Y Hosoda, Y Hosokawa, M Hosokawa, M Houberg, W Howard, J	
Honda, M 4 Hong, G. H Hong, J Hong, SH Honrubia, J Horrubia, J Horruchi, R Horiuchi, R Horiuchi, R Horiuchi, R Horiuchi, R Horiuchi, R Hosea, J. C Hosea, J. C Hoseda, T Hosoda, Y Hosoda, Y Hosoda, Y Hosokawa, M Hosokawa, M Houberg, W Howard, J Howard, J	
Honda, M 4 Hong, G. H Hong, J Hong, SH Honrubia, J Horrubia, J Hopf, C Horiuchi, R Horiuchi, R Horiuchi, R Horiuchi, R Horiuchi, R Hosea, J. C Hosea, J. C Hosoda, T Hosoda, Y Hosoda, Y Hosoda, Y Hosokawa, M Hosokawa, M Houlberg, W Howard, J Howard, J Howard, J Hu, C	
Honda, M 4 Hong, G. H Hong, J Hong, SH Honrubia, J Honrubia, J Horiuchi, R Horiuchi, R Horiuchi, R Horiuchi, R Hosoa, J Hosoda, T Hosoda, T Hosoda, Y Hosoda, Y Hosokawa, M Hosokawa, M Hosokawa, M Hosokawa, M Hosokawa, M Houlberg, W Howard, J Howard, N Hu, C	
Honda, M 4 Hong, G. H Hong, J Hong, SH Honrubia, J Horrubia, J Horrubia, J Horruchi, R Horiuchi, R Horiuchi, R Horiuchi, R Hosea, J. C Hosoda, T Hosoda, T Hosoda, Y Hosoda, Y Hosokawa, M Hosokawa, M Hosokawa, M Hosokawa, M Hosokawa, M Hosokawa, M Hosokawa, M Howard, J Howard, J Hu, D Hu, J	

Hu, X	132
Huang, J	
Huang, M	
Huang, Y121, 174, 3	25, 327, 330
Huang, Z174, 2	
Hubbard, A 43, 145, 297, 2	99 , 510, 558
Huber, A158, 278, 2	
Hudson, S	
Hülsewede, R	
Hughes, J 27, 35, 145, 295–2	97, 299, 558
Hughes, P	
Huijsmans, G 57, 240, 365, 369, 32	70, 415, 421,
427, 460	
Humphreys, D	
Humphreys, D. A	54, 658, 670
Hussain, S	30, 254
Hutchinson, I.	
Huynh, P	
Hwang, HS	
Hwang, Y	
Hwang, YS	
Hyatt, A 2	
Hyatt, A. W160, 2	10, 654, 659

— I —

Imadera, K	3	36, 448
Imai, T	35, 192, 50)9 , 570
Imamura, K		
Imazawa, R		53, 557
Imbeaux, F	25, 293, 42	24 , 547
In, Y		18, 344
Inada, T		294
Inagaki, S22,		
Ingenito, F		694
Innocente, P.	12	28, 244
Inomoto, M	17, 20)5, 604
Inoue, H		609
Inoue, S)1, 691
Irby, J		97, 558
Irzak, M 1	133, 186, 187, 20)4, 389
Isaev, M		
Isayama, A		508
Ishida, S		
Ishihara, K		
Ishii, G		
Ishii, K		
Ishii, Y		
Ishikawa, H		
Ishizawa, A	4	14, 474
Islam, M. K		
Islas, O		579
Isler, R. C		
Isobe, K		643
Isobe, M121, 1	169, 311, 323, 32	29, 587
Itagaki, H		,
Itami, K		
Ito, A		
Ito, A. M		6 1, 62 9
Ito, S)9, 577
Itoh, K124, 141, 174, 3	334, 338, 402, 4	53, 491
Itoh, S141, 174, 3	334, 338, 402, 4	53, 491
Ivanov, A 1		
Ivanov, D		
Ivanov, N		
Ivanov, S		
Ivanova, D.		36, 523
Ivanova-Stanik, I		
Iwakiri, H		
Iwamoto, A		
Iwamoto, M		
Iwamoto, Y	• • • • • • • • • • • • • • • • • • • •	618
Izacard, O		466
Izzo, V. A		J8, 36 5

1zacard, O	00
Izzo, V. A	5
— I —	
Jaboulay, JC	7
Jachmich, S 151, 278, 280, 285, 423, 455, 45	<i>i</i> 6
Jackson, G. L 217, 660, 662, 68	. 9
Jacquemot, S)1

Jacquet, P	. 38, 277,	280, 290
Jacquot, J		464
Jadav, H		321
Jadeja, K		152, 321
Jaeger, E. F		438
Jagannathan, G		237
Jakubowski, L		
Jakubowski, M		137.241
James, C		586
Jang, J		
[arboe, T	478.	580,600
Jardin, S	,	404
Jardin, S. C	139	437, 478
[arrott, C		610
Järvinen, A. E	38	280 455
Jayswal, S. P		
Jenkins, I		
Jenko, F 18 , 144, 359, 3	268 206	660 600
Jeon, Y. 13 , 23 , 139, 140 , 161,	200, 390 , 241, 245	246 671
Jeon, I. 13, 23 , 139, 140 , 101,	241, 343,	340, 071
Jeong, J	•••••	100
Jeong, J. H JET-EFDA Contributors,	•••••	
[ha, R	152,	321, 322
Iha, S		
[ha, S. K	• • • • • • • • •	152
Ihang, H Ii, X 40, 48 , 121, 156 , 174, 3		343, 374
ji, X 40, 48, 121, 156, 174, 3	323, 324,	326–328,
330–332, 334		
Jia, H	• • • • • • • • • •	235
Jiang, H		401
Jiang, J		.681,682
Jiang, M 51 , 156, 3	324, 325,	326 , 328
Jie, Y		232
Jiménez-Rey, D		269
Jimenez-Ramos, M. C		
Jin, F		529
Jin, S. W		505
Jin, X. Z		680
Jiolat, G		576
[itsuno, T	117,	609,613
lo, J		605
Joanne, F		
Juanne, F		
loaquim, L		146 363
loaquim, L		146 363
Joaquim, L Joffrin, E 38 , 146, 163, 164, 1	 276, 277,	146 363 291 , 428
Joaquim, L		146 363 291 , 428 521
Joaquim, L. Joffrin, E 38 , 146, 163, 164, 1 Johnson, D. Johnson, M.	276, 277,	146 363 291, 428 521 608
Joaquim, L. Joffrin, E 38 , 146, 163, 164, 1 Johnson, D. Johnson, M. Johnson, R. D.		146 363 291 , 428 521 608 658
Joaquim, L. Joffrin, E 38 , 146, 163, 164, 1 Johnson, D. Johnson, M. Johnson, R. D.		146 363 291 , 428 521 608 658
Joaquim, L Joffrin, E 38 , 146, 163, 164, 1 Johnson, D Johnson, M Johnson, R. D Johnson, T Johzaki, T 45 , 117, 609, 1	276, 277, 276, 277, 285, 613, 616 ,	146 363 291, 428 521 608 658 368, 396 617, 693
Joaquim, L Joffrin, E 38 , 146, 163, 164, 1 Johnson, D Johnson, M Johnson, R. D Johnson, T Johzaki, T 45 , 117, 609, 1 Joisa, S	276, 277, 276, 277, 285, 613, 616 , 152,	146 363 291 , 428 521 608 658 368, 396 617, 693 321, 322
Joaquim, L Joffrin, E38, 146, 163, 164, 1 Johnson, D Johnson, M Johnson, R. D Johnson, T Johzaki, T45, 117, 609, 1 Joisa, S Joisa, Y. S	276, 277, 285, 613, 616 , 152,	146 363 291 , 428 521 608 658 368, 396 617, 693 321, 322 130
Joaquim, L Joffrin, E 38 , 146, 163, 164, 1 Johnson, D Johnson, M Johnson, R. D Johnson, T Johzaki, T 45 , 117, 609, 1 Joisa, S Joisa, Y. S Jolliet, S	276, 277, 285, 613, 616 , 152,	146 363 291, 428 521 608 658 368, 396 617, 693 321, 322 130 363
Joaquim, L Joffrin, E 38 , 146, 163, 164, 1 Johnson, D Johnson, M Johnson, R. D Johnson, T Johzaki, T 45 , 117, 609, 1 Joisa, S	276, 277, 285, 613, 616 , 152,	146 363 291 , 428 521 608 658 368, 396 617, 693 321, 322 130 363 264

Jucker, P	
Juhn, JW	
Jun, C	
Jun-Gyo, B	
Jung, B	605, 672
Jung, HC	
Jung, KJ	.505, 530, 531
Jurczynski, S	586
Justice Fletcher, J.	634

— K —

Kadia, B			321
Kado, S	258-	261,	570
Kadomtsev, M			275
Kadowaki, M			512
Kagei, Y			452
Kaita, R	316,	476,	586
Kajino, T		621,	623
Kajita, S			629
Kajitani, H			500
Kajiwara, K			
Kakeno, M		620,	622
Kakuda, H			
Kakurin, A			
Kalal, M			
Kallenbach, A 47, 56, 157, 165,			
Kamada, Y59,			
Kamendje, R			
Kamentsev, K			
Kamio, S159, 205,			
Kamiya, K141,			
Kamlah, M			
Kammel, A			
Kan, H	117,	620-	-623
Kaneko, J			
Kaneko, O			
Kang, D. K			
Kang, K. O			
Kantor, M			
Kargin, N			
Kariya, T	192,	509,	570
Karpushov, A	226,	246,	247
Kasahara, H.47, 56, 159, 227, 294,			
Kasajima, K			
Kashiwa, Y			
Kashiwagi, M			
Kasuya, N	37,	141,	453
Katanuma, I			
Kato, D			
Kato, S			
Kato, T			509
Kaveeva, E			
Kavin, A	581,	666,	667

Kaw, P 321, 376,	
Kaw, P. K	
Kawahata, K245,	
Kawamura, G	473
Kawanaka, J 117, 609,	
Kawano, Y 32, 525,	
Kawasaki, S.	191
Kawashima, T117, 620-	-623
Kawazura, Y	684
Kaye, S 123 , 313, 315, 316, 586,	590
Keeling, D164,	264
Kemp, R	516
Kenmochi, N	
Kessel, C 162, 520, 543–545, 558, 590,	
Kevin, O	
Khan, M. S	
Khan, Z	
Khayrutdinov, R	
Khilkevitch, E	
Khirwadkar, S.	
Khitrov, S	
Khodak, A.	
Khokhlov, M	
Khorshid, P	
Khrabrykh, N.	
Khripunov, B.	642
	044
Vhristi V C	120
Khristi, Y. S.	130
Khristi, Y. S	130 652
Khristi, Y. S	130 652 540
Khristi, Y. S	130 652 540 688
Khristi, Y. S	130 652 540 688 247
Khristi, Y. S	130 652 540 688 247 531
Khristi, Y. S. Khromov, N. 133, 188, 389, 390, Khvostenko, P. 204, 515, Kikuchi, M. Kim, D. 226, Kim, DH. Kim, G.	130 652 540 688 247 .531 344
Khristi, Y. S	130 652 540 688 247 531 344 505
Khristi, Y. S	130 652 540 688 247 531 344 505 664
Khristi, Y. S. Khromov, N. 133, 188, 389, 390, Khvostenko, P. 204, 515, Kikuchi, M. Kim, D. 226, Kim, DH. Kim, G. Kim, G. H. Kim, H. Kim, H. Kim, HS. 44, 343, 504, 505, 520,	130 652 540 688 247 531 344 505 664 671
Khristi, Y. S. Khromov, N	130 652 540 688 247 531 344 505 664 671 672
Khristi, Y. S. Khromov, N	130 652 540 688 247 531 344 505 664 671 672 612
Khristi, Y. S. Khromov, N	130 652 540 688 247 .531 344 505 664 671 672 .612 393
Khristi, Y. S. Khromov, N	130 652 540 688 247 531 344 505 664 671 672 612 393 695
Khristi, Y. S. Khromov, N	130 652 540 688 247 531 344 505 664 671 672 612 393 695 350
Khristi, Y. S. Khromov, N	130 652 540 688 247 531 344 505 664 671 672 612 393 695 350 161
Khristi, Y. S. Khromov, N. 133, 188, 389, 390, Khvostenko, P. 204, 515, Kikuchi, M. Kim, D. Kim, DH. Kim, G. Kim, G. H. Kim, HS. Kim, J. 57, 150, 344, 344, 345, 347, 348, 393, Kim, J. S. Kim, J. Y. Kim, K. 41, 49, 52, 520, 543, 544, 545, 671, Kim, M.	130 652 540 688 247 531 344 505 664 671 672 612 393 695 350 .161 671
Khristi, Y. S. Khromov, N	130 652 540 688 247 531 344 505 664 671 672 612 393 695 350 161 671 665
Khristi, Y. S. Khromov, N. 133, 188, 389, 390, Khvostenko, P. 204, 515, Kikuchi, M. Kim, D. Kim, DH. Kim, G. Kim, G. Kim, G. H. Kim, HS. Kim, J. 57, 150, 344, 344, 345, 347, 348, 393, Kim, J. S. Kim, J. Y. Kim, K. 41, 49, 52, 520, 543, 544, 545, 671, Kim, M. Kim, S. Kim, SH. 424, 664,	130 652 540 688 247 531 344 505 664 671 672 612 393 695 350 161 .671 665 671
Khristi, Y. S. Khromov, N. 133, 188, 389, 390, Khvomov, N. 133, 188, 389, 390, Khvostenko, P. 204, 515, Kikuchi, M. Kim, D. Kim, D. Kim, G. Kim, G. Kim, G. Kim, G. Kim, JH. Kim, G. Kim, G. Kim, G. Kim, JH. Kim, G. Kim, G. Kim, JH. Kim, J. S. Kim, J. S. Kim, J. Y. Kim, K. 41, 49, 52, 520, 543, 544, 545, 671, Kim, M. Kim, M. Kim, M. H. Kim, M. H. Kim, S. Kim, SH. 424, 664, Kim, SW. 32,	130 652 540 688 247 531 344 505 664 671 672 612 393 695 350 161 671 665 671 531
Khristi, Y. S. Khromov, N	130 652 540 688 247 531 344 505 664 671 672 612 393 695 350 161 .671 665 671 531 374
Khristi, Y. S. Khromov, N	130 652 540 688 247 531 344 505 664 671 672 612 393 695 350 161 671 665 671 531 374
Khristi, Y. S. Khromov, N	130 652 540 688 247 531 344 505 664 672 612 393 350 161 671 665 671 531 374 505 605
Khristi, Y. S. Khromov, N	130 652 540 688 247 531 344 505 664 672 612 393 350 161 671 671 665 671 374 505 605 678
Khristi, Y. S. Khromov, N	130 652 540 688 247 531 344 505 664 671 672 612 393 695 635 671 671 531 374 505 605 678 354
Khristi, Y. S. Khromov, N	130 652 540 688 247 531 344 505 664 671 672 612 393 695 635 671 671 531 374 505 605 678 354
Khristi, Y. S. Khromov, N	130 652 540 688 247 531 344 505 664 671 672 672 393 695 350 161 671 665 671 374 505 605 678 354 354 354 354 354 354 354 354 355 355

King, J. D	212
Kinsey, J.	662
Kiptily, V151, 277,	278
Kirillov, I	554
Kirillov, I	443.
460	,
Kirneva, N	585
Kirschner, A	281
Kisaki, M.	655
Kishimoto, Y.	
Kiss, G.	506
Kißlinger, J.	
Kitagawa, Y 117, 620–623,	693
Kiviniemi, T	446
Kizane, G	
Kizu, K	574
Klabacha, J.	
Kleiber, R	
Klepper, C	
Klimek, I Klimov, N	204
Klishchenko, A. V.	
Klyuchnikov, L 16,	198
Knaster, J	
Knaup, M	423
Knitter, R.	
Ко, Ј	299
Ko, S Ko, WH 57 , 139, 140, 155, 214, 343, 345,	155
Ko. WH., 57, 139, 140, 155, 214, 343, 345.	
	346,
349, 350, 353	
349, 350, 353 Kobayashi, M 11, 17, 124 , 300, 301, 331,	
349, 350, 353 Kobayashi, M 11, 17, 124 , 300, 301, 331,	473,
349, 350, 353 Kobayashi, M 11, 17, 124 , 300, 301, 331,	473,
349, 350, 353 Kobayashi, M 11, 17, 124 , 300, 301, 331, 517 Kobayashi, R	473, 629 261
349, 350, 353 Kobayashi, M 11 , 17 , 124 , 300, 301, 331, 517 Kobayashi, R	473, 629 261 508
349, 350, 353 Kobayashi, M 11, 17, 124 , 300, 301, 331, 517 Kobayashi, R	473, 629 261 508
349, 350, 353 Kobayashi, M 11 , 17 , 124 , 300, 301, 331, 517 Kobayashi, R	473, 629 261 508 448 499
349, 350, 353 Kobayashi, M 11 , 17 , 124 , 300, 301, 331, 517 Kobayashi, R	473, 629 261 508 448 499 677
349, 350, 353 Kobayashi, M 11 , 17 , 124 , 300, 301, 331, 517 Kobayashi, R	473, 629 261 508 448 499 677
349, 350, 353 Kobayashi, M 11 , 17 , 124 , 300, 301, 331, 517 Kobayashi, R	473, 629 261 508 448 499 677 117
349, 350, 353 Kobayashi, M 11 , 17 , 124 , 300, 301, 331, 517 Kobayashi, R. Kobayashi, S. Kobayashi, T. Kobayashi, T. Kocan, M. Kochergin, M. Kodama, R. Kodera, R.	473, 629 261 508 448 499 677 117 245
349, 350, 353 Kobayashi, M 11 , 17 , 124 , 300, 301, 331, 517 Kobayashi, R. Kobayashi, S 30 , 258, 259, 260 , Kobayashi, T 35 , 51 , 141, 154, 183, 338 , Kobiki, T. Kocan, M	473, 629 261 508 448 499 677 117 245 668
349, 350, 353 Kobayashi, M 11 , 17 , 124 , 300, 301, 331, 517 Kobayashi, R. Kobayashi, S 30 , 258, 259, 260 , Kobayashi, T 35 , 51 , 141, 154, 183, 338 , Kobiki, T. Kocan, M	473, 629 261 508 448 499 677 117 245 668 444
349, 350, 353 Kobayashi, M 11 , 17 , 124 , 300, 301, 331, 517 Kobayashi, R. Kobayashi, S 30 , 258, 259, 260 , Kobayashi, T 35 , 51 , 141, 154, 183, 338 , Kobiki, T	473, 629 261 508 448 499 677 117 245 668 444 575
349, 350, 353 Kobayashi, M 11 , 17 , 124 , 300, 301, 331, 517 Kobayashi, R. Kobayashi, S 30 , 258, 259, 260 , Kobayashi, T 35 , 51 , 141, 154, 183, 338 , Kobiki, T	473, 629 261 508 448 499 677 117 245 668 444 575 117
349, 350, 353 Kobayashi, M 11 , 17 , 124 , 300, 301, 331, 517 Kobayashi, R. Kobayashi, S 30 , 258, 259, 260 , Kobayashi, T 35 , 51 , 141, 154, 183, 338 , Kobiki, T	473, 629 261 508 448 499 677 117 245 668 444 575 117 245
349, 350, 353 Kobayashi, M 11, 17, 124, 300, 301, 331, 517 Kobayashi, R Kobayashi, S	473, 629 261 508 448 499 677 117 245 668 444 575 117 245 276
349, 350, 353 Kobayashi, M 11 , 17 , 124 , 300, 301, 331, 517 Kobayashi, R. Kobayashi, S 30 , 258, 259, 260 , Kobayashi, T 35 , 51 , 141, 154, 183, 338 , Kobiki, T. Kocan, M	473, 629 261 508 448 499 677 117 245 668 444 575 117 245 276 570
349, 350, 353 Kobayashi, M 11, 17, 124, 300, 301, 331, 517 Kobayashi, R Kobayashi, S	473, 629 261 508 448 499 677 117 245 668 444 575 117 245 276 570 642
349, 350, 353 Kobayashi, M 11, 17, 124, 300, 301, 331, 517 Kobayashi, R. Kobayashi, S. Sobayashi, S. 30, 258, 259, 260, Kobayashi, T. Kobayashi, T. Sobayashi, T. Sobayashi, T. Sobayashi, T. Kobayashi, T. Sobayashi, T. Sobayashi, T. Sobayashi, T. Kobayashi, T. Sobayashi, T. Sobayashi, T. Kobayashi, T. Sobayashi, T. Kocan, M. Sobayashi, T. Kodama, R. Kodera, R. Köchl, F. Köchl, F. Sobayashi, A. Sobayashi, Soba	473, 629 261 508 448 499 677 117 245 668 444 575 117 245 276 570 642 574
349, 350, 353 Kobayashi, M 11, 17, 124, 300, 301, 331, 517 Kobayashi, R. Kobayashi, S. Sobayashi, S. 30, 258, 259, 260, Kobayashi, S. Kobayashi, S. 30, 258, 259, 260, Kobayashi, T. Kobayashi, T. Sobayashi, T. Sobayashi, T. Kobayashi, T. Sobayashi, T. Kobayashi, T. Kobayashi, T. Sobayashi, T. Sobayashi, T. Sobayashi, T. Kocan, M. 240, 363, Kochergin, M. Kodera, R. Kodera, R. Kodera, R. Kodera, R. Kogen, M. Kogu, M. Kogu, M. Kogu, M. Kogu, M. Kogu, D. Koidan, V. Koidan, V. Koidan, V. Koizumi, N. Sobaya, M. Koizumi, N.	473, 629 261 508 448 499 677 117 245 668 444 575 117 245 276 570 642 574 500
349, 350, 353 Kobayashi, M 11, 17, 124, 300, 301, 331, 517 Kobayashi, R. Kobayashi, S. Sobayashi, S. 30, 258, 259, 260, Kobayashi, T. Kobayashi, T. Sobayashi, T. Sobayashi, T. Sobayashi, T. Kobayashi, T. Kobayashi, T. Sobayashi, T. Kobayashi, T. Kobayashi, T. Kochar, R. Kochergin, M. Kodera, R. Kodera, R. Köchl, F. Köppen, M. Soga, M. Koguchi, H. Kogut, D. Koidan, V. Koidan, V. Koidan, V. Koidan, V. Koizumi, N. Sojuma, A.	473, 629 261 508 448 499 677 117 245 668 444 575 117 245 276 570 642 574 500 513
349, 350, 353 Kobayashi, M 11, 17, 124, 300, 301, 331, 517 Kobayashi, R. Kobayashi, S. Sobayashi, S. 30, 258, 259, 260, Kobayashi, T. Kobayashi, T. 30, 258, 259, 260, Kobayashi, T. Kobayashi, T. Sobayashi, T. Kobayashi, T. Sobayashi, T. Kobayashi, T. Kobayashi, T. Kobayashi, T. Sobayashi, T. Kochergin, M. Kochergin, M. Kodera, R. Kodera, R. Köchl, F. Köppen, M. Koga, M. Koguchi, H. Kogut, D. Koidan, V. Koidan, V. Koidan, V. Koidan, N. Kojuma, A. Sojima, S.	473, 629 261 508 448 499 677 117 245 668 444 575 117 245 276 570 642 570 642 574 500 513 613
349, 350, 353 Kobayashi, M 11, 17, 124, 300, 301, 331, 517 Kobayashi, R. Kobayashi, S. Sobayashi, S. 30, 258, 259, 260, Kobayashi, T. Kobayashi, T. Sobayashi, T. Sobayashi, T. Sobayashi, T. Kobayashi, T. Kobayashi, T. Sobayashi, T. Kobayashi, T. Kobayashi, T. Kochar, R. Kochergin, M. Kodera, R. Kodera, R. Köchl, F. Köppen, M. Soga, M. Koguchi, H. Kogut, D. Koidan, V. Koidan, V. Koidan, V. Koidan, V. Koizumi, N. Sojuma, A.	473, 629 261 508 448 499 677 117 245 668 444 575 117 245 276 570 642 570 642 574 500 513 613 648

Kolemen, E 20 , 47 , 57 , 136, 160, 210, 6 661, 673		
Kolesnikova, T	685,	686
Koliner, J.	128,	244
Kolodeshnikov, A		572
Komarov, A.		320
Komarov, V.		
Komata, M		
Komeda, O		
Komm, M.		
Komori, A	141,	655
Kondo, K		
Kondo, T	520-	623
Kong, D	327,	335
Kong, H. J	42.	612
Konopleva, R.		527
Konoshima, S	258–	261
Konovalov, S 25, 415, 418, 4	421,	422
Konovalov, V		
Kopchenkov, B.		685
Korbla Gbadago, J		634
Koresheva, E		
Kornev, V 45, 189, 318, 3	319,	320
Kornienko, S.		642
Korobov, K.	198,	585
Korolev, V	,	198
Korotaev, A.		
Korpilo, T.		446
Koshelev, E		611
Koskela, T		
Koslowski, H. R.		
Koslowski, R.	151,	356
Kost, Y		527
Kosuga, Y 19 , 50 , 141, 402 , 440, 4	485,	491
Kotov, V	275,	526
Kotschenreuther, M. T 25, 417, 482, 5	558,	590
Kouprienko, D	186,	187
Koval, A	531,	677
Kovalenko, Y		253
Kowalska-Strzeciwilk, E		646
Kozintseva, M		
Kozulya, M.		
Kramer, G. J.	136,	168
Krämer-Flecken, A	289,	356
Krasheninnikov, S 34, 42, 57, 4	196 ,	610
Krashevskaya, G	. 51,	336
Krasikov, Y.		
Krasilnikov, A 10, 11, 1	112,	541
Krasnov, S.	133,	581
Krat, S		281
Kravchuk, S		201
Kravtsova, M		637
Kreter, A 28,		
Krieger, K 183, 184, 2	287,	423

Krikunov, S	319
Krivska, A	
Kruezi, U 151, 278,	386
Kruezi, U	479
100	568
Krupin, V	585
Krupnik, L 199,	320
Krylov, S 173,	
Krylov, V	515
Ku, SH	
Kubic, M	
Kubkowska, M	646
Kubo, H.	
Kubo, S	655
Kubota, R	387
Kugel, H.	
Kuiroukidis, A.	
Kukhtin, V.	
Kukushkin, A	
Kukushkin, A. B	
Kukushkin, A. S275, 410, 413, 668,	677
Kulaga, A.	342
Kuley, A	308
Kulikauskas, V.	642
Kulikov, E	
Kulikov, G	
Kulkarni, S	200
Kulsartov, T.	651
Kunsartov, 1	321
$Ruillal, A, \ldots, Ruillal, A, \ldots, Ruillal, A, Ruillal, Ruillal$	521
Kumar M	120
Kumar, M	
Kumar, M Kumar, R	559
Kumar, M Kumar, R Kumar, S	559 322
Kumar, M. Kumar, R. Kumar, S. 128, 321, Kumazawa, R. 227,	559 322 294
Kumar, M. Kumar, R. Kumar, S. 128, 321, Kumazawa, R. 227, Kuprienko, D.	559 322 294 185
Kumar, M. Kumar, R. Kumar, S. 128, 321, Kumazawa, R. 227, Kuprienko, D. Kurita, T. 620–	559 322 294 185 623
Kumar, M. Kumar, R. Kumar, S. 128, 321, Kumazawa, R. 227, Kuprienko, D. Kurita, T. 620– Kuriyama, M.	559 322 294 185 623 512
Kumar, M. Kumar, R. Kumar, S. 128, 321, Kumazawa, R. 227, Kuprienko, D. Kurita, T. 620– Kuriyama, M. Kurki-Suonio, T. 25,	559 322 294 185 623 512 414
Kumar, M. Kumar, R. Kumar, S. 128, 321, Kumazawa, R. 227, Kuprienko, D. Kurita, T. 620– Kuriyama, M. Kurki-Suonio, T. 25, Kurkin, G.	559 322 294 185 623 512 414 541
Kumar, M. Kumar, R. Kumar, S. 128, 321, Kumazawa, R. 227, Kuprienko, D. Kurita, T. 620– Kuriyama, M. Kurki-Suonio, T. 25, Kurkin, G. Kurnaev, V. 563,	559 322 294 185 623 512 414 541 632
Kumar, M. Kumar, R. Kumar, S. Kumar, S. Kumazawa, R. 227, Kuprienko, D. Kurita, T. Kurita, T. Kursia, M. Kurki-Suonio, T. Kurnaev, V. 563, Kuroda, K.	559 322 294 185 623 512 414 541 632 340
Kumar, M. Kumar, R. Kumar, S. 128, 321, Kumar, S. Kumazawa, R. 227, Kuprienko, D. Kurita, T. Kurita, T. Kurki-Suonio, T. Sturkin, G. Kurnaev, V. Kuroda, K. Kurskiev, G. Star, 133, 188, 189, 283, 631,	559 322 294 185 623 512 414 541 632 340 677
Kumar, M. Kumar, R. Kumar, S. 128, 321, Kumar, S. Kumazawa, R. 227, Kuprienko, D. Kurita, T. Kurita, T. Kurki-Suonio, T. Sturkin, G. Kurnaev, V. Kuroda, K. Kurskiev, G. Star, 133, 188, 189, 283, 631,	559 322 294 185 623 512 414 541 632 340 677
Kumar, M. Kumar, R. Kumar, S. Kumar, S. Kumar, S. Kumar, S. Kumar, S. Kumar, S. Kurar, S. Kurita, T. Kurita, T. Kurita, T. Kurita, T. Kurita, T. Kurita, T. Kurki-Suonio, T. Kurki-Suonio, T. Kurki-Suonio, T. Kurki-Suonio, T. Kurki-Suonio, T. Kurki-Suonio, T. Kurakev, V. Kurnaev, V. Kuroda, K. Kurskiev, G. Kurzan, B. Kuteev, B Kuteev, B Si, 134, 550, 553, 562, 593, 562, 593, 562, 593, 563, 563, 563, 563, 563, 563, 563, 56	559 322 294 185 623 512 414 541 632 340 677
Kumar, M. Kumar, R. Kumar, S. 128, 321, Kumar, S. Kumar, S. 128, 321, Kumar, S. Kumar, S. 128, 321, Kumar, S. Kurpienko, D. Kurita, T. Kurita, T. Kurita, T. Kurita, T. Kurita, T. Kurki-Suonio, T. Kurki-Suonio, T. Sturnaev, V. Kurnaev, V. Kuroda, K. Kurskiev, G. Sturey, B. Kuteev, B. Stuteev, B. Stuteev	559 322 294 185 623 512 414 541 632 340 677 144 596,
Kumar, M. Kumar, R. Kumar, S. 128, 321, Kumar, S. Kumar, S. Kumar, S. Kumar, S. Kurata Kurita, T. Kursian, G. Kurskiev, G. Stronda, K. Kurskiev, G. Kurzan, B. Kuteev, B. Stronda, K. Kuteev, B. Stronda, Strong, Str	559 322 294 185 623 512 414 541 632 340 677 144 596, 205
Kumar, M. Kumar, R. Kumar, S. 128, 321, Kumar, S. Kumar, S. Kumar, S. Kurita, T. Kurki-Suonio, T. Sturita, G. Kurnaev, V. Kuroda, K. Kuroda, K. Kurzan, B. Kuteev, B. Kuteev, B. S1, 702 Kuwahata, A. Kuzenov, V.	559 322 294 185 623 512 414 541 632 340 677 144 596, 205 692
Kumar, M. Kumar, R. Kumar, S. Kumar, S. Kumar, S. Kumar, S. Kumar, S. Kurita, T. Kursion, M. Kurnaev, V. Kurnaev, V. Kurnaev, V. Kurskiev, G. Sturey, G. Kurzan, B. Kuteev, B. S1, 702 Kuwahata, A. Kuzenov, V. Kuzmin, A.	559 322 294 185 623 512 414 541 632 340 677 144 596, 205 692 190
Kumar, M. Kumar, R. Kumar, S. 128, 321, Kumar, S. Kumar, S. Kumar, S. Kuraita, S. Kurita, T. Kursian, M. Kurnaev, V. Kurskiev, G. Sturnaev, V. Kurskiev, G. Stura, B. Kuteev, B. Stuteev, B.	559 322 294 185 623 512 414 541 632 340 677 144 596, 205 692 <i>190</i> 504
Kumar, M. Kumar, R. Kumar, S. Kumar, S. Kumar, S. Kumar, S. Kumar, S. Kumar, S. Kurnawa, R. Suprimedo, D. Kurita, T. Kurita, T. Kurita, T. Kurita, T. Kurita, T. Kurita, G. Kurnaev, V. Kurskiev, G. Kurskiev, G. States,	559 322 294 185 623 512 414 541 632 340 677 144 596, 205 692 190 504 652
Kumar, M. Kumar, R. Kumar, S. Kumar, S. Kumar, S. Kumar, S. Kumar, S. Kurnawa, R. Surita, T. Kurita, S. Kurita, G. Kurnaev, V. Kurskiev, G. Kurskiev, G. States, S. Kuraen, B. Kuteev, B. Kutaen, S. Kuzenov, V. Kuzenov, V. Kuzenov, V. Kuzmin, A. Kuznetsov, V. 498, Kuznetsov, Y. K.	559 322 294 185 623 512 414 541 632 340 677 144 596, 205 692 190 504 652 341
Kumar, M. Kumar, R. Kumar, S. Kurnawa, R. Surrita, T. Kurita, G. Kurnaev, V. Kuraev, V. Kuraev, S. Kuraev, S. States, 133, 188, 189, 283, 631, Kurzan, B. Kuteev, B. Kuzenov, V. Kuzenov, V. Kuzmetsov, V. Kuznetsov, V. Kuznetsov, Y. K. Kwak, J.	559 322 294 185 623 512 414 5512 632 340 677 144 596, 205 692 190 504 652 341 346
Kumar, M. Kumar, R. Kumar, S. Kuprienko, D. Kurita, T. Kurskiev, G. Kurnaev, V. Kurskiev, G. Kurskiev, G. Kurskiev, G. Kurskiev, G. Kurskiev, G. Kurskiev, G. Statestow, S. Kuzenov, V. Kuzenov, V. Kuzenov, V. Kuznetsov, V. Kuzaletsov, Y. K. Kwak, J. Kwak, JG. Kuzhetsov, Y. K.	559 322 294 185 623 512 414 541 632 340 677 144 596, 205 692 190 504 652 341 346 348
Kumar, M. Kumar, R. Kumar, S. Kurnawa, R. Surrita, T. Kurita, G. Kurnaev, V. Kuraev, V. Kuraev, S. Kuraev, S. States, 133, 188, 189, 283, 631, Kurzan, B. Kuteev, B. Kuzenov, V. Kuzenov, V. Kuzmetsov, V. Kuznetsov, V. Kuznetsov, Y. K. Kwak, J.	559 322 294 185 623 512 414 541 632 340 677 144 596, 205 692 190 504 652 341 346 348 465

Kwon, S545	
— L —	
La Haye, R. J 210, 212, 217, 218, 660, 661	
Labik, G	
Labit, B	
LaBombard, B 43, 53, 145, 295, 296, 363, 510	,
558	
Labusov, A	
Laggner, F	
Lamalle, P. U	

LaBombard, B	43 , 53 , 145, 295, 296, 363, 510,
558	
Labusov, A	
Lamalle, P. U	
Lampert, M	
Lan, T	
Lanctot, M	
Lang, J	
Lang, P	
Lanza, R	
Lashkul, S	15 , 172, 185, 186 , 187
Lasnier, C	
Lasnier, C. J	
Latu, G	
Latushkin, S	
Lauber, P	
Lauro Taroni, L	
Lawon, J	
Lawrence, D	
Lawson, K	
Lazarus, E	
Lazzaretti, M	
Lazzaro, E	
Lebedev, S	
LeBlanc, B. P	
	17 , 339, 374, 391
Lee, GS	
	60, 261, 346, 347, 348, 349 , 349,
	993, 605
	505, 530, 531
Lee, H. J	
Lee, J. D	
Lee, K	

Lee, KD	155
Lee, K. C 43 , 44 , <i>313</i> ,	471
Lee, K. D	140
Lee, S	161
Lee, S. G 58, 120, 140, 155, 229, 343, 345,	347,
348, 354 , 355, 471	
Lee, S. H	609
Lee, W 58, 161, 343, 352, 353, 355, 471,	496
Lee, Y.	520
Leem, J	
Leem, JE	353
Leerink, S	
Lehnen, M150, 151, 240 , 278, 415, 418,	426
455, 456	120,
Lei, G	121
Leichtle, D.	50/
Leipold, F.	631
Lenpholm, M	2051
Leonard, A. W 45 , 47 , 56 , <i>160</i> , 210, 211,	205
	361,
476, 654, 689	
Leonov, V	665
Leonov, V. M.	664
Lepikhov, S	652
Lerche, E153, 239, 280, 285,	290
Lerche, E. A	277
Lescinskis, B.	
Lestz, J	375
Lesur, M 50, 402,	
Levashova, M	
Levesque, J	257
Levesy, B	592
Lewis, E	
Leybros, R.	459
Leys, O	
Li Puma, A	547
Li, B	121
Li, C	608
	466
Li, G	100
Li, G 23 , 121, 231 , 235, 407, Li, H121,	
Li, H 121,	335
Li, H	335
Li, H	335 263,
Li, H	335 263, 326
Li, H	335 263, 326 235
Li, H	 335 263, 326 235 121
Li, H	 335 263, 326 235 121 522
Li, H	335 263, 326 235 121 522 330
Li, H	 335 263, 326 235 121 522 330 329
Li, H	 335 263, 326 235 121 522 330 329 394
Li, H	 335 263, 326 235 121 522 330 329 394 332
Li, H	 335 263, 326 235 121 522 330 329 394 332 529
Li, H	 335 263, 326 235 121 522 330 329 394 332 529 681
Li, H	 335 263, 326 235 121 522 330 329 394 332 529 681 236
Li, H	 335 263, 326 235 121 522 330 329 394 332 529 681 236 234

Lilley, S	Lilley, M. K	
Lin, T		
Lin, Y	Lin, L	128, 243, 244
Lin, Y	Lin, T	535, 588
Lin, Z	Lin, Y	227.510.558
Liniers, M	Lin. Z. 49	55, 373, 398
Linsmeier, C		
Lipschultz, B		
Lischitz, A	Linschultz B 177 281	455 510 558
Lisgo, S	Lischitz A	379
Lisitsa, V	Lisgo S	237 275 287
Lister, J		
Litaudon, X	-	
Litnovský, A		
Litunovsky, N		
Litvinov, A		
Liu, A		
Liu, C		
Liu, D		
Liu, F	Liu, C	121, 327 126 175 520
Liu, H		
Liu, L	Liu, F	235,369,670
Liu, S		
Liu, W	Liu, L	
Liu, X		
Liu, Y 14, 25, 50, 121, 137, 156, 174, 180, 317 323, 325, 326, 328–330, 332–334, 377, 427, 433, 449 Liu, Y. Q		
323, 325, 326, 328–330, 332–334, 377, 427, 433, 449 Liu, Y. Q. 450 Liu, Z. 231, 233, 236, 299, 323 Livshits, A. 68 Lizunov, A. 255 Loarer, T. 37, 276, 282, 299 Loarer, J. 527 Logan, N. 211 Loizu, J. 256 Logan, N. 211 Loizu, J. 256 Lomas, P. 146, 163, 242, 276, 277, 280, 284 López-Fraguas, A. 271 Lorer, J. 315 Lorenzini, R. 16, 128, 199 Lotte, P. 144 Loureho, F. 472 Loureiro, N. F. 411 Lowry, C. 146, 158, 163, 456 Lozin, A. 342 Lozin, A. 342 Lozin, A.<	Liu, X	, 61, 529, 628
377, 427, 433, 449 Liu, Y. Q. 450 Liu, Z. 231, 233, 236, 299, 328 Livshits, A. 687 Lizunov, A. 255 Loarer, T. 37, 276, 282, 299 Loarer, J. 527 Logan, N. 212 Logan, N. 211 Loizu, J. 256 Lomas, P. 146, 163, 242, 276, 277, 280, 284 López-Fraguas, A. 277 Lorer, J. 315 Lorenzini, R. 16, 128, 199 Lotte, P. 144 Loureno, N. F. 417 Lowry, C. 146, 158, 163, 456 Lozin, A. 342 Lozin, A. 342 Lowry, C. 146, 158, 163, 456 Lozin, A. 342 Lu, P. 336		
Liu, Y. Q		
Liu, Z		, 332–334,
Livshits, A	<i>377</i> , 427 , 433, 449	
Lizunov, A	<i>377</i> , 427 , 433, 449 Liu, Y. O.	
Loarer, T	<i>377</i> , 427 , 433, 449 Liu, Y. Q Liu, Z	
Loarte, A.234, 240, 284, 299, 365, 369, 410, 413 426, 427, 435, 663, 664, 668 Lobanov, K	377, 427, 433, 449 Liu, Y. Q Liu, Z	
426, 427, 435, 663, 664, 668 Lobanov, K. 666 Loesser, D. 527 Logan, N. 212 Loizu, J. 250 Lomas, P. 146, 163, 242, 276, 277, 280, 284 López-Fraguas, A. 277 Lore, J. 315 Lorenzini, R. 16, 128, 199 Louche, F. 479 Loureiro, N. F. 411 Lowry, C. 146, 158, 163, 450 Lozin, A. 342 Lu, L. 227, 466 Lu, P. 33 Lu, Z. 396	377, 427, 433, 449 Liu, Y. Q Liu, Z	
Lobanov, K	377, 427, 433, 449 Liu, Y. Q Liu, Z	
Loesser, D	377, 427, 433, 449 Liu, Y. Q. Liu, Z. 231, 233, Livshits, A. Lizunov, A. Loarer, T. 37, Loarte, A.234, 240, 284, 299, 365, 5	
Logan, N	377, 427, 433, 449 Liu, Y. Q	
Loizu, J	377, 427, 433, 449 Liu, Y. Q	
Lomas, P 146, 163, 242, 276, 277, 280, 284 López-Fraguas, A	377, 427, 433, 449 Liu, Y. Q	
López-Fraguas, A	377, 427, 433, 449 Liu, Y. Q	
Lore, J	377, 427, 433, 449 Liu, Y. Q. Liu, Z. Liu, Z. Livshits, A. Lizunov, A. Loarer, T. Loarte, A.234, 240, 284, 299, 365, 3 426, 427, 435, 663, 664 Lobanov, K. Loesser, D. Logan, N. Loizu, J.	
Lorenzini, R	377, 427, 433, 449 Liu, Y. Q. Liu, Z. Liushits, A. Lizunov, A. Loarer, T. Loarte, A.234, 240, 284, 299, 365, 3 426, 427, 435, 663, 664 Lobanov, K. Loesser, D. Logan, N. Loizu, J. Lomas, P. 146, 163, 242, 276,	
Lotte, P	377, 427, 433, 449 Liu, Y. Q. Liu, Z. Liushits, A. Lizunov, A. Loarer, T. Loarte, A.234, 240, 284, 299, 365, 3426, 427, 435, 663, 664 Lobanov, K. Loesser, D. Logan, N. Loizu, J. Lomas, P. 146, 163, 242, 276, López-Fraguas, A.	
Louche, F	377, 427, 433, 449 Liu, Y. Q	
Loureiro, N. F	377, 427, 433, 449 Liu, Y. Q	
Lowry, C	377, 427, 433, 449 Liu, Y. Q	
Lozin, A	377, 427, 433, 449 Liu, Y. Q	
Lozin, A	377, 427, 433, 449 Liu, Y. Q. Liu, Z. Liushits, A. Lizunov, A. Loarer, T. Loarte, A.234, 240, 284, 299, 365, 426, 427, 435, 663, 664 Lobanov, K. Loesser, D. Logan, N. Loizu, J. Lomas, P. Lore, J. Lorer, J. Lorenzini, R. Lorenzini, R. Louche, F. Louche, F. Louche, N. F.	
Lu, P	377, 427, 433, 449 Liu, Y. Q	
Lu, P	377, 427, 433, 449 Liu, Y. Q. Liu, Z. Livshits, A. Lizunov, A. Loarer, T. Loarer, T. 426, 427, 435, 663, 664 Lobanov, K. Loesser, D. Logan, N. Loizu, J. Lomas, P. Lofez-Fraguas, A. Loren, J. Lorenzini, R. Lotte, P. Louche, F. Loureiro, N. F. Lowry, C. Lozin, A.	
Lu, Y	377, 427, 433, 449 Liu, Y. Q. Liu, Z. Liunov, A. Loarer, T. Loarer, T. Loarer, T. 426, 427, 435, 663, 664 Lobanov, K. Loesser, D. Logan, N. Loizu, J. Lomas, P. Lofez-Fraguas, A. Lore, J. Lorenzini, R. Lotte, P. Louche, F. Loureiro, N. F. Lowry, C. Lozin, A. Lu, L. Lozin, A. Loure, J. Lowry, C. Lowry, C. Lozin, A. Lu, L.	
Lu, Z	377, 427, 433, 449 Liu, Y. Q. Liu, Z. Livshits, A. Lizunov, A. Loarer, T. 37, Loarer, T. 426, 427, 435, 663, 664 Lobanov, K. Loesser, D. Logan, N. Loizu, J. Logan, N. Loizu, J. Lomas, P. Lore, J. Lore, J. Lore, J. Loureino, N. F. Lowry, C. Luwry, C. Lowry, C. Luwr, P.	
Luce, T. C. 20, 142, 162, 210, 658, 660, 661, 662	377, 427, 433, 449 Liu, Y. Q. Liu, Z. Livshits, A. Lizunov, A. Loarer, T. 37, Loarer, T. 426, 427, 435, 663, 664 Lobanov, K. Loesser, D. Logan, N. Loizu, J. Logan, N. Loizu, J. Lomas, P. Lore, J. Lore, J. Lore, J. Loureino, N. F. Lowry, C. Luwry, C. Lowry, C. Luwr, P.	
, , , , , , , , , , , , , , , , , , , ,	377, 427, 433, 449 Liu, Y. Q. Liu, Z. Livshits, A. Lizunov, A. Loarer, T. Joarer, T. 37, Loarer, J. Logan, N. Loizu, J. Loizu, J. Loizu, J. Lorenzini, R. Lorer, J. Lorenzini, R. Loureiro, N. F. Lowry, C. Lowry, C. Lowry, C. Lu, Y. Lu, P. Lu, Y. Lu, Z.	

Luhmann, Jr., N. C 143,	161.352.353.355
Lukash, V	
Lunt, T	
Luo, G	
Luo, X	
Luo, Y	
Luo, Z	
Lupelli, I	
Lv, B	
Lysenko, S	
Lyssoivan, A	
Lyttle, M.	
Lyu, B	
Lyublinski, I	

– M –

Ma, C	231
Ma, Z	468
Macklin, B	503
Maddaluno, G	221
Maddison, G146, 280, 4	
Maejima, T	512
Maekawa, T	34(
Maeyama, S 22, 36, 358, 4	
Maget, P 293, 368, 0	669
Maggi, C 27, 35, 146, 153, 158, 239, 277, 2	279
435, 456	
Maggiora, R.	464
Mahajan, S 558,	590
Mahavar, K	
Mahesuria, G. I	
Mailloux, J146,	164
Maingi, R.136, 207, 209, 210, 299, 315, 316, 3	362
586, 590, 654, 689	
Maistrello, A	578
Makhankov, A	
Makido, O	
Makowski, M. A160, 0	654
Makwana, A. R	
Malard, P	182
Malinowski, K	
Malkov, M 14 ,	380
Maltzev, S	
Manchanda, R130, 152,	
Manduchi, G	
Mansfield, D	
Mansuri, I. A	
Mantica, P 153, 277, 368, 3	
Mantovani, S	583
Manz, P	299
Manzanares, A 151, 276, 2	278
Mao, W	
Mao, Y	227

Marandet, Y 293,	459
Maraschek, M	
Marchetto, C 164,	220
Marcuzzi, D	
Marechal, JL	576
Marenkov, E.	496
Margairaz, F	249
Marinoni, A 142,	
Marinucci, M	225
Markin, A	
Marklin, G	
Marmar, E 10, 11, 116, 296, 297, 299,	558
Marocco, D	
Marot, L	523
Marrelli, L	218
Marsen, S	456
Martin, E. H	
Martin, P	218
Martin, R	592
Martin-Solis, J. R	126
Martines, E	120
Martinez, J.	120 570
Martinez, M	510
Martovetsky, N	501
Martynov, A.	688
Marushchenko, N.	309
Maruyama, M	261
Maruyama, S	
Masamune, S 26,	
Masand, H.	
Masashi, K	604
Masiello, A 22, 35,	
Mastrostefano, S	
Masuzaki, S124, 159, 300, 301, 308, 473,	570
Masyukevich, S 283, 631,	677
Matejicek, J	646
Matsui, K.	
Matsukawa, M	578
Matsumoto, T	604
Matsunaga, G	493
Matsuura, H	570
Matsuyama, A 36, 367, 400, 403,	452
Mattei, M.	669
Matthew, L	146
Matthews, G 28, 35, 147, 277, 278, 280,	281.
286, 291, 423, 455	,
Matthias, B	238
Matveeva, M.	
Mauel, M.	
Mavrin, A	
Maximov, V.	
Mayer, M.	281
Mayoral, ML	
Mayuko, K	
1VIA Y UKO, IX	014

Mazon, D		32
Mazul, I		
Mazul, I. V		50
Mazzitelli, G.	20, 219, 65	51
Mazzotta, C	21, 220, 223, 22	25
Mazzucato, E		13
McCarthy, K. J		
McCarv, E		10
McCary, E McClements, K		2
McColl, D		92
McCollam, K		
McCormick, K.		
McDermott, R17	7, 179, 181, 299, 34	13
McDonald, D		
McFadden, G.		
McGarry, M.	128 24	14
McGuffey, C		10
McIntosh, S.		
McKee, G. R.22, 35, 136, 14	142 175 012 04	פנ 1
299, 660	2, 143, 173, 213, 24	.1,
Mckee, G. R.	()	20
McLean, A. G. 160, 210, 21		22
McLean, H		
Meadows, A.		
Medina, F.		
Mednikov, A.		53
Medvedev, S		
Medvedev, S. Y.		54
Meier, E		76
Meigs, A 158, 27	9, 364, 423, 455, 45	56
Meitner, S.		
Mellera, V		
Melnik, A		39
Melnikov, A 16, 19		
Menard, J 47	6, 478, 586, 590 , 67	73
Meneghini, O		
Meneses, L		
Menmuir, S		
Menon, V		
Merle, A		
Merlo, G		19
Merriman, L.		
Mertens, P		23
Messiaen, A		79
Mesyats, G.		
Meusel, J		24
Meyer, H.		79
Meyer, O.		93
Meyer, W. H	16	50
Meyerhofer, D		
Miao, X		38
Michel, F.		
Migliori, S		

Miki, K	200
Miki, K	
Miklaszewski, R	
Mikov, V.	
Milanesio, D	
Militello Asp, E	
Militello, F.	
Miller, D	
Milovanovic, M	
Mima, K	
Minaev, V	60 , 133, 188, 189, 581
Minami, R	
Minami, T	
Minashin, P	
Mineev, A	
Minelli, D	
Minello, V	
Minervini, J.	
Mirnov, S	
Mirnov, V.	
Mironov, M.	180 420 524
Mironov, Y.	
Miroshnikov, I	
Mishchenko, O	
Mishra, K	
Missirlian, M	
Mitarai, O	
Mitchell, N	
Mito, T	
Mitsunaka, Y	
Miura, E	
Miura, H	
Miura, Y	
Miyamoto, M	
Miyanaga, N	
Miyato, N	
Miyazawa, J	.159.300.307.556.577
Mizuguchi, N	245
Mizuuchi, T	30 , 258–260, 261
Mlynář, J.	151 153 277 278
Moeller, C	294 405
Mogaki, K	
Mohri, K	
Moiseenko, V.	
Molchanov, P	
Molchanov, P. A	
Molvik, A	
Momo, B	
Monakhov, I	276, 277, 285, 290
Monier-Garbet, P	
Monni, G	
Montag, P	
Monticello, D.	
Mooney, R	
Morace, A	

Moradi, S	
Morales, J	
Mordijck, S	19 , 136, 214
Moreau, D	
Moreno, C	
Morgan, K	
Mori, Y 46, 117,	620 , 621–623, 693
Morisaki, T	
Morishita, K	641
Morita, S 121, 124,	303, 306, 331, 655
Moriyama, S	
Morlock, C	
Moro, A	
Moro, F	
Morones, J.	
Morozov, D	
Morris, J.	
Morris, W	
Morton, L	128 243 244
Mosconi, M.	
Mosetto, A.	
Motohiro, T	
Motojima, G	159 266 300 301
Motojima, O	0 11 100
Moulton, D	
Moyer, R 168, 207, 208,	
Moyer, R. A	
Wi0yer, K. A	100
Mualton T	107
Mualton, T	
Müller, H. W	
Müller, H. W Müller, S	
Müller, H. W Müller, S Mueller, D	
Müller, H. W Müller, S Mueller, D Mukai, K	
Müller, H. W Müller, S Mueller, D Mukai, K Mukhin, E	
Müller, H. W Müller, S Mueller, D Mukai, K Mukhin, E	
Müller, H. W Müller, S Mueller, D Mukai, K Mukhin, E	
Müller, H. W Müller, S Mueller, D Mukai, K Mukhin, E	
Müller, H. W Müller, S Mueller, D Mukai, K Mukhin, E	
Müller, H. W Müller, S Mueller, D Mukai, K Mukhin, E	
Müller, H. W Müller, S Mueller, D Mukai, K Mukhin, E	
Müller, H. W. Müller, S. Mueller, D. Mukai, K. Mukhin, E. Muksunov, A. Mumgaard, R. Munaretto, S. Muñoz, O. Muraglia, M. Muraglia, M.	
Müller, H. W. Müller, S. Mukler, D. Mukai, K. Mukhin, E. Muksunov, A. Mumgaard, R. Munaretto, S. Muñoz, O. Muraglia, M. Murakami, H. Murakami, I.	
Müller, H. W Müller, S Mueller, D Mukai, K. Mukhin, E	
Müller, H. W. Müller, S. Mueller, D. Mukai, K. Mukhin, E. Muksunov, A. Mumgaard, R. Munaretto, S. Munaretto, Munaretto, S. Muraglia, M. Murakami, H. Murakami, J. Murakami, S. Murakami, S.	
Müller, H. W. Müller, S. Mukai, K. Mukhin, E. Muksunov, A. Mumgaard, R. Munaretto, S. Muraglia, M. Murakami, H. Murakami, S. Murakami, S. Murakhtin, S.	
Müller, H. W. Müller, S. Mukai, K. Mukhin, E. Muksunov, A. Mumgaard, R. Munaretto, S. Munaretto, S. Muraglia, M. Murakami, H. Murakami, S. Murakami, S. Murakami, S. Murakami, A.	
Müller, H. W. Müller, S. Mukai, K. Mukhin, E. Muksunov, A. Mungaard, R. Munaretto, S. Muñoz, O. Muraglia, M. Murakami, H. Murakami, I. Murakami, S. Murakami, S. Murakhtin, S. Murashtin, S. Murashtin, S. Murashima, T.	
Müller, H. W. Müller, S. Mukai, K. Mukhin, E. Muksunov, A. Mungaard, R. Munaretto, S. Muñoz, O. Muraglia, M. Murakami, H. Murakami, I. Murakami, S. Murakami, S. Murakhtin, S. Murashima, T. Muraga, T.	
Müller, H. W. Müller, S. Mukai, K. Mukkin, E. Muksunov, A. Mumgaard, R. Mumaretto, S. Munaretto, S. Muraglia, M. Murakami, H. Murakami, S. Murakami, S. Murakami, S. Murakami, S. Murakami, N. Murakami, S. Murakami, N. Murakami, N. Murakami, N. Murakami, S. Murakami, N. Murakami, S. Murakami, S. Murakami, N. Murakami, N. Murakami, N. Murakami, N. Murakin, S. Murakin, N.	
Müller, H. W. Müller, S. Mukai, K. Mukkin, E. Muksunov, A. Mumgaard, R. Mumaretto, S. Munaretto, S. Muraglia, M. Murakami, H. Murakami, S. Murakami, S. Murakami, S. Murakami, S. Murakami, N. Murakami, S. Murakami, N. Murakami, N. Murakami, N. Murakami, S. Murakami, N. Murakami, S. Murakami, S. Murakami, N. Murakami, N. Murakami, N. Murakami, N. Murakin, S. Murakin, N.	
Müller, H. W. Müller, S. Mukai, K. Mukki, K. Mukkin, E. Muksunov, A. Mumgaard, R. Mumgaard, R. Munaretto, S. Murayard, R. Murakami, H. Murakami, S. Murakami, S. Murakami, S. Murakari, S. Murakari, S. Murakari, S. Murakari, S. Murakari, S. Murayari, A. Murashima, T. Murashima, T. Mustafin, N. Mutoh, S. Mutoh, T. Mutoh, T. Mutakari, Songara Mutakari, N. Mutah, T. Mutah, T. Mutoh, T. Mutah, T. <td>$\begin{array}{c} & & & 197 \\ & & & & & 364 \\ & & & & & 364 \\ & & & & & & & 364 \\ &$</td>	$\begin{array}{c} & & & 197 \\ & & & & & 364 \\ & & & & & 364 \\ & & & & & & & 364 \\ & & & & & & & & & & & & & & & & & & $
Müller, H. W. Müller, S. Mukai, K. Mukki, K. Mukkin, E. Muksunov, A. Mumgaard, R. Mumgaard, R. Mumgaard, R. Munaretto, S. Muraglia, M. Murakami, H. Murakami, I. Murakami, S. Murakatin, S. Murakami, S. Murakami, A. Murakatin, S. Murakatin, S. Murakatin, N. Mutoh, T. 159, 294, 308,	$\begin{array}{c} & & 197 \\ & & & 364 \\ & & & 364 \\ & & & 364 \\ & & & & 478, 673 \\ & & & & 43, 261, 300 \\ 283, 631, 652, 677 \\ & & & & & 297 \\ & & & & & 297 \\ & & & & & 297 \\ & & & & & & 297 \\ & & & & & & & 297 \\ & & & & & & & 297 \\ & & & & & & & & 297 \\ & & & & & & & & & & & 297 \\ & & & & & & & & & & & & & \\ & & & & $
Müller, H. W. Müller, S. Mukai, K. Mukki, K. Mukkin, E. Muksunov, A. Mumgaard, R. Mumgaard, R. Munaretto, S. Murayard, R. Murakami, H. Murakami, S. Murakami, S. Murakami, S. Murakari, S. Murakari, S. Murakari, S. Murakari, S. Murakari, S. Murayari, A. Murashima, T. Murashima, T. Mustafin, N. Mutoh, S. Mutoh, T. Mutoh, T. Mutakari, Songara Mutakari, N. Mutah, T. Mutah, T. Mutoh, T. Mutah, T. <td></td>	

— N —	
Na, D	. 343
Na, Y	
Na, YS	. 672
Nabais, F	411
Nabara, Y.	
Nagae, Y	261
Nagai, K.	117
Nagai, T	
Nagao, K	
Nagaoka, K. 49 , 55 , 169, 259, 305, 311, 472	655
Nagasaki, K. 159, 169, 258–261, 309, 509,	539
688	,
Nagashima, Y	.338
Nagata, M	262
Nagata, S.	570
Nagatomo, H 45 , 117, 609, 613, 616, 617	693
Nagayama, Y	
Naidenov, V.	
Nakahira, M.	500
Nakai, M	-615
Nakajima, N 12, 131	
Nakamata, H.	
Nakamura, H.	
Nakamura, K	
Nakamura, M	
Nakamura, N	
Nakamura, Y	
Nakanishi, A	. 294
Nakashima, H	
Nakashima, Y	. 191
Nakashiina, 1	, 570
Nakata, M	
Nakayama, K	
Nakayama, S117, 621 Nakazato, T	, 623
Nam, K	471
Nam, 1U 140, 347, 332, 333	,4/1
Napoli, F.	
Napoli, R	. 583
Nardon, E	,460
Narushima, Y 44, 301, 310, 312, 371	,604
Nascimento, I. C.	
Natsume, K.	
Naumenko, N.	. 198
Nave, M. F	, 341
Navratil, G	
Navratil, G. A	,217
Nazikian, R 136 , 168, 207, 361, 654, 659,	663,
689 Neilson, G520, 543, 544	E A F
Nelson, B	
Nemets, A.	198

Nemoto, S	.513
Nesenevich, V 25	
Nespoli, F	. 363
Nesterenko, V.	. 201
Neubauer, O	
Neudatchin, S 16	, 197
Neumeyer, C 586	
Neverov, V.	. 275
Newman, D	.431
Ni, M	
Nicollet, S	
Nie, B	
Nie, L	
Nielsen, S.	
Nieto, A	
Nikitenko, A.	611
Nikolaev, V.	611
Nikulin, V.	102
Nilsson, E	
Nimavat, H. D.	
Nindval, n. D	. 150
Nishiguchi, A.	. 017
Nishijima, D	. 149
Nishimura, H 117, 609, 613	
Nishimura, K.	
Nishimura, S	,310
Nishimura, Y 46, 117, 620, 621, 622	
Nishino, N	. 570
	1.1.1
Nishioka, K.	. 260
Nishiura, M 309	. 260 , 684
Nishiura, M	. 260 , 684 , 446
Nishiura, M	. 260 , 684 , 446 .529
Nishiura, M	. 260 , 684 , 446 . 529 . 522
Nishiura, M	. 260 , 684 , 446 . 529 . 522 . 370
Nishiura, M. 309 Niskala, P. 172 Niu, E. 172 Niu, L. Nkonga, B. Noble, C. 172	. 260 , 684 , 446 .529 .522 . 370 . 277
Nishiura, M. 309 Niskala, P. 172 Niu, E. 172 Niu, L. 172 Nkonga, B. 172 Noble, C. 172 Nocente, M. 172	. 260 , 684 , 446 .529 .522 . 370 . 277 . 180
Nishiura, M. 309 Niskala, P. 172 Niu, E. 172 Niu, L. 172 Nkonga, B. 172 Noble, C. 172 Nocente, M. 172 Noda, A. 172	. 260 , 684 , 446 .529 .522 . 370 . 277 . 180 .620
Nishiura, M. 309 Niskala, P. 172 Niu, E. 172 Niu, L. Nonga, B. Noble, C. Nocente, M. Noda, A. Nogami, S.	. 260 , 684 , 446 .529 .522 . 370 . 277 . 180 .620 .630
Nishiura, M. 309 Niskala, P. 172 Niu, E. 172 Niu, L. Nonga, B. Noble, C. Nocente, M. Noda, A. Nogami, S. Nogami, T. Nogami, T.	. 260 , 684 , 446 .529 .522 . 370 . 277 . 180 .620 .630 .684
Nishiura, M. 309 Niskala, P. 172 Niu, E. 172 Niu, L. Nkonga, B. Noble, C. Nocente, M. Noda, A. Nogami, S. Nogami, T. Noguchi, N.	. 260 , 684 , 446 .529 .522 . 370 . 277 . 180 .620 .630 .684 . 261
Nishiura, M. 309 Niskala, P. 172 Niu, E. 172 Niu, L. Nonga, B. Noble, C. Nocente, M. Noda, A. Nogami, S. Nogami, T. Nogami, T.	. 260 , 684 , 446 .529 .522 . 370 . 277 . 180 .620 .630 .684 . 261
Nishiura, M. 309 Niskala, P. 172 Niu, E. 172 Niu, L. 172 Nkonga, B. 172 Noble, C. 172 Nocente, M. 172 Nogami, S. 172 Nogami, T. 172 Noguchi, N. 172 Noiri, Y. 172	. 260 , 684 , 446 .529 .522 . 370 . 277 . 180 .620 .630 .684 . 261 .530 . 629
Nishiura, M. 309 Niskala, P. 172 Niu, E. 172 Niu, L. Nkonga, B. Noble, C. Nocente, M. Noda, A. Nogami, S. Nogami, T. Noguchi, N. Noh, C. H. Noh, C. H.	. 260 , 684 , 446 .529 .522 . 370 . 277 . 180 .620 .630 .684 . 261 .530 . 629
Nishiura, M. 309 Niskala, P. 172 Niu, E. 172 Niu, L. 172 Nkonga, B. 172 Noble, C. 172 Nocente, M. 172 Nogami, S. 172 Nogami, T. 172 Noguchi, N. 172 Noiri, Y. 172	. 260 , 684 , 446 .529 .522 . 370 . 277 . 180 .620 .630 .684 . 261 .530 .629 .159
Nishiura, M. 309 Niskala, P. 172 Niu, E. 172 Niu, L. Nkonga, B. Noble, C. Nocente, M. Noda, A. Nogami, S. Nogami, S. Nogami, T. Noguchi, N. Noh, C. H. Noiri, Y. Nomura, G. Norajitra, P. Norajitra, P.	. 260 , 684 , 446 .529 .522 . 370 . 277 . 180 .620 .630 .684 .261 .530 .629 .159 .128 .567
Nishiura, M. 309 Niskala, P. 172 Niu, E. 172 Niu, L. Nkonga, B. Noble, C. Nocente, M. Noda, A. Nogami, S. Nogami, S. Nogami, T. Noguchi, N. Noh, C. H. Noiri, Y. Nomura, G. Norajitra, P. Norajitra, P.	. 260 , 684 , 446 .529 .522 . 370 . 277 . 180 .620 .630 .684 .261 .530 .629 .159 .128 .567
Nishiura, M. 309 Niskala, P. 172 Niu, E. 172 Niu, L. Nkonga, B. Noble, C. Nocente, M. Noda, A. Nogami, S. Nogami, S. Nogami, T. Noguchi, N. Noh, C. H. Noiri, Y. Nomura, G. Norajitra, P. Norimatsu, T. Norimatsu, T. 117	. 260 , 684 , 446 .529 .522 . 370 .620 .630 .630 .684 .261 .530 .629 .159 .128 .567 , 609
Nishiura, M. 309 Niskala, P. 172 Niu, E. 172 Niu, L. 172 Nkonga, B. 172 Noble, C. 172 Nocente, M. 172 Noda, A. 172 Nogami, S. 172 Nogami, S. 172 Noguchi, N. 172 Noh, C. H. 117 Nomura, G. 117 Norajitra, P. 117 Nornberg, M. 26, 128	. 260 , 684 , 446 .529 .522 . 370 . 277 . 180 .620 .630 .684 . 261 .530 . 629 .128 .567 , 609 , 244
Nishiura, M. 309 Niskala, P. 172 Niu, E. 172 Niu, L. 172 Nkonga, B. 172 Noble, C. 172 Nocente, M. 172 Noda, A. 172 Nogami, S. 172 Nogami, S. 172 Noguchi, N. 172 Noh, C. H. 172 Nomura, G. 171 Nornajitra, P. 117 Normatsu, T. 117 Norscini, C. 26, 128	. 260 , 684 , 446 .529 .522 . 370 . 277 . 180 .620 .630 .684 . 261 .530 . 629 .159 .128 .567 , 609 , 244 .431
Nishiura, M. 309 Niskala, P. 172 Niu, E. 172 Niu, L. 172 Nkonga, B. 172 Noble, C. 172 Nocente, M. 172 Noda, A. 172 Nogami, S. 172 Nogami, S. 172 Noguchi, N. 173 Noiri, Y. 174 Nomura, G. 117 Nornajitra, P. 117 Nornberg, M. 26, 128 Norscini, C. 227, 251, 276	. 260 , 684 , 446 .529 .522 . 370 .620 .630 .630 .684 .261 .530 .629 .128 .567 , 609 , 244 .431 , 290
Nishiura, M. 309 Niskala, P. 172 Niu, E. 172 Niu, L. 172 Noin, L. 172 Noda, A. 172 Nogami, S. 172 Nogami, S. 172 Nogami, T. 100 Noguchi, N. 117 Noiri, Y. 117 Norn, P. 117 Norimatsu, T. 117 Norrimerg, M. 26, 128 Norscini, C. 127, 251, 276 Noterdaeme, JM. 227, 251, 276	. 260 , 684 , 446 .529 .522 . 370 . 277 . 180 .620 .630 .684 . 261 .530 . 629 .128 .567 , 0 69 , 244 .431 . 290 . 578
Nishiura, M. 309 Niskala, P. 172 Niu, E. 172 Niu, L. 172 Nola, A. 172 Nocente, M. 172 Nogami, S. Nogami, S. Nogami, S. Nogami, T. Nogami, T. Nogami, T. Nogami, T. Noguchi, N. Noh, C. H. Noiri, Y. Nomura, G. Nonn, P. Norrajitra, P. 117 Nornberg, M. 26, 128 Norscini, C. 227, 251, 276 Novello, L. Novohatsky, A.	. 260 , 684 , 446 .529 .522 . 370 .620 .630 .630 .630 .629 .128 .567 , 609 .241 .350 .567 .241 .578 .578 .578 .578 .578 .579 .578 .579 .577 .579 .577 .579 .577 .579 .577 .579 .577 .579 .577 .579 .577 .579 .577 .579 .577 .579 .577 .579 .577
Nishiura, M. 309 Niskala, P. 172 Niu, E. 172 Niu, L. 172 Noble, C. 172 Noda, A. 172 Nogami, S. Nogami, T. Nogami, T. Nogami, T. Noguchi, N. Noh, C. H. Noiri, Y. Nomura, G. Norn, P. Norrajitra, P. Norimatsu, T. 117 Nornberg, M. 26, 128 Nosteridaeme, JM. 227, 251, 276 Novello, L. Novokhatsky, A. Novokhatsky, A. 59, 133	. 260 , 684 , 446 .529 .522 . 370 .620 .630 .620 .630 .684 .261 .530 .629 .128 .567 .269 .244 .431 .290 .578 .677 , 652
Nishiura, M. 309 Niskala, P. 172 Niu, E. 172 Niu, L. 172 Noble, C. 172 Noda, A. 172 Nogami, S. Nogami, T. Nogami, T. Nogami, T. Noguchi, N. Noh, C. H. Noiri, Y. Nomura, G. Norn, P. Norrajitra, P. Norimatsu, T. 117 Nornberg, M. 26, 128 Nosteridaeme, JM. 227, 251, 276 Novello, L. Novokhatsky, A. Novokhatsky, A. 59, 133	. 260 , 684 , 446 .529 .522 . 370 .620 .630 .620 .630 .684 .261 .530 .629 .128 .567 .269 .244 .431 .290 .578 .677 , 652
Nishiura, M. 309 Niskala, P. 172 Niu, E. 172 Niu, L. 172 Nola, A. 172 Nocente, M. 172 Nogami, S. Nogami, S. Nogami, S. Nogami, T. Nogami, T. Nogami, T. Nogami, T. Noguchi, N. Noh, C. H. Noiri, Y. Nomura, G. Nonn, P. Norrajitra, P. 117 Nornberg, M. 26, 128 Norscini, C. 227, 251, 276 Novello, L. Novohatsky, A.	. 260 , 684 , 446 .529 .522 .370 .620 .630 .620 .630 .624 .530 .629 .128 .567 .264 .3567 .264 .357 .644 .307 .258 .578 .677 .622 .578 .577 .578 .577 .578 .577 .578 .577 .578 .578 .577 .5788 .57888 .57888 .57888 .578888 .57888 .5788888 .57888888888888888888888888888888888888

Numakura, T	509, 570
Nunami, M.	50, 487, 494
Nunio, F	576
Nunoya, Y	33, 501, 534
Nusbaum, M	
Nygren, R	
Nyqvist, R	

- 0 -

U	
O'Mullane, M	
Oberkofler, M	
Obukhov, D	
Ochando, M. A	
Oda, Y	35.507.508.629
Odstrcil, T	
Ogata, S	629
Ogawa, K	
Ogawa, Y	
Oh, DK.	
Oh, J	
Oh, S	
Oh, Y	
Oh, YK	
Ohasa, K	
Ohdachi, S43, 138	3. 304 . 310–312. 371
Ohno, N43, 53, 124, 300	
636	
Ohsako, T	
Ohshima, K	
Ohshima, S	
Oijerholm, J	
Oishi, T	
Ojha, A	
Okabayashi, M	
Okada, H	
Okajima, S	
Okano, K	
Oki, K	
Okihara, S	
Okulov, G	
Okuyama, Y	
Oliva, S	
Olivares, C	
Oliver, H. J. C	411
Oliver, J	
Olofsson, K. E. J	
Omori, T	
Onchi, T	
Ongena, J	
Onjun, T	
Ono, M	. 478, 509, 586 , 590
Ono, Y	
Orain, F	

Orlov, D	19, 136, 207, 315
Orlov, D. M	
Orsitto, F. P.	
Osakabe, M.48, 55, 169,	302, 305, 309, 311, 382,
472, 539, 655	5
Osborne, T	
Osborne, T. H	136, 160, 361, 689
Osei-Mensah, W	
Oshikiri, M	
Oshima, S	
Osipov, I	
Ovchinnikov, S	
Owsiak, M	
Oyaidzu, M	
Ozaki, T	311, 609, 613, 614, 620

– P –

— I —	
Paccagnella, R	37
Pace, D	30
Pace, D. C16	68
Paduch, M 64	6
Pak, S	92
Pal, R 32	22
Palak, B	
Pamela, S	50
Pan, C	54
Panaccione, L	23
Panasenkov, A 20)4
Panayotis, S14	8
Panchal, A. G 13	
Panchal, P. N	30
Panchal, R. N 13	30
Panchal, V	52
Pandya, S	21
Pandya, S. P	30
Panek, R 46	
Panin, A	26
Pankin, A145, 38	36
Pankin, A. Y	54
Panov, A)2
Panov, V 53	33
Paolucci, F	1
Parail, V	
Paravastu, Y	30
Parekh, T. J	30
Parghi, B. R 13	30
Parihar, M	21
Park, B	93
Park, BH 120, 34	
Park, C. K)5
Park, G 57, 62, 140, 35	74
Park, H	51
Park, H. K 58, 345, 352, 353, 355, 52	
Park, J	54

Park, JK			
Park, J. M		66	1
Park, J. S		, 543, 54 5	5
Park, S		612	2
Park, SH			
Park, Y			1
Park, YS 57,	139, 345, 353	3, 355, 673	3
Parke, E		3, 243, 244	4
Parker, R. R	235, 295, 296	6, 297, 558	3
Parker, S	2	7, 36, 362	2
Parkin, W.			
Parks, P			
Parmar, K.			
Parra, F			
Passeron, C			
Pasternak, A.			
Pastor, I			
Pastukhov, V		18 390	5
Patel, A			
Patel, D. J.			
Patel, H. S.			
Patel, J. C			
Patel, K. B			
Patel, N			
Patel, P. J.			
Patel, R. J.			
Pathak, R.	•••••	504	1
Pathak, S.	• • • • • • • • • • • • • • •		1
Pathak, S. K			
Pathan, F. S			
Patrov, M			
Pavlichenko, R			2
Paz-Soldan, C 19, 136,		, 212 , 217	',
365, 659, 660			_
Peebles, J		610)
Peebles, T			
Peebles, W			
Peebles, W. A.			
Pégourié, B			
Penaflor, B. G.			
Peng, J			
Peng, M			1
Peng, Q		257	7
Peng, X		449	9
Pereira, R.		278	3
Pereslavtsev, P			1
Perevalov, A.		172	2
Perez, R. V			
Perfilov, S			
Pericoli Ridolfini, V			
Perkins, R.			
Perona, A.			
Perona, G.			
Perry, E			
2 · · · · · · · · · · · · · · · · · · ·			

Pertsev, D	
Peterson, B 124,	300
Petersson, P 281, 286,	523
Petr, S	
Petrasso, R. D.	608
Petrie, T. W 19 , 45 , 160, 210 , <i>315</i> , 654,	660
Petrov, A	
Petrov, M	
Petrov, S	
Petrov, V.	642
Petrov, V. S	
Petrov, Y	652
Petrzilka, V	
Petty, C. C 20 , 142, 143, 175, 213, 214,	662
Peysson, Y	
Pfefferle, D	
Philipps, V. P	
Phillips, C. K.	
Phillips, G.	
Phillips, P	
Picha, R	297
Pierattini, S.	
Piergotti, V.	220
Pietrzak, A.	
Pigarov, A	
Pimenov, V.	
Pinches, S	
Pinsker, R	660
Pinsker, R. I	
Pinzhin, Y	
Piovan, R	578
Piovesan, P 128, 217,	
Piron, C 217,	218
Piron, L	218
Pironti, A	583
Pisarev, A	496
Pistner, C.	
Pitcher, C. S.	592
Pitcher, C. S Pitts, R 147, 237, 240, 242, 290, 423, 499,	677
Pitts, R. A.	464
Platacis, E 58,	
Plociennik, M.	
Plunk, G. G	
Plyusnin, V. V	278
Pochelon, A.	246
Podda, S	
Podestá, M	
Poitevin, Y.	
Polevoi, A	
Polevoi, A. R	
Poli, F	
Polli, G	
Polosatkin, S.	
Polosatkin, S Polunovskii I	
T OIUHOVSKIL I	024

Ponkratov, Y	
Poolyarat, N	
Popov, A	
Popova, E	
Popovic, Z	
Porkolab, M	.145, 296, 405, 558, 660
Porte, L	26 , 246, 249
Poshekhonov, Y	
Potanina, L	
Poyé, A	
Pradhan, S	12, 18, 130, 559
Pragash, R	
Prasad, U	
Prater, R	405, 438, 466, 670
Praveenlal, E. V	
Pretty, D	
Privalova, E	
Proll, J. H. E	
Prusakova, M	
Pucella, G 12, 18, 129 ,	, 164, 196, 220–222, 225,
226	
	, 128, 243, 368, 396, 690
	, 177, 179, 182, 239, 277,
360, 423	
	12, 18, 127, 128, 153
	50, 490
Putvinski, S	

— Q —

Qian, J	
Qiao, B	610
Qiu, X	
Qiu, Y	
Qiu, Z	332, 468, 470
Õu, H	
Õu, Z	,
Quercia, A	
2	

— R —

Rabinski, M	222
Rack, M	232
Radhakrishnan, S.	559
Raeder, J	680
Rafiq, T	4, 386
Raftopoulos, S	
Raghunathan, M.	
Rajkovic, M14	

Raju, D	130,	152,	322
Ramaiya, N.	152,	321,	322
Ramakrishnan, R			586
Raman, R 208, 365,	478,	586,	590
Ramogida, G 220, 223, 224,	228,	583,	669
Rao, B			132
Rao, C			
Rao, J		121,	330
Rapisarda, D			
Rasmussen, D			506
Raspon, C			
Rathgeber, S			
Rathgeber, S. K.			144
Raval, D. C			130
Raval, J	152,	321,	504
Raval, T. Y			
Razdobarin, A			
Razumenko, D			319
Razumova, K	<mark>20</mark> ,	216,	432
Reale, M			
Reich, J			504
Reich, M 15, 178,	277,	285,	656
Reichle, R	. <mark>24</mark> ,	237,	631
Reiman, A			
Reimerdes, H		226,	248
Reimold, F	157,	183,	238
Reinhart, M Reinke, M.145, 153, 158, 295, 297,			149
Reinke, M.145, 153, 158, 295, 297,	427,	510,	558
Reiter, D			124
Remi, D			
Ren, Q		466,	657
Ren, Y			
Reusch, J			128
Reux, C 34, 48,	151,	278,	547
Reynolds-Barredo, J			431
Rhee, T	. 18,	374,	397
Rhee, TN			
Rhodes, D			257
Rhodes, T		142,	213
Rhodes, T. L 143,	175,	660,	689
Ricapito, I		. <mark>32</mark> ,	528
Riccardo, V			
Ricci, D			224
Ricci, P	8, <mark>36</mark> ,	250,	363
Rice, J 295,	297,	299,	558
Riemann, J			359
Rimini, F 146, 163, 277,	279,	280,	284
Rimini, F. G			285
Rinderknecht, H			608
Riva, F	••••		363
Riva, M		221,	223
Roach, C 265,	266,	268,	443
Robin, F			
Roccella, S			219

Rocipon, H	576
Rodrigues, P 24,	411
Rognlien, T	558
Roh, B. R	505
Rohde, V	242
Romanelli, F	110
Romanelli, M	668
Romano, A 220,	223
Romanov, V	342
Ronald, S	586
Ronchi, G	341
Roquemore, A. L	689
Roquemore, L	
Rosenberg, M.	608
Rossel, J.	
Rossi, P	574
Rost, J. C	143
Rouault, G	424
Rowan, W	
Rowley, C. W	139
Roy, I 17, 198,	204
Roy, I	204 390
Rozhansky, V	390 550
Rozhansky, V	390 550
Rozhansky, V	390 550 319
Rozhansky, V	390 550 319 536
Rozhansky, V. 27, 36, 133, 360, Rozhansky, V. A. 802 Rozhdestvensky, V. 15, 185, Rozov, V. 33,	390 550 319 536 523
Rozhansky, V. 27, 36, 133, 360, Rozhansky, V. A. 80, 15, 185, Rozhdestvensky, V. 15, 185, Rozov, V. 33, Rubel, M. 281, 286, Rubinacci, G. 288, Rudakov, D. L. 19,	390 550 319 536 523 583 211
Rozhansky, V. 27, 36, 133, 360, Rozhansky, V. A. 80, 15, 185, Rozhdestvensky, V. 15, 185, Rozov, V. 33, Rubel, M. 281, 286, Rubinacci, G. 288,	390 550 319 536 523 583 211
Rozhansky, V. 27, 36, 133, 360, Rozhansky, V. A. 80, 15, 185, Rozhdestvensky, V. 15, 185, Rozov, V. 33, Rubel, M. 281, 286, Rubinacci, G. 288, Rudakov, D. L. 19,	390 550 319 536 523 583 211 528
Rozhansky, V. 27, 36, 133, 360, Rozhansky, V. A. 80, 15, 185, Rozov, V. 33, Rubel, M. 281, 286, Rubinacci, G. 288, Rudakov, D. L. 19, Rueda, A. 10,	390 550 319 536 523 583 211 528 694
Rozhansky, V. 27, 36, 133, 360, Rozhansky, V. A. 80, 15, 185, Rozov, V. 33, Rubel, M. 281, 286, Rubinacci, G. 288, Rudakov, D. L. 19, Rupasov, A. 19,	390 550 319 536 523 583 211 528 694 477
Rozhansky, V. 27, 36, 133, 360, Rozhansky, V. A. 80, 15, 185, Rozov, V. 33, Rubel, M. 281, 286, Rubinacci, G. 288, Rudakov, D. L. 19, Rupasov, A. 81, 285, Rupasov, A. 45,	390 550 319 523 583 211 528 694 477 427
Rozhansky, V. 27, 36, 133, 360, Rozhansky, V. A. 80, 15, 185, Rozov, V. 33, Rubel, M. 281, 286, Rubinacci, G. 288, Rudakov, D. L. 19, Rueda, A. 19, Rupsov, A. 45, Ryan, D. 45,	 390 550 319 536 523 583 211 528 694 477 427 438
Rozhansky, V. 27, 36, 133, 360, Rozhansky, V. A. Rozhdestvensky, V. Rozhdestvensky, V. 15, 185, Rozov, V. 33, Rubel, M. 281, 286, Rubinacci, G. 288, Rudakov, D. L. 19, Rueda, A. 19, Rupasov, A. 45, Ryan, D. Ruanting and another statements	390 550 319 523 523 523 528 694 477 427 438 642
Rozhansky, V. 27, 36, 133, 360, Rozhansky, V. A. Rozhansky, V. A. Rozhdestvensky, V. 15, 185, Rozov, V. 33, Rubel, M. 281, 286, Rubinacci, G. 288, Rudakov, D. L. 19, Rueda, A. 19, Russell, D. 45, Ryan, D. Ryanov, A. Ryazanov, A. 10,	390 550 319 523 583 211 528 694 477 427 427 438 642 173
Rozhansky, V. 27, 36, 133, 360, Rozhansky, V. A. Rozhansky, V. A. Rozhdestvensky, V. 15, 185, Rozov, V. 33, Rubel, M. 281, 286, Rubinacci, G. 288, Rudakov, D. L. 19, Rueda, A. 19, Russell, D. 45, Ryan, D. Ryazanov, A. Ryaakov, D. Ruzenov, A.	 390 550 319 536 523 583 211 528 694 427 427 428 642 173 299
Rozhansky, V. 27, 36, 133, 360, Rozhansky, V. A. Rozhansky, V. A. Rozhdestvensky, V. 15, 185, Rozov, V. 33, Rubel, M. 281, 286, Rubinacci, G. 288, Rudakov, D. L. 19, Rueda, A. 19, Russell, D. 45, Ryan, D. Ryazanov, A. Ryazanov, A. 165, 178, 179,	390 550 319 536 523 583 211 528 694 477 427 438 642 173 299 160
Rozhansky, V. 27, 36, 133, 360, Rozhansky, V. A. Rozhansky, V. A. Rozhdestvensky, V. 15, 185, Rozov, V. 33, Rubel, M. 281, 286, Rubinacci, G. 288, Rudakov, D. L. 19, Rueda, A. 19, Russell, D. 45, Ryan, D. Ryaznov, A. Ryaznov, A. Ryakov, D. Ryter, F. 165, 178, 179, Ryutov, D. 19,	390 550 319 536 523 583 211 528 694 477 427 438 642 173 299 160 692

— S —

Sa, J. W	504, 505
Saarelma, S.31, 137, 146, 164, 265,	280, 284, 443
Sabbagh, S. A 11, 13, 17, 23, 60,	123, 139, 344,
345, 355, 586, 590, 673	3
Sabot, R	38, 289
Sadaoki, K	609
Sadowski, M. J.	
Sadykov, A.	29, 434
Safronov, A.	677
Sagara, A556,	570, 577, 587
Sagisaka, A	615
Saibene, G	284, 410

Saigusa, M	. 508
Saint-Laurent, F151	. 278
Saito, K	655
Saito, S	
Saitoh, H	
Sakagami, H	693
Sakai, A	
Sakakibara, S	
Sakamoto, K	
Sakamoto, M.	
Sakamoto, R	
Sakamoto, T	.294
Sakamoto, Y 49	
Sakata, S	
Sakaue, H. A	. 303
Sakawa, Y	
Sakharov, N 133, 188, 189, 389, 581	, 652
Sakurai, T	. 500
Salahutdinov, G.	. 563
Saldaña, C.	
Salewski, M	
Salmi, A	
Salvador, M	
Samm, U	<i>'</i>
Samsonov, D	
Sánchez, J	
Sanchez, R.	
Sanna, S.	.579
Sano, F	
Sano, H	
Sano, R.	
Sano, T	
Sanpei, A	
Sanromán, M	
Santos, J	.609
Santra, P	. 130
Sanz, J	. 618
Saoutic, B	, 547
Sarazin, Y 29, 431	
Sarff, J 126, 128 , 243	, 244
Särkimäki, K	.414
Sartori, R	, 668
Sarukura, N.	.117
Sasaki, M141	
Sasaki, S.	
Sassano, M	
Sassi, M.	
Satake, S	
Satake, S	
Satiryanarayana, K	
Sato, N	
Sato, N 11/ Sato, S	
Sato, S	
Sato, I	
Saton, N 620, 622	., 623

Sauppe, J Sauter, O226, 246, 247, 424, 489, 656	.128
Sauter, O226, 246, 247, 424, 489, 656	, 688
Savel'ev, V	. 685
Saveliev, A 133, 186, 204, 366	, 389
Savelyev, V	. 686
Savkin, V	.253
Savoldi Richard, L	.538
Savrukhin, P504	, 585
Sawada, H	
Sawada, Y	.486
Sawahata, M	. 508
Saxena, Y	.322
Saxena, Y. C	.152
Sborchia, C 29 , 503, 504	, 530
Scannell, R	, 443
Scarabosio, A	. 238
Schauer, F 573	, 575
Schekochihin, A	.268
Scherbak, A.	. 201
Schettini, G	
Schlutt, M	. 381
Schmid, K	, 287
Schmitz, L 56, 62, 142, 143, 175, 214	, 299
Schmitz, O 124, 241	, 315
Schneider, H	. 586
Schneider, M	. 293
Schneider, P. A144	, 178
Schneller, M	, 395
Scholz, M	. 549
Schuster, E	. 658
Schwander, F Schwarz-Selinger, T	.459
Schwarz-Selinger, T	. 242
Schweer, B	. 479
Schweinzer, J	, 239
Scott, B	
Scott, S	. 297
Scotti, F	
Sebastian, J	.624
Sedlak, K	
Seguin, F	
Seino, Y	. 577
Sekachev, I	
Seki, N 512	, 513
Seki, R 159, 169, 260, 261, 302, 308, 311,	, 539,
556, 584, 655	
Seki, T 39 , 159, 169, 294, 308, 539	, 655
Seki, Y10, 29	
Sekiguchi, J	. 604
Sekine, T 46, 117, 620–622	
Seltzman, A	
Semenov, E	.642
Semenov, V	, 677
Semwal, P	
Sen, A63, 152, 430, 439	, 699

Senichenkov, I16,	133,	390
Sentoku, Y	620-	-623
Seo, SH		155
Seol, J 57, 344, 347, 348,	354,	393
Sergeev, D	173,	197
Sergeev, V	593,	652
Sergienko, G 158, 276, 278,	423.	456
Serikov, A		
Serna, J		
Serre, E		
Sertoli, M		
Sestero, A.		
Setiadi, C. A		252
Severo, J. H.	52	341
Shafer, M.		
Shafer, M. W.		
Shah, P. R.		
Shaing, K		139
Shan, J	. 14,	381
Snan, J	232,	233
Shang, J.		
Shao, L.		
Shapoval, A		342
Shapovalov, G	572,	651
Shapovalov, M.		685
Sharapov, S 31 ,		
Sharma, A.		
Sharma, A. L.		130
Sharma, A. N		130
Sharma, D. K		
Sharma, M		
Sharma, P. K		
Sharma, R		130
Sharples, R		
Shatalin, S		.186
Shaw, A	277,	290
Shchegolev, P133,	188,	189
Shcherbak, A	. 16,	202
Shcherbinin, O	204,	389
Sheikh, H.		285
Shelukhin, D		
Shen, B.	<i>.</i>	232
Shen, H		
Shen, J		522
Shen, L		
Shen, Y.		
Sheng, P.		236
Sheng, X.		
Sheng, Z.		
Shestakov, E		585
Shesterikov, I		
Shevelev, A	279	500
Shevelev, A 185, Shi, N	210,	024 021
Shi, N		
JIII, 1		. 232

Shi, W	(EO
	658
Shi, Y 40, 48, 132, 155, 229,	339
Shi, Z.121, 156, 323, 325, 326, 328, 330-332,	492
Shibanuma, K	
Shibutani, K	
Shigemori, K	609
Shigemura, T	340
Shigin, P.	237
Shiina, D.	512
Shikama, T	
Shim, S. B	672
Shimada, M	677
Shimizu, A169, 311,	
Shimizu, K	
Shimizu, T117,	513
Shimkevich, A53,	
Shimozuma, T 44, 141, 159, 309, 509,	655
Shinohara, K 180, 367, 493,	495
Shinya, K	676
Sillitya, K	0/0
Shinya, T	294
Shiraga, H.45, 117, 609, 613, 614, 615-617,	693
Shiraishi, J 42, 403,	467
Shiraiwa, S 295, 297, 510,	558
Shiraki, D	219
Shishko, A	
Shmatov, M46,	625
Shmelev, A	563
Shoji, M 44, 159, 308, 473,	E70
5001. VI	D/U
Shpanskii, Y. S	550
Shpanskii, Y. S Shu, W	550 237
Shpanskii, Y. S Shu, W Shukla, B	550 237 152
Shpanskii, Y. S Shu, W Shukla, B	550 237 152
Shpanskii, Y. S Shu, W Shukla, B Shukla, B. K	550 237 152 130
Shpanskii, Y. S Shu, W Shukla, B Shukla, B. K Shurygin, F	550 237 152 130 527
Shpanskii, Y. S Shu, W Shukla, B Shukla, B. K Shurygin, F Shurygin, V	550 237 152 130 527 275
Shpanskii, Y. S Shu, W Shukla, B Shukla, B. K Shurygin, F Shurygin, V Shutov, K	550 237 152 130 527 275 502
Shpanskii, Y. S. Shu, W. Shukla, B. Shukla, B. K. Shurygin, F. Shurygin, V. Shutov, K. Sid, A.	550 237 152 130 527 275 502 619
Shpanskii, Y. S. Shu, W. Shukla, B. Shukla, B. K. Shurygin, F. Shurygin, V. Shutov, K. Sid, A. Sidorov, A.	550 237 152 130 527 275 502 619 204
Shpanskii, Y. S. Shu, W. Shukla, B. Shukla, B. K. Shurygin, F. Shurygin, V. Shutov, K. Sid, A. Sidorov, A.	550 237 152 130 527 275 502 619 204
Shpanskii, Y. S. Shu, W. Shukla, B. Shukla, B. Shurygin, F. Shurygin, V. Shutov, K. Sid, A. Sidorov, A. Sieglin, B. 455, 456,	550 237 152 130 527 275 502 619 204 669
Shpanskii, Y. S. Shu, W. Shukla, B. Shukla, B. K. Shurygin, F. Shurygin, V. Shutov, K. Sid, A. Sidorov, A. Sieglin, B. Sigov, A.	550 237 152 130 527 275 502 619 204 669 686
Shpanskii, Y. S. Shu, W. Shukla, B. Shukla, B. K. Shurygin, F. Shurygin, F. Shutov, K. Sid, A. Sidorov, A. Sieglin, B. Sigov, A. Silburn, S.	550 237 152 130 527 275 502 619 204 669 686 267
Shpanskii, Y. S. Shu, W. Shukla, B. Shukla, B. K. Shurygin, F. Shurygin, V. Shutov, K. Sid, A. Sidorov, A. Sieglin, B. Sigov, A. Silburn, S. Silva, A.	550 237 152 130 527 275 502 619 204 669 686 267 549
Shpanskii, Y. S. Shu, W. Shukla, B. Shukla, B. K. Shurygin, F. Shurygin, V. Shutov, K. Sid, A. Sidorov, A. Sieglin, B. Silburn, S. Silva, A. Silva, C.	 550 237 152 130 527 275 502 619 204 669 686 267 549 363
Shpanskii, Y. S. Shu, W. Shukla, B. Shukla, B. K. Shurygin, F. Shurygin, V. Shutov, K. Sid, A. Sidorov, A. Sieglin, B. Silburn, S. Silva, A. Silva, C.	 550 237 152 130 527 275 502 619 204 669 686 267 549 363
Shpanskii, Y. S. Shu, W. Shukla, B. Shukla, B. Shurygin, F. Shurygin, V. Shutov, K. Sidorov, A. Sieglin, B. Silburn, S. Silva, A. Silva, C. Simon, M.	550 237 152 130 527 275 502 619 204 669 686 267 549 363 511
Shpanskii, Y. S. Shu, W. Shukla, B. Shukla, B. Shurygin, F. Shurygin, V. Shutov, K. Sidorov, A. Sidorov, A. Sieglin, B. Silburn, S. Silva, A. Silva, C. Simon, M.	550 237 152 130 527 502 619 204 669 686 267 549 363 511 176
Shpanskii, Y. S. Shu, W. Shukla, B. Shukla, B. Shukla, B. Shukla, B. Shukla, B. Shurygin, F. Shurygin, V. Shutov, K. Sid, A. Sidorov, A. Sieglin, B. Silburn, S. Silburn, S. Silva, A. Simon, M. Simon, P. Simonen, T.	550 237 152 130 527 275 502 619 204 669 686 267 549 363 511 176 597
Shpanskii, Y. S. Shu, W. Shukla, B. Shukla, B. Shukla, B. Shukla, B. Shukla, B. Shukla, B. Shurygin, F. Shurygin, V. Shutov, K. Sid, A. Sidorov, A. Sieglin, B. Sigov, A. Silburn, S. Silva, A. Silva, C. Simon, M. Simon, P. Simonen, T. Simpson, J.	550 237 152 130 527 275 502 619 204 669 686 267 549 363 511 176 597 443
Shpanskii, Y. S. Shu, W. Shukla, B. Shukla, B. Shukla, B. Shukla, B. Shurygin, F. Shurygin, V. Shutov, K. Sid, A. Sidorov, A. Sieglin, B. Silburn, S. Silva, A. Silva, C. Simon, M. Simon, P. Simonon, J. Singh, A. K.	550 237 152 130 527 275 502 619 204 669 686 267 549 363 511 176 597 443 130
Shpanskii, Y. S. Shu, W. Shukla, B. Shukla, B. Shukla, B. Shukla, B. Shurygin, F. Shurygin, V. Shutov, K. Sid, A. Sidorov, A. Sieglin, B. Silburn, S. Silva, A. Silva, C. Simon, M. Simon, P. Simonon, J. Singh, A. K.	550 237 152 130 527 275 502 619 204 669 686 267 549 363 511 176 597 443 130
Shpanskii, Y. S. Shu, W. Shukla, B. Shurygin, F. Shurygin, Y. Shurygin, V. Silva, A. Silburn, S. Silva, A. Silva, A. Silva, C. Simon, M. Simon, P. Simonen, T. Simpson, J. 146, 164, Singh, A. K. Singh, R. 14, 376,	550 237 152 237 275 502 619 204 669 686 267 549 363 511 176 597 443 130 385
Shpanskii, Y. S. Shu, W. Shukla, B. Shukla, B. K. Shurygin, F. Shurygin, V. Shutov, K. Sid, A. Sidorov, A. Sieglin, B. Silva, A. Silva, A. Simon, M. Simonen, T. Simonen, J. 146, 164, Singh, R. Sio, H.	550 237 152 237 275 502 619 204 669 686 267 549 363 511 176 597 443 130 385 608
Shpanskii, Y. S. Shu, W. Shukla, B. Shukla, B. K. Shurygin, F. Shurygin, V. Shutov, K. Sid, A. Sidorov, A. Sieglin, B. Silva, A. Silva, A. Simon, M. Simonen, T. Simonen, J. 146, 164, Singh, R. Sio, H.	550 237 152 207 502 619 204 669 686 267 549 363 511 176 597 443 130 385 608
Shpanskii, Y. S. Shu, W. Shukla, B. Shurygin, F. Shurygin, F. Shurygin, V. Shurygin, V. Shurygin, V. Shutov, K. Sid, A. Sidorov, A. Sieglin, B. Sigov, A. Silburn, S. Silburn, S. Silva, A. Silva, A. Silva, C. Simon, M. Simon, P. Simonen, T. Simpson, J. Singh, A. K. Singh, R. Singh, R. Sipilä, S. Sips, A.48, 55, 146, 158, 162, 163, 239, 277,	550 237 152 237 275 502 619 204 669 686 267 549 363 511 176 597 443 130 385 608 414 284,
Shpanskii, Y. S. Shu, W. Shukla, B. Shurygin, F. Shurygin, F. Shurygin, V. Shurygin, V. Shurygin, V. Shutov, K. Sid, A. Sidorov, A. Sieglin, B. Sigov, A. Silburn, S. Silburn, S. Silva, A. Silva, A. Silva, C. Simon, M. Simon, P. Simonen, T. Simpson, J. Singh, A. K. Singh, R. Singh, R. Sipilä, S. Sips, A.48, 55, 146, 158, 162, 163, 239, 277,	550 237 152 237 275 502 619 204 669 686 267 549 363 511 176 597 443 130 385 608 414 284,
Shpanskii, Y. S. Shu, W. Shukla, B. Shukla, B. K. Shurygin, F. Shurygin, F. Shurygin, K. Shutov, K. Sid, A. Sidorov, A. Sidorov, A. Silourn, S. Silva, A. Silva, C. Simon, M. Simonen, T. Simonen, T. Singh, A. K. Singh, R. Sipila, S. Sipila, S. Sipila, S. Sips, A.48, 55, 146, 158, 162, 163, 239, 277, 285, 290, 291 Siren, P.	550 237 152 275 502 619 204 669 686 267 549 363 511 176 597 443 130 385 608 414 284, 279
Shpanskii, Y. S. Shu, W. Shukla, B. Shukla, B. K. Shurygin, F. Shurygin, V. Shutov, K. Sid, A. Sidorov, A. Sieglin, B. Silburn, S. Silva, A. Silva, C. Simonen, T. Simonen, T. Simpson, J. 146, 164, Singh, R. Sioje, A. Singson, J. Singh, R. Sigi, S. Sipilä, S. Sips, A.48, 55, 146, 158, 162, 163, 239, 277,	550 237 152 275 502 619 204 669 686 267 549 363 511 176 597 443 130 385 608 414 284, 279

Sivak, P	639
Sizyuk, T 53, 211,	635
Skakov, M	
Skokov, V. G.	550
Skoric, M	.378
Skosyrev, Y	173
Skovoroda, A457,	
Smirnov, A	
Smirnov, D	399
Smirnov, I.	637
Smirnov, R	
Smith, M	
Smith, S 19, 209, 213, 466,	
Smith, S. P	
Snicker, A.	
Snipes, J	667
Snipes, J. A.	
Snyder, P.	
Snyder, P. B.27, 36, 136, 145, 231, 361, 466,	663
689	000,
Sokolov, M.	515
Solano, E	
Soldatkina, E	
Solomakhin, A.	
Solomatin, R.	
Solomon, W.	
Solomon, W. M136, 142, 210, 212, 361,	657
659–661, 663	0.57,
Soloviev, V	200
Someya, Y	679
Sonara, D. P	
Sonehara, M.	294
Song, S.	
Song, X	334
Song, Y	227
Sonnendrucker, E.	270
Sorbom, B	200
Sorokina, E	602
Sorokovikova, A.	
Soukhanovskii, V. 160 , 210, 315, 316, 476,	586
590, 654	560,
Soures, J	608
Sovinec, C	433
Sozzi, C 20, 151, 220, 224–226, 278,	285
Spineanu, F	431
Spitsyn, A	553
Spitsyn, A. V.	550
Spizzo, G	196
Spolaore, M	10/
Spong, D	169
Srikant, G. L. N.	
Srinivas, Y	
Srinivas, 1	
Stinivasan, K	
Jt j01111, 11	400

Staebler, G. M 36, 386, 451, 466,	657
Stahle, P Stamp, M.158, 275, 279–281, 364, 423, 455,	298
Stamp, M.158, 275, 279–281, 364, 423, 455,	456
Stangeby, P. C.	211
Stankiewicz, R	384
Steinhauer, L	604
Stepanov, A	
Stepanov, B	
Stepanov, I.	
Stephens, H.	
Stepniewski, W	201
Stevenson, T	
Stieglitz, R.	
Stoafer, C.	257
Stober, J 162,	
Stöckel, J	
Stolberg, K	
Stolyarova, V	
Stotler, D	362
Strait, E. J	218
Strait, T	
Strand, P	424
Stratten, B	
Strauss, H	
Strauss, H. R	
Striebig, A.	
Stuilchamary M	527
Strikhanov, M	183
Stroth, U 56, 62, 171, 177,	183
Stroth, U 56, 62, 171, 177, Strumberger, E	183 180
Stroth, U	183 180 128
Stroth, U	183 180 128 592
Stroth, U	183 180 128 592 173
Stroth, U. 56, 62, 171, 177, Strumberger, E. Stupishin, N. Suarez, A. Subbotin, G. Subbotin, S. 561,	183 180 128 592 173 562
Stroth, U. 56, 62, 171, 177, Strumberger, E. Stupishin, N. Suarez, A. Subbotin, G. Subbotin, G. 561, Sudo, S. 44, 303,	183 180 128 592 173 562 307
Stroth, U. 56, 62, 171, 177, Strumberger, E. Stupishin, N. Suarez, A. Subbotin, G. Subbotin, G. 561, Sudo, S. 44, 303, Sugama, H. 474,	 183 180 128 592 173 562 307 487
Stroth, U. 56, 62, 171, 177, Strumberger, E. Stupishin, N. Suarez, A. Subbotin, G. Subbotin, G. 561, Sudo, S. 44, 303, Sugama, H. 474, Sugiyama, L. 14, 50, 60, 383, 404, 437, 488,	183 180 128 592 173 562 307 487 <i>583</i>
Stroth, U. 56, 62, 171, 177, Strumberger, E. Stupishin, N. Suarez, A. Subbotin, G. Subbotin, S. 561, Sudo, S. 44, 303, Sugama, H. 474, Sugiyama, L. 14, 50, 60, 383, 404, 437, 488, Sugiyama, L. E. 43,	183 180 128 592 173 562 307 487 <i>583</i> <i>297</i>
Stroth, U. 56, 62, 171, 177, Strumberger, E. Stupishin, N. Suarez, A. Subbotin, G. Subbotin, G. 561, Subbotin, S. 561, Sudo, S. 44, 303, Sugama, H. 474, Sugiyama, L. 14, 50, 60, 383, 404, 437, 488, Sugiyama, L. E. 43, Sukhanova, M. 50,	183 180 128 592 173 562 307 487 <i>583</i> <i>297</i> 533
Stroth, U. 56, 62, 171, 177, Strumberger, E. Stupishin, N. Suarez, A. Subbotin, G. Subbotin, S. 561, Subotin, S. 561, Sugama, H. 474, Sugiyama, L. 14, 50, 60, 383, 404, 437, 488, Sugiyama, L. E. 43, Sukhanova, M. 324,	183 180 128 592 173 562 307 487 <i>583</i> <i>297</i> 533 492
Stroth, U. 56, 62, 171, 177, Strumberger, E. Stupishin, N. Suarez, A. Subbotin, G. Subbotin, G. 561, Sudo, S. 561, Sugama, H. 474, Sugiyama, L. 14, 50, 60, 383, 404, 437, 488, Sugiyama, L. E. 43, Sukhanova, M. 324, Sun, A. 324, Sun, P. 30,	183 180 128 592 173 562 307 487 583 297 533 492 331
Stroth, U. 56, 62, 171, 177, Strumberger, E. Stupishin, N. Suarez, A. Subbotin, G. Subbotin, S. 561, Subotin, S. 561, Sugama, H. 474, Sugiyama, L. 14, 50, 60, 383, 404, 437, 488, Sugiyama, L. E. 43, Sukhanova, M. 324,	183 180 128 592 173 562 307 487 583 297 533 492 331
Stroth, U. 56, 62, 171, 177, Strumberger, E. Stupishin, N. Suarez, A. Subbotin, G. Subbotin, S. 561, Sudo, S. 44, 303, Sugama, H. 474, Sugiyama, L. 14, 50, 60, 383, 404, 437, 488, Sugiyama, L. E. 43, Sukhanova, M. Sun, A. Sun, A. 324, Sun, P. 50, 324,	183 180 128 592 173 562 307 487 583 297 533 492 331 492
Stroth, U. 56, 62, 171, 177, Strumberger, E. Stupishin, N. Suarez, A. Subbotin, G. Subbotin, S. 561, Subbotin, S. 561, Subotin, S. 44, 303, Sugama, H. 474, Sugiyama, L. 14, 50, 60, 383, 404, 437, 488, Sugiyama, L. E. 43, Sukhanova, M. 324, Sun, A. 324, Sun, T. 156, 324, Sun, X. 156, 324,	183 180 128 592 173 562 307 583 297 533 492 331 492 335
Stroth, U. 56, 62, 171, 177, Strumberger, E. Stupishin, N. Suarez, A. Subbotin, G. Subbotin, S. 561, Sudo, S. 44, 303, Sugama, H. 474, Sugiyama, L. 14, 50, 60, 383, 404, 437, 488, Sugiyama, L. E. 43, Sukhanova, M. 324, Sun, A. 324, Sun, T. 156, 324, Sun, X. 139, 232, 339,	183 180 128 592 173 562 307 487 583 297 533 492 331 492 335 449
Stroth, U. 56, 62, 171, 177, Strumberger, E. Stupishin, N. Suarez, A. Subbotin, G. Subbotin, S. 561, Sudo, S. 44, 303, Sugama, H. 474, Sugiyama, L. 14, 50, 60, 383, 404, 437, 488, Sugiyama, L. E. 43, Sukhanova, M. 324, Sun, P. 50n, 7. Sun, Y. 156, 324, Sun, X. 309, 232, 339, Sun, Z. 234,	183 180 128 592 173 562 307 487 583 297 533 492 331 492 335 449 335
Stroth, U. 56, 62, 171, 177, Strumberger, E. Stupishin, N. Suarez, A. Subbotin, G. Subbotin, S. 561, Subbotin, S. 561, Sudo, S. 44, 303, Sugama, H. 474, Sugiyama, L. 14, 50, 60, 383, 404, 437, 488, Sugiyama, L. E. 43, Sukhanova, M. 324, Sun, A. 324, Sun, Y. 139, 232, 339, Sun, Z. 234, Sunahara, A. 117, 609, 613, 617, 620–623,	183 180 128 592 173 562 307 487 583 297 533 492 331 492 335 449 316 693
Stroth, U. 56, 62, 171, 177, Strumberger, E. Stupishin, N. Suarez, A. Subbotin, G. Subbotin, S. 56, 61, Subbotin, S. 56, 62, 171, 177, Subbotin, G. Subbotin, S. Subbotin, S. 56, 61, Sudo, S. 44, 303, Sugama, H. 474, Sugiyama, L. 14, 50, 60, 383, 404, 437, 488, Sugiyama, L. E. 43, Sukhanova, M. 324, Sun, A. 324, Sun, P. 30n, 7. Sun, X. 139, 232, 339, Sun, Z. 234, Sunahara, A. 117, 609, 613, 617, 620–623, Supe, A. 317, 609, 613, 617, 620–623,	1833 1800 1288 5922 1733 5622 307 4877 5333 2977 5333 4922 3311 4922 3355 4499 3166 693 6488
Stroth, U. 56, 62, 171, 177, Strumberger, E. Stupishin, N. Suarez, A. Subbotin, G. Subbotin, S. 56, 61, Subbotin, S. 56, 62, 171, 177, Subbotin, G. Subbotin, S. Subbotin, S. 56, 61, Sudo, S. 44, 303, Sugama, H. 474, Sugiyama, L. 14, 50, 60, 383, 404, 437, 488, Sugiyama, L. E. 43, Sukhanova, M. 324, Sun, A. 324, Sun, T. 156, 324, Sun, X. 39, 232, 339, Sun, Z. 234, Sunahara, A. 117, 609, 613, 617, 620–623, Supe, A. 546,	1833 1800 1288 5922 1733 562 307 4877 5833 2977 5333 4922 3311 4922 3316 693 6488 569
Stroth, U. 56, 62, 171, 177, Strumberger, E. Stupishin, N. Suarez, A. Subbotin, G. Subbotin, S. 561, Subbotin, S. 561, Sudo, S. 44, 303, Sugama, H. 474, Sugiyama, L. 14, 50, 60, 383, 404, 437, 488, Sugiyama, L. E. 43, Sukhanova, M. 324, Sun, P. 50n, T. Sun, Y. 139, 232, 339, Sun, X. 234, Sunatara, A. 117, 609, 613, 617, 620–623, Supe, A. 546, Sushkov, A. 60, 515,	1833 1800 1288 5922 1733 562 307 4877 5333 4922 3314 492 335 4492 3166 693 6488 569 585
Stroth, U. 56, 62, 171, 177, Strumberger, E. Stupishin, N. Suarez, A. Subbotin, G. Subbotin, S. 561, Subbotin, S. 561, Subbotin, S. 561, Sugama, H. 474, Sugiyama, L. 14, 50, 60, 383, 404, 437, 488, Sugiyama, L. E. 43, Sukhanova, M. 324, Sun, A. 324, Sun, Y. 139, 232, 339, Sun, X. 234, Sunahara, A. 117, 609, 613, 617, 620–623, Supe, A. Surey, E. 546, Sushkov, A. 60, 515, Sutherland, D. 59, 580,	1833 1800 1288 5922 1733 562 307 4877 5333 4922 3314 492 335 4499 3166 693 6488 569 585 600
Stroth, U. 56, 62, 171, 177, Strumberger, E. Stupishin, N. Suarez, A. Subbotin, G. Subbotin, S. 561, Subbotin, S. 561, Subbotin, S. 561, Subotin, S. 561, Subotin, S. 561, Sudo, S. 44, 303, Sugama, H. 474, Sugiyama, L. 14, 50, 60, 383, 404, 437, 488, Sugiyama, L. E. 43, Sukhanova, M. 324, Sun, A. 324, Sun, T. 156, 324, Sun, X. 234, Sunahara, A. 117, 609, 613, 617, 620–623, Supe, A. 34, Surrey, E. 546, Sushkov, A. 60, 515, Sutherland, D. 59, 580, Suttrop, W. 15, 137, 180, 181,	183 180 128 592 173 562 307 487 583 297 533 492 331 492 335 4 92 3316 693 648 569 585 600 241
Stroth, U. 56, 62, 171, 177, Strumberger, E. Stupishin, N. Suarez, A. Subbotin, G. Subbotin, S. 561, Sudo, S. 44, 303, Sugama, H. 474, Sugiyama, L. 14, 50, 60, 383, 404, 437, 488, Sugiyama, L. 14, 50, 60, 383, 404, 437, 483, Sugiyama, L. 14, 50, 60, 383, 404, 437, 483, Sugiyama, L. 20, 60, 383, 404, 437, 483, Sugiyama, L. 14, 50, 60, 383, 404, 437, 483, Sugiyama, L. 14, 50, 60, 383, 404, 437, 483, Sugiyama, L. 14, 50, 60, 383, 404, 437, 483, Sugiyama, L. 20, 60, 383, 404, 437, 483, Sugiyama, L. 14, 50, 60, 383, 404, 437, 483, Sugiyama, L. 14, 50, 60, 383, 404, 437, 483, Sugiyama, L. 20, 60, 383, 404, 437, 483, Sugiyama, L. 20, 60, 383, 404, 437, 483, Sun, T. 139, 232, 339, Sun, T. 139, 232, 339, Sun, Y. 139, 232, 339, Sun, Y. 139, 232, 339, Sun, Y. 139, 232, 339, Sun, Z. 234, Sunahara, A. 117, 609, 613, 617, 620–623, Supe, A. 546, Sushkov, A. 60, 515, Sutherland, D.	183 180 128 592 173 562 307 487 583 297 533 492 331 492 335 648 569 585 600 241 534
Stroth, U. 56, 62, 171, 177, Strumberger, E. Stupishin, N. Suarez, A. Subbotin, G. Subbotin, S. 561, Subbotin, S. 561, Subbotin, S. 561, Subotin, S. 561, Subotin, S. 561, Sudo, S. 44, 303, Sugama, H. 474, Sugiyama, L. 14, 50, 60, 383, 404, 437, 488, Sugiyama, L. E. 43, Sukhanova, M. 324, Sun, A. 324, Sun, T. 156, 324, Sun, X. 234, Sunahara, A. 117, 609, 613, 617, 620–623, Supe, A. 34, Surrey, E. 546, Sushkov, A. 60, 515, Sutherland, D. 59, 580, Suttrop, W. 15, 137, 180, 181,	183 180 128 592 173 562 297 533 492 331 492 335 492 331 6 693 6 693 6 693 669 585 600 2411 534 655

Suzuki, Y 52, 138, 261, 304, 310-312, 36	57, 371,
433, 493 , 584, 655	
Svalov, G	502
Svennson, L	512
Svensson, J	456
Svidzinski, V	38, 603
Sychevsky, S.	537
Sychugov, D	34, 593
Sysoeva, E	366
Sytchevsky, S	666
Szherbak, A	203

 Т	_

Tabares, F	Ŀ
Tafalla, D124	E.
Taga, M)
Taguchi, T117, 609, 616	5
Tahiliani, K)
Takagi, I)
Takagi, M	
Takahashi, H 159, 305, 309, 472, 509, 655	5
Takahashi, K	
Takahashi, T	E.
Takahashi, Y534	
Takamura, J	E.
Takamura, S)
Takase, Y	ł.
Takayama, A)
Takeda, H)
Takeda, N	2
Takeiri, Y	
Takemura, Y	2
Takenaga, H154	Ł
Takizuka, T	3
Tal, B246	5
Tala, T 15, 179)
Tamain, P	
Tamura, H 577	7
Tamura, N141, 159, 300, 303, 307, 655	;
Tamura, T)
Tan, Y45, 317	
Tanaka, H 52, 159, 245, 300, 301, 340, 517	7
Tanaka, K.138, 141, 159, 241, 261, 305, 307, 311	,
312, 474, 655	
Tanaka, S	2
Tanaka, T630)
Tanaka, Y	
Tanchuk, V 133, 581, 652	
Tang, W43, 469	
Tanigawa, H 679	
Tank, J. K130	
Tanna, R	
Tanna, R. L	
Tanna, V. L)

	630
Tavani, M	
Taylor, D	
Taylor, G.	438, 475, 586, 660
Tazhibayeva, I	
Telesca, G	
Tendler, M	
Teplova, N	
Terakado, M	
Terazaki, Y	
Terranova, D	
Terry, J	145, 295, 296, 510, 558
	12, 18, 126, 128, 243, 244
Terzolo I	
Theiler C	145, 250, 299, 363, 558
Thomas, J	
Thomas, M	
	G. N
Titus, J	
Titus, P	520, 543, 544, 558, 586
Tiwari, S. K	
Tobari, H	35, 512, 513
Tobias, B. J	
Tobita, K	517, 518, 555, 679
Todd, T	
Todo, Y	. 49, 55, 371, 372, 382, 495
Toi, K	
Toigo, V	
Tokunaga. S.	
Told, D.	
Tolstvakov S 133 1	88, 189, 283, 631, 652, 677
Tomarchio, V	

— U —

Uchida, M	340
Uder, C	579
Udintsev, V	
Udintsev, V. S.	
Ueba, R	
Ueda, Y	
Uesugi, Y	
Umansky, M.	
Umeda, N	512, 513
Unezhev, V	642

Unterberg, B	
Unterberg, E. A	.136, 138, 315, 654
Urano, H 146, 154, 284	, 367, 368, 493, 494
Uron, K	
Ushiki, T	
Usui, K	
Utin, Y	
Utoh, H	517, 518, 555
Utsugi, M	609

— V —

Vadim, Y	437
Vafin, S	
Valanju, P	590
Valeo, E. J	
Valisa, M40, 48, 153,	277
Vallet, JC53, 560,	
Valovic, M 31 , 137,	266
Valtenbergs, O	648
Van Eester, D	290
Van Oost, G	134
van Rooij, G 280,	456
Van Schoor, M	479
van Wyk, F	
Van Zeeland, M. 48, 55, 167, 168, 180, 372, 3	375,
657	
Van Zeeland, M. A	
Varadarajulu, A	
Varfolomeev, V133, 188, 389,	
Varia, A	
Varmora, P	130
Varoutis, S	568
Vasilevskiy, I	
Vayakis, G 237, 525,	677
Vdovin, V	541
Vekshina, E133,	390
Velasco, J. L	270
Velikhov, E. P	
Veranda, M	450
Verdoolaege, G	251
Verger, J. M	576
Vergote, M	356
Vermare, L	
Vernay, T	
Verona Rinati, G	
Verona, C.	
Verrecchia, M	574
Vershkov, V	173
Vertkov, A17, 201, 203, 219,	651
Vertongen, P.	504
Vervier, M	
Veselova, I.	360
Veshchev, E	275

Vezinet, D	182
Victor, B	
Vieira, R	5, 558
Viezzer, E14, 27, 35, 144, 177, 179, 181	, 299
360, 690	
Vijvers, W	248
Vildjunas, M	3-320
Vilemova, M.	
Villard, L	1,688
Villari, R	. 549
Villone, F 228, 288, 583	
Vincenzi, P.	
Vinnichenko, A	
Vinyar, I	234
Viola, B	9,228
Vitale, V	
Vitupier, G.	504
Vlad, G	
Vlad, M	431
Vladimir, K	. 529
Voitsekhovitch, I163	
Voitsenya, V	342
Volpe, F252	2, 259
Volpe, F. A	. 218
von Halle, A	. 586
von Hellermann, M.	
von Nessi, G	. 442
Vora, M. M.	130
Vorobyov, G. M.	. 254
Voronin, A 133, 389	9,652
Voronova, A	
Voskoboinikov, S 133, 360), 390
Vostner, A	501
Vuille, V	5, 249
Vukolov, D.	275
Vukolov, K.	. 275
Vysotsky, V 29	9, <mark>50</mark> 2

• W –

Wada, K	
Wada, M	
Wade, M. R	13, 23 , 136
Wagner, C	610
Wagner, D	
Wagner, F.	
Wahb, E	
Wakasa, A	
Wakatsuki, T	
Waksman, J	128
Walk, J	
Walker, M. L.	
Wallace, G.	295, 297, 558
Walsh, M.	

Waltz, R. E	
Wampler, W. R.	
Wan, B. 11, 13, 119, 166, 215,	227, 229, 232, 234,
235, 316, 657	
Wan, L	
Wang, A	
Wang, E	
Wang, F	229
Wang, G	
Wang, H 14 , 166	.230.232.234.382
Wang, L 23, 132	230 232 234 339
Wang, M	229 232 235 535
Wang, M. X	588
Wang, N	
Wang, P	E0 520 650
Wang, Q	101
Wang, S	
wang, 5	
Wang, W	
Wang, X	
Wang, X. G	
Wang, Y 33, 121	
Wang, Z 51 , 132, 156, 398	, 408, 427, 449, 492
Wang, Z. R	
Wanner, M	
Ward, D	
Wash, M	
Watanabe, H	
Watanabe, K 260, 261, 304	, 310, 312, 512, 513
Watanabe, O	
Watanabe, T	378, 494
Watanabe, TH	
Watanabe, T. G	
Watanabe, Y	
Watari, T	
Watkins, J. G.	.136, 160, 210, 211
Wauters, T	
Wehner, W. P	
Wei, L	
Wei, M	
Wei, R	
Wei, W	
Wei, Y	
Wei, Z	
Weiland, M	178 395
Weinhorst, B.	594
Weisen, H.	
Weller, A.	
Wenninger, R	30 516 660
Wenzel, U	
Wesley, J	
Wessel, F	
Whalen C	106 109 044
Whelan, G.	145 200 206 552
White, A	
White, R	

White, R. B	
Whyte, D	43, 295, 298, 299, 558
Widdowson, A	
Wiesen, S.	
Wikman, S	
Wilgen, J.	
Wilks, S	
Willensdorfer, M	
Williams, G. J	
Williams, M.	
Wilson, H. R	
Wilson, J	
Wilson, J. R	
Wilson, R	
Wingen, A.	136, 207, 315
Wischmeier, M 24, 47,	
669	
Wölz, M	
Wolf, R	
Wolfe, S. M	296, 297, 299, 558, 659
Wolfrum, E 144, 177, 1	180, 181, 183, 299, 690
Wong, C. P	
Woolley, R	
Wright, J. C	
Wu, J	
Wu, Y	597, 681, 682, 688
Wu, Z	
Wukitch, S 22, 35, 2	227, 290, 297, 510 , 558

v	
 Λ	

Xanthopoulos, P359	
Xi, P	5
Xia, F	ł
Xia, T 20 , 231, 407 , 492	2
Xiang, L	Ł
Xiao, B	
Xiao, C	
Xiao, Y 20 , 166, 174, 40 6	
Xie, H	
Xie, H. S	2
Xie, J	;
Xie, Y 236	5
Xin, W	;
Xiong, Y)
Xu, G 45, 48, 55, 119, 166, 232, 234, 235, <i>316</i>	,
657	
Xu, H	5
Xu, H. B 60, 588	3
Xu, J)
Xu, M 11 , 17 , 121 , 327, 328, 332, 335, 449, 492	2
Xu, X 161, 166, 231, 374, 385, 407, 492	2
Xu, X. Y)
Xu, Y 24, 50, 58, 121, 124, 156, 236 , 323, 324	,
327, 328, 331, 333, 334, 356 , 449	

Xu, Z	650
Xuan, W	121

- Y —

— 1 —	
Yabuuchi, K	
Yadav, R	321
Yagi, M358, 400, 430, 452, 453,	
Yajima, M	
Yakovlev, D	253
Yamada, H 124, 141, 302, 307, 312,	655
Yamada, I	312
Yamada, T	
Yamaguchi, H	472
Yamaguchi, K	512
Yamaguchi, T	294
Yamamoto, S 30, 258, 259, 260,	261
Yamanaka, H	513
Yamanoi, K	
Yamasaki, K	205
Yamasaki, M.	
Yamauchi, K.	578
Yamoto, S	486
Yan, L121, 174, 325, 327, 328, 330, 331,	334,
335 339	
Yan, L. W	332
Yan, N	
Yan, Z142, 175, 299,	689
Yanagi, N	
Yanai, R	205
Yang, C	
Yang, J	
Yang, Q 121, 156, 174, 324, 325, 327–332,	
Yang, Q. W	326
Yang, S	
Yang, SM.	
Yang, Y	
Yang, Z	
Yano, Y	
Yao, K	
Yao, L	
Yarim, C	
Yashin, A	
Yasuhara, R	
Yatsu, K.	
Ye, M	
Yeom, J	
Yi, S	465
Yokokura, K	
Yokoyama, K	
Yokoyama, M 43 , 169, 260, 261, 302 , 307,	+70 172
10K0yallia, IVI 43, 109, 200, 201, 302, 307, 556, 584, 655	±/ 4,
556, 584, 655 Yoo, J	348
Yoo, J. W	35/
100, j. **	554

Yoo, MG.	572
Yoon, S	
Yoon, SW 11 , 13 , 120 , 140, 345, 349, 6	573
Yoshida, H 1	
Yoshida, K.	574
Yoshida, M 40, 48, 154, 367, 494, 5	513
Yoshida, N 1	191
Yoshida, Z	584
Yoshikawa, M	570
Yoshimoto, Y	
Yoshimura, Y 159, 309, 509, 6	555
Yoshinuma, M. 43, 305, 307, 310, 311, 472, 6	555
You, K	348
You, KI	345
Young, W 2	243
Yu, C 121, 263, 3	335
Yu, D 50 , 121, 174, 325 , 327, 328, 334, 4	192
Yu, J4	108
Yu, L 51 , 121, 328, 330 , 332, 4	
Yu, W	
Yu, Y	
Yuan, B121, 1	156
Yuan, G	329
Yuan, X	
Yuh, H	313
Yukhimchuk, A	
Yun, G 155, 161, 344–346, 352 , 353, 3	
Yurchenko, E4	109

	Ζ	
--	---	--

Zabeo, L	667
Zaccaria, P	511
Zadvitskiy, G	133, 189, 390
Zagorski, R	.26, 293, 384, 428, 441
Zakharov, A	
Zakharov, L	
Zalavutdinov, R	
Zamanov, N	
Zanca, P	
Zang, L	
Zang, Q	
Zani, L	
Zanino, R	
Zaniol, B	
Zarins, A.	
Zarzoso, D	
Zatekin, V	
Zaytsev, K	
Zebrowski, J	
Zemedkun, S	
Zeng, L 142, 143, 1	150, 175, 213, 232, 333
Zenin, V	
Zhai, Y	32, 520, 521, 544

Zhang, C	638
Zhang, H	229
Zhang, J	121, 649
Zhang, L	
Zhang, S	32 233 335
Zhang, T	32,233,333
Zhang, W	
Zhang, X 23, 227, 229, 290, 33	39, 468, 564
Zhang, Y 51 , 323, 326, 32	29 , 332, 333
Zhang, Z	45, 609, 613
Zhao, C	
Zhao, H	
Zhao, J.	
Zhao, K 52 , 132, 174, 325, 327, 33	24 220 401
ZIIdO, N52, 152, 174, 525, 527, 50	54, 559 , 401
Zhao, L.	
Zhao, Y	
Zhap, Y	235
Zharkov, M	
Zheng, G	
Zheng, L	50 128 482
Zheng, P.	54 408 638
Zheng, S	
Zhilin, E	133, 581
Zhirkin, A	53 , 596
Zhogolev, V	15, 418, 421
Zhogolev V F	661
Zilogoicv, v. L	
Zhong, W. 51 , 121, 174, 323–325, 32	
Zhogolev, V. E Zhong, W. 51 , 121, 174, 323–325, 32 334, 492	27, 328 , 332,
334, 492	
334, 492 Zhou, C	
334, 492 Zhou, C Zhou, H	
334, 492 Zhou, C Zhou, H Zhou, J	
334, 492 Zhou, C Zhou, H Zhou, J Zhou, T	
334, 492 Zhou, C Zhou, H Zhou, J	
334, 492 Zhou, C Zhou, H Zhou, J Zhou, T	
334, 492 Zhou, C Zhou, H Zhou, J Zhou, T Zhou, Y Zhou, Y	
334, 492 Zhou, C Zhou, H Zhou, J Zhou, T Zhou, Y Zhou, Y Zhu, G Zhu, J	
334, 492 Zhou, C. Zhou, H. Zhou, J. Zhou, J. Zhou, Y. Zhou, Y. Zhu, G. Zhu, J. Zhu, P.	
334, 492 Zhou, C. Zhou, H. Zhou, J. Zhou, T. Zhou, Y. Zhu, G. Zhu, J. Zhu, P. Zhu, X.	
334, 492 Zhou, C. Zhou, H. Zhou, J. Zhou, J. Zhou, Y. Zhou, Y. Zhu, G. Zhu, G. Zhu, P. Zhu, Y. Zhu, R. Zhu, R. Zhuang, G. 12, 12	504 331 121 488 25, 328, 330
334, 492 Zhou, C. Zhou, H. Zhou, J. Zhou, J. Zhou, Y. Zhou, Y. Zhu, G. Zhu, J. Zhu, P. Zhu, X. Zhuang, G. Lu, 12, 13 Zhuang, H.	504 331 121 488 25, 328, 330 327 42, 468 433 529 32 , 333, 339 333
334, 492 Zhou, C. Zhou, H. Zhou, J. Zhou, Y. Zhou, Y. Zhou, Y. Zhu, G. Zhu, J. Zhu, J. Zhu, Y. Zhu, X. Zhuang, G. Zhuang, H. Zhubr, N.	504 331 121 488 25, 328, 330 327 42, 468 433 529 32, 333, 339 333 319, 320
334, 492 Zhou, C. Zhou, H. Zhou, J. Zhou, J. Zhou, Y. Zhou, Y. Zhu, G. Zhu, J. Zhu, P. Zhu, R. Zhuang, G. Zhuang, H. Zhuang, H. Zhuang, K. Zielinska, E.	504 331 121 488 25, 328, 330 327 42, 468 32, 328, 330 529 32, 333, 339 333 319, 320 646
334, 492 Zhou, C. Zhou, H. Zhou, J. Zhou, J. Zhou, Y. Zhou, Y. Zhu, G. Zhu, J. Zhu, P. Zhu, R. Zhuang, G. Zhuang, H. Zhuang, H. Zhuang, K. Zielinska, E.	504 331 121 488 25, 328, 330 327 42, 468 32, 328, 330 529 32, 333, 339 333 319, 320 646
334, 492 Zhou, C. Zhou, H. Zhou, J. Zhou, J. Zhou, Y. Zhou, Y. Zhu, G. Zhu, G. Zhu, P. Zhu, P. Zhu, X. Zhuang, G. Zhuang, H. Zhuang, H. Zielinska, E. Zocco, A.	504 331 121 488 25, 328, 330
334, 492 Zhou, C. Zhou, H. Zhou, J. Zhou, Y. Zhu, G. Zhu, G. Zhu, P. Zhu, P. Zhu, X. Zhuang, G. Zhuang, H. Zhus, N. Zielinska, E. Zocco, A. Zohm, H. Zhou, N. Zhu, J. Zhu, G. Zhu, J. Zhu, S. Zhu, P. Zhu, P. Zhuang, G. 12, 12 Zhuang, H. Zhubr, N. Zielinska, E. Zocco, A. Zohm, H. Zhu, T. Zhubr, N. Zielinska, E. Zohm, H. Zohm, H. Zohm, H. Zhubr, H. Zhubr, H. Zhubr, M. Zhubr, M. Zohubr, M. Zohubr, H. Zhubr, H. Zhubr, M. Zhubr, M. Zhubr, M. Zhubr, M. <td>504 331 121 488 25, 328, 330 327 42, 468 529 32, 333, 339 333 319, 320 646 444 13, 165, 669</td>	504 331 121 488 25, 328, 330 327 42, 468 529 32, 333, 339 333 319, 320 646 444 13, 165, 669
334, 492 Zhou, C. Zhou, H. Zhou, J. Zhou, Y. Zhu, G. Zhu, G. Zhu, P. Zhu, P. Zhu, X. Zhuang, G. Zhuang, H. Zhubr, N. Zielinska, E. Zocco, A. Zoletnik, S.	504 331 121 488 25, 328, 330 327 42, 468 433 529 32, 333, 339 333 319, 320 646 444 13, 165, 669 471, 525
334, 492 Zhou, C. Zhou, H. Zhou, J. Zhou, T. Zhou, Y. Ill, J. Zhu, G. Zhu, G. Zhu, P. Zhu, P. Zhu, X. Zhuang, G. Zhuang, H. Zhubr, N. Zielinska, E. Zocco, A. Zoletnik, S. Zolfaghari, A.	
334, 492 Zhou, C. Zhou, H. Zhou, J. Zhou, T. Zhou, Y. Ill, J. Zhu, G. Zhu, G. Zhu, P. Zhu, P. Zhu, X. Zhuang, G. Zhuang, H. Zhubr, N. Zielinska, E. Zocco, A. Zoletnik, S. Zolfaghari, A.	
334, 492 Zhou, C. Zhou, J. Zhou, J. Zhou, Y. Zhou, Y. Zhu, G. Zhu, G. Zhu, J. Zhu, P. Zhu, X. Zhuang, G. Zhus, N. Zielinska, E. Zoco, A. Zoletnik, S. Zolfaghari, A. Zonca, F. Zou, X. 121, 174, 232, 22	504 331 121 488 25, 328, 330 529 32, 333, 339 3319, 320 42, 468 433 529 32, 333, 339 3319, 320 444 13, 165, 669 471, 525 586, 590 76, 468, 470 34, 328, 334
334, 492 Zhou, C. Zhou, J. Zhou, J. Zhou, Y. Zhu, G. Zhu, G. Zhu, J. Zhu, P. Zhu, X. Zhuang, G. Zhuz, Y. Zhuz, S. Zorco, A. Zoletnik, S. Zoletnik, S. Zolfaghari, A. Zouz, F. Zucchi, L.	504 331 121 488 25, 328, 330 327 42, 468 433 529 32, 333, 339 333 319, 320 444 13, 165, 669 471, 525 586, 590 76, 468, 470 34, 328, 334
334, 492 Zhou, C. Zhou, J. Zhou, J. Zhou, Y. Zhu, G. Zhu, G. Zhu, J. Zhu, J. Zhu, J. Zhu, Y. Zhu, S. Zoenco, A. Zolfaghari, A. Zou, X. I21, 174, 232, 22 Zucchi, L. Zuin, M.	504 331 121 488 25, 328, 330 327 42, 468 433 529 32, 333, 339 333 319, 320 444 13, 165, 669 471, 525 586, 590 76, 468, 470 34, 328, 334 583 583 196
334, 492 Zhou, C. Zhou, J. Zhou, J. Zhou, Y. Zhou, Y. Zhu, G. Zhu, J. Zhu, J. Zhu, P. Zhu, X. Zhuang, G. Zhusr, M. Zhusr, M. Zhuang, G. Zhusr, M. Zhusr, M. Zhuang, H. Zhusr, N. Zielinska, E. Zocco, A. Zohm, H. Zoletnik, S. Zolfaghari, A. Zonca, F. Zou, X. Zucchi, L. Zuro, B.	504 331 121 488 25, 328, 330 225, 328, 330 327, 42, 468 433 529 32, 333, 339 32, 333, 339 3319, 320 646 444 13, 165, 669 471, 525 5586, 590 76, 468, 470 76, 468, 470 34, 328, 334 583 196 31, 269, 270
334, 492 Zhou, C. Zhou, H. Zhou, J. Zhou, Y. Zhou, Y. Zhou, Y. Zhou, Y. Zhu, G. Zhu, J. Zhu, J. Zhu, Y. Zhu, S. Zhu, Y. Zhu, S. Zhu, Y. Zhuang, G. Zhuang, G. Zhubr, N. Zielinska, E. Zocco, A. Zohm, H. Zolfaghari, A. Zonca, F. Zurchi, L. Zuro, B. Zushi, H. 334, 492	504 331 121 488 25, 328, 330 327 42, 468 333 329 32, 333, 339 333 319, 320 646 441 13, 165, 669 471, 525 5, 586, 590 76, 468, 470 34, 328, 334 583 196 31, 269, 270 93, 509, 688
334, 492 Zhou, C. Zhou, H. Zhou, J. Zhou, Y. Zhou, Y. Zhou, Y. Zhou, Y. Zhu, G. Zhu, J. Zhu, J. Zhu, Y. Zhu, S. Zhu, Y. Zhu, S. Zhu, Y. Zhuang, G. Zhuang, G. Zhubr, N. Zielinska, E. Zocco, A. Zohm, H. Zolfaghari, A. Zonca, F. Zurchi, L. Zuro, B. Zushi, H. 334, 492	504 331 121 488 25, 328, 330 327 42, 468 333 329 32, 333, 339 333 319, 320 646 441 13, 165, 669 471, 525 5, 586, 590 76, 468, 470 34, 328, 334 583 196 31, 269, 270 93, 509, 688
334, 492 Zhou, C. Zhou, J. Zhou, J. Zhou, Y. Zhou, Y. Zhu, G. Zhu, J. Zhu, J. Zhu, P. Zhu, X. Zhuang, G. Zhusr, M. Zhusr, M. Zhuang, G. Zhusr, M. Zhusr, M. Zhuang, H. Zhusr, N. Zielinska, E. Zocco, A. Zohm, H. Zoletnik, S. Zolfaghari, A. Zonca, F. Zou, X. Zucchi, L. Zuro, B.	504 331 121 488 25, 328, 330 225, 328, 330 327, 42, 468 433 529 32, 333, 339 32, 333, 339 32, 333, 339 32, 333, 339 444 13, 165, 669 444 13, 165, 669 4471, 525 586, 590 76, 468, 470 76, 468, 470 34, 328, 334 583 583 196 31, 269, 270 93, 509, 688 62, 477, 558